BIOSENSORS – EMERGING MATERIALS AND APPLICATIONS

Edited by **Pier Andrea Serra**

INTECHWEB.ORG

Biosensors – Emerging Materials and Applications
Edited by Pier Andrea Serra

Published by InTech
Janeza Trdine 9, 51000 Rijeka, Croatia

Publishing Process Manager Mirna Cvijic
Technical Editor Teodora Smiljanic
Cover Designer Jan Hyrat
Image Copyright Goran Kuzmanovski, 2010. Used under license from Shutterstock.com

First published June, 2011
Printed in Croatia

A free online edition of this book is available at www.intechopen.com
Additional hard copies can be obtained from orders@intechweb.org

Biosensors – Emerging Materials and Applications, Edited by Pier Andrea Serra
p. cm.
ISBN 978-953-307-328-6

Contents

Preface

A biosensor is defined as a detecting device that combines a transducer with a biologically sensitive and selective component. When a specific target molecule interacts with the biological component, a signal is produced, at transducer level, proportional to the concentration of the substance. Therefore biosensors can measure compounds present in the environment, chemical processes, food and human body at low cost if compared with traditional analytical techniques.

This book covers a wide range of aspects and issues related to biosensor technology, bringing together researchers from 19 different countries. The book consists of 27 chapters written by 106 authors and divided in three sections. The first section, entitled Biosensors Technology and Materials, is composed by 17 chapters and describes emerging aspects of technology applied to biosensors. The subsequent section, entitled Biosensors for Health and including six chapters, is devoted to biosensor applications in the medical field. The last section, composed by four chapters, treats of the environmental and biosecurity applications of biosensors.

I want to express my appreciation and gratitude to all authors who contributed to this book with their research results and to InTech team, in particular to the Publishing Process Manager Ms. Mirna Cvijic that accomplished its mission with professionalism and dedication.

Pier Andrea Serra
University of Sassari
Italy

Part 1

Biosensor Technology and Materials

1

Signal Analysis and Calibration of Biosensors for Biogenic Amines in the Mixtures of Several Substrates

Toonika Rinken, Priit Rinken and Kairi Kivirand
University of Tartu, Institute of Chemistry
Estonia

1. Introduction

In real life we should often conduct analyses, where several compounds with similar properties are simultaneously present in solutions. In traditional analytical chemistry, this problem is usually solved by the pre-treatment of probes, enabling to eliminate the interference effect of different compounds. This process requires skilled labour, resources and time and eliminates the possibility to carry out on-line analyses.

A promising option for the conduction of on-line analyses is the application of biosensors, which are considered to provide reliable results, at least concerning the issues of selectivity. As biosensors are based on a selective bio-recognition of assessable compounds, there are typically only a restricted number of molecules (besides the ones of the analyte) present in a probe, which can induce measurable signals. However, in cases we have several competing compounds which can generate identical measurable effects, the selectivity of a biosensor can be quite poor and the results illusory. This phenomenon occurs clearly in the studies with enzyme inhibition-based biosensors (Luque de Castro & Herrera, 2003), but can be also well observed with biosensors, based on enzymes having activity towards several substrates, e.g. biosensors measuring biogenic amines (Kivirand & Rinken, 2009), different sugars etc.

Biogenic amines (BAs) are natural nitrogenous compounds formed mainly in the process of decarboxylation and aging of free amino acids. The detection of these compounds is a valuable tool for assessing the freshness and quality of a wide variety of protein-containing products like fish, meat, cheese, wine etc. (Yano *et al*, 1996;Vinci & Antonelli, 2002;Önal, 2007). The most common biogenic amines, used for the indication of food quality are histamine, putrescine and cadaverine (Kivirand & Rinken, 2011). Other BAs, commonly determined in foodstuff are trimethylamine (Mitsubayashi *et al*, 2004), spermidine, spermine and tyramine (Alonso-Lomillo *et al*, 2010). At present, regulations have been established only for the intake of histamine, but no accordant limits are set for other BA-s, including putrescine and cadaverine, although several studies have indicated that putrescine and cadaverine could increase the toxicity of histamine by inhibiting the enzymes involved in histamine biodegradation (Niculescu *et al*, 2000). The allowed maximum residue level of histamine in food according to EEC regulations is 100 mg/kg (EEC, 2001); the international food safety organization FDA has established the histamine level to 50 mg/kg (FDA, 2001).

Biosensors for BAs comprise different amine - selective enzymes, like amine oxidase (previously copper-containing amine oxidase EC 1.4.3.6, in 2008 EC entry deleted and replaced by monoamine oxidase EC 1.4.3.21 and diamine oxidase EC 1.4.3.22), putrescine oxidase (EC 1.4.3.10), methylamine dehydrogenase (EC 1.4.99.3) and flavin-containing mono-oxygenase type-3 (EC 1.14.13.8) in combinations with a variety of signal transduction systems and are based on different signal rising mechanisms. No other bio-recognition systems beside enzymes are known to have been used in BA biosensors at present (Kivirand & Rinken, 2011).

The selectivity of the most widely used enzyme diamine oxidase is relatively poor. The available data about the substrate specificity of this enzyme towards different amines varies within a wide range for enzyme preparations from different sources, and even seems to be dependent on the applied experimental method. The best substrates for diamine oxidase from the seedlings of different papilionaceuos (*Pisum sativum, Lathyrus sativus, Lens culinaris, Vicia faba*) are cadaverine (1,5-diaminopentane) and putrescine (1,4-diaminobutane); other BAs have much lower affinities. The relative specific activity of pea seedlings' diamine oxidase (PSAO) is found to be 100 % towards putrescine, 111 % towards cadaverine, 56 % towards agmatine and spermidine, 44 % towards 1,6-diaminohexane, 30 % towards histamine, 8 % towards spermine and no activity has been found towards 1,3-diaminopropane (Kenten & Mann, 1952). Characterizing the relative specificity of this enzyme with the help of a oxygen sensor, it was found to be 100 % towards cadaverine, 86.2 % towards putrescine, 42.6 % towards 1,6-diaminohexane, 37.7 % towards 1,7-diaminoheptane, 11.6 % towards dopamine and 9.8 % towards histamine (Kivirand & Rinken, 2007). It has also been reported that PSAO has at least 3 times higher specificity towards histamine than other plant amine oxidases (Medda *et al*, 1995). According to literature, PSAO has very low activity towards 1,3-diaminopropane (Matsuda & Suzuki, 1977) and 1,2-diaminoethane (Kivirand & Rinken, 2007).

The above - presented data concerns studies, where only one substrate has been present in solution. In real probes, there are several BAs, produced in the process of putrefaction of proteins, simultaneously present and the inhibition phenomenon by competing substrates (amines) has to be considered, since the enzyme accepts different BAs as alternatives. The competing substrates generate analogous signals, measured with a reaction signal transduction system. In the case of oxidases, the enzyme actually requires a second substrate (oxygen) or a substance, which can act as an electron acceptor in the oxidation reaction and makes the reaction possible.

In BA biosensors the most commonly used signal transducers are various electrochemical sensors. According to the electron transfer mechanism utilized (with or without an additional mediator), electrochemical biosensors are classified into three generations (Eggins, 1996;Freire *et al*, 2003). An overview of the studied to date BA biosensors, all based on an amine-selective enzyme and some electrochemical signal transduction system, is given in (Kivirand & Rinken, 2011). A big problem for most BA biosensors is that it is not possible to differentiate between different BAs. As the ratio of BAs in a probe is resulting from the amino-acidic consistence of proteins, the results of BA analyses with biosensors are sometimes vague and reflect the combination of the levels of several BAs.

The studies with biosensors are usually based on the steady state response of the measuring system, where the system generates the maximum response. Most authors claim that with this method of data acquisition, the sensitivity of biosensor systems towards certain amines is not interfered by other biogenic amines, present in the sample. For example, Carsol et al.

studied a pool of different amines instead of a single amine substrate with amine oxidase based biosensors and detected no interactions of different amines (Carsol & Mascini, 1999). Albrecht-Ruiz et al. used diamine oxidase based colorimetric method for histamine detection and found that the absorbances of putrescine, cadaverine and histamine are additive, as the measured absorbances were less than 10 % smaller than their expected values. According to the presented data, the absorbances were smaller in all cases, where putrescine and/or cadaverine were present (Albrecht-Ruiz, 1999). Simultaneous analyses of the total BA content in fish probes with diamine oxidase based biosensor and ion-chromatography (conductivity detection) showed, that the obtained results with both methods were similar in cases when the BA contents were low. When BA concentrations began to rise during the storage of fish samples, differences between the results, obtained with diamine oxidase biosensor and ion-chromatography, began to increase (Carelli *et al*, 2007). There exists also a report about enzyme-based BA biosensor array, using an artificial neural network for the pattern recognition (Lange & Wittmann, 2002).
In the present study we analyze the output currents of BA biosensors, based on pea seedlings diamine oxidase and an electrochemical oxygen sensor to find the potential impact of different biogenic amines into the biosensor response and propose several models for the calibration of these biosensors in case of simultaneous presence of these amines in solutions The biosensor response has been characterized by the maximum signal change parameter of the reaction, calculated from the transient phase data (Rinken, 2003).

2. Materials and methods

2.1 Materials and experimental procedures

Diamine oxidase was isolated from *Pisum sativum* seedlings (PSAO, EC 1.4.3.22), purified as described earlier (Kivirand & Rinken, 2007) and used in soluble form (PSAO activity in the enzyme extract was 5.43 IU/mg solid; 7.55 mg/mL). All other reagents used in the study were of analytical grade.
PSAO catalyzes the oxidation of amines by dissolved oxygen:

$$R\text{-}CH_2NH_2 + H_2O + O_2 \xrightarrow{PSAO} RCHO + NH_3 + H_2O_2 \quad (1)$$

The change of dissolved oxygen concentration in reaction medium in the course of reaction was followed with a simple Clark - type oxygen sensor. All kinetic measurements were carried out under continuous stirring in a closed and thermostated glass cell in air-saturated 0.1 M phosphate buffer (pH 7.0) at 25° C. The reaction was started by injection of 100 µl PSAO solution into reaction medium, which was containing amine(s) and the sensor output signal was registered at 1 sec intervals (final PSAO concentration 0.108 IU/ml). Each experimental curve consisted of minimum 800-1600 data points, allowing the calculation of the biosensor response parameters according to the dynamic biosensor model (Rinken & Tenno, 2001). For these calculations, SigmaPlot® 9.0 (SPSS Software, USA) and GraphPad Prism® 5.0 (GraphPad Software, San Diego, USA) software were used.

2.2 The basic principles of the applied dynamic biosensor model

The dynamic model for biosensors is designed to take into account the kinetics of enzyme reactions with ping-pong mechanism, the diffusion of substrates and the inertia of the

diffusion – limited sensors (or the whole bio-sensing system). It enables the calculation of steady state parameters from the biosensor transient response with errors less than 3 % and with no need for additional determination of the system's geometrical, diffusion or partition parameters (Rinken & Tenno, 2001). According to this model, the normalized biosensor output current $I(t)/I_0$ (corresponding to the normalized dissolved oxygen concentration $c_{O_2}(t)/c_{O_2}(0)$, as I depend linearly on c_{O_2}) is expressed as a 3-parameter function of time t:

$$\frac{I(t)}{I_0} = \frac{c_{O_2}(t)}{c_{O_2}(0)} = Aexp(-Bt) + (1-A) - 2A\sum_{n=1}^{\infty}(-1)^n \frac{\tau_S}{\frac{n^2}{B-\tau_S}} \left[\exp(-Bt) - exp\left(-n^2\frac{t}{\tau_S}\right)\right] \quad (2)$$

where $I(t)$ is the biosensor output current and $c_{O_2}(t)$ the corresponding dissolved oxygen concentration at time moment t; I_0 is the output current and $c_{O_2}(0)$ the corresponding dissolved oxygen concentration at the start of the reaction. Parameters A and B are complex parameters characterizing the ongoing chemical reaction, both depending hyperbolically on substrate concentration. Parameter A corresponds to the maximum possible biosensor signal change in case time $t \to \infty$ (normalized signal change at steady – state) and parameter B is the kinetic parameter (the initial maximal slope of the enzyme – catalyzed process curve); τ_s is the time constant of the internal processes of oxygen transducer taken together and characterizes the inertia of the transducer's (system's) response (Rinken & Tenno, 2001). Parameters A, B and τ_s are independent on each other. The most suitable parameter for the characterization of results obtained with different biosensors and the calibration of these biosensors, is the maximum signal change parameter A, as the kinetic parameter B includes an intercept (diffusion constant of oxygen) resulting from its definition and is more sensitive to experimental noise (Rinken, 2003). The application of the dynamic model enables to calculate the biosensor response parameters quickly from the transient signal, minimizing the influence of side processes, going on in the system (H_2O_2 degradation, oxygen absorption through the liquid – air surface etc.) and to avoid the uncertainty of determining the steady state.

2.3 Correlation analysis of the biosensor data

The biosensor data (the values of maximum signal change parameters) was obtained over a longer period from experiments, carried out with different diamine oxidase – based biosensors in solutions, where one, two or three different biogenic amines (cadaverine, putrescine and/or histamine), which concentrations varied from 0 to 2 mmol/L, were present. For data analysis with different models we used the results of overall 112 measurements. The multivariate concentration – biosensor signal correlation analyses were carried out using DataFit 9.0 software (Oakdale Engineering, USA).

3. Discussion

3.1 Inhibition of diamine oxidase by a competing substrate

The selectivity towards different amines of diamine oxidase from pea seedlings (PSAO, EC 1.4.3.22), used in our studies, was characterized with the normalized maximum signal change parameter A, calculated from the decrease of oxygen concentration due to the oxidation of a particular substrate. The dependences of this parameter A on the concentrations of 1,5-diaminopentane (cadaverine), 1,4-diaminobutane (putrescine) and histamine in single substrate solutions are shown on Fig. 1 (a-c).

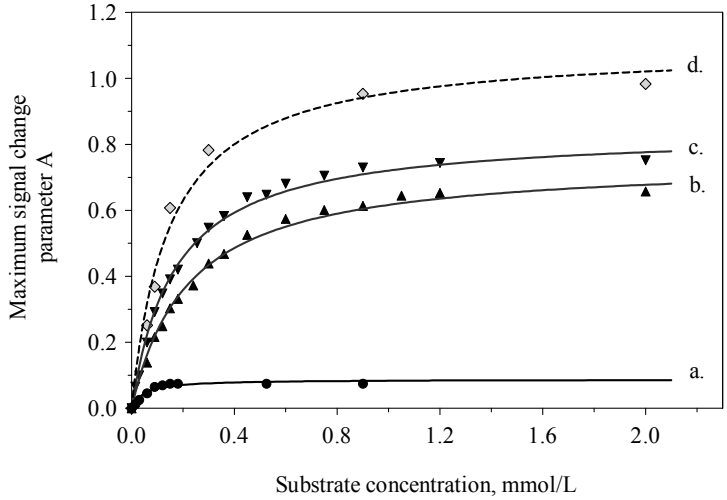

Fig. 1. The maximum signal change parameter *A* for (a) histamine; (b) putrescine; (c) cadaverine and (d) cadaverine and putrescine equimolar mixtures. Measurements were carried out in 0.1 M phosphate buffer (pH 7.00) at 25°C, [PSAO] = 0.108 IU/mL

As expected, all these curves were hyperbolas (Rinken, 2003). The maximum values of these hyperbolic curves indicate the PSAO activity towards particular amines and were used for the characterization of PSAO selectivity. Among the studied three substrates, PSAO showed the highest specific activity towards cadaverine – the normalized maximal signal decrease was 76% of the initial signal. Taking the PSAO specific activity towards cadaverine as 100%, the relative activity of PSAO towards other common BAs was 86.2% for putrescine and 9.8% for histamine. These results showed that concerning BAs, PSAO was highly selective towards cadaverine and putrescine and its activity towards histamine was approximately 10 times smaller. Applying a different method, spectrophotometrical studies, a much higher (27%) selectivity of PSAO towards histamine in comparison with cadaverine has been reported (Medda *et al*, 1995).

The selectivity of PSAO determines the relative speed of oxidation of different amines and has to be taken into consideration if PSAO is exploited for bio-recognition for analytical purposes in solutions, which simultaneously contain several biogenic amines, which oxidation is catalyzed by PSAO.

To study the inhibition of PSAO by a competing substrate, we followed the biosensor signal in the mixtures of two different amines. In equimolar solutions of cadaverine and putrescine, the resulting signal was considerably higher than the signals of cadaverine and putrescine by themselves, but lower than the sum of the signals of single substrates at similar concentrations (Fig.1 c-d). Comparing the parameter *A* values, obtained from solutions, containing only cadaverine or putrescine and from their different mixtures, it turned out that, as an average, the values of parameter *A* for mixtures were 1.14 ± 0.02 times smaller than the summarized parameter *A* values for single substrates (Fig.2).

The analysis of the values of parameter *A* in mixtures at different substrates' concentration rates showed that neither cadaverine nor putrescine had a 100 % impact into the parameter

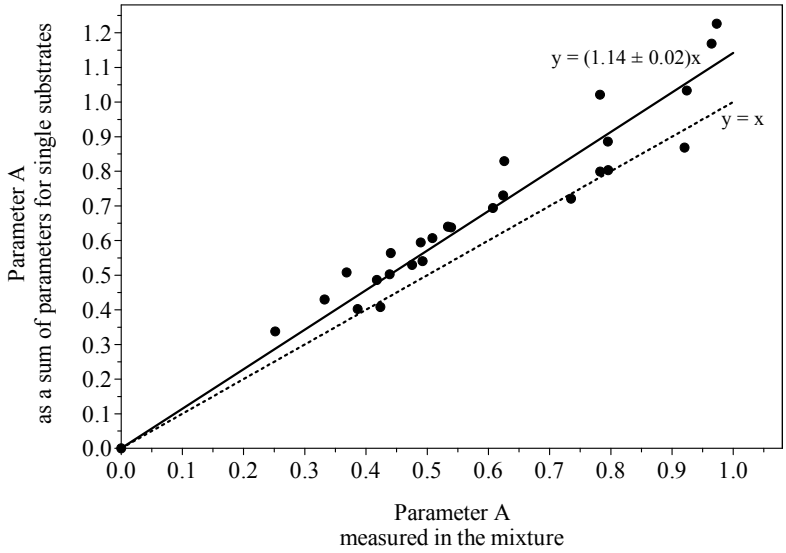

Fig. 2. The curve of the signal change parameter *A* as the sum of cadaverine and putrescine signals vs. the same parameter, measured in the mixture of cadaverine and putrescine, at similar substrate concentrations

A value. Both these substrates had an impact between 60 and 85 % of the maximum effect at a certain concentration and the impact was smaller at concentrations below their particular K_M value. It is interesting to notice that the effect of one of these substrates was not dependent on the concentration of the other, as for example the putrescine effect in the resulting value of parameter *A* in the mixture was not dependent on the cadaverine concentration.

The biosensor response was also studied in mixtures, which besides cadaverine and/or putrescine contained histamine. In case the solution contained cadaverine and/or histamine, even at low cadaverine concentrations it was not possible to detect any histamine effect on the maximum signal change parameter *A* of the biosensor response (Fig. 3).

The calculated values of the parameter *A* were constant at fixed cadaverine concentrations, even if the histamine concentrations in the mixture varied from 0.01 – 3.0 mmol/L, the latter being over 20 times above histamine K_M value and exceeding several times the histamine maximum residue level in foods allowed by EEC regulations (100 mg/kg, corresponding to 0.9 mmol/L). Similar "screening" effect of histamine was also found in the mixtures of putrescine/histamine and cadaverine/putrescine/histamine.

These studies indicate that applying a PSAO based biosensor for the detection of histamine or the content of total amines, the concentrations of some amines are underestimated in case there are several BAs simultaneously present in the sample. This "screening" phenomenon and the dependence of the output signal on the rate and relative concentrations of different biogenic amines in the sample can lead to the underestimation of the content of biogenic amines in food, especially in cases when some particular biogenic amines become dominant in the course of putrefaction, like putrescine and cadaverine in decomposing of white fish.

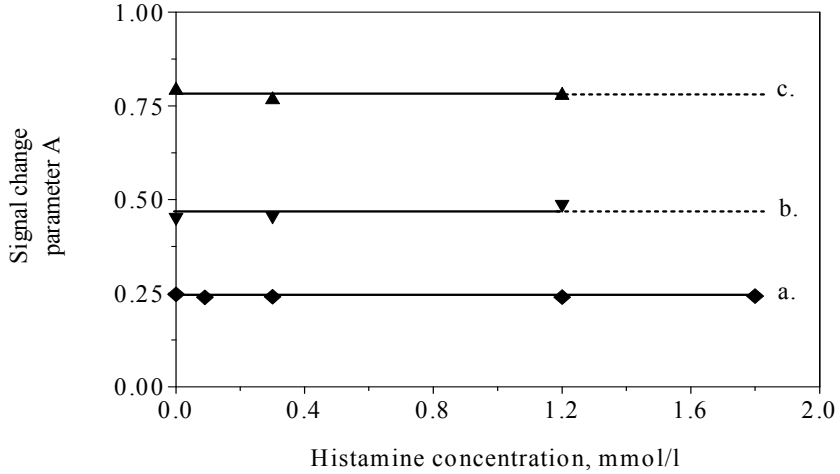

Fig. 3. The calculated maximum signal change (parameter *A*) in the mixtures of cadaverine and histamine at different concentration rates: histamine concentration is shown on x-axis and cadaverine concentration is (a) 0.15 mmol/L; (b) 0.30 mmol/L; (c) 0.60 mmol/L. Measurements were carried out in 0.1 M phosphate buffer (pH 7.00) at 25°C, [PSAO] = 0.108 IU/mL

The mechanism of PSAO - catalyzed oxidation of different amines follows a similar ping-pong pattern (Yamasaki *et al*, 1970) and the enzyme accepts different amines as alternatives to each other. For the characterization of the individual impact of the studied BAs into the biosensor output signal, which is a lump sum of several parallel reactions, we applied multivariate correlation analysis.

3.2 Multivariate correlation analysis

As different substrates generate analogous signals, a proper model should characterize the impact of these substrates into the resulting signal, enabling the application of the signal parameters for the calibration of a biosensor for several substrates. This task of calibration inescapably requires signal measurements in solutions with varying concentration ratios of BAs, which can be achieved by addition of a certain amount of definite amine to the probe and so producing a series of BA solutions with variable concentrations. A good model in combination with a vital number of measurements (equal to the number of coefficients in a model) in different solutions forms a solid base for the calibration of biosensors, which selectivity is relatively poor, e.g. PSAO-based biosensors for biogenic amines. Similar models for biosensor calibration can be applied for other low selectivity biosensors, like in the case of inhibition – based biosensors, where the catalytic action of an enzyme is modified not only by the presence of given species, but also by very different compounds like metal cations, various inorganic and organic species etc (Luque de Castro & Herrera, 2003).

3.2.1 Hyperbolic model

In single substrate solutions, the biosensor maximum signal change parameter *A* depends on the substrate concentration hyperbolically (Rinken & Tenno, 2001):

$$A = \frac{k_{cat}^{*}[E]_{total} c_S^{bulk}}{k_{diff}^{O_2} K_{O_2} K_S + (k_{cat}^{*}[E]_{total} + k_{diff}^{O_2} K_{O_2}) c_S^{bulk}} \quad (3)$$

In Eq.(3), k_{cat}^{*} denotes the apparent catalytic constant of the enzyme-catalyzed reaction, $[E]_{total}$ is the overall concentration of the enzyme in biosensor, $k_{diff}^{O_2}$ is the apparent diffusion constant of oxygen, K_{O_2} is the dissociation constant for the enzyme-oxygen complex, K_S is dissociation constant for the enzyme-substrate complex and c_S^{bulk} is substrate concentration in solution.

As the reaction mechanism for competing BAs is similar, we used the sum of three hyperbolas, each describing the impact of an individual substrate. After transformation, the dependence of parameter A on substrate concentration (Eq.3) can be presented as a function with 2 coefficients (Rinken, 2003), which is the minimal number of coefficients to determine one normalized hyperbola, which maximum value equals to 1:

$$A = \frac{m c_S^{bulk}}{K_S + (m+1) c_S^{bulk}} \quad (4)$$

In Eq. (4), the meaning of K_s is as defined above and the parameter m is a combination of 3 different physical constants and the total amount of enzyme $[E]_{total}$:

$$m = \frac{k_{cat}^{*}[E]_{total}}{k_{diff}^{O_2} K_{O_2}} \quad (5)$$

The resulting biosensor signal's maximum change parameter A in the mixture of 3 substrates can be expressed as a function of 3 variables (the number of variables corresponds to the number of competing substrates in solution) and 6 coefficients as following:

$$A = \frac{m_1 x}{K_1 + (m_1+1)x} + \frac{m_2 y}{K_2 + (m_2+1)y} + \frac{m_3 z}{K_3 + (m_3+1)z} \quad (6),$$

where x, y and z are the variables denoting the concentrations of cadaverine, putrescine and histamine accordingly; m and K are appropriate coefficients. Applying Eq. 6 as a model for the biosensor parameter A, we got a good correlation with the experimental results with standard deviation σ = 0.097 and correlation coefficient R= 0.93. The basic problem with this approximation was the great absolute values of coefficients m_3 and K_3 characterizing the effect of histamine, which were up to 10^{20} times higher than the coefficients m_1 and K_1 for cadaverine and m_2 and K_2 for putrescine (Table 1, model 1). This may lead to the distortion of the assumption that the reaction mechanism is similar for all substrates and amplification of experimental noise.

To avoid this obstacle, we transformed Eq. 6 so, that the values of coefficients characterizing the impact of different substrates were in the same order, although we had to add 3 additional coefficients:

$$A = \frac{a_1 x}{b_1 + (a_1 + c_1)x} + \frac{a_2 y}{b_2 + (a_2 + c_2)y} + \frac{a_3 z}{b_3 + (a_3 + c_3)z} \quad (7)$$

In Eq. (7) coefficients a_1-a_3, b_1-b_3 and c_1-c_3 have the following physical meanings:

$$a = k^{*}_{cat}[E]_{total} \tag{8}$$

$$b = k^{O_2}_{diff} K_{O_2} K_S \tag{9}$$

$$c = k^{O_2}_{diff} K_{O_2} \tag{10}$$

Resulting from Eqs. 9 & 10, the quotient of coefficients b and c equals to $b/c = K_S$.
Applying Eq. 7 as a model for the biosensor parameter *A*, we got similar fit as with Eq. 6, but the values of the equation coefficients, characterizing different substrates were in the same order (Table 1, model 2).

	Model	**n**	**Coefficient values**	**σ**	**R^2**
1.	$A = \frac{m_1 x}{K_1 + (m_1+1)x} + \frac{m_2 y}{K_2 + (m_2+1)y} + \frac{m_3 z}{K_3 + (m_3+1)z}$	6	m_1= 6.05 K_1=1.48 m_2=1.65 K_2=0.48 m_3=5.12·10^{18} K_3=6.26·10^{20}	0.097	0.871
2.	$A = \frac{a_1 x}{b_1 + (a_1+c_1)x} + \frac{a_2 y}{b_2 + (a_2+c_2)y} + \frac{a_3 z}{b_3 + (a_3+c_3)z}$	9	a_1=1.57 b_1=0.39 c_1=0.26 a_2=1.42 b_2=0.41 c_2=0.86 a_3=0.26 b_3=2.06 c_3=10.73		

Table 1. The number and values of the calculated coefficients, the value of standard deviation σ and square of the correlation coefficient R^2 for studied hyperbolic models of the BA biosensor

The correlation of the calculated and experimental values of parameter *A* is graphically shown on Fig. 4, where the ideal correlation is shown with a solid line. It can be seen that the calculated with hyperbolic model values of parameter *A* correlate normally with the experimental data and there are no systematic drifts, except in case of very low reaction effects.
The main disadvantage of this hyperbolic model is the rather high number of coefficients, which is 9 (6); 3 (2) coefficients for each substrate. So for the calibration of the BA biosensor towards 3 substrates, it is necessary to carry out measurements at least 9 (6) different BA concentration ratios: with the original sample and 8 (5) additional solutions, where a definite amount of one or more substrates has been added. This procedure is time-consuming and may also lead to notable experimental noise, although it enables the calibration of biosensors in mixtures of several substrates.

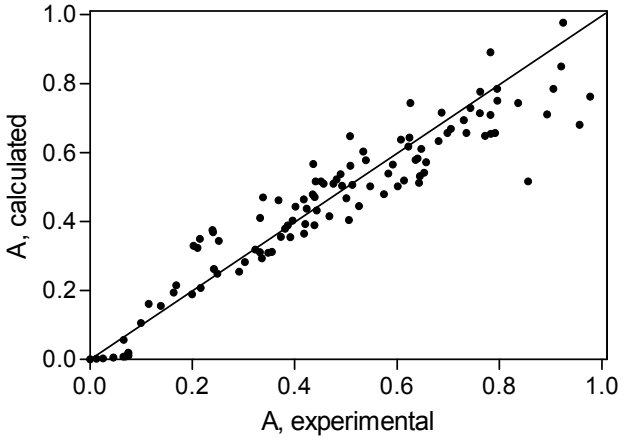

Fig. 4. Correlation of the values of maximum signal change parameter *A*, calculated with the help of the hyperbolic model and from experimental data. Line x=y marks the ideal correlation.

3.2.2 Quantitative Concentration – Signal Relationship (QCSR)

We also studied the application of some more formal models with a potentially smaller number of variables to characterize the biosensor signal parameter *A*. The QCSR model for the characterization of the biosensor maximum signal parameter *A* included different addends as "descriptors" of reactions, going on in the biosensor and taking into account the individual concentrations of BAs and the interference phenomena (inhibition by a competing substrate) of these compounds. The interference was described with 3 different types of "descriptors", such as the products of duplicate substrate concentrations along with the quadrates and exponents of each single BA concentration:

$$A = ax + by + cz + dxy + fxz + gyz + hx^2 + jy^2 + kz^2 + le^x + me^y + ne^z + p \quad (11).$$

In Eq. 11, *x*, *y* and *z* are the variables denoting the concentrations of cadaverine, putrescine and histamine accordingly; coefficients *a, b..... n* denote the impact of each "descriptor" and *p* is the constant term.

The correlation studies were performed with 5 models composed of different number of "descriptors", symmetrical towards all three studied substrates. The simplest model with 4 variables comprised the concentration terms of the three BAs and the constant term ($A = ax + by + cz + p$). As expected, this simple model showed systematic deviations from the experimental data and the correlation was rather poor (R^2=0.437), as it didn't include the interference of the substrates (Fig. 5, blue dots). The value of standard deviation was 0.198 (Table 2, model 3).

Complementing the model with the addends of the products of duplicate substrate concentrations ($A = ax + by + cz + dxy + fxz + gyz + p$), the number of "descriptors" increased to 7 and the correlation improved (R^2=0.547), but not sufficiently to be applicable for practical purposes (Fig. 5, green dots). Model $A = ax + by + cz + hx^2 + jy^2 + kz^2 + p$, also comprising of 7 "descriptors" resulted in a bit better correlation (R^2=0.777) (Fig. 5, lilac dots). Combining the 2 abovementioned models together, the number of "descriptors" increased to 10 resulting in the square correlation coefficient R^2=0.784 (Fig. 5, black dots). As

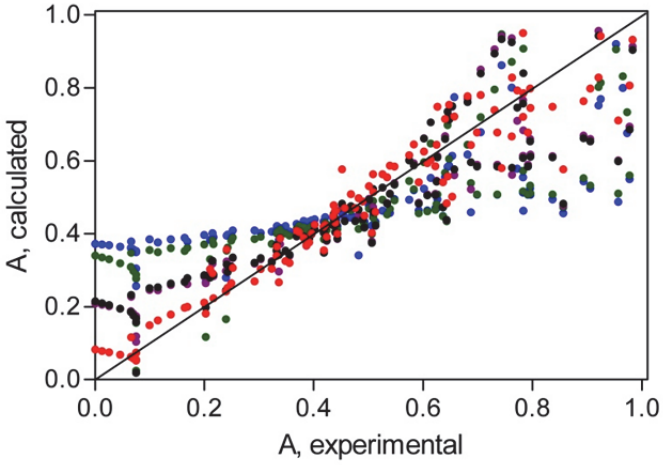

- $A = ax + by + cz + p$
- $A = ax + by + cz + dxy + fxz + gyz + p$
- $A = ax + by + cz + hx^2 + jy^2 + kz^2 + p$
- $A = ax + by + cz + dxy + fxz + gyz + hx^2 + jy^2 + kz^2 + p$
- $A = ax + by + cz + dxy + fxz + gyz + hx^2 + jy^2 + kz^2 + le^x + +me^y + ne^z + p$

Fig. 5. Correlation of the values of maximum signal change parameter *A*, calculated with the help of different QCSR models and from experimental data. Line x=y marks the ideal correlation.

the correlation was not sufficiently improved with the addition of the products of duplicate substrate concentrations, these "descriptors" do not describe the interference of substrates in solution satisfactorily and need not be considered in models, applied for the calibration of BA biosensors.

	Model	**n**	**Coefficient values**	**σ**	**R^2**
3.	$A = ax + by + cz + p$	4	a=0.41 b=0.20 c=-0.13 p=0.37	0.198	0.437
4.	$A = ax + by + cz + dxy + fxz + gyz + p$	7	a=0.51 b=0.34 c=-0.35 d=-0.24	0.180	0.547

			f=0.95 g=2.66 p=0.34		
5.	$A = ax + by + cz + hx^2 + jy^2 + kz^2 + p$	7	a=1.26 b=0.86 c=-0.25 h=-0.54 j=-0.34 k=0.15 p=0.21	0.127	0.777
6.	$A = ax + by + cz + dxy + fxz + gyz + hx^2 + jy^2 + kz^2 + p$	10	a=1.22 b=0.84 c=-0.33 d=-0.01 f=0.41 g=2.48 h=-0.52 j=-0.33 k=0.13 p=0.21	0.126	0.784
7.	$A = ax + by + cz + dxy + fxz + gyz + hx^2 + jy^2 + kz^2 + le^x + me^y + ne^z + p$	13	a=0.40 b=0.34 c=1.97 d=-0.13 f=0.27 g=-0.35 h=-2.98 j=-2.16 k=1.87 l=1.86 m=1.35 n=-2.26 p=-0.87	0.079	0.917
8.	$A = ax + by + cz + hx^2 + jy^2 + kz^2 + le^x + me^y + ne^z + p$	10	a=0.49 b=0.42 c=1.24 h=-2.87 j=-1.99 k=1.28 l=1.73 m=1.18 n=-1.48 p=-1.35	0.086	0.901

Table 2. The number of "descriptors" n, the values of the calculated coefficients, the values of standard deviations σ and squares of the correlation coefficients R^2 for studied models of the BA biosensor

Addition of the exponential "descriptors" to the model improved the correlation and the fit of the model with the experimental data was similar to that of the hyperbolic model (Eq. 6). We used two different models, including the exponential terms, with overall 13 or 10 "descriptors" (Table 2, models 7 & 8). Similarly to the earlier results (Table 2, models 5 & 6), the products of duplicate substrate concentrations didn't improve considerably the correlation and could be omitted. The QCSR model, including 10 "descriptors" (Table 2, model 8) resulted in R^2=0.901, which value is similar to that obtained from hyperbolic model (R^2= 0.871; Table 1 model 2).

According to data on Figs. 4 & 5 and Tables 1 & 2, the smallest divergence of the calculated values from the experimental ones were achieved with the application of the hyperbolic models (models 1 & 2) and the more complicated QCSR models (models 7 & 8), although among the QCSR models one should prefer the one including smaller number of "descriptors". All these models could theoretically be used for the calibration and measurements with BA biosensors in the presence of different amines simultaneously.

4. Conclusions

The application of diamine oxidase based biosensors is a good option for the rapid determination of food quality, although in the case of simultaneous presence of several biogenic amines, the sensor signal is influenced by the rate of concentrations of different amines, formed during the process of protein putrefaction. In the presence of cadaverine and putrescine, the effect of histamine on the biosensor response is totally screened and the interaction of cadaverine and putrescine partially eliminates their own impact into the signal, causing the decrease of the resulting signal output, which is not an additive sum of the signals of single substrates. This screening effect can be successfully characterized with different multivariate models of biosensor signal. These models enable the calibration of biosensors towards several substrates in mixtures of different biogenic amines, which generate analogous biosensor response. Similar methodology can be applied in other systems, where the selectivity of a biosensor is low and the traditional ways of calibration do not enable to determine the concentrations of individual compounds in mixtures.

5. Acknowledgements

This work was supported by Estonian Science Foundation (grant no. 7465).

6. References

Albrecht-Ruiz,M. (1999) Rapid method for biogenic amines evaluation in fish meal. *Journal of Aquatic Food Product Technology*, 8, 71-83.

Alonso-Lomillo,M.A.N., Dominguez-Renedo,O., Matos,P., & Arcos-Martinez,M.J. (2010) Disposable biosensors for determination of biogenic amines. *Analytica Chimica Acta*, 665, 26-31.

Brenda. The Comprehensive Enzyme Information System (www.brenda-enzymes.org, 2011).

Carelli,D., Centonze,D., Palermo,C., Quinto,M., & Rotunno,T. (2007) An interference free amperometric biosensor for the detection of biogenic amines in food products. *Biosensors and Bioelectronics*, 23, 640-647.

Carsol,M.-A. & Mascini,M. (1999) Diamine oxidase and putrescine oxidase immobilized reactors in flow injection analysis: a comparison in substrate specificity. *Talanta*, 50, 141-148.

EEC (2001) Directive 91/493/EEC - laying down the health conditions for the production and the placing on the market of fishery products. *EEC-Regulations*.

Eggins,B.R. (1996) *Biosensors: An Introduction,* Wiley Teubner "Chemistry".

FDA (2001) Scombrotoxin (Histamine) formation. In Fish and fishery products hazard and controls guidance (3.rd. ed.). *Food and Drug Administration, Center for Food Safety and Applied Nutrition*.

Freire,R.S., Pessoa,C.A., Mello,L.D., & Kubota,L.T. (2003) Direct electron transfer: an approach for electrochemical biosensors with higher selectivity and sensitivity. *Journal of Brazilin Chemical Society*, 14, 230-243.

Kenten,R.H. & Mann,P.J.G. (1952) The oxidation of amines by extracts of pea seedlings. *The Biochemical Journal*, 50, 360-369.

Kivirand,K. & Rinken,T. (2007) Purification and properties of amine oxidase from pea seedlings. *Proceedings of the Estonian Academy of Sciences. Chemistry*, 56, 164-171.

Kivirand,K. & Rinken,T. (2009) Interference of the Simultaneous Presence of Different Biogenic Amines on the Response of an Amine Oxidase-Based Biosensor. *Analytical Letters*, 42, 1725-1733.

Kivirand,K. & Rinken,T. (2011) Biosensors for Biogenic Amines: the Present State of Art. *Analytical Letters*, in press.

Lange,J. & Wittmann,C. (2002) Enzyme sensor array for the determination of biogenic amines in food samples. *Analytical &Bioanalitycal Chemistry*, 372, 276-283.

Luque de Castro,M.D. & Herrera,M.C. (2003) Enzyme inhibition-based biosensors and biosensing systems: questionable analytical devices. *Biosensors and Bioelectronics*, 18, 279-294.

Matsuda,H. & Suzuki,Y. Some properties of the amine oxidase in Vicia faba seedlings. *Plant Cell Physiol*. 18[5], 1131-1137. 1977.

Medda,R., Padiglia,A., & Floris,G. (1995) Plant copper-amine oxidases. *Phytochemistry*, 39, 1-9.

Mitsubayashi,K., Kubotera,Y., Yano,K., Hashimoto,Y., Kon,T., Nakakura,S., Nishi,Y., & Endo,H. (2004) Trimethylamine biosensor with flavin-containing monooxygenase type 3 (FMO3) for fish-freshness analysis. *Sensors and Actuators B: Chemical*, 103, 463-467.

Niculescu,M., Nistor,C., Frébort,I., Peč,P., Mattiasson,B., & Csöregi,E. (2000) Redox hydrogel-based amperometric bienzyme electrodes for fish freshness monitoring. *Analytical Chemistry,* 72, 1591-1597.

Önal,A. (2007) A review: Current analytical methods for the determination of biogenic amines in foods. *Food Chemistry*, 103, 1475-1486.

Rinken,T. (2003) Determination of kinetic constants and enzyme activity from a biosensor transient signal. *Analytical Letters*, 36, 1535-1545.

Rinken,T. & Tenno,T. (2001) Dynamic model of amperometric biosensors. Characterisation of glucose biosensor output. *Biosensors & Bioelectronics*, 16, 53-59.

Vinci,G. & Antonelli,M.L. (2002) Biogenic amines: quality index of freshness in red and white meat. *Food Control*, 13, 519-524.

Yamasaki,E.F., Swindell,R., & Reed,D.J. (1970) Some aspects of catalysis by the amine oxidase of pea seedlings. *Biochemistry*, 9, 1206-1210.

Yano,Y., Yokoyama,K., Tamiya,E., & Karube,I. (1996) Direct evaluation of meat spoilage and the progress of aging using biosensors. *Analytica Chimica Acta*, 320, 269-276.

2

Molecular Design of Multivalent Glycosides Bearing GlcNAc, $(GlcNAc)_2$ and LacNAc - Analysis of Cross-linking Activities with WGA and ECA Lectins

Makoto Ogata, Yoshinori Misawa and Taichi Usui
Shizuoka University
Japan

1. Introduction

The cross-linking properties of a variety of plant and animal lectins with multivalent carbohydrates and glycoproteins have been reviewed (Sacchettini et al., 2001; Brewer 1997; Dessen et al., 1995; Pieters 2004). These studies show that a number of lectins form cross-linked complexes with branched chain oligosaccharides [Bhattacharyya et al., 1988(a); Bhattacharyya et al., 1990], glycopeptides [Bhattacharyya et al., 1987(a); Bhattacharyya et al., 1990], and glycoproteins (Gupta & Brewer, 1994; Gupta et al., 1996). High affinity lectin ligands are of great interest in the cross-linking activities of such carbohydrate-mediated processes. The generation of high affinity ligands, however, is not trivial because the interaction of individual carbohydrate epitopes with lectin is, in many cases, weak and undiscriminating. The binding affinity can be dramatically increased by clustering lectin binding sites and carbohydrate recognition units (Mammen et al., 1998; Roy 2003; Lindhorst 2002; Houseman & Mrksich, 2002; Lee & Lee, 2000). The observation that binding affinity increases exponentially with the number of binding sites has been termed the glycoside cluster effect (Lee & Lee, 1995; Lundquist & Toone, 2002). In general, monovalent carbohydrate-protein interactions often occur with low binding affinities ($Kd \sim 10^{-3}$ M) (Mandal et al., 1994). However, multivalent interactions have several advantages over monomeric ones and are often used by nature to control a wide variety of cellular processes. With this in mind, multivalent carbohydrate analogs for high affinity binding to target lectins have been designed (Maierhofer et al., 2007; Roy 1996; Kiessling & Pohl, 1996; Mammen et al., 1995; Toone 1994; Kitov et al., 2000). It is becoming increasingly clear that multivalency is a powerful design approach to increase the binding strength of synthetic ligands. Considering that strong binding is required for practical application of interference strategies, the synthesis and evaluation of multivalent carbohydrates is a topic of increasing prominence. The multivalency effect can lead to truly large rate enhancement, even for systems of low valency, such as a divalent system (Dam et al., 2005). We are interested in developing an efficient synthetic route to multivalent glycosides, for glycomimetics, as they tend to have enhanced affinity due to their multivalency for specific lectins. Here we describe a simple strategy to design di- and tetravalent glycosides of *N*-acetylglucosamine (GlcNAc), *N*,*N*'-diacetylchitobiose [$(GlcNAc)_2$] and *N*-acetyllactosamine (LacNAc), which

have an enhanced multivalent effect due to a scaffold structure when bound to wheat germ (*Triticum vulgaris*) agglutinin (WGA) and coral tree (*Erythrina cristagalli*) agglutinin (ECA). Using these di- and tetravalent glycosides, interactions with lectins were analyzed using a hemagglutination inhibition assay, a precipitation assay, double-diffusion test, and surface plasmon resonance analysis.

2. Enzymatic synthesis of spacer-O-linked divalent glycosides and their cross-linking activities with WGA lectin

This section describes a convenient enzymatic synthesis of divalent spacer-O-linked GlcNAc-glycosides carrying alkyl spacers and their binding property with WGA.

2.1 Enzymatic synthesis of divalent spacer-O-linked GlcNAc-glycosides

Amycolatopsis orientalis (IFO 12806^T) was cultured with colloidal chitin. Increasing the activities of both *N*-acetylhexosaminidase (NAHase) and chitinase was observed in course of culture (Usui et al., 1987). When NAHase activity reached a maximum, the culture was centrifuged, and then the supernatant was desalted and freeze-dried. The dried powder was directly used for transglycosylation without purification. The enzyme catalyzed the synthesis of target spacer-O-linked divalent glycoside **1** together with monovalent 6-hydroxyhexyl β-D-*N*-acetylglucosaminide and 6-hydroxyhexyl β-D-*N*,*N*′-diacetylchitobioside through *N*-acetylglucosaminyl transfer from $(GlcNAc)_4$ to 1,6-hexanediol (Scheme 1). The target glycoside was separated by successive chromatographies of charcoal-Celite and silica gel columns to obtain in a 10.5% overall yield based on donor added. The synthesis of short length (1,3-propanediol) of spacer-O-linked divalent glycoside **2** was achieved in a similar manner by using chitinolytic enzyme (Scheme 1).

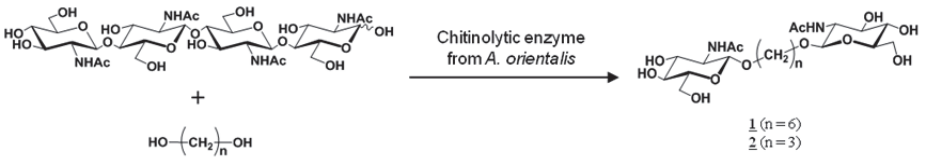

Scheme 1. Enzymatic synthesis of spacer-O-linked divalent GlcNAc-glycosides.

2.2 Cross-linking property of spacer-O-linked divalent glycosides as divalent ligand

Interaction of the resulting spacer-O-linked divalent glycosides carrying GlcNAc with WGA was analyzed by two different methods: precipitation and biosensor analysis. The avility of the syhthetic divalent glycosides (**1** and **2**) to bind to WGA was first analyzed by precipitation analysis. WGA (128 μM) and divalent glycoside (0.025-12.8 mM) were mixed on a 96-well microplate. When each divalent GlcNAc glycoside was added to the WGA solution under appropriate conditions, glycoside **1** with the long spacer (C-6) formed a precipitate within a few minutes, whereas glycoside **2** with the short spacer (C-3) did not little. However, the presence of chitin oligosaccharide [$(GlcNAc)_2$ and $(GlcNAc)_3$] prevented the formation of precipitates with **1**. The precipitates with glycoside **1** dissolved upon addition of the di- and trisaccharide (data not shown). These results indicate that the divalent GlcNAc glycoside bind specifically to WGA. Monovalent glycosides carrying GlcNAc and $(GlcNAc)_2$ on one side did not form a precipitate. Precipitin curves for WGA in

the presence of the divalent glycosides **1** and **2** were prepared by measuring the lectin concentration in the supernatant (Fig. 1). Spacer-O-linked divalent glycoside **2** with the short spacer did little form precipitate. By contrast, the concentration of **1** at the equivalence point was in the region of 0.1-2.5 mM, although the value was not accurately determined under the present conditions. Precipitation analysis showed that spacer-O-linked divalent GlcNAc glycoside specifically binds to WGA. Furthermore, the length of spacer group between the two GlcNAc residues appears to affect the ability to precipitate WGA. From these results, the length of spacer might be important in allowing the molecule to adopt a favorable orientation during interaction with the GlcNAc binding site on WGA. Some reserchers reported that the binding and cross-linking properties of lectin are sensitive to the degree of flexibility and spacing between the carbohydrate epitopes of the analogs (Krishnamurthy et al., 2007), which are entirely consistent with the present results.

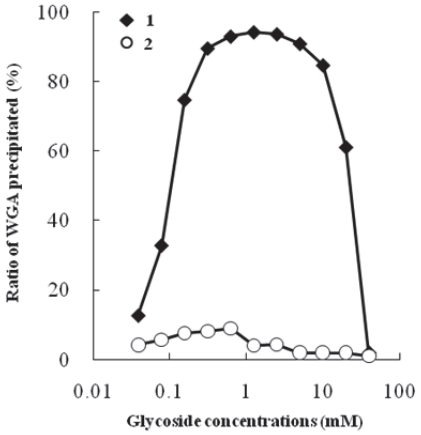

Fig. 1. Precipitin curves for the precipitation of WGA with spacer-O-linked divalent glycosides. The percentage of precipitated WGA was calculated by subtracting the amount of WGA in the supernatant from the total amount of WGA.

We have already reported that by surface plasmon resonance (SPR) analysis, spacer-linked divalent glycoside promotes, rather than inhibits, binding of WGA to surface-bound asialofetuin on a sensor chip (Misawa et al., 2008). This result is dramatically different from that of the corresponding monovalent glycoside, which inhibits the binding of the lectin. In the part, a SPR binding assay was used to monitor the cross-linking effect of synthetic divalent glycosides on the interaction of soluble WGA with a surface-bound WGA, which was directly immobilized onto the surface of a sensor chip using the amine coupling method. Cross-linking of the spacer-O-linked divalent glycosides with WGA in solution was minotored by coinjecting an equilibrium mixture of a fixed amount of WGA with a variable amount of glycoside onto a surface-bound WGA. The surface was regenerated at the end of each cycle using 50 mM H_3PO_4. Based on the sensorgrams, we plotted the RUs (response units) at 190 s, corrsponding to the cross-linking maximum responses for the divalent glycosides to the surface-bound WGA, against glycoside concentration (Fig. 2). As anticipated, injection of a solution of WGA in the absence of divalent glycoside (*i.e.*, negative control) resulted in no change of RU. However, as the concentration of divalent glycoside (**1**

and **2**) increased (*i.e.*, from 0.001 mM to 0.1 mM) there was an increse in RU (Fig. 2). GlcNAc, $(GlcNAc)_2$ and monovalent glycoside carrying GlcNAc were also injected as a control and then ploted (Fig. 2). They were not seen on a top of the peak as seen in **1** and **2**, although they seemed to show a silght increase of RU. It suggests that these control samples cannot cross-link between surface- and free-WGA. The maximal RU of glycoside **1**, was 5 times greater than that of **2**. Our data suggests that coinjection of divalent glycoside and tetravalent WGA as analyse results in simultaneous cross-linking. The cross-linking complexes presumably also bind to the surface-bound WGA through unbound divalent glycoside (Fig. 3). Burke *at al.* used SPR to show the trivalent mannose macrocycle, which is more potent than the corresponding monovalent derivative, functions by cross-linking Con A in solution (Burke et al., 2000). This is consistent with our results.

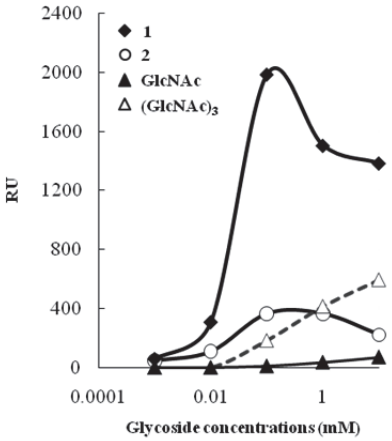

Fig. 2. Cross-linking formation of WGA with spacer-O-linked divalent glycosides on the sensor chip. WGA corresponding to 5700 response units was immobilized onto the sensor chip.

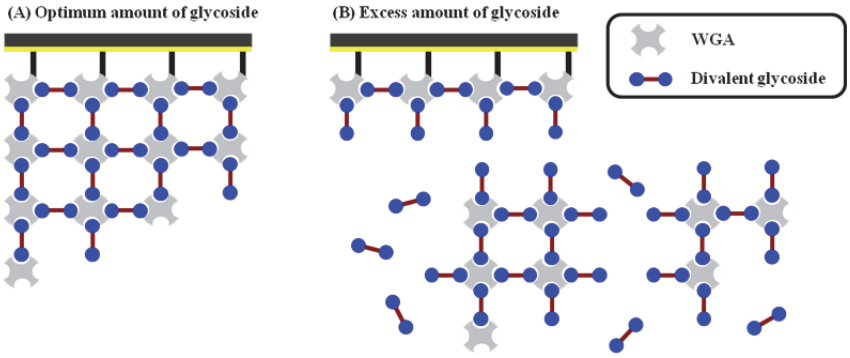

Fig. 3. Diagrams of cross-linking formation and collapse of cross-linking complex on the chip. (A) The formation of complex under optimum amount of spacer-O-linked divalent glycosides. (B) The collapse of complex under excess amount of spacer-O-linked divalent glycosides.

3. Synthesis of spacer-N-linked divalent glycosides and their cross-linking activities with WGA lectin

We showed an enzymatic method for preparing spacer-O-linked divalent glycosides bearing GlcNAc by chitinolytic enzyme-mediated transglycosylation (Scheme 1) [Misawa et al., 2008(a); Misawa et al., 2009]. The enzyme catalyzes the direct transfer of GlcNAc residue to a primary diol acceptor. The divalent glycoside was shown to bind, cross-link and precipitate WGA. These results encouraged us to prepare spacer-N-linked divalent GlcNAc, $(GlcNAc)_2$ and LacNAc-glycosides as ligands that possess cross-linking activity with target lectins [Misawa et al., 2008(b)].

3.1 Synthesis of spacer-N-linked divalent glycosides

As represented in Scheme 2, an amino function was introduced into the anomer position of GlcNAc, $(GlcNAc)_2$, and LacNAc with ammonia according to the method of Hiratake and co-workers (Kato et al., 2005). The resulting *N*-β-mono- and diglycosylamines were then condensed with one of the three dicarboxylic acids (n = 3, 4 or 5) with HBTU and diisopropyl ethanolamine (DIEA) in DMSO. The *N*-glycosylation proceeded stereoselectively within a few hours to give only the β-glycoside without the need for any protection and deprotection step. The yields of **3**-**8** were 50-60%, based on the amount of dicarboxylic acid added. The target compounds were purified by chromatography on a single silica gel column and their structures were determined by ^{1}H and ^{13}C NMR absorptions on the basis of two dimensional C-H COSY techniques. The compounds were soluble in water and DMSO. This method affords an easy and efficient synthesis of spacer-N-linked divalent glycosides bearing GlcNAc, $(GlcNAc)_2$, and LacNAc from the corresponding glycosylamine.

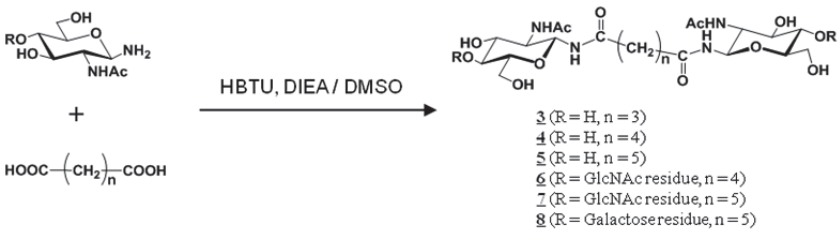

Scheme 2. Synthesis of spacer-N-linked divalent glycosides.

3.2 Interaction of spacer-N-linked divalent glycoside with WGA

3.2.1 Precipitation analysis

The interaction of the resulting spacer-N-linked divalent glycosides carrying GlcNAc or $(GlcNAc)_2$ with WGA was analyzed by two different methods: precipitation and biosensor analyses. Spacer-O-linked divalent glycoside **1**, which has the ability of precipitating WGA as a divalent ligand, was used as a control. The ability of the synthetic spacer-N-linked divalent glycosides (**3**-**7**) to bind to WGA was first analyzed by precipitation analysis. WGA (256 μM) and divalent glycoside (0.025-12.8 mM) were mixed on a 96-well microplate. When each divalent GlcNAc- and $(GlcNAc)_2$-glycoside was added to the WGA solution under appropriate conditions, **3**-**7** formed a precipitate within a few mnites. However, the presence of chitooligosaccharide [$(GlcNAc)_2$ and $(GlcNAc)_3$] prevented the formation of precipitates with **3**-**7**. Furthermore, the precipitates formed with **3**-**7** dissolved upon the addition of the

oligomer. These results indicate that the divalent glycosides **3**-**5** were prepared by measuring the lectin concentration in the supernatant (Fig. 4A).

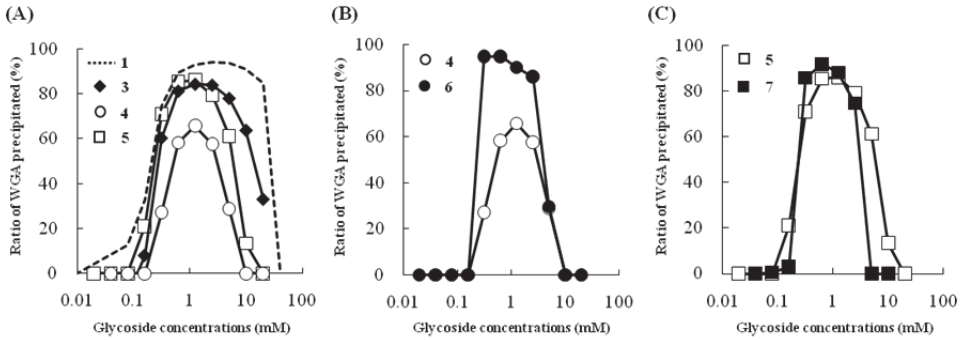

Fig. 4. Precipitin curves for the precipitation of WGA with spacer-N-linked divalent glycosides. The percentage of precipitated WGA was calculated by subtracting the amount of WGA in the supernatant from the total amount of WGA. (A) Spacer-N-linked divalent GlcNAc-glycosides **3**-**5** precipitated WGA. The curve corresponding to spacer-O-linked divalent glycoside **1** is shown by a dashed line for comparison. (B) Spacer-N-linked divalent GlcNAc- and $(GlcNAc)_2$-glycosides bearing $-(CH_2)_4-$ on the spacer precipitated WGA. (C) Spacer-N-linked divalent GlcNAc- and $(GlcNAc)_2$-glycosides bearing $-(CH_2)_5-$ on the spacer precipitated WGA.

The ability to form a precipitate was compared with that of spacer-O-linked divalent glycoside **1**. The concentration of **3**, **4** or **5** at the equivalence point (region of maximum precipitation) of the precipitin curve for 128 μM of WGA was about 1 mM. By constract, the concentration of **1** at the equivalence point was in the region of 0.1-2.5 mM, although the value was not accurately determined under the present conditions. Figure 4B compares the precipitin curves of **4** and **6** bearing GlcNAc or $(GlcNAc)_2$, respectively, with the same spacer group. These results clearly show that the addition of GlcNAc to **4** increases the amount of precipitate obtained in the assay. On the other hand, the addition of GlcNAc to **5** did not substantially increase the amount of precipitate generated in the assay (Fig. 4C). Precipitation analysis showed that spacer-N-linked divalent GlcNAc glycosides specifically bind to WGA in an analogy with spacer-O-linked divalent GlcNAc glysoides. However, the effect of the spacer-N-linked divalent GlcNAc glycosides on the interaction with the lectin was somewhat weaker than that of sapcer-O-linked divalent GlcNAc glycoside **1**. Our results demonstrate that divalent analogs with flexible spacer groups (O-linked) between the two GlcNAc residues possess higher affinity for the lectin compared to those bearing an inflexible spacer group (N-linked) through an NHCO linkage. Furthermore, the length of the spacer group between the two GlcNAc residues appears to affect the ability to precipitate WGA. The maximum amount of precipitate generated with divalent glycosides increased 30-33% when the spacer unit contained an odd number of methylene groups (**3** and **5**) compared to a corresponding glycoside with an even number of methylene groups in the spacer unit (**4**). From these results, the length of the spacer might be important in allowing the molecule to adopt a favorable orientation during interaction with the GlcNAc binding site. It has been reported that the binding and cross-linking properties of lectins are sensitive to the degree of

flexibility and spacing between the carbohydrate epitopes of the analogs (Dam et al., 2005; Krishnamurthy et al., 2007), which is entirely consistent with the present results.

3.2.2 SPR analysis

We have already reported that by SPR analysis, spacer-O-linked divalent glycoside **1** promotes, rather than inhibits, binding of WGA to surface- bound asialofetuin on a sensor chip [Misawa et al., 2008(a); Misawa et al., 2009]. Thus, we plotted the RUs at 190 s, which corresponds to the cross-linking maximum responses for the divalent glycosides to the surface-bound WGA, against glycoside concentration (as shown in Fig. 5), although some of the sensorgrams did not reach equilibrium. Our main purpose was to prove its ability to act as a divalent ligand through SPR analysis. In this case, the amount corresponded to 5700 RU of WGA (Figs. 5A and 5B) immobilized onto the surface, while 8700 RU in Fig. 5C. The cross-linking activity with the GlcNAc divalent glycosides increased in the order of **1** > **3** = **5** > **4** (Fig. 5A). The maximal RU of compound **6**, bearing (GlcNAc)$_2$, was 30% greater than that of **4**, bearing a single GlcNAc with the same spacer unit (Fig. 5B). In contrast, the maximal RU of compound **7** bearing (GlcNAc)$_2$ was 30% smaller than that of **5** bearing GlcNAc (Fig. 5C). The binding activity corresponds to the results from the precipitation analysis. Our data suggest that co-injection of divalent glycoside and tetravalent WGA as analyte results in simultaneous cross-linking. This result shows that the length of the spacer group between two terminal residues greatly influences the cross-linking activity.

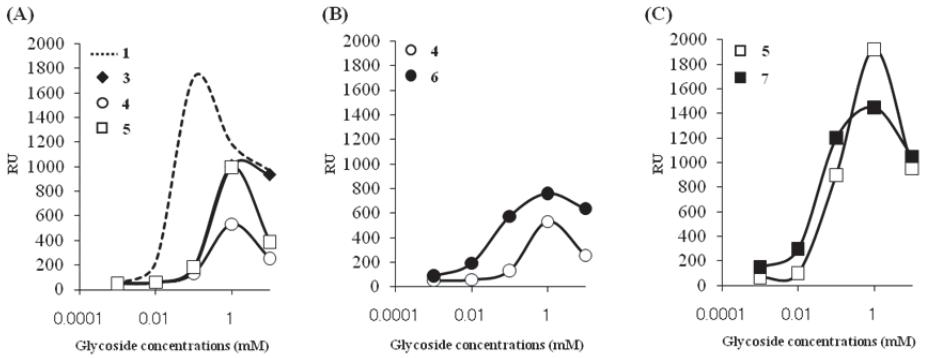

Fig. 5. Cross-linking formation of WGA with spacer-N-linked divalent glycosides on the sensor chip. In case of (A) and (B), WGA corresponding to 5700 response units was immobilized onto the sensor chip. In case of (C), WGA corresponding to 8700 response units was immobilized onto the sensor chip. (A) Spacer-N- and O-linked divalent GlcNAc-glycosides **1** and **3**-**5**. (B) Spacer-N-linked divalent GlcNAc- and (GlcNAc)$_2$-glycosides bearing -$(CH_2)_4$- on the spacer. (C) Spacer-N-linked divalent GlcNAc- and (GlcNAc)$_2$-glycosides bearing -$(CH_2)_5$- on the spacer.

4. Molecular design of spacer-N-linked tetravalent glycosides and their cross-linking activities with WGA and ECA lectins

We showed a synthetic method for generating spacer-O/N-linked divalent glycosides bearing GlcNAc, (GlcNAc)$_2$ and LacNAc with different spacer groups. The divalent

glycosides were shown to be capable of precipitating WGA and jack bean (*Canavalia ensiformis*) agglutinin (Con A) as divalent ligands. They were even able to achieve divalency in systems of low valency. These results encouraged us to prepare multivalent carbohydrate analogs for high affinity binding to target lectins (Masaka et al., 2010).

4.1 Synthesis of tetravalent glycosides

We designed two types of nonspacer- and spacer-N-linked tetravalent glycosides to increase the binding strength with specific lectins. Two types of N-linked tetravalent glycosides bearing GlcNAc, $(GlcNAc)_2$ and LacNAc were designed and prepared using ethylene glycol bis (β-aminoethyl ether)-*N*,*N*,*N*′,*N*′-tetraacetate (EGTA) as a precursor, which is widely used as a calcium-specific chelator, Scheme 3.

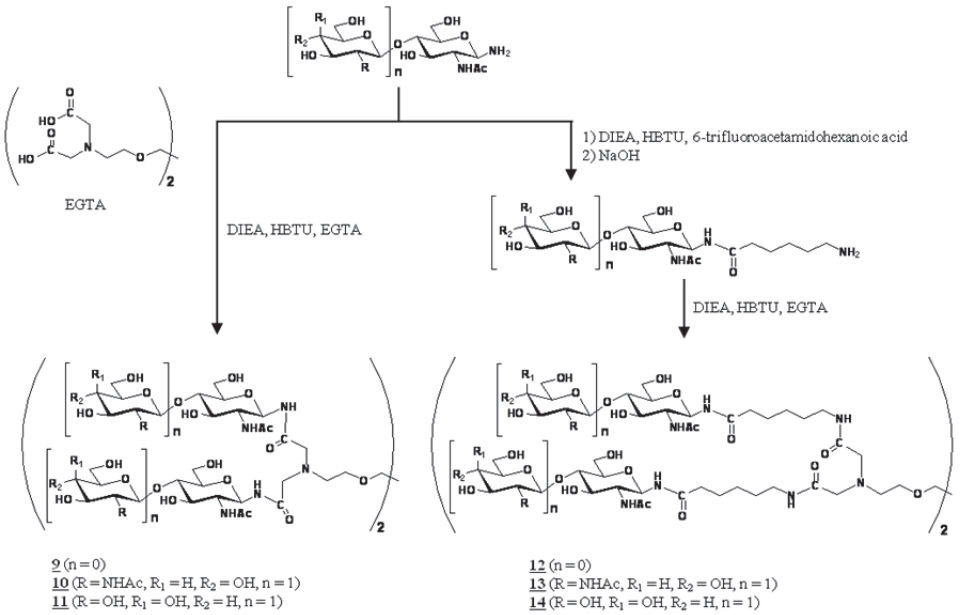

Scheme 3. Synthesis of nonspacer- and spacer-N-linked tetravalent glycosides.

Nonspacer-N-linked tetravalent glycosides were firstly prepared as follows. The *N*-β-mono- and diglycosylamines bearing GlcNAc, $(GlcNAc)_2$ and LacNAc were directly condensed with tetra-acetate EGTA in DMSO containing HBTU and DIEA. The tetravalent glycosides **9**, **10** and **11** were purified by chromatography on a Bio-Gel P-2 column and a charcoal-Celite column, producing yields of 55, 26 and 23%, respectively, based on the amount of EGTA added (Scheme 3). For an alternative design, we made a spacer-N-linked tetravalent glycoside by insertion of a spacer group between the sugar and EGTA. Thus, the corresponding *N*-β-glycosylamines were first condensed with the carboxyl group of 6-trifluoroacetamidohexanoic acid as in Scheme 3. The resulting spacer-N-linked glycosides were then deacylated to the corresponding amino group by alkali treatment, and the amino group was reacted with EGTA, as described above. Targets **12**, **13** and **14** were purified by chromatography on a Bio-Gel P-2 column and an ODS column producing high yields of 71,

74 and 67%, respectively, based on the amount of EGTA added. The tetravalent glycosides were elucidated by ^1H and ^{13}C NMR analyses, as described previously [Misawa et al., 2008(b); Ogata et al., 2009]. Structures of tetravalent glycosides bearing $(GlcNAc)_2$ were used as a reference in the analysis of ^1H NMR spectra. In the ^1H NMR spectra of **10** and **13**, two types of glycosidic proton signals were clearly observed in the lower field with larger coupling constants (**10**, δ 5.11, $J_{1,2}$ 9.8 Hz, H-1 and δ 4.63, $J_{1',2'}$ 8.6 Hz, H-1'; **13**, δ 5.06, $J_{1,2}$ 9.0 Hz, H-1 and δ 4.62, $J_{1',2'}$ 8.5 Hz, H-1'). In ^{13}C NMR spectra, two types of glycosidic signals were also characterized by the lower field (**10**, δ 104.2, C-1'β and δ 81.0, C-1β; **13**, δ 104.2, C-1'β and δ 81.1, C-1β). The spectra showed only the separated and overlapping resonances corresponding to respective sugar moieties. This simplicity suggests that these four sugar moieties can be superposed upon each other. ESI-MS analysis of tetra-headed glycosides **9**, **10**, **11**, **12**, **13** and **14** showed molecular ions at *m/z* 1211.5, 2023.8, 1859.7, 1663.8, 2477.4 and 2312.3, respectively, arising from the $[M + Na]^+$ ions. These results indicate that the resulting tetravalent glycosides consist exclusively of stereoregular sugars with tetravalent units. These compounds were soluble in water and the solubilities were 5 ~ 10%. Our synthetic methods are easy and efficient in the synthesis of tetravalent glycosides with stereoregular sugars through tetravalent carboxyl groups.

4.2 Interaction of tetravalent glycosides with specific lectins

The resulting tetravalent glycosides were used in the analysis of WGA and ECA: Interactions were measured using four methods: hemagglutination inhibition assay, precipitation assay, double-diffusion test, and biosensor analysis.

4.2.1 Hemagglutination inhibition assay

The interaction abilities of a series of divalent N^1,N^7-di-(2-acetamido-2-deoxy-β-D-glucopyranosyl-(1→4)-2-acetamido-2-deoxy-β-D-glucopyranosyl)-pimeamide (**7**) and tetravalent glycosides related to GlcNAc were compared with those of $(GlcNAc)_2$ and $(GlcNAc)_3$, which were used as control samples and are potent inhibitors of the hemagglutination of WGA (Table 1). In the hemagglutination inhibition assay, a multivalency effect was observed for **10**, **12** and **13**, but not for **9** bearing GlcNAc, when compared with $(GlcNAc)_2$, $(GlcNAc)_3$ and divalent **7**. Compounds **10**, **12** and **13** acted as inhibitors and their activities were 2 ~ 1042 fold higher than the reducing sugars $(GlcNAc)_2$ and $(GlcNAc)_3$ and 1 ~ 260 fold higher than divalent **7**. Compound **13** was the most effective inhibitor at a low concentration among the tetravalent glycosides: IC_{50} was 0.18 μM. Inhibition by flexible tetravalent **13**, bearing tandem GlcNAc**,** was much higher than the analog **12**, bearing a single GlcNAc and rigid nonspaced **10**, bearing tandem GlcNAc. The inhibition activity of the tetravalent glycosides increased in the order of **13 > 10 > 12 > 9**. It is worth noting that **13**, despite its low molecular weight, increases binding by a factor of 4 ~ 8 when compared with ovalbumin and asialofetuin.

In contrast, multivalency effects were not much detected in ECA (Table 2). The minimal inhibitory concentrations of the lectin mediated hemagglutination of ECA were: 47 μM for divalent LacNAc-glycoside (**8**), 12 μM for **11** and 5.9 μM for **14**. The relative binding affinity of **14** was one hundred and thirty times less than the binding affinity of asialofetuin. We suggest that ECA has a small multivalency enhancement ability, when comparing with WGA. This would be due to a difference of the binding mode on sugar sequence. ECA acts in an exo-manner on LacNAc sequence, while WGA both in endo and exo-manner on

GlcNAc sequence (Goldstein & Poretz, 1986). We have already reported the ECA is much less subject to the cluster effect by glycopolymer than WGA (Zeng et al., 2000).

Inhibitors	Sugar moiety	Valency	IC_{50}[a] (μM)	IC_{50}[b] (μM)
$(GlcNAc)_2$	-	Mono	750	750 (1)[d]
$(GlcNAc)_3$	-	Mono	375	375 (2)
7	$(GlcNAc)_2$	Di	93.8	188 (4)
9	GlcNAc	Tetra	>4000	-
10	$(GlcNAc)_2$	Tetra	5.86	23.4 (32)
11	LacNAc	Tetra	>4000	-
12	GlcNAc	Tetra	46.9	188 (4)
13	$(GlcNAc)_2$	Tetra	0.18	0.72 (1042)
14	LacNAc	Tetra	ND[c]	-
Ovalbumin	-	-	1.46	-
Asialofetuin	-	-	0.73	-

[a] Minimum concentrations required for complete inhibition of hemagglutination.
[b] Concentration of sugar units.
[c] ND: not determined.
[d] Relative inhibitory potency. (All data normalized to those of $(GlcNAc)_2$. Higher values indicate greater inhibitory potency.)

Table 1. Inhibition of WGA-mediated hemagglutination by di- and tetravalent glycosides.

Inhibitors	Sugar moiety	Valency	IC_{50}[a] (μM)	IC_{50}[b] (μM)
LacNAc	-	Mono	94	94 (1)[c]
8	LacNAc	Di	47	94 (1)
11	LacNAc	Tetra	12	48 (2)
14	LacNAc	Tetra	5.9	24 (4)
Asialofetuin	-	-	0.092	-
Fetuin	-	-	0.37	-

[a] Minimum concentrations required for complete inhibition of hemagglutination.
[b] Concentration of LacNAc units.
[c] Relative inhibitory potency. (All data normalized to those of LacNAc. Higher values indicate greater inhibitory potency.)

Table 2. Inhibition of ECA-mediated hemagglutination by di- and tetravalent glycosides.

4.2.2 Precipitation analysis

In the quantitative precipitation assay, tetravalent glycosides were shown to be capable of precipitating WGA/ECA as tetravalent ligands. The result is consistent with the sugar specificities of the corresponding lectins reported for naturally occurring glycoproteins, glycolipids and oligosaccharides. The precipitin profiles (Figs. 6 and 7) are similar to antigen-antibody (Kabat 1976), lectin-polysaccharide (Usui et al., 1981), and lectin-glycopeptide [Bhattacharyya et al., 1988(a)] and complex-type oligosaccharide-Con A precipitin curves [Bhattacharyya et al., 1987(b)] which suggests similar multivalent interactions between the tetravalent glycosides and WGA/ECA, despite the low molecular weights as ligands. The precipitin profile between flexible **12**/**13** with spacer and WGA was shown to proceed stoichiometrically, compared with rigid **9** and **10** with no spacer.

Compounds **12** and **13** behaved tetravalently in WGA binding. Similar precipitation experiments with spacer-linked **14** showed that it is divalent for ECA binding. No precipitates were observed between divalent glycoside and ECA. The results suggested the spacer-linked glycosides effectively bind and promote cross-linking of WGA in solution, rather than inhibiting the binding of lectin. Precipitation of WGA with **10**, **12** and **13** occurs at room temperature, whereas precipitation of ECA with **11** and **14**, which bind more weakly, requires a lower temperature (4°C). In general, the precipitation data for ligand with lectin reflects the relative affinities of carbohydrate for the proteins. The binding activities of lectins, including WGA and ECA, produced cross-linked complexes with the tetravalent glycosides. The results were supported by the double diffusion test. However, ECA has a much smaller multivalency enhancement than WGA. The present results are easily predictable by previous our reports. Because we have already reported that artificial glycopolymers bearing (GlcNAc)$_2$ unit shows a strong interaction with WGA, because of a cluster effect of multivalent oligosaccharide chains in the polymer, whereas ECA is much less subject to cluster effect by glycopolymer bearing LacNAc unit (Zeng et al., 1998).

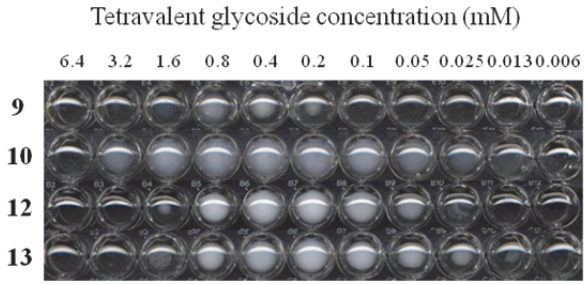

Fig. 6. Photographs of precipitate formed by addition of tetravalent glycosides to WGA-PBS solution.

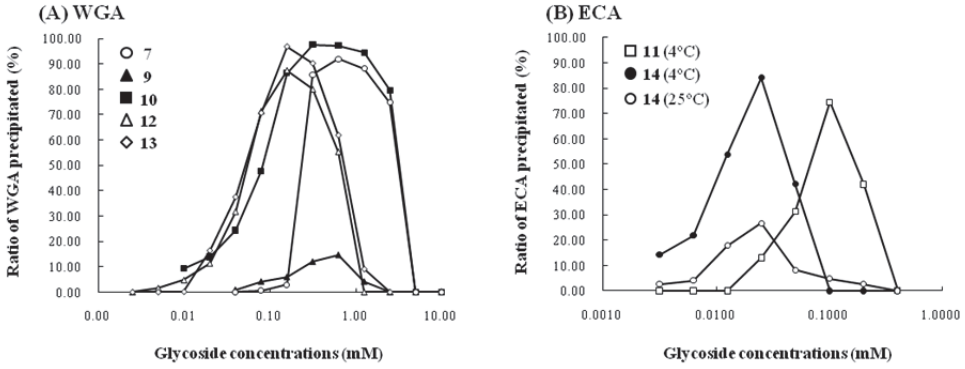

Fig. 7. Precipitin curves for the precipitation of WGA (A) and ECA (B) with tetravalent glycosides. The percentage of precipitated WGA or ECA was calculated by subtracting the amount of WGA/ECA in the supernatant from the total amount of WGA/ECA, respectively.

4.2.3 Double diffusion test

Figure 8 shows the results of double diffusion reactions using tetravalent glycosides **9-14** with WGA and ECA lectins. In general, precipitate is formed by the reaction between two specific high molecular weight compounds, such as lectin-glycoprotein and lectin-polysaccharide (Ogata et al., 2007; Zeng et al., 2000; Usui et al., 1981). Interestingly, sharp precipitin bands are seen between the central well with WGA and the surrounding wells containing tetravalent glycosides **10**, **12** and **13** (Fig. 8A). Precipitin bands were not observed with **9**, **11** and **14**. Weak precipitin bands were observed between the central well with ECA and the surrounding wells containing **11** and **14** bearing LacNAc at 4°C (Fig. 8B). These reactivities correlate well with the results of the hemagglutination inhibitory assay.

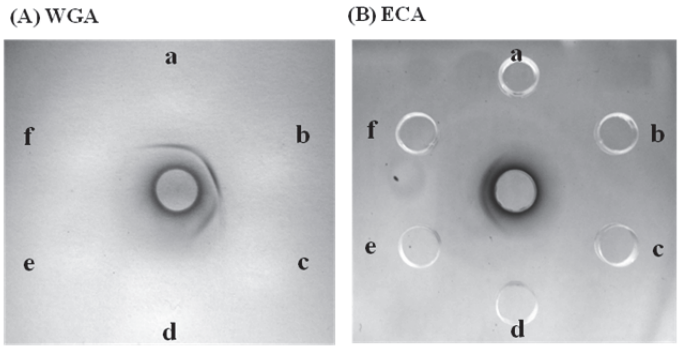

Fig. 8. Double diffusion reaction of tetravalent glycosides with WGA (A) and ECA (B) in agar gel. Lectin solutions were put in the center wells. Portions of tetra-headed glycoside solutions were added to the peripheral wells. a: **13**; b: **10**; c: **12**; d: **9**; e: **14**; f: **11**.

4.2.4 SPR analysis

SPR competition binding assays were used to monitor the effect of tetravalent glycosides on the interaction of soluble WGA with surface-bound WGA. The dissociation rate of **10** and **13** at maximal RU bearing tandem GlcNAc was much slower than that of **9** and **12** bearing single GlcNAc (Fig. 9). The dissociation rates can be summarized as: **13** > **10** >> **12** > **9**. The slow down of the dissociation rate enhances binding affinity, and is due to multivalency effects (Lee & Lee, 2000). This relationship is consistent with the hemagglutination inhibition activity mention above. Thus, it indicates that the binding affinity is not only enhanced by the existence of a spacer on the tetravalent glycosides, but also a sugar length. In our study, RU increased as the concentration of the tetravalent glycosides increased from 0.1 μM to 0.1 mM. Thus, the tetravalent glycosides promoted, rather than inhibited, binding of WGA to a surface-bound WGA. Our data suggests co-injection of tetravalent glycoside and tetravalent WGA as analyte results in simultaneous cross-linking. The cross-linking complexes presumably bind to the surface-bound WGA through unbound tetravalent glycosides. Compounds **12** and **13**, with flexible spacer, clearly show maximum binding at 0.1 mM and spacer-N-linked divalent GlcNAc-glycoside (**5**) displayed maximum binding at 1 mM (Fig. 10). The results of SPR analysis corresponded with the results of the precipitation assay.

Our results show flexible tetravalent **13** has particularly high-affinity for WGA. Gour and Verma with the help of AFM (atomic force microscope) imaging demonstrated strong,

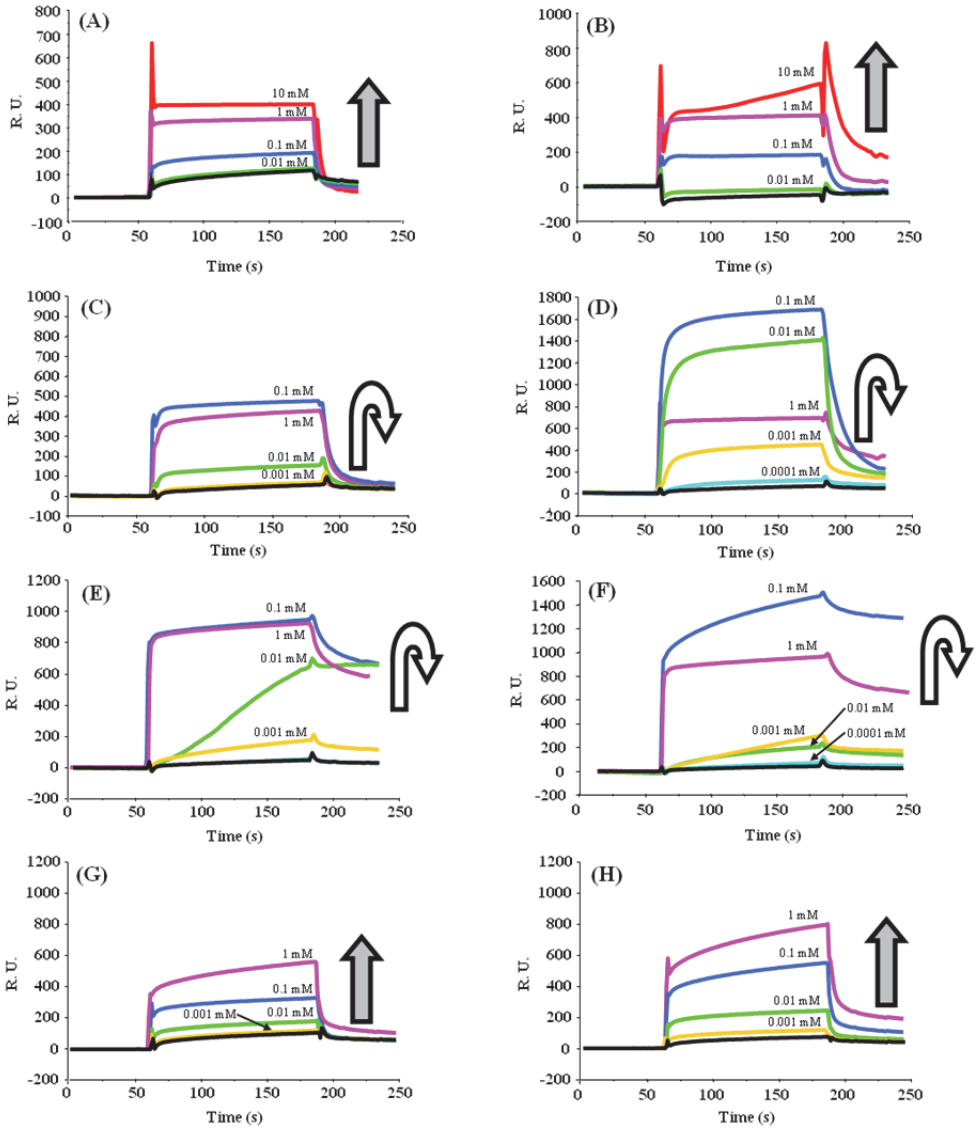

Fig. 9. Sensorgrams showing the interactions of the glycosides with WGA. WGA corresponding to 8100 (A and B) or 6700 (C to H) response units was directly immobilized onto the sensor chip. WGA was co-injected with glycoside: (A) $(GlcNAc)_2$, (B) $(GlcNAc)_3$, (C) **9**, (D) **12**, (E) **10**, (F) **13**, (G) **11**, and (H) **14** [Color lines show increased and decreased RU, or injected without glycoside as a negative control (black line)].

complex interactions between a trivalent mannose conjugate and Con A (Gour & Verma, 2007). Their results suggest the orientation of a tetravalent glycoside as ligand was highly compatible with the formation of cross-linked complexes, which is the likely cause of binding enhancement for this class of lectin. The chelate effect leads to large rate enhancement in tetravalent systems, with favorable orientation of ligands. In the chelation mechanism, neighboring binding sites are simultaneously occupied by ligands bridged by suitable spacers (Rao et al., 1998). Typically, binding of the first ligand is thought to reduce the entropic barriers for binding the second and further ligands. The chelate effect can lead to a large rate enhancement for the tetravalent system of **13**, so that the spacer is optimal in terms of flexibility. On closer inspection, it was found that binding enhancement was due to a combination of multivalency effects and spacer effects.

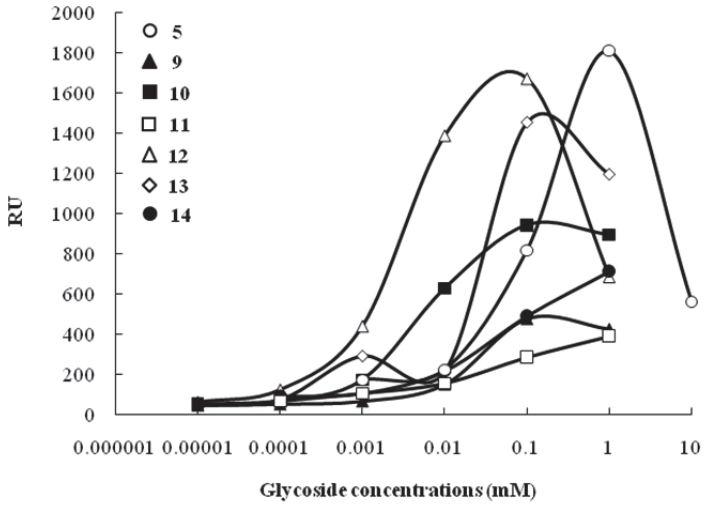

Fig. 10. Cross-linking formation of WGA with tetravalent glycosides on the sensor chip. WGA corresponding to 6700 response units was immobilized onto the sensor chip.

5. Summary

We designed various type di- and tetravalent glycosides to increase the binding strength of synthetic ligands for WGA and ECA. Synthesized di- and tetravalent glycosides bearing GlcNAc, $(GlcNAc)_2$ and LacNAc were found to be capable of binding and precipitating specific lectins as di- or tetravalent ligand. Especialy, spacer-N-linked tetravalent glycoside bearing flexible tandem GlcNAc (**13**) showed a strong multivalency effect for WGA, as studied through lectin-ligand interactions. Our results suggest that even small synthetic conjugates could act as potential ligands for lectin binding, producing similar multivalent interactions with glycoprotein. Future studies on the interaction of synthetic multivalent glycoside conjugates with lectins for the generation of cross-linking complexes are planned and are expected to complement other biophysical studies of lectin-multivalent carbohydrate interactions.

6. Acknowledgment

We thank professor Jun Hiratake of Kyoto University for useful suggestions.

7. References

Bhattacharyya, L.; Ceccarini, C.; Lorenzoni, P. & Brewer, C. F. (1987(a)). Concanavalin A interactions with asparagine-linked glycopeptides. *J. Biol. Chem.*, Vol.262, pp. 1288-1293.

Bhattacharyya, L.; Fant, J.; Lonn, H. & Brewer, C. F. (1990). Binding and precipitating activities of *Lotus tetragonolobus* isolectins with L-fucosyl oligosaccharides. Formation of unique homogeneous cross-linked lattices observed by electron microscopy. *Biochemistry*, Vol.29, pp. 7523-7530.

Bhattacharyya, L.; Haraldsson, M. & Brewer, C. F. (1987(b)). Concanavalin A interactions with asparagine-linked glycopeptides. *J. Biol. Chem.*, Vol.262, pp. 1294-1299.

Bhattacharyya, L.; Haraldsson, M. & Brewer, C. F. (1988(a)). Precipitation of galactose-specific lectins by complex-type oligosaccharides and glycopeptides: studies with lectins from *Ricinus communis* (agglutinin I), *Erythrina indica*, *Erythrina arborescens*, *Abrus precatorius* (agglutinin), and *Glycine max* (soybean). *Biochemistry*, Vol.27, pp. 1034-1041.

Bhattacharyya, L.; Khan, M. I. & Brewer, C. F. (1988(b)). Interactions of concanavalin A with asparagine-linked glycopeptides: formation of homogeneous cross-linked lattices in mixed precipitation systems. *Biochemistry*, Vol.27, pp. 8762-8767.

Brewer, C. F. (1997). Cross-linking activities of galectins and other multivalent lectins. *Trends Glycosci. Glycotechnol.*, Vol.9, pp. 155-165.

Burke, S. D.; Zhao, Q.; Schuster, M. C. & Kiessling, L. L. (2000). Synergistic formation of soluble lectin clusters by a templated multivalent saccharide ligand. *J. Am. Chem. Soc.*, Vol.122, pp. 4518-4519.

Dam, T. K.; Oscarson, S.; Roy, R.; Das, S. K.; Page, D.; Macaluso, F. & Brewer, C. F. (2005). Thermodynamic, kinetic, and electron microscopy studies of concanavalin A and *Dioclea grandiflora* lectin cross-linked with synthetic divalent carbohydrates. *J. Biol. Chem.*, Vol.280, pp. 8640-8646.

Dessen, A.; gupta, D.; Sabesan, S.; Brewer, C. F. & Sacchettini, J. C. (1995). X-ray crystal structure of the soybean agglutinin cross-linked with a biantennary analog of the blood group I carbohydrate antigen. *Biochemistry*, Vol.34, pp. 4933-4942.

Goldstein, I. J. & Poretz, R. D. (1986). in *The Lectins*: Liener, I. E.; Sharon, N. & Goldstain, I. J. Eds.: Academic Press, Orlando, FL, pp. 35-244.

Gour, N. & Verma, S. (2007). Synthesis and AFM studies of lectin-carbohydrate self-assemblies. *Tetrahedron*, Vol.64, pp. 7331-7337.

Gupta, D. & Brewer, C. F. (1994). Homogeneous aggregation of the 14-kDa β-galactosidase specific vertebrate lectin complex with asialofetuin in mixed systems. *Biochemistry*, Vol.33, pp. 5526-5530.

Gupta, D.; Kaltner, H.; Dong, X.; Gabius, H.-J. & Brewer, C. F. (1996). Comparative cross-linking activities of lactose-specific plant and animal lectins and a natural lactose-

binding immunoglobulin G fraction from human serum with asialofetuin. *Glycobiology*, Vol.6, pp. 843-849.

Houseman, B. T. & Mrksich, M. (2002). Model systems for studying polyvalent carbohydrate binding interactions. *Top. Curr. Chem.*, Vol.218, pp. 1-44.

Kabat, E. A. (1976). in *Structural Concepts in Immunology and Immunochemistry, 2nd ed.*: Rinehart, H. New York.

Kato, M.; Uno, T.; Hiratake, J. & Sakata, K. (2005). α-Glucopyranoimidazolines as intermediate analogue inhibitors of family 20 β-*N*-acetylglucosaminidases. *Bioorg. Med. Chem.*, Vol.13, pp. 1563-1571.

Kiessling, L. L. & Pohl, N. L. (1996). Strength in numbers: non-natural polyvalent carbohydrate derivatives. *Chem. Biol.*, Vol.3, pp. 71-77.

Kitov, P. I.; Sadowska, J. M.; Mulvey, G.; Armstrong, G. D.; Ling, H.; Pannu, N. S.; Read, R. J. & Bundle, D. R. (2000). Shiga-like toxins are neutralized by tailored multivalent carbohydrate ligands. *Nature*, Vol.403, pp. 669-672.

Krishnamurthy, V. M.; Semetey, V.; Bracher, P. J.; Shen, N. & Whitesides, G. M. (2007). Dependence of effective molarity on linker length for an intramolecular protein-ligand system. *J. Am. Chem. Soc.*, Vol.129, pp. 1312-1320.

Lee, R. T. & Lee, Y. C. (2000). Affinity enhancement by multivalent lectin-carbohydrate interaction. *Glycoconjugate J.*, Vol.17, pp. 543-551.

Lee, Y. C. & Lee, R. T. (1995). Carbohydrate-protein interactions: Basis of glycobiology. *Acc. Chem. Res.*, Vol.28, pp. 321-327.

Lindhorst, T. K. (2002). Artificial multivalent sugar ligands to understand and manipulate carbohydrate-protein interactions. *Top. Curr. Chem.*, Vol.218, pp. 201-232.

Lundquist, j. J. & Toone, E. J. (2002). The cluster glycoside effect. *Chem. Rev.*, Vol.102, pp. 555-578.

Maierhofer, C.; Rohmer, K. & Wittmann, V. (2007). Probing multivalent carbohydrate-lectin interactions by an enzyme-linked lectin assay employing covalently immobilized carbohydrates. *Bioorg. Med. Chem.*, Vol.15, pp. 7661-7676.

Mammen, M.; Choi, S.-K. & Whitesides, G. M. (1998). Polyvalent interactions in biological system: Implications for design and use of multivalent ligands and inhibitors. *Angew. Chem. Int. Ed.*, Vol.37, pp. 2754-2794.

Mammen, M.; Dahmann, G. & Whitesides, G. M. (1995). Effective inhibitors of hemagglutination by influenza virus synthesized from polymers having active ester groups. Insight into mechanism of inhibition. *J. Med. Chem.*, Vol.38, pp. 4179-4190.

Mandal, D. K.; Kishore, N. & Brewer, C. F. (1994). Thermodynamics of lectin-carbohydrate interactions. Titration microcalorimetry measurements of the binding of N-linked carbohydrates and ovalbumin to concanavalin A. *Biochemistry*, Vol.33, pp. 1149-1156.

Masaka, R.; Ogata, M.; Misawa, Y.; Yano, M.; Hashimoto, C.; Murata, T.; Kawagishi, H. & Usui, T. (2010). Molecular design of N-linked tetravalent glycosides bearing *N*-acetylglucosamine, *N*,*N'*-diacetylchitobiose and *N*-acetyllactosamine: Analysis of cross-linking activities with WGA and ECA lectins. *Bioorg. Med. Chem.*, Vol.18, pp. 621-629.

Misawa, Y.; Akimoto, T.; Amarume, S.; Murata, T. & Usui, T. (2008(a)). Enzymatic synthesis of spacer-linked divalent glycosides carrying *N*-acetylglucosamine and *N*-acetyllactosamine: Analysis of cross-linking activities with WGA. *J. Biochem. (Tokyo)*, Vol.143, pp. 21-30.

Misawa, Y.; Masaka, R.; Maeda, K.; Yano, M.; Murata, T.; Kawagishi, H. & Usui, T. (2008(b)). Efficient synthesis of spacer-N-linked double-headed glycosides carrying *N*-acetylglucosamine and *N*,*N*′-diacetylchitobiose and their cross-linking activities with wheat germ agglutinin. *Carbohydr. Res.*, Vol.343, pp. 434-442.

Misawa, Y.; Masaka, R.; Yano, M.; Murata, T. & Usui, T. (2009). Synthesis of spacer-linked divalent glycosides by chitinolytic enzyme form *Amycolatopsis orientalis*. *J. Appl. Glycosci.*, Vol.56, pp. 89-95.

Ogata, M.; Hidari, K. I.-P.-J.; Kozaki, W.; Murata, T.; Hiratake, J.; Park, E. Y.; Suzuki, T. & Usui, T. (2009). Molecular design of spacer-*N*-linked sialoglycopolypeptide as polymeric inhibitors against influenza virus infection. *Biomacromolecules*, Vol.10, pp. 1894-1903.

Ogata, M.; Murata, T.; Murakami, K.; Suzuki, T.; Hidari, K. I.-P.-J.; Suzuki, Y. & Usui, T. (2007). Chemoenzymatic synthesis of artificial glycopolypeptides containing multivalent sialyloligosaccharides with a γ-polyglutamic acid backbone and their effect on inhibition of infection by influenza viruses. *Bioorg. Med. Chem.*, Vol.15, pp. 1383-1393.

Pieters, R. J. (2004). Interference with lectin binding and bacterial adhesion by multivalent carbohydrates and peptidic carbohydrate mimics. *Trends Glycosci. Glycotechnol.*, Vol.16, pp. 243-254.

Rao, J.; Lahiri, J.; Lsaacs, L.; Weis, R. M. & Whitesides, G. M. (1998). A trivalent system from vancomycin-D-Ala-D-Ala with higher affinity than avidin-biotin. *Science*, Vol.280, pp. 708-711.

Roy, R. (2003). A decade of glycodendrimer chemistry. *Trends Glycosci. Glycotechnol.*, Vol.15, pp. 291-310.

Roy, R. (1996). Syntheses and some applications of chemically defined multivalent glycoconjugates. *Curr. Opin. Struct. Biol.*, Vol.6, pp. 692-702.

Sacchettini, J. C.; Baum, L. G. & Brewer, C. F. (2001). Multivalent protein-carbohydrate interactions. A new paradigm for supermolecular assembly and signal transduction. *Biochemistry*, Vol.40, pp. 3009-3015.

Toone, E. J. (1994). Structure and energetics of protein-carbohydrate complexes. *Curr. Opin. Struct. Biol.*, Vol.4, pp. 719-728.

Usui, T.; Iwasaki, Y. & Mizuno, T. (1981). Isolation and characterization of two kind of heterogalactan from the fruit bodies of *ganodernra applannatum* by employing a column of concan. *Carbohydr. Res.*, Vol.92, pp. 103-114.

Usui, T.; Hayashi, Y.; Nanjo, F.; Sakai, K. & Ishido, Y. (1987). Transglycosylation reaction of a chitinase purified from *Nocardia orientalis*. *Biochim. Biophys. Acta*, Vol.923, pp. 302-309.

Zeng, X.; Murata, T.; Kawagishi, H.; Usui, T. & Kobayashi, K. (1998). Analysis of specific interactions of stnthetic glycopolypeptides carrying *N*-acetyllactosamine and related compounds with lectins. *Carbohydr. Res.*, Vol.312, pp. 209-217.

Zeng, X.; Nakaaki, Y.; Murata, T. & Usui, T. (2000). Chemoenzymatic synthesis of glycopolypeptides carrying α-Neu5Ac-(2→3)-β-D-Gal-(1→3)-α-D-GalNAc, β-D-Gal-(1→3)-α-D-GalNAc, and related compounds and analysis of their specific interactions with lectins. *Arch. Biochem. Biophys.*, Vol.383, pp. 28-37.

3

Determination of Binding Kinetics between Proteins with Multiple Nonidentical Binding Sites by SPR Flow Cell Biosensor Technology

Kristmundur Sigmundsson[1,4], Nicole Beauchemin[3],
Johan Lengqvist[2,5] and Björn Öbrink[1]
[1]*Department of Cell and Molecular Biology, Karolinska Institutet, Stockholm,*
[2]*Department of Medical Biophysics and Biochemistry, Karolinska Institutet, Stockholm,*
[3]*Goodman Cancer Research Centre, McGill University, Montreal, QC,*
[4]*Present address: Department of Medical Biophysics and Biochemistry, Karolinska Institutet, Stockholm,*
[5]*Present address: Department of Molecular Toxicology, Safety Assessment, AstraZeneca Research and Development, Södertälje,*
[1,2,4,5]*Sweden*
[3]*Canada*

1. Introduction

Protein-protein binding interactions are crucial in signaling networks that regulate cellular functions in health and disease. A large number of membrane and cytoplasmic proteins participate in those networks, and a complete understanding of their functional activities at the cellular level would require comprehensive analysis of the kinetics of the various protein interactions. This is, however, a herculean task due to both the multitude of interacting proteins and the complexity of the individual pairwise binding interactions. The latter are in many cases not simple 1:1 binding reactions but a result of simultaneous interactions between several distinct binding sites. In an initial attempt to tackle this challenge we have developed new algorithms and experimental procedures to determine the binding kinetics of the cell adhesion receptor CEACAM1-L and the protein tyrosine phosphatase SHP-1 (Fig. 1). CEACAM1-L is a signal-regulating cell surface-associated transmembrane protein that regulates a plethora of basic biological events including cell proliferation and motility, apoptosis, tissue morphogenesis, immune reactions and microbial infections, vasculogenesis and angiogenesis, and cancer growth and invasion (Gray-Owen & Blumberg, 2006; Müller et al., 2009; Singer et al., 2010). Many of CEACAM1-L's regulatory activities are a result of its binding and activation of Src-family kinases and the protein tyrosine phosphatases SHP-1 and SHP-2. The cytoplasmic domain of CEACAM1-L contains two phosphotyrosine-based ITIM sequences, pY488 and pY515, that bind to SH2 domains in the kinases and phosphatases (Fig. 1). The kinases have one SH2 domain whereas the phosphatases have two SH2 domains, N-SH2 and C-SH2, arranged in tandem. Thus, there is a potential for at least four different binding interactions between CEACAM1-L and SHP-1 or SHP-2. Here we have focussed on the binding interactions between the cytoplasmic domain of

CEACAM1-L and the SH2 domains of SHP-1, which were studied in an SPR-based flow cell biosensor.

To be able to analyze such a complex system, with several distinct binding sites in both of the interacting molecules, we started by characterizing the interactions between the single binding sites, using peptides and protein domains. The resulting parameters were then used as building blocks for more elaborate analyses of the interactions of the tandem N,C-$(SH2)_2$ domain with the double-tyrosine-phosphorylated cytoplasmic domain of CEACAM1-L. The major questions that we addressed with this approach were: which complexes are formed between the CEACAM1-L cytoplasmic domain and the tandem SH2-domain of SHP-1, what kind of kinetics do they obey, and which of them are of physiological relevance. To that end we had to develop new reaction schemes based on plausible interactions, and translate them into equations and algorithms that could be used for curve fitting analysis of recorded sensorgrams. The analyses demonstrated that both the N-SH2 and C-SH2 domains of SHP-1 participated in binding to the two ITIM sequences in CEACAM1-L. Interestingly, our approach led to the discovery of a second phosphotyrosine binding site in the C-SH2 domain, which differed kinetically from the other C-SH2 binding site. At physiological temperature, the most pronounced complex that was formed was a double-docked form, in which the CEACAM1-L pY488 motif occupied the N-SH2 binding site and the pY515 motif occupied one of the two phosphotyrosine binding sites in the C-SH2 domain.

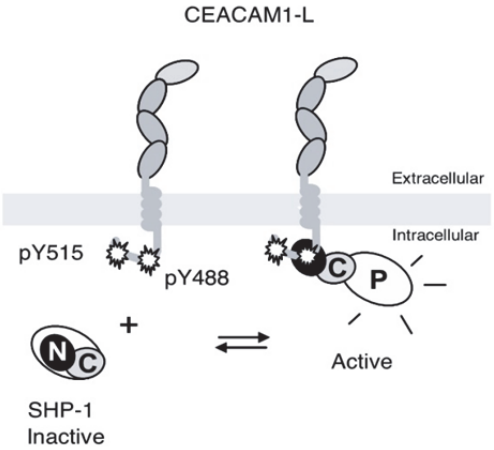

Fig. 1. Cartoon of CEACAM1-L, SHP-1 and a hypothetical interaction complex. Murine CEACAM1-L has an intracellular domain of 73 amino acids including two phosphorylatable tyrosine residues, Y488 and Y515. SHP-1 has two SH2 domains (labelled N and C) and a C-terminal phosphatase domain (P). The phosphatase is autoinhibited when undocked. SH2-domain interactions with phosphotyrosine-containing sequence motifs initiate a conformational change leading to phosphatase activation.

2. Experimental procedures

2.1 Peptides

Peptides spanning the Y488 and Y515 regions of mouse CEACAM1-L were purchased from K. J. Ross-Petersen AS (Horsholm, Denmark). These included both unphosphorylated and

tyrosine-phosphorylated forms of N-terminally biotinylated dodecameric peptides: VDDVAY(488)TVLNFN, ATETVY(515)SEVKKK, and N-terminally cysteinylated eicosameric and pentadecameric peptides: CKVDDVAY(488)TVLNFNSQQPNR and CPRATETVY(515)SEVKKK, respectively. Additionally, a scrambled derivative of the unphosphorylated Y488 dodecapeptide, Biotin-LANDFVNDTVYV, was purchased from the same producer. All peptides were highly homogeneous and > 95 % pure as demonstrated by amino acid analysis, HPLC, and MALDITOF mass spectrometry.

2.2 Recombinant proteins

The construction of recombinant proteins of single SH2 domains and the tandem form N,C-$(SH2)_2$ of mouse SHP-1, and of the cytoplasmic part of mouse CEACAM1-L fused with GST using the pGEX-2T vector system, has been described previously (Beauchemin et al. 1997). Proteins were produced in *Escherichia coli* BL21. Protein synthesis was induced with IPTG (0.2 mM). The tyrosine phosphorylated cytoplasmic part of CEACAM1-L (GST-Lcyt-[pY488/pY515]) was produced in *Epicurian coli* TKX1 (#200124, Stratagene), inducing protein synthesis simultaneously with IPTG (0.2 mM) and IAA (0.1 mM). Purification of the GST fusion proteins was performed by affinity adsorption on glutathione-Sepharose according to a standard protocol from the manufacturer (Amersham). Buffer exchange and further purification of recombinant proteins was carried out on a Superose 12 prepacked column attached to a FPLC 500 system (Pharmacia AB), equilibrated in 10 mM Hepes, 150 mM NaCl, 3.4 mM EDTA, and 0.005% surfactant P20, pH 7.4 (HBS). Protein purity was confirmed by SDS-PAGE. Concentrations of purified GST-N-SH2, GST-C-SH2, GST-N,C-$(SH)_2$ and GST-Lcyt proteins were determined by absorption spectroscopy, using the following molar absorptivity values (ε in $M^{-1}cm^{-1}$, at 280 nm): 51730, 57480, 69630 and 43480, respectively. In the protein interaction measurements, the active concentrations of the analyte proteins were double-checked by the BIAcore-based procedure described in (Sigmundsson et al., 2002). For GST removal, recombinant proteins were treated with 100 units of thrombin per 3 mg fusion protein per 1 ml at 4 ˚C, for 48 h, with mild swirling. The calculated molecular masses of non-cleaved fusion proteins were: GST-N-SH2 = 37.5 kDa, GST-C-SH2 = 39.0 kDa and GST-N,C-$(SH)_2$ = 51.1 kDa. The calculated molecular masses of thrombin cleaved products were: N-SH2 = 11.3 kDa, C-SH2 = 12.9 kDa, N,C-$(SH)_2$ = 24.9 kDa and GST = 26.2 kDa. The tyrosine phosphorylation of GST-Lcyt was determined by nanoelectrospray ionization mass spectrometry using a QTQF1 instrument (Waters), analysing both intact full size protein and trypsinized fragments.

2.3 Protein interaction measurements

Interaction measurements based on surface plasmon resonance (SPR) detection were carried out with a BIAcore 2000 instrument (BIAcore AB, Uppsala, Sweden).

2.4 Ligand immobilization

Peptides were immobilized on CM5 Sensor Chips, either by binding via the N-terminal biotin groups to immobilized streptavidin (SA), or via direct coupling by thiol-disulphide exchange. Carboxymethyl-modified dextran surfaces were activated according to a standard procedure, with an injection of 0.05 M NHS/0.2 M EDC for 7 min. High density streptavidin chips (SA ≈ 2000 RU) were prepared by injection of 140 µl of freshly prepared SA (50 µg/ml in 5 mM acetate buffer, pH 4.5) at 10 µl/min. This resulted in 1995 – 2025 RU of immobilized streptavidin per lane after blocking of remaining reactive esters with two injections of 1 M

ethanolamine-HCl, pH 8.5 for 2 min each. Low density streptavidin chips (SA ≈ 1000 RU) were prepared by injection of 40 µl of SA (50 µg/ml) and blocking as described above, which resulted in 980 – 1100 RU of SA per lane. N-terminally biotinylated dodecameric peptides were dissolved in DMSO to give stock solutions of 3.5 g/l. Prior to immobilization, the stocks were diluted to 50 µg/ml in HBS and then injected into separate lanes at 20 µl/min for one minute. Finally, the lanes were washed separately by four injections of 6 M guanidine-HCl/HBS, pH 7.4 for 1 min each and injections of 4 M LiCl/HBS for 1 min and 0.25 % P20/HBS for 1 min, respectively. The levels of stably immobilized peptides were 200 – 240 RU and 65-80 RU per lane, for high and low density SA surfaces, respectively.
For preparation of low density peptide surfaces, N-terminally cysteinylated peptides were immobilized via direct coupling by thiol-disulphide exchange. For this purpose, NHS/EDC activated surfaces were modified by interaction with a freshly prepared solution of 80 mM PDEA (thiol coupling reagent) in 0.1 M borate buffer pH 8.5 for 4 min, by injection of 40 µl at 10 µl/min, followed by a 4 min blocking step with 1 M ethanolamine-HCl, pH 8.5, prior to peptide injections. Peptides were dissolved in DMSO at 2 mM concentration and were diluted with 5 mM acetate buffers to the indicated concentrations immediately before immobilization as follows: CKVDDVAY(488)TVLNFNSQQPNR 0.4 µM at pH 4.5, CKVDDVA-pY(488)-TVLNFNSQQPNR 10.0 µM at pH 3.9, CPRATETVY(515)SEVKKK 0.2 µM at pH 4.5, and CPRATETV-pY(515)-SEVKKK 0.5 µM at pH 4.5. Levels of stably immobilized peptides were 35 ± 5 RU per lane 1 and 2 for the pY515 and Y515 peptides respectively, and 16 ± 5 RU for the pY488 peptide on lane 3, as determined after blocking of remaining reactive surface 2-pyridinyldithio-groups with freshly prepared 6 mM L-cysteine in 5 mM acetate, pH 4.5 for 2 min, followed by washing with 0.25% P20/HBS. If assuming 100% binding capacity of these two surfaces the theoretical saturation level, i.e. R_{Max} with regard to N,C-$(SH)_2$ as the analyte, was c:a 120 RU and 510 RU, for the pY488 and pY515 surfaces, respectively. The non-phosphorylated Y515 peptide on lane 2 was applied as the reference surface. For preparation of peptide-free reference surfaces (lane 4), blocking was performed by injection of the L-cysteine solution for 15 min at 10 µl/min.
For immobilization of the GST-Lcyt-pY protein, anti-GST antibody was amine-coupled to CM5 Sensor Chips. For this purpose the carboxymethyl-modified dextran surfaces were activated according to standard procedures. The antibody was diluted in 10 mM Na-acetate buffer, pH 5.0, according to a standard protocol from the manufacturer and injected at 10 µl/min to a final immobilization level of 1000 ± 100 RU per lane. The surfaces were washed ten times with 20 µl of 20 mM glycine, pH 2.2, followed by two washes with 20 µl 2 M LiCl/HBS and one wash with 20 µl of 0.2 % P20/HBS, at a flow rate of 10 µl/min. GST-Lcyt-pY was immobilized on lane 2 at a concentration of 0.2 mg/ml in HBS at a flow rate of 10 µl/min, for 6 min. A saturation level of c:a 112 RU was reached, and verified by an additional injection of 20 µl of 0.5 mg/ml GST-Lcyt-pY, which did not add to the immobilized amount of ligand. Lane 1 was saturated with GST and used as the reference lane. When loading the reference lane, 0.4 mg/ml GST in HBS was flushed over both lane 1 and lane 2, for 10 min. This resulted in c:a 95 RU binding of GST to lane 1, while no change was obtained in lane 2. Surfaces were washed 10 times with 1.5 M LiCl/HBS with no detectable decrease in ligand levels.

2.5 Protein interaction analyses

Samples were kept at 2° C prior to injection. All interaction analyses were performed in HBS at a flow of 20 µl/min. In all SPR assays involving peptide ligands, phosphorylated

peptides were placed in flow cells 1 and 3. Flow cell 2 was loaded with unphosphorylated peptide or a scrambled unphosphorylated peptide and was used as a reference for unspecific binding and background subtraction. Flow cell 4 was kept free of ligand (peptide), but received the complete treatment of activation and inactivation. This flow cell was used as an independent control to monitor differences in refractive indices of sample and running buffer and to monitor background adsorption to the dextran (or dextran-SA) surface. A monoclonal anti-phosphotyrosine antibody (PY99) was used to confirm equal loadings of phosphotyrosine peptides in flow cells 1 and 3. For qualitative binding studies non-cleaved and cleaved recombinant proteins were flushed over N-terminally biotinylated dodecameric peptides at 25° C, immobilized on both high and low density SA chips. Low density surfaces with N-terminally cysteinylated peptides (15-30 RU) were used in SPR assays aimed to determine kinetic constants. For this purpose, recombinant proteins cleaved from GST were injected at different concentrations in a randomized order with a total of 3 injections per concentration. This process was repeated at 5°, 15°, 25°, 35°, and 37° C. Regeneration of ligand surfaces containing disulfide-linked peptides was performed with a 1 min pulse of 4 M LiCl/HBS, followed by a 1 min pulse of 0.25 % P20/HBS, at 20 µl/min. Interactions with the GST-Lcyt-pY ligand were performed in triplicates at 25° C. The GST-Lcyt-pY ligand surface was regenerated with a 1 min pulse of 1.5 M LiCl/HBS, followed by a 1 min pulse of 0.20 % P20/HBS. To optimize the interaction profiles used for kinetic calculations, the recorded primary responses were processed in a double background subtraction routine. For this purpose, triplicate injections of running buffer were recorded at all temperatures. Thereafter, the averaged buffer profile of each flow cell, at a given temperature, was subtracted from the primary response profiles of individual sample injections. Then, the reference lane response was subtracted from the ligand lane response.

2.6 Interaction models

The recorded profiles of N,C-$(SH2)_2$ interactions with immobilized CEACAM1 peptides (pY488 and pY515) were compared with three models, based on plausible interaction mechanisms. The interaction of N,C-$(SH2)_2$ with GST-Lcyt-[pY488/pY515] required a specific model, described below as Model 4. All the models assumed a mass transport limited process based on the two compartment model (Myszka et al., 1997).

2.6.1 Model 1: A simple bimolecular interaction

The primary model for a simple interaction of two components, where one is in solution (analyte: A) and the other is attached to a surface (ligand: L) is defined as a two step process

$$A_{\text{bulk}} \underset{k_c}{\overset{k_c}{\rightleftharpoons}} A_{\text{surface}} + L \underset{k_d}{\overset{k_a}{\rightleftharpoons}} AL$$

where the first step is the mass transport of the analyte between the bulk flow and the surface (characterized by the k_c coefficient). The second step describes the interactions at the surface, i.e. the rate of complex (AL) formation and dissociation.

2.6.2 Model 2: A bimolecular interaction of an analyte with two binding sites

The tandem shaped N,C-$(SH2)_2$ of SHP-1 represents a type of analyte, carrying at least two binding sites per molecule. These two sites can possibly compete in binding to the same phosphotyrosine motif (ligand: L). Model 1 cannot be applied to such an interaction, except in the rare case where both sites (domains) would have identical interaction kinetics. A model which takes into account the different kinetics of two binding sites on the same analyte, interacting with a uniform ligand, has the form

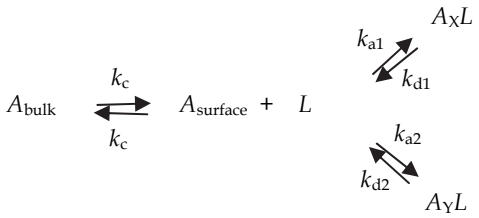

Referring to N,C-$(SH)_2$ as the analyte, the rate constant pairs k_{a1}, k_{d1} and k_{a2}, k_{d2} describe the kinetics of complexes formed via the N-SH2 and C-SH2 domains, respectively. This model assumes a stoichiometry of 1:1 and a low density of the surface bound ligand.

2.6.3 Model 3: A bimolecular interaction of an analyte with three binding sites

This is an extension of Model 2, accounting for a third binding site in the analyte molecule. The rate constant pair k_{a3} and k_{d3}, characterizes the kinetics of a complex (A_ZL) formed via this additional site, resulting in

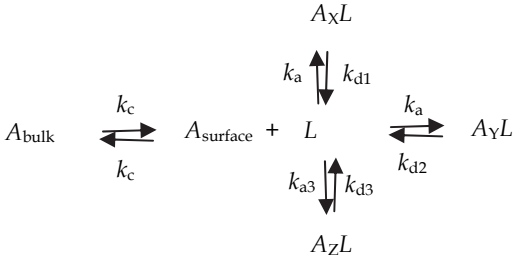

2.6.4 Model 4: A bimolecular interaction between a ligand with two binding sites and an analyte with three binding sites

A specific model was designed to address the interaction of the N,C-$(SH2)_2$ tandem domain with the entire CEACAM1-L cytoplasmic domain phosphorylated on both tyrosine residues. The model was restricted to AL binary complex forms, i.e. simultaneous binding of one A molecule to two L molecules, or of two A molecules to one L molecule, was excluded. All combinations of single docking between one of the three analyte sites and one of the two ligand sites were included. Furthermore, we included all permutations of second docking events allowing the formation of double docked AL forms from single docked forms. The reactions in this model are displayed in Figure 4C.

2.6.5 Mathematical description of models 1-4

A mathematical description of the interaction models is provided here in sets of coupled first order differential equations. These equations were used in curve fit routines for kinetics analyses, including the estimation of rate constants from experimentally obtained data. The analyte concentration in the bulk and at the surface is defined by $[A_B]$ and $[A_S]$, respectively, the concentration of free ligand binding sites as $[L]$, and a surface bound complex of analyte and ligand as $[AL]$, all in the unit of μM. Different binding sites in the analyte molecule are referred to as X, Y and Z. Association and dissociation rate constants are defined as k_a or k_{ax}, and k_d or k_{dx}, respectively, where x defines a particular reaction. Unless stated differently, k_a and k_d are in the units of $M^{-1}s^{-1}$ and s^{-1}, respectively. The mass transport between the bulk flow and the surface is defined by a coefficient k_c. h_d is a characteristic height of the diffusion layer that links the change in concentration expressed per surface area ($[AL]$) and per volume ($[A_S]$). Calculations of h_d and k_c were performed in the same manner as we have described previously (Sigmundsson et al., 2002).

Model 1:

$$d[A_S]/dt = (k_c([A_B] - [A_S]) - k_a[A_S][L] + k_d[AL])/h_d \quad (1.1)$$

$$d[AL]/dt = k_a[A_S][L] - k_d[AL] \quad (1.2)$$

Model 2:

$$d[A_S]/dt = (k_c([A_B] - [A_S]) - (k_{a1} + k_{a2})[A_S][L] + k_{d1}[A_X L] + k_{d2}[A_Y L])/h_d \quad (2.1)$$

$$d[A_X L]/dt = k_{a1}[A_S][L] - k_{d1}[A_X L] \quad (2.2)$$

$$d[A_Y L]/dt = k_{a2}[A_S][L] - k_{d2}[A_Y L] \quad (2.3)$$

$$d[AL_{Total}]/dt = (k_{a1} + k_{a2})[A_S][L] - k_{d1}[A_X L] - k_{d2}[A_Y L] \quad (2.4)$$

Model 3:

$$d[A_S]/dt = (k_c([A_B] - [A_S]) - (k_{a1} + k_{a2} + k_{a3})[A_S][L] + k_{d1}[A_X L] + k_{d2}[A_Y L] + k_{d3}[A_Z L])/h_d \quad (3.1)$$

$$d[A_X L]/dt = k_{a1}[A_S][L] - k_{d1}[A_X L] \quad (3.2)$$

$$d[A_Y L]/dt = k_{a2}[A_S][L] - k_{d2}[A_Y L] \quad (3.3)$$

$$d[A_Z L]/dt = k_{a3}[A_S][L] - k_{d3}[A_Z L] \quad (3.4)$$

$$d[AL_{Total}]/dt = (k_{a1} + k_{a2} + k_{a3})[A_S][L] - k_{d1}[A_X L] - k_{d2}[A_Y L] - k_{d3}[A_Z L] \quad (3.5)$$

Model 4:

The two ligand binding sites are referred to as α (pY488) and β (pY515). The three analyte binding sites are referred to as X, Y and Z (N-SH2, C2-SH2 and C1-SH2, respectively). The model takes into account three different ligand forms, which in our case refer to the tyrosine-phosphorylation status of the ligand. In this respect the ligand is divided into three populations: L^{α}, L^{β} and $L^{\alpha\beta}$, for mono- and di-phosphorylated forms. The fractions of these forms with regard to the total amount of phosphorylated ligand units are defined with **Π**, **Ψ** and **Ω**, respectively. The detected response signal R, measured by an SPR-based sensor is proportional to the amount of complex formed at the detector surface multiplied by the factor MwG, i.e., $R = MwG[AL]$, where Mw is the molecular mass of the analyte and G is a factor converting the concentration to R values ($G = 10000\ R\ \mathrm{cm^2/g}$ of protein). When all the immobilized ligand has been fully bound into an AL complex, $R = R_{\mathrm{Max}}$ (i.e., a theoretical maximum value). The contribution of the different $[AL]$ complexes to the response signal (R) can now be referred to as follows: $R^{\alpha X} = [A^X L^{\alpha}]$, defines the amount of a complex docked via the α-site in the ligand and the X-site in the analyte. The total response of complexes docked via the α site is defined as R^{α}. The amount of a double docked complex with a [α-X/β-Z] configuration, is defined as $R^{\alpha X\beta Z}$. The total response of all double docked forms is defined as $R^{\alpha\beta}$. Complexes of di-phosphorylated single-docked ligands are defined with the subscription 2P, eg. $R^{\alpha X}{}_{2P}$. Association constants labeled with stars (k_a^* and k_a^{**}) define the second association steps giving rise to double docked forms. These constants have the unit of s^{-1}. To keep the amount of fit parameters at minimum it is assumed that a binding between two interacting sites, whether formed via a primary or a secondary docking event, dissociates with the same probability. Thus, the interactions described by k_{a1}, k_{a1}^*, k_{a1}^{**}, all share the same dissociation constant, k_{d1}. The full size model includes 32 parameters. Thereof 24 are rate constants. The model is easily adjusted for fewer reactions. The version used to calculate the data presented in Figure 4 included 20 parameters, of which 16 were rate constants. After the identification and elimination of non-existing reactions, and after the identification of parameters which could be fixed, the fit variables could be limited to 5, 4 of which representing unknown rate constants, and R_{Max} being the fifth global variable.

$$\frac{d[A_S]}{dt} = (k_c([A_B] - [A_S]) - (k_{a1} + k_{a2} + k_{a3})[A_S]\frac{(\Pi R_{Max} - R^{\alpha})}{M_w G}$$

$$+\frac{(k_{d1}R^{\alpha X} + k_{d2}R^{\alpha Y} + k_{d3}R^{\alpha Z})}{M_w G} - (k_{a4} + k_{a5} + k_{a6})[A_S]\frac{(\Psi R_{Max} - R^{\beta})}{M_w G}$$

$$+\frac{(k_{d4}R^{\beta Y} + k_{d5}R^{\beta Z} + k_{d6}R^{\beta X})}{M_w G}$$

$$-(k_{a1} + k_{a2} + k_{a3} + k_{a4} + k_{a5} + k_{a6})[A_S]\frac{(\Omega R_{Max} - R_{2P}^{1\times Docked} - R^{\alpha\beta})}{M_w G}$$

$$+\frac{(k_{d1}R_{2P}^{\alpha X} + k_{d2}R_{2P}^{\alpha Y} + k_{d3}R_{2P}^{\alpha Z} + k_{d4}R_{2P}^{\beta Y} + k_{d5}R_{2P}^{\beta Z} + k_{d6}R_{2P}^{\beta X})}{M_w G})/h_d \tag{4.1}$$

$$dR^{\alpha X}/dt = k_{a1}[A_S](\Pi R_{Max} - R^{\alpha}) - k_{d1}R^{\alpha X} \tag{4.2}$$

$$dR^{\alpha Y}/dt = k_{a2}[A_S](\Pi R_{Max} - R^{\alpha}) - k_{d2}R^{\alpha Y} \tag{4.3}$$

$$dR^{\alpha Z}/dt = k_{a3}[A_S](\Pi R_{Max} - R^{\alpha}) - k_{d3}R^{\alpha Z} \tag{4.4}$$

$$\frac{dR^{\alpha}}{dt} = \frac{dR^{\alpha X}}{dt} + \frac{dR^{\alpha Y}}{dt} + \frac{dR^{\alpha Z}}{dt} \tag{4.5}$$

$$dR^{\beta Y}/dt = k_{a4}[A_S](\Psi R_{Max} - R^{\beta}) - k_{d4}R^{\beta Y} \tag{4.6}$$

$$dR^{\beta Z}/dt = k_{a5}[A_S](\Psi R_{Max} - R^{\beta}) - k_{d5}R^{\beta Z} \tag{4.7}$$

$$dR^{\beta X}/dt = k_{a6}[A_S](\Psi R_{Max} - R^{\beta}) - k_{d6}R^{\beta X} \tag{4.8}$$

$$\frac{dR^{\beta}}{dt} = \frac{dR^{\beta X}}{dt} + \frac{dR^{\beta Y}}{dt} + \frac{dR^{\beta Z}}{dt} \tag{4.9}$$

$$\frac{dR_{2P}^{\alpha X}}{dt} = k_{a1}[A_S](\Omega R_{Max} - R_{2p}^{1\times Docked} - R^{\alpha\beta})$$
$$-(k_{d1} + k_{a4}^{\star\star} + k_{a5}^{\star})R_{2P}^{\alpha X} + k_{d4}R^{\alpha X\beta Y} + k_{d5}R^{\alpha X\beta Z} \tag{4.10}$$

$$\frac{dR_{2P}^{\alpha Y}}{dt} = k_{a2}[A_S](\Omega R_{Max} - R_{2p}^{1\times Docked} - R^{\alpha\beta})$$
$$-(k_{d2} + k_{a5}^{\star\star} + k_{a6}^{\star})R_{2P}^{\alpha X} + k_{d5}R^{\alpha X\beta Y} + k_{d6}R^{\alpha X\beta Z} \tag{4.11}$$

$$\frac{dR_{2P}^{\alpha Z}}{dt} = k_{a3}[A_S](\Omega R_{Max} - R_{2p}^{1\times Docked} - R^{\alpha\beta})$$
$$-(k_{d3} + k_{a4}^{\star} + k_{a6}^{\star\star})R_{2P}^{\alpha Z} + k_{d4}R^{\alpha Z\beta Y} + k_{d6}R^{\alpha Z\beta X} \tag{4.12}$$

$$\frac{dR_{2P}^{\beta Y}}{dt} = k_{a4}[A_S](\Omega R_{Max} - R_{2p}^{1\times Docked} - R^{\alpha\beta})$$
$$-(k_{d4} + k_{a1}^{\star\star} + k_{a3}^{\star})R_{2P}^{\beta Y} + k_{d1}R^{\alpha X\beta Y} + k_{d3}R^{\alpha Z\beta Y} \tag{4.13}$$

$$\frac{dR_{2P}^{\beta Z}}{dt} = k_{a5}[A_S](\Omega R_{Max} - R_{2p}^{1\times Docked} - R^{\alpha\beta})$$
$$-(k_{d5} + k_{a1}^{\star} + k_{a2}^{\star})R_{2P}^{\beta Z} + k_{d1}R^{\alpha X\beta Z} + k_{d2}R^{\alpha Y\beta Z} \tag{4.14}$$

$$\frac{dR_{2P}^{\beta X}}{dt} = k_{a6}[A_S](\Omega R_{Max} - R_{2p}^{1\times Docked} - R^{\alpha\beta})$$
$$-(k_{d6} + k_{a2}^{\star\star} + k_{a3}^{\star\star})R_{2P}^{\beta X} + k_{d2}R^{\alpha Y\beta X} + k_{d3}R^{\alpha Z\beta X} \tag{4.15}$$

$$\frac{dR_{2P}^{1\times Docked}}{dt} = \frac{dR_{2P}^{\alpha X}}{dt} + \frac{dR_{2P}^{\alpha Y}}{dt} + \frac{dR_{2P}^{\alpha Z}}{dt} + \frac{dR_{2P}^{\beta X}}{dt} + \frac{dR_{2P}^{\beta Y}}{dt} + \frac{dR_{2P}^{\beta Z}}{dt} \tag{4.16}$$

$$\frac{dR^{\alpha X\beta Y}}{dt} = k_{a1}^{\star\star} R_{2P}^{\beta Y} + k_{a4}^{\star\star} R_{2P}^{\alpha X} - (k_{d1} + k_{d4}) R^{\alpha X\beta Y} \tag{4.17}$$

$$\frac{dR^{\alpha X\beta Z}}{dt} = k_{a1}^{\star} R_{2P}^{\beta Z} + k_{a5}^{\star} R_{2P}^{\alpha X} - (k_{d1} + k_{d5}) R^{\alpha X\beta Z} \tag{4.18}$$

$$\frac{dR^{\alpha Y\beta Z}}{dt} = k_{a2}^{\star} R_{2P}^{\beta Z} + k_{a5}^{\star\star} R_{2P}^{\alpha Y} - (k_{d1} + k_{d5}) R^{\alpha Y\beta Z} \tag{4.19}$$

$$\frac{dR^{\alpha Y\beta X}}{dt} = k_{a2}^{\star\star} R_{2P}^{\beta X} + k_{a6}^{\star} R_{2P}^{\alpha Y} - (k_{d2} + k_{d6}) R^{\alpha Y\beta X} \tag{4.20}$$

$$\frac{dR^{\alpha Z\beta X}}{dt} = k_{a3}^{\star\star} R_{2P}^{\beta X} + k_{a6}^{\star\star} R_{2P}^{\alpha Z} - (k_{d3} + k_{d6}) R^{\alpha Z\beta X} \tag{4.21}$$

$$\frac{dR^{\alpha Z\beta Y}}{dt} = k_{a3}^{\star} R_{2P}^{\beta Y} + k_{a4}^{\star} R_{2P}^{\alpha Z} - (k_{d3} + k_{d4}) R^{\alpha Z\beta Y} \tag{4.22}$$

$$\frac{dR^{\alpha\beta}}{dt} = \frac{dR^{\alpha X\beta Y}}{dt} + \frac{dR^{\alpha X\beta Z}}{dt} + \frac{dR^{\alpha Y\beta Z}}{dt} + \frac{dR^{\alpha Y\beta X}}{dt} + \frac{dR^{\alpha Z\beta X}}{dt} + \frac{dR^{\alpha Z\beta Y}}{dt} \tag{4.23}$$

$$\frac{dR_{Total}}{dt} = \frac{dR^{\alpha}}{dt} + \frac{dR^{\beta}}{dt} + \frac{dR_{2P}^{1\times Docked}}{dt} + \frac{dR^{\alpha\beta}}{dt} \tag{4.24}$$

2.7 Determination of kinetic constants

Data modification including scale transformation and background subtraction was performed with the program BIAevaluation 4.1. Data analyses and calculations based on numerical approaches, including global curve fitting to interaction models for estimation of kinetic constants, were performed with IGOR Pro (version 4.09.0, WaveMetrics, Inc.). Curve fit functions based on models 1, 2, 3, and 4 were created as external operation routines, compiled in C, using CodeWarrior IDE (version 5.1.1.1105, Metrowerks Corporation) and applied together with the Global Fit Procedure in IGOR Pro, based on a nonlinear least-squares method, utilizing the Levenberg-Marquard algorithm (Press et al., 1999). For numerical integration, a fifth order Runge-Kutta-Fehlberg method was applied (Press et al., 1999). Previous mathematical analysis has demonstrated that this numerical procedure, used in the curve fitting routine, gives precise and accurate solutions of the underlying differential equations (Sigmundsson et al., 2002).

2.8 Computational analysis of SHP-1 binding to mono- and di-phosphorylated CEACAM1-L

The kinetic rate constants determined by the BIAcore analyses were used to compute the binding kinetics of the SHP-1 tandem N,C-$(SH2)_2$ domain to CEACAM1-L phosphorylated on Y488 only, or on both Y488 and Y515. This was done by setting up complete reaction

schemes for all possible pathways leading to the reversible formation of all complexes that were identified by the experimental BIAcore analyses (see Tables 1 and 2 and Fig. 4C). The coupled, non-linear differential equations that were formulated from these reaction schemes were solved numerically, utilizing IGOR Pro.

3. Results

3.1 Interaction profiles

Interaction profiles of uncleaved and cleaved GST-fusion constructs of SHP-1 N-SH2, C-SH2, and N,C-$(SH)_2$ domains with biotinylated peptides were recorded at 25° C. The SH2 domains interacted specifically with the two phosphorylated ITIM-like peptide motifs, whereas responses with unphosphorylated ITIM-like sequences involving Y488 and Y515, and a scrambled Y488 sequence, were insignificant and resembled the background profiles of a ligand-free streptavidin surface (Fig. 2A-F). No binding was observed between GST and the ligand surfaces (Fig. 2H). The N-SH2, C-SH2 and N,C-$(SH2)_2$ domains all interacted with the pY488 ligand. However, the dissociation of the GST-fusion proteins was significantly slower compared with that of the GST-free N-SH2, C-SH2 and N,C-$(SH2)_2$ domains (blue curves in Figure 2: A vs. B, C vs. D, E vs. F). In fact, the binding of GST-C-SH2 and GST-N,C-$(SH2)_2$ to pY488 gave rise to severe difficulties in regeneration of the ligand surface. These results indicate that the GST moiety caused secondary interactions between the analyte molecules at the surface.

No interaction was detected between pY515 and GST-N-SH2 or the N-SH2 domain (Fig. 2A-B: red curves). The GST-C-SH2 and GST-N,C-$(SH2)_2$ proteins gave minor responses with the pY515 ligand, while the free C-SH2 and N,C-$(SH2)_2$ domains showed significant interaction (Fig. 2C-F: red curves). These results indicate that the GST part of these fusion proteins blocked the access to a pY515 interaction site, which became available for binding in the GST-free C-SH2 and N,C-$(SH2)_2$ domains. Together, Figures 2C and 2D indicate that the C-SH2 domain holds 2 different binding sites. One of these is accessible (C1-site) and the other is blocked (C2-site) in the GST-C-SH2 form. The accessible C1-site interacts with the pY488 ligand (blue), while the response to pY515 (red) is minimal (Fig. 2C). The C2-site on the C-SH2 domain becomes accessible after cleavage from the GST fusion partner (Fig. 2D), giving a characteristic binding profile to the pY515 ligand (red). This same site gives rise to an additional profile in response to the pY488 ligand (blue), characterized by a sharp change in the start of the association and dissociation phases (marked by arrows in Fig. 2D). The same blockage of interaction with pY515 was seen for the GST-N,C-$(SH2)_2$ protein (Fig. 2E) when compared with the response patterns of free N,C-$(SH2)_2$ (Fig. 2F). Figure 2G shows an interaction with the anti-phosphotyrosine antibody (PY99), confirming identical immobilization levels for the pY488 (blue) and pY515 (red) ligands.

3.2 Determination of kinetic constants for SH2 domains binding to distinct phosphotyrosine ligands

Due to high avidity and problems with surface regeneration, it was not possible to collect data for kinetic evaluation of the interactions of GST-C-SH2 and GST-N,C-$(SH2)_2$ with the biotinylated pY488 and pY515 ligands. Furthermore, the interaction of GST-N-SH2 with the biotinylated pY488 peptide could not be evaluated by any simple interaction models. The free N-SH2 and C-SH2 domains were also unsuitable for kinetic analysis because they underwent slow inactivation after cleavage of the GST moiety. Thrombin cleavage of the GST-N,C-$(SH2)_2$ protein on the other hand provided a stable N,C-$(SH2)_2$ tandem domain,

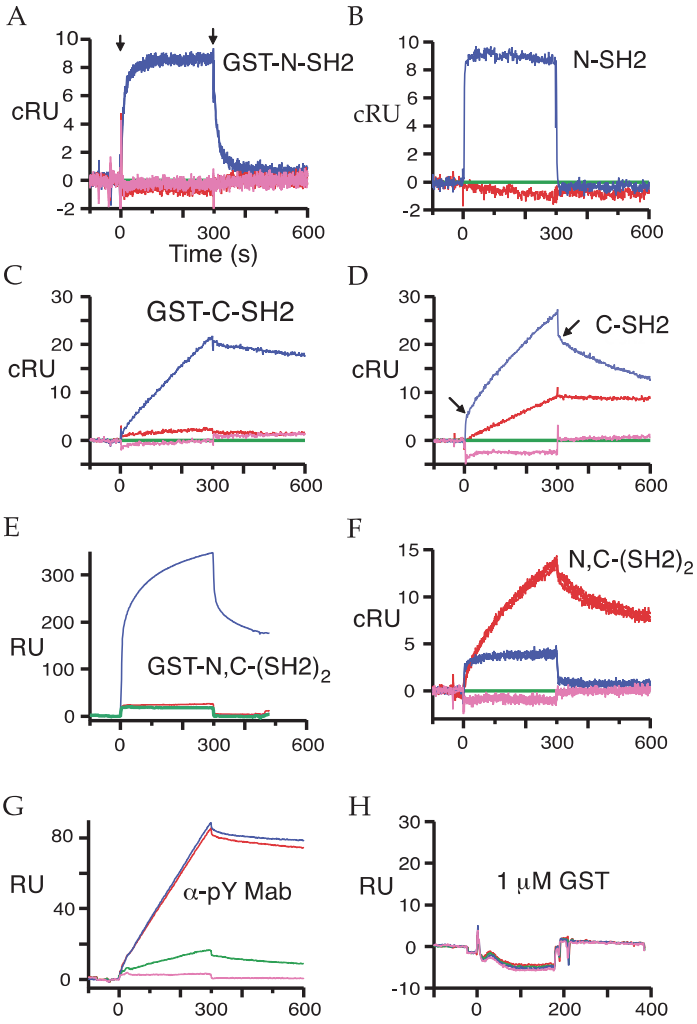

Fig. 2. Sensorgrams showing interaction profiles for SH2 domains derived from SHP-1 (non-cleaved and cleaved from GST). Responses to the different CEACAM1-L-derived biotinylated peptide ligands have the following colours: pY488 = blue, pY515 = red, Y488 = green (reference lane) and a free streptavidin surface = pink. Analyte: A) GST-N-SH2, 2 nM (3 × repeat), arrows indicate the start and end of sample injection. B) N-SH2, 4 nM. C) GST-C-SH2, 10 nM. D) C-SH2, 15 nM, arrows indicate the two different profiles seen in the start of the association and dissociation phases. E) GST-N,C-$(SH2)_2$, 15 nM. F) N,C-$(SH2)_2$, 20 nM (3 × repeat). G) PY99 Mab, 1 nM. H) GST, 1 μM. RU: Response units, cRU: corrected response units (response from the reference lane has been subtracted). Measurements were performed in HBS, pH 7.4, 25° C, at a flow of 20 μl/min. Low density ligand surfaces were used in A, B, C, D, F, G, H. A high density ligand surface was used in E.

which could be used for kinetic interaction analysis. For this purpose we used ligand surfaces with N-terminally cysteinylated peptides, to circumvent the regeneration problems with the biotinylated peptide ligands. Recordings at five different temperatures showed that the interactions of N,C-$(SH2)_2$ with the pY488 and pY515 motifs were strongly temperature-dependent, exhibiting an overall increase in both association and dissociation rates with increasing temperature (Fig. 3). However, the interaction patterns were complex and could not be fitted to the simple interaction model 1, or to a two-state version of model 1 in which the primary binding is followed by a more stable binding (not shown). Thus, in order to work out the kinetics, we designed and applied fit routines based on plausible interaction paths and the information obtained from the experiments described in Figure 2. These routines were denoted models 2 and 3. The resulting curve fittings are shown in Figure 3, and the respective rate constants from these fits are listed in Table 1. Using these rate constants, the curve fit for the highest concentration of each data set (plotted red) was subjected to profile analysis of the underlying, contributing binding reactions (plotted black, blue and green), as shown in Figure 3. In addition, we estimated the surface-to-bulk analyte concentration ratio ($[A_{surface}]/[A_{bulk}]$) during the interval of sample injection, by applying the same parameters and rate constants as used and obtained in the fit approaches. These profiles (not shown) indicated the data recordings to be essentially free of mass transport limitation.

Recordings of the interaction of N,C-$(SH2)_2$ with the pY488 motif indicated some higher degree of complexity. At 5° and 15° C model 3 matched best with this interaction, whereas applying model 3 at 25° and 35° C, resulted in a reduction to model 2. Similarly, at 37° C the interaction was best described by model 2, although a reduction towards model 1 was indicated. The profile that contributed the most to the total signal at all temperatures was the N-SH2-site interacting with the pY488 motif (Fig. 3, black dashed curve). This interaction is characterized by rapid association and dissociation (Table 1; see also Figs. 2A and B). Competition from one or two additional binding sites on the N,C-$(SH2)_2$ protein (belonging to the C-SH2 domain) leads to slight profile changes. In the inserted graph in Figure 3 at 25° C (black: N-SH2 site binding to pY488), we demonstrate with a simulation based on the observed rate constants, how the profile for the N,C-$(SH2)_2$ molecule would appear if only the N-SH2 site was active, and the other binding sites were inactive. The similarity of this profile with that observed for the isolated N-SH2 domain in Figure 2B is striking. From comparison with the binding profiles of the single SH2 domains (Figs. 2A-D) we conclude that the second binding reaction, plotted as green dashed profiles in Fig. 3 (left panels), represents the C1-SH2 site interaction with the pY488 motif. This interaction showed slow association and dissociation, resembling the observed binding profile for the interaction of the GST-C-SH2 accessible site with pY488 (Figs. 2C and D, blue curves). Interestingly, this interaction was most pronounced at 25° C and decreased with further rise in temperature, and therefore appears to be less relevant at physiological temperature (37° C). The third binding reaction (blue dashed profiles in Fig. 3, left panels) corresponded to the interaction of pY488 with the C2-SH2 site (the inaccessible site in GST-C-SH2, according to Fig. 2C and D, which is the part of the blue curve characterized by a fast on/off profile, indicated by arrows in Fig 2D). This interaction was also highly temperature-dependent. From 15° to 25° C its magnitude decreased markedly, and at temperatures ≥ 35° C it no longer existed. This is shown in Figure 3, where the data recorded at 25° and 35° C were analyzed with a function based on model 3 (returning an infinitely small k_{a3}). It should be pointed out that in contrast to the results displayed in Figure 3, Figure 2D shows that the C2-site of the isolated C-SH2 domain interacted with the pY488 ligand at 25° C, and provided a minor but detectable contribution to the recorded signal. Thus, this interaction might only occur for the

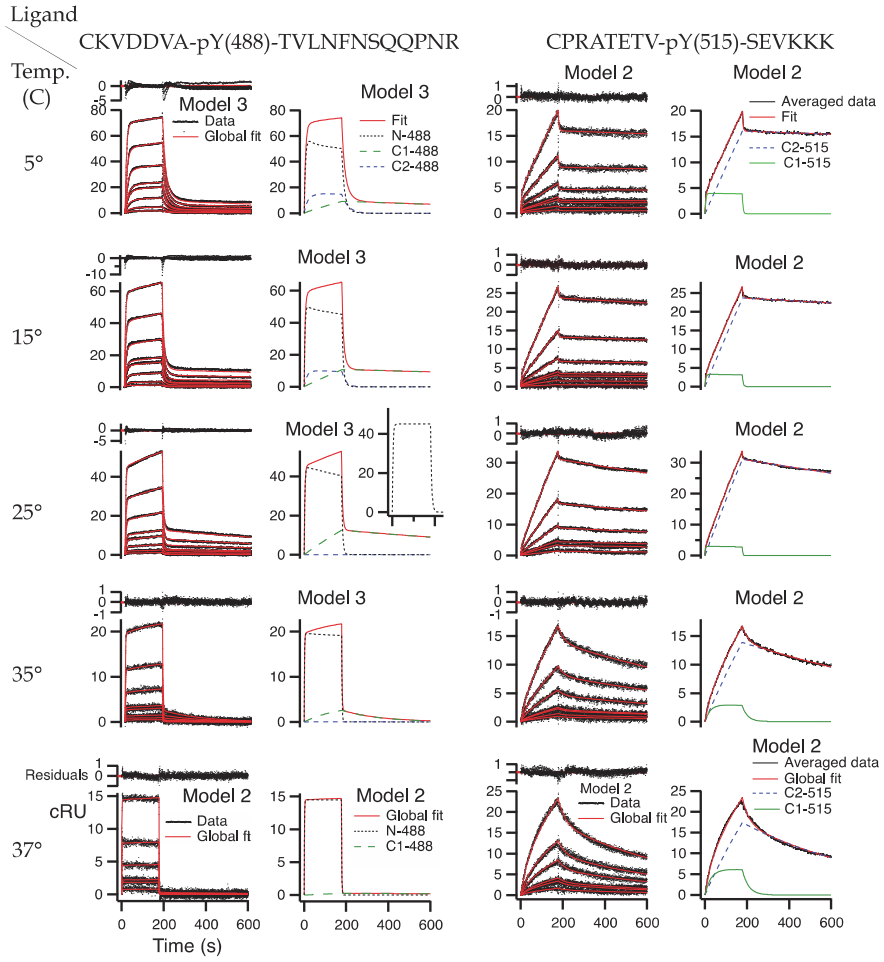

Fig. 3. Sensorgrams for the interactions of N,C-$(SH2)_2$ with the CEACAM1-L-derived cysteinylated phosphopeptides pY488 (left panel) and pY515 (right panel), at various temperatures. At each temperature samples were injected for 3 minutes in a randomized order with a total of three injections per concentration. All data are shown (black) together with global curve fits (red). Residuals are shown above each global fit result. For the pY488 ligand at 5°, 15°, 25° and 35°, fits were based on model 3. Fits for pY488 at 37° and for pY515 at all temperatures, were based on model 2. Analyte concentrations were defined as fit variables, with the initial values of 120, 60, 30, 15, 12, 6, 3, and 1.5 nM, as estimated from dilution factors and applied with constraints of ± 30 %, in global fit approaches. Flow rate was 20 µl/min. R_{Max} was 120 and 510 RU for the pY488 and pY515 surfaces, respectively. For the 24.9 kDa analyte, diffusion coefficients and h_d at 5°, 15°, 25°, 35° and 37° C were: (9.5, 9.8, 10.2, 10.5, 10.6)×10^{-7} cm^2s^{-1}, and 6.84, 6.92, 7.00, 7.08, 7.10 µm, respectively. Profile analysis for the 120 nM concentration responses is provided to the right of each fit panel. cRU: corrected response units. The results are tabulated in Table 1.

isolated C-SH2 domain at 25° C and above, disappearing in the N,C-$(SH2)_2$ domain for conformational/stability reasons.

At 37° C the interaction of the C1-SH2 site with pY488 also disappeared almost completely. The decrease in binding of the C1-SH2 and C2-SH2 sites to pY488 with increasing temperature represents a true temperature-dependence and was not caused by denaturation of the C-SH2 domain, since both of these sites bound significantly to pY515, even at 37° C (Fig. 3, right panels; Table 1). Thus, at 37° C, the interaction of the N,C-$(SH2)_2$ tandem domain with pY488 approached model 1, in which the rapid association/dissociation between the N-SH2 domain and the pY488 motif dominated.

The analysis of the N,C-$(SH2)_2$ binding to the pY515 peptide gave excellent curve fittings applying model 2, at all temperatures. From the data shown in Figures 2A and B (red curves), we know that the N-SH2 domain did not interact with pY515. Therefore, it is unlikely that the N-SH2 domain was involved in the interaction of N,C-$(SH2)_2$ with pY515. Accordingly, and by comparing with the binding profiles of the single SH2 domains (Figs. 2C-F), we refer to the major reaction of the N,C-$(SH2)_2$ with pY515 (Fig. 3, right panels: blue dashed profile) as the C2- site, i.e. the GST-C-SH2-inaccessible site in the pY515 interaction (Fig. 2 C,D: red profiles). The less pronounced reaction (Fig.3: green profiles) we refer to as the C1-SH2 site, i.e. the GST-C-SH2 accessible site in the interaction with pY515. While the interaction of the C1-SH2 site with pY515 appears minimal at 25° C, it becomes significant at 35° and 37° C.

Interaction	Temp	k_a	k_d	K_d
	°C	$M^{-1}\ s^{-1}$	s^{-1}	M
N-SH2:pY488	5	$1.45\times10^{6}\pm1.6\times10^{5}$	$1.0\times10^{-1}\pm 5\times10^{-3}$	7.4×10^{-8}
	15	$1.72\times10^{6}\pm3.6\times10^{5}$	$2.3\times10^{-1}\pm2\times10^{-2}$	1.4×10^{-7}
	25	$1.83\times10^{6}\pm1.6\times10^{4}$	$3.2\times10^{-1}\pm3\times10^{-3}$	1.8×10^{-7}
	35	$2.00\times10^{6}\pm1.5\times10^{2}$	$9.9\times10^{-1}\pm1\times10^{-3}$	5.0×10^{-7}
	37	$2.17\times10^{6}\pm1.7\times10^{5}$	$1.5\ \pm5\times10^{-2}$	6.9×10^{-7}
C1-SH2:pY488	5	$1.37\times10^{4}\pm9.8\times10^{2}$	$7.1\times10^{-4}\pm6\times10^{-5}$	5.2×10^{-8}
	15	$9.48\times10^{3}\pm1.3\times10^{3}$	$3.5\times10^{-4}\pm3\times10^{-5}$	3.7×10^{-8}
	25	$1.01\times10^{4}\pm0.6\times10^{1}$	$8.0\times10^{-4}\pm1\times10^{-5}$	7.9×10^{-8}
	35	$2.33\times10^{3}\pm3.6\times10^{1}$	$5.5\times10^{-3}\pm8\times10^{-5}$	2.4×10^{-6}
	37	$1.39\times10^{2}\pm1.8\times10^{1}$	$3.8\times10^{-4}\pm2\times10^{-4}$	2.8×10^{-6}
C2-SH2:pY488	5	$1.52\times10^{5}\pm5.1\times10^{4}$	$3.9\times10^{-2}\pm5\times10^{-3}$	2.6×10^{-7}
	15	$1.00\times10^{5}\pm4.0\times10^{3}$	$7.0\times10^{-2}\pm1\times10^{-2}$	6.5×10^{-7}
C1-SH2:pY515	5	$2.54\times10^{4}\pm1.8\times10^{3}$	$2.9\times10^{-1}\pm9\times10^{-3}$	1.1×10^{-5}
	15	$1.86\times10^{4}\pm1.0\times10^{3}$	$2.6\times10^{-1}\pm1\times10^{-2}$	1.4×10^{-5}
	25	$2.18\times10^{4}\pm4.1\times10^{3}$	$4.2\times10^{-1}\pm3\times10^{-2}$	2.1×10^{-5}
	35	$2.68\times10^{3}\pm5.0\times10^{1}$	$4.2\times10^{-2}\pm1\times10^{-3}$	1.6×10^{-5}
	37	$3.98\times10^{3}\pm6.3\times10^{1}$	$3.5\times10^{-2}\pm6\times10^{-4}$	8.8×10^{-6}
C2-SH2:pY515	5	$1.95\times10^{3}\pm1.3\times10^{2}$	$9.4\times10^{-5}\pm4\times10^{-6}$	4.8×10^{-8}
	15	$2.94\times10^{3}\pm1.2\times10^{2}$	$1.43\times10^{-4}\pm3\times10^{-6}$	4.9×10^{-8}
	25	$3.25\times10^{3}\pm6.0\times10^{2}$	$3.72\times10^{-4}\pm3\times10^{-6}$	1.2×10^{-7}
	35	$1.83\times10^{3}\pm5.0\times10^{1}$	$9.01\times10^{-4}\pm 8\times10^{-6}$	4.9×10^{-7}
	37	$2.08\times10^{3}\pm1.4\times10^{1}$	$1.58\times10^{-3}\pm1\times10^{-5}$	7.6×10^{-7}

Table 1. Kinetic parameters for the interactions between the SHP-1 N,C-$(SH2)_2$ domain and CEACAM1-L derived pY488 and pY515 peptides.

3.3 Determination of the mechanism and kinetic constants for the interaction of the N,C-$(SH2)_2$ domain with the CEACAM1-Lcyt cytoplasmic domain

Finally, we analyzed the interaction at 25˚ C of the tandem N,C-$(SH2)_2$ domain with the full size cytoplasmic domain of CEACAM1-L, phosphorylated on both tyrosine residues (Y488 and Y515). According to mass spectrometry analysis c:a 75% of the GST-Lcyt ligand, produced in the *E. coli* TKX1 strain, was phosphorylated. Approximately 34% of the phosphorylated fraction was accounted for by di-phosphorylated GST-Lcyt (pY488, pY515), 63 % was mono-phosphorylated on Y488, and c:a 3 % was mono-phosphorylated on Y515. The phosphorylated GST-Lcyt ligand (34.2 kDa) was immobilized to give 112 RU. This provided a theoretical R_{Max} of c:a 115 RU with respect to N,C-$(SH2)_2$ (24.9 kDa) binding, assuming a binding ratio of 1:1 and 100% ligand access. The N,C-$(SH2)_2$ domain showed no detectable interaction with the GST reference surface.

		Ligand			
		CEACAM1-L cytoplasmic domain		pY-peptide	
Parameter	Fixed	Value	± SD	Value	Interaction
k_{a1} ($M^{-1}s^{-1}$)	●	1.83×10^{6}		1.83×10^{6}	N-SH2 to pY488
k_{d1} (s^{-1})		2.69×10^{-1}	3.7×10^{-3}	3.20×10^{-1}	N-SH2 off pY488
k_{a2} ($M^{-1}s^{-1}$)	●	0		Negligible	C2-SH2 to pY488
k_{d2} (s^{-1})	●	0		Negligible	C2-SH2 off pY488
k_{a3} ($M^{-1}s^{-1}$)	●	1.01×10^{4}		1.01×10^{4}	C1-SH2 to pY488
k_{d3} (s^{-1})	●	8.00×10^{-4}		8.00×10^{-4}	C1-SH2 off pY488
k_{a4} ($M^{-1}s^{-1}$)	●	3.25×10^{3}		3.25×10^{3}	C2-SH2 to pY515
k_{d4} (s^{-1})	●	3.72×10^{-4}		3.72×10^{-4}	C2-SH2 off pY515
k_{a5} ($M^{-1}s^{-1}$)	●	2.18×10^{4}		2.18×10^{4}	C1-SH2 to pY515
k_{d5} (s^{-1})		2.32×10^{-2}	1.4×10^{-3}	4.20×10^{-1}	C1-SH2 off pY515
k_{a1*} (s^{-1}) *i)*		0.35	0.12		N-SH2 to pY488 on C1-SH2:pY515
k_{a5*} (s^{-1}) *i)*		4.81	0.14		C1-SH2 to pY515 on N-SH2:pY488
k_{a1*} (s^{-1}) *ii)*		3.94	2.19		N-SH2 to pY488 on C1-SH2:pY515
k_{a5*} (s^{-1}) *ii)*		0.50	0.02		C1-SH2 to pY515 on N-SH2:pY488

Table 2. Kinetic parameters for the interaction between the SHP-1 N,C-$(SH2)_2$ domain and the tyrosine-phosphorylated CEACAM1-L cytoplasmic domain. The experimental data shown in Figure 4A were analyzed by Model 4. The kinetic parameters are defined in Model 4. The parameters labelled (●) were kept fixed during the curve fitting runs. The parameter values for the pY-peptide ligand were taken from Table 1.

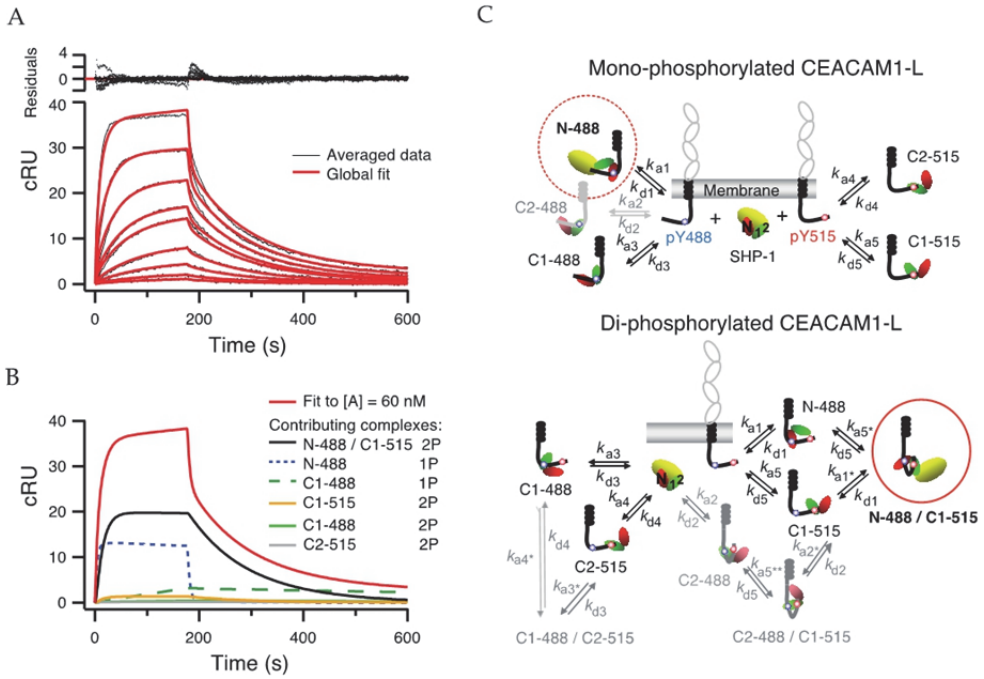

Fig. 4. The interaction of N,C-$(SH2)_2$ with mono- and di-phosphorylated CEACAM1-L cytoplasmic domain. The N,C-$(SH2)_2$ domain of SHP-1 was injected at 25° C for 3 min, at 20 µl/min. Ligand with the composition of 63 % GST-Lcyt-pY488, 3 % GST-Lcyt-pY515 and 34 % GST-Lcyt-[pY488/pY515], according to mass spectrometry analysis, was immobilized (112 RU) on a low density anti-GST-Ab surface. Reference surface was saturated with GST. A) Sensorgram showing averaged responses of three runs per concentration (black) of 60, 30, 15, 12, 6, 3, 1.5, 0.75, 0.375 nM, together with a global curve fit (red), based on an optimized interaction model described in C. The averaged squared residual per data point, $\overline{r}^{\,2}$, was 0.188. The results are tabulated in Table 2. B) Profile analysis showing the contribution of the different complex forms to the response obtained at [Analyte] = 60 nM. Complexes are indicated with N-488/C1-515: N-SH2 bound to pY488 and C1-SH2 bound to pY515 in tandem; N-488: N-SH2 bound to pY488; C1-488: C1-SH2 bound to pY488; C1-515: C1-SH2 bound to pY515; C2-515: C2-SH2 bound to pY515. The tyrosine-phosphorylation status of the ligand in a particular complex is indicated by 1P and 2P, for mono- and di-phosphorylation, respectively. C) A scheme for the interactions predicted by the global fit results in A. The N-SH2 domain is coloured red, the C-SH2 domain is coloured green, and the phosphatase domain is coloured yellow. For simplicity reasons the phosphatase domain (yellow) was omitted from all but two complexes, and the CEACAM1 extracellular domain (grey) is only shown on the non-complexed molecules. Interactions suggested by the global fit-results are indicated in black. Interactions excluded by the fit results are indicated in grey. Red circles are drawn around the most ubiquitous complexes (dashed circle for a mono-phosphorylated ligand and solid circle for a di-phosphorylated ligand).

A special curve fit approach was designed for an interaction model which allowed testing of all combinations of single and double dockings (model 4). Constraints were introduced to exclude non-permissible interactions, such as N-SH2 interactions with pY515. Initial values for confirmed interactions were obtained from Table 1 and the number of fit parameters and variables were trimmed to a minimum. Despite our efforts to provide various initial values for the pY488 binding to the C2-site (represented in our model by k_{a2}), the fit-routine consistently repressed this parameter to zero, indicating a non-existant or irrelevant interaction, in agreement with the results obtained with the mono-phosphorylated pY488 peptide (Table 1). This eliminated two variables (k_{a2} and k_{d2}) from the model. Likewise, all forms of double-docked complexes could be eliminated except the N-488/C1-515, which was mandatory for adequate quality fit results. According to this analysis, a total of five complexes were formed. Four of these belonged to the single-docked forms, observed earlier on the mono-phosphorylated peptide surfaces at 25° C. The fifth form was the double-docked N-488/C1-515 complex. The results from this analysis are shown in Figure 4 and tabulated in Table 2. Importantly, the primary rate constants diverged minimally from those obtained with the mono-phosphorylated peptides. However, the results included two indistinguishable solutions for the secondary rate constants, k_{a1*} and k_{a5*}, which describe the second docking event, during the formation of a double-docked complex (Fig. 4C). Both solutions are listed in Table 2, labelled with superscripts: $^{i)}$ $k_{a1*} < k_{a5*}$ and $^{ii)}$ $k_{a1*} > k_{a5*}$. Although the fit approach could not distinguish between these two solutions, it seems logical that the second alternative, $k_{a1*} > k_{a5*}$, is more probable, because the corresponding primary rate constants showed the relation $k_{a1} >> k_{a5}$ for all conditions (Table 1). A profile analysis is provided in Fig. 4B. According to this result the most pronounced complex was the double-docked form with the N-SH2 site bound to pY488 and the C1-SH2 site bound to pY515. Complexes with two analyte molecules bound per di-pY-ligand were rejected by all fit algorithms. Such complexes probably do not form for steric reasons. The interaction model that satisfied the global curve fit result is schematized in Figure 4C.

3.4 Kinetics of the binding of the N,C-$(SH2)_2$ domain to mono- and di-phosphorylated CEACAM1-L

We wanted to determine both the kinetics and the equilibrium of all the types of complexes that SHP-1 could form with the CEACAM1-L cytoplasmic domain, either mono-phosphorylated on Y488, or fully di-phosphorylated on both Y488 and Y515. This could not be done by direct BIAcore experiments because experimental phosphorylation of the recombinant CEACAM1-L cytoplasmic domain always resulted in a mixture of mono- and di-phosphorylated protein. Therefore, we applied computational analysis utilizing the rate constant values from Table 2 for the 25° C condition. At 37° C, a compromise solution was applied, since experimental data did not exist for k_{a1*} and k_{a5*}. Primary rate constants from Table 1 for 37° C were thus applied together with the $^{ii)}$ $k_{a1*} > k_{a5*}$ values of Table 2. The computation was done for a reaction volume that consists of a shell including the lipid bilayer contained within a 20 nm thick extracellular layer and a 15 nm thick intracellular layer (Öbrink et al., 2002). CEACAM1 is anchored in the lipid bilayer, and based on earlier biochemical data we assumed the concentration of CEACAM1-L in the reaction volume to be 1.0 μM. An overall cellular concentration of SHP-1 was determined to 1.84 μM in cultured epithelial cells (unpublished results). This concentration value was kept constant during the computation, assuming non-limiting diffusion of SHP-1 from the inner bulk cytoplasmic region to the 15 nm thick cytoplasmic reaction volume. The results are displayed in Figure 5.

For CEACAM1-L mono-phosphorylated on Y488 the temperature is an essential factor, affecting which type of complex will govern the system (Fig. 5A, C). At 25° C, the N-SH2:pY488 complex (N-488) dominated during the first eight minutes, but thereafter the C1-SH2:pY488 form (C1-488) became predominant. Equilibrium was reached in 40 minutes, with 31 % N-488 and 69 % C1-488. At 37° C, the N-488 complex dominated the system at all times, providing an opposite equilibrium of 80 % N-488 and 20 % C1-488.
The binding kinetics to CEACAM1-L phosphorylated on both Y488 and Y515 were somewhat more complex (Fig. 5B, D). Immediately after phosphorylation, the binding of the N-SH2 domain to pY488 accounted for c:a 80 % of total complexes. This complex then underwent a second docking to provide the double-docked N-488/C1-515 form. At both 25° and 37° C, the N-488/C1-515 form already dominated from the first minute and to equilibrium. At equilibrium at 37° C, N-488/C1-515 accounted for 62% of all complexes and the single-docked C1-515 form accounted for 24 %. The single-docked N-488 and C2-515 forms accounted for c:a 6 % each. These results indicate the N-488 complex and the N-488/C1-515 complex to be the biologically relevant forms.

4. Discussion

The impetus for this work was to advance our understanding of the signaling by the cell adhesion molecule CEACAM1-L. Because of the central role of SHP-1 in CEACAM1-L-mediated signaling, we chose to initiate this line of studies with a thorough analysis of the binding interactions between SHP-1 and the CEACAM1-L tyrosine-phosphorylated cytoplasmic domain. We applied a surface plasmon resonance-based technique (the BIAcore flow cell biosensor) to investigate the key patterns and kinetics of the binding interactions of SHP-1 with CEACAM1-L. Because CEACAM1-L has two phosphotyrosine binding motifs and SHP-1 has two SH2 domains, there is potential for several combinations of simultaneously forming binding complexes. To analyze such a combinatorial system we applied a classical reductionistic approach, starting by characterizing interactions between single binding sites. Results from these analyses were then used as building blocks for more elaborate analyses of the interactions of the tandem N,C-$(SH2)_2$ domain of SHP-1 with the CEACAM1-L double-tyrosine-phosphorylated cytoplasmic domain.
Initially, we used GST-fusion proteins of the SHP-1 SH2 domains. An unforeseen complication with this approach was that the GST moiety blocked some binding sites in both the GST-C-SH2 and the GST-N,C-$(SH2)_2$ proteins, which was discovered when the GST moiety was cleaved from the fusion proteins. However, this blocking effect had a positive consequence, because it led to the discovery of an additional binding site for phosphotyrosine motifs in the C-SH2 domain. Thus, there are three binding sites for tyrosine-phosphorylated CEACAM1-L in the SH2 domains of SHP-1. Finding a third phosphotyrosine recognition site was not anticipated, but was a consequence of the unique detectability of the SPR-based approach, which demonstrates one of the advantages of our strategy and the novel algorithms for binding analysis.
Most SH2 domains are believed to have one binding site for phosphotyrosine motifs, involving ArgαA2 and ArgβB5 (Waksman et al., 1993). However, our finding of an additional binding site for phosphotyrosine in the C-SH2 domain of SHP-1 is supported by the work of Weber et al. (Weber et al., 2000). By detailed NMR analysis of a doubly tyrosine-phosphorylated peptide (from the polyoma middle T antigen) complexed with the N-SH2 domain of the p85 subunit of phosphoinositide 3-kinase, they found a second site, in which

the phosphotyrosine is coordinated by a network of hydrogen bonds with the three amino acids, E411, S412 and the ε-amino group of K423. Sequence alignment of the p85 N-SH2 domain with the C-SH2 domain of SHP-1 demonstrates that the latter has two lysine residues, K198 and K199 (Yang et al., 2003), in the positions corresponding to E411 and S412 in the former one. Thus, this region of the SHP-1 C-SH2 domain has two positively charged amino acids, which could interact with the CEACAM1-L negatively charged phosphotyrosine residues. Site localization and further characterization of the two phosphotyrosine binding sites in the SHP-1 C-terminal SH2 domain require structural analysis of co-crystals of SHP-1 SH2 domains with mono- and double-phosphorylated CEACAM1-L cytoplasmic domains.

Experiments with single SH2 domains binding to mono-phosphotyrosine peptides showed that some interactions, e.g. the binding of the N-SH2 domain to the pY488 motif, had very rapid association and dissociation phases. Because of the relatively small number of reading points in such phases, the curve fit algorithm could not distinguish between several sets of solutions for k_a and k_d. This called for constraints to be introduced in the curve fitting procedure. To that end we assumed that the combination of the smallest possible rate constants, which satisfied the curve fitting, represented the most accurate description of these fast reactions.

Because single N-SH2 and C-SH2 domains were unstable we performed all detailed kinetic analyses with the N,C-$(SH2)_2$ protein. The interactions of N,C-$(SH2)_2$ with the pY488 and pY515 peptides followed the binding profiles and patterns predicted by the binding interactions of the individual N-SH2 and C-SH2 domains (see Figs. 2 and 3). The design and utilization of appropriate interaction schemes (models 2 and 3) were thus straightforward. Kinetic analysis at several different temperatures, analyzed by models 2 and 3, confirmed the existence of two binding sites in the C-SH2 domain, and one binding site in the N-SH2 domain. However, the different binding interactions had different temperature-dependencies. The interaction of the C2-SH2 site with the pY488 motif, which according to our analysis was significant at and below 15° C, no longer existed at and above 25° C. Similarly, the interaction of the C1-SH2 site with the pY488 motif had a fairly slow dissociation rate at all tested temperatures, but its association rate decreased by two orders of magnitude, upon temperature change from 5° to 37° C. Thus, at 37° C the contribution of this interaction was markedly decreased. In contrast, the interaction of the C1-SH2 site with the pY515 motif, which barely was detectable at 25° C, became significant enough at 37° C to claim physiological relevance.

The kinetic binding properties of the different complexes between tyrosine-phosphorylated CEACAM1-L and SHP-1 lead to interesting conclusions about *in vivo* complex formation between these signaling proteins. In many cell types CEACAM1-L tyrosine-phosphorylation is transient, with a peak 5-10 minutes after the triggering event. Thus, binding of SH2 domain-containing tyrosine kinases and phosphatases to CEACAM1-L can only happen within this time span. Complexes characterized by rapid association, such as N-SH2 binding to the pY488 site, will dominate early after tyrosine-phosphorylation relative to complexes with similar equilibrium binding affinities but slower association and dissociation. Computational analysis of the binding data obtained with the double-tyrosine-phosphorylated CEACAM1-L cytoplasmic domain and the tandem N,C-$(SH2)_2$ domain provided interesting insights into the time-dependent formation of the various CEACAM1-L:SHP-1 complexes. One finding was that the binding of SHP-1 to CEACAM1-L mono-phosphorylated on Y488 and to CEACAM1-L phosporylated on both Y488 and Y515, was

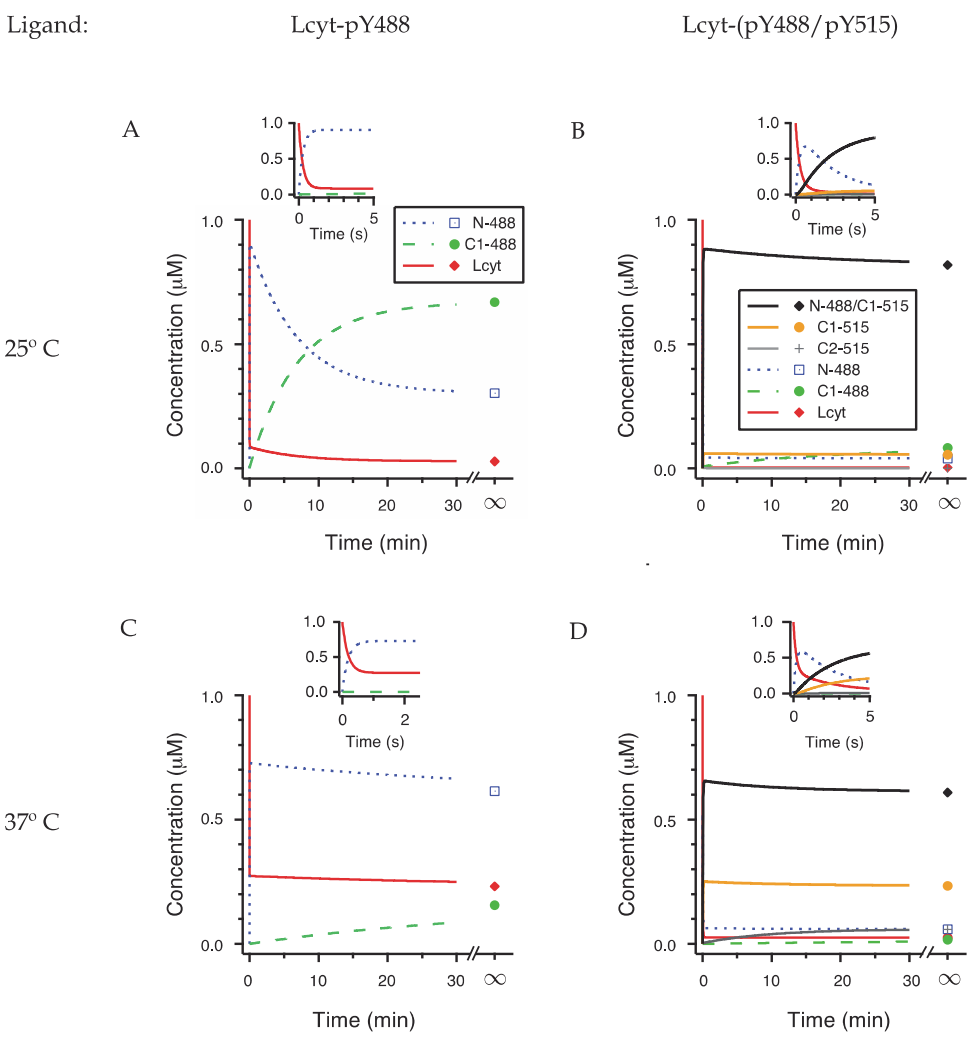

Fig. 5. Kinetics of the N,C-$(SH2)_2$ domain binding to mono- and di-phosphorylated CEACAM1-L. Interactions of CEACAM1-L mono-phosphorylated on Y488 (A,C) or di-phosphorylated on Y488 and Y515 (B,D), were analyzed computationally for two temperature conditions, 25° and 37° C, applying the model described in Fig. 4C. The initial membrane concentration of non-complexed phosphorylated CEACAM1-L was set to 1 µM; the cytoplasmic concentration of SHP-1 was kept constant, at 1.84 µM. For 25° C, the rate constants were taken from Table 2. For 37° C, the primary rate constants from Table 1 were used, together with k_{a1^*} [ii)] and k_{a5^*} [ii)] from Table 2. The notions provided in A are valid also for C. The notions provided in B are valid also for D. Complexes are indicated with N-488: N-SH2 bound to pY488; C1-488: C1-SH2 bound to pY488; C2-515: C2-SH2 bound to pY515; C1-515: C1-SH2 bound to pY515; N-488/C1-515: N-SH2 bound to pY488 and C1-SH2 bound to pY515 in tandem.

fairly similar. For CEACAM1-L mono-phosphorylated on Y488, binding of the N-SH2 domain dominated early after phosphorylation at 25° C (Fig. 5A), and at all times after phosphorylation at 37° C (Fig. 5C). At equilibrium the C1-SH2 site also contributed significantly. This binding pattern changed minimally for CEACAM1-L phosphorylated on both Y488 and Y515 (Fig. 5D). In this case the mono-docked N-488 complex dominated during the first few seconds, but gradually decreased as it served as a precursor for the double docked N-488/C1-515 complex, which became the dominant form (> 62 %) already within the first minute and ever after. The second most pronounced complex under these phosphorylation conditions was the mono-docked C1-515 form (24%).

It is believed that the N- and the C-SH2 domains have different functional roles in SHP-1, and that activation of the phosphatase is primarily due to engagement of the N-SH2 domain (Yang et al., 2003). Our data support this notion, and furthermore suggest that the role of the C-SH2 domain is primarily to stabilize the complex via engagement of the C1-SH2 site. Our data also suggests that phosphorylation of the membrane proximal tyrosine, Y488, in CEACAM1-L is the important reaction for activation of SHP-1, whereas phosphorylation of the distal tyrosine, Y515, primarily serves to stabilize the complex and sustain the activation state of the enzyme. This has functional implications, since it has been found that CEACAM1-L is preferentially phosphorylated on Y488 in some cell types, whereas in other cell types it becomes phosphorylated on both tyrosines (Brümmer et al., 1995; Huber et al., 1999). The transient versus stable CEACAM1-L tyrosine-phosphorylation also varies in different cell types. However, to fully understand the activation kinetics of SHP-1 it is necessary to also include CEACAM1-L's interactions with SHP-2 and c-Src, since these enzymes compete for the same binding sites in tyrosine-phosphorylated CEACAM1-L (Müller et al., 2009). Therefore, the kinetics and activation patterns of the binding of SHP-2 and c-Src to mono- and di-phosphorylated CEACAM1-L need to be investigated in future analyses.

The SPR-based approach is different from earlier approaches used to determine binding specificity and affinity of phosphopeptides to SH2 domains. In previous analyses, combinatorial libraries of short phosphopeptides have been used in pull-down assays, to characterize high affinity peptide sequence motifs for various SH2 domains (Songyang et al., 1993; Songyang et al., 1994). However, although providing optimal motifs with regard to stable binding, this method may not result in unbiased identification of physiologically relevant recognition motifs, since interactions dominated by slow dissociation rates are favored due to the obligatory washing steps included in the experimental procedures. Ligands with high dissociation rates, which will not be detected by the combinatorial peptide binding pull-down approach, may be of equally high affinity as ligands with slow dissociation, if they have fast association rates, since the equilibrium binding constant, K_d, equals the ratio k_d/k_a of the dissociation and association rate constants. Examples of binding reactions with similar equilibrium binding affinity, but with association and dissociation rates differing by three orders of magnitude are found in Table 1 (compare N-488 with C2-515). Such fast association/dissociation reactions, identified by our SPR-based procedure, may play very important roles in the control of signal cascades, because the resulting complexes will dominate early after tyrosine phosphorylation and will allow rapid switches between active and inactive enzyme states.

Finally, the interaction data presented in this paper (Figs. 3 and 5) emphasize that temperature is an important factor worth considering for all biochemical interactions. For various reasons, interaction studies involving mammalian proteins are routinely performed at temperatures considerably lower than physiological. Our data indicate that this can sometimes be misleading with regard to physiological relevance.

5. Conclusion

Signaling networks are at the heart of cellular functions in multicellular organisms. Such networks are composed of a large number of proteins that interact with each other in a complex and highly dynamic manner. Many of these interactions are characterized by rapid association/dissociation reactions between molecules having several distinct binding sites for each other. To initiate a deeper understanding of cell signaling we developed novel tools for characterizing the kinetics of macromolecules interacting through several distinct binding sites. This approach was based on utilization of SPR-based flow cell biosensors. It comprised a reductionistic approach starting with simple binding site interactions moving to molecules with multiple binding sites, and the development of novel algorithms for curve fitting analysis. By this approach we demonstrated that it is possible to make detailed analyses of the binding kinetics between macromolecules having 2-3 distinct binding sites for each other. We applied it to characterize the interactions of the signal regulating cell adhesion molecule CEACAM1-L with the protein tyrosine phosphatase SHP-1. Several new discoveries, with important implications for cell-cell recognition-mediated regulation of cellular signaling, were made. A novel binding site for phosphotyrosine-based motifs was discovered in the C-teminal SH2 domain in SHP-1. Some of the binding interactions were strongly temperature dependent, and disappeared at 37°C. This showed which of the binding interactions that are physiologically important. The detailed kinetic characterization together with computational analysis made it possible to determine the different roles of both the two tyrosine residues in the cytoplasmic domain of CEACAM1-L and of the two SH2 domains in SHP-1. Engagement of the N-terminal SHP-1 SH2 domain with the membrane proximal CEACAM1-L phosphotyrosine motif proved to be the most important interaction, whereas the C-terminal SHP-1 SH2 domain and the membrane-distal CEACAM1-L phosphotyrosine motif primarily served to stabilize and sustain the CEACAM1-L/SHP-1 interaction. Finally, our results demonstrate and emphasize the importance of binding kinetics in the action of cellular signalling networks. Some of the fast binding interactions dominated during the first few minutes after CEACAM1-L tyrosine phosphorylation and then disappeared. Since CEACAM1-L tyrosine phosphorylation is transient in some cell types, it is these transient interactions that play a dominant role in initiation of CEACAM1-L-mediated signal cascades. Such fast but transient kinetic interactions most likely have important roles in many other cell signaling events.

6. Acknowledgement

The present investigation was supported by grants from the Swedish Research Council, the Swedish Cancer Foundation, Karolinska Institutet, and the Canadian Institutes of Health Research.

7. References

Beauchemin, N., Kunath, T., Robitaille, J., Chow, B., Turbide, C., Daniels, E., & Veillette, A. (1997). Association of biliary glycoprotein with protein tyrosine phosphatase SHP-1 in malignant colon epithelial cells. *Oncogene,* 14, 783-790.

Brümmer, J., Neumaier, M., Göpfert, C., & Wagener, C. (1995). Association of pp60c-src with biliary glycoprotein (CD66a), an adhesion molecule of the carcinoembryonic antigen family downregulated in colorectal carcinomas. *Oncogene,* 11, 1649-1655.

Gray-Owen, S.D., & Blumberg, R.S. (2006). CEACAM1: contact-dependent control of immunity. *Nature Reviews Immunology,* 6, 433-446.

Huber, M., Izzi, L., Grondin, P., Houde, C., Kunath, T., Veillette, A., & Beauchemin, N. (1999). The carboxyl-terminal region of biliary glycoprotein controls its tyrosine phosphorylation and association with protein-tyrosine phosphatases SHP-1 and SHP-2 in epithelial cells. *J. Biol. Chem.,* 274, 335-344.

Müller, M.M., Klaile, E., Vorontsova, O., Singer, B.B., & Öbrink, B. (2009). Homophilic adhesion and CEACAM1-S regulate dimerization of CEACAM1-L and recruitment of SHP-2 and c-Src. *J. Cell Biol.*, 187, 569-581.

Myszka, D.G., Morton, T.A., Doyle, M.L., & Chaiken, I.M. (1997). Kinetic analysis of a protein antigen-antibody interaction limited by mass transport on an optical biosensor. *Biophys. Chem.,* 64, 127-137.

Öbrink, B., Sawa, H., Scheffrahn, I., Singer, B.B., Sigmundsson, K., Sundberg, U., Heymann, R., Beauchemin, N., Weng, G., Ram, P., & Iyengar, R. (2002). Computational analysis of isoform-specific signal regulation by CEACAM1 - a cell adhesion molecule expressed in PC12 cells. *Ann. N. Y. Acad. Sci.,* 971, 597-607.

Press, W.H., Teukolsky, S.A., Vetterling, W.T., & Flannery, B.P. (1999). *Numerical Recipies in C* (2nd ed), Cambridge University Press, Cambridge, U.K.

Sigmundsson, K., Másson, G., Rice, R., Beauchemin, N., & Öbrink, B. (2002). Determination of active concentrations and association and dissociation rate constants of interacting biomolecules: an analytical solution to the theory for kinetic and mass transport limitations in biosensor technology and its experimental verification. *Biochemistry,* 41, 8263-8276.

Singer, B.B., Scheffrahn, I., Kammerer, R., Suttorp, N., Ergun, S., & Slevogt, H. (2010). Deregulation of the CEACAM expression pattern causes undifferentiated cell growth in human lung adenocarcinoma cells. *PLoS ONE*, 5(1): e8747. doi:10.1371/journal.pone.0008747.

Songyang, Z., Shoelson, S.E., Chaudhuri, M., Gish, G., Pawson, T., Haser, W.G., King, F., Roberts, T., Ratnofsky, S., Lechleider, R.J., Neel, B., Birge, R.B., Fajardo, J.E., Chou, M.M., Hanafusa, H., Schaffhausen, B., & Cantley, L.C. (1993). SH2 domains recognize specific phosphopeptide sequences, *Cell,* 72, 767-778.

Songyang, Z., Shoelson, S.E., McGlade, J., Olivier, P., Pawson, T., Bustelo, X.R., Barbacid, M., Sabe, H., Hanafusa, H., Yi, T., Ren, R., Baltimore, D., Ratnofsky, S., Feldman, R.A., & Cantley, L.C. (1994). Specific motifs recognized by the SH2 domains of Csk, 3BP2, fps/fes, GRB-2, HCP, SHC, Syk, and Vav. *Mol. Cell. Biol.,* 14, 2777-2785.

Waksman, G., Shoelson, S.E., Pant, N., Cowburn, D., & Kuriyan, J. (1993). Binding of a high affinity phosphotyrosyl peptide to the Src SH2 domain: crystal structures of the complexed and peptide-free forms. *Cell,* 72, 779-790.

Weber, T., Schaffhausen, B., Liu, Y., & Günther, U.L. (2000). NMR structure of the N-SH2 of the p85 subunit of phosphoinositide 3-kinase complexed to a doubly phosphorylated peptide reveals a second phosphotyrosine binding site. *Biochemistry,* 39, 15860-15869.

Yang, J., Liu, L., He, D., Song, X., Liang, X., Zhao, Z.J., & Zhou, G.W. (2003) Crystal structure of human protein-tyrosine phosphatase SHP-1, *J. Biol. Chem.,* 278, 6516-6520.

4

Sum-frequency Generation Spectroscopy in Biosensors Technology

Volcke Cédric, Caudano Yves and Peremans André
Research centre in Physics of Matter and Radiation (PMR), University of Namur
Belgium

1. Introduction

As there is need for detection of chemical and biochemical substances in many important areas (e.g. medicine, biotechnology, security, drug and food monitoring), the development of devices allowing such detection grows up rapidly. *Such devices are known under the generic name of "biosensor", revealing a combination of two components: a biological element and a sensor device. Practically, in a biosensor, a bioelement recognises an analyte and the sensor transduces the variations in the biomolecule into a measurable signal*. The selected bioelement is specific to the analyte, whose presence and concentration is expected to be determined.
Since the first preliminary devices, research groups from various areas worked together to develop more sophisticated, reliable and mature biosensors. *However, despite intensive attempts, these have not been so successful, partially due to a lack of technology for assembling biomolecules in an oriented, ordered, or site directed manner on solid surfaces. Indeed, many problems have to be fixed.* First of all, the active biomolecule (protein, antibody or nucleic acid) must be immobilised onto the selected surface at the appropriate surface density while maintaining its activity. The way they are immobilised (physical adsorption (Dreesen et al., 2004a; Ekblad & Liedberg, 2010; Kidoaki & Matsuda, 2002; Nakanishi et al., 2001) versus covalent binding (Brady & Jordaan, 2009; Frasconi et al., 2010; Gandhiraman et al., 2009; Stutz, 2009)) and the surface substrate properties (wettability, roughness… (Gandhiraman et al., 2010a)) are, amongst others, parameters affecting biomolecule density and activity. Also, once proteins are attached to surfaces, different factors are affecting their biomolecular recogition (specific binding), i.e. environment (Gubala et al., 2010), immobilisation strategy (Gandhiraman et al., 2010b), protein orientation (Xu et al., 2007; Araci et al., 2008)… Further, non-specific binding on biosensor surface is decreasing/affecting its limit-of-detection (Gandhiraman et al., 2009, 2010b). So, protein immobilisation/adsorption and orientation therefore appear to play a crucial role, highly affecting biosensor performances.
In this context, several analytical techniques were used to characterise adsorbed/immobilised proteins, to determine their identity, concentration, conformation and/or spatial density. However, relatively few data are available concerning protein orientation particularly. Indeed, this issue remains relatively marginal, mainly due to a lack of appropriate characterisation techniques availability. Despite its primary interest, protein orientation is generally only discussed *a posteriori* as an hypothesis to explain variable protein activity efficiency.

Since the last ten years, specifically dedicated investigations to protein orientation were performed. In such cases, adapted characterisation techniques were used. For example, the orientation of heme complex in *Cytochrome C* proteins were determined by Raman spectroscopy, therefore deducing the overall protein orientation (Mc Donald et al., 1996; Edminston et al., 1997; Keating et al., 1998; Yu et al., 2007; Sonois et al., 2009; Grosserueschkamp et al., 2009). Unfortunately, such investigations were limited to heme groups containing proteins. Characterisation techniques more easily applicable to a larger range of proteins were developped by Castner's (Xia et al., 2002; Wagner et al., 2003, 2004; Belu et al., 2003; H. Wang et al., 2004; Cheng et al., 2006; Baugh et al., 2010; Liu et al., 2010) and Aoyagi's (Aoyagi et al., 2008a, 2008b, 2009; Okada et al., 2008) groups. They successfully adapted time-of-flight secondary ion mass spectroscopy (ToF-SIMS) in order to discriminate protein orientation by precisely probing ionised fragments peaks associated to particular amino acids (by using principal component analysis). Unfortunately, this technique can only be performed under ultra-high vacuum conditions, which is not adequate for biological species.

Recently, an emerging technique, sum-frequency generation vibrational (SFG) spectroscopy was applied to the analysis of proteins adsorbed at various interfaces. The technique relies on a second-order nonlinear optical process forbidden in centrosymmetric media. Therefore, SFG is intrinsically specific to the interfacial media where the centrosymmetry of the bulk substrate is broken. Practically, in a SFG experiment, two pulsed laser beams (one in the infrared and the other in the visible range) are focused on a surface or an interface. The spatial overlap and temporal synchronisation of both incident laser pulses –the duration of which lays in the picosecond or femtosecond spectral ranges- induces the generation of SFG photons (Humbert et al., 2008; Y.R. Shen, 1989; Vidal & Tadjeddine, 2005; Williams & Beattie, 2002), which frequency is the sum of the frequencies of both initial ones (Howell et al., 2008; Ye et al., 2009). The SFG signal is enhanced while the IR beam excites a vibrational mode of the molecules adsorbed on the sample surface. Therefore, SFG allows identification of molecular species and chemical groups, but also provides information on the interfacial structures, such as molecular orientation. This all-optical technique presents the advantages of being non-invasive, order-sensitive, and of requiring small sample volumes. SFG can be performed in situ and in real-time, for a large variety of substrates (metals, insulators, semiconductors) and of buried interfaces (solid-liquid, liquid-liquid, liquid-gaseous, solid-high pressure) (Buck et al., 2001; Z. Chen et al., 2002; Lambert et al., 2005; H.F. Wang et al., 2005; Z. Chen et al., 2007; Kubota et al., 2007).

A few number of research group have demonstrated the possibility to record SFG spectra from proteins, leading to the differentiation of protein conformations, (sub)structures and functional groups orientation distributions (J. Wang et al., 2002a, 2002b, 2003a, 2003b, 2004a, 2004b, 2005, 2007; Koffas et al., 2003; J. Kim et al., 2004; Dreesen et al., 2004b; Paszti et al., 2004; X. Chen et al., 2005a; Clarke et al., 2005; Mermut et al., 2006; Phillips et al., 2007; York et al., 2007; Weidner et al., 2009, 2010; Baugh et al., 2010; Boughton et al., 2010; Ye et al., 2010; Nguyen et al., 2010). We believe it is important to summarise these protein related SFG studies and make it accessible to researchers in the fields of biosensors, biomaterials and biomedical diagnostic devices. Although we tried to be as exhaustive as possible regarding the literature, authors apologise for any possible omission.

In this review, we propose to describe this technique as well as its application and utility in biological species analysis and biosensor technology. After a brief introduction to the SFG

we illustrate the performance of SFG using selected studies on protein thin films. Thereafter, we present precursor studies using SFG spectroscopy as a detection system in biosensor devices. In each section, we shall detail what kind of information can be extracted from SFG data, based on recent experimental results. Finally, SFG prospects in biosensor, biomedical diagnostic devices or biomaterials will conclude this review.

2. Sum-frequency generation - theoretical background

Detailed theoretical and technical considerations on SFG spectroscopy can be found in numerous reviews and books (Shen, 1984; Tadjeddine & Peremans, 1998; Lambert et al., 2005; Zheng et al., 2008). We shall briefly describe the necessary theoretical background for the understanding of the following sections. We'll then focus on the SFG phenomenon and its application to the investigations of adsorbate properties. Sum-frequency generation vibrational spectroscopy is a second-order nonlinear optical process. Just like a low-intensity external electric field induces a linear polarisation in materials such as

$$\vec{P} = \varepsilon_0 \chi \vec{E} \tag{1}$$

(where $\varepsilon_0, \chi, \vec{E}$ respectively represent the dielectric permittivity of free space, the electric susceptibility of the material and the external electric field), when this electric field is intense enough, higher-order terms in the polarisation can no longer be neglected and become sufficiently large to be observed. The polarisation can therefore be expressed as :

$$\vec{P} = \varepsilon_0 \chi^{(1)} \vec{E} + \varepsilon_0 \chi^{(2)} \vec{E}\vec{E} + \varepsilon_0 \chi^{(3)} \vec{E}\vec{E}\vec{E} + \ldots \tag{2}$$

where $\chi^{(n)}$ represents the n^{th} -order susceptibility, which is a tensor with 3^{n+1} components. Let's consider two incident electromagnetic waves polarised in the Z direction and propagating in the X direction such as:

$$E_1 = E_{1z} \cos \omega_1 t \text{ and } E_2 = E_{2z} \cos \omega_2 t \tag{3}$$

(the spatial phase *kx* in the cosinus is ignored for simplicity). We shall try to evaluate the components of the polarisation, based on the above-mentioned equation (2) limited to the 1st and 2nd -order susceptibilities. For example, the component along the X axis of the polarisation can be rewritten as

$$\begin{aligned} P_x &= \varepsilon_0 \chi_{xz} \left(E_{1z} \cos \omega_1 t + E_{2z} \cos \omega_2 t \right) + \varepsilon_0 \chi^{(2)}_{xzz} \left(E_{1z} \cos \omega_1 t + E_{2z} \cos \omega_2 t \right)^2 \\ &= P_x^L + P_x^{NL} \end{aligned} \tag{4}$$

with P_x^L and P_x^{NL} are respectively the linear and nonlinear terms of the X component of the polarisation. The nonlinear terms proportional to $\chi^{(2)}$ in equation (4) can be expressed as:

$$P_x^{NL} = \varepsilon_0 \chi^{(2)}_{xzz} \tfrac{1}{2} \left(E_{1z}^2 + E_{2z}^2 \right) \tag{5}(a)$$

$$+ \varepsilon_0 \chi^{(2)}_{xzz} \tfrac{1}{2} \left(E_{1z}^2 \cos 2\omega_1 t + E_{2z}^2 \cos 2\omega_2 t \right) \tag{b}$$

$$+ \varepsilon_0 \chi^{(2)}_{xzz} E_{1z} E_{2z} \cos\left(\omega_1 + \omega_2 \right) t \tag{c}$$

$$+ \varepsilon_0 \chi^{(2)}_{xzz} E_{1z} E_{2z} \cos\left(\omega_1 - \omega_2 \right) t \tag{d}$$

The nonlinear term is now composed of:

- Two components $E_{1z}^2/2 + E_{2z}^2/2$ at nul frequency, i.e. the term (a) in equ. (5). This process is called *optical rectification* and is responsible of the apparition of a static bias voltage at the edges of the material.
- One component at the frequency $2\omega_1$ and one component at the frequency $2\omega_2$, i.e. the term (b) in equation (5). This phenomenon is called *second-harmonic generation (SHG)* and is doubling the frequency of the incident beams.
- One component at a frequency $(\omega_1 + \omega_2)$, i.e. the term (c) in equation (5). This is the *sum-frequency generation (SFG)* phenomenon.
- One component at a frequency $(\omega_1 - \omega_2)$, i.e. the term (d) in equation (5). This phenomenon is called *difference-frequency generation (DFG)*.

This equation explains the origin of the SFG signal. Indeed, as the nonlinear polarisation oscillates at the SFG frequency in the probed material, it will emit an electromagnetic radiation at that frequency. So, practically, in a typical SFG spectroscopy experiment, two input pulsed laser beams (at frequencies ω_1 and ω_2) are focused and overlapped spatially and synchronised temporally on a sample surface (J. Wang et al., 2002a). The laser beams are intense enough to reveal 2nd -order components of the sample susceptibility. These will mix the frequencies of both input beams and give rise to nonlinear effects like optical rectification, SHG, SFG and DFG. We only focus here on the generated SFG light. Generally, ω_1 and ω_2 are in the visible and infrared range, respectively. Interestingly, the SFG signal is enhanced while the IR beam excites a resonance mode of molecules on the sample surface (the condition is that the vibration must be both infrared and Raman active). Therefore, if ω_2 is scanned over the SFG-active vibrational resonances of adsorbates on the sample surface, the SFG signal is resonantly enhanced, thus producing a vibrational spectrum characteristic of the adsorbates (J. Wang et al., 2002a). It therefore allows identification of molecular species and chemical groups, but also provides information about interfacial structures, such as order and orientation distribution of functional groups.

2.1 SFG signal properties

Several important properties of the SFG spectroscopic signal makes it very advantageous for surface analysis:

1. It can be demonstrated that this technique is intrinsically surface-sensitive. This is a consequence of the fact that 2nd -order nonlinear processes, including SFG spectroscopy, are forbidden in media presenting an inversion symmetry. As most usual materials present any inversion symmetry, they do not generate an SFG nonlinear signal from their volume. So only their surface or the interface between two media, which can be viewed as a symmetry break, is an important source of surface nonlinear polarisation, and therefore of SFG signal. Moreover, due to its high interface sensitivity, a reference spectrum is not required, unlike for surface IR spectroscopy for example.
2. As a photon based technique, it is not limited to vacuum but can also be performed through gases and transparent liquids and solids.
3. As a vibrational spectroscopy, it yields very specific physico-chemical information on the interface structure and composition via the molecular vibrations of the adsorbates.
4. From a general point of view, the SFG signal is proportional to the absolute square of the nonlinear susceptibility, $|\chi|^2$. Moreover, if the IR beam frequency is coinciding with

a vibrational resonance of adsorbates, the vibrationally enhanced SFG susceptibility can be estimated to be roughly proportional to the product of the IR and Raman transition moments. Therefore, the SFG signal is resonantly enhanced only if the vibrational mode is both Raman and IR active (Shen et al., 1994; Yenageh et al., 1995; Tadjeddine et al., 1995; Himmelhaus et al., 2000; Mani et al., 2004a).

5. The SFG response is sensitive to orientation and ordering of surface species (Himmelhaus et al., 2000; Rao et al., 2004). More precisely, the SFG spectrum of an isotropic layer adsorbed on a surface can be modelled, assuming a lorentzian response of molecular vibrations as

$$I_{ppp/ssp}^{\mathrm{SFG}} \infty \left| \chi_{ppp/ssp}^{(2)\mathrm{NR,eff}} + \chi_{ppp/ssp}^{(2)\mathrm{R,eff}} \right|^2 \tag{6}$$

where $\chi^{(2)NR,\,eff}$ and $\chi^{(2)R,\,eff}$ represent the effective non-resonant (NR) susceptibility of the interface and the effective resonant (R) contribution from the adsorbed molecular vibrations. The effective macroscopic resonant susceptibility $\chi^{(2)R,\,eff}$ can be expressed as:

$$\begin{aligned} \chi_{ppp/ssp}^{(2)\mathrm{R,eff}} \infty & \frac{\omega_{\mathrm{SFG}}}{c} \frac{N_s}{\cos\theta_{\mathrm{SFG}}} \sum_{i,j,k} F_{p/s}^{\mathrm{SFG},i} F_{p/s}^{\mathrm{Vis},j} F_{p/p}^{IR,k} \times \\ & \left\{ \sum_{\mathrm{v}} \frac{1}{\omega_{\mathrm{v}}} \frac{1}{(\omega_{\mathrm{v}} - \omega_{\mathrm{IR}} - i\Gamma_{\mathrm{v}})} \left\langle \sum_{i,m,n} T_{ijk}^{lmn} \frac{\partial \alpha_{lm}(\omega_{Vis})}{\partial Q_{\mathrm{v}}} \frac{\partial \mu_n}{\partial Q_{\mathrm{v}}} \right\rangle \right\} \end{aligned} \tag{7}$$

where $\partial\alpha_{lm}(\omega_{vis})/\partial Q_v$ and $\partial\mu_n/\partial Q_v$ are the Raman susceptibility and the infrared dipole associated to each vibration. T_{ijk}^{lmn} rotates the molecule in the surface coordinate system and the bracket $\sum_{lmn}\left\langle T_{ijk}^{lmn}\right\rangle$ represents a sum-average over the molecule orientation distribution. N_s is the density of molecules on the surface. Γ_v is the half width at half-maximum of the Lorentzian band shape. *F* are called the Fresnel factors and connect the electric field components of the three coherent beams to the fields inside the interfacial layer. Assuming an azimuthally isotropic ad-layer, only four components of the susceptibility tensor are independent. In principle, these components can be selectively probed with four sets of polarisations (*ppp*, *ssp*, *sps* and *pss*). However, on metallic surfaces, the *pss* and *sps* polarisation sets yield negligeable SFG signals due to efficient screening of the IR beam component parallel to the surface. The *ssp* polarisation combination on metallic surface gives an SFG signal typically more than one order of magnitude weaker than that of the *ppp* polarisation combination. However comparing SFG spectra with these two different polarisation combination enables to refine the determination of the admolecule orientation as discussed in the following parapgraph.
By comparison, the IR absorption spectrum is obtained using the following equation:

$$Abs(\omega_{IR}) \propto N_S \sum_{v} \mathrm{Im} \frac{1}{(\omega_v - \omega_{IR} - i\Gamma_v)} \sum_{k} \left| F^{IR,k} \right|^2 \left\langle \left(\sum_{n} T_k^n \frac{\partial \mu_n}{\partial Q_v} \right)^2 \right\rangle I^{IR} \tag{8}$$

So, interpreting SFG data requires the Raman tensor $\partial\alpha_{lm}(\omega_{vis})/\partial Q_v$ and IR dipole $\partial\mu_n/\partial Q_v$ to be determined for each vibrational mode. These molecular properties can be inferred from *ab initio* calculations and calculated SFG spectra can be compared to

experimental data, acquired for different polarisation combinations, to determine admolecule orientation (Cecchet et al., 2010a, 2010b).

3. SFG signal of proteins

In the last two decades, SFG vibrational spectroscopy has been applied to structure and orientation analysis of adsorbed molecules (Cecchet et al., 2010; Kudelski et al., 2005; Lin et al., 1995; Mani et al., 2004b; Watanabe et al., 1994). For example, alkanethiol molecules adsorbed on gold, silver or platinum surfaces were extensively studied (Yeganeh et al., 1995; Kudelski et al., 2005; Humbert et al., 2006; Dreesen et al., 2006a; Sartenaer et al., 2007). SFG allowed the determination of molecular adsorption and orientation phenomenon to be better understood. Although the understanding of protein adsorption on the molecular level is crucial for design of future applications in coating technology or biosensor device for example, SFG spectroscopy was applied only recently to the investigation of biological samples such as phospholipid bilayers (Pohle et al., 1999; X. Chen et al., 2007; X. Chen et al., 2010; Kett et al., 2010), model peptides (York et al., 2007; Phillips et al., 2007) or amino acids (Mermut et al., 2005). Several proteins like bovine serum albumin (BSA) (J. Wang et al., 2003b), immunoglobulin G (IgG) (X. Chen et al., 2005b), collagen (Rocha et al., 2007) or fibrinogen (Jung et al., 2003) were investigated by SFG at various surfaces/interfaces.
Initially, such studies mainly focused on –CH and –NH vibrational features (J. Wang et al, 2002a, 2002b, 2003a, 2004a; Paszti et al., 2004; Dreesen et al., 2004b; Clarke et al., 2006), providing, amongst others, structural informations about hydrophobic side chains. Nowadays, a few groups have demonstrated the possibility to detect SFG signals from protein amide I groups, leading to the differentiation of protein secondary structures and protein orientation. These three growing steps (C-H, N-H and amide I bands analysis) in the understanding and interpretation of protein SFG signal are detailed in the next three subsections.

3.1 CH bands

The C-H stretching vibration region (between 2800-3000 cm^{-1} for aliphatic and 3000-3100 cm^{-1} for aromatic C-H) is the most regarded region while studying adsorbed molecules or biological species. Proteins are composed of a succession of amino acids, where the most important amount of C-H groups are located in their side chains. The average orientation of such side chains, and even some kinetic changes can therefore be deduced.
Most SFG investigations on proteins are performed in their native environment, i.e. liquid (mainly water or PBS solutions). For example, the first analysis of protein layers by SFG spectroscopy was published in the 2000's by J. Wang et al. (J. Wang et al., 2002a, 2002b). Bovine serum albumin (BSA) layers (J. Wang et al., 2002a, 2002b) adsorbed on three different substrates (fused silica, deuterated-polystyrene (d-PS) and deuterated-polymethylmetacrylate (d-PMMA)). As depicted in Figure 1 a and c, no SFG vibration in the CH stretching region is observed at the fused silica/BSA solution or at fused silica/water interfaces, which was interpreted as a lack of protein adsorption or no net alignment of functional groups of adsorbed BSA proteins. After washing and drying, SFG spectra highlighted a strong C-H vibration when collected in air (Fig. 1 b and d), revealing for the first time adsorption of BSA molecules using SFG spectroscopy (J. Wang et al., 2002b). From these observations, orientation information was inferred. Indeed, in solution, adsorbed BSA molecules are in contact with two hydrophilic environments, silica and water (or BSA

solution). Therefore, BSA molecules adopt an hydrophilic conformation, i.e., the hydrophobic groups (mainly C-H) tend to stay inside the film with no net alignment: thus they induce no SFG signal. Oppositely, when exposed to air, hydrophobic parts of the molecules are assumed to face towards the air, which is also hydrophobic (J. Wang et al., 2002b). Such experiments were also performed on various substrates (PS, PMMA…) and various environments (hydrophobic solvents like benzene, carbon tetrachloride or FC-15…) (J. Wang et al., 2002b), revealing various protein conformations (including conformation and/or orientation changes) according to environmental conditions (substrate and surrounding medium). Moreover, the effect of pH solution for example on protein side chain conformation was also revealed (J. Wang et al., 2002a; G. Kim et al., 2002).
This highlights the primary importance of hydrophobic effects towards protein adsorption behaviours. Since acidity also influences the orientation distribution of functional groups in proteins, this parameter is also important for properties like biocompatibility or molecular recognition efficiency.
On another hand, air/solid interfaces were also investigated and provided some interesting results. For example, ambient contaminations while working in air are of primary concern. In this context, SFG is totally adapted for studying effects of contaminations in air on protein adsorption. Such experiments were performed on titanum surfaces, where SFG was also able to determine the role of natural hydrocarbon contamination on protein adsorption behaviour. Actually, it highlighted its relatively poor influence in the protein adsorption phenomenon on Ti-oxide surfaces, only based on SFG C-H vibrations (Paszti et al., 2004).

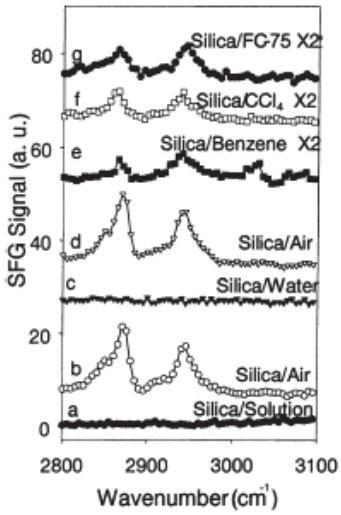

Fig. 1. SFG Spectra collected from (a) silica/BSA solution interface; (b) silica/air interface after silica was removed from solution and washed by water; (c) silica/water interface after the sample contacted water again; (d) silica/air interface after the sample was again removed from water; (e,f,g) silica/benzene or silica/ CCl_4 or silica/FC-75 interface after procedures (a) and (b) and contacting the sample with benzene, CCl_4, or FC-75. Spectral intensities in spectra e,f,g are multiplied by 2. (a) . Reprinted with permission from Ref (J. Wang et al., 2002b). Copyright 2002 American Chemical Society.

These examples highlight the importance for the careful analysis of SFG C-H vibration modes of adsorbed proteins. The experiments should be performed with caution and precision. The model used in the interpretation of data is important and needs to be selected considering each experimental parameter. Using this, C-H vibrational range in SFG spectra can provide very useful information on functional groups conformation of adsorbed proteins, protein and/or substrate surface changes.

3.2 NH bands

Another spectral region of interest in protein SFG spectra is the N-H vibrational range. Indeed, until 2009 and the investigations of Weidner et al. (Weidner et al., 2009, 2010), the attribution of this mode was unclear. The dominant peak near 3300 cm^{-1} observed in SFG spectra of adsorbed proteins or peptides was either attributed to amide A mode (related to protein backbone structure) or to amine resonances (related to side chains) (Jung et al., 2003; Clarke et al., 2005; Mermut et al., 2006; Phillips et al., 2007; york et al, 2007). In order to solve this controversy, Weidner et al. used isotope-labelled Lkα14 peptides adsorbed on SiO_2 (negatively charged) and CaF_2 (positively charged) surfaces (Weidner et al., 2009). These peptides are composed of leucine (L) side chains (hydrophobic) and lysine (K) side chains hydrophilic) assuming an α-helix structure. The amine groups of the lysine side chains were labelled with ^{15}N isotopes, which is supposed to result in an estimated 8 cm^{-1} red-shift of the NH_3 resonance frequency. Authors observed a red-shift of the ~ 3300 cm^{-1} vibrational mode of about 9 cm^{-1} (on SiO_2) and of ~ 13 cm^{-1} (on CaF_2), while comparing unlabelled and labelled peptides SFG spectra. This clearly demonstrates that this peak can be unambiguously associated to the NH_3 amine stretching mode. However it is still under controversy if its origin is associated to backbone, side chains or both NH groups orientation (G. Kim et al., 2002; Clarke et al., 2005).

3.3 Amide I band

The major drawback of the previous experiments is their difficulty to deduce overall structure, conformation or orientation of adsorbed proteins only from C-H and/or N-H SFG stretching vibrations. Previously, protein structures were successfully studied using infrared spectroscopy and Raman scattering. These investigations revealed that amide vibrational bands are very sensitive to protein secondary structures (Singh, 2000). Unfortunately, in situ detection of such bands is made difficult due to limited sensitivity of such techniques and possible interferences from the environment (i.e. water signals). In 2003, J. Wang et al. (J. Wang et al., 2003b) first demonstrated the possibility of using SFG to observe amide I signals from proteins or peptides adsorbed at solid/liquid interfaces. The advantages of using SFG rather than other spectroscopic techniques are its ability to provide the amide I signals without interference from the environmental signals (i.e. from water for example). Spectroscopic data on the amide also provide supplementary structural information since the related second-order nonlinear optical susceptibility tensor contains more elements than the linear susceptibility tensor. However, in order to improve the recording of the weak amide I SFG signal, Wang et al. (J. Wang et al., 2003b) adopted a "near total reflection" experimental configuration for their SFG set up using a CaF_2 prism, leading to an enhancement of the SFG intensity. SFG signature of amide I was obtained in situ from various proteins (Fig. 2 Left). All proteins presented very specific amide I SFG signature, which can be due to variations in protein surface coverage, orientation and secondary structure. The attribution of each SFG feature needed more investigations as detailed below.

3.3.1 β-turns structures

Further, at this stage, a correlation between SFG amide I spectral characteristics and protein interfacial structures, with particular attention to the β-sheets conformation, was still needed. This was performed by X. Chen et al. early after while demonstrating the feasibility of using SFG to identify protein/peptide secondary structures (β-sheets) (X. Chen et al., 2005a). Particularly, tachyplesin I, a peptide having an antiparallel β-sheet structure, was investigated. SFG spectra of tachyplesin I adsorbed on polystyrene surface are shown in Fig. 2 Right (a). Several characteristic peaks can be observed at 1664 cm^{-1} and 1688 cm^{-1}. After addition of dithiothreitol (DTT) in the solution, the SFG amide I region appears as presented in Fig. 2 Right (b). DTT is often used to elucidate disulfide bonds function in proteins, as it is known to reduce it. So, contacting proteins/peptides with DTT will induce a reduction of disulfide bonds and destroy the β-sheet structures. The disappearance of the 1688 cm^{-1} peak after contact with DTT demonstrated its relationship with β-sheet structures. This analysis first validated SFG as a powerful technique for determining the detailed β-sheet structures of proteins.

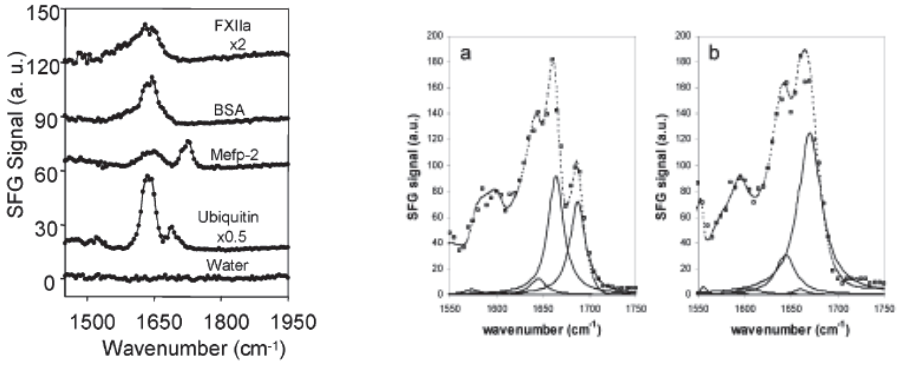

Fig. 2. (Left) SFG spectra collected from interfaces between polystyrene and various protein solutions. Reprinted with permission from Ref (J. Wang et al., 2003b). Copyright 2003 American Chemical Society. (Right) SFG spectra (squares) and fitting results (dotted lines) for tachyplesin I adsorbed at solution/polystyrene interface. The solid lines represent the component peaks used to fit the spectra. (a) SFG spectra obtained before contacting with dithiothreitol and (b) after contacting with dithiothreitol. Reprinted with permission from Ref (X. Chen et al., 2005a). Copyright 2005 American Chemical Society.

3.3.2 α-helix structures

Similarly to the β-sheets, X. Chen et al. (X. Chen et al., 2005a) investigated the SFG fingerprints of α-helical structures in adsorbed proteins. They focused on a peptide, MSI594, consisting of 24 amino acids residues and adopting a α-helical structure. In this case, the main peak in the SFG signal of the amide I region is centred at 1650 cm^{-1}, and was attributed to α-helical structure, as confirmed by ATR-FTIR experiments. Those examples clearly demonstrated that SFG amide I signals can differentiate various protein secondary structures, such as α-helices and β-sheets. Based on such considerations, α-helix and β-turn secondary structures of several proteins and peptides have been analysed by SFG spectroscopy (Weidner et al., 2010; Baugh et al., 2010; Boughton et al., 2010).

4. Protein orientation

Considering the above-mentioned investigations, we can now expect to infer the protein orientation from SFG data, as demonstrated by Clarke et al. on blood proteins like fibrinogen (Clarke et al., 2005; J. Wang et al., 2006). Such results are of primary interest in biomaterials science for example as it can help in-depth understanding of biocompatibility properties of the studied materials. Fibrinogen is a protein composed of a central hydrophobic domain (E domain, Fig. 3 Left) connected to two hydrophobic domains (D domains, Fig. 3 Left) by coiled coils of α-helices (Fig. 3 Left) (Clarke et al., 2005; J. Wang et al., 2006). The dominant contribution to SFG amide I signal (Fig. 3 Right) is associated to the presence of α-helices (at 1650 cm^{-1}). Minor contributions from β-sheets and turn structures are also observed and are in agreement with protein structure. The orientation of the protein parts can be deduced from those signals. Indeed, the majority of the α-helices can be found in the coiled coils. The strong SFG signal is assumed to appear when a large orientation of α-helices is occurring, i.e. an ordering of α-helices in coiled coils. This can be explained from the fact that : (1) the net dipole of an α-helix arises from the N- to the C-terminus; (2) the ssp (SFG signal is s-polarised, the visible light is s-polarised and the IR beam is p-polarised) polarisation combination is sensitive to functional groups presenting an orientation perpendicular to sample surface. In such a case, the authors conclude that the SFG signal originates from fibrinogen proteins adsorbed in a bent conformation (Clarke et al., 2005; J. Wang et al., 2006). Such orientation determination of protein substructures were also performed on tachyplesin I, where SFG combined with ATR-FTIR data allowed the quantitative determination of the tilt angle (θ) and the twist angle (ψ) of the β-sheet structure at various interfaces.

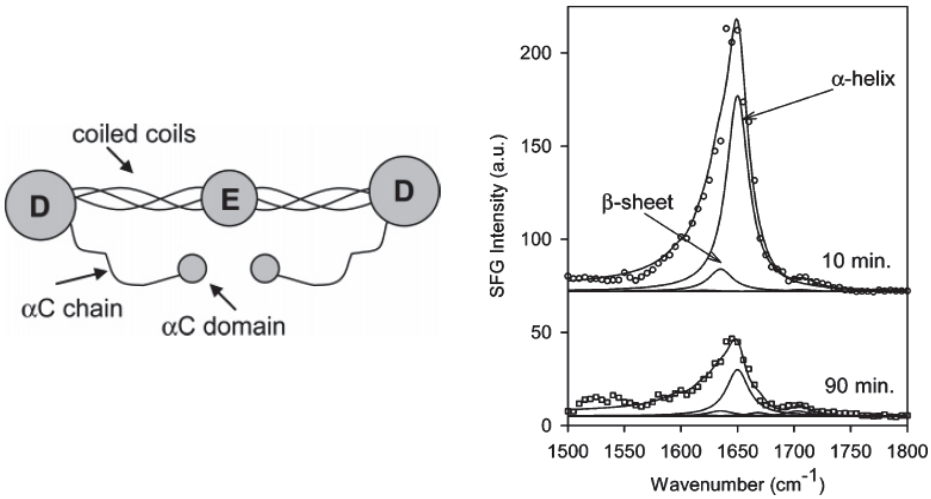

Fig. 3. (Left) Fibrinogen structure (with labelled domains). (Right) Amide I spectral range in SFG spectra of fibrinogen adsorbed at PBS/poly(ether urethane) interface collected after 10 and 90 min. Points are experimental data while lines are fitting results (or represent components of the fit). Reprinted with permission from Ref (Clarke et al., 2005). Copyright 2005 American Chemical Society.

Moreover, conformational changes with time were also observed. These changes encountered after adsorption on surfaces are of primary interest in biomedical materials and biomaterials science. For example, protein adsorption is the first phenomenon occurring when implants are integrated into living tissues. Moreover, these changes can also affect their recognition efficiency with regards to other biomolecules. Similar investigations were also performed on diverse proteins like bovine serum albumin, ubiquitin, factor XII and some other deuterated proteins (J. Wang et al., 2005).

4.1 Polarisation mapping

Since proteins are large molecules, their vibrational spectra can be composed of many vibrational modes, resulting in complex spectra, which may be difficult to interpret. In order to circumvent this difficulty, a new method, referred *as polarisation mapping method*, was developed by J. Wang et al. in 2005 (J. Wang et al., 2005). In this method, the input and output signals polarisations were modified compared to usual polarisations used (ssp or ppp). Indeed, it was shown that fitting parameters only derived from ssp and ppp fitted spectra may not always be reliable (J. Wang et al., 2004b). So, in the polarisation mapping method, SFG spectra are in this case collected using a p-polarised IR beam and a 45° polarised visible beam (i.e. between s- and p-polarisation). A continuous change of the SFG output signal polarisation is performed. Such configuration, combined with model calculations (J. Wang et al., 2005), allowed an improvement of reliability and resolution of SFG measurements, from which more structural information (orientation and orientation distribution of functional groups) can be deduced. This is particularly true for complex molecules like proteins or polymers.

Orientation of proteins/peptides on surface is relevant for applications where biological recognition events are involved. Indeed, protein/peptide orientations are crucial since recognition sites can be blocked due to inappropriate protein orientation on surface. This can drastically decrease the signal-to-noise ratio (and consequently degrade the limit-of-detection) of the derived biosensor or biomedical diagnostic device, for example. A first step in this direction was put forward by Ye et al. only recently (Ye et al., 2010). Using amide I SFG signal, they observed peptide orientation variations according to protein deposition method. Indeed, differences were noticed between physically adsorbed and chemically immobilised peptides regarding its orientation.

5. SFG as a biosensor technique

The analysis and information obtained using SFG on proteins/peptides using C-H, N-H and amide I vibrational modes have been described and its importance for biosensor revealed. Further, as only molecular groups in proteins/peptides at interfaces that have a net organisation will contribute to the measured SFG signal, it is expected to be an excellent probe to identify the side chains involved in biomolecular recognition events. Indeed, surface interactions can introduce significant ordering in the binding regions of proteins/peptides. However, in order to be applied to biosensors and/or biomedical diagnostic devices, biomolecular recognition should also be detected by SFG spectroscopy.

This was first highlighted by Dreesen et al. in 2004 (Dreesen et al., 2004a, 2004b). Indeed, the authors were interested in the vibrational information of an adsorbed derivated vitamin (biocytin) on diverse substrates (Au, Pt, Ag and CaF_2) and its subsequent recognition by a protein (avidin). The SFG signal (obtained in the total internal reflection configuration) in

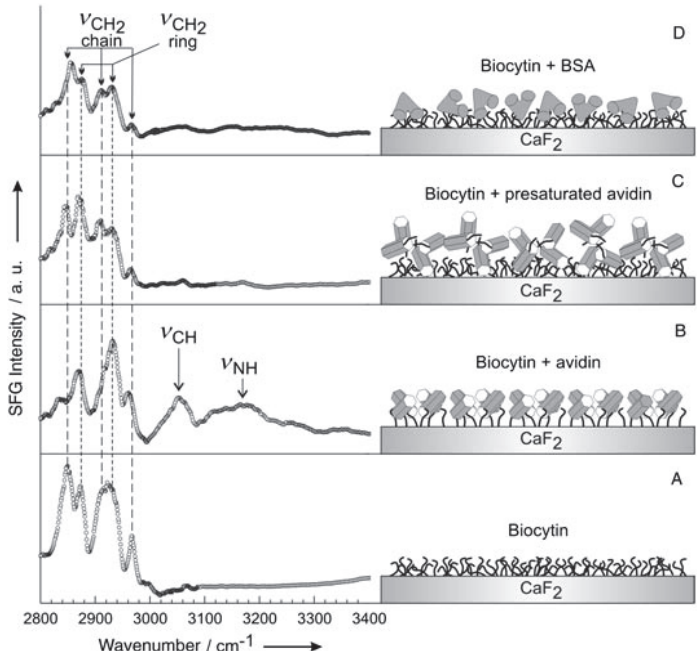

Fig. 4. SFG spectra of biocytin layers adsorbed on CaF_2 substrates (a) before and (b) after contacting with avidin solution, (c) presaturated avidin solution and (d) BSA solutions. Reprinted from Ref (Dreesen et al., 2004b), Copyright 2004, with permission from Elsevier.

the C-H vibrational range of the biocytin layer revealed, despite some structural gauche defects, that the adsorbed layer presents an organisation relatively similar to usual self-assembled monolayers of alkanethiols on gold surfaces (Dreesen et al., 2006a; Sartenaer et al., 2007). The biocytin layer only exhibits the SFG fingerprints of CH_2 groups included into the molecular backbone (CH_2 chain) and to the ureido ring (CH_2 ring). When comparing the SFG spectra of the biocytin layer alone to the (biocytin + avidin) layer, important changes were observed: (1) only CH_2 ring peaks are visible (CH_2 chain peaks are drastically reduced); (2) two signals in the 3000 - 3300 cm^{-1} region appear. The disappearance of CH_2 chain peaks was explained by a reorganisation of biocytin conformation after avidin binding.

The most interesting feature demonstrating the biomolecular recognition between biocytin and avidin are the appearance of two peaks in the 3000 - 3300 cm^{-1} region. Although an unambiguous attribution of those peaks is difficult, the authors' results demonstrated that the SFG signal observed is due to the interaction between both biological species. Indeed, complementary measurements were performed in order to address the specificity of the molecular recognition highlighted by the SFG signals observed: (1) immersing a biocytin layer in avidin solution presaturated with biotin (preventing recognition events between avidin in solution and the biocytin layer on surface); (2) immersing a biocytin layer in a BSA solution (for which no molecular recognition can occur with biocytin). The resulting SFG spectra recorded are similar to biocytin layers without spectral features associated to recognition events (i.e. in the 3000 – 3300 cm^{-1} range) (Dreesen et al. 2004b).

Further, a new experimental setup, developed by Tourillon et al. (Tourillon et al., 2007, 2009), allowed to significantly enhance the SFG signal recorded, compared to usual external reflection configuration. Their concept was first demonstrated on self-assembled monolayers (SAMs) of alkanethiol (Tourillon et al., 2007). Indeed, authors first compared the SFG intensity on dodecanethiol SAMs adsorbed on a dense gold nanoparticle array in an external reflection and in a total internal reflection (TIR) configuration. Both exhibited clear SFG spectra but the TIR-SFG configuration presented intensities by one order of magnitude higher than external reflection configuration. This enhanced intensity SFG configuration was further applied to the recognition of biocytin molecules by avidin proteins (Tourillon et al., 2009). Again, they observed an excellent signal-to-noise as well as a high signal-to-background ratio. TIR-SFG spectrum of biocytinilated thiols adsorbed on the nanoparticles array only exhibit mainly CH bonds attached to the tetrahydrothiophene ring, CH_2 and a Fermi resonance-enhanced overtone of the 1550 cm^{-1} band coming from amide II entities. These observations highlight a well ordered SAMs on gold nanoparticle surfaces. After immersing the sample in an avidin solution, drastic changes in TIR-SFG spectra were observed. The 2882 cm^{-1}, 2942 cm^{-1} and 2975 cm^{-1} peaks intensities greatly decreased and were associated to a reorganisation of the biocytinilated thiol layer in order to match the bonding pocket of avidin proteins. Oppositely, the 3079 cm^{-1} band intensity increased while the 2859 cm^{-1} peak was mainly unchanged. This indicates the molecular chains of the biocytinilated thiols remain unmodified and that only the apex biotin ring has to change its orientation for the recognition with avidin binding pocket. Finally, as previously tested, supplementary experiments were performed in order to address the specificity of the molecular recognition highlighted by the SFG. These recent results can lead to the emergence of a new label-free detection system for biosensor applications.

6. Conclusion

In this review, the recent experimental and theoretical developments in sum-frequency generation spectroscopy analysis of proteins and peptides adsorbed on surfaces were detailed. Our goal was to demonstrate the applicability and usefulness of such nonlinear optical spectroscopic technique to biological science and biotechnology.

Indeed, during the last 6 years, SFG spectroscopy was shown to be able to record the vibrational signature of biomolecule thin films through signals from protein –CH vibrations, allowing the determination of the "hydrophobic" or "hydrophilic" conformation of adsorbed proteins/peptides. The modification of surface structure and/or protein conformation was revealed as well. The N-H vibration mode (~ 3300 cm^{-1}) was also identified and appropriate peak attribution performed. Moreover, the amide I band of proteins was observed. This spectroscopic range is very interesting as it allows to identify (using adequate modelling) the presence, conformation and orientation distribution of some functional groups, but also of protein secondary structures (i.e. α-helix, β-sheets and turns). It allows to infer the overall protein orientation/conformation as well.

Based on such considerations, it can be reasonably assumed that recognition events between complementary biomolecules could also be detected, introducing SFG spectroscopy into the biosensor world. This exciting perspective was recently developed (Dreesen et al., 2004b; Tourillon et al., 2009) in unambiguously identifying the SFG fingerprint of molecular recognition events between biocytin molecules and avidin proteins.

This constitutes the basis for new developments of SFG spectroscopy in biotechnology. Indeed, in biosensor devices, the relationship between protein orientation and molecular recognition can for example now be determined on a wide range of substrates in a wide range of environments. The effects of the surface properties, environmental conditions, protein immobilisation procedures… could easily be related in situ to protein orientation and protein activity (recognition) only by using SFG spectroscopy. Further in biomedical devices, deeper understanding of the properties of materials biocompatibility can be inferred by analysing protein changes, conformation, orientation and activity once adsorbed on surfaces.

7. Acknowledgments

Y. Caudano and A. Peremans are respectively research associate and research director of the Belgian Fund for Scientific Research F.R.S.-FNRS. C. Volcke aknowledges the Walloon Region for financial support.

8. References

Aoyagi, S.; Rouleau, A.; and Boireau, W. (2008a). TOF-SIMS structural characterization of self-assembly monolayer of cytochrome *b5* onto gold substrate. *Appl. Surf. Sci.*, Vol. 255, No 4, (2008), pp 1071-1074, ISSN 0169-4332.

Aoyagi, S.; Okada, K.; Shigyo, A.; Man, N.; and Karen, A. (2008b). Evaluation of oriented lysozyme immobilized with monoclonal antibody. *Appl. Surf. Sci.*, Vol. 255, No 4, (2008), pp 1096-1099, , ISSN 0169-4332.

Aoyagi, S.; and Inoue, M. (2009). An orientation analysis method for protein immobilized on quantum dot particles. *Appl. Surf. Sci.*, Vol. 256, No 4, (2009), pp 995-997, ISSN 0169-4332.

Araci, Z.O.; Runge, A.F.; Doherty III, W.J.; and Saavedra, S.S. (2008). Correlating molecular orientation distributions and electrochemical kinetics in subpopulations of an immobilized protein film. *J. Am. Chem. Soc.*, Vol. 130, No 5, (2008), pp 1572-1573, ISSN: 0002-7863.

Baugh, L.; Weidner, T.; Baio, J.E.; Nguyen, P.-C.T.; Gamble, L.J.; Stayton, P.S.; and Castner, D.G. (2010). Probing the Orientation of Surface-Immobilized Protein G B1 Using ToF-SIMS, Sum Frequency Generation, and NEXAFS Spectroscopy. *Langmuir*, Vol. 26, No 21, (2010), pp 16434-16441, ISSN: 0743-7463.

Belu, A.M.; Graham, D.J.; and Castner, D.G. (2003). Time-of-flight secondary ion mass spectrometry: techniques and applications for the characterization of biomaterial surfaces. *Biomaterials*, Vol. 24, No 21, (2003), pp 3635-3653, ISSN 0142-9612.

Boughton, A.P.; Andricioaei, I.; and Chen, Z. (2010). Surface orientation of magainin 2: Molecular dynamics simulation and sum frequency generation vibrational spectroscopic studies. *Langmuir*, Vol. 26, No 20, (2010), pp 16031-16036, ISSN 0743-7463.

Brady, D.; and Jordaan, J. (2009). Advances in enzyme immobilisation. *Biotechnol. Lett.*, Vol. 31, No 11, (2009), pp 1639-1650, ISSN 0141-5492.

Buck, M.; and Himmelhaus, M. (2001). Vibrational spectroscopy of interfaces by infrared-visible sum frequency generation. *J. Vac. Sci. Technol. A*, Vol. 19, No 6, (2001), pp 2717-2736, ISSN 0734-2101.

Cecchet, F; Lis, D.; Guthmuller, J.; Champagne, B; Caudano, Y. ; Silien, C. ; Mani, A.A. ; Thiry, P.A.; and Peremans, A. (2010a). Orientational analysis of dodecanethiol and p-nitrothiophenol SAMs on metals with polarisation-dependent SFG spectroscopy. *ChemPhysChem*, Vol. 11, No 3, (2010), pp 607-615. ISSN 1439-7641.

Cecchet, F; Lis, D.; Guthmuller, J.; Champagne, B; Fonder, G.; Mekhalif, Z.; Caudano, Y. ; Mani, A.A. ; Thiry, P.A.; and Peremans, A. (2010b). Theoretical calculations and experimental measurements of the vibrational response of p-NTP SAMs: An orientational analysis. *J. Phys. Chem. C*, Vol. 114, No 9, (2010), pp 4106-4113.

Chen, X.; Wang, J.; Sniadecki, J.J.; Even, M.A.; and Chen, Z. (2005a). Probing α-helical and β-sheet structures of peptides at solid/liquid interfaces with SFG. *Langmuir*, Vol. 21, No 7, (2005), pp 2662-2664. ISSN 0743-7463.

Chen, X.; Clarke, M.L.; Wang, J.; and Chen, Z. (2005b). Sum frequency generation vibrational spectroscopy studies on molecular conformation and orientation of biological molecules at interfaces. *Int. J. Mod. Phys. B*, Vol. 19, No 4, (2005), pp 691-713, ISSN 0217-9792.

Chen, X.; Wang, J.; Boughton, A.; Kristalyn, C.B.; and Chen, Z. (2007). Multiple orientation of melittin inside a single lipid bilayer determined by combined vibrational spectroscopic studies. *J. Am. Chem. Soc.*, Vol. 129, No 5, (2007), pp 1420-1427, ISSN: 0002-7863.

Chen, X.; Hua, W.; Huang, Z.; and Allen, H.C. (2010). Interfacial water structure associated with phospholipid membranes studied by phase-sensitive vibrational sum frequency generation spectroscopy. *J. Am. Chem. Soc.*, Vol. 132, No 32, (2010), pp 11336-11342, ISSN: 0002-7863.

Chen, Z.; Shen, Y.R.; and Somorjai, G.A. (2002). Studies of polymer surfaces by sum frequency generation vibrational spectroscopy. *Ann. Rev. Phys. Chem.*, Vol. 53, (2002), pp 437-465, ISSN 0066-426X.

Chen, Z. (2007a). Understanding surfaces and buried interfaces of polymer materials at the molecular level using sum frequency generation vibrational spectroscopy. *Polym. Int.*, Vol. 56, No 5, (2007), pp 577-587, ISSN 1097-0126.

Cheng, X.; Canavan, H.E.; Graham, D.J.; Castner, D.G.; and Ratner, B.D. (2006). Temperature dependent activity and structure of adsorbed proteins on plasma polymerized *N*-isopropyl acrylamide. *Biointerphases*, Vol. 1, No 1, (2006), pp 61-72, ISSN 1934-8630.

Clarke, M.L.; Wang, J.; and Chen, Z. (2005). Conformational changes of fibrinogen after adsorption. *J. Phys. Chem. B*, Vol. 109, No 46, (2005), pp 22027-22035, ISSN 1520-6106.

Clarke, M.L.; and Chen, Z. (2006). Polymer surface reorientation after protein adsorption. *Langmuir*, Vol. 22, No 21, (2006), pp 8627-8630, ISSN 0743-7463.

Dreesen, L.; Humbert, C.; Sartenaer, Y.; Caudano, Y.; Volcke, C.; Mani, A.A.; Peremans, A.; Thiry, P.A.; Hanique, S.; and Frère, J.-M. (2004a). Electronic and molecular properties of an adsorbed protein monolayer probed by two-color sum-frequency generation spectroscopy. *Langmuir*, Vol 20, No 17, (2004), pp 7201-7207, ISSN 0743-7463.

Dreesen, L.; Sartenaer, Y.; Humbert, C.; Mani, A.A.; Lemaire, J.-J.; Methivier, C.; Pradier, C.-M.; Thiry, P.A.; and Peremans, A. (2004b). Sum-frequency generation spectroscopy applied to model biosensors systems. *Thin Solid Films*, Vol. 464-465, (2004), pp 373-378, ISSN 0040-6090.

Dreesen, L.; Volcke, C.; Sartenaer, Y.; Peremans, A.; Thiry, P.A.; Humbert, C.; Grugier, J.; and Marchand-Brynaert, J. (2006a). Comparative study of decyl thiocyanate and decanethiol self-assembled monolayers on gold substrates. *Surf. Sci.*, Vol. 600, No 18, (2006), pp 4052-4057, ISSN 0039-6028.

Dreesen, L.; Silien, C.; Volcke, C.; Sartenaer, Y.; Thiry, P.A.; Peremans, A.; Grugier, J.; Marchand-Brynaert, J.; Brans, A.; Grubisic, S.; and Joris, B. (2007). Adsorption Properties of the Penicillin Derivative DTPA on Gold Substrates. *ChemPhysChem*, Vol. 8, No 7, (2007), pp 1071-1076, ISSN 1439-7641.

Edmiston, P.L.; Lee, J.E.; Cheng S.-S.; and Saavedra, S.S. (1997). Molecular orientation distributions in protein films. 1. Cytochrome c adsorbed to surfaces of variable surface chemistry. *J. Am. Chem. Soc.*, Vol. 119, No 3, (1997), pp 560-570, ISSN: 0002-7863.

Ekblad, T.; and Liedberg, B. (2010). Protein adsorption and surface patterning. *Curr. Op. Coll. Interf. Sci.*, Vol. 15, No 6, (2010), pp 499-509, ISSN 1359-0294.

Frasconi, M.; Mazzei, F.; and Ferri, T. (2010). Protein immobilization at gold-thiol surfaces and potential for biosensing. *Anal. Bioanal. Chem.*, Vol. 398, No 4, (2010), pp 1545-1564, ISSN 1618-2642.

Gandhiraman, R.P.; Volcke, C.; Gubala, V.; Doyle, C.; Basabe-Desmonts, L.; Dotzler, C.; Toney, M.; Iacono, M.; Nooney, R.; Daniels, S.; James, B.; and Williams, D.E. (2009). High efficiency amine functionalization of cycloolefin polymer surfaces for biodiagnostics. *J. Mater. Chem.*, Vol. 20, No 20, (2009), pp 4116-4127, ISSN 0959-9428.

Gandhiraman, R.P.; Muniyappa, M.K.; Dudek, M.M.; Coyle, C.; Volcke, C.; Burham, P.; Daniels, S.; Barron, N.; Clynes, M.; and Cameron, D. (2010). Interaction of plasma deposited HMDSO based coatings with fibrinogen and human blood plasma: the correlation between bulk plasma, surface characteristics and biomolecule interaction. *Plasma Process. Polym.*, Vol. 77, No 5, (2010), pp 4111-421, ISSN 1612-8869.

Gandhiraman, R.P.; Gubala, V.; Nam, L.C.H.; Volcke, C.; Doyle, C.; James, B.; Daniels, S.; and Williams, D.E. (2010b). Deposition of chemically reactive and repellent sites on biosensor chips for reduced non-specific binding. *Coll. Surf. B-Biointerfaces*, Vol. 79, No 1, (2010), pp 270-275, ISSN 0927-7765.

Grosserueschkamp, M.; Friedrich, M.C.; Plum, M.; Knoll, W.; and Naumann, R.L.C. (2009). Electron transfer kinetics of cytochrome c probed by time-resolved surface enhanced resonance Raman spectroscopy. *J. Phys. Chem. B*, Vol. 113, No 8, (2009), pp 2492-2497, ISSN 1520-6106.

Gubala, V.; Gandhiraman, R.P.; Volcke, C.; Doyle, C.; Coyle, C.; James, B.; Daniels, S.; and Williams, D.E. (2010). Functionalization of cyclo olefin polymer surfaces by plasma-enhanced chemical vapour deposition: Comprehensive characterization and analysis of the contact surface and the bulk of aminosiloxane coatings. *Analyst*, Vol. 135, No 6, (2010), pp 1375-1381, ISSN 0003-2654.

Himmelhaus, M.; Eisert, F.; Buck, M.; and Grunze, M. (2000). Self-assembly of n-alkanethiol monolayers: A study by IR-visible sum frequency spectroscopy. *J. Phys. Chem. B*, Vol. 104, No 3, (2000), pp 576-584, ISSN 1520-6106.

Humbert, C.; Volcke, C.; Sartenaer, Y.; Peremans, A.; Thiry, P.A.; and Dreesen, L. (2006). Molecular conformation and electronic properties of protoporphyrin-IX self-assembled monolayers adsorbed on a Pt(111) surface. *Surf. Sci.*, Vol. 600, No 18, (2006), pp 370-3709, ISSN 0039-6028.

Humbert, C.; Busson, B.; Six, C.; Gayral, A.; Gruselle, M.; Villain, F.; and Tadjeddine, A. (2008). Sum-frequency generation as a vibrational and electronic probe of the electrochemical interface and thin films. *J. Electroanal. Chem.*, Vol. 621, No 2, (2008), pp 314-321, ISSN 1572-6657.

Howell, C.; Diesner, M.-O.; Grunze, M.; Koelsch, P. (2008). Probing the extracellular matrix with sum-frequency-generation spectroscopy. *Langmuir*, Vol. 24, No 24, (2008), pp 13819-13821, ISSN 0743-7463.

Ji, N.; Ostroverkhov, V.; Chen, C.Y.; and Shen, Y.R. (2007). Phase-sensitive sum-frequency vibrational spectroscopy and its application to studies of interfacial alkyl chains. *J. Am. Chem. Soc.*, Vol. 129, No 33, (2007), pp 10056-10057, ISSN: 0002-7863.

Ji, N.; Ostroverkhov, V.; Tian, C.S.; and Shen, Y.R. (2008). Characterization of vibrational resonances of water-vapor interfaces by phase-sensitive sum-frequency spectroscopy. *Phys. Rev. Lett.*, Vol. 100, No 9, (2008), p 096102 (4 pages) , ISSN 0031-9007.

Jung, S.Y.; Lim, S.-M.; Albertorio, F.; Kim, G.; Gurau, M.C.; Yang, R.D.; Holden, M.A.; and Cremer, P.S. (2003). The Vroman Effect: A molecular level description of fibrinogen displacement. *J. Am. Chem. Soc.*, Vol. 125, No 42, (2003), pp 12782-12786, ISSN: 0002-7863.

Keating, C.D.; Kovaleski, K.M.; Natan, M.J. (1998). Protein:colloid conjugates for surface enhanced Raman scattering: stability and control of protein orientation. *J. Phys. Chem. B*, Vol. 102, No 47, (1998), pp 9404-9413, ISSN 1520-6106.

Kett, P.J.; Casford, M.T.L.; and Davies, P.B. (2010). Sum frequency generation (SFG) vibrational spectroscopy of planar phosphatidylethanolamine hybrid bilayer membranes under water. *Langmuir*, Vol. 26, No 12, (2010), pp 9710-9719, ISSN 0743-7463.

Kidoaki, S.; and Matsuda, T. (2002). Mechanistic aspects of protein/material interactions probed by atomic force microscopy. *Colloids Surfaces B: Biointerfaces*, Vol. 23, No 2-3, (2002), pp 153-163, ISSN 0927-7765.

Kim, G.; Gurau, M.; Kim, J.; and Cremer, P.S. (2002). Investigations of lysozyme adsorption at the air/water and quartz/water interfaces by vibrational sum frequency spectroscopy. *Langmuir*, vol. 18, No 7 (2002), pp 2807-2811, ISSN 0743-7463.

Kim, J.; Koffas, T.S.; Lawrence, C.C.; and Somorjai, G.A. (2004). Surface structural characterization of protein- and polymer-modified polystyrene microspheres by infrared-visible sum frequency generation vibrational spectroscopy and scanning force microscopy. *Langmuir*, Vol. 20, No 11, (2004), pp 4640-4646, ISSN 0743-7463.

Koffas, T.S.; Kim, J.; Lawrence, C.C.; and Somorjai, G.A. (2003). Detection of immobilized protein on latex microspheres by IR-visible sum frequency generation and scanning force microscopy. *Langmuir*, Vol. 19, No 9, (2003), pp 3563-3566, ISSN 0743-7463.

Kubota, J.; and Domen, K. (2007). Study of the dynamics of surface molecules by time-resolved sum frequency generation spectroscopy. *Anal. Bioanal. Chem.*, Vol. 388, No 1, (2007), pp 17-27, ISSN 1618-2642.

Kudelski, A. (2005). Characterization of thiolate-based mono- and bilayers by vibrational spectroscopy: A review. *Vibr. Spectr.*, Vol. 39, No 2, (2005), pp 200-213, ISSN 0924-2031.

Lambert, A.G.; Davies, P.B.; and Neivandt, D.J. (2005). Implementing the theory of sum frequency generation vibrational spectroscopy: A tutorial review. *Appl. Spectr. Rev.*, Vol. 40, No 2, (2005), pp 103-145, ISSN 0570-4928.

Lin, S.H.; Hayashi, M.; Lin, C.H.; Yu, J.; Villaeys, A.A.; and Wu, G.Y.C. (1995). Theoretical-studies of IR-UV sum-frequency generation applied to adsorbed molecules. *Mol. Phys.*, Vol. 84, No 3 (1995), pp 453-468. ISSN: 0026-8976.

Liu, F.; Dubey, M.; Takahashi, H.; Castner, D.G., and Grainger, D.W. (2010). Immobilized Antibody Orientation Analysis Using Secondary Ion Mass Spectrometry and Fluorescence Imaging of Affinity-Generated Patterns. *Anal. Chem.*, Vol. 82, No 7, (2010), pp 2947-1958, ISSN 0003-2700.

MacDonald, I.D.G.; and Smith, W.E. (1996). Orientation of cytochrome c adsorbed on a citrate-reduced silver colloid surface. *Langmuir*, Vol. 12, No 3, (1996), pp 706-713, ISSN 0743-7463.

Mani, A.A.; Schultz, Z.D.; Champagne, B.; Humbert, C.; Dreesen, L.; Gewirth, A.A.; White, J.O.; Thiry, P.A.; Peremans, A.; and Caudano, Y. (2004a). Molecule orientation in self-assembled monolayers determined by infrared-visible sum-frequency generation spectroscopy. *Appl. Surf. Sci.*, Vol. 237, No 1-4, (2004), pp 444-449, ISSN 0169-4332.

Mani, A.A.; Schultz, Z.D.; Caudano, Y.; Champagne, B.; Humbert, C.; Dreesen, L.; Gewirth, A.A.; White, J.O.; Thiry, P.A.; and Peremans, A. (2004b). Orientation of thiophenol adsorbed on silver determined by nonlinear vibrational spectroscopy of the carbon skeleton. *J. Phys. Chem. B*, Vol. 108, No 41 (2004), pp 16135-16138, ISSN 1520-6106.

Mermut, O.; Phillips, D.C.; York, R.L.; McCrea, K.R.; Ward, R.S.; and Somorjai, G.A. (2006). In situ adsorption studies of a 14-amino acid leucine-lysine peptide onto hydrophobic polystyrene and hydrophilic silica surfaces using quartz crystal microbalance, atomic force microscopy, and sum frequency generation vibrational spectroscopy. *J. Am. Chem. Soc.*, Vol. 128, No 11, (2006), pp 3598-3607, ISSN: 0002-7863.

Nakanishi, K.; Sakiyama, T.; and Imamura, K. (2001). On the adsorption of proteins on solid surfaces, a common but very complicated phenomenon. *J. Biosc. Bioengin.*, Vol. 91, No 3 (2001), pp 233-244, ISSN 1389-1723.

Nguyen, K.T.; King, J.T.; and Chen, Z. (2010). Orientation determination of interfacial β-sheet structures in situ. *J. Phys. Chem. B*, Vol. 114, No 25, (2010), pp 8291-8300, ISSN 1520-6106.

Okada, K.; Aoyagi, S.; Dohi, M.; Kato, N.; Kudo, M.; Tozu, M.; Miyayama, T.; and Sanada, N. (2008). Evaluation of immobilized-lysozyme by means of TOF-SIMS. *Appl. Surf. Sci.*, Vol. 255, No 4, (2008) pp 1104-1106, ISSN 0169-4332.

Ostroverkhov, V.; Waychunas, G.A.; and Shen, Y.R. (2005). New information on water interfacial structure revealed by phase-sensitive surface spectroscopy. *Phys. Rev. Lett.*, Vol. 94, No 4, (2005), p 046102 (4 pages) , ISSN 0031-9007.

Paszti, Z.; Wang, J.; Clarke, M.L.; and Chen, Z. (2004). Sum frequency generation vibrational spectroscopy studies of protein adsorption on oxide-covered Ti surfaces. *J. Phys. Chem. B*, Vol. 108, No 23, (2004), pp 7779-7787, ISSN 1520-6106.

Pohle, W.; Saβ, M.; Selle, C.; Wolfrum, K.; and Lobau, J. (1999). Probing phospholipid chain fluidity by vibrational spectroscopy including sum-frequency generation. *Vibr. Spectr.*, Vol. 19, No 2, (1999), pp 321-327, ISSN 0924-2031.

Phillips, D.C.; York, R.L.; Mermut, O.; McCrea, K.R.; Ward, R.S.; and Somorjai, G.A. (2007). Side chain, chain length, and sequence effects on amphiphilic peptide adsorption at hydrophobic and hydrophilic surfaces studied by sum-frequency generation vibrational spectroscopy and quartz crystal microbalance. *J. Phys. Chem. C*, Vol. 111, No 1, (2007), pp 255-261, ISSN 1932-7447.

Rao, A.; Rangwalla, H.; Varshney, V.; and Dhinojwala, A. (2004). Structure of poly(methyl methacrylate) chains adsorbed on sapphire probed using infrared-visible sum frequency generation spectroscopy. *Langmuir*, Vol. 20, No 17, (2004), pp 7183-7188, ISSN 0743-7463.

Rocha-Mendoza, I.; Yankelevich, D.R.; Wang, M.; Reiser, K.M.; Frank, C.W.; and Knoesen, A. (2007). Sum frequency vibrational spectroscopy: The molecular origin of the optical second-order nonlinearity of collagen. *Biophys. J.*, Vol. 93, No 12, (2007), pp 4433-4444, ISSN 0006-3495.

Sartenaer, Y.; Dreesen, L.; Humbert, C.; Volcke, C.; Tourillon, G.; Louette, P.; Thiry, P.A.; and Peremans, A. (2007). Adsorption properties of decyl thiocyanate and decanethiol on platinum substrates studied by sum-frequency generation spectroscopy. *Surf. Sci.*, Vol. 601, No 5, (2007), pp 1259-1264, ISSN 0039-6028.

Shen, Y.R. (1984). The principles of nonlinear optics, John Wiley & Sons, New York, USA, ISBN 0-471-88998-9.

Shen, Y.R. (1989). Surface properties probed by second-harmonic and sum-frequency generation. *Nature*, Vol. 337, No 6207 (1989), pp 519-525, ISSN 0028-0836.

Shen, Y.R. (1999). Surfaces probed by nonlinear optics. *Surf. Sci.*, Vol. 299/300, No (1994), pp 551-562, ISSN 0039-6028.

Singh, B. R. (2000). *Infrared Analysis of Peptides and Proteins Principles and Applications*; ACS Symposium Series 750; Oxford University Press: Washington, DC, 2000, ISBN 9780841236363.

Sonois, V.; Bacsa, W.; and Faller, P. (2009). Intense Raman bands and low luminescence of thin films of heme proteins on silica. *Chem. Phys. Lett.*, Vol. 48, No 1-3, (2009), pp 66-69, 009-2614.

Stutz, H. (2009). Protein attachment onto silica surfaces – A survey of molecular fundamentals, resulting effects and novel preventive strategies in CE. *Electrophoresis*, Vol. 30, No 12 (2009), pp 2032-2061. ISSN: 0173-0835.

Tadjeddine, A.; Peremans, A.; and Guyot-Sionnest, P. (1995). Vibrational spectroscopy of the electrochemical interface by visible-infrared sum-frequency generation. *Surf. Sci.*, Vol. 335, No 1-3, (1995), pp 210-220, ISSN 0039-6028.

Tadjeddine, A.; and Peremans, A. (1998). Non linear optical spectroscopy of the electrochemical interface. *Advances in Spectroscopy*, Collection Spectroscopy for Surface Science, Vol 26 (1998), pp 159-217, ISSN 0892-2888.

Tourillon, G.; Dreesen, L.; Volcke, C.; Sartenaer, Y.; Thiry, P.A.; and Peremans, A. (2007) Total internal reflection sum-frequency generation spectroscopy and dense gold nanoparticles monolayer: a route for probing adsorbed molecules. *Nanotechnology*, Vol. 18, No 41, (2007), p 415301 (7pp), ISSN 0957-4484.

Tourillon, G.; Dreesen, L.; Volcke, C.; Sartenaer, Y.; Thiry, P.A.; and Peremans, A. (2009). Close-packed array of gold nanoparticles and sum frequency generation spectroscopy in total internal reflection: a platform for studying biomolecules and biosensors. *J. Mater. Sci.*, Vol. 44, No 24, (2009), pp 6805-6810, ISSN 0022-2461.

Vidal, F.; and Tadjeddine, A. (2005). Sum-frequency generation spectroscopy of interfaces. *Rep. Progr. Phys.*, Vol. 68, No 5, (2005), pp 1095-1127. ISSN 0034-4885.

Wagner, M.S.; Horbett, T.A.; and Castner, D.G. (2003). Characterization of the structure of binary and ternary adsorbed protein films using electron spectroscopy for chemically analysis, time-of-flight secondary ion mass spectrometry, and radiolabeling. *Langmuir*, Vol. 19, No 5, (2003), pp 1708-1715, ISSN 0743-7463.

Wagner, M.S.; and Castner, D.G. (2004). Analysis of adsorbed proteins by static time-of-flight secondary ion mass spectrometry. *Appl. Surf. Sci.*, Vol. 231-232, (2004), pp 366-376, ISSN 0169-4332.

Wang, H.; Castner, D.G.; Ratner, B.D.; and Jiang, S. (2004). Probing the Orientation of Surface-Immobilized Immunoglobulin G by Time-of-Flight Secondary Ion Mass Spectrometry. *Langmuir*, Vol. 20, No 5, (2004), pp 1877-1887, ISSN 0743-7463.

Wang, H.F.; Gan, W.; Lu, R.; Rao, Y.; and Wu, B.H. (2005). Quantitative spectral and orientational analysis in surface sum frequency generation vibrational spectroscopy (SFG-VS). *Int. Rev. Phys. Chem.*, Vol. 24, No 2, (2005), pp 191-256, ISSN 0144-235X.

Wang, J.; Buck, S.M.; and Chen, Z. (2002a). Sum frequency generation vibrational spectroscopy studies on protein adsorption. *J. Phys. Chem. B*, Vol. 106, No 44, (2002), pp 11666-11672, ISSN 1520-6106.

Wang, J.; Buck, S.M.; Even, M.A.; and Chen, Z. (2002b). Molecular response of proteins at different interfacial environments detected by sum frequency generation vibrational spectroscopy. *J. Am. Chem. Soc.*, Vol. 124, No 44, (2002), pp 13302-13305, ISSN: 0002-7863.

Wang, J.; Clarke, M.L.; Zhang, Y.; Chen, X.; and Chen, Z. (2003a). Using isotope-labeled proteins and sum frequency generation vibrational spectroscopy to study protein adsorption. *Langmuir*, Vol. 19, No 19, (2003), pp 7862-7866, ISSN 0743-7463.

Wang, J.; Even, M.A.; Chen, X.; Schmaier, A.H.; Waite, J.H.; and Chen, Z. (2003b). Detection of amide I signals of interfacial proteins in situ using SFG. *J. Am. Chem. Soc.*, Vol. 125, No 33, (2003), pp 9914-9915, ISSN: 0002-7863.

Wang, J.; Paszti, Z.; Even, M.A.; and Chen, Z. (2004a). Interpretation of sum frequency generation vibrational spectra of interfacial proteins by the Thin Film Model. *J. Phys. Chem. B*, Vol. 108, No 11, (2004), pp 3625-3632, ISSN 1520-6106.

Wang, J.; Clarke, M.L.; and Chen, Z. (2004b). Polarization mapping: A method to improve sum frequency generation spectral analysis. *Anal. Chem.*, Vol. 76, No 8, (2004), pp 2159-2167, ISSN 0003-2700.

Wang, J.; Clarke, M.L.; Chen, X.; Even, M.A.; Johnson, W.C.; and Chen, Z. (2005). Molecular studies on protein conformations at polymer/liquid interfaces using sum frequency generation vibrational spectroscopy. *Surf. Sci.*, Vol. 587, No 1-2, (2005), pp 1-11, ISSN 0039-6028.

Wang, J.; Chen, X.; Clarke, M.L.; and Chen, Z. (2006). Vibrational spectroscopic studies on fibrinogen adsorption at polystyrene/protein solution interfaces: hydrophobic side chain and secondary structure changes. *J. Phys. Chem. B*, Vol. 110, No 10, (2006), pp 5017-5024, ISSN 1520-6106.

Wang, J.; Paszti, Z.; Clarke, M.L.; Chen, X.; Chen, Z. (2007). Deduction of structural information of interfacial proteins by combined vibrational spectroscopic methods. *J. Phys. Chem. B*, Vol. 111, No 21, (2007), pp 6088-6095, ISSN 1520-6106.

Watanabe, N.; Yamamoto, H.; Wad a, A.; Domen, K.; Hirose, C.; Ohtake, T.; and Mino, N. (1994). Vibrational sum-frequency generation (VSFG) spectra of n-alkyltrichlorosilanes chemisorbed on quartz plate. *Spectrochem. Acta Part A: Mol. Spectr.*, Vol. 50, No 8-9 (1994), pp 1529-1537, ISSN 1386-1425.

Weidner, T.; Breen, N.F.; Drobny, G.P.; and Castner, D.G. (2009). Amide or amide: Determining the origin of the 3300 cm^{-1} NH mode in protein SFG spectra using ^{15}N isotope labels. *J. Phys. Chem. B*, Vol. 113, No 47, (2009), pp 15423-15426, ISSN 1520-6106.

Weidner, T.; Apte, J.S.; Gamble, L.J.; and Castner, D.G. (2010). Probing the orientation and conformation of α-helix and β-strand model peptides on self-assembled monolayers using sum frequency generation and NEXAFS spectroscopy. *Langmuir*, Vol. 26, No 5, (2010), pp 3433-3440, ISSN 0743-7463.

Williams, C.T.; and Beattie, D.A. (2002). Probing buried interfaces with non-linear optical spectroscopy. *Surf. Sci.*, Vol 500, No 1-3 (2002), pp 545-576, ISSN 0039-6028.

Xia, N.; May, C.J.; McArthur, S.L.; and Castner, D.G. (2002). Time-of-flight secondary ion mass spectrometry analysis of conformational changes in adsorbed protein films. *Langmuir*, Vol. 18, No 10, (2002), pp 4090-4097, ISSN 0743-7463.

Xu, H.; Zhao, X.; Lu, J.R.; and Williams, D.E. (2007). Relationship between the structural conformation of monoclonal antibody layers and antigen binding capacity. *Biomacromol.*, Vol. 8, No 8, (2007), pp 2422-2428, ISSN 1525-7797.

Ye, S.; Nguyen, K.T.; Le Clair, S.V.; and Chen, Z. (2009). In situ molecular level studies on membrane related peptides and proteins in real time using sum frequency generation spectroscopy. *J. Struct. Biol.*, Vol. 168, No 1, (2009) pp 61-77, ISSN 1047-8477.

Ye, S. Nguyen, K.T. Boughton, A.P. Mello, C.M. Chen, Z. (2010). Orientation difference of chemically immobilized and physically adsorbed biological molecules on polymers detected at the solid/liquid interfaces in situ. *Langmuir*, Vol. 26, No 9, (2010), pp 6471-6477, ISSN 0743-7463.

Yeganeh, M.S.; Dougal, S.M.; Polizzotti, R.S.; and Rabinowitz, P. (1995). Interfacial atomic structure of a self-assembled alkyl thiol monolayer on Au(111) – A sum-frequency generation study. *Phys. Rev. Lett.*, Vol. 74, No 10, (1995), pp 1811-1814, ISSN 0031-9007.

York, R.L.; Mermut, O.; Phillips, D.C.; McCrea, K.R.; Ward, R.S.; and Somorjai, G.A. (2007). Influence of ionic strength on the adsorption of a model peptide on hydrophilic

silica and hydrophobic polystyrene surfaces: Insight from SFG vibrational spectroscopy. *J. Phys. Chem. C*, Vol. 111, No 25, (2007), pp 8866-8871, ISSN 1932-7447.

Yu, Q.; and Golden, G. (2007). Probing the protein orientation on charged self-assembled monolayers on gold nanohole arrays by SERS. *Langmuir*, Vo. 23, No 17, (2007), pp 8659-8662, ISSN 0743-7463.

Zheng, D.S.; Wang, Y.; Liu, A.A.; and Wang, H.F. (2008). Microscopic molecular optics theory of surface second harmonic generation and sum-frequency generation spectroscopy based on the discrete dipole lattice model. *Int. Rev. Phys. Chem.*, Vol. 27, No 4, (2008), pp 629-664, ISSN 0144-235X.

5

How to Make FRET Biosensors for Rab Family GTPases

Nanako Ishido, Hotaka Kobayashi, Yasushi Sako, Takao Arai, Mitsunori Fukuda and Takeshi Nakamura
Tokyo University of Science; Tohoku University; RIKEN Japan

1. Introduction

Genetically-encoded Förster resonance energy transfer (FRET) biosensors enable us to visualize a variety of signaling events, such as protein phosphorylation and G protein activation in living cells (Miyawaki, 2003). Using FRET-based biosensors we can obtain spatiotemporal information on the changes in activity of signaling molecules in living cells. From this viewpoint, FRET imaging of signaling molecules that regulate membrane traffic is one of the most suitable applications of this technique. The Rab family GTPases constitute the largest branch of the Ras GTPase superfamily. Rab GTPases use the guanine nucleotide-dependent switch mechanism common to the Ras superfamily to regulate each of the four major steps in membrane trafficking: vesicle budding, vesicle delivery, vesicle tethering, and fusion of the vesicle membrane with that of the target compartment (Zerial and McBride, 2001; Grosshans et al., 2006; Stenmark, 2009). Recently, we developed a FRET sensor for Rab5, and demonstrated that live-cell imaging with FRET sensors enables us to pinpoint the activation and inactivation of Rab5, and thereby to understand its relationship with other events linked to vesicle transport (Kitano et al., 2008).
In the first half of this chapter, we describe step-by-step strategies to develop unimolecular-type FRET biosensors for Rab family GTPases. We use the development of a Rab35 sensor as an example. Although improvements to FRET sensors are still made on a trial-and-error basis, we provide practical tips for their optimization. In the second half of this chapter, we introduce FRET imaging with total internal reflection fluorescence (TIRF) microscopy. TIRF microscopy is particularly well suited to visualize the dynamics of molecules and events near the plasma membrane (Mattheyses et al., 2010). We have used FRET imaging with TIRF microscopy to show that the activity of TC10, a Rho family GTPase, at tethered vesicles drops immediately before vesicle fusion in HeLa cells stimulated with epidermal growth factor (EGF) (Kawase et al., 2006). We describe how to set up and use TIRF-FRET to visualize local changes in GTPase activity on vesicles during membrane fusion.

2. Unimolecular FRET sensors

2.1 Overview of FRET biosensors

FRET is a process by which a fluorophore (donor) in an excited state transfers its energy to a neighboring fluorophore (acceptor) non-radiatively (Tsien and Miyawaki, 1998; Pollok and

Heim, 1999). Although an understanding of the physical principles underlying FRET is not necessarily required for biological experiments, researchers who try to develop and/or use FRET sensors must note that FRET depends on a proper spectral overlap between the donor and the acceptor, the distance between both fluorophores, and their relative orientation. The physical principles underlying FRET have been extensively reviewed elsewhere (Periasamy and Day, 1999; Jares-Erijman and Jovin, 2003).

2.2 Advantages of unimolecular FRET sensors

In general, green fluorescent protein (GFP)-based FRET sensors are classified into two types: bimolecular and unimolecular sensors (Miyawaki, 2003; Kurokawa et al., 2004). For bimolecular sensors, donor (CFP) and acceptor (YFP) are fused to protein A (e.g., the sensor domain) and protein B (e.g., the detector domain), respectively (Fig. 1a). In this case, protein

(a) Bimolecular sensor, in which YFP and CFP are fused to protein A and protein B, respectively. Upon stimulation, the association of proteins A and B brings YFP in close proximity to CFP, and FRET occurs. (b) Unimolecular sensor, in which protein A and protein B are 'sandwiched' between YFP and CFP.

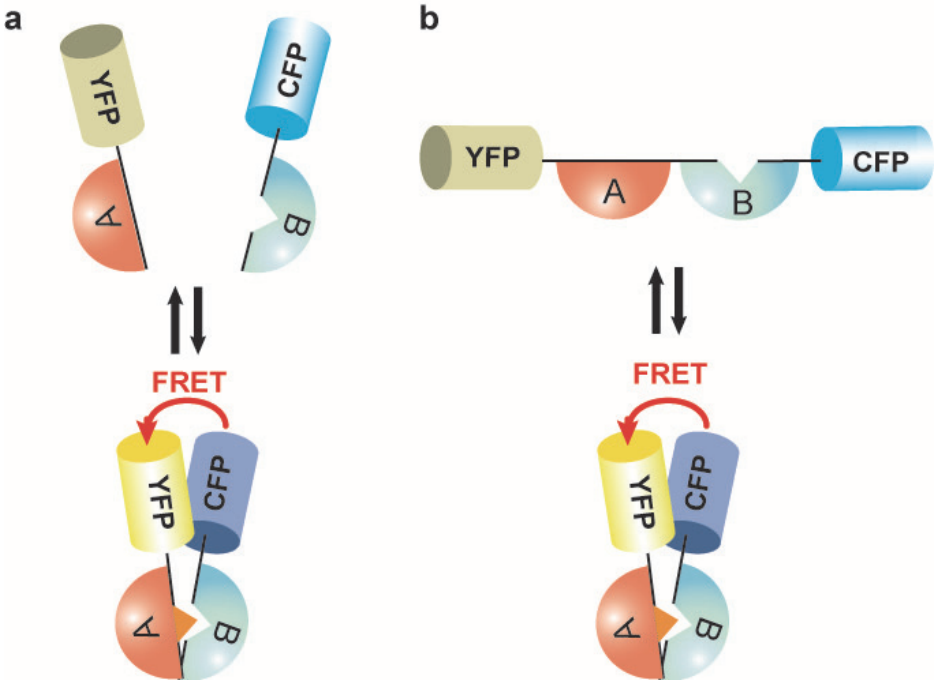

Fig. 1. Two types of FRET biosensors

A changes its conformation following stimulation. Then, protein A binds to protein B and FRET occurs. The change in distance between the fluorophores is critically important for bimolecular sensors (Fig. 1a). In contrast, for unimolecular sensors, all four modules are combined into a single chain (Fig. 1b). Also for unimolecular sensors, protein A changes its conformation following stimulation. Then, protein A binds to protein B and FRET occurs.

However, the change in distance between both fluorophores is not so large, as shown in Fig. 1b. Thus, developers of unimolecular sensors have to consider how to induce a large change in relative orientation between the fluorophores. At present, it is almost impossible to design retionally an optimal structure for a particular unimolecular sensor, and therefore its design is still labor-intensive (described in detail below).

Nevertheless, in our opinion, if good sensors are available, it is preferable to use a unimolecular sensor. This is because with a unimolecular sensor protein A and protein B are placed in close proximity, and thus, protein B can easily find protein A. This will increase the percentage of real FRET signals *versus* undesired signals arising from donor emission bleedthrough and direct acceptor excitation (Hailey et al., 2002; Kurokawa et al., 2004). Furthermore, perturbation of endogenous signaling is reduced when using a unimolecular sensor instead of a bimolecular sensor (Miyawaki, 2003). An additional drawback of bimolecular sensors is that it is difficult to conrol their expression levels, because the ideal molecular ratio of YFP-protein A and CFP-protein B is 1:1 for quantitative FRET imaging.

It should be noted that, from a general point of view, the suitable applications for bimolecular and unimolecular sensors are different. Thus, in practice, the type of sensors is chosen based on the aim of the experiment. In the case of monitoring an interaction between protein A and protein B, it is natural to select a bimolecular sensor. Correction of FRET signals obtained with a bimolecular sensor is elaborate but attainable (Kraynov et al., 2000; Sekar and Periasamy, 2003). Unimolecular sensors are preferable for visualizing changes in the activity of a protein, pH, Ca^{2+} concentration, *etc.*.

3. How to make FRET biosensors for Rab family GTPases

3.1 Raichu sensors

Unimolecular FRET sensors, which can visualize the 'on' and 'off' states of Ras GTPase superfamily proteins, were first developed in Matsuda's laboratory and are collectively designated "Ras and interacting protein chimaeric unit (Raichu)" sensors (Mochizuki et al., 2001). Similar FRET sensors for Ras GTPase superfamily proteins have been reported by other groups (Pertz et al., 2006).

Raichu sensors comprise four modules: a donor (CFP), an acceptor (YFP), a GTPase and the GTPase-binding domain of its binding partner. In the Raichu sensors for Ras family GTPases, YFP, the GTPase, the GTPase-binding domain, and CFP are sequentially connected from the N-terminus by spacers (Mochizuki et al., 2001). In the inactive GDP-bound form of the GTPase, CFP and YFP in the sensor are located at a distance from each other, mostly resulting in emission from CFP. Upon stimulation, GDP on the GTPase is exchanged for GTP, which induces an interaction between the GTP-bound GTPase and the GTPase-binding domain. This intramolecular binding brings CFP close to YFP, thereby permitting energy transfer from CFP to YFP. FRET is simultaneously manifested by a quenching of CFP fluorescence and an increase in YFP fluorescence; therefore, the YFP/CFP ratio of Raichu sensors is conveniently used as a representation of FRET efficiency. Previous experiments have shown that the YFP/CFP ratio of a Raichu sensor correlates with the GTP/GDP ratio (Mochizuki et al., 2001; Yoshizaki et al., 2003). Raichu sensors for Ras family GTPases (Ras, Rap1, Ral, R-Ras) (Mochizuki et al., 2001; Takaya et al., 2004; Takaya et al., 2007), Rho family GTPases (RhoA, Rac1, Cdc42, TC10)(Itoh et al., 2002; Yoshizaki et al., 2003), and Rab family GTPase (Rab5) (Kitano et al., 2008) have been published to date.

3.2 FRET imaging using Raichu-Rab5

Rab5 is a key regulator of a broad range of early endocytic pathway components (Zerial and McBride, 2001) including apoptotic cell engulfment (Nakaya et al., 2006). However, the precise spatio-temporal dynamics of Rab5 activity during endocytosis remain unknown. To make Rab5 activity visible in living cells, we developed a FRET biosensor for Rab5, Raichu-Rab5 (Fig. 2a). The difference between Raichu sensors for Ras and Rho GTPases and Raichu-Rab5 is the order of the four modules that constitute the FRET sensors. In the case of Raichu-Rab5, we placed Rab5 at the C-terminus, because the *in vivo* lipid modification of Rab5 requires access of Rab5-bound Rab escort protein (REP) to the lipid modification site of Rab5 located at the C-terminus of the FRET sensor. We confirmed that Raichu-Rab5 colocalized with red fluorescent protein (RFP)-Rab5 and bound to Rab guanine dissociation inhibitor (a) Schematic representation of Raichu-Rab5 bound to GDP or GTP. RBD indicates the N-terminal Rab5-binding domain of early endosome antigen 1 (EEA1). (b) $\alpha_v\beta_3$ integrin-expressing Swiss3T3 cells were transfected with pRaichu-Rab5/PM and co-cultured with apoptotic thymocytes in the presence of MFG-E8. Thereafter, images were obtained every 1 min. The top panels show PC and FRET/CFP ratio images at the indicated time-points (min). In the intensity-modulated display mode shown here, eight colors from red to blue are used to represent the FRET/CFP ratio, with the intensity of each color indicating the mean intensity of FRET and CFP. The upper and lower limits of the ratio range are shown at the bottom. Time sequences in the bottom panels show the PC, FRET/CFP ratio, and CFP images of the engulfed sites marked by white squares in the top panels. Scale bar: 20 μm. Figure reproduced with permission from Nature Publishing Group (Kitano et al., 2008).
(RabGDI). The dynamic range, *i.e.*, the percentage increase in the YFP/CFP ratio, of Raichu-Rab5 is 96%; thus, Raichu-Rab5 has the widest dynamic range among the Raichu biosensors that have been reported thus far.

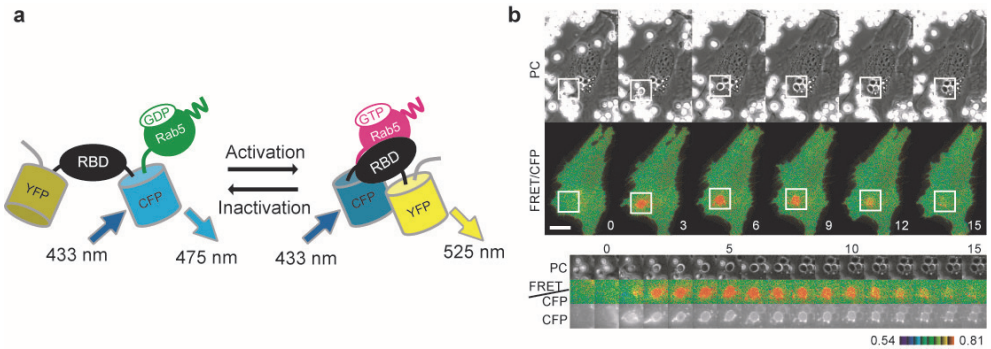

Fig. 2. FRET imaging using Raichu-Rab5

Using Raichu-Rab5 fused to the C-terminus of K-Ras protein (Raichu-Rab5/PM), we visualized Rab5 activation during milk fat globule epidermal growth factor 8 (MFG-E8)-mediated engulfment of apoptotic cells by Swiss3T3 cells stably-expressing integrin $\alpha_v\beta_3$ (Fig. 2b). The progress of phagocytosis was monitored by phase-contrast (PC) images, in which the completion of engulfment was recognizable by the transition of the engulfed apoptotic cells from phase-bright to phase-dark (Diakonova et al., 2002). We set the zero time-point to be the frame immediately before the initiation of the phase shift, which lasted

approximately 3 minutes on average. Rab5 activation started during this period of phase shift and reached a peak within an average of 4 minutes. Very similar results were obtained in the macrophage cell line, BAM3.
Visualization of the activation and inactivation of Rab5 on phagosomes has enabled us to understand its relationship with other events during phagocytosis. Engulfment of apoptotic cells and accumulation of actin filaments around nascent phagosomes preceded Rab5 activation, which occurred in parallel with actin disassembly. Microtubules were required for Rab5 activation on phagosomes, suggesting that the actin coat around the phagosome behaves as a physical barrier to microtubule extension. This view was supported by the finding that Gepex-5, which was located at microtubule tips through binding to EB1, was responsible for Rab5 activation on phagosomes.

3.3 Development of Raichu-Rab35

3.3.1 Overview of Rab35

Rab35, whose transcripts are apparently ubiquitously expressed (Zhu et al., 1994), bears the closest homology with yeast Ypt1p and mammalian Rab1a and Rab1b, which function in endoplasmic reticulum-Golgi transport. However, Rab35 does not show an endoplasmic reticulum-Golgi localization. Endogenous Rab35 in HeLa cells is found mainly at the plasma membrane and in the cytosol, with labeling of intracellular endosomal structures identifiable at the ultrastructural level (Kouranti et al., 2006).
Recent analyses in different systems have revealed an amazingly diverse array of Rab35 functions (Table 1). Acting in the context of endosomal trafficking and recycling, Rab35 has been shown to regulate cytokinesis of *Drosophila* S2 cells and HeLa cells (Kouranti et al., 2006), oocyte receptor recycling in *Caenorhabditis elegans* (Sato et al., 2008), and Ca^{2+} activated potassium channel recycling (Gao et. al., 2010). In immune cells, Rab35 is implicated in T-cell receptor recycling, immunological synapse formation (Patino-Lopez et al., 2008), and major histocompatibility complex (MHC) class II molecule recycling (Walseng et al., 2008). Connecdenn/DENND1A, a guanine nucleotide exchange factor (GEF) for Rab35, plays a role in synaptic vesicle endocytosis/recycling (Allaire et al., 2006) and cargo-specific exit from early endosomes (Allaire et al., 2010).
Another facet of Rab35's function is the promotion of cellular protrusions. In baby hamster kidney (BHK) cells, overexpression of wild type or a constitutively active mutant of Rab35 induced the formation of long cell extensions, while the GDP-locked mutant of Rab35 constitutively active mutant of Rab35 also induced neurite outgrowth in N1E-115 and PC12 cells (Chevallier et al., 2009; Kanno et al., 2009). Expression of wild-type Rab35 in S2 cells induced filopodia-like cellular extensions, a process that was blocked with an inhibitor of actin polymerization (Zhang et al., 2009). The authors claimed that Rab35 controls actin bundling. Very recently, Rab35 has been reported to regulate exosome secretion in oligodendrocytes. These authors suggested that Rab35 might function in docking or tethering (Hsu et al., 2010)
Key questions in the understanding of the wide range of Rab35 functions are (i) what exactly is the role of Rab35 in recycling endosome-cell surface transport, and (ii) how does its function intersect with that of Rab11? The membrane localization patterns of Rab35 and Rab11 show a large degree of overlap. It also appears that Rab35 and Rab11's gross membrane traffic functions overlap substantially, and manipulation of their activities affects common recycling cargos such as the transferrin receptor (Chua et al., 2010). One scenario is

Function	Animal/Cell	Reference
endosomal trafficking and recycling		
cytokinesis	*Drosophila* S2 cells, HeLa cells	Kouranti et al. (2006)
transferrin recycling	HeLa cells	Kouranti et al. (2006)
synaptic vesicle recycling	hippocampal neurons	Allaire et al. (2006, 2010)
york receptor recycling	*C. elegans*	Sato et al. (2008)
T cell receptor recycling	Jurkat cells	Patino-Lopez et al. (2008)
MHC-II recycling	HeLa cells expressing MHC-II	Walseng et al. (2008)
immunological synapse formation	Jurkat and Raji cells	Yuseff et al. (2009)
Ca^{2+}-activated K channel recycling	HEK and HMEC-1 cells	Gao et al. (2010)
peripheral protrusion formation	BHK cells	Chavallier et al. (2009)
neurite outgrowth	N1E-115 and PC12 cells	Chavallier et al. (2009)
bristle formation	*Drosophila*	Zhang et al. (2009)
exosome secretion	Oli-neu cells	Hsu et al. (2010)

Table 1. The broad range of functions of Rab35

that Rab11 and Rab35 function sequentially in recycling endosomes to plasma membrane transport, similarly to the Rab11 to Rab8 pathway in AMPA receptor trafficking in dendritic spines (Brown et al., 2007). On the other hand, transport carried from recycling endosomes could require both Rab11 and Rab35 in proportions determined by the types of membrane cargo in a cell type specific, or cell physiology-dependent manner. Defining the pathways and factors involved in Rab11 and Rab35 functions in different endocytic recycling systems is clearly of immediate interest. Furthermore, we emphasized that FRET imaging is the most suitable and reliable tool to examine local activity regulation in these dynamic systems.

3.3.2 A practical guide to making FRET biosensors for Rab family GTPases

The following is an abridged procedure for developing Raichu-type FRET sensors for Rab GTPases essentially based on the protocol to make Raichu sensors for Ras and Rho GTPases (Nakamura et al., 2006; Nakamura and Matsuda, 2009; Kiyokawa et al., 2011).

Design of a candidate sensor

As described above, it is almost impossible to design rationally an optimal structure for a desired unimolecular sensor. Thus, at first, developers should identify as many proteins as possible that bind to the target Rab in a GTP-dependent manner. Empirically, we like to collect three to five binding proteins that have different affinities for the target Rab protein. The developers should also collect informations about the protein motifs required for the binding.

One way to make a sensor with a wide dynamic range is to search for a GTPase-binding domain that has a moderate affinity for the GTPase (Yoshizaki et al., 2003). One explanation for this is that the GTPase-binding domain competes with the GTPase activating proteins (GAPs) in cells (Kurokawa et al., 2004). Strong inhibition of GAPs would lead to a relatively high GTP level in the sensor, even in the unstimulated state, which may cause a narrowing of the dynamic range.

Crystallographic data for the GTPase and GTPase-binding domain can help to determine the minimum regions to incorporate into the sensor. Unfortunately, there is currently insufficient crystallographic data for the optimal design of a Raichu sensor in most cases. Therefore, trying various lengths of the GTPase and GTPase-binding domain is highly recommended. In addition, various sequential combinations of the four modules (YFP, CFP, GTPase, and GTPase-binding domain) should be tested. YFP is usually located before CFP because an excess of the acceptor (YFP) does not greatly decrease the signal-to-noise ratio, even when translation of the sensor is prematurely terminated. Eleven amino acids at the C-terminus of GFP can be truncated without affecting its fluorescence profile. In most Raichu sensors, we have removed the 11 C-terminal residues of YFP, hoping to reduce the flexibility between YFP and the subsequent module. The length and sequence of the spacers are also critical. If the FRET efficiency of a prototype sensor changes to some extent upon activation, the possibility of further improvement by changing the spacer should be considered. As spacers, we usually use one to six repeats of the sequence Gly-Gly-Ser-Gly-Gly; however, we intend to reexamine this in a future. It is considered that Gly provides flexibility, while Ser prevents aggregation of peptide chains. Misfolding of CFP occasionally occurs, and this can sometimes be rectified by modifying the spacer before the CFP.

If developers obtain a candidate sensor whose dynamic range is broad enough, the next step is further optimization. At present, the principle of this optimization step is a matter of debate. Recently, Nagai's group reported two strategies for sensor optimization (Kotera et al., 2010). They claim that the balance between the enhancement of dimerization and the maintenance of free dissociation is critical; among the *Aequorea* fluorescent protein variants they examined, those with alanine at 206 most closely matched the requirements. Kotera and collegues also claimed that developers should note the relative orientation of the fluorescent proteins. For the fluorescent proteins to dimerize, they must be bound in an antiparallel configuration. Because wildtype GFP has both N- and C-termini in close proximity, at least in the crystal (Palm et al., 1997), simple fusion of fluorescent proteins with a short linker will not result in antiparallel dimerization. Nagai's group presumed that the effectiveness of circular permutation (cp) mutants in several FRET sensors, such as yellow cameleon 3.6 (Nagai et al., 2004), might come from the ease of dimerization of fluorescent proteins in an antiparallel configuration.

The ideal location for a sensor in a cell has also been a matter of debate. The most persuasive idea is that the sensor should be colocalized with the endogenous protein; for this purpose, the GTPase's own CAAX-box should be added to the C-terminus of the sensor. As described for Raichu-Rab5, it is necessary to place Rab protein at the C-terminus because *in vivo* lipid modification of Rab requires access by Rab-bound REP to the lipid modification site of the Rab protein located at the C-terminus of the FRET sensor. Alternatively, addition of the CAAX-box of K-Ras4B to the C-terminus enables the sensor to be located at the plasma membrane; this approach mostly yields a high signal-to-noise ratio, especially when only a limited fraction of the GTPase is activated upon stimulation. If a fraction of the target Rab protein resides in the plasma membrane and is expected to change its activity there upon stimulation, this type of FRET sensor might be useful as shown for Raichu-Rab5.

Characterization of candidate sensors

We usually transfect candidate sensors into the FreeStyle 293-F cell line (Invitrogen), which is a variant of the 293 cell line adapted for suspension growth. Following a 2-day incubation, the cell culture is poured into 3-ml cuvettes and the cuvettes are placed in a

spectrophotometer (for example, a JASCO FP-6200). Next, we illuminate the cell culture with an excitation wavelength of 433 nm, and obtain a fluorescence spectrum from 450 nm to 550 nm. The background is subtracted using the spectrum of the mock-transfected cell culture.

If developers do not use 293-F cells, 293T cells plated on 100-mm collagen-coated dishes should be transfected with candidate sensors, and cell lysates prepared according to a standard procedure should be used for fluorescence spectrometry (Nakamura and Matsuda, 2009).

For characterizing a candidate sensor, we introduce a constitutively active or inactive mutation into the GTPase in the sensor for comparison with the same sensor containing the wild-type GTPase. Alternatively, we co-transfect the candidate sensor with a GEF or GAP for the GTPase, and compare the spectrum with those of samples transfected with the sensor alone. Under our criteria, Raichu-type sensors are considered suitable for FRET imaging when the dynamic range exceeds 30%.

Practically, further evaluation of a sensor is recommended before widespead use. We recommend that developers check the following: (i) whether the sensor shows a linear correlation between its GTP loading and FRET efficiency upon cotransfection with various quantities of GEFs or GAPs and (ii) whether the sensor and its endogenous counterpart show comparable responses to physiological stimulations when examined by biochemical methods.

3.3.3 Example: development of Raichu-Rab35

To make Rab35 activity visible in living cells, we developed FRET sensors, designated Raichu-Rab35s. We used centaurinβ2 (Kanno et al., 2010) and Rab35BP2 (Kobayashi et al., submitted) for the Rab35 effector proteins. We constructed sensors based on either the basic structure of Raichu-Rab5 containing m1Venus and m1SECFP as fluorescent proteins (Kitano et al., 2008) or the newly-developed design in Matsuda's laboratory (Komatsu et al., unpublished) containing YPet (Nguyen and Daugherty, 2005) and SECFP.

In the initial tests, Raichu-A011 showed the broadest dynamic range over 30% (Table 2). However, the FRET/CFP ratio of the sensor containing wild-type Rab35 is almost similar to that of the sensor containing Rab35-Q67L, suggesting that Raichu-A011 might be almost insensitive to Rab35GEF. The dynamic range of Raichu-A018 was relatively high (24.3%) and the cellular localization of Raichu-A018 resembled that of EGFP-Rab35. As shown in the left panel of Fig. 3, Raichu-A018 is expected to respond to both GEFs and GAPs.

Although the dynamic range of Raichu-A008 and Raichu-A015 was promisingly broad, the FRET/CFP ratio of the sensor containing Rab35-S22N was higher than that of the sensor containing Rab35-Q67L. Based on our experience, we tentatively excluded these two candidates because sensors with these characteristics cannot generally respond to GEFs and GAPs. At this stage, we thought that Rab35BP2 might be more suitable than centaurinβ2 as an effector protein. Thus, in the next step, we prepared candidate sensors containing Rab35BP2-RBD.

Next, we tried two approaches. First, we used the minimal Rab35-binding domain, Rab35BP2-RBDΔC2, which was identified during the course of Raichu-Rab35 development. Second, we replaced YPet with cp mutants of Venus to change the relative orientation of the fluorescent proteins. As a result, we obtained two more promising candidate sensors: Raichu-A033 and Raichu-A050. Raichu-A033 has a remarkably broad dynamic range

Sensor name	Basic design	Binding domain	Yellow FP	Dynamic range
Raichu-A008	Raichu-Rab5 type	centaurinβ2-RBD	m1Venus	-22.5%
Raichu-A011	Raichu-Rab5 type	Rab35BP2-RBD	m1Venus	33.7%
Raichu-A015	Long-linker type	centaurinβ2-RBD	YPet-M	-23.3%
Raichu-A018	Long-linker type	Rab35BP2-RBD	YPet-M	24.3%
Raichu-A030	Raichu-Rab5 type	Rab35BP2-RBD-ΔC2	m1Venus	21.6%
Raichu-A033	Long-linker type	Rab35BP2-RBD-ΔC2	YPet-M	92.7%
Raichu-A036	Long-linker type	Rab35BP2-RBD	cp195Venus	24.8%
Raichu-A039	Long-linker type	Rab35BP2-RBD	cp173Venus	16.9%
Raichu-A047	Long-linker type	Rab35BP2-RBD-ΔC2	cp195Venus	41.1%
Raichu-A050	Long-linker type	Rab35BP2-RBD-ΔC2	cp173Venus	37.0%

Table 2. Summary of candidate FRET sensors for Rab35

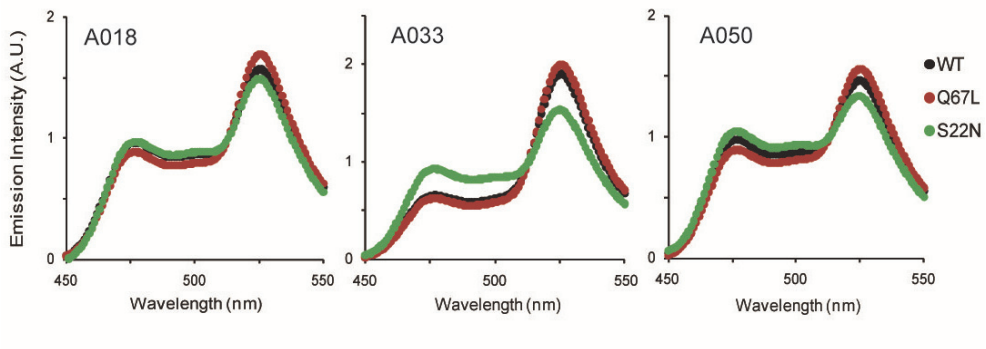

Fig. 3. Emission spectra of Raichu-Rab35s

Sensor name	Binding domain	Yellow FP	Dynamic range	Presumed property
Raichu-A018	Rab35BP2-RBD	YPet-M	24.3%	highly sensitive to GEF
Raichu-A033	Rab35BP2-RBD-ΔC2	YPet-M	92.7%	highly sensitive to GAP
Raichu-A050	Rab35BP2-RBD-ΔC2	cp195Venus	37.0%	sensitive to GEF and GAP

Table 3. Summary of FRET sensors for Rab35

(92.7%), which is comparable to that of Raichu-Rab5 described above. However, as shown in Fig. 3, the FRET/CFP ratio of this sensor containing wild-type Rab35 is very similar to that of the sensor containing Rab35-Q67L, suggesting that Raichu-A033 might be somewhat insensitive to Rab35GEF (Fig. 3, middle). For the other candidate, Raichu-A050, the dynamic range is sufficiently high (37.0%) and it is expected to respond to both GEFs and GAPs (Fig. 3, right), although its cellular localization is somewhat different from that of EGFP-Rab35. Table 3 shows a summary of the features of our newly developed Rab35 sensors. We believe that different Rab35 sensors may suit different situations.
293-F cells expressing Raichu-A018, A033, and A050 were excited at 433 nm and a fluorescent spectrum from 450 nm to 550 nm was obtained. WT, Q67L, and S22N denote wild-type, constitutively active mutant, and GDP-locked mutant, respectively.

4. How to use the TIRF-FRET system

4.1 General considerations

TIRF microscopy provides a means to excite fluorophores selectively near the adherent cell surface while minimizing fluorescence from intracellular regions. TIRF primarily illuminates only fluorophores very near (*i.e.*, within 100 nm of) the cover slip–sample interface. Background fluorescence is minimized because excitation of fluorophores further away from the cover slip is drastically reduced. For this reason, TIRF has been employed to address numerous questions regarding the dynamics of the cytoskeleton or intracellular signaling near the plasma membrane, endocytosis, exocytosis, and cell–substrate contacts (Mattheyses et al., 2010).
Several studies using FRET imaging under TIRF microscopy have been reported since 2003. However, all of these studies have used bimolecular FRET sensors to investigate protein–protein interaction (Bal et al., 2008; Lam et al., 2010) or cAMP signaling (Dyachok et al., 2006). In 2006, we reported FRET imaging using the unimolecular sensor Raichu–TC10 under TIRF microscopy during EGF-induced exocytosis (Kawase et al., 2006). To our knowledge, this was the first report of TIRF imaging using a unimolecular FRET sensor.

4.2 Visualization of GTP hydrolysis of TC10 during exocytosis using TIRF-FRET system

TC10, a Rho-family GTPase, plays a significant role in the exocytosis of GLUT4 (Chiang et al., 2001; Saltiel and Pessin, 2002) and other proteins (Cuadra et al., 2004; Cheng et al., 2005). Furthermore, TC10 is mainly localized to vesicular structures (Michaelson et al., 2001), which makes it suitable for monitoring activity changes on vesicles. In Kawase et al. (2006), we reported visualization of GTP hydrolysis of TC10 immediately before vesicle fusion, using a combination of a newly developed unimolecular FRET sensor, Raichu-TC10, and TIRF microscopy (Fig. 4). We postulated that hydrolysis of GTP-TC10 triggers vesicle fusion. In support of this model, a GTPase-deficient TC10 mutant potently inhibited EGF-induced vesicular fusion in HeLa cells and depolarization-induced secretion of neuropeptide Y in PC12 cells. Our study also indicated that GTP-TC10 is indispensable for loading its binding partners onto vesicles, and for the delivery of vesicles to target membranes. Thus, TC10 could play roles in three separate steps of exocytosis: loading of the cargo, tethering to the plasma membrane, and triggering vesicle fusion. Of note, both GTP-loading and GTP

hydrolysis of TC10 play important roles and occur simultaneously in different subcellular compartments. Therefore, functional imaging of GTPases using FRET-based sensors is very powerful for the analysis of parallel events within the same cell.

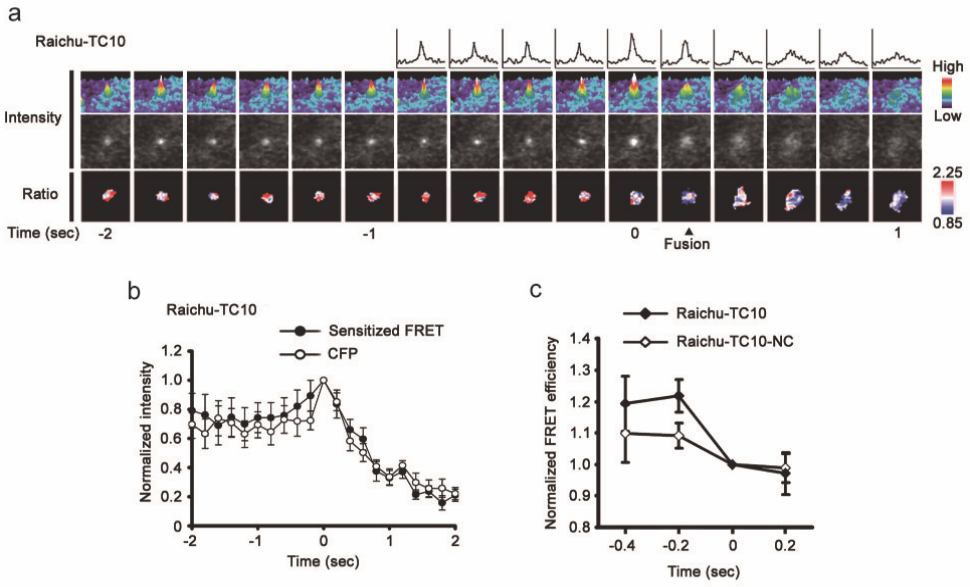

Fig. 4. GTP hydrolysis of TC10 immediately before fusion

(a) Sensitized FRET intensity and ratio images of Raichu-TC10 in fusing vesicles obtained by TIRF microscopy. The first and second rows show plots of the sensitized FRET intensity scanned across the center of the fusing vesicles, and pseudocolored 3D-plots of the sensitized FRET intensity, respectively. (b) Time-course of normalized sensitized FRET and CFP intensities of vesicles containing Raichu-TC10. (c) Time-dependent changes in the normalized FRET efficiency of Raichu-TC10- or Raichu-TC10-NC- (a negative control)-expressing vesicles. The bars in (b,c) are SEM (Raichu-TC10, n = 8; Raichu-TC10-NC, n = 11). Reprinted from Developmental Cell, Vol. 11, Kawase, Nakamura, Takaya, Aoki, Namikawa, Kiyama, Inagaki, Takemoto, Saltiel, and Matsuda, "GTP hydrolysis by the Rho family GTPase TC10 promotes exocytic vesicle fusion", 411–421, ©2006, with permission from Elsevier.

4.3 Setting up of a TIRF-FRET system

Although many researchers use 'home-made' TIRF set-ups, commercial TIRF systems are available from major microscopy companies (Olympus, Nikon, Zeiss, and Leica). These systems have the same fundamental ability to deliver a through-the-objective TIRF illumination and can be used to obtain TIRF-FRET images. Prism-based TIRF has several benefits, including lower cost and a clearer evanescent field; however most cell biologists use a through-the-objective TIRF system, because it is more user-friendly, requiring minimal maintenance and alignment.

One important requirement in through-the-objective TIRF is the use of high numerical aperture (NA) objectives. The NA of an objective describes its light-gathering power and also describes the maximum angle at which the excitation light can emerge from the objective. Therefore, the NA of the objective must be greater than the refractive index of the sample, preferable by a substantial margin. There are several commercial TIRF objectives with an NA greater than 1.4. The most common TIRF objectives are 1.45 NA and 1.49 NA, and both are available in 60× and 100× options.

There is a wide range of charge-coupled device (CCD) cameras from conventional CCDs to electron-multiplying (EM) CCDs. For TIRF-FRET imaging in the field of membrane traffic, EMCCDs are strongly recommended because rapid imaging in very low light situations is required. In addition, an image splitter, which allows simultaneous acquisition of emission from two spectrally distinct fluorophores, offers great benefit in obtaining FRET from moving vesicles. However, users should note that the image splitter can cause a problem, known as a misregistration, when generating FRET images.

In TIRF-FRET imaging using Raichu-TC10, we used an Olympus IX70 inverted microscope equipped with a 442-nm HeCd laser (Omnichrome), a TIRF illuminator (Olympus), and an Olympus 100x objective (NA 1.45). The CFP and sensitized images were obtained simultaneously using an image splitter (Dual-View; Optical Insights) and an EMCCD camera (iXon DV887; Andor) as shown in Fig. 5.

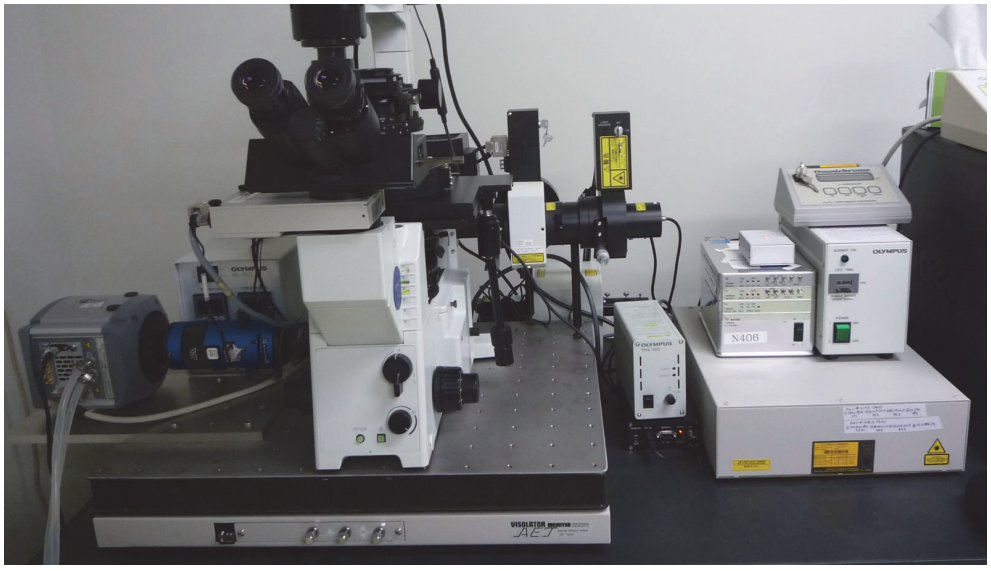

Fig. 5. One example of a TIRF-FRET system

Commercially available TIRF microscopes use one-sided laser illumination. However, in this method, the interference patterns of lasers sometimes reduce the quality of the image. Furthermore, the concave shape of cells and anisotropic cellular structures might reduce the image quality. These issues can be overcome by illumination from several directions using multiple beams or a circular laser beam (Sako, 2006).

4.4 Image acquisition

TIRF-FRET imaging is conducted similarly to conventional FRET imaging (Nakamura and Matsuda, 2009). In the case of Raichu-TC10 imaging (Fig. 4), plasmids encoding Raichu-TC10 were transfected into HeLa cells plated on glass-bottomed dishes. After 24 h, the cells were starved for 3 h and then stimulated with 50 ng/ml of EGF. The FRET efficiency (sensitized FRET/CFP ratio) in the subcellular compartments was determined as follows. For vesicles and perinuclear compartments, regions showing higher CFP intensity than an appropriate threshold level were selected, and their sensitized FRET and CFP intensities were obtained. For the plasma membrane, three appropriate regions were selected manually and the averages of their sensitized FRET and CFP intensities were obtained. Images were obtained in a stream (free-run) mode using MetaMorph software (Universal Imaging); stacked images containing 500 planes were continually acquired with a 200-ms exposure.

The most common problem with TIRF microscopy is contamination of the image with propagating light (Matteyses et al., 2010). The most likely reason for this is an improperly aligned excitation source. This will be readily recognized as a field that is half in and half out of TIRF, or the complete inability to obtain TIRF. The excitation laser beam must be focused on the back focal plane of the objective. If this is not the case, light will emerge from the objective at multiple angles. It is important to follow the manufacturer's instructions to check and correct the focus onto the back focal plane.

4.5 Image analysis

Images obtained during vesicular fusion (Kawase et al., 2006) were analyzed using MetaMorph software according to Tsuboi et al. (2004), with some modifications. Image analysis is described in detail in Fig. 6.

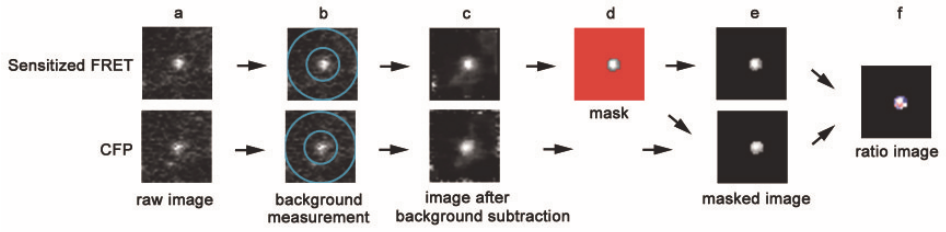

Fig. 6. Method of image processing to obtain ratio images of FRET sensors in vesicles obtained by TIRF microscopy

Single exocytotic events were selected manually, and vesicular fusion was distinguished from vesicle retreat as described previously (Fix et al., 2004). The fusing vesicle was centerd in the image (Fig. 6a). The local background was determined as the average fluorescence of the region between two concentric rings with diameters of 2 μm (inner) and 5 μm (outer) (Fig. 6b). This background was subtracted from a raw image (Fig. 6c). Next, in the sensitized FRET image, the threshold value appropriate for extracting vesicles was determined manually (Fig. 6d). This threshold mask was applied to both the sensitized FRET and the CFP images (Fig. 6e). Finally, a ratio image was obtained by dividing the sensitized FRET image by the CFP image (Fig. 6f). Reprinted from Developmental Cell, Vol. 11, Kawase, Nakamura, Takaya, Aoki, Namikawa, Kiyama, Inagaki, Takemoto, Saltiel, and Matsuda,

"GTP hydrolysis by the Rho family GTPase TC10 promotes exocytic vesicle fusion", 411-421, ©2006, with permission from Elsevier.

5. Conclusion

FRET-based biosensors for Rab family GTPases have become very powerful tools for the analysis of molecular mechanisms regulating a broad range of membrane trafficking events. In this chapter, we have provided a practical guide to making FRET sensors for Rab GTPases. In the near future, we expect further improvements in sensor design and optimization, because FRET techniques are becoming essential tools in cell biology.

6. Acknowledgments

We thank Sayaka Yoshiki and Hiroko Koizumi for technical help and their input, and members of the Matsuda laboratory for fruitful discussions. This work was supported by grants from the Ministry of Education, Culture, Sports, Science, and Technology of Japan, the Uehara Memorial Foundation, the Research Foundation for Opto-Science and Technology, and the Naito Foundation.

7. References

Allaire, P. D.; Ritter, B.; Thomas, S.; Burman, J. L.; Denisov, A. Y.; Legendre-Guillemin, V.; Harper, S. Q. ; Davidson, B. L.; Gehring, K. & McPherson, P. S. (2006). Connecdenn, a novel DENN domain-containing protein of neuronal clathrin-coated vesicles functioning in synaptic vesicle endocytosis. *Journal of Neuroscience,* 26, 13202-13212.

Allaire, P. D.; Marat, A. L.; Dall'Armi, C.; Di, P. G.; McPherson, P. S. & Ritter, B. (2010). The Connecdenn DENN domain: a GEF for Rab35 mediating cargo-specific exit from early endosomes. *Molecular Cell,* 37, 370-382.

Bal, M.; Zaika, O.; Martin, P. & Shapiro, M. S. (2008). Calmodulin binding to M-type K+ channels assayed by TIRF/FRET in living cells. *Journal of Physiology* 586, 2307-2320.

Brown, T. C.; Correia, S. S.; Petrok, C. N. & Esteban, J. A. (2007). Functional compartmentalization of endosomal trafficking for the synaptic delivery of AMPA receptors during long-term potentiation. *Jounal of Neuroscience,* 27, 13311-13315.

Cheng, J.; Wang, H. & Guggino, W. B. (2005). Regulation of Cystic Fibrosis Transmembrane Regulator Trafficking and Protein Expression by a Rho Family Small GTPase TC10. *Journal of Biological Chemistry,* 280, 3731-3739.

Chevallier, J.; Koop, C.; Srivastava, A.; Petrie, R. J., Lamarche-Vane, N. & Presley, J. F. (2009). Rab35 regulates neurite outgrowth and cell shape. *FEBS Letters,* 583, 1096-1101.

Chiang, S. H.; Baumann, C. A.; Kanzaki, M.; Thurmond, D. C.; Watson, R. T.; Neudauer, C. L.; Macara, I. G.; Pessin, J. E. & Saltiel, A. R. (2001). Insulin-stimulated GLUT4 translocation requires the CAP-dependent activation of TC10. *Nature,* 410, 944-948.

Chua, C. E. L., Lim, Y. S. & Tang, B. L. (2010). Rab35 - a vesiclular traffic-regulating small GTPase with actin modulating roles. *FEBS Letters,* 584, 1-6.

Cuadra, A. E.; Kuo, S. H.; Kawasaki, Y.; Bredt, D. S. & Chetkovich, D. M. (2004). AMPA Receptor Synaptic Targeting Regulated by Stargazin Interactions with the Golgi-Resident PDZ Protein nPIST. *Journal of Neuroscience,* 24, 7491-7502.

Diakonova, M.; Bokoch, G. & Swanson, J. A. (2002). Dynamics of cytoskeletal proteins during Fcgamma receptor-mediated phagocytosis in macrophages. *Molelular Biology of the Cell,* 13, 402-411.

Dyachok, O.; Isakov, Y.; Sagetorp, J. & Tengholm, A. (2006). Oscillations of cyclic AMP in hormone-stimulated insulin-secreting beta-cells. *Nature,* 439, 349-352.

Fix, M.; Melia, T. J.; Jaiswal, J. K.; Rappoport, J. Z.; You, D.; Sollner, T. H., Rothman, J. E. & Simon, S. M. (2004). Imaging single membrane fusion events mediated by SNARE proteins. *Proceedings of the National Academy of Science of the United Staes of America,* 101, 7311-7316.

Gao, Y., Balut, C. M., Bailey, M. A., Patino-Lopez, G., Shaw, S. & Devor, D. C. Recycling of theCa^{2+}-activated K^+ channel, KCa2.3, is dependent upon RME-1, Rab35/EPI64C, and an N-terminal domain. *Journal of Biological Chemistry,* 285, 17938-17953.

Grosshans, B. L.; Ortiz, D. & Novick, P. (2006). Rabs and their effectors: achieving specificity in membrane traffic. *Proceedings of the National Academy of Science of the United Staes of America,* 103, 11821-11827.

Hailey, D. W.; Davis, T. N. & Muller, E. G. (2002). Fluorescence resonance energy transfer using color variants of green fluorescent protein. *Methods in Enzymology,* 351, 34-49.

Hsu, C., Morohashi, Y., Yoshimura, S., Manrique-Hoyos, N., Jung, S., Lauterbach, M. A., Bakhti, M., Grønborg, M., Möbius, W., Rhee, J., Barr, F. A. & Simons, M. (2010) Regulation of exosome secretion by Rab35 and its GTPase-activating proteins TBC1D10A-C. Journal of Cell Biology 189, 223-232.

Itoh, R. E.; Kurokawa, K.; Ohba, Y.; Yoshizaki, H.; Mochizuki, N. & Matsuda, M. (2002). Activation of rac and cdc42 video imaged by fluorescent resonance energy transfer-based single-molecule probes in the membrane of living cells. *Molecular and Cellular Biology,* 22, 6582-6591.

Jares-Erijman, E. A. & Jovin, T. M. (2003). FRET imaging. *Nature Biotechnoogy,* 21, 1387-1395.

Kanno, E.; Ishibashi, K.; Kobayashi, H.; Matsui, T.; Ohbayashi, N. & Fukuda, M. (2010). Comparative screening for novel Rab-binding proteins by GST pull-down assay using 60 different mammmalian Rabs. *Traffic,* 44, 491-507.

Kawase, K.; Nakamura, T.; Takaya, A.; Aoki, K.; Namikawa, K.; Kiyama, H.; Inagaki, S.; Takemoto, H.; Saltiel, A. R. & Matsuda, M. (2006). GTP hydrolysis by the Rho family GTPase TC10 promotes exocytic vesicle fusion. *Developmental Cell,* 11, 411-421.

Kitano, M.; Nakaya, M.; Nakamuta, T.; Nagata, S. & Matsuda, M. (2008). Imaging of Rab5 activity identifies essential regulators for phagosome maturation. *Nature,* 453, 241-245.

Kiyokawa, E.; Aoki, K.; Nakamura, T. & Matsuda, M. Spatiotemporal regulation of small GTPases as revealed by probes based on the principle of Förster resonance energy transfer (FRET): implications for signaling and pharmacology. *Annual Review of Pharmacology and Toxicology,* in press.

Kotera, I.; Iwasaki, T.; Imamura, H.; Noji, H. & Nagai, T. (2010). Reversible dimerization of Aequorea victoria fluorescent proteins increases the dynamic range of FRET-based indicators. *ACS Chemical Biology,* 5, 215-222.

Kouranti, I.; Sachse, M.; Arouche, N.; Goud, B. & Echard, A. (2006). Rab35 regulates an endocytic recycling pathway essential for the terminal steps of cytokinesis. *Current Biology,* 16, 1719-1725.

Kraynov, V. S.; Chamberlain, C.; Bokoch, G. M.; Schwartz, M. A.; Slabaugh, S. & Hahn, K. M. (2000). Localized Rac activation dynamics visualized in living cells. *Science,* 290, 333-337.

Kurokawa, K.; Takaya, A.; Fujioka, A.; Terai, K. & Matsuda, M. Visualizing the signal transduction pathways in living cells with GFP-based FRET probes. (2004.) *Acta Histochemica Cytochemica,* 37, 347-355.

Lam, A. D.; Ismail, S.; Wu, R.; Yizhar, O.; Passmore, D. R.; Ernst, S. A. & Stuenkel, E. L. (2010). Mapping dynamic protein interactions to insulin secretory granule behavior with TIRF-FRET. *Biophysical Journal,* 99, 1311-1320.

Mattheyses, A .L.; Simon, S. M. & Rappoport, J. Z. (2010). Imaging with total internal reflection fluorescence microscopy for the cell biologist. *Journal of Cell Science,* 123, 3621-3628.

Michaelson, D., Silletti, J., Murphy, G., D'Eustachio, P., Rush, M. & Philips, M. R. (2001). Differential localization of Rho GTPases in live cells: regulation by hypervariable regions and RhoGDI binding. *Journal of Cell Biology,* 152, 111-126.

Miyawaki, A. (2003). Visualization of the spatial and temporal dynamics of intracellular signaling. *Developmental Cell, 4,* 295-305.

Mochizuki, N.; Yamashita, S.; Kurokawa, K.; Ohba, Y.; Nagai, T.; Miyawaki, A. & Matsuda, M. (2001). Spatio-temporal images of growth-factor-induced activation of Ras and Rap1. *Nature,* 411, 1065-1068.

Nagai, T.; Yamada, S.; Tominaga, T.; Ichikawa, M. & Miyawaki, A. (2004). Expanded dynamic range of fluorescent indicators for Ca2+ by circularly permuted yellow fluorescent proteins. *Proceedings of the National Academy of Science of the United Staes of America,* 101, 10554-10559.

Nakamura, T.; Kurokawa, K.; Kiyokawa, E. & Matsuda, M. (2006) Analysis of the spatio-temporal regulation of Rho GTPases using Raichu probes. *Methods in Enzomology,* 406, 315-332.

Nakamura, T. & Matsuda, M. (2009). In vivo imaging of signal transduction cascades with probes based on Forster Resonance Energy Transfer (FRET). In: *Current Protocol in Cell Biology,* Bonifacino, J. S.; Dasso, M.; Harford, J. B.; Lippincott-Schwartz, J. & Yamada, K. M., 45, Chapter 14, Unit14.10. 1-14. John Wiley & Sons, 9780471143031, Hoboken.

Nakaya, M.; Tanaka, M.; Okabe, Y.; Hanayama, R. & Nagata,S. (2006). Opposite effects of rho family GTPases on engulfment of apoptotic cells by macrophages. *Journal of Biological Chemistry,* 281, 8836-8842.

Nguyen, A. W. & Daugherty, P. S. (2005). Evolutionary optimization of fluorescent proteins for intracellular FRET. *Nature Biotechnology,* 23, 355-360.

Palm, G. J.; Zdanov, A.; Gaitanaris, G. A.; Stauber, R.; Pavlakis, G. N. & Wlodawer, A. (1997). The structural basis for spectral variations in green fluorescent protein. *Nature Structural Biology,* 4, 361-365.

Patino-Lopez, G.; Dong, X.; Ben-Aissa, K.; Bernot, K. M.; Itoh, T.; Fukuda, M.; Kruhlak, M. J.; Samelson, L. E. & Shaw, S. (2008). Rab35 and its GAP EPI64C in T cells regulate receptor recycling and immunological synapse formation. *Journal of Biological Chemistry,* 283, 18323-18330.

Periasamy, A. & Day, R. N. (1999). Visualizing protein interactions in living cells using digitized GFP imaging and FRET microscopy. *Methods in Cell Biology,* 58, 293-314.

Pertz, O.; Hodgson, L.; Klemke, R. L. & Hahn, K. M. (2006). Spatiotemporal dynamics of RhoA activity in migrating cells. Nature, 440, 1069-1072.

Pollok, B. A. & Heim, R. (1999). Using GFP in FRET-based applications. Trends in Cell Biology, 9, 57-60.

Saltiel, A. R. & Pessin, J. E. (2002). Insulin signaling pathways in time and space. *Trends in Cell Biology,* 12, 65-71.

Sako, Y. (2006). Imaging single molecules in living cells for systems biology. *Molecular Systtems Biology,* 2, 56-61.

Sato, M.; Sato, K.; Liou, W.; Pant, S.; Harada, A. & Grant, B. D. (2008). Regulation of endocytic recycling by C. elegans Rab35 and its regulator RME-4, a coated-pit protein. *EMBO Journal*, 27, 1183-1196.

Sekar, R. B. & Periasamy, A. (2003). Fluorescence resonance energy transfer (FRET) microscopy imaging of live cell protein localizations. *Journal of Cell Biology,* 160, 629-633.

Stenmark, H. (2009). Rab GTPases as coordinators of vesicle traffic. *Nature Reviewes Moelcular Cell Biology,* 10, 513-525.

Takaya, A.; Ohba, Y.; Kurokawa, K. & Matsuda M. (2007). R-Ras regulates exocytosis by Rgl2/Rlf-mediated activation of RalA on endosomes. *Molecular Biology of the Cell* 18, 1850-1860.

Takaya, A.; Ohba, Y.; Kurokawa, K. & Matsuda, M. (2004). RalA activation at nascent lamellipodia of epidermal growth factor-stimulated Cos7 cells and migrating Madin-Darby canine kidney cells. *Molecular Biology of the Cell* 15, 2549-2557.

Tsien, R. Y. & Miyawaki, A. (1998). Seeing the machinery of live cells. *Science,* 280, 1954-1955.

Tsuboi, T.; McMahon, H. T. & Rutter, G. A. (2004). Mechanisms of Dense Core Vesicle Recapture following "Kiss and Run" ("Cavicapture") Exocytosis in Insulin-secreting Cells. *Journal of Biological Chemistry,* 279, 47115-47124.

Walseng, E.; Bakke, O. & Roche, P. A. (2008). Major histocompatibility complex class II-peptide complexes internalize using a clathrin- and dynamin-independent endocytosis pathway. *Journal of Biological Chemistry,* 283, 14717-14727.

Yoshizaki, H;, Ohba, Y.; Kurokawa, K.; Itoh, R. E.; Nakamura, T.; Mochizuki, N.; Nagashima, K. & Matsuda, M. (2003). Activity of Rho-family G proteins during cell divison as visualized with FRET-based probes. *Journal of Cell Biology*, 162, 223-232.

Yuseff, M. I., Lankar, D. & Lennon-Duménil, A. M. (2009) Dynamics of membrane trafficking downstream of B and T cell receptor engagement: impact on immune synapses. *Traffic,* 10, 629-636.

Zerial, M. & McBride, H. (2001). Rab proteins as membrane organizers. *Nature Review of Molecular and Cellular Biology,* 2, 107-117.

Zhang, J.; Fonovic, M.; Suyama, K.; Bogyo, M. & Scott, M. P. (2009). Rab35 controls actin bundling by recruiting fascin as an effector protein. *Science,* 325, 1250-1254.

Zhu, A. X.; Zhao, Y. & Flier, J. S. (1994). Molecular cloning of two small GTP-binding proteins from human skeletal muscle. *Biochemica Biophysica Research Communications,* 205, 1875-1882.

6

Chiral Biosensors and Immunosensors

Marzena Kaniewska and Marek Trojanowicz
University of Warsaw
Poland

1. Introduction

Investigation of compounds having the asymmetric carbon in their structure has a fundamental significance for understanding all processes that occur in living organisms. Biologically active compounds as amino acids, sugars, peptides, proteins and polysaccharides posses a different stereochemistry. All of these compounds are involve in chiral interactions in biochemical systems functioning in living organisms. Animal and human peptides consist of almost only left-handed (L) amino acids as building blocks for peptides. Right-handed (D) amino acids occur in unicellular lower organisms. A huge interest in chirality results also from the fact that present pharmaceutical and chemical industry to large extent is based on the synthesis of compounds that may have a different stereochemistry. Enantiomeric pharmaceuticals, pesticides or food additives can have a different influence on living organisms. The first observations on the pharmacological role of enantiomers are assigned to Abderhalde and Müller, who described in 1908 a difference in raising blood pressure by enantiomers of epinephrine. These observation started research on the effects of the enantiomers in the context of the pharmacological effect.

Clinical tests indicate that the replacement of racemate by a single active enantiomer of pharmaceutical allows to use of lower doses of drugs, increasing the therapeutic efficacy of individual doses. It helps to avoid possible harmful interactions with other drugs, to minimize the differences in drug metabolism between species and reduce the toxicity caused by supplementation of inactive isomers (Agranat et al., 2002; Baumann et al., 2002). There has been a trend towards to ensure that pharmaceuticals that were invented, approved and marketed as a racemate or a mixture of diastereomers, have been re-marketed as single enantiomers. Such compounds are called "chiral switches" (Caner et al., 2004; Hutt & Valentová, 2003)

The enantiomers of the same compound, indistinguishable by physical and chemical properties show sometimes different physiological effects. There are a number of examples demonstrated the need to test the impact of individual enantiomers, and in some cases, the chiral purity control of the compound. Enantiomers may differ in smell which can be exemplified by carvone, S and R-enantiomer have the scent of caraway and mint respectively (Laska et al., 1999). They may have a different taste - for example, isoleucine and asparagine, have a bitter taste as a form of L and sweet in the form of D (Zawirska-Wojtasiak, 2006) and activity effects on organisms, such as ephedrine and adrenaline. The stimulating effect of (+) ephedrine is 80% of the effect caused by (-) ephedrine (Herráez-Hernández & Campíns-Falco, 2001). There have also been known cases in which one of the enantiomers of a compound have a beneficial influence for the body and the other caused

serious problems. The most famous example was the drug with analgesic and calming effect - thalidomide administered to pregnant women in the racemic form. It was found that the R enantiomer has a therapeutic effect, while the other enantiomer was strongly teratogenic. It elicited phocomelia, disease involving the disappearance of the long bones of limbs (Nakanishi et al., 2004; Lenz, 1988). Currently, researches on the use of this drug for cancer are conducted. It is used to treat multiple myeloma, especially in the elderly. Its inhibiting effect on the formation of blood vessels around tumours was also noted. Also, the enantiomers of many other drugs have different effects. L-DOPA is used to treat Parkinson's disease, while the D-enantiomer exhibits strong toxicity. Similarly, in the case of penicillamine, D-enantiomer is used as an antiarthritic drug, and the L-enantiomer is highly toxic (Eichelbaum & Gross, 1996). Also, a number of drugs belonging to the group of antidepressants and psychotropic drugs have a different effect of both enantiomers (Lane & Baker, 1999).

Literature presents many examples showing that enantiomers differ in activity, rate of reaction or time of dissolution. The example of difference in time of dissolution can be fungicide metalaxyl. In a neutral pH the R enantiomer in its active form shows over four times higher dissolution constant than S enantiomer. (R)-(+)-isomer of organophosphorus pesticide methamidophos reveals the higher insecticidal activity against flies than other enantiomer and racemate (Miyazaki et al.,1988). On the other hand (S)-(-)-methamidophos appear more toxic after application against German cockroaches in a short time. During first 5 hours the same dose of S enantiomer caused death of 75% of insects whereas R enantiomer caused death of only 20%.

Research of the individual enantiomers can be a valuable indicator of the quality of different food products. D amino acid content in natural samples of milk, juice and honey is an indication of bacterial contamination, prolonged storage time of products or poor quality of fruit used in the production of juice. The content of D or L enantiomers of lactic acid in fermented products provides the type of bacteria responsible for the process. Similarly the presence of D-asparagine in yogurt samples indicates the presence of specific bacteria. Also, chiral alcohols can be used to control product quality. For determination of 2-butanol in distilled spirits, R-enantiomer derived from bacteria that may be present in the mash, and S enantiomer is produced only by yeast. The content of R-2-butanol is a marker of bacterial contamination. Also from chiral linalool (affecting the taste of oranges), the S form is present in sweet oranges, and R is the typical to bitter. It can be an indicator of adulteration of the concentrate's composition (Marchelli et al., 1996).

Enantiomers of some compounds can be used also to trace sources of water contamination. A non-selective beta blocker mainly used in the treatment of hypertension-propranolol exists in untreated sewage as a racemate. During successive steps of sewage treatment the amount of R enantiomer in relation to both enantiomers decreased to even less then 40% regardless the concentration of compound. Determination of enantiomeric fraction (the ratio of the concentration of one of the isomers to the total concentration) can be useful indicator to evaluate if examined water is significantly affected by untreated sewage, for example as a result of leaking sewers and to apportion the contribution of treated and untreated sewage into surface waters (Fono & Sedlak, 2005).

In a similar manner the source of groundwater contamination in Switzerland by specifying the content of enantiomers of the herbicide Mecoprop was determined. In order to protect crops in agriculture, it is sold as a pure enantiomer, while the same compound was also used to protect roofs against fouling by plants. In latter case a racemate was used.

Enantiomer ratio of 0.5 was an indication that about 50% of the herbicide in surface water origin from roofs security system, and not - as expected - mostly from agriculture (Bucheli et al., 1998).
There are also works in which attempts to use information about the racemization rate in the study to determine the age of archaeological finds on the basis of the ratio of amino acids enantiomers contained in samples of bone, shell or teeth. In living organisms, the ratio of amino acid D / L is zero. After the death of the body's proteins break down and the process of racemization begins. It leads to increase the ratio of amino acids D / L up to one. This process is lengthy and depends on many factors such as the structure of the amino acid sequence of amino acids in the protein, pH, buffering effect, humidity, temperature, as well as the presence of catalysts. Due to the large number of parameters that must be controlled, this technique is challenged by many researchers, even though it is used for 30 years and has resulted in many interesting publications (Robins et al. 2001).
Optically pure compounds are also used in chiral synthesis. In 2001, Sharpless, Knowles and Noyori received the Nobel Prize for research on the oxidation and hydrogenation reactions using optically active compounds which have found application in the production of many antibiotics and anti-inflammatory and cardiac drugs (Kaniewska 2009).
The enantiomers of the same compound are characterized by almost identical physical properties. For this reason they can not be separated by widely used methods such as fractional distillation or fractional crystallization except that the solvent is optically active. Methods used for separation and determination of individual isomers are based on interaction with substances exhibiting optical activity. Currently used methods for the analysis of optically active compounds are mainly separation methods such as gas chromatography (GC), liquid chromatography (LC) and high performance liquid chromatography (HPLC) using chiral stationary phases, chiral selectors in the mobile phase or flow reactors for derivatization and highly efficient electromigration techniques as capillary electrophoresis (CE) using chiral selectors. Other methods are mass spectroscopy, NMR to the study of molecular recognition, as well as some spectroscopic techniques. These techniques require expensive equipment and the analysis is in most cases time-consuming.
Biosensors are widely used for analytical application for example in clinical of food analysis, environmental monitoring or chemical processes. They are characterized by good precision and sensitivity. The measurement is fast and stable. Biosensors can be miniaturized and used in portable analysers. They contain the biological material which often has the stereoselective or stereospecific properties. For this reason, biosensors may be competitive to the separation methods for the analysis of optically active compounds.

2. Enantioselective enzymatic biosensors

2.1 Electrochemical biosensors

Among natural receptors in construction of biosensors most often enzymes are employed. The reasons are the wide range of measurable parameters that can be utilized as result of biocatalytic process (chemical products, ions, protons, light, electrons) and a large number of available, isolated enzymes (Subrahmanyam et al. 2002). Numerous number of enzymes employed for long years in design of biosensors catalyses enantioselectively reactions of particular isomers of substrates, but very few reports can be found on their enantioselectivity and potential applications. The most examples can be find in reviews (Schlügerl et al. 1996; Stefan et al. 1999)).

Enzymes as compounds involved in life processes catalyze the reactions in which the substrate is a compound in the form of pure enantiomer. Enzymes may exhibit, depending on the method and mechanism of interaction with substrates, the absolute, or stereochemical specificity. The specificity may relate the D and L forms, geometric isomers, the position of binding, the coenzyme spatial settings, and the asymmetry of the complex enzyme-substrate. Stereochemical specificity is the perfect matching of the substrate configuration of the spatial points of interaction in the active centre. Active complex is generated only in the case of appropriate size. Enzymes catalyse reactions by creating new reaction pathways of lower energy transition state. The first step is usually to produce an enzyme-substrate complex. Substrate binds to the enzyme active site, which is a small recess or slot for the characteristic structure of the enzyme. Binding specificity depends on the specific arrangement of atoms in the active site. The fit is possible only if the substrate have an appropriate shape. In the case of chiral compounds the velocity of the reaction of substrate molecule with the enzyme is usually different for both enantiomers. Enantioselectivity factor value (E) can be determined from the equation (1) (Chen C. S. et al. 1982)

$$E = \frac{V_{\max 1} / K_{M1}}{V_{\max 2} / K_{M2}} \tag{1}$$

The difference of reaction rates of competing substrates due to the difference in Gibbs free energy of the subsequent stages of the reaction (Fig. 1) (Overbeeke et al., 1998).

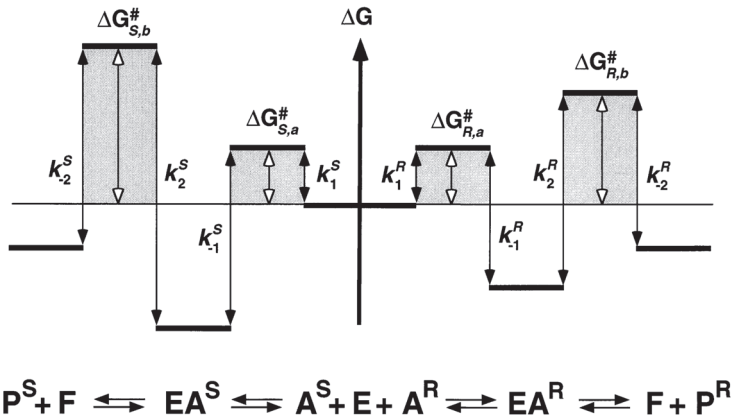

Fig. 1. Gibbs free energy change in subsequent reactions catalysed by the enantioselective enzyme

Then the enantioselectivity is determined from the expression (2):

$$-RT \ln E = \Delta\Delta G^{\neq}_{R,S} \cong \Delta G^{\neq}_{Rb} - \Delta G^{\neq}_{Sb} \tag{2}$$

2.1.1 Chiral catalysis

The most often developed, so far, are systems with pair of enzymes specific for each enantiomer. One of the mostly used examples are amino acid oxidases. D-amino acid oxidase, by the presence of adenine flavin dinucleotide (FAD) as cofactor, catalyses the

oxidation of D amino acids to imino acids which are immediately hydrolyzed to the corresponding α-keto acids and ammonium ions (Moreno et al. 1996). D-AAOx does not catalyze the oxidation of the opposite enantiomer and it is not inhibited by L amino acids. The properties of D-amino acid oxidase differ depending on the species. For example, the structure of the active centre of enzyme derived from mould is more open, which is the cause of a much broader range of catalytic activity (Pollegioni et al. 2002).

Enantiomers of amino acids were determined electrochemically with the biosensors that differ by way of immobilization, enzyme systems, or a kind of mediator. D-AAOx or L-AAOx were involved to the construction of biosensor sensitive to D or L amino acids. Value of the signal obtained for over 20 common L-amino acids and six important D-amino acids were presented in (Sarkar et al. 1999) and compared with the results obtained in (Kacaniklic et al. 1994). In the first case an enzyme was immobilized on the screen-printed electrode with the addition of polyethylamine (PEI) to the working electrode paste. The working electrode incorporated rhodinized carbon to facilitate hydrogen peroxide oxidation. Sensor showed response to six of the seven tested D amino acids, except D-proline. Only the average response of the biosensor for the relevant amino acid at a concentration of 0.1 mol L-1 was presented. In the latter case the enantioselective enzyme was coimmobilized with the horseradish peroxidase in the graphite paste with the addition of polyethylamine. In another example D-or L-AAOx were immobilized together with horseradish peroxidase and ferrocene as a mediator in the graphite-Teflon paste. The sensor consists of two electrodes – each with a different amino acid oxidase, L or D was used to determine amino acids in the racemic samples, or to determine the L amino acid in samples of grapes. Measurements were carried out in batch and flow (Dominguez et al. 2001). For the rapid determination of D and L amino acids the system of D-or L-AAOx biosensors immobilized in a membrane protein with glutaraldehyde was used. The chiral selectivity of the reactor was checked. The system was used for determination of amino acids in samples of two beers during the process of fermentation (Varadi et al. 1999). For determination of D-alanine a system of two sensors was used. System contained a reactor with DAAOx immobilized by glutaraldehyde on glass porous CPG (long chain alkyl amino-controlled pore glass) coupled with a sensor with the pyruvate oxidase (PyOx). D-amino acid oxidase catalysed the oxidation of D-amino acids, including the formation of pyruvate from D-alanine. This compound was then oxidized in a reaction catalysed by the pyruvate oxidase and the amount of oxygen consumed in this reaction corresponded to the contents of D-alanine in the sample (Inaba et al. 2003a). A different design of a sensor based on the same reactions was also used. Pyruvate oxidase was immobilized in the membrane on the surface of the Clark oxygen electrode. Suitable amino acid oxidase D-or L- in the buffer was added to a sample of amino acids and oxygen-saturated solution was incubated with catalase. After a specified time, the concentration of pyruvic acid formed was measured using electrode with PyOx (Inaba et al. 2003a). DAAOx was also immobilized on Prussian blue film by electrochemical codeposition. The electroactive layer was covered with Nafion. Biosensor was calibrated with D-alanine, but had no specific answer to this amino acid (Shi & Dong, 1995)

The screen-printed electrodes with the Prussian Blue as a mediator were used to prepare the biosensor for D-amino acids (Wcislo et al. 2007). The surface of the working electrode covered with the mediator has been additionally protected by the Nafion layer and then modified by evaporation of mixture containing DAAOx, bovine serum albumin and glutaraldehyde. The short response time and good reproducibility was obtained in

measurements of D-alanine and some chosen D-amino acids. Biosensor showed the linear response to D-alanine in the phosphate buffer with addition of FAD in the concentration range 10-300 μM. L-alanine did not give any response (Fig. 2). The biosensor was examined towards some other D amino acids and all L amino acids. The total amount of D-amino acids was estimated for the samples of milk and juices.

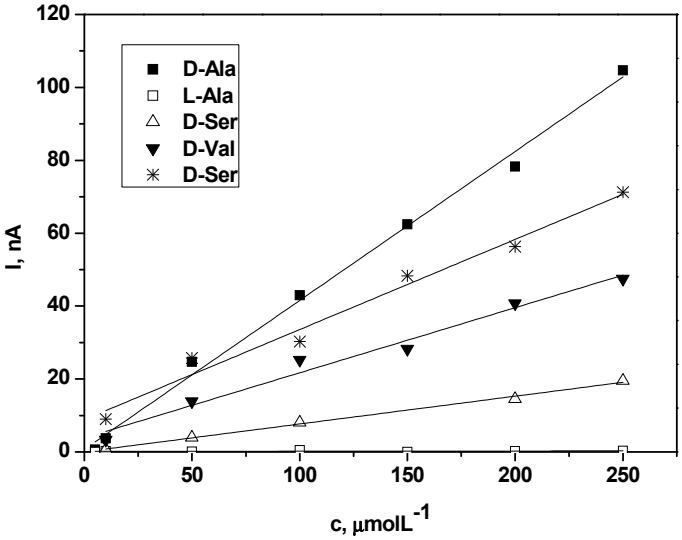

Fig. 2. The amperometric response of screen-printed enzymatic biosensor to enantiomers of alanine. Measurements made by placing a drop of measuring solution on the SPE sensor at – 0.05 V polarizing potential. Solution of alanine made in 50 mM phosphate buffer of pH 7.4 containing 0.1 M KCl and 10 μM FAD (Wcislo et al. 2007) .

The graphite paste biosensors with immobilized L-AAOx were employed for enantioselective detection of S-capropril (Stefan et al. 2003a). With amino acid oxidases also multi-enzyme biosensors were developed for determination of various drugs from the group of angiotensin-converting enzyme inhibitors such as cilizapril, pentopril (Aboul-Enein et al., 1999a), enalapril, ramipril, trandolapril (Stefan et al., 1998) and perindopril (Aboul-Enein et al., 1999b). For determination of D- or L-methotrexate (substituted glutamic acid) D-AAOx or L-AAOx were immobilized together with glutamate oxidase and horseradish peroxidase in the graphite paste. Different combinations of enzymes were examined. Mono-, bi- and trienzyme electrodes were constructed. The best enantioselectivity was obtained for three enzyme system with L-AAOx (selectivity coefficient $pK^{amp} = 3.09$). The selectivity of all biosensors was checked by both separate and mixed solution method. In mixed solution method the ratio between the concentration of the main and the interfering enantiomer was 1:10 (Stefan et al. 2003b). For the same multi-enzymatic system also a covalent immobilization with glutaraldehyde on the graphite support was examined with carbodiimide and thermal hardening, but immobilization in graphite paste was found simpler and providing better results in terms of enantioselectivity. Similar methods of enzyme immobilization have been used for detection of pipecolic acid.

The graphite paste biosensor consist D or L amino acid oxidase or the one of the amino acid oxidase combined with horseradish peroxidase in order to improve detection of hydrogen peroxide. The best result was obtained for bienzyme biosensor containing L-AAOx with HRP (selectivity coefficient $pK^{amp} = 3.82$). The values of amperometric selectivity coefficients for all the biosensors designed for L and D pipecolic acid were higher than 2. Proposed biosensors were used in clinical analysis to detect L or D-pipecolic acid in serum samples (Stefan et al. 2003c).

Another similar pair of enzymes sensitive to enantiomers is D- and L-lactate dehydrogenases (D-, L-LDH). Biosensors with these enzymes immobilized on porous carbon electrodes with the use of osmium complex $(Os(bpy)_3)(PF_6)_2$ as mediator have been used for determination of D and L-lactic acids. Changes in the concentration of lactic acid enantiomers measured by cyclic voltammetry were linear for L-enantiomer in the range of 0.1 -10 mmol L-1 and D-enantiomer of 1-20 mmol L-1. The enantioselectivity was determined by marking of error of one of the enantiomers determination at 10 fold excess of another. In the case of biosensor with L-lactate dehydrogenase, L-lactic acid was determined with an error of 4.9% with 10 fold excess of D-lactic acid. In the opposite situation the error was 5.4% (Motonaka et al. 1998). In the design of enzyme field effect transistor with D-LDH, the enzyme was immobilized on pH sensitive gate. The enantioselectivity of the biosensor is presented in Fig. 3. The authors admited, however, that the equilibrium of these reactions was shifted to the left and therefore the reaction product had to be removed. The signals were also influenced by pH, buffer capacity, temperature and flow-rate (Kullick et al. 1994). In a similar way biosensors with D- and L-malate dehydrogenases have been prepared (Schlügerl et al 1996).

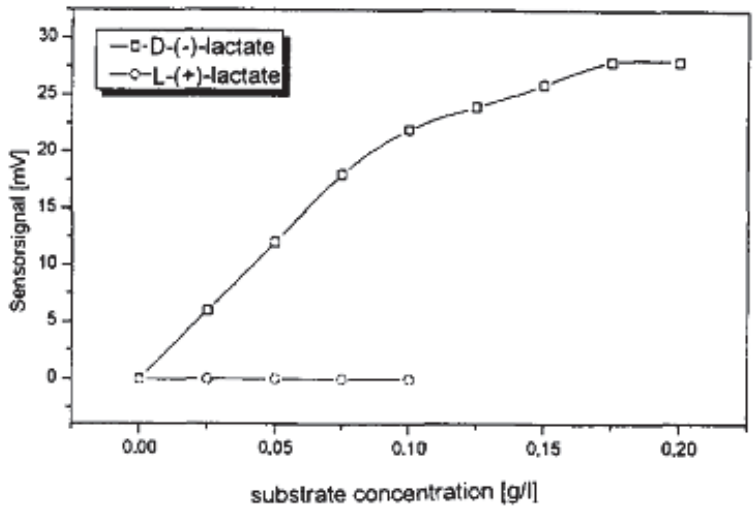

Fig. 3. The potentiometric response of D-LDH FET biosensor to enantiomers of lactate (Kullick et al. 1994).

In cases where there are no specific enzymes for both enantiomers another method of determination can be used. Two biosensors can be simultaneously employed – one sensing

with similar sensitivity both D and L species, and another one, sensitive to particular enantiomer. A multichannel system with eight pH field effect transistors has been developed for determination of hydrophobic esters of amino acids. Esterase EC 3.1.1.1 was used as a non-enantioselective enzyme while α-chymotrypsin only catalysed the reaction of L-amino acid esters. The first biosensor could detect the total amount of amino acid esters and the second gave the information about the enantiomeric ratio in the sample. The same authors present the example of the sensor containing the esterase and lipase for the enantioselective determination of β-hydroxy acid esters, where lipase catalysed the reaction of D-β-hydroxy esters (Kullick et al. 1994). The authors also mention the possibility of construction of system of two enzymes – amidase and aminoacylaze - which catalyze the reactions of deacylation. Amidase catalyzes the non-selective reaction of N-acetyl amino acids and aminoacylaze selectively catalyses only N-acetyl-L-amino acids (Schlügerl et al. 1996)

Also a biosensor design has been reported, where with the use of non-enantioselective enzyme, the enantioselectivity has been gained by the modification of sensing electrode surface with appropriate conducting polymer, which additionally serves as support for immobilization of enzyme. The surface of glassy carbon electrode was modified by electropolymerization of the chiral dicarbazole-biotin. The modification provided differentiation of current magnitude for anodic oxidation of L- and D-norepinephrine of about 50% at 0.5 V *vs.* SCE. Electrode was modified by six enzyme layers constructed by six cycles of sussesive deposition of avidine and biotinylated polyphenol oxidase (PPO). The immobilization resulted in obtaining of biosensor for measurements of D-norepinephrine with 4.8 times larger sensitivity than for L isomer at 0.2 V *vs.* SCE (Cosnier et al. 2003).

Finely there are enzymes with well defined enantioselectivity still not involved to biosensor design. One of the examples is Quinohaemoprotein alcohol dehydrogenase (Jongejan et al., 2000). The enzyme is enantioselective in the oxidation of secondary alcohols. A strong preference is observed for the S-2-alcohols. The enantioselectivity increases with increasing chain length. The same enzyme was immobilized on the surface of electrode and used in that form for preparative purposes (Somers et al., 1998). Although another type of alcohol dehydrogenases were used for biosensor design (Jiang et al. 2009) Quinohaemoprotein alcohol dehydrogenase as yet didn't find any analytical application.

2.1.2 Chiral inhibition

There is a large representation of chiral compounds among pesticides. 25% of the active pesticide ingredients appear in the form of enantiomers (Garrison, 2006). A vast majority of these compounds is produced and sold as a racemate. The operating principle for a large number of phosphoogranic pesticides is precisely acetylcholinesterase inhibition. Unimmobilized enzyme inhibition studies using phosphoogranic pesticides in solution and in vivo in water microorganisms, indicate differences in the inhibition rate and toxicity against selected organisms for the enantiomers of the compounds used for tests. These differences may depend on the origin of the enzyme. Depending on whether it was tested in vitro or in living organisms opposite inhibition was observed. (-)-Profenofos has more than 8-fold greater toxicity on Daphnia manga in vivo, while (+)-Profenofos in vitro shows a rate of inhibition over 71 times stronger towards HR-AChE (Nillos et al., 2007). In the case of fenoxon sulfoxide, IC50 (half maximal inhibitor concentration) has been presented. This factor was estimated for two enzymes: HR-AChE and EE AChE with the average figures at

6.9 μM and 6.5 μM for R (+) fenoxon sulfoxide and 230 μM and 111 μM for S (-) fenoxon sulfoxide respectively (Gadepalli et al., 2007). Another example of chiral phosphoogranic pesticide is the nematicide fosthiazate. The examination of individual enantiomers' reactivity showed a 1.4 difference in the inhibition of EE AChE in vitro and a 3.1 fold difference in toxicity against Daphnia manga (Lin K. D. Linet al., 2007). Significant differences of AChE inhibition can also be observed for the insecticide chloramidofos, which has 2 pairs of diastereoisomers; depending on the chosen pair of enantiomers the differences range from 1.1 to 18.1 (for measurements in vitro) and from 1.2 to 13 (in vivo) (Zhou et al., 2007).
The operating principle of malathion and malaoxon also is based on the inhibition of acetylcholinesterase. The differences in the inhibition rate dependent on the enantiomer applied, as well as on the origin of the enzyme have been observed. R malaoxon inhibited RB AChE (rat brain) 8.6 times faster than S malaoxon (Berkman et al., 1993a). In turn, BE AChE (bovine erythrocytes) difference in the rate of inhibition of R / S is 22.5 (Rodriguez et al., 1997).
Below we present for the first time in literature a screen printed biosensor which can be used to measure the inhibition of the immobilized enzyme in both batch and flow analysis.
Screen printed electrode mediated with Prussian Blue and protected by Nafion layer was used to prepare the bienzymatic biosensor. The membrane was obtained by mixing acetylcholinesterase, choline oxidase and BSA solution phosphate buffer with the addition of KCl, and then with glutaraldehyde solution in water. The scope of straightness for the signal received in batch measurements was 10-500 μM for acetylcholine chloride. Static measurements indicated that the enzyme immobilized by the R-enantiomer is inhibited stronger than the one immobilized with the S-enantiomer by approximately 1.25 times. For malathion the inhibition ratio for the enantiomers R / S was 1.3 (Fig 4A).
Batch measurements were also carried out for B394-strain acetylcholinesterase – a mutant strain of the enzyme isolated from the fruit fly. The biosensor with immobilized B394 strain acetylcholinesterase showed practically no difference in inhibition by the two pesticides (malaoxon and malathion) (Fig 4B)
For the flow measurements the biosensor with EEAChE showed linear response to the analyte in the range of concentration from 50 to 800 μM. The ratio of the original signal of the biosensor inhibited by R and S enantiomers of malaoxon in flow analysis after the first injection was 2.7. Then, after the second injection of the inhibitor solution, it was as high as 22 and the subsequent injections caused practically no signal from the enzyme immobilized on the surface of the biosensor by R-enantiomer (Fig 4C). The enzyme inhibited by S-enantiomer, on the other hand, still showed some activity. The presented study also confirms that the differences in inhibition depend on the chiral origin of the enzyme (Kaniewska, 2009).

3. Enantioselective immunosensors

It is well known that antibodies can differentiate enantiomers of antigens (Landsteiner & van der Scheer, 1928). Bedsides numerous other selectors as cyclodextrins, crown ethers, macrocyclic antibiotics, Pirkles, proteins or cellulose commonly used for obtaining a chiral stationary phases for HPLC, chiral separation can be obtained by immobilizing suitably raised stereoselective antibodies onto a stationary phase (Hofstetter et al., 2002; Kim H. et al., 2004).
The development of the affinity-based biosensors is on of the fastest growing area in the biosensor field (Rogers 2000). Various strategies have been developed for design of separation-free electrochemical immunosensors, based mostly on heterogeneous immunoassay procedures (Killard & Smyth, 2000).

3.1 Electrochemical immunosensors

The possibility of the construction of enantioselective immunosensors was indicated by the use a stereoselective antibody sensitive to the chiral centre of α-amino acids (Hofstetter et al., 1998). The interactions of rabbit antibodies was detected for amino acids in an enzyme-linked immunosorbent assay (ELISA). The enantiospecificity was observed for free amino acids p-aminophenylalanine and phenylalanine, whose structures overlap with the hapten, but also it was exhibited for other amino acids, aromatic and aliphatic. The same antibodies were employed for the development of a highly enantioselective electrochemical immunosensor. Stereoselective binding of an anti-D-amino acid antibody to the hapten-modified sensor surface resulted in capacitance changes that were detected with high sensitivity by a potentiostatic step method enabled to detect impurities of D-phenylalanine as low as 0.001%. The L-enantiomer was not bound by the antibody (Zhang S. et al. 2006).
Another example of electrochemical sensor is based on the stereoselective interaction of proline with carcinoembrionic antibody (anti-CEA). The selected pure enantiomer of proline was assembled on the glassy carbon electrode surface. Then the anti-CEA was loaded and

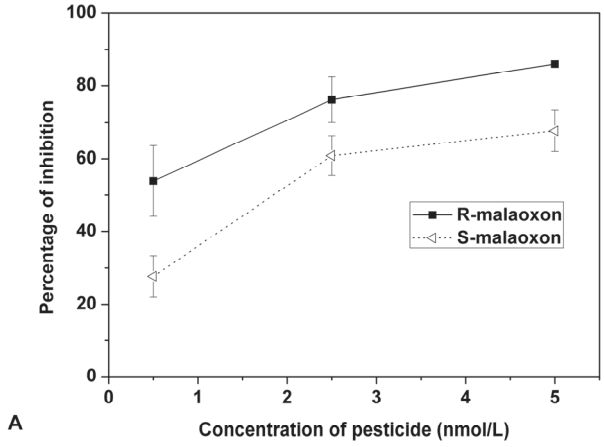

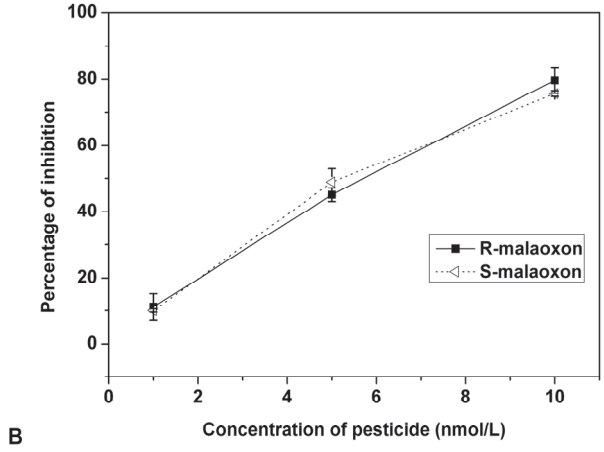

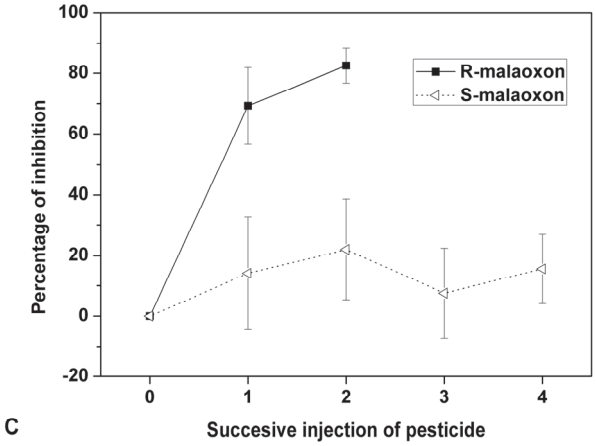

Fig. 4. The percentage of inhibition of AChE immobilized on the surface of the biosensors by malaoxon enantiomers. (A) Inhibition of EE AChE in batch measurement. A signal measurement was performed for three samples of the substrate (concentration 100 µM), preceded by baseline measurements. Then the electrode was incubated for 20 minutes in a solution of a given concentration of the pesticide. (B) Inhibition of B394 strain AChE in batch measurements. Signal measurement was performed for three samples in the substrate concentration of 1mmol L^{-1} preceded by baseline measurements. (C) Inhibition of EE AChE immobilized on the surface of biosensors inhibited by malaoxon enantiomers (40 nM concentration) in the flow system. 100 µL of solution of the substrate at a concentration of 400 µM and 100 µL of inhibitor solution were injected. Subsequent injections were preceded by rinsing the biosensor phosphate buffer (Kaniewska, 2009).

the ready immunosensors were tested over different concentration of carcinoembryonic antigen (CEA) (Fig 5.). The experimental results demonstrated that electrodes modified with D-proline had a better recognition function to anti-CEA, which is in good correlation with images of electrode surface obtained by atomic force microscopy. Authors suggested that designing chiral surfaces of amino acids may bring a new direction for biomaterials and help to understand the origin of stereoselectivity in pharmaceutical systems and clinic diagnoses (Chen M. et al.2009).

An amperometric immunosensor based on a graphite paste was presented in (Stefan & Aboul-Enein 2002). Mouse monoclonal anti-(+)-3,3′,5,5′-tetraiodo-L-thyronine (anti-L-T4) was used to the construction of immunosensor sensitive to thyroid hormone L-T4 known also as L-thyroxine. The selectivity coefficient obtained over D-T4 was $1.7 \cdot 10^{-4}$.

3.2 Other type of detection

Anti-D-AA antibodies have been employed for the determination of trace amounts of enantiomeric impurities of amino acids in the design of immunosensor based on different detection methods. The binding of stereoselective antibodies sensitive to the chiral centre of D-phenylalanine tested by a competitive enzyme-linked immunosorbent assay enabled to detect D- phenylalanine concentrations as low as 0.1 mM in the presence of 10 mM L-phenylalanine which corresponds to an enantiomer excess of 99.998% (Hofstetter et al., 2000).

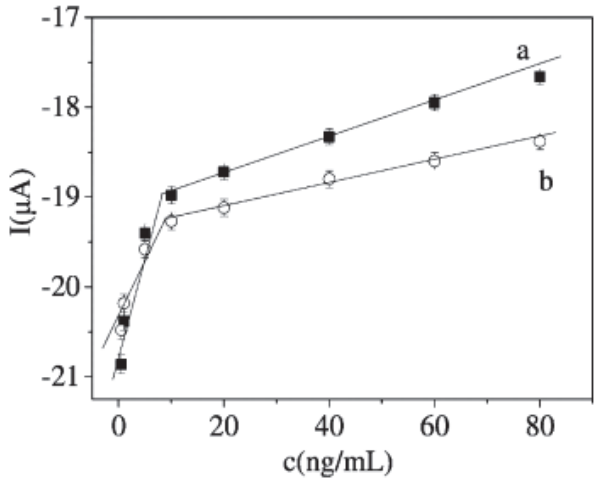

Fig. 5. Calibration plots of the cathodic peak current response vs. concentration of CEA (0.5-80 ng/mL) with D (closed squares) and L (open circles) modified immunoelectrodes under optimal conditions (Chen M. et al.2009).

The same interactions were used in construction of immunosensors based on surface plasmon resonance detection. Applications of immunoglobulins in a sensor design allowed to detect a low-molecular-weight analytes as amino acids by the SPR method. Compounds called D1 (p-amino-D-phenylalanine) and L1 (p-amino-L-phenylalanine) were immobilized onto separate channels of the sensor coated by the streptavidin covalently linked to carboxymethyl-dextran. Polyclonal rabbit antibody sensitive to D-amino acids interacted with the sensor while no increase of the SPR signal was observed for antibody sensitive to L-amino acids. Chiral discrimination was shown for the enantiomers of tyrosine, DOPA (3,4-dihydroxyphenylalanine), norleucine (Fig 6.) and tryptophan. The immunosensor allowed to detect 0.01% of the minor enantiomer present in the major enantiomer sample (Hofstetter et al., 1999).

Also a magnetic relaxation switching appears can be applied as a detection method for the construction of chiral immunosensors. This method allows for a rapid determination of enantiomeric excess in a high-throughput format. The MRS immunosensor was based on magnetic nanoparticles consisted of superparamagnetic iron oxide core with an aminated cross-linked dextran coating (CLIO) labelled with a derivative of D-phenylalanine. A decrease of more than 100 ms in the relaxation time was obtained by self-assembly of antibodies specific to D-amino acids (anti-D-AA) added to the CLIO-D-Phe. Upon addition of mixtures of the phenylalanine enantiomers to the CLIO-D-Phe/anti-D-AA self assembled structures, the presence of D-Phe impurities resulted in the dispersion of the nanoparticles by competing with the CLIO-D-Phe conjugates for antibody binding sites. The immunosensor allowed to detect 0.1 μM D-Phe in the presence of 10 mM L-Phe, which is an equivalent to 99,998% enantiomer excess (Fig 7.) (Tsourkas et al., 2004).

For the less sensitive determination of enantiomeric impurities a simple and inexpensive membrane-based optical immunosensor was invented. The immunosensor was based on a competitive reaction between an analyte and a biotin-derivatized analogue for the binding

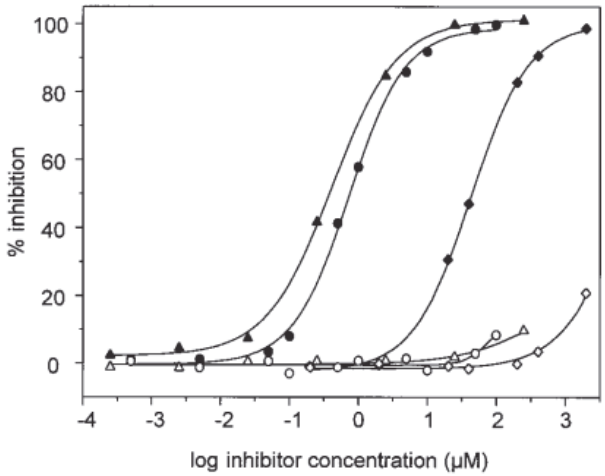

Fig. 6. Stereoselective binding of antibody to various amino acids: D-tyrosine (closed triangles), L-tyrosine (open triangles), D-DOPA (open circles), L-DOPA (closed circles), D-norleucine (closed diamonds), L-norleucine (open diamonds). The SPR values were converted into percentage of inhibition.

sites of a stereoselective membrane immobilized antibody. The antibody-bound was detected with peroxidase-conjugated avidin that converted a colourless substrate into an insoluble dye. The colour intensity was inversely related to the concentration of an analyte. The immunosensor allowed for quantitative determination of chiral phenylalanine up to an enantiomer excess 99.9% (Hofsetter et al. 2005)

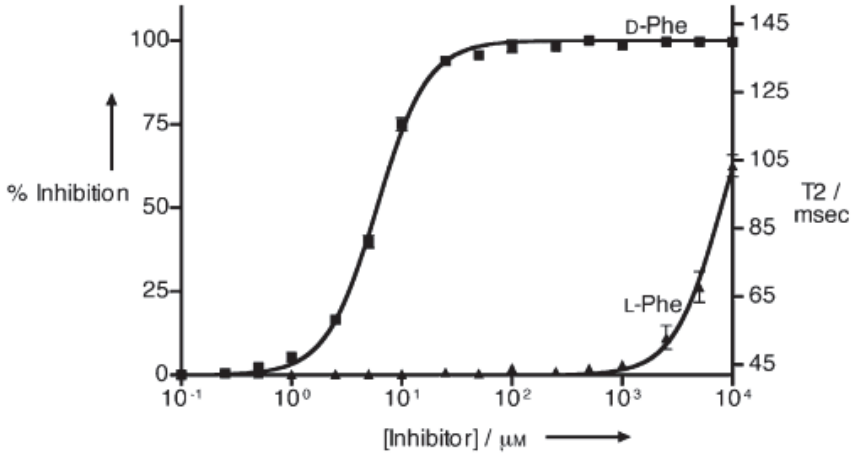

Fig. 7. Inhibition of the CLIO-D-Phe/anti-D-AA self assembly in the presence of increasing concentrations of L- or D-Phe as detected by changes in the T2 relaxation time (Tsourkas A. et al 2004)

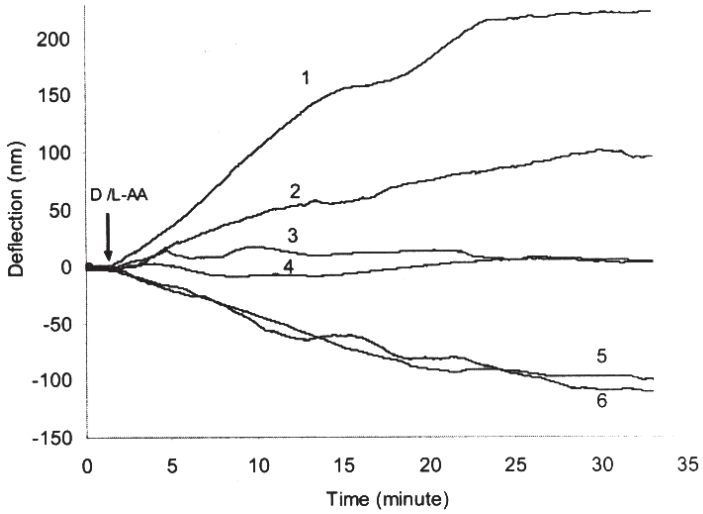

Fig. 8. Time trace of cantilever defections resulting from the binding of enantiomers of amino acids to micro cantilevers modified with covalently anti-L-amino acid antibody (1-4) or human immunoglobulin G (5,6) 1-50 mg/L L-tryptophan, 2,5- 50mg/L L-phenylalanine, 3- 50 mg/L D-tryptophan, 4,6- 50 mg/L D-phenylalanine. (Dutta et al. 2003).

These antibodies have been also employed for enantioselective sequential-injection chemiluminescence immunoassay of triiodothhyronine and tetraiodothyronine with immunoreactor with immobilized haptens. It has been shown that the detection of <0.01% of the L enantiomers in samples of D enantiomers is possible in less than 5 minutes including regeneration of immunoreactor (Silvaieh et al. 2002). Anti-D-AA was used in microfabricated cantilevers for enantioselective detection of amino acids based on inducing surface stress by intermolecular forces arising from analyte adsorption on surface-immobilized antibodies (Dutta et al. 2003). The temporal response of the cantilever allowed the quantitative determination of enantiomeric purity up to an enantiomeric excess of 99.8%. Based on the slope of response curves or anti-D-amino acid antibody, the selectivity coefficients for D- enantiomer towards L-isomer were 6.5, 7.7, and 37.5 for D-phenylalanine, D-tryptophan (Fig 8.) and D-methionine respectively. The largest enantioselectivity has been observed for D-valine (104).

4. Enantioselective bioreceptors

4.1 Mass-based biosensors

There are many examples of sensors exhibiting the enantioselective properties based on quartz crystal microbalance technique for example sensor for L-histidine (Zhang Z. et al. 2005), (+) methyl lactate (Ng et al. 2002), L-cysteine (Chen Z. et al. 2000), L-phenylalanine (Huang et al. 2003) or (-) menthol (Tanese et al. 2004). However the combination of biological macromolecules and QCM technique has been rarely reported for the studies of chiral discrimination.

Two sensors were developed by immobilization of human serum albumin (HAS) and bovine serum albumin (BSA) onto gold electrode combined with quartz plate by self-

assembled monolayer technique. The decreased frequency demonstrated interactions between albumines and enantiomers of R,S-1-(3-Metoxyphenyl)ethylamine (R,S-3-MPEA), R,S-1-(4-Metoxyphenyl)ethylamine (R,S-4-MPEA), R,S-tetrahydronaphthylamine (R,S-TNA), R,S-2-octanol (R,S-2-OT) and R,S-methyl lactate (R,S-MEL). The binding affinity of BSA and HSA for all five pairs of enantiomers was stereodependent. The effectiveness of the QCM sensor was described by the chiral discrimination factor $\alpha_{QCM,}$ defined as a quotient of the frequency decrease for enantiomer R and S respectively. For both sensors the highest discrimination factor were obtained for R,S-TNA. The value were for BSA sensor α_{QCM} =1.34 while for HSA sensor α_{QCM} =1.57 (Su et al. 2009).

4.2 Optical biosensors

The Surface Plasmon Resonance method was used for monitoring real time interactions of enantiomeric drug compounds to biomolecules immobilized on the surface of the sensor chip. The example of such biosensor for the first time was used to check the binding of the unnamed chiral drugs to human and rat albumins. However the enantiomers showed slight differences in their affinities towards the immobilized albumins, authors admitted that they were not able to detect whatever subtle differences could be due to differences in the enantiomers or it could be due to experimental errors (Ahmad et al. 2003). The next SPR biosensors were used to a detailed investigation of enantioselective interactions between protein and chiral small drugs. The binding of β-blockers alprenolol and propranolol to Cel7a cellulase was used as a model system. Cel7a was immobilized onto the sensor chip by PDEA-mediated thiol coupling. The single enantiomers of β-blockers were injected in a series with broad concentration range and a different pH of the solution was examined. The results were compared with the previously validated HPLC perturbation method. (Arnell et al., 2006). Similar interactions of drugs were examined for the SPR biosensors with two types of proteins-transport and target, immobilized onto the sensor chip. Different type of strong, intermediated and week interactions were exhibited by the models of binding of propranolol enantiomers to α_1-acid glycoprotein (AGP), R- and S-warfarin to human serum albumin (HSA) and RS and SR-melagratan to thrombin, AGP and HSA. Strong binding occurred in the case of RS-melagratan-trombin interaction. The other enantiomer did not interact at all with the protein (Sandblad et al., 2009)

4.3 Ion channel biosensors

The enantioselectivity was also reported for coulometric ion channel sensor for glutamic acid. The sensor was based on the use of glutamate receptor ion channel protein. The glutamate receptor was immobilized within an artificial bilayer lipid membrane formed by applying the folding method across a small circular aperture bored through a thin polyimide-film. The detection of L-glutamic acid was performed at a concentration as low as 10^{-8} M. The observed enantioselectivity for the channel activation was attributed to a combined effect of both the relative strength of binding isomers to the receptor protein and the relative potency of bound isomers to induce the ion channel current (Minami et al., 1991).

5. Enantioselective aptamers

DNA aptamers are a new group of chiral selectors. They are a single-stranded oligonucleotide sequences that can fold into a 3D shape with binding pocket and clefts that

allow them to bind many molecular targets as proteins, amino acids, peptides, cells and viruses with specificity that allows them to distinguish even strictly structurally related molecules. Aptamers are able to bind the target molecules with a very high affinity, equal or sometimes even superior to those of antibodies. Comparing to antibodies they present also some important advantages as well defined sequences produced by reproducible solid phase synthesis which allows an accurate modulation of their selectivity and binding parameters. Aptamers are much smaller than antibodies, permitting a higher density of molecules to be attached to surfaces. Their production does not require animal's immunization. It's also possible to obtain aptamers towards molecules that do not stimulate immunoresponce or that are toxic. Selections are not limited by physiological constraints allowing aptamers that bind their targets in extreme conditions to be isolated. Aptamers will refold to regain functionality after exposure to denaturing conditions (Mosing & Bowser, 2007). They are attractive host molecules, because they can be tailored to a variety of guest targets by the method of systematic evolution of ligands by exponential enrichment (SELEX) (Giovannoli et al., 2008).

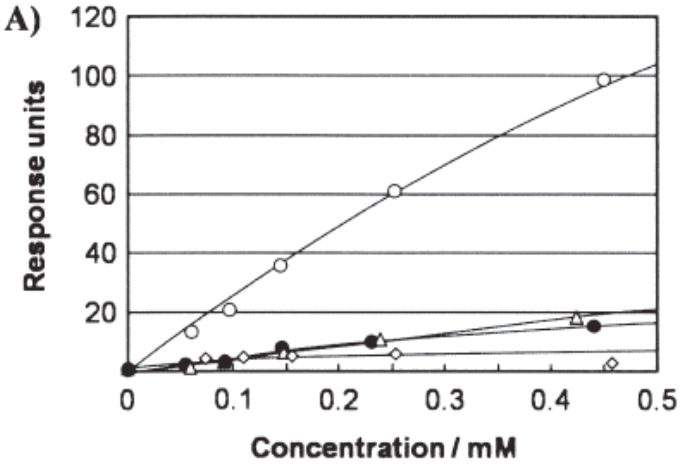

Fig. 9. SPR analyses of enantioselective binding interactions of selected aptamer with complex of avidine and biotinylated L-glutamic acid- α,γ-di-t-butylester (closed circles), D-glutamic acid- α,γ-di-t-butylester (open circles), glycine t-butyl ester (open triangles) and aptamers complex with avidine and biotin (open diamonds) (Ohsawa et al., 2008)

Aptamers can be successfully used to the biosensor design. As a biocomponents in biosensors they offers a multitude of advantages, such as the possibility of easily regenerate the function of immobilized aptamers, their homogeneous preparation and the possibility of using different detection methods due to easy labeling (Tombelli et al., 2005). A different detection techniques can be use for the aptasensor design as for example electrochemical (Liu et al., 2010), optical (Lee & Walt, 2000) or mass-based (Minunni et al., 2004). Although many examples of aptamer biosensor are presented in the literature only few of them considers the enantioselective properties.

The enzymatically prepared the biotinylated aptamers were immobilized on the sensor chip attached with streptavidin. Two of three selected amptamers showed enantioselective

recognition of the dicarboxylic acid moiety of glutamic acid. The binding affinity and enantioselectivity were successfully evaluated by SPR measurements, and the binding ability of these aptamers was eliminated by the absence of arginyl groups, indicating that modified groups are indispensable due to their binding affinity and enantioselectivity. The enantioselective response of selected aptamer is presented in Fig 9. (Ohsawa et al., 2008).
Another example presented in (Perrier et al., 2010) is based on the induced-fit binding mechanism of end-labelled nucleic acid aptamers to the small molecule. The anti-adenosine DNA aptamer, labelled by a single fluorescein dye was employed as a model functional nucleic acid probe. Target binding is converted into a significant increase of the fluorescence anisotropy signal presumably produced by the reduction of the local motional freedom of the dye and detected by fluorescence polarization sensor. In case of target molecule the difference in the anisotropy fluorescence signal generated by D and L enantiomers was not enough to allow the enantioselective detection of adenosine. The presented DNA aptamer was also able to bind the adenine nucleotides such as adenosine monophosphate AMP. In latter case aptasensor exhibited important enantioselective properties. Titration curves obtained by the addition of D-AMP show an FP response while for L-AMP does not cause any significant response Fig 10.

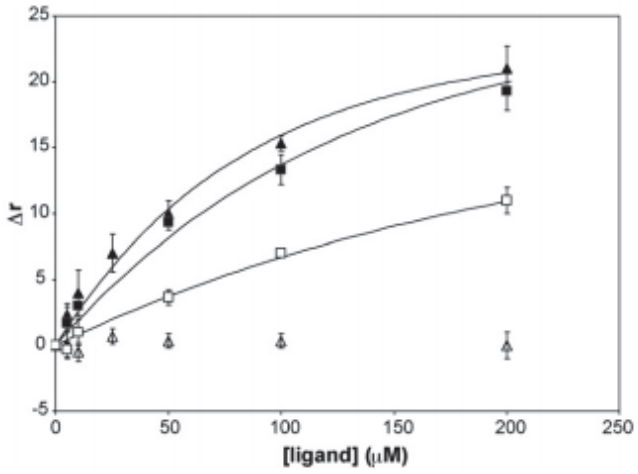

Fig. 10. Titration curves of the 3′-F-21-Apt probe with increasing concentration of enantiomers D-Ade (closed squares), L-Ade (open squares), D-AMP (closed triangles) and L-AMP (open triangles). Δr is a difference between the measured anisotrophy in the presence and in the absence of analyte (Perrier et al., 2010).

Aptamers are increasingly being used as chiral selectors in separation techniques as capillary electrophoresis or HPLC. Recently new aptamers for different specific molecular targets are selected. Some of them posses enantioselective properties for example for D-peptides (Michaud et al., 2003), histidine (Ruta et al., 2007a), arginine (Ruta et al., 2007b; Brumbt et al., 2005), thalidomide (Shoji et al., 2007) or ibuprofen (Kim Y. S. et al., 2010). These aptamers can potentially be used to construct chiral biosensors. Despite of successful chiral separation by aptamer modified stationary phase (Ravelet et al., 2005) or aptamers

based capillary electrophoresis there still exists deficiencies in the understanding of the molecular basis of their chiral recognition. In (Lin P. H. et al., 2009) authors study the binding mechanism of DNA aptamers with L-argininamide by spectroscopic and calorimetric methods.

5. Conclusion

The design and optimization of sensors based on the use of active biological materials, biosensors and immunosensors for rapid, selective and sensitive determination of chiral compounds seems to be an extremely promising direction of development. As it was presented to the construction of such sensors a different detection methods may be involved. Guideline in the selection of biologically active material can be results of research conducted by separation methods using chiral antibodies or aptamers. Especially development of aptasensor which are a relatively new technique seems to be promising. The number of available biological active materials suitable to the construction of biosensors could be increased by enzyme screening and protein design. It is quite possible that with very well optimized enantioselectivity, stability and reproducibility biochemical sensors may become in the future valuable instruments for quick control of chiral purity for biotechnology and pharmaceutical industry.

6. References

Aboul-Enein, H. Y., Stefan, R. I. & Radu, G. L. (1999a) Biosensor for enantioselective analysis of S-cilazapril, S-trandolapril, and S-pentopril Pharmacuetical Development and Technology Vol. 4, No. 2, (May 1999), pp. 251-255, ISSN 1083-7450

Aboul-Enein, H. Y., Stefan, R. I. & Radu, G. L. (1999b) Biosensor for the enantioselective analysis of S-perindopril *Preparative Biochemistry & Biotechnology* Vol. 29, No 1, (February 1999), pp. 55-61, ISSN 1082-6068

Agranat, I., Caner, H. & Caldwell, J. (2002) Putting chirality to work: the strategy of chiral switches. *Nature Reviews Drug Discovery*, Vol. 1, No. 10, (October 2002), pp. 753-768, ISSN 1474-1776

Ahmad, A., Ramakrishnan, A., McLean, M. A. & Breau, A. P. (2003) Use of surface plasmon resonance biosensor technology as a possible alternative to detect differences in binding of enantiomeric drug compounds to immobilized albumins. *Biosensors and Bioelectronics,* Vol. 18, No. 4, (April 2003), pp. 399-404, ISSN 0956-5663

Arnell, R., Ferraz, N. & Fornstedt, T. (2006) Analytical characterization of chiral drug-protein interactions: Comparison between the optical biosensor (Surface Plasmon Resonance) assay and HPLC perturbation method. *Analytical Chemistry* Vol. 78, No. 5, (March 2006), pp. 1682-1689, ISSN 00032700

Baumann, P., Zullino, D. F. & Eap, C. E. (2002) Enantiomers' potential in psychopharmacology. A critical analysis with special emphasis on the antidepressant escitalopram., *European Neuropsychopharmacology*, Vol. 12, No. 5, (October 2002), pp.433-444, ISSN 0924-977

Berkman, C. E., Quinn, D. A. & Thompson, C. M. (1993) Synthesis, absolute configuration, and analysis of malathion, malaoxon, and isomalathion enantiomers. *Chemical Research in Toxicology*. Vol. 6, No. 5, (September 1993), pp. 724-730. ISSN 0893-228X

Brumbt, A., Ravelet, C., Grosset, C., Ravel, A., Villet, A. & Peyrin, E. (2005) Chiral stationary phase based on a biostable L-RNA aptamers. *Analytical Chemistry* Vol. 77, No. 7, (April 2005), pp. 1993-1998, ISSN 00032700

Bucheli, T., Müller, S. R., Voegelin, A. & Schwarzenbach, R. P. (1998) Bituminous Roof Sealing Membranes as Major Source of Herbicide (R, S)-Mecoprop in roof Runoff waters: Potential contamination of groundwater and surface waters., *Environmental Science and Technology* Vol. 32, No. 22, (September 1998), pp. 3465-3471, ISSN 0013-936X

Caner, H., Groner, E. & Levy, L. (2004) Trends in the development of chiral drugs. *Drug Discovery Today*, Vol. 9, No. 3, (February 2004), pp. 105-110, ISSN 1359-6446

Chen, C. S., Fujimoto, Y., Girdaukas, G. & Sih C. J. (1982) Quantitative analyses of biochemical kinetic resolution of enantiomers *Journal of the American Chemical Society* Vol. 104, No. 25, (December 1982), pp. 7294-7299, ISSN 0002-7863

Chen, M., Fu, Y., Ciu, X., Wang, L. & Li, M. (2009) Comparative Analysis of Proline Enantiomer in Chiral Recognition of Biological Macromolecule in Immunoassay *Electroanalysis* Vol. 21, No. 21, (November 2009), pp. 2339-2344, ISSN 1040-0397

Chen, Z., Takei, Y., Deore, B. A. & Nagaoka, T. (2000) Enantioselective uptake of amino acid with overoxidized polypyrrole colloid templated with L-lactate. *Analyst*, Vol. *125*, No. 12, (n.d.), pp. 2249-2254, ISSN 0003-2654

Cosnier, S., Le Pellec, A., Marks, R.S., Périé, K. & Lellouche, J-P. (2003) A permselective biotinylated polydicarbazole film for the fabrication of amperometric enzyme electrodes. *Electrochemistry Communications*, Vol. 5, No. 11, (November 2003), pp. 973-977, ISSN 1388-2481

Dominguez, R., Serra, B., Reviejo, A.J. & Pingarrón, J.M. (2001) Chiral analysis of amino acids using electrochemical composite bienzyme biosensors. *Analytical Biochemistry*, Vol. 298, No. 2, (November 2001), pp. 275-282, ISSN 0003-2697

Dutta, P., Tipple, C. A., Lavrik, N. V., Datskos, P. G., Hofstetter, H., Hofstetter, O. & Sepaniak, M. J. (2003) Enantioselective Sensors Based on Antibody-Mediated Nanomechanics. *Analytical Chemistry*, Vol. 75, No. 10, (May 2003), pp. 2342-2348, ISSN 00032700

Eichelbaum, M. & Gross, S. A. (1996) Sterochemical aspects of drug action and disposition., *Advances in Drug Research.* Vol. 28, (n.d.). pp. 1-64, ISSN 0065-2490

Fono, L. J. & Sedlak, D. L. (2005) Use of the Chiral Pharmaceutical Propranolol to Identify Sewage Discharges into Surface Waters., *Environmental Science and Technology*, Vol. 39, No. 23, (December 2005), pp. 9244-9252, ISSN 0013-936X

Gadepalli, R.S., Rimoldi, J.M., Fronczek, F.R., Nillos, M., Gan, J., Deng, X., Rodriguez-Fuentes, G. & Schlenk, D. (2007) Synthesis of fenthion sulfoxide and fenoxon sulfoxide enantiomers: Effect of sulfur chirality on acetylcholinesterase activity. *Chemical Research in Toxicology,* Vol. 20, No. 2, (January 2007), pp. 257-262, ISSN 0893-228X

Garrison, A.W. (2006) Probing the enantioselectivity of chiral pesticides. Environmental Science and Technology, Vol. 40, No. 1, (January 2006), pp. 16-23. ISSN 0013-936X

Giovannoli, C., Baggiani, C., Anfossi, L. & Giraudi, G. (2008) Aptamers and molecularly imprinted polymers as artificial biomimetic receptors in affinity capillary electrophoresis and electrochromatography. *Electrophoresis,* Vol. 29, No. 16, (August 2008), pp. 3349-3365, ISSN 0173-0835

Herráez-Hernández, R. & Campíns-Falco, P. (2001) Chiral Separation of Ephedrines by Liquid Chromatography Using β-cyclodextrins., *Analytica Chimica Acta*, Vol. 434, No. 2, (May 2001), pp. 315-324, ISSN 0003-2670

Hofstetter, O., Hertweck, J. K. & Hofstetter, H. (2005) Detection of enantiomeric impurities in a simple membrane-based optical immunosensors Journal of Biochemical and Biophysical Methods Vol. 63, No. 2, (May 2005), pp. 91-99, ISSN 0165-022X

Hofstetter, O., Hofstetter, H., Schurig, V., Wilchek, M. & Green, B. S. (1998) Antibodies Can Recognize the Chiral Center of Free α-Amino Acids. *Journal of the American Chemical Society,* Vol. 120, No. 13, (April 1998), pp. 3251-3252, ISSN 0002-7863

Hofstetter, O., Hofstetter, H., Wilchek, M., Schurig, V. & Green, B. S. (2000) An immunochemical approach for the determination of trace amounts of enantiomeric impurities. *Chemical Communications*, Vol. n. a., Iss 17, (n.d.) pp. 1581-1582, ISSN 1359-7345

Hofstetter, O., Hofstetter, H., Wilchek, M., Schurig, V. & Green, B. S. (1999) Chiral discrimination using an immunosensor. *Nature Biotechnology*, Vol. 17, No. 4, (April 1999), pp. 371-374, ISSN 1087-0156

Hofstetter, O., Lindstrom, H. & Hofstetter, H. (2002) Direct Resolution of Enantiomers in High-Performance Immunoaffinity Chromatography under Isocratic Conditions. *Analytical Chemistry*; Vol 74, No. 9, (May 2002), pp. 2119-2125, ISSN 00032700

Huang, J., Egan, V., Guo, H., Yoon,J. Y., Briseno, A. L., Rauda, I. E., Garrell, R. L., Knobler, C. M., Zhou, F. & Kaner, R. B. (2003) Enantioselective discrimination of D- and L-phenylalanine by chiral polyaniniline thin films. *Advanced Materials*. Vol. 15, No. 14, (July 2003) pp. 1158-1161, ISSN 0935-9648

Hutt, A.J. & Valentová, J. (2003) The Chiral Switch: The Development of single enantiomer drugs from racemates. *Acta Facultatis Pharmaceuticae Universitatis Comenianae*, Vol. 50, (n.d.), pp. 7-23, ISSN 0301-2298

Inaba, Y., Hamada-Sato, N., Kobayashi, T., Imada, C. & Watanabe, E. (2003b) Determination of D- and L-alanine concentrations using a pyruvic acid sensor., *Biosensors and Bioelectronics*, Vol. 18, No. 8, (August 2003), pp. 963-971, ISSN 0956-5663

Inaba, Y., Mizukami, K., Hamada-Sato, N., Kobayashi, T., Imada, C. & Watanabe, E. (2003a) Development of a D-alanine sensor for the monitoring of a fermentation using improved selectivity by the combination of D-amino acid oxidase and pyruvate oxidase *Biosensors and Bioelectronics*, Vol. 19, No. 5, (December 2003), pp. 423-431, ISSN 0956-5663

Jiang, X.Y., Zhu, L.D., Yang, D.X., Mao, X.Y. & Wu, Y.H. (2009) Amperometric Ethanol Biosensor Based on Integration of Alcohol Dehydrogenase with Meldola's Blue/Ordered Mesoporous Carbon Electrode. *Electroanalysis* Vol. 21, Iss 14, (July 2009), pp. 1617-1623, ISSN 1040-0397

Jongejan, A., Machado, S. S. & Jongejan, J. A., (2000) The enantioselectivity of quinohaemoprotein alcohol dehydrogenases: mechanistic and structural aspects, *Journal of Molecular Catalysis B: Enzymatic*, Vol. 8, No. 1-3, (January 2000), pp. 121-163, ISSN 1381-1177

Kacaniklic, V., Johansson, K., Marko-Varga, G., Gorton, I., Jonsson-Pettersson G. & Csoregi, E. (1994) Amperometric biosensors for detection of L- and D-amino acids based on coimmobilized peroxidase and L and D- amino acid oxidase in carbon paste electrodes. *Electroanalysis,* Vol. 6, No. 5-6, (May-June 1994), pp. 381-390, ISSN 1040-0397

Kaniewska M. PhD Thesis, University of Warsaw, 2009

Killard, A.J. & Smyth, M.R. (2000) Separation-free electrochemical immunosensor strategies. *Analytical Letters*, Vol. 33, No. 8, (n.d.), pp. 1451-1465, ISSN 0003-2719

Kim, H., Gritti, F. & Guiochon, G. (2004) Effect of the temperature on the isotherm parameters of phenol in reversed-phase liquid chromatography. *Journal of Chromatography A*, Vol. 1049, No. 1-2, (September 2004), pp. 25-36, ISSN 0021-9673

Kim, Y. S., Hyun, C. J., Kim, I. A. & Gu, M. B. (2010) Isolation and characterization of enantioselective DNA aptamers for ibuprofen *Bioorganic & Medicinal Chemistry*. Vol. 18, No. 10, (May 2010), pp. 3467-3473, ISSN 0968-0896

Kullick, T., Ulber, R., Meyer, H. H., Scheper, T. & Schlügerl, K. (1994) Biosensors for enantioselective analysis. *Analytica Chimica Acta,* Vol. 293, No. 3, (July 1994), pp. 271-276, ISSN 0003-2670

Landsteiner, K. & van der Scheer, J. (1928) Serological Differentiation of steric isomers. *Journal of Experimental Medicine*, Vol. 48, No. 3, (September 1928), pp. 315-320, ISSN 0022-1007

Lane, R. M. & Baker, G. B., (1999) Chirality and Drugs Used in Psychiatry: Nice to Know or Need to Know?, *Cellular and Molecular Neurobiology*, Vol. 19,No. 3, (June 1999), pp. 355-372 ISSN 0272-4340

Laska, M., Liesen, A. & Teubner, P. (1999) Enantioselectivity of odor perception in squirrel monkey and humans. *American Journal of Physiology Regulatory Integrative Comperative Physiology*, Vol. 277, No. 4, (October 1999), pp. R1098-R1103, ISSN 0363-6119

Lee, M. & Walt, D.R. (2000) A fiber-optic microarray biosensor using aptamers as receptors. *Analytical Biochemistry* Vol. 282, No. 1, (June 2000), pp. 142–146, ISSN 0003-2697

Lin, K. D., Zang, F., Zhou, S.S., Lui, W., Gan, J. & Pan, Z. (2007) Stereoisomeric separation and toxicity of the namaticide fosthiazate *Environmental Toxicology and Chemistry,* Vol. 26, No. 11, (November 2007), pp. 2339-2344, ISSN 0730-7268

Lin, P. H., Tong, S. J., Louis, S. R., Chang, Y., Chen, W. Y. (2009) Thermodynamic basis of chiral recognition in a DNA aptamers. *Physical Chemistry Chemical Physics* Vol. 11, No. 42, (November 2009), pp. 9744-9750, ISSN 1463-9076

Liu, Y., Tuleouva, N., Ramanculov, E. & Revzin, A. (2010) Aptamer-Based Electrochemical Biosensor for Interferon Gamma Detection. *Analytical Chemistry,* Vol. 82, No. 19, (October 2010), pp. 8131-8136 , ISSN 0003-2697

Lenz, W. (1988) A short history of thalidomide embryopathy. *Teratology*, Vol. 38, No. 3, (n.d.), pp. 203-215, ISSN 0040-3709

Marchelli, R., Dossena, A. & Palla, G. (1996) The potential of enantioselective analysis as a quality control tool., *Trends in Food Science and Technology*, Vol. 7, No. 4, (April 1996), pp. 113-119, ISSN 0924-2244

Michaud, M., Jourdan, E., Villet, A., Ravel, A., Grosset, C. & Peyrin, E.(2003) A DNA aptamers as a new target-specific chiral selector for HPLC. *Journal of the American Chemical Society,* Vol. 125, No. 28, (July 2003), pp. 8672-8679, ISSN 0002-7863

Minami, H., Sugawara, M., Odashima, K., Umezawa, Y., Uto, M., Michaelis, E. K. & Kuwana, T. (1991) Ion channel sensors for glutamic acid. *Analytical Chemistry*, Vol. 63, No. 23, (December 1991), pp. 2787-2795, ISSN 00032700

Minunni, M., Tombelli, S., Gullotto, A., Luzi, E. & Mascini, M., 2004. Development of biosensors with aptamers as bio-recognition element: the case of HIV-1 Tat protein.

Biosensors and Bioelectronics, Vol. 20, No. 6, (December 2004), pp. 1149–1156, ISSN 0956-5663

Miyazaki, A., Nakamura, T., Kawaradani, M. & Marumo, S. (1988) Resolution and Biological Activity of Both Enantiomers of Methamidophos and Acephate. *Journal of Agricultural and Food Chemistry*, Vol. 36, No. 4, (July 1988), pp. 835-837, ISSN 0021-8561

Moreno, J. A., Montes, F. J., Catakin, J. & Gahln M. A. (1996) Inhibition of D-amino acid oxidase by alpha-keto acids analogs of amino acids. *Enzyme and Microbial Technology,* Vol. 18, No. 5, (April 1996), pp. 379-382, ISSN 0141-0229

Mosing, R. K. & Bowser, M. T. (2007) Microfluidic selection and applications of aptamers. *Journal of Separation Science*, Vol. 30, No. 10, (July 2007), pp. 1420-1426, ISSN 1615-9306

Motonaka, J., Katumoto, Y. & Ikeda, S. (1998) Preparation and properties of enzyme sensors for L-lactic and D-lactic acids in optical isomers. *Analytica Chimica Acta.* Vol. 368, No. 1-2, (July 1998), pp. 91-95, ISSN 0003-2670

Nakanishi, T., Yamakawa, N., Asahi, T., Shibata, N., Ohtani, B. & Osaka, T. (2004) Chiral Discrimination Between Thalidomide Enantiomers Using a Solid Surface With Two-Dimensional Chirality. *Chirality* Vol. 16, (n.d.), pp.S36-S39, ISSN 0899-0042

Ng, S-C., Sun, T. & Chan, H.S.O. (2002) Chiral discrimination of enantiomers with a self-assembled monolayer of functionalized β-cyclodextrins on Au surfaces. *Tetrahedron Letters*, Vol. 43, No. 15, (April 2002), pp. 2863-2866. ISSN 0040-4039

Nillos, M.G., Rodriguez-Fuentes, G., Gan, J. & Schlenk, D. (2007) Enantioselective acetylcholinesterase inhibition of the organophosphorous insecticides profenofos, fonofos, and crotoxyphos. *Environmental Toxicology and Chemistry*, Vol. 26, No. 9, (September 2007), pp. 1949-1954, ISSN 0730-7268

Ohsawa, K., Kasamatsu, T., Nagashima, J., Hanawa, K., Kuwahara, M., Ozaki, H. & Sawai, H. (2008) Arginine-modified DNA aptamers that show enantioselective recognition of the dicarboxylic acid moiety of glutamic acid *Analytical Sciences*, Vol. 24, No. 1, (January 2008), pp. 167-172, ISSN 0910-6340

Overbeeke, P.L.A., Orrenius, S.C., Jongejan, J.A. & Duine J.A. (1998) Enthalpic and entropic contributions to lipase enantioselectivity *Chemistry and Physics of Lipids*, Vol. *93*, No. 1, (June 1998), pp 81-93, ISSN 0009-3084

Perrier, S., Ravelet, C., Guieu, V., Fize, J., Roy, B., Perigaud, C. & Peyrin, E. (2010) Rationally designed aptamer-based fluorescence polarization sensor dedicated to the small target analysis. *Biosensors and Bioelectronics,* Vol. 25, No. 7, (March 2010), pp. 1652-1657, ISSN 0956-5663

Pollegioni, L., Diederichs, K, Molla, G., Umhau, S., Welte, W., Ghisla, S. & Pilone, M. S. (2002) Yeast D amino Acid Oxidase: Structural basis of its catalytic properties., *Journal of Molecular Biology*, Vol. 324, No. 3, (November 2002), pp. 535-546, ISSN 0022-2836

Ravelet, C., Boulkedid, R., Ravel, A., Grosset, C., Villet, A., Fize, J. & Peyrin, E. (2005) A L-RNA aptamer chiral stationary phase for the resolution of target and related compounds. *Journal of Chromatography A,* Vol. 1076, Iss 1-2, (May 2005), pp. 62-70, ISSN 0021-9673

Robins, J., Jones, M. & Matisoo-Smith, E., 2001, Amino Acid Racemization Dating in New Zealand: An Overview., Auckland University, Private Bag 92019, pp.1-45 Available from http://www.detectingdesign.com/PDF%20Files/amino%20acid%20racemization%20dating.pdf

Rodriguez, O.P., Muth, G.W., Berkman, C.E., Kim, K. & Thompson, C.M. (1997) Inhibition of various cholinesterases with the enantiomers of malaoxon. *Bulletin of Environmental Contamination and Toxicology,* Vol. 58, No. 2, (n.d.), pp. 171-176, ISSN 0007-4861

Rogers, K.R. (2000) Principles of affinity-based biosensors. *Molecular Biotechnology*, Vol. 14, No. 2, (February 2000), pp. 109-129, ISSN 1073-6085

Ruta, J., Grosset, .C, Ravelet, C., Fize, J., Villet, A., Ravel, A. & Peyrin, E. (2007a) Chiral resolution of histidine using an anti-D-histidine L-RNA aptamers microbore column. *Journal of Chromatography B-Analytical Technologies in the Biomedical and Life Sciences,* Vol. 845 No. 2, (January 2007), pp. 186-190 ISSN 1570-0232

Ruta, J., Ravelet, C., Baussanne, I., Decout, J.L. & Peyrin, E. (2007b) Aptamer-based enantioselective competitive binding assay for the trace enantiomer detection. *Analytical Chemistry,* Vol. 79, No. 12, (June 2007), pp. 4716-4719, ISSN 00032700

Sandblad, P., Arnell, R., Samuelsson, J. & Fornstadt, T. (2009) Approach for Reliable Evaluation of Drug Proteins Interactions Using Surface Plasmon Resonance Technology. *Analytical Chemistry,* Vol. 81, No. 9, (May 2009), pp. 3551-3559, ISSN 00032700

Sarkar, P., Tothill, I. E., Setford, S. J. & Turner, A. P. F. (1999) Screen-printed amperometric biosensors for the rapid measurement of l- and d-amino acids. *The Analyst,* Vol. 124, No. 6, (June 1999), pp. 865-870, ISSN 0003-2654

Schlügerl, K., Ulber, R., & Scheper, T. (1996) Developments of biosensors for enantiomeric analysis. *Trends in analytical chemistry*, Vol. 15, No. 2, (n.d.), pp. 56-62, ISSN 0165-9936

Shi, Q. & Dong, S. (1995) Amperometric biosensors based on the immobilization of oxidases in Prussian blue film by electrochemical codeposition. *Analytica Chimica Acta,* Vol. 310, No. 3, (July 1995), pp. 429-436, ISSN 0003-2670

Shoji, A., Kuwahara, M., Ozaki, H. & Sawai, H. (2007) Modified DNA aptamers that binds the (R)-Isomer of a thalidomide derivative with high enantioselectivity *Journal of the American Chemical Society* Vol. 129, No. 5, (February 2007), pp. 1456-1464, ISSN 0002-7863

Silvaieh, H., Wintersteiger, R., Schmid, M.G., Hofstetter, O. & Schurig, V. (2002) Enantioselective sequential-injection chemiluminescence immunoassays for 3,3',5-triiodothyronine (T_3) and thyroxine (T_4) *Analytica Chimica Acta*, Vol. 463, No. 1, (July 2002), pp. 5-14, ISSN 0003-2670

Somers, W. A. C., Stigter, E. C. A, van Hartingsveldt, W. & van der Lugt, J. P. (1998) Enantioselective oxidation of secondary alcohols at a quinohaemoprotein alcohol dehydrogenase electrode. *Applied Biochemistry and Biotechnology,* Vol. 75, No. 2-3, (November/December 1998), pp. 151-162, ISSN 0273-2289

Stefan, R.I., Aboul-Enein, H.Y. & Radu, G.L. (1998) Biosensors for the enantioselective analysis of S-enalapril and S-ramipril *Preparative Biochemistry & Biotechnology* Vol. 28, No. 4, (n.d.), pp. 305-312, ISSN 1082-6068

Stefan, R.I. & Aboul-Enein, H.Y. (2002) The construction and characterization of an amperometric immunosensor for the thyroid hormone (+)-3,3 ',5,5 '- tetraiodo-L-thyronine (L-T-4) Journal of Immunoassay & Immunochemistry Vol. 23, No. 4, (November 2002) pp. 429-437, ISSN 1532-1819

Stefan, R.I., Bala, C. & Aboul-Enein, H.Y. (2003a) Biosensor for the enantioselective analysis of S- captopril. *Sensors and Actuators* B, Vol. 92, No. 1-2, (July 2003), pp. 228-231, ISSN 0925-4005

Stefan, R.I., Bokretsion, R.G., van Staden, J.F. & Aboul-Enein, H.Y. (2003b) Determination of L- and D- enantiomers of methotrexate using amperometric biosensors. *Talanta*, Vol. 60, No. 5, (July 2003), pp. 983-990. ISSN 0039-9140

Stefan, R.I., Najem, R.M., van Staden, J.F. & Aboul-Enein, H.Y. (2003c) Biosensors for the enantioselective analysis of pipecolic acid *Sensors and Actuators B*, Vol. 94, No. 3, (October 2003), pp. 271-275, ISSN 0925-4005

Stefan, R.I., van Staden, J.F. & Aboul-Enain, H.Y. (1999) Analysis of chiral drugs with enantioselective biosensors. An overview. *Electroanalysis*, Vol. 11, No. 16, (November 1999), pp. 1233-1235, ISSN 1040-0397

Su, W. C., Zhang, W.G., Zhang, S., Fan, J., Yin, X.,. Luo, M.L & Ng, S.C. (2009) A novel strategy for rapid real-time chiral discrimination of enantiomers using serum albumin functionalized QCM biosensor. *Biosensensors and Bioelectronics* Vol. 25, No. 2, (October 2009), pp. 488-492, ISSN 0956-5663

Subrahmanyam, S., Piletsky, S. A & Turner, A. P. F. (2002) Application of Natural Receptors in Sensors and Assays- Review *Analytical Chemistry*; Vol. 74, No. 16, (August 2002), pp. 3942-3951, ISSN 00032700

Tanese, M.C., Torsi, L., Cioffi, N., Zotti, L.A., Colangiuli, D., Farinola, G.M., Babudri, F., Naso, F., Giangregorio, M.M., Sabbatini, L. & Zambonin, P.G. (2004) Poly(phenyleneethynylene) polymers bearing glucose substituents as promising active layers in enantioselective chemiresistors., *Sensors and Actuators B*, Vol. 100, No. 1-2, (June 2004) pp. 17-21, ISSN 0925-4005

Tombelli, S., Minunni, M. & Mascini, M. (2005) Review. Analytical applications of aptamers. *Biosensors and Bioelectronics,* Vol. 20, No. 12, (June 2005), pp. 2424–2434, ISSN 0956-5663

Tsourkas, A., Hofstetter, O., Hofstetter, H. Weissleder, R. & Josephson, L. (2004) Magnetic relaxation swich immunosensors detect anantiomeric impurities. *Angewandte Chemie-International Edition*, Vol. 43, No. 18, (n.d.), pp. 2395-2399, ISSN 0044-8249

Varadi, M., Adanyi, N., Szabó, E.E. & Trummer, N. (1999) Determination of the ratio of D- and L-amino acids in brewing by an immobilised amino acid oxidase enzyme reactor coupled to amperometric detection. *Biosensors and Bioelectronics*, Vol. 14, No. 3, (March 1999), pp. 335-340, ISSN 0956-5663

Wcisło, M., Compagnone, D. & Trojanowicz, M. (2007) Enantioselective screen-printed amperometric biosensor for determination of D-amino acids. *Bioelectrochemistry* Vol. 71, No. 1, (September 2007), pp. 91-98, ISSN 1567-5394

Zawirska-Wojtasiak, R. (2006) Chirality and the nature of food authenticity of aroma., *Acta Scientiarum Polonorum, Technologia Alimentaria*, Vol. 5, No. 1, (n.d.), pp. 21-36, ISSN 1644-0730

Zhang, S., Ding, J., Liu, Y., Kong, J. & Hofstetter, O. (2006) Development of a highly enantioselective capacitive immunosensor for the detection of alpha-amino acids. *Analytical Chemistry* Vol. 78, No. 21, (November 2006), pp. 7592-7596, ISSN 0003-2700

Zhang, Z., Liao, H., Li,H., Nie, L. & Yao, S. (2005) Stereoselective histidine sensor based on molecularly imprinted sol-gel films., *Analytical Biochemistry*, Vol. 336, No. 1, (January 2005), pp. 108-116, ISSN 0003-2697

Zhou, S., Lin, K., Yang, H., Li, L., Liu, W. & Li, J. (2007) Stereoisomeric Separation and Toxicity of a New Organophosphorus Insecticide Chloramidophos *Chemical Research in Toxicology,* Vol. 20, No. 3, (March 2003), pp. 400-405, ISSN 0893-228X

7

Recent Progress in the Construction Methodology of Fluorescent Biosensors Based on Biomolecules

Eiji Nakata, FongFong Liew, Shun Nakano and Takashi Morii
Institute of Advanced Energy, Kyoto University
Kyoto, Japan

1. Introduction

The creation of novel molecular tools for detection and monitoring of the transitional concentration and localization changes of biologically important molecules, such as biomacromolecules, signaling small molecules and biologically important ions, is a great challenge in the field of chemical biology. Therefore, much attention has been devoted by chemists and biologists to develop sensing tools that allow real-time tracking of the molecules of interests *in vivo* or *in vitro*. (Thevenot, D. R. et al., 2001; Jelinek, R. et al., 2004; Borisov, S. M. et al., 2008) Among them, the fluorescent biosensor, which is defined as the sensor that converts a molecular recognition event to a measurable fluorescent signal change, has recently emerged as a powerful tool for the following reasons. (Hellinga, H.W. et al., 1998; Johnsson, N. et al., 2007; Johnsson, K., 2009; Wang, H. et al., 2009; Liu, J. et al., 2009) Biomacromolecular receptors, such as nucleic acids (DNA or RNA) or proteins, have superior characteristics as the recognition platform because they play crucial roles in numerous biological processes to mediate and regulate a range of strict recognition and chemical reactions within cells. As for the tools for the transducer, the fluorescence detection has the superior physical properties, such as high sensitivity, excellent spatial resolution, good tissue penetration and low cost for the detection system, in contrast to the other detection method including optical, electrical, electrochemical, thermal, magnetic detections. Thus, transducing the molecular recognition events with the fluorescence signals is very appealing and has been one of the most widely adapted methods. (Giepmans, B.N. et al., 2006; Rao, J. et al., 2007) The rational design strategies of fluorescent biosensors have not been matured as generally considered by the researchers in the biological field. A simple strategy to construct a biosensor with tailored characteristics would be to conjugate a recognition module with a signal transducer unit, although there is no simple methodology to conjugate the recognition module and the transducer unit to afford a usable fluorescent biosensor. Here we focus to overview the progress in the design strategy of fluorescent biosensors, such as the auto-fluorescent protein-based biosensor, protein-based biosensor covalently modified with synthetic fluorophores and signaling aptamers.

2. Auto-fluorescent proteins (AFPs) based biosensors

Auto-fluorescent proteins (AFPs) such as green fluorescent protein (GFP) from jellyfish (Shimomura, O. et al., 1962) are widely used as noninvasive fluorescent markers for gene expression, protein localization, and intracellular protein targeting (Chalfie, M. et al., 1994; Lippincott-Schwartz, J. et al., 2001). The application of AFPs is not limited to the fluorescent markers. Various kinds of AFP-based biosensors have recently been developed by fusion of reporter proteins or mutation of AFPs for imaging and sensing important molecules and key events in living cell. (Zhang, J. et al. 2002; Zhang, J. et al. 2007; Mank, M. et al., 2008; VanEngelenburg, S. B. et al. 2008; Lawrence, D. S. et al. 2007; Ozawa, T. 2006; Prinz, A. et al. 2008) The advantage of AFP-based biosensor is that it can be endogenously expressed in cells or tissues simply by transfection of the plasmid DNA encoding it. This approach is a noninvasive method and therefore avoids damage to the cell. Because AFPs based biosensor can be produced automatically, the influence of dilution due to vital activity, such as cell growth and division, is minimal. Moreover, it is possible to control the localization of biosensors to the sites of interest within cell by introducing a certain organelle-specific targeting signal. These biosensors have been powerful tool for in vivo applications.

2.1 Single AFP based biosensor

In the case of biosensors based on a single AFP, analyte binding events affect directly or indirectly to fluorescent properties or formation, respectively, of the chromophore moiety of AFP. The former is classified as analyte-sensitive sensors and the latter as conformation-sensitive sensors.

The design of analyte-sensitive sensors utilizes AFP variants, whose fluorescent properties are directly affected by the interaction between a target molecule and a chromophore moiety in AFP. In general, the fluorescence of most of AFP variants is affected reversibly by moderate acidification of the chromophore. To exploit such intrinsic properties of AFPs, pH sensitive AFP variants have been developed. (Kneen, M. et al. 1998; Llopis, J. et al. 1998; Miesenbock, G. et al. 1998; Matsuyama, S. et al. 2000) Mutants of YFPs showing pH sensitivity bind to halide ion selectively and the binding of anion leads to fluorescence quenching due to the induced pKa shift. (Wachter, R. M. et al. 1999; Jayaraman, S. et al. 2000; Wachter, R. M. et al. 2000) The fluorescence of AFP becomes sensitive to other signals by the introduction of specific mutation in close proximity to the chromophore or within the barrel structure. In this manner, biosensors specific for Mercury (II) ion (Chapleau, R.R. et al. 2008) and Zinc (II) ion (Barondeau, D. P. et al. 2002) have been created. The receptor function of the sensor was directly integrated into the chromophore by alteration of the chemical nature around the chromophore.

Another design strategy of a single AFP based biosensor relies on circularly permutated AFP (cpAFP), which is classified as a conformation-sensitive sensor, that is, a conformational change of the receptor associated with the ligand-binding event results a formation of the AFP chromophore. The cpAFP is a regenerated AFP variant, in which the original N- and C termini are connected with a flexible peptide linker to regenerate novel N and C termini at specific positions. (Baird, G. S. et al. 1999) A number of cpAFPs with novel termini retained their fluorescence even when a foreign receptor was inserted at the termini. Indeed, cpAFP variants that detect Ca^{2+} (Nakai, J. et al. 2001; Souslova, E. A. et al. 2007; Baird, G. S. et al. 1999, Nagai, T. et al. 2001), cGMP (Nausch, L. W. et al. 2008), H_2O_2 (Belousov, V. V. et al. 2006; Dooley, C. T. 2004), Zn^{2+} (Mizuno, T. et al. 2007) and an inositol

phosphate derivative (Sakaguchi, R. et al. 2009), have been developed by inserting appropriate receptor modules.

Morii and coworkers developed a cpAFP-based sensor for D-*myo*-inositol-1,3,4,5-tetrakisphosphate, Ins(1,3,4,5)P_4, by utilizing a newly designed split PH domain of Bruton's tyrosine kinase (Btk) and cpGFP (Sakaguchi, R. et al. 2009) (Figure 1). Interestingly, the conjugate Btk-cpGFP realized a ratiometric fluorescence detection of Ins(1,3,4,5)P_4 by the excitation of each distinct absorption band, and retained ligand affinity and selectivity of the original PH domain.

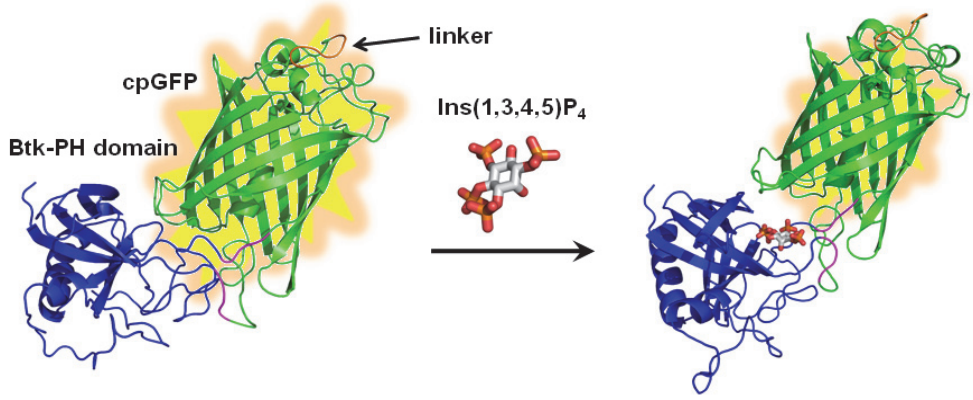

Fig. 1. Schematic illustration shows a fluorescent biosensor for Ins(1,3,4,5)P_4 based on the split Btk PH domain-cpGFP conjugate (Sakaguchi, R. et al. 2009). The original N and C termini of GFP were linked with a short peptide linker (orange), and the novel terminal of cpGFP (purple) was fused to the split Btk PH domain (blue). The conformational change of the PH domain induced by the ligand-binding event was transduced to the structural change of the chromophore of cpGFP, and then resulted in the ratiometric fluorescence change of cpGFP.

2.2 Split AFP based biosensor

It is considered that the formation of a AFPs chromophore requires a properly folded and an intact structure. However, many experimental data indicate that slight structural modifications of AFPs, like circular permutation and insertion of recognition domains as described in the previous section, still give fluorescent AFPs constructs. Therefore, AFP sensors in the absence of targets often reveal unavoidable background fluorescence. An excellent strategy to accomplish full suppression of the initial fluorescence utilizes an AFP variant that was split into two non-fluorescent fragments.(Shyu, Y.J. et al. 2008; Kerppola T. K. 2006) Regan and co-workers first demonstrated that a split GFP displayed a quite low background fluorescence in the separated state and a fluorescence emission was significantly recovered by the reassembly of the two fragments when they were placed in close proximity by strongly interacting antiparallel leucine zippers.(Ghosh, I. et al. 2000) Based on this strategy, a receptor composed of two subunits that are associated by binding to the analyte can be converted into a fluorescent biosensor by connecting each of the two subunits with each split AFP fragment (Figure 2). Actually, several types of biosensors have

been developed for fluorescent detection of specific DNA sequences (Stains, C. I. et al. 2005; Demidov, V. V. et al. 2006), DNA methylation(Stains, C. I. et al. 2006), mRNA(Ozawa, T. et al. 2007; Valencia-Burton, M. et al. 2007) and protein interactions (Nyfeler, B. et al. 2005; Hu, C. -D. et al. 2003; Wilson, C. G. et al, 2004).

Unlike the above-mentioned split AFP reconstitution, in which split AFP halves reform into a fluorescent structure via noncovalent association, another reconstitution strategy, intein-mediated reconstitution, has been developed by Ozawa and co-workers (Ozawa, T. et al. 2000). In this strategy, split inteins were fused to split EGFPs. Each split intein-EGFP fusion is attached to a protein of interest. The split inteins are brought into close proximity to trigger protein splicing when an analyte induces the association between proteins of interest. As a result, the two EGFP fragments are linked with a covalent bond and emit fluorescence. More comprehensive information on this reconstitution strategy is available in other excellent reviews (Ozawa, T. 2006; Awais, M. et al. 2011).

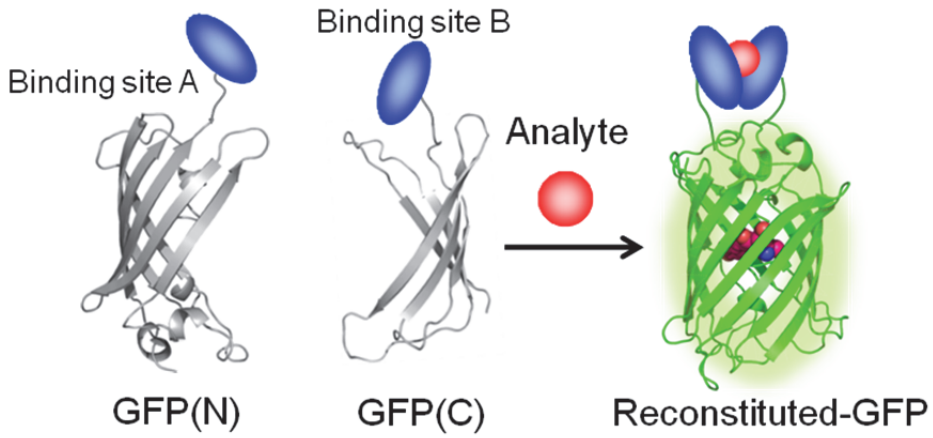

Fig. 2. Schematic illustration shows split AFP based fluorescent biosensor. A fluorescent protein such as GFP is split into two halves [GFP(N) and GFP(C)], which connect each of the two binding subunits, are associated by binding to the analyte.

2.3 FRET based biosensor

Non-radiative transfer of energy from an excited donor fluorophore to an acceptor chromophore is known as fluorescence resonance energy transfer (FRET). In order to induce FRET, the excitation spectrum of the acceptor must overlap with the emission spectrum of the donor, and the two fluorophores must be close in proximity (< 10 nm) and in a favorable orientation (Sapsford, K. E. et al. 2006). The efficiency of FRET is sensitive to the distance and the orientation between the donor and acceptor groups. To obtain the expected energy transfer efficiency for biological applications, the following two issues in the sensor design should be considered. First, suitable FRET pairs in which the donor emission spectrum overlaps the acceptor absorption spectrum should be chosen. In the AFP-based FRET strategy, CFP and YFP mutants have been favorably utilized as a FRET donor and an acceptor, respectively (Piston, D.W. et al. 2007). Second, the donor and the acceptor fluorophores should be placed at a rational distance which can drastically change

the efficiency of FRET before and after the sensing event.(Ohashi, T. et al. 2007) Therefore, a FRET based biosensor can sense the analyte in a ratiometric manner by comparing the donor and acceptor emission intensities that are result from the analyte induced distance and/or conformational changes. Based on the mechanism by which FRET efficiency changes, AFP-based FRET biosensors can be divided into two classes, that is, an intramolecular and an intermolecular FRET systems (Figure 3). In the case of intramolecular FRET biosensors, the two fluorophores are attached at two ends of a peptide sequence in the receptor protein or the concatenation of interacting domains. The feasibility of this strategy strongly depends on the magnitude of the structural change of the receptor. In the case of a receptor that displays a large structural change upon binding to the substrate, this strategy would be the most straightforward way to integrate the signal transduction function into the receptor of interest. Based on this strategy, various FRET biosensor for imaging intracellular events such as enzyme activities [e.g. protease (Mahajan, N. P. et al. 1999; Luo, K. Q. et al. 2001; Rehm, M. et al. 2002; Ai, H. W. et al. 2008), kinase (Sato, M. et al. 2002; Nagai, Y., et al. 2000), phosphatase (Newman, R. H. et al. 2008)] and dynamics of intracellular second messengers [e.g.Ca^{2+}(Miyawaki, A. et al. 1997; Romoser, V. A. et al. 1997), cAMP (Nikolaev,V. et al. 2004), cGMP (Sato, M. et al. 2000), IP_3 (Sato, M. et al. 2005)] have been developed. It should be noted that careful optimization, such as tuning the position of AFPs relative to the sensing domain by changing the linker between each of protein units, is frequently necessary to realize the satisfactory response of the FRET change. Most importantly, the

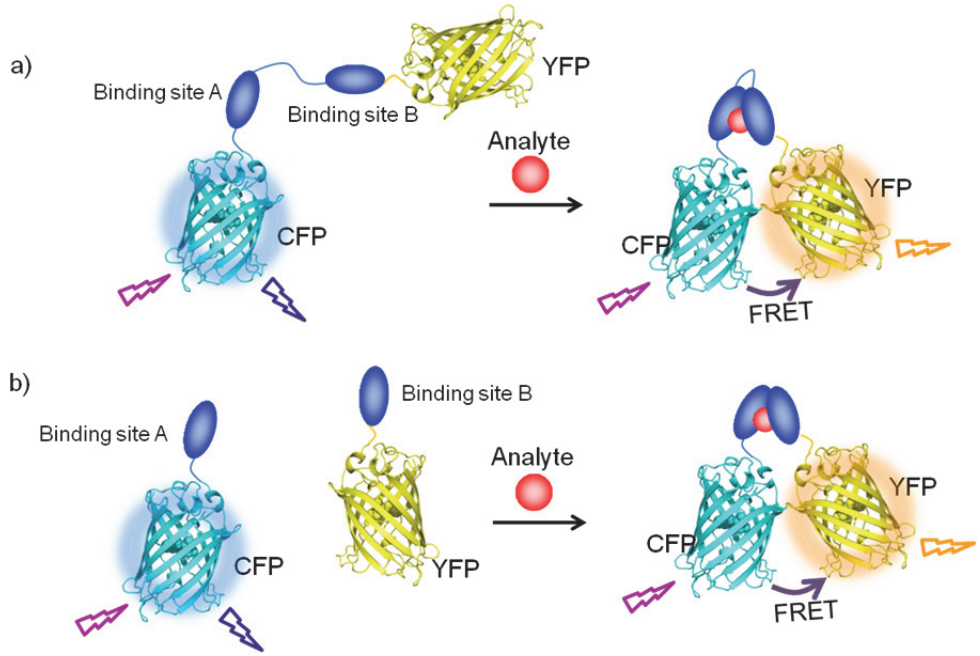

Fig. 3. AFP-fused FRET based biosensors. (a) Intramolecular FRET-based biosensor: The protein domains with a large structural change upon the analyte binding event. (b) Intermolecular FRET-based biosensor: The change of FRET efficiency is induced by the dissociation or association of the subunit upon the analyte-binding event.

obligatory conformational change in the receptor protein severely limits the choice of proteins available for the construction of FRET biosensors by this strategy. Recently, Johnsson and co-workers have demonstrated a new type of FRET biosensor based on their SNAP-tag technique, for which conformational changes upon analyte binding were not required (Brun, M. A. et al. 2009). Intermolecular FRET biosensors have been developed by employing two protein domains separated from each other, to which AFPs of FRET donor and acceptor are attached, respectively. Zaccoro and co-workers constructed FRET biosensor for cAMP by applying this strategy to the regulatory and catalytic subunit of protein kinase A (PKA) (Zaccolo, M. et al. 2000; Zaccolo, M et al. 2002). This biosensor can detect the rise of intracellular cAMP concentration by the decrease in the FRET efficiency induced by dissociation of the catalytic subunit from the regulatory subunit. Although this strategy shows a potential to effect a dynamic FRET change by the analyte-induced association and/or dissociation of protein subunits, the stoichiometry of the FRET donor and acceptor may vary between either cells or intracellular compartments. In these cases, they cause difficulty in analysis of the FRET efficiency changes. More comprehensive information on dual FRET-based biosensors is available in other excellent reviews (Souslova, E. A. et al. 2007; VanDngelenburg, S. B. et al. 2008; Carlson, H. J. et al. 2009).

3. Protein-based biosensor covalently modified with fluorescent artificial molecules

Another useful strategy to construct fluorescent biosensors is a structure-based design of a protein covalently modified with a fluorescent dye. Advantages for the use of fluorescent dyes are as follows. First, the relatively smaller size of the synthetic fluorophore is likely to less perturb the property of the original receptor protein. Second, a superior characteristic of dye, that is, the fluorescence changes in intensity and wavelength and the microenvironmental sensitivity such as pH, polarity or molecular recognition, could be introduced to the receptor protein. Not only simple dyes but also functional molecules, such as artificial receptors, can be incorporated. Third, the attachment of dye to the protein framework is more flexible than the use of AFPs. While the attaching positions of AFP are generally limited to the N- and C termini of receptor proteins, the incorporation of small dye to proteins is also possible in the middle of loop regions or at close proximity to the binding pocket. On the other hands, unlike AFPs based biosensor, this type of protein-based biosensor generally require the invasive technique for translocating across the plasma membrane, such as electroporation (Marrero, M.B. et al. 1995; Fenton, M. et al. 1998; Sakaguchi, R. et al. 2010), lipofection (Zelphati, O., et al. 2001; Zheng, X. et al. 2003), microinjection (Abarzua, P. et al. 1995), and tagging cell-permeable peptide sequences (Wadia, J.S. et al 2005; Sugimoto, K. et al 2004). In addition, the central issue for the construction of these types of biosensors is the way to introduce a dye into the receptor protein site-selectively. Here, a variety of fluorescent biosensors that use fluorescent molecules is described according to a classification of the incorporation methodologies of fluorescent dye.

3.1 Introduction of a thiol reactive fluorophore on a unique cysteine residue of engineered receptor protein

The most important process to success this methodology is that all of the original cysteine residue of the receptor protein must be initially substituted with other amino acids to avoid

the nonspecific labeling of cysteine reactive fluorophores. Following the process, a unique cysteine residue was introduced at specific position. The position to introduce a fluorophore is most conveniently determined by the three-dimensional structure of the receptor protein.
As a pioneering work, bPBPs (bacteria periplasmic binding protein), a representative protein scaffold, were converted to fluorophore-modified biosensors by Hellinga *et al*. (Dwyer, M. A. et al. 2004) or others (Gilardi, G. et al. 1994; Brune, M. et al. 1998; Hirshberg, M. et al. 1998). Most of bPBPs consist of two domains connected by a hinge region, with a ligand binding site located at the interface between the two domains, which can permit dynamic conformational changes induced upon ligand binding. Therefore, two distinct approaches are used to establish an efficient signal transduction mechanism that would sense the ligand-binding event. In the first approach, an environmentally sensitive fluorophore is positioned in the binding pocket so that the ligand-induced changes in the fluorescence are produced by the direct fluorophore-ligand interactions. This approach often has a disadvantage that unfavorable steric interactions between the introduced fluorophore and the ligand lower the binding affinity. The second approach introduces environmentally sensitive fluorophore at the region that is distant from the ligand-binding site but exhibits dynamic domain movement in response to the ligand binding. This allosteric sensing mechanism shows an advantage that the ligand binding is essentially unaffected by introducing a fluorophore.
On the other hand, there are number of proteins that do not undergo such a dynamic conformational change upon ligand binding, but they are capable of recognizing the various substances of biological importance. The useful methodology to convert such non-allosteric proteins to fluorescent biosensors is to introduce an environmentally sensitive fluorophore within the proximity of the ligand-binding site, though this strategy might have some drawbacks as mentioned above. But several successful examples demonstrated that such a methodology is applicable for obtaining biosensors (Chan, P. H. et al. 2004; Nalbant, P. et al. 2004; Chan, P. H. 2008). Morii and coworkers constructed novel biosensors for inositol 1,4,5-trisphosphate [Ins(1,4,5)P_3] and 1,3,4,5-tetrakisphosphate [Ins(1,3,4,5)P_4] by utilizing the pleckstrin homology (PH) domain of phospholipase C (PLC) δ_1 (Morii, T. et al. 2002) and the general receptor for phosphoinositides 1 (GRP1) (Sakaguchi, R. et al. 2010) (Figure 4), respectively. In these biosensors a synthetic fluorophore was attached at the proximity of the ligand-binding site based on the three dimensional structures of proteins so that the changes in orientation of the fluorophore induced by the substrate binding lead to a sufficient fluorescence response. This structure-based design of synthetic fluorophore-modified biosensors is a powerful method to produce biosensors with high selectivity and appropriate affinity to target inositol derivatives in living cells (Sakaguchi, R. et al. 2010; Sugimoto, K. et al. 2004; Nishida, M. et al. 2003).

3.2 Site-specific unnatural amino acid mutagenesis with an expanded genetic code

As mentioned above, the post-labeling of unique cysteine residues required preliminary preparation that all of the original cysteine residue of the receptor protein must be substituted with other amino acids. The process might cause the instability of the receptor protein mutant. A mutagenesis technique for direct incorporation of synthetic fluorophores as unnatural amino acids into desired positions in proteins can avoid such a problem. A site-specific mutagenesis with an expanded genetic code that employed an amber suppression method (Wang, L. 2005; et al. Xie, J. et al. 2006) or a four-base codon method (Hohsaka, T. et al., 2002) in cell-free translation systems has provided a variety of fluorescently modified

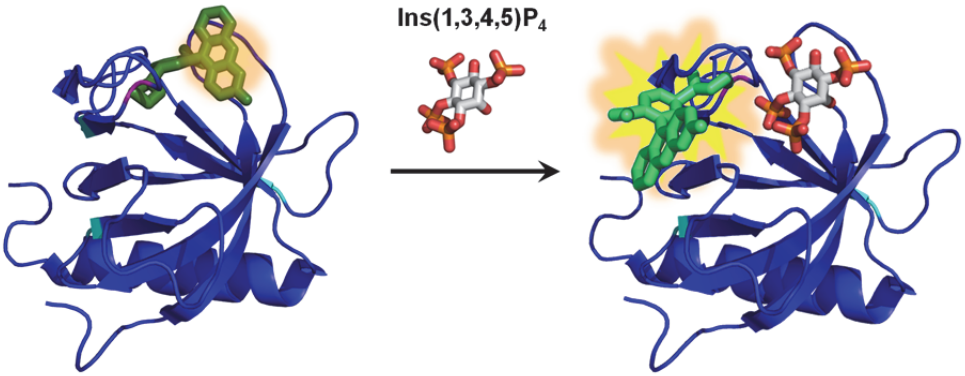

Fig. 4. A schematic illustration shows a fluorescent biosensor for Ins(1,3,4,5)P_4 based on the GRP1 PH domain (Sakaguchi, R. et al. 2010). Firstly, the original cysteine residues (cyan) of GRP PH domain were replaced with other amino acids. Second, a unique cysteine residue (magenta) was introduced to the resultant mutant followed by labeling with thiol reactive fluorescein (green) as an environment sensitive fluorophore to give Ins(1,3,4,5)P_4 sensor. The local environmental change of the fluorophore induced by the ligand-binding event was transduced to the fluorescence enhancement.

proteins (Anderson, R. D. et al. 2002; Taki, M. et al. 2002; Kajihara D. et al. 2006). As an excellent example, Hohsaka and co-workers prepared a series of semisynthetic calmodulins, two different position of which were replaced with unnatural amino acids bearing a FRET pair of BODIPY derivatives by using two sets of four-base codons. Some of the doubly modified calmodulin sensed calmodulin-binding peptide by substantial FRET signal changes. This is a powerful tool for site-specific introduction of unnatural amino acids into protein, though the examples of the construction of fluorescent biosensor based on these methods are still limited.

3.3 Covalent introduction of fluorescent molecules by chemical modification

Modification of a protein by using genetic method often causes the lower activity or instability of the mutated protein as mentioned in the previous section. In addition, the method is not appropriate when the three dimensional structure of a receptor protein is not known. In that case, an approach to site-specifically incorporate a signal transducer proximal to the binding pocket of intact receptor protein by using selective chemical modifications is valid.

As the primary example, Schultz and co-workers constructed an antibody-based fluorescent biosensor by using an affinity-labeling method (Pollack, S. J. et al. 1988). The chemically engineered antibody, of which the proximal antigen-recognition site was modified by fluorescent molecule, can detect antigen binding by fluorescence decrease. Hamachi and co-workers constructed a lectin-based fluorescent biosensor using an improved photo affinity labeling method, termed as P-PALM (post-photoaffinity labeling modification) (Hamachi, I. et al. 2000; Nagase, T. et al. 2001, Nagase, T. et al. 2003). This methodology can introduce artificial molecules (e.g. fluorophore, artificial receptor) proximal to the active site of a target protein without genetically modifying the protein framework. In a proof-of-principle experiment, P-PALM was demonstrated by using concanavalin A (Con A), an extensively

studied lectin (saccharide-binding protein). Introduction of a thiol group as a chemoselective modification site in proximity of the ligand-binding pocket of Con A is conducted by a designed photoaffinity labeling molecule, which is composed of a ligand module, a photo reactive module and a cleavable disulfide module. Depending on the nature of the subsequent modification by a thiol reactive artificial molecule, not only environmental sensitive fluorophore (Koshi, Y. et al. 2005; Nakata, E. et al. 2005; Nakata, E. et al. 2008) but also fluorescent artificial receptor (Nakata, E. et al. 2004) can be introduced to Con A. Intact Con A can be converted to a various type of fluorescent biosensors that successfully sense the saccharide derivatives in different manners. Because the initial P-PALM strategy based on thiol chemistry shows limited bioorthogonality, this method is not applicable to many proteins. To overcome this drawback, Hamachi group adopted the ketone/aldehyde-based hydrazone/oxime exchange reaction (Takaoka, Y. et al. 2006) and the organometallic Suzuki reaction (Wakabayashi, H. 2008) as bioorthogonal chemoselective modifications. Recently, Hamachi and co-workers also developed ligand-directed tosyl (LDT) chemistry-based approach as a more general and simple strategy of target selective chemical modification (Tsukiji, S. 2009). A detailed description of their strategies is described in other review articles (Nakata, E. et al. 2007; Wang. H. et al. 2009).

4. Signaling aptamers

Protein based biosensors are generally constructed by using native or slightly modified proteins as the scaffold. Therefore, the function of the constructed biosensor, such as the specificity and the affinity toward the substrate, depends on that of the native receptor. Unlike receptor proteins, DNA or RNA based receptors (aptamers) which have appropriate affinity and specificity for various targets ranging from small molecules to proteins can be generated by using *in vitro* selection, also known as SELEX (systematic evolution of ligands by exponential enrichment) (Ellington, A. D. 1994; Ellington, A. D. et al. 1990; Gold, L. et al. 1995; Osborne, S. E. et al. 1997; Wilson, D. S. et al. 1999). That is, aptamers that bind to the substrate of interest with tailor made functions, such as the specificity and the affinity, can potentially be generated through *in vitro* selection. Previous work indicated that most of the structurally characterized aptamers underwent induced-fit type of conformational change upon ligand binding [Westhof, E. et al. 1997]. Introduction of the signal transduction module such as a fluorophore at an appropriate site of the aptamer enables a read out of the ligand-binding event as a local environmental change of the fluorophore. Thus, the design of aptamer-based fluorescent sensors represents an attractive and promising alternative to the protein-based sensors. Some excellent reviews of aptamer sensors have already covered the selection and evolution techniques and sophisticated applications of the aptamer sensors [Liu, J. et al 2009; Mok, W. et al. 2008]. Here we focus on unique modular strategies to construct aptamer sensors, which would avoid the cumbersome trial-and-error process to construct a sensor with an optimized function.

4.1 Modular strategies for tailoring aptamer sensors

Sophisticated design strategies have successfully provided fluorescent biosensors based on biomolecules such as DNA, RNA or proteins, but these strategies usually require the redundant optimization of sensor functions. For example, introduction of the fluorophore often impairs the original receptor function and does not always ensure the fluorophore-labelled receptor to act as an expected sensor. It is quite difficult to empirically apply the

obtained findings from the previously constructed biosensor to the other one, because the communication between the substrate binding and the signal-transduction is not so simple and is unique to the individual biosensor. On the other hand, a modular strategy that permits facile preparation of biosensors with tailored characteristics by a simple combination of a receptor and a signal transducer has recently emerged as a new paradigm for a versatile design of fluorescent biosensors. Stojanovic and co-workers have proposed a modular design of signaling aptamers based on the allosteric regulation of binding events (Stojanovic, M. N. et al. 2004). The target binding aptamers were fused with the reporter dye binding aptamers, which can drastically increase the fluorescent intensity of reporter dye, and the reporter dye binding was significantly enhanced upon target binding. Fluorescent sensors for adenosine triphosphate (ATP), flavin mononucleotide (FMN) and theophylline have been demonstrated based on this design, showing the generality of the approach. Later, several groups reported various allosteric aptamer sensors based on the methodology (Kolpashchikov, D. M. 2005; Xu, W. et al. 2010; Furutani, C. et al. 2010).

The application of the selection and evolution technique is not limited to obtain functional macromolecules solely composed of RNA or DNA. Morii and co-workers have recently developed a conceptually new strategy for preparation of fluorescent biosensors with diverse functions based on a framework of ribonucleopeptide (RNP), such as the structurally well characterized complex of the Rev Responsive Element (RRE)-HIV Rev peptide (Rev peptide) and RRE RNA (Figure 5) (Tainaka, K. et al. 2010). In the first step to construct the fluorescent RNP sensor, a randomized nucleotide sequence was introduced into the RNA subunit of RNP to construct RNP library. In vitro selection method was applied to the RNP library to afford a series of RNP receptors for a given target (Morii, T. et al. 2002). In the second step, the Rev peptide was modified with a fluorophore as the transducer of binding event without greatly disturbing the affinity and specificity of the RNP receptor. The constructed fluorescent RNP sensor showed the fluorescent intensity changing upon binding to the target molecule as the result of the conformational change of RNA subunit by inducing target binding. In similar to RNA aptamers, the RNP receptors, which obtained by in vitro selection, are considered as a RNP receptor library, because a variety of RNA structures and reveal different affinity to the target molecule were included. The combined peptide subunit is also easily converted to functionalized Rev peptide libraries, such as various fluorophore modified Rev peptide libraries with a variety of excitation and emission wavelengths. By taking the advantage of such the noncovalent nature of the RNP complex, RNP sensors with desired affinity, selectivity and optical sensing properties could be selected in a high-throughput manner by combining a series of RNA subunits derived from each of the library. Actually, a variety of fluorescent biosensors for targeting ATP (Hagihara, M. et al. 2006), GTP (Hagihara, M. et al. 2006), histamine (Fukuda, M. et al. 2009), phosphotyrosine (Hasegawa, T. et al. 2005), and phosphotyrosine-containing peptide fragment (Hasegawa, T. et al. 2008) have been produced by the group, showing the generality of the approach. Recently, the group showed that ATP-binding RNP sensor was rationally converted to GTP-binding RNP sensor to have realized the detail of the recognition mechanism (Nakano, S. et al. 2011). Though the noncovalent configuration conveniently provides fluorescent RNP sensors in the selection stage, it have a possibility to becomes a disadvantage for the practical measurements after optimization of the sensor function, for instance, the RNP complex would dissociate to each component under reducing condition such as the nanomolar range. A covalently linking of RNA and peptide subunits without sacrificing the sensing function would overcome such disadvantages.

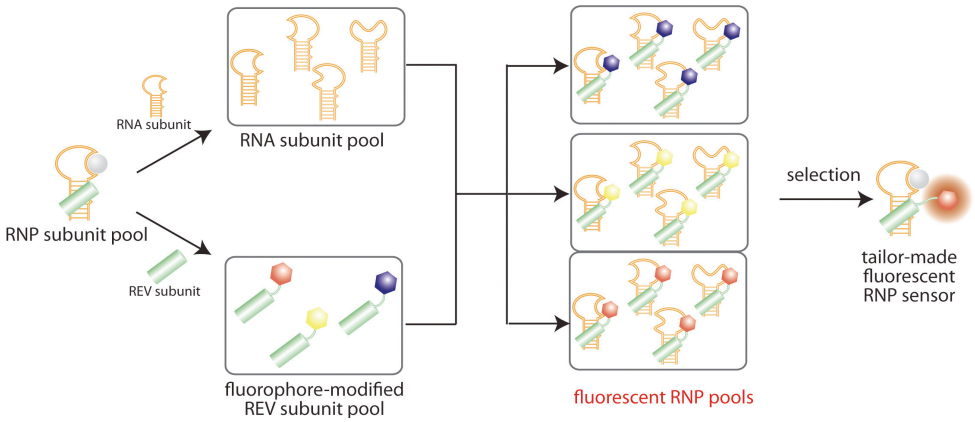

Fig. 5. Screening methodology of a tailor-made RNP fluorescent sensor [Hagihara, M. et al. 2006]. Combination between the RNA subunit library and several dye-labeled Rev peptide subunits generates combinatorial fluorescent RNP receptor libraries, from which RNP sensors with desired function, such as optical property, affinity and selectivity, are selected.

5. Perspective

Here we overviewed construction methodologies of fluorescent biosensor based on biomolecules, that is, protein-based biosensor and aptamer-based biosensor. The systematic developments of these technologies have expanded the applicability of fluorescent biosensors. In the case of the protein based biosensor, there is no doubt that these sensors represent the most practical and reliable tools for the real-time measurements of various biologically important molecules in living cells. Actually, the function of second messengers, for example, in the cell has been progressively clarified owing to significant contribution of these new biosensors. However, the wide varieties of the construction strategies, which have both the advantages and drawbacks as mentioned above, strongly indicated the lack of general approach to conjugate a recognition module with a signal transducer unit. Further effort in the fields for establishing a general and simple strategy to construct usable biosensors will realize tailor-made fluorescent biosensors.

Aptamer-based biosensors have potential to realize the tailor-made biosensor with finely tuneable affinity and selectivity based on in vitro selection technique, and to visualize intracellular molecules. However, this type of sensor is practically passive with challenges in cell application owing to the inherent liability of RNA molecules in the intracellular condition. Such the drawbacks will be overcome by the improved selection and evolution technique to construct the aptamers that resist to the cellular degradation activity.

6. Reference

Abarzua, P., LoSardo, J. E., Gubler, M. L., & Neri, A. (1995). Microinjection of Monoclonal Antibody PAb421 into Human SW480 Colorectal Carcinoma Cells Restores the Transcription Activation Function to Mutant p53. *Cancer Res.*, 55(16), 3490–3494.

Ai, H. W., Hazelwood, K. L., Davidson, M. W., & Campbell, R. E. (2008). Fluorescent protein FRET pairs for ratiometric imaging of dual biosensors. *Nat. Methods*, 5(5), 401–403.

Anderson, R. D., 3rd, Zhou, J., & Hecht, S. M. (2002). Fluorescence Resonance Energy Transfer between Unnatural Amino Acids in a Structurally Modified Dihydrofolate Reductase. *J. Am. Chem. Soc.* 124(33), 9674–9675.

Awasis, M., & Ozawa, T. (2011). Illuminating Intracellular Signaling and Molecules for Single Cell Analysis. *Molecular Biosystems*, in press

Baird, G.S., Zacharias, D.A., & Tsien, R.Y. (1999). Circular Permutation and Receptor Insertion within Green Fluorescent Proteins. *Proc. Natl. Acad. Sci. USA*, 96(20), 11241–11246.

Barondeau, D. P., Kassmann, C. J., Tainer, J. A., & Getzoff, E. D. (2002). Structural Chemistry of a Green Fluorescent Protein Zn Biosensor. *J. Am. Chem. Soc.,* 124(14), 3522–3524.

Belousov, V. V., Fradkov, A. F., Lukyanov, K. A., Staroverov, D. B., Shakhbazov, K. S., Terskikh, A. V., & Lukyanov, S. (2006). Genetically Encoded Fluorescent Indicator for Intracellular Hydrogen Peroxide. *Nat. Methods,* 3(4), 281–286.

Borisov, S. M., & Wolfbeis,O. S., S. M. & Wolfbeis,O. S. (2008) Optical Biosensors. *Chem. Rev.,* 108(2), 423–461.

Brun, M. A., Tan, K. T., Nakata, E., Hinner, M. J., Johnsson, K. (2009). Semisynthetic Fluorescent Sensor Proteins Based on Self-Labeling Protein Tags. *J. Am. Chem. Soc.,* 131(16), 5873–5884.

Brune, M., Hunter, J. L., Howell, S. A., Martin, S. R., Hazlett, T. L., Corrie, J. E., & Webb, M. R. (1998). Mechanism of Inorganic Phosphate Interaction with Phosphate Binding Protein from Escherichia Coli. *Biochemistry,* 37(29), 10370–10380.

Carlson, H. J., &Campbell, R. E., (2009) Genetically Encoded FRET-Based Biosensors for Multiparameter Fluorescence Imaging. *Curr. Opin. Biotechnol.* 20(1), 19–27.

Chalfie, M., Tu, Y., Euskirchen, G., Ward, W. W., & Prasher, D. C. (1994). Green Fluorescent Protein as a Marker for Gene Expression. *Science*, 263(5148), 802–805.

Chan, P. H., Liu, H. B., Chen, Y. W., Chan, K. C., Tsang, C. W., Leung, Y. C.,& Wong, K. Y. (2004). Rational Design of a Novel Fluorescent Biosensor for β-Lactam Antibiotics from a Class a β-Lactamase. *J. Am. Chem. Soc.,* 126(13), 4074–4075.

Chan, P. H., So, P. K., Ma, D. L., Zhao, Y., Lai, T. S., Chung, W. H., Chan, K. C., Yiu, K. F., Chan, H. W., Siu, F. M., Tsang, C. W., Leung, Y. C., Wong, K. Y. (2008). Fluorophore-Labeled β-Lactamase as a Biosensor for β-Lactam Antibiotics: A Study of the Biosensing Process. *J. Am. Chem. Soc.,* 130(20), 6351–6361.

Chapleau, R. R., Blomberg, R., Ford, P. C., Sagermann, M., (2008). Design of a Highly Specific and Noninvasive Biosensor Suitable for Real-Time in Vivo Imaging of Mercury (II) Uptake. *Protein Sci.,* 17(4), 614–622.

Demidov, V. V., Dokholyan, N. V., Witte-Hoffmann, C., Chalasani, P., Yiu, H. W., Ding, F., Yu, Y., Cantor, C. R., & Broude, N. E. (2006). Fast Complementation of Split Fluorescent Protein Triggered by DNA Hybridization. *Proc. Natl. Acad. Sci. USA* ,103(7), 2052–2056.

Dooley, C. T., Dore, T. M., Hanson, G. T., Jackson, W. C., Remington, S.J., & Tsien, R. Y. (2004). Imaging Dynamic Redox Changes in Mammalian Cells with Green Fluorescent Protein Indicators. *J. Biol. Chem.* 279(21), 22284–22293.

Dwyer, M. A., & Hellinga, H. W. (2004). Periplasmic Binding Proteins: A Versatile Superfamily for Protein Engineering. *Curr. Opin. Struct. Biol.*, 14(4), 495–504.

Ellington, A. D. (1994). RNA Selection. Aptamers Achieve the Desired Recognition. *Curr. Biol.* 4(5), 427–429.

Ellington, A. D., & Szostak, J. W. (1990). In Vitro Selection of RNA Molecules That Bind Specific Ligands. *Nature*, 346(6287), 818–822.

Fenton, M., Bone, N., & Sinclair, A. J. (1998). The Efficient and Rapid Import of a Peptide into Primary B and T Lymphocytes and a Lymphoblastoid Cell Line. *J. Immunol. Methods,* 212(1), 41–48.

Fukuda, M., Hayashi, H., Hasegawa, T., & Morii, T. (2009). Development of a Fluorescent Ribonucleopeptide Sensor for Histamine. *Trans. Mat. Res. Soc. Jpn.* 34, 525–527.

Furutani, C., Shinomiya, K., Aoyama, Y., Yamada, K., & Sando, S. (2010). Modular blue fluorescent RNA sensors for label-free detection of target molecules. Mol Biosyst., 6(9),1569-1571.

Ghosh, I., Hamilton, A.D., & Regan, L. (2000) Antiparallel Leucine Zipper-Directed Protein Reassembly: Application to the Green Fluorescent Protein. *J. Am. Chem. Soc.* 122(23), 5658–5659.

Giepmans, B.N., Adams, S.R.,Ellisman, M.H., & Tsien, R.Y. (2006) The Fluorescent Toolbox for Assessing Protein Location and Function. *Science*, 312(5771), 217–224.

Gilardi, G., Zhou, L. Q., Hibbert, L., & Cass, A. E. (1994). Engineering the Maltose Binding Protein for Reagentless Fluorescence Sensing. *Anal. Chem.* 66(21), 3840–3847.

Gold, L., Polisky, B., Uhlenbeck, O., & Yarus, M. (1995). Diversity of Oligonucleotide Functions. *Annu. Rev. Biochem.*, 64, 763–797.

Hagihara, M., Fukuda, M., Hasegawa, T., & Morii, T. (2006). A Modular Strategy for Tailoring Fluorescent Biosensors from Ribonucleopeptide Complexes. *J. Am. Chem. Soc.* 128(39), 12932–12940.

Hamachi, I., Nagase, T., & Shinkai, S. (2000). A General Semisynthetic Method for Fluorescent Saccharide-Biosensors Based on a Lectin. *J. Am. Chem. Soc.* 122(48), 12065–12066.

Hasegawa, T., Hagihara, M., Fukuda, M., Nakano, S., Fujieda, N., Morii, T. (2008). Context-Dependent Fluorescence Detection of a Phosphorylated Tyrosine Residue by a Ribonucleopeptide. *J. Am. Chem. Soc.* 130(27), 8804–8812.

Hasegawa, T., Ohkubo, K., Yoshikawa, S., & Morii, T. (2005). A Ribonucleopeptide Receptor Targets Phosphotyrosine. *J. Surf. Sci. Nanotech.*, 3, 33–37.

Hellinga, H.W. & Marvin, J.S. (1998) Protein Engineering and the Development of Generic Biosensors. *Trends Biotechnol.* 16(4), 183–189.

Hirshberg, M., Henrick, K., Haire, L. L., Vasisht, N., Brune, M., Corrie, J. E., & Webb, M. R. (1998). Crystal Structure of Phosphate Binding Protein Labeled with a Coumarin Fluorophore, a Probe for Inorganic Phosphate. *Biochemistry,* 37(29), 10381–10385.

Hohsaka, T., &Sisido, M. (2002). Incorporation of Non-Natural Amino Acids into Proteins. *Curr. Opin. Chem. Biol.* 6(6), 809–815.

Hu, C.-D. T. & Kerppola, K. (2003). Simultaneous visualization of multiple protein interactions in living cells using multicolor fluorescence complementation analysis. *Nat. Biotechnol.*, 21(5), 539–545.

Jayaraman, S., Haggie, P., Wachter, R. M., Remington, S. J., &Verkman, A. S. (2000). Mechanism and Cellular Applications of a Green Fluorescent Protein-based Halide Sensor. *J. Biol. Chem.* 275(9), 6047–6050.

Jelinek, R. & Kolusheva, S. (2004). Carbohydrate biosensors. *Chem. Rev.* 104(12), 5987–6015.

Johnsson, K. (2009). Visualizing Biochemical Activities in Living Cells. *Nat. Chem. Biol.* 5(2), 63–65.

Johnsson, N., & Johnsson, K. (2007) Chemical Tools for Biomolecular Imaging. *ACS Chem. Biol.*, 2(1), 31–38.

Kajihara, D., Abe, R., Iijima, I., Komiyama, C., Sisido, M., & Hohsaka, T. (2006) FRET Analysis of Protein Conformational Change through Position-Specific Incorporation of Fluorescent Amino Acids. *Nat. Methods,* 3(11), 923–929.

Kerppola, T. K. (2006) Visualization of molecular interactions by fluorescence complementation, *Nature Rev. Mol. Cell Biol.*, 7(6), 449-456

Kneen, M., Farinas, J., Li, Y., & Verkman, A. S. (1998). Green fluorescent protein as a noninvasive intracellular pH indicator. *Biophys. J.* 74(3), 1591–1599.

Kolpashchikov, D. M. (2005). Binary Malachite Green Aptamer for Fluorescent Detection of Nucleic Acids. *J. Am. Chem. Soc.*, 127(36), 12442–12443

Koshi, Y., Nakata, E., & Hamachi, I. (2005). Luminescent Saccharide Biosensor by Using Lanthanide-Bound Lectin Labeled with Fluorescein. *ChemBioChem*, 6(8), 1349–1352.

Lawrence, D. S., & Wang, Q. (2007). Seeing Is Believing: Peptide-Based Fluorescent Sensors of Protein Tyrosine Kinase Activity. *ChemBioChem* 8(4), 373–378.

Lippincott-Schwartz, J., Snapp, E., & Kenworthy, A. (2001). Studying Protein Dynamics in Living Cells. *Nat. Rev. Mol. Cell Biol.*, 2(6), 444–456.

Liu, J., Cao, Z., & Lu, Y. (2009). Functional Nucleic Acid Sensors. *Chem. Rev.* 109(5), 1948–1998.

Liu, J., Cao, Z., & Lu, Y. (2009). Functional Nucleic Acid Sensors. *Chem. Rev.,* 109(5), 1948–1998.

Llopis, J., McCaffery, J. M., Miyawaki, A., Farquhar, M. G., & Tsien, R. Y. (1998). Measurement of cytosolic, mitochondrial and Golgi pH in single living cells with green fluorescent protein. *Proc. Natl. Acad. Sci. USA,* 95(12), 6803–6808.

Luo, K. Q., Yu, V. C., Pu, Y., & Chang, D. C. (2001). Application of the fluorescence resonance energy transfer method for studying the dynamics of caspase-3 activation during UV-induced apoptosis in living HeLa cells. *Biochem. Biophys. Res. Commun.* 283(5), 1054–1060.

Mahajan, N. P., Harrison-Shostak, D. C., Michaux, J., & Herman, B. (1999). Novel mutant green fluorescent protein protease substrates reveal the activation of specific caspases during apoptosis. *Chem. Biol.* 6(6), 401–409.

Mank, M. Griesbeck,O. (2008) Genetically Encoded Calcium Indicators. *Chem. Rev.* 108(5), 1550–1564.

Marrero, M. B., Schieffer, B., Paxton, W. G., Schieffer, E., & Bernstein, K. E., (1995). Electroporation of pp60$^{c\text{-}src}$ Antibodies Inhibits the Angiotensin II Activation of Phospholipase C-γ1 in Rat Aortic Smooth Muscle Cells. *J. Biol. Chem.,* 270(26), 15734–15738.

Matsuyama, S., Llopis, J., Deveraux, Q. L., Tsien, R. Y., & Reed, J. C. (2000). Changes in intramitochondrial and cytosolic pH: early events that modulate caspase activation during apoptosis. *Nature Cell Biol.* 2(6), 318–325.

Miesenböck, G., De Angelis, D. A., & Rothman, J. E. (1998). Visualizing secretion and synaptic transmission with pH-sensitive green fluorescent proteins. *Nature,* 394(6689), 192–195.

Miyawaki, A., Llopis, J., Heim, R., McCaffery, J. M., Adams, J. A., Ikura, M., & Tsien, R.Y. (1997). Fluorescent Indicators for Ca^{2+} Based on Green Fluorescent Proteins and Calmodulin. *Nature,* 388(6645), 882–887.

Mizuno, T., Murao, K., Tanabe, Y., Oda, M., & Tanaka, T. (2007). Metal-Ion-Dependent GFP Emission in Vivo by Combining a Circularly Permutated Green Fluorescent Protein with an Engineered Metal-Ion-Binding Coiled-Coil. *J. Am. Chem. Soc.* 129(37), 11378–11383.

Mok, W., & Li, Y. (2008). Recent Progress in Nucleic Acid Aptamer-Based Biosensors and Bioassays. *Sensors*, 8, 7050–7084.

Morii, T., Hagihara, M., Sato, S., & Makino, K. (2002). In Vitro Selection of ATP-Binding Receptors Using a Ribonucleopeptide Complex. *J. Am. Chem. Soc.*, 124(17), 4617–4622.

Morii, T., Sugimoto, K., Makino, K., Otsuka, M., Imoto, K., & Mori, Y. (2002). A New Fluorescent Biosensor for Inositol Trisphosphate. *J. Am. Chem. Soc.,* 124(7), 1138–1139.

Nagai, T., Sawano, A., Park, E.S., & Miyawaki, A. (2001). Circularly Permuted Green Fluorescent Proteins Engineered to Sense Ca^{2+}. *Proc Natl Acad Sci U S A* 98(6), 3197–3202.

Nagai, Y., Miyazaki, M., Aoki, R., Zama, T., Inoue, S., Hirose, K., Iino, M., & Hagiwara, M. (2000). A fluorescent indicator for visualizing cAMP-induced phosphorylation in vivo. Nat. Biotechnol. 18(3), 313-316.

Nagase, T. Shinkai, S. & Hamachi, I. (2001). Post-Photoaffinity Labeling Modification Using Aldehyde Chemistry to Produce a Fluorescent Lectin toward Saccharide-Biosensors Chem. Commun., 229-230

Nagase, T., Nakata, E., Shinkai, S. & Hamachi, I. (2003). Construction of Artifical Signal Transducers on a Lectin Surface by Post-Photoaffinity-Labeling Modification for Fluorescent Sccharide Biosensors. *Chem. Eur. J.*, 9(15), 3660-3669.

Nakai, J., Ohkura, M., & Imoto, K. (2001) A High Signal-to-Noise Ca^{2+} Probe Composed of a Single Green Fluorescent Protein. *Nat. Biotechnol.* 19(2), 137–141.

Nakano, S., Mashima, T., Matsugami, A., Inoue, M., Katahira, M. & Morii, T. (2011). Structural Aspects for the Recognition of ATP by Ribonucleopeptide Receptors. *J. Am. Chem. Soc. 133(12), 4567-4579*.

Nakata, E., Koshi, Y., Koga, E., Katayama, Y., Hamachi, I. (2005). Double-Modification of Lectin Using Two Distinct Chemistries for Fluorescent Ratiometric Sensing and Imaging Saccharides in Test Tube or in Cell. *J. Am. Chem. Soc.* 127(38), 13253–13261.

Nakata, E., Nagase, T., Shinkai, S., & Hamachi, I. (2004). Coupling a Natural Receptor Protein with an Artificial Receptor to Afford a Semisynthetic Fluorescent Biosensor. *J. Am. Chem. Soc.,* 126(2), 490–495.

Nakata, E., Tsukiji, S., &Hamachi, I. (2007). Development of New Methods to Introduce Unnatural Functional Molecules into Native Proteins for Protein Engineering. *Bull. Chem. Soc. Jpn.,* 80, 1268–1279.

Nakata, E., Wang, H., & Hamachi, I. (2008). Ratiometric Fluorescent Biosensor for Real-Time and Label-Free Monitoring of Fine Saccharide Metabolic Pathways. *ChemBioChem*, 9(1), 25–28.

Nalbant, P. Hodgson, L. Kraynov,V. Toutchkine, A. Hahn, K. M. (2004). Activation dynamics of endogenous Cdc42 visualized in living cells. *Science*. 305(5690), 1615-1619.

Nausch, L. W., Ledoux, J., Bonev, A. D., Nelson, M. T., Dostmann, W. R. (2008). Differential Patterning of cGMP in Vascular Smooth Muscle Cells Revealed by Single GFP-Linked Biosensors. *Proc. Natl. Acad. Sci. USA,* 105(1), 365–370.

Newman R. H., & Zhang J. (2008). Visualization of phosphatase activity in living cells with a FRET-based calcineurin activity sensor. Mol. BioSyst., 4(6), 496-501 .

Nikolaev, V., Bunemann, O. M., Hein, L., Hannawacker , A. & Lohse, M. J. (2004). Novel Single Chain cAMP Sensors for Receptor-induced Signal Propagation *J. Biol. Chem.*, 279 (36), 37215–37218

Nishida, M., Sugimoto, K., Hara, Y., Mori, E., Morii, T., Kurosaki, T., & Mori, Y. (2003). Amplification of Receptor Signaling by Ca^{2+} Entry-Mediated Translocation and Activation of PLCγ2 in B Lymphocytes. *EMBO J*, 22(18), 4677–4688.

Nyfeler, B. Michnick, S. W. & Hauri, H.-P. (2005). Capturing protein interactions in the secretory pathway of living cells. *Proc. Natl. Acad. Sci. USA,* 102(18), 6350–6355.

Ohashi, T., Galiacy, S. D., Briscoe, G., & Erickson, H. P. (2007). Experimental Study of GFP-Based FRET, with Application to Intrinsically Unstructured Proteins. *Protein Sci.* 16(7), 1429–1438.

Osborne, S. E., Ellington, A. D. (1997). Nucleic Acid Selection and the Challenge of Combinatorial Chemistry. *Chem. Rev.* 97(2), 349–370.

Ozawa, T. (2006). Designing split reporter proteins for analytical tools. *Analytic Chimica Acta,* 556(1), 58–68.

Ozawa, T., Natori, Y., Sato, M., & Umezawa, Y. (2007). Imaging Dynamics of Endogenous Mitochondrial RNA in Single Living Cells. *Nat. Methods* 4(5), 413–419.

Ozawa, T., Nogami, S., Sato, M., Ohya, Y., & Umezawa, Y. (2000). A fluorescent indicator for detecting protein-protein interactions in vivo based on protein splicing. *Anal. Chem.* 72(21), 5151–5157.

Piston, D. W., & Kremers, G. J. (2007). Fluorescent Protein FRET: The Good, the Bad and the Ugly. *Trends Biochem. Sci.,* 32(9), 407–414.

Pollack, S. J., Nakayama, G. R., & Shultz, P. G. (1988). Introducion of Nucleophiles and Spectroscopic Probes into Antibody Combining Sites. *Science*, 242(4881), 1038.

Prinz, A., Reither, G., Diskar, M., & Schultz, C. (2008). Fluorescence and bioluminescence procedures for functional proteomics. *Proteomics,* 8(6), 1179–1196.

Rao, J., Dragulescu-Andrasi, A., & Yao, H. (2007). Fluorescence Imaging in Vivo: Recent Advances. *Curr. Opin. Biotechnol.,* 18(1), 17–25.

Rehm, M., Dussmann, H., Janicke, R. U., Tavare, J. M., Kogel, D., & Prehn, J. H. (2002). Single-cell fluorescence resonance energy transfer analysis demonstrates that caspase activation during apoptosis is a rapid process. Role of caspase-3. *J Biol. Chem.,* 277(27), 24506–24514.

Romoser, V. A., Hinkle, P.M., & Persechini, A. (1997) Detection in Living Cells of Ca^{2+}-Dependent Changes in the Fluorescence Emission of an Indicator Composed of Two Green Fluorescent Protein Variants Linked by a Calmodulin-Binding Sequence. A New Class of Fluorescent Indicators. *J. Biol. Chem.,* 272(20), 13270–13274.

Sakaguchi, R., Endoh, T., Yamamoto, S., Tainaka, K., Sugimoto, K., Fujieda, N., Kiyonaka, S., Mori, Y., & Morii, T. (2009). A Single Circularly Permuted GFP Sensor for Inositol-1,3,4,5-Tetrakisphosphate Based on a Split PH Domain. *Bioorg. Med. Chem.*, 17(20), 7381–7386.

Sakaguchi, R., Tainaka, K., Shimada, N., Nakano, S., Inoue, M., Kiyonaka, S., Mori, Y., & Morii, T. (2010). An in Vivo Fluorescent Sensor Reveals Intracellular $Ins(1,3,4,5)P_4$ Dynamics in Single Cells. *Angew. Chem., Int. Ed.,* 49(12), 2150-2153.

Sapsford, K.E., Berti, L., & Medintz, I. L. (2006). Materials for Fluorescence Resonance Energy Transfer Analysis: Beyond Traditional Donor-Acceptor Combinations. *Angew. Chem., Int. Ed.,* 45(28), 4562–4589.

Sato, M. Ozawa, T. Inukai, K. Asano T., & Umezawa, Y. (2002). Fluorescent Indicators for Imaging Protein Phosphorylation in Single Living Cells. *Nature Biotechnol.*, 20(3), 287–294.

Sato, M., Hida, N., Ozawa T., & Umezawa, Y. (2000). Fluorescent Indicators for Cyclic GMP Based on Cyclic GMP-Dependent Protein Kinase Iα and Green Fluorescent Proteins. *Anal. Chem.*, 72(24), 5918–5924.

Sato, M., Ueada, Y., Shibuya, M. & Umezawa, Y., (2005). Locating Inositol 1,4,5-trisphosphate in the Nucleus and Neuronal Dendrites with Genetically Encoded Fluorescent Indicators *Anal. Chem.*, 77(15), 4751–4758.

Shimomura, O., Johnson, F. H., & Saiga, Y. (1962). Extraction, Purification and Properties of Aequorin, a Bioluminescent Protein from the Luminous Hydromedusan, Aequorea. *J. Cell Comp. Physiol.*, 59, 223–239.

Shyu, Y. J., & Hu, C.-D. (2008). Fluorescence complementation: an emerging tool for biological research. *Trends in Biotechnology*, 26 (11), 622-630.

Souslova, E. A., & Chudakov, D. M. (2007). Genetically Encoded Intracellular Sensors Based on Fluorescent Proteins. *Biochemistry (Mosc)*, 72(7), 683–697.

Souslova, E. A., Belousov, V. V., Lock, J. G., Stromblad, S., Kasparov, S., Bolshakov, A. P., Pinelis, V. G., Labas, Y. A., Lukyanov, S., Mayr, L. M., & Chudakov, D. M. (2007). Single Fluorescent Protein-Based Ca^{2+} Sensors with Increased Dynamic Range. *BMC Biotechnol.* 7, 37.

Stains, C. I., Furman, J. L., Segal, D. J., & Ghosh, I. (2006). Site-Specific Detection of DNA Methylation Utilizing mCpG-SEER. *J. Am. Chem. Soc.*, 128(30), 9761–9765.

Stains, C. I., Porter, J. R., Ooi, A. T., Segal, D. J., & Ghosh, I. (2005). DNA Sequence-Enabled Reassembly of the Green Fluorescent Protein. *J. Am. Chem. Soc.* 127(31), 10782–10783.

Stojanovic, M. N., & Kolpashchikov, D. M. (2004). Modular Aptameric Sensors. *J. Am. Chem. Soc.* 126(30), 9266–9270.

Sugimoto, K., Nishida, M., Otsuka, M., Makino, K., Ohkubo, K., Mori, Y., & Morii, T. (2004). Novel Real-Time Sensors to Quantitatively Assess in Vivo Inositol 1,4,5-Trisphosphate Production in Intact Cells. *Chem. Biol.* 11(4), 475–485.

Sugimoto, K., Nishida, M., Otsuka, M., Makino, K., Ohkubo, K., Mori, Y., & Morii, T. Novel Real-Time Sensors to Quantitatively Assess in Vivo Inositol 1,4,5-Trisphosphate Production in Intact Cells. (2004). *Chem. Biol.* 11(4), 475–485.

Tainaka, K., Sakaguchi, R., Hayashi, H., Nakano, S., Liew, F.-F., & Morii, T., (2010). Design Strategies of Fluorescent Biosensors Based on Biological macromolecular Receptors. *Sensors*, 10, 1355-1376.

Takaoka, Y. Tsutsumi, H. Kasagi, N. Nakata, E. & Hamachi, I. (2006). One-pot and Sequential Organic Chemistry on an Enzyme Surface to Tether a Fluorescent Probe at the Proximity of the Active Site with Restoring Enzyme Activity. *J. Am. Chem. Soc.*, 128(10), 3273-3280

Taki, M., Hohsaka, T., Murakami, H., Taira, K., & Sisido, M. (2002). Position-Specific Incorporation of a Fluorophore-Quencher Pair into a Single Streptavidin through Orthogonal Four-Base Codon/Anticodon Pairs. *J. Am. Chem. Soc.* 124(49), 14586–14590.

Thevenot, D. R., Toth, K., Durst, R. A., & Wilson, G. S. (2001). Electrochemical biosensors: recommended definitions and classification. *J. Biosci. Bioeng.* 16(1-2), 121–131.

Tsukiji, S., Miyagawa, M., Takaoka, Y., Tamura, T., & Hamachi, I. (2009). Ligand-Directed Tosyl Chemistry for Protein Labeling in Vivo. *Nat. Chem. Biol.*, 5(5), 341–343.

Tsukiji, S., Wang, H., Miyagawa, M., Tamura, T., Takaoka, Y., & Hamachi, I. (2009). Quenched Ligand-Directed Tosylate Reagents for One-Step Construction of Turn-on Fluorescent Biosensors. *J. Am. Chem. Soc.*, 131(25), 9046–9054.

Valencia-Burton, M., McCullough, R. M., Cantor, C. R., & Broude, N. E. (2007). RNA Visualization in Live Bacterial Cells Using Fluorescent Protein Complementation. *Nat. Methods,* 4(5), 421–427

VanEngelenburg, S. B., & Palmer, A. E., (2008). Fluorescent Biosensors of Protein Function. *Curr. Opin. Chem. Biol.* 12(1), 60–65.

Wachter, R. M., & Remington, S. J. (1999). Sensitivity of the YFP Form of Green Fluorescent Protein to Halides and Nitrate. *Curr. Biol.*, 9, R628–R629.

Wachter, R. M., Yarbrough, D., Kallio, K., Remington, S. J. (2000). Crystallographic and energetic analysis of binding of selected anions to the yellow variants of green fluorescent protein. *J. Mol. Biol*., 301(1), 157–171.

Wadia, J. S., Dowdy, S. F. (2005). Transmembrane Delivery of Protein and Peptide Drugs by TAT-Mediated Transduction in the Treatment of Cancer. *Adv. Drug. Deliv. Rev.*, 57(4), 579–596.

Wakabayashi, H. Miyagawa, M. Koshi, Y. Takaoka, Y. Tsukiji, S. & Hamachi, I. (2008). Affinity Labeling-Based Introduction of a Reactive Handle for Natural Protein Modification, Chem.-An Asian J., 3(7), 1134-1139.

Wang, H., Nakata, E., & Hamachi, I. (2009). Recent Progress in Strategies for the Creation of Protein-Based Fluorescent Biosensors. *ChemBioChem*, 10(16), 2560–2577.

Wang, L., & Schultz, P. G. (2005). Expanding the Genetic Code. *Angew. Chem., Int. Ed.* 44(1), 34–66.

Westhof, E., Patel, D. J. (1997). Nucleic Acids. From Self-Assembly to Induced-Fit Recognition. *Curr. Opin. Struct. Biol.,* 7(3), 305–309.

Wilson, C. G., Magliery, T. J., & Regan, L. (2004). Detecting protein-protein interactions with GFP-fragment reassembly. *Nat. Methods*, 1(3), 255–262.

Wilson, D. S., Szostak, J. W. (1999). In Vitro Selection of Functional Nucleic Acids. *Annu. Rev. Biochem.,* 68, 611–647.

Xie, J., & Schultz, P. G. (2006). A Chemical Toolkit for Proteins--an Expanded Genetic Code. *Nat. Rev. Mol. Cell Biol.* 7(10), 775–782.

Xu, W., & Lu, Y. (2010). Label-free fluorescent aptamer sensor based on regulation of malachite green fluorescence. Anal Chem ., 82(2), 574-578

Zaccolo, M. & Pozzan, T. (2002). Discrete Microdomains with High Concentration of cAMP in Stimulated Rat Neonatal Cardiac Myocytes. *Science,* 295(5560), 1711–1715.

Zaccolo, M., De Giorgi, F., Cho, C. Y., Feng, L., Knapp, T., Negulescu, P.A., Taylor, S. S., Tsien, R. Y., & Pozzan, T. (2000). A Genetically Encoded, Fluorescent Indicator for Cyclic AMP in Living Cells. *Nat. Cell Biol.,* 2(1), 25–29.

Zelphati, O., Wang, Y., Kitada, S., Reed, J. C., Felgner, P. L., & Corbeil, J. (2001). Intracellular Delivery of Proteins with a New Lipid-Mediated Delivery System. *J. Biol. Chem.,* 276(37), 35103–35110.

Zhang, J., & Allen, M. D. (2007). FRET-based biosensors for protein kinases: illuminating the kinome. *Mol. BioSyst.* 3(11), 759–765.

Zhang, J., Campbell, R. E., Ting, A. Y., & Tsien, R. Y. (2002). Creating new fluorescent probes for cell biology. *Nat. Rev. Mol. Cell Biol.,* 3(12), 906–918.

Zheng, X., Lundberg, M., Karlsson, A., Johansson, M. (2003). Lipid-Mediated Protein Delivery of Suicide Nucleoside Kinases. *Cancer Res.* 63(20), 6909–6913.

8

"No Calibration" Type Sensor in Routine Amperometric Bio-sensing - An Example of a Disposable Hydrogen Peroxide Biosensor

C. Creanga[1], S. Serban[2], R.W. Pittson[2] and N. El Murr[1]
[1]CNRS – University of Nantes, (CEISAM Lab. UMR 6230)
2 rue de la Houssinière, BP 92208, Nantes
[2]Gwent Group, Monmouth House, Mamhilad Park, Pontypool NP4 OHZ
[1]France
[2]U.K.

1. Introduction

The predicted potential market size for the use of biosensors in the biomedical sector has correlated closely to the actual global market sales of biosensor devices. Unlike glucose measurement in blood, biosensors for environmental or food analysis are niche markets in which the demand varies and the sale volumes are low. Until now the use of biosensors in these markets has been limited. In contrast, spectrophotometric methods, and particularly enzyme-coupled assays, packaged in simple to use kit form, have proved successful in such fragmented markets and have become, in many cases, the recommended standard method for industrial analysis. The popularity of such kits is the result of disposable consumables, reliable detection methods and most importantly, no requirement for tedious calibration steps (if the Beer-Lambert law is applicable). Disadvantages include sample preparation, multiple and sequential addition of several reagents during the analysis process. We believe that within the environmental and agri-food industries, amperometric biosensor technology could be a valid competitor to the standard spectrophotometric methods; provided that cheap and easy to use methods are proposed. According to industrial users within these fragmented markets, the biggest obstacle for the take up of biosensor technology as a standard method is the requirement for complex pre-calibration. It seems that, to meet the demand of these markets, an essential improvement would be the removal of calibration steps before the use of the biosensor.

The electrochemical signal of a large number of amperometric biosensors is dependent upon enzymatic or chemical kinetics that are reliant on operating conditions (enzyme concentrations, temperature, pH) and so necessarily requires a calibration step prior to use. Despite their excellent analytical performances this makes them unattractive for industries that want to use these analytical tools in remote locations using unskilled operators. With spectroscopic methods these calibration steps are unnecessary because, for a given wavelength and a fixed light path, the measured absorbance is directly proportional to the concentration of sample material. This is true for a concentration range for which the Beer-

Lambert law is applicable. Theoretically, electrochemistry offers similar opportunities, providing certain parameters are set, where the amount of charge or the current passed through an electrochemical cell is proportional to the concentration of an electroactive product. This is particularly applicable in the case of amperometric biosensors using disposable screen printed electrodes as transducers: controlled-potential coulometry which obeys Faraday's law and chronoamperometry ruled by the Cottrell equation.
After evaluation of both electrochemical methods we have chosen chronoamperometry. This has allowed us to develop a new strategy to achieve the objective of preparing disposable biosensors that can be used without prior calibration. Our preference to validate this strategy was that of horseradish peroxidase (HRP) based biosensors for the analysis of hydrogen peroxide (H_2O_2).
This choice is motivated by the fact that hydrogen peroxide is widely used in many industrial applications and is also involved in very large number of analytical procedures. H_2O_2 is commonly used in fields such as sterilization, textile and paper bleaching, or food and pharmaceutical industries. In addition H_2O_2 is the product of many biological reactions involving oxidase enzymes. Therefore, it is the key product to the analysis of many oxidase substrates particularly when using electrochemical sensors and biosensors for health, environment and biosecurity.

2. Disposable amperometric biosensors

Typically, a biosensor may be defined as a measurement device that contains a biological element whose role is to recognize, often specifically, a product that is desired to detect or to quantify. This recognition is accompanied by changes which are converted by the transducer into a signal to be amplified, processed and displayed. The biosensor consists of all the components that make this chain, though very often the word is given to the single transducer associated with the biological element (as we will do in this article).
Various types of biosensors have been described and developed; they differ mainly according to their biological components, their transducers and to the physicochemical method that generates the signal. The most studied biosensors are undoubtedly those which associate enzymes with electrochemical transducers operating in amperometric mode. The main driving force for the development of this type of biosensors is certainly the great success of the very popular home-care device used by diabetics to measure glucose in blood. This successful development was due to the fact that the sensor met two keys needs: the disposable electrochemical transducers fully met the needs of the user and the mass production techniques met the low cost requirement for the producer. The way to associate the biological element to the transducer depends on the intended use of the biosensor. In many cases it is necessary to add other components to the active surface for the proper functioning of the biosensor (activator, buffer pH, redox mediator, membrane). The easiest way to accomplish this is via deposition onto the transducer surface, either in one shot or successively, via solutions of different components, followed by the evaporation of the liquid.

2.1 Screen printing transducers

2.1.1 Short history of screen printing

Several conflicting theories have been put forward relating to the screen printing process. One of them suggests that screen printing originated in China and was used for textile

printing. These prints, believed to have been produced using some form of stencil printing, are over 2000 years old; hence there is no corroborative evidence to prove how they were made.
It was in the textiles printing industry that the first modern form of the process originated, in both England and France, about 1850. The details of the method are now unclear but it seemed to incorporate the use of a stencil system for the production of continuous lengths of printed fabric.
By the beginning of the 20th century, this process has become somewhat more refined, with use of the silk stretched on frames to support hand–made stencils. Ink was applied through the silk by means of a brush. This system was developed further by 1920, with the introduction of a rubber-bladed squeegee to force ink through the screen.
A major breakthrough was achieved in 1940 when the first photographic stencil was developed. The screen printing method used today relies on the same principle as these early systems.

2.1.2 Screen printing process

The basic process involves forcing an ink or paste through a screen comprising a mesh stretched over a frame. The mesh is left open in areas to be printed but occluded in areas where no deposit is required (Figure 1).
The size of the holes in the screen mesh is determined by the thread diameter of the mesh material and the spacing of the threads in the weave. During the print cycle, the squeegee pushes the ink through the mesh. The ink must pass freely through these holes in order to give a repeatable pattern and avoid problems with blocking. After pushing the ink into the open area, the surplus is removed by the edge of the squeegee. The mesh should peel away from the surface immediately behind the squeegee, leaving all the ink that was in the mesh deposited on the printing surface (Website 1).
Screen-printed carbon electrodes can be mass produced at low cost and are readily adaptable as base transducers. Nowadays the use of automatic and semi-automatic machines for screen printing has made the entire process fast and clean, allowing the manufacture of billions of screen printed sensors, per year, worldwide. Nearly the entire production of glucose strips for glucose monitoring in blood is manufactured by means of screen printing. There are also many other types of sensors being manufactured using this technique.
There are several advantages attributed to the use of screen printing process for high volume sensor manufacture. Some of them are related to fact that the technique is versatile in its ability to print on almost all materials in a variety of shapes. Moreover it is a relatively fast technique and precise, giving highly reproducible devices. There are a large number of functional inks (pastes) available and they can be used for manufacturing electrochemical base transducers.

2.1.3 Screen printing inks (pastes)

Many terms are used to describe the printing medium, for example: ink, paste, dye, conductive epoxy, adhesive, etc. However, the general terms 'ink' and 'paste' cover most needs. Ink is generally low in viscosity, paste is high, but the words are used interchangeably.
Ink formulation is a specialised field, and most inks are proprietary compounds.
All inks or pastes consist of two main ingredients: the pigment or other active element and a vehicle to convey the pigment throughout the process to its position on the printed surface.

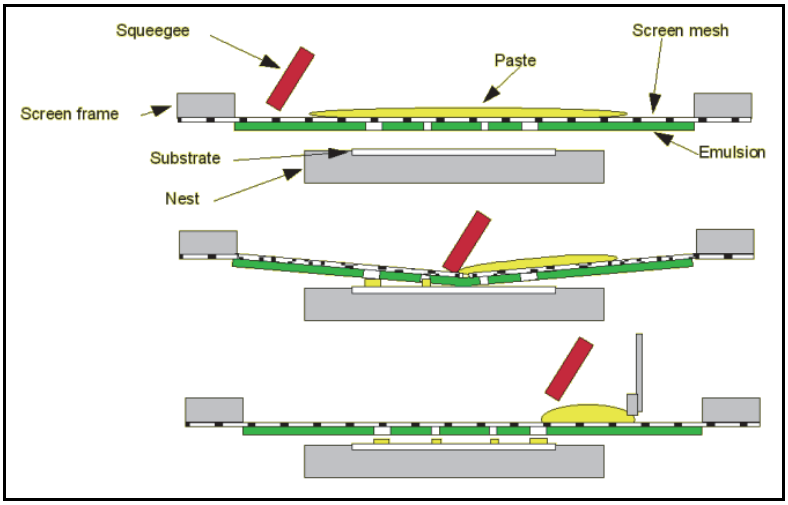

Fig. 1. Screen printing process – the basic.

The vehicle must be of a sticky, elastic nature so that the ink can be pushed about, change shape, yet hold together as a body until the required amount is separated from the remainder by the squeegee. The vehicle contains a combination of solvents, resins, humectants, antifoaming agents, preservatives, thickeners etc. One role of the vehicle is to allow the dispersion of the pigment or functional element into the ink. The functional element, whether carbon powder or metallic powders, has to be evenly distributed in the vehicle without any agglomerates and present final particle sizes that would allow the ink to go through the screen printing process without blocking the screen.
There is a minimum of two processes used to ensure the dispersion of components in the screen printing ink preparation. Mixing of the ingredients allows good dispersion of the active particles in the vehicle and triple-roll milling ensures a reduced particle size and no agglomerates in the ink (Website 2).
The repeatability of the final screen printed transducer depends not only on the quality of the screen printing process but also on a thorough dispersion of the active ingredient into the ink. At Gwent Group we ensure that both ink manufacturing and screen printing processes are performed following the highest levels of quality control to provide the most repeatable electrochemical sensors.

2.2 Screen printed electrochemical transducers

2.2.1 Design and production

One of the advantages of manufacturing transducers by the method of screen printing is the ability to produce them in large numbers at once. Industrially speaking, mass production techniques significantly lower the fabrication costs. But such production can only be successful if it results in reproducible transducers. This is a crucial condition because of the nature of the single use of the biosensor and the impossibility to carry out calibration before its use to make the measurement.
The electrochemical transducers we have generally used in our work are 2 electrode systems with a working electrode (WE) in carbon /graphite and a common reference and counter

electrode in Ag/AgCl. A typical screen printing production batch was made of 20 cards (Figure 2) each containing 220 transducers. The WE is circular with a diameter of 6 mm surrounded by an Ag/AgCl ring electrode. The two electrodes are extended by connectors and are isolated using an insulating ink which creates a flat circular electrochemical cell of 10 mm diameter.

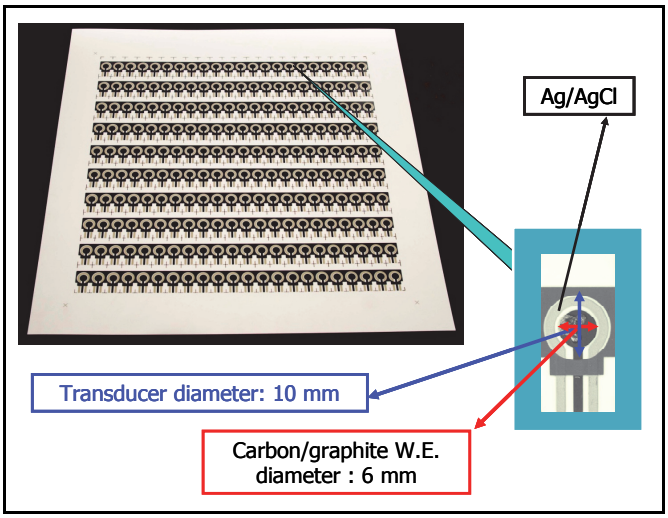

Fig. 2. Design of screen-printed electrochemical transducers

2.2.2 Reproducibility tests

One of the major challenges for the screen printing technique, in the mass production of transducers, is without doubt, that of reproducibility. This is even more crucial when producing single use transducers. Indeed, a good reproducibility offers the possibility to apply to the whole batch manufactured, with a minimum of error, the parameters of a calibration curve obtained either by measurements of standard solutions or imposed by a mathematical formula defined in advance.

To examine the reproducibility of the electrochemical transducers that we prepared, we have taken at random three of the twenty cards of the same batch on which we conducted comparative studies by chronoamperometry. Twenty transducers were taken from each of the three cards and every ten were used to analyze the electrochemical behaviour of ferrocene derivative (Fc-R) solution of definite concentration. Figure 3 illustrates the results of ten chronoamperometry experiments for each ferrocene solutions. In the insert is shown the expansion of the current area showing that each ten curves are superimposed indicating excellent reproducibility of the electrochemical transducers.

The overall results of the statistical study on the reproducibility of fabrication of the electrochemical transducers are recorded in Tables 1 and 2.

In this study, the electrochemical experiments were performed using the transducers in a two electrodes configuration. 40 µL of the test solution is deposited on the surface of the transducer in the area delimiting the planar electrochemical cell, a potential of +0.5 V is imposed, using a potentiostat, on the surface of the WE and the collected current (i) is

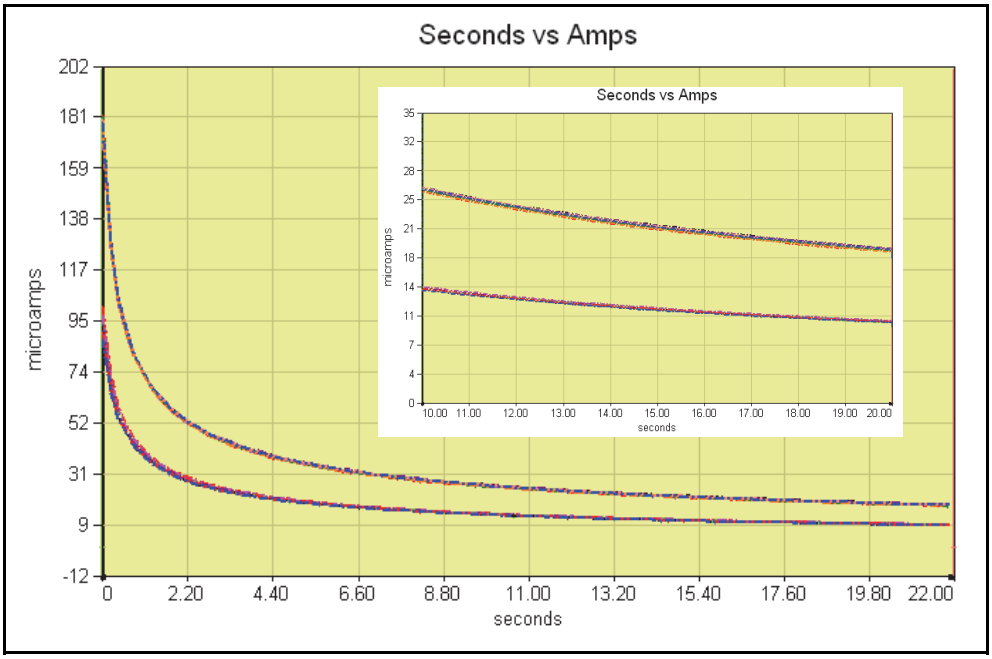

Fig. 3. Superposition of the signals obtained by chronoamperometry at +0.5 V *vs.* Ag / AgCl, with ten different transducers for two ferrocene derivative solutions.

	Card N° 1		Card N° 2		Card N° 3	
	Solution 1	Solution 2	Solution 1	Solution 2	Solution 1	Solution 2
Current (µA) (mean of 10 measures)	9.44	18.44	9.78	18.69	9.52	18.64
Standard deviation (µA)	0.14	0.15	0.07	0.25	0.11	0.19
Coefficient of variation (%)	1.53	0.82	0.71	1.32	1.12	1.03

Table 1. Reproducibility of transducers from each screen-printed card

	Solution 1			Solution 2		
	Card N° 1	Card N° 2	Card N° 3	Card N° 1	Card N° 2	Card N° 3
Current means (µA)	9.44	9.78	9.52	18.44	18.69	18.64
Mean (µA)	9.58			18.59		
Standard deviation (µA)	0.15			0.11		
Coefficient of variation (%)	1.55			0.59		

Table 2. Reproducibility of transducers between screen-printed cards

recorded versus time (t). In the case of ferrocenes solutions the curve obeys the Cottrell equation which states that the product ($it^{1/2}$) is constant for a diffusion-controlled reaction at a planar electrode.

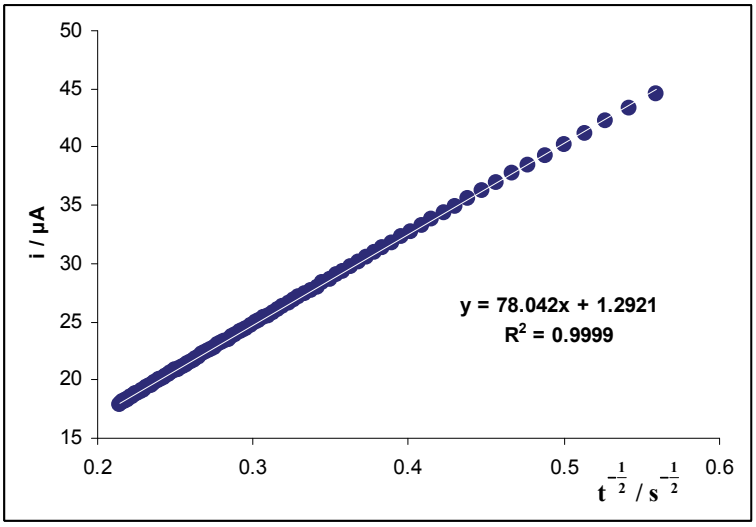

Fig. 4. Correlation curve as a function of $t^{-1/2}$ of the current (i) measured by chronoamperometry of a solution of ferrocene derivative

The results of one of the chronoamperometric experiments run with ferrocene derivative solution on the electrochemical transducer is shown in Figure 4, where the graphical representation of the relationship i = f ($t^{-1/2}$) shows a perfect linearity indicating that the electrochemical reaction (1), taking place at the surface of the transducer, is controlled by diffusion in accordance with the Cottrell equation.

$$Fc - R \rightleftarrows Fc - R^{+} + e^{-} \tag{1}$$

2.3 Disposable amperometric peroxidase mediated biosensor

The concentration of hydrogen peroxide can be measured directly using amperometric detection. Electrochemical oxidation is commonly achieved at a potential of approximately +0.6 to +0.7 V *vs.* Ag/AgCl on a platinum electrode. A number of electroactive chemical species can interfere since they are oxidised within the same potential range. Several electrochemical sensors and biosensors have been described to minimize the interferences (Giannoudi et al., 2006) by modifying the transducers particularly by Prussian blue and its analogous (Karyakin, 2001; Ricci & Palleschi, 2005), carbon nanotubes (Wang, 2005; Zagal et al., 2009) and peroxidase enzymes. The latter are based on electron transfer reactions between the enzyme and the working electrode either directly (Ferapontova, 2004) or through redox mediators (Ruzgas et al., 1996). This last concept of mediated electron transfer reaction is the basis of our work on "no calibration" type biosensor.

Numerous small redox active molecules exchanging one or two electrons with the oxidized form of peroxidase have been used to construct peroxidase-modified electrodes that can

measure H_2O_2 in a cathodic way (Ruzgas et al., 1996). The ferrocene derivatives are typical examples of one-electron mediators that are used for the bio-electrocatalytic reduction of peroxidases. In earlier research, we published the preparation of modified electrode with HRP and ferrocenes for hydrogen peroxide measurement (Charpentier & El Murr, 1995a), which can be combined with oxidase enzymes to permit the detection of their substrates in cathodic mode (Charpentier & El Murr, 1995b; Rondeau et al., 1999; Guémas et al., 2000; Serban et al., 2004; Serban & El Murr, 2006; Dai et al., 2007). The ferrocene mediated hydrogen peroxide biosensor is based on the reactions scheme shown in Figure 5.

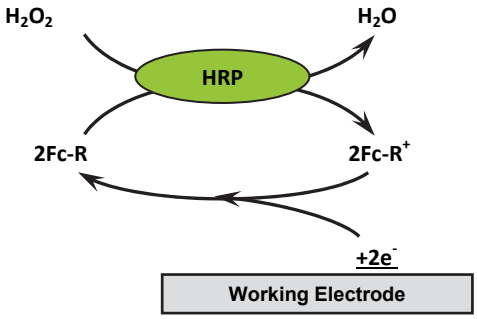

Fig. 5. Reactions scheme of ferrocene mediated peroxidase biosensor

2.3.1 Biosensor preparation

Starting from screen printed electrochemical transducers the general procedure for preparation of biosensors is as follows: three aqueous solutions were prepared separately, the first containing the horseradish peroxidase (HRP) enzyme, the second the ferrocene derivative (Fc-R) and the third a 0.4 M phosphate buffer solution + KCl. A total of 10 µL of each of the three solutions was deposited on the surface of the working electrode of screen-printed electrochemical cells, which were dried and stored at 6°C. In general, biosensors batches were made consisting of 100 to 200 units. The surface of each biosensor was usually modified by 0.5 U HRP, 16.10^{-8} moles ferrocene derivative, and a mixture of K_2HPO_4, KH_2PO_4, and KCl, which after addition of 40 µL of test solution produces a 0.1 M buffered solution at pH 7.2.

2.3.2 Choice of redox mediator

The ferrocenes are very popular as redox mediators particularly for reactions involving glucose oxidase or peroxidases. This popularity is mainly the result of the large number of derivatives previously synthesized, the commercial availability of many of them, the stability both in reduced and oxidized forms of a great number of derivatives, and particularly because they can cover a full range of redox potential depending on the nature and the number of substituents carried by the two cyclopentadienyl rings. During our work on the behaviour of hydrogen peroxide biosensors, we considered several ferrocene derivatives mono- or di-substituted by organic groups with varied electronic effects. Finally, the derivative that was selected is the carboxymethyl ferrocene; $(C_5H_5)Fe(C_5H_4\text{-}CH_2\text{-}COOH)$. The reasons for this choice include the high solubility of its both reduced and oxidized forms and the electronic effect brought by its substituent which results in an adequate redox potential which guaranty high reactivity towards the enzyme. Very good reactivity and solubility of the mediator are essential requirements for the preparation of "no calibration" type biosensor.

2.3.3 "No calibration" type hydrogen peroxide biosensor

For amperometric biosensors, the detection method most commonly used is chronoamperometry. In practice, measurements can be performed in various modes depending on the positioning of the working electrode with respect to the sample solution: the most frequently used are (1) stationary electrode in a relatively large volume of solution, (2) stationary electrode in a stirred or flow solution (e.g. flow injection analysis), and (3) stationary electrode with a very low volume of solution. For single-use biosensors, the third method is the one usually implemented. Very often the area of the working electrode in such a configuration is relatively large compared to the volume of substrate added. The measured current, related to the concentration of the substance to be analyzed, depends on the method applied and on the kinetics that take place in solution as well as on the surface of the working electrode during the chronoamperometric detection. Thus currents controlled by chemical kinetics are different from those controlled only by the diffusion of electroactive substances and undergo differently the effects of physicochemical parameters (temperature, reagents concentrations, enzymes activities)

For the reagentless disposable peroxidase biosensor described above, all reagents and enzymes are on the surface of the electrochemical transducer. The assay procedure is as follow: a total of 40 µL of the test solution is added to the biosensor surface and left to react for a given time (reaction time: t_r) before applying the potential at the working electrode in chronoamperometry mode for 20 seconds. The reaction time (t_r) is very important and can be critical on the current result. It should be long enough when a chemical reaction is required prior to the electrochemical one. This is the case when the measure is based on the detection related to an end-point reaction. Considering the reaction scheme shown in Figure 5, if this time (t_r) is very short H_2O_2 will remain in solution so a homogenous enzymatic reaction will accompany the heterogeneous electron-transfer process occurring at the electrode-solution interface. A catalytic regeneration mechanism (EC') takes place for which the resulting current will be dependent on the enzyme reaction kinetics (Savéant & Vianello, 1967). If sufficient time is allowed so that the enzymatic reaction is completed, H_2O_2 will be totally consumed and the equivalent of twice its concentration of ferricinium cation Fc-R^+ will be generated in solution. No enzymatic reaction can then take place and the electrochemical response $i_{(t)}$ of the planar transducer is controlled by the diffusion of Fc-R^+ according to the Cottrell equation (2) where **F** is Faraday's constant, **A** the electrode area, **n** the number of electrons involved in the electrochemical process, **D** the diffusion coefficient of the electroactive ferricinium species and **[Fc-R^+]** its concentration. A comprehensive study has allowed us to show that, for a time (t_r) equal to 30 seconds, it was possible to achieve an end-point reaction for H_2O_2 concentrations above 2 mM. A comprehensive study showed that the end-point of the enzymatic reaction shown in Figure 5 could be reached within 30 seconds for concentrations above 2 mM H_2O_2. Therefore, for all tests with hydrogen peroxide biosensors, a time (t_r) = 30 s has been fixed before running the chronoamperometric experiments.

$$i_{(t)} = \pi^{-1/2} \cdot F \cdot A \cdot n \cdot \left[Fc - R^+ \right] \cdot D \cdot t^{-1/2} \tag{2}$$

Because the hydrogen peroxide tests are carried out with disposable biosensors using reproducible transducers (as already shown above) the electrode area **A** is always constant As the electrochemical reaction involved is always the same (reaction 1), the diffusion coefficient **D** is always constant and the number of electrons **n** equal to 1. Thus, for the same

batch of transducers the current obtained by chronoamperometry at a time **t** (20 s) depends only on the ferricinium concentration [Fc-R+] and equation (2) becomes:

$$i_{(t)} = k \cdot \left[Fc - R^{+} \right] \tag{3}$$

Considering the equation (3) **k** is simply the slope of the calibration curve that can be obtained beforehand with standard solutions of Fc-R using transducers from the same batch. Provided that the enzymatic reaction, shown in Figure 5, is completed (end-point reaction) in the time (t_r) the initial concentration of hydrogen peroxide is then equal to half of that of Fc-R+. The final equation to calculate the concentrations of hydrogen peroxide solutions using the biosensor, without prior calibration, is:

$$\left[H_2O_2 \right] = i_{(t)} / 2k_{(t)} \tag{4}$$

where $\mathbf{i_{(t)}}$ is the chronoamperometric current measured at the time (t), typically 20 seconds, with the biosensor and $\mathbf{k_{(t)}}$ is the slope of the calibration curve obtained by chronoamperometry with standard ferrocene mediator solutions at the same time (t) using transducers from the same batch that was used for the preparation of disposable hydrogen peroxide biosensors.

2.3.4 Prior determination of $k_{(t)}$ for a given batch of transducers

Several standard solutions of carboxymethyl ferrocene Fc-CH_2-COOH covering the range from 0 to 4 mM were prepared. After deposition of 40 µL of each on the surface of a transducer of the same batch as those used to prepare the biosensors, a potential of +0.5 V *vs.* Ag/AgCl was applied to the working electrode and the faradic current generated was measured at t = 20 s. The slope ($\mathbf{k_{(t)}}$ = 11.64 µA/mM of Fc-CH_2-COOH) of the calibration curve (Figure 6) resulting from these measurements transforms the equation (4) in:

$$\left[H_2O_2 \right] = i_{(t)} / 23.28 \tag{5}$$

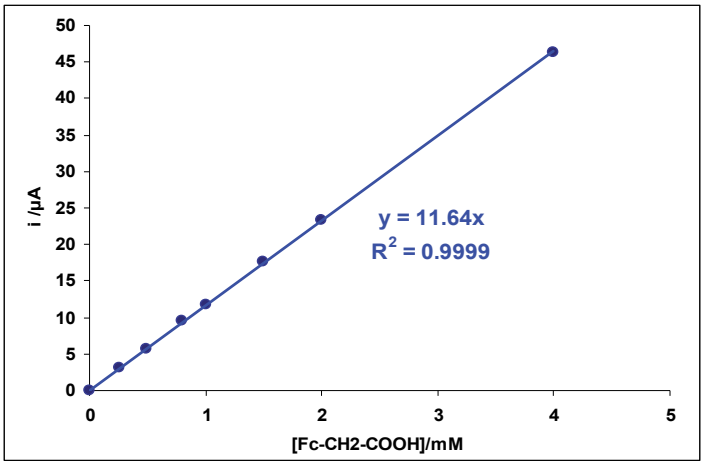

Fig. 6. Calibration curve of carboxymethyl ferrocene

For the batch of transducers used in this study, equation (5) enables by a simple calculation to determine the concentration of H_2O_2 solutions by chronoamperometric tests using disposable hydrogen peroxide biosensors.

2.3.5 Validation of the "No calibration" concept

To validate the concept, based on equation (5), to measure hydrogen peroxide without a preliminary calibration step with H_2O_2 standard solutions, we prepared from a stock solution titrated with $KMnO_4$ five H_2O_2 solutions of known concentrations, that we measured with the disposable biosensors.

In Table 3 are collected the results of this study, which shows that the deviations observed when using the equation (5) are low and remain anyway in the same order of magnitude as measurement errors obtained by biosensors in general. This shows that the proposed method provides reliable measurements, without the need to perform a tedious calibration step before each test.

$[H_2O_2]$ (mM)	i (µA)	$[H_2O_2]$ (mM) calculated with equation (5)	Deviation (%)
0.158	-3.78	0.162	2.69
0.316	-7.389	0.317	0.44
0.553	-12.49	0.537	-3.07
0.790	-18.54	0.796	0.80
0.988	-22.75	0.977	-1.05

Table 3. Results of measurements of H_2O_2 solutions by means of "no calibration" type biosensors

3. Conclusion

Amperometric enzyme based biosensors using redox mediators capable of shuttling electrons from the redox centre of the enzyme to the surface of the electrode are by far the most popular and the most studied. In addition, this type of biosensor is the one that has had the greatest commercial success, following the launch into the market of glucose biosensors devices for the control of diabetics' glycemia. From the perspective of electrochemistry, these biosensors are based on the measurement of a kinetic current controlled by the enzymatic reaction that detects the substrate. This current depends on the activity of the enzyme and is therefore sensitive to several physicochemical factors that may influence the kinetics of the reaction. For this, a calibration step is necessary to obtain, in the operating conditions, reliable measurements. This calibration step, often considered tedious and time consuming, makes these biosensors unattractive for industries that want to use these analytical tools in remote locations utilising unskilled workers. The development of "no calibration" type biosensor concept could be considered as the important step to overcome this difficulty. We have validated this concept in producing reliable and reproducible disposable biosensors for H_2O_2 that operate with horse radish peroxidase and carboxymethyl ferrocene as redox mediator which are commercially available, cheap and stable. Such a "no calibration" type H_2O_2 biosensor will serve as a general platform for a very large number of biosensors that use enzymes such as oxidases or combination of dehydrogenases and NADH oxidase.

4. Acknowledgment

This work was supported financially by the European Commission under Grant N°: COOP-CT-31588. The authors thank Mrs. Sheila Pittson for her help on revising the manuscript.

5. References

Charpentier, L. & El Murr, N. (1995a). Electrode enzymatique pour l'analyse du peroxyde d'hydrogène.*Analusis*, Vol. 23, pp. 265, ISSN 0365-4877

Charpentier, L. & El Murr, N. (1995b). Amperometric determination of colesterol in serum with use of a renewable surface peroxidase electrode. *Analytica Chimica Acta*, Vol. 318, Issue 1, pp. 89-93, ISSN 0003-2670

Dai, Z., Serban, S., El Murr, N. (2007). Layer-by-layer construction of hydroxymethyl ferrocene modified screen-printed electrode for rapid one-step α-fetoprotein amperometric flow/stop flow-injection immunoassay. *Biosensors and Bioelectronics,* Vol. 22, Issue 8, (March 2007), pp. 1700-1706, ISSN 09565663

Ferapontova, E. E. (2004). Direct peroxidase bioelectrocatalysis on a variety of electrode materials. *Electroanalysis*, Vol. 16, Issue 13-14, (July 2004), pp. 1101-1112, ISSN 10400397

Giannoudi, L., Piletska, E. V. & Piletsky, S. A. (2006). Development of Biosensors for the Detection of Hydrogen Peroxide, In *Biothechnological Applications of Photosynthetic Proteins: Biochips, Biosensors and Biodevices,* M.T. Giardi & E. V. Piletska, (Ed.), 175-191, Springel, ISBN: 0387330097

Guémas, Y., Boujtita, M., El Murr, N. (2000). Biosensor for determination of glucose and sucrose in fruit juices by flow injection analysis. *Applied Biochemistry and Biotechnology*, Vol. 89, Numbers 2-3, pp. 171-181

Karyakin, A. (2001). Prussian Blue and Its Analogues: Electrochemistry and Analytical Applications. *Electroanalysis*, Vol. 13, Issue 10, (June 2001), pp. 813-819, ISSN 10400397

Ricci, F. & Palleschi, G. (2005). Sensor and biosensor preparation, optimisation and applications of Prussian Blue modified electrodes. *Biosensors and Bioelectronics*, Vol. 21, Issue 3, (September 2005), pp. 389–407, ISSN 09565663

Rondeau, A., Larrson, N., Boujtita, M., Gorton, L., El Murr, N. (1999). The synergetic effect of redox mediators and peroxidise in a bioenzymatic biosensor for glucose. *Analusis*, Vol. 27, Issue 7, (September 1999), pp. 649-656, ISSN 0365-4877

Ruzgas, T., Csöregi, E., Emneus, J., Gorton, L., Marko-Varga, G. (1996). Peroxidase-modified electrodes: fundamentals and application: A Rewiew. *Analytica Chimica Acta*, Vol. 330, n° 2-3, pp. 123-138, ISSN 0003-2670

Savéant, J.M. & Vianello, E. (1967). Potential-sweep voltammetry: general theory of chemical polarisation. *Electrochimica Acta*, Vol. 12, Issue 6, (June 1967), pp. 629-646, ISSN 0013-4686

Serban, S., Danet, A.F., El Murr, N. (2004). Rapid and Sensitive Automated Method for Glucose Monitoring in Wine Processing. *J. Agric. Food Chem.*, Vol. 52, Issue 18, (8 September 2004), pp. 5588-5592

Serban, S., El Murr, N. (2006). Redox-flexible NADH oxidase biosensor: A platform for various dehydrogenase bioassays and biosensors. *Electrochimica Acta*, Vol. 51, Issue 24, (15 July 2006), pp. 5143-5149, ISSN 0013-4686

Wang, J. (2005). Carbon-Nanotube Based Electrochemical Biosensors: A Review. *Electroanalysis*, Vol. 17, Issue 1, (January 2005), pp. 7–14, ISSN 10400397

Website 1: http://www.gwent.org/Gem/index.html

Website 2: http://www.exakt.de/Three-Roll-Mills.25+M52087573ab0.0.html

Zagal, J. H., Griveau, S., Ozoemena, K. I., Nyokong, T., Bedioui, F. (2009). Carbon nanotubes, phthalocyanines and porphyrins: attractive hybrid materials for electrocatalysis and electroanalysis. *Journal of Nanoscience and Nanotechnology*, Vol. 9, No. 4, (April 2009), pp. 2201-2214, ISSN: 1550-7033.

9

QCM Technology in Biosensors

Yeison Montagut[1], José Vicente García[1], Yolanda Jiménez[1],
Carmen March[2], Ángel Montoya[2] and Antonio Arnau[1]
[1]*Grupo de Fenómenos Ondulatorios, Departamento de Ingeniería Electrónica*
[2]*Instituto Interuniversitario de Investigación en Bioingeniería y Tecnología Orientada al Ser Humano (I3BH, Grupo de Inmunotecnología)*
Universitat Politècnica de Valéncia,
Spain

1. Introduction

In the fields of analytical and physical chemistry, medical diagnostics and biotechnology there is an increasing demand of highly selective and sensitive analytical techniques which, optimally, allow an in real-time direct monitoring with easy to use, reliable and miniaturized devices. Biomolecular interactions such as: antigen-antibody, pathogen detection, cell adhesion, adsorption and hybridization of oligonucleotides, characterization of adsorbed proteins, DNA & RNA interactions with complementary strands and detection of bacteria and viruses, among others, are typical applications in these areas.
Conventionally, analytical methods include different techniques depending on the application. For instance, for low molecular weight pollutants detection, gas and liquid chromatography are classical techniques. These techniques precise of sophisticated sample pre-treatment: extraction of crude sample with large amounts of organic solvent, which is expensive and needs to be discarded; precolumn filtration and extensive purification (De Kok et al., 1992). Due to these shortcomings the analysis of a large number of samples may be both cost and time prohibitive (Ahmad et al., 1986).
Immunoassays for low molecular weight compounds (pesticides, industrial chemical pollutants, etc.) have already gained a place in the analytical benchtop as alternative or complementary methods for routine classical analysis as they are simple, fast, inexpensive, and selective as well as highly sensitive although, in general, not as much as chromatographic techniques. Immunoassays are able to detect specifically one target analyte in a complex sample. Moreover, immunoassays can be performed on portable devices, irrespective of centralized laboratories, which turn them into a suitable tool for quantification analysis in on-line applications. These techniques are based on the interaction of one antigen (analyte) with an antibody which recognizes it in a specific way. Currently, Enzyme Linked ImmunoSorbent Assay (ELISA) and Immunosensors are the most popular immunoassays. In ELISAs the detection of the analyte is always indirect because one of the immunoreagents is labeled. In immunosensors, or immunological biosensors, the detection is direct, one of the immunoreagents is immobilized on the surface of the transducer, and a direct physical signal is produced when interaction occurs (Marty et al, 1998; Byfield et al, 1994; Montoya et al, 2008). In those techniques where labels are necessary, the actual

quantitative measurement is only done after the biochemical recognition step. Moreover, label can compromise the biochemical activity (Hawkins et al., 2006). This label-free direct detection represents an essential advantage of immunosensors as compared to label-dependent immunoassays (Janshoff et al., 2000).

Immunosensors combine the selectivity provided by immunological interactions with the high sensitivity achieved by the signal transducers and are being proposed and proving to be powerful analytical devices for the monitoring of low molecular weight compounds such as organic pollutants in food and the environment (Su, et al., 2000; Fung et al., 2001).

Different sensing technologies are being used for biochemical sensors. Categorized by the transducer mechanism, electrochemical, optical and acoustic wave sensing techniques have emerged as the most promising biochemical sensor technologies (Coté et al., 2003). Common to most optical and electrochemical principles popular exceptions are Surface Plasmon Resonance (SPR) or electrochemical impedance spectroscopy, is the requirement of a label, as in the case of ELISAs, equipped with the physical information to stimulate the transducer, but increasing the complexity and thus the cost for analysis. Examples of labels are the coupling with an enzyme, a fluorescent molecule, a magnetic bead or a radioactive element (Asch et al., 1999).

Acoustic sensing has taken advantage of the progress made in the last decades in piezoelectric resonators for radio-frequency (RF) telecommunication technologies. The piezoelectric elements used in: radars, cellular phones or electronic watches for the implementation of filters, oscillators, etc., have been applied to sensors (Lec, 2001). The so-called gravimetric technique is based on the change in the resonance frequency experimented by the resonator due to a mass attached on the sensor surface (Sauerbrey, 1959); it has opened a great deal of applications in bio-chemical sensing in both gaseous and liquid media.

Most of the biochemical interactions described above are susceptible of being evaluated and monitored in terms of mass transfer over the appropriate interface. This characteristic allows using the gravimetric techniques based on acoustic sensors for a label-free and a quantitative time-dependent detection. Acoustic sensor based techniques combine their direct detection, real-time monitoring, high sensitivity and selectivity capabilities with a reduced cost in relation to other techniques. As mentioned previously, optical techniques, like Surface Plasmon Resonance (SPR), depend on the optical properties of the materials used; on the contrary, the most applied principle of detection in acoustic sensing for biochemical applications is based on mass (gravimetric) properties and it is, therefore, independent of the optical properties of the materials, allowing to perform studies over a great variety of surfaces and suitable for direct measurement on crude, unpurified samples. This eliminates the need for sample preparation and therefore reduces the number of steps involved in the process – bringing many benefits, including significant time and cost-savings. Additionally, acoustic systems provide information on the real binding to a receptor and not simply proximity to a receptor, as could be the case with SPR techniques. Furthermore, the key measuring magnitude of acoustic wave devices is the frequency of a signal which can be processed easily and precisely, unlike other devices.

The classical quartz crystal microbalance (QCM) has been the most used acoustic device for sensor applications; however, other acoustic devices have been, and are being used, for the implementation of nano-gravimetric techniques in biosensor applications. Although this chapter is focused on QCM technology, a broader view of the different techniques used in the implementation of acoustic biosensors could be very useful for three reasons: first because it gives a complete updated sight of the acoustic techniques currently used in

biosensors, second because some of the challenges remaining for QCM can be applied to other acoustic devices, and third because the new aspects presented in this chapter, mainly in relation to the new sensor characterization interfaces, can be considered for the other devices as well. With this purpose, a brief description of the state of the art of the different acoustic techniques used in biosensors is included next.

Different types of acoustic sensing elements exist, varying in wave propagation and deflection type, and in the way they are excited (Ferrari & Lucklum, 2008). They can be classified into two categories: bulk acoustic waves (BAW) and surface-generated acoustic waves (SGAW). Moreover they may work with longitudinal waves (with the deflection in the direction of propagation) or shear waves (with the deflection perpendicular to the direction of propagation). The number of biochemical applications is extended for in-liquid applications; in these cases it is necessary to minimize the acoustic radiation into the medium of interest and the shear wave is mostly used.

1.1 Bulk acoustic wave devices (BAW)

Bulk acoustic wave (BAW) devices utilize waves travelling or standing in the bulk of the material. They are mostly excited through the piezoelectric or capacitive effects by using electrodes on which an alternative voltage is applied. The three important BAW devices are: quartz crystal microbalances (QCM), film bulk acoustic resonators (FBAR) and cantilevers. Figure 1 shows their basic structure and typical dimensions. Because the vibrating mode of cantilevers is not suited for operation in liquids due to the high damping we will focus our discussion on QCM and FBAR devices.

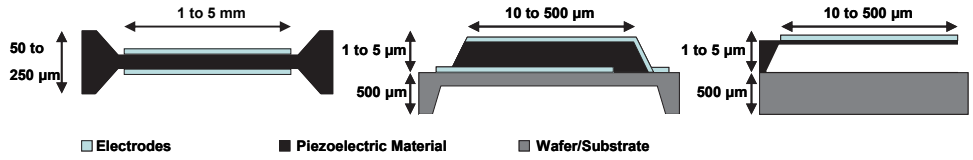

Fig. 1. Bulk acoustic devices: a) QCM, b) FBAR and c) Cantilevers

1.1.1 QCM for biosensing applications

The classical QCM is formed by a thin slice of AT-cut quartz crystal. Acoustic waves are excited by a voltage applied to an electrode structure where the quartz crystal is sandwiched (see Figure 1a). Shear waves are excited which makes the operation in liquids viable (Kanazawa & Gordon, 1985). QCM has been the most used acoustic device for sensor applications since 1959, when Sauerbrey established the relation between the change in the resonance frequency and the surface mass density deposited on the sensor face. The theoretical absolute mass sensitivity for this shift is proportional to the square of the resonant frequency, according to the following expression (Sauerbrey, 1959):

$$S_a = \frac{\Delta f}{\Delta m} = -\frac{2}{\rho v}\frac{f_n^2}{n} \text{ (Hz cm}^2 \text{ ng}^{-1}\text{)} \quad (1)$$

where Δf is the frequency shift, Δm is the surface mass density change on the active sensor's surface, ρ is the quartz density, v the propagation velocity of the wave in the AT cut crystal,

f_n is the frequency of the selected harmonic resonant mode and n is the harmonic number (n=1 for the fundamental mode). Theoretical mass sensitivity, i.e., the lineal relationship between the frequency variation and the mass surface density change so obtained in Sauerbrey's equation, is right only on ideal conditions, where only inertial mass effects contribute on the resonant frequency shift of the QCM sensor (Voinova et al., 2002; Kankare, 2002; Jiménez et al., 2008; Jiménez et al., 2006). For AT cut quartz crystals, the limit of detection (LOD) or surface mass resolution for a minimum detectable frequency shift $\Delta f_{\min}$ will be given by:

$$\Delta m_{\min} = \frac{\Delta f_{\min}}{S_a} \tag{2}$$

Many commercial systems are already on the market (Coté et al., 2003). Absolute sensitivities of a 30 MHz QCM reach 2 Hz cm^2 ng^{-1}, with typical mass resolutions around 10 ng cm^{-2} (Lin et al., 1993). Lower mass resolutions down to 1 ng cm^{-2} seem possible by improving the characterization electronic interface as well as the fluidic system.

This technique has extensively been employed in the literature just for the monitoring of many substance absorption and detection processes (Janshoff et al., 2000). QCM technology has a huge field of applications in biochemistry and biotechnology. The availability for QCM to operate in liquid has extended the number of applications including the characterization of different type of molecular interactions such as: peptides (Furtado et al., 1999), proteins (BenDov et al., 1997), oligonucleotides (Hook et al., 2001), bacteriophages (Hengerer et al., 1999), viruses (Zhou et al., 2002), bacteria (Fung & Wong, 2001) and cells (Richert et al., 2002); recently it has been applied for detection of DNA strands and genetically modified organisms (GMOs) (Stobiecka et al., 2007).

Despite of the extensive use of QCM technology, some challenges such as the improvement of the sensitivity and the limit of detection in high fundamental frequency QCM, remain unsolved; recently, an electrodeless QCM biosensor for 170MHz fundamental frequency, with a sensitivity of 67 Hz cm^{-2} ng^{-1}, has been reported (Ogi et al, 2009); this shows that the classical QCM technique still remains as a promising technique. Once these aspects are solved the next challenge would be the integration; in this sense, commercial QCM systems are mostly based on single element sensors, or on multi-channel systems composed of several single element sensors (Tatsuma et al., 1999). They are to date expensive, mainly because currently their manufacturing is complex, especially for high frequencies, and their application for sensor arrays is difficult due to lack of integration capability. Most of these shortcomings could be overcome with the appearing of film bulk acoustic resonators (FBAR).

1.1.2 FBAR devices for biosensing applications

A typical film bulk acoustic resonator (FBAR) consists of a piezoelectric thin film (such as ZnO or AlN) sandwiched between two metal layers. A membrane FBAR is shown in Figure 1b. In the past few years, FBARs on silicon substrates have been considered for filter applications in RF devices (Vale et al., 1990). Gabl et al. were the first to considerer FBARs for gravimetric bio-chemical sensing applications (Gabl et al., 2003). They basically function like QCMs; however, unlike QCMs, typical thicknesses for the piezoelectric thin film are between 100 nm and a few μm, allowing FBARs to easily attain resonance frequencies in the GHz range. The main advantage of FBAR technology is its integration compatibility with CMOS technologies, which is a prerequisite for fabrication of sensors and sensor arrays

integrated with the electronics, and hence low cost mass fabrication of miniature sensor systems. However, the miniaturization of sensor devices should go in parallel with the miniaturization and optimization of the microfluidic system which is of extreme importance for reducing the noise and increasing the stability of the complete system; the main problems of the microfluidics are the complexity of integration and the cost. Moreover, due to higher resonance frequency of these devices and according to (1), higher sensitivities than for QCMs could be reached; however, the higher sensitivity does not mean necessarily that a higher LOD or mass resolution is achieved. Effectively, thin film electroacoustic technology has made possible to fabricate quasi-shear mode thin film bulk acoustic resonators (FBAR), operating with a sufficient electromechanical coupling for use in liquid media at 1-2 GHz (Bjurstrom et al., 2006; Gabl et al., 2004); however, the higher frequency and the smaller size of the resonator result in that the boundary conditions have a much stronger effect on the FBAR performance than on the QCM response. This will result in a higher mass sensitivity, but in an increased noise level as well, thus moderating the gain in resolution (Wingqvist 2007, 2008). So far only publications of network analyzer based FBAR sensor measurements have been published in the literature, which show that the FBAR mass resolution is very similar if not better than for oscillator based QCM sensors (Weber et al., 2006; Wingqvist 2007, 2008, 2009). The first shear mode FBAR biosensor system working in liquid environment was reported in 2006 (Weber et al., 2006). The device had a mass sensitivity of 585 Hz cm^2 ng^{-1} and a limit of detection of 2.3 ng cm^{-2}, already better than that obtained with QCM (5.0 ng cm^{-2}) for the same antigen/antibody recognition measurements. However, these results have been compared with typical 10MHz QCM sensors; therefore high fundamental frequency QCM sensors working, for instance, at 150MHz could have much higher resolution than the reported FBAR sensors. In 2009 a FBAR for the label-free biosensing of DNA attached on functionalized gold surfaces was reported (Nirsch et al., 2009). The sensor operated at about 800 MHz, had a mass sensitivity of about 2000 Hz cm^2 ng^{-1} and a minimum detectable mass of about 1ng cm^{-2}. However, studies of the mass sensitivity only do not provide a comprehensive view of the major factors influencing the mass resolution. For instance in FBAR sensors, in contrast to the conventional QCM, the thickness of the electrodes is comparable to that of the piezoelectric film and hence cannot be neglected. The FBAR must, therefore, be considered like a multilayer structure, where the acoustic path includes the piezoelectric film as well as an acoustically "dead" material, e.g. electrodes and additional layers such as for instance Au, which is commonly used as a suitable surface for various biochemical applications, or SiO_2 which also is used for temperature compensation (Bjurstrom et al., 2007). In general there is a set of factors which must be considered and affects the quality factor of a FBAR sensor such as: loss mechanisms, multilayer effects, lateral structure, spurious modes, etc.
Another approach used to get higher mass sensitivities by increasing the frequency is by using surface generated acoustic wave devices (SGAW)

1.2 Surface generated acoustic wave devices (SGAW)

SGAW devices have been used as chemical sensors in both gaseous and liquid media. The input port of a SGAW sensor is comprised of metal interdigital electrodes (IDTs), with alternative electrical polarity, deposited or photodesigned on an optically polished surface of a piezoelectric crystal. Applying a RF signal, a mechanical acoustic wave is launched into the piezoelectric material due to the inverse piezoelectric phenomenon. The generated acoustic wave propagates through the substrate arriving at an output IDT. The separation

between the IDTs defines the sensing area where biochemical interactions at the sensor surface cause changes in the properties of the acoustic wave (wave propagation velocity, amplitude or resonant frequency) (Ballantine et al., 1997). Thus, at the output IDT the electrical signal can be monitored after a delay in an open loop configuration. Figure 2, shows a schematic view of different SGAW devices

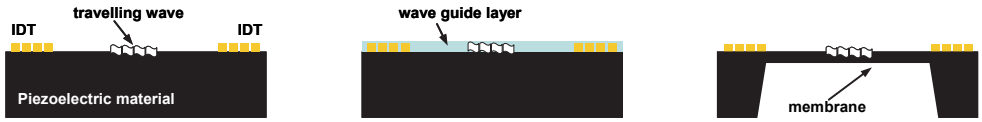

a) b) c)

Fig. 2. Different types of SGAW devices: a) typical SAW configuration, b) Love-wave SGAW device and c) flexural plate SGAW device

In SGAW devices the acoustic wave propagates, guided or unguided, along a single surface of the substrate. SGAW devices are able to operate, without compromising the fragility of the device, at higher frequencies than QCMs (Länge et al., 2008) and the acoustic energy of these devices is confined in the surface layer of about one wave length, therefore, the base-mass of the active layer is about one order of magnitude smaller than that of the QCM, increasing dramatically the sensitivity (Gronewold, 2007; Francis 2006; Fu et al., 2010). The longitudinal or Rayleigh mode SAW device has a substantial surface-normal displacement that easily dissipates the acoustic wave energy into the liquid, leading to excessive damping, and hence poor sensitivity and noise. Waves in a shear horizontal SH-SAW device propagate in a shear horizontal mode, and do not easily radiate acoustic energy into the liquid and thus maintain a high sensitivity in liquids (Barie & Rapp, 2001). Shear Horizontal Surface Acoustic Wave (SH-SAW), Surface Transverse Wave (STW), Love Wave (LW), Shear Horizontal Acoustic Plate Mode (SH-APM) and Layered Guided Acoustic Plate Mode (LG-APM), have recently been reported as more sensitive than the typical QCM-based devices (Rocha-Gaso et al., 2009).

In most cases, Love-wave devices operate in the SH wave mode with the acoustic energy trapped within a thin guiding layer (typically submicrometer). This enhances the detection sensitivity by more than one order of magnitude as compared with a different SAW device owing to a much-reduced base-mass (Josse et al., 2001; McHale, 2003). In addition, the wave guide layer in the Love mode biosensor could, in principle, also protect and insulate the IDT from the liquid media which might otherwise be detrimental to the electrode. Therefore, they are frequently utilized to perform bio-sensing in liquid conditions (Lindner, 2008; Jacoby & Vellekoop, 1997; Bisoffi et al., 2008; Andrä et al., 2008; Moll et al., 2007, 2008; Branch & Brozik, 2004; Tamarin et al., 2003; Howe & Harding, 2000), arising as the most promising SGAW device for this purpose due to its high mass sensitivity and electrode isolation characteristics from liquid media (Rocha-Gaso et al., 2009; Francis et al., 2005).

The mass sensitivity of LW sensors can be evaluated by different techniques based on incremental modifications of the surface density on the sensing area of the device (Francis et al., 2004). Experimental and theoretical techniques to evaluate mass sensitivity of Love Wave sensors are reported in literature (Francis et al., 2004; Harding, 2001; Wang et al., 1994). Kalantar and coworkers reported a sensitivity of 95 Hz cm^2ng^{-1} for a 100MHz Love mode sensor, which is much better than the values reported for QCM technology (Kalatar et al., 2003); however, Moll and coworkers reported a LOD for a Love sensor of 400 ng cm^{-2},

this reveals once again that an increase in the sensitivity does not mean, necessarily, an increase in the LOD (Moll et al., 2008). Moreover, in spite of the initial advantage of the guiding layer for isolating the IDTs, in real practice the capacitive coupling between the IDTs due to the higher permittivity of the liquid makes necessary to avoid the contact of the liquid with the guiding layer just over IDTs, at the same time that it is necessary to allow the contact of the central area between the IDTs with the liquid medium. This increases the complexity of the design and practical implementation of the flow cell for LW acoustic devices; this is one of the reasons why there are very few commercial microgravimetric systems based on LW-devices for in-liquid applications.

Consequently, although acoustic techniques have been improved in terms of robustness and reliability and allow measuring molecular interactions in real time, the main challenges remain on the improvement of the sensitivity, but with the aim of getting a higher mass resolution, multi-analysis and integration capabilities and reliability, as well as the availability of a functional system, specifically designed for each application, which permits the use of acoustic based techniques in a flexible and reliable way.

This chapter is focused on QCM technology applied to Biosensors. The main aspect of improving the sensitivity and the limit of detection is treated in detail and can be mostly applied to other type of acoustic devices. A new concept for the sensor characterization along with its electronic implementation is included and compared with an improved oscillator configuration. The different biochemical steps included in a typical biosensor application are covered as well in this chapter, through a case study of a QCM immunosensor for the detection of low molecular weight pollutants. The obtained results validate the new sensor characterization concept and system as a new QCM characterization technique. Moreover, this technique offers the opportunity of undertaking the remaining challenges in the acoustic biosensor technologies: 1) improvement in the sensitivity and limit of detection by working with very high frequency QCM sensors; and 2) the possibility to easily implement a QCM sensor array system with integration capabilities.

2. Fundamentals of QCM: physical bases and instrumentation techniques

2.1 Physical bases

The use of the AT-cut quartz crystal resonator as the so-called QCM (quartz-crystal microbalance) sensor has been based on the Sauerbrey equation (Sauerbrey, 1959), generalized in (1) for harmonic resonant frequencies. When a Newtonian semi-infinite liquid medium is in contact with the resonator surface, Kanazawa equation provides the associated frequency shift due to the contacting fluid (Kanazawa & Gordon, 1985). For a QCM sensor one face in contact with an "acoustically thin layer" contacting a semi-infinite fluid medium, as it is the normal case in biosensor applications, the contribution of the coating and the liquid properties can be considered additive and Martin's equation (3) can be applied (Martin et al., 1991), which combines both effects on the frequency shift, the mass effect of the coating (Sauerbrey effect) and the mass effect of the liquid (Kanazawa effect)

$$\Delta f = -\frac{2 f_o^2}{Z_{cq}} \left(m_c + m_L \right) \tag{3}$$

In the former equation, written for fundamental resonant frequencies f_o, the first term of the second member corresponds to the Sauerbrey effect and the second to the Kanazawa effect,

where Z_{cq} is the characteristic acoustic impedance of the quartz, m_c is the surface mass density of the coating and $m_L=\rho_L\delta_L/2$ where ρ_L and δ_L are, respectively, the liquid density and the wave penetration depth of the acoustic wave in the liquid: m_L is, in fact, the equivalent surface mass density of the liquid, which moves in an exponentially damped sinusoidal profile, due to the oscillatory movement of the surface of the sensor. Assuming constant properties of the liquid medium, which can be accepted in most of QCM biosensing applications, the frequency shift provides a measuring parameter to monitor the interactions occurring at the coating interface and which can be evaluated in terms of surface mass changes.

According to (2), for a certain surface mass density of the coating, the associated frequency shift increases directly proportional to the square of the resonance frequency – only for fundamental frequencies (1). Consequently, it seems logic to think that the higher the resonance frequency the higher the sensitivity. In fact the resonance frequency of the resonator has been always the main parameter for sensor characterization.

2.2 Instrumentation techniques

In practice, all the QCM sensor characterization techniques provide, among other relevant parameters, the resonance frequency shift of the sensor (Arnau et al., 2008; Eichelbaum et al., 1999): network or impedance analysis is used to sweep the resonance frequency range of the resonator and determine the maximum conductance frequency (Schröder et al., 2001; Doerner et al., 2003), which is almost equivalent to the motional series resonance frequency of the resonator-sensor; impulse excitation and decay method techniques are used to determine the series-resonance or the parallel-resonance frequency depending on the measuring set-up (Rodahl & Kasemo, 1996); oscillator techniques are used for a continuous monitoring of a frequency which corresponds to a specific phase shift of the sensor in the resonance bandwidth (Ehahoun et al., 2002; Barnes, 1992; Wessendorf, 1993; Borngräber et al., 2002; Martin et al., 1997), this frequency can be used, in many applications, as reference of the resonance frequency of the sensor; and the lock-in techniques, which can be considered as sophisticated oscillators, are designed for a continuous monitoring of the motional series resonance frequency or the maximum conductance frequency of the resonator-sensor (Arnau et al., 2002, 2007; Ferrari et al., 2001, 2006; Jakoby et al., 2005; Riesch & Jakoby 2007). In order to assure that the frequency shift is the only parameter of interest, a second parameter providing information of the constancy of the properties of liquid medium is of interest, mainly in piezoelectric biosensors; this parameter depends on the characterization system being: the maximum conductance or the conductance bandwidth in impedance analysis, the dissipation factor in decay methods and a voltage associated with the sensor damping in oscillator techniques

The different characterization methods mentioned can be classified in two types: 1) those which passively interrogate the sensor, and 2) those in which the sensor forms part of the characterization system. In the first group impedance or network analyzers and decay methods are included. Advantages of impedance analyzers are mainly related to the fact that the sensor is almost characterized in isolation and no external circuitry influences its electrical behaviour; additionally, electrical external influences can be excluded by calibration. The accuracy of decay methods is high provided that the accuracy in the data acquisition is high as well, both in phase and amplitude, which becomes very complicated for high resonance frequencies; therefore, for high frequency resonators only impedance analysis provides accurate results, but its high cost and large dimensions, prevent its use for

sensor applications. Consequently, oscillators are taken as alternative for sensor resonance frequency monitoring; the low cost of their circuitry as well as the integration capability and continuous monitoring are some features which make the oscillators to be the most common alternative for high resonance frequency QCM sensors. However, in spite of the efforts carried out to build oscillator configurations suitable for in-liquid applications (Barnes, 1991; Auge et al., 1994, 1995; Chagnard et al., 1996; Paul & Beeler, 1998; Rodríguez-Pardo, 2004, 2006; Wessendorf, 2001; Benes et al., 1999) the poor stability of high frequency QCM systems based on oscillators has prevented increasing the limit of detection despite the higher sensitivity reported (Rabe et al., 2000; Uttenthaler et al., 2000; Zimmermann et al., 2001; Sagmeister et al., 2009).

3. A new concept for sensor characterization

In QCM based biosensors, in which this chapter is focused, the experimental frequency shifts expected are usually small, in the order of tens of Hertz. Therefore, the great efforts performed to improve the sensitivity of the sensor are useless if they are not accompanied with an increase in the limit of detection. As mentioned, increasing the sensor frequency has not carried a parallel improve in the resolution; this suggests that the resonant frequency is not the only parameter to take into account to get our purposes.
Effectively, the sensitivity will not be improved if the frequency stability is not improved as well. Two aspects should be distinguished: on one hand on the experimental set-up which must be designed to minimize the disturbances or interferences which can affect the resonance frequency of the resonator such as: temperature, vibrations, pressure changes due to the fluid pumps, etc.; and on the other hand on the ability of the characterization system for an accurate measuring of the parameter of interest, in this case the appropriate resonance frequency of the resonator-sensor. Assuming that the experimental set-up is maintained under maximum control, the frequency stability depends on the measuring system.

3.1 Problem outline

The measuring systems used for high fundamental frequency QCM applications, apart from routing impedance analysis, have been oscillators for the reasons mentioned above. It is important to realize that the role of crystal resonators in radio-frequency oscillators is to improve the frequency stability. The oscillation frequency in an oscillator is the result of a delicate balance among the phase responses of each one of the elements in the oscillator (Arnau et al., 2008, 2009); if the phase response in one of the elements changes, the oscillation frequency shifts to find the new balance point. Therefore the origin of the frequency instability is the phase instability and a direct relationship exists between a phase shift and the corresponding frequency shift. This relationship can be easily obtained through the definition of the stability factor S_F of a crystal resonator operating at its series resonance frequency f_o:

$$S_F = \frac{\Delta\phi}{\Delta f} f_o = 2Q \tag{4}$$

where Δf is the frequency shift necessary to provide a phase shift $\Delta\varphi$ in the phase-frequency response of the resonator, around f_o, and Q is the series quality factor of the resonator.
According to (4) the frequency noise Δf_n associated to a phase noise in the circuitry $\Delta\varphi_n$ is:

$$\Delta f_n = \frac{f_o}{2Q}\Delta\varphi_n \tag{5}$$

Consequently, because the quality factor is normally reduced proportionally to $1/f_o$, the frequency instability is increased in relation to the square of frequency. Moreover, the phase response of the electronic components of an oscillator gets worse with increasing the frequency, which increases, even more, the noise. Furthermore, if the limit of the detection is assumed to be three times the level of noise ($\Delta\varphi_{min}=3\Delta\varphi_n$), the minimum detectable surface mass density change of a QCM, according to (2) and (5) will be:

$$\Delta m_{\min} = \frac{f_o}{2QS_a}\Delta\varphi_{\min} \tag{6}$$

The former equation seems to indicate that for a given minimum detectable phase of the measuring system, the surface mass limit of detection does not depend on the frequency. Fortunately this is not completely true; the liquid medium has not been taken into account in the obtaining of the previous equation. Recently, the following phase-mass relationship has been obtained for a QCM in contact with a liquid medium (Arnau et al., 2009):

$$\Delta m_{\min} \approx -m_L\Delta\varphi_{\min} \tag{7}$$

Therefore, because $m_L=\rho_L\delta_L/2$ and $\delta_L=(\eta_L/\pi f\rho_L)^{1/2}$, where η_L is the liquid viscosity, is reduced proportionally to $1/f^{1/2}$, so does m_L and then the resolution of the surface mass density Δm_{min} increases with $f^{1/2}$ for a given $\Delta\varphi_{min}$.

Effectively, the ratio between the limits of detection of surface mass density at two different frequencies, $f_2 > f_1$, for a given phase limit of detection of the monitoring system, according to (7), is:

$$\frac{\Delta m_{\min}(f_2)}{\Delta m_{\min}(f_1)} = \sqrt{\frac{f_1}{f_2}} \tag{8}$$

Therefore, the surface mass limit of detection, for a constant phase limit of detection of the measuring system, reduces proportionally to $f^{1/2}$ and so the resolution increases correspondingly. This is not in contradiction with (6), simply the effective reduction of the quality factor of the sensor in liquid, is proportional to $1/f^{1/2}$ instead to $1/f$ when the contacting liquid is considered. This is not true in air because the approximation given in (7) is not acceptable. In air, an increase in frequency does not improve the limit of detection unless the stability and the phase limit of detection of the measuring system are improved.

The previous analysis allows concluding the following important remarks: 1) The sensitivity of a QCM always increases with increasing the frequency; however, the mass resolution, which is the parameter of interest, only increases with the frequency if the noise is, at least, maintained constant or reduced. Moreover, this increase in the mass resolution is only valid for in-liquid QCM and not for in-gas QCM; and 2) Once all the cares have been taken into account to reduce the perturbations on the resonator-sensor such as: temperature and pressure fluctuations, etc., the mass resolution is only depending on the interface system, its stability and its phase detection limit.

Consequently, unlike in RF-oscillators, in QCM sensor oscillators the quality factor of the resonator is strongly reduced, and any phase instability in the rest of the elements of the oscillator is compensated with a much larger frequency-shift of the sensor, which contributes in a frequency noise increase. Therefore for high frequency QCM sensor applications in liquid, the components which from part of the oscillator, apart from the resonator-sensor, should be selected as ideal as possible to avoid the phase noise which is transferred into frequency noise. Unfortunately to design and implement an ideal oscillator for high frequency QCM sensors in liquid is not an easy task as mentioned.

3.2 Concept description

The great sensitivity of the QCM sensors is due to the great acceleration suffered by the mass layer deposited on the sensor surface (for 10MHz sensors in air, it is around 10^7 times the gravity). This big acceleration is due to two parameters: frequency and displacement amplitude of sensor surface; therefore, it is very important to work at maximum displacements and this occurs at resonance. However, the important part of this argument is that we have a resonance bandwidth in which the amplitude of displacement is reasonably big. Therefore, taking into account that the expected frequency shifts in QCM biosensors are very small, it could be possible to interrogate the sensor at an appropriate fixed frequency in the resonance bandwidth and then measure the change in the phase response of the sensor, due to the experimental process to be monitoring, without losing the resonance; Fig.3a depicts this idea. The advantage of this approach is that the sensor is interrogated with an external source which can be designed to be very stable and with extremely low phase and frequency noises. A similar approach has been already applied by some authors (Dress et al., 1999; Pax et al., 2005), but recently a simple relationship between the surface mass change and the corresponding sensor phase shift, for a sensor operating at its motional series resonant frequency, has been already obtained as follows (Arnau et al., 2009):

$$\Delta\varphi(\text{rad}) = -\frac{\Delta m_c}{m_q + m_L} \tag{9}$$

where $m_q=\eta_q\pi/2v_q$, being η_q the effective quartz viscosity and v_q the wave propagation speed in the quartz. In liquid applications $m_q << m_L$ and (9) reduces into (7).

The former equation is very simple but, apart from introducing the mathematical quantification of the phase-mass approach, makes clear a very important aspect: in contrast with Sauerbrey equation in which the frequency shift associated with a change in the surface mass density of the coating does not depend on the medium, (9) includes the additional effect of the medium. From the previous equation it is clear that the bigger m_L the bigger Δm_c for a given phase-shift detection limit. In other words, Sauerbrey equation predicts the same shift in the resonant frequency for a sensor in vacuum or in liquid for a given change in the surface mass of the coating; however the corresponding phase-shift is much smaller for the sensor in liquid than in vacuum. Therefore, although the Sauerbrey equation predicts the same frequency-mass sensitivity in both cases, much higher phase stability of the system is necessary for the case of the sensor in liquid than in vacuum to have, in practice, the same mass resolution.

In principle, the new method based on monitoring the phase shift of the sensor at an appropriate fixed frequency in the resonance bandwidth, allows characterizing the sensor almost in isolation with a RF signal of lowest phase and frequency noises, even at very high frequencies, in a simple way.

3.3 System description

A simple circuit to implement the phase-mass characterization approach is depicted in Fig.3b, where a mixer is used as a phase detector. A more specific circuit has been recently proposed (Fig.4) (Arnau et al., 2009) and a practical implementation of the sensor circuit part is shown in Fig.5.

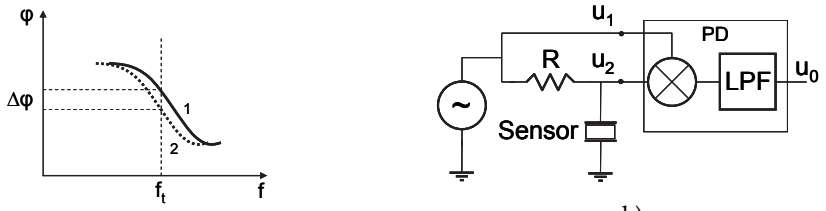

Fig. 3. a) Description of the phase approach and b) Simple implementation

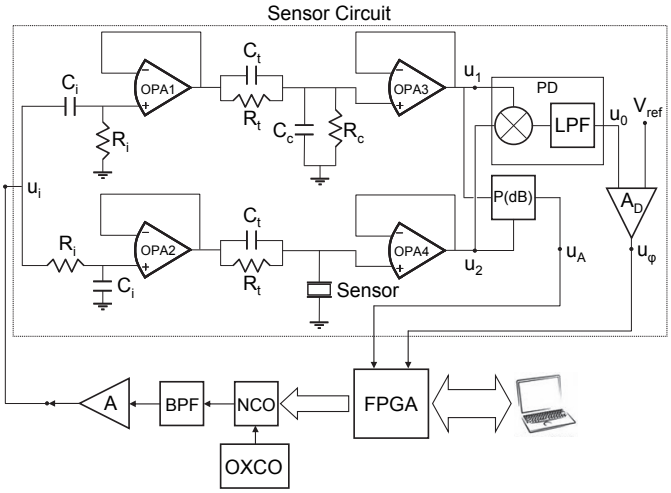

Fig. 4. Proposed system (Arnau et al. 2009)

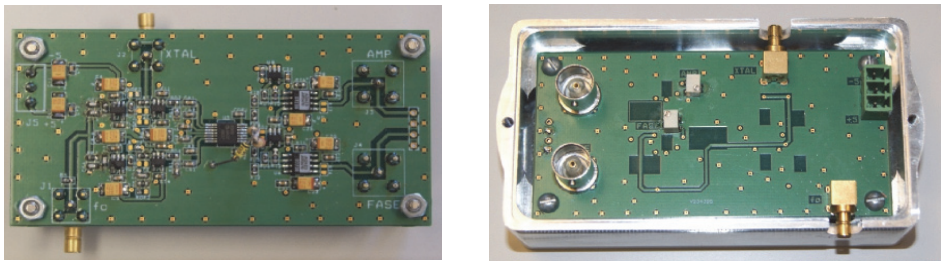

Fig. 5. Implemented system: a) bottom b) top

4. Case study: QCM immunosensor for carbaryl detection. Concept validation

A biosensor can be defined as an analytical device in which a biological receptor, such as: an enzyme, an antibody, a tissue portion, a whole cell, etc., is immobilized onto the surface of an electronic, optic or optoelectronic transducer. When a target analyte, from a complex mixture, is recognized by the immobilized biological material, a biochemical interaction is produced and transformed into a quantifiable signal by means of the transducer.
An immunosensor is a particular type of a biosensor in which the biological component and the target analyte are immunoreagents involved in an immunoassay. The term "immunoassay" refers to and comprises all the analytical procedures based on the specific antigen-antibody recognition. With regards to the immunoreagents, several antigens (free analytes, protein-hapten conjugates) can be involved in the reaction, whereas usually only one antibody takes part in the immunoassay (Montoya et al, 2008).

4.1 Piezoelectric immunosensors for low molecular weight pollutants

An antibody is a protein produced by the immune system of mammals as a natural defence reaction against the exposure to an external agent (an antigen). Antibodies can be obtained in the laboratory in order to be used in immunoassays for analytical purposes. For antibody production against low-molecular weight compunds, these analytes must be chemically modified (haptens), and covalently bound to proteins. Subsequently, the hapten-protein conjugates obtained are used both as antigens for mammal immunization and as assay conjugates in immunoassays.
In the most popular immunoassay configuration one of the immunoreagents (the antigen or the antibody) is immobilized on a solid support. Depending on the immobilized molecule, two main solid-phase immunoassay formats can be defined: the conjugate-coated; and the antibody-coated formats. With low-molecular weight compounds, the conjugate coated format (when the immobilized immunoreagent is the hapten-protein conjugate) must preferably be chosen (Montoya et al, 2008; March et al, 2009). In this type of assay, the detection of the analyte is based on a binding inhibition test and thus a competitive assay is performed; the free analyte competes with the immobilized conjugate for binding to a fixed, limited amount of the antibody. As in any competitive assay, the signal decreases as the analyte concentration increases. This inverse relationship allows us to obtain the typical dose-response curves of a competitive immunoassay.
In QCM piezoelectric immunosensors the transducer is a piezoelectric acoustic device, usually a quartz crystal resonator, although other acoustic sensing technologies are used as mentioned. The most common electrode-configuration of quartz resonators for biosensor applications implements gold electrodes which can be used as the support for immobilization of immunoreagents (antibodies, antigens, or hapten-conjugates), in such a way that a subsequent immunoreaction (antigen-antibody binding) could be detected as a mass variation.

4.1.1 Immunoreagent immobilization

The immobilization of biomolecules on the transducer surface is essential to ensure sensor's performance, playing an important role on the specificity, sensitivity, reproducibility and recycling ability of the immunosensor. As a consequence of that some of the requirements that should be fulfilled by an immobilization process include: (1) retention of biological activity of biomolecules; (2) achievement of reproducible and stable attachment with the

substrate against variations of pH, temperature, ionic strength, and chemical nature of the microenvironment; and (3) uniform, dense, and oriented localization of the biomolecules.
Among all the immobilization methods reported in the literature (Bizet et al., 1998; Su et al., 2000; Tombelli & Mascini, 2000), covalent binding (Pribyl et al., 2003; Prohanka & Skládal, 2005) is the most promising technique because it fulfils most of the requirements mentioned above.
Great effort has been devoted to achieve and optimize the conditions for covalent binding. Self-assembled monolayer (SAM) technology has been providing the best results (Vaughan et al., 1999; Ferreti et al., 2000; Mauriz et al., 2006; Briand et al., 2006). SAM is the generic name given to the methodologies and technologies that allow the generation of monomolecular layers, also called monolayers, of biological molecules on a variety of substrates. This technique allows a reliable control over both the packing density and the environment of an immobilized recognition centre or multiple centres at a substrate surface.
Many organic compounds are adequate to self-assemble: long chain carboxylic acids or alcohols (RCOOH, ROH), where R is an alkyl chain, reacting with metal oxide substrates; organosilane species ($RSiX_3$, R_2SiX_2 or R_3SiX), where X is a chlorine atom or an alkoxy group, reacting with hydroxylated substrates (glass, silicon and aluminium oxide, etc.); and organosulfur-based species reacting with noble metal (gold, silver) surfaces. Up to date, the latest system has been the most widely studied being the best characterized in terms of stability and physicochemical properties. Moreover, sulfur-containing compounds (alkanethiols, dialkyl disulfides and dialkyl sulfides) have a strong affinity for noble metal surfaces as they are spontaneously chemisorbed, with a regular organisation and high thermal, mechanical and chemical stability, on perfectly cleaned gold surfaces (Ferreti et al., 2000). Their adsorption to the surface has been shown to proceed by two methods: by ionic dissociation (10a) and, more favourably, by radical formation (10b) (Vaughan et al., 1999).

$$RSH + Au \rightarrow AuRS^- + H^+ \quad (10a)$$

$$RSH + Au \rightarrow AuRS\cdot + H\cdot \quad (10b)$$

Because of its stability, orientation and ability to functionalize the terminal groups on the molecules, SAMs can offer a very convenient and versatile method for covalent immobilization of biomolecules on gold surfaces for biosensor development. Being in intimate contact with the support surface, SAMs do not have the problems associated with mass transport, thus providing the advantage of a faster and potentially more intense response when exposed to external stimuli (Vaughan et al., 1999; Ferreti et al., 2000).
The covalent binding of a protein to a gold surface by means of SAM formation, basically consists on the following stages: (1) SAM formation with an ethanolic solution of a long chain thiolated acid which is adsorbed onto the gold sensor surface; (2) activation of the terminal carboxylic groups of the thiolated acid, to an intermediate reagent (N-hydroxy-succinimide ester), which takes place by means of an ethanolic or aqueous mixture of N-hydroxi-succinimide (NHS) and carboxi-diimide (EDC); (3) covalent attachment of the active intermediate, thus obtained, to the amine groups of the hapten-protein conjugates; and (4) addition of ethanolamine to deactivate all the unreacted intermediate NHS-esters remaining on the sensor surface. This procedure ensures that only covalently bound analyte

derivatives (hapten-conjugates) remain on the sensor surface (Duan & Meyerhoff, 1995; Disley et al., 1998; Mauriz et al., 2006; Briand et al., 2006; March et al., 2009).
The process described can be done with simple or mixed SAMs. Mixed SAMs are generally formed by co-adsorption of mixtures of two thiols, one of them providing a functional terminal group (like a carboxylic acid, COOH) at a low molar fraction, and the other one being the "diluting" thiol (with, for example, CH_3 or OH terminal groups) at a high molar fraction. The second thiol reduces the surface concentration of functional groups, thus minimizing steric hindrance, partial denaturation of the potential immobilized protein and non-specific interactions that could produce interference signals. Also the diluting thiol can be used to tailor the overall physico-chemical properties of the interface (such as its hydrophobic/hydrophilic character). Consequently, the use of mixed SAMs of alkanethiols (long chain thiols) on gold is particularly recommended in order to minimize steric hindrances, to prevent denaturation, and hence to improve the activity of immobilized proteins (Subramanian & Irudayarj, 2006; Bonroy et al., 2006; Briand et al., 2006, 2007).

4.2 Characterization of a piezoelectric immunosensor

The resonance frequency shift is usually handled as monitoring parameter in piezoelectric immunosensors; however the phase-shift monitoring has been proposed above as a new QCM monitoring parameter for high resolution QCM applications. A comparison between the classical technique based on frequency shift monitoring and the new one based on phase shift monitoring, under the same experimental conditions, is presented next to validate the proposed technique. Only with this purpose, a piezoelectric immunosensor for the detection of the pesticide carbaryl, as a validation model, has been developed.

4.2.1 Experimental set-up and methodology

AT-cut quartz crystals with gold electrodes (10 MHz, International Crystal Manufacturing) were functionalized by immobilizing BSA-CNH carbaryl hapten conjugate on the sensor surface through the formation of a thioctic acid self-assembled monolayer (March et.al.,2009). The crystal was placed in a custom-made flow cell and included in a flow-through setup, controlled by a peristaltic pump (Minipuls 3, Gilson), with the injection loop and solutions at the input of the flow cell exchanged by manual Rheodyne valves (models 5020 and 5011, Supelco). The whole fluidic system was placed inside a custom made thermostatic chamber and all the experiments were performed at 25ºC ±0.1ºC. To avoid unwanted disturbances the chamber was placed on an anti-vibration table. The sensor characterization circuit, shown in the previous section, was connected to the piezoelectric sensor and it was also placed in the thermostatic chamber. A RF signal generator model HP8664A (Hewlet Packard) generated the signal applied to the circuit and the voltage variations related to the phase shift and attenuation were measured with a digital multimeter HP 34401A (Agilent) and sent to a PC via GPIB bus. The experimental set-up is presented in figure 6.
The immunoassay developed to determine carbaryl was an inhibition test based on the conjugate coated format, in which the hapten-conjugate was immobilized on the sensor surface. A fixed amount of the respective monoclonal antibody was mixed with standard solutions of the analyte and pumped over the sensor surface. Since the analyte inhibits antibody binding to the respective immobilized conjugate, increasing concentrations of analyte will reduce the phase shift induced on the piezoelectric sensor and the corresponding demodulated voltage.

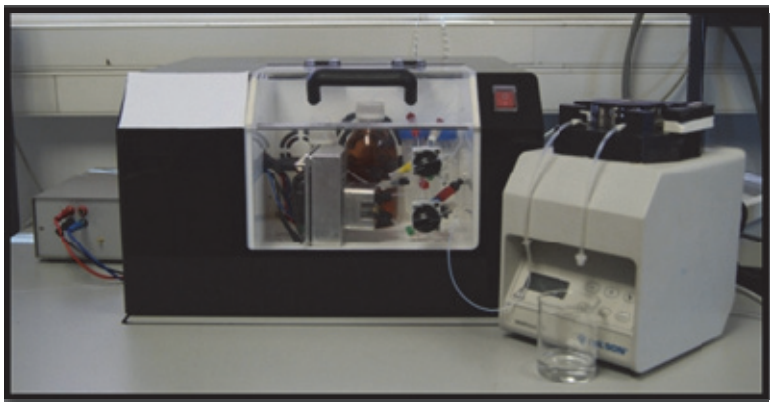

Fig. 6. Experimental set-up

Different standard concentrations of carbaryl were prepared by serial dilutions in PBS, from a 1 mM stock solution in dimetylformamide at -20ºC. The standards were mixed with a fixed concentration of the monoclonal antibody LIB-CNH45 (from I3BH-UPV, Abad et al., 1997) in PBS. Analyte-antibody solutions were incubated for one hour at chamber temperature and then injected onto the sensor surface. The phase-shift was monitored in real-time for each analyte concentration, as the binding between free antibody and the immobilized conjugate took place. For each assay, after stabilization of the initial signal at a flow rate of 30 µL/min for 2 min, the sample (250 µL) was injected for 12 min to measure the immunoreaction. Once each assay was finished, regeneration of the sensing surface was performed using diluted hydrochloric acid, HCl, 0.1M at a flow rate of 280 µL/min for 4 min to break the antibody-hapten linkage. After the regeneration, buffer solution was again flown-through for 2 min at the same flow rate.

4.2.2 Results and discussion

Figure 7 shows the typical real-time signals obtained in the immunoassay developed for the detection of carbaryl with the phase shift concept. As it can be seen on the figure, the typical inverse relationship for a competitive assay is obtained between the phase-shift voltage (ΔV_φ) and the pesticide concentration in the sample. Only a representative part of the signals obtained in the immunoassay, corresponding to concentrations of antibody-analyte of 10, 20, 100 and 500µg/L are shown in Fig. 7.

A representative standard curve (Fig. 8) was finally obtained by averaging three individual standard curves starting from samples that were run at least in duplicate. In Fig. 8 the decrement of the phase voltage has been normalized and represented as a percentage of the maximum decrement obtained ($100x\Delta V_\varphi/\Delta V_{\varphi 0}$, being ΔV_φ the voltage variation of each sample and $\Delta V_{\varphi 0}$ the variation for the zero analyte concentration sample, which provides maximum signal). The experimental points were fitted to a four-parameter logistic equation, then showing the typical decreasing sigmoidal shape of binding inhibition immunoassays.

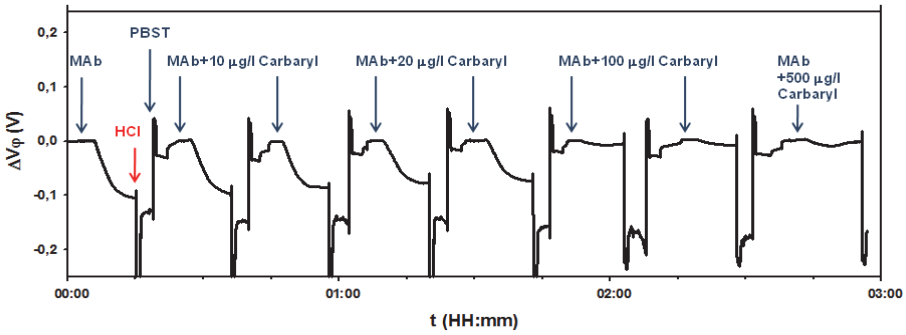

Fig. 7. Real time piezoelectric immunosensor response to different concentrations of analyte

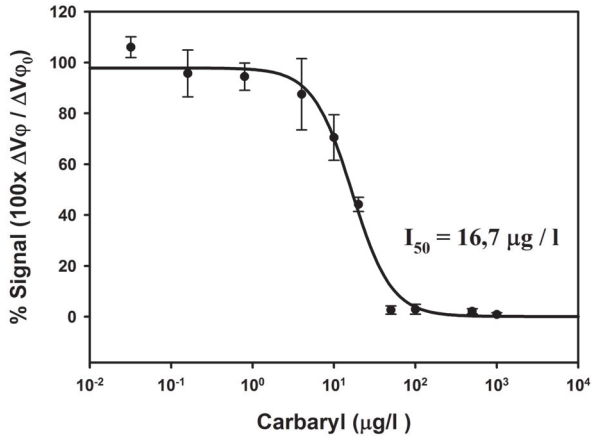

Fig. 8. Average standard curve for the carbaryl piezoelectric immunosensor based on phase-shift characterization method

One of the parameters of interest of the immunosensor, generally accepted as a good approach of the immmunosensor sensitivity, is the I_{50} value. This point is related to the analyte concentration giving 50% inhibition of the maximum signal. In this case, the I_{50} value obtained was 16.7 µg/L. The limit of detection (LOD), another parameter of interest calculated as the pesticide concentration that provides 90% of the maximum signal (I_{90} value) was 4 µg/L. The quantification range, this is, the working range in which the signal inhibition is linear (between 20% and 80% of the maximum), covered concentrations of analyte between 7 and 35 µg/L.

These results were compared with those obtained in the same immunoassay format and conditions for carbaryl detection but using a different characterization circuit (Table 1).

As it can be observed, both the sensitivity and limit of detection of the developed immunosensor were of the same order of magnitude as compared to previously reported results (March et al., 2009; Montagut et al., 2011). These results validate the new characterization concept and the developed interface. An improvement trend of the analytical parameters (I_{50} and LOD), due to the reduction of the noise in the new system, is

	Phase Shift Method	Oscillator (Montagut, 2011)	(March et al, 2009)
Sensitivity I_{50} (µg/L)	16.7	24.0	30.0
L.O.D. I_{90} (µg/L)	4.0	6.5	11.0
Linear Range (µg/L)	7 – 35	11 – 42	15 - 53

Table 1. Comparative results obtained for the QCM immunosensor using different electronic characterization techniques

observed as well. Effectively, the noise level in the oscillator technique was of 2Hz for a maximum signal of 137Hz, while for the phase-shift interface was of 1mV for a maximum signal of 200mV, this indicates an improvement of three times the noise to maximum signal, which could provide a better improvement of the immunosensor sensitivity and limit of detection by optimizing the biochemical parameters, although this is not the main purpose of this work. Moreover, it is important to notice that the improvement trend has been got even with relative low frequency sensors (10MHz), where electronic components and circuits have a very good performance. Recent preliminary results, not shown, using the new concept with high fundamental frequency resonator sensors seem to indicate that a significant improvement, both in sensitivity and limit of detection, could be found with very high fundamental frequency sensors.

5. Conclusions and future lines

The new method for QCM biosensors characterization, based on the monitoring of the phase-shift experimented by a signal of constant frequency in the resonant bandwidth of the sensor, has been validated under real-experimental conditions, and compared with classical interface techniques. An improvement trend, both in sensitivity and limit of detection, is observed, even for relative low frequency resonators (10MHz), due to the signal to noise ratio improvement. Moreover, the new characterization system, particularly useful for biosensor applications, has special advantages which make it ideal for addressing the remaining challenges in high resolution QCM applications: a) the sensor is passively interrogated by an external source, which can be designed with high frequency stability an very low phase noise, even at very high frequencies, b) the sensor circuit can be made very simple with high integration capabilities, and c) sensors working at the same fundamental resonance frequency could be characterized, in principle, with only one source, opening the possibility of working with sensor arrays for multianalysis detection.
Following the results presented here, the next step is to perform experiments with high fundamental frequency BAW resonators based on inverted mesa technology.

6. Acknowledgment

The authors are grateful to the Spanish Ministry of Science and Technology the financial support to this research under contract reference AGL2009-13511, and to the company Advanced Wave Sensors S.L. (www.awsensors.com) for the help provided in the development of some parts of this work.

7. References

Abad, A.; Primo, J. & Montoya, A. (1997). Development of an enzyme-linked immunosorbent assay to carbaryl. 1. Antibody production from several haptens and characterization in different immunoassay formats. *J. Agric. Food Chem*. Vol. 45, pp.1486-1494

Ahmad, N.; Marolt, R.S. (1986). One-step extraction and cleanup procedure for determination of p,p'-DDT, p,p'-DDD, and p,p'-DDE in fish. *J. Assoc. Off. Anal. Chem.* Vol. 69, pp. 581-586

Andrä, J.; Böhling, A.; Gronewold, TMA.; Schlecht, U.; Perpeet, M. & Gutsmann, T. (2008). Surface acoustic wave biosensor as a tool to study the interactions of antimicrobial peptides with phospholipid and lipopolysaccharide model membranes. *Langmuir*, Vol. 24, pp. 9148-9153

Arnau, A.; Ferrari, V.; Soares, D. & Perrot, H. (2008). *Piezoelectric Transducers and Applications*, 2nd ed., ch.5, pp. 117-186, A Arnau ed., ISBN: 978-3-540-77507-2, Ed. Springer Verlag Berlin Heidelberg

Arnau, A.; García, J.V.; Jiménez, Y.; Ferrari, V. & Ferrari, M. (2007). Improved Electronic Interfaces for Heavy Loaded at Cut Quartz Crystal Microbalance Sensors. *Proceedings of Frequency Control Symposium Joint with the 21st European Frequency and Time Forum. IEEE International*, pp. 357-362

Arnau, A.; Montagut, Y.; García, J.V. & Jimenez, Y. (2009). A different point of view on the sensitivity of quartz crystal microbalance sensors. *Meas. Sci. Technol*., Vol. 20, 124004 (11pp.)

Arnau, A.; Sogorb, T. & Jiménez, Y. (2002). Circuit for continuous motional series resonant frequency and motional resistance monitoring of quartz crystal resonators by parallel capacitance compensation. *Rev. Sci. Instrum.,* Vol. 73, No. 7, pp. 2724-2737

Asch, G. et al. (1999) *Les capteurs en instrumentation industrielle*, 5eme édition, Dunod, ISBN 2-1000-4758-2, Paris

Auge, J.; Hauptmann, P.; Eichelbaum. F. & Rösler, S. (1994). Quartz crystal microbalance sensor in liquids. *Sensor and Actuators B*, Vol. 18-19, pp. 518-522

Auge, J.; Hauptmann, P.; Hartmann, J.; Rösler, S. & Lucklum, R. (1995). New design for QCM sensors in liquids. *Sensors and Actuators B*, Vol. 24-25, pp. 43-48

Ballantine, DS.; White, RM.; Martin, SJ.; Ricco, AJ.; Zellers, ET.; Frye, GC. & Wohltjen, H. (1997). *Acoustic Wave Sensors: Theory, Design and Physico-Chemical Applications*. ISBN: 0-12-077460-7, 436 pp. Academic press, San Diego

Barie, N. & Rapp, M. (2001). Covalent bound sensing layers on surface acoustic wave (SAW) biosensors. *Biosens. Bioelectron*., Vol. 16, pp. 979-987

Barnes, C. (1991). Development of quartz crystal-oscillators for under liquid sensing. *Sensors and Actuators A-Physical*, Vol. 29, No. 1, pp. 59-69

Barnes, C. (1992). Some new concepts on factors influencing the operational frequency of liquid- immersed quartz microbalances. *Sensors and Actuators A-Physical*, Vol. 30, No. 3, pp. 197-202

BenDov, I,; Willner, I.; & Zisman, E. (1997). Piezoelectric immunosensors for urine specimens of chlamydia trachomatis employing quartz crystal microbalance microgravimetric analyses. *Anal Chem*, Vol. 69, pp. 3506-3512

Benes, E.; Schmid, M.; Gröschl, M.; Berlinger, P.; Nowotny, H. & Harms, K.C. (1999). Solving the cable problem between crystal sensor and electronics by use of a balanced

bridge oscillator circuit. *Proceedings of the Joint Meeting of the European Frequency and Time Forum and the IEEE International Frequency Control Symposium*, Vol. 2, pp. 1023-1026

Bisoffi, M.; Hjelle, B.; Brown, DC.; Branch, DW.; Edwards, TL.; Brozik, SM.; Bondu-Hawkins, VS. & Larson, RS. (2008). Detection of viral bioagents using a shear horizontal surface acoustic wave biosensor. *Biosens Bioelectron*., Vol. 23, No. 9, pp. 1397-1403

Bizet, K.; Gabrielli, C.; Perrot, H. & Therasse J. (1998). Validation of antibody-based recognition by piezoelectric transducers through electroacoustic admittance analysis. *Biosens. Bioelectron.* ,Vol. 13. No. 3-4, pp. 259-269.

Bjurstrom, J.; Wingqvist, G. & Katardjiev, I. (2006). Synthesis of textured thin piezoelectric AlN films with a nonzero c-axis mean tilt for the fabrication of shear mode resonators. *IEEE Trans. Ultrason. Ferroelectr. Freq. Control*, Vol. 53, No. 11, pp. 2095–2100

Bjurstrom, J.; Wingqvist, G.; Yantchev, V. & Katardjiev, I. (2007). Temperature compensation of liquid FBAR sensors. *Journal of Micromechanics and Microengineering*, Vol. 17, pp. 651–658.

Bonroy, K.; Frederix, F.; Reekmans, G.; Dewolf, E.; De Palma, R.; Borghs, G.; Declerck, P. & Goddeeris, B. (2006). Comparision of random oriented immobilisation of antibody fragments on mixed self-assembled monolayers. *J. Immunol. Methods,* Vol. 312, No. 1-2, pp. 167-181.

Borngräber, R.; Schröder, J.; Lucklum, R. & Hauptmann, P. (2002). Is an oscillator-based measurement adequate in a liquid environment? *IEEE Trans. Ultrason. Ferroelect. Freq. Contr.*, Vol. 49, No. 9, pp. 1254-1259

Branch, DW. & Brozik, SM. (2004). Low-level detection of a Bacillus anthracis simulant using Love-wave biosensors on 36° YX LiTaO3. (2004). *Biosens Bioelectron*., Vol. 19, pp. 849-859

Briand, E.; Salmain, M.; Henry, J.; Perrot, H.; Compère, C. & Pradier C. (2006). Building of an immunosensor: How can the composition and structure of the thiol attachment affect the immunosenor efficiency? *Biosens. Bioelectron.,* Vol. 22, pp. 440-448.

Briand, E.; Salmain, M.; Compère, C. & Pradier C. M. S. (2007). Anti-rabbit immunoglobulin G detection in complex medium by PM-RAIRS and QCM influence of the antibody immobilization method. *Biosens. Bioelectron.,* Vol. 22, pp. 2884-2890.

Byfield, MP. & Abuknesha R.A. (1994). Biochemical aspects of biosensors. *Biosens Bioelectron*, Vol. 9, No. 4-5, pp. 373-400

Chagnard, C.; Gilbert, P.; Watkins, A. N.; Beeler, T. & Paul, D.W. (1996). An electronic oscillator with automatic gain control: EQCM applications. *Sensors and Actuators B*, Vol. 32, pp.129-136

Coté, L. ; Lec, R. M. & Pishko, M. V. (2003). Emerging Biomedical Sensing Technologies and Their Applications. *IEEE Sensors Journal*. Vol. 3, pp. 251-265, ISSN 1530-437X/03

De Kok, A.; Hiemstra, M.; Brinkman, U. A. T. (1992). Low ng/l level determination of twenty N-methylcarbamate pesticides via SPE and HPLC, *J. Chromatogr*. Vol. 623, pp. 265 276

Disley, D.M.; Cullen, D.C.; You, H.X. & Lowe, C.R. (1998). Covalent coupling of immunoglobulin G to self-assembled monolayers as method for immobilizing the

interfacial-recognition layer of a surface plasmon resonance immunosensor. *Biosens. Bioelectron.,* Vol. 13, No. 11, pp. 1213-1225.

Doerner, S.; Schneider, T.; Schröder, J. & Hauptmann, P. (2003). Universal impedance spectrum analyzer for sensor applications. *Proceedings of IEEE Sensors*, pp. 596-594

Dress, D.M., Shanks, H.R.; Van Deusen, R.A. & Landin, A.R. (1999). *Method and system for detecting material using piezoelectric resonators.* US Patent 5932953

Duan, Ch. & Meyerhoff, M.E. (1995). Immobilization of proteins on gold coated porous membranes via activated self-assembled monolayer of thioctic acid. *Mikrochim. Acta,* Vol. 117, No. 3-4, pp. 195-206.

Ehahoun, H.; Gabrielli, C.; Keddam, M.; Perrot, H. & Rousseau, P. (2002). Performances and limits of a parallel oscillator for electrochemical quartz crystal microbalances. *Anal Chem.,* Vol. 74, pp. 1119-1127

Eichelbaum, F.; Borngräber, R.; Schröder, J.; Lucklum, R. & Hauptmann, P. (1999). Interface circuits for quartz crystal microbalance sensors. *Rev. Sci. Instrum*., Vol. 70, pp. 2537-2545

Ferrari, V.; Marioli, D. & Taroni, A. (2001). Improving the accuracy and operating range of quartz microbalance sensors by purposely designed oscillator circuit. *IEEE Trans. Instrum. Meas.*, Vol. 50, pp. 1119-1122

Ferrari, M.; Ferrari, V.; Marioli, D.; Taroni, A.; Suman, M. & Dalcanale, E. (2006). In-liquid sensing of chemical compounds by QCM sensors coupled with high-accuracy ACC oscillator. *IEEE Trans. Instrum. Meas*., Vol. 55, No. 3, pp. 828-834

Ferrari, V. & Lucklum, R. (2008) *Piezoelectric Transducers and Applications* 2nd ed., ch.2, pp. 39-62, A Arnau ed., ISBN: 978-3-540-77507-2, Ed. Springer Verlag Berlin Heidelberg

Ferreti, S.; Paynter, S.; Russell, D.A.; Sapsford, K.E. & Richardson, D.J. (2000). Self-assembled monolayers: a versatile tool for the formulation of bio-surfaces. *Trends in Anal.Chem.,* Vol. 19, No. 9, pp. 530-540.

Francis, LA.; Friedt, J-M.; De Palma, R.; Zhou, C.; Bartic, C.; Campitelli, A. & Bertrand, P. (2004). Techniques to evaluate the mass sensitivity of Love mode surface acoustic wave biosensors. Frequency Control Symposium and Exposition, 2004. *Proceedings of the 2004 IEEE International* pp.241-249

Francis, LA.; Friedt, J-M. & Bertrand, P. (2005). Influence of electromagnetic interferences on the mass sensitivity of Love mode surface acoustic wave sensors. *Sensors and Actuators A*, Vol. 123-124, pp. 360-369

Francis, LA. (2006). *Thin film acoustic waveguides and resonators for gravimetric sensing applications in liquid*. PhD Thesis. Université Catholique de Louvain.

Fu, Y.Q.; Luo, J.K.; Du, X.Y.; Flewitt, A.J.; Li, Y.; Markx, G.H.; Walton, A.J. & Milne, W.I. (2010) Recent developments on ZnO films for acoustic wave based bio-sensing and microfluidic applications: a review. *Sensors and Actuators B*, Vol. 143, pp. 606–619

Fung, YS. & Wong, YY. (2001). Self-assembled monolayers as the coating in a quartz piezoelectric crystal immunosensor to detect Salmonella in aqueous solution. *Anal Chem*, Vol. 73, pp. 5302-5309

Furtado, LM.; Su, HB.; Thompson, M.; Mack, DP. & Hayward, GL. (1999). Interactions of HIV-1 TAR RNA with Tat-derived peptides discriminated by on-line acoustic wave detector. *Anal Chem,* Vol. 71, pp. 1167-1175

Gabl, R.; Feucht, H.D.; Zeininger, H.; Eckstein, G.; Schreiter, M.; Primig, R.; Pitzer, D. & Wersing, W. (2004). First results on label-free detection of DNA and protein

molecules using a novel integrated sensor technology based on gravimetric detection principles. *Biosens. Bioelectron*, Vol. 19, No. 6, pp. 615–620

Gabl, R.; Schreiter, M.; Green, E.; Feucht, H.-D.; Zeininger, H.; Runck, J.; Reichl, W.; Primig, R. ; Pitzer, D.; Eckstein, G. & Wersing, W. (2003) Novel integrated FBAR sensors: a universal technology platform for bio-and gas-detection *Proc. IEEE Sensors*, Toronto,Canada, Vol. 2, pp. 1184-1188

Gronewold, T.M.A. (2007) Surface acoustic wave sensors in the bioanalytical field: Recent trends and challenges. *Analytica Chimica Acta*, Vol. 603, No. 2, pp. 119-128

Harding, GL. (2001). Mass sensitivity of Love-mode acoustic sensors incorporating silicon dioxide and silicon-oxy-fluoride guiding layers. *Sensors and Actuators A*, Vol. 88, pp. 20-28

Hawkins, E.; Cooper, M. & Campbell, I. (2006). Acoustic detection technology in the analysis of biomolecular interactions. *Innovations in Pharmaceutical Technology*, Vol. 21, pp. 30-34

Hengerer, A.; Kosslinger, C.; Decker, J.; Hauck, S.; Queitsch, I.; Wolf, H. & Dubel, S. (1999). Determination of phage antibody affinities to antigen by a microbalance sensor system. *Biotechniques,* Vol. 26, pp. 956-960

Hook F, Ray A, Norden B, and Kasemo B (2001). Characterization of PNA and DNA immobilization and subsequent hybridization with DNA using acoustic-shear-wave attenuation measurements. *Langmuir*, 17, 8305-8312

Howe, E. & Harding, G. (2000). A comparison of protocols for the optimisation of detection of bacteria using a surface acoustic wave (SAW) biosensor. *Biosens Bioelectron*., Vol. 15, No. 11-12, pp. 641-649

Jacoby, B. & Vellekoop, M. (1997). Properties of Love waves: applications in sensors. *Smart Materials and Structures*, Vol. 6, No. 6, pp.668–679

Jakoby, B.; Art, G. & Bastemeijer, J. (2005). A novel analog readout electronics for microacoustic thickness shear-mode sensors. *IEEE Sensors Journal*, Vol. 5, pp. 1106-1111

Janshoff, A.; Galla, H.-J. & Steinem, C. (2000). Piezoelectric mass-sensing devices as biosensors - an alternative to optical biosensors?, *Angew. Chem. Int. Ed*., Vol. 39, pp. 4004-4032

Jiménez, Y.; Fernández, R.; Torres, R.; Arnau, A.; Otero, M. & Calvo, E. (2006). Viscoelastic characterization of electrochemically prepared conducting polymer films by impedance analysis at quartz crystal. Study of the surface roughness effect on the effective values of the viscoelastic properties of the coating. *Journal of Electroanalytical Chemistry*, Vol 153, No. 7, pp 455-466

Jiménez, Y.; Otero, M. & Arnau, A. (2008) *Piezoelectric Transducers and Applications* 2nd ed., Ch 14, pp. 331-398, A Arnau ed., ISBN: 978-3-540-77507-2, Ed. Springer Verlag Berlin Heidelberg

Josse, F.; Bender, F. & Cernosek, R.W. (2001). Guided Shear Horizontal Surface Acoustic Wave Sensors for Chemical and Biochemical Detection in Liquids. *Anal. Chem*., Vol. 73, pp. 5937-5944

Kalantar-Zadeh, K.; Wlodarski, W.; Chen, Y. Y.; Fry, B. N. & Galatsis, K. (2003). Novel Love mode surface acoustic wave based immunosensors. *Sens. Actuators B*, Vol. 91, pp. 143-147.

Kanazawa, K.K. & Gordon II, J.G. (1985). The oscillation frequency of a quartz resonator in contact with a liquid. *Analytica Chimica Acta*, Vol. 175, pp. 99-105

Kankare J. (2002). Sauerbrey equation of quartz crystal microbalance in liquid medium. *Langmuir*, Vol. 18, pp. 7092-7094

Länge, K.; Rapp, BE. & Rapp, M. (2008). Surface acoustic wave biosensors: a review *Anal Bioanal Chem,* Vol. 391, No. 5, pp. 1509-1519

Lec, R. M. (2001) Piezoelectric Biosensors: Recent Advances and Applications. *Frequency Control Symposium and PDA Exhibition, 2001. Proceedings of the 2001 IEEE International* , ISBN: 0-7803-7028-7, pp. 419-429, Seattle, WA, USA, 06 jun 2001

Lin, Z.; Yip, C. M.; Joseph, I. S. & Ward M. D. (1993). Operation of an Ultrasensitive 30 MHz Quartz Crystal Microbalance in Liquids. *Anal. Chem*, Vol. 65, pp. 1546-1551

Lindner, G. (2008). Sensors and actuators based on surface acoustic waves propagating along solid–liquid interfaces. *Journal of Physics D: Applied Physics,* Vol. 41, No. 12, 123002

March, C.; Manclús, J. J.; Jiménez, Y.; Arnau, A. & Montoya, A. (2009). A piezoelectric immunosensor for the determination of pesticide residues and metabolites in fruit juices. *Talanta ,* Vol. 78, No. 3, pp. 827-833

Martin, S.J.; Granstaff, V.E. & Frye, G.C. (1991). Characterization of quartz crystal microbalance with simultaneous mass and liquid loading. *Anal. Chem*., Vol. 63, pp. 2272-2281

Martin, S.J.; Spates, J. J.; Wessendorf, K. O.; Schneider, T. W. & Huber, R. J. (1997). Resonator/oscillator response to liquid loading. *Anal. Chem*., Vol. 69, pp. 2050-2054

Marty, J.L.; Leca, B. & Noguer, T. (1998). Biosensors for the detection of pesticides. *Analusis Magazine*, Vol. 26, No. 6, pp. M144-M149

Mauriz, E.; Calle, A.; Abad, A.; Montoya, A.; Hildebrandt, A.; Barceló, D. & Lechuga, L.M. (2006). Determination of carbaryl in natural water samples by a surface plasmon resonance flow-through immunosensors. *Biosens. Bioelectron.,* Vol. 21, No. 11, pp. 2129-2136.

Mchale, G. (2003). Generalized concept of SH-APM and Love wave sensors. *Meas. Sci. Technol*., Vol. 14, No. 11, pp. 1847-1853

Moll, N.; Pascal, E.; Dinh, DH.; Pillot. JP.; Bennetau, B.; Rebiere, D.; Moynet, D.; Mas, Y.; Mossalayi, D.; Pistre, J. & Dejous, C. (2007). A Love wave immunosensor for whole E. coli bacteria detection using an innovative two-step immobilisation approach. *Biosens Bioelectron*., Vol. 22, No. 9-10, pp. 2145-2150

Moll, N.; Pascal, E.; Dinh, DH.; Lachaud, J-L.; Vellutini, L.; Pillot, J-P.; Rebière, D.; Moynet, D.; Pistré, J.; Mossalayi, D.; Mas, Y.; Bennetau, B. & Déjous, C. (2008). Multipurpose Love acoustic wave immunosensor for bacteria, virus or proteins detection. *ITBM-RBM*, Vol. 29, pp. 155-161

Montagut, Y.J. (2011). *Improved oscillator system for QCM applications in-liquid media and a proposal for a new characterization method for piezoelectric biosensors characterization*. Doctoral Thesis. Universitat Politècnica de Valéncia

Montoya, A.; Ocampo, A. & March, C. (2008) *Piezoelectric Transducers and Applications* 2nd ed., Ch 12, pp. 289-306, A Arnau ed., ISBN: 978-3-540-77507-2, Ed. Springer Verlag Berlin Heidelberg

Nirschl, M.; Blüher, A.; Erler, C.; Katzschner, B.; Vikholm-Lundin, I.; Auer, S; Vörös, J.; Pompe, W; Schreiter, M. & Mertig, M. (2009). Film bulk acoustic resonators for

DNA and protein detection and investigation of in-vitro bacterial S-layer formation. *Sens. Actuators A*, Vol. 156, pp. 180-184

Ogi, H.; Nagai, H.; Fukunishi, Y.; Hirao, M. & Nishiyama, M. (2009). 170MHz electrodeless quartz crystal microbalance biosensor: capability and limitation of higher frequency measurement. *Analytical Chemistry*, Vol. 81, pp. 8068-8073

Paul, D.W. & Beeler, T.L. (1998). Piezoelectric sensor Q-loss compensation. US Patent No. 4788466

Pax, M.; Rieger, J.; Eibl, R. H.; Thielemann, C. & Johannsmann, D. (2005). Measurements of fast fluctuations of viscoelastic properties with the quartz crystal microbalance. *Analyst,* Vol. 130, pp. 1474-1477

Pribyl, J.; Hepel, M.; Halámek, J. & Skládal, P. (2003). Development of piezoelectric immunosensor for competitive and direct determination of atrazine. *Sensors and Actuators B,* Vol. 91, pp. 333-341.

Prohanka, M. & Skládal, P. (2005). Piezoelectric immunosensor for francisella tularensis detection using immunoglobulin m in a limited dilution. *Anal. Lett.,* Vol. 38, No. 3, pp. 411-422.

Rabe, J.; Büttgenbach, S.; Zimmermann, B. & Hauptmann, P. (2000). Design, manufacturing, and characterization of high-frequency thickness-shear mode resonators. *2000 IEEE/EIA International Frequency Control Symposium and Exhibition*, ISBN: 0-7803-5838-4, pp.106-112.

Richert, L.; Lavalle, P.; Vaultier D, Senger, B.; Stoltz, F.; Schaaf, P.; Voegel, J.C. & Picart, C. (2002). Cell interactions with polyelectrolyte multilayer films *Biomacromolecules*, Vol. 3, pp. 1170-1178

Riesch, C. & Jakoby, B. (2007). Novel Readout Electronics for Thickness Shear-Mode Liquid Sensors Compensating for Spurious Conductivity and Capacitances. *IEEE Sensors Journal*, Vol. 7, No. 3, pp. 464-469

Rocha-Gaso, MI.; March-Iborra, C.; Montoya-Baides, A. & Arnau-Vives, A. (2009) Surface Generated Acoustic Wave Biosensors for the Detection of Pathogen Agents: A review. *Sensors*, Vol. 9, pp. 5740-5769

Rodahl, M. & Kasemo, B. (1996). A simple setup to simultaneously measure the resonant frequency and the absolute dissipation factor of a quartz crystal microbalance. *Rev. Sci. Instrum.,* Vol. 67, pp. 3238-3241

Rodríguez-Pardo, L.; Fariña, J.; Gabrielli, C. ; Perrot, H. & Brendel, R. (2004). Resolution in quartz oscillator circuits for high sensitivity microbalance sensors in damping media. *Sensors and Actuators B*, Vol. 103, pp. 318-324

Rodríguez-Pardo, L.; Fariña, J.; Gabrielli, C.; Perrot, H. & Brendel, R. (2006). Quartz crystal oscillator circuit for high resolution microgravimetric sensors. *Electronics Letters*, Vol. 42, No. 18, pp. 1065-1067

Sagmeister, B.P.; Graz, I.M.; Schwödiauer, R.; Gruber, H. & Bauer, S. (2009). User-friendly, miniature biosensor flow cell for fragile high fundamental frequency quartz crystal resonators. *Biosensor and Bioelectronics*, Vol. 24, pp. 2643-2648

Sauerbrey, G. (1959). Verwendung von schwingquarzen zur wägung dünner schichten und zur mikrowägung. *Zeitschrift Fuer Physik*, Vol. 155, No. 2, pp. 206-222

Schröder, J.; Borngräber, R.; Lucklum, R. & Hauptmann, P. (2001). Network analysis based interface electronics for quartz crystal microbalance. *Review Scientific Instruments*, Vol. 72, No. 6, pp. 2750-2755

Stobiecka, M.; Jarosław, M.; Janowska, B.; Tudek, B. & Radecka, H. (2007). Piezoelectric Sensor for Determination of Genetically Modified Soybean Roundup Ready in Samples not Amplified by PCR. *Sensors*, Vol. 7, pp. 1462-1479

Su, X.; Li, S. F. Y.; Liu, W. & Kwang, J. (2000). Piezoelectric quartz crystal based screening test for porcine reproductive and respiratory syndrome virus infection in pigs. *Analyst*, Vol. 125, pp. 725-730

Subramanian, A. & Irudayaraj, J. (2006). A mixed self-assembled monolayer-based surface plasmon immunosensor for the detection of E. coli O157:H7. *Biosens. Bioelectron.,*Vol. 21, No. 7, pp. 998-1006.

Tamarin, O.; Comeau, S.; Déjous, C.; Moynet, D.; Rebière, D.; Bezian, J. & Pistré, J. (2003). Real time device for biosensing: design of a bacteriophage model using love acoustic wave *Biosens Bioelectron*., Vol. 18, pp. 755-763

Tatsuma, T.; Watanabe, Y.; Oyama, N.; Kitakizaki, K. & Haba, M. (1999). Multichannel Quartz Crystal Microbalance. *Anal. Chem*., Vol. 71, pp. 3632-3636

Tombelli, S. & Mascini, M. (2000). Piezoelectric quartz crystal biosensors: recent immobilization schemes. *Anal. Letters,* Vol. 33, No. 11, pp. 2129-2151.

Uttenthaler, E.; Schräml, M.; Mandel, J. & Drost, S. (2001). Ultrasensitive quartz microbalance sensors for detection of M13-Phages in liquids. *Biosensors & Bioelectronics*, Vol. 16, pp. 735-743

Vale, C.; Rosenbaum, J.; Horwitz, S.; Krishnaswamy, S. & Moore, R. (1990) FBAR filters at GHz frequencies. *Procceding of the 44th Annual Symposium on Frequency Control.* pp. 332-336, Baltimore, MD, USA, 23 May 1990

Vaughan, R.D.; O'Sullivan, C.K. & Guibault, G.G. (1999). Sulfur-based self assembled monolayers (SAM`s) on piezoelectric crystals for immunosensors development. *Fresenius J. Anal. Chem.,* Vol. 364, pp. 54-57.

Voinova, M. V.; Johnson, M. & Kasemo, B. (2002). Missing mass effect in biosensor's QCM applications. *Biosensors and Bioelectronics* Vol. 17, pp. 835-841

Wang, Z.; Cheeke, JDN. & Jen, CK. (1994). Sensitivity analysis for Love mode acoustic gravimetric sensors. *Applied Physics Letter*, Vol. 64, pp. 2940-2942

Weber, J.; Albers, W.M.; Tuppurainen, J.; Link, M.; Gabl, R.; Wersing, W. & Schreiter, M. (2006). Shear mode FBARs as highly sensitive liquid biosensors, *Sensors Actuat. A: Phys*, Vol. 128, No. 1, pp. 84–88

Wessendorf, K.O. (1993). The lever oscillator for use in high resistance resonator applications. *Proceedings of the 1993 IEEE International Frequency Control Symposium*, pp. 711-717

Wessendorf, K.O. (2001). The active-bridge oscillator for use with liquid loaded QCM sensors. *Proceedings of IEEE International Frequency Control Symposium and PDA Exhibition*, pp. 400-407

Wingqvist, G.; Anderson, H.; Lennartsson, C.; Weissbach, T.; Yanchtev, V. & Lloyd Spetz, A. (2009) On the applicability of high frequency acoustic shear mode biosensing in view of thickness limitations set by the film resonance. *Biosens. Bioelectron*., Vol. 24, pp. 3387-3390

Wingqvist, G.; Bjurstrom, J.; Liljeholm, L.; Yantchev, V. & Katardjiev, I. (2007). Shear mode AlN thin film electro-acoustic resonant sensor operation in viscous media. *Sensors and Actuators B: Chemical*, Vol. 123, No. 1, pp. 466–473

Wingqvist, G.; Yantchev, V. & Katardjiev, I. (2008). Mass sensitivity of multilayer thin film resonant BAW sensors. *Sensors Actuat. A: Phys*, Vol. 148, No. 1, pp. 88–95

Zhou, XD.; Liu, LJ. & Hu, M. ; Wang, L. & Hu, J. (2002). Detection of hepatitis B virus by piezoelectric biosensor. *Jounal of Pharmaceutical and Biomedical Analysis*, Vol. 27, No.1-2, pp. 341-345

Zimmermann, B.; Lucklum, R. & Hauptmann, P. (2001). Electrical characterization of high-frequency thickness-shear-mode resonators by impedance analysis. *Sensors and Actuators B*, Vol. 76, pp.47-57

10

Electrodeposition of Insulating Thin Film Polymers from Aliphatic Monomers as Transducers for Biosensor Applications

Guillaume Herlem and Tijani Gharbi
Institute FEMTO-ST/Department of Optic, UMR CNRS 6174,
University of Franche-Comte
France

1. Introduction

Molecules can be oxidized anodically or reduced cathodically depending on their chemical functions but only some of them can be electropolymerized. The electropolymerization process of organic molecules leading to conductive, semiconducting or insulating polymer takes place at the surface of a biased electrode. In this case, a modification of an electrode surface, that can be a semiconductor or a conductive one, occurs in an irreversible way.
Electrodes coated with conducting polymer films, have attracted considerable interest in the last two decades. A multitude of reviews and monographs have been written on the subject (Adhikari et al., 2004). Many electrochemical works were performed with aromatic or conjugated compounds yielding insulating polymer too. But few studies were made up to now with aliphatic molecules concerning their electropolymerization behavior. One of the reasons comes from the problem to study thin film which requires characterizations with expansive and not widespread spectroscopic analysis methods such as x-ray photoelectron spectroscopy and AFM imaging for instance. Furthermore, thin coatings at the electrode surface which could occur during a reaction, were neglected for a long time and regarded as a baneful interference hushing a possible insulating polymer up.
Electropolymerized thin film polymers possess a wide range of applications in electroanalysis (Kalimuthu et al., 2009), energy storage (Granqvist, 2007), electrocatalysis (Xiao et al., 2009), biosensing (Merkoci, 2009), corrosion protection (Medrano-Vaca et al., 2008), sensors and electronic devices (Liu et al., 2010), electrochromic displays (Reiter et al., 2009), etc. Although polymer films on a surface can be formed in several chemical ways, electropolymerization is one of the most convenient and advantageous especially the thickness control during the film growth.
On one hand, poly(thiophene), poly(pyrrole), poly(aniline) and their derivatives are amongst the most widely studied conducting polymers. This is probably due to the high conductivities of their oxidized forms and their ability to reversibly switch between conducting and insulating states by doping and undoping. On the other hand, insulating polymers have not paid so much attraction. Their electrochemical growth on an electrode surface is limited to thin film especially for aliphatic molecules due to the resulting current drop. If their thickness does not reach more than tens of nanometers, the surface electrode is

modified durably and uniformly. But advantageous properties such as biocompatibility or proton affinity for these polymers compared to previous ones will be of prime importance for sensor and biosensor applications.
Consequently, the aim of this chapter is to draw up recent research studies concerning the electrochemistry of aliphatic molecules leading to thin film polymer coatings. These thin film are of interest in sensor and biosensor developments as we can see further.

2. Electrochemistry of bi-functional aliphatic molecules

The origin of the work concerning the electropolymerization of aliphatic bifunctional molecule comes back to the study of simple ω-amines which are known to form aminates (analog to hydrates' name) which are highly conductive electrolytes (Herlem et al. 2000). Despite the potential window of primary amines (about 3.5 V on platinum electrode), ethylenediamine (EDA) shown abnormal electrochemical behavior when biased anodically. In this case the electrode passivation occurs. This is the reason why we studied amine compounds with great interest. In addition, some combinations have been made with different functional groups as shown of the Figure 1.

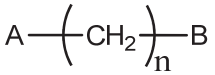

H_2N-	-NH_2
HS-	-SH
H_2N-	-COOH
H_2N-	-$OSi(OC_2H_5)_3$

Fig. 1. Bifunctional molecule with a combination of groups A and B leading to electrodeposition.

The choice of the functional groups depicted Figure 1 was done in the light of some observations made concerning substituted ω-amines. This is also an attempt to generalize the particular electrochemical behavior of some bifunctional aliphatic molecules which can be electropolimerized.
In a first part, a description of the electrochemistry of ω-amine based electrolytes will be given, followed with the electrochemical behavior of ethanedithiol. Then, in a third part, we will discuss on the electrochemistry of concentrated glycine based electrolytes. At last, we will see in which conditions the electrodeposition of 3-aminopropyltriethoxy silane occurs.

2.1 Anodic oxidation of primary di and tri amines

It was pointed out previously that the passivation of electrodes such as smooth platinum and gold, titanium and glassy carbon occurs during the anodic oxidation of an electrolyte composed with one salt dissolved in one pure di or tri amine. The originality resides here in the use of the solvent which is also the monomer. No co-solvent has to be added in the electrolyte because of the good solubility of salts and the excellent conductivities reached. The electrode passivation only occurs with unsubstituted primary di and tri amines H_2N-(CH_2)n-NH_2 where primary amino groups are at the two ends of the alkyl chain (Herlem et al., 1999). The method of choice underlying this phenomenon is the electrochemical quartz

crystal microbalance (EQCM) technique coupled to cyclic voltammetry measurement (Figure 2):

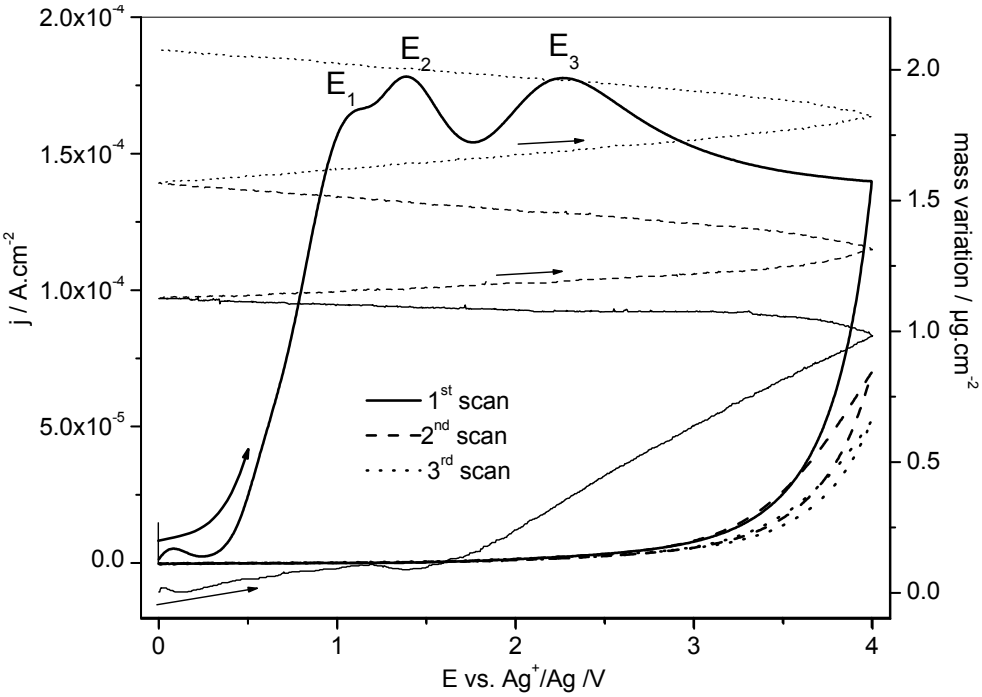

Fig. 2. Mass variation coupled to cyclic voltammetry of 1,3-DAP charged with KPF6 0.1 M on 5 MHz Au quartz coated electrode (scan rate: 20mV/s, counter-electrode: Pt, reference electrode: Ag wire).

During the first scan, as soon as the anodic peak E2 at +1.4 V is reached, the mass increases at the electrode surface as shown Figure 2. This is the case for 1,3-diaminopropane (1,3-DAP) based electrolytes and observed experimentally for EDA and diethylenetriamine (DETA) based electrolytes too. Beyond 3V, there is a plateau where the current is constant. At the second scan (and also for the next ones) there is a drastic drop of current density. All the peaks have disappeared but the mass deposition still increases. The broadness of the peaks on the voltammograms (E1=1.1 V, E2= 1.4 V, E3= 2.2 V vs. Ag^+/Ag for 1,3-DAP) are characteristic of the electrochemical behavior of primary amines. Notice that for 1,4-diaminobutane and other diamines with increasing alkyl length chain between the two amino groups, the melting points are decreased drastically.

The electropolymerization process of primary di or tri amines is possible on different metallic or semiconducting electrodes such as smooth gold, smooth platinum, glassy carbon, p or n-type silicon, Fluorine Tin Oxide (FTO). It does not happen with Iron or Copper electrodes for instance. Copper and silver cations are known to be remarkably chelated by EDA and consequently the corresponding metals are oxidized anodically at a lower potential than those of EDA or DETA. From the HSAB principle from Parr and Pearson, metallic copper electrode cannot be used as working electrode in amine based electrolytes

because of its cationic hardness which is very close to that of the amine giving a reaction between the two species (Table 1).

	Cu+	Ag^+	Pt^{2+}	Pt	EDA	1,3-DAP	DETA
η (eV)	6.3	7	8.0	3.5	6.2	6.3	6

Table 1. Chemical hardnesses of Pt and some metallic ions and amines calculated at the Hartree-Fock level of theory using 6-31G basis sets.

On the other hand, the hardness value of Pt^{2+} means that Pt will not be ionized anodically and complexed by the amines having lower hardness value. This is one of the reasons why noble metals like Pt are used in the electrochemistry of amines for example.
Two parameters have to be taken into accounts that prevent the electropolymerization of the primary di or triamines during their anodic oxidation. First, amines based electrolytes must be anhydrous. Addition of water in these media dramatically modify the voltammograms by generating an anodic wall, instead of the plateau observed previously, that appears at a lower potential particularly as the water concentration increases (Figure 3).

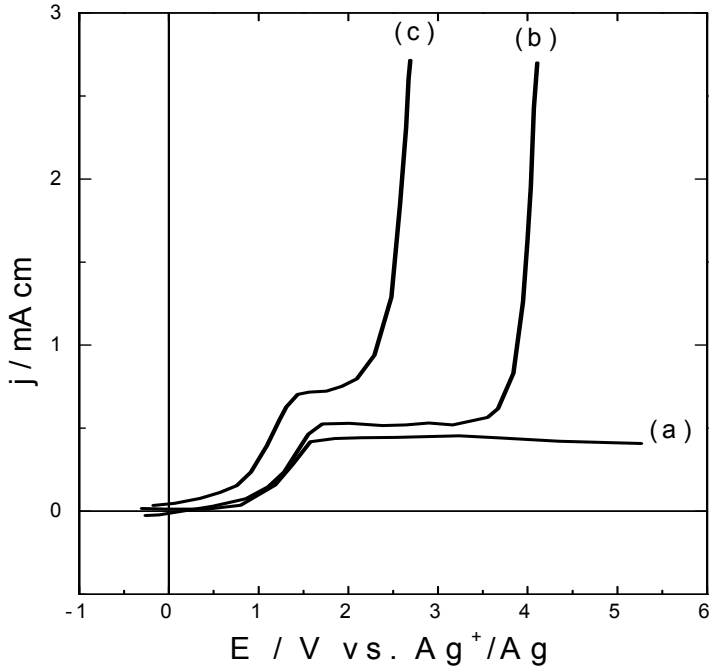

Fig. 3. Electrochemical behavior (reverse scans are not presented) of a smooth Pt electrode in pure EDA vs. Ag+/Ag, as a function of increasing quantity of water (supporting electrolyte: LiSO2CF3 0.1 M; Scan rate 10mVs-1).(a) : 0 % of water. (b) : 17 % of water. (c) : 29 % of water.

Secondly, the anodic oxidation takes place only with primary amines and the vicinal carbon does not have to be substituted. The resulting thin films are insoluble in various solvents as cold water, acetone, propylene carbonate, ethanol, ω-alkylamine, etc, modifying durably the electrochemical behavior of the electrode.

Spectroscopic analysis such as FT-IR (Fourier Transform-Infrared), IRAS (Internal Absorption), IR-ATR (Attenuated Total Reflection), Raman and XPS (X-Ray Photoelectron spectroscopy) revealed the polymeric structure of the thin film coating during the anodic oxidation of an ω-alkylamine. For instance, ethylenediamine leads to linear polyethylenimine (L-PEI) while 1,3-DAP gives linear polypropylenimine (L-PPI). DETA, which is the dimer of EDA, induces L-PEI too.
IR-ATR spectra from electropolymerized and from organic synthesized L-PEI (and L-PPI) fit in good agreement each other's (Saegusa et al., 1972), (Biçak et al., 1998), (). ν(NH): 3200-3400 cm^{-1}, ν(CH_2): 2800-2950 cm^{-1}, ν(NH): 1450-1600 cm^{-1}, δ(CH): 1300-1450 cm^{-1}, ν(C-NH-C): 1050-1150 cm^{-1}. Wavelength number values can fluctuate because of the mass weight variations of the polymers depending on the experimental conditions in particular the bias time.
Raman spectroscopy discarded, from the mechanism, a possible formation of substituted hydrazine(s) due to the doubling of the radical formed after the loss of a proton and an electron.
XPS spectra of L-PEI coating from EDA electropolymerization match well those already published (Beamson et al., 1992). C1s and N1s peaks at BE = 285.7 eV and 399.7 eV respectively corresponds to the C-N bond in –CH_2-CH_2-N– pattern. XPS confirms also the presence of –C=N– and –C=O bonds in a small extent located at the surface electrode.
Spectroscopic results from the electropolymerized polyalkylenimine can be compared to those synthesized via organic chemistry. Linear polyethyleneimine (L-PEI) was first synthesized by chemical route in 1970 by Dick (Dick et al., 1970). L-PEI can be obtained by the cationic polymerization of 2-substituted-2-oxazolines or by aqueous polymerization of aziridine (Gembitskii et al., 1978) but the electrochemical synthesis is far less complicated than the organic one.
In the light of ab initio calculations, the probable mechanism for the anodic oxidation of EDA described elsewhere (Lakard et al., 2002) is essentially as shown in Figure 4. The reaction, based on studies by Mann and others (Mann et al., (1970), consists of the monomer adsorption on the electrode surface in the two first steps. In a third step there is the monomer oxidation with a departure of one electron followed, in a fourth step, by the cleavage of the C-N bond. The fifth step is the attack of another ω-amines by the former primary carbocation. The following steps are the expulsion of the proton from the protonated amine, a loss of one electron like in step 3 and then the breaking of the C-N bond like in step 4. Step 5 can goes on to give the chain growth.

2.2 Anodic oxidation of ethanedithiol

According to Figure 1, another interesting bifunctional molecule is 1,2-ethanedithiol (EDT) (Lakard et al., 2008). Its electrochemical behavior was studied by mean of cyclic voltammetry in anodic oxidation. Although EDT is liquid at ambient temperature, conducting salts are insoluble and EDT was dissolved in a co-solvent. In acetonitrile Figure 5 a typical cyclic voltammogram shows two peaks at 1.79 V and 2.16 V versus Ag^+/Ag, but only during the first scan. During additional scans, the oxidation peaks are less pronounced but the anodic peaks remains nearly the same from one scan to other. These observations underline that EDT is oxidized under anodic potentials leading to the electrode passivation.
Electrochemical Quartz Crystal Microbalance experiment performed on a Pt coated quartz shows Figure 6 that it is not necessary to scan out to a potential greater than 3 V vs. Ag+/Ag since the film grows after the second oxidation peak.

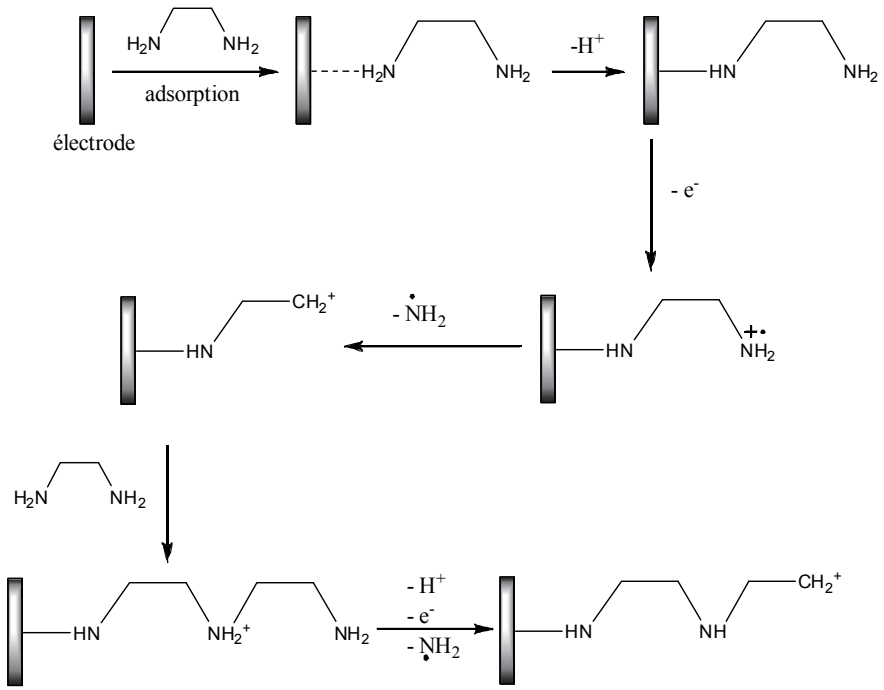

Fig. 4. Anodic oxidation mechanism of EDA

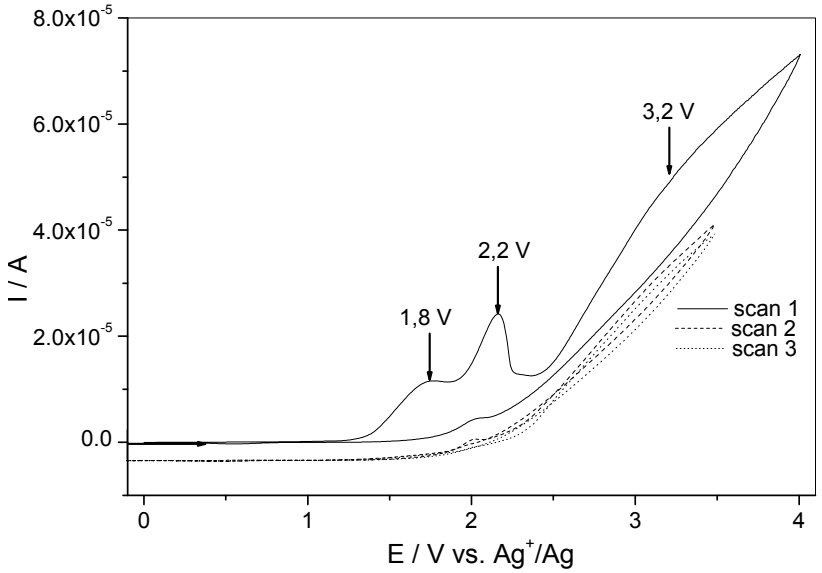

Fig. 5. Cyclic voltammogram of EDT 2.34M charged with LiTFSI 1 mM in acetonitrile on Pt. Scan rate: 20 mV/s.

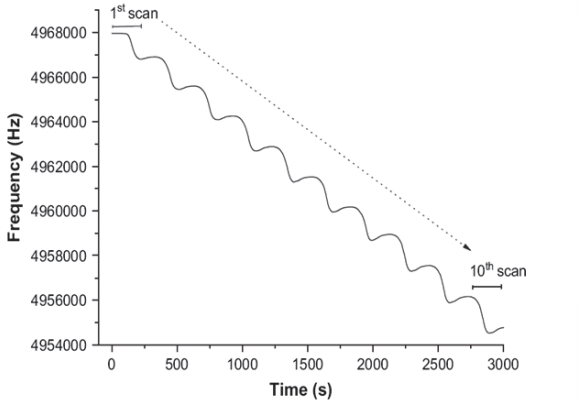

Fig. 6. Frequency changes as a function of time during the anodic oxidation of EDT.

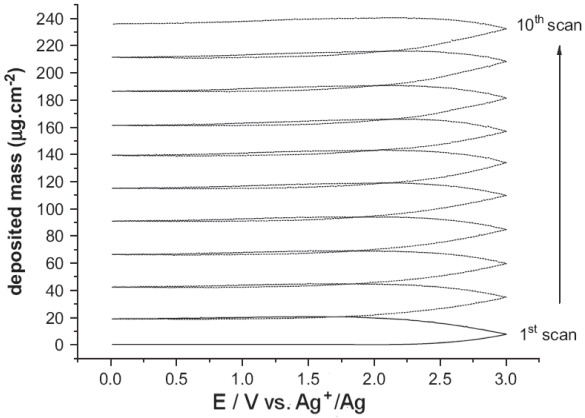

Fig. 7. Frequency changes as a function of the potential during the anodic oxidation of EDT

From the Figure 6 it can be observed also that the oxidation of EDT leads to a general decrease of the platinum-coated quartz frequency. The deposited mass on the electrode surface as a function of the potential is displayed Figure 7. The weight increase is observed at the second peak (2.16 V) of the first cycle. The deposited mass continues to increase as far as the potential is superior to 2.0 V. It can be noticed too that the deposited mass increases for subsequent scans and that the deposited mass is about the same for each cycle. So, the film synthesized at the electrode surface grows as much as repeated cycles.

X-ray photoelectron, Raman and IR analysis, were made on films deposited on platinum electrodes by anodic oxidation of EDT in acetonitrile charged with LiTFSI. Even after rinsing by pure water and ethyl alcohol, then drying under vacuum, the surface of the coating showed the presence of the supporting salt LiTFSI as shown by one O1s peak at a binding energy of 535.0 eV and one N1s peak at 403.9 eV (Figure 8a). Moreover, the XPS spectrum indicates that oxidized EDT gave one C1s peak at 288.5 eV, one S2s peak at 231.0 eV and two S2p3/2 peaks 165.3 eV and 164.0 eV (these binding energies fit well with those already

published (Rosado et al., 1998; Taga et al., 1997). Figure 8bcd shows narrow range scans for C1s, S2s and S2p3/2, respectively. Comparing these binding energies with those already published, it can be deduce that C1s peak is indicative of C-C or C-S bonds, that S2p3/2 peaks at 165.3 eV and 164.0 eV correspond to S-S bond and C-S bond of R-S-S-R molecule, respectively, and that the C/S atomic ratio deduced from XPS intensities is 1 for the film formed by oxidation of EDT.

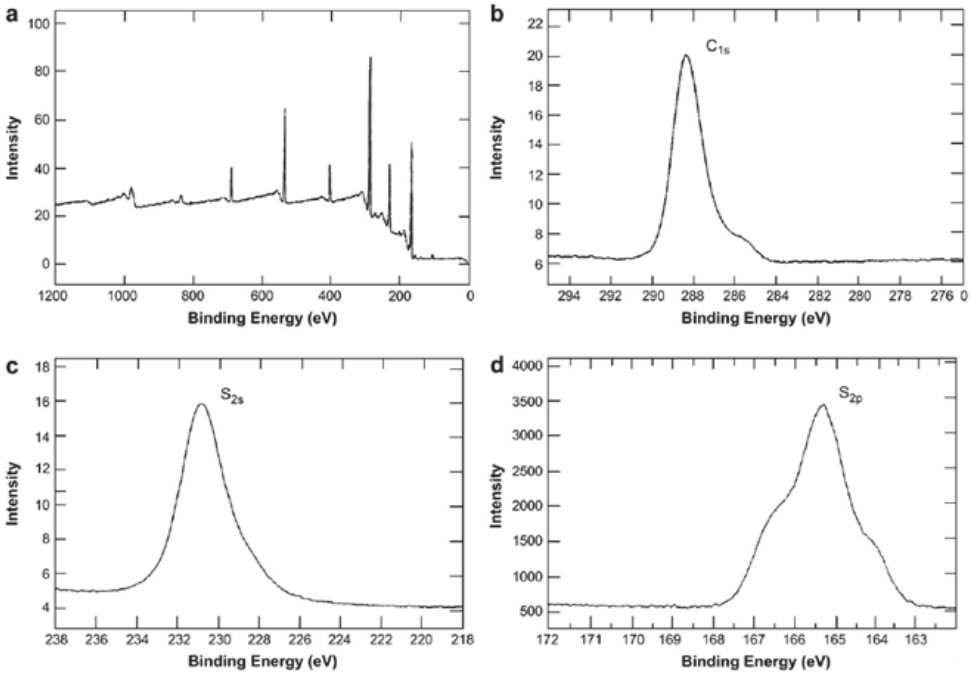

Fig. 8. xps spectra of anodically oxidazed EDT on smooth platinum.

Raman spectra from oxidized EDT gave additional information about the electrosynthesized films on the platinum electrode surfaces. A typical spectrum of the resulting film from the anodic oxidation of EDT in acetonitrile is shown Figure 9. Some characteristic vibration bands of polydisulfides can be underlined: asymmetric and symmetric -CH stretching modes at 2948 and 2904 cm^{-1}, respectively, -CH deformations at 1410 and 1280 cm^{-1}, C-C stretching at 1051 cm^{-1}, C-S out of plane vibration band at 731 cm^{-1} and S-S stretching at 505 cm^{-1}. No SH vibration band was observed between 2500 and 2600 cm^{-1}.

IRRAS spectroscopy (Figure 10) confirms Raman and XPS analyses. The main characteristic vibration bands of the polysulfide film are: -CH deformation at 1410 cm^{-1} and 1260 cm^{-1}, C-S vibration bands at 1200 cm^{-1} and 1100 cm^{-1} and C-S out of plane vibrations at 700 cm^{-1}. These peaks fit well with those obtained from similar compounds such as polyethylenesulfide or polypropylenesulfide. We could also notice that no -SH vibration band was observed in the IRRAS spectra (localized between 2500 and 2600 cm^{-1}).

From these spectroscopic studies, the product of anodic oxidized EDT leads to a polyethylenedisulfide film whose structure is similar to $(S\text{-}S\text{-}CH_2\text{-}CH_2)_n$.

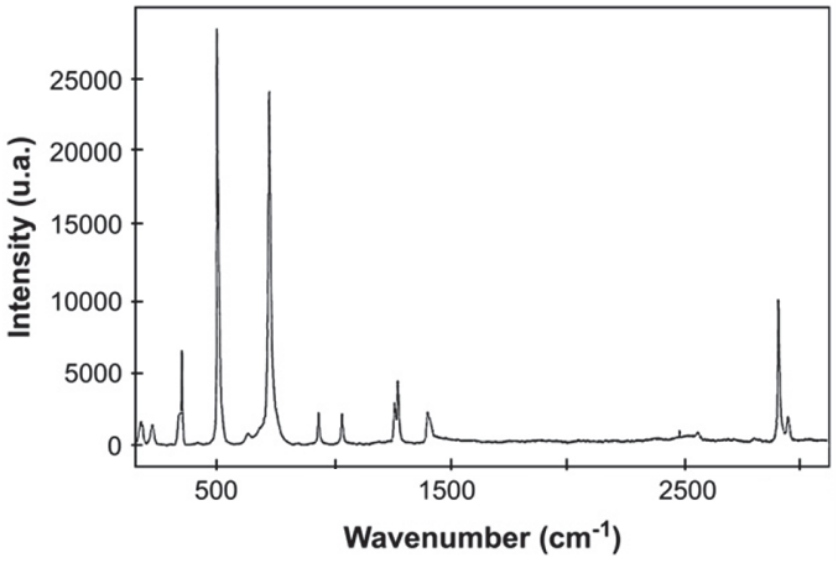

Fig. 9. Raman spectrum of oxidized EDT modified platinum surface.

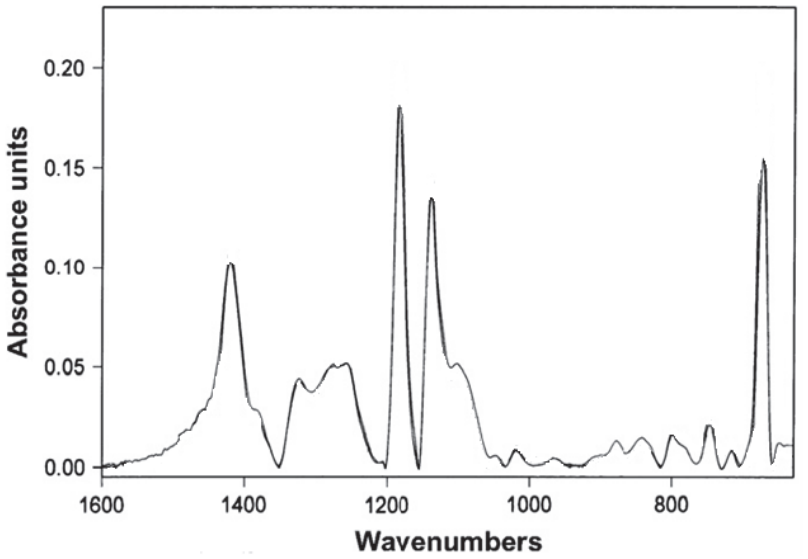

Fig. 10. IRRAS spectrum of oxidized EDT modified platinum surface.

Previous studies (Svensmark et al., 1991) on the electrochemical oxidation of thiols and related compounds on noble metal electrodes have shown that the electrochemical oxidation process of a thiol, noted R-SH, involves the initial formation of the $RS^{+\bullet}$ radical cation, followed by the formation of the $RS^{\bullet}$ radical and by the dimerization to the disulfide. This reaction was used as the first steps of the proposed mechanism (Figure 11). The first step is

adsorption of monomer on the platinum surface electrode. Then the monomer is oxidized with the loss of an electron and the formation of a cation radical. This step corresponds to the oxidation peaks observed in Figure 5. This step is followed by a deprotonation with formation of a radical, which dimerizes to the disulfide. Then, other sequences of oxidation, deprotonation, oligomerization take place yielding a polymer film. Therefore, a polyethylenedisulfide $(CH_2\text{-}CH_2\text{-}S\text{-}S)_n$ grows progressively on the electrode surface.

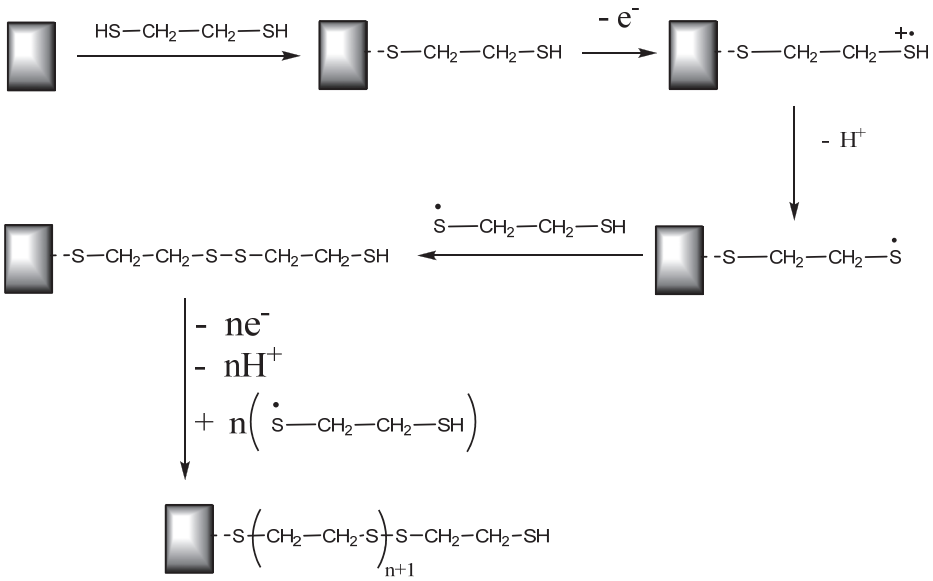

Fig. 11. Proposed mechanism of the anodic oxidation of EDT.

2.3 Anodic oxidation of glycine

The first electrochemical studies of amino acids date back to the 60 s and focused on their behavior in strong acid solutions where amino acids leads to carboxylic acids, aldehydes, ammonia and carbon dioxide (Lund et al., 1991). Electrochemistry of amino acids spread out until a renewal of interest at the end of the 90 s for studying the adsorption, reactivity and protein-surface interactions. From the literature, glycine has attracted extensive attention in recent years with investigations on single crystal electrodes (Huerta et al., 1997; Zhen et al., 2004) as well as on polycrystalline electrodes (MacDonald et al., 1997) due to its small size and chemical and biological importance. Many voltammetry studies on single crystal electrode coupled to several in situ techniques such as infrared (FTIRS) or Raman (Xiao et al., 2002) SERS spectroscopy and quartz crystal microbalance were performed. Different electrode materials were used. For instance, on monocrystalline electrode such as Pt(111) electrode, strongly bonded cyanide is formed above 0.5 V/RHE with CO_2 generation from the carboxyl group oxidation (Kolbe reaction). In addition, reversible adsorption of glycinate anions has been detected at potentials higher than 0.3 V. On Au(111) surface in alkaline solution, there is a dissociative adsorption of glycine leading to adsorbed cyanide from -0.6 to 0.0 V/SCE to give aurous cyanide at 0.3 V. Above 0.3 V several reactions may occur: (1)

direct oxidation of bulk glycine, (2) consumption of HO^- from H_2O hydrolysis for carbonate and bicarbonate formation and (3) gold atom dissolution from electrode surface.

For other electrode materials there are quite different results from some other works undertaken in the same period as those evocated previously. For instance, the anodic oxidation of glycine on glassy carbon electrodes (GCE) was carried out for elaborating amperometric sensors. The first application (Yu et al., 1997; Chen et al., 1997; Zhang et al., 2001) concerned the use of modified GCE from anodic oxidation of glycine 10^{-2}M dissolved in phosphate buffered solution of pH=7 for monitoring uric acid concentration. It was stated that the GCE was coated by polyglycine with no obvious proof, e. g. spectroscopic characterizations.

No data concerning the electrochemistry of highly concentrated glycine based electrolytes and their electrochemical behavior on smooth platinum electrode can be found. Indeed, the use of concentrated glycine solutions allow to enhance interaction between the electrode surface and their oxidation products.

Among usual solvents, only water dissolves glycine in great quantity. In our experiments the concentration was fixed to 0.5 M. Despite their electrochemical stability in a wide potential window, nonaqueous solvents such as propylene carbonate and N-methyl-pyrrolidinone were discarded because of the weak solubility reached in these solvents (less than 0.1 M). $NaBF_4$ 0.01 M was used as supporting electrolyte which is a salt with high solubility and high electrochemical stability. The different pH values of the electrolyte were adjusted either with H_2SO_4 or NaOH as needed.

EQCM experiments coupled to cyclic voltammetry technique were performed on smooth platinum electrode in aqueous solutions only. Due to the different forms that glycine can have (acidic, basic or zwitterion) as shown Figure 12, it was necessary to take into account the pH influence.

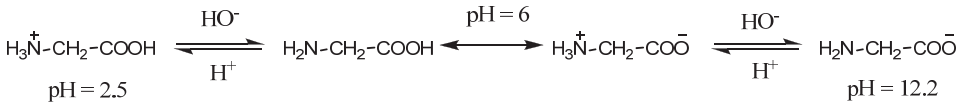

Fig. 12. The different glycine forms versus pH values

Different electrochemical studies were carried out at three different pH solutions which were 1, 6 and 13. Between 0 and 2.5 V vs. Ag^+/Ag as shown Figure 13, there is a faradaic peak corresponding to the glycine oxidation. Its potential position depends strongly on the pH value. The higher the pH, the higher the anodic oxidation potential E. The different peak potential values found are E=0.88 V at pH=1, E=0.95 V at pH=6 and E=1.70 V at pH=13.

The gravimetric curves obtained simultaneously allow correlating the mass variation at the electrode surface to the pH and the potential values (Figure 14). It can be seen that only at pH above 13 there is a drastic mass increase beyond the anodic peak potential at 1.7 V vs. Ag^+/Ag during the forward scan and the mass deposition goes on during the reverse scan. At pH=1, the slight mass increase that occurred beyond 0.55 V during the forward scan is totally cancelled during the reverse scan.

At pH=13 (above pKa=12.2) and between 1.4 and 1.9 V (Figure 15), there is a current drop with decreasing peak intensity as the scans proceed. No reverse peak is observed suggesting an irreversible reaction at the platinum surface that yields an insulating coating.

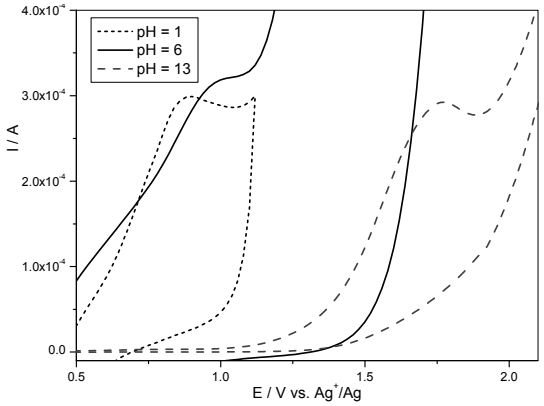

Fig. 13. Cyclic voltammogram of glycine 0.5 M in water at three different pH values. Scan rate: 20 mV/s.

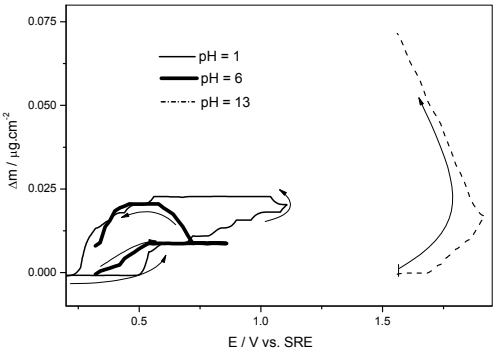

Fig. 14. Gravimetric curves coupled to cyclic voltammetry of glycine 0.5 M in water at three different pH values. Scan rate: 20 mV/s.

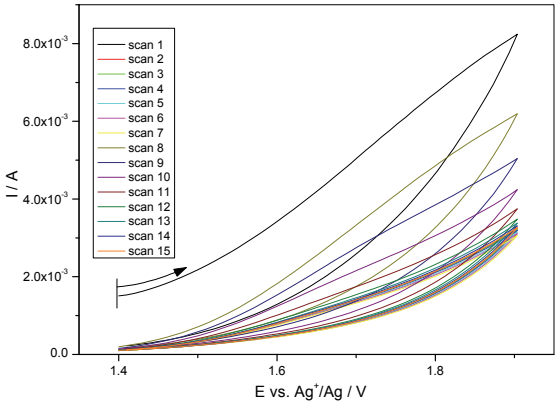

Fig. 15. Ten cyclic voltammograms of glycine 0.5 M in water at pH 13.

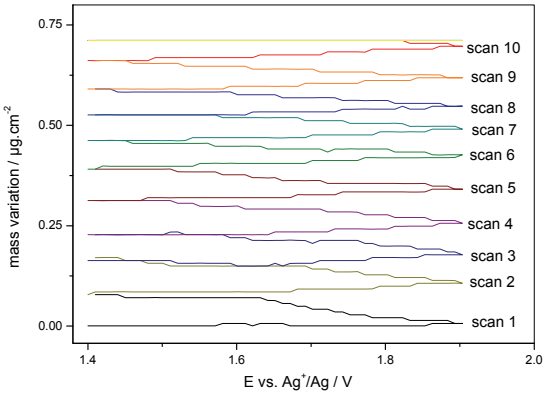

Fig. 16. The simultaneous gravimetric curves obtained with the EQCM.

Simultaneous EQCM measurements (Figure 16) show the constant mass increase at the platinum surface between 1.4 and 1.9 V vs. Ag^+/Ag as the scans proceed. It can be also noticed that the mass deposition is more important for the first scan than for the others.
The influence of glycine concentration on the mass electrodeposited at the electrode surface at pH = 13 shows that the mass increases with increasing concentration of glycine in a quite linear way up to 1 M. Before and after the electrochemical experiments, no pH change in the electrolyte solution is detected.
After ten scans, the electrode surface, rinsed with water, sonicated during 30 s and dried at 300 K, it is possible to distinguish with naked eye, a slight milky-white complexion.
Topographic AFM image Figure 17 shows a complete change compared to Figure 18 depicting the bare platinum surface. The typical platinum nodules (about 50 nm diameter) have disappeared suggesting an important thickness of the coating. We are not in presence of a monolayer of adsorbed species. In addition, the scare lines observed are characteristic of stick – slipping interactions between the tip and the coating denoting its polymeric structure.
ATR-FTIR spectra at air after electrochemical experiments at pH =1, 6 and 13 are very similar. Thus, only the spectrum of the coating performed at pH=13, which corresponds to the most abundant electrodeposited mass among the three pH values, is shown Figure 19. The anodic oxidation of concentrated glycine based electrolyte leads to a passivated electrode surface with a polypeptide coating. These peptide bond formations are probably electrocalysed during the anodic oxidation of primary amine in water. Effectively, the anodic oxidation of R-CH_2-NH2 in water yields aldehyde R-CHO. And the reaction between aldehyde and primary amine leads to amide. In addition, the ATR-FTIR spectra from our coatings are different from the glycine (or glycine salt) one (Rosado et al., 1998).
The spectral features of our coating displayed Figure 4 are almost identical to those of polyglycine II (PGII) oligomers (Taga et al., 1997). Due to the tight binding of our coating with the platinum surface, some vibration modes can disappear and some others can be enhanced, e.g. the amide III mode in the region 1290 - 1240 cm^{-1} and the primary amine at 1100 cm^{-1}, respectively. The presence of –CH_2 bending vibrations at 1450 – 1400 cm^{-1} is in favor of oligomers. But the characteristic skeletal stretching band for PGII (bulk) at 1027 cm^{-1} is not visible in our case since –NH_2 band is broad in this region.

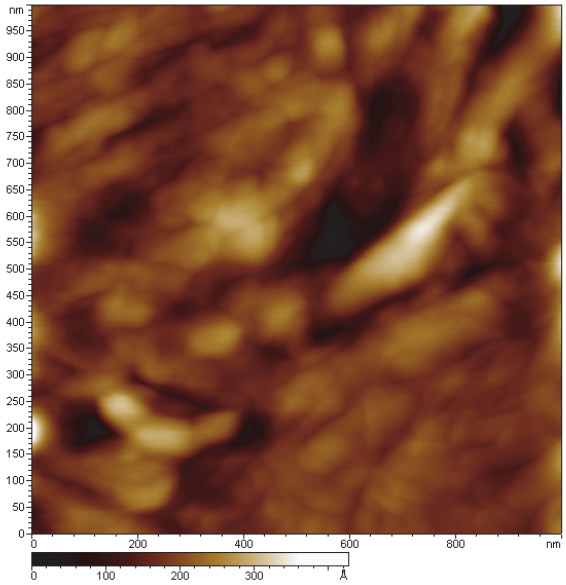

Fig. 17. AFM topography in contact mode of the platinum coated quartz after 20 voltammetric sweeps.

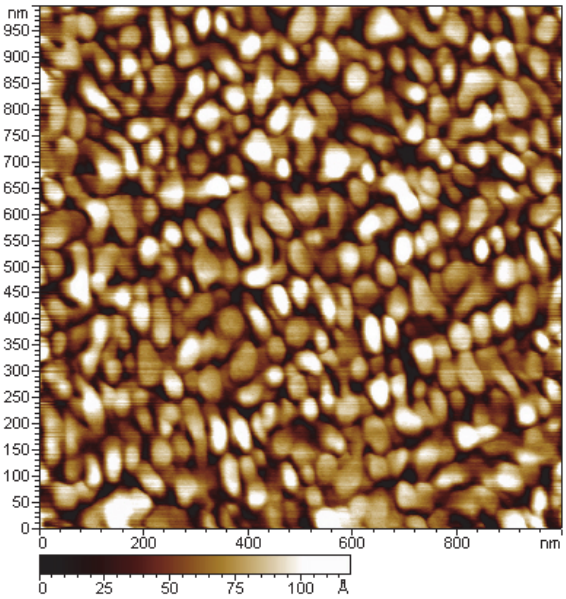

Fig. 18. The bare platinum surface.

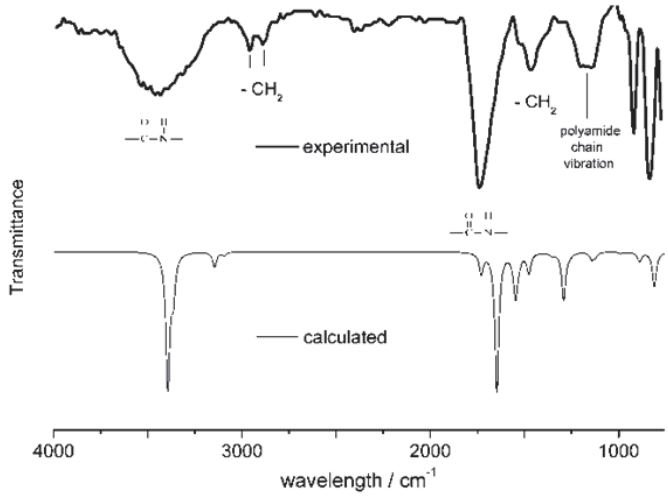

Fig. 19. IR-ATR spectroscopy of anodic oxidation of glycine and theoretical spectrum

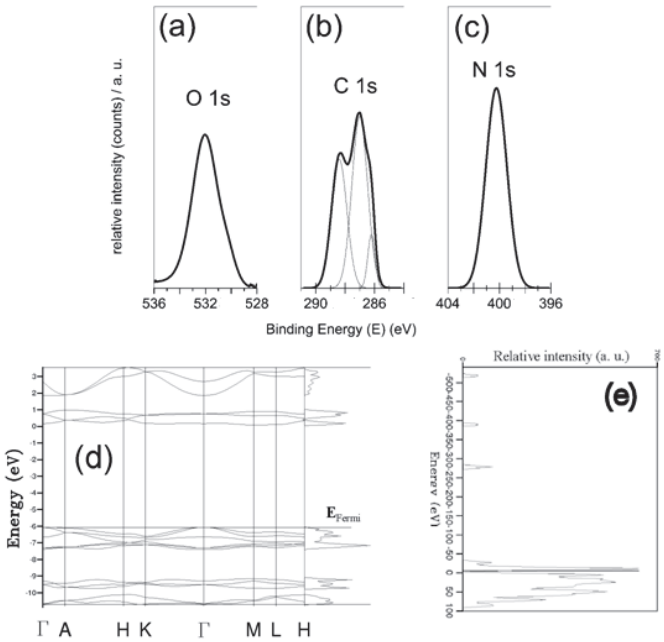

Fig. 20. xps spectroscopy of the anodic oxidation of glycine on Pt and calculated band structure and density of states.

The changes in the chemical environment of platinum surface were analyzed by XPS. If ATR-FTIR can detect chemical groups within few micrometers, XPS can probe only depth of ten nanometers. Figure 20 shows the XPS survey spectrum (a) and the C 1s (b), N 1s (c) and

(d) O 1s regions. The pre-peak at 5 eV in the onset in figure 5a is characteristic of a polymeric structure. Two C 1s peaks are clearly resolved Figure 20b. The peak at 285.5 eV can be attributed to -CH_2, while the other at 288.8 can be assigned to –C=O. The peak areas give a ratio of 1 –C=O for 2 –CH_2. The peak at 287.3 eV seems to be intrinsic to glycine system and remains unclear (Löfgren et al., 1997). As shown Figure 20c there is one asymmetric peak in the N 1s region. Peak deconvolution gave two different environments at 400.4 eV and 399.2 eV. The lowest energy binding corresponds to amide bond whereas the other at 400.4 eV is related to -(C=O)-NH-(CO)-. The IR band absorption of C=O in -(C=O)-NH-(CH_2)- is strong between 1670 and 1790 cm-1. There is effectively strong but large band absorption on the spectra in this wave number window. In these conditions, XPS is best suitable to analyze this coating. The Figure 20d in the O 1s region reveals two peaks at 531.8 eV and 536 eV. The asymmetric peak at 531.8 eV is attributed to –C=O in polyamide bond and the deconvoluted peak at 532.7 eV agrees well carboxylate energy binding. The peak at 536 eV remains unresolved.

The XPS data shown in Figure 20 are very different from those concerning glycine adsorbed on Pt(111) (18). Cyanide group is not present.

A possible mechanism can be proposed in the Figure 21 taking into account the chemisorption via the carboxylate group at pH=13, the anodic oxidation of primary amine that yields aldehyde and its reaction with amine from glycine leading to amide bond. This later step was deduced from XPS results and specifically that at 400.4 eV in the N 1s region. Further reactions with peptide formation lead to a product which looks like polyglycine composition.

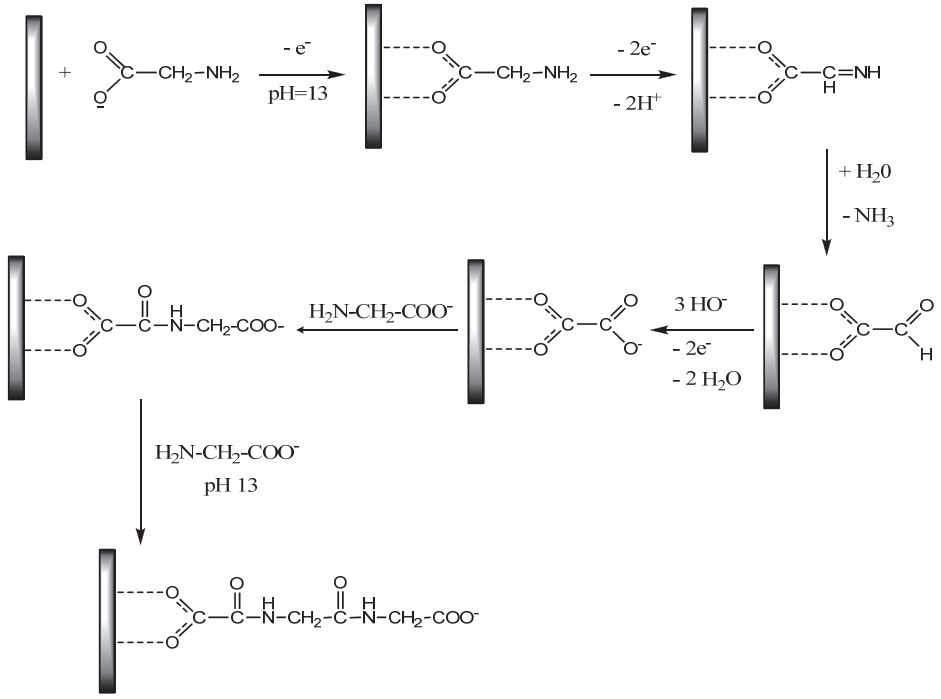

Fig. 21. Possible mechanism of the anodic oxidation of glycine leading to PG II.

2.4 Cathodic reduction of 3-aminopropyltriethoxy silane

The sol-gel process has been extensively investigated over the last twenty years especially to develop organically modified silicate (ormosils) films yielding the first industrial applications (Schmidt et al., 1988). The interest in sol-gel chemistry stems from the easy way to produce advanced materials with desirable properties including optics, protective films, dielectric and electronic coatings, high temperature superconductors, reinforcement fibers, fillers, and catalysts (Keefer et al., 1990). The very mild reaction conditions (particularly the low reaction temperatures) plus the possibility to incorporate inorganic and organic materials to each other led to a conceptually novel class of precursor materials.

Two years ago, the electrodeposition of trimethoxysilane (TMOS) on cathodically negatively biased conducting electrode surfaces to form thin silane films was reported (Deepa et al., 2003). Compared to spin-casting or dip coating methods, electrochemistry offers several advantages such as film thickness and porosity controls.

3-APTES which is among the most widely used chemicals in direct surface modification (Diao et al., 2005) based on silanization for biomolecule immobilization (Blasi et al., 2005), was rarely used until now for biosensor applications as chemically modified electrodes (Pauliukaite et al., 2005; Kandimalla et al., 2005). The present research seeks to explore on the basis of the Figure 1, the electrochemical behavior of pure or diluted nonaqueous 3-APTES based electrolytes for the preparation of ultra thin 3-APTES films on gold surfaces.

Many pure liquid state trialkoxyalkylsilanes exist as well as some organofunctional silanes such as 3-APTES. But due to their low dielectric constant (between 0.7 and 3) (Carré et al., 2003; Weast et al., 1968), they have never been regarded as solvents of interest in electrochemistry. $N(C_4H_9)_4PF_6$ dissolved in 3-APTES yields a conductivity of about 1 µS/cm at room temperature. The amino group presence in 3-APTES molecule does not enhance the salt solubility considerably as it is observed in pure 1,3-DAP where highly concentrated electrolytes can be reached up to 4M for instance.

Cyclic voltammetry (Figure 22) performed in 3-APTES charged with $N(C_4H_9)_4PF_6$ (10^{-3} M) plus freshly added water (10^{-3} M), between -4 V and 4 V versus Ag^+/Ag and shows neither net faradic peak nor gas evolving on the electrode surfaces (both working and counter electrodes). It can be observed thanks to EQCM experiment (Figure 23) coupled to cyclic

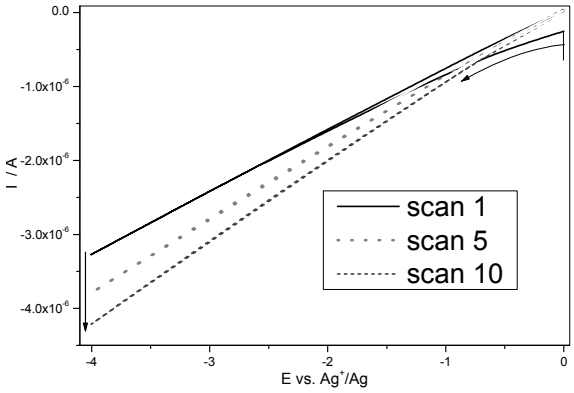

Fig. 22. Cyclic voltammogram in cathodic reduction of 3-APTES containing 1 mM of N(C4H9)4PF6 plus 1 mM of water.

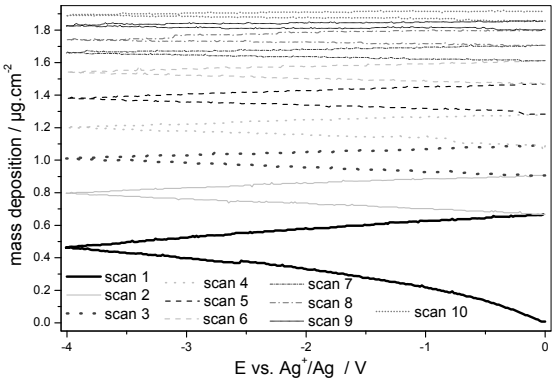

Fig. 23. Corresponding mass deposition as a function of the potential applied to a 5 MHz gold coated AT cut quartz crystal.

voltammetry that there is a mass deposition on gold electrode surface up to 2 µg.cm^{-2} at the end of the 10th scan according to the Lewis and Lu relationship (Lewis et al., 1972). This corresponds to a frequency change of 115 Hz which is in excellent agreement with the 5 MHz quartz crystal AT cut sensitivity of 56.6 Hz.cm^2.µg^{-1}. From the anhydrous 3-APTES based electrolyte (charged only with $N(C_4H_9)_4PF_6$) synthesized in a glove box under argon stream, no net mass deposition was observed on gold surface when biased cathodically but strong adsorption/desorption phenomena as a function of time occurs at zero current.
The electrochemical behavior of 3-APTES was also investigated in tetrahydrofurane (THF) because of the very negative cathodic wall reched in this solvent, and good solubilities of siloxane and ammonium salt (Lund et al., 1991). The electrogenerated hydroxide ions during the cathodic reduction process due to the water decomposition, acts as the catalyst for the hydrolysis and condensation of 3-APTES. Actually, amino groups are not reduced during this process. Figure 24 shows a cathodic voltammogram quite similar to that obtained Figure 22 without any reduction wave but showing a curve inflexion around -1.2 V

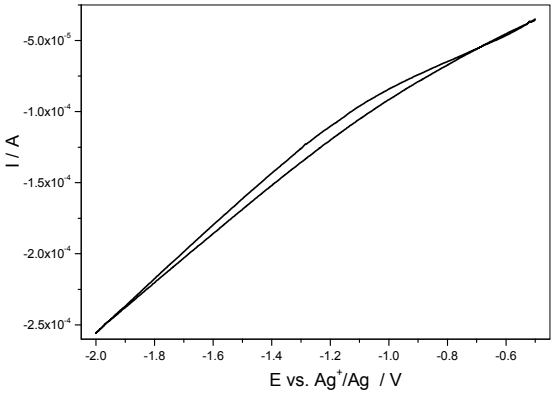

Fig. 24. Cyclic voltammogram of THF based electrolyte containing 1 mM of N(C4H9)4PF6 plus 1 mM of water.

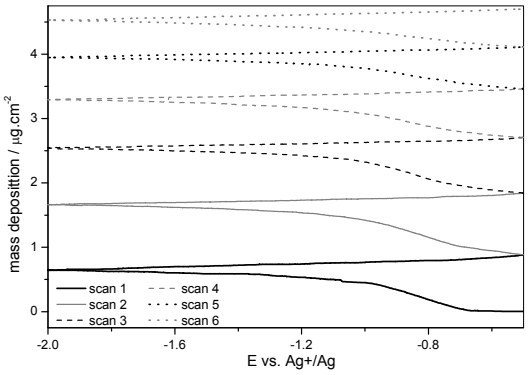

Fig. 25. Corresponding mass deposition as a function of the potential applied to a 5 MHz gold coated AT cut quartz crystal.

corresponding to the beginning of the cathodic limit of THF. Considering the mass variation curve recorded simultaneously (Figure 25) during cyclic voltammetry experiment, there was no need to go down to -4V and potential scans were limited in the potential range -0.5 to -2 V. Effectively, the mass deposition rate is optimum between -0.7 V and -1 V, evolving in an asymptotic manner beyond -1V as illustrated Figure 2b. At the end of the 10th scan, the mass deposition is more important than in pure 3-APTES electrolyte, reaching 4.7 µg.cm^{-2}. Clearly, 3-APTES has not to be concentrated in THF because the mass deposition is twice in THF based electrolyte than that in pure 3-APTES one and water concentration has to be in the same range.

The film thicknesses versus the biased electrode durations determined ex situ by ellipsometry measurements in air are reported Figure 26, as a function of cycles. There is a

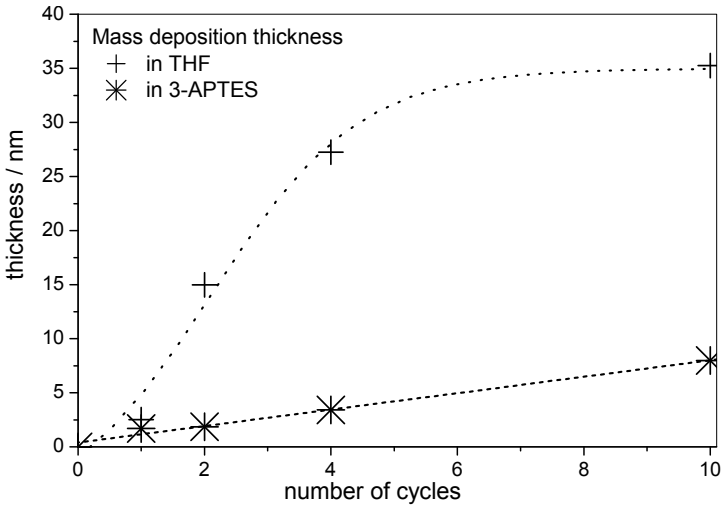

Fig. 26. 3-APTES layer thickness as a function of the number of cyclic voltammetry cycles in either 3-APTES based or THF based electrolytes.

noticeable difference, for the same potential range cycling [-0.5 to -2V], between the mass deposition in THF and in pure 3-APTES. The thickness versus the cycle numbers in THF based electrolyte is best fitted with a sigmoid curve, whereas in pure 3-APTES a linear regression matches very well the experimental data. Moreover, at the end of ten cycles the coating thickness is still growing up either in THF or in pure 3-APTES but of lesser importance than for the first cycles.

The IR-ATR characterization performed on the electrochemically modified gold coated quartz crystal in THF based electrolyte is given Figure 27 (raw spectra without any correction). The recorded spectrum of the pure 3-APTES shows typical absorption bands at 3374 cm^{-1} and 3282 cm^{-1} (νN-H for $-NH_2$), noteworthy is a considerable decrease in signal on gold surface. But IR-ATR enables us to detect $-NH_2$ groups despite the noisy band at about 1600 cm^{-1}. This noise is often observed at this frequency for IR-ATR spectra of electrodeposited linear polyethylenimine thin films from the anodic oxidation of ethylenediamine based electrolytes. The strong doublet at 1104 and 1084 cm^{-1} as well as the stronger band at 1022 cm^{-1} give evidence of the $Si\text{-}OCH_2CH_3$ presence. Between 1000 and 900 cm^{-1}, shoulders at 972 and 933 cm^{-1} are in favor of Si-O-metal formation.

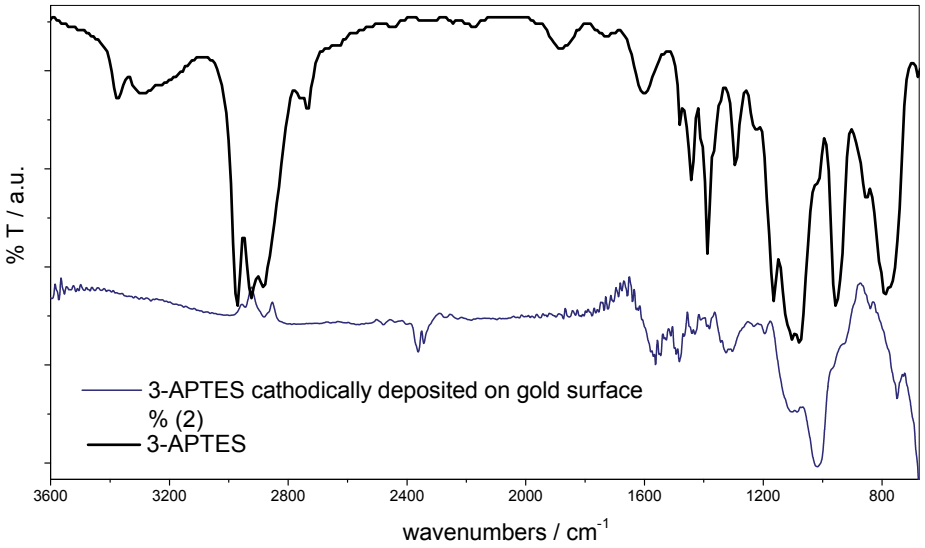

Fig. 27. FT-IR-ATR spectra of pure liquid 3-APTES and cathodic reduction of 3-APTES in THF on gold surface.

The topography and electrical properties of the 3-APTES thin film were examined with scanning tunneling microscopy. Figure 28a shows a typical STM image of freshly annealed Au(111) substrate; the presence of atomically flat Au(111) terraces over hundreds of nanometers. Figure 28b shows an image in water of the former gold substrate, biased between -0.5 and -2 V during one cycle in THF based electrolyte, where dot coverage takes place with a high density. When biased between -0.5 and -2 V during three cycles in THF based electrolyte, Figure 28c, the gold substrate is uniformly passivated. In fact, it was

impossible to image the 3-APTES coating at this stage in water but only in air (with difficulty). For this reason and as many insulating thin film coatings, 3-APTES ensure uniform thickness coatings without pinhole.

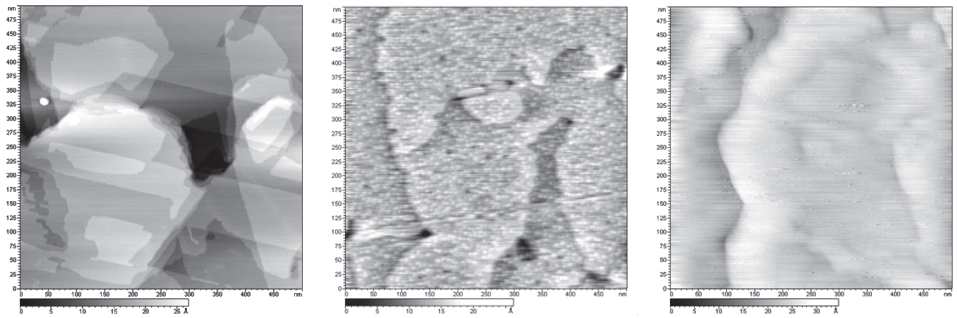

(a) (b) (c)

Fig. 28. STM picture recorded in (a) air of freshly annealed Au(111) on mica; (b) water of cathodically electrodeposited 3-APTES between -0.5 and -2V during one cycle at 20 mV/s in THF based electrolyte and (c) in air of cathodically electrodeposited 3-APTES during three cycles at 20 mV/s between -0.5 and -2V in THF based electrolyte.

The possible reactions of the cathodic reduction of water are

$$2\ H_2O + 2e^- \rightarrow 2\ HO^- + H_2$$

$$O2 + 2\ H_2O + 4e^- \rightarrow 4\ HO^-$$

$$O2 + 2\ H_2O + 2e^- \rightarrow H_2O_2 + 2\ HO^-$$

The hydrolysis of 3-APTES (1) and its condensation (2) on the hydroxyl covered surface HO-| lead to the following mechanisms :

$$(H_2N\text{-}C_3H_6)Si(OC_2H_5)_3 + mH_2O \rightarrow (H_2N\text{-}C_3H_6)Si(OC_2H_5)_{(3-m)}(OH)_m + mROH \quad (1)$$

$$(H_2N\text{-}C_3H_6)Si(OC_2H_5)_{(3-m)}(OH)_m + HO\text{-}| \rightarrow (H_2N\text{-}C_3H_6)Si(OC_2H_5R)_{(3-m)}(OH)_{(m-1)}\text{-}O\text{-}| + H_2O \quad (2)$$

In summary, gold surfaces can be modified electrochemically from the cathodic reduction of 3-APTES. This siloxane is not only grafted covalently to gold metal via oxo bond but is also electrodeposited over several nanometer thicknesses on gold surface suggesting a multilayer coating. Electrochemical studies of 3-APTES based electrolytes showed that gold surface modification is irreversible and mass deposition is larger in THF than in 3-APTES based electrolyte. In addition, the deposition catalyzed electrochemically in presence of water occurs on different electrode material such as Pt, Ti, glassy carbon, etc.

3. Insulating polymer thin film based biosensors

Immobilized enzyme on electrode surface is of prime importance when used as biosensors since their selectivity and selectivity for analyte detection. Molecule recognition requires also a good accessibility of the enzyme catalytic site. Consequently the simpler the enzyme attachment is, the more efficient the biosensor is. Until now, several solutions were

developed for immobilizing enzyme onto a surface using rather chemical protocols in water (Cosnier et al., 1999) than possibilities supplied by nonaqueous chemistry and/or electrochemistry which remain in great part unexplored (Kröger et al., 1998; Dumont et al., 1996).
The electrochemical deposition of thin film polymers presented previously allows directly and in one step the covalently grafting of films belonging functional groups of interest on metallic (Au, Pt, Fe, Ti, glassy carbon) or semiconducting surfaces (Si-p type, fluorine doped tin oxide). This part illustrates how to take advantage of the functional group presence in the thin film coatings presented previously for sensor and biosensor applications following the scheme displayed in Figure 29.

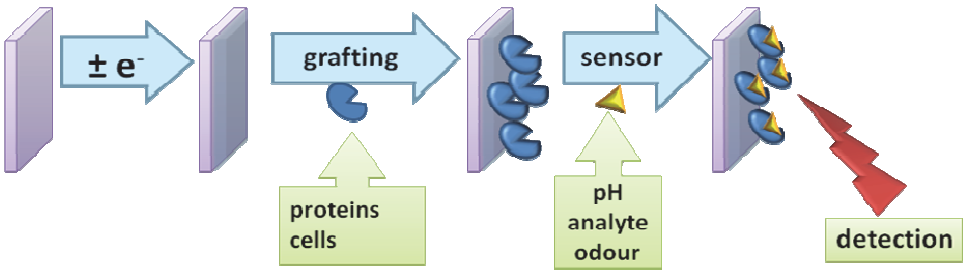

Fig. 29. general scheme of a thin film coating based (bio)sensor.

3.1 pH and ion sensors

The covalent grafting of amine based thin films on the electrode surface and their affinity towards protons makes them good candidates for pH receptor. PG behavior as pH sensor is compared to L-PEI and polyaniline (PANI).
In this purpose, the realization of a micro-sensor composed of two microelectrodes (Pt: working electrode; Ag^+/Ag: reference electrode) deposited on a glass substrate (Figure 30) was achieved via a conventional photolithography process (Figure 31).

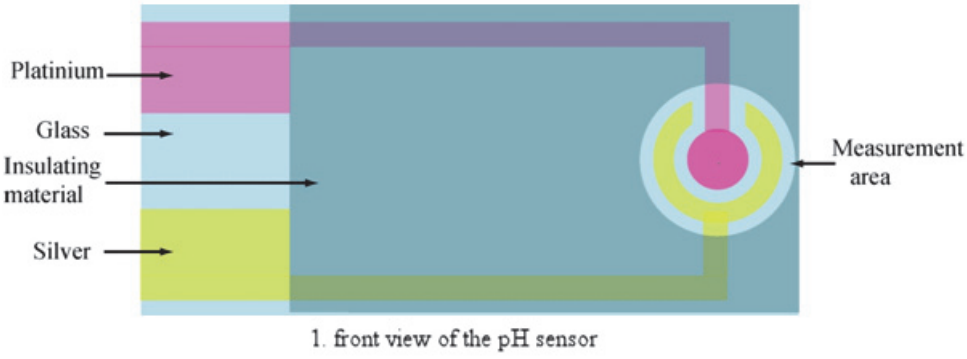

Fig. 30. pH sensor with two electrodes: a thin film based Pt electrode and a reference electrode (silver).

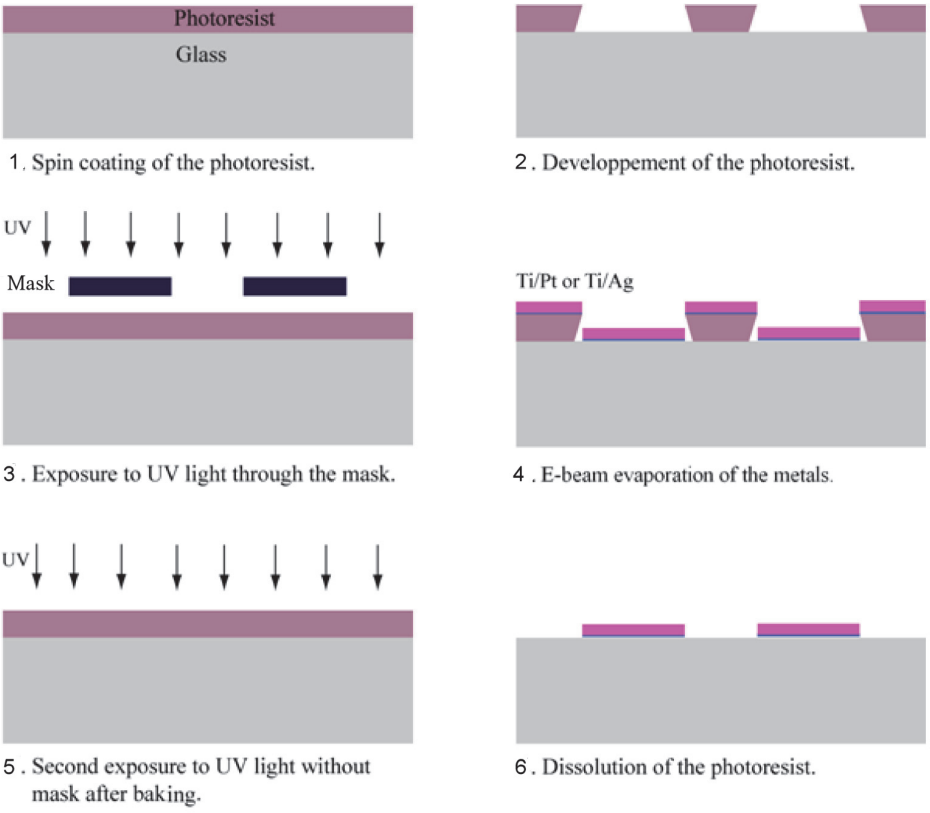

Fig. 31. Photolithography process of the pH sensor

The microelectrode connexions have rectangular ends which can be plugged to the digital voltmeter. The pH sensor architecture has been chosen for studying the effect of the geometry (diameters of the working electrode: 1000, 500, 125 and 10 µm) and to optimize the interaction between the two electrodes. A silica layer is deposited at the final step on the substrate excepted on the measuring area and the two ends allowing an effective electrical insulation. Thus, only the measure areas (Pt and AgCl) are in contact with the solution.
According to the works described previously, different thin polymer films (PGII, L-PEI and PANI) on smooth Pt were electrodeposited by cyclic voltammetry: ten scans are sufficient to coat irreversibly the platinum surface for PG and L-PEI modified electrodes whereas two scans are carried out for PANI. The resulting coatings, due to the amino group presence, act as proton receptors where the variation of the charge density occurs depending on the proton concentration.
The Pt/PG modified electrodes were tested in potentiometric mode as pH receptor when dipped in different buffered solutions at 293 K. In all the cases, there are large potential variations in the considered pH range. For PGII coating (Figure 32a), at the millimeter scale the potentiometric response is quasi Nernstian (52.4 mV/pH) but decreases down to 41.1 mV/pH for 10 µm electrode size which is a loss of sensitivity of about 20%. Despite this smaller sensitivity, pH measurements are still possible and reliable with a 10 µm electrode size.

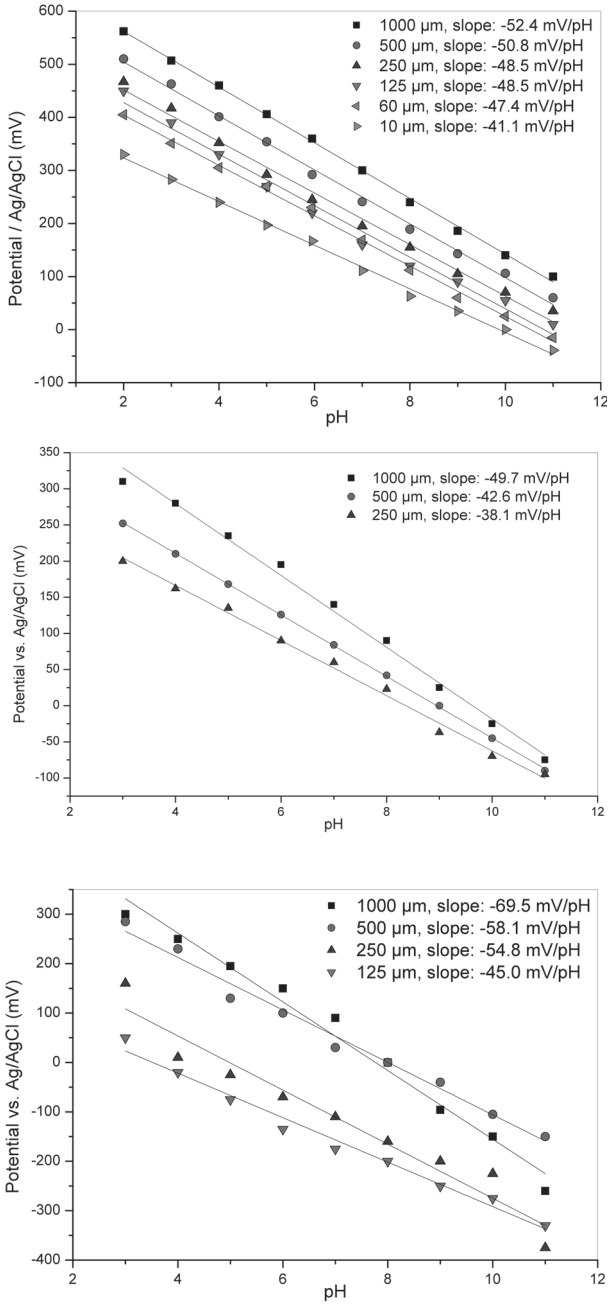

Fig. 32. pH measurements on Pt electrode of different sizes in the pH range: (a) for Pt/PG, (b) for Pt/PEI-L and (c) for Pt/PANI.

Concerning Pt/L-PEI electrodes, the same trends can be observed as for Pt/PG ones since L-PEI but is stable in a narrower pH range [3- 11] than that of PG (Figure 32b). Compared to Pt/PG and Pt/PEI-L, Pt/PANI (Figure 32c) modified electrodes have quasi to sub Nernstian (69.5 mV/pH) behaviors, depending on the electrode size. In fact, the potential response characterizes not only the transduction of proton concentration vs. pH but also the redox sensitivity of PANI to ionic species in the buffered solutions. This chemical environment can lead to doped PANI that switches to conducting state, yielding in return side electrochemical reactions responsible for over voltage and then sub Nernstian response. Another drawback in using this redox polymer is its tendency to peel off in acidic medium.

Response time of the pH measurements, linear relationship between pH and electrode potential, and the reproducibility are also important factors to take into account. Concerning the reversibility of the potentiometric measurements versus pH, the equilibrium potential response time decreases with the decreasing electrode size. In fact, at least two parameters are essential at this stage: the thickness of the polymer coating and the electrode area. Ellipsometric measurements have shown that after the electrodeposition process described previously, the PG coating thickness is around 15 nm (Table 2). Beyond this thickness value, the response time is increased and below, the pH sensitivity is decreased. The smaller the electrode size, the smaller the sensitivity (slope). For instance, at the millimeter size, the response time is about 30 s and less than 10 s for 10 µm electrode size. The response time which is comparable to that of a glass pH electrode with millimeter size electrode (30 s), is shorten drastically at the micrometer scale. We adjusted the parameters for the other electropolymerization process in order to have polymer thickness for PEI-L and PANI in the same range than that of PG.

The reversibility of the pH measurement is directly related to the response time. Reversible tests on Pt/PG with 10 µm diameter electrode were made by comparing the potential responses after a pH scan from 2 to 11 and return to 2. No noticeable difference was detected. For Pt/PEI-L and Pt/PANI, the difference is barely noticeable with 10 µm electrode size too. Globally, the potential variations vs. pH of all the modified electrodes present a linear response. The linear correlation coefficients are near 1 for Pt/PG and Pt/PEI-L modified electrodes and between 0.93 and 0.98 for Pt/PANI.

The ageing of the Pt/PG electrode was examined by testing the responses of a newly prepared Pt/PG 60 µm size over a period of thirty days. The sensitivity of this system is slightly decreased to 42 mV/pH unit with a potential shift of +120 mV, which is suitable for monitoring the pH in the range [2 – 12]. Notice that the ageing of PANI [13] has a large impact on its electronic properties which is not in favor of its use as pH transducer for a long period of time.

Electrodeposited polymer	Number of cycles (cyclic voltammetry)	Thickness (nm)
PG II	10	15 ± 0.4
L-PEI	10	18 ± 0.4
PANI	2	50 ± 1

Table 2. Polymer thickness versus the number of cycles (cyclic voltammetry).

3.2 Biosensors

Bare gold surfaces from Biacore can be electrochemically modified with 3-APTES when biased negatively below –0.7V/SRE. The resulting polysiloxane film is coated covalently to gold metal via oxo bridges. The interest of such surface covered with amino groups is its grafting (cross-linking) thereafter biological molecules in mild conditions. As an example, α-lactalbumin was grafted on the 3-APTES based film electrodeposited on a bare gold chip (corresponding to 2 CV cycles deposition from the Figure 25). This reaction was monitored by means of the SPR shift (Figure 33). After rinsing with distilled water (quoted 1 on the graph), 1% glutaraldehyde was injected on the surface (arrow A) during 1400 s (quoted 2). The sensor chip was rinsed three times with water (quoted 1) and α-lactalbumin (2mg/mL) was injected on the 3-APTES surface (arrow B) during 1700 s (quoted 3). The injection of -lactalbumin is then stopped (arrow C) and the difference in resonance units before and after α-lactalbumin injection corresponded to the amount of protein covalently attached to the 3-APTES surface (quoted 4). This result confirms that primary amino groups on the top of the 3-APTES thin film are available for covalent binding of proteins. Furthermore, the electrodeposited 3-APTES thin film on gold surface for SPR experiments allows graft and detection of macromolecules such as α-lactalbumin.

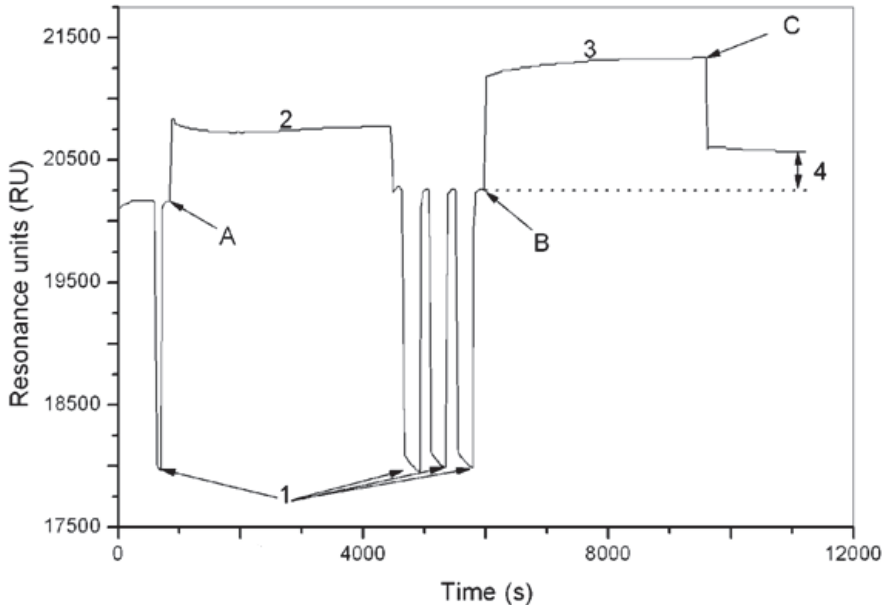

Fig. 33. SPR sensorgram from Biacore 3000 illustrating the binding of α-lactalbumin to electrodeposited 3-APTES on bare gold. The surface was first rinsed with water (1), then 1% glutaraldehyde (2) and α-lactalbumin at 2 mg/mL (3) were injected on the surface. Difference in resonance units before and after α-lactalbumin injection (4) corresponds to the amount of this protein covalently attached to the 3-APTES surface.

4. Outlook

The present review describes a new way for synthesizing thin film coatings from aliphatic bifunctional monomer, their characterization and their use as tranducers for sensor and biosensor applications. These thin film coatings can be electrosynthsized during anodic oxidation experiments (EDA, 1,3-DAP, DETA, 1,2-EDT, glycine) or during cathodic reduction (3-APTES).
The electrochemical synthesis of such polymers offers some advantages over chemical oxidation of aziridine or oxazoline for instance because on the electrode surface, the polymer is directly deposited and the adhesion creates tight binding allowing further grafting.
Although it has been shown the interest of such electropolymerization reactions, the combinations proposed Figure 1 can be continued with other functional groups such as alcohol, etc. It is possible by this way to explore deeply the scope of thin film coatings and use them in sensor and biosensor applications.

5. References

Adhikari, B.; Majumdar, S. (2004). Polymers in sensor applications. Progress in Polymer Science Vol.29, No.7, pp. 699-766.

Kalimuthu, P.; John, SA. (2009). Electropolymerized film of functionalized thiadiazole on glassy carbon electrode for the simultaneous determination of ascorbic acid, dopamine and uric acid. Bioelectrochemistry, Vol.77, No.1, pp. 13-18.

Granqvist, CG. (2007). Solar Energy Materials and Solar Cells, Vol.91, No.17, pp. 1529-1598.

Xiao, L.; Wildgoose, GG.; Compton, RG. (2009). Exploring the origins of the apparent "electrocatalysis" observed at C-60 film-modified electrodes. Sensors and Actuators B: Chemical, Vol.138, No.2, pp. 524-531.

Merkoci, A. (Ed) (2009). Biosensing using nanomaterials, ISBN: 978-0-470-18309-0, Wiley.

Medrano-Vaca, MG.; Gonzalez-Rodriguez, JG.; Nicho, ME.; Casales, M.; Salinas-Bravo, VM. (2008). Corrosion protection of carbon steel by thin films of poly (3-alkyl thiophenes) in 0.5 M H_2SO_4. Electrochimica Acta, Vol.53, No.9, pp. 3500-3507.

Liu, B.; Chen, X.; Fang, D.; Perrone, A.; Pispas, S.; Vainos, NA. (2010). Environmental monitoring by thin film nanocomposite sensors for cultural heritage preservation. J. Alloys and Compounds, Vol.504, No.1, pp. S405-S409.

Reiter, J; Krejza, O.; Sedlaříková, M (2009). Electrochromic devices employing methacrylate-based polymer electrolytes. Solar Energy Materials and Solar Cells, Vol.93, No.2, pp. 249-255.

Herlem, G.; Fahys, B.; Herlem, M.; Penneau, JF. (1999). A new relation between the maxima conductivities of nonaqueous concentrated electrolytes and chemical hardness of solvents and salts. J. Sol. Chem., Vol.28, No.3, pp. 223–235.

Herlem, G.; Reybier, K.; Trokourey, K; Fahys, B. (2000). Electrochemical oxidation of ethylenediamine: New way to make polyethyleneimine-like coatings on metallic or semiconducting materials. J. Electrochem. Soc., Vol.147, No.2, p. 597.

Saegusa, T., Ikeda, H., Fujii, H. (1972). Crystalline polyethylenimine. Macromol., Vol.5, pp. 108.

Biçak, N.; Senkal, BF. (1998). Removal of nitrite ions from aqueous solutions by cross-linked polymer of ethylenediamine with epichlorohydrin, Reactive & Functional Polymers Vol.36, No.1, pp. 71-77.

Aldrich FT-IR Handbook, Milwaukee, USA (1997).

Beamson, G.; Briggs, D. (1992). High Resolution XPS of Organic Compounds, The Scienta ESCA300 Database, pp. 182-183, Wiley Interscience.

Dick, CR.; Ham, GE. (1970). Characterization of polyethylenimine, J. Macromol. Sci. Chem., Vol.A4, p. 1301.

Gembitskii, PA.; Kleshcheva, NA. , Chhmarin, AI.; Zhuk, DS. (1978). Polymerization of ethylenimine to linear polyethylenimine. Polum. Sci. USSR (Engl. Trans.) Vol.A20, 2982 (1978).

Lakard, B.; Herlem, G.; Fahys, B. (2002). Ab initio study of the electrochemical polymerization mechanism leading from DETA to PEI, J. Mol. Struct. (Theochem), Vol.593, pp. 133–141.

Mann, CK.; Barnes, KK. (1970). Electrochemical Reactions in Non Aqueous Systems, Chapt. 8, p. 271, Dekker, NewYork, USA.

Lakard, B.; Herlem, G., Fahys, B. (2008). Electrochemical polymerization of 1,2-ethanedithiol as a new way to synthesize polyethylenedisulfide, Polymer, Vol.49, No.7, pp. 1743–1747.

Svensmark, BO; Hammerich, O (1991). Organic electrochemistry, 3rd edition. Lund, H; Baizer, MM (Eds), Dekker, New York, USA, ISBN 0-8247-8154-6; pp. 660-698.

Lund, H; Baizer MM. (1991). Organic Electrochemistry, 3rd edition, Lund, H; Baizer, MM (Eds), Dekker, New York, USA, ISBN 0-8247-8154-6, p. 601 and 3 references therein (1991).

Huerta, F., Morallón, E., Cases, F., Rodes, E; Vásquez, JL; Aldaz, A. (1997). Electrochemical behaviour of amino acids on Pt(h,k,l): A voltammetric and in situ FTIR study .1. Glycine on Pt(111). J. Electroanal. Chem., Vol.421, pp. 179-185.

Zhen, CH.; Sun, SG.; Fan, CJ.; Chen, SP.; Mao, BW.; Chen, YP. (2004). In situ FTIRS and EQCM studies of glycine adsorption and oxidation on Au(111) electrode in alkaline solutions, Electrochem. Acta, Vol.49, pp. 1249-1255.

MacDonald, SM.; Roscoe, SG. (1997). Electrochemical oxidation reactions of tyrosine, tryptophan and related dipeptides, Electrochem. Acta, Vol.42, No. 8, pp. 1189-1200.

Xiao, XY.; Sun, SG.; Yao, JL.; Wu, QH; Tian, ZQ. (2002). Surface-enhanced Raman spectroscopic studies of dissociative adsorption of amino acids on platinum and gold electrodes in alkaline solutions, Langmuir, Vol.18, 6274-6279.

Yu, AM.; Zhang, HL.; Chen, HY. (1997). Catalytic oxidation of uric acid at the polyglycine chemically modified electrode and its trace determination, Analyst, Vol.122, pp. 839-841.

Chen, HY.; Yu, AM.; Zhang, HL. (1997). Electrocatalytic oxidation of dopamine at the polyglycine chemically modified carbon fibre bundle electrode and its voltammetric resolution with uric acid, Fresenius J. Anal. Chem., Vol.358, pp. 863-864

Zhang, L.; Lin, X. (2001). Covalent Modification of Glassy Carbon Electrodes with Glycine for Voltammetric Separation of Dopamine and Ascorbic Acid, Fresenius J. Anal. Chem, Vol.370, pp. 956-962.

Rosado, M.; Duarte, MLTS; Fausto, R. (1998), Vibrational spectra of acid and alkaline glycine salts Vibrational Spectroscopy Vol.16, No.1, p.35-54.

Taga, K.; et al. (1997). Vibrational analysis of 3-chloropropylsilane, Vibrational Specroscopy Vol.14, No.2, pp. 143-146.

Löfgren, P. (1997), Glycine on Pt(111): A TDS and XPS study, Surface science Vol.370, 277.

Schmidt, H.; Seiferling, B.; Philipp,G.; Deichmann, K. (1988). Ultrastructure Processing of Advanced Ceramics, J. MacKenzie, D. & Ulrich, DR. (Eds), J. Wiley & Sons, Chichester, p. 651.

Keefer, KD (1990). Silicon Based Polymer Science: A Comprehensive Resource; Zeigler, JM. & Fearon, FWG., ACS Advances in Chemistry Ser. , American Chemical Society, Washington, DC, USA, No.224, p. 227.

Deepa, PN., Kanungo, M.; Claycomb, G.; Sherwood, PMA, Collinson, MM. (2003). Electrochemically deposited sol-gel-derived silicate films as a viable alternative in thin-film design, Anal. Chem., Vol.75, No.20, p. 5399-5405.

Diao, J.; Ren, D.; Engstrom, J. R.; Lee, K. H. (2005); A surface modification strategy on silicon nitride for developing biosensors, Anal. Biochem., Vol.343, No.2, pp. 322-328.

Blasi, L.; Longo, L.; Vasapollo, G.; Cingolani, R.; Rinaldi, R.; Rizzello, T.; Acierno, R.; Maffia, M. (2005). Characterization of glutamate dehydrogenase immobilization on silica surface by atomic force microscopy and kinetic analyses, Enzyme and Microbial Technology, Vol.36, No.5-6, pp. 818-823.

Pauliukaite, R.; Brett, CMA. (2005). Characterization of novel glucose oxysilane sol-gel electrochemical biosensors with copper hexacyanoferrate mediator, Electrochimica Acta, Vol.50, No.25-26, pp. 4973-4980.

Kandimalla, VB; Tripathi, VS.; Ju, H. (2006). A conductive ormosil encapsulated with ferrocene conjugate and multiwall carbon nanotubes for biosensing application, Biomaterials, Vol.27, No.7, pp. 1167-1174.

Carré, A.; Lacarrière, V; Birch, W (2003). Molecular interactions between DNA and an aminated glass substrate, J. Colloid and Interface Science, Vol.260, pp. 55.

Weast, RC. (Ed.) (1968). Handbook of chemistry and physics, E60, 49th edition, , the chemical rubber co.

Lewis, O.; Lu, C. (1972). Investigation of film-thickness determination by oscillating quartz resonators with large mass load, J. Appl. Phys., Vol.43, pp.4385.

Lund, H.; Baizer MM. (Eds) (1991). Organic Electrochemistry: an introduction and guide-3rd edition, ISBN 0-8247-8154-6, Marcel DEKKER Inc., p. 856.

Cosnier, S. (1999). Biomolecule immobilization on electrode surfaces by entrapment or attachment to electrochemically polymerized films. A review, Biosensors & Bioelectronics Vol.14, pp. 443-456.

Kröger, S.; Setford, SJ.; Turner, APF. (1998). Assessment of glucose oxidase behaviour in alcoholic solutions using disposable electrodes, Anal. Chim. Acta Vol.368, pp. 219-231.

Dumont, J.; Fortier, G. (1996). Behavior of glucose oxidase immobilized in various electropolymerized thin films, Biotechnology and Bioengineering Vol.49, pp. 544-552.

11

Surface Modification Approaches for Electrochemical Biosensors

Jin Shi and D. Marshall Porterfield
Purdue University
United States

1. Introduction

Electrochemical biosensors are transducers that convert biological information into electrical information. Electrochemical biosensors provide qualitative and quantitative information (Wang 1999) on the existence and concentration of the target compounds in the analyte in the form of current (amperometric biosensor) or voltage (potentiometric biosensor).

A typical amperometric biosensor consists of three components: the analyte, the transduction element (electrode and conductive nanomaterials) and the biorecognition element (enzyme) (McLamore et al., 2010a; McLamore et al., 2010b; McLamore et al., ; Shi et al., 2010). During biosensor operation, target compound in the sample is specifically recognized by the enzymes immobilized on the electrode. Electrooxidative intermediate is produced by this enzyme-substrate interaction. The produced electrooxidative intermediate is oxidized or reduced by the voltage applied on the biosensor, and current proportional to substrate concentration is generated and recorded. By calibrating the biosensor using solutions with known concentration, the relationship between measured current and substrate concentration is obtained. The sensitivity and specificity of the sensor is ensured by the high selectivity of enzymes.

Considering the functional mechanism of biosensors, surface modification of the electrode is vital to biosensor performance. The most straightforward and also widely used approach is to immobilize enzymes on the electrode with a polymer layer. However, this method has two major limitations. One is that the activity of the enzymes can be affected by structural change due to the polymer layer, and affected by the pH of the layer (Zou et al., 2008). The other is that the thickness of the polymer layer cannot be precisely controlled, so the response time and sensitivity of the biosensor could be affected (Li et al., 1996). To overcome these limitations, some groups used polymers with neutral pH such as silicate sol-gel for enzyme immobilization to preserve enzyme activity (Salimi et al., 2004) while some groups used electric methods such as cyclic voltammetry to control layer deposition (Llaudet et al., 2005; Smutok et al., 2006). Furthermore, to obtain better performance, nanomaterials including carbon nanotubes (CNTs) and metal nanomaterials are often involved in surface modification (McLamore et al., 2010a; McLamore et al., 2010b; McLamore et al., ; Shi et al., 2010). Since different modification approaches result in quite distinct biosensor performance, problems with evaluating and comparing different approaches, and sorting out the optimal ones have arisen. To solve this problem, a standardization method which evaluates the performance of biosensors constructed by different approaches is needed.

In this chapter, followed by a comprehensive literature review of surface modification approaches, a tentative protocol for comparing different approaches will be discussed.

2. Immobilization approaches for enzymes

As was mentioned previously, enzymes are the biorecognition element of biosensors. Biosensors function based on the highly selective enzyme-substrate interactions. Thus, the enzymes immobilized on electrode determine the target compound, the activity of the enzymes determines the sensitivity, and the selectivity of the enzymes determines the specificity of the biosensors. As a result, it is important to develop proper enzyme immobilization approaches with high enzyme loading and well-preserved enzyme activity.

2.1 Enzyme based biosensing

Enzymes are usually immobilized on the electrode by polymer encapsulation or covalent linking (McLamore et al., 2010b; McLamore et al., 2011; Rickus et al., 2002; Shi et al., 2010). During biosensor operation, when analyte solution diffuses into the enzyme layer, a series of biochemical and electrochemical reactions will take place. Take the *de facto* enzyme glucose oxidase (GOx) as an example. GOx based biosensors function through the following steps:

In the first step (biorecognition), GOx converts glucose into H_2O_2 and gluconic acid. The main purpose of this step is to produce the electrooxidative intermediate H_2O_2, because glucose cannot be directly electrooxidized. Because the enzyme-substrate interaction in this step is specific to glucose, biorecognition step ensures the selectivity of the biosensors.

$$\text{Step 1. Glucose} + O_2 \xrightarrow{GOx} \text{Gluconic acid} + H_2O_2$$

In the second step (transduction), an electric potential is applied to the electrode. The value of the potential is determined by the type of electrode used, and the type of the electroactive intermediate produced in *step 1*. In this particular example, for measuring H_2O_2 with a Pt electrode, the potential used is usually +500 mV-+800 mV (McLamore et al., 2010b; McLamore et al., 2011; Shi et al., 2010). The main purpose of this step is to measure the concentration of H_2O_2 by measuring current.

$$\text{Step 2. } H_2O_2 \rightarrow O_2 + 2H^+ + 2e^-$$

Since the concentration of H_2O_2 is proportional to glucose according to *step 1*, glucose concentration can be determined. By modifying the electrode with conductive nanomaterials, the electron transfer rate during electrooxidizing H_2O_2 can be significantly increased. So the biosensor will have increased sensitivity, which is the reason why surface modification with nanomaterials is important to biosensor performance.

2.2 Enzyme immobilization approaches

One of the most widely used approach for immobilizing enzymes is to entrap enzymes within polymer layers. The layer containing enzymes can be deposited on electrodes by cast-and-dry, or electropolymerization. Many polymers have been reported for such applications, including nafion (Fortier et al., 1992; Vaillancourt et al., 1999) , polypyrrole (Branzoi & Pilan 2008; Ekanayake et al., 2007), polytyramine (Situmorang et al., 1999) and silicate sol-gels (Llaudet et al., 2005; Rickus et al., 2002; Salimi et al., 2004).

Nafion is a negatively charged sulfonated tetrafluorethylene copolymer, which possesses a strong surface adhesion to electrode surface and a low swelling capability in aqueous media (Gong et al., 2005; Liaw et al., 2006; Wang et al., 2003b). Thus, nafion is quite appropriate for enzyme immobilization. Biosensors based on nafion/enzyme composite for the detection of glucose and other compounds have been reported (Fortier et al., 1992; Vaillancourt et al., 1999). One noticeable advantage of nafion over other polymers is that the negative charges repel the diffusion of many negatively charged compounds such as ascorbate and acetaminophen into the layer (Ni et al., 1999), significantly enhancing biosensing selectivity .
Polypyrrole (PPy) is a conductive polymer mainly made up of pyrroles. Polypyrroles can be formed through electropolymerization using cyclic voltammetry, resulting in a uniformly doped PPy film with positive charges on electrode surface (Schuhmann 1991; Schuhmann & Kittsteiner-Eberle 1991; Schuhmann et al., 1990). One advantage with PPy is that enzymes with negative charges can be absorbed into PPy layers via electrostatic forces (Gao et al., 2003). Another advantage is that the thickness of the PPy layer can be quantitatively controlled by controlling the number of cycles during cyclic voltammetry. The selectivity of polypyrrole film can be enhanced by the addition of various counter ions (Sadik 1999; Teasdale & Wallace 1993; Zotti 1992). Biosensors based on PPy for versatile sensing applications have been reported (Dumont & Fortier 1996; Ekanayake et al., 2007; Umana & Waller 2002). Excellent reproducibility in amperometric response and resistance towards high temperature have been reported for PPy over a number of polymers including polyaniline, poly(aniline/p-phenylediamine) , polyindole , and poly(o-phenylediamine) (Dumont & Fortier 1996). The major disadvantage with PPy is that the layer is most stable under pH range of 5.5-6.0 (Dumont 1996), which may greatly lower the activities of certain enzymes that favor basic pH, such as glycerol kinase (optimal pH=9.8) and glycerol-3-phosphate oxidase (optimal pH=8.1), both of which are used in adenosine-3-phosphate (ATP) sensing (Llaudet et al., 2005). In addition, Schuhmann et al. reported that the enzyme loading capability of PPy was low (Schuhmann 1991), which may result in a low biosensor sensitivity.
Silicate sol-gels are polymers formed by ethyl esters of orthosilicic acid, among which tetraethyl orthosilicate (TEOS) and tetramethyl orthosilicate (TMOS) are most commonly used in the immobilization of enzymes (Llaudet et al., 2005; Salimi et al., 2004; Yang et al., 1998). The hydrolysis and condensation of sol-gels at low temperature (usually 4 °C) generate a 3-dimensional polymer matrix of silica, which can entrap enzymes (Rickus et al., 2002). Biosensors based on sol-gel approach for the detection of glucose (Salimi et al., 2004), ATP (Llaudet et al., 2005) and other compounds with linear response range covering physiological concentrations have been reported. One advantage of sol-gel immobilization is that enzymes are entrapped within the matrix with no covalent linking involved, thus enzyme activity may be better preserved. Another advantage is that the porous structure of sol-gel matrix facilitates the diffusion of substrates into the matrix and provides space for the interaction between substrates and enzymes. However, since immobilization approaches based on sol-gels require dip coating and the distribution of dissolved enzymes in the sol-gel is not uniform, the thickness of the layer and the amount of loaded enzymes may vary a lot, affecting the reproducibility of biosensors.
Other polymers such as chitosan (Kang et al., 2007; Miscoria et al., 2006) have been used for enzyme immobilization as well. Some approaches directly entrap enzymes in the polymer. The common drawback with these approaches is the relatively low efficacy of enzyme loading that often results in inconsistency in amperometric response and reduced sensitivity

during long-term biosensor operation (Schuhmann 1991; Schuhmann & Kittsteiner-Eberle 1991). Thus, cross-linking agents have been combined with polymer layers for better enzyme loading. These agents include glutaraldehyde (GA) (via NH_2- bond) (Guerrieri et al., 1998), 1-ethyl-3-(3-diamino)propyl-carbodiimide (EDC) and *N*-hydroxysulfosuccinimide (NHS) (via –COOH bond) (Limbut et al., 2006), and 3-mercapto-1-propanesulfonic acid (MPS) (via –SR^- bond and electrostatic forces) (Miscoria et al., 2006). Increased amperometric sensitivity has been reported for biosensors when cross-linking agents are used for enzyme immobilization (Guerrieri et al., 1998; Miscoria et al., 2006). Some agents such as GA (McLamore et al., 2010b) and thiol linker [dithiobis (succinimidyl undecanoate)] (Claussen et al., 2009) can directly link enzymes to the electrode surface with no polymer layer involved, providing alternatives to polymer immobilization.

3. Immobilization of nanomaterials

One problem with biosensors based only on polymers and enzymes is the undesired low signal-to-noise ratio, because catalytic ability of enzymes is limited. Consequently, biosensor's amperometric response may be submerged by noise. One of the most commonly used approaches to resolve this problem is to modify biosensors with nanomaterials. Two most commonly used nanomaterials are carbon nanotubes and metal nanomaterials (McLamore et al., 2010a; McLamore et al., 2010b; McLamore et al., 2011; Shi et al., 2010).
Ever since Iijima reported the synthesis method for CNT in 1991(Iijima 1991) , this allotrope of carbon has demonstrated versatile applications in biomedical imaging (Choi et al., 2007b), chemical batteries (Wang et al., 2003a), and biosensing (McLamore et al., 2010a; McLamore et al., 2010b; McLamore et al., 2011; Shi et al., 2010). CNTs have two types: single-walled CNT (SWNT) and multi-walled CNT (MWNT). SWNT is a seamless cylinder formed by rolling-over a one-atom-thick layer of graphite namely graphene (Iijima & Ichihashi 1993) (Fig. 1a), while MWNT has the structure of sheets of graphite arranged in concentric cylinders (Ajayan 1999; Dai 2002) (Fig . 1b). SWNT has a diameter on the order of 1.2 nm (Fig. 1d) while MWNT has a diameter on the order of 10 nm to 20 nm with concentric nanotubes 0.34 nm apart (Ajayan 1999; Dai 2002) (Fig. 1c).

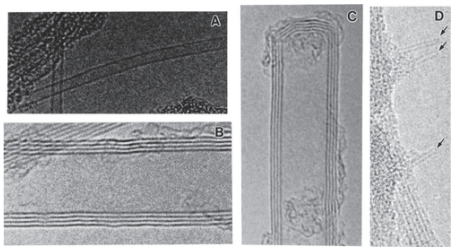

Fig. 1. High-resolution transmission electron microscopy images of typical SWNT (A) and MWNT (B). Closed nanotube tips are also shown in panel C (MWNT tips) and panel D (SWNT tip, shown by arrows). The inner space corresponds to the diameter of the inner hollow in the tube. The separation between the closely spaced fringes in the MWNT (B, C) is 0.34 nm, close to the spacing between graphite planes. The diameter of the SWNT (A, D) is ~1.2 nm. Every layer in the image (fringe) corresponds to the edges of each cylinder in the nanotube assembly. (Reprinted with permission from (Ajayan 1999). Copyright (1999) from American Chemical Society)

3.1 Electrochemical basis for CNT

STM/STS studies have shown that CNTs consist of both metallic and semi-conductive tubes (Odom et al., 1998; Wilder et al., 1998). Both SWNTs (Wang et al., 2003b) and MWNTs (McLamore et al., 2010a; McLamore et al., 2010b; McLamore et al., 2011; Shi et al., 2010) have been widely used in biosensing . CNTs have been demonstrated to possess the ability to facilitate the electron transfer process during electroreduction and electrooxidation of electroactive species, such as NADH and hydrogen peroxide (Hrapovic et al., 2004; Wang et al., 2003b), and the electron transfer process during enzyme-substrate interaction, even when the enzyme redox center is deeply embedded (Gooding et al., 2003).

Researches have been carried out to explore the underlying mechanism for CNT to enhance biosensor performance. The reasons for CNT to greatly improve biosensor's response are summarized as follows:

First, CNTs enlarge the effective surface area when immobilized on the surface of the electrodes. The electrode impedance is decreased, and the current is increased due to the increase in surface area (Azamian et al., 2002). Another advantage due to enlarged surface area is that more enzymes can be immobilized. MWNTs have been used as a matrix for enzyme immobilization (Shi et al., 2010).

Second, CNTs act as a catalyst that increases electron transfer rate. The carbon atoms at the ends of CNT behave like the edge plane of highly oriented pyrolytic graphite (HOPG) from a mechanistic point of view (Li et al., 2002). When CNTs are pretreated by purifying and refluxing using strong acid such as nitric acid (McLamore et al., 2010a), the tube ends will be connected with oxygenated species, such as carboxylic acids, alcohols and quinines (Gooding 2005; Koehne et al., 2003). The oxygenated tube ends allow efficient electron transfer (Gooding 2005; Koehne et al., 2003), which is the origin for the catalytic ability of CNTs. This underlying mechanism is further supported by comparing peak separation in cyclic voltammogram of potassium ferricyanide between one electrode with aligned SWNTs perpendicular to its surface and another electrode with SWNTs with random orientations. The former has much a smaller separation than the latter, indicating improved electrochemical property (Liu et al., 2005).

Third, the electrodes are endowed with better wetting properties due to the porous structure of CNTs (Nugent et al., 2001). As a result, analyte solution will diffuse into the CNT bundles with lower friction (Verweij et al., 2007), which contributes to a higher current sensitivity when biosensing is diffusion limited (Cambiaso et al., 1996).

3.2 Surface modification approaches using CNTs

3.2.1 Abrasive immobilization

CNT, as an allotrope of carbon, can be attached to carbon electrode surface by non-covalent forces. Salimi et al. prepared glucose biosensor based on abrasive immobilization approach, by gently rubbing the polished basal plane pyrolytic graphite (bppg) electrode surface on a filter paper containing MWNTs (Salimi et al., 2004). Decreased oxidation and reduction potentials for H_2O_2 were discovered compared with bare bppg electrodes, indicating the improvement in electrocatlytic activities of the electrodes due to CNT immobilization (Salimi et al., 2004). In amperometric tests, well-defined response to glucose addition was reported for the bppg/CNT/sol-gel/GOx biosensor while hardly any response could be observed with the bppg/sol-gel/GOx electrodes (Salimi et al., 2004), demonstrating that the low signal-to-noise issue with biosensors based on conventional materials could be resolved by adding nanomaterials. In addition, compared with glucose biosensors with no CNT

involved (Wang et al., 1997; Yang et al., 1998), the analytical parameters (sensitivity, detection limit, response time and linear range) for bppg/CNT/sol-gel/GOx biosensor were comparable or better (Salimi et al., 2004).

3.2.2 Immobilization with MPS

(3-Mercaptopropyl) trimethoxysilane (MPS), a silanization reagent with methoxy and thiol functional groups, has been applied to attach MWNTs to electrodes (McLamore et al., 2010a; Zeng & Huang 2004). The thiol groups form covalent bonds to link CNTs to electrodes. Biosensors based on this approach exhibited increased peak current in cyclic voltammetry with potassium ferricyanide, and high sensitivity towards the direct oxidation of IAA, due to the CNTs on electrode surface which facilitated electron transfer. MPS immobilization of CNTs provides an alternative to abrasive immobilization which can be applied to metal electrodes. Desirable reproducibility has been reported for biosensors based on this approach (Zeng & Huang 2004).

3.2.3 Immobilization with polymer entrapment

The major obstacle to immobilizing CNTs for biosensing is that CNTs tend to aggregate due to van der Walls forces among tubes. As a result, CNTs are insoluble in almost all solvents (Chen et al., 1998; Star et al., 2001). Since almost all conventional approaches for building enzyme based biosensors rely on polymer layers to entrap enzymes, similar approaches can be developed to immobilize CNT. Researches have shown that many polymer layers can suspend CNT, including nafion (McLamore et al., 2010b; McLamore et al., 2011; Shi et al., 2010 ; Tsai et al., 2005; Wang et al., 2003b), chitosan (Kang et al., 2007, 2008) and silicate sol-gels (Chen & Dong 2007; Gavalas et al., 2004) .

Nafion is a conductive sulfonated tetrafluorethylene copolymer and its negatively charged layer is capable of suspending CNTs and enzymes. SEM image showed that MWNTs were well dispersed within nafion layer, and formed a conductive network which will facilitate electron transfer during electrochemical reactions (Shi et al., 2010) (Fig. 2).

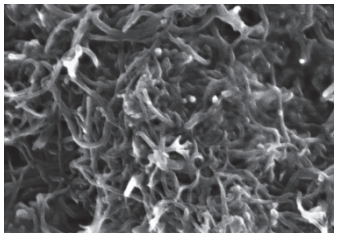

Fig. 2. SEM image for a MWNTs/Nafion layer on a biosensor. (Reprinted with permission from (Shi et al., 2010). Copyright (2010) from Elsevier Inc.)

Chitosan is a linear polysaccharide with fine biocompatibility and adhesive capability to chemically modified surfaces. Pretreated CNTs with –COOH groups on tube ends could disperse among chitosan containing $–NH_2$ groups due to the peptide bonds formed between –COOH and $–NH_2$ (Kang et al., 2007). Biosensors based on chitosan polymers with CNT and enzymes involved have been reported (Kang et al., 2007, 2008). Similar to other CNT modified electrodes, the oxidation potential for electrooxidative species is significantly lowered (Zhang 2004). A low oxidation potential ensures that interferences such as

acetaminophen and ascorbic acid, that can only be oxidized at high voltages, are excluded, which greatly enhances the selectivity of the biosensors. However, one disadvantage with chitosan is that the peptide bonds formed between CNTs and chitosan eliminate the –COOH groups on CNT, which may lower the catalytic ability of CNTs, as the ability mainly comes from the oxidative species at tube ends.

Polypyrrole (PPy) is a highly conductive polymer formed from a number of connected pyrrole rings. Wang et al. reported that "oxidized CNT" together with enzymes could act as combined dopants to form a covalently linked PPy-CNT-Enzyme layer (Wang & Musameh 2005). When electro-oxidized at +650 mV using platinum (Pt) or glass carbon (GC) electrodes as working electrodes, each pyrrole ring will carry one positive charge. With the presence of charge balancing anionic dopants, such as negatively charged enzymes (Kang et al., 2007; Umana & Waller 2002) or –COOH modified CNTs (Wang & Musameh 2005), polymer layers with enzymes or CNTs will form on the working electrode surface after electropolymerization (Wang & Musameh 2005) . Glucose biosensors based on this approach showed significantly increased response to glucose compared with no MWNT involved. In addition, thanks to irreversibly oxidized PPy's special property to reject electroactive interferences (Malitesta et al., 1990), glucose biosensors based on PPy/MWNT exhibited no response towards uric and ascorbic acids even at +900 mV (Wang & Musameh 2005), showing excellent selectivity. Besides PPy, immobilization approaches based on similar electropolymerization process using polyaniline (PAN) was also reported (Ma et al., 2006). In addition, the auto-assembly linking of negatively charged oxygenated groups on modified CNTs to positively charged polyelectrolyte poly(diallyldimethylammonium chloride) (PDDA) layer with no need of electropolymerization was reported (Mamedov et al., 2002; Rouse & Lillehei 2002).

Silicate sol-gels, including tetramethyl orthosilicate (TMOS) and tetraethyl orthosilicate (TEOS), have been widely used in enzyme immobilization due to the formed porous 3-D matrix structure which physically entraps enzymes (Llaudet et al., 2005; Salimi et al., 2004; Yang et al., 1998). The use of sol-gels to immobilize CNTs on biosensors have been reported by directly dispersing CNTs within pretreated methyltriethoxysilane (MTEOS) (Gavalas et al., 2004), Propyltrimethoxysilane (PTMOS) (Gong et al., 2004) and methyltrimethoxysilane (MTMOS) (Chen & Dong 2007) solutions. Homogeneous suspensions were obtained after ultrasonication and sol-gel/CNT layers were formed on electrodes. TEM image of CNT and the CNT/sol-gel composite (Gong et al., 2004) showed that small MWNT bundles were separated into several independent nanoelectrodes, which greatly increased the contacting area between CNTs and analytes.

3.2.4 CNT paste electrodes

Almost all previously reviewed approaches immobilized CNTs on a substrate electrode, such as glassy carbon (GC), platinum (Pt) and gold (Au). CNTs can be directly packed into a carbon electrode with or without binder materials (Britto et al., 1996; Rubianes & Rivas 2003; Valentini et al., 2003; Wang & Musameh 2003a; Zare et al., 2010) (Wang & Musameh 2003b; Zhao et al., 2003). Britto et al. first reported biosensors based on CNT paste electrode by packing a paste of MWNTs with bromoform into a glass tube for dopamine detection, and the resulted paste electrode showed desirable electrochemical reversibility in cyclic voltammetry compared with conventional carbon electrodes (Britto et al., 1996). Enhanced amperometric response was also reported for CNT paste electrodes compared with carbon paste electrodes (Wang & Musameh 2003b).

3.2.5 Immobilization of aligned CNTs

As has been discussed previously, the catalytic activities of CNTs are mainly due to the carbon atoms at the end of the tubes, especially when tube ends are attached with oxygenated species (Chou et al., 2005; Gooding 2005; Koehne et al., 2003; Nugent et al., 2001). If the CNTs are perpendicular to the electrode surface, carbon atoms at tube ends will be sufficiently exposed and the catalytic activities of CNTs can be further increased. Almost none of the approaches reviewed previously had control over the orientation of CNTs. Take the polymer layer approach as an example, when CNTs are dispersed in the polymer layer, the orientations of CNTs are completely random. Huang et al. developed a method of preparing aligned CNT thin film on a quartz plate which can be easily transferred to other surfaces, such as electrode surface (Huang et al., 1999). Gao et al. developed a glucose biosensor based on this approach using gold electrodes (Gao et al., 2003). Increased glucose sensitivity was reported and a decreased irreversible single oxidation peak was observed compared with glassy carbon electrodes with no CNTs. Yun et al. developed a needle biosensor for H_2O_2 based on the same approach with modifications, and enhanced amperometric and voltammetric properties were observed (Yun et al., 2006). Wang et al. reported another CNT alignment approach by microwave plasma enhanced chemical vapor deposition using nickel as a catalyst (Wang et al., 2003c). Resulted CNTs grew densely and vertically along the grain of the catalytic particles (Yudasaka et al., 2009) and the CNTs were aligned straight by virtue of the nickel used, except for few entangled and cross-linked tubes. Wang et al. further reported that by controlling the thickness of the nickel layer, the diameter of aligned CNTs could be controlled (Wang et al., 2003c). Glucose biosensor based on this approach with direct absorption of glucose oxidase by MWNTs has been reported and more than 91% of the initial sensitivity towards glucose remained after three months, indicating good stability (Wang et al., 2003c). Liu et al. developed a self-assembled SWNT alignment method under room temperature, which was much easier to implement compared with Dai and Wang's approaches requiring high temperature (Liu 2000). Derivative CNT alignment approaches have been reported (Chattopadhyay et al., 2001; Kim & Sigmund 2003).

3.2.6 Other surface modification approaches using CNTs

Other surface modification approaches using CNTs have been reported, including CNT-nanoelectrode ensembles (NEE) (Lin et al., 2004) and screen-printed CNT (Wang & Musameh 2004), which all provided biosensors with enhanced performance by virtue of the unique structure and properties of CNTs.

3.3 Combination of CNTs and metal nanomaterials

Transition metal nanomaterials possess high catalytic activities and facilitate electron transfer for many electrochemical reactions. Metal nanomaterials also enhance the performance of the biosensors by enlarging the effective surface area (Hrapovic et al., 2004). Biosensors incorporating metal nanomaterials, including platinum black (McLamore et al., 2010a; McLamore et al., 2010b; McLamore et al., 2011; Shi et al., 2010), copper (Xu et al., 2006), silver (Ren et al., 2005), palladium (Claussen et al., 2009; Lim et al., 2005) and gold (Daniel 2004) have exhibited well biocompatibility and enhanced performance. Especially the combination of metal nanomaterials and CNTs for surface modification of biosensors has proved to be feasible and more effective than using either nanomaterial alone (Evans et al., 2002; Hrapovic et al.,

2004; McLamore et al., 2010a; McLamore et al., 2010b; McLamore et al., 2011; Shi et al., 2010 ; Zou et al., 2008). Increased H_2O_2 sensitivity and effective surface area have been demonstrated for Pt black/MWNT/Nafion electrodes over bare electrodes (Shi et al., 2010) (Fig. 3).

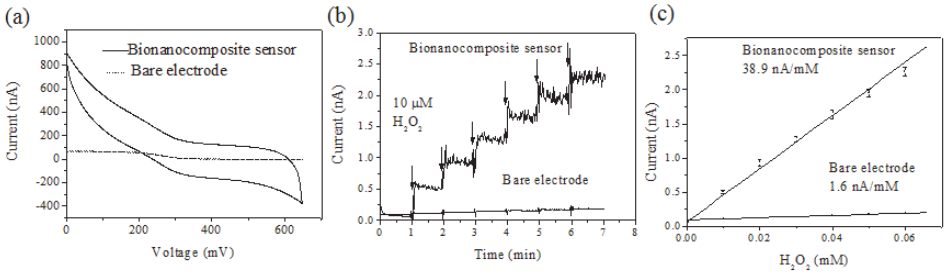

Fig. 3. (a) CV in 4 mM $Fe(CN)_6^{3-}$ /1M KNO_3 for a bare micro electrode and a bionanocomposite sensor at a scan rate 20mV/s. (Reprinted with permission from (Shi et al., 2010). Copyright (2010) from Elsevier Inc.)
(b) Representative current response to H_2O_2 for a bionanocomposite sensor and a bare electrode. (Reprinted with permission from (Shi et al., 2010). Copyright (2010) from Elsevier Inc.)
(c) Average linear regression result for averaged current versus molar concentration of H_2O_2. (Reprinted with permission from (Shi et al., 2010). Copyright (2010) from Elsevier Inc.)

Due to the high hydrophobicity of CNTs, most metal nanomaterials would not attach to CNTs via physical absorption. Hrapovic et al. linked Pt nanoparticles to SWNTs using the charge interaction between Pt and nafion-suspended SWNT, where Pt was positively charged and nafion was negative. A uniform layer containing Pt-CNT was formed (Hrapovic et al., 2004) (Fig. 4a). Kang et al. reported glucose biosensors based on a uniform Pt-CNT-chitosan film because the amino group of chitosan facilitates the dissolving of both Pt nanoparticles and –COOH modified CNT. Pt nanoparticles and CNT were dispersed in chitosan sol–gel as shown in the TEM image (Kang et al., 2008) (Fig. 4b). Electrodeposition of Pt and Au nanoparticles on CNT modified electrodes using H_2PtCl_6 and $HAuCl_4$ as Pt and Au source for glucose biosensing has also been reported, and SEM image showed that the porous MWNT film provided an ideal matrix for the distribution of Pt nanoparticles (Kang et al., 2007; Zou et al., 2008) (Fig. 4c).
The combination of metal nanomaterials and CNTs in biosensor surface modification integrates the catalytic capabilities of both nanomaterials and has been proved to be more effective in enhancing the biosensor's performance than using either material alone, including amperometric response, detection limit, linear range and stability (Claussen et al., 2009; Claussen et al., 2010; Hrapovic et al., 2004; McLamore et al., 2010a; McLamore et al., 2010b; McLamore et al., 2011; Shi et al., 2010).

3.4 Attaching enzymes to nanomaterials

Various surface modification approaches based on CNTs and metal nanomaterials have been reviewed in the previous sections. A good question is how to immobilize enzymes on

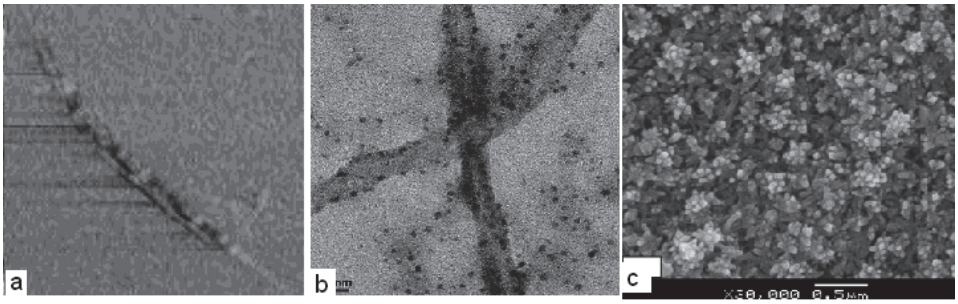

Fig. 4. (a). AFM tapping-mode phase image (size, 1 μm × 1 μm; data scale, 20 nm) of one SWCNT in the presence of Pt nanoparticles. (Reprinted with permission from (Hrapovic et al., 2004). Copyright (2004) from American Chemical Society)
(b). TEM image of CNT–PtNP–CS–MTOS sol–gel. (Reprinted with permission from (Kang et al., 2008). Copyright (2007) from Elsevier B.V)
(c). SEM image of a Pt/MWNTs/GC electrode. (Reprinted with permission from (Zou et al., 2008). Copyright (2007) from Elsevier B.V)

nanomaterial modified electrodes, so that the biosensors have biorecognition capability while the catalytic activities of nanomaterials are preserved. Existing methods include direct absorption of enzymes by MWNTs due to the porous structure (McLamore et al., 2011; Shi et al., 2010), encapsulating enzymes and nanomaterials in the same polymer layer (Chen & Dong 2007; Choi et al., 2007a; Lim et al., 2005; Tsai et al., 2005), depositing multiple layers containing nanomaterials and enzymes (Zou et al., 2008) and attaching enzymes to modified electrodes via cross-linking agents (Claussen et al., 2009; Claussen et al., 2010). Gooding et al. reported a self-assembled attachment approach by incubating CNTs in microperoxidase MP-11 solution in HEPES buffer and showed that the enzymes were attached to the ends of the tubes via covalent bonds instead of being entrapped in the gaps among tubes (Gooding et al., 2003). They further demonstrated that no enzymes were linked to the side walls of CNTs with AFM showing that the number of CNTs was almost the same as the number of MP-11 enzymes (Gooding et al., 2003). Peak current of cyclic voltammetry in PBS for biosensors with MP-11 linked to SWNT was more than three times that of biosensors with no SWNT, demonstrating the electrochemical catalytic activities of CNTs (Gooding et al., 2003). Willner et al. reported similar approaches and linked the enzyme redox active center of flavin adenine dinucleotide (FAD) to the end of CNTs (Fernando et al., 2004). The attachment of enzyme redox center not only provided increased biosensing sensitivity due to enhanced electron transfer, but also allowed the direct electron transfer between enzymes and CNTs, which was the basis for third generation biosensors measuring direct electron transfer.
Attaching enzymes to nanomaterials facilitates the "electrical communication" between enzymes and nanomaterials, resulting in improved biosensor response. However, one potential drawback associated this technique is that the structure of enzymes may be changed due to the covalent bonds which link enzymes to CNTs. The catalytic activities of enzymes may be affected due to the structural change.

4. Conclusions

Almost all the literatures reviewed in this chapter reported biosensor performance in terms of amperometric and/or voltammetric response to the target compounds. Due to the large

amount of existing surface modification approaches, problems with evaluating and comparing different approaches, and sorting out the optimal ones have arisen.

For biosensors, two important biophysical factors will affect amperometric response: 1.Enzyme activity. When covalent bonds exist between the enzymes and cross-liking agents, polymer layers, nanomaterials or the electrode surface, the structural change of enzymes will decrease the catalytic activities. 2. Diffusion properties of layer immobilized on the surface of the electrode, including polymers, enzymes and nanomaterials. The ideal case is that the layer is most permeable to target compounds, while most resistant to the interfering compounds that will otherwise generate interference. For surface modification approaches aimed at enhancing the performance of biosensors, such as the immobilization of CNTs, two factors should be considered as well: 1. Enlarged surface area. Both CNTs and metal nanomaterials can enlarge the effective surface area of the electrodes. 2. Enhanced electron transfer rate due to the catalytic ability of nanomaterials.

The complexity arising from the many factors affecting biosensing has posed great difficulty for comparing different surface modification approaches considering analyzing various configurations of membranes, the underlying connections and interactions among components within membranes. Consequently, certain standards should be set up to evaluate the performance of the biosensors. Amperometric response is the commonly used standard. However, different approaches are based on electrodes of different geometric shape, such as disk electrode, wire electrode, and needle electrode, with quite distinct effective surface area. Therefore, it is more reasonable to use the current density (current per surface area) to evaluate the performance of biosensors instead of amperometric response. Current density is defined as:

$$j=i/A \quad (1)$$

Where j is the current density, I is the amperometric sensitivity of the biosensor and A is the effective surface area. For macro biosensors, A can be determined by cyclic voltammetry with potassium ferricyanide. According to the Randles-Sevcik equation (Bard & Faulkner 2000):

$$i_p=(2.69*10^5)n^{3/2}D^{1/2}CAv^{1/2} \quad (2)$$

where n is the number of transferred electrons during the oxidation and reduction of potassium ferricyanide, D is the diffusion coefficient (6.70 X 10^{-6} cm^2 sec^{-1}), C is the molar concentration of ferricyanide, A is the effective surface area (cm^2), and v is the scan rate (V sec^{-1}). By varying v and measuring i_p, A can be determined after linear regression. For microelectrodes, surface area can be determined by cyclic voltammetry with potassium ferricyanide as well. The diffusion limited current i_{lim} is defined as (Heinze 1993):

$$i_{lim} = KnFDCr \quad (3)$$

where K is the geometric constant, F is the faradic constant, r is the radius of the electrode tip, and other constants have the same meanings as in equation (2).

5. References

Ajayan, P.M., 1999. Nanotubes from Carbon. Chem. Rev, pp. 1787-1800.

Azamian, B.R.; Davis, J.J.; Coleman, K.S.; Bagshaw, C.B. & Green, M.L.H. (2002). Bioelectrochemical Single-Walled Carbon Nanotubes. *J. Am. Chem. Soc.,* Vol.124, No.43, (2002), pp. 12664-12665.

Bard, A.J. & Faulkner, L.R. (2000). *Electrochemical methods : fundamentals and applications*, (2nd), Wiley, ISBN 9780471055426, New York.

Branzoi, V. & Pilan, L. (2008). Electropolymerization Compounds Used for the Obtainment of Modified Electrodes and Electrochemical Biosensors. *Mol. Cryst. Liq. Cryst.,* Vol.484, (2008), pp. 303-321.

Britto, P.J.; Santhanam, K.S.V. & Ajayan, P.M. (1996). Carbon nanotube electrode for oxidation of dopamine. *Bioelectrochem. Bioenerg.,* Vol.41, No.1, (1996), pp. 121-125.

Cambiaso, A.; Delfino, L.; Grattarola, M.; Verreschi, G.; Ashworth, D.; Maines, A. & Vadgama, P. (1996). Modelling and simulation of a diffusion limited glucose biosensor. *Sensors and Actuators B: Chemical,* Vol.33, No.1-3, (1996), pp. 203-207.

Chattopadhyay, D.; Galeska, I. & Papadimitrakopoulos, F. (2001). Metal-Assisted Organization of Shortened Carbon Nanotubes in Monolayer and Multilayer Forest Assemblies. *J. Am. Chem. Soc.,* Vol.123, No.38, (2001), pp. 9451-9452.

Chen, H. & Dong, S. (2007). Direct electrochemistry and electrocatalysis of horseradish peroxidase immobilized in sol-gel-derived ceramic-carbon nanotube nanocomposite film. *Biosens. Bioelectron.,* Vol.22, No.8, (2007), pp. 1811-1815.

Chen, J.; Hamon, M.A.; Hu, H.; Chen, Y.; Rao, A.M.; Eklund, P.C. & Haddon, R.C. (1998). Solution Properties of Single-Walled Carbon Nanotubes. *Science.,* Vol.282, No.5386, (1998), pp. 95.

Choi, H.N.; Han, J.H.; Park, J.A.; Lee, J.M. & Lee, W.-Y. (2007a). Amperometric Glucose Biosensor Based on Glucose Oxidase Encapsulated in Carbon Nanotube–Titania–Nafion Composite Film on Platinized Glassy Carbon Electrode. *Electroanalysis,* Vol.19, No.17, (2007a), pp. 1757-1763.

Choi, J.H.; Nguyen, F.T.; Barone, P.W.; Heller, D.A.; Moll, A.E.; Patel, D.; Boppart, S.A. & Strano, M.S. (2007b). Multimodal Biomedical Imaging with Asymmetric Single-Walled Carbon Nanotube/Iron Oxide Nanoparticle Complexes. *Nano Lett.,* Vol.7, No.4, (2007b), pp. 861-867.

Chou, A.; Bocking, T.; Singh, N.K. & Gooding, J.J., 2005. Demonstration of the importance of oxygenated species at the ends of carbon nanotubes for their favourable electrochemical properties. pp. 842-844.

Claussen, J.C.; Franklin, A.D.; ul Haque, A.; Porterfield, D.M. & Fisher, T.S. (2009). Electrochemical Biosensor of Nanocube-Augmented Carbon Nanotube Networks. *ACS Nano,* Vol.3, No.1, (2009), pp. 37-44.

Claussen, J.C.; Kim, S.S.; Haque, A.U.; Artiles, M.S.; Porterfield, D.M. & Fisher, T.S. (2010). Electrochemical Glucose Biosensor of Platinum Nanospheres Connected by Carbon Nanotubes. *J Diabetes Sci Technol.* , Vol.4, No.2, (2010), pp. 312.

Dai, H. (2002). Carbon nanotubes: opportunities and challenges. *Surf. Sci.,* Vol.500, No.1-3, (2002), pp. 218-241.

Daniel, M.C. (2004). Gold nanoparticles: assembly, supramolecular chemistry, quantum-size-related properties, and applications toward biology, catalysis, and nanotechnology. *Chem. Rev.,* Vol.104, No.1, (2004), pp. 293.

Dumont, J. & Fortier, G., 1996. Behavior of glucose oxidase immobilized in various electropolymerized thin films. pp. 544-552.

Dumont, J., G. Fortier (1996). Behavior of Glucose Oxidase Immobilized in Various Electropolymerized Thin Films. *Biotechnology and Bioengineering,* Vol.49, (1996), pp. 544-552.

Ekanayake, E.M.I.M.; Preethichandra, D.M.G. & Kaneto, K. (2007). Polypyrrole nanotube array sensor for enhanced adsorption of glucose oxidase in glucose biosensors. *Biosens. Bioelectron.,* Vol.23, No.1, (2007), pp. 107-113.

Evans, S.A.G.; Elliott, J.M.; Andrews, L.M.; Bartlett, P.N.; Doyle, P.J. & Denuault, G. (2002). Detection of Hydrogen Peroxide at Mesoporous Platinum Microelectrodes. *Anal. Chem.,* Vol.74, No.6, (2002), pp. 1322-1326.

Fernando, P.; Yossi, W. & Itamar, W., 2004. Long-Range Electrical Contacting of Redox Enzymes by SWCNT Connectors. pp. 2113-2117.

Fortier, G.; Vaillancourt, M. & Belanger, D., 1992. Evaluation of nafion as media for glucose oxidase immobilization for the development of an amperometric glucose biosensor. pp. 275-283.

Gao, M.; Dai, L. & Wallace, G. (2003). Biosensors Based on Aligned Carbon Nanotubes Coated with Inherently Conducting Polymers. *Electroanalysis.,* Vol.15, No.13, (2003), pp. 1089.

Gavalas, V.G.; Law, S.A.; Christopher Ball, J.; Andrews, R. & Bachas, L.G. (2004). Carbon nanotube aqueous sol-gel composites: enzyme-friendly platforms for the development of stable biosensors. *Analytical biochemistry.,* Vol.329, No.2, (2004), pp. 247.

Gong, K.; Yan, Y.; Zhang, M.; Su, L.; Xiong, S. & Mao, L. (2005). Electrochemistry and Electroanalytical Applications of Carbon Nanotubes: A Review. *Anal. Sci.,* Vol.21, (2005), pp. 1383-1394.

Gong, K.; Zhang, M.; Yan, Y.; Su, L.; Mao, L.; Xiong, S. & Chen, Y. (2004). Sol-Gel-Derived Ceramic-Carbon Nanotube Nanocomposite Electrodes: Tunable Electrode Dimension and Potential Electrochemical Applications. *Anal. Chem.,* Vol.76, No.21, (2004), pp. 6500-6505.

Gooding, J.J. (2005). Nanostructuring electrodes with carbon nanotubes: A review on electrochemistry and applications for sensing. *Electrochim. Acta,* Vol.50, No.15, (2005), pp. 3049-3060.

Gooding, J.J.; Wibowo, R.; Liu, J.; Yang, W.; Losic, D.; Orbons, S.; Mearns, F.J.; Shapter, J.G. & Hibbert, D.B. (2003). Protein electrochemistry using aligned carbon nanotube arrays. *J. Am. Chem. Soc.,* Vol.125, No.30, (2003), pp. 9006-9007.

Guerrieri, A.; De Benedetto, G.E.; Palmisano, F. & Zambonin, P.G. (1998). Electrosynthesized non-conducting polymers as permselective membranes in amperometric enzyme electrodes: a glucose biosensor based on a co-crosslinked glucose oxidase/overoxidized polypyrrole bilayer. *Biosens. Bioelectron.,* Vol.13, No.1, (1998), pp. 103-112.

Heinze, J. (1993). Ultramicroelectrodes in Electrochemistry. *J. Angew. Chem., Int. Ed. Engl.,* Vol.32, No.9, (1993), pp. 1268-1288.

Hrapovic, S.; Liu, Y.; Male, K.B. & Luong, J.H. (2004). Electrochemical biosensing platforms using platinum nanoparticles and carbon nanotubes. *Anal. Chem.,* Vol.76, No.4, (2004), pp. 1083-1088.

Huang, S.; Dai, L. & Mau, A.W.H. (1999). Patterned Growth and Contact Transfer of Well-Aligned Carbon Nanotube Films. *The Journal of Physical Chemistry B,* Vol.103, No.21, (1999), pp. 4223-4227.

Iijima, S. (1991). Helical microtubules of graphitic carbon. *Nature,* Vol.354, No.6348, (1991), pp. 56-58.

Iijima, S. & Ichihashi, T. (1993). Single-shell carbon nanotubes of 1-nm diameter. *Nature,* Vol.363, No.6430, (1993), pp. 603-605.

Kang, X.; Mai, Z.; Zou, X.; Cai, P. & Mo, J. (2007). A novel glucose biosensor based on immobilization of glucose oxidase in chitosan on a glassy carbon electrode modified with gold-platinum alloy nanoparticles/multiwall carbon nanotubes. *Anal. Biochem.,* Vol.369, No.1, (2007), pp. 71-79.

Kang, X.; Mai, Z.; Zou, X.; Cai, P. & Mo, J. (2008). Glucose biosensors based on platinum nanoparticles-deposited carbon nanotubes in sol-gel chitosan/silica hybrid. *Talanta,* Vol.74, No.4, (2008), pp. 879-886.

Kim, B. & Sigmund, W.M. (2003). Self-Alignment of Shortened Multiwall Carbon Nanotubes on Polyelectrolyte Layers. *Langmuir,* Vol.19, No.11, (2003), pp. 4848-4851.

Koehne, J.; Chen, H.; Li, J.; Cassell, A.M.; Ye, Q.; Ng, H.T.; Han, J. & Meyyappan, M. (2003). Ultrasensitive label-free DNA analysis using an electronic chip based on carbon nanotube nanoelectrode arrays. *Nanotechnology,* Vol.14, (2003), pp. 1239.

Li, J.; Cassell, A.; Delzeit, L.; Han, J. & Meyyappan, M. (2002). Novel Three-Dimensional Electrodes: Electrochemical Properties of Carbon Nanotube Ensembles. *J. Phys. Chem. B,* Vol.106, No.36, (2002), pp. 9299-9305.

Li, J.; Tan, S.N. & Ge, H. (1996). Silica sol-gel immobilized amperometric biosensor for hydrogen peroxide. *Anal. Chim. Acta,* Vol.335, No.1-2, (1996), pp. 137-145.

Liaw, H.W.; Chen, J.M. & Tsai, Y.C. (2006). Development of an amperometric ethanol biosensor based on a multiwalled carbon nanotube-Nafion-alcohol dehydrogenase nanobiocomposite. *J. Nanosci. Nanotechnol.,* Vol.6, No.8, (2006), pp. 2396-2402.

Lim, S.H.; Wei, J.; Lin, J.; Li, Q. & KuaYou, J. (2005). A glucose biosensor based on electrodeposition of palladium nanoparticles and glucose oxidase onto Nafion-solubilized carbon nanotube electrode. *Biosens. Bioelectron.,* Vol.20, No.11, (2005), pp. 2341-2346.

Limbut, W.; Kanatharana, P.; Mattiasson, B.; Asawatreratanakul, P. & Thavarungkul, P. (2006). A comparative study of capacitive immunosensors based on self-assembled monolayers formed from thiourea, thioctic acid, and 3-mercaptopropionic acid. *Biosens. Bioelectron.,* Vol.22, No.2, (2006), pp. 233-240.

Lin, Y.; Lu, F.; Tu, Y. & Ren, Z. (2004). Glucose Biosensors Based on Carbon Nanotube Nanoelectrode Ensembles. *Nano Lett.,* Vol.4, No.2, (2004), pp. 191-195.

Liu, J.; Chou, A.; Rahmat, W.; Paddon-Row, M.N. & Gooding, J.J. (2005). Achieving Direct Electrical Connection to Glucose Oxidase Using Aligned Single Walled Carbon Nanotube Arrays. *Electroanalysis,* Vol.17, No.1, (2005), pp. 38-46.

Liu, Z., Ziyong Shen, Tao Zhu, Shifeng Hou, and Lizhen Ying (2000). Organizing Single-Walled Carbon Nanotubes on Gold Using a Wet Chemical Self-Assembling Technique. *Langmuir,* Vol.16, (2000), pp. 3569- 3573.

Llaudet, E.; Hatz, S.; Droniou, M. & Dale, N. (2005). Microelectrode biosensor for real-time measurement of ATP in biological tissue. *Anal. Chem.,* Vol.77, No.10, (2005), pp. 3267-3273.

Ma, Y.; Ali, S.R.; Dodoo, A.S. & He, H. (2006). Enhanced Sensitivity for Biosensors: Multiple Functions of DNA-Wrapped Single-Walled Carbon Nanotubes in Self-Doped Polyaniline Nanocomposites. *The Journal of Physical Chemistry B,* Vol.110, No.33, (2006), pp. 16359-16365.

Malitesta, C.; Palmisano, F.; Torsi, L. & Zambonin, P.G. (1990). Glucose fast-response amperometric sensor based on glucose oxidase immobilized in an electropolymerized poly (o-phenylenediamine) film. *Anal. Chem.,* Vol.62, No.24, (1990), pp. 2735-2740.

Mamedov, A.A.; Kotov, N.A.; Prato, M.; Guldi, D.M.; Wicksted, J.P. & Hirsch, A. (2002). Molecular design of strong single-wall carbon nanotube/polyelectrolyte multilayer composites. *Nat. Mater.,* Vol.1, No.3, (2002), pp. 190-194.

McLamore, E.S.; Diggs, A.; Calvo Marzal, P.; Shi, J.; Blakeslee, J.J.; Peer, W.A.; Murphy, A.S. & Porterfield, D.M. (2010a). Non-invasive quantification of endogenous root auxin transport using an integrated flux microsensor technique. *The Plant Journal,* Vol.63, No.6, (2010a), pp. 1004-1016.

McLamore, E.S.; Mohanty, S.; Shi, J.; Claussen, J.; Jedlicka, S.S.; Rickus, J.L. & Porterfield, D.M. (2010b). A self-referencing glutamate biosensor for measuring real time neuronal glutamate flux. *J. Neurosci. Methods,* Vol.189, No.1, (2010b), pp. 14-22.

McLamore, E.S.; Shi, J.; Jaroch, D.; Claussen, J.C.; Uchida, A.; Jiang, Y.; Zhang, W.; Donkin, S.S.; Banks, M.K.; Buhman, K.K.; Teegarden, D.; Rickus, J.L. & Porterfield, D.M. (A self referencing platinum nanoparticle decorated enzyme-based microbiosensor for real time measurement of physiological glucose transport. *Biosens. Bioelectron.,* Vol.In Press, Corrected Proof.

McLamore, E.S.; Shi, J.; Jaroch, D.; Claussen, J.C.; Uchida, A.; Jiang, Y.; Zhang, W.; Donkin, S.S.; Banks, M.K.; Buhman, K.K.; Teegarden, D.; Rickus, J.L. & Porterfield, D.M. (2011). A self referencing platinum nanoparticle decorated enzyme-based microbiosensor for real time measurement of physiological glucose transport. *Biosens. Bioelectron.,* Vol.26, No.5, (2011), pp. 2237-2245.

Miscoria, S.A.; Desbrieres, J.; Barrera, G.D.; Labb, P. & Rivas, G.A. (2006). Glucose biosensor based on the layer-by-layer self-assembling of glucose oxidase and chitosan derivatives on a thiolated gold surface. *Anal. Chim. Acta,* Vol.578, No.2, (2006), pp. 137-144.

Ni, J.-A.; Ju, H.-X.; Chen, H.-Y. & Leech, D. (1999). Amperometric determination of epinephrine with an osmium complex and Nafion double-layer membrane modified electrode. *Anal. Chim. Acta,* Vol.378, No.1-3, (1999), pp. 151-157.

Nugent, J.M.; Santhanam, K.S.V.; Rubio, A. & Ajayan, P.M. (2001). Fast Electron Transfer Kinetics on Multiwalled Carbon Nanotube Microbundle Electrodes. *Nano Lett.,* Vol.1, No.2, (2001), pp. 87-91.

Odom, T.W.; Huang, J.-L.; Kim, P. & Lieber, C.M. (1998). Atomic structure and electronic properties of single-walled carbon nanotubes. *Nature,* Vol.391, No.6662, (1998), pp. 62-64.

Ren, X.; Meng, X.; Chen, D.; Tang, F. & Jiao, J. (2005). Using silver nanoparticle to enhance current response of biosensor. *Biosens. Bioelectron.,* Vol.21, No.3, (2005), pp. 433-437.

Rickus, J.L.; Dunn, B.; Zink, J.I.; Frances, S.L. & Chris, A.R.T., 2002book. Optically Based Sol-Gel Biosensor Materials. Optical Biosensors, pp. 427-456. Elsevier Science, Amsterdam.

Rouse, J.H. & Lillehei, P.T. (2002). Electrostatic Assembly of Polymer/Single Walled Carbon Nanotube Multilayer Films. *Nano Lett.,* Vol.3, No.1, (2002), pp. 59-62.

Rubianes, M.D. & Rivas, G.A. (2003). Carbon nanotubes paste electrode. *Electrochem. Commun.,* Vol.5, No.8, (2003), pp. 689-694.

Sadik, O.A. (1999). Bioaffinity Sensors Based on Conducting Polymers: A Short Review. *Electroanalysis,* Vol.11, No.12, (1999), pp. 839-844.

Salimi, A.; Compton, R.G. & Hallaj, R. (2004). Glucose biosensor prepared by glucose oxidase encapsulated sol-gel and carbon-nanotube-modified basal plane pyrolytic graphite electrode. *Anal. Biochem.,* Vol.333, No.1, (2004), pp. 49-56.

Schuhmann, W. (1991). Amperometric substrate determination in flow-injection systems with polypyrrole- enzyme electrodes. *Sensors & Actuators B,* Vol.4, (1991), pp. 41-49.

Schuhmann, W. & Kittsteiner-Eberle, R. (1991). Evaluation of polypyrrole/glucose oxidase electrodes in flow-injection systems for sucrose determination. *Biosens. Bioelectron.,* Vol.6, No.3, (1991), pp. 263-273.

Schuhmann, W.; Lammert, R.; Uhe, B. & Schmidt, H.L. (1990). Polypyrrole, a new possibility for covalent binding of oxidoreductases to electrode surfaces as a base for stable biosensors. *Sensors and Actuators B: Chemical,* Vol.1, No.1-6, (1990), pp. 537-541.

Shi, J.; McLamore, E.; Jaroch, D.; Claussen, J.; Rickus, J. & Porterfield, D.M. (Oscillatory glucose flux in INS1 pancreatic [beta] cells: A self-referencing microbiosensor study. *Anal. Biochem.,* Vol.411, (2010), pp. 185-193.

Situmorang, M.; Gooding, J.J. & Hibbert, D.B. (1999). Immobilisation of enzyme throughout a polytyramine matrix: a versatile procedure for fabricating biosensors. *Anal. Chim. Acta,* Vol.394, No.2-3, (1999), pp. 211-223.

Smutok, O.; Ngounou, B.; Pavlishko, H.; Gayda, G.; Gonchar, M. & Schuhmann, W. (2006). A reagentless bienzyme amperometric biosensor based on alcohol oxidase/peroxidase and an Os-complex modified electrodeposition paint. *Sensors and Actuators B: Chemical,* Vol.113, No.2, (2006), pp. 590-598.

Star, A.; Stoddart, J.F.; Steuerman, D.; Diehl, M.; Boukai, A.; Wong, E.W.; Yang, X.; Chung, S.W.; Choi, H. & Heath, J.R. (2001). Preparation and Properties of Polymer-Wrapped Single-Walled Carbon Nanotubes. *ANGEWANDTE CHEMIE - INTERNATIONAL EDITION IN ENGLISH-,* Vol.40, (2001), pp. 1721-1725.

Teasdale, P.R. & Wallace, G.G. (1993). Molecular recognition using conducting polymers: basis of an electrochemical sensing technology柳lenary lecture. *The Analyst,* Vol.118, No.4, (1993), pp. 329-334.

Tsai, Y.C.; Li, S.C. & Chen, J.M. (2005). Cast thin film biosensor design based on a Nafion backbone, a multiwalled carbon nanotube conduit, and a glucose oxidase function. *Langmuir,* Vol.21, No.8, (2005), pp. 3653-3658.

Umana, M. & Waller, J. (2002). Protein-modified electrodes. The glucose oxidase/polypyrrole system. *Anal. Chem.,* Vol.58, No.14, (2002), pp. 2979-2983.

Vaillancourt, M.; Chen, J.W.; Fortier, G. & Beanger, D., 1999. Electrochemical and Enzymatic Studies of Electron Transfer Mediation by Ferrocene Derivatives with Nafion-Glucose Oxidase Electrodes. pp. 23-31.

Valentini, F.; Amine, A.; Orlanducci, S.; Terranova, M.L. & Palleschi, G. (2003). Carbon Nanotube Purification: Preparation and Characterization of Carbon Nanotube Paste Electrodes. *Anal. Chem.,* Vol.75, No.20, (2003), pp. 5413-5421.

Verweij, H.; Melissa, S. & Ju, L., 2007. Fast Mass Transport Through Carbon Nanotube Membranes. pp. 1996-2004.

Wang; J; Pamidi & P. V, A. (1997). *Sol-gel-derived gold composite electrodes*, American Chemical Society Washington, DC, ETATS-UNIS.

Wang, G.X.; Ahn, J.h.; Yao, J.; Lindsay, M.; Liu, H.K. & Dou, S.X. (2003a). Preparation and characterization of carbon nanotubes for energy storage. *J. Power Sources,* Vol.119/121, (2003a), pp. 16-23.

Wang, J. (1999). Amperometric biosensors for clinical and therapeutic drug monitoring: a review. *J. Pharm. Biomed. Anal.,* Vol.19, No.1-2, (1999), pp. 1-2.

Wang, J. & Musameh, M. (2003a). Carbon Nanotube/Teflon Composite Electrochemical Sensors and Biosensors. *Anal. Chem.,* Vol.75, No.9, (2003a), pp. 2075-2079.

Wang, J. & Musameh, M. (2003b). Enzyme-dispersed carbon-nanotube electrodes: a needle microsensor for monitoring glucose. *Analyst (Cambridge, U. K.),* Vol.128, No.11, (2003b), pp. 1382-1385.

Wang, J. & Musameh, M. (2004). Carbon nanotube screen-printed electrochemical sensors. *Analyst,* Vol.129, No.1, (2004), pp. 1-2.

Wang, J. & Musameh, M. (2005). Carbon-nanotubes doped polypyrrole glucose biosensor. *Anal. Chim. Acta,* Vol.539, No.1-2, (2005), pp. 209-213.

Wang, J.; Musameh, M. & Lin, Y. (2003b). Solubilization of carbon nanotubes by Nafion toward the preparation of amperometric biosensors. *J. Am. Chem. Soc.,* Vol.125, No.9, (2003b), pp. 2408-2409.

Wang, S.G.; Zhang, Q.; Yoon, S.F. & Ahn, J. (2003c). Synthesis and characterization of MWNTs with narrow diameter over nickel catalyst by MPCVD. *Scripta materialia.,* Vol.48, No.4, (2003c), pp. 409.

Wilder, J.W.G.; Venema, L.C.; Rinzler, A.G.; Smalley, R.E. & Dekker, C. (1998). Electronic structure of atomically resolved carbon nanotubes. *Nature,* Vol.391, No.6662, (1998), pp. 59-62.

Xu, Q.; Zhao, Y.; Xu, J.Z. & Zhu, J.-J. (2006). Preparation of functionalized copper nanoparticles and fabrication of a glucose sensor. *Sensors and Actuators B: Chemical,* Vol.114, No.1, (2006), pp. 379-386.

Yang, S.; Lu, Y.; Atanossov, P.; Wilkins, E. & Long, X. (1998). Microfabricated glucose biosensor with glucose oxidase entrapped in sol-gel matrix. *Talanta,* Vol.47, No.3, (1998), pp. 735-743.

Yudasaka, M.; Kikuchi, R.; Ohki, Y.; Ota, E. & Yoshimura, S. (2009). Behavior of Ni in carbon nanotube nucleation. *Appl. Phys. Lett.,* Vol.70, No.14, (2009), pp. 1817-1818.

Yun, Y.; Bange, A.; Shanov, V.N.; Heineman, W.R.; Halsall, H.B.; Dong, Z.; Jazieh, A.; Yi, T.; Wong, D.; Pixley, S.; Behbehani, M. & Schulz, M.J., 2006. Fabrication and Characterization of a Multiwall Carbon Nanotube Needle Biosensor. Nanotechnology, 2006. IEEE-NANO 2006. Sixth IEEE Conference on, pp. 280-283.

Zare, H.R.; Shishehbore, M.R.; Nematollahi, D. & Tehrani, M.S. (2010). Electrochemical behavior of nano-composite containing 4-hydroxy-2-(triphenylphosphonio)phenolate and multi-wall carbon nanotubes spiked in carbon paste and its application for electrocatalytic oxidation of hydrazine. *Sensors and Actuators B: Chemical,* Vol.151, No.1, (2010), pp. 153-161.

Zeng, B. & Huang, F. (2004). Electrochemical behavior and determination of fluphenazine at multi-walled carbon nanotubes/(3-mercaptopropyl)trimethoxysilane bilayer modified gold electrodes. *Talanta.,* Vol.64, No.2, (2004), pp. 380-386.

Zhang, M., A. Smith and W. Gorski (2004). Carbon nanotube–chitosan system for electrochemical sensing based on dehydrogenase enzymes. *Anal. Chem. ,* Vol.76, (2004), pp. 5045–5050.

Zhao, Y.-D.; Zhang, W.-D.; Chen, H. & Luo, Q.-M. (2003). Electrocatalytic oxidation of cysteine at carbon nanotube powder microelectrode and its detection. *Sensors and Actuators B: Chemical,* Vol.92, No.3, (2003), pp. 279-285.

Zotti, G. (1992). Electrochemical sensors based on polyconjugated conducting polymers. *Synth. Met.,* Vol.51, No.1-3, (1992), pp. 373-382.

Zou, Y.; Xiang, C.; Sun, L.-X. & Xu, F. (2008). Glucose biosensor based on electrodeposition of platinum nanoparticles onto carbon nanotubes and immobilizing enzyme with chitosan-SiO2 sol-gel. *Biosens. Bioelectron.,* Vol.23, No.7, (2008), pp. 1010-1016.

12

Aptamer Sensors Combined with Enzymes for Highly Sensitive Detection

Koichi Abe and Kazunori Ikebukuro
Tokyo University of Agriculture and Technology
Japan

1. Introduction

Diagnostics have taken on a larger role in patient care, with diagnostics for point-of-care testing (POCT) having greatly expanded during the last two decades. The expectation is that POCT will continue to grow because it can help to expand personalized therapy and theranostics, which will provide the right medicine to the right person, with the right dosage at the right time. For POCT, it will be necessary to construct miniaturized biosensors at a low cost that have high sensitivity with rapid sensing.
Affinity-based techniques that are used in clinical diagnostics rely on the high affinity and specificity of antibodies for highly sensitive detection of target molecules. Antibody-based diagnostic systems are well established, and enable the detection of various molecules. However, aptamers are expected to be the next-generation elements for molecular recognition.
Aptamers are short strands of nucleic acids that have been designed to specifically bind to various target molecules, and have comparable affinity and specificity to antibodies. They are selected using the SELEX (Systematic Evolution of Ligands by Exponential Enrichment) technique (Tuerk & Gold, 1990), also referred to as "in vitro selection" or "in vitro evolution." SELEX is a combinatorial chemistry technique that produces single-stranded oligonucleotides of DNA or RNA, which specifically bind to a target ligand(s).
It has been two decades since the first report on aptamers became public (Ellington & Szostak, 1990; Tuerk & Gold, 1990). During these two decades, many aptamers have been reported and an aptamer has been approved as a therapeutic medicine by the US Food and Drug Administration (FDA). Aptamers have many advantages as biosensors that antibodies do not have, such as:

1. The ability to be selected by SELEX.
2. The ability to be synthesized and modified.
3. The ability to renature.
4. More stability than antibodies.
5. The ability to change conformation upon binding to target molecules.

For theranostics, the first advantage is important when it is necessary to obtain affinity probes against various novel biomarkers. SELEX has many advantages, and is an excellent method to evolve aptamers so that they have an extremely high binding affinity to a variety of target ligands. We were able to successfully achieve the automatic in vitro screening of aptamers, which enabled us to obtain aptamers against more than 100 proteins per month (Cox & Ellington, 2001). Aptamers can therefore be developed more rapidly than antibodies.

In addition, since there is virtually no shortage of targets for aptamers, we can obtain aptamers against small molecules, peptides, proteins and even cells.
Aptamers selected by SELEX against purified membrane proteins often do not bind to native membrane proteins on the cell because the membrane protein will change its conformation after purification. Since Cell-SELEX enables us to treat native membrane proteins as target molecules, we can obtain more useful aptamers for cell identification (Pestourie et al., 2006). SELEX against unpurified protein, including Cell-SELEX, can be utilized to identify biomarkers as well (Berezovski et al., 2008; Noma et al., 2006a). Although in vitro selection is a powerful method to obtain aptamers, selected aptamers often require optimization for the best affinity and specificity. We can perform post-optimization of their sequences after SELEX through iterative cycles of mutated DNA synthesis and evaluation of their functions, which would be a cumbersome process for antibodies (Ikebukuro et al., 2005b; Ikebukuro et al., 2006; Knight et al., 2009; Noma & Ikebukuro, 2006; Noma et al., 2006b; Savory et al., 2010).
The fifth advantage is important so that aptamers can be perceived as unique reagents for analytical applications, not as alternatives to antibodies. Since aptamers are a kind of biopolymer consisting of nucleic acids that have many negative charges, their tertiary structures are destabilized by repulsion between phosphate backbones. In addition, since aptamers are formed by Watson-Crick base pairing, some aptamers have the ability to form different structures. Target molecule binding stabilizes a particular structure, even though the structure would have little chance of forming without the target molecules. Aptamers have the potential to change structures, and in some cases, drastically. Many aptameric sensors have been reported that rely on the transduction of structural changes into detectable signals (Han et al., 2010; Li et al., 2010).
In this chapter, we focus on enzymes that are combined with aptamer sensors. Since enzymes catalyze various kinds of reactions, they are used as biosensors for many biomarkers. In addition, since catalytic turnover of enzymes enables signal amplification at moderate temperatures, it enables affinity-based biosensors to measure target molecules with high sensitivity, and without the need for radioisotopes. Most antibody-based diagnostics systems use enzyme-labeled antibodies. For the combination of aptamers with enzymes, aptamers would work not only as a replacement molecule for antibodies, but also as a part of a new device that can exploit the unique properties of aptamers. First, we categorize aptamer sensors based on how to combine enzymes with aptamer sensors. Second, we describe the detail of the enzymes and discuss them based on biosensors for highly sensitive detection and POCT.

2. Strategy of enzyme combination with aptamer sensors

The key point of combining an aptamer sensor with an enzyme is the ability to distinguish aptamer–target molecular complexes from unbound aptamers before signal amplification. Figure 1 shows how aptamer sensors using enzymes are divided into two groups based on how to distinguish aptamer-protein complexes from unbound aptamer. Bound free (B/F) separation can easily purify aptamer-protein complexes by eliminating unbound aptamer. Ordinarily, to eliminate unbound aptamer and detect an aptamer-protein complex by its enzyme activity, a sandwich assay is applied. Most clinical diagnostic methods use an antibody-based sandwich assay such as the enzyme-linked immunosorbent assay (ELISA). However, we constructed a biosensor using an aptamer which had the unique properties of

aptamers, as well as their ability to bind to the target molecule. When we perform B/F separation using an antibody, we apply a competitive assay. However, a competitive assay requires purified target molecules, and the process is difficult when the purification of a target molecule is laborious. As mentioned above, aptamers have unique features: their structural change is accompanied by target binding. Therefore, we can construct an aptamer based B/F separation system that is not a competitive assay.
The second group does not require B/F separation, and regulates enzymatic activity by using target molecules. It can be divided into two subgroups. One group regulates enzymatic activity directly by using target molecules. The other group changes the input DNA structure into an output DNA structure that can serve as a substrate for polymerase. Since the polymerase can replicate the substrate DNA, we can control the polymerase reaction via regulation of the substrate DNA.
We will describe the details of each group separately.

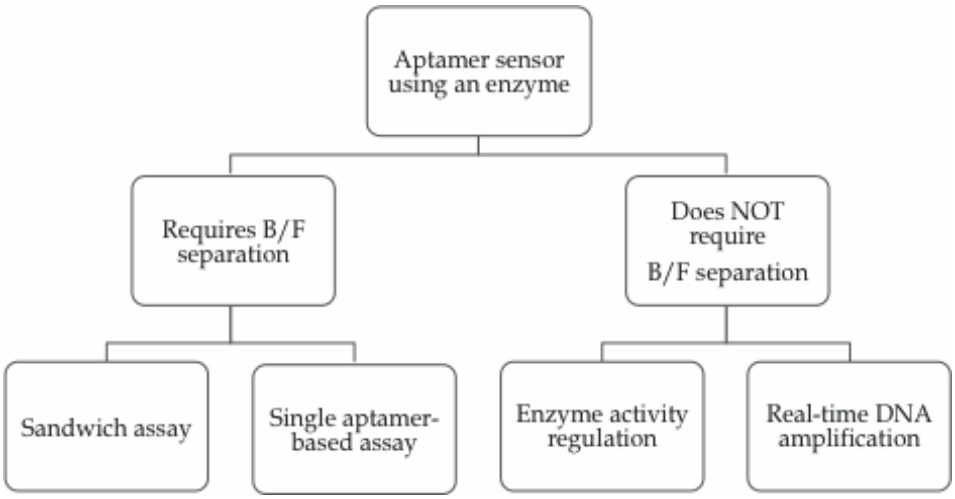

Fig. 1. A schematic of the two categories of aptamer sensors that use enzymes. Aptamer sensors that use enzymes are divided into two main groups. The first group requires B/F separation, and the second group does not require it. The first group is divided into two subgroups based on how the B/F separation is performed. The second group is divided into two subgroups based on how enzymatic activity is regulated. In one subgroup, enzymatic activity is regulated directly by the activity of the aptamer, and in the other, the structure of the aptamer is regulated by target binding for DNA amplification.

2.1 Sensing with bound free separation

2.1.1 Sandwich assay

B/F separation is an attractive process because it can eliminate not only unbound enzyme-modified molecular recognition elements, but also nonspecific binding and some molecules that affect noise. Since B/F separation reduces background signal and noise, it enables highly sensitive detection. Most clinical diagnostic methods using antibodies are based on the sandwich strategy. A sandwich assay requires two molecular recognition elements that bind to the target molecule simultaneously. One is immobilized on a solid support such as

beads or plates, and the other one is modified with enzymes. Using them, unbound molecular recognition elements modified with enzymes can be removed, and the target molecule can be detected without the need to label target molecules via enzyme activity measurements (Fig. 2). There have been many reports that describe the sandwich assay (Han et al., 2010) and many types of enzymes have been mentioned in these reports, as we will discuss later. Sometimes, the aptamers modified with enzymes are used as detection reagents, and antibodies are used for capturing the target reagent. A chemical crosslink is required when antibodies are modified with enzymes, and it often causes a loss of function. However, since aptamers can be easily modified with various molecules, they can simply be connected with any enzyme via interaction with modified molecules and their partner molecules, such as biotin and avidin.

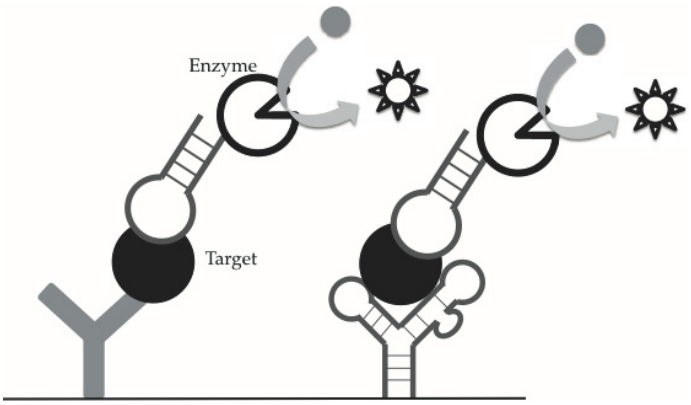

Fig. 2. Sandwich assay using an aptamer. On the left side, the antibody is used as a capture reagent and the enzyme-modified aptamer is used as a detection reagent. On the right side, different aptamers are used as capture reagents and detection reagents. For the sandwich assay, both reagents should recognize different regions of the target protein if the target protein is not a homomultimeric protein.

2.1.2 B/F separation based on a single aptamer

Since the sandwich assay requires two molecular recognition elements that can bind to the target molecule simultaneously, it is difficult to apply it to the sensing of small molecules and proteins that have only one superior molecular recognition element. Therefore, we constructed a simple B/F separation system based on single aptamers using a conformational change of aptamer. This system consists of two parts: an aptamer and its complementary DNA. We previously described two types of single aptamer-based B/F separation systems (Abe et al., 2011; Fukasawa et al., 2009; Ogasawara et al., 2009) (Fig. 3).

The first type of system makes use of the stability feature of aptamers by providing target molecules so that the aptamer will bind to them and stabilize its structure (Fig. 3(a)). Structures of aptamers are destabilized by repulsion between negative charges. Therefore, an aptamer can be easily hybridized with its complementary DNA without target molecule binding. On the other hand, since target binding stabilizes the whole structure of the aptamer, the aptamer-target complex inhibits hybridization with complementary DNA. We designed a complementary DNA named CaDNA that will bind to a part of an aptamer that

is amenable to hybridization inhibition upon binding to the aptamer target. We modified the aptamer with an avidin-conjugated enzyme and we succeeded in detecting thrombin, IgE (Fukasawa et al., 2009), and vascular endothelial growth factor (VEGF) (in preparation) via enzymatic activity measurement.

The second system makes use of the structural changes that aptamers undergo upon binding to their target molecules (Fig. 3(b)). We created a "capturable" aptamer by adding a sequence to it that gave it a new structure. Capturable aptamers cannot hybridize with CaDNA unless their target molecules are present. In this case, the structure of a capturable aptamer in the presence of its target molecule changes to a different structure from that which was present in the absence of the target molecule. We succeeded in the design of a capturable aptamer for thrombin (Abe et al., 2011) and a mouse prion protein (Ogasawara et al., 2009). In these studies, although fluorescent labeling was used for detection, enzyme labeling enabled a 10-fold lower detection of mouse prion protein than fluorescent labeling (unpublished data).

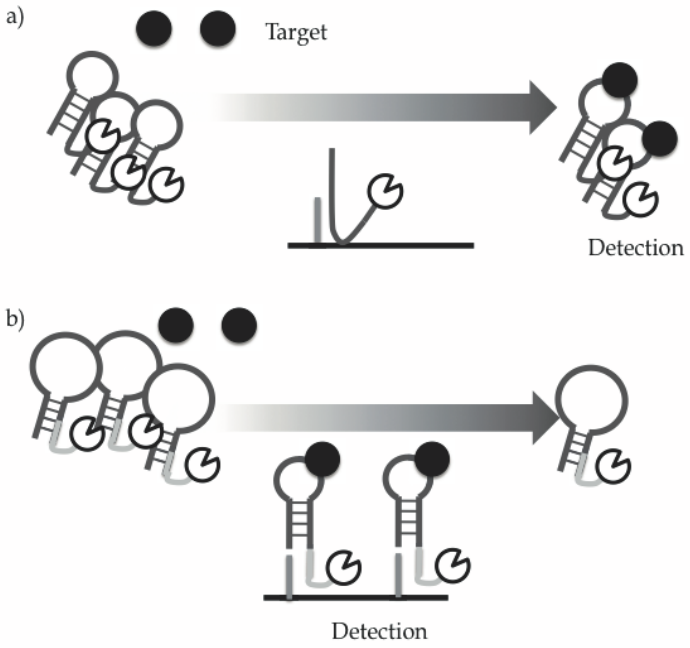

Fig. 3. The scheme of a single aptamer-based B/F separation system. (a) In the absence of a target molecule, the aptamers are trapped by the immobilized beads containing CaDNA, whereas in the presence of the target protein, aptamers that bind to the target are not trapped. The target protein can therefore be detected by means of simple B/F separations, and by measuring the fluorescence or enzymatic activity of the labeled aptamer in the supernatant. (b) The aptamer, which is able to be captured, undergoes a conformational change upon binding to the target molecule. This change induces the exposure of a partial single-strand that hybridizes with the CaDNA. Otherwise, any unbound capturable aptamer does not hybridize with the CaDNA and is removed by the bound/free separation.

Of these two types of single aptamer-based B/F separation systems, the first can be easily designed, because it does not require any additional sequences, whereas the second system requires careful design of the additional sequence of the aptamer with structural prediction. However, the benefit of the second system is that it can eliminate many interfering compounds. The first system can eliminate enzyme-modified aptamers that do not bind to the target molecule, but it is difficult to eliminate interfering compounds because aptamers that bind to the target molecule are present in the supernatant. It is therefore necessary to select a particular system to suit the needs of each particular target molecule.
Wei et al. reported a different type of single aptamer based B/F separation system without complementary DNA being present (Wei & Ho, 2009). They utilized steric hindrance between enzyme-modified antibodies and antigen-modified target-binding aptamers. They used fluorescein-modified aptamers and anti-fluorescein horseradish peroxidase (HRP)-conjugated antibody. The antibody cannot bind to the fluorescein-modified aptamer due to steric hindrance without its target molecule. The aptamers change conformation upon binding to the target molecule, and then the antibodies can bind to them. Since the aptamers were immobilized on the solid support, this sensing system enabled B/F separation to occur using an aptamer.

2.2 Homogeneous sensing

To measure the target molecules without B/F separation, regulation of signal output is required. Jhaveri et al. reported aptamers that changed their structure upon binding to the target molecule, which resulted in the regulation of fluorescent signals (Jhaveri et al., 2000). If we can introduce enzyme signal amplification into a signaling aptamer, a highly sensitive detection can be performed without the need for B/F separation. Reported homogeneous detection systems using enzymes are based on two strategies: enzyme activity regulation by the target molecule, and DNA amplification accompanied by the target molecule binding to aptamers.

2.2.1 Enzyme activity regulation by the target molecule

If we can find an enzyme that catalyzes a reaction with a target molecule, we can construct an effective sensing system such as the glucose sensor, which is already on the market and is being used daily. However, it is difficult to screen an enzyme that reacts with a given target molecule. Protein engineering allows us to improve the enzyme substrate specificity, and we have reported such examples (Igarashi et al., 2004), but it is still difficult to change the substrate specificity dramatically. Then we constructed an enzyme that has a novel subunit that can regulate enzymatic activity allosterically based on the aptamer. If the target molecule activates enzymatic activity, we can quantify the target molecule via an enzyme activity measurement. We named this sensing system the Aptameric Enzyme Subunit (AES) (Ikebukuro et al., 2008; Yoshida et al., 2009; Yoshida et al., 2006a, b, 2008).
An AES consists of two aptamers: an enzyme-inhibiting aptamer and a target molecule-binding aptamer. The enzyme does not generate signals because the AES inhibits enzymatic activity when it is not bound to the target molecules. However, upon binding of the target molecules to the AES, the AES changes its conformation, which results in a loss of enzyme inhibitory activity. Then we can measure the target molecule concentration via enzyme activity measurements without the need for B/F separation. Therefore, an AES acts as an enzyme subunit that can regulate its activity via the target molecule binding allosterically.

Figure 4 shows a design strategy for an AES. To act as an AES, the binding ability of an enzyme-inhibiting moiety against an enzyme should decrease upon binding of the target molecule to the target molecule-binding moiety. We used a 31-mer thrombin-binding aptamer (TBA) that we optimized as the enzyme-inhibiting aptamer (Fig. 4(a)) (Ikebukuro et al. 2005b). The TBA forms a G-quadruplex structure that plays an important role in its inhibitory activity. Then we inserted the target molecule-binding moiety into a loop region of the G-quadruplex that does not critically affect its binding ability against thrombin. This was done by inserting the DNA-binding domain into the TBA (Yoshida et al., 2006b) (Fig. 4(b)). DNA binding would disrupt the TBA's structure, resulting in an increase of thrombin activity. Next, we inserted an adenosine-binding aptamer into the TBA (Yoshida et al., 2006a) (Fig. 4(c)). We expected that adenosine binding would stabilize the TBA structure rather than disrupt it. As expected, we observed a decrease in thrombin activity that was dependent on the adenosine concentration. However, it was not obvious whether most aptamer stabilization occurred because of the aptamer's structure, or whether there was also influence from the TBA's structure upon binding to the target molecule. Then, we designed different types of AESs for the purpose of universal molecule sensing (Fig. 4(d)).

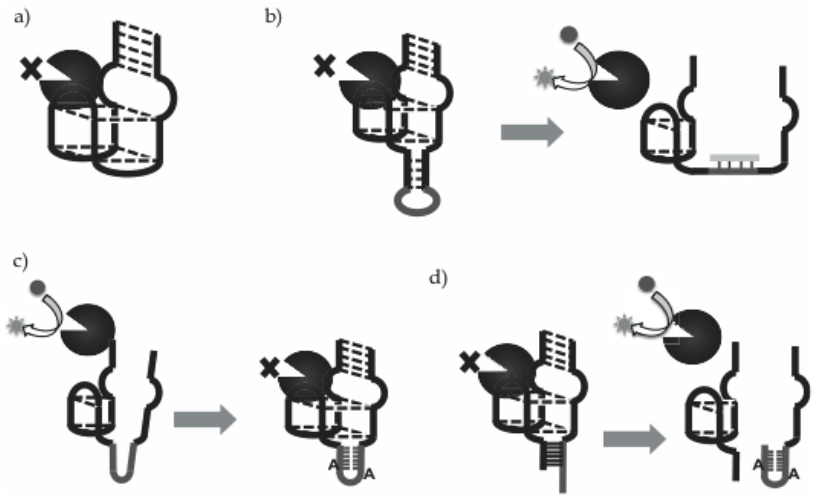

Fig. 4. Aptameric enzyme subunits using a thrombin-inhibiting aptamer. The target-binding aptamer was inserted into a loop of thrombin-inhibiting aptamer that was not a critical region for thrombin recognition. a) The structure of 31-mer thrombin-inhibiting aptamer b) The AES inhibits thrombin activity without a target DNA. Target DNA hybridization induces a destruction of the structure of thrombin-inhibiting aptamer, resulting in an increase of thrombin activity. c) There is more inhibition of thrombin activity when the AES binds to the target molecule as compared to when there is no target binding. d) The AES inhibits thrombin activity without a target molecule. Target molecule binding induces a break in hybridization between the target molecule binding aptamer and additional complementary DNA, resulting in an increase of thrombin activity.

We split the TBA into two parts in the same region where a target-binding aptamer was inserted. One strand is connected with the target-binding aptamer and another strand is

connected with its complementary strand (Fig. 4(d)). Without the target molecule, the target-binding aptamer moiety hybridizes with its complementary strand, which results in the stabilization of the TBA conformation. Then the TBA moiety inhibits thrombin enzymatic activity. Target molecule binding disrupts complementary base pairing and results in a single-stranded nucleic acid structure, which would destabilize the structure of TBA and increase thrombin enzymatic activity. Compared with former AESs, we would be able to design a type of AES that is easily split. We succeeded in designing a type of split AES for sensing adenosine (Yoshida et al., 2006a), IgE (Yoshida et al., 2008) and insulin (Yoshida et al., 2009).

Chelyapov and Fletcher et al. reported similar sensing systems for AESs (Chelyapov, 2006; Fletcher et al., 2010). Chelyapov used an aptamer that inhibited Russell's viper venom factor X activator (RVV-X), and Fletcher et al. used an aptamer that inhibited *Eco*RI.

AESs are advantageous because they sense rapidly and easily. Target molecule binding transduces enzymatic activity immediately. In addition, an AES does not require the modification of an enzyme with an aptamer. Therefore, enzymatic activity can be fully utilized. To design AESs for highly sensitive detection, it is most important that the aptamer has powerful enzyme inhibitory activity. When we used an aptamer with weak inhibitory activity, we had to add a large quantity of it in order to completely inhibit thrombin activity. Then most of the aptamer in solution will not bind to enzyme It is difficult to detect low concentrations of target molecules because target molecules bind to AESs that do not bind to enzyme. Therefore, we should use enzyme-inhibiting aptamers that have a high inhibitory activity.

2.2.2 Real-time PCR or RCA assay

Fredriksson et al. reported a proximity ligation assay (PLA) (Fredriksson et al., 2002). The PLA depends on the simultaneous and proximate recognition of target molecules by pairs of affinity probes modified with oligonucleotides. Each modified oligonucleotide can be hybridized with connector DNA, resulting in the formation of amplifiable DNA through ligation between modified oligonucleotides. Then we can detect target molecules through PCR amplification without B/F separation. Fredriksson et al. reported a PLA using an aptamer (Fig. 5(a)). Although PLA and immuno-PCR require oligonucleotide modification with affinity probes, oligonucleotide modification with an antibody is a cumbersome process. On the other hand, the aptamer can be easily connected to oligonucleotides by DNA synthesis. Therefore, the aptamer is more suitable for immuno-PCR and the PLA than the antibody.

Di Giusto et al. reported protein detection by rolling cycle amplification (RCA) based on proximity extension (Di Giusto, 2005) (Fig. 5(b)). This method used a circular aptamer and an aptamer that had a complimentary sequence with a part of a circular aptamer that could bind to the target molecule simultaneously. They reported circularization of the aptamer, enabling it to stabilize without loss of function. When both aptamers bind to the target molecule, complementary DNA hybridizes with a part of the circular DNA, and the rolling cycle amplification reaction starts. This method can detect protein, without the need for carrying out B/F separation or ligation.

Although proximity ligation or an extension assay will achieve highly sensitive detection of proteins without B/F separation, they require two aptamers that can bind to the target molecule simultaneously. There are some reports of protein detection by PCR or RCA that employs the conformational change of an aptamer. For PCR, binding to the target molecule

should induce a conformational change of the aptamer, and when the aptamer hybridizes to its complementary DNA, this will serve as a primer binding site (Yang & Ellington, 2008) (Fig. 5(c)). Then we can detect the target molecule by ligation of the aptamer to complementary DNA followed by PCR amplification. On the other hand, for RCA, Yang et al. designed an aptamer sequence for proximity ligation within the internal aptamer (Yang et al., 2007) (Fig. 5(d)). Upon binding of the target molecule, both the 5′ end and 3′ end form a stem and join with each other. Then an aptamer is formed by ligation of circular DNA, and it is amplified by RCA

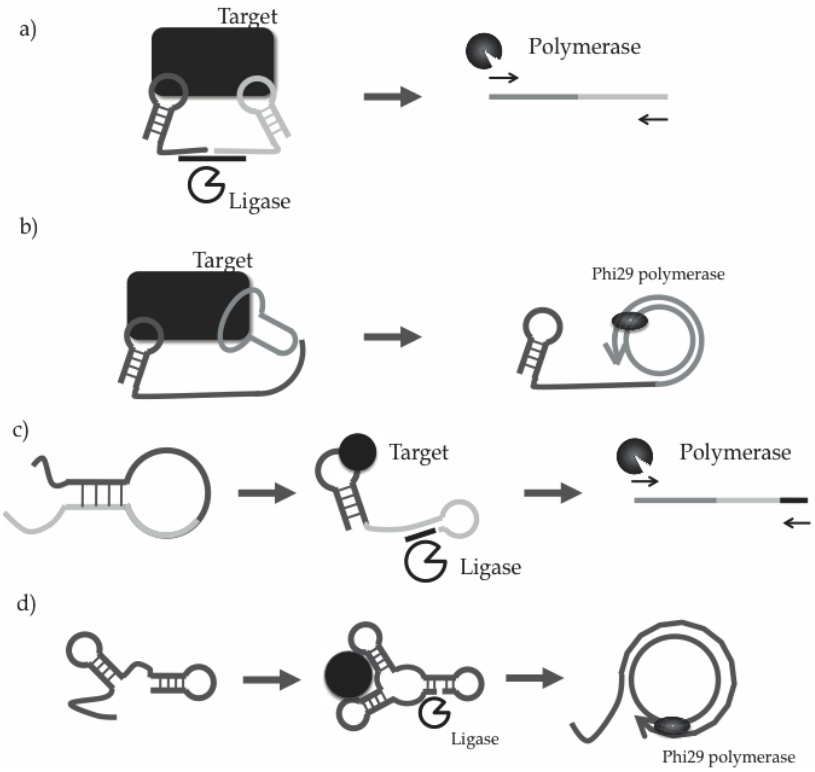

Fig. 5. Biosensing based on different methods of DNA amplification, accompanied by target molecule binding. a) Proximity ligation assay. Two aptamers are ligated after binding to the proximate site of target molecules, resulting in the detection of the target through PCR amplification. b) Proximity extension assay. An aptamer is circularized and a primer sequence that is complementary to a part of the circularized aptamer is added to the other aptamer. Proximate binding of both aptamers to the target molecules induce a RCA reaction. c) Target molecule binding induces a conformational change in the aptamers. Then, the aptamer hybridizes and ligates with probe DNA, resulting in the formation of amplifiable DNA, which enables detection of the target through PCR amplification. d) Target molecule binding induces a conformational change of the aptamer, resulting in the formation of circular DNA by intramolecular ligation. Circular DNA is amplified by RCA.

Conformational change of an aptamer is an attractive strategy for biosensing because only one aptamer is required. However, to design drastic conformational changes of the aptamer would be time-consuming. Although there are many reports of biosensing using conformational changes of aptamers, only a few target protein-binding aptamers are used because their conformational changes have been thoroughly studied. Wu et al. reported a universal aptamer sensing system using RCA (Wu et al., 2010). As previously mentioned, the structure of aptamers is stabilized upon binding to a target molecule, resulting in inhibition of hybridization with the captured DNA that is a part of the complimentary DNA of the aptamer. Wu et al. utilized free capture DNA that was not hybridized with an aptamer for formation of circular DNA by ligation, followed by RCA. This sensing system does not require careful design of the aptamer's desired conformational change. However, the addition of DNA to an aptamer or hybridization with an aptamer before target molecule binding results in decreasing binding affinity of the aptamer.

3. Transduction of binding events into measurable signals by enzymes

Enzymes can transduce binding events to various measurable signals and amplify them. As mentioned above, enzymes are combined with aptamer sensors using various sensing schemes. Table 1 shows a list of enzymes combined with aptamer sensors. There are many reports that aptamer sensors have been combined with ribozyme or deoxyribozyme (Breaker, 2002; Kuwabara et al., 2000). (Deoxy)ribozyme is attractive for use as a labelling tool of aptamer sensors because it can easily be connected to an aptamer by synthesis, whereas enzyme connections often require chemical crosslinking that sometimes causes a decrease in enzymatic activity. However, compared with enzymes, there is limited use for (deoxy)ribozyme combinations in detection schemes because their activities are much less than that of enzymes and they catalyze fewer types of reactions than enzymes. In the following subsection, we describe the features of enzymes and detection schemes. We have focused on electrochemical biosensors because they can be constructed with low cost and high sensitivity.

3.1 Oxidoreductase

Electrochemical sensing applications using aptamers are rapidly increasing (Cho et al., 2009). Electrochemical sensing systems enable highly sensitive detection of target molecules, and these systems can be readily miniaturized at a low cost. Therefore, an electrochemical sensing system is suitable for POCT. In fact, the most frequently used biosensor is a glucose biosensor, based on electrochemical sensing using glucose dehydrogenase. Since glucose-sensing systems are well-established and used commercially, they are attractive tools for sensing systems of various biomarkers that use aptamers.

We first reported thrombin sensing using an aptamer conjugated with pyrroloquinoline quinone-dependent glucose dehydrogenase (PQQGDH) (Ikebukuro et al., 2004; Ikebukuro et al., 2005a). PQQGDH has a high catalytic activity (about 5000 U/mg protein). We used glutaraldehyde to crosslink PQQGDH with avidin. Biotin-modified aptamers were labeled by PQQGDH through avidin-biotin interaction. Thiol-modified aptamers were immobilized on an Au electrode. A sandwich structure was formed on the Au electrode, and we observed a current that was dependent on the target molecule concentration via PQQGDH activity mediated by 1-methoxy-5-methylphenazinium methyl sulfate with a low detection limit of 10 nM. However, cross-linking between PQQGDH and avidin resulted in a decrease in enzymatic activity. Then we reported the accomplishment of PQQGDH labeling without

Name	Detection type
Polymerase	Fluorescence
Phi29 polymerase	Fluorescence or electrochemical
Dehydrogenase	Electrochemical
Peroxidase (HRP)	Electrochemical, Chemiluminescence or Fluorescence
Alkaliphosphatase	Electrochemical, Chemiluminescence or Fluorescence
Nuclease	Fluorescence
Protease	Fluorescence or others

Table 1. Enzyme list for signal amplification in aptamer sensors

crosslinking using a PQQGDH-binding aptamer (Abe et al., 2010; Osawa et al., 2009). The PQQGDH-binding aptamer that we screened was bound to PQQGDH with high affinity (K_d: c.a. 40 nM) and specificity, and it did not affect PQQGDH activity. Enzyme labeling of target-binding aptamer via noncovalent bonding with enzyme-binding aptamer would help us to make a construct for highly sensitive detection.

3.2 Polymerase

Since the development of Immuno-PCR in 1992 (Sano et al., 1992), polymerases have been used as biosensor signal amplification tools. As contrasted with the cumbersome step of antibody modification using oligonucleotides, aptamers are easily applicable to similar assays that use immuno-PCR. If the aptamer has sufficient length for primer binding, it can be amplified directly (Fischer et al., 2008). Since a PCR reaction can amplify DNA exponentially, signal amplification by polymerase enables more highly sensitive detection than by ELISA. The limit of detection of a given ELISA is, in general, enhanced 100 to 10000-fold by the use of PCR as a signal amplification system. The disadvantage of PCR is the requirement of a longer reaction time than for other enzyme reactions. Many researchers have attempted time reduction of PCR, and they succeeded in a PCR that took 20 minutes using Lab-on-a-chip technology (Kim et al., 2009; Kopp et al., 1998).

Phi29 polymerase has been used to catalyze RCA, and it is also used for signal amplification. As contrasted with a typical DNA polymerase, Phi29 polymerase can amplify hundreds of copies of a circular DNA template isothermally. This unique amplification was utilized for biosensing that could not be performed by a typical DNA polymerase. Isothermal amplification has a great advantage for use with biosensing because there is no requirement for specific devices.

The reaction products are ordinarily measured by fluorescence using Sybr® Green I or a related molecule that can generate a fluorescent signal upon specific recognition of double-stranded DNA. In addition, since RCA can isothermally produce a long strand of DNA that is connected to the aptamer, the aptamer can be labelled by fluorescence or enzymatic methods via DNA probe hybridization. A molecular beacon that can recognize DNA with more specificity than Sybr® Green I and can generate a fluorescent signal upon DNA binding will enable real-time detection with high specificity. Since RCA products have many probe binding

sites, multiple enzyme labelling in a RCA product will enable a 10 to 100-fold signal amplification compared with modification of an aptamer with an enzyme (Zhou et al., 2007).

3.3 Alkaline phosphatase and horseradish peroxidase

Alkaline phosphatase (ALP) and HRP are mainly used as biosensors when combined with an antibody and an aptamer. The most important advantage of these enzymes is that we can use commercial avidin conjugates, as well as commercial antibody conjugates. Then we can easily apply them to various sensing systems.

ALP catalyzes the dephosphorylation of various substrates, and is used in various sensing systems such as chemiluminescent detection, fluorescence detection and electrochemical detection. ALP allows a nonreductive substrate, ascorbic acid 2-phosphate, to be converted into reducing agent ascorbic acid at an electrode's surface. Finally, silver ions were reduced and deposited on the electrode surface as metallic silver, which was determined by linear sweep voltammetry. Zhou et al. combined RCA, to be used for the detection of Platelet-Derived Growth Factor (PDGF), with ALP by using an electrochemical assay based on silver deposition (Zhou et al., 2007). They succeeded in the detection of PDGF with a low detection limit of 10 fM. Xiang et al. combined diaphorase with ALP for further signal amplification (Xiang et al., 2010). They used *p*-aminophenylphosphate (*p*-APP) as a substrate for ALP. ALP catalyzes the dephosphorylation of *p*-APP to *p*-aminophenol (*p*-AP), and the *p*-AP was then subjected to an electrochemical oxidation process that caused it to change to *p*-quinonimine (*p*-QI) on the electrode. Diaphorase catalyzes the reduction of *p*-QI to *p*-AP, coupled with NADH oxidation. Successful thrombin detection occurred with a low detection limit of 8.3 fM. The dual amplified detection strategy substantially lowered the detection limit by four orders of magnitude compared to common single enzyme-based schemes.

HRP catalyzes reduction of various substrates that is accompanied by hydrogen peroxide oxidation. Using a specific mediator such as 3,3',5,5'-tetramethylbenzidine (TMB), HRP has been applied to electrochemical detection. TMB was also used for enhancement of surface plasmon resonance imaging (SPRI) (Li et al., 2007).

3.4 Nuclease

Specific nucleases are used for fluorescence signal amplification using a molecular beacon as the substrate. The molecular beacon is a stem-loop type of DNA that is labeled with a fluorescent molecule and has a quencher at each termini (Tyagi & Kramer, 1996). Although fluorescence is quenched with stem-loop structure formation, fluorescence is observed upon binding to the target DNA or the target molecule when structural disruption of the molecular beacon is induced. Although most molecular beacons bind to DNA, we can design the transduction of any molecule by controlling the binding event of the molecule to an aptamer so that specific DNA signals are transmitted, which are then detected by a molecular beacon. A simple example is the modification of complementary DNA of a molecular beacon with an aptamer in a sandwich assay. Xue et al. used Nb.*BbvC* I, which is one of the nick-end labeling nucleases used for fluorescence signal amplification (Xue et al., 2010). The molecular beacon recognizes the modified DNA of the aptamer, and then Nb.*BbvC* I cleaves the hybrid of the molecular beacon with the aptamer. Since Nb.*BbvC* I introduces a nick to the strands of the molecular beacon, the molecular beacon then dissociates from the aptamer. The released target strand could then hybridize to another

molecular beacon and initiate a second cycle of cleavage. Each DNA strand modified by an aptamer has the capability to go through many such cycles.
Fletcher et al. also used a molecular beacon inserted into the *Eco*RI recognition sequence (Fletcher et al., 2010). They used *Eco*RI to inhibit the aptamer and DNA, which consisted of target-binding of the DNA and the complementary DNA of *Eco*RI that would inhibit the aptamer. The binding of the target DNA induces hybridization of the complementary DNA to the *Eco*RI-inhibiting aptamer, resulting in an increase of fluorescence via cleaving of the molecular beacon by active *Eco*RI.

3.4 Protease

Since TBA is well characterized, some researchers, including ourselves, have used thrombin as a detection enzyme, utilizing ability of TBA inhibiting thrombin activity (Pavlov et al., 2005; Yoshida et al., 2006a). Protease activity was measured using a synthetic peptide labeled with a fluorescent molecule as the substrate. In the case of a protease such as thrombin and RVV-X factor X activator, we can measure protease activity via observation of the coagulation that results from enzymatic activity. Chelyapov constructed a biosensor that can evaluate RVV-X activity with the naked eye, using microspheres for signal amplification (Chelyapov, 2006). Chelyapov succeeded in the detection of VEGF with a low detection limit of 5 fmol. Despite semi-quantitative or qualitative assays, visible detection is suitable for POCT because it does not require specific devices.

4. Conclusion

Many aptamer sensors have been reported for the past two decades. However, antibodies are still commonly used for diagnostics because unlike aptamers, many kinds of antibodies can be utilized. Although different kinds of aptamers have been increasing every year, it is difficult to replace aptamer sensors with existing antibody-based devices. Therefore, we should not use aptamers as alternatives for antibodies, but instead, we should utilize their unique properties accompanied with their molecular structure for constructing sensors. There is a strong need for aptamer sensors to be developed for theranostics and POCT, since there is substantial growth in the demand for biomarkers that will be used in drug development and in vitro diagnosis.
As mentioned above, certain properties of aptamers enable us to construct biosensors that are suitable for POCT. They can easily measure target molecules with high sensitivity and rapidity. Aptamers enable us to construct homogeneous biosensors that can use any enzyme. Most homogeneous sensing systems that use antibodies require specific devices or are based on the aggregation of beads, resulting in a sandwich formation. However, we can construct various homogeneous biosensors, including those based on electrochemical systems, utilizing various enzyme activities. The AES is a most ideal sensing system because it can amplify signals without any cumbersome processes, although optimization would require rigorous control of the structural change of the aptamer in order to enable highly sensitive detection. If we can obtain the aptamer that inhibits glucose dehydrogenase, we would be able to construct attractive biosensors.
One of advantages of aptamers for theranostics is that they can measure target molecules by binding to them. Homogeneous detection with capturable aptamers enable the detection of a target molecule using a single aptamer. We can detect any molecules, from cells to small molecules, based on the same sensing strategies, and we do not have to select and optimize

two affinity probes. As a short-term goal, we should develop biosensors for novel biomarkers, since aptamers would be excellent candidates for affinity probes that facilitate the construction of a biosensing system for any biomarker.

5. Acknowledgment

This work was supported by the 2009 Industrial Technology Research Grant Program of the New Energy and Industrial Technology Development Organization (NEDO) of Japan.

6. References

Abe, K.; Ogasawara, D.; Yoshida, W.; Sode, K. & Ikebukuro, K., (2011). Aptameric sensors based on structural change for diagnosis. Faraday Discuss. Vol. 149, pp. 93-106.

Abe, K.; Sode, K. & Ikebukuro, K., (2010). Constructing an improved pyrroloquinoline quinone glucose dehydrogenase binding aptamer for enzyme labeling. Biotechnol. Lett. Vol. 32, No. 9, pp. 1293-1298.

Berezovski, M.V.; Lechmann, M.; Musheev, M.U.; Mak, T.W. & Krylov, S.N., (2008). Aptamer-facilitated biomarker discovery (AptaBiD). J. Am. Chem. Soc. Vol. 130, No. 28, pp. 9137-9143.

Breaker, R.R., (2002). Engineered allosteric ribozymes as biosensor components. Curr. Opin. Biotechnol. Vol. 13, No. 1, pp. 31-39.

Chelyapov, N., (2006). Allosteric Aptamers Controlling a Signal Amplification Cascade Allow Visual Detection of Molecules at Picomolar Concentrations†. Biochemistry Vol. 45, No. 7, pp. 2461-2466.

Cho, E.J.; Lee, J.W. & Ellington, A.D., (2009). Applications of aptamers as sensors. Annu. Rev. Anal. Chem. Vol. 2, pp. 241-264.

Cox, J.C. & Ellington, A.D., (2001). Automated selection of anti-protein aptamers. Bioorg. Med. Chem. Vol. 9, No. 10, pp. 2525-2531.

Di Giusto, D.A., (2005). Proximity extension of circular DNA aptamers with real-time protein detection. Nucleic. Acids. Res. Vol. 33, No. 6, pp. e64.

Ellington, A.D. & Szostak, J.W., (1990). In vitro selection of RNA molecules that bind specific ligands. Nature Vol. 346, No. 6287, pp. 818-822.

Fischer, N.; Tarasow, T. & Tok, J., (2008). Protein detection via direct enzymatic amplification of short DNA aptamers. Anal. Biochem. Vol. 373, No. 1, pp. 121-128.

Fletcher, S.J.; Phillips, L.W.; Milligan, A.S. & Rodda, S.J., (2010). Toward specific detection of Dengue virus serotypes using a novel modular biosensor. Biosen. Bioelectron. Vol. 26, No. 4, pp. 1696-1700.

Fredriksson, S.; Gullberg, M.; Jarvius, J.; Olsson, C.; Pietras, K.; Gústafsdóttir, S.; Östman, A. & Landegren, U., (2002). Protein detection using proximity-dependent DNA ligation assays. Nat. Biotechnol. Vol. 20, No. 5, pp. 473-477.

Fukasawa, M.; Yoshida, W.; Yamazaki, H.; Sode, K. & Ikebukuro, K., (2009). An Aptamer-Based Bound/Free Separation System for Protein Detection. Electroanalysis Vol. 21, No. 11, pp. 1297-1302.

Han, K.; Liang, Z.Q. & Zhou, N.D., (2010). Design Strategies for Aptamer-Based Biosensors. Sensors Vol. 10, No. 5, pp. 4541-4557.

Igarashi, S.; Okuda, J.; Ikebukuro, K. & Sode, K., (2004). Molecular engineering of PQQGDH and its applications. Arch. Biochem. Biophys. Vol. 428, No. 1, pp. 52-63.

Ikebukuro, K.; Kiyohara, C. & Sode, K., (2004). Electrochemical detection of protein using a double aptamer sandwich. Anal. Lett. Vol. 37, No. 14, pp. 2901-2909.

Ikebukuro, K.; Kiyohara, C. & Sode, K., (2005a). Novel electrochemical sensor system for protein using the aptamers in sandwich manner. Biosens. Bioelectron. Vol. 20, No. 10, pp. 2168-2172.

Ikebukuro, K.; Okumura, Y.; Sumikura, K. & Karube, I., (2005b). A novel method of screening thrombin-inhibiting DNA aptamers using an evolution-mimicking algorithm. Nucleic. Acids. Res. Vol. 33, No. 12, pp. e108.

Ikebukuro, K.; Yoshida, W.; Noma, T. & Sode, K., (2006). Analysis of the evolution of the thrombin-inhibiting DNA aptamers using a genetic algorithm. Biotechnol. Lett. Vol. 28, No. 23, pp. 1933-1937.

Ikebukuro, K.; Yoshida, W. & Sode, K., (2008). Aptameric enzyme subunit for homogeneous DNA sensing. Biotechnol. Lett. Vol. 30, No. 2, pp. 243-252.

Jhaveri, S.; Kirby, R.; Conrad, R.; Maglott, E.; Bowser, M.; Kennedy, R.; Glick, G. & Ellington, A., (2000). Designed signaling aptamers that transduce molecular recognition to changes in fluorescence intensity. J. Am. Chem. Soc Vol. 122, No. 11, pp. 2469-2473.

Kim, H.; Dixit, S.; Green, C.J & Faris, G.W., (2009). Nanodroplet real-time PCR system with laser assisted heating. Optics Express Vol. 17, No. 1, pp. 218-227

Knight, C.G.; Platt, M.; Rowe, W.; Wedge, D.C.; Khan, F.; Day, P.J.; McShea, A.; Knowles, J. & Kell, D.B., (2009). Array-based evolution of DNA aptamers allows modelling of an explicit sequence-fitness landscape. Nucleic. Acids. Res. Vol. 37, No. 1, pp. e6.

Kopp, M.U.; Mello, A.J. & Manz, A., (1998). Chemical amplification: continuous-flow PCR on a chip. Science Vol. 280, No. 5366, pp. 1046-1048.

Kuwabara, T.; Warashina, M. & Taira, K., (2000). Allosterically controllable ribozymes with biosensor functions. Curr. Opin. Chem. Biol. Vol. 4, No. 6, pp. 669-677.

Li, D.; Song, S. & Fan, C., (2010). Target-responsive structural switching for nucleic acid-based sensors. Acc. Chem. Res. Vol. 43, No. 5, pp. 631-641.

Li, Y.; Lee, H.J. & Corn, R.M., (2007). Detection of protein biomarkers using RNA aptamer microarrays and enzymatically amplified surface plasmon resonance imaging. Anal. Chem. Vol. 79, No. 3, pp. 1082-1088.

Noma, T. & Ikebukuro, K., (2006). Aptamer selection based on inhibitory activity using an evolution-mimicking algorithm. Biochem. Biophys. Res. Commun. Vol. 347, No. 1, pp. 226-231.

Noma, T.; Ikebukuro, K.; Sode, K.; Ohkubo, T.; Sakasegawa, Y.; Hachiya, N. & Kaneko, K., (2006a). A screening method for DNA aptamers that bind to specific, unidentified protein in tissue samples. Biotechnol. Lett. Vol. 28, No. 17, pp. 1377-1381.

Noma, T.; Sode, K. & Ikebukuro, K., (2006b). Characterization and application of aptamers for Taq DNA polymerase selected using an evolution-mimicking algorithm. Biotechnol. Lett. Vol. 28, No. 23, pp. 1939-1944.

Ogasawara, D.; Hachiya, N.S.; Kaneko, K.; Sode, K. & Ikebukuro, K., (2009). Detection system based on the conformational change in an aptamer and its application to simple bound/free separation. Biosens. Bioelectron. Vol. 24, No. 5, pp. 1372-1376.

Osawa, Y.; Takase, M.; Sode, K. & Ikebukuro, K., (2009). DNA Aptamers that Bind to PQQGDH as an Electrochemical Labeling Tool. Electroanalysis Vol. 21, No. 11, pp. 1303-1308.

Pavlov, V.; Shlyahovsky, B. & Willner, I., (2005). Fluorescence detection of DNA by the catalytic activation of an aptamer/thrombin complex. J. Am. Chem. Soc. Vol. 127, No. 18, pp. 6522-6523.

Pestourie, C.; Cerchia, L.; Gombert, K.; Aissouni, Y.; Boulay, J.; De Franciscis, V.; Libri, D.; Tavitian, B. & Duconge, F., (2006). Comparison of different strategies to select aptamers against a transmembrane protein target. Oligonucleotides Vol. 16, No. 4, pp. 323-335.

Sano, T.; Smith, C.L. & Cantor, C.R., (1992). Immuno-PCR: very sensitive antigen detection by means of specific antibody-DNA conjugates. Science Vol. 258, No. 5079, pp. 120-122.

Savory, N.; Abe, K.; Sode, K. & Ikebukuro, K., (2010). Selection of DNA aptamer against prostate specific antigen using a genetic algorithm and application to sensing. Biosens. Bioelectron. Vol. 26, No. 4, pp. 1386-1391.

Tuerk, C. & Gold, L., (1990). Systematic evolution of ligands by exponential enrichment: RNA ligands to bacteriophage T4 DNA polymerase. Science Vol. 249, No. 4968, pp. 505-510.

Tyagi, S. & Kramer, F.R., (1996). Molecular beacons: probes that fluoresce upon hybridization. Nat. Biotechnol. Vol. 14, No. 3, pp. 303-308.

Wei, F. & Ho, C.-M., (2009). Aptamer-based electrochemical biosensor for Botulinum neurotoxin. Anal. Bioanal. Chem. Vol. 393, No. 8, pp. 1943-1948.

Wu, Z.-S.; Zhang, S.; Zhou, H.; Shen, G.-L. & Yu, R., (2010). Universal aptameric system for highly sensitive detection of protein based on structure-switching-triggered rolling circle amplification. Anal. Chem. Vol. 82, No. 6, pp. 2221-2227.

Xiang, Y.; Zhang, Y.; Qian, X.; Chai, Y.; Wang, J. & Yuan, R., (2010). Ultrasensitive aptamer-based protein detection via a dual amplified biocatalytic strategy. Biosens. Bioelectron. Vol. 25, No. 11, pp. 2539-2542.

Xue, L.; Zhou, X. & Xing, D., (2010). Highly sensitive protein detection based on aptamer probe and isothermal nicking enzyme assisted fluorescence signal amplification. Chem. Commun. Vol. 46, No. 39, pp. 7373.

Yang, L. & Ellington, A., (2008). Real-time PCR detection of protein analytes with conformation-switching aptamers. Anal. Biochem. Vol. 380, No. 2, pp. 164-173.

Yang, L.; Fung, C.W.; Cho, E.J. & Ellington, A.D., (2007). Real-time rolling circle amplification for protein detection. Anal Chem Vol. 79, No. 9, pp. 3320-3329.

Yoshida, W.; Mochizuki, E.; Takase, M.; Hasegawa, H.; Morita, Y.; Yamazaki, H.; Sode, K. & Ikebukuro, K., (2009). Selection of DNA aptamers against insulin and construction of an aptameric enzyme subunit for insulin sensing. Biosens. Bioelectron. Vol. 24, No. 5, pp. 1116-1120.

Yoshida, W.; Sode, K. & Ikebukuro, K., (2006a). Aptameric enzyme subunit for biosensing based on enzymatic activity measurement. Anal. Chem. Vol. 78, No. 10, pp. 3296-3303.

Yoshida, W.; Sode, K. & Ikebukuro, K., (2006b). Homogeneous DNA sensing using enzyme-inhibiting DNA aptamers. Biochem. Biophys. Res. Commun. Vol. 348, No. 1, pp. 245-252.

Yoshida, W.; Sode, K. & Ikebukuro, K., (2008). Label-free homogeneous detection of immunoglobulin E by an aptameric enzyme subunit. Biotechnol. Lett. Vol. 30, No. 3, pp. 421-425.

Zhou, L.; Ou, L.-J.; Chu, X.; Shen, G.-L. & Yu, R.-Q., (2007). Aptamer-based rolling circle amplification: a platform for electrochemical detection of protein. Anal. Chem. Vol. 79, No. 19, pp. 7492-7500.

13

Enhancing the Performance of Surface-based Biosensors by AC Electrokinetic Effects - a Review

Protiva Rani Roy, Matthew R. Tomkins and Aristides Docoslis
Department of Chemical Engineering, Queen's University, Kingston, ON Canada

1. Introduction

Miniaturized surface based biosensors are a cost effective and portable means for the sensing of biologically active compounds. With advents in micro- and nanotechnology, the design of surface based biosensors can be adapted for various detection goals and for integration with multiple detection techniques. In particular, the issue of pathogen detection is an important challenge with applications in defence, health care, food safety, diagnostics and clinical research. The research of micro-fluidic analytical systems, such as surface based biosensors or "lab-on-a-chip" designs, have gained increasing popularity, not only due to the enhancement of the analytical performance, but also due to their reduced size, decreased consumption of reagents and the ability to integrate multiple technologies within a single device. Although conventional pathogen detection methods are well established, they are greatly restricted by the assay time. For pathogens that typically occur at low concentrations, the mass transfer required for detection is diffusion limited and incubation is often needed in order to enhance the concentration of the target analyte. AC electrokinetic effects provide a means for biosensors to detect pathogens quickly and at lower concentrations, thus overcoming these bottlenecks.

2. Overview of AC electrokinetic phenomena

AC electrokinetics deals with the movement of a particle and/or the fluid by means of an AC electric field and has received considerable attention for improving the capture of analytes. An example of an AC electrokinetic force is dielectrophoresis (DEP) where a non-uniform electric field acts on an uncharged particle. When acting on a fluid, AC electrokinetic forces can induce AC electroosmosis and AC electrothermal effects. These forces can create non-uniform streamlines to convex and mix (Li, 2004), or even to separate a mixture of particle sizes (Green & Morgan, 1998). Most bioparticles, such as cells and viruses, behave as dielectrically polarized particles in the presence of an external field. Using AC electric fields for particle manipulation offers several advantages, such as allowing operation at low voltages, which is important for portable devices and minimizing electrolysis and chemical reactions. The following will provide a brief overview of AC electrokinetic forces with applications for use in biosensors, as comprehensive reviews of AC electrokinetic forces in general are available elsewhere (Ramos *et al.*, 1998).

DEP is a force acting on the induced dipole of a polarizable particle in a suspending fluid in the presence of a non-uniform electric field (Pohl, 1951). It was first defined by Pohl in 1951, and was used to remove suspended particles from a polymer solution. Pethig & Markx (1997) provides a review of applied DEP in the field of biotechnology. In brief, if a particle, such as a bacterium or virus, is more polarizable than the surrounding medium, the particle undergoes positive DEP (pDEP) and tends towards areas of high electric field strength (Fig 1a–Left). If a particle is less polarizable than the surrounding medium, it undergoes negative DEP (nDEP) and tends towards areas of electric field minima (Fig 1a–Right).

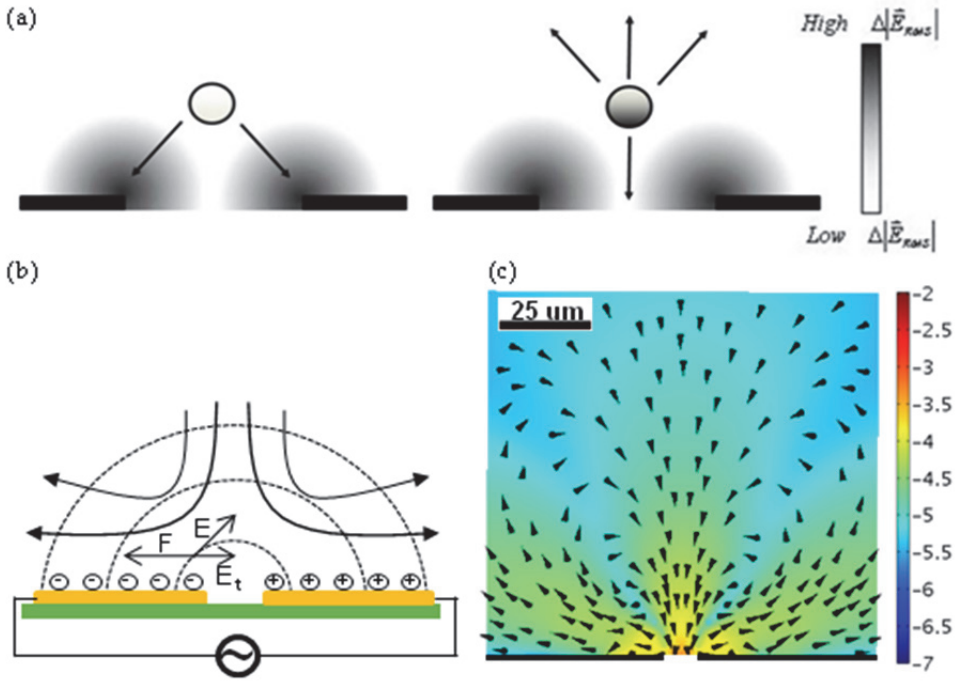

Fig. 1. AC electrokinetic effects generated by a pair of electrodes (horizontal gold or black bars) located on the surface of a non-conductive substrate. a) A schematic representation of a particle undergoing pDEP (left) and nDEP (right) in a non-uniform electric field. b) The reported mechanism for AC-electroosmosis where the arrows indicate fluid flow driven down towards the electrode gap and out along the surface of the electrode due to the force of the tangential component of the electric field on the ions in solution. Adapted from Morgan & Green (2003). c) Circulation pattern of fluid near the electrode edge created by electrothermal effects where the arrows indicate the net force on a suspended particle with an r_p of 200 nm. The colour intensity indicates the magnitude of the fluid velocity with an scale bar in $\log_{10}$m/s. The circulation zones appear to be similar to a microfluidic system subjected to AC electroosmotic flow. (Tomkins *et al.*, 2008).

The time averaged dielectrophoretic force for a spherical particle in an electric field with a constant phase is presented in equation 1.

$$< F_{DEP} >= 2\pi r_p^3 \,\mathrm{Re}\left[\frac{\varepsilon_p^* - \varepsilon_m^*}{\varepsilon_p^* + 2\varepsilon_m^*}\right]\nabla^2 \left|E_{RMS}\right|^2 \quad (1)$$

The equation shows that the DEP force (F) is a function of a particle's size (r_P), both the particle and the medium's complex permittivities (ε_p^* & ε_m^*) as well as the gradient of the applied electric field (E). Since the force of DEP varies with particle size and the electric field gradient, it allows for the separation between different sized cells. Alternatively, by measuring the velocities of single cells as a function of distance and voltage, DEP can be used to characterize their electrical properties (Pohl & Pethig, 1977; Burt *et al.*, 1990; Humberto *et al.*, 2008). However, the most attractive application of DEP is that it can be integrated within a biosensor with a pair of electrodes in order to amplify a pathogen's concentration at a sensor surface. The use of either pDEP or nDEP causes the deterministic motion of particles towards the desired location; yet, it is a short range force. The same electric field for applied DEP can have an effect on the medium as well by causing fluid flows and thereby overcoming limitations due to diffusion by enhancing the movement of particles from the bulk to the local area of the sensor (Sigurdson *et al.*, 2005).

AC electroosmosis and AC electrothermal effects produce similar flow patterns in some cases, but they are of different origin. AC electroosmotic flow is typically produced from the interaction of the nonuniform electric field and the diffuse electrical double layer formed by the polarization of the electrode by the counter ions in an electrolyte solution (Fig 1b). The tangential component of the electric field (E_t) at the electrode surface applies a force (F) on the ions present, pushing them out across the surface of the electrode and thus dragging fluid down into the center of the gap. The time averaged fluid velocity due to AC electroosmosis is presented in equation 2.

$$< u_x >= \frac{1}{2}\mathrm{Re}\left[\frac{\sigma_{qo} E_t^*}{\eta\kappa}\right] \quad (2)$$

AC electroosmosis is a function of the surface charge density (σ_{qo}), fluid viscosity (η) and the reciprocal debye length (κ). At low frequencies, the majority of the potential drop occurs at the double layer near the electrodes. Therefore, the remaining voltage drop across the electrodes is small in comparison and since the tangential component of the electric field must be continuous the resulting velocity due to AC electroosmosis is negligible. At high frequencies, the potential across the double layer is very small and results in virtually no induced charge, again causing negligible AC electroosmosis effects. AC electroosmosis dominates at frequencies between 100 and 100,000 Hz while above 100,000 Hz, AC electrothermal flow is predominant. AC electrothermal flow arises by uneven Joule heating of the fluid, which gives rise to nonuniformities in conductivity and permittivity. These nonuniformities interact with the electric field to generate flow, often in circulating patterns (Fig. 1c) (Feng *et al.*, 2007). The time averaged body force on the medium responsible for the generation of AC electrothermal fluid flow for a constant phase electric field is presented in equation 3.

$$< \vec{f}_e >= \frac{1}{2}\frac{\varepsilon_m(\alpha - \beta)}{\sigma_m^2 + (\omega\tau_{CR})^2}(\nabla T \cdot \vec{E})\vec{E} - \frac{1}{4}\varepsilon_m \alpha \left|\vec{E}\right|^2 \nabla T \quad (3)$$

AC electrothermal fluid flow is a function of: α and β the effects of temperature on the gradients of permittivity and conductivity respectively; and τ_{CR}, the charge relaxation time of the medium defined as the ratio of a medium's permittivity to its conductivity. The first term on the right hand side of equation 3 is the Coloumbic contribution while the second term is the dielectric contribution to the total force. The Columbic term dominates at frequencies below the charge relaxation time.

Due to the range of effective frequencies, voltages and ease of application, a number of researchers have proposed techniques to enhance the activity of microfluidic sensors by using AC electrohydrodynamic flows (Sigurdson *et al.*, 2005; Hoettges *et al.*, 2003; Gagnon & Chang, 2005; Wu *et al.*, 2005a; Sauli *et al.*, 2005; Hou *et al.*, 2007; Wu *et al.*, 2005b). This chapter will review the use of AC electrokinetics to develop biosensors for pathogens as well as the different detection techniques employed.

3. Manipulation of bioparticles by AC Electrokinetics

Before surface based biosensors can identify a target bioparticle, that bioparticle must first move from the bulk sample towards the sensing element and then become captured or detected. As demonstrated in the previous section, AC electrokinetics effects can be used to affect both the movement of bioparticles from the bulk. Through AC electroosmosis or AC electrothermal flows bioparticles are continuously brought towards the sensing element overcoming any diffusion limitations. With DEP, the bioparticles are retained in proximity to the sensing element allowing for more time for capturing or detection to take place. Without these driving forces, biosensors can suffer from poor detection limits because of the low number distribution of molecules in the detection region and limited physical sensitivity of the transducer. The literature presented will demonstrate how AC electrokinetics has been employed to manipulate cells, viruses and DNA for the performance enhancement of surface based biosensors.

3.1 Biological cells

Cells, including bacteria and yeast, represent the largest sized bioparticles in the category of pathogens and are generally the most easily influenced by AC electrokinetic effects. One of the first reports dealing with the manipulation of cells was presented by Dimitrov & Zhelev (1987) where the manipulation, dielectrophoretic mobility, and dielectrophoretic coefficients of individual cells were examined under different conditions. The capability to move cells based on their dielectric properties allowed for DEP to be useful in the separation of mammalian cells (Gascoyne *et al.*, 1992), viable and nonviable cells (Markx *et al.*, 1994; Oblak *et al.*, 2007; Li & Bashir, 2002; Talary *et al.*, 1996; Jen & Chen, 2009), microorganisms (Markx *et al.*, 1995) and human breast cancer cells from blood cells (Becker *et al.*, 1995). This cell sorting allows for the screening of cells prior to exposure to a biosensor's surface thus providing a means of rapid sample sorting.

Depending on the sensing location and the dielectric properties of the pathogen of interest, the electrode design can be important consideration. Interdigitated castellated microelectrodes have been widely used for cell manipulation and separation (Betts, 1995; Oblak *et al.*, 20007; Pethig *et al.*, 1992; Pethig, 1996) as this design allows for the differential focusing and collection of cells at distinct electrodes areas under the influence of both positive and negative dielectrophoretic forces (Gascoyne *et al.*, 1992). In 1991 the first

polynomial electrode design was reported to produce a well defined non-uniform electric field for the study and application of nDEP (Huang & Pethig, 1991). An example of this is presented in Fig. 2 where *E. coli* and *M. Lysodeikticus* are separated using a polynomial electrode setup. Recently, a simple and novel curved electrode design has been used for the separation of airborne microbes from beads or dust that are present in airborne environmental samples, an important task prior to the real-time detection of airborne microbes (Sungmoon *et al.*, 2009).

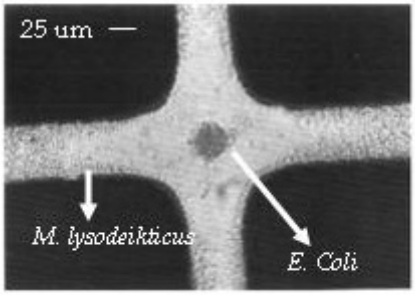

Fig. 2. Separation of *E. coli* (experiencing nDEP) and *M. lysodeikticus* (experiencing pDEP) in a polynomial electrode after application of a 4 $V_{PP,}$ 100 kHz signal in a suspending medium of 280 mM mannitol with a conductivity of 550 μS cm-1 (Markx *et al.*, 1994). Reused with permission.

In order for quantitative and qualitative studies to take place on a single cell or a small population of cells, the isolation and accurate positioning of the target must first be accomplished. Negative dielectrophoresis in particular has emerged as a powerful tool for this role. Under the influence of nDEP bioparticles are typically driven to regions away from the electrodes. The *E. Coli* in fig. 2 are collected in a nDEP "trap" or "cage" at the center because the electric field at that point is a localized minimum. This concept can be expanded to arrays of microelectrodes, thus enabling the precise placement and retention of multiple pathogenic samples (Frenea *et al.*, 2003).

3.2 Viruses

Representing some of the smallest size pathogenic bioparticles, the manipulation of virus particles is made difficult due to the presence of Brownian motion. To overcome the random stochastic motion, the manipulation of submicron sized particles requires large deterministic forces. Since DEP scales with a particle's volume, an electric field gradient of sufficient magnitude must be generated to provide a powerful enough force and necessitates the use of electrodes separated by only a few microns (Mullery *et al.*, 1996; Green & Morgan, 1997). Reducing the dimensions of the electrodes in a biosensor will decrease the voltage required to produce a given electrical field strength and, as a result, reduce both the power dissipated in the system and the temperature increment (Castellanos *et al.*, 2003). This is particularly beneficial for portable systems that run on low power.

A number of reports currently exist on the subject of AC electrokinetic manipulation of viruses (Park *et al.*, 2007; Akin *et al.*, 2004; Wu *et al.*, 2005a; de la Rica *et al.*, 2008; Müller *et al.*, 1996; Schnelle *et al.*, 1996). In many of these cases, successful virus collection results from

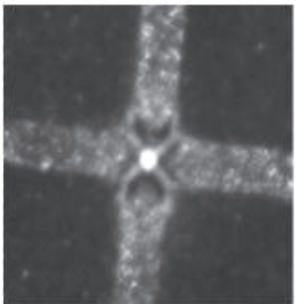

Fig. 3. Fluorescence image of nDEP collected vesicular stomatitis virus in TSE after fluorescent staining. The microelectrodes have a central gap measuring 2 μm across.

a combination of DEP and electrohydrodynamic flows (Ramos *et al.*, 1999). In 1998, Green & Morgan reported the manipulation of a mammalian virus, herpes simplex virus type 1, both by positive and negative DEP over a frequency range of 10 kHz-20 MHz using a polynomial microelectrode array with a gap of 2 μm. More recently, Docoslis *et al.* (2007) demonstrated the collection of vesicular stomatitis virus in buffered solutions of physiologically relevant conductivity using microelectrodes with a gap measuring 2 μm across (Fig. 3).

3.3 DNA

DNA offers a potential tool for the selective detection of pathogens by means of detecting the presence or absence of genetic sequences found in specific pathogens. A DNA molecule consists of two strands of deoxyribonucleotides held together by hydrogen bonding and takes a random conformation in water. Under slightly basic conditions the DNA molecule becomes negatively charged and a counter ion cloud surrounds the molecule. This counter ion cloud can be displaced in the presence of an electric field, increasing the ionic polarizability of the molecule (Hölzel & Bier, 2003). When an electrostatic field is applied, DNA polarizes, and every part of the DNA orients along the field lines, stretching it into an approximately straight shape. Due to the field non-uniformity, stretched DNA dielectrophoretically moves towards the electrode edge until one end comes into contact. On the basis of this behaviour many researchers have used AC electrokinetics to manipulate DNA (Walti *et al.*, 2007; Lapizco-Encinas & Palomares, 2007; Washizu *et al.*, 1995 & 2004; Dewarrat *et al.*, 2002; Asbury *et al.*, 2002; Washizu, 2005; Tuukkanen *et al.*, 2006; Chou *et al.*, 2002; Kawabata & Washizu, 2001; Yamamoto *et al.*, 2000; Wang *et al.*, 2005). For example, a modified interdigitated microelectrode array, termed "zipper electrode" by the authors, has been reported to concentrate a wide range of nanoparticles of biological interest, such as the influenza virus and DNA (Hübner *et al.*, 2007). Fig. 4 shows the fluorescence microscopy recorded for the trapping of stained λ-phage DNA in a floating electrode device. The figure shown here is recorded 10 sec after the application of an electric field with a voltage of 200 V_{pp} and a frequency of 30 Hz.

The manipulation of DNA by AC electrokinetic effects has been applied in the biological field and reviewed recently by Washizu (2005). The versatility of DNA allows for it to be used as a sensing, or analytical device and AC electrokinetic effects play an important role in the manipulation of this biological tool. AC Electrokinetics has been used to perform molecular surgery for the reproducible cutting of DNA at any desired position along the

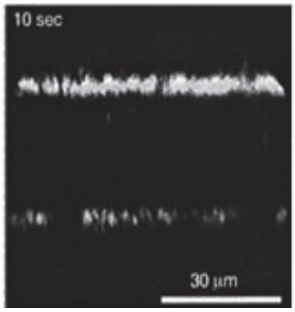

Fig. 4. Dielectrophoretic trapping of λ-phage DNA molecule when 30 Hz, 200 Vpp signal was applied in a floating electrode device (Asbury *et al.*, 2002). Reused with permission.

DNA molecule (Yamamoto *et al.*, 2000). Gene mapping has also found AC electrokinetics useful as a means for manipulating DNA to bring it into contact with enzymes in order to search for binding locations, and thus mapping the gene (Kurosawa *et al.*, 2000). Similarly manipulating and stretching DNA is useful for determining the order of the nucleotide bases for gene sequencing (Washizu *et al.*, 2005), and for measuring molecular sizes by counting base pairs (Washizu & Kurosawa, 1990). AC electrokinetically manipulated DNA can still undergo molecular interactions and has been used to achieve the selective binding of foreign single stranded DNA (Kawabata & Washizu, 2001). As a detection and sensing tool, once the DNA is brought close enough to touch an electrode, if the electrode edge consists of an electrochemically active metal, such as aluminum, then the DNA becomes permanently anchored there (Washizu *et al.*, 2004). Alternatively, the DNA can be trapped dielectrophoretically and it has been demonstrated by a number of researchers that trapped DNA can be used as a selective bioreceptor towards the development of pathogen biosensors (Gagnon *et al.*, 2008; Lagally *et al.*, 2005; Cheng *et al.*, 1998a; Cheng *et al.*, 1998b).

4. Detection of AC-electrokinetically trapped particles

Research over the last decade has shown that there is no shortage of analytical methods that can be successfully interfaced with AC electrokinetically enhanced sampling in a surface-based biosensor. The most promising candidates include methods that rely on optical (absorbance measurement, Raman, confocal microscopy, fluorescent intensity, etc.), mass based (quartz crystal microbalance, surface acoustic wave, etc.), electrical, or electrochemical (potentiometric, amperometric, conductometric, coulometric, impedimetric) (Velusamy *et al.*, 2010) detection. Optical and electrochemical sensors tend to be the most popular for pathogen analysis due to their selectivity and sensitivity. In general it is convenient to incorporate conventional optical or electrochemical devices with microfluidic detection systems. Successful implementation of these methods requires that the concentration amplification effect achieved by AC electrokinetics be combined with a selective target retention method. The latter can be accomplished with the immobilization of a target-specific molecule, such as a strand of DNA, an antibody, a protein, or an enzyme, or a more complex biological system such as a membrane, cell or tissue (Velusamy *et al.*, 2010). This type of molecular recognition ensures that the captured bioparticle will remain on the sensor surface even after the electric field is turned off. The sensitivity of a surface based biosensor

is thus directly affected by the packing density of the sensing element bound to the surface. Methods for surface functionalization have included the use of thiol interactions (Park & Kim, 1998; Radke & Alocilja, 2005; Bhatia *et al.*, 1989), avidin-biotin interactions (Costanzo *et al.*, 2005), self-assembled monolayer coated electrodes (Wana *et al.*, 2009), polymer coated electrodes (Livache *et al.*, 1998) and size specific capillary flow trapping (Hamblin *et al.*, 2010). A number of proof-of-principle studies have demonstrated that a combination of AC electrokinetics with a molecular recognition method can substantially improve the sensitivity of a biosensor (Yang, 2009; Yang *et al.*, 2006; Yang *et al.*, 2008). In principle, decorating the surface of the biosensor with antibodies allows for easy substitution when targeting a multitude of pathogens. The ability to replace specific bioreceptors on demand for the particular screening of a target pathogen gives this method high flexibility.

4.1 Optical detection

Optical based detections vary in their type and application. This section will focus on the most commonly used, namely: absorbance measurement, surface enhanced Raman scattering, and fluorescence.

4.1.1 Absorbance based measurements

An optical system was first described by Price *et al.*, (1988) to detect dielectrophoretically trapped bacterial cells by monitoring the changes in light absorbance through the suspension as bacteria collected at an electrode array by pDEP. Later on, Pethig *et al.* (1992) reported a dual beam optical spectrometer with improved sensitivity for the detection of yeast cells collected by both nDEP and pDEP (Talary & Pethig, 1994). The mechanism of pathogen detection by absorbance measurements based on dielectrophoretic immuno-capture is illustrated in Fig. 5. The immuno-capture of the bacterial cells under DEP after 15 and 30 min of sampling was found to be 82% and 74% more efficient than that achieved without DEP. The immuno-captured bacterial cells were detected by sandwich format ELISA on the chips. The absorbance signals by DEP assisted immuno-capture were reported to be enhanced by 64.7–105.2% for samples containing 10^3–10^6 cells/20 μL (Yang, 2009).

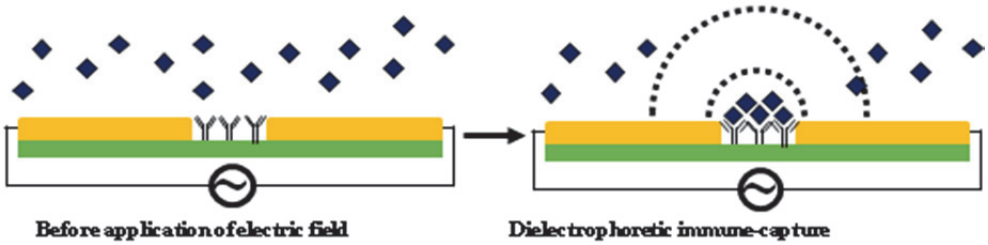

Fig. 5. Mechanism of nDEP immuno-capture: The area of collection (inter-electrode gap) is functionalized with a target-specific reactive component, an antibody in this case. Application of a spatially non-uniform electric field (dashed lines) causes nearby antigens to undergo nDEP and collect midway between the electrodes. Once collected, the immobilized antigens can be reacted with an optically active component.

4.1.2 Fluorescence-based detection

Fluorescence is by far the most frequently used optical signalling method for the monitoring and detection of AC-electrokinetically trapped bioparticles due to its high level of sensitivity and low background noise (Hübner *et al.*, 2007; Wong *et al.*, 2004b; Cui *et al.*, 2002; Yang *et al.*, 2008). Using fluorescent imaging, Docoslis *et al.* (2007) detected captured virus (vesicular stomatitis virus) and later explored numerical simulations of the system to better understand the processes involved (Wood *et al.*, 2007). The virus was captured from physiologically relevant ionic strength media (880 mS m^{-1}) at low concentrations (<10^6 PFU mL^{-1}). The numerical simulations revealed that with a quadrupolar microelectrode the capturing of the virus was achieved by both DEP for the short range capture and electrothermal fluid flow to overcome diffusion limitations. Others were also able to achieve virus capture at low ionic strengths (1-100 mS m^{-1}) and higher particle concentrations (>10^6 particles mL^{-1}) (Hughes *et al.*, 1998; Hughes *et al.*, 2001; Pethig *et al.*, 1992; Grom *et al.*, 2006; Morgan & Green, 1997). The dielectrophoretic capture and detection of a food borne pathogen, *Listeria monocytogenes*, was accomplished with the aid of the heat shock protein 60 (Hsp60) immobilized on a sensor's surface (Koo *et al.*, 2009). Hsp60 is a receptor for the Listeria adhesion protein (LAP), a house keeping enzyme of *Listeria monocytogenes* during the intestinal phase infection. Both fluorescent microscopy and ELISA were used to detect the binding of target cells with the receptor. The enhancement of binding with the aid of DEP was found to be 60% higher than without. As discussed in section 3.3, single stranded DNA can be used as a receptor to detect the specific sequence of a pathogen's genetics. Lagally *et al.* (2005) described an integrated system where bacterial cells where electrokinetically concentrated from a continuous-flow and detected via DNA-rRNA hybridization. After pDEP trapping the bacterial cells, the cells were lysed by chaotropic salt and the released DNA was denatured by endonuclease. The *E. Coli* cells were detected by fluorescent detection via the sequence specific hybridization of an rRNA-directed optical molecular beacon with the denatured DNA. This integrated microsystem is capable of the sequence specific genetic detection of 25 cells within 30 min. After hybridization, the percentage of the fluorescence was observed to increase with time and a linear relationship was found between the number of trapped cells and the percentage of maximum fluorescence. Others have reported the optical detection of cells (e.g., carcinoma cells, malarially-parasitized cells) where DEP was used to separate infected cells from healthy cells. Once lysed, the infected cells were identified with fluorescent probes on a bioelectronic chip (Gascoyne *et al.*, 2004; Cheng *et al.*, 1998a, 1998b).

4.1.3 Raman spectroscopy

Raman spectroscopy allows for analyte identification through the inspection of its "chemical fingerprint" on the basis of the vibrational, rotational and other low-frequency modes. Typically, for Raman detection, the signal provided by a low concentration surface based biosensor is not strong enough for detection. The use of surface enhanced Raman scattering (SERS) is often needed and can be achieved through the use of metal nanoparticles. The metal nanoparticles must be either chemically bonded to the bacteria or settle in the proximity of the bacteria in order to increase the scattering (Hou *et al.*, 2007; Cheng *et al.*, 2007). An on-chip detection of pathogens using surface enhanced raman spectroscopy (SERS) has been reported recently by Hou *et al.* (2007), where the Raman signals of the pathogens were enhanced by the presence of ~80–100 nm silver

nanoparticles. Combined with a discharge driven vortex for target concentration, SERS was successfully used in the detection of bioparticles at a concentration of 10^4 CFU/mL in the presence of silver nanoparticles (Hou *et al.*, 2007). A continuous flow system for bioparticle sorting was presented by Cheng *et al.* (2007) where, once sorted, the detection of the pathogen was accomplished via SERS. This integrated chip used DEP for a combination of filtering, focusing, sorting and trapping with a throughput of 500 particles/s (Cheng *et al.*, 2007).

4.2 Mass based detection

Pathogenic particles with length scales on the order of nanometers can individually weight as little as tens of picograms. In order for mass based detection to succeed, either very sensitive detection methods or significant pathogen amplification is necessary. The following sections will examine how AC electrokinetics has been used to improve the mass based detection sensitivity and sampling for quartz crystal microbalances and cantilever based detection methods.

4.2.1 Quartz crystal microbalance detection

A quartz crystal microbalance (QCM) utilizes a piezoelectric quartz crystal that has a fundamental resonance frequency which changes in accordance to the amount of mass attached to the crystal surface. Fatoyinbo *et al.* (2007) developed for the first time an integrated system where yeast cells were concentrated on an electrode surface by DEP and then quantified by a QCM system. The steady-state response predicted from the frequency shift analysis of nanoparticle-loaded DEP-QCM has shown significant improvements in rates of particle detection. The work was done at a concentration of 10^8 nano-spheres/mL and detection was achieved five times faster than other QCM surface loading techniques described in the literature.

4.2.2 Cantilever detection

Similar in concept to the QCM, a cantilever acts as a free-standing platform whose resonant frequency decreases with the addition of mass. As more bioparticles become deposited on the surface, the shift becomes more pronounced. The combination of AC electrokinetics with a cantilever beam was recently achieved and allowed for the rapid collection of human cancer cells (Park *et al.*, 2008). Using two conductive cantilevers situated across from one another over a well, Park *et al.* used pDEP to direct the human cancer cells onto the cantilever surface. Fig. 6 demonstrates the setup of a series of cantilevers where the change in resonant frequency is measured using a laser Doppler vibrometer. However, sensitivity remained an issue as culturing of up to 7 days was required in order for the cell mass to be detected. nDEP collection of *E. Coli* was achieved by Tomkins *et al.* (submitted, 2011) through the use of polynomial electrodes on a cantilever surface. By using a poly-L-lysine layer on the cantilever to act as a non-specific layer for the electrostatic retention of bacteria, a shift in frequency was detected after 30 minutes of collection from a concentration of 10^8 particles /mL. In order to maximize the sensitivity of a cantilever beam, the most desirable location for collection is at the cantilever tip, furthest away from the anchor. However, Islam *et al.* (2007) successfully applied AC electroosmotic flow to drive polystyrene particles to a point near the anchor and detected a mass change after drying.

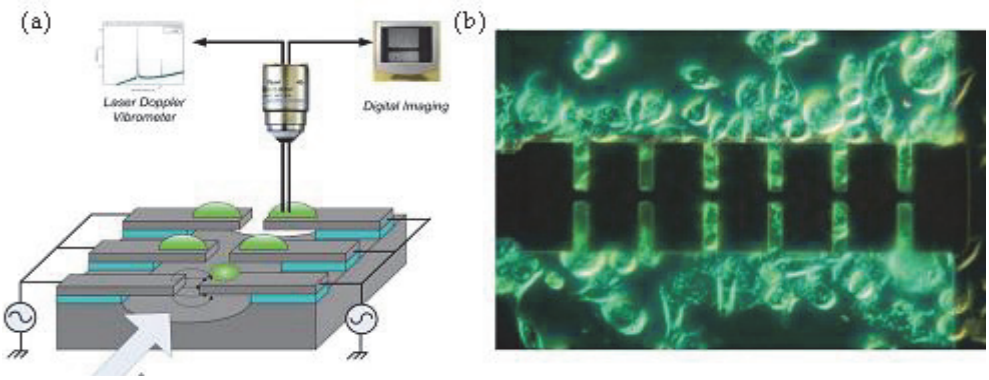

Fig. 6. (a) A schematic diagram of pairs of cantilevers. Each opposing cantilever acted as one half of an electrode pair when inducing pDEP. The arrow indicates the direction of flow. (b) A 'living' cantilever with human cervical cancer cells (Park *et al.*, 2008). Reused with permission.

4.3 Electrical or electrochemical detection

When biosensors employ an electrical or electrochemical sensing element, many of the features needed for AC electrokinetics are already present. These methods are easier to interface with miniaturized devices than optical methods because they employ electrical signals and do not need an often bulky optical measuring system. Microelectrodes for applied AC electrokinetics can be easily added into a microfluidic channel using standard photolithographic techniques and their integration with an electrical diagnostic chip allows for the sharing of features or power sources. Moreover, some electrical sensing methods do not require a labelling step for sensing target pathogens which makes the on-chip enhanced sampling provided by AC electrokinetics an attractive asset. Electrical sensing methods can be separated into 4 subclasses depending on the type of signal being measured: amperometric (changes in current), conductometric (changes in conductance or resistance), impedimetric (changes in resistance to an AC current), and coulometric (changes in capacitance). This section will focus on recent electrical or electrochemical sensing methods that have used AC electrokinetics.

4.3.1 Amperometric detection

By measuring the change in current as pathogens pass between a pair of sensing electrodes, it is possible to detect single cells in solution. AC elecktrokinetics can be used to position or manipulate these single cells into the proper location to achieve sensing. Utilizing the Coulter-counter principle Pandey & White (2004) used dielectrophoresis to detect a single cell (Chinese hamster ovary, CHO) as it was driven to pass through a micro-aperture (10-25μm in diameter, comparable to the size of the cells being tested) in a silicon nitride membrane. Detection of a cell was achieved by recording the decrease in the ionic current caused from the passage of a single cell as it passed through the micro-aperture. Live bacteria were also detected amperometrically by first using pDEP to trap the bacteria and then using AC induced fluid flow to move the cells until they formed a bridge across micron-sized electrode gaps (Beck *et al.*, 2005). The cells were first captured at the electrode edges by applying an electric field (1.5 V_{PP}, 1MHz). The cells were then transported along

the length of the electrode into the gap by exploiting an electric field induced flow at a lower voltage (0.5 V). The two electrodes tapered to a point small enough that a single bacterium would completely bridge the electrodes and detection could be achieved.

4.3.2 Conductometric detection

Direct measurement of the conductance between two electrodes with a nano-sized gap can be a highly sensitive technique for detecting bioparticles. A series of reports have been published by Suehiro *et al.* to detect dielectrophoretically trapped bacteria by measuring changes in conductance (1999; 2003a; 2003b; 2003c; 2005; 2006). The bacteria were collected within a small gap (5μm) between the microelectrode arrays by trapping the cells at the electrode edge with pDEP. After collection, an improved detection method was described by this group using electropermeabilization (Suehiro *et al.*, 2003b; 2005). While cells can be destroyed using AC electric fields within a specific frequency window (Menachery & Pethig, 2005), electropermeabilization causes the cell membrane to become permeable in order to increase the apparent conductivity of the trapped bacteria. Once applied, the bacterial cell wall leaks intracellular ions into the surrounding medium and transiently increases the conductance (Fig. 7). Using this method, the detection time of yeast cells and *E. Coli* cells was observed to shorten by two orders of magnitude to 15 min and 3 hr, respectively and the sensitivity was improved to 10^2 CFU/mL.

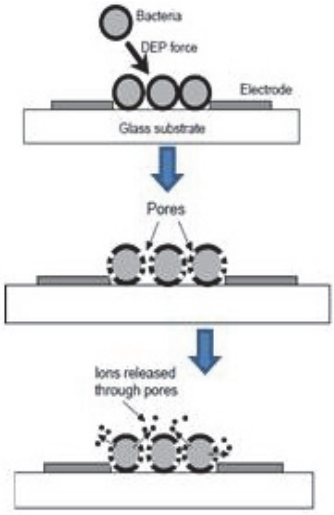

Fig. 7. A schematic diagram of electropermeabilization. The cells are first trapped, and then ruptured via an increased electric field followed by the subsequent release of intercellular ions to the surrounding area (Suehiro *et al.*, 2003b). Reused with permission.

Selectivity for these detection methods was demonstrated by exploiting the different dielectric properties of cell mixtures. Selective detection of viable cells from a mixture of viable and non-viable cells was achieved using DEP collection at two different electric field frequencies. At 100 kHz the viable and nonviable bacteria were trapped near an electrode corner due to positive DEP and their conductances changed proportionally with time. At 1

MHz only viable bacterial cells were trapped by positive DEP as the conductance change over time was less remarkable (Suehiro *et al*., 2003c). The increase in conductance indicated that certain areas of the electrode gap had been bridged by trapped bacteria.
To enhance the detection of dielectrophoretically collected particles, metal nanoparticles have been used to transform nonconductive trapped particles into conductive interparticle-connected entities through metal deposition. For example, silver particles attached to DEP trapped bioparticles bridged the gap between two microelectrodes by silver nucleation (Velev & Kaler, 1999). Latex particles coated with protein A were dielectrophoretically trapped between micron-sized gold electrodes and stabilized by a non-ionic surfactant. Adsorption of protein A onto the latex surface yielded a sensing interface for the specific association of the human immunoglobulin (IgG) antigen. The association of the human immunoglobulin on the surface was probed by the binding of secondary gold labelled anti-human IgG antibodies, followed by the catalytic deposition of a silver layer on the gold nanoparticles. The silver layer bridged the gap between the two microelectrodes, resulting in a resistance of 50-70 Ω, whereas the negative control gave a resistance of 10^3 Ω. The lower detection limit for this model sensor was calculated at 2×10^{-13}- 2×10^{-14} M.

4.3.3 Impedimetric detection

Impedimetric detection is one of the most promising techniques for developing label-free, real time, and non-invasive methods for bioparticle detection. Milner *et al.* (1998) first proposed a differential impedance method for the quantitative detection of DEP captured bacteria and opened the door for biosensors where non-visible sub-micrometer bioparticles, such as viruses and DNA fragments, could be quantitatively investigated. This is not to suggest that impedimetric detection can only be used in isolation. In conjunction with optical monitoring, impedance has been used for the characterization of prohibitively small bioparticles (Guan *et al*., 2004).
Dielectrophoretic impedence measurement (DEPIM), a new method reported by Suehiro *et al*., occurs when there is an impedance change as interdigitated microelectrodes are connected due to the trapping and pearl-chain formation of cells by DEP (Suehiro *et al*., 1999). A 'pearl-chain' occurs during capture when bioparticles become dielectrophoretically attracted towards one another and form strings of particles resembling a chain of pearls. This pearl chain can enhance sensing by being electrically connected in parallel within the electrode gap, thus increasing the conductance and capacitance between the electrodes. The conductance, G_T and capacitances, C_T between the electrodes are found to increase proportionally with the increase in cell concentration. By fitting the measured G_T and C_T values, a linear calibration chart was derived that enables the absolute measurements of cell concentration. This method accurately assayed *E. Coli* cells suspended in solution at a concentration of 10^5 CFU/mL within 10 min. DEPIM has been used to concentrate bacterial cells (*L. monocytogenes)* from dilute solutions (10^5 cfu/mL) in order to detect the metabolic activity of the bacteria and provide enhanced sensitivity for the biosensor. (Sjöberg *et al*., 2005). After trapping the cell on the sensor surface, impedance sensing arose from the differences in the physical properties, *i.e.*, differences in conductivity and permittivity, between the particles and the suspending medium as well as the changes in the geometric form of the collected particle on the electrode array. Other studies found that the changes in the permittivity of the dielectric between the electrodes are proportional to the total volume of the suspending medium replaced by the DEP collected particles (Allsopp *et al*., 1999). Thus, a linear relationship between the capacitance change and cell concentration was found.

The DEPIM method was further developed with improved selectivity and sensitivity by applying electropermeabilization (Suehiro *et al.*, 2003b), antibody-antigen interactions (Suehiro *et al.*, 2003a; Suehiro *et al.*, 2006; Suehiro *et al.*, 2005) and different DEP forces (Suehiro *et al.*, 2003c). In a series of publications, this group reported the detection of cells with high selectivity by using antigen-antibody reactions (Suehiro *et al.*, 2006). This phenomenon was employed with DEPIM measurement via agglutination and immobilization and is illustrated in Fig. 8. An antibody specific to the target bacteria was added to the cell suspension to cause agglutination. pDEP was employed to attract particles to an electrode tip. At the electrode tips, the antibody was in a region of high concentration of the target bacteria, thereby increasing the amount of agglutination. After washing, a second round of DEP collection was used where the conditions of the DEP force and the drag forces were adjusted by varying the strength of the electric field so that only agglutinated products of the target bacteria were selectively trapped. A second method was proposed where immobilization for DEPIM relied on an electrode coated with immobilized antibodies prior to the experiment. The DEP force was then adjusted to be strong enough to bring bacteria to the chip surface, but not enough to overcome the drag force exerted by the flowing liquid. This allowed for simultaneously trapping the target bacteria by the antibody-antigen and suppressed non-specific bacteria binding.

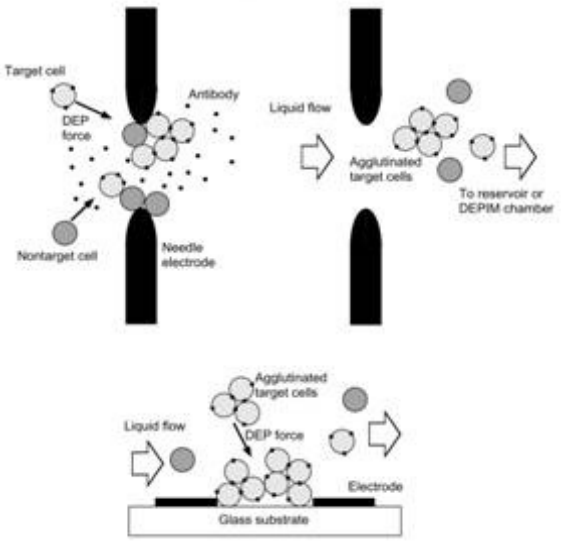

Fig. 8. A schematic diagram of DEPIM for agglutinated bacteria. The top schematic demonstrates trapping between electrode tips assisted with pDEP. The target bacteria become agglutinated at the tips and are then washed away to the reservoir. The agglomerates can then be collected more easily as shown in the bottom schematic (Suehiro *et al.*, 2003a; 2003b). Reused with permission.

To miniaturize the analytical procedures for microorganism detection, a lab-on-a-chip device integrated with DEP based moving cages was demonstrated where the movement of the cages was achieved through actuation. Coupled with impedance based detection this

lab-on-a-chip had no need for fluid flow or external optical components (Medoro *et al.*, 2003). The cells are trapped in a stable levitation under the influence of an electric field and were then moved to a target location. The DEP cages were observed to shift and merge, consequently increasing the particle concentration within the cage. Impedance detection of *E. Coli* in tap water has also been achieved with the AC electroosmotic trapping of the bacteria using 1 V_{RMS} at 100 Hz (Wu *et al.*, 2005b). Detection was possible for *E. Coli* suspended in tap water at a concentration of 5×10^3 CFU/ml after trapping by AC electroosmosis. From the impedance results it was concluded that the system could detect pathogenic cells at a concentration of 10^4 cell/mL.
Single wall carbon nanotubes (SWCNTs) polarize in the presence of an electric field and can undergo self-assembled aggregation due to dipole-dipole interactions. Furthermore, they are good conductors and can change the conductance between the two microelectrodes by forming a bridge across the electrode gap, acting as a super capacitor. The strong dipoles of SWCNTs allow them to absorb onto the bioparticles and in a mixture of SWCNTs with bacteria, the impedimetric detection of bacteria was enhanced. Without CNT under the conditions applied, no bacteria were collected, however, with CNT enhanced DEP capture bacteria were collected and detected, as shown in Fig. 9 (Zhou *et al.*, 2006). The authors suggested that the enhanced DEP trapping of bacteria was probably due to the stronger electric fields, and hence stronger DEP forces, generated near the dispersed SWCNTs. The transport time between the bioparticles and the sensor was shown to be greatly reduced and that the bacteria were concentrated and detected in less than 10 min at a concentration of 10^4 particles/mL. Dielectrophoretic collection, impedence detection and characterization of DNA have also been reported by a number of researchers (Hölzel & Bier, 2004; Linko *et al.*, 2009).

Fig. 9. CNT (0.2 mg/mL) enhanced collection of *E. Coli* bacteria (10^5 CFU/mL) (Zhou *et al.*, 2006). Reused with permission.

4.3.4 Coulometric detection

In capacitance cytometry, a change in the total capacitance across a pair of microelectrodes is measured as the individual cell is allowed to pass through a microfluidic channel. As previously mentioned in section 3.3, DNA polarizes in an applied low frequency AC electric field. Capacitance measurement is employed by means of detecting and quantifying the polarization response of DNA as the cell passed through a 1 kHz electric field. Capacitance detection of DNA in solution has been applied by measuring the capacitance change between the planar microelectrodes (Henning *et al.*, 2008). Total DNA content of a cell has

also been quantified by using capacitance cytometry, a termed coined by the authors to describe the linear relationship between the AC-capacitance and the DNA content (Sohn *et al*., 2000). A new method was recently published where the capacitive detection of viruses was achieved with an extremely low detection limit by using peptide nanotubes, a concept similar to the enhancement provided by CNT for bacteria that was discussed earlier (de la Rica *et al*., 2008). Self assembled peptide nanotubes coated with a virus specific antibody were trapped between a pair of electrodes by pDEP. Binding of the virus to the antibody caused a decrease in the permittivity as well as the capacitance between the electrodes due to the lower dielectric constant of the virus than that of the medium. Compared to other label free optical based transducers, this peptide nanotube based electrical transducer demonstrates a better detection limit for the herpes simplex virus type 2 with a detection limit of 10^2 PFU/mL achieved within 1 hr.

5. Conclusions

The use of surface based biosensors with enhanced collection via AC electrokinetics allows for miniaturized, portable systems for the detection and characterization of potential pathogens. The research presented here has shown that the diffusion limitation bottleneck of traditional biosensors can be overcome with the aid of microelectrode arrays embedded on the sensor's surface. AC electrokinetic amplification for the enhanced bioparticle collection at virtually any location on a biosensor's surface can be achieved through positive or negative dielectrophoresis, AC electroosmosis or electrothermal flow, all of which provide a versatility of application for microelectromechnical devices. Furthermore, this technique is compatible with a range of detection methods including optical, mass and electrical based sensing. With the proliferation of micro- and nanotechnologies, and the need for onsite detection, a portable miniaturized system capable of detecting low concentrations of potentially dangerous pathogens is desirable. Commercially available lab-on-a-chip sensors capable of processing samples for the detection of multiple pathogenic compounds via an array of biosensors where the role of AC electrokinetics provides both sample amplification and transportation is quickly approaching reality.

6. References

Akin, D., Li, H., & Bashir, R. (2004). Real-Time Virus Trapping and Fluorescent Imaging in Microfluidic Devices. *Nano Lett.,* Vol. 4, pp. (257-259)

Allsopp, D.W.E., Milner, K.R., Brown, A.P., & Betts, W.B. (1999). Impedance technique for measuring dielectrophoretic collection of microbiological particles. *J. Phys. D: Appl. Phys*., Vol. 32, pp. (1066-1074)

Asbury, C.L., Diercks, A.H., & Engh, G.V.D. (2002). Trapping of DNA by dielectrophoresis. *Electrophoresis,* Vol. 23, pp. (2658-2666)

Beck, J.D., Shang, L., Marcus, M.S., & Hamers, R.J. (2005). Manipulation and Real-Time Electrical Detection of Individual Bacterial Cells at Electrode Junctions: A Model for Assembly of Nanoscale Biosystems*Nano Lett.,* Vol. 5, pp. (777-781)

Becker, F.F., Wang, X-B., Huang, Y., Pethig, R., Vykoukal, J., & Gascoyne, P. R. (1995). Separation of human breast cancer cells from blood by differential dielectric affinity. *Proc. Natl. Acad. Sci. USA, Cell Biology*, Vol. 92, pp. (860-864)

Betts, W. B. (1995). The potential of dielectrophoresis for the real-time detection of microorganisms in foods. *Trends in Food Sci. Technol*., Vol. 6, pp. (51-58)

Bhatia, S.K., Shriver-Lake, L.C., Prior, K.J., Georger, J.H., Calvert, J.M., Bredehorst, R., & Ligler, F.S. (1989). Use of Thiol-terminated silanes and heterobifunctional crosslinkers for immobilization of antibodies on silica surfaces. *Anal. Biochem.,* Vol. 178, pp. (408-413)

Burt, J.P. H., Al-Ameen, T.A.K, & Pethig, R. (1989). An optical dielectrophoresis spectrometer for low –frequency measurements on colloidal suspensions. *J. Phys. E: Sci. Instrum*., Vol. 22, pp. (952-957)

Castellanos, A., Ramos, A., Gonzalez, A., Green, N.G., & Morgan, H. (2003). Electrohydrodynamics and dielectrophoresis in Microsystems: scaling laws. *J. Phys. D: Appl. Phys*., Vol. 36, pp. (2584-2597)

Cheng, J., Sheldon, E.L., Wu, L., Uribe, A., Gerrue, L.O., Carrino, J., Heller, M.J., & O'Connell, J.P. (1998a). Preparation and hybridization analysis of DNA/RNA from E. coli on microfabricated bioelectronic chips. Nature Biotechnology, Vol. *16,* pp. (*541-546)*

Cheng, J., Sheldon, E.L., Wu, L., Heller, M.J., & O'Connell, J.P. (1998b). Isolation of Cultured Cervical Carcinoma Cells Mixed with Peripheral Blood Cells on a Bioelectronic Chip. *Anal. Chem*., Vol. 70, pp. (2321-2326)

Cheng, I–F., Chang, H–C., Hou, D., & Chang, H–C. (2007). An integrated dielectrophoretic chip for continuous bioparticle filtering, focusing, sorting, trapping, and detecting. *Biomicrofluidics*, Vol. 1, pp. (021503:1-15)

Chou, C-F., Tegenfeldt, J. O., Bakajin, O., Chan, S. S., Cox, E. C., Darnton, N., Duke, T. & Austin, R. H. (2002). Electrodeless Dielectrophoresis of Single- and Double-Stranded DNA. *Biophysical Journal*, Vol. 83, pp. (2170-2179)

Costanzo, P. J., Liang, E., Patten, T. E., Collins, S. D., & Smith., R. L. (2005). Biomolecule detection via target mediated nanoparticle aggregation and dielectrophoretic impedance measurement. *Lab Chip*, Vol. 5, pp. (606-610)

Cui, L., Zhang, T., & Morgan, H. (2002). Optical particle detection integrated in a dielectrophoretic lab-on-a-chip. *J. Micromech. Microeng*., Vol. 12, pp. (7-12)

Dewarrat, F., Calame, M., & Schönenberger, C. (2002). Orientation and Positioning of DNA Molecules with an Electric Field Technique. *Single Mol*., Vol. 3, pp. (189-193)

Dimitrov, D.S., & Zhelev, D.V. (1987). Dielectrophoresis of individual Cells: experimental Methods and results, *Bioelectrochemistry and Bioenergetics,* Vol. 17, pp. (549-557)

Docoslis, A., Espinoza, L.A.T., Zhang, B., Cheng, L-L., Israel, B.A., Alexandridis, P., & Abbott, N.L. (2007) Using Nonuniform Electric Fields To Accelerate the Transport of Viruses to Surfaces from Media of Physiological Ionic Strength. *Langmuir*, Vol. 23,, pp. (3840-3848)

Fatoyinbo, H.O., Hoettges, K.F., Reddy, S.M., & Hughes, M.P. (2007). An integrated dielectrophoretic quartz crystal microbalance (DEP-QCM) device for rapid biosensing applications. *Biosensors and Bioelectronics,* Vol. 23, pp. (225-232)

Feng, J.J., Krishnamoorthy, S., & Sundaram, S. (2007). Numerical analysis of mixing by electrothermal induced flow in microfluidic systems. *Biomicrofluidics*, Vol. 1, pp. (024102:1-8)

Frenea, M., Faure, S.P., Le Pioufle, B., Coquet, Ph., & Fujita, H. (2003). Positioning living cells on a high-density electrode array by negative dielectrophoresis. *Materials Science and Engineering C*, Vol. 23, pp. (597-603)

Gagnon, Z., & Chang, H-C. (2005). Aligning Fast Alternating Current Electroosmotic Flow Fields and Characteristic Frequencies with dielectrophoretic Traps to Achieve Rapid Bacteria detection. *Electrophoresis,* Vol. 26, pp. (3725-3737)

Gagnon, Z., Senapati, S., Gordon, J., & Chang, H–C. (2008). Dielectrophoretic detection and quantification of hybridized DNA molecules on nano-genetic particles. *Electrophoresis,* Vol. 29, pp. (4808-4812)

Gascoyne, P.R.C., Huang, Y., Pethig, R., Vykoukal, J., & Becker, F. F. (1992). Dielectrophoretic separation of mammalian cells studied by computerized image analysis. *Meas. Sci. Technol.*, Vol. 3, pp. (439-445)

Gascoyne, P., Satayavivad, J., & Ruchirawat, M. (2004). Microfluidic approaches to malaria detection. *Acta Tropica*, Vol. 89, pp. (357-369)

Green, N.G., & Morgan, H. (1997). Dielectrophoretic investigations of sub-micrometre latex spheres. *J. Phys. D: Appl. Phys.*, Vol. 30, pp. (2626-2633)

Green, N.G., & Morgan, H. (1998). Separation of submicrometre particles using a combination of dielectrophoretic and electrohydrodynamic forces. *J. Phys. D: Appl. Phys*., Vol. 31, pp. (L25-L30)

Green, N.G., Ramos, A., Gonzalez, A., Morgan, H., & Castellanos, A. (2002). Fluid flow induced by nonuniform ac electric fields in electrolytes on microelectrodes. III. Observation of streamlines and numerical simulation. *Physical Review E,* Vol. 66, pp. (026305:1-11)

Grom, F., Kentsch, J., Müller, T., Schnelle, T., & Stelzle, M. (2006). Accumulation and trapping of hepatitis A virus particles by electrohydrodynamic flow and dielectrophoresis. *Electrophoresis,* Vol. 27, pp. (1386-1393)

Guan, J.G., Miao, Y.Q., & Zhang, Q.J. (2004). Impedimetric Biosensors. *Biosci. Bioeng*., Vol. 97, pp. (219-226)

Hamblin, M.N., Xuan, J., Maynes, D., Tolley, H. D., Belnap, D. M., Woolley, A. T., Leeb, M. L., & Hawkins, A. R. (2010). Selective trapping and concentration of nanoparticles and viruses in dual-height nanofluidic channels. *Lab Chip*, Vol. 10, pp. (173-178)

Henning, A., Henkel, J., Bier, F.F., & Hölzel, R. (2008). Label-free electrical quantification of the dielectrophoretic response of DNA. *PMC Biophysics* Vol. 1, No. 4

Hoettges, K.F., McDonnell, M.B., & Hughes, M.P. (2003). Use of combined dielectrophoretic/electrohydrodynamic forces for biosensor enhancement. *J. Phys. D: Appl. Phys*., Vol. 36, pp. (L101-L104)

Hölzel, R., & Bier, F.F. (2003). Dielectrophoretic manipulation of DNA. *IEE Proc-Nanobiotechnol.,* Vol. 150, pp. (47-53)

Hölzel, R., & Bier, F.F. (2004). Monitoring Dielectrophoretic Collection of DNA by Impedance Measurement. *AIP Conference Proceedings,* Vol. 725, pp. (77-83)

Hou, D., Maheshwari, S., & Chang, H.C. (2007). Rapid bioparticle concentration and detection by combining a discharge driven vortex with surface enhanced Raman scattering. *Biomicrofluidics*, Vol. 1, pp. (014106:1-13)

Huang, Y., & Pethlg, R. (1991). Electrode design for negative dielectrophoresis. *Meas. Sci. Technol.,* Vol. 2, pp. (1142-1146)

Hübner, Y., Hoettges, K.F., McDonnell, M.B., Carter, M.J., & Hughes, M.P. (2007). Applications of dielectrophoretic/electro-hydrodynamic "zipper" electrodes for detection of biological nanoparticles. *Int J Nanomedicine*., Vol. 2, No. 3, pp. (427-431)

Hughes, M. P., Morgan, H., Rixon, F. J., Burt, J. P. H., & Pethig, R. (1998). Manipulation of herpes simplex virus type 1 by dielectrophoresis, *Biochim. Biophys. Acta.*, Vol. 1425, pp. (119-126)

Hughes, M. P., Morgan, H., & Rixon, F. J. (2001). Dielectrophoretic manipulation and characterization of herpes simplex virus-1 capsids. *Eur. Biophys. J.*, Vol. 30, pp. (268-272)

Humberto, F., Morales, F., Duarte, J. E., & Martí, J. S. (2008). Non-uniform electric field-induced yeast cell electrokinetic behavior. *Revista Ingenieria E Investigacion,* Vol. 28, pp. (116-121)

Islam, N., Lian, M., W & u, J. (2007). Enhancing microcantilever capability with integrated AC electroosmotic trapping. *Microfluid. Nanofluid.,* Vol. 3, pp. (369-375)

Jen, C–P., & Chen, T–W. (2009). Selective trapping of live and dead mammalian cells using insulator-based dielectrophoresis within open-top microstructures. *Biomed. Microdevices,* Vol. 11, pp. (597-607)

Kawabata, T., & Washizu, M. (2001). Dielectrophoretic Detection of Molecular Bindings. *IEEE Transactions on Industry Applications*, Vol. 37, pp. (1625-1633)

Koo, O.K., Liu, Y., Shuaib, S., Bhattacharya, S., Ladisch, M.R., Bashir, R., & Bhunia, A.K. (2009). Targeted Capture of Pathogenic Bacteria Using a Mammalian Cell Receptor Coupled with dielectrophoresis on a Biochip. *Anal. Chem.,* Vol. 81, pp. (3094-3101)

Kurosawa, O., Okabe, K., & Washizu, M. (2000). DNA analysis based on physical manipulation. *Proceedings of 13th Micro Electro Mechanical Systems.*, pp. (311-316)

Lagally, E.T., Lee, S-H., & Soh, H.T. (2005). Integrated microsystem for dielectrophoretic cell concentration and genetic Detection. *Lab Chip*, Vol. 5, pp. (1053-1058)

Lapizco-Encinas, B. H., & Palomares, M. R. (2007). Dielectrophoresis for the manipulation of Nanobioparticles. *Electrophoresis*, Vol. 28, pp. (4521-4538)

Li, H., & Bashir, R. (2002). Dielectrophoretic separation and manipulation of live and heat-treated cells of *Listeria* on microfabricated devices with interdigitated electrodes. *Sensors and Actuators B: Chemical,* Vol. 86, pp. (215-221)

Li, D. (2004). *Electrokinetics in microfluidics*, Elsevier

Linko, V., Paasonen, S–T., Kuzyk, A., Torma, P., & Toppari, J.J. (2009). Characterization of the Conductance Mechanisms of DNA Origami by AC Impedance Spectroscopy. *Small,* Vol. 5, pp. (2382-2386)

Livache, T., Bazin, H., Caillat, P., & Roget., A. (1998). Electroconducting polymers for the construction of DNA or peptide arrays on silicon chips. *Biosensors & Bioelectronics*, Vol. 13, pp. (629-634)

Markx, G.H., Huang, Y., Zhou, X-F., & Pethig, R. (1994). Dielectrophoretic characterization and separation of micro-organisms. *Microbiology,* Vol. 140, pp. (585-591)

Markx, G.H., & Pethig, R. (1995). Dielectrophoretic Separation of Cells: Continuous Separation. *Biotechnology and Bioengineering*, Vol. 45, pp. (337-343)

Medoro, G., Manaresi, N., Leonardi, A., Altomare, L., Tartagni, M., & Guerrieri, R. (2003). A Lab-on-a-Chip for Cell Detection and Manipulation. *IEEE Sensors Journal,* Vol. 3, No. 3, pp. (317-325)

Menachery, A., & Pethig, R. (2005). Controlling cell destruction using dielectrophoretic Forces. *IEE Proc. Nanobiotechnol.*, Vol. 152, pp. (145-149).

Milner, K.R., Brown, A.P., Allsopp, D.W.E., & Betts, W.B. (1998). Dielectrophoretic classification of bacteria using differential impedance measurements. *Electronics Letters,* Vol. 3, pp. (66-68)

Morgan, H., & Green, N.G. (1997). Dielectrophoretic manipulation of rod-shaped viral particles. *Journal of Electrostatics*, Vol. 42, pp. (279-293)

Morgan, H. & Green, N.G. (2003). *AC electrokinetics: colloids and nanoparticles*, Research Studies Press Ltd.

Müller, T., Fiedler, S., Schnelle, T., Ludwig, K., Junga, H., & Fuhr, G. (1996). High frequency electric fields for Trapping viruses. *Biotechnology Techniques,* Vol. 10 pp. (221-226)

Mullery, T., Gerardinoz, A., Schnelley, T., Shirleyy, S. G., Bordoniz, F., Gasperisz, G. D., Leonix, R., & Fuhr, G. (1996). Trapping of micrometre and sub-micrometre particles by high-frequency electric fields and hydrodynamic forces. *J. Phys. D: Appl. Phys.*, Vol. 29, pp. (340-349)

Oblak, J., Krizaj, D., Amon, S., Macek-Lebar, A., & Miklavcic, D. (2007). Separation of electroporated and non-electroporated cells by means of dielectrophoresis. *IFMBE Proceedings*, Vol. 16, pp. (178-181)

Pandey, S., & White, M.H. (2004). Detection of Dielectrophoretic Driven Passage of Single Cells through Micro-Apertures in a Silicon Nitride Membrane. *Conf. Proc. IEEE Eng. Med. Biol. Soc.*, Vol. 3, pp. (1956-1959)

Park, I-S., & Kim, N. (1998). Thiolated *Salmonella* antibody immobilization onto the gold surface of piezoelectric quartz crystal. *Biosensors & Bioelectronics,* Vol. 13, pp. (1091-1097)

Park, K., Akin, D., & Bashir, R. (2007). Electrical capture and lysis of vaccinia virus particles using silicon nano-scale probe array. *Biomed. Microdevices,* Vol. 9, pp. (877-883)

Park, K., Jang, J., Irmia, D., Sturgis, J., Lee, J., Robinson, P., Tonerd, M., & Bashir, R. (2008). 'Living cantilever arrays' for characterization of mass of single live cells in fluids. *Lab on a Chip*, Vol. 8, pp. (1034-1041)

Pethig, R. (1996). Dielectrophoresis: Using In homogeneous AC Electrical Fields to Separate and Manipulate Cells. *Crirical Reviews in Biotechnology,* Vol. 16, pp. (331-348)

Pethig, R., & Markx, G.H. (1997). Applications of dielectrophoresis in biotechnology. *Trends Biotechnol.*, Vol. 15, pp. (426-432)

Pethig, R., Huang, Y., Wang, X-B., & Burt, J.P. H. (1992). Positive and negative dielectrophoretic collection of colloidal particles using interdigitated castellated microelectrodes. *J. Phys. D: Appl. Phys.*, Vol. 24, pp. (881-888)

Pohl, H. A. (1951). The motion and precipitation of suspensoids in divergent electric fields. *Journal of Applied Physics*, Vol. 22, pp. (869-871)

Pohl, H.A., & Pethig, R. (1977). Dielectric measurements using non-uniform electric field (dielectrophoretic) effects. *J. Phys. E: Sci. Instrum.,* Vol. 10, pp. (190-193)

Price, J.A.R., Burt, J. P.H., & Pethig, R. (1988). Applications of a new optical technique for measuring the dielectrophoretic behaviour of micro-organisms. *Biochim. Biophys. Acta,* Vol. 964, pp. (221-230)

Radke, S.M., & Alocilja, E.C. (2005). A microfabricated biosensor for detecting foodborne bioterrorism agents. *IEEE Sensors Journal*, Vol. 5, pp. (744-750)

Ramos, A., Morgan, H., Green, N.G., & Castellanos, A. (1998). Ac electrokinetics: a review of forces in microelectrode structures. *J. Phys. D: Appl. Phys.*, Vol. 31, pp. (2338-2353)

Ramos, A., Morgan, H., Green, N.G., & Castellanos, A. (1999). AC Electric-Field-Induced Fluid Flow in Microelectrodes. *J.Coll. Int. Sci.*, Vol. 217, pp. (420-422)

de la Rica, R., Mendoza, E., Lechuga, L.M., & Matsui, H. (2008). Label-Free Pathogen Detection with Sensor Chips Assembled from Peptide Nanotubes. *Angew. Chem. Int. Ed.*, Vol. 47, pp. (9752-9755)

Sauli, U.S., Panayiotou, M., Schnydrig, S., Jordan, M., & Renaud, P. (2005). Temperature measurements in microfluidic systems: Heat dissipation of negative dielectrophoresis barriers. *Electrophoresis,* Vol. 26, pp. (2239-2246)

Schnelle, T., Müller, T., Fiedler, S., Shirley, S. G., Ludwig, K., Herrmann, A., Fuhr, G., Wagner B., & Zimmermann, U. (1996). Trapping of viruses in high-frequency electric field cages. *Naturwisswnschaften*, Vol. 83, pp. (172-176)

Sigurdson, M., Wang, D., & Meinhart, C.D. (2005). Electrothermal stirring for heterogeneous immunoassays. *Lab Chip*, Vol. 5, pp. (1366-1373)

Sjöberg, R. G., Morisette, D. T., & Bashir, R. (2005). Impedance Microbiology-on-a-Chip: Microfluidic Bioprocessor for Rapid Detection of Bacterial Metabolism. *J. Microelectromech. Syst.*, Vol. 14, pp. (829-838)

Sohn, L.L., Saleh, O.A., Facer, G.R., Beavis, A.J., Allan, R.S., & Notterman, D.A. (2000). Capacitance cytometry: Measuring biological cells one by one. *Proc Natl Acad Sci,*, Vol. 97, pp. (10687-10690)

Suehiro, J., Yatsunami, R., Hamada, R., & Hara, M. (1999) Quantitative estimation of biological cell concentration suspended in aqueous medium by using dielectrophoretic impedance measurement method. *J. Phys. D: Appl. Phys.*, Vol. 32, pp. (2814-2820)

Suehiro, J., Noutomi, D., Shutou, M., & Hara, M. (2003a). Selective detection of specific bacteria using dielectrophoretic impedance measurement method combined with an antigen–antibody reaction. *Journal of Electrostatics*, Vol. 58, pp. (229-246)

Suehiro, J., Shutou, M., Hatano, T., & Hara, M. (2003b). High sensitive detection of biological cells using dielectrophoretic impedance measurement method combined with electropermeabilization, *Sensors and Actuators B*, Vol. 96, pp. (144-151)

Suehiro, J., Hamada, R., Noutomi, D., Shutou, M., & Hara, M. (2003c). Selective detection of viable bacteria using dielectrophoretic impedance measurement method. *Journal of Electrostatics,* Vol. 57, pp. (157-168)

Suehiro, J., Hatano, T., Shutou, M., H & ara, M. (2005). Improvement of electric pulse shape for electropermeabilization assisted dielectrophoretic impedance measurement for high sensitive bacteria detection. *Sensors and Actuators B,* Vol. 109, pp. (209-215)

Suehiro, J., Ohtsubo, A., Hatano, T., & Hara, M. (2006). Selective detection of bacteria by a dielectrophoretic impedance measurement method using an antibody-immobilized electrode chip. *Sensors and Actuators B,* Vol. 119, pp. (319-326)

Sungmoon, H., Woonam, Y., Park, J. C., & Jung., H. Y. (2009). Dielectrophoretic Separation of Airborne Microbes and Dust Particles Using a Microfluidic Channel for Real-Time Bioaerosol Monitoring. *Environ. Sci. Technol.*, Vol. 43, pp. (5857-5863)

Talary, M.S., & Pethig, R. (1994). Optical technique for measuring the positive and negative dielectrophoretic behaviour of cells and colloidal suspensions. *IEE Proc. Sci. Meas. Technol.*, Vol. 141, pp. (395-399)

Talary, M.S., Burt, J.P.H., Tame, J.A., & Pethig, R. (1996). Electromanipulation and separation of cells using travelling electric fields. *J. Phys. D: Appl. Phys.*, Vol. 29, pp. (2198-2203)

Tomkins, M.R., Wood, J.A., & Docoslis, A. (2008). Observations and Analysis of Electrokinetically Driven Particle Trapping in Planar Microelectrode Arrays. *The Canadian Journal of Chemical Engineering*, Vol. 86, pp. (609-621)

Tomkins, M.T., Chow, J., Lai, Y-J., Docoslis, A., (submitted, 2011) A coupled cantilever-microelectrode biosensor for enhanced pathogen detection.

Tuukkanen, S., Toppari, J. J.,Kuzyk, A. Hirviniemi, L., Hytönen, V.P. Ihalainen, T. & Törmä, P. (2006). Carbon Nanotubes as Electrodes for Dielectrophoresis of DNA. *Nano Lett.*, Vol. 6, pp. (1339-1343)

Velev, O.D., & Kaler, E.W. (1999). In Situ Assembly of Colloidal Particles into Miniaturized Biosensors, *Langmuir*, Vol. 15, pp. (3693-3698)

Velusamy, V., Arshak, K., Korostynska, O., Oliwa, K., & Adley, C. (2010). An overview of foodborne pathogen detection: In the perspective of biosensors. *Biotechnology Advances,* Vol. 28, pp. (232-254) 0734-9750

Walti, C. W¨, Germishuizen, W. A., Tosch, P., Kaminski, C. F., & Davies, A. G. (2007). AC electrokinetic manipulation of DNA. *J. Phys. D: Appl. Phys.*, Vol. 40, pp. (114-118)

Wana, Y., Zhanga, D., & Hou, B. (2009). Monitoring microbial populations of sulfate-reducing bacteria using an impedimetric immunosensor based on agglutination assay. *Talanta*, Vol. 80, pp. (218-223)

Wang, T–H., Peng, Y., Zhang, C., Wong, P. K., & Ho, C–M. (2005). Single-Molecule Tracing on a Fluidic Microchip for Quantitative Detection of Low-Abundance Nucleic Acids. *J Am Chem Soc.,* Vol. 127, pp. (5354-2365)

Washizu, M., & Kurosawa, O. (1990). Electrostatic Manipulation of DNA in Microfabricated Structures. *IEEE Transactions on Industry Applications*, Vol. 26, pp. (1165-1172)

Washizu, M., Kurosawa, O., Arai, I., Suzuki, S., & Shimamoto, N. (1995). Applications of electrostatic stretch and-positioning of DNA *IEEE Trans. Ind. Appl.,* Vol. 31, No. 3, pp. (447-456)

Washizu, M., Kimura, Y., Kobayashi, T., Kurosawa, O., Matsumoto, S., & Mamine, T. (2004). Stretching DNA as a template for molecular construction. *AIP Conference Proceedings Series,* Vol. 725, pp. (67-77)

Washizu., M. (2005). Biological applications of electrostatic surface field effects. *Journal of Electrostatics*, Vol. 63, pp. (795-802)

Wong, P.K., Chen, C.Y., Wang, T.H., & Ho, C.M. (2004b). Electrokinetic bioprocessor for concentrating cells and molecules. *Anal. Chem.*, Vol. 76, pp. (6908-6914)

Wood, J. A., Zhang, B., Tomkins, M. R., & Docoslis, A. (2007). Numerical investigation of AC electrokinetic virus trapping inside high ionic strength media. *Microfluid Nanofluid,* Vol. 3, pp. (547-560)

Wu, J., Ben, Y., Battigelli, D., & Chang, H–C. (2005a). Long-Range AC Electroosmotic Trapping and Detection of Bioparticles. *Ind. Eng. Chem. Res.,* Vol. 44, pp. (2815-2822)

Wu, J., Ben, Y., & Chang, H.C. (2005b). Particle detection by electrical impedance spectroscopy with asymmetric-polarization AC electroosmotic trapping. *Microfluid Nanofluid,* Vol. 1, pp. (161-167)

Yamamoto, T., Kurosawa, O., Kabata, H., Shimamoto, N., & Washizu, M. (2000). Molecular Surgery of DNA Based on Electrostatic Micromanipulation. *IEEE Transactions on Industry Applications,* Vol. 36, pp. (1010-1017)

Yang, L. (2009). Dielectrophoresis assisted immuno-capture and detection of foodborne pathogenic bacteria in biochips. *Talanta,* Vol. 80, pp. (551-558)

Yang, L., Banada, P.P., Bhunia, A.K., & Bashir, R. (2008). Effects of Dielectrophoresis on Growth, Viability and Immuno-reactivity of *Listeria monocytogenes*. *J Biol Eng* Vol. 2, No. 1, Record (6)

Yang, L., Banada, P.P., Chatni, M.R., Lim, K.S., Bhunia, A.K., Ladischde, M., & Bashir, R. (2006). A multifunctional micro-fluidic system for dielectrophoretic concentration coupled with immuno-capture of low numbers of *Listeria monocytogenes*. *Lab Chip*, Vol. 6, pp. (896-905)

Zhou, R., Wang, P., & Chang, H-C. (2006). Bacteria Capture, concentration and detection by alternating current dielectrophoresis and self-assembly of dispersed single-wall carbon nanotubes. *Electrophoresis,* Vol. 27, pp. (1376-1385)

14

New Concepts of Integrated Photonic Biosensors Based on Porous Silicon

Cécile Jamois[1] et al[*]
[1]*Institut des Nanotechnologies de Lyon (INL), CNRS UMR 5270, INSA-Lyon*
[2]*Institut des Nanotechnologies de Lyon (INL), CNRS UMR 5270, Ecole Centrale de Lyon*
Université de Lyon
France

1. Introduction

A biosensor is a device that uses specific biochemical reactions mediated by isolated tissues, enzymes, immunosystems, organelles or whole cells to detect chemical compounds (IUPAC: http://goldbook.iupac.org/B00663.html). Biosensors integrate two functions, i) a bio-receptor functionalized with probes able to specifically recognize the targeted species and ii) a transducer converting the specific biological interaction into a quantitatively measurable signal. One way to classify biosensors relates on the transduction mode, such as optical (fluorescence, surface-enhanced Raman scattering, chemiluminescence, colorimetry, dual polarization interferometry and surface plasmon resonance), electrochemical (amperometry, potentiometry, field-effect transistor and conductimetry) and gravimetric transduction (quartz crystal microbalance, cantilever) (Sassolas et al., 2008).
The evaluation of biosensor performances relies on the following criteria: high sensitivity, operational and linear concentration range, detection and quantitative determination limits, high selectivity, steady-state and transient response times, sample throughput, reliability, reproducibility, stability and long lifetime (Thévenot et al., 1999). Other aspects like cost of test, ease of use, time of analysis including all the steps required for sample preparation should also be taken into account. Some biosensors are based on the use of labels such as colorimetric, fluorescent, enzymatic moieties or redox species... However, the current trends aim to develop on-chip integrated and label free detection systems. In this framework, porous silicon (PSi) offers high potential for biosensing:

- PSi physical properties directly depend on the structure. The optical properties are linked to the variation of refractive index with a change of porosity while the electrochemical properties rely on surface chemistry modification. Thus, PSi based transducers can be sensitive both to surface or volume biomolecular recognition.
- PSi surface chemistry is essentially governed by the high reactivity of Si-H bond, which can form both Si-alkyle or Si-OH bond (Stewart & Buriak, 2000). Thus, the surface can be either hydrophobic or hydrophilic, and a large range of biomolecules can be immobilized.

[*]Cheng Li[1], Emmanuel Gerelli[1], Régis Orobtchouk[1], Taha Benyattou[1], Ali Belarouci[2], Yann Chevolot[2], Virginie Monnier[2] and Eliane Souteyrand[2]

- The porosity of PSi can vary from 15 to 90%, yielding high specific surface and pore size ranging from nanopores (< 2 nm) to macropores (> 50 nm) (Canham, 1990). Mesopores (with 2-50 nm diameter) are the most suitable for biosensing, because they are large enough to allow for good biomolecule diffusion and they yield large specific surfaces ranging from 100 m^2/g to 350 m^2/g, which strongly increases the amount of biomolecules that can be immobilized on the transducer compared to a 2D surface immobilization. It is worthwhile to point out that the accessibility of the probes by the target molecules (to be detected) depends both on the pore size and on the surface energy of PSi (Tinsley-Bown et al., 2000).
- Finally, PSi is fully compatible with standard microprocessing techniques and can be micromachined, etched, and on-chip integrated.

The scope of this chapter is to present new concepts of integrated PSi biosensors, as well as the tools used for their study and realization, and a discussion on their performances.

2. Biosensors based on porous silicon

In the field of biosensors, PSi is mainly used for its large surface area. As an example, functionalized PSi was used in a modified single-tube format chemiluminescent assay to catalyze an enzymatic reaction indicating the presence of *Escherichia coli* bacteria. A lower detection limit of 10 cells within 40 min was obtained using PSi, compared to 10^3 cells for "classical" tube chemiluminescence assay (Mathew & Alocija, 2005). PSi thin films functionalized with covalently grafted antibodies were also used to selectively capture dye-labelled MS2 bacteriophage viruses (Rossi et al., 2007). Although pore penetration and binding efficiency depend on PSi surface wettability, fluorescence measurements showed a detection limit of $2x10^7$ pfu/ml (pfu: plaque-forming units) and a dynamic range for the measurement of viral concentrations from $2x10^7$ to $2x10^{10}$ pfu/ml. In these two cases, the targeted species are detected by chemiluminescent or fluorescent intensity measurements.

Biosensors can be advantageously based on electrical or electrochemical transducer properties when the biological recognition involves the conversion of an electroactive substance in contact with the target to be detected, e.g., in the case of enzymatic reaction. The current generated by electron transfer can be directly measured by amperometry if a conductive working electrode is used. A limiting factor for the sensitivity and the dynamic range is the amount of catalyzing species entrapped at the surface of the working electrode. Hence, a way to improve amperometric biosensor performances is the enlargement of the electrode area. Using a platinum-coated PSi layer to determine cholesterol concentration, a 3-fold increase of sensitivity was obtained compared to a planar electrode (Song et al. 2006).

A second class of electrical biosensors takes advantage of the semiconducting properties of Si substrates. In 1970, it was shown that a Field Effect Transistor (FET) can be adapted to work in aqueous media to build a so-called ISFET device that is sensitive to the ionic interactions with the SiO_2 surface (Bergveld, 1970). In the ENFET proposed in 1980, the sensing surface of FET is modified with enzymatic species (Caras & Janata, 1980). In 1994, we proposed the GENFET, a device using the intrinsic properties of negatively charged DNA strands for in-situ and direct label-free detection of DNA hybridization (Martin et al., 1994). In order to detect simultaneously different DNA sequences, we showed that the photopotential of electrolyte/SiO_2/Si semiconducting device is sensitive to the variation of the surface charge induced by DNA hybridization and could be used as a transducer for DNA chips (Souteyrand et al., 1997, 2000). In 1996, a PSi layer was added at the surface of

the bulk Si potentiometric device to measure penicillin concentration. An enlarged linear range of the calibration curve and higher signals were obtained, which were attributed to the larger amount of enzyme immobilised on the PSi substrate compared to planar structures (Thust et al., 1996, 1999). To conclude, in the case of electrical transducers, the improvement of biosensor performances achieved with PSi layers is usually only due to an increase of the specific working area and not to improvement of the electrical properties.

In the case of label-free optical detection, biosensors exploit the refractive index variations induced by the presence of target biomolecules specifically bound to probes immobilized at the sensor surface. Among the large family of PSi optical biosensors, the simplest devices are Fabry-Perot interferometers constituted of a few μm-thick PSi monolayers. Large shifts of the interference fringes induced by the binding of target molecules have been observed for a large variety of molecules such as DNA, proteins or small organic biomolecules (Lin et al., 1997). Multilayer structures exhibiting high reflectivity in well-defined frequency ranges, such as Bragg mirrors (Rendina et al., 2007) or rugate filters (Chapron et al., 2007; Cunin et al., 2002), have also been widely studied for biosensing applications. These devices usually yield increased sensitivity due to multiple reflections of light within the multilayers, which enhance light-matter interactions. When a layer is introduced inside the multilayer structure with a different width or a different porosity from the PSi layers constituting the multilayer, a microcavity is built. Such a device enables to obtain very narrow resonances that are highly confined inside the microcavity and thus are very sensitive to any variation in refractive index induced by the presence of target biomolecules in this layer. It has been demonstrated that molecule layers as thin as 0.01 nm could be detected using microcavities (Ouyang et al., 2006). These devices are also suitable for antibodies detection in whole blood samples with high specificity and good sensitivity (Bonanno & DeLouise, 2007).

As an alternative to biosensors based on multilayers, planar waveguides have also been proposed. They consist of a thin waveguiding layer with medium porosity on top of a highly porous substrate. Contrary to interferometers or multilayers that are usually used at normal incidence, planar waveguides support light modes that are propagating within the waveguide parallel to the surface. These modes are confined by total internal reflection due to the refractive index difference between the waveguide and the surrounding air or the highly porous substrate, respectively. In order to excite such propagating modes, light is usually coupled through a prism at very particular incidence angles. Refractive index variation in the waveguide layer can be observed by monitoring the variation in coupling angle. Very high sensitivities corresponding to detection limits of 5 pg/mm^2 have been reported using such sensors for DNA detection (Rong et al., 2008).

In the PSi-based optical biosensors cited above, red shifts are usually expected because the presence of the target biomolecules should increase the PSi refractive index. However, it has been demonstrated that a competing mechanism can lead to strong blue shifts. If Si-H or Si-OH bonds are present on the PSi surface, a transfer of negative charges from the bound molecules to the PSi can catalyze oxidation by the surrounding water molecules and results in strong corrosion of the PSi, thus in strong reduction of refractive index. The resulting blue shifts have often been observed in the case of DNA hybridization (Lin et al., 1997), and DNA biosensors based on catalytic corrosion were proposed and shown to yield much higher sensitivities than red-shift sensors (Steinem et al., 2004). The transduction mechanism was recently generalized to non-charged molecules by oxidation hydrolysis via metal catalysts in presence of oxidants, and avidin detection on biotinized PSi surfaces was demonstrated

(Völcker et al., 2008). It is important to point out that this type of biosensors is restricted to single-use, as the corrosion leads to destruction of the PSi structure.
More complete reviews on PSi-based biosensors (Jane et al., 2009) or on label-free optical biosensors (Fan et al., 2008) can be found in the literature.

3. Novel photonic-crystal-based biosensors

As presented above, most PSi optical sensors share the particularity that their active region for sensing is either buried – e.g., micro-cavities in multilayers – or very thick – as in the case of interferometric devices. This leads to limitations of the diffusion of biomolecules inside the porous structure, which introduce delays in the device response and alter the optical properties due to in-depth inhomogeneity of infiltration. These issues can be reduced if the sensing layer is at the device surface and relatively thin, as in the case of planar waveguides. The sensitivity of such planar sensors could be greatly enhanced if the surface configuration of planar waveguides could be combined with stronger light confinement and/or strong slowing down of light in order to increase light-matter interactions. The use of gratings (Ryckman et al., 2010) constitutes a first step towards improving the optical properties. Another way is to design new sensors using photonic crystals (PCs) concepts.
Photonic crystals are periodic arrangements of dielectric media (Joannopoulos et al., 1995; Viktorovitch et al., 2007, 2010). The periodicity can be either along one direction for one-dimensional (1D) PCs, in a plane for two-dimensional (2D) PCs, or in all dimensions for three-dimensional (3D) PCs. In this sense, periodic multilayers such as Bragg mirrors constitute 1D PCs. PCs have the great property to exhibit band structures for photons, i.e., light in such structures can only have discrete frequency states called photonic bands. Convenient engineering of photonic bands enables to control light velocity. Moreover, photonic band gaps (PBGs) can exist, i.e., frequency regions where light propagation is prohibited inside the PC. Hence, through a careful design of the PC it is possible to tailor its optical properties in order to strongly confine light in a given region of the device and to strongly reduce its propagation velocity.
In the following, we will present two different concepts of planar biosensors using PCs properties to increase sensitivity: a surface wave biosensor and a planar 1D PC device.

3.1 Surface-wave biosensor

The surface wave (SW) biosensor consists of a periodic multilayer with a defect layer at its surface. It can be understood as a hybrid between a planar waveguide and a microcavity device. Similarly to the planar waveguide, light can be excited within the PSi structure, e.g. through a prism, and confined due to the refractive index contrast between the dielectric structure and the lower-index environment. Similarly to the microcavity sensor, the periodic multilayer exhibits a PBG which prohibits light propagation inside the multilayer. Hence, light excited in such a device is forced to propagate within the thin defect top layer, leading to very strong light confinement and intensity within this surface layer. The sensitivity of SW devices has already been demonstrated for sensing applications (Liscidini & Sipe, 2007; Shinn & Robertson, 2005). It can be enhanced further if the devices are made in a material with much greater specific surface like PSi (Guillermain et al., 2006, 2007).
The principle of the SW biosensor is illustrated in fig. 1. Light is coupled to the PSi device through a prism. In this configuration, the SW can only be excited at a given frequency for a particular angle of incidence θ_0, when its wave vector is matching the parallel wave vector

of the incident beam inside the prism. At the particular angle of incidence θ_0, most light is coupled to the SW, leading to a strong intensity decrease of the reflected beam. As the coupling conditions to the SW strongly depend on the surface layer configuration, in particular its refractive index, any change in refractive index induced by the presence of the target molecules should lead to a variation of the coupling angle, as illustrated in fig. 1b.

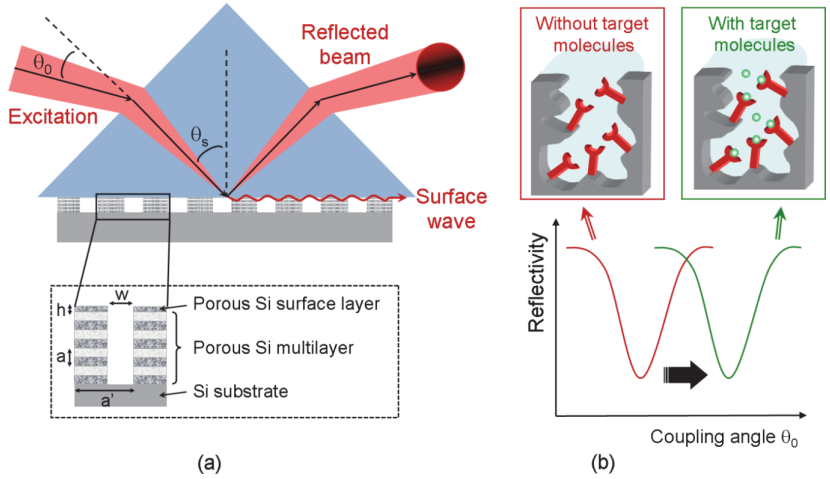

Fig. 1. Principle of the surface wave sensor: (a) device description, and (b) principle of optical sensing.

When compared to planar waveguides, the SW device presents the great advantage that the top layer can be of any porosity, provided that the layer thickness is correspondingly adjusted to optimize the optical properties. This means that the porosity of the top layer can be chosen depending on the size and properties of the biomolecules to detect. This is not the case in planar waveguides where the porosity of the top layer is limited, since the refractive index of the waveguide should be higher than that of the underlying PSi substrate. Moreover, we will demonstrate in section 6.1 that strong decrease of light velocity can be achieved via a lateral patterning of the multilayer with air slits as shown in fig. 1a, leading to strong enhancement of the biosensor sensitivity (Jamois et al., 2010a).
In the configuration shown in fig. 1a, the surface of the PSi device is facing the prism. In the case where in-situ experiments should be performed, the same biosensor could be used, provided that it is reported onto a transparent substrate in order to couple light from the backside and leave the PSi device in contact with the analyte.

3.2 Planar photonic-crystal biosensor

The planar 1D PC biosensor consists of a PSi layer with low or medium porosity on top of a higher-porosity substrate. As illustrated in fig. 2a, the top layer is patterned by a periodic array of air slits that extend in the depth down to the underlying porous substrate. When excited by a light beam at normal incidence, such a device can support particular modes, called Fano resonances that result from the coupling between the discrete bands of the 1D PC and the continuous states of the surrounding medium seen by the incident beam. These resonances are highly confined within the top layer and can have very high spectral finesse

(Jamois et al., 2010b; Viktorovitch et al., 2007, 2010). If the device is conveniently designed, the excitation of the Fano resonance can lead to a complete switch of the reflectivity from zero reflection (i.e. complete transmission) to total reflection. Hence, any change in the refractive index of PSi induced by the presence of target molecules will lead to a shift of the resonance and to an abrupt change of reflectivity, as shown in fig. 2b.

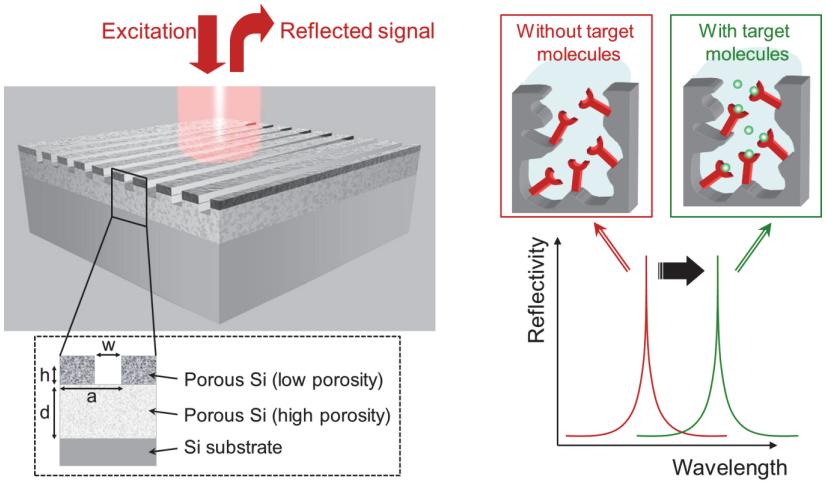

Fig. 2. Principle of the planar photonic crystal sensor: (a) device description, and (b) principle of optical sensing.

This type of biosensor presents the advantage to be used at normal incidence with relatively simple optical setups and no need for a prism. It can be directly integrated into an optical microchip in case multiple parallel sensing is desired. As will be discussed later in this chapter, its fabrication is easier than for the surface wave device, since only the top layer is patterned in this case.

The biosensor configuration presented in fig. 2 aims at monitoring reflection properties. This is the configuration that will be considered in the following sections. However, the same device could also be used in transmission, provided that it is reported onto a transparent substrate. Transmission configuration is particularly interesting when in-situ measurements are desired, as it prevents the incident beam from going through the analyte, which could lead to strong light absorption and sensitivity decrease. In-situ measurements could also be performed in reflection configuration if the design of the biosensor is carefully optimized in order to position the resonance in a wavelength range where the analyte absorption is low.

4. Experimental realization

The experimental realization of the PC-based biosensors requires several main steps. The first step is anodization of the substrate to form the PSi layers. It is the focus of section 4.1. Anodization is followed by lateral patterning of the PSi using standard nanolithography and dry etching techniques in order to fabricate the PC, as will be detailed in section 4.2. After

cleaning of the PSi devices to remove the remains from the patterning process, the PSi structure is slightly thermally oxidized (≤ 1 nm SiO_2) in order to enable subsequent silane-based functionalization. The details of PSi functionalization are discussed in section 4.3. In the following, we will consider the case of DNA sensing via hybridization of single-strand DNA targets with their complementary strands immobilized on the PSi surface. After immobilization of the DNA probes, the last required step is a capping to prevent non-specific absorption. The main steps in the biosensor realization are summarized again below:

anodization → patterning → oxidation → silanization → immobilization → capping → hybridization.

The influence of each step on the optical properties of the PSi is characterized by reflectivity measurements on 5 µm-thick PSi monolayers. After each step, the amounts of molecules infiltrated inside the pores can be quantitatively evaluated by fitting the reflectivity spectra with the refractive index models presented in section 5.1. The success of DNA immobilization and hybridization has also been verified by fluorescence measurements using probe and target molecules labelled with Cy3 and Cy5, respectively.

4.1 Porous silicon anodization

Anodization of silicon substrates to produce PSi is a well-described process in the literature. It takes place in hydrofluoric acid (HF) solution, where the silicon is dissolved by the fluorine ions thanks to the positive charges reaching the electrolyte/silicon interface (Kochergin & Föll, 2009; Lehmann & Gösele, 1991). Depending on substrate doping, current density and electrolyte concentration, the porosity and morphology of the fabricated PSi can be varied (Lehmann et al., 2000). In particular, PSi structures constituted of successive layers with different porosities, such as planar waveguides or multilayers, can be fabricated by controlled variation of the current density during anodization.

Fig. 3a shows a schematic view of the cell used to prepare our PSi samples. In order to fabricate meso-PSi, highly P-doped silicon substrates are used. The substrate is placed at the bottom of the anodization cell on a copper electrode, and in contact with the HF/H_2O/ethanol (35%/35%/30%) electrolyte. The second electrode made of platinum is immersed in the electrolyte at the top of the cell.

When preparing PSi layers for optical application, good care has to be taken that the roughness at the interfaces between the layers is low enough to prevent light scattering. Hence, anodization takes place at low temperature (-40°C) in order to enhance the viscosity of the electrolyte, which has been shown to strongly reduce interface roughness (Setzu et al., 1998). Working at low temperature also allows for a better control of the anodization velocities, thus for a better control of the layer thicknesses. Fig. 3b presents a scanning electron microscope (SEM) picture of a fabricated SW device consisting of PSi layers with alternative porosities of 80% and 35% and a small surface layer with 35% porosity. In spite of the roughness due to sample cleaving, very smooth interfaces between the layers can be seen. The surface layer has a well-controlled thickness as thin as 60 nm.

After fabrication, the PSi structures are systematically characterized by reflectivity measurements in the 900-1700 nm infra-red range, in order to check the porosity, layer thickness and homogeneity. Fits of the reflectivity spectra are performed using the refractive index models and the optical simulation methods presented in section 5.

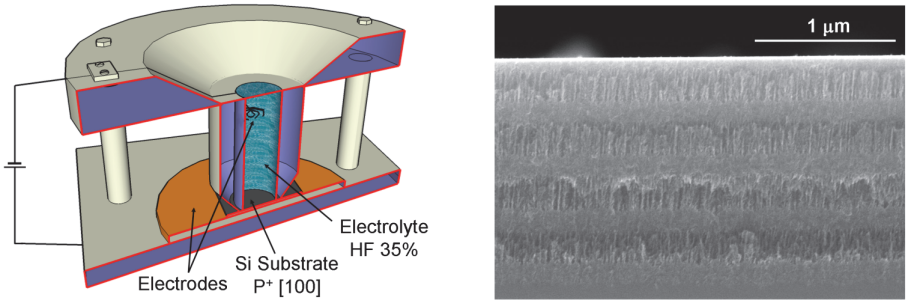

Fig. 3. (a) Schematic view of the anodization cell used to prepare the PSi samples, and (b) SEM picture showing an example of PSi multilayer.

4.2 Porous silicon patterning

After fabrication of the PSi layers, the next step in biosensor realization is PSi patterning to build the PC devices. The challenge here consists in deeply patterning a material that is itself nanostructured, anisotropic, and highly insulating, at a submicron scale. The desired air slits should have perfectly vertical walls, a typical width of 200 to 400 nm, a period below 1 μm, and an aspect ratio – i.e. depth/width ratio – of 2 to 4.

Different ways have been explored to obtain patterns in PSi at a submicron scale. Among them, photo-dissolution appears to be a promising technique, which uses holographic setups to create light patterns into the material and locally dissolve the material (Lerondel et al., 1997). Similarly, photo-oxidation has also been proposed as an alternative to locally oxidize and selectively etch patterns into PSi layers (Park et al., 2008).

Different nanoimprint techniques have also been proposed, such as soft lithography where PSi is put in contact with a polymer stamp and selectively detached from the substrate (Sirbuly et al., 2003). Very recently, patterning of PSi layers via nanoimprint using silicon stamps has been proposed (Ryckman et al., 2010). This technique allows for the realization of very well defined gratings; however, the PSi inside the patterns might get damaged. The pattern aspect ratio that can be reached using imprinting techniques is also quite limited.

In order to reach the desired depth required for our PC devices, a patterning process based on electron-beam lithography and reactive ion etching (RIE) has been selected. Very few reports on PSi patterning using dry etching techniques can be found in literature. The processes proposed are based on fluorine (Arens-Fischer et al., 2000; Tserepi et al., 2003) or chlorine plasmas (Meade & Sailor, 2007) and have been used to realize patterns with widths in the 10-100 μm range. In spite of these encouraging achievements, PSi patterning at sub-micrometer scale with high aspect ratios remains a real challenge for many reasons: the porous nanostructure of the material and its anisotropic morphology leading to poor efficiency in the case of such directional etching processes, the large internal surface of PSi favouring high sensitivity to contaminations such as polymer deposition during plasma etching, as well as the strongly insulating nature of the material.

The different steps in the realization of the PSi PCs are presented in fig. 4. After fabrication of the PSi by anodization, a silica layer is deposited by sputtering. This layer serves a triple purpose, since it helps homogenising the surface of the sample for subsequent resist spin-coating and lithography, it prevents the resist from penetrating into the material pores, and

it is used as a hard mask for RIE. After deposition of the silica layer, electron-beam lithography is carried out using PMMA A4 resist, and the resist patterns are transferred into the underlying silica layer by a CHF_3-based RIE process. The patterned silica layer is then used as a hard mask for PSi etching which occurs in SF_6/Ar plasma.

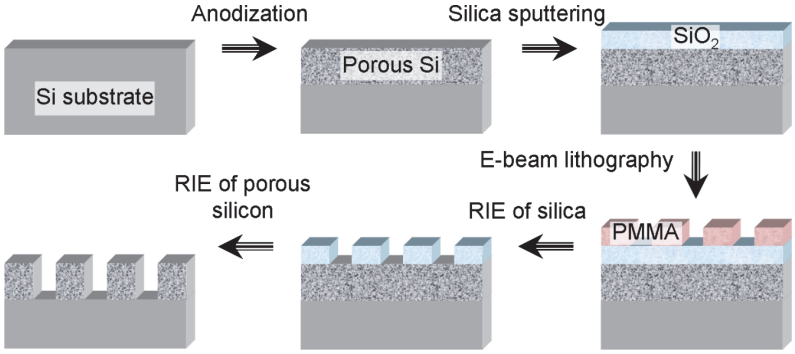

Fig. 4. The different steps of the patterning process used to realize PCs in PSi.

After careful optimization of each step of the PC realization process, in particular PSi patterning in SF_6-based RIE, deep trenches with vertical walls and aspect ratio of about 2 were successfully etched into the PSi. Fig. 5a shows an example of trenches realized in a PSi structure constituted of two layers with different porosity, 35% and 80% for the top and bottom layer, respectively. It can be observed that the RIE process enables to etch both porosities with perfectly vertical walls and no visible transition between the two layers in spite of their very different morphological and electrical properties.

The etching efficiency of the RIE process strongly decreases with increasing porosity. Hence, the pattern depth that can be reached is limited in the presence of 80% porosity layers, and the process presented above has to be adapted to allow for the devices fabrication.

In the case of planar PC fabrication where only the top layer with 35% porosity is patterned, the limitation in etching efficiency is induced by the presence of the underlying highly-insulating 80%porosity substrate. In order to reach deeper patterns, anodization of the high-porosity substrate can be performed after patterning of the top layer. Fig. 5b shows a SEM view of a fabricated planar PC device which consists of a 700 nm-thick PSi layer with 35% porosity on top of a substrate with 80% porosity. The width and period of the trenches are 400 nm and 900 nm, respectively. The high-porosity substrate was anodized after patterning of the top layer. A very smooth interface between the two porous layers can be observed.

In the case of the SW device, much deeper trenches are required, since at least 3 multilayer periods should be patterned. A well-known way to achieve deep etching is to use cyclic processes including passivation steps to provide both sidewall verticality and protection of the etching mask. However, such a process should be avoided in the case of PSi, as it would lead to strong polymerization inside the PSi pores that would harden considerably the material etching over time, as well as prohibit any subsequent biochemical functionalization. In order to reach the desired number of patterned multilayer periods, a new process using a more selective hard mask has to be developed. One way would be to consider metallic masks; however, the issue of metal contamination of the internal PSi surface exposed to the RIE environment has to be carefully investigated, as it may also influence subsequent biochemical functionalization.

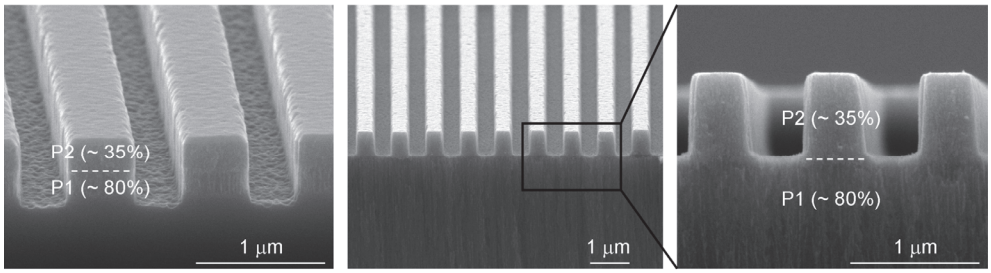

Fig. 5. (a) SEM image showing a preliminary result of patterning of PSi layers with different porosities P1 (80%) and P2 (35%). (b) SEM images of fabricated planar PC in PSi. The period of the patterns is 900 nm, and the device has a total size of 100 μm x 100 μm.

Another issue to tackle is the contamination of the PSi by fluorine during the RIE process. Indeed, the fluorine contained in the plasma can react with inevitable carbon contamination to form a fluorocarbon layer that deposits onto the PSi walls in the depth of the material. Special treatments are currently under development to clean the PSi walls from this contamination. Anodizing the substrate after RIE like in the case of the planar PC device is also a good way to avoid this contamination.

4.3 Porous silicon functionalization for DNA sensing

The bioselective element of biosensors is usually based on the immobilization of biomolecules on the surface of the transducer. The immobilization reaction can be achieved by physisorption through weak interactions (van der Waals, coulombic forces), by crosslinking with glutaraldehyde via an aminated surface (Rong et al., 2008) or SMCC via a thiolated surface, by entrapment or by chemisorption via covalent bonding.

Covalent immobilization reactions of biomolecules require chemical functionalization of the surface. These chemical groups can be introduced by plasma, polymer coatings… Hetero-cross linkers are also widely used. These molecules have two functional groups: one reacting with the material and one reacting with the biomolecules to be immobilized.

PSi has already been used as a large surface area matrix for immobilization of different kinds of biomolecules including enzymes (Drott et al., 1997), DNA fragments (De Stefano et al., 2007) and antibodies (Betty, 2009). Chemical functionalization of PSi can either involve the native Si-H terminated surfaces or the Si-O bond resulting from PSi oxidation.

Native Si-H surfaces can lead to Si-C or Si-Si bonds via organometallic reactions or via dehydrogenative silane coupling, respectively (Stewart & Buriak, 2000). The hydrosilylation reaction of alkyne and alkene with Si-H leads to the formation of Si-C bond with reduction of the C-C multiple bond. It proceeds with appreciable rate in the presence of white light, Lewis acid or by thermal activation. Similarly, formation of Si-C can be obtained by reaction of Grignard (Stewart & Buriak, 2000) or by electrografting reactions with organo halide (Gurtner et al., 1999) or alkyne (Robins et al., 1999). Si-C bonds can also be formed by cleavage of Si-Si linkage by reacting organolithium (Kim & Laibinis, 1998) or by electrochemical reduction of alkynes (Robins et al., 1999).

Oxidation of silicon results in the incorporation of oxygen, leading to a surface bearing terminal silanol groups. These groups can readily react with silazane, alkoxy silane or

organo silyl halide to form a siloxane bridge Si-O-Si. Organo silane can be mono or multifunctional (tri or di-chloro or -alkoxysilane). Multifunctional silane is usually preferred due to its higher reactivity and because it can lead to lower non-specific binding. Silanization with aminopropyl triethoxy silane or 3-glycidopropyl trimethoxy silane is well documented in the literature (Dugas et al., 2010a).

With multifunctional silane, additional intermolecular dehydration reactions between adjacent organo silanols lead to a 2D network. This polycondensation reaction needs to be perfectly monitored, otherwise it will lead to an anarchic 3D network and consequently to non-reproducible surface chemistry and obstruction of the PSi pores. An alternative solution is the use of monofunctional silane. Indeed, in this case each silane molecule can only react with the surface to form a siloxane bridge or with another silane molecule to form a dimer (Dugas et al., 2010b). The dimer is eliminated by subsequent washing. Therefore, no polymeric network is formed. The lower reactivity of monofunctional silane can be compensated by the use of silazane groups allowing for the complete reaction of all surface accessible silanols as demonstrated by Dugas (Dugas & Chevalier, 2003). The obtained layer was demonstrated to be reproducible and stable under harsh conditions.

Our process uses a monofunctional silane, *tert*-butyl-11-(dimethylamino)silylundecanoate which is an organo silazane bearing an ester function. Chemical functionalization of silica (Bras et al., 2004), PSi (Bessueille et al., 2005) and glass have been reported using this molecule from solution in pentane or from gas phase (Phaner-Goutorbe et al., 2011). As illustrated in fig. 6, after silanization, the *tert*-butyl ester is converted into the corresponding carboxylic acid by acidolysis in formic acid and activated with N-hydroxy succinimide. The obtained NHS ester surfaces can be employed for amine coupling. The resulting surface has a molecule density of $2x10^{14}$ molecules/cm^2. Immobilization of amino-modified oligonucleotide from diluted solution (25 µM) yielded to 3 – $4x10^{11}$ strands/cm^2. Hybridization yield with single stranded synthetic oligonucleotide is 10-20% (Dugas et al., 2004).

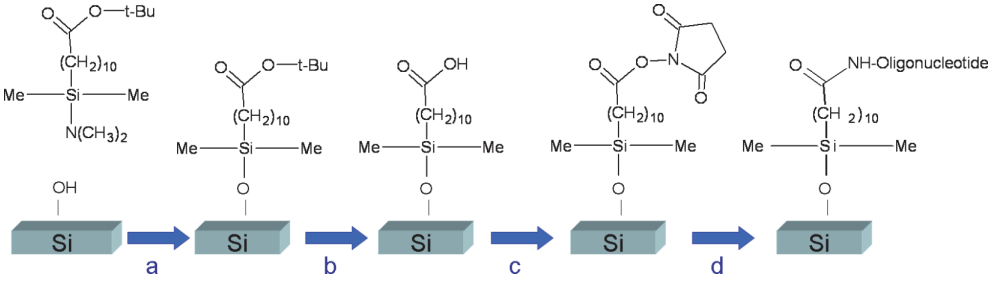

Fig. 6. Amino modified oligonucleotide are covalently immobilized by formation of an amide bond. After surface silanization with the monovalent silane uses *tert*-butyl-11-(dimethylamino)silylundecanoate (a), the *tert*-butyl ester group is removed leading to the corresponding carboxylic function (b). Activation (c) with diisoprpyl carbodiimide/ N-hydroxysuccinimide allows for the reaction with amino modified oliganucleotide (d) leading to the formation of an amide bond.

The resulting covalent immobilization of oligonucleotides can withstand 25 successive cycles of hybridization/denaturation (in 0.1 N NaOH) onto the same surface without observing any degradation, as well as deprotection/oxidation steps performed during

phosphoramidite oligonucleotide synthesis (Bessueille et al., 2005; Cloarec et al., 2008). Immobilization of peptides (Soultani-Vigneron et al., 2005), histones (El Khoury et al., 2010) or carbohydrates (Chevolot et al., 2007; Moni et al., 2009; Zhang et al., 2009) has also been achieved.

5. Modeling of optical properties

Modelling of PSi based PCs includes two different aspects: the calculation of the refractive index, and the simulation of the optical properties. They are presented in the following.

5.1 Calculation of porous silicon refractive index

PSi is a composite medium with a pore size much smaller than the wavelength of light. Hence, the dielectric response can be described through an effective dielectric function. A complete review of the different isotropic and anisotropic models used for the calculation of PSi refractive index has recently been published (Kochergin & Föll, 2009). In the isotropic approximation, the main models used for the calculation of the effective dielectric function are the Bruggeman and Landau Lifshitz Looyenga (LLL) effective medium approximations (EMA) that can be defined by the following expressions (Bruggeman, 1935; Looyenga, 1965):

$$Bruggeman: \sum_i f_i \frac{\varepsilon_i - \varepsilon_{eff}}{\varepsilon_i + 2\varepsilon_{eff}} = 0 \qquad LLL: \ \varepsilon_{eff} = \left(\sum_i \left(\varepsilon_i^{1/3} - \varepsilon_{Si}^{1/3} \right) f_i + \varepsilon_{Si}^{1/3} \right)^3 , \ \sum_i f_i = 1 \qquad (1)$$

where f_i and ε_i are the volume fraction and the complex dielectric function of material i, respectively. The refractive index of materials is related to the permittivity ε with $\varepsilon = n^2$. The refractive indices of Si and SiO_2 can be obtained from the Palik handbook (Palik, 1998). As the materials are used in their transparency domain, the variations of their refractive indices with the wavelength are deduced from a Cauchy law, using the parameters given in table 1:

$n = A + \frac{B}{\lambda^2} + \frac{C}{\lambda^4}$		A	B	C
	Si	3.4227	0.1104	0.041
	SiO_2	1.4213	0.0856	-0.0735

Table 1. Cauchy law and values of the Cauchy coefficients used for the modelling.

In order to consider absorption of light in the doped silicon substrate, variations of the refractive index induced by free carriers absorption have to be taken into account. The relation proposed by Soref is used (Soref & Bennett, 1987), which requires calculation of the electron and holes mobilities depending on substrate doping (Sedra & Smith, 1997).

The models presented above have been implemented to fit experimental data, in particular the reflectivity measurements performed on PSi layers. As an example, the reflectivity spectra of a PSi monolayer before and after an oxidation step are plotted on fig. 7. The parameters of the Bruggeman and LLL models and the thickness of the PSi monolayer are obtained using a Levenberg Marquardt nonlinear fitting method (Press et al., 1992). The results obtained using the Bruggeman and LLL models reproduce well the experimental indices deduced from reflectivity measurements. For this particular sample, the PSi layer was found to have an initial porosity of 70% and 73%, respectively, and a thickness of 4.735 and 4.741 µm, respectively, for the Bruggeman and LLL models. Both models gave a silica

fraction of 11% after oxidation. Hence, the fitted parameters are very close for both models, with a relative variation below 5%.

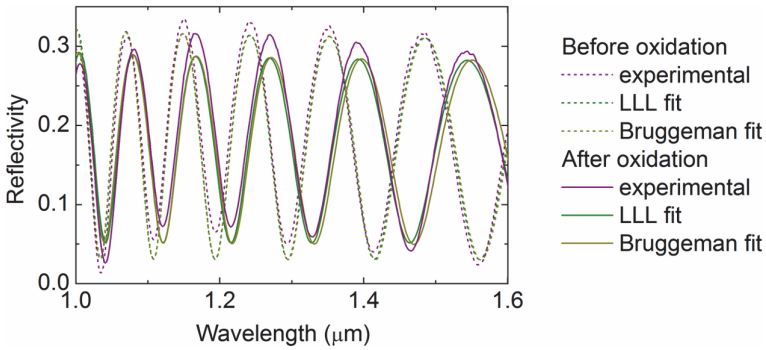

Fig. 7. Evolution of the reflectivity of a PSi monolayer before (dash) and after (straight) oxidation step. The experimental data has been fitted with the Bruggeman and LLL models.

In the following sections, the refractive indices will be determined using the LLL model. Fitting all experimental data using the LLL model, we could evaluate that the volume fractions of silica after oxidation correspond to the formation of a layer having a thickness of 1 nm on the internal PSi walls, for both porosities considered (35% and 80%). This is consistent with the experimental calibrations of the oxidation process. Similarly, the volume fractions of silane molecules deduced from the experimental spectra after silanization are equivalent to the formation of dense layers with refractive index 1.4 and thickness around 1.7 nm covering the internal PSi walls. This layer thickness is similar for both porosities and consistent with the developed length of the silane molecules used (~ 1.7 nm).

5.1 Simulation of optical properties

Numerical modelling is a major concern for the study of PC structures. Along the years, two main approaches have emerged: the plane wave expansion (PWE) and the finite difference in the time domain (FDTD) method.

The PWE method relies on the translation symmetry of the PC structure. The method assumes a time harmonic evolution of the electromagnetic fields. In this case, the Maxwell equations lead to the following general Helmoltz equation:

$$\vec{\nabla}\times\left(\frac{1}{\varepsilon_r(\vec{r})}\vec{\nabla}\times\vec{H}(\vec{r})\right)=\left(\frac{\omega}{c}\right)^2\vec{H}(\vec{r}) \tag{2}$$

where $\boldsymbol{H}$ stands for the magnetic field, ω the pulsation and ε_r is the relative dielectric permittivity.

This is an eigenvalue problem, which can be solved using a Fourier expansion along the vectors of the reciprocal lattice. It leads to the dispersion relation $\omega = \omega(\boldsymbol{k})$ where $\boldsymbol{k}(k_x,k_y,k_z)$ is the light wave vector. This approach enables a very efficient calculation of the band diagram, giving information on photonic band gaps, group and phase velocity… of the infinite periodic structure. However, this useful approach suffers from some limitations. In its common formulation, it could not easily handle losses (lossy material, leaky modes…). In

the following sections, a free software package is used, MIT Photonic Bands (MPB) (Johnson & Joannopoulos, 2001).
When it comes to real finite devices, the FDTD method is more suited. This method relies on the discretization in time and space of the Maxwell equations (Taflove & Hagness, 2005):

$$\frac{\partial \vec{E}}{\partial t} = \frac{1}{\varepsilon} \nabla \times \vec{H} \quad and \quad \frac{\partial \vec{H}}{\partial t} = -\frac{1}{\mu} \nabla \times \vec{E} \tag{3}$$

where $\boldsymbol{E}$ and $\boldsymbol{H}$ stand for the electric and magnetic field, respectively, and ε and μ for the dielectric and magnetic permittivity, respectively.
The numerical experiments generally consist in sending an electromagnetic pulse onto the structure and to monitor its response with time. A single simulation run is necessary to get the frequency response thanks to the Fourier transform of the time response. It gives access to the spectral response of the system (transmission, reflection). The ability of FDTD to solve open problems is very useful for the study of microcavities and leaky modes. It gives access to the quality factor (Q factor = $\lambda/\Delta\lambda$) of resonances. Moreover, an electromagnetic field map at a given frequency could be easily obtained thanks to the discrete Fourier transform. As this method has achieved its full maturity, it can handle dispersive and lossy materials, non-uniform mesh, non-linear effects… Another interesting development is the implementation of periodic boundary conditions which enable the study of infinite PCs. Compared to the PWE, the FDTD method is less efficient; however, it allows for the study of leaky modes (modes above the light line, i.e. in the free-state continuum). The FDTD method also requires a lot of computing resources which are now available, thanks to ever evolving microprocessor power, and it can be by nature easily parallelized.

6. Performance study of photonic-crystal-based biosensors

In this section, a performance study of the two PC-based biosensors is discussed, using the tools and methods presented above. Both devices are considered for use in the infra-red range at around 1300-1500 nm wavelength where absorption losses in the material can be neglected. In this case, the main source of losses in PSi devices is expected to be scattering at the interface of the silicon nanocrystallites (Ferrand & Romestain, 2000). Experimental measurements show that the losses are only a few cm^{-1} in this wavelength range and should not alter significantly the sensor response. Therefore, we expect our theoretical predictions to be in good agreement with experimental results.

6.1 Surface-wave biosensor

The very high sensitivity of the SW sensor in the 1D – i.e., unpatterned – configuration has been demonstrated both theoretically and experimentally. In particular, we have observed angular variations as large as 20° after grafting of amine molecules inside the PSi device (Guillermain et al., 2007). In further studies, much smaller amounts of biomolecules were considered, in order to evaluate the limit of detection of the biosensor. It was demonstrated that convenient lateral patterning could enhance the sensitivity of the biosensor by an order of magnitude (Jamois et al., 2010a). In these previous studies, we focussed on SW sensors having a high-index surface layer with porosity 35%. Such porosity enables to reach very high sensitivities due to very large PSi internal surface. However, due to the small pore size (< 10 nm) sensing is limited to small biomolecules. In the following, we consider the case of

SW sensors having a surface layer with larger porosity 55%, which might yield a slightly lower sensitivity due to smaller PSi internal surface, but enables sensing of larger molecules. The devices consist of a multilayer with period a and standard porosities P1 = 80% and P2 = 35%, respectively, with corresponding refractive indices n1 = 1.4 and n2 = 2.5 deduced from the LLL model. The multilayer is terminated by a surface layer with porosity P_{surf} = 55% and refractive index 2.0. Fig. 8 shows the band diagram of the 1D PC for the propagation direction parallel to the surface. As the 1D PC is homogeneous in the direction of propagation, the bands of the 1D structure shown in fig. 8 are continuous. However, the continuity of the bands can be broken by introducing a periodic perturbation. If a periodic pattern is introduced in the direction of propagation, bands are back-folded at the edge of the lateral Brillouin zone – for wave vectors $k = \pi/a$ – resulting in local band flattening, i.e., a strong decrease of light velocity. After careful optimization of both the multilayer and the array of air slits, a 2D structure was obtained with a PBG large enough to assure a good confinement of the SW. The optimized parameters of the resulting 2D PC are thicknesses d1 = d2 = 0.5a for the multilayer, and w = 0.8a and a' = 1.2a for the width and period of the air slits, respectively. For a good comparison of the sensor performances, the layer thicknesses are the same for the 1D sensor as for the 2D device. Because the surface mode position within the PBG is highly sensitive to the thickness of the surface layer (Guillermain et al., 2006), optimization of the surface layer thickness has also been necessary to position the SW in the middle of the PBG and thus provide a good light confinement within the surface layer. The optimized thickness of the surface layer is h = 0.4a for both 1D and 2D devices. Fig. 8 shows the band structures for the optimized 1D and 2D SW devices.

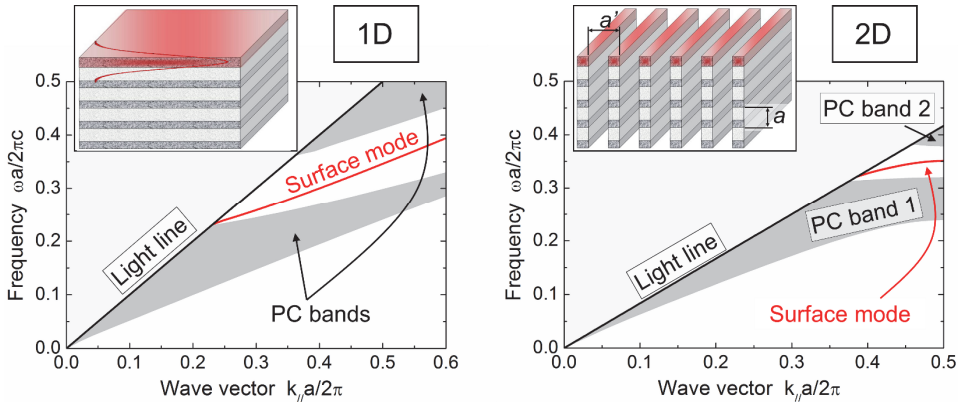

Fig. 8. Simulated band structures (MPB) of the SW sensor in air environment for the unpatterned (1D) and patterned (2D) configurations.

As plane-wave simulations consider a semi-infinite structure that is not experimentally achievable, periodic FDTD simulations were also performed to evaluate the performances of more realistic devices. Considering a multilayer consisting of 6 periods and varying the depth of the air slits, it could be verified that the optical properties of the device do not vary significantly with an increase of the slits depth, provided that the air slits are at least 3 multilayer periods deep. Hence, our band structure calculations can well describe the expected device performances, if the depth of the patterns in the experimental 2D sensor reaches 3 multilayer periods.

In order to demonstrate the high device sensitivity, a comparative study of the optical response in the 1D and the 2D cases has been performed in air environment, considering as an initial state a slightly oxidized porous structure (~ 1 nm SiO_2) and varying the amount of molecules grafted onto the pore walls. Note that similar results would be obtained in the case of specific biomolecular recognition, provided that the initial refractive index of PSi is adjusted to take into account biochemical functionalization. Moreover, we consider the limiting case where molecule grafting is restricted to the surface layer in order to take into account the inhomogeneous infiltration of liquids and biomolecules inside meso-PSi, which is the largest close to the surface and decreases in the depth of the multilayer, as was demonstrated using labelled proteins (De Stefano & D'Auria, 2007). We should point out that this restriction is underestimating the response of the biosensors.

The shift in the band structure induced by the grafting of 2.5%biomolecules inside the PSi is presented in fig. 9 for both 1D and 2D devices. It can be seen that the much flatter surface band of the 2D sensor leads to much larger variations in wave vector and in resulting coupling angle. In the presence of the biomolecules, the shift in coupling angle is 0.7° for the unpatterned device and as large as 4.0° for the patterned sensor. This corresponds to an increase in sensitivity of the 2D device by a factor 6 compared to the 1D case.

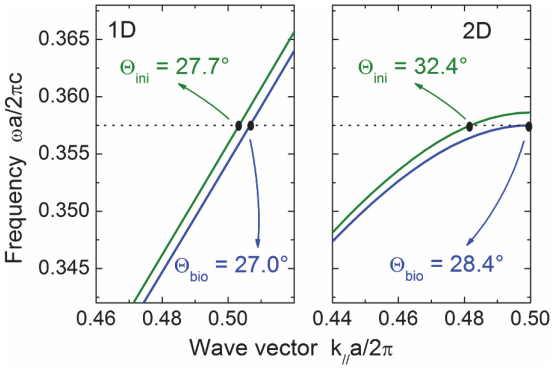

Fig. 9. Optical response of the surface wave sensor to the grafting of 2.5% biomolecules in air environment for the unpatterned (1D) and patterned (2D) configurations.

The variation in coupling angle and in refractive index depending on the amount of biomolecules is presented in fig. 10 for the 2D biosensor. For a better understanding of the amount of biomolecules infiltrated inside the pores, it is also expressed as the equivalent thickness d_{bio} of a dense monolayer having the same volume and homogeneously coating the internal surface of the pores. This formalism has already been used in other studies of photonic sensors based on PSi, and has proven to yield good agreement between theoretical predictions and experimental results (Ouyang et al., 2006). As can be seen in fig. 10a, a variation in coupling angle as large as 13.5° is expected for the grafting of a dense monolayer of biomolecules with thickness 1.7, which corresponds to the case of our silanization process. A much smaller amount of molecules of 0.1% – equivalent to a dense layer with thickness 0.01 nm – would still induce a variation in coupling angle of 1°, with a corresponding variation in refractive index of $6x10^{-4}$. Considering that high-performance SPR setups can detect angular variations as small as 0.001°, we can conclude that the limit of detection of the SW sensor is very low.

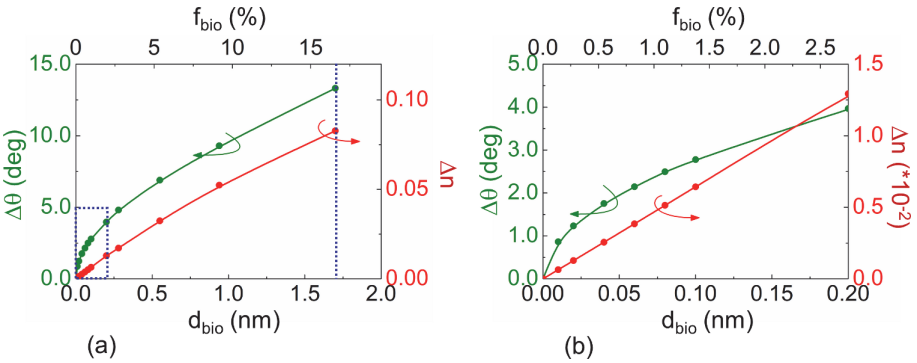

Fig. 10. Simulated optical response (MPB) of the SW sensor in air environment as a function of the amount of detected biomolecules: (a) for large amounts, and (b) for smaller amounts. The optical response is expressed both as a shift in coupling angle ($\Delta\theta$) and as the corresponding refractive index variation in the top layer (Δn). The amount of biomolecules is given as a volume fraction inside the PSi (f_{bio}) and as an equivalent thickness (d_{bio}). The blue dashed line indicates the expected device response to silane grafting.

6.2 Planar photonic-crystal biosensor

The optical response of the planar PC observed at normal incidence shows the superposition between interferences occurring inside the PSi layers and the excited Fano resonances. In order to maximize the variation of reflection induced by biosensing events, the structure has to be optimized to position the resonance in a zero of reflectivity corresponding to destructive interferences within the PSi layers. This way, the reflected signal at resonance can be switched between 0% and 100%. The device optimization was performed combining plane-wave and FDTD simulations for the TE polarization where the electric field is parallel to the slits (Jamois et al., 2010b). After optimization, the band structure presented in fig. 11a was obtained, yielding a Fano resonance with very sharp features at a relative frequency $a/\lambda = 0.66$ very close to the Γ point, where it can be excited at normal incidence. The Q factor of the resonance can be as high as 1200 for the optimized 1D PC with top layer thickness $h = 0.75a$ and trench width $w = 0.4a$. Note that the Q factor is very sensitive to the thickness of the top PSi layer: increasing or decreasing the thickness by only 50 nm results in a reduction of the Q factor by several hundred. As our fabrication process enables a very good control of the layer thicknesses, the sensitivity of the Q factor should not have a significant impact on the device performances. The Q factor also strongly varies with the filling factor, i.e., the relative width of the air slits, which means that the experimental fabrication process should be carefully calibrated to obtain the desired slit widths.

In order to evaluate the performance of the device for biosensing, a similar study was performed as in the case of the SW sensor, considering as an initial state a slightly oxidized porous structure (~ 1 nm SiO_2) and varying the amount of molecules grafted onto the pore walls. Fig. 11b shows the shift of the resonance depending on the amount of biomolecules. Due to the finesse of the resonance, the presence of only 0.35% biomolecules leads to a shift of the resonance large enough to induce a dramatic decrease in reflectivity from 100% (green curve) down to 32% (red curve). The wavelength variation of the resonance depending on the amount of biomolecules is presented in fig. 12a-b, where the amount of biomolecules is

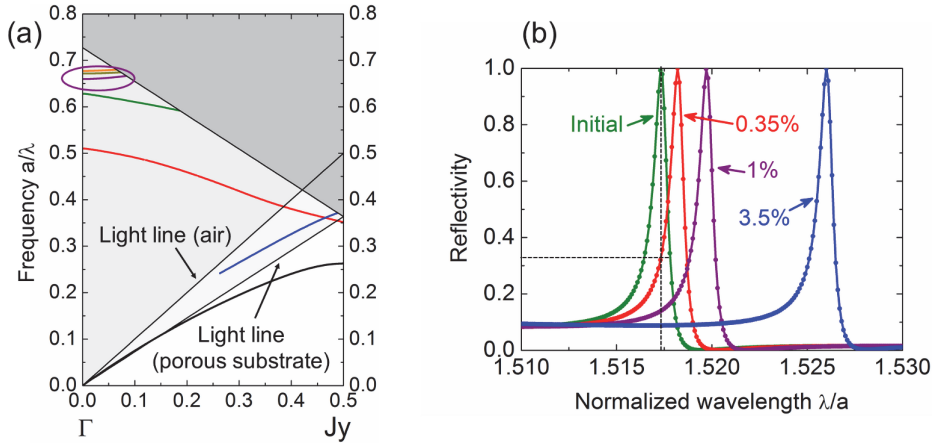

Fig. 11. (a) Band structure of the planar photonic crystal device (MPB simulation). The resonance of interest for biosensing is marked by a purple circle. (b) Reflectivity behaviour showing the resonance shift depending on the amount of biomolecules (FDTD simulation).

again expressed both as a volume fraction f_{bio} and as an equivalent thickness d_{bio}. The corresponding refractive index variation of the top PSi layer is also shown. As this study is performed in air environment, the wavelength variation is determined for an initial resonance centred at 1500 nm. Fig. 12a highlights the very large sensitivity of the device; indeed, in the case of grafting of a dense monolayer of silane molecules with a length of 1.7 nm, the expected shift of the resonance is larger than 50 nm. Fig. 12b demonstrates that smaller amounts of biomolecules can be well detected as well, since the grafting of 0.35% of molecules – equivalent to a dense monolayer with only 0.02 nm thickness – would induce a wavelength shift larger than 1 nm, which is in good agreement with fig. 11b. The induced refractive index variation for this small amount of biomolecules would be below $2x10^{-3}$.

In order to evaluate the performances of the sensor for in-situ measurements, the same study has been performed in aqueous environment. In this case, all the pores of the PSi layers as well as the trenches are completely filled with water. The presence of water inside the pores induces an increase of the oxidized PSi refractive index to 2.52 and 1.63, respectively, for the top layer and the substrate. Hence, the index contrasts remain quite large between the layers of different porosities, as well as between the PSi and the water-filled slits. After a new optimization of the photonic crystal to take into account the new index configuration, a similar Fano resonance was found to yield a Q factor above 1000 if the thickness of the top layer is adjusted to $0.8a$. This means that the presence of water does not dramatically alter the device performances. Fig. 12c-d shows the optical response of the sensor in aqueous environment with varying amount of biomolecules. For a better comparison with the results obtained in air environment, the wavelength shifts have been calculated for a resonance centred at 1500 nm. When using the device at shorter wavelength (e.g., at 1300 nm where water absorption is strongly reduced) the wavelength shift of the resonance is correspondingly slightly smaller. Due to the lower refractive index difference between biomolecules and water ($\Delta n < 0.1$) than between biomolecules and air ($\Delta n \sim 1.4$), it is expected that the same volume of molecules induces a lower optical response in aqueous environment. In this case, silane grafting shown in fig. 12c would induce a shift of the

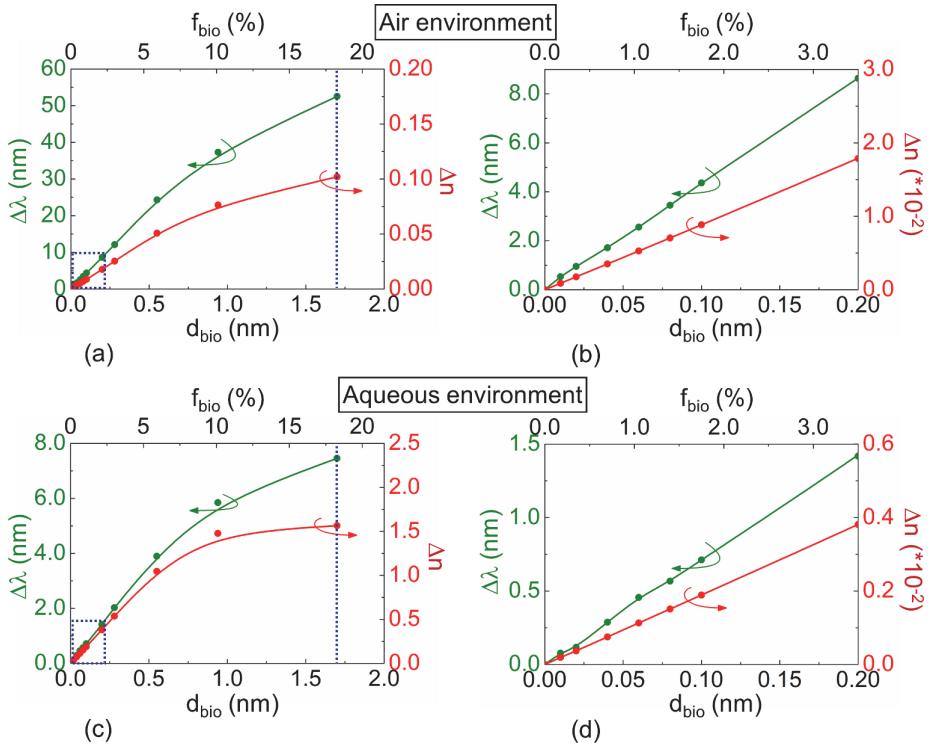

Fig. 12. Simulated optical response (MPB) of the planar photonic crystal biosensor in air and aqueous environment, respectively: (a), (c) for large amounts of biomolecules, and (b), (d) for smaller amounts. The optical response is expressed both in wavelength shift (Δλ) and in corresponding refractive index variation in the top layer (Δn). The amount of biomolecules is given as a volume fraction (f_{bio}) and as an equivalent thickness (d_{bio}). The blue dashed line indicates the expected device response to silane grafting.

resonance by 7.5 nm, which corresponds to a decrease in sensitivity by a factor 7 compared to the sensor in air environment. However, we can see in fig. 12d that very small amounts of biomolecules can still be detected, as the grafting of 1% of biomolecules, equivalent to a dense monolayer with 0.06 nm thickness, would induce a wavelength shift of 0.5 nm.

In order to study the experimental response of the biosensor, the process discussed in section 4 was used to realize devices similar to the one shown in fig 5b. The fabricated devices were then functionalized and their optical properties were characterized by reflectivity measurements at each main functionalization step. The optical setup used for the reflectivity measurements, presented in fig. 13a, is equipped with a wide band 1200-1600 nm laser diode source and an InGaAs detector. Light is focussed on the 100 µm x 100 µm size device via a microscope objective. Nano-positioning of the sample is achieved via an XYZ piezoelectric table and is monitored with a visualization camera.

The optical response of the device is presented in fig. 13b. The green spectrum shows the reflectivity of the device after oxidation. The oscillations in reflectivity due to the interferences in the PSi substrate are clearly visible. Superimposed to these oscillations, 2

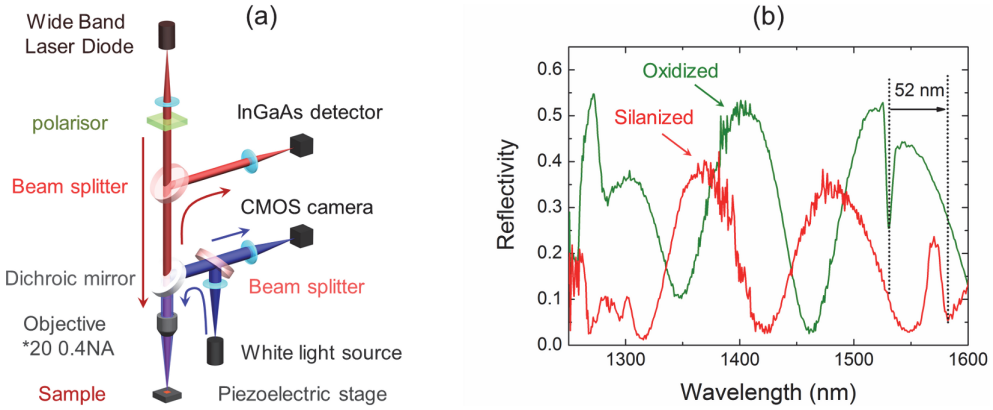

Fig. 13. (a) Schematic view of the optical setup. (b) Reflectivity measurements of the planar PC device, after oxidation (green curve) and after subsequent silanization (red curve).

main resonances can be seen, the first one around 1280 nm and a sharper resonance at 1530 nm. This second resonance is the Fano resonance of interest for biosensing. After silanization, the same device has been characterized again and the red spectrum has been obtained. Comparing the two spectra, it can be observed that the interference fringes have shifted, indicating a change in refractive index of the PSi layer and successful silane grafting. Moreover, the second resonance that was initially at 1530 nm shows a strong 52 nm red shift, which is in perfect agreement with the simulated expectations discussed in fig. 12.
After immobilization of DNA probes on the silanized PSi surface, the devices show strong 20 nm blue shifts, which are a signature of PSi corrosion due to remaining Si-H bonds (Steinem et al., 2004). Although the amount of Si-H and Si-OH bonds is very low – almost invisible on FTIR spectra – their presence is sufficient to induce a damage of the PSi structure with the resulting blue shift, and to prevent any quantitative measurement of the immobilized DNA molecules. Hence, both our oxidation process and the surface capping by the silane molecules should be further improved to completely eliminate the Si-H bonds or to prevent access from the water molecules to these H-bonds.

7. Conclusion

In this chapter, new concepts for meso-PSi integrated optical biosensors based on photonic crystals have been presented, as well as the study of their performances.
The first biosensor is based on the excitation of SW at the surface of a PC device. Such devices yield very high sensitivity that can be further enhanced by the introduction of lateral patterning. We demonstrated a gain in sensitivity by a factor 6 between the 1D and 2D biosensors. Another great property of this biosensor is the possibility to adjust the porosity of the surface layer depending on the size of the target biomolecules. One disadvantage of the SW device is that prism coupling requires large optical setups that are not convenient for mass applications. It also requires large device areas and is not compatible with on-chip multiple parallel sensing. These limitations can be overcome if the prism is replaced, e.g., by a grating and if a detection principle similar to SPRI setups is used. The other limitation of the SW sensor in its 2D configuration is a quite challenging technological realization due to

the depth of the slits that have to be patterned into the PSi multilayer. New processes are currently been developed to enable the fabrication and experimental study of these sensors.
The second biosensor is based on the excitation of Fano resonances in planar PCs at normal incidence. Such devices require simpler optical setups, they are very compact and can be directly integrated into optical microchips, enabling for multiple parallel sensing. They yield high sensitivity and their experimental realization is less challenging than in the case of SW devices. We demonstrated perfect agreement between the theoretical and experimental performances and shift of the resonance wavelength as large as 52 nm after grafting of a silane monolayer. Because the porosity of the top layer cannot be too large in order to yield good optical properties, these sensors are restricted to the detection of small biomolecules. Further optimization of the sensor design will help to overcome this limitation.
Therefore, PCs in PSi are a very promising route to realize high performance biosensors that can be fully integrated into optical microchips and used for in-situ analysis. As both the experimental realization and the theoretical design of the devices are still at the focus of intensive research, new exciting developments will certainly occur in a near future.

8. Acknowledgments

The experimental work is performed at the technological platform Nanolyon. R. Mazurczyk, P. Crémillieu, C. Seassal, A. Sabac and J.-L. Leclercq are kindly acknowledged for fruitful discussions on fabrication techniques and technical support. We are also very grateful to C. Martinet, G. Grenet, C. Botella, N. Blanchard, P. Regreny and D. Leonard for their help on physico-chemical characterization of PSi.
Financial support by the French ANR in the framework of the research project BiP BiP (JC09_440814), and the INSA-Lyon in the framework of a BQR project, as well as the CSC for PhD stipend funding are acknowledged.

9. References

Arens-Fischer, R.; Krüger, M.; Thönissen, M.; Ganse, V.; Hunkel, D.; Marso, M. & Lüth, H. (2000). Formation of porous silicon filter structures with different properties on small areas. *Journal of Porous Materials*, Vol. 7, pp. 223–225, ISSN 1380-2224

Bergveld, P. (1970). Development of an ion-sensitive solid state device for neurophysiological measurements, *IEEE Transactions on Biomedical Engineering* Vol. 17, pp. 70–71

Bessueille, F.; Dugas, V.; Vikulov, V.; Cloarec, J.-P.; Souteyrand, E. & Martin, J.R. (2005). Assessment of PSi substrate for well-characterised sensitive DNA chip implement. *Biosensors & Bioelectronics,* Vol. 21, No. 6, pp. 908-916, ISSN 01694332

Betty, C.A. (2009). Highly sensitive capacitive immunosensor based on PSi-polyaniline structure: Bias dependence on specificity. *Biosensors and Bioelectronics,* Vol. 25, No. 2, pp. 338-343, ISSN 0956-5663

Bonanno, L.M. & DeLouise, L.A. (2007). Whole blood optical sensor. *Biosensors & Bioelectronics,* Vol. 23, No. 3, pp. 444-448, ISSN 0956-5663

Bras, M.; Dugas, V.; Bessueille, F.; Cloarec, J.-P.; Martin, J.R.; Cabrera, M.; Chauvet, J.-P.; Souteyard, E. & Garrigues, M. (2004). Optimisation of a silicon/silicon dioxide substrate for a fluorescence DNA microarray. *Biosensors and Bioelectronics,* Vol. 20, No. 4, pp. 797-806, ISSN 09565663

Bruggeman, D.A.G. (1935). Berechnung Verschiedener Physikalischer Konstanten von Heterogenen Substanzen. *Annalen der Physik*, Vol. 24, pp. 636-664

Canham, L.T. (1990). Silicon quantum wire array fabrication by electrochemical and chemical dissolution of wafers. *Applied Physics Letters,* Vol. 57, No. 10, pp. 1046-1048, ISSN 0003-6951

Caras, S. & Janata, J. (1980). Field effect transistor sensitive to penicillin. *Analytical Chemistry*, Vol. 52, No. 12, pp. 1935-1937, ISSN 0003-2700

Chapron, J.; Alekseev, S.A.; Lysenko, V.; Zaitsev, V.N. & Barbier, D. (2007). Analysis of interaction between chemical agents and porous Si nanostructures using optical sensing properties of infra-red Rugate filters. *Sensors and Actuators B,* Vol. 120, No. 2, pp. 706-711, ISSN 0925-4005

Chevolot, Y.; Bouillon, C.; Vidal, S.; Morvan, F.; Meyer, A.; Cloarec, J.-P.; Jochum, A.; Praly, J.-P.; Vasseur, J.-J. & Souteyrand, E. (2007). DNA-Based Carbohydrate Biochips: A Platform for Surface Glyco-Engineering. *Angewandte Chemie-International Edition,* Vol. 46, No. 14, pp. 2398-2402, ISSN 1433-7851

Cloarec, J.-P.; Chevolot, Y.; Laurenceau, E.; Phaner-Goutorbe, M. & Souteyrand, E. (2008). A multidisciplinary approach for molecular diagnostics based on biosensors and microarrays. *IRBM,* Vol. 29, No. 2-3, pp. 105-127, ISSN 12979562

Cunin, F.; Schmedake, T. A.; Link, J.R.; Li, Y.Y.; Koh, J.; Bhatia, S.N. & Sailor, M.J. (2002). Biomolecular screening with encoded porous-silicon photonic crystals. *Nature Materials*, Vol. 1, No.1, pp. 39-41, ISSN 1476-1122

De Stefano, L.; Arcari, P.; Lamberti, A.; Sanges, C.; Rotiroti, L.; Rea, I. & Rendina, I. (2007). DNA Optical Detection Based on PSi Technology: from Biosensors to Biochips. *Sensors,* Vol. 7, No. 2, pp. 214-221, ISSN 1424-8220

De Stefano, L. & D'Auria, S. (2007). Confocal imaging of protein distributions in PSi optical structures. *Journal of Physics: Condensed Matter*, Vol. 19, pp. 395009, ISSN 0953-8984

Drott, J.; Lindstrom, K.; Rosengren, L. & Laurell, T. (1997). PSi as the carrier matrix in microstructured enzyme reactors yielding high enzyme activities. *Journal of Micromechanics and Microengineering,* Vol. 7, No. 1, pp. 14-23, ISSN 0960-1317

Dugas, V. & Chevalier, Y. (2003). Surface hydroxylation and silane grafting on fumed and thermal silica. *Journal of Colloid and Interface Science,* Vol. 264, No. 2, pp. 354-361, ISSN 00219797

Dugas, V.; Depret, G.; Chevalier, B.; Nesme, X. & Souteyrand, E. (2004). Immobilization of single-stranded DNA fragments to solid surfaces and their repeatable specific hybridization: covalent binding or adsorption? *Sensors and Actuators, B: Chemical,* Vol. 101, No. 1-2, pp. 112-121, ISSN 0925-4005

Dugas, V.; Elaissari, A. & Chevalier, Y. (2010a). *Surface Sensitization Techniques and Recognition Receptors Immobilization on Biosensors and Microarrays,* Recognition Receptors in Biosensors, M. Zourob, Springer Verlag, pp. 47-134, ISBN 978-1-4419-0918-3, New York (USA)

Dugas, V.; Demesmay, C.; Chevolot, Y. & Souteyrand, E. (2010b). *Use of Organosilanes in Biosensors*, Biotechnology in Agriculture, Industry and Medecine, Nova Science Publishers, Inc., ISBN 978-1-61668-029-9, New York (USA)

El Khoury, G.; Laurenceau, E.; Chevolot, Y.; Merieux, Y.; Desbos, A.; Fabien, N.; Rigal, D.; Souteyrand, E. & Cloarec, J.-P. (2010a). Development of miniaturized immunoassay: Influence of surface chemistry and comparison with enzyme-linked

immunosorbent assay and Western blot. *Analytical Biochemistry,* Vol. 400, No. 1, pp. 10-18, ISSN 0003-2697

Fan, X.; White, I.M.; Shopova, S.I.; Zhu, H.; Suter, J.D. & Sun, Y. (2008). Sensitive optical biosensors for unlabeled targets: A review. *Analytica Chimica Acta*, Vol. 620, pp. 8-26

Ferrand, P. & Romestain, R. (2000). Optical losses in PSi waveguides in the near-infrared: Effects of scattering. *Applied Physics Letters*, Vol. 77, pp. 3535-3537, ISSN 0003-6951

Guillermain, E.; Lysenko, V. & Benyattou, T. (2006). Surface wave photonic device based on PSi multilayers. *Journal of Luminescence,* Vol. 121, pp. 319-321, ISSN 0022-2313

Guillermain, E.; Lysenko, V.; Oroubtchouk, R.; Benyattou, T.; Roux, S.; Pillonnet, A. & Perriat, P. (2007). Bragg surface wave device based on PSi and its application for sensing. *Applied Physics Letters*, Vol.90, No. 24, pp. 241116, ISSN 0003-6951

Gurtner, C.; Wun, A.W. & Sailor, M.J. (1999). Surface modification of PSi by electrochemical reduction of organo halides. *Angewandte Chemie-International Edition,* Vol. 38, No. 13-14, pp. 1966-1968, ISSN 1433-7851

Jamois, C.; Li, C.; Orobtchouk, R. & Benyattou, T. (2010a). Slow Bloch surface wave devices on PSi for sensing applications. *Photonics and Nanostructures: Fundamentals and Applications*, Vol. 8, No. 2, pp. 72-77, ISSN 1569-4410

Jamois, C.; Li, C.; Gerelli, E.; Chevolot, Y.; Monnier, V.; Skryshevskyi, R.; Orobtchouk, R.; Souteyrand, E. & Benyattou, T. (2010b). Porous-silicon based planar photonic crystals for sensing applications, *Proceedings SPIE 7713, Conference on Photonic Crystal Materials and Devices IX*, 7713OU pp. 1-10, Brussels, Belgium, April 12-15, 2010, ISSN 0277-786X

Jane, A.; Dronov, R.; Hodges, A. & Völcker, N.H. (2009). Porous silicon biosensors on the advance. *Trends in Biotechnology*, Vol. 27, No. 4, pp. 230-239, ISSN 0167-7799

Joannopoulos, J.D.; Meade, R.D. & Winn, J.N. (1995). *Photonic crystals, molding the flow of light*. Princeton Academic Press, Princeton, NJ, ISBN 0-691-03744-2

Johnson, S.G., & Joannopoulos, J.D. (2001). Block-iterative frequency-domain methods for Maxwell's equations in a planewave basis. *Optics Express*, Vol. 8, No. 3, pp. 173-190, ISSN 1094-4087

Kim, N.Y. & Laibinis, P.E. (1998). Derivatization of PSi by Grignard reagents at room temperature. *Journal of the American Chemical Society,* Vol. 120, No. 18, pp. 4516-4517, ISSN 0002-7863

Kochergin, V. & Föll, H. (2009). *Porous Semiconductors Optical Properties and Applications*. Springer, ISBN 978-1-84882-577-2, London

Lehmann, V. & Gösele, U. (1991). Porous silicon formation: A quantum wire effect. *Applied Physics Letters*, Vol. 58, No. 8, pp. 856-858, ISSN 0003-6951

Lehmann, V.; Stengl, R. & Luigart, A. (2000). On the morphology and the electrochemical formation mechanism of mesoporous silicon. *Materials Science and Engineering*, Vol. B 69–70, pp. 11-22, ISSN 0921-5107

Lerondel, G.; Setzu, S.; Thönissen, M. & Romestain, R. (1997). Holography in PSi. *Journal of Imaging Science and Technology*, Vol. 41, No .5, pp. 468-473, ISSN 8750-9237

Lin, V.S.–Y.; Motesharei, K.; Dancil, K.-P.S.; Sailor, M.J. & Ghadiri, M.R. (1997). A porous silicon-based optical interferometric biosensor. *Science*, Vol. 278, pp. 840-842

Liscidini, M. & Sipe, J.E. (2007). Enhancement of diffraction for biosensing applications via Bloch surface waves. *Applied Physics Letters*, Vol. 91, pp. 253125, ISSN 0003-6951

Looyenga, H. (1965). Dielectric constants of heterogeneous mixtures. *Physica*, Vol. 31, pp. 401–406

Martin, J.R.; Souteyrand, E.; Lawrence, M.F. & Mikkelsen, S.R. (1994). Procedure for the analysis of biological substances in a conductive liquid medium (GENFET). 1994 French Patent n° 94 0868, US Patent Application: USSN 08/ 649,985

Mathew, F.P. & Alocilja, E.C. (2005) Porous silicon based biosensor for pathogen detection. *Biosensors and Bioelectronics*, Vol. 20, No. 8, pp. 1656-1661, ISSN 0956-5663

Meade, S.O. & Sailor, M.J. (2007). Microfabrication of freestanding PSi particles containing spectral barcodes, *Physica Status Solidi*, Vol. 1, No. 2, pp. R71–R73, ISSN 1862-6254

Moni, L.; Pourceau, G.; Zhang, J.; Meyer, A.; Vidal, S.; Souteyrand, E.; Dondoni, A.; Morvan, F.; Chevolot, Y.; Vasseur, J.-J. & Marra, A. (2009). Design of Triazole-Tethered Glycoclusters Exhibiting Three Different Spatial Arrangements and Comparative Study of their Affinities towards PA-IL and RCA 120 by Using a DNA-Based Glycoarray. *Chembiochem,* Vol. 10, No. 8, pp. 1369-1378, ISSN 1439-4227

Ouyang, H.; Striemer, C.C. & Fauchet, P.M. (2006). Quantitative analysis of the sensitivity of PSi optical biosensors. *Applied Physics Letters*, Vol. 88, pp. 163108, ISSN 0003-6951

Palik, E.D. (1998). *Handbook of optical constants of solids*. Academic Press New York, ISBN 0-12-544423-0

Park, H.; Dickerson, J.H; & Weiss, S.M. (2008). Spatially localized one-dimensional PSi photonic crystals. *Applied Physics Letters*, Vol. 92, No. 1, pp. 011113, ISSN 0003-6951

Phaner-Goutorbe, M.; Dugas, V.; Chevolot, Y. & Souteyrand, E. (2011). Silanization of silica and glass slides for DNA microarrays by Impregnation and Gas phase Protocols: A comparative study. *Material Science and Engineering C,* Vol. 31, No. 2, pp. 384-390, ISSN 0928-4931

Press, W.H.; Flannery, B.P.; Teukolsky, S.A. & Vetterling, W.T. (1992). *Numerical Recipes in C: The art of Scientific Computing*. Cambridge University Press, ISBN 0-521-43108-5

Rendina, I.; Rea, I.; Rotiroti, L. & De Stefano, L. (2007). Porous silicon-based optical biosensors and biochips. *Physica E*, Vol. 38, pp. 188-192, ISSN 1386-9477

Robins, E.G.; Stewart, M.P. & Buriak, J.M. (1999). Anodic and cathodic electrografting of alkynes on PSi. *Chemical Communications,* No. 24, pp. 2479-2480, ISSN 1359-7345

Rong, G.; Najmaie, A.; Sipe, J.E. & Weiss, S.M. (2008). Nanoscale PSi waveguide for label-free DNA sensing. *Biosensors and Bioelectronics,* Vol. 23, No. 10, pp. 1572-1576, ISSN 0956-5663

Rossi, A.M.; Wang, L.; Reipa, V & Murphy, T.E. (2007). Porous silicon biosensor for detection of virus. *Biosensors and Bioelectronics*, Vol. 23, pp. 741-745, ISSN 0956-5663

Ryckman, J.D.; Liscidini, M.; Sipe, J.E. & Weiss, S.M. (2010). PSi structures for low-cost diffraction-based biosensing. *Applied Physics Letters*, Vol. 96, pp. 171103

Sassolas, A.; Leca-Bouvier, B.D. & Blum, L.J. (2008). DNA Biosensors and Microarrays. *Chemical Reviews,* Vol. 108, No. 1, pp. 109-139, ISSN 00092665

Sedra, A.S. & Smith, K.C. (1997). *Microelectronics Circuits*. 4th Edition, Oxford University Press, ISBN 978-0195116632

Setzu, S.; Lerondel, G. & Romestain, R. (1998). Temperature effect on the roughness of the formation interface of p-type PSi. *Journal of Applied Physics*, Vol. 84, No. 6, pp. 3129-3133, ISSN 0021-8979

Shinn, M. & Robertson, W.M. (2005). Surface plasmon-like sensor based on surface electromagnetic waves in a photonic band-gap material. *Sensors and Actuators B*, Vol. 105, No. 2, pp. 360-364, ISSN 0925-4005

Sirbuly, D.J.; Lowman, J.M.; Scott, B.; Stucky, G.D & Buratto, S.K. (2003). Patterned microstructures of PSi by dry-removal soft lithography. *Advanced Materials*, Vol. 15, No. 2, pp. 149-152, ISSN 0935-9648

Song, M.-J.; Yun, D.-H.; Min, N.-K. & Hong, S.-I. (2006). Comparison of effective working electrode areas on planar and porous silicon substrates for Cholesterol Biosensor. *Japanese Journal of Applied Physics*, Vol. 45, N°9A, pp. 7197-7202, ISSN 0021-4922

Soref, R.A. & Bennett, B.R. (1987). Electrooptical effect in Silicon. *IEEE Journal of Quantum Electronics*, Vol. 23, pp. 123-129, ISSN 0018-9197

Soultani-Vigneron, S.; Dugas, V.; Rouillat, M.H.; Fedolliere, J.; Duclos, M.C.; Vnuk, E.; Phaner-Goutorbe, M.; Bulone, V.; Martin, J.R.; Wallach, J. & Cloarec, J.-P. (2005). Immobilisation of oligo-peptidic probes for microarray implementation: Characterisation by FTIR, Atomic Force Microscopy and 2D fluorescence. *Journal Of Chromatography B-Analytical Technologies In The Biomedical And Life Sciences,* Vol. 822, No. 1-2, pp. 304-310, ISSN 1570-0232

Souteyrand, E.; Cloarec, J.-P.; Martin, J.R.; Wilson, C; Lawrence, I.; Mikkelsen, S.R. & Lawrence, M.F. (1997). Direct detection of the hybridization of specific DNA sequences by field effect. *Journal of Physical Chemistry*, Vol. 101, No.15, pp.2980-2985

Souteyrand, E.; Chen, C.; Cloarec, J;-P.; Nesme, X.; Simonet, P.; Navarro, I. & Martin, J.R. (2000). Comparison between the electrochemical and optoelectrochemical impedance measurement for the detection of DNA hybridization. *Applied Biotechnology and Biochemistry*, Vol. 89, pp. 195-207, ISSN 0273-2289

Steinem, C.; Janshoff, A.; Lin, V.S.-Y.; Völcker, N.H. & Ghadiri, M.R. (2004). DNA hybridization-enhanced porous silicon corrosion: mechanistic investigations and prospect for optical interferometric biosensing. *Tetrahedron*, Vol. 60, pp. 11259, ISSN 0040-4020

Stewart, M.P. & Buriak, J.M. (2000). Chemical and Biological Applications of PSi Technology. *Advanced Materials,* Vol. 12, No. 12, pp. 859-869, ISSN 0935-9648

Taflove, A & Hagness, S.C. (2005). *Computational Electrodynamics: The Finite-Difference Time-Domain Method*. Third Edition, Artech House, Boston, ISBN 978-1-58053-832-9

Thévenot, D.R.; Roth, K.; Durst, R.A. & Wilson, G.S. (1999). Electrochemical biosensors: recommended definitions and classification. *Pure and Applied Chemistry,* Vol. 71, No. 12, pp. 2333-2348, ISSN 0033-4545

Thust, M.; Schöning, M.J; Frohnhoff, S.; Arens-Fischer, R.; Kordos, P. & Lüth, H. (1996). Porous silicon as a substrate material for potentiometric biosensors. *Measurements Science and Technology*, Vol. 7, pp. 26-29, ISSN 0957-0233

Thust, M.; Schöning, M.J; Schroth, P.; Malkoc, U.; Dicker, C.I.; Steffen, A.; Kordos, P. & Lüth, H. (1999). Enzyme immobilisation on planar and porous silicon substrates for biosensors applications. *Journal of molecular Catalysis B*, Vol.7, pp.77, ISSN 1381-1177

Tinsley-Bown, A.M.; Canham, L.T.; Hollings, M.; Anderson, M.H.; Reeves, C.L.; Cox, T.I.; Nicklin, S.; Squirrell, D.J.; Perkins, E.; Hutchinson, A.; Sailor, M.J. & Wun, A. (2000). Tuning the Pore Size and Surface Chemistry of PSi for Immunoassays. *Physica Status Solidi (a),* Vol. 182, No. 1, pp. 547-553, ISSN 0031-8965

Tserepi, A.; Tsamis, C.; Gogolides, E. & Nassiopoulou, A.G. (2003). Dry etching of PSi in high density plasmas, *Physica Status Solidi (a)*, Vol. 197, pp.163-167, ISSN: 0031-8965

Viktorovitch, P.; Drouard, E.; Garrigues, M..; Leclercq, J.-L.; Letartre, X.; Rojo-Romeo, P. & Seassal, C. (2007). Photonic crystals: basic concepts and devices. *Comptes Rendus Physique*, Vol.8, pp. 253-266

Viktorovitch, P.; Ben Bakir, B.; Boutami, S.; Leclercq, J.-L.; Letartre, X.; Rojo-Romeo, P.; Seassal, C.; Zussy, M.; Di Cioccio, L. & Fedeli, J.-M. (2010). 3D harnessing of light with 2.5D photonic crystals. *Laser & Photonics Reviews*, Vol.4, No.3, pp. 401–413

Völcker, N.H.; Alfonso, I. & Ghadiri, M.R. (2008). Catalyzed oxidative corrosion of porous silicon used as an optical transducer for ligand–receptor interactions. *ChemBioChem*, Vol.9, pp.1176-1186

Zhang, J.; Pourceau, G.; Meyer, A.; Vidal, S.; Praly, J.-P.; Souteyrand, E.; Vasseur, J.-J.; Morvan, F. & Chevolot, Y. (2009a). DNA-directed immobilisation of glycomimetics for glycoarrays application: Comparison with covalent immobilisation, and development of an on-chip IC50 measurement assay. *Biosensors and Bioelectronics,* Vol.24, No.8, pp. 2515, ISSN 0956-5663

15

Porous Silicon Sensors - from Single Layers to Multilayer Structures

J.E. Lugo, M. Ocampo, R. Doti and J. Faubert
Visual Psychophysics and perception laboratory School of Optometry
University of Montreal
Canada

1. Introduction

1.1 Origin and discovery

Silicon, one of the more common elements in nature, is defined as a metalloid, which corresponds to the number 14 in the Mendeleyev Periodic Table. It is heavier than Carbon (element number 6 in the periodic table and a key component in biochemistry), but both have chemical characteristics that are very close. Since human civilization began, volcanic stones containing this metalloid in the form of dioxide were used to create the first tools and weapons. Roman historian Plinio the Elder (23AD-79AD) mentioned the *Silex-Silicis* (silicon stones) in one of his works as very hard stones. These roman words are the *Latin* origin of the name Silicon (Tomkeieff, 1941).

J.J.Berzelius was credited for the discovery of this element in 1824 in Stockholm, Sweden, but Gay-Lussac and Thenard had already prepared impure amorphous silicon by 1811. After World War II, once the applied mechanical technology was ready to produce very pure silicon wafers (under the form of monolithic crystals) and succeeded to manage the problem of the surface impurities and contamination (Hull, 1999), the electronic industry jumped from the Germanium diodes to the Silicon integrated circuits and metal-oxide-semiconductor (MOS) microprocessors that helped man reach the Moon. In summary, it is safe to say that Silicon's role along our evolution extends from prehistoric times to the exploration of the Solar System.

In 1956 at the U.S. Bell Laboratories, Arthur Uhlir Jr. and Ingeborg Uhlir while trying a new technique for polishing Silicon crystalline wafers observed for the first time a red-green film formed on the wafer surface (Kilian et al, 2009). Since the discovery of its luminescence properties by Leigh Canham in 1990 (Kilian et al, 2009), researchers started to study the nonlinear optical, electric and mechanical properties of this nanostructure. This effort has permitted the fabrication of uniform porous layers with diameters as small as one nanometer, and permitting an enormous inner surface density.

2. How to prepare porous silicon (p-Si)

Several techniques exist to form this structure from a pure Silicon crystalline wafer. The most popular are: electrochemical etching, stain etching and photochemical etching. Here we introduce two versions of the etching process (Anglin, n.d).

2.1 Electrochemical etching

As shown in the figure 1, we have a Si wafer (single crystalline) with the top face in contact with a hydrofluoric acid solution and where an immersed platinum electrode is placed at certain distance from the wafer and parallel to it. In the bottom face of the wafer we find a flat metallic electrode that is in close electric contact. Between the two electrodes there is a controlled voltage supply with its negative pole connected to the platinum immersed electrode. A current is established from the anodic electrode (back of the wafer) and the catodic electrode (platinum immersed). Modulating four variables: the intensity and interval of application of this current, the HF solution concentration, and the concentration and type of dopant previously applied to the Si wafer (type-n, type-p, or highly doped: type-pp and type nn) it is then possible to control the porous size and p-Si layer geometric parameters, as well as the number of layers. Dopant refers to a different element atom that replaces a percentage of the Si atom inside the wafer and that is compatible with it in a crystallographic way, but that presents an electron in excess (type n) or an electron lack (type p). This introduces a number of properties that modify the material behavior when an electric field is applied, mainly the resistivity, that will influence the etching process performance. The electric current oxidizes the surface silicon atoms permitting a fluoride attack on them generating the pores. It is also possible to create multilayer structures by alternating different current densities. For instance, if we start making the first layer with a current density J_1 then the final porosity (and the refractive index) is going to be approximately determined by this current density. The electrochemical reaction time determines the thickness. By switching the current density to a different value J_2, something amazing happens, the reaction continues mostly at the crystalline silicon interface, leaving an almost intact first layer. Then the second layer will have a different refractive index and thickness (if we readjust the reaction time). Porosity can be measured by gravimetrical means. That is, the original crystalline silicon wafer is weighted first, then p-Si is formed and the wafer is weighted again, finally the p-Si layer is removed by adding KOH (Potassium hydroxide) and the wafer is weighted once more. With these three measurements is possible to determine the porosity. To measure the thickness, SEM (scanning electronic microscopy) techniques are normally used giving the best resolution and accuracy. Refractive index is usually determined by optical interference methods, where the refractive index can be estimated by taking adjacent maxima or minima from interference fringes coming from the p-Si sample.

Stain etching: In this procedure the power supply action is replaced by the chemical oxidant action of nitric acid. The reaction control is performed trough the addition of other additives. Results are less homogeneous than those of the first process described, but they still permit to have the material quality compatible with several applications.

3. Different types of p-Si sensors. Overview

Sensors allow our systems and devices to be in relation with the real events that we need to register or control. So, precision (same response to the same stimuli: repeatability) and accuracy (indicating magnitude value as close as possible to the real magnitude of the stimulus to be sensed: minimum absolute error spread) are two main requirements for any sensor when the industry selects its type or structure for market use. However, other properties will define the success of a new kind of sensor in the market. These are:

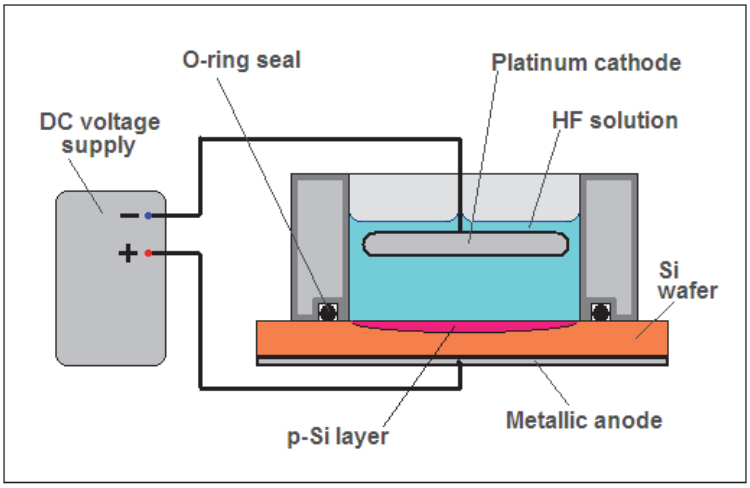

Fig. 1. Experimental setup for porous silicon fabrication.

technological compatibility with the existing devices, geometric dimension requirements, low noise insertion, ease of adjustment and setup, low power consumption, performance standardization (linear if possible), low thermal or aging characteristic drifts, robustness, reliability, low obsolescence, and very wide field of applications. P-Si is a material that accomplishes all of these requirements with enough margins to think that it will become increasingly popular in the short term.

For instance, integrated circuits (IC) are made of crystalline Silicon, which means it is fully compatible for associating a p-Si sensor to any electronic device. The electrochemical technology used to create a p-Si layer does not collide with the IC lithography. The geometric dimensions required to create this type of sensor are sufficiently small to be integrated in an IC. The homogeneity of the porous and its radius control (internal surface density control) as well as its layer stability is improving very fast. We can create a vast range of p-Si structures ranging from photonic crystals, a diffusive absorption electric material, a characterized geometry surface chemical reactor material, etc. The number of potential sensing applications is very large and is still growing daily (Angelucci et al, 1997).

In this section we present an overview of several types of p-Si sensors. Although not an exhaustive description, we cover a wide range of applications to illustrate the possibilities of putting the special characteristics of this material to work. We must consider that the p-Si application field is object of new developments practically everyday.

3.1 P-Si Biosensors: optical properties changes

Medical automated diagnostic, specific biological fluid concentration dynamics and molecular recognition are some of the expanding needs to be satisfied in the biomedical, veterinary and food industry. All of them could be achieved by this kind of sensors.

Research in this field was pushed by the discovery of the light emission capacity of the p-Si material (Cullis & Canham, 1991). The main consequence of this fact was considering the p-Si optical properties changes to detect target substances in function of the ability to trap molecules given by the boundary chemistry that occurs in the inner porous surface and its special characteristics (800 m^2 per gram).

3.1.1 Refractive index transduction

The mechanism referred to the absorption or diffusion of a complex molecule substance into the p-Si material could be complex and dependent on the geometry of the porous layer, the surface chemistry activity and the physical conditions present. We will try an intuitive simplified description of this type of detectors.

As shown in figure 2, a cell equipped with a transparent window contains a p-Si specimen which surface is in contact with a solution flow. The window is swiped by a special fiber optic tip linked to an interferometer. The fibers have two functions: a) providing white light from a special lamp, and b) picking up the reflected light to send it into the interferometer

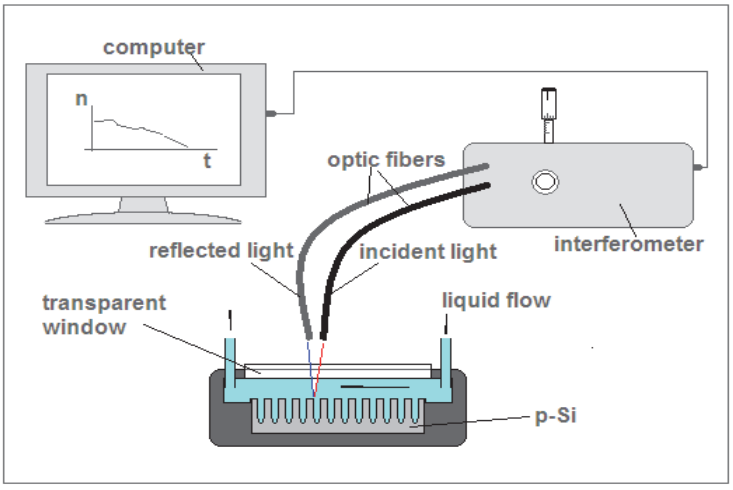

Fig. 2. Scheme showing the refractive index transduction.

that will let to obtain the System Reflectance Spectrum. This specific online info will give us, by means of a computerized algorithm, the evolution in time of the p-Si refraction index **n.** In this case the change in the reflectivity spectrum is a function of the DNA hybridization between an immobilized reference DNA (molecules attached to the porous surface) and a target DNA in solution (Jane et al, 2009). This event modifies the reflected light spectra in a way that is suitable of being quantified, thus configuring a bio-sensor.

3.2 One-dimensional photonic crystals (1 D)

When the specimen structure corresponds to a one-plane multi layer p-Si crystal we are in presence of a 1D photonic crystal (see figure 3). This geometry offers better reflectance spectra (without side lobes) if compared with a mono-layer structure. Combining the layers dimensions (layer thickness, porous density and radius, number of layers, etc.) we can tune the different layer's refraction index **n,** and according to the global geometry we can tune the average refraction index, $\mathbf{n_m}$ for the specimen. This kind of geometry permits create Bragg reflectors and Micro cavities (Lee & Fauchet, 2009**)** which reflectivity shows defined functional dependence when liquid solutions or gases are in contact with the p-Si specimen.

Once again the set up configuration is similar to the figure showing the fiber optic interferometer. The figure below refers to the characteristic reflectance spectra for these two

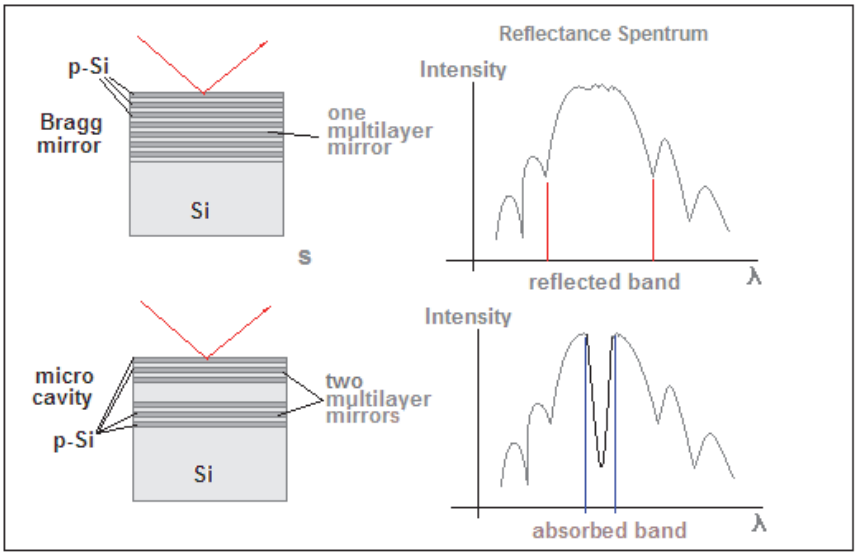

Fig. 3. Scheme showing two different one-dimensional photonic arrays of sensors.

types of photonic crystals. The difference between the incident light spectrum and the Reflectance Spectrum is the energy absorbed (refracted light) by the crystal bulk (Jalkanen et al, 2010). Finally, we would like to mention that this reflection mechanism shows in addition another important characteristics as the polarization of the reflected light (TE or TM) where the Transversal Electric or Transversal Magnetic components of the traveling electromagnetic wave (in our case the incident light) are discriminated by the photonic crystal reflection mechanism.

3.2.1 Reflectance spectrum shifting mechanism

The presence or absence of a target molecule in the liquid solution can be determined as follows:

First, we obtain the reflected light spectrum with the device filled only with the solution solvent: for instance: water (this is equivalent to zeroing our instrument). It will be the reference reflectance spectrum.

In the next step we introduce into the liquid flow the substance containing the target molecule, while computing the modified reflected light spectrum.

The modified spectra will be shifted (Baratto et al, 2002) in the light wavelength domain with respect to the reference spectrum depending on:

- whether or not the solution is capable to go into the channels of p-Si, or it's rejected
- the surface chemistry creates bonds that attach or not the target molecules against the channels walls (this can be controlled by a previous surface oxidation)
- the type of bond attaching the molecules to the surface: ionic, covalent, etc.

-the refraction index of the substances involved, that is function of their solution concentration and that depending on the device geometry will result in a global refraction index valid for the device considered as an unit. In the figure 4, we present, as an example, the detection two types of molecules together.

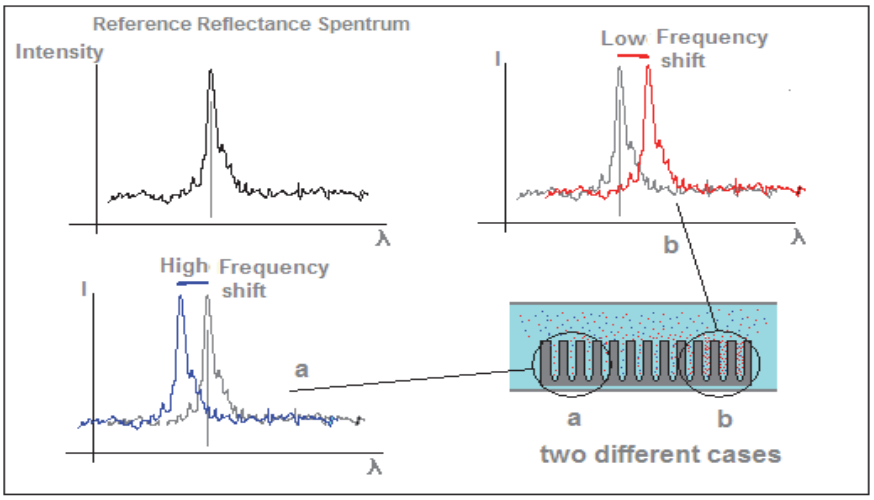

Fig. 4. Optical detection examples for two different types of molecules.

In the case a) the blue molecules are kept outside of the p-Si structure due to the surface chemistry bonds and reducing their presence inside de structure channels. The resulting lowered density of blue molecules inside the channels reduces the global refraction index, as well. This change in the device refraction index shifts the reflected spectrum towards the higher frequencies (shorter wave length). This effect is called blue shifting.
In the case b) instead, the red molecules are induced to get into the channels increasing their density. As result, this time the global refraction index is increased and the reflected spectrum will be shifted toward the lower frequencies (longer wavelength). This is called red shifting.
The reader must have into account that in the above discussion both types of situation were introduced together in order to improve the comprehension of this mechanism. In real life, and due to the complexity of the conditions and detection thresholds to achieve, only one type of target molecule is present in the experiment. Furthermore, the whole device is conceived and designed to increase its detection capabilities in function of the specific target molecule.

3.2.2 Photoluminescence transduction

This refers to the emission of photons (called secondary photons) when the p-Si specimen is excited by a light beam (primary photons). This phenomenon was verified at room temperature around twenty years ago. The principle for this type of biosensors is based in the photoluminescence quenching (PQ) that takes place when the specimen is in contact with a target substance. Applications cover from organic solvents, biological waste, and molecular recognition (Di francia et al, 2005). This type of sensors is delicate and sensible to interfacial charging that can affect their performance. The experimental set up is similar to that shown in the figure 4. The comparison between the returned light spectrum, whether is present or not the target substance in contact with the p-Si, is the parameter that lets scale the sensor. We could say that this is a Frequency Converter mechanism. From the incident energy, normally a short wavelength close to, one part is reflected and from the absorbed

portion a fraction is origin of a longer wavelength light emission: normally red. This new component is not present in the incident spectrum, but it appears in the reflectance spectrum as shown in figure 5.

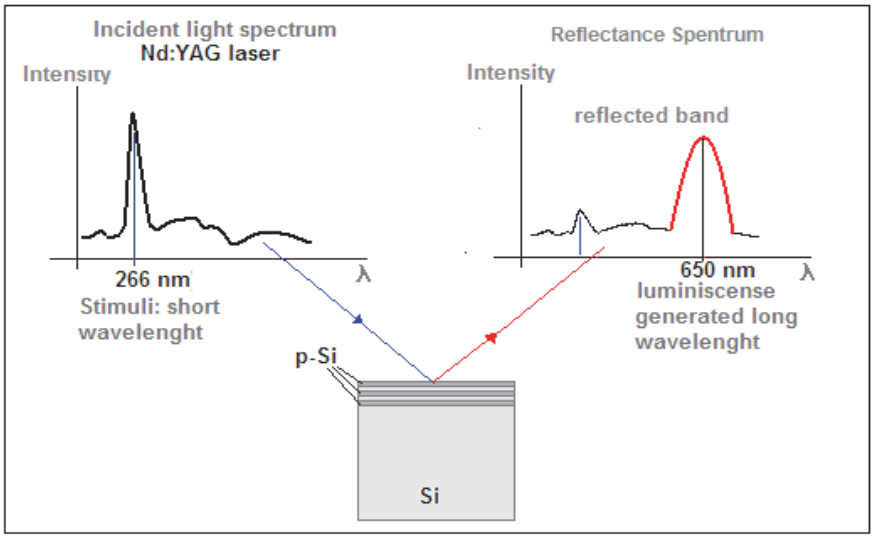

Fig. 5. Scheme for the photoluminescence transduction.

3.2.3 Capacitive transduction

The physic property by which it is possible to storage electric charge between two conductive materials, or the equivalent that is to storage electrostatic energy, is called capacity. The simplest geometry for configuring a capacitor, device which has this property, is to have two flat metallic surfaces separated by a dielectric material (typically an isolator). The relationship between the superficial electric charge density accumulated in both metallic planes and the external electric field applied to a planar p-Si specimen is known as the Dielectric Constant. When considering a particular geometry, this constant lets measure the Capacitance of the whole device. The arrangement fundamentals are shown in the figure 6.
The capture of target substances molecules in the surface of the specimen varies the Surface Charge Density, thus the Capacity of the whole device. This effect lets to scale the system as a biosensor by correlating the device electric capacity to the presence and solution density of the target molecule. The complete electric model for the sensor is composed by a capacitance associated to a parallel and a serial conductance (representing relaxation constants of the material according to the working frequency) that make necessary to assess the impedance spectroscopy (Baratto et al, 2001) to determine the particular frequency at which we have the maximum gas sensitivity.

3.2.4 Conductance transduction

The relationship between the current in Amperes circulating trough a piece of a given resistive material and the value of the potential difference in Volts applied to originate that current is defined as the conductance of that resistive piece. This could be interpreted as the

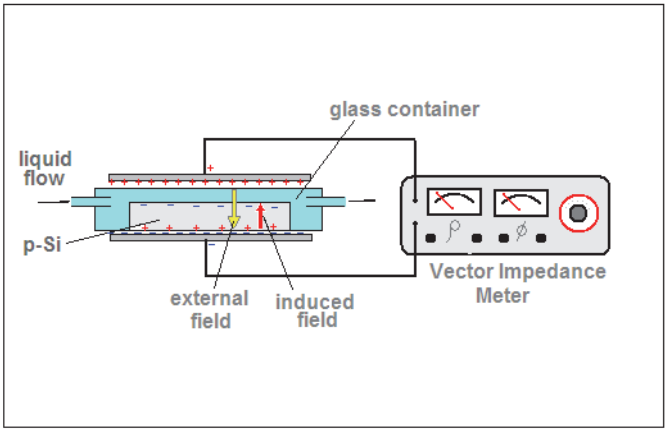

Fig. 6. Scheme showing the capacitive transduction mechanism.

facility that a material offers to let a current circulate trough it per unit of Volt applied. The conductance unit is the Siemens (S).

The phenomenon is related to divers mechanisms by which the electrons contained in a, for instance, crystalline structure are enable to circulate trough that structure. These mechanisms could cover from a simple action of the external electric field applied, to complex electron interactions between specific energy levels inside the atoms.

The existence of a dominant geometrical characteristic such as the inner porous, and its inherent enormous surface density, makes p-Si very susceptible for conductance dependence on the environmental conditions. And from the beginning several types of sensors were conceived on this basis to detect: relative humidity, gases, alcohol, and organic vapors in general (Choi et al, 2009).

With this objective, p-Si geometric parameters have been tuned to maximize conductance detection of different target molecules, presenting each resulting device a big discrimination between targets, even if the response has a systematic fading in the time domain. In figure 7 you can see the specimen with two gold plated surface terminals that let connect it to a DC source by means of an ammeter and a resistor of 1 kilo ohm. A voltmeter reads the resistor voltage drop: V_R. This is the output signal of the system when the vapor or gas flow is in contact with the specimen. The graphic represents the normalized value of V_R in function of time, where '**m**' (blue) represents the output for *Methanol*, ' **i** ' (green) for *Isopropyl Alcohol*, and '**a**' for *Acetone* (Choi et al, 2009) .

As you can see the response of the sensor is specific for each molecule. But the output is not constant along the time because of the vapor penetration in the porous. Exist a delay (several minutes) after the flow is enabled (valve open) to get the maximum output voltage level. We observe an override of the output signal (peak) after the valve is closed (flux off). In addition exist a recovery time (not indicated) needed by the sensor for returning to the initial sensibility. Another aspect to consider is the **t**hermal drift (that can be manage by controlling the environmental temperature), and the aging effect that reduces sensibility in few month of use. Engineers have to overcome all these difficulties and unexpected behaviors to produce a reliable sensor, even if its performance is based on a simple and stable principle. This situation extends, and somehow in a more complex way, to all the other types of p-Si sensors discussed.

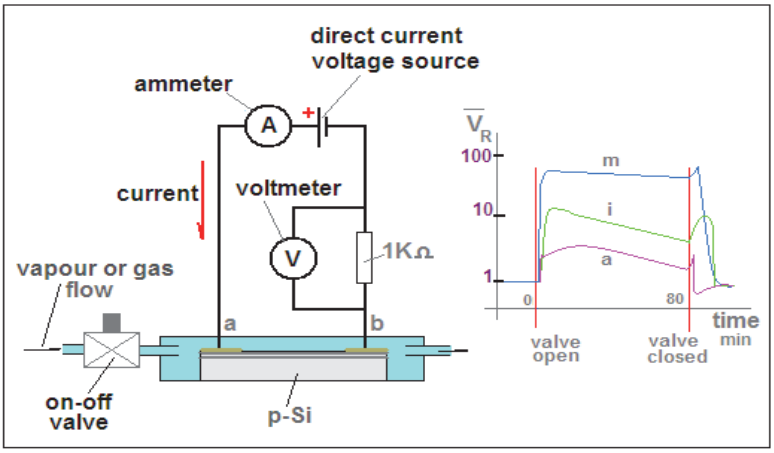

Fig. 7. Conductance transduction scheme.

4. How to make p-Si selective to different chemical and biological compounds in three specific examples

P-Si possesses a large internal surface area ranges from 90 to 783 m^2/cm^3 (Chan et al 2001) which provides numerous sites for many potential species to attach. It has been proposed as the substrate material for sensing applications because it can readily be integrated with silicon technology. Different methods and mechanisms were used for p-Si formation, the bulk of which can be classified as electrochemical (Chan et al, 2001; Lugo et al, 2007; Archer et al, 2005), photoelectrochemical and 'stain etching' methods that do not require light or electrical bias. The most common method used is the anodisation under galvanostatic conditions. Both phosphorous (n-type) and boron (p-type) doped silicon can be electrochemically etched in aqueous and/or organic electrolyte solutions containing HF to yield a range of nano- to micro-scale structures by simply selecting the appropriate dopant concentration of the Si substrate and/or adjusting the anodisation conditions (Kilian et al, 2009). According to its pore sizes, p-Si can be classified as macroporous (pore diameter $d > 50$ nm), mesoporous ($2 \text{ nm} < d < 50$ nm) and microporous ($d < 2$ nm). Diameter of DNA molecules is approximately 5 angstroms. Therefore, the p-Si pores size must be in the order of nanometers to allow infiltration of the biomolecules to be useful to optical biosensing. This is the main reason to focuses on mesoporous silicon to accommodate biological species. The sensitivity of the surface to chemical species has been demonstrated by exposing porous silicon layers to different compounds, such as vapors, molecules with different dipole moments, DNA, small viruses and bacteria (Ben-Chorin et al, 1994; Schechter et al, 1995; Chan et al, 2001; Archer & Fauchet, 2001). In the development of a sensor, selectivity is a very important issue because the sensor must be able to distinguish the element being sensed. For biosensors the bioselective element is usually immobilized on some sort of support (Chan et al, 2001), p-Si in this case. The sensor is then exposed to the species being sensed and the output signal is detected. To obtain a high quality sensor the p-Si layers must be made by choosing the appropriate anodization conditions. DNA biosensors based on nucleic acid recognition processes are rapidly being developed with the goal of rapid and

inexpensive testing of genetic and infectious diseases. The use of DNA recognition layers represents an exciting development in analytical chemistry (McGown et al, 1995). Electrochemical biosensors have received a great deal of attention due to their high sensitivity and rapid speed of detection. In addition, electrochemical techniques are ideally suited to miniaturization and have the potential to simplify nucleic acid analysis using low-cost electronics (Yan et al, 2001). Nowadays, they are being used in many reports for detecting the DNA hybridization event, due to their high sensitivity, small dimensions, low cost, and compatibility with microfabrication technology (Yan et al, 2001; Kara et al, 2002; Wang, 1999; Erdem et al, 1999; Marraza et al, 2000; Maruyama et al, 2001; Shi et al, 2004).

4.1 First example: an electrical sensor

To prepare the porous silicon layers, Archer et al (Archer et al, 2005) use N,N dimelthylformamide (DMF) under galvanostatic conditions of p-type silicon (resistivity ~ 10-20 Ohm-cm) with a current density of 4 mA/cm^2. The electrolyte could be a 4 wt% hydrofluoric acid (49 wt%) in N, N dimethylformamide (DMF). The use of a mild oxidizer, such as DMF, results in a straight and smooth pore walls with pore diameter in the micrometer range (Archer et al, 2005). These conditions were selected to increase the pore diameter and to enhance the sensitivity to changes in the space charge region. The porous layers were etched for 70 min resulting in 20 microns thick layers. To stabilize the p-Si device a thin layer of surface oxide is required for proper operation. The layers were thus chemically oxidized by immersion in 30 wt.% of hydrogen peroxide (H_2O_2) for a period of 48 h at room temperature (22 Celsius degrees). Although the oxide layer produced by this oxidation technique is very thin. The oxide is hydrophilic enough to allow the infiltration of water soluble molecules without the need of a thicker thermally grown oxide. After oxidation the porous layers were rinsed with deionized water and ethanol and dried under a stream of nitrogen. The oxide on the backside of the crystalline silicon substrate was stripped with a 15% HF solution (7:1, water: 49 wt % HF) prior to the contact placement. The wafers were cleaved into sections of 4 × 7 mm and two coplanar electrical contacts were placed 700 μm apart on the crystalline silicon substrate. In this approach, the p-Si surface is completely exposed to the sensing molecules and no metal contacts are made to it, avoiding the introduction of foreign materials into the porous matrix (Archer et al , 2005). In order to avoid any of the solvents tested from reaching the backside contacts, the sensors were fixed on a glass slide, which ensures a horizontal surface for a uniform distribution of the solvent on the porous layer and protects the backside of the device.

4.2 Second example: an optical sensor

Precise control of the nanocrystalline size distribution is extremely difficult; therefore, an alternative method is required to reduce the luminescence bandwidth (typical fwhm ~ 150 nm). Selena Chan et al. (Chan et al, 2001) developed a device nanostructure, which solves this problem. It consists of a microcavity resonator composed of various porous silicon layers, prepared electrochemically (Chan et al 2001). By confining the luminescence generated in the central layer of the microcavity by two Bragg reflectors, the photoluminescence spectrum is composed of multiple sharp and narrow peaks with fwhm values = 3 nm. Upon a refractive index change, the photoluminescent spikes shift, thereby generating a large, detectable differential signal. Selena Chan (Chan et al, 2001) presented an optical approach to detecting Gram-(-) bacteria based on the principles of light interference

across multilayers of varying refractive indices. By properly functionalizing the inner surface of a porous silicon layer with highly selective receptor molecules aimed at specific targets, multisensor arrays can be designed to quickly determine the presence of certain pathogens. The porous silicon surface was treated with a 3-glycidoxypropyltrimethoxy silane subsequent exposure of this epoxide-terminated surface to an aqueous solution of tetratryptophan *ter*-cyclo pentane (TWTPC) at 6%, dimethyl sulfoxide (DMSO) provide a surface functionalized with the lipid A-bonding receptor. However were found that the procedure with purified diphosphoryl lipid A do not produce a functional devices (Chan et al, 2001). This conduces to an assumption that all four groups of the tetratryptophan receptor react with the functionalized porous silicon surface, thus blocking access to the binding face of the receptor molecule. If this were indeed the case, we hypothesized that exposure of the epoxide-terminated surface to a mixture of TWTCP and a "blocking" amine would allow for the generation of a functional sensor. Using glycine methyl ester as the blocking amine and examining the response of the sensor to purified lipid A, they found that the optimal ratio of receptor to blocker molecules was 1:10 TWTCP:glycine methyl ester (Chan et al, 2001). In this case, incubation of the sensor with a solution of lipid A produces an 8 nm redshift in the photoluminescence peak wavelength. When a 100% solution of TWTCP or a 100% solution of glycine methyl ester is immobilized in the porous matrix, no shifting of the luminescence peaks is detected after exposure to lipid A.
To determine the ability of this sensor to differentiate between two classes of bacteria, independent overnight cultures of Gram- (-) bacteria *(Escherichia coli)* and Gram-(+) bacteria *(Bacillus subtilis*) were grown up, centrifuged, and then individually lysed following resuspension in phosphate buffer solution (PBS, pH 7.4). Upon exposure of the lysed Gram-(-) cells to the immobilized TWTCP biochip, a 4 nm photoluminescence red-shift was detected. However, when the microcavity sensor was exposed to a solution of lysed Gram-(+) bacteria, no shifting of the luminescence peaks was observed. We attribute the large shift to the recognition and binding of the TWTCP receptor with the lipid A present in the bacterial cell wall. Analogous results were obtained with several other species of Gram-(+) and Gram-(-) bacteria. These results demonstrate the ability of a p-Si biosensor to distinguish between Gram-(-) and Gram-(+) bacteria. Clear modulation of the photoluminescence spectra from microcavity device structures illustrates their application as biosensors that can translate the recognition of lipid A present in bacterial cell walls into an optical signal. The remarkable features of these silicon sensors (integratable, high surface-to-volume ratio, robust, inexpensive, small, ease of use) should allow arrays to be constructed to simultaneously identify a variety of analytes by simply functionalizing the surface with arrays of specific, high affinity receptor molecules.

4.3 Third example: an electrochemical sensor

Lugo et al (Lugo et al, 2007) describes the use of p-Si layers to transduce hybridization of DNA into a chemical oxidation of guanine by $Ru(bpy)_3^{2+}$, the reduced form of which is then detected electrochemically. Nucleic acid modified p-Si electrodes were used in combination of voltammetry for the detection of DNA. $Ru(bpy)_3^{2+}$ were used as electrochemical hybridization indicator for DNA detection. It has been shown (Johnston et al, 1994; Johnston et al, 1995; Johnston & Thorp, 1996; Napier et al, 1997) that Ruthenium $Ru(bpy)_3^{2+}$ is a better indicator for quantitative determination of short gene sequence such as the ones used in those experiments. The DNA probe sequence, immobilized at the electrodes, was

engineered in a similar way as in (Napier et al, 1997) to decrease the oxidation of the probe DNA with $Ru(bpy)_3^{2+}$. Such a sequence does not contain the guanine but inosine. Inosine is three orders of magnitude less reactive than guanosine and still recognizes cytidine which is very important for sensing all four bases in the DNA target sequence.
In another experiment (Lugo et al, 2007) p-Si samples were prepared from p+-type, boron doped silicon wafers with a resistivity of 0.008-0.012 Ohm.cm by standard anodization (electrolyte: 15% of HF) at a current density of 30 $mA.cm^{-2}$. The porosity was measured by the gravimetrical method given a porosity of approximately 62%. The pore size was estimated by TEM and ranged from 50 nm-75 nm in diameter. These diameters are large enough to allow the sensing molecules to penetrate and attach. For DNA, the diameter of the nucleotides is approximately 5Å, which is small enough to fit into the porous matrix. Stabilization of p-Si is necessary to passivate its surface and this was done by thermal oxidation. Thermal oxidation of p-Si requires several precautions and high temperatures (>700ºC). Covering the whole internal surface with a thin SiO_2 layer stabilizes the structure, permits water penetration into the pores, and facilitates probe and target penetration (Archer & Fauchet, 2007). All p-Si samples were thermally oxidized in oxygen ambient at 900ºC for 10 minutes.
Measurement set up used for these experiments is an electrochemical instrumentation that includes a BAS 100B/W Electrochemical Analyzer. A BAS VC-2 voltammetry cell (model MF-1065) was used for the electrochemical experiments. It is well suited to small sizes and has a special micro-cell for volumes as small as 50 microliters. The micro-cell, which includes the working electrode, separates a small volume containing the sample from a bulk solution containing the reference and auxiliary electrode with a salt bridge. A platinum wire serves as auxiliary electrode and the modified p-Si samples function as working electrodes. It is important to mention that p-Si, especially oxidized p-Si, is not conducting and it is in fact the p+ doped silicon that is conducting the electrical current. The top area of the exposed p-Si samples was 0.8 cm^2 and all lateral areas were insulated with a commercial epoxy resin (see figure1). The epoxy resin was deposited very carefully and dried for one hour. The samples were attached to the electrochemical system as shown in figure 1. Potentials were measured relative to an aqueous, saturated Ag/AgCl double junction (reference electrode). The voltammetry experiments were carried out at different scan rates in an electrochemical buffer solution composed by 50 mM sodium phosphate (pH 7) with 0.7 M NaCl. A schematic representation of the electrochemical measurement set up and the electrode arrangement is shown in figure 8.

4.3.1 DNA electrochemical detection procedure steps: p-Si, silanization, probe immobilization, hybridization, and voltammetric detection

p-Si Silanization. Several methods maybe employed to bind DNA to different supports (Archer & Fauchet, 2007). One method commonly used for binding DNA involves silanization of an oxidized surface. The function of silane coupling agents is to provide stable bond between two non-bonding surfaces: for example, an inorganic surface to an organic molecule. 3-glycidoxypropyltrimethoxysilane was used to silanize the oxidized p-Si. A 5% aqueous solution of silane was prepared (pH 4.0). This converts silane into a reactive silanol through hydrolysis. The p-Si samples were then immersed into the continuosly stirred solution and left overnight. 3-glycidoxypropyltrimethoxysilane is hydrolyzed to a reactive silanol by using double distilled water (pH 4). Porous silicon samples were then submerged into silanol solution for approximately 17 hours. Constant stirring of the solution was necessary to continuously mix the solution.

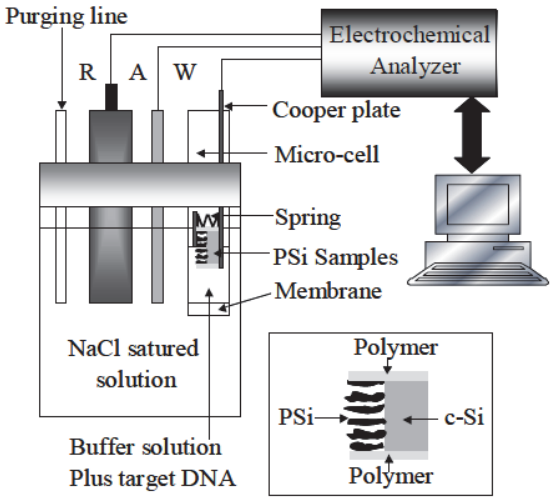

Fig. 8. Measurement system: the p-Si electrode is used as working electrode. A platinum wire is the auxiliary electrode and Ag/AgCl the reference electrode. Inset: cross section showing the different parts of the working electrode.

Probe immobilization After successful silanization, DNA is immobilized onto the surface of p-Si through diffusion. Aqueous solutions of DNA containing 150 microliters of DNA (50 microM) were carefully placed directly above de p-Si layer. The DNA molecules covalently bond to the silanized surface, where they become immobilized. The samples were then placed in a steam container where they were heated in an oven at 37ºC for approximately 20 hours. The DNA attached samples then should be rinsed in double distilled water and dried with nitrogen.

Hybridization. The DNA attached to p-Si was exposed to its complementary strand DNA (target), the mismatch sequence (mismatch probe) and itself (probe). Binding was allowed to proceed for 1 hour at room temperature into hybridization buffer containing 1 M NaCl, 10-20 mM sodium cacodylate, 0.5 mM EDTA, 150 mM KCl and 5 mM $MgCl_2$. Throughout the steps, binding is confirmed using Fourier Transform Infrared Spectroscopy.

Voltammetric detection. Cyclic voltammetry (CV) was carried out having the DNA modified, p-Si electrode as working electrode, an Ag/AgCl as the reference electrode, and platinum wire as the counter electrode. 6 microliters of (0.1microM) was poured into 150 microliters of electrochemical buffer solution. After allowing the solution to diffuse into the samples for 15 minutes, CV was performed. Solutions were deoxygenated via purging with nitrogen for 10 minutes prior to measurements.

p-Si DNA-electrodes and $Ru(bpy)_{32+}$ were used for specific gene detection. $Ru(bpy)_{32+}$ exhibits a reversible redox couple at 1.05 V and oxidizes guanine in DNA at high salt concentration (Chan et al, 2001) according to:

$$Ru(bpy)_3^{2+} \rightarrow Ru(bpy)_3^{3+} + e^- \quad (1)$$

$$Ru(bpy)_3^{3+} + DNA \rightarrow DNA_{Ox} + Ru(bpy)_3^{2+} \quad (2)$$

where DNA_{ox} is a DNA molecule in which guanine has been oxidized by $Ru(bpy)_3^{3+}$. If the DNA probe contains guanine then $Ru(bpy)_3^{3+}$ will oxidize guanine in DNA, even without the presence of the target DNA. In order to prevent that the DNA probe reacts with $Ru(bpy)_3^{2+}$ the guanine has been replaced for another less reactive nucleotide. Some previous results show that the addition of an oligonucleotide that does not contain guanine produces a small enhancement in the oxidation current (Napier et al, 1997). Those results have shown that the inosine 5′-monophosphate is 3 orders of magnitude less electrochemically reactive than guanosine 5′-monophosphate and still recognizes cytidine (Napier et al, 1997). This fact is very important if we want to recognize all four bases in the target sequence. Nevertheless there is a drawback that can have consequences on the hybridization efficiency. Since the deaminated hypoxanthine in the ionosine can only form two of the three hydrogen bonds in a Watson-Crick base pair, it may be desirable to use a guanine derivative that is redox-inert but capable of forming all three hydrogen bonds. However some studies have shown (Napier et al, 1997) that the specificity afforded by inosine substitution was sufficient but they propose 7- deazaguanine as alternative. For this reason the DNA probe sequence does not contain the guanine base but the target does. Figure 2 (top) shows the CV obtained in solution for the hybrid DNA (probe-target) at different scan rates (target DNA concentration of 0.5×10^{-10}M). Figure 2 (bottom) shows that the anodic current of $Ru(bpy)_3^{2+}$ is linearly proportional to the scan rate. This result is congruent with a process that is controlled by adsorption. Figure 3 (top) shows the CV (scan rate of 50 $mV.s^{-1}$) of varied concentrations of target DNA (probe-target sequence, curves 2 to 5) and different targets (probe-mismatch target sequence, curve 1 and probe-probe sequence, curve 6). In curve 1, the mismatch target sequence contains two more pairs of base G than the target sequence and that is why the current in this case is bigger than the current obtained in the probe-target sequence cases (curves 2 to 5) or the probe-probe sequence (curve 6). Moreover in curve 6 the current intensity decreases as a consequence of the absent of the base G in the probe. Nevertheless a significant increase in current was observed for curves 2 to 5 where the target DNA undergoes hybridization to the complementary DNA. This current increase suggests that the hybridization was successful and that the electron transfer from the guanines of the hybridized strand to $Ru(bpy)_3^{2+}$ is responsible for the increase in the current. If we compare curves 1, 2 and 6 (same DNA concentration but different target sequence) we observe that the sensor responds differently to each target and therefore a good selectivity is achieved. Figure 3 (bottom) shows the anodic peak currents of $Ru(bpy)_3^{2+}$ at four different concentrations (curves 2 to 5). The peaks are linearly related to the concentration of the target DNA sequence between 0.5×10^{-10} and 500×10^{-10}M. The detection limit of this approach was 5×10^{-11}M. The sensitivity achieved in this work is similar to the one obtained in reference (Jalkanen et al, 2010), where a sensitivity of $9.0\text{x}10^{-11}$M was reported for a sensor that uses gold substrates instead. In summary this results clearly show that the electrochemical p-Si sensor shown here has a good selectivity and sensitivity to the target compound, two very important characteristics that a sensor ought to have.

5. Future optical sensors

Recently our group has studied the Negative refraction phenomenon in p-Si photonic crystals (Lugo et al, 2009; Lugo et al, 2011). Negative refraction refers that it is possible to bend light to the wrong direction of the normal at some interface between two materials. Let α be the incident angle of light. According to Snell's law, light impinging from air to a

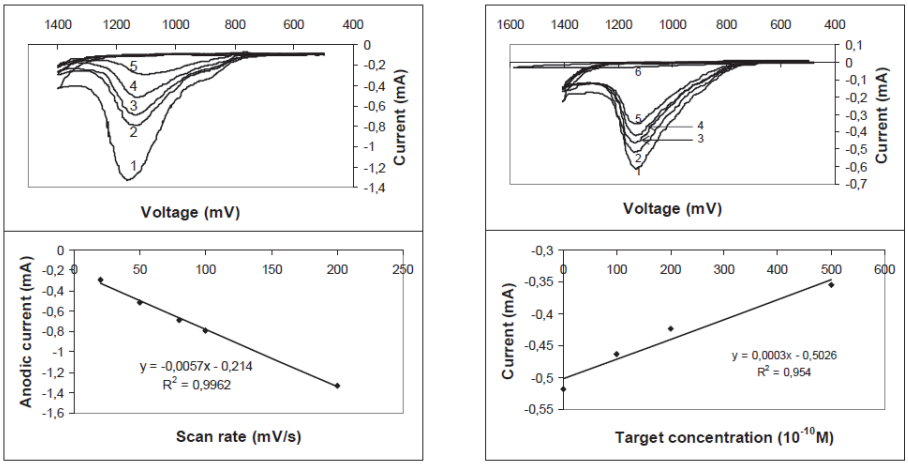

Fig. 9. (Left column, top) Cyclic voltammograms of the probe-target DNA sequence in 0.1 μM $Ru(bpy)_3^{2+}$ solution at different scan rates (mV.s-1): (1) 20; (2) 50; (3) 80; (4) 100; (5) 200. (Left column, bottom) The anodic current changes with the scan rate. The target concentration was 0.5×10-10M. (Right column, top) Cycled voltammograms of different concentrations of target DNA: (2) 0.5×10-10M, (3) 100×10-10M, (4) 200×10-10M, (5) 500×10-10M. Curve 1 shows the CV for the probe-mismatch target DNA sequence (0.5×10-10M) and curve 6 for the probe DNA sequence (0.5×10-10M). (Right column, bottom) The anodic current changes with the concentration of the target DNA. In all cases we have used 0.1 μM of $Ru(bpy)_3^{2+}$.

different material with bigger refractive index (like in figure 10) should cross the interface and continue traveling in the other side of the normal and actually bending towards the normal (the normal direction in this case is the line from where the angle alpha is measured). However in a one-dimensional photonic crystal that consists of a series of layers (80 in this case) "a" and "b" with indices of refraction n_a and n_b, it is possible to bend the light to the same side of the normal once the light crosses the interface (angle β'). This particular condition is found close to the bandgap edges corresponding to low energy or frequency edges of the second and fourth photonic bands once the indices of refraction and thickness have been properly tailored.

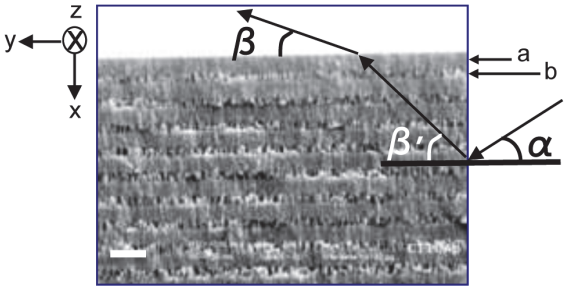

Fig. 10. One-dimensional photonic crystal picture. Showing the light path that a negative refraction beam follows.

Experimentally, the way to observe the negative refraction beam is described in figure 11. The sample (Component 6) with the pinhole (Component 4) was illuminated by a broad band source (Component 1) and to obtain the desired monochromatic light we have used two band-pass filters (Component 3) at 633 nm and 1350 nm (both have a 10 nm bandwidth). The TE or TM polarization was selected by using two linear polarizers (Component 2), and the negative refractive transmitted light was captured by two CCD cameras, one for the visible range and a second for the infrared region coupled with a singlet lens (Component 9) placed at 8 mm from the sample. The sample and the camera were mounted on linear and rotary mechanical stages. The XYZ linear stages had a resolution of 1 micron and the rotary stages had a resolution of 2.5 arc minutes. The TE or

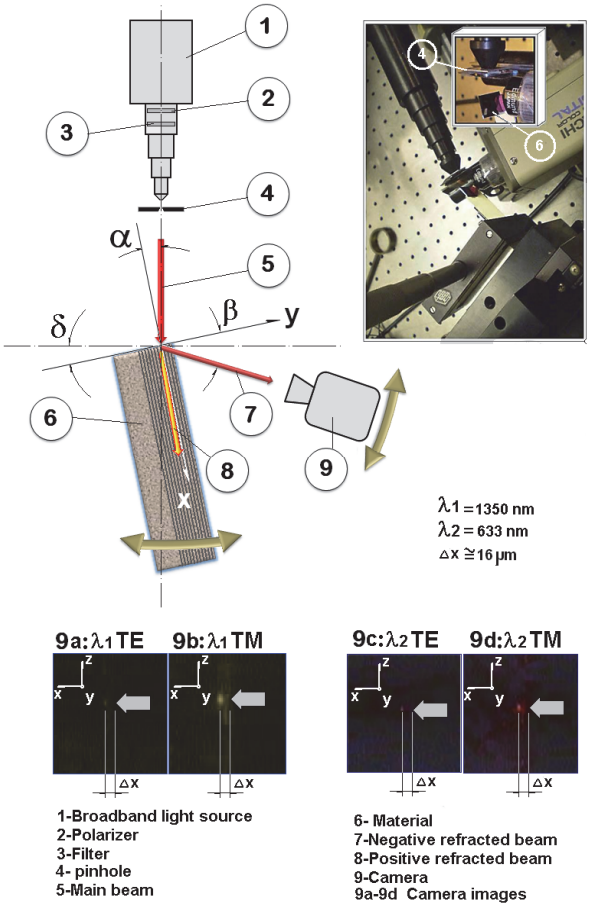

Fig. 11. A cartoon of the experimental setup (with the nine components) for the negative refraction observation and a picture of the real experimental setup. Both the sample and the camera are placed in translational and rotational stages. A broadband source along with bandpass filters and linear polarizers were used to explore the infrared and visible negative refraction bands. Captured images for the different conditions are shown in 9a-9d.

TM Polarized monochromatic light beam (Component 5) illuminated the sample at an angle of 25 degrees through a 1 mm pinhole placed at 3 mm from the sample. The beam was focused in the x-direction interface in a way that light never hit the y-direction interface. This was performed very carefully by scanning the focused light beam from the crystalline silicon substrate towards the y-direction interface. The cameras were centered at 25 degrees (angle β') but their positions were compensated to account for the positive refraction that the negative refraction beam (Component 7) suffers at the exit of the y-direction interface (angle β'). This was done by using Snell's law and an effective refractive index value of 1.6 for the multilayer structure. Once everything was in place we scanned the sample on the z-direction (see component 9) and when a spot image was captured we measured the distance from the x-direction interface to the image (Δx was corrected due to the sample rotation) by using the micrometer screw of the linear stage. This was possible because our imaging system was capable to give us enough resolution to mark on a screen the x-direction interface and the spot image. The components 9a-9d shows four images corresponding to 1350 nm and 633 nm (TE and TM polarizations). The spots are located at a distance of approximately Δx = 16 microns from the interface (x-direction) which agreed with our numerical simulations.

Now, how we can implement a sensor based on this wonderful property? One answer is that we can introduce a chemical compound or a biological agent that would increase the refractive index of each layer. As a consequence the negative refraction condition (at certain angle of incidence) would be altered and the output angle β would not be the same. Since, this angular difference is proportional to the increment on the refractive indices and this refractive index increment is proportional to compound concentration, therefore compound concentration would be proportional to the angular difference. We performed full-wave simulations for TE polarization light considering the experimental thickness and refractive indices we found in references (Lugo et al, 2009; Lugo et al, 2011). The optical losses were neglected and we simulated 80 periods. The first results are shown in Figure 12 (Top). We can observe that for visible light (633 nm) with an incidence angle of 15 degrees there are three beams propagating inside the multilayer. The one that travels to the top of the multilayer is the negative refraction beam, the one that travels parallel to the multilayers is known as a waveguide mode and the last one that goes downwards is the positive refraction beam. What happens if we increase the refractive indices of the layers by 0.1 %. The answer is displayed in figure 12 (Bottom). Where we can see that beam propagation directions drastically change. The negative refraction angular change is of the order of 30 degrees, which shows that this sensor might be very sensitive when working with this beam and we believed can achieve a sensitivity similar to the one found in (Saarinen et al, 2005). The waveguide mode can be used for sensing applications as well because the beam intensity decreases and shifts spatially. Although the change is not dramatic as in the precedent case, it is still useful for sensing higher compound concentrations, for instance. Finally the positive refraction angular change is of the order of 12 degrees and this beam can be used in a similar way as the waveguide mode.

Final remarks:

Porous silicon has been demonstrated as a suitable host for different sensing applications. Porous silicon has been shown to be an ideal sensor material for various compounds and the variety of sensing applications ranges from alcohols to bacteria. On the other hand p-Si has

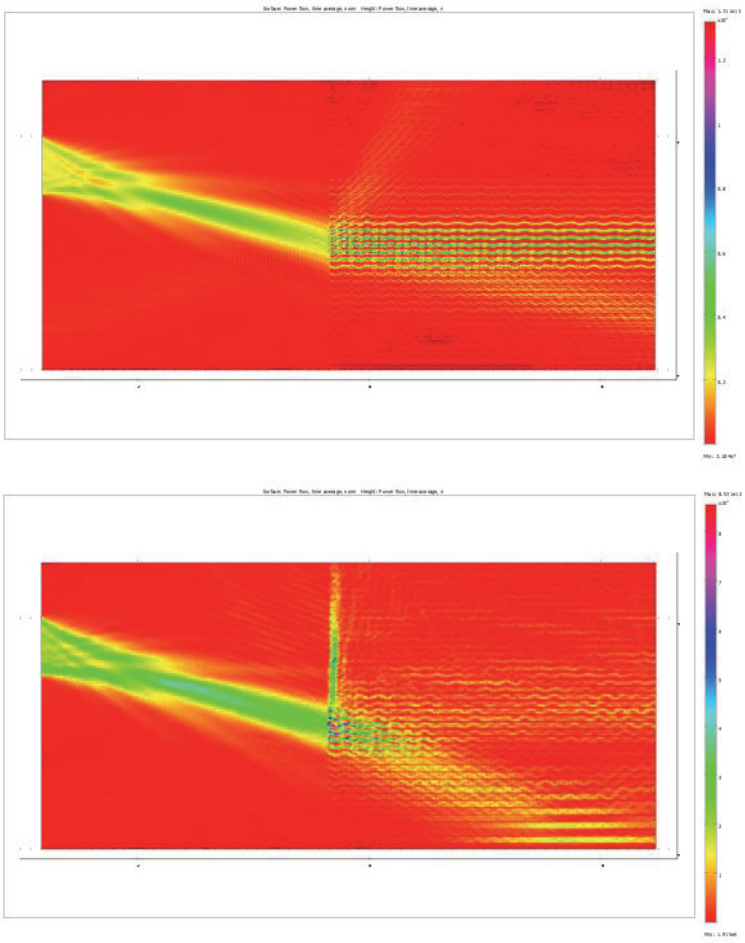

Fig. 12. (Top) Finite element simulation of a one-dimensional photonic crystal consisting of 80 layers with alternated refractive indices. Light of 633 nm impinges at an angle of 15 degrees and then splits up in three beams. The negative refraction beams goes towards the top of the structure. The waveguide mode beam travels parallel to the surface of the layers. The positive refraction beam goes downwards. (Bottom) After increasing 0.1% the refractive indices in the structure the negative refraction beam changes drastically its direction. The waveguide mode and the positive refraction beam change their direction as well but it is less pronounced than in the negative refraction case.

originated several proof-of-principle studies such as electrochemical, electrical and optical transducers. The latter have been intensively studied and are based on photoluminescence effects, reflective interference, or photonic resonance. Porous silicon sensors are promising platforms for pharmaceutical applications because it is highly absorbed by our bodies and also has low toxicity properties. Porous silicon technology allows us to control pore size from a few nanometers to several hundreds of nanometers in diameter. Porous silicon surface can be

modified by chemical methods with different compounds ranging from organic to biological molecules (proteins, bacteria, peptides, antibodies, etc.). The impressive optical properties of this material may provide us with a wonderful tool for in vivo sensing or therapeutics. For instance, its luminescence and the unique reflectivity spectra of multilayers are two features that allow p-Si to exhibit a signal that is modified in a predictable way when exposed to environmental changes. Another important property is that p-Si may be easily integrated into standard silicon microelectronics techniques. This integration would be beneficial for medical applications because we would be able to create more sophisticated active devices. However, there are several challenges that p-Si sensing technology has to overcome before having the first commercial products based on it. First, there is a cost effective problem that involves the use of relatively small areas of p-Si and the safe handling of HF waste. Our group has used the specificity of DNA and the sensitivity of electrochemical detection to develop a novel, silicon compatible detection sensor for the identification of DNA. DNA hybridization has been detected voltammetrically by using ruthenium bipyridine in p-Si samples. In order to prevent the DNA probe from reacting $Ru(bpy)_3^{2+}$ with the guanosine 5'-monophosphate has been replaced from the DNA probe sequence for inosine 5'-monophosphate, which is much less reactive to oxidization. Ruthenium bipyridine showed a catalytic effect on the anodic peak current which is related to the concentration of target DNA in the hybridization reaction. The results confirmed that the DNA sensing method used here is a quick and convenient way for the specific and quantitative detection of DNA. Recently we have studied negative refraction in p-Si photonic crystals. Since negative refraction is a non-linear phenomenon, as we have shown from our simulations, the fabrication of a high sensitivity sensor that uses this effect is possible. Finally, the future will tell us whether p-Si sensing technology will reach the market giving us new and wonderful devices for medical applications or security.

6. References

Anglin E. J.; Cheng K.; Freeman W.R.; Sailor M.J. Porous silicon in drug delivery devices and materials. Advanced Drug Delivery Reviews, Vol. 60, No. 11, pp. 1266-1277.

Angelucci, R.; Poggi, A.; Critelli, C.; Dori, L.; Cavani, F.; Parisini, A.; Garulli, A.; Cardinali, G.C.; Fiorini, M. (1997). A novel gas sensor for hydrocarbons detection based on porous silicon permeated with Sn-V mixed oxides. Solid-State Device Research Conference, pp. 684 – 687.

Archer M. and Fauchet P.M. (2003). phys. Status Solidi A-Appl.Mat., Vol. 198, pp. 503.

Archer M.; Christohersen M. and Fauchet P.M. (2005). Sensors and Actuators B, Vol. 106, pp. 347-357.

Baratto C.; Faglia G.; Comini E.; Sberveglieri G.; Taroni A.; La Ferrara V.; Quercia L. and Di Francia G. (2001). A novel porous silicon sensor for detection of sub-ppm NO_2 concentrations. Sensors and Actuators B: Chemical, Vol. 77, pp. 62-66.

Baratto C.; Faglia G.; Sberveglieri G.; Gaburro Z.; Pancheri L. Oton C.J.; L. Pavesi. (2002). Multiparametric porous silicon sensors. Sensors, Vol. 2, pp. 121-126.

Ben-Chorin M.; Kux A.; and Schechter I. (1994). Appl. Phys. Lett., Vol. 64, pp. 481.

Chan S.; Li Y.; Rothberg L.J.; Miller B.L. and Fauchet P.M. (2001). Mater. Sci. Eng. C-Biomimetic Supramol.Syst., Vol. 15, pp. 2777.

Chan Selena; Horner Scott R.; Fauchet Philippe M. and Miller Benjamin L. (2001). J. Am. Chem. Soc., Vol. 123, pp. 11797-11798.

Cullis A. G. and Canham L.T. (1991). Visible light emission due to quantum size effects in highly porous crystalline silicon. Nature, Vol. 353, pp. 335-338.

Choi SH.; Cheng H.; Park SH.; Kim H.J.; Kim Y.Y and Lee K.W. (2009). A study of the gas specificity of porous silicon sensors for organic vapors. Materials science–Poland, Vol. 27, pp. 603-610

Di Francia G.; Castaldo A.; Massera E.; Nasti I.; Quercia L. and Rea I. (2005). A very sensitive porous silicon based humidity sensor. Sensors and Actuators B: Chemical Vol. 111 No. 112, pp. 135-139.

Erdem A.; Kerman K.; Meri B.; Akarca U.S. and Ozsoz M. (1999). Electroanalysis, Vol. 11, pp. 586.

Hull R. (1999). Properties of Crystalline Silicon (INSPEC, London).

Jalkanen Tero; Tuura Jaani; Mäkilä Ermei and Salonen Jarno. (2010). Electro-optical porous silicon gas sensor with enhanced selectivity. Sensors and Actuators B: Chemical Vol. 147, No. 1, pp. 100-104.

Jane A.; Dronov R.; Hodges A. and Voelcker N.H. (2009). Trends in Biotechnology - Porous silicon biosensors on the advance. Trends in Biotechnology, Vol. 27, No. 4, pp. 230-239.

Johnston D. H.; Cheng C. C.; Campbell K. J. and Thorp H. H. (1994). Inorg. Chem., Vol. 33, pp. 6388.

Johnston D. H.; Glasgow K. C. and Thorp H. H. (1995). J. Am. Chem. Soc., Vol. 117, pp. 8933.

Johnston D. H., and Thorp H. H. (1996). J. Phys. Chem., Vol. 100, pp. 13837.

Kara P.; Kerman K.; Ozkan D.; Meric B.; Erdem A.; Ozkan Z. and Ozsoz M. (2002). Electrochem. Commun., Vol. 4, pp. 705.

Kilian K. A; Böcking T. and Gooding J. J. (2009). The importance of surface chemistry in mesoporous materials: lessons from porous silicon biosensors. Chem. Commun., pp. 630-640.

Lee Mindy R. and Fauchet Philippe M. (2007). Two-dimensional silicon photonic crystal based biosensing platform for protein detection. Optics. Express, Vol. 8, pp. 4530–4535.

Lugo J.E.; Ocampo M.; Kirk A.G.; Plant D.V. and Fauchet P.M. (2007). Journal of new materials for Electrochemical Systems, Vol. 10, pp. 113-116.

Lugo J. E., de la Mora B., Doti R., Nava R., Tagueña J., del Rio A., and Faubert J., 2009, 'Multiband negative refraction in one-dimensional photonic crystals', Optics Express, Vol. 17, Issue 5, pp. 3036-3041.

Lugo J.E., Doti R. and Faubert J., 2011, 'Negative Refraction angular characterization in one dimensional photonic crystals, Plos One, to be publish.

Marraza G., Chiti G., Anichimi M., 2000, Clin. Chem., Vol. 46, 31.

Maruyama K., Motonaka J., Mishima Y., Matsuzaki Y., Nakabayashi I., Nakabayashi Y., 2001, Sens. Actuator, B-Chem., Vol. 76, 215.

McGown L, M. Joseph, J. Pitner, G. Vonk, C. Linn, 1995, Anal. Chem., Vol. 67, 663A.

Napier M. E., Loomis C. R., Sistare M. F., Kim J., Eckhardt A. E., and Thorp H. H., 1997, Bioconjugate Chem., Vol. 8, 906.

Saarinen J.J., Sipe J.E., Weiss S. and Fauchet P.M., 2005, 'Optical sensor based on resonant porous silicon structures' Quantum Electronics and Laser Science Conference, JWB38.

Schechter I., Ben-Chorin M., and Kux A., 1995,Anal. Chem., Vol. 67, 3727.

Shi L., Xiao Y., Willner I., 2004, Electrochem. Commun., Vol. 6, 1057.

Tomkeieff S.I., 1941, On the origin of the name 'quartz' .University of Durham , Newcastle upon Tyne.

Wang J., 1999, Chem. Eur. J., Vol. 5, 1681.

Yan F., Erdem A., Meric B., Kerman K., Ozsoz M., Sadik O. A., 2001, Electrochem. Commun., Vol. 3, 224.

16

Organic-inorganic Interfaces for a New Generation of Hybrid Biosensors

Luca De Stefano[1], Ilaria Rea[1], Ivo Rendina[1], Michele Giocondo[3], Said Houmadi[3], Sara Longobardi[2] and Paola Giardina[2]
[1]*CNR-IMM Institute for Microelectronics and Microsystems, National Research Council*
[2]*Department of Organic Chemistry and Biochemistry, University of Naples "Federico II"*
[3]*CNR-IPCF Institute for Chemical and Physical Processes, National Research Council*
Italy

1. Introduction

Biosensors have by far moved from laboratories benches to the point of use, and, in some cases, their represent technical standards and commercial successes in applications of social interest, such as medical diagnostic or environmental monitoring. Based on biological molecules, but also on their bio-inspired synthetic counterparts, biosensors employ different transducers (optical, potentiometric, volt-amperometric, colorimetric, and so on) converting the molecular interaction information into a measurable electric signal. As the result of a real multi-disciplinary field of science and technology, biosensors can take advantage from each improvement and progress coming from other disciplines: new features and better performances have been reached in the last year due to simplified fabrication methodologies, deep integration of optical or electrical transducers, and, last but not least, microfluidic circuits. More recently, nanostructured components dramatically increased biosensors reliability especially in public health and environmental monitoring. Nevertheless, there is still a pressing demand of innovations which could lead to smaller, faster, and cheaper biosensors systems with ability to provide not only accurate information but also feedback actions to the real world. The fabrication of a new generation of hybrid biodevices, where biological, or bio-inspired, molecules are fully integrated with a micro or a nano technological platform, strongly depends on the bio-compatibilization treatments of the devices surfaces. The design and the realization of bio/non-bio interfaces with specific properties, such as chemical stability, wettability, and biomolecules immobilization ability, are key features in the miniaturization and optimization processes of biosensors. In particular, protein immobilization is a hot topic in biotechnology since commercial solutions, as in the case of DNA microarrays, are not still available. Proteins are, due to their composition, a class of very heterogeneous macromolecules with variable properties. For these reasons, it is extremely difficult to find a common surface suitable for different proteins with a broad range in molecular weight and physical–chemical properties such as charge and hydrophobicity. A further aspect is the orientation of the bound proteins, that could be of crucial relevance for quantitative analysis, interaction studies, and enzymatic reactions. Many different surfaces, and chemical treatments of these surfaces, have been

investigated in the last years, but an universal solution for all the applications aforementioned could not be identified.
Following this very actual theme, our main focus in this chapter is to discuss different applications in biosensing of a special class of amphiphilic proteins: the hydrophobins. These proteins self-assemble in a nanometric biofilm at the interfaces between water and air, or on the surfaces covered by water solution. New functionalities can be added to the biosensors surfaces without using any chemical or physical treatment, just covering them by a self-assembled protein biofilm.
The main topics covered in the following paragraphs are: origin and properties of the hydrophobins; deposition methods of the hydrophobins biofilm on different surfaces and the characterizations techniques we use to determine the physical properties of these bio-interfaces; the features exhibited by the hydrophobins covered surfaces, and finally, the biosensors systems based on hydrophobins biofilms.
We outline in this chapter how the peculiarities of these proteins can be of interest in the technological field, beyond their large utilization in biotechnology, nowadays at industrial level. Moreover, the experience matured on this subject can be the paradigm of a new kind of approach in design and realization of the next generation of biosensors.

2. Hydrophobins: surface active proteins

Proteins are actually polymers whose basic monomer units are amino acids, the so called *residues*. In nature, the building blocks of the protein structure are 20 different amino acids that, on the base of their physical-chemical properties, can be classified as hydrophobic or hydrophilic. The sequence of hydrophobic and hydrophilic residues in the primary structure will give rise to an hydropatic pattern on the protein. As consequence, in water, they behave like amphiphilic molecules, giving rise to structures that maximize the number of interactions between hydrophilic groups and water and, at the same time, minimize those between hydrophobic groups and water.
Hydrophobins (HFBs) are a large family of small proteins (about 100 amino acids) that appear to be ubiquitous in the Fungi kingdom. The name *hydrophobin* was originally introduced because of the high content of hydrophobic amino acids (Wessels J.G.H, *et al*., 1991). They fulfil a broad spectrum of functions in fungal growth and development. They are ubiquitously present as a water-insoluble form on the surfaces of various fungal structures, such as aerial hyphae, spores, and fruiting bodies, etc., and mediate attachment to hydrophobic surfaces. HFBs are very efficient in lowering the surface tension of water allowing the hyphae to escape from the aqueous medium and grow into the air. As the fungal hyphae grow through the air-water interface into the air, the hydrophobins at the interface are believed to coat the emerging hyphae as they penetrate through the interface, as shown in Figure 1. *In vitro* hydrophobins are able to self-assemble at hydrophilic/hydrophobic interfaces into an amphipathic membrane, resulting in the change of nature of surfaces.
Hydrophobins have been split in two groups, class I and class II, based on the differences in their hydropathy patterns, spacing of aminoacids between the eight conserved cysteine residues and properties of the aggregates they form (Linder *et al*. 2005). Class I hydrophobins generate very insoluble assemblies, which can only be dissolved in strong acids (i.e. 100% trifluoroacetic acid) and form rodlet structures outside the fungal cell wall. Assemblies of Class II can be more easily dissolved in ethanol or sodium dodecyl sulphate

and form assemblies that lack a distinct rodlet morphology. Despite these morphological differences, no obvious distinction between the functions of class I and class II hydrophobins within the fungal life cycle has yet emerged.

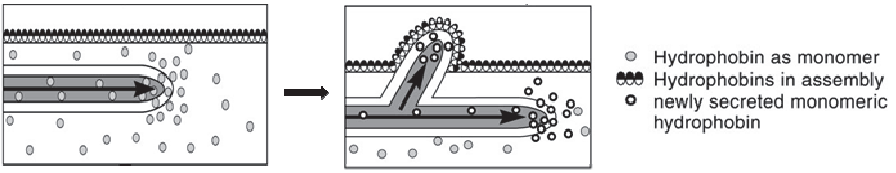

Fig. 1. Schematic of HFB role in fungal hyphae growth.

2.1 Hydrophobins structures

In order to provide a complete molecular description of hydrophobins, two complementary points of view have to be considered: the structure of non-assembled hydrophobins and the features of the assembled form. The structure of a protein is characterized in four ways: the primary structure is the order of the different amino acids in a protein chain, whereas the secondary structure consists of the geometry of chain segments; the main types of secondary structure are two, called the α-helix and the β-sheets. The tertiary structure describes how the full three dimensional arrangement of the chains and all its side groups, revealing how a protein folds in on itself, and finally the quaternary structure of a protein describes how different protein chains hook up with each other.

HFBs of both types I and II, although share quite a low sequence similarity, feature a clear signature, namely eight Cys residues in a characteristic pattern. In this pattern, the third and fourth as well as the sixth and seventh Cys residues are always adjacent in the sequence. In the protein folded state, this special pattern gives rise to four disulfide bonds spanning over the entire structure of the protein.

Class I HFBs consist of a four-stranded β-barrel core, an additional two-stranded β-sheet and two sizeable disordered regions, as it can be seen in Figure 2. Notably, the charged residues are localized at one side of the surface of the protein. This strongly suggests that the water-soluble form is amphipathic (Zampieri *et al*., 2010). This structure is consistent with its ability to form an amphipathic polymer.

Class II HFBs consist of a core with a β-barrel structure (Fig. 2), nevertheless do not contain the two disordered loops. Furthermore, the additional two-stranded β-sheet in class I hydrophobins is replaced with an α-helix, in the same region (Kwan, A.H.Y *et al*., 2006; Hakanpää, J, *et al*., 2006). One side of the monomer surface contains only aliphatic side chains. This creates a hydrophobic patch which constitutes 12% of the total surface area (situated on the top of the structure showed in figure 2). The protein surface is otherwise mainly hydrophilic, and thus the surface is segregated into a hydrophobic and a hydrophilic part. This amphiphilic structure governs the properties of class II hydrophobins, such as surface activity and surface adsorption.

2.2 The assembly process

The characteristic property of HFBs is adsorption at hydrophobic-hydrophilic interfaces, at which they form amphiphilic films (Wessels J.G.H, *et al*., 2007; Wösten H.A.B, *et al*., 2007). The interface can occur between solid and liquid, liquid and liquid or liquid and vapour. In early studies, hydrophobins were found to self-assemble into aggregates and form various

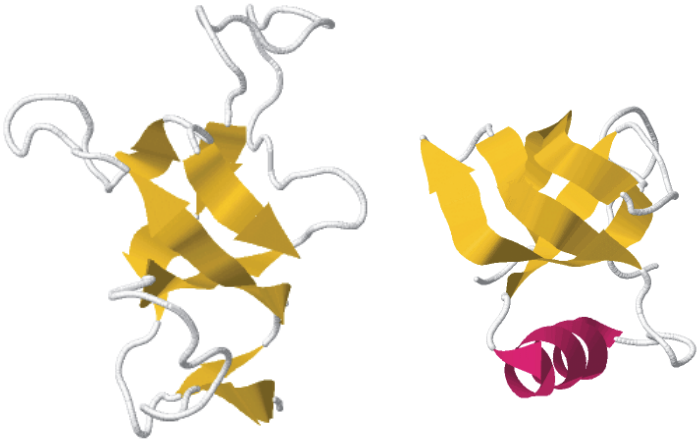

Class I **Class II**

Fig. 2. HFBs structures.

types of self-assembled structures. Rodlets were first observed on the outer surface of spores from *Penicillium* (Sassen *et al*., 1967; Hess *et al*.,1968) and *Aspergillus* (Hess *et al*., 1969; Ghiorse and Edwards, 1973).

Class I HFBs at low concentration are in monomeric form, while at higher concentrations they are mainly in a dimeric form (Wang, X *et al*., 2002; Wang, X *et al*., 2004). Self-assembly proceeds through the formation of an intermediate form, the α- helical state (De Vocht, M.L *et al*., 2005, Wang, X *et al*., 2005). Upon transfer to the β-sheet state, the content of β-sheet structures increases. This is accompanied by the formation of a mechanically stable protein film. However, during this transition the proteins forms nanometric wide fibrils, which are known as rodlets. SE measurements have shown that the film is about 3 nm thick (Wang, X *et al*., 2005). This and the fact that the diameter of the β-barrel of the protein is approximately 2.5 nm suggest that the rodlets could be formed by a molecular monolayer (Kwan, A.H.Y *et al*., 2006). The charged patch on the protein surface would face the hydrophilic side of the interface, while the hydrophobic diametrically opposite site would face the hydrophobic side of the interface. This arrangement is consistent with the way other surface active molecules orient themselves at hydrophilic-hydrophobic interfaces (Kwan, A.H.Y *et al*., 2006).

Like class I, class II HFBs exist as monomers at low concentration (Szilvay, G.R et al., 2006). When the concentration is increased, they form dimers and, at higher concentrations, tetramers (Torkkeli, M et al., 2002). The monomers have a higher affinity for surfaces than for formation of oligomers (Linder *et al*. 2005; Szilvay, G.R et al., 2006). These oligomers would dissociate at a hydrophilic-hydrophobic interface, which would result in the formation of a film which consists of a monolayer of the class II HFB: a scheme of these differences is reported in Figure 3. In contrast to class I, self-assembly of class II HFB at the water-air interface is not accompanied by a change in secondary structure (Askolin, S. et al., 2006), furthermore this layer is not rodlet-like as in the case of class I HFBs.

Moreover, as described above, the end state of class I HFBs is very stable and cannot be dissociated by pressure, detergent or 60% ethanol. In contrast, the end form of class II HFBs readily dissolves under these conditions.

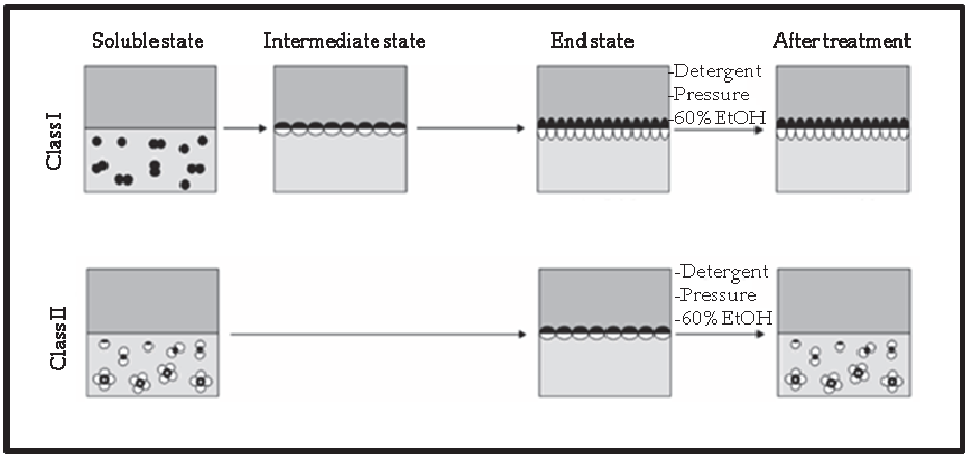

Fig. 3. Main differences between class I and class II HFBs.

3. Hydrophobins self-assembling on solid surface: methods and characterizations

A simple technique used to induce the self-assembling of the HFB biofilm on a solid substrate is the drop-deposition method, where the drop is a micro-litre volume of a liquid solution containing the proteins in their monomeric state. Even if this kind of film casting is not a perfectly controlled process, i.e. the protein concentration increases in an uncontrollable way during solvent evaporation, it is possible, by using proper starting conditions of some parameters, such as temperature, surface cleaning, and so on, to obtain reproducible results in term of film thickness and surface wettability. By using this technique, different kind of surfaces have been conditioned: in the next paragraph we report the main experiences in worldwide laboratories on this subject. Here, we present the standard processes to obtain self-assembled HFB biofilms and the main characterization methods we use. Biofilm drop casting is normally used in our laboratory to give new functionalities to silicon surface: silicon, and silicon related materials, is the most used solid support in the microelectronic industry. For this reason, silicon is widely used in all the application of electro-optic and photonic devices. At this aim, highly doped p^+ silicon wafer, <100> oriented, 0.003 Ω cm resistivity, 400 μm tick, was cut into 2 x 2 cm^2 pieces. The silicon substrates were cleaned using the standard RCA process and dried in a stream of nitrogen gas. RCA is based on a combination of two cleaning steps, one using solutions of ammonium hydroxide/hydrogen peroxide/deionized water, and the other using hydrochloric acid/hydrogen peroxide/deionized water, both at the temperature of 80 °C. The samples were prepared by coating the silicon chips with 200 μl of HFB solution (0.2 mg/ml of protein dissolved in an ethanol-deionized water (60/40 v/v) mixture) for 1 h, drying for 10 min on a hot plate at 80°C, and then washing with the ethanol-water mixture. The incubation process was repeated two times. Then, the samples were treated for 10 min at 100°C in 2% Sodium Dodecyl Sulfate (SDS), so as to remove the protein not assembled into the biofilm, and again washed in deionized water.

The Langmuir technique is the most accurate way to get mono-molecular films of amphiphilic molecules. A known quantity of the material is spread on the free surface of a suitable liquid (the subphase) contained in a trough. The quantity of the material has to be predetermined on

the base of the molecular and trough areas, in order to know the surface molecular concentration. In doing this, one should take care to use a sufficiently low surface concentration in order to have an interfacial film of non-interacting molecules (the so-called gas phase). Moreover, as one desires to have all molecules at the interface, it is very important to adjust the subphase pH in order to match the isoelectric point of the used protein.
Once the interfacial film is formed, the presence of movable barriers on the Langmuir trough allows to compress the film in a controlled manner, varying in this way the surface molecular density and consequently the surface tension. The latter can be measured with several techniques, but the most used is the Wilhelmy plate tensiometer, consisting of a thin plate made from glass, platinum or even paper, attached to a scale or balance via a thin metal wire.

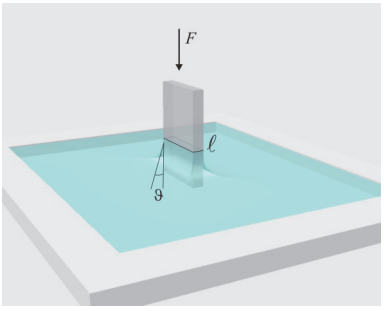

Fig. 4. Scheme and reference angle for Wilhelmy equation.

The force on the plate due to wetting is measured via a microbalance and used to calculate the surface tension (σ) using the Wilhelmy equation (see Figure 4):

$$\sigma = \frac{F}{\ell \cos \vartheta}$$

where λ is the wetted perimeter of the Wilhelmy plate and θ is the contact angle between the liquid phase and the plate. In practice the contact angle is rarely measured, instead either literature values are used, or complete wetting (θ = 0) is assumed.
The most important feature of the interfacial film is the pressure Vs. area isotherm, obtained by recording the surface pressure as a function of the trough area. If the number of molecules present at the interface is known, as in the case of water insoluble amphiphiles, the surface pressure can be plotted as a function of water surface available to each molecule. This curve can reveal several details about the interfacial film properties, in particular phase transitions and collapses of the molecular film. In such cases the steric factor plays a relevant role in the film stability and the entire sequence of phases transitions can be sperimentally observed (see Fig. 5).

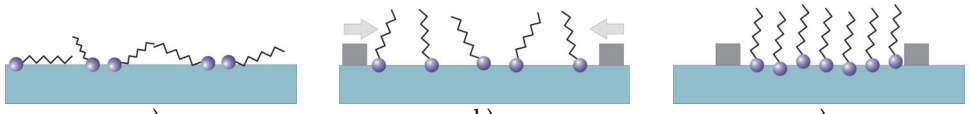

Fig. 5. Cartoon sequence of the possible molecular arrangement for an amphiphile monolayer as function of the molecular density: a) gas phase; b) liquid-expanded phase; c) condensed phase.

When proteins are used for making a Langmuir film things can be quite different, as a considerable number of other factors has to be took into account: the state of the protein (folded or unfolded) and her shape (in general almost globular), the presence of multiple hydrophobic patches. In figure 6 a typical isotherm for Vmh-2 from *Pleorotus Ostreatus* is shown. It is evident that many features are missing with respect to the case of a fatty acid. In particular only one critical point is present. If one keeps in mind the quasi-globular shape of this protein can easily realize that the gas - expanded liquid – solid transitions are in some way continuous, without any abrupt molecular rearrangement as in the case of an elongated molecule.

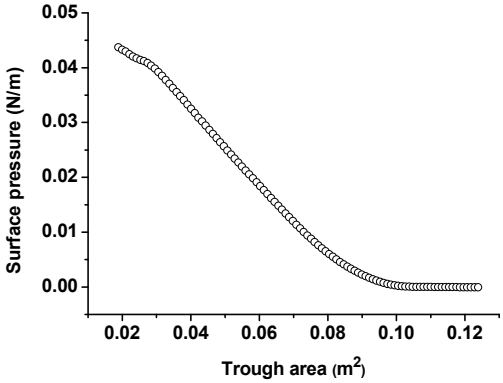

Fig. 6. Typical isotherm measured for the hydrophobin Vmh-2 during film formation.

If the used amphiphilic protein is even only partially soluble in water, although the isotherm features still hold, one has to face with the problem to determine the number of molecules present at the interface and hence the surface molecular density. This occurrence can be made evident by isobaric measurements, in which the ratio between the trough surface S and the initial trough surface S_0 is plotted as a function of time at a given constant surface pressure value. The plot shown in Fig. 7 refers to Vmh2 HFB from the fungus *Pleurotus Ostreatus*. The decreasing of the trough area in time is due to a surface molecular depletion that could be ascribed both to a bare solubilisation of the film or to some more complex process involving the creation of soluble assemblies. From the same plot one can also argue that an increasing in the surface pressure has the effect of stabilizing the film, reducing the molecular depletion ratio, as the decreasing in the curve slope with the increasing of the surface pressure demonstrate.

One possible method for at least estimate the surface molecular concentration is the fitting of the experimental isotherm with a suitable 2-D equation of state, leaving the surface density as fitting parameter. In the simplest case holds a Vollmer-like equation of the kind.

$$\Pi = \frac{mkT}{A - \omega} - \Pi_{coh} \tag{1}$$

where Π is the surface pressure, k is the Boltzmann constant, T is the temperature, ω is the limiting area of a molecule in the gaseous state, A is the area per molecule, Π_{coh} is the

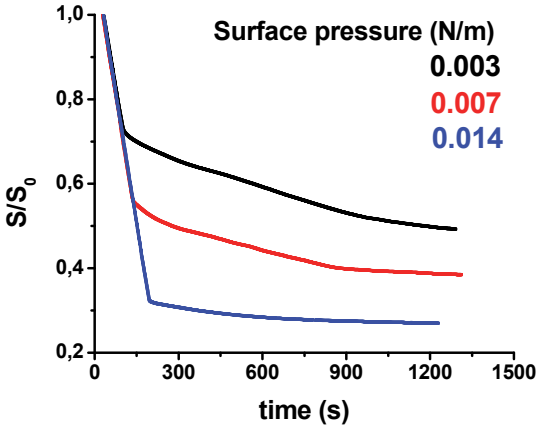

Fig. 7. Isobaric measurement at different surface pressures for the Vmh-2 hydrophobin.

cohesion pressure accounting for the intermolecular interactions, and m is a parameter accounting for the number of kinetically independent units (fragments or ions). The parameter A is actually the inverse of the surface molecular density and can hence be expressed as

$$A = \frac{S}{n}, \tag{2}$$

where S is the trough area and n the number of molecules present at the interface.
Once the Langmuir film has been characterized, it can be transferred onto a solid substrate for applications or subsequent analyses. The most used methods are the vertical lift/dipping of the substrate through the interfacial film (Langmuir-Blodgett technique) and the horizontal plate lift from the interface (Langmuir-Shaeffer technique). When hydrophilic subphases are used, the lift method allows to transfer the monolayer with his hydrophilic side facing the substrate (also hydrophilic), leaving the hydrophobic side exposed to the air.

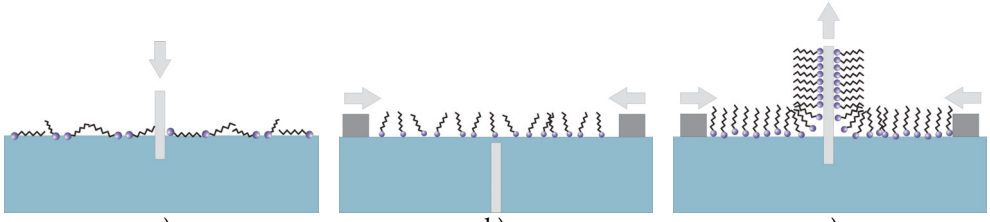

Fig. 8. Schematic of Langmuir-Blodgett technique: with the barriers opened, in the gas phase, the substrate is dipped in the subphase (a); then the film is compressed at the desired surface pressure (b); finally the substrate is lifted through the interfacial film, dragging a portion of it. In the meanwhile the closed-loop control closes the barriers in order to keep constant the surface pressure (c).

Alternatively, the film can be transferred with his hydrophobic side facing an hydrophobic substrate by dipping the latter through the interfacial film. The monolayer side exposed to the air in this case will be hydrophilic. In the Langmuir-Blodgett deposition technique, the trough control system allows to perform the film transfer at constant surface pressure, closing the barriers in order to compensate the surface molecular depletion due to the film transfer itself.

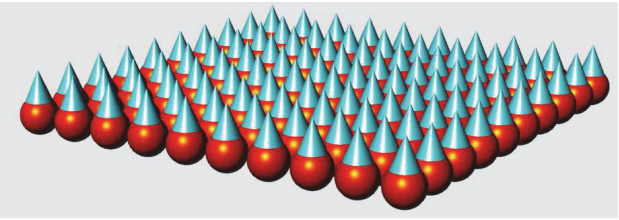

Fig. 9. Cartoon of ordered protein monolayer for Langmuir- Schaefer

The Langmuir-Shaeffer technique allows to remove a whole patch of the interfacial film at once. Under the same initial conditions as above, this method allows the film sticking from the hydrophobic side onto an hydrophobic substrate, leaving thus the hydrophilic side of the monolayer exposed to the air. In this case, the closed-loop active surface pressure control isn't strictly required, providing that the monolayer is stable at the interface.

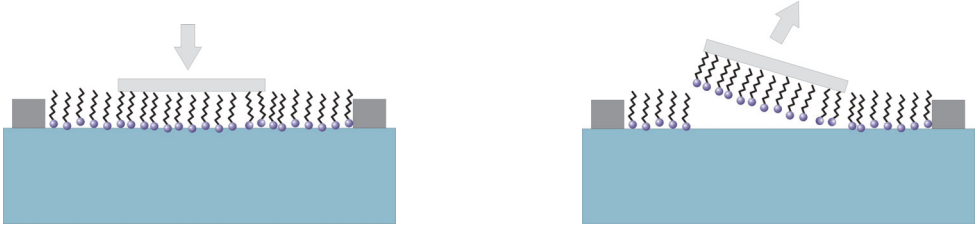

Fig. 10. Schematic of Langmuir-Shaeffer technique.

Sometimes it can be useful to lift the molecular film as self-standing, in order to eliminate the interactions between molecules and an underlying substrate. This task is often accomplished using metallic grids, of the kind used in TEM specimen preparation, featuring a suitably fine mesh.
The HFBs film self-assembled on the silicon surface or by LB methods can be characterized by means of several methods; the most common characterization techniques are the spectroscopic ellipsometry, the atomic force microscopy, and the water contact angle.

3.1 Spectroscopic ellipsometry

Spectroscopic ellipsometry (SE) allows to determine the optical properties (i. e., the refractive index n and extinction coefficient k) and the thickness of the HFB biofilm assembled on a solid surface. The method is based on the measurement of the change in the polarization state of the light over the spectral range after the reflection from the sample surface. Ellipsometry measures the complex reflectance ratio (ρ) defined by:

$$\rho = \frac{R_p}{R_s} = \tan\psi e^{i\Delta} \tag{3}$$

where R_p and R_s are the complex reflection coefficients of the light polarized parallel and perpendicular to the plane of incidence. Thus, ψ and Δ are, respectively, the amplitude ratio and the phase shift between *s* and *p* components of polarized light.

We have used a Jobin Yvon UVISEL-NIR phase modulated spectroscopic ellipsometer, at an angle of incidence of 65° over the range 320-1600 nm with a resolution of 5 nm. The properties of the biofilm have been extracted from the SE measurements using the analysis software Delta Psi (Horiba Jobin Yvon).

The optical properties, *n* and *k*, as functions of the wavelength have been determined by fitting the experimental results using the Tauc-Lorentz model, firstly proposed in 1996 by Jellison and Modine as a new parameterization of the optical functions of amorphous materials. The imaginary part of the dielectric function is based on the Lorentz oscillator model and the Tauc joint density of states:

$$\varepsilon_2 = \begin{cases} \frac{1}{E}\frac{AE_0C(E-E_g)^2}{(E^2-E_0^2)^2+C^2E^2} & E > E_g \\ 0 & E \le E_g \end{cases} \tag{4}$$

The real part of the dielectric function is given by Kramers-Kronig integration:

$$\varepsilon_1 = \varepsilon_\infty + \frac{2}{\pi} P \int_{E_g}^{\infty} \frac{\xi\varepsilon_2(\xi)}{\xi^2 - E^2} d\xi \tag{5}$$

These equations include five fitting parameters: the peak transition energy E_0, the broadening term *C*, the optical energy gap E_g, the transition matrix element related *A*, and the integration constant ε_∞.

In Figure 11, *n* and *k*, as functions of the wavelength, are reported for the Vmh2 biofilm self-assembled on silicon together with the values of the fitting parameters and the χ^2.

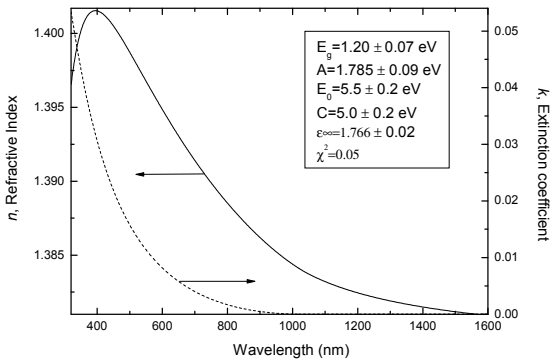

Fig. 11. Optical properties, *n* and *k*, of the Vmh2 biofilm self-assembled on silicon surface as functions of the wavelength.

Starting from these results, we can use the ellipsometric technique to estimate the thickness of the biofilm depending on the concentration or on the post deposition washing procedure, for example. We notice that before SDS washing the thickness of Vmh2 biofilm could be of

tenths of microns, also depending on protein concentration in the starting solution. We have verified that a step-by-step deposition allows the assembling of biofilms of increasing thicknesses: after three consecutive depositions, for a total time of three hours, we have obtained biofilms assembled on crystalline silicon up to 40 nm thick, that is, thicker than those reported in literature. After hot SDS washing the biofilm is very much thinner: a value of 3.91 ± 0.06 nm has been calculated modelling the HFB sample by a simple homogeneous layer. We believe that this is the thickness of a monolayer of HFBs when self-assembled on hydrophobic silicon: this value is consistent with a typical molecular size and comparable to atomic force microscopy measurements. According to the above described model, the washing step of the chip is strong enough to remove the proteins aggregates deposited on the HFB monolayer that directly interacts with the hydrophobic silicon surface. This behaviour points out the stronger interactions between the silicon surface and the HFB monolayer with respect to those between the HFB aggregates and the HFB monolayer. The experimental spectra Ψ and Δ, together with the calculated ones, are shown in Figure 12. The persistence of Vmh2 biofilm on the silicon surface depends strongly on its chemical nature: we have thus verified that the same deposition procedure on silicon dioxide, which is a hydrophilic surface, does not give the same results in terms of biofilm chemical stability. After washing the biofilm in hot SDS solution only sparse islands of protein biofilm can be found on the silicon dioxide chip. This different behaviour can be ascribed to the greater number of hydrophobic residues constituting the protein with the respect to those hydrophilic.

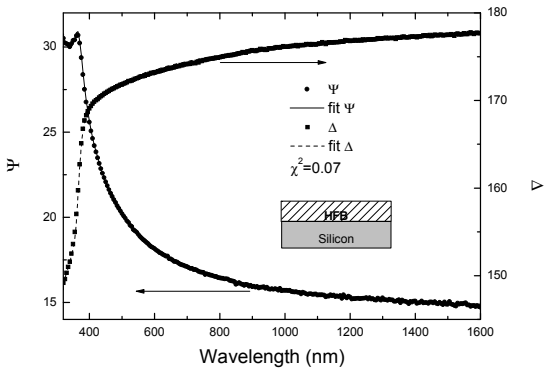

Fig. 12. Measured and calculated spectra (Ψ, Δ) of the HFB biofilm self-assembled on a silicon surface.

3.2 Atomic force microscopy

In the early 1980s the first Scanning Probe Microscope (SPM) has been introduced. It was actually a Scanning Tunneling Microscope, exploiting the tunnelling current between the surface sample and a very sharp conductive tip sweeping back and forth a few tens nanometers over the sample surface. The electron tunnelling is a quantistic effect connected to the probability for an electron to cross a gap between two conductive solids. Its development was driven by the need of the semiconductors industry to characterize the semiconductor inhomogeneities at the nanoscale, this issue becoming of increasing importance with the

progresses in the miniaturization of the electronic devices. A few years later, a similar instrument was released, the Atomic Force Microscope (AFM) exploiting the van der Waals-like interaction forces between the sample surface and the tip, instead of the tunnelling current and allowing the imaging of non-conductive samples as well, down to the atomic scale.

In their essential parts, an AFM is made of a closed loop controlled scanning head and an acquisition/digital signal processing board slotted in a PC running a devoted software. Samples are under the form of small chips or thin films with *x-y* size ranging from the sub-millimiter to a centimeter. The *z* size is usually in the order of a nm. The sample is placed at the free end of a piezoelectric scanner; depending on the piezo characteristics, the scanned area can range from a few tens nm^2 to ~10^4 sq. microns with a resolution down to a few tenth nm. The AFM probes can feature pyramidal or conical shape, with a height in the range of a few microns and a tip radius down to a couple nanometers; this makes a really sharp tip, carring only a few atoms at the end! The tip is placed at the end of a flexible cantilever; both the tip and the cantilever are usually made of silicon, although other materials are now available, as diamond or carbon nanotubes.

When the tip is brought close to the sample surface, the van der Waals-like forces between the sample surface and the tip cause the cantilever bending; if one knows the cantilever spring constant, the bending measurements allows to deduce the interaction force. The detection technique exploits the reflection of a laser beam from the upper side of the cantilever; the bending is measured by the laser spot displacement over a two or four quadrants photodetector.

An AFM can operate essentially in two different modes according to the sample surface-tip distance range. When this distance is small, in the order of few Angstrom, one operates in the repulsive region of the interaction potential and the operating mode is named *contact mode*. On the contrary, when this distance is "large", in the order of 1 – 10 nm , the attractive region of the interaction potential is involved and the corresponding mode is named *no-contact mode*. The difference between the contact and the no-contact mode is remarkable, because of the difference in the range of the forces involved in the interaction between the AFM tip and the sample surface; in the contact mode case, the repulsive forces are in the order of tens of nN, al least one order of magnitude stronger than the case of the attractive forces involved in the no-contact mode. Because of the extreme force weakness, the detection technique used in no-contact AFM is very sensitive: driven by a piezo element, the cantilever oscillates with a typical amplitude of few nm at a frequency slightly above the resonance, while "flies over" the surface of the sample. The presence of Van der Waals and other long-range attractive forces shifts the cantilever resonant frequency which, in turn, causes the oscillation amplitude to decrease.

The NC-mode is useful in imaging soft samples, as is the case of biologic molecules, given the weakness of the involved forces that prevents or minimizes the sample damage.

An evolution of the AFM no-contact operating mode is the *tapping* or *intermittent mode*.

In tapping mode the cantilever oscillates at its resonant frequency or slightly below. The amplitude of oscillation typically ranges from 20 nm to 100 nm. Differently from the case of no-contact mode, in which the tip never comes in contact with the sample surface, in the tapping mode the tip lightly "taps" on the sample surface during scanning, contacting the surface at the bottom of its oscillation.

Beside the bare imaging of soft samples, the AFM dynamical modes (NC and tapping) can supply information about other features of the sample at the nano scale, as its wetting and visco-elastic properties. In order to achieve such information, a fundamental measurement is

the phase lag between the signal driving the cantilever piezo element and the cantilever response. Then the experimental curves are fitted with a model describing the cantilever dynamics. The recording of the phase lag at constant amplitude for each point of the acquisition *x*-*y* grid will produce a phase image that closely relates to a dissipation map.
In our experience, a NanoScope V Multimode AFM (Digital Instruments/Veeco) was used for the imaging of the HFB biofilm. The sample was imaged in air in tapping mode. The scan frequency was tipically 1 Hz per line and images were flattened to a second order polynomial.
The AFM images of the HFB silicon coated sample are reported in Figure 13; the formation of a homogeneous biofilm can be observed in the phase image (right picture in Figure 13). The AFM characterization also reveals the presence of rodlets-like structures on top of the biofilm (Rodlet average height 4.11 ± 0.08 nm; Rodlet average width 23.9 ± 0.6 nm; Rodlet average length 64 ± 3 nm; Mean roughness 3.32 nm).

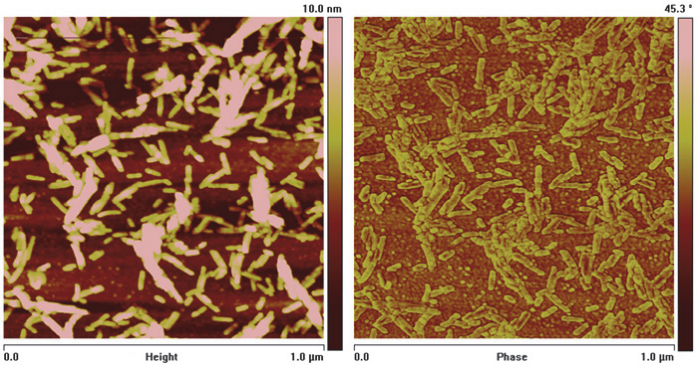

Fig. 13. Height and phase atomic force microscopy images of silicon surface coated with HFB biofilm.

3.3 Water contact angle measurements

The most common method for the determination of the surface wettability is the water contact angle (WCA) measurement. The technique simple, quick, and cheap is based on the analysis of the contact angle formed between a surface and a water droplet placed on it.
At the aim to determine the wettability of the HFB biofilm, we have used the sessile drop method for WCA measurements on a OCA 30 – DataPhysics coupled with a drop shape analysis software. Five measurements were analyzed for each sample.
The silicon surface, after the removal of the native oxide layer in hydrofluoridric acid, is characterized by a WCA of (90.0±0.3)° (Figure 14 (A)). The presence of the HFBP biofilm lowers the WCA down to (44±1)° (Figure 14 (B)): this interface is more hydrophilic due to the assembly of the protein into a film with apolar groups disposed towards the hydrophobic silicon and the polar groups on the other side.

4. Functional surfaces based on hydrophobins biofilms

The capability of hydrophobins to adhere to various surfaces was one of the first observations among hydrophobins functions. An early finding on the behaviour of the class I hydrophobin SC3 from *Schizophyllum commune* was that when it binds to for example

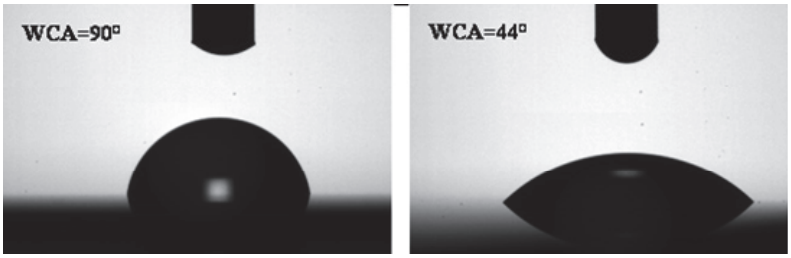

Fig. 14. Water contact angle measurements of bare silicon (A) and silicon coated with HFB (B).

Teflon, it can form a very insoluble layer (de Vocht et al. 2002). All hydrophobins adhere to surfaces, but there is a difference in the binding characteristics (Askolin et al. 2006). While class I members adhere very strongly, this is not seen for class II members which dissociate more easily.

Glass has been one of the widely used substrates for protein chips. Qin et al (2007a) have compared two methods for protein immobilization on glass slides, one is the traditional method of silanization (Mezzasoma et al. 2002); the other is the coating with the class II hydrophobin HFBI from *Trichoderma reesei*. The modified glass surfaces were characterized with X-ray photoelectron spectroscopy (XPS), water contact angle measurement (WCA) and immunoassay. The results have shown that HFBI coating can achieve the same result of protein immobilization on glass slides as silanization did, or even better. Moreover the HFBI coating does not require the complex procedure and strict surface cleanness as the silanization needs. HFBI-coated surfaces can be used immediately or preserved for some days prior to use. Therefore hydrophobin self-assemblies seems to be a simple and generic way for protein immobilization on glass slides.

Mica and polydimethylsiloxane (PDMS) are other substrates used for patterning of biomolecules. Freshly cleaved mica is a promising substrate for patterning applications, because it is the most readily available surface with atomic-scale flatness. Biomolecules, such as proteins, could not be immobilized on mica surfaces effectively without surface modification. PDMS is a kind of soft polymer with attractive physical and chemical properties: elasticity, optical transparency, flexible surface chemistry, low permeability to water, low toxicity, and low electrical conductivity. Thus, it has been widely used in microfluidic devices and microcontact printing technology. A simple method to modify both mica and PDMS surfaces by HFBI for protein immobilization has been recently developed (Qin et al. 2007b). XPS and WCA measurements illustrated that the wettability surface can be changed from superhydrophobic (PDMS) or superhydrophilic (mica) to moderately hydrophilic. The same surfaces, mica, glass, and PDMS, have been modified using the class I hydrophobin HGFI from *Grifola frondosa* (Hou et al. 2009). The surface wettability was efficiently changed by HGFI modification, as XPS and WCA measurements indicated. Furthermore data showed that self-assembled HGFI has better stability than type II hydrophobin HFBI: HGFI self-assembly was stable against rinsing by several solutions, i.e. 2% hot SDS solution and 60 vol.% ethanol.

Polystyrene and its variations are extensively used as solid supports to produce, for example, polystyrene-microtitre plates and tubes in immunoassays. Wang et al. (2010a) have

used the Class I hydrophobin HGFI to increase the hydrophilicity of polystyrene for facilitating immobilization of biomolecules. The adsorption process of HGFI on the polystyrene surfaces was studied by quartz crystal microbalance at different pH values, by XPS, WCA measurements and AFM analyses. By self-assembling, hydrophobin easily formed an intact charged film on the hydrophobic polystyrene that enhanced the hydrophilicity of the polystyrene for a long time (Wang et al. 2010a).
Silicon is the most used solid support in all micro- and nanotechnologies developed for the integrated circuits industry. For this reason, silicon is also used in many commercial technological platforms for biomedical and biosensing applications. The anisotropic wet micromachining of silicon, based on a water solution of potassium hydroxide (KOH), is a standard fabrication process that is extensively exploited in the realization of very complex microsystems such as cantilevers or membranes. A nanostructured self-assembled biofilm of Vmh2, was deposited on crystalline silicon and since this procedure formed chemically and mechanically stable layers of self-assembled proteins, the biomolecular membrane has been tested as masking material in the KOH wet etch of the crystalline silicon. The process has been monitored by SE and atomic force microscopy measurements. Because of the high persistence of the protein biofilm, the hydrophobin-coated silicon surface is perfectly protected during the standard KOH micromachining process (De Stefano et al. 2007). In Figure 15 the optical photos of the two silicon samples after this treatment, are shown: on the A image is clearly visible the etched surface whereas in the B image the HFB covered surface is perfectly homogeneous.

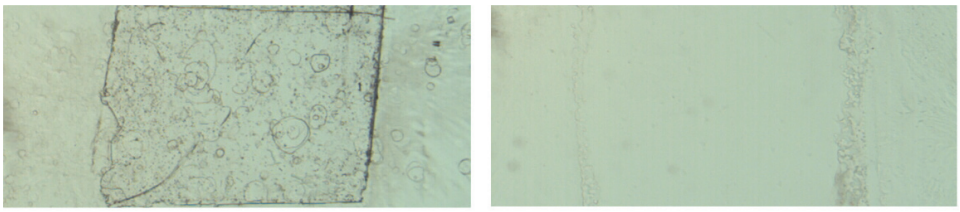

Fig. 15. Optical images of the silicon surface after the KOH etching: (A) bare silicon; (B) silicon coated with HFB.

This qualitative result is quantitative confirmed by ellipsometric and profilometric measurements: an 8.40 (0.05) nm biofilm of hydrophobins is still optically detected by the ellipsometer and the profilometer cannot detect any dig into the hydrophobins shielded sample, as it can be seen in Figure 16.
Porous silicon (PSi), a silicon related material obtained by silicon dissolution in an electrochemical cell in hydrofluoridic water solution, is really a versatile material owing to its peculiar morphological, physical, and chemical properties, allowing the easy fabrication of sophisticated optical multilayers, such as one-dimensional photonic crystals, by a simple electrochemical etching process. The reflectivity spectrum of the photonic crystals shows characteristic shapes, which are very useful in many applications, from biochemical sensing to medical imaging. The major drawback of the ''as etched'' PSi is its chemical instability: it has been shown that a PSi wafer can be dissolved under the physiological conditions that are very often used in biological experiments. De Stefano et al. (2008) have covered the Psi

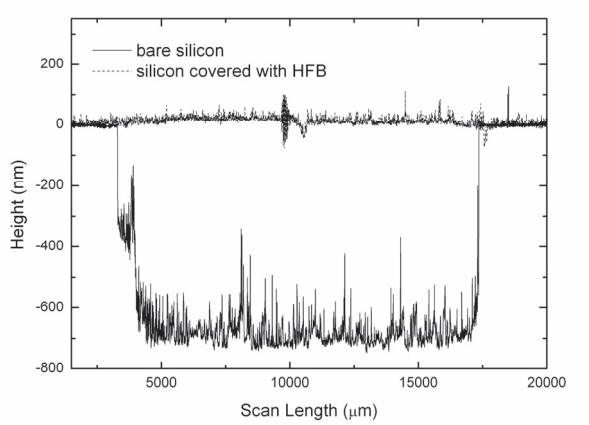

Fig. 16. Profilometric measurements of bare silicon (solid line) and silicon covered with HFB (dash line).

surface with the highly stable and resistant biofilm resulting from the self-assembly of Vmh2. The hydrophobin penetrates the whole stack, accumulating at the bottom and modifies strongly the wettability of the PSi surface. Moreover, the protein membrane not only protects the nanocrystalline material from basic dissolution in NaOH, but also leaves unaltered the sensing ability of such an optical transducer, adding chemical stability, which can be key in biomolecular experiments.

Gold is an excellent electric conductor with fine ductility and chemical inertness, thus an ideal choice for developing bioelectronic devices. HFBI modification on smooth gold surfaces has been proven to effectively enhance the surface hydrophilicity. The unmodified bare gold surface exhibited a weak hydrophilicity, while the surface hydrophilicity was remarkably improved after HFBI processing, as demonstrated by WCA measurements. The increase of surface wettability was not affected by the presence of washing procedures (Zhao et al. 2009).

Carbon nanotubes (CNTs, hollow cylinders made of sheets of carbon atoms) have recently emerged as building blocks of novel nanoscale structures and devices. CNTs have a variety of electronic properties that can be exploited for a variety of applications. Nanotubes have been functionalized to be biocompatible and to be capable of recognizing proteins (Shim et al. 2002). Often this functionalization has involved noncovalent binding between a bifunctional molecule and a nanotube in order to anchor a bioreceptor molecule with a high degree of control and specificity. Furthermore, CNTs are commonly insoluble in all solvents and usually form tangled network structures containing various impurities (Wu et al., 2010). To overcome these limits, CNT surfaces are often tailored using either covalent (Wu et al., 2007) or noncovalent modification (Hecht et al., 2006) strategies. A novel noncovalent approach has been developed for the functionalization of multi-wall carbon nanotubes (MWNTs, many layers to form concentric cylinders) using the class II hydrophobin, HFBI. The HFBI–MWNTs nanocomposite was characterized by scanning electron microscopy (SEM), transmission electron microscopy (TEM) and WCA. The hydrophobin HFBI demonstrates to be an efficient solubilizing agent for MWNTs. The resulting HFBI–MWNTs nanocomposite film with both merits of HFBI and MWNTs exhibited high hydrophilicity, fast electron-transfer kinetics and excellent electrocatalytic activity (Wang et al. 2010b).

The deposition of ceramic thin films from aqueous solutions at low temperature using biopolymers as templates has attracted much attention due to economic and environmental benefits. Titanium dioxide is one of the most attractive functional materials and shows a wide range of applications across vastly different areas because of its unique chemical, optical, and electrical properties. Santhia et al. (2010) deposited smooth, nanocrystalline titania thin films by an aqueous deposition method on a hydrophobin film. Firstly, the hydrophobins were self-assembled on a silicon substrate and characterized by XPS, AFM and surface potential measurements. Hydrophobin-modified silicon substrates were then used to deposit from aqueous solution at near-ambient conditions highly uniform, crack-free nanocrystalline TiO_2 thin films. Nanoindentation tests showed the high resistance against mechanical stress of the deposited titania films. The determined averaged hardness value and the Young's modulus highlight the compatibility of these films for coating implants and other biomedical applications.

5. Biosensors based on organic/inorganic interfaces

In recent times, there has been an increasing interest in interfacing biological molecules with nanomaterials and in understanding, controlling, and applying biomolecule-nanomaterial interactions for sensing. If the biomolecule of interest is a protein, a critical issue is the retention of its structure and activity on the nanoscale supports. It is of fundamental interest to understand how nanomaterial properties affect the structure, activity, and stability of conjugated proteins and identify optimal conditions to preserve functionality following protein immobilization. A similar argument is also important in the case of antibodies: all immunoassay based on the interaction between an antigen and its specific antibody critically depend on how the antibodies are immobilized on solid supports. In particular, it should be possible to bond the antibodies by their constant region, since the variable portion should be free in order to recognize and link the antigen. In general, the adsorption of any biomolecule to solid surfaces often induces structural changes that may affect the native functionality. This is a frequently observed phenomenon, and the resulting changes in structure, and function, can have profound consequences. When biomolecules are immobilized on hydrophobic surface, they can suffer considerable denaturation and lose biological activity due to strong hydrophobic interactions (Butler, 2004). In contrast, biomolecules have less conformational change and retain functional activity when are immobilized on hydrophilic surfaces, as the major driving force between biomolecules and the hydrophilic surface is the electrostatic force (Goddard and Hotchkiss, 2007; Kaur et al., 2004; Lubarsky et al., 2005). Moreover the strength and selectivity of protein-protein interactions make proteins excellent candidates to serve as linkers to form ordered structures (Wang 2010).

Taking into consideration the above mentioned evidences, self assembling proteins like hydrophobins that have the remarkable property of adhering to almost any surface forming stable amphiphylic films are very good candidates to easily manufacture stable, enzyme-based catalytic surfaces for applications in biosensing. This approach has a bearing for preparing stable enzyme-based catalytic surfaces in an easy, rapid, and reliable way. Within very short times, without resorting to covalent chemistry, enzymes can be stably immobilized on a solid surface. As a matter of fact several papers have been published reporting the use of hydrophobins to immobilize proteins.

Palomo et al. (2003) reported the binding of *Pleurotus ostreatus* hydrophobins to a hydrophilic matrix (agarose) to construct a support for noncovalent immobilization and activation of lipases. Lipase immobilization on agarose-bound hydrophobins resulted in increased lipase activity and stability. Its enantioselectivity was similar to that of lipases interfacially immobilized on conventional hydrophobic supports.

Two redox enzymes, glucose oxidase from *Aspergillus niger* (GOX) and horseradish peroxidase (HRP), were immobilized on glassy carbon electrodes coated with SC3 (Corvis 2005). It was shown that the immobilized GOX kept its activity on the 99th day of repeated use while HRP was active on the 36th day after immobilization. The affinity for the substrate was comparable for the immobilized and dissolved GOX and HRP, while the kinetic measurements indicate that the enzyme specific activity is lower for the immobilized, compared to the dissolved enzymes. The contact angle measurements suggest that the major contribution to the interactions involved in the immobilization of the enzymes on the SC3 layers comes from polar amino acids.

The Vmh2 modified silicon surface has been tested by BSA immobilization: solutions containing a rhodamine labelled BSA at different concentration, between 3 and 12 μM, have been spotted on the HFB film (De Stefano et al. 2009). The labelled bioprobes have been spotted also on other bare silicon samples, as a negative control on the possible aspecific binding between the silicon and the probe. All the samples have been washed in deionized water to remove the excess of biological matter and observed by the fluorescence microscopy system. Under lamp illumination, we found that the fluorescence of silicon-HFB-BSA system is brighter than the negative control. The fluorescence signal is also quite homogeneous on the whole surface also after a overnight washing in deionized water, which means that the strength of the affinity bond between the HFB and the BSA is enough to conclude that the HFB-BSA system is very stable.

Protein immobilization on the Vmh2 biofilm on silicon has been also verified and analyzed using an enzyme, POXC laccase. The enzymatic assay on the immobilized enzyme has been performed by dipping the chip into the buffer containing the substrate and by following the absorbance change during several minutes (pH 5 buffer, DMP as a substrate: a good trade-off between stability and activity of the enzyme). A 30 μl drop of the enzyme solution (about 700 U/ml) has been deposited on protein modified chips (1cmx1cm) and, after several washing, an activity between 0.1 and 0.2 U has been determined on each chip, resulting in an immobilization yield of 0.5÷1%. This value is comparable to that one (7%) obtained in the optimized conditions for laccase immobilization on EUPERGIT C 250L© (Russo et al. 2008). Taking into account the specific activity of the free enzyme (430 Umg^{-1}) and its molecular mass (59 kDa), 0.5μg of laccase corresponds to about 8 pmol (5 x 10^{12} molecules) immobilized on each chip. A reasonable evaluation of the surface occupied by a single protein molecule can be based on crystal structures of laccases. This surface should be 28 x 10^{-12} mm^2, considering the protein as a sphere with radius of 3 x 10^{-6} mm. On this basis, the maximum number of laccase molecule on each chip should be 3 x 10^{12}. These data indicate that the number of active immobilized laccase molecules on each chip is of the same order of magnitude than the maximum expected. Laccase assays have been repeated on the same chip after 24 and 48 hours in the same conditions. About one half of the activity has been lost after one day, but no variation of the residual activity has been observed after the second day. Moreover, comparison of these data with those of the free enzyme, stored at the same temperature, showed that the immobilized enzyme is significantly more stable than the free form.

A class I hydrophobin, HGFI purified by *Grifola frondosa*, has been used in modifying polystyrene wettability and also as a functional interface for immunofluorimetric assay. In particular, time resolved fluorescence assay has been used for the quantitative determination of carcinoembryonic antigen. A detection limit of 0.24 ng/mL is claimed by authors (Wang et al. 2010).
Even if class II is less chemically stable, HFBI has been used in glucose biosensing once decorated by multi wall carbon nanotube and glucose oxidase (Wang et al. 2010). A detection limit of 8.2 μM has been reached by amperometric measurements.
HFBI has also been used in coating gold surfaces for applications in electrochemical biosensing (Zhao et al. 2009). Choline oxidase has been immobilized on the gold electrode functionalized by HFBI and a very large current response as been registered on exposure to a choline substrate.
More futuristic applications of organic/inorganic interfaces based on hydrophobins on solid support can be forecasted by thinking at the new hydrophobins molecules that can be obtained by fusion proteins. Recently, HFBII, another hydrophobin from *Trichoderma reesei*, was employed as molecular carrier: it was tagged genetically onto a functional protein molecule, a Maltose binding protein (MBP), in order to construct a molecular interface. HFBII fusion proteins were intermingled with native HFBII molecules at the optimal ratio: the superfluous native HFBII molecules acted as nanospacers, resulting in the formation of a tight self-organized protein layer on both an air/water interface and a solid surface (Asakawa et al. 2009).

6. Conclusion

Beside improvement in transduction systems, readout electronics, and integrated microfluidics, the next generation of biosensors requires strong advances in fabrication and control of the organic/inorganic interfaces which are the first key issue to be developed for achieving reliable commercial devices. Understanding the fundamentals physico-chemical properties of these interfaces is the first step towards more performing instrumentation. The role of self-assembling, natural amphiphilic biomolecules, as hydrophobins are, could be of great impact on this multidisciplinary field of science and technology. The results obtained in research and industrial laboratories, reported in this chapter, are very promising, especially in biosensing applications. Hydrophobins –inorganic interfaces could be a kind of paradigm for the development of bio/non-bio based innovative devices.

7. References

Askawa, H., Tahara, S., Nakamichi, M., Takehara, K., Ikeno, S., Linder, M.B., Haruyama, T. (2009) The amphiphilic protein HFBII as a genetically taggable molecular carrier for the formation of a self-organised functional protein layer on a solid surface, *Langmuir* 25 (16), 8841-8844.

De Vocht, M.L.; Reviakine, I.; Ulrich, W.P.; Bergsma-Schutter, W.; Wosten, H.A..B.; Vogel, H.; Brisson, A.; Wessels, J.G.H.; & Robillard, G.T. (2002) Self-assembly of the hydrophobin SC3 proceeds via two structural intermediates. *Protein Science* 11: 1199-1205.

Askolin, S.; Linder, M.; Scholtmeijer, K.; Tenkanen, M.; Penttilä, M.; de Vocht, M.L.; & Wösten, H. A. B. (2006) Interaction and comparison of a class I hydrophobin from

Schizophyllum commune and class II hydrophobins from Trichoderma reesei. *Biomacromolecules* 7: 1295-301.

Qin, M.; Hou, S.; Wang, L.K.; Feng, X.Z.; Wang, R.;. Yang, Y.L.; Wang, C.; Yu, L.; Shao, B.; & Qiao M.Q. (2007a) Two methods for glass surface modification and their application in protein immobilization. *Colloids and surfaces. B, Biointerfaces* 60: 243-9.

Jellison, G.E., Jr; Modine, F.A. (1996) Parameterization of the optical functions of amorphous materials in the interband region. *Applied Physics Letters*, 69, 371.

Jellison, G.E., Jr; Modine, F.A. (1996) Erratum: ''Parameterization of the optical functions of amorphous materials in the interband region'' [Appl. Phys. Lett. 69, 371 (1996)] *Applied Physics Letters*, 69, 2137.

Mezzasoma, L.; Bacarese-Hamilton, T.; Di Cristina, M.; Rossi, R.; Bistoni, F.; & Crisanti, A. (2002) Antigen Microarrays for Serodiagnosis of Infectious Diseases. *Clinical Chemistry* 48: 121-130

Qin, M.; Wang, L. K.; Feng, X. Z.; Yang, Y. L.; Wang, R.; Wang, C.; Yu, L.; Shao, B.; & Qiao, M. Q. (2007b) Bioactive surface modification of mica and poly(dimethylsiloxane) with hydrophobins for protein immobilization. *Langmuir* 23: 4465-71.

Hou, S.; Li, X.; Li, X.; Feng, X. Z.; Wang, R.; Wang, C.; Yu, L.; & Qiao, M. Q. (2009) Surface modification using a novel type I hydrophobin HGFI. *Analytical and Bioanalytical Chemistry* 394: 783-9.

Wang, Z.; Huang, Y.; Li, S.; Xu, H.; Linder, M.B.; & Qiao, M. (2010) Hydrophilic modification of polystyrene with hydrophobin for time-resolved immunofluorometric assay. *Biosensors and Bioelectronics* 26: 1074-9.

De Stefano, L.; Rea, I.; Armenante A.; Giardina, P.; Giocondo, M.; & Rendina I. (2007) Self-assembled Biofilm of Hydrophobins Protect the Silicon Surface in the KOH Wet Etch Process. *Langmuir* 23: 7920-2

De Stefano; L.; Rea, I.; Giardina, P.; Armenante, A.; & Rendina I. (2008) Protein modified porous silicon nanostructures *Advanced Materials* 20: 1529–1533

Russo M.E., Giardina P., Marzocchella A., Salatino P., Sannia G. (2008) *Enzimology and Microbiology Biotechnology 42*, 521–530

Zhao, Z.X.; Wang, H.C.; Qin, X.; Wang, X.S.; Qiao, M.Q.; Anzai, J.I.; & Chen, Q. (2009) Self-assembled film of hydrophobins on gold surfaces and its application to electrochemical biosensing. *Colloids and surfaces. B, Biointerfaces* 71: 102-6.

Shim, M.;, Shi Kam, N. W.; Chen, R.J.; Li, Y.; & Dai H (2002) Functionalization of carbon nanotubes for biocompatibility and biomolecular recognition. *Nano Letters* 2:285-288

Wu, H.C.; Chang, X.L., Liu, L., Zhao, F., Zhao, Y.L., (2010) Chemistry of carbon nanotubes in biomedical applications. *Journal of Materials Chemistry* 20:1036–1052.

Wu, B.Y.; Hou, S.H.; Yin, F.; Zhao, Z.X.; Wang, Y.Y.; Wang, X.S.; & Chen, Q. (2007) Amperometric glucose biosensor based on multilayer films via layer-by-layer self-assembly of multi-wall carbon nanotubes, gold nanoparticles and glucose oxidase on the Pt electrode. *Biosensors and Bioelectronics* 22: 2854–2860.

Kern, W., Ed., (1993) *Handbook of Semiconductor Cleaning Technology*; Noyes Publishing Park Ridge, NJ, Chapter 1.

W. van der Vegt, H.C. van der Mei, H.A.B. Wösten, J.G.H. Wessels , H.J. Busscher (1996) A comparison of the surface activity of the fungal hydrophobin SC3p with those of other proteins. *Biophysical Chemistry* 57 253-260

S. O. Lumsdon, J. Green, B. Stieglitz (2005) Adsorption of hydrophobin proteins at hydrophobic and hydrophilic interfaces. *Colloids and Surfaces B: Biointerfaces* 44 172–178

H.A.B. Wösten, T.G. Ruardy, H.C. van der Mei, H.J. Busscher, J. G.H. Wessels (1995) Interfacial self-assembly of a Schizophyllum commune hydrophobin into an insoluble amphipathic protein membrane depends on surface hydrophobicity. *Colloids and Surfaces B: Biointerfaces* 5 189 195

K. Kisko, G.R. Szilvay, E. Vuorimaa, H. Lemmetyinen, M.B. Linder, M. Torkkelia and R. Serimaaa (2007) Self-assembled films of hydrophobin protein HFBIII from Trichoderma reesei. *Journal of Applied Crystallography* 40, s355–s360

K. Kisko, G.R. Szilvay, E. Vuorimaa, H. Lemmetyinen, M.B. Linder, M. Torkkelia and R. Serimaaa (2009) Self-Assembled Films of Hydrophobin Proteins HFBI and HFBII Studied in Situ at the Air/Water Interface. *Langmuir*, *25,* 1612-1619

Szilvay GR, Nakari-Setala T, and. Linder MB (2006) Behavior of Trichoderma reesei hydrophobins in solution: Interactions, dynamics, and multimer formation. *Biochemistry*, 45, 8590-8598

V. B. Fainerman and D. Vollhardt (1999) Equations of state for Langmuir monolayers with two-dimensional phase transitions. *Journal of Physical Chemistry B*, 103, 145-150.

D. Vollhardt, V. B. Fainerman, and S. Siegel (2000) Thermodynamic and textural characterization of DPPG phospholipid monolayers. *Journal of Physical Chemistry B*, 104, 4115-4121.

D. Vollhardt*, and V. B. Fainerman (2002) Temperature dependence of the phase transition in branched chain phospholipid monolayers at the air/water interface. *Journal of Physical Chemistry B*, 106, 12000-12005.

Houmadi S, Ciuchi F, De Santo MP, De Stefano L, Rea I, Giardina P, Armenante A, Lacaze E, and Giocondo M. (2008) Langmuir-Blodgett Film of Hydrophobin Protein from Pleurotus ostreatus at the Air-Water Interface *Langmuir*, 24 (22), 12953–12957.

Binnig, G., Rohrer, H., Gerber, C., and Weibel, E. (1982) Tunneling through a controllable vacuum gap. *Applied Physics Letters* 40, 178.

Binnig, G., Quate, C. F., and Gerber, Ch. (1986) Atomic Force Microscope. *Physical Review Letters* 56, 9, 930.

J. P. Cleveland, B. Anczykowski, A. E. Schmid, V. B. Elings (1998) Energy dissipation in tapping-mode atomic force microscopy. *Applied Physics Letters*, 72, 2613–5

B. Anczykowski, D. Krüger, and H. Fuchs (1996) Cantilever dynamics in quasinoncontact force microscopy: Spectroscopic aspects. *Physical Review B* 53, 23

J. Tamayo and R. García (1996) Deformation, Contact Time, and Phase Contrast in Tapping Mode Scanning Force Microscopy. *Langmuir*, *12,* 4430-4435

Burnham, N.A., Behrend, O.P., Oulevey, F., Gremaud, G., Gallo, P-J., Gourdony, D., Dupas, E., Kuliky, A.J., Pollockz, H.M., and Briggsx, G.A.D. (1997) How does a tip tap? *Nanotechnology* 8 67–75.

García, R., and San Paulo, A., (1999) Attractive and repulsive tip-sample interaction regimes in tapping-mode atomic force microscopy. *Physical Review B* 60, 7, 4961.

Anczykowski, B., Gotsmann, B., Fuchs, H., Cleveland, J.P., Elings, V.B., (1999) How to measure energy dissipation in dynamic mode atomic force microscopy - *Applied Surface Science* 140 376–382.

Wang, X.; de Vocht, M.L.; de Jonge, J.; Poolman, B.; Robillard, G.T. (2002) Structural changes and molecular interactions of hydrophobin SC3 in solution and on a hydrophobic surface. *Protein Science 11*, 1172-1181.

De Vocht, M.L.; Reviakine, I.; Ulrich, W.P.; Bergsma-Schutter, W.; Wösten, H.A.B.; Vogel, H.; Brisson, A.; Wessels, J.G.H.; Robillard, G.T. (2002) Self-assembly of the hydrophobin SC3 proceeds via two structural intermediates. *Protein Science*, *11*, 1199-1205.

Wang, X.; Shi, F.; Wösten, H.A.B.; Hektor, H.J.; Poolman, B.; Robillard, G.T. The SC3 hydrophobin self-assembles into a membrane with distinct mass transfer properties (2005) *Biophysical Journal*, *88*, 3434-3443.

Szilvay, G.R.; Nakari-Setälä, T.; Linder, M.B. (2006) Behavior of *Trichoderma reseei* hydrophobins in solution: Interactions, dynamics and multimer formation. *Biochemistry*, *45*, 8590-8598.

Torkkeli, M.; Serimaa, R.; Ikkala, O.; Linder, M.B. (2002) Aggregation and self-assembly of hydrophobins from *Trichoderma reesei*: Low-resolution structural models. *Biophysical Journal*, *83*, 2240-2247.

17

Porous Silicon-based Electrochemical Biosensors

Andrea Salis[1], Susanna Setzu[2], Maura Monduzzi[1] and Guido Mula[2]
[1]*Dipartimento di Scienze Chimiche, Università di Cagliari–CSGI and CNBS*
[2]*Dipartimento di Fisica, Università di Cagliari*
Italy

1. Introduction

There is a growing need of highly efficient compact devices for a wide range of applications in several fields. Among the candidate materials, porous silicon (PSi) has attracted an increasing research interest, apart from its obvious potentially straightforward integration with standard Si technologies, thanks to its unique properties, and its present applications span from biomedicine (Anglin et al. 2008) to biosensing, from photonics (Huy et al. 2009) to photovoltaic devices (Xiong et al. 2010).
After its discovery (Uhlir 1956), porous silicon hasn't attracted much attention until the discovery of its room temperature luminescence properties (Canham 1990). However, the porous silicon-based photonics with all-silicon light-emitting devices never showed, to date, high enough efficiency for real applications. Nevertheless, many other applications have since been the object of much research, thanks to the many advantages of porous silicon: the flexibility of its formation process (Föll et al. 2002), the extensive tailoring of its structural properties (Lehmann et al. 2000), the very large specific surface (Halimaoui 1993) and also its biocompatibility, mandatory for both drug delivery devices and several biosensing applications (Low et al. 2009; Park et al. 2009). The deep knowledge of silicon chemistry is easily applicable to porous silicon (Buriak 2002; Salonen and Lehto 2008) and allows functionalization of the internal pore surface for the chemical bonding of the biological molecules of interest or for a better stabilization of the structure. The relevance for the field of PSi biosensors of a well controlled surface chemistry has been detailed by Lees and coworkers and by Kilian and coworkers (Lees et al. 2003; Kilian et al. 2009) and will be treated more deeply later in this article.
The very large internal surface of porous silicon proved to be a great advantage since, like other porous materials, it allows the bonding of active molecules over a large surface in a small volume (e.g. a 20 μm thick PSi sample with a specific surface area of 500 m^2/cm^3 may offer 1 m^2 of developed surface with only 1 cm^2 of external surface), with a sensible increase of the efficiency of the devices. Moreover, the large internal surface is important when there is the need of dispersing the active molecules, as happened in the case of laser dye dispersed in a PSi matrix (Setzu et al. 1999). Differently from other materials, however, PSi may be easily prepared either in powder or wafer, depending on the specific application. This allows for the fabrication of devices that can be dispersed in a given medium or that can be reusable. Devices integrating PSi layers with specific enzymes or with molecules with

specific target allow the realization of label free biosensors. Examples of this kind of devices have been demonstrated, for instance, for DNA sensing (Rong et al. 2008) and for triglycerides quantitative measurements (Setzu et al. 2007).
Porous silicon was successfully used in the development of a quite large variety of new biosensors, mainly using optical detection (Chan et al. 2001; Jane et al. 2009). It is surprising that porous silicon electrochemical sensors didn't get as much attention as the optical sensors. This is likely due to the fact that much research efforts have been devoted to the development of optical PSi devices in the field of optoelectronics. Then, a natural transfer of this knowledge to the field of biosensing has occurred when PSi-based biosensors become an interesting research field. However, the general field of electrochemical sensors (Bakker and Telting-Diaz 2002; Privett et al. 2008) is the most developed sensor branch and also PSi electrochemical sensors have been developed showing interesting characteristics and sensitivity properties.
Several reviews describe the state of the art of PSi biosensors (Anglin et al. 2008; Jane et al. 2009; Kilian et al. 2009) mainly based on optical signal transduction. The remarkable development of optical PSi biosensor has been triggered by the ability to modulate the porous silicon refractive index in the etch direction, and therefore to tailor the optical properties of the devices to one's needs, that has stimulated the research in the field of signal transduction by optical means. Optical transduction through either Fabry-Perot fringes, microcavity resonators or rugate filters has been widely investigated (Lin et al. 1997; Chan et al. 2001; Sailor 2007). There are several examples of quantitative determination of a given DNA strain by using optical detection on a single or multiple-layer PSi sample (Chan et al. 2000; De Stefano et al. 2007). Other examples show in-body detection of drug release (Anglin et al. 2008). Optical detection may be extremely useful when there is the need of a very high sensitivity for small amount of molecules to be detected, since the refractive index of the porous layer is highly affected by a change in the refractive index of the liquid in the pores (Anderson et al. 2003). The measured sensitivity of the optical biosensors strongly depends on the chosen optical structure and on the analyte (Haes and Van Duyne 2002; DeLouise et al. 2005).
It is, however, rather surprising that very little research has been made in the field of electrochemical porous silicon-based sensors even if electrochemical sensors have several important advantages: low cost and high sensitivity, together with a low power requirement and relatively simple detection instruments. Moreover they can be miniaturised more easily than optical biosensors. All these considerations make particularly worthwhile to review the advantages of PSi electrochemical biosensors. This is the main aim of the present chapter.

2. Porous silicon formation, oxidation, functionalisation, and biomolecules immobilisation

2.1 Formation process and main properties of porous silicon

Porous silicon samples are mainly produced by an electrochemical etch in the dark of a bulk single crystalline silicon substrate (Lehmann 1996). Fig. 1 shows a typical electrochemical cell used for PSi formation (Fig. 1a). A PSi sample is also shown (Fig. 1b). There are also various alternative preparation methods (Kolasinski 2005), i.e. chemical vapour etching (Ben Jaballah et al. 2005), metal-assisted etching (Harada et al. 2001; Chattopadhyay et al. 2002), and stain etching (Steckl et al. 1993; Ünal et al. 2001).

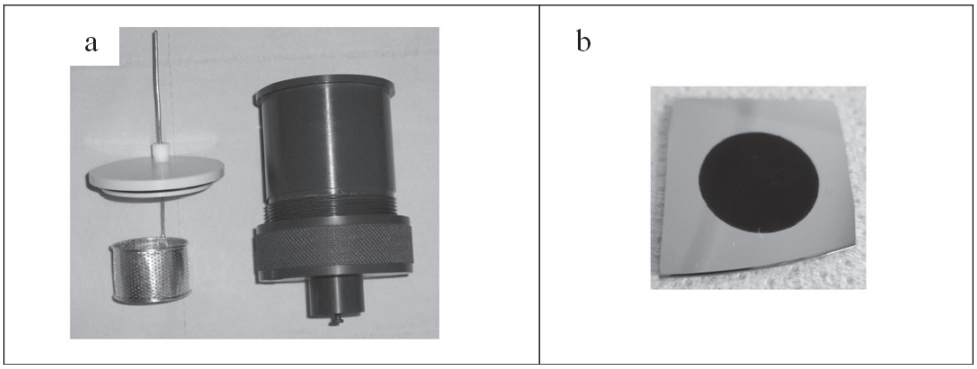

Fig. 1. Electrochemical cell used of PSi formation (a) and a PSi sample (b).

These methods give, at present, less reproducible results with respect to electrochemical etch, even though stain etch PSi is already commercially available. The etching solutions are prepared using HF, ethanol and pure water in different concentrations. The concentration of HF in the solution is one of the parameters controlling the structural properties of the samples and gives different porosities and pores' densities for a given current density used in the fabrication process. The HF concentration is also a fundamental parameter for the porosity range available. Halimaoui (Halimaoui 1993) studied the PSi layer porosities as a function of the applied current density for different HF concentrations, and observed that the porosity range between the lowest and highest current densities available for the porous layer formation varied for different HF concentrations. It has also been demonstrated that the PSi characteristics depend on the HF concentration of the etching solution (Dian et al. 2004; Kumar et al. 2009) from pores shape to density. In particular, Dian and coworkers showed that, for the same formation current density, varying the HF concentration leads to layers with different characteristics and porosities whose variations may reach about 30% in their experimental conditions. Kumar and coworkers studied the variations of the physical and electronic properties of PSi layers prepared using etching solutions with various HF contents by means of a combination of volumetric sorption isotherms, visual colour observation, photoluminescence, scanning electron microscopy, and Raman spectroscopy.

2.2 PSi layers morphology and design

Critical parameters for the defining of the PSi layers pores morphology are the doping type and the doping level of the crystalline silicon substrates used for the preparation of the samples (Föll et al. 2002). These parameters affect the kind of porosity, starting from the pores' diameter that can span from nanopores (a few nm) to mesopores (a few tens of nm to a few hundreds of nm) up to macropores (a few μm).

Only the nanoporous *p*- and p^+-type porous silicon show room temperature photoluminescence (Cullis et al. 1997). p^+ and n^+-type PSi are mesoporous and suitable for immobilisation of bio-macromolecules with a few nm diameter, while *p*-type PSi, whose pore diameter is of the order of a few nm, is suitable only for very small molecules. Macroporous *n*-type PSi may accommodate larger molecules, whose size depends on the pores' diameter. It can be prepared with pores in the 100 nm – few μm range, depending on

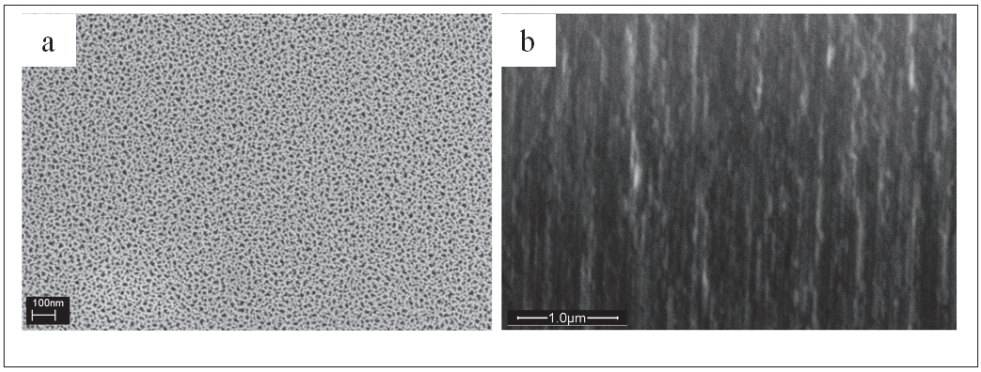

Fig. 2. SEM micrographs of n^+-PSi sample. Top view (a) and the side view (b) of the nano-pores.

the formation condition (Gruning and Lehmann 1996; Ouyang and Fauchet 2005). The pores' diameter can be further modified after formation by means of one or more of the several available techniques able to enlarge the pores' diameter to better adapt to the size of the molecule of interest. Tinsley-Bown and co-workers (Tinsley-Bown et al. 2000) described a method based on immersing the porous layers in an ethanol-rich alkali (KOH) solution, whose effect on the pores' diameter may be controlled by the immersion time. Hamm and coworkers (Hamm et al. 2003) used a similar method by immersing the PSi samples in a NaOH etching (0.1 and 1 M) solution. To avoid problems due the hydrophobic nature of the PSi walls, an ethanol drop is put on the samples' surface before the immersion in the NaOH solution. These methods add a significant flexibility in the tailoring of the PSi layers structural properties in view of the realization of biosensors. More details about the dependence of the kind, shape and size of the PSi pores on the substrate doping may be found in the scientific literature (Smith and Collins 1992; Lehmann et al. 2000; Föll et al. 2002).

A relevant characteristic of porous silicon is that once the porous layer is formed it will play no longer any role in the ongoing formation process: the electrochemical etch is essentially an interface process taking place only at the porous/crystalline interface (Chazalviel et al. 2000). Since the structural and optical features of the formed layers depend on the formation parameters, and in particular on the formation current density, it is possible to design structures well tailored on the needs of the application. In particular, knowing that higher formation current densities lead to layers with higher porosities and lower refractive index, PSi multilayers with an in-the-depth modulation have been realised. A periodic variation of the formation current density will lead to a periodic variation of the porosity in the formation direction and then to a corresponding periodic refractive index variation (Setzu et al. 2000), leading to the realization of 1D photonic bandgap in the formation direction.

2.3 Oxidation of PSi surface

Surface chemistry of PSi is a feature of fundamental interest (Kilian et al. 2009). Chemical modifications at the air-solid interfaces strongly affect the biosensing performance (Dancil et al. 1999). Indeed, freshly prepared PSi is unstable due to the presence of highly reactive silicon hydride (Si-H_x, x = 1, 2 and 3) species that are very reactive both in air and in water

(Anderson et al. 2003). Thus, in order to use PSi as a matrix for a biosensing device, a stable surface must be obtained. Several procedures addressed to this purpose have been reported. The most common is to grow an oxide layer on the PSi surface - to avoid spontaneous oxidation either in air or in water media – through a thermal (Reddy et al. 2003), or a chemical (ozone) treatment (Dancil et al. 1999). Oxidation treatment can be followed by a silanisation step to introduce suitable functional groups (Kilian et al. 2009). The biomolecule needed for biosensing can be adsorbed either after the oxidation (physical adsorption) or the silanisation (chemical adsorption) steps. Whatever the kind of interactions between the PSi and the biomolecule, the oxidation step affects the operative behaviour of potentiometric biosensors. The formation of the SiO_2 layer during thermal or ozone oxidation cannot be controlled; therefore, it is not possible to obtain a reproducible surface in different PSi wafer samples preparation. And reproducibility, clearly, is a crucial step in the fabrication of a biosensor.

Anodic oxidation is a technique commonly used to stabilize the very reactive surface of fresh porous silicon (Bsiesy et al. 1991; Petrova-Koch et al. 1992; Cantin et al. 1996). Compared to other oxidation techniques, it allows the obtainment of highly reproducible oxidised samples. Recently, we reported a study where PSi layers were oxidised through this electrochemical procedure (Salis et al. 2010). Anodic oxidation is realised through a controlled procedure where a given current intensity is made to flow into an electrochemical cell until a fixed oxidising potential or a given oxidation time is reached. A typical anodic oxidation curve is shown in Fig. 3.

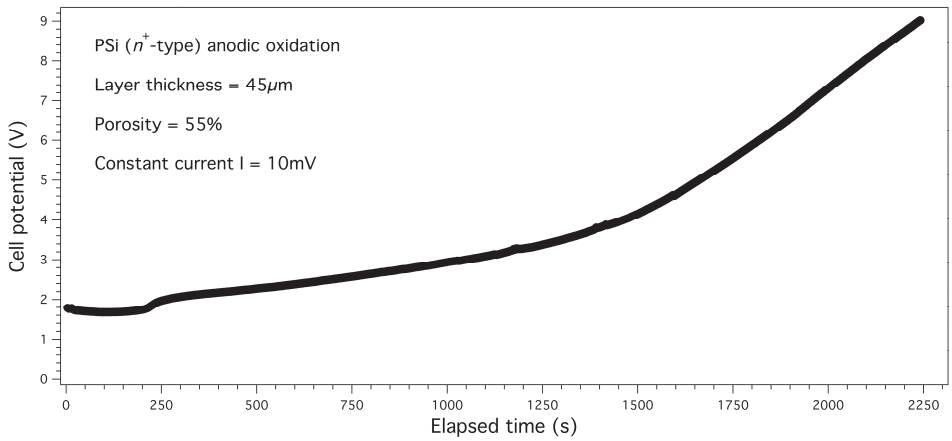

Fig. 3. A typical anodic oxidation curve.

2.4 PSi surface functionalisation and biomolecules immobilisation

As reported above, the surface of fresh PSi is almost completely covered by highly reactive hydride species (Petrova-Koch et al. 1992). Indeed, when PSi is put in contact with alkaline solutions, and even with buffer solutions at physiological pH, it dissolves giving orthosilicic acid ($Si(OH)_4$) (Anderson et al. 2003). Neglecting this phenomenon can lead to confuse a signal drift, due to the oxidation phenomenon, with the biosensing signal (Lin et al. 1997; Janshoff et al. 1998; Dancil et al. 1999). Besides oxidation, a strategy to improve PSi stability

is the modification of the surface by mean of functionalising agents. This is usually done as a preliminary step which ends with the biomolecule immobilisation.
Xia and coworkers published a study where porous silicon surfaces were bio-functionalised by a simple three-step method (Xia et al. 2006). A scheme of the functionalising procedure is shown in Fig. 4. First the hydrogen-terminated porous silicon was oxidised and amino-silanised in a one-pot reaction by 3-aminopropyl(triethoxyl)silane (APTES) with the aid of an organic base, diisopropylethylamine. Then, the primary amine reacted with a two homobifunctional cross-linker, bis(N-succinimidyl)carbonate. By modulating the reaction conditions, a high surface coverage of linking groups, succinimidyl ester, could be obtained. A similar functionalisation could be done by using (N,N′-bis(p-maleimidophenyl)methylene instead of bis(N-succinimidyl)carbonate. Succinimidyl ester is an amino-reactive group, therefore mouse monoclonal antibody bearing amino groups was grafted (Xia et al. 2006). An enzyme (Horseradish peroxidise) linked immunosorbent assay was used to evaluate the surface density of antibody. The other linker, (N,N′-bis(p-maleimidophenyl)methylene, after reflux in acetonitrile with surface amines, resulted in maleimide-terminated surfaces. Then a reduced urokinase bearing accessible thiol groups was grafted and its enzymatic activity determined.

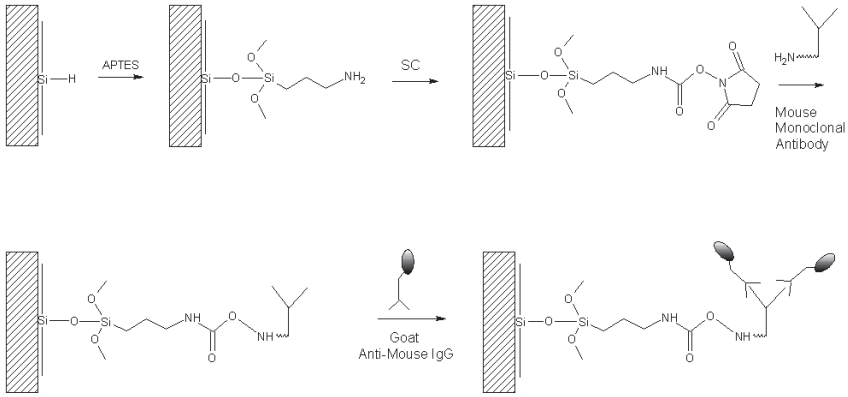

Fig. 4. An example of PSi functionalisation and enzyme immobilisation. Adapted from (Xia et al. 2006).

Another procedure was followed by Fernandez and coworkers (Fernandez et al. 2008). PSi surface was firstly oxidised then modified with APTES and with the bifunctional reagent gluharaldehyde. This procedure allowed to immobilise covalently *Pseudomonas cepacia* lipase as confirmed by means of FTIR spectroscopy.
Although these procedures confer a high degree of chemical stability to PSi surface, they may have some drawbacks. As will be seen below, the presence of silica layers at solid/liquid interface confers sensitivity to pH variations. The functionalisation steps, which substitutes silica with other chemical groups may lead to the loss of pH sensitivity and hence to the impossibility to use it for the realisation of potentiometric biosensor (Hamann and Lewis 2006). This is not, in any case, a problem for other types of signal transduction.
As noted earlier, all porous materials have a large specific surface that can reach very high area values, such as 2000 m^2/g e.g. in case of activated carbon (Kaneko et al. 1992). This high value, considering an activated carbon density of about 0.5 g/cm^3 (it depends on the

characteristics of the activated carbon), is analogous to that obtainable with porous silicon, whose specific surface may reach more than 900 m^2/cm^3 in the case of *p*-type nanoporous silicon (Halimaoui 1993). This large specific surface area allows the immobilisation of a large amount of active molecules in a very small space. The choice of the pore's morphology best adapted to the size of the molecule to be loaded into the PSi matrix is crucial for the optimisation of the device's properties. Karlsson and coworkers (Karlsson et al. 2003) studied the penetration depth of human serum albumin as a function of the PSi pores' size and demonstrated that there is a threshold pore diameter for the pores' filling. This diameter is related not only to the original molecule's size but also to the immobilisation method, that can help or impede the molecule's penetration within the pores by modifying the molecule's shape and/or the chemical environment.

DeLouise and coworkers (DeLouise and Miller 2004) studied the enzyme immobilisation capacity of porous silicon samples using glutathione-*s*-transferase (GST) to quantify the amount of enzyme bound to the PSi pores' surface. Using a simple geometric model of the columnar PSi pores they estimated the total available internal surface and the maximum amount of enzyme that can be immobilised onto this surface by simply assuming that the GST molecules, considered as spheres, will form a compact monolayer coverage. This model showed to be quite effective in estimating the minimum pores' depth (and then internal surface) needed to accommodate a given number of enzyme's moles dissolved into the immobilisation solution. Another point of interest in the immobilisation of molecules within the PSi pores is the fact that it is possible to distribute the molecules in such a way that the interaction between them may be reduced to a minimum. This can be a key point when these interactions may impede the molecule's activity relevant for the application being studied. For instance, this is the case for laser dyes, where their ability to emit light significantly depends on a sufficient dispersion of the molecules and is quenched when the molecules aggregate. Setzu and coworkers (Setzu et al. 1999) showed how the inclusion of a laser dye (Rhodamine 6G) into a porous silicon microcavity was an effective method to improve significantly its emission efficiency, demonstrating at the same time the good dispersion of the dye molecules.

The insertion of active molecules in nano- or mesoporous structures also showed an improvement of enzyme stability in several materials thanks to the spatial confinement and to the interaction with the pores' walls (Sotiropoulou et al. 2005; Kima et al. 2006). This enhanced stability is relevant for increasing shelf life, allowing the reusability of the devices and improving the biosensor-related measurement reliability.

3. Electrochemical biosensors

There are two main types of electrochemical transduction in biosensors: potentiometry and amperometry/voltammetry. They have been used for the analysis of different kinds of substances as shown in table 1.

3.1 PSi-based potentiometric biosensors

Potentiometric biosensors use porous silicon as an electrode of an electrochemical cell (Thust et al. 1996). The PSi wafer has the function both to immobilise the biological element and to be sensitive to the chemical variations produced by the immobilised biomolecule in the electrolyte solution, transducting them in a detectable electric signal. The measured parameter is the potential difference between the cathode (i.e. a platinum electrode) and the

anode (PSi electrode) of the electrochemical cell. This voltage is affected both by the chemical composition of the electrolyte solution (i.e. pH) and on the semiconducting properties of PSi, which depend on the flat-band potential (V_{fb}). In the absence of an electric field, in a semiconductor V_{fb} is related to the Fermi level of the semiconductor E_F, by:

$$E_F = eV_{fb} \tag{1}$$

where e is the charge of the electron. V_{fb} depends on the phenomena occurring at the PSi surface. Thus, when the semiconductor constitutes one of the electrodes of an electrochemical cell, the measured cell voltage is related to V_{fb}. Besides, the principle of the potentiometric transduction is based on the presence of silicon oxide at the solid/liquid interface. Indeed, in oxidised samples the porous silicon surface is covered by a silica layer which is in direct contact with the electrolyte solution. The silica layer chemically adsorbs water producing silanol (Si-OH) groups. According to the 'site binding model' of the electrical double layer at the oxide/water interface (Yates et al. 1974), silanol groups display an amphoteric behaviour being differently charged according to the pH of the electrolyte solution adsorbing/desorbing H^+ ions onto the surface of oxidised silicon.

Type of transduction	Type of PSi	Biological element	Analyte	Reference
Potentiometry (C-V)	p-type	Penicillase	Penicillin	(Thust et al. 1996)
Potentiometry (C-V)	p-type	*Porcine pancreatic* lipase	Triglycerides	(Reddy et al. 2001; Reddy et al. 2003)
Potentiometry (C-V)		Lipase Urease	Triglycerides Urea	(Basu et al. 2005)
Potentiometry (OCP)	n^+-type	*Candida rugosa* lipase	Triglycerides	(Setzu et al. 2007)
Amperometry	p-type	Cholesterol oxidase, Biliriubin oxidase, Glutamate oxidase	Cholesterol/ bilirubin	(Song et al. 2007)
Cyclic Voltammetry	p-type	Glutamate oxidase	ALT/AST	(Song et al. 2009)
Cyclic Voltammetry	p-type	Laccase/Azurin	-	(Ressine et al. 2010)
Cyclic Voltammetry	p-type	DNA	tDNA	(Jin et al. 2010)
Conductivity	p-type	Tyrosinase	Catechol	(Tembe et al. 2008)

Table 1. Type and principle of functioning of developed electrochemical biosensors.

The site binding model is commonly applied to metal oxide sites which may either bind with a hydrogen ion at the surface,

$$MOH + H^+ \rightleftarrows MOH_2^+$$

with equilibrium constant K_{a1}, or the oxide sites may release a hydrogen ion,

$$MOH \rightleftarrows MO^- + H^+$$

with equilibrium constant K_{a2}.

Indeed, silicon oxide surface in contact with aqueous solutions is positively charged, negatively charged or neutral depending on the pH of the solution and on the point of zero charge ($pH_{pzc}=1/2(pK_{a1} + pK_{a2})$) of the solid surface.
Nernst law predicts an ideal shift of surface potential of 59 mV per pH unit at 298 K.[1] In fact, the slope of potential/pH curves is usually lower (Madou et al. 1981; Nakato et al. 1987; Reddy et al. 2003) since a dependence ≈ 30 mV/pH for oxidised silicon was found. This seems to be a general phenomenon for semiconductors in contact with electrolyte solutions whose surface potential shows a linear dependence on pH. Deviations from the Nernst law are often observed. For example, for TiO_2 the dependence of flat-band potential on pH is 50 mV/pH unit (van de Lagemaat et al. 1998), for 6H-SiC is 40 mV/pH unit, for GaP is 37 mV/pH unit. On these bases, PSi-based potentiometric biosensors can detect substances which produce a change of pH of the electrolyte solution in contact with the electrode surface. This has been first hypothesised about 15 years ago (Thust et al. 1996).
Thust and coworkers immobilised penicillinase, an enzyme sensitive to penicillin, on oxidised *p*-type PSi through physical adsorption. To characterise the electrochemical properties of their penicillin biosensor, capacitance-voltage (C-V) measurements were carried out. The response of the sensor to penicillin was explained by the pH change of the electrolyte near the silica surface which originates from the enzymatic reaction where penicillin G is hydrolysed to liberate H^+. Depending on the resulting pH value of the electrolyte solution, the position of the C-V curve shifts along the voltage axis. As shown in Fig. 5, the shifts were evaluated at 60% of the maximum capacitance value.

[1] The surface potential drop across the interface is described by the equation (Yates et al. 1974):

$$2.303\Delta pH = -\frac{e\Psi_0}{kT} - \frac{1}{2}\ln\left[\frac{(v+u)\alpha_-}{(v-u)\alpha_+}\right] \tag{1}$$

Where ΔpH= pH-pH_{pzc},Ψ_0 is the surface potential, e = 1.602×10^{-19} C, k is the Boltzmann constant, T is the absolute temperature, and the parameters inside square brackets are functions of the surface charge σ_0 that we indicate as $f(\sigma_0)$. After few passages we can write:

$$\Psi_0 = 2.303\frac{\mathrm{kT}}{\mathrm{e}}(\mathrm{pH} - \mathrm{pH}_{\mathrm{pzc}}) - \frac{2.303}{2}\frac{\mathrm{kT}}{\mathrm{e}}\log \mathrm{f}(\sigma_0) \tag{2}$$

At T=298K

$$\Psi_0 = 0.059[\mathrm{pH} - \mathrm{pH}_{\mathrm{pzc}} - \frac{1}{2}\log \mathrm{f}(\sigma_0)] \tag{3}$$

Calculating the derivative of surface potential respect to pH

$$\frac{\mathrm{d}\Psi_0}{\mathrm{dpH}} = 0.059\left(1 - \frac{\mathrm{dpH}_{\mathrm{pzc}}}{\mathrm{dpH}} - \frac{1}{2}\frac{\mathrm{d}(\log \mathrm{f}(\sigma_0))}{\mathrm{dpH}}\right) \tag{4}$$

Since pH_{pzc} depends on the intrinsic acid-base properties of the oxide surface (K_{a1} and K_{a2}), it can be considered constant with pH. Thus, only if σ_0 is independent by pH the difference of potential between the surface of the oxide and the electrolyte solution follows the Nernst law, and a slope ($d\Psi_0/dpH$)) of 59 mV is obtained. The results of Yates et al. showed that σ_0 strongly depends on pH, hence the third term of equation (4) is not generally zero. Moreover σ_0 is different for different oxides depending on the difference ΔpK (=pK_{a1}-pK_{a2}) and on the concentration and the type of the supporting electrolyte.

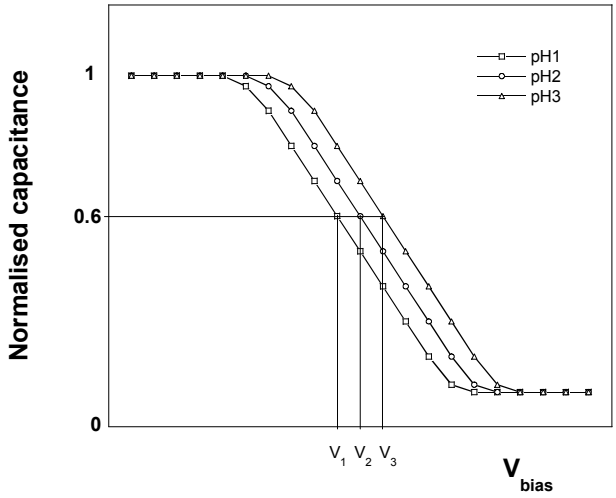

Fig. 5. Typical behaviour of the C-V curves for different pH values. Increasing the pH of the solution, causes a shift of the C-V curves to higher values along the potential axis. Adapted from (Thust et al. 1996).

Following this pioneering work, Chadha and coworkers published a series of papers aimed to the development of a potentiometric PSi-based biosensor for the analysis of triglycerides. The active biomolecule was a *Porcine pancreatic* lipase that catalyses the hydrolysis of tributyrin, thus producing butyric acid whose dissociation causes a pH decrease (Reddy et al. 2001; Reddy et al. 2003). Although the authors claimed that the lipase was immobilised on the PSi surface, it is hard to believe that this would happen in the stated experimental conditions, since the lipase solution was added to the tributyrin emulsion and then dropped on the electrode surface for the measurement. It is more likely that in this configuration the lipase acts as a homogeneous biocatalyst producing butyric acid which promotes the pH shift that is detected by the electrochemical cell and read as a potential change. In a successive work this system was used also for the analysis of urea by means of an urease enzyme instead of the lipase (Basu et al. 2005).
Finally, the system was implemented since *Pseudomonas cepacia* lipase was effectively immobilised through a preliminary chemical modification of the surface of oxidised PSi (APTS, glutaraldehyde). All steps were confirmed by means of FTIR spectroscopy (Fernandez et al. 2008).
Most of the works described used *p*-type PSi whereas only our group focused the attention on n^+-type PSi (Setzu et al. 2007). This kind of substrate was used for the realisation of a potentiometric biosensor for triglycerides quantification. The working configuration for this sensor is an electrochemical cell where the anode is a PSi sample loaded with *Candida rugosa* lipase which was physically adsorbed into the mesopores. The electrodes configuration used for the potentiometric measurement is shown in Fig. 6.
In this configuration the PSi sample was used as an electrode, while a platinum electrode was used as the second electrode. Moreover, a reference electrode (saturated calomel electrode) was used to take into account properly the variations of the cell's open circuit potential (*OCP*). The emulsion was kept under constant stirring. The hydrolysis of an

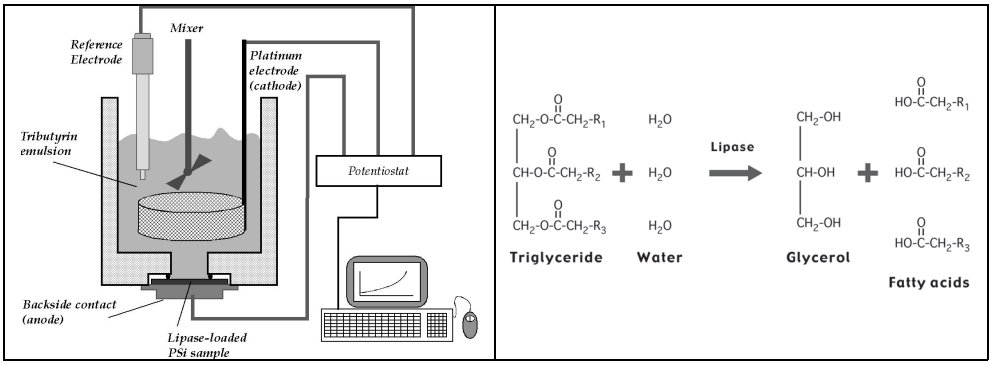

(a) (b)

Fig. 6. PSi-based Potentiometric biosensor setup (a). Lipase catalysed hydrolysis of triglycerides (b).

aqueous emulsion of tributyrin was used to ascertain the activity of the immobilised lipase. The butyric acid formed, as a result of the biocatalyst action, produces a pH change that is measured by the variation of the open circuit potential at the electrodes of the electrochemical cell (Okorn-Schmidt 1999). The open-circuit potential, also referred to as equilibrium potential or rest potential, is the overall voltage generated in the electrochemical cell measured with respect to the potential of a reference electrode. This voltage is measured in the open circuit configuration using a high-impedance voltmeter, so that only a negligible current can flow through the cell. The *OCP* is an easily measurable electrochemical parameter, but at the same time is a complex quantity since it is the sum of all possible potential drops in the system. Indeed, in such experimental setup additional potential drops (V_0) are involved in addition to the flat band potential, V_{fb}, for example potential drops at electrolyte/reference electrode and semiconductor/metal interfaces.

The absolute value of *OCP* gives no useful information about interface reactions. On the contrary, *OCP* variation is a good parameter to investigate interfacial phenomena. Indeed, the only contribution to *OCP* that can vary as a consequence of a reaction at the electrode surface is V_{fb}, since all other possible potential drops are, in first approximation, not affected by interface modifications. The study of the time evolution of the *OCP* is then equivalent to the study of the time evolution of the flat-band potential. This type of biosensor is in principle re-usable, thus allowing a significant cost reduction while maintaining high detection efficiency.

3.1.1 Comparison of PSi triglycerides biosensors with others literature detectors

It is interesting to compare the performances of PSi biosensors with other kinds of sensors described in the scientific literature. We will do here a brief comparison with a few literature examples of devices using completely different methods, with no pretention of exhaustivity and limited to triglycerides biosensors, to better understand how PSi bisensors place themselves with respect to other devices for the same applications. The literature values are to be compared to those reported for PSi. The PSi potentiometric detectors show, in the paper of Setzu and coworkers (Setzu et al. 2007), a linear regime, dependent on the amount of lipase immobilised within the PSi pores, up to about 10 mM. In the paper of Reddy and co-workers (Reddy et al. 2003) the authors show a calibration curve up to a few tens of mM.

These results can also be compared with the human blood normal triglycerides level which is below 1.69 mM (150 mg/dL) in the normal regime and above 5.56 mM (500 mg/dL) for a very high risk.

Method	Sensitivity	Detection range	Reference
Potentiometric - Immobilised lipase in PSi	-	<15mM	(Setzu et al. 2007)
Potentiometric, PSi electrode, lipase in solution	30mV/pH unit	5-40mM	(Reddy et al. 2003)
Impedimetric - Polyanilyne nanotubes	2.59×10^{-3} $K\Omega^{-1}$ mg^{-1} dL	25–300 mg dL^{-1}	(Dhand et al. 2009)
pH measurements – lipase on silica beads - tributyrin	0.478 pH/mM	<4 mM	(Pijanowsk et al. 2001)
pH measurements – lipase on silica beads - triacetin	0.022 pH/mM	<30 mM	(Pijanowsk et al. 2001)
Potentiometric - EISCAP	500 μM	8mM	(Fernandez et al. 2009)
Micromechanical	10 μM	500μM	(Fernandez et al. 2009)
ENFET – lipase on magnetic nanoparticles	-	5-30mM	(Vijayalakshmi et al. 2008)

Table 2. Comparison between sensitivity and detection range for several methods of triglycerides analysis.

Dhand and coworkers (Dhand et al. 2009) using a polianilyne nanotube film obtained a linear response range of 25–300 mg dL^{-1}, a sensitivity of 2.59×10^{-3} $K\Omega^{-1}$ mg^{-1} dL, with a response time of 20 s and regression coefficient of 0.99. Pijanowsk and coworkers studied a pH detector based on silica gel beads immobilised with a lipase in a microreactor (Pijanowsk et al. 2001). The authors tested three different methods for immobilising the lipase and compared the detector sensitivity on three different triglycerides. The higher sensitivity was obtained for tributyrin with 0.478 pH/mM for concentration < 4 mM, while the widest linear range, up to 30 mM, was obtained using triacetin but with a significantly lower sensitivity (0.022pH/mM). Fernandez and coworkers compared two kind of Si-based biosensors (Fernandez et al. 2009).
The first one was an EISCAP (electrolyte–insulator–semiconductor capacitor) sensor built depositing silicon nitride on *p*-type Si substrate and used for potentiometric transduction, while the second was a Si-based micromechanical sensor whose detection method is based on the measurement of the resonance frequency of a cantilever immersed in a solution containing the enzyme substrate. While the EISCAP sensor showed a sensitivity of about 500μM and a linear range up to about 8 mM, the micromechanical sensor had a sensitivity of about 10 μM and a detection range tested up to 500 μM. Vijayalakshmi and co-workers (Vijayalakshmi et al. 2008) used an ion-selective field effect transistor (ISFET) for detection of pH changes induced by lipase immobilised onto magnetic $NiFe_2O_4$ nanoparticles dispersed in a triglyceride's solution obtaining a linear measurement range of 5–30 mM. These results, summarised in Table 2, evidence that the reported values for PSi biosensors compare well with literature results even with completely different systems.

3.2 Other types of PSi-based electrochemical biosensors

PSi can be used for the realisation of amperometric and voltammetric biosensors, besides potentiometric ones. In this case the immobilised enzyme catalyses a redox reaction involving analyte oxidation/reduction which produces a flux of electrons measured, in terms of current intensity, by the electrodes of the electrochemical cell. In these systems, PSi is usually one of the involved electrodes. In fact, due to its low conductivity properties, the PSi surface has to be modified using a conducting material as gold (Ressine et al. 2010), platinum (Song et al. 2007), or a conductive polymer (Jin et al. 2010; Zhao and Jiang 2010). In that case the main function of PSi is to act as a high surface area substrate to enhance the sensitivity of biosensing. Indeed, it has been reported that porous electrodes can increase biosensor sensitivity in comparison with flat surface electrodes. Song and coworkers (Song et al. 2006) conducted a series of experiments using a planar silicon electrode and a porous silicon electrode. Cholesterol oxidase was covalently immobilised on each electrode by silanisation. The calculated effective surface area and sensitivity of the porous electrode were about 3.1-fold larger than those of the planar electrode. Successive works of the same group were devoted to develop an electrochemical biosensor array system for the diagnosis and monitoring of liver diseases (Song et al. 2007; Song et al. 2009). This biosensor array was able to simultaneously detect four different biomarkers of liver disease, namely: cholesterol, bilirubin, alanineaminotransferase (ALT) and aspartateaminotransferase (AST) levels in aqueous fluid samples. The aim of the work was to design a miniaturised measurement system using electrodes processed by porous silicon and array technology. Enzymes (cholesterol oxidase, bilirubin oxidase and glutamate oxidase) were covalently immobilised to Pt thin-film electrodes based on the PSi substrate. The immobilisation procedure involved few steps, namely: Pt oxidation; silanisation of hydroxilated Pt film electrode with APTES (aminopropyltriethoxysilane); silanised surface activation with glutaraldehyde; covalent binding of enzymes through reaction of amino groups of lysines with aldehydic group of activated electrode surface (Fig. 7). All the immobilised enzymes catalyse the oxidation of their respective analytes yielding hydrogen peroxide. This molecule is oxidised at the Pt thin film electrode, according to:

$$H_2O_2 \rightarrow O_2 + 2H^+ + 2e^-$$

The control of the level of these analytes in human serum is important in the diagnosis and monitoring of liver diseases and myocardial infarction.

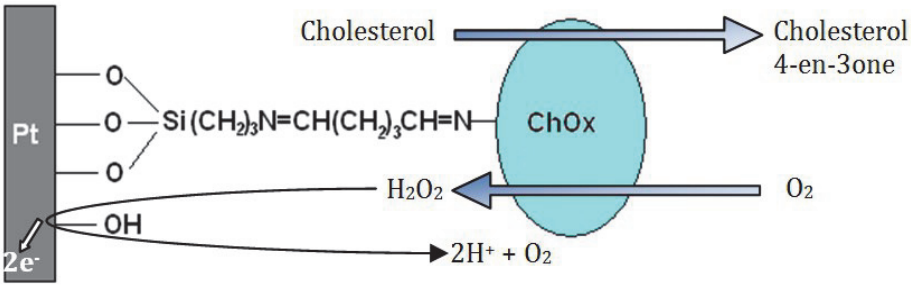

Fig. 7. Schematic illustration of electron transfer mechanism in silanised Pt thin film electrode with Cholesterol Oxidase (ChOx) immobilisation. Adapted from (Song et al. 2007).

Ressine and coworkers fabricated a novel three-dimensional chip with high surface area from double side porous silicon wafers by a sequential two-step anodic dissolution process (Ressine et al. 2010). Double-sided three-dimensional porous silicon chips, 6 mm × 6 mm, covered with a 40 nm gold (nano)layer, were fabricated from a porous silicon wafer. These devices, characterised by scanning electron microscopy along with electrochemical characterisation, showed ample conductivity, mechanical stability, and high surface area (10 times higher electrochemically active surface area compared with the geometric area). The three-dimensional gold coated silicon chips were further modified with thiol layers, followed by immobilisation of a simple copper-containing redox protein, azurin, or a complex multicopper redox enzyme, laccase. The bioelectrochemical studies showed very high surface concentrations of azurin and laccase, *i.e*. close to the theoretical monolayer coverage. However, direct electron transfer reactions between the biomolecules and gold surfaces were observed only for a small percentage of the immobilised redox protein and enzyme, respectively. Thus, highly efficient oxygen-bioelectroreduction on laccase-modified 3D thiol-gold-porous silicon chips (as compared to planar laccase-modified gold electrodes, 42 μA/cm^2 versus 7 μA/cm^2, respectively) was obtained only in the presence of an efficient soluble redox mediator. The bioelectrochemical studies provided unequivocal evidence of efficient O_2-bioelectrocatalysis by laccase in the three-dimensional chip structure.

Jin and co-workers fabricated and electrochemically characterised a label-free DNA sensor based on a porous silicon substrate (Jin et al. 2010). A *p*-type silicon wafer was electrochemically anodised in an ethanolic hydrofluoric (HF) solution to construct a PS layer on which polypyrrole (PPy) film was directly electropolymerised. To achieve direct electropolymerisation of PPy on PSi substrate without pre-deposition of any metallic thin-film underlayer, a low resistivity wafer was used. The rough surface of the PSi layer allowed for a strong adsorption of the PPy film. Intrinsic negative charge of the DNA backbone was exploited to electrostatically adsorb 26 base pairs of probe DNA (pDNA) into the PPy film by applying positive potential. The pDNA was designed to hybridise with the target DNA (tDNA) which is the insertion element (*Iel*) gene of *Salmonella enteric serovar Enteritidis*. Dependence of peak current around 0.2 V versus Ag/AgCl on tDNA concentration and incubation time were shown from the cyclic voltammograms of PS/PPy + pDNA + tDNA substrates. Scanning electron microscopy (SEM) image of the cross-section of a PS/PPy + pDNA + tDNA multilayered film showed successful direct electropolymerisation of PPy for a nano-PS DNA biosensor.

Tembe and coworkers developed a conductivity-based catechol biosensor using porous silicon as the immobilisation matrix for enzyme tyrosinase (Tembe et al. 2008). The enzyme was immobilised in an electrochemically etched surface of *p*-type silicon. The presence of enzyme in a porous structure and the retention of enzyme activity were confirmed by scanning electron microscopy and spectrophotometric studies, respectively. The principle of the sensor is based on the change in the conductivity of the tyrosinase-entrapped porous silicon matrix. When the entrapped tyrosinase interacts with catechol, the change in the current voltage (I-V) characteristics is obtained, which is proportional to analyte concentration.

4. Conclusions

In this chapter an overview of the recent advances on the use of porous silicon as a matrix for the realisation of biosensors is given. The main advantages of PSi biosensors, both with

electrochemical or optical transduction, are the large developed surface, the relative simplicity of the fabrication process, the easy integration with standard technology, the wide range of possible applications. We focused here our attention on electrochemical (particularly potentiometric) biosensors since, despite their easy realisation, for both potentiometric and amperometric/voltammetric biosensors, few research efforts have been devoted to these devices compared with optical biosensors. Nevertheless, there is a number of promising works concerning PSi-based electrochemical biosensors now available in the literature.

The key points discussed here concern the techniques used for PSi formation, the importance of surface stabilisation by oxidation techniques, the different strategies for enzyme/biomolecule immobilisation, and the realisation of the electrochemical biosensors. Concerning the last point, we showed that the realisation of potentiometric biosensors is based on the oxidation of the PSi pores' walls needed for both stabilising the PSi layers and confer them pH sensitivity. The transduction is due the formation of and acidic/basic substance as the result of the reaction catalysed by a suitable enzyme immobilised on the PSi surface.

Amperometric/voltammetric PSi-based biosensors, instead, measure the current intensity produced by the action of a redox reaction on the analyte of interest by an enzyme immobilised on the electrode surface. The importance of PSi is due the sensitivity enhancement due to the higher surface area of PSi compared to flat electrodes. The main difficulty in these biosensors is due to the low conductivity of PSi compared to metal electrodes. This can be overcome by coupling PSi with a Pt, Au, or a conductive polymer thin film to enhance its conductivity.

In conclusion, porous silicon constitutes an interesting matrix for the realisation of biosensing devices. Due to the recent growing interest it is very likely that previously neglected electrochemical transduction will reach a similar level of development as that obtained with optical transduction.

5. Acknowledgment

MIUR, PRIN 2008 grant number 2006030935 and Fondazione Banco di Sardegna are thanked for financial support.

6. References

Anderson, M. A., A. Tinsley-Bown, P. Allcock, E. Perkins, P. Snow, M. Hollings, R. G. Smith, C. Reeves, D. J. Squirrell, S. Nicklin and T. I. Cox (2003). Sensitivity of the optical properties of porous silicon layers to the refractive index of liquid in the pores *Physica Status Solidi a-Applications and Materials Science*, Vol.197, pp. 528-533

Anderson, S. H. C., H. Elliot, D. J. Wallis, L. T. Canham and J. J. Powell (2003). Dissolution of different forms of partially porous silicon wafers under simulated phsiological conditions. *Physica Status Solidi a-Applications and Materials Science*, Vol.197, pp. 331-335

Anglin, E. J., L. Cheng, W. R. Freeman and M. J. Sailor (2008). Porous silicon in drug delivery devices and materials. *Advanced Drug Delivery Reviews*, Vol.60, pp. 1266-1277

Bakker, E. and M. Telting-Diaz (2002). Electrochemical Sensors. *Analytical Chemistry*, Vol.74, pp. 2781-2800

Basu, I., R. V. Subramanian, A. Mathew, A. M. Kayastha, A. Chadha and E. Bhattacharya (2005). Solid state potentiometric sensor for the estimation of tributyrin and urea. *Sensors and Actuators B: Chemical*, Vol.107, pp. 418-423

Ben Jaballah, A., M. Hassen, M. Hajji, M. Saadoun, B. Bessaïs and H. Ezzaouia (2005). Chemical vapour etching of silicon and porous silicon: silicon solar cells and micromachining applications. *Physica Status Solidi a-Applications and Materials Science*, Vol.202, pp. 1606

Bsiesy, A., J. C. Vial, F. Gaspard, R. Herino, M. Ligeon, F. Muller, R. Romestain, A. Wasiela, A. Halimaoui and G. Bomchil (1991). Photoluminescence of high porosity and of electrochemically oxidized porous silicon layers. *Surface Science*, Vol.254, pp. 195-200

Buriak, J. M. (2002). Organometallic Chemistry on Silicon and Germanium Surfaces. *Chemical Reviews*, Vol.102 pp. 1271-1308

Canham, L. T. (1990). Silicon quantum wire array fabrication by electrochemical and chemical dissolution of wafers. *Applied Physics Letters*, Vol.57, pp. 1046

Cantin, J. L., M. Schoisswohl, A. Grosman, S. Lebib, C. Ortega, H. J. von Berdeleben, É. Vázsonyi, G. Jalsovszky and J. Erostyák (1996). Anodic oxidation of p- and p+-type porous silicon: surface structural transformations and oxide formation. *Thin Solid Films*, Vol.276, pp. 76-79

Chan, S., P. M. Fauchet, Y. Li, L. J. Rothberg and B. L. Miller (2000). Porous Silicon Microcavities for Biosensing Applications. *Physica Status Solidi (a)*, Vol.182, pp. 541-546

Chan, S., Y. Li, L. J. Rothberg, B. L. Miller and P. M. Fauchet (2001). Nanoscale silicon microcavities for biosensing. *Materials Science & Engineering C-Biomimetic and Supramolecular Systems*, Vol.15, pp. 277-282

Chattopadhyay, S., X. Li and P. Bohn (2002). In-plane control of morphology and tunable photoluminescence in porous silicon produced by metal-assisted electroless chemical etching. *Journal of Applied Physics*, Vol.91, pp. 6134

Chazalviel, J.-N., R. B. Wehrspohn and F. Ozanam (2000). Electrochemical preparation of porous semiconductors: from phenomenology to understanding. *Materials Science and Engineering B*, Vol.69-70, pp. 1-10

Cullis, A., L. Canham and D. Calcott (1997). The structural and luminescence properties of porous silicon. *Journal of Applied Physics*, Vol.82, pp. 909-965

Dancil, K.-P. S., D. P. Greiner and M. J. Sailor (1999). A Porous Silicon Optical Biosensor: Detection of Reversible Binding of IgG to a Protein A-Modified Surface. *Journal of the American Chemical Society*, Vol.121, pp. 7925-7930

De Stefano, L., P. Arcari, A. Lamberti, C. Sanges, L. Rotiroti, I. Rea and I. Rendina (2007). DNA optical detection based on porous silicon technology: from biosensors to biochips. *Sensors*, Vol. 7, pp. 214-221

DeLouise, L. A., P. M. Kou and B. L. Miller (2005). Cross-correlation of optical microcavity biosensor response with immobilized enzyme activity. Insights into biosensor sensitivity. *Analytical Chemistry*, Vol.77, pp. 3222-3230

DeLouise, L. A. and B. L. Miller (2004). Quantatitive assessment of enzyme immobilization capacity in porous silicon. *Analytical Chemistry*, Vol.76, pp. 6915-6920

Dhand, C., P. R. Solanki, K. N. Sood, M. Datta and B. D. Malhotra (2009). Polyaniline nanotubes for impedimetric triglyceride detection. *Electrochemistry Communications*, Vol.11, pp. 1482-1486

Dian, J., A. Macek, D. Niznansky, I. Nemec, V. Vrkoslavc, T. Chvojka and I. Jelinek (2004). SEM and HRTEM study of porous silicon-relationship between fabrication, morphology and optical properties. *Applied Surface Science*, Vol.238 pp. 169-174

Fernandez, R. E., E. Bhattacharya and A. Chadha (2008). Covalent immobilization of Pseudomonas cepacia lipase on semiconducting materials. *Applied Surface Science*, Vol.254, pp. 4512-4519

Fernandez, R. E., V. Hareesh, E. Bhattacharya and A. Chadha (2009). Comparison of a potentiometric and a micromechanical triglyceride biosensor. *Biosensors and Bioelectronics*, Vol.24, pp. 1276-1280

Föll, H., M. Christophersen and J. Carstensen (2002). Formation and application of porous silicon. *Materials Science and Engineering: R: Reports*, Vol.39, pp. 93-141

Gruning, U. and V. Lehmann (1996). Two-dimensional infrared photonic crystal based on macroporous silicon. *Thin Solid Films*, Vol.276 pp. 151

Haes, A. J. and R. P. Van Duyne (2002). *Journal of the American Chemical Society*, Vol.124, pp. 10596-10604

Halimaoui, H. (1993). Electrochemical and chemical behavior of porous silicon layers: the role of the material wettability and its high specific surface area. In: *Optical Properties of low dimensional silicon structures*, D. C. Bensahel (Ed.), The Netherlands, Kluwer Academic Publisher: 11

Hamann, T. W. and N. S. Lewis (2006). Control of the Stability, Electron-Transfer Kinetics, and pH-Dependent Energetics of Si/H/O Interfaces through Methyl Termination of Si(111) Surfaces. *The Journal of Physical Chemistry B*, Vol.110, pp. 22291-22294

Hamm, D., T. Sakka and Y. H. Ogata (2003). Etching of porous silicon in basic solution. *Physica Status Solidi a-Applications and Materials Science*, Vol.197, pp. 175-179

Harada, Y., X. Li, P. Bohn and R. Nuzzo (2001). Catalytic amplification of the soft lithographic patterning of Si. Nonelectrochemical orthogonal fabrication of photoluminescent porous Si pixel arrays. *Journal of the American Chemical Society*, Vol.123, pp. 8709

Huy, B., P. V. Hoi, P. H. Khoi, D. K. Van, P. T. Binh and T. T. Cham (2009). Porous silicon as a low dimensional and optical material. *Journal of Physics: Conference Series*, Vol.187, pp. Article number 012033

Jane, A., R. Dronov, A. Hodges and N. H. Voelcker (2009). Porous silicon biosensors on the advance. *Trends in Biotechnology*, Vol.27, pp. 230-239

Janshoff, A., K.-P. S. Dancil, C. Steinem, D. P. Greiner, V. S.-Y. Lin, C. Gurtner, K. Motesharei, M. J. Sailor and M. R. Ghadiri (1998). Macroporous p-Type Silicon Fabry-Perot Layers. Fabrication, Characterization, and Applications in Biosensing. *Journal of the American Chemical Society*, Vol.120, pp. 12108-12116

Jin, J.-H., E. Alocilja and D. Grooms (2010). Fabrication and electroanalytical characterization of label-free DNA sensor based on direct electropolymerization of pyrrole on p-type porous silicon substrates. *Journal of Porous Materials*, Vol.17, pp. 169-176

Kaneko, K., C. Ishii, M. Ruike and H. kuwabara (1992). Origin of superhigh surface area and microcrystalline graphitic structures of activated carbons. *Carbon*, Vol.30 pp. 1075-1088

Karlsson, L. M., P. Tengvall, I. Lundstrom and H. J. Arwin (2003). Penetration and loading of human serum albumin in porous silicon layers with different pore sizes and thicknesses. *Journal of Colloid and Interface Science*, Vol.266, pp. 40-47

Kilian, K. A., T. Boecking and J. J. Gooding (2009). The importance of surface chemistry in mesoporous materials: lessons from porous silicon biosensors. *Chemical Communications*, pp. 630-640

Kima, J., J. W. Grate and P. Wang (2006). Nanostructures for enzyme stabilization. *Chemical Engineering Science* Vol.61 pp. 1017-1026

Kolasinski, K. (2005). Silicon nanostructures from electroless electrochemical etching. *Current Opinion in Solid State and Materials Science*, Vol.9, pp. 73-83

Kumar, P., P. Lemmens, M. Ghosh, F. Ludwig and M. Schilling (2009). Effect of HF Concentration on Physical and Electronic Properties of Electrochemically Formed Nanoporous Silicon. *Journal of Nanomaterials*, Vol. 7, pp.

Lees, I. N., H. Lin, C. A. Canaria, C. Gurtner, M. J. Sailor and G. M. Miskelly (2003). Chemical Stability of Porous Silicon Surfaces Electrochemically Modified with Functional Alkyl Species. *Langmuir*, Vol.19, pp. 9812-9817

Lehmann, V. (1996). Porous silicon formation and other photoelectrochemical effects at silicon electrodes anodized in hydrofluoric acid. *Applied Surface Science*, Vol.106, pp. 402-405

Lehmann, V., R. Stengl and A. Luigart (2000). On the morphology and the electrochemical formation mechanism of mesoporous silicon. *Materials Science and Engineering B*, Vol.69-70, pp. 11-22

Lin, V. S.-Y., K. Motesharei, K.-P. S. Dancil, M. J. Sailor and M. R. Ghadiri (1997). A Porous Silicon-Based Optical Interferometric Biosensor. *Science*, Vol.278, pp. 840-843

Low, S. P., N. H. Voelcker, L. T. Canham and K. A. Williams (2009). The biocompatibility of porous silicon in tissues of the eye. *Biomaterials*, Vol.30, pp. 2873-2880

Madou, M. J., B. H. Loo, K. W. Frese and S. R. Morrison (1981). Bulk and surface characterization of the silicon electrode. *Surface Science*, Vol.108, pp. 135-152

Nakato, Y., T. Ueda, Y. Egi and H. Tsubomura (1987). Decomposition Potentials of Crystalline Silicon as Related to the Photocurrent Stability of p-n Junction Silicon Semiconductor Electrodes. *Journal of the Electrochemical Society*, Vol.134, pp. 353-358

Okorn-Schmidt, H. F. (1999). Characterization of silicon surface preparation processes for advanced gate dielectrics. *IBM Journal Research Development*, Vol.43, pp. 351-365

Ouyang, H. and P. M. Fauchet (2005). Biosensing using porous silicon photonic bandgap structures. *SPIE Optics East*, pp. 600508-600515

Park, J.-H., L. Gu, G. v. Maltzahn, E. Ruoslahti, S. N. Bhatia and M. J. Sailor (2009). Biodegradable luminescent porous silicon nanoparticles for in vivo applications. *Nature Materials*, Vol. 8, pp. 331-336

Petrova-Koch, T. Muschik, A. Kux, B. K. Meyer, F. Koch and V. Lehman (1992). *Applied Physics Letters*, Vol.61, pp. 943

Pijanowsk, D. G., A. Baraniecka, R. Wiatera, G. Ginalska, J. Lobarzewski and W. Torbicz (2001). The pH-detection of triglycerides. *Sensors and Actuators B: Chemical* Vol.78, pp. 263-266

Privett, B. J., J. H. Shin and M. H. Schoenfisch (2008). Electrochemical sensors. *Analytical Chemistry*, Vol.80, pp. 4499-4517

Reddy, R. R. K., I. Basu, E. Bhattacharya and A. Chadha (2003). Estimation of triglycerides by a porous silicon based potentiometric biosensor. *Current Applied Physics*, Vol.3, pp. 155-161

Reddy, R. R. K., A. Chadha and E. Bhattacharya (2001). Porous silicon based potentiometric triglyceride biosensor. *Biosensors and Bioelectronics*, Vol.16, pp. 313-317

Ressine, A., C. Vaz-Domínguez, V. M. Fernandez, A. L. De Lacey, T. Laurell, T. Ruzgas and S. Shleev (2010). Bioelectrochemical studies of azurin and laccase confined in three-dimensional chips based on gold-modified nano-/microstructured silicon. *Biosensors and Bioelectronics*, Vol.25, pp. 1001-1007

Rong, G., J. D. Ryckman, R. L. Mernaugh and S. M. Weiss (2008). Label-free porous silicon membrane waveguide for DNA sensing. *Applied Physics Letters*, Vol.93, pp. 161109

Sailor, M. J. (2007). Color me sensitive: amplification and discrimination in photonic silicon nanostructures. *ACS nano*, Vol.1, pp. 248-252

Salis, A., F. Cugia, S. Setzu, G. Mula and M. Monduzzi (2010). Effect of oxidation level of n+-type mesoporous silicon surface on the adsorption and the catalytic activity of candida rugosa lipase. *Journal of Colloid and Interface Science*, Vol.345, pp. 448-453

Salonen, J. and V.-P. Lehto (2008). Fabrication and chemical surface modification of mesoporous silicon for biomedical applications. *Chemical Engineering Journal*, Vol.137, pp. 162-172

Setzu, S., P. Ferrand and R. Romestain (2000). Optical properties of multilayered porous silicon. *Materials Science and Engineering B*, Vol.69-70, pp. 34-42

Setzu, S., S. Salis, V. Demontis, A. Salis, M. Monduzzi and G. Mula (2007). Porous silicon-based potentiometric biosensor for triglycerides. *Physica Status Solidi a-Applications and Materials Science*, Vol.204, pp. 1434-1438

Setzu, S., P. Solsona, S. Létant, R. Romestain and J. C. Vial (1999). Microcavity effect on dye impregnated porous silicon samples. *European Physics Journal A*, Vol.7, pp. 59-63

Smith, R. and S. Collins (1992). Porous silicon formation mechanisms. *Journal of Applied Physics*, Vol.71, pp. 1-22

Song, M.-J., D.-H. Yun, J.-H. Jin, N.-K. Min and S.-I. Hong (2006). Comparison of Effective Working Electrode Areas on Planar and Porous Silicon Substrates for Cholesterol Biosensor. *Japanese Journal of Applied Physics*, Vol.45, pp. 7197-7202

Song, M. J., D. H. Yun and S. I. Hong (2009). An Electrochemical Biosensor Array for Rapid Detection of Alanine Aminotransferase and Aspartate Aminotransferase. *Bioscience Biotechnology and Biochemistry*, Vol.73, pp. 474-478

Song, M. J., D. H. Yun, N. K. Min and S. I. Hong (2007). Electrochemical Biosensor Array for Liver Diagnosis Using Silanization Technique on Nanoporous Silicon Electrode. *Journal of Bioscience and Bioengineering*, Vol.103, pp. 32-37

Sotiropoulou, S., V. Vamvakaki and N. A. Chaniotakis (2005). Stabilization of enzymes in nanoporous materials for biosensor applications. *Biosensors and Bioelectronics*, Vol.20 pp. 1674-1679

Steckl, A. J., J. Xu, H. C. Mogul and S. Mogren (1993). *Applied Physics Letters*, Vol.62 pp. 1982

Tembe, S., P. S. Chaudhari, S. V. Bhoraskar, S. F. D'Souza and M. S. Karve (2008). Conductivity-Based Catechol Sensor Using Tyrosinase Immobilized in Porous Silicon. *IEEE Sensors Journal*, Vol.8, pp. 1593-1597

Thust, M., M. J. Schöning, S. Frohnhoff, R. Arens-Fischer, P. Kordos and H. Lüth (1996). Porous silicon as a substrate material for potentiometric biosensors. *Measurements Science and Technology*, Vol.7, pp. 26-29

Tinsley-Bown, A. M., L. T. Canham, M. Hollings, M. H. Anderson, C. L. Reeves, T. I. Cox, S. Nicklin, D. J. Squirrel, E. Perkins, A. Hutchinson, M. J. Sailor and A. Wun (2000). Tuning the pore size and surface chemistry of porous silicon for immunoassays. *Physica Status Solidi a-Applications and Materials Science*, Vol.182, pp. 547-553

Uhlir, A. (1956). Electrolytic Shaping of Germanium and Silicon. *Bell System Techonolgy Journal*, Vol.35, pp. 333-347

Ünal, B., A. N. Parbukov and S. C. Bayliss (2001). Photovoltaic properties of a novel stain etched porous silicon and its application in photosensitive devices. *Optical Materials*, Vol.17, pp. 79-82

van de Lagemaat, J., VanmaekelberghD. and J. J. Kelly (1998). Photoelectrochemical characterization of 6H-SiC. *Journal of Applied Physics*, Vol.83, pp. 6089-6095

Vijayalakshmi, A., Y. Tarunashree, B. Baruwati, S. V. Manorama, B. L. Narayana, R. E. C. Johnson and N. M. Rao (2008). Enzyme field effect transistor (ENFET) for estimation of triglycerides using magnetic nanoparticles *Biosensors and Bioelectronics*, Vol.23, pp. 1708-1714

Xia, B., S.-J. Xiao, D.-J. Guo, J. Wang, J. Chao, H.-B. Liu, J. Pei, Y.-Q. Chen, Y.-C. Tang and J.-N. Liu (2006). Biofunctionalisation of porous silicon (PS) surfaces by using homobifunctional cross-linkers. *Journal of Materials Chemistry*, Vol.16, pp. 570-578

Xiong, Z., F. Zhao, J. Yang and X. Hu (2010). Comparison of optical absorption in Si nanowire and nanoporous Si structures for photovoltaic applications. *Applied Physics Letters*, Vol.96, pp. 181903

Yates, D. E., S. Levine and T. W. Healy (1974). Site-binding model of the electrical doble layer at the oxide/water interface. *Journal of the Chemical Society, Faraday Transactions*, Vol.70, pp. 1807-1818

Zhao, Z. and H. Jiang (2010). Enzyme-based Electrochemical Biosensors. In: *Biosensors*, P. A. Serra, InTech.

Part 2

Biosensors for Health

18

Minimally Invasive Sensing

Patricia Connolly, David Heath and Christopher McCormick
Bioengineering, University of Strathclyde
United Kingdom

1. Introduction

The key causes of mortality today include cardiovascular disease, infectious diseases, cancer and diabetes. Figure 1, from the World Health Organisation's Global Burden of Disease Report (World Health Organisation [WHO], 2006), illustrates the proportion of deaths due to the major causes. When these statistics are taken together with the age at death data as shown in Figure 2 (WHO, 2006) it can be seen that in the higher income countries, the burden of caring for the ageing population with chronic conditions will dominate healthcare needs and budgets. In the lower income countries there are still significant problems with childhood illness and infectious diseases and the challenge here is to protect the health of their younger populations.

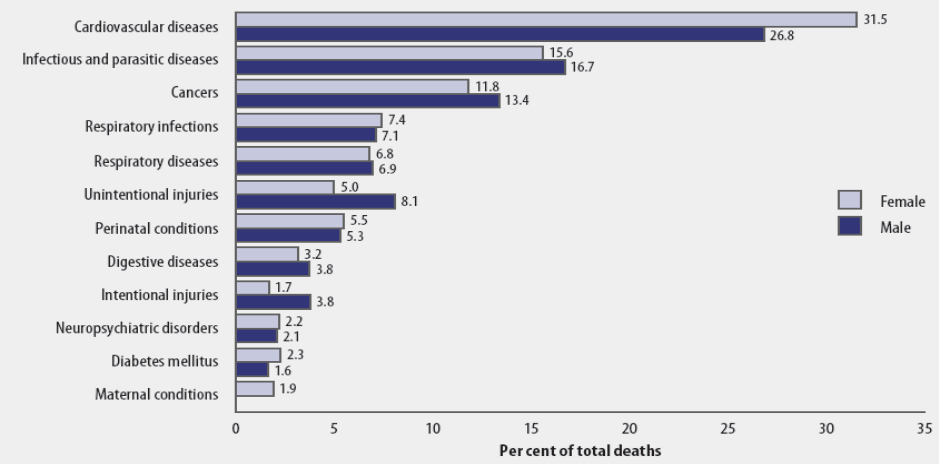

Fig. 1. Distribution of deaths by leading cause groups, male and female, worldwide, 2004 (WHO, 2006, reprinted with permission).

Whilst there are differences in the nature of the healthcare challenges between high and low-income countries, it is clear that both groups must find more effective ways of delivering healthcare into their populations at reasonable cost. This is critically important if countries are going to continue to provide effective healthcare for their citizens, whether this is privately or publicly funded. This presents challenges to pharmaceutical research, drug

delivery, medical devices, hospital care, community care and community medicine. Chronic disease takes many people out of the community and workplace and creates an enormous and unseen group of patients requiring long term intervention and care. Secondary effects of chronic conditions generate problems in wound care, nutrition, provision of home-based medical equipment and community treatment, creating additional burdens for healthcare systems. As an example, in the UK alone the cost of chronic wounds is estimated to be £2.6 billion per annum, with 200,000 patients experiencing a chronic wound at any one time (Posnett & Franks, 2008).

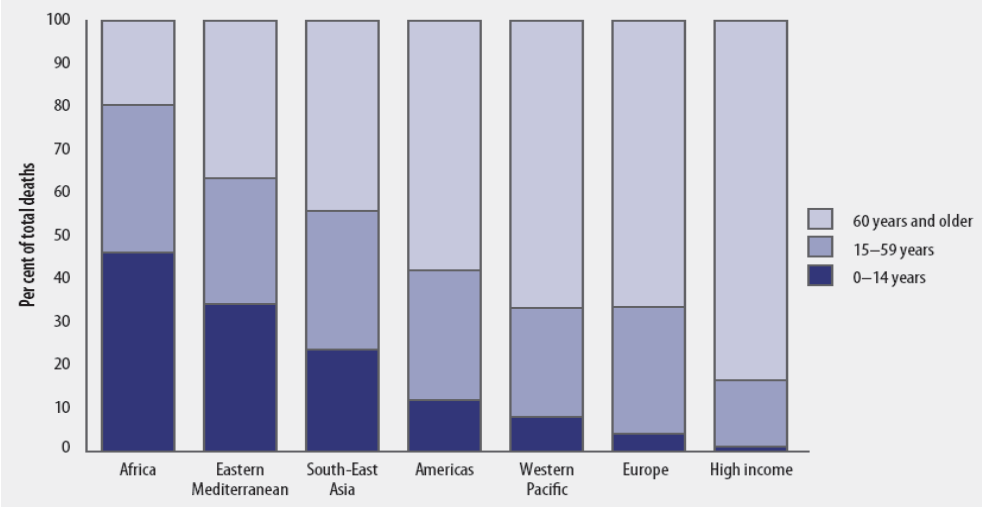

Fig. 2. Percentage deaths by age group in different global regions, 2004 (WHO, 2006, reprinted with permission)

Diagnostics and monitoring have key roles to play in optimising care, and the expectation in the biosensors community that developed in the 1980s and 1990s was that biosensors would be deployed extensively to address some of these needs. It is clear however, that despite the widespread (and frequently ingenious) development of new sensor types and technology, and the advances in device miniaturisation, there is still a notable gap between laboratory biosensing and commercially viable medical or consumer diagnostic devices. The biosensor community needs to find ways of bringing its work to the wider population for telemedicine or telehealthcare. To do this some of the fundamental problems in biosensors, which have impeded their useful deployment in healthcare, must be overcome. Some of the key challenges for practical use of clinical biosensors will now be highlighted. It is proposed that further use of minimally invasive sampling techniques for patient monitoring will allow flexibility in biosensor selection, and provide a wider range of diagnostic systems for use in the home, community or clinic.

2. Home or frequent monitoring via wearable or minimally invasive sensors

The field of wearable sensors that report via wireless systems is advancing, but biosensors are notably missing from current systems. Pantelopoulos & Bourbakis, (2010) have recently

surveyed this area and report the potential for wearable sensors for mainly ECG, EEG, blood pressure, and pO2, but glucose sensing is the only biosensor application mentioned (Pantelopoulos & Bourbakis, 2010). Consideration of wearable sensors highlights two different clinical questions. Firstly, what are the types of parameters that would be useful to monitor, and secondly, why are there so few clinical 'on body' biosensors?

In addressing the first question, what parameters are useful for wearable sensors, there are several important factors to consider. The answer to this question requires an interdisciplinary approach. There is a question to be put to healthcare providers on what would be useful as a wearable, disposable sensor for home monitoring. Working with clinical groups, it is possible to create a profile of what would be most beneficial to their patient groups in terms of medical technology and monitoring. At present, the three leading causes of death worldwide are cancer, ischaemic heart disease, and cerebrovascular disease. It is projected that deaths attributable to these diseases will continue to rise between now and 2030, with the increase in cancer deaths being most marked (WHO, 2006). In each case, early identification of the disease has been shown to improve survival rates. High blood pressure is strongly correlated with increased risk of heart disease and stroke, and therefore technologies to enable better monitoring and early identification of these conditions may have a positive impact on reducing cardiovascular related deaths. Similarly, it has been shown in several studies that survival rates from cancer are linked to time of diagnosis. Diagnostic technologies for this purpose have been developed and are being applied in home testing kits for bowel cancer (Walsh & Terdiman, 2003). Of great relevance to any analysis of potential parameters are the changes in lifestyle that have occurred in recent years and which are expected to continue. Most notably, obesity is an emerging problem across many developed and developing societies. It has been linked to a variety of metabolic disorders, including Type II Diabetes, cardiovascular diseases, and certain cancers. With increasingly sedentary lifestyles, it is likely to remain a major issue, and is therefore receiving considerable focus as a target for the preventative healthcare strategies increasingly being adopted. Similarly, Hospital Acquired Infections (HAI) remain an unfortunate feature across many healthcare systems, with their impact not only being felt by the affected patients, but also in driving up the treatment costs to healthcare providers. There is considerable debate about the best preventative measures to adopt to reduce HAI but any technology that proves capable of rapidly detecting such infections, or the bacteria that cause them, would be a powerful tool in such preventative strategies.

The above discussion is not comprehensive but its purpose is to provide a background to common issues facing healthcare systems across the world, and to stimulate thoughts on what parameters might usefully be measured. Looking ahead, and accepting that home monitoring is set to become a major feature of healthcare systems, what parameters could be usefully checked at home and used to adjust lifestyle or medication? As an example, if some of the key health challenges and medical conditions identified by the WHO are mapped to relevant clinical parameters, then a selection of parameters that would be useful to measure regularly and locally emerges, as shown in Table 1.

Whichever field of health is considered, a key component of any parameter analysis must be a market evaluation. The financial investment that is required to take a biosensor concept to a final product is substantial and may in itself be an explanation as to the lack of available biosensors for home settings or continuous monitoring. In this context, the question that Kissinger posed in 2005 remains key: "Do enough people want or need to have a sensor for the analyte of interest?" (Kissinger, 2005). When one considers the size of the diabetic

market for glucose monitoring, around $7bn (with a small but growing segment of this given to continuous monitoring) (HSBC, 2006), it is perhaps not surprising that the glucose biosensor is the most successful of all known biosensors today, representing around 85% of the biosensors' market. In addressing the question of what type of parameter to measure the answer must clearly come from an analysis of the population base for the parameter, the clinical need, the advantages to the patient and the cost savings to be made from its proper integration in healthcare provision. This in turn will drive a true market for the sensor and ensure its uptake if properly deployed.

Condition	**Parameter**
Dehydration (elderly)	electrolytes
Obesity (weight loss)	ketones, tryglycerides, insulin
Asthma	blood parameters, compliance
Wound management	wound moisture, pH, bacteria
Diabetes	glucose, insulin, ketones
Cardiovascular	electrolytes, cardiac markers
Stress	cortisol
Poor nutrition	vitamins, electrolytes
Drug abuse	drugs of abuse
Drug compliance	specific sensors for medicines
Cancer	markers for therapy, recurrence

Table 1. Parameters potentially useful for home or community clinic monitoring

It is also necessary to understand the different types of markets within healthcare and alternative models of delivery within these markets. Across the world, there has been a movement towards an increasing role for Primary Health Care (WHO, 2008), with a growth in patient-centred approaches which aim to put people at the centre of their own healthcare. The practical implementation of this is causing a decentralisation of healthcare provision away from the hospital to the home, local surgeries, and pharmacies. This coincides with demands for better prevention, and early diagnosis. The driving force behind these trends is the downward pressure on the unit cost of treatment that is a major feature of today's healthcare systems.

Many of the influences identified above are well established. It is therefore pertinent to consider why such a limited number of biosensors have made an impact within this apparently favourable climate. The regulatory environment which governs such devices is an important consideration. It is beyond the scope of this chapter to detail the regulatory requirements in each region. Whatever the precise nature of the regulatory framework in any region, it is clear that it represents a significant barrier standing between a promising research result and subsequent translation into a marketable medical device product. This is certainly one explanation for the discrepancy between the volume of academic research papers reporting on biosensor development, and the rather limited number of commercially successful biosensors. Crucially, gaining regulatory approval represents a significant cost, the bulk of which is necessarily incurred at a point when the device is unable to generate sales revenue. These costs are mainly related to obtaining proof of clinical performance and generating biocompatibility or toxicology data, and to ensuring that large scale manufacture of devices is highly quality controlled. Consideration of the regulatory requirements from the outset of any medical device programme can help to minimise such costs by the correct selection of acceptable materials, and by adoption of approved design practices from the start of the process.

This takes us to a discussion of the key biological challenges in the deployment of biosensors, either in wearable format or as implanted systems.

3. Home use biosensors

3.1 State of the art

The parameter that continues to set the pace for personal use of biosensors is glucose and it will be used in this chapter to illustrate what can be achieved in minimally-invasive biosensing. The extent of the diabetic market is such that there are considerable commercial and healthcare incentives to drive new developments in monitoring in this field. The WHO statistics from 2004 indicated that there were 170 million diabetics worldwide at that point and lifestyle changes are raising the rate of the development of the condition significantly, with an expected world population of 300 million by 2025 (WHO 2004). The development of portable glucose sensors for diabetics has been reviewed in detail by Newman & Turner, in 2005, tracing the path of glucose sensing from the Yellow Springs Glucose Analyser developed by Leyland Clark through the introduction of amperometric, mediated glucose sensors that provide reliable and portable glucose sensing up to the 'minimally invasive' sensors on offer today. The frequent blood sampling required by diabetics who use blood testing devices has led to problems for users, including pain and damage to sampling sites, and companies have tried to overcome this by devising better lance systems and looking for alternative sampling sites to the fingertips. Ideally no blood sampling would take place for diabetic home testing and the field is moving towards this.

3.2 Subcutaneous glucose sensors

Currently the state of the art in minimally invasive technology is provided by subcutaneous sensors that the user must inject under their skin and clip to a skin mounted transmitter. Systems are available from Medtronic (Guardian® REAL-Time), Abbot (FreeStyle Navigator®) and Dexcom (Cox, 2009). The sensors can be left in body for up to seven days before removal or replacement and will transmit glucose readings to a meter from the skin mounted transmitter. This is a clear advance in glucose monitoring and the best yet that biosensing has been able to offer the diabetic field.

Other point of care systems are available for some parameters but are all based on blood sampling, such as devices for monitoring of anti-coagulation therapy e.g. HemoSense INRatio meter (Meurin et al., 2009) and lactate measurement devices for sports monitoring and general medicine e.g. Roche Accutrend (Acierno et al., 2008). Thus it is clear that there is no widespread availability of biosensors that are capable of either full or subcutaneous long term implantation and a brief consideration of the reasons for this is appropriate.

3.3 Device implantation responses

The host response in the human body to any foreign material is a stimulation of the inflammatory response. Body fluid contact with the device and protein adhesion stimulates cellular activity on the implant surfaces, commencing with leukocyte contact and a cell cascade reaction. This further stimulates protein deposition and fibrous encapsulation of the foreign material, creating a barrier to analyte diffusion and a degradation of device performance. Miniaturisation of devices has not removed these fundamental biological problems. The smaller sensors developed through nanotechnology are not immune to this

response despite improvements in biomaterials and the use of biocompatible coatings, such as polyethylene glycol, and the use of tissue response modifiers (mainly anti-inflammatory drugs) embedded in devices for local release. Vaddiraju et al., (2010) have reviewed the challenges facing nanosensors for implantation and conclude that while the reduction in size of implant through nanotechnology has lowered the immune response it has not been removed. Nevertheless, they recommend continued research in this field and the development of multianalyte devices for early disease detection.

In addition there may be opportunities to introduce temporary implanted sensors where tissue needs local monitoring over shorter times. An example of such a device is an implantable sensor for cancer marker proteins that can be left in situ during tumour surgery to monitor local tissue response (Daniel et al., 2009). The sensor contains an implanted magnetic label sensitive to cancer markers which can diffuse into the device. It has been demonstrated in a murine model for the monitoring of cancer markers following tumour resectioning. With adjustment of the magnetic label it could equally be deployed for monitoring of metabolites or chemotherapy agents.

Subcutaneous sensors do not fare much better when the host response is considered and are also subject to protein attachment. Gifford et al., (2006) have studied the encapsulation of a subcutaneous needle-type biosensor for glucose using a rat model and concluded that the absorption and infiltration of larger molecules, such as IgG (169 kDa) and serum albumin (66KDa), creates barriers to the diffusion of glucose and is the main cause of loss of sensitivity in these devices. Regular calibration is needed to account for this loss in sensitivity.

3.4 Less invasive approaches to health monitoring

If *in vivo* and subcutaneous biosensors are eventually thwarted by the host response then less invasive methods of obtaining biological samples directly from the subject must be the answer to many diagnostic requirements. There is a great deal of research presently underway to address this. The use of less invasive sensing methods for glucose are explored below, as an example of how minimally invasive monitoring is developing. Methods of non-invasive and continuous glucose monitoring are regularly reviewed (see for example Ferrante do Amaral & Wolf, 2008; Girardin et al., 2009; Pickup et al., 2005; Tura et al., 2007; Wickramasinghe et al., 2004)

3.5 Measurement of glucose in body fluids other than blood or interstitial fluid

Although blood glucose concentrations are of interest, noninvasive methods for measuring glucose have been attempted using a number of different fluids in the body. The following discussion concentrates on fluids that are most readily accessible, such as sweat, saliva, tear fluid and urine while sampling of interstitial fluid will be discussed in later sections. Sweat is an example of a body fluid that is readily accessible through non-invasive means. Glucose levels in sweat have been reported to be similar to glucose levels found in blood. Sweat may therefore represent one option for non invasive measurement (Pellett et al., 1999) of glucose and other parameters. Patches have been developed for sweat collection, and these devices have been trialled for use in the detection of substance abuse (Liberty et al., 2003; Uemura et al., 2004).

The measurement of glucose in urine, urinalysis, has also been used as an indication of blood glucose levels. This has been used clinically for some time and is often the method by which diabetics are first identified (Pickup & Williams, 1997). Although this method of

analysis is useful it does not lend itself to continuous, quantitative, blood glucose measurements. Aside from the practical issues of regularly measuring urine glucose levels, storage times in the bladder lead to significant lag times between glucose levels excreted in the urine and those found in the blood. Similarly, glucose levels in other biological fluids, such as saliva, also lag behind blood (Pellett et al., 1999).
Even if this lag time between blood and body fluid glucose was considered insignificant, there are few devices reported in the literature for non-invasive, near continuous, monitoring of glucose levels from sampled human body fluids other than interstitial fluid. An example of a system for human body fluid measurement is a contact lens that reacts to tear glucose levels (Badugu et al., 2003). Contact lenses embedded with a form of boronic acid that contains fluorophores have been investigated as a medium for sensing the amount of glucose in tear fluid. It has been suggested that this approach may be suitable for the continuous monitoring of tear glucose levels, which typically correlate to blood glucose levels. A potential tear glucose operating range of 50μM – 1000μM was reported (Badugu et al., 2003). It has been proposed that users could assess their glucose concentration by comparing the colour of their contact lens against pre-calibrated colour strip (Badugu et al., 2005). Further work is needed to address issues of resolution, lifetime and biocompatibility (Moschou et al., 2004). The main issues concerning this method are, firstly, it seems that glucose fluctuation would only be detected if its concentration increased over what was expected. If this were the case, then the onset of hypoglycaemia would not be detected. The second issue is that this method does not provide a quantitative measure of blood glucose levels so could not be used in conjunction with hypo- or hyper-glycaemic alarms or give indication of insulin dose countermeasures.

4. Human skin and minimally invasive monitoring

Due to the potential for access through skin, the majority of approaches taken to minimally invasive blood glucose monitoring have concentrated on this organ. Skin is an effective barrier to the transport of molecules into the body or out of the body, due to the structure of the dermis, epidermis and stratum corneum, but does allow some molecular transport, interstial fluid collection and subcutaneous access. The remainder of the chapter will deal with methods of non-invasive monitoring based on dermal or transdermal analysis of the analytes that can be obtained through the skin.

4.1 Dermal monitoring approaches

4.1.1 Non-invasive – electromagnetic analysis

Electromagnetic radiation provides the possibility for truly non-invasive glucose measurement with a very low risk of adverse side effects. Electromagnetic (EM) wave radiation can be observed over a wide range of different wavelengths. The range of wavelengths gives rise to the electromagnetic spectrum as shown in Figure 3.
Electromagnetic radiation will interact with molecules and atoms. These energetic interactions can be used to probe glucose, and potentially other parameters, in various ways depending on the chosen wavelength. As sensing of blood glucose has to be non-harmful to the body, shorter wavelengths than the optical region cannot be used as radiation below these wavelengths becomes ionising.
Optical methods (between the visible and far-infrared parts of the electromagnetic spectrum) are largely based upon focusing a beam of light onto a tissue test site and measuring how the

light is modified by the target tissue. Light will interact with biological tissues in a number ways including absorption, reflection, scattering, transmission, polarisation or modification in wavelength. The nature of this interaction and the degree to which it occurs will depend upon the components of the tissue (e.g. water, fat, glucose) and their respective concentrations within the target sample. These compounds have recognisable optical signature responses to incident light and many forms of analysis have been investigated to relate these optical signatures to the concentration of glucose in tissue samples.

When the glucose concentration of the sample site has been measured, this then has to be related to blood glucose concentration. This is not a straightforward process as within a chosen sample site there will be a number of compartments each containing a different concentration of glucose. Each of these different compartments will contribute to the measured signal. For sites chosen on the skin, the signal is likely to be dominated by the compartments containing intracellular fluid, interstitial fluid and capillary blood. The ratio of these three groups will also vary depending on site location leading to very site specific measurement calibrations.

Two of the most popular areas for investigation of glucose by electromagnetic spectroscopy are near-infrared spectroscopy and mid-infrared spectroscopy.

4.1.2 Near-Infrared Spectroscopy (NIR)

The near-infrared range used for investigating blood glucose spans an electromagnetic wavelength range of approximately 1000nm -2500nm. This region is a very popular range for investigation of glucose as it permits penetration into deep tissue (~1-100mm) depending on the chosen wavelength. The depth of penetration will decrease with increasing

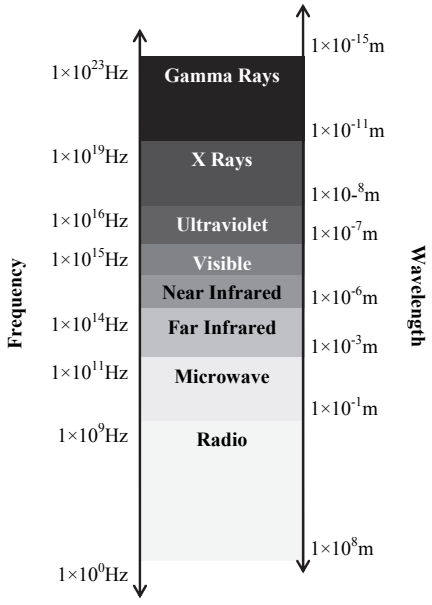

Fig. 3. An illustration of the regions of the electromagnetic spectrum with approximate corresponding frequency and wavelength.

wavelength. Another advantage is that the absorption coefficient of water is weaker in near-infrared region when compared with the mid-infrared region

There are challenges to glucose measurement by near-infrared spectroscopy and a variety of tissue test sites have been researched (Oliver et al., 2009). From a physiological perspective, the challenges are compound. Firstly this arises from the relatively low concentrations of glucose in the body when compared with the presence of other substances that affect the NIR signal such as fats and water. Secondly, the absorption coefficient of glucose is low in the near-infrared region and, finally, the spectral bands due to glucose overlap with bands due to water, fat, haemoglobin and proteins. This introduces significant technical challenges for signal sensitivity and signal interference, which will need to be addressed in order to demonstrate sufficient accuracy of glucose measurement (Pickup et al., 2005; Tura et al., 2007; Ferrante do Amaral & Wolf, 2008). The cost and physical size of equipment required for infrared spectroscopy measurements may also limit its application in continuous monitoring, particularly in the context of wearable sensors. Despite these challenges, there is still a large amount of commercial activity in this area.

4.1.3 Mid-infrared region

The mid-infrared region can span between 2500nm – 10,000nm. As this radiation is at longer wavelengths than Near-Infra Red, the depth of penetration is reduced to the micrometer range (Tura et al., 2007). At these wavelengths, less of the light is scattered and the majority of light is absorbed. In this region the absorption peaks are sharper and more defined when compared with the broader weaker peaks seen in the NIR region. This is observed for both glucose and other compounds (Ferrante do Amaral & Wolf, 2008). However, hydration level of the skin can has a strong impact on such absorption signals and this is subject to variation.

4.2 Transdermal monitoring approaches

The transdermal route has clear attractions and can be divided into two approaches: interstitial fluid sampling, and transdermal extraction. In the first method, the intention is to directly sample interstitial fluid and this can be done via microneedle technology, sonophoresis or thermal ablation. For the second approach, transdermal extraction of molecules is achieved by electrically sampling the skin interface. This largely makes use of the existing skin transport routes in the hair follicles, sweat glands and in nano and micoporous structures in the skin. This is the realm of iontophoresis and electroporation. Both approaches could lend themselves to combined extraction and sensing using micro and nano electromechanical systems (MEMS and NEMS technology) and therefore should be of interest to those developing miniaturised sensors. Much of the literature in the field has been generated from research into transdermal drug delivery, but it is equally applicable to the extraction of molecules via the skin. Arora et al., (2008) comprehensively review Microsystems for transdermal drug delivery and describe state of the art skin delivery techniques that could easily be adapted for the collection of, or access to, interstitial fluid. They point out that creating micrometre-scale breaches in the skin is well tolerated and the skin will recover quickly from such breaches. Thus, it is possible to temporarily reduce the skin barrier for molecular collection and analysis. This means that the accepted passive limits of drug delivery (or molecular extraction) of 500 Da can be surpassed and large molecules could be detected as well as small.

4.2.1 Interstitial Fluid Sampling (ISF)

The most easily understood of the device types for transdermal extraction are microneedle devices. Microneedle arrays can be fabricated and pressed onto skin or scraped over it to create the necessary breach in the stratum corneum. Successful application of a microneedle array can increase skin permeability in that region by up to 4 orders of magnitude. Microneedles can be solid or hollow and therefore such devices could offer a degree of flexibility in terms of location of biosensors. Combined sensors and microneedles are already being suggested by some groups. For example, Mukerjee et al., (2004) demonstrated successful collection of interstitial fluid from a microneedle and capillary device which enabled glucose measurement. Further investigation of how interstitial fluid levels of specific analytes compare with blood levels is required, but early signs are encouraging. Mitragotri et al., (2000) also investigated a range of other parameters in rats, with ISF collected by sonophoresis taken together with simultaneously collected serum samples, and found good agreement between glucose, albumin and triglycerides in ISF and serum, but higher than expected lactate and calcium in the ISF as compared to serum.

4.2.2 Ultrasound (sonophresis/phonophoresis)

Ultrasound has been explored as a method for enhancing drug transport across the skin. Various power levels, duty cycles, and frequencies have been examined. Drug delivery for a range of hydrophilic and hydrophobic compounds enhanced by sonophoresis has been comprehensively reviewed by Escobar-Chavez et al., who conclude that the use of sonophoresis in skin permeation enhancement and drug delivery is likely to increase (Escobar-Chavez et al., 2009)

Various frequencies of ultrasound can be chosen, from low frequencies (20 kHz) to very high frequencies (low MHz), to be applied to the skin to enhance permeability. It has been suggested that in the lower frequency range (approximately 20 - 90 kHz) there exists a threshold intensity below which no detectable skin permeability enhancement will be observed. This threshold intensity increased with frequency (Tezel et al., 2001). It has also been suggested by the same authors that low frequencies (20 kHz) induced localised transport compared to a more dispersed effect seen with higher frequencies (58.9 kHz). Other authors (Ueda et al., 1995) have suggested that high frequency (10 and 16 MHz) ultrasonication can concentrate the ultrasonic energy on the stratum corneum *in vivo*. They also reported that electron microscopy indicated that the intercellular route of the stratum corneum is influenced by ultrasonication at these frequencies.

Cavitation, the growth and collapse of gas bubbles, is generally reported to be the dominant mechanism of sonophoresis. Cavitation is thought to disorder the lipid bilayers in the stratum corneum creating mass transfer pathways and thus increasing the diffusion coefficient of solutes. However, it has been suggested that cavitation alone cannot account for the total enhancement effect observed (Cancel et al., 2004). Several mechanisms have been suggested to contribute to this transport phenomenon. Among these are structural changes caused by cavitation, thermal effects, mixing in the liquid phase and acoustic streaming through hair follicles and sweat ducts. In addition, a convective mechanism of enhancement has also been suggested, although no quantitative analysis has been proposed.

Cavitational and mechanical effects increase tissue temperature and skin permeability is increased by an increase in temperature. The ultrasonic apparatus used in one study (Ueda et al., 1995), raised the temperature in the donor compartment (*in vitro*) by 3 - 4°C during the application of ultrasound. This may account for some reversible effects accompanying

ultrasound. *In vivo*, raising tissue temperature should not exceed an increase of 1°C as anything above this can cause irreversible damage to tissue. Such unwanted effects may account for the irreversible effects observed such as a decrease in barrier function of stratum corneum.
Successful application of ultrasound to skin for the sampling of interstitial fluid and detection of glucose has already been successfully demonstrated by Kost et al., (2000) and it remains a topic of research interest.
In summary, the sonophoresis approach to skin permeability enhancement is clearly of interest although physical size and cost of ultrasound based enhancement technology may limit its use in the field of continuous monitoring, particularly with application to wearable sensors.

4.2.3 Radiofrequency (RF) thermal ablation

Radiofrequency thermal ablation has been used in microsurgery for treatment of conditions such as tumours. This method consists of an array of needle like electrodes that are placed on the skin which deliver heat that kills the tumour while leaving the surrounding healthy tissue unharmed. This method has been tested in a similar way for aiding transdermal drug delivery. This works by using high voltage radiofrequency currents to create aqueous microchannels in the skin (Sintov et al., 2003). This study examined this effect *in vitro* (across porcine skin) and *in vivo* in rats. The study reports increased delivery of the chosen drug (diclofenac) by a factor of 30 compared with the control over a 12 hour period. As RF thermal ablation has been demonstrated an effective method of increasing skin permeability, it is conceivable that it could be adapted for use in transdermal extraction or assisted diffusion.

4.2.4 Electroporation

Electroporation refers to the application of high electric fields for short bursts to skin causing the formation of micropores in the skin. A cell bilayer can be electroporated by the application of transmembrane voltages in the range 0.3-1V and thus 1ms pulses of between 100- and 1500V have been used to electroporate the stratum corneum which contains approximately 100 bilayers (Vanbever & Preat, 1999). However, there is evidence that even application of moderate voltages up to 60V across the skin causes electroporation (Chizmadzhev et al., 1998) and thus it should be expected that some poration will occur during iontophoresis. The formation of micron feature openings in the SC by electroporation leads to the possibility of extraction of higher molecular weight molecules. There is considerable scope for localised electroporation of skin by microdevices and microelectrodes that is yet to be exploited.

4.2.5 Iontophoresis

Iontophoresis is a process where two electrodes, with good interface conductivity (such as silver chloride and conducting gel), are placed upon a membrane and a small voltage is applied to deliver a low current through the membrane (or skin in human applications). This voltage usually seeks to drive a constant DC current in the range of 300 – 500 $\mu A/cm^2$. This method can be used to enhance transport of ionic elements, or molecules and compounds through the skin as a result of the interaction of the charged ions and molecules with the imposed electric field. Uncharged molecules are also transported by

electroosmosis. The skin is a permselective membrane that, at physiological pH (~5.0-6.0), supports a net negative charge (Manabe et al., 2000). As a result, a positively charged ion will penetrate more easily across the skin than a comparably sized negative ion. An electroosmotic solvent flow will also be established. This electroosmotic effect predominates in the anode to cathode direction because current is preferentially carried by cations and momentum is transferred to the solvent by cation movement. This momentum causes a net convective flow (electroosmosis) from anode to cathode and, as a result, there will be enhanced transport of dissolved, uncharged solutes in the same direction.

Iontophoresis may also enhance the transdermal movement of larger molecules (> 1000 Da) (Delgado-Charro et al., 1994). However, the transport numbers of such molecules (i.e., the fraction of the total current flowing which is carried by the large molecule of interest) are very small because of competition from smaller, more mobile ions such as the background electrolytes and/or receptor solutions. Research in this field is ongoing and unexpected behaviour has sometimes been reported with larger molecules such as peptides. For example, a very weak dependence of flux upon applied current density, and even an inverse relationship between transport and applied peptide concentration, has been observed (Delgado-Charro et al., 1994).

5. Minimally invasive monitoring by reverse iontophoresis

Reverse iontophoresis is where the application of electric current across the skin is used to extract a substance of interest from within or beneath the skin to the surface (Santy & Guy, 1996a,b). Figure 4 illustrates the application of a constant current via two skin mounted electrodes. The electrodes are housed in electrically conducting gel chambers. The diagram also illustrates the resultant solvent flow that is generated. Circles with a '+' represent positive ions and circles with a '-' represent negative ions. Circles with a 'G' represent the glucose that is caught in the solvent flow and carried into the gel chamber for analysis via an imbedded sensor.

Transdermal molecular extraction by reverse iontophoresis has a distinct appeal as it is an electronically controlled and programmable method of extraction, that can be turned on and off at different points in the diagnostic cycle. Because there is no deliberate breach of the skin there are four separate routes of molecular transmission that are available for molecular transport; transcellular, intercellular, via hair follicles and via eccrine (sweat) glands (Riviere & Heit, 1997). The mechanism of extraction is non-specific; there are a great number of potential analytes that could be measured and therefore a great number of potential uses for reverse iontophoresis. An example of this has been shown by Sieg et al., where glucose and urea were simultaneously extracted (Sieg et al., 2004b). We have demonstrated good levels of simultaneous lactate and glucose extraction in healthy volunteers by application of iontophoresic current of 300uA cm^{-2} in 15 minute cycles for periods up to 1 hour as shown in Figure 5 (Ching & Connolly, 2008b). Others have shown the simultaneous extraction of a range of amino acids in human subjects (Sieg et al., 2009).

Investigations into methods of optimising the analyte extraction have revealed that cathodic extraction is enhanced as pH increases as far as can be feasibly maintained in contact with the skin surface; the reverse is true for anodal extraction (Santi & Guy, 1996b). In-vitro, electroosmosis increases with decreasing ionic strength in the electrode chambers. However, sufficient electrolyte must be present to sustain the necessary electrochemical reactions occurring at the electrode surfaces.

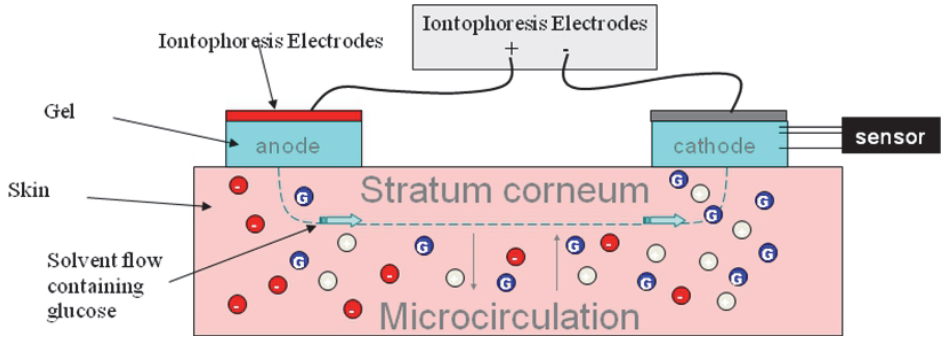

Fig. 4. Schematic illustration of the principle of reverse iontophoresis showing an iontophoresis extraction device supplying a constant current to an anode and cathode.

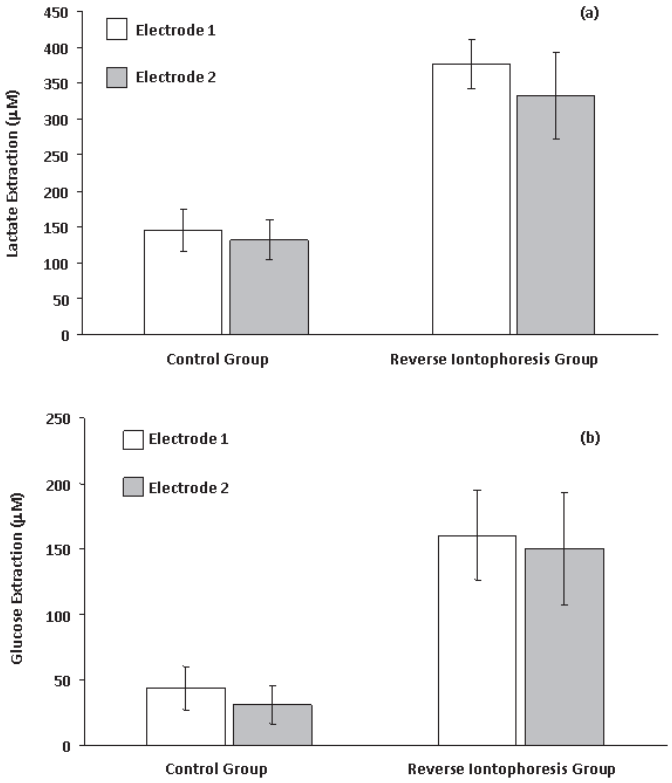

Fig. 5. Average results of long duration bipolar direct current application (current density of 0.3mA/cm^2, polarity of electrodes reversed at intervals of 15 minutes, experimental time of 60 minutes) on human transdermal extraction of **(a)** lactate and **(b)** glucose (mean ± SD; n=10). Extraction of lactate or glucose by reverse iontophoresis was significantly higher ($p<0.001$ for both cases) than that of the control sample. Reprinted from Ching & Connolly, 2008b with permission.

Further work by Santi & Guy used a non-metabolizable sugar mannitol as a marker and found that decreasing the pH in the anodal chamber and increasing that in the cathode chamber improved the total quantity of electroosmotic flow from beneath the skin (Santi & Guy, 1996a). The authors also fixed pH, and reduced the ionic strength of the electrode chamber solutions (relative to the physiological level), confirming again enhanced reverse extraction, most notably at the cathode.

5.1 Effects of iontophoresis on human skin and skin recovery

The successful clinical application of iontophoresis will require minimal or no side effects as well as the rapid recovery of the skin barrier after the current flow has been terminated. Curdy et al., (2001) has reviewed non-invasive methods for skin integrity assessment. These methods include Transepidermal water loss (TEWL), Impedance spectroscopy (IS), Attenuated total reflectance-Fourier transform infrared (ATR-FTIR) spectroscopy and Laser Doppler flowmetry (or velocimetry) (LDF). Curdy et al., used a variety of these methods to assess skin function following iontophoresis *in vivo* (Curdy et al., 2002). The paper demonstrated a reduction in skin barrier impedance, as desired and expected, post-iontophoresis. However, the paper concludes that there is no evidence of an association between the observed reduction in impedance and skin damage.

The potential for reverse iontophoresis as a technology for transdermal extraction has been most noticeably demonstrated by the Glucowatch (Cygnus Inc). Significantly, the GlucoWatch gained FDA approval for diabetic monitoring in 2001. The FDA approval was based on nine pivotal clinical studies, seven assessed the effectiveness of the device and two assessed safety. A summary of these studies and the criteria on which the GlucoWatch achieved FDA approval can be found in the relevant FDA approval documentation (Summary of safety and effectiveness data, PMA No. P990026, FDA 2011). In 2002, the second generation device (GlucoWatch G2) obtained FDA approval (Summary of safety and effectiveness data, PMA No. P990026S008b, FDA 2011) Further details on this device can be found in the literature (see for example Tierney et al., 2001). Despite obtaining FDA approval in 2001 the GlucoWatch did not secure market adoption. Technical or user-related issues, such as sweating on the skin under the device causing a short circuit that (when detected by two electrodes specifically designed for this) stopped glucose readings, impeded its widespread uptake

5.2 Reverse iontophoresis challenges

If reverse iontophoresis is going to make the impact that many expect in the field of minimally invasive monitoring, it is clear that key technical challenges will have to be overcome. It is now worth exploring each in some detail and examining what research is underway to address each challenge. The following analysis is largely based on glucose sensing, although other parameters are mentioned where appropriate. However, many of the technology challenges are common across a range of potential parameters, and therefore the discussion should be of relevance to all readers engaged in minimally-invasive sensor development.

5.2.1 Comfort

It is clear that one of the major advantages of minimally invasive sensors is an ability to perform monitoring that is relatively pain free. This is clearly understood when the

replacement of frequent, fingerstick blood sampling is considered. Any device that can provide the same information without the requirement for blood samples would represent a real advance and facilitate better disease management strategies, which are known to reduce secondary complications of diabetes (UK Prospective Diabetes Study Group (1998a; 1998b; 1998c; 1998d)). It is therefore essential that any proposed technology does not in itself introduce new barriers to adoption, such as pain or inconvenience associated with its use. The level of pain experienced during iontophoresis is related to the current density, and it is generally accepted that currents in excess of 300μA / cm^2 cannot be readily tolerated for extended periods (Ledger, 1992). This places limits on the type of molecule that can be extracted transdermally for analysis, with molecules over 500Da being unlikely to cross the skin at this level of current. In addition, the applied current density has also been directly correlated with the transdermal flux (Delgado-Charro et al., 1994). Using the neutral molecule, Mannitol, Delgado-Charro et al., were able to demonstrate that flux was linearly correlated with applied current density over a range of 0.14 – 0.55 mA / cm^2 (Delgado-Charro et al., 1994). Therefore, any efforts to reduce the current level must be balanced with the need to extract a quantifiable amount of the analyte of interest, and for biosensing this is limited by the range of the sensor to be deployed in the gel electrode. Consequently, technologies that can enable efficient transdermal extraction at low current levels are particularly appealing

Since one of the potential benefits of minimally invasive sensors is the ability to monitor continuously over extended periods, it is worth examining in more detail how the skin interface responds to the process of reverse intophoresis over prolonged extraction periods. On a practical level, there is evidence of localised skin irritation over prolonged durations of reverse iontophoresis (Howard et al., 1995). There are two main reasons for this beyond the localized heating that can occur at higher levels of current. Firstly, the use of direct current (DC) and secondly, the use of embedded biosensors within the skin gel.

Direct current (DC) is believed to generate high concentrations of hydroxyl ions within the anodal gel compartment, with the production of hydrogen ions within the cathodal compartment. Since both gel compartments are in intimate contact with the skin surface, the resultant localized alterations in pH may be, at least in part, responsible for the erythema and stinging that has been reported in some studies (Howard et al., 1995). In efforts to address this, polarity reversal has been introduced. Here, the polarity of the electrodes is regularly alternated, such that the current flow changes direction. In addition to reducing the effects of local pH imbalances, it has also been shown in several studies, including our own, to actually enhance iontophoretic transport (Ching et al., 2008a). DC current can cause electrical polarization of the skin, thus inhibiting molecular transport across it, and it has been proposed that the enhanced transport, produced by switching electrode polarity, is likely due to a reversal of this skin polarisation process (Ching et al., 2008a). It is worth mentioning, however, that not all studies have demonstrated such an enhancement effect on transdermal flux (Santi & Guy, 1996a; Santi & Guy, 1996b). It is likely that the optimum extraction conditions are molecule dependent. Careful consideration of current level, duration, and delivery mode are therefore required.

Another factor to be considered in transdermal extraction is the accumulation of reaction intermediates and products resulting from the detection technology. The extent to which this represents a barrier to clinical adoption depends on the molecule of interest, and how it is to be measured. If one considers the detection of electrolytes collected at the skin surface by reverse iontophoresis, a relatively simple embedded ion-selective potentiometric sensor

could be used to measure the ion concentration without the production of any deleterious reaction products. However, the situation was quite different with the first generation of reverse-iontophoresis based continuous glucose monitors. The biosensors employed in these devices used glucose oxidase enzyme that was distributed throughout the gel (Tierney et al., 2001). Considering that the product of the glucose-glucose oxidase reaction is hydrogen peroxide, a known irritant (Watt et al., 2004), it is clear that irritation is a risk with prolonged use of these types of embedded sensors. The use of mediated enzyme electrodes for analyte detection, where the detection enzyme is bonded to the electrode alongside a mediator (Liu & Okuma, 1998; Sato et al., 2006), or where the components are dispersed in the ink of a printed electrode (Saby et al., 1995), has removed this particular limitation. These mediated biosensors, which do not produce hydrogen peroxide, are now the most common method of glucose detection used today.

At this stage, it is worth repeating that one of the main aims of minimally invasive sensors, is to replace existing invasive measurement methods where this will be of real clinical benefit. If this replacement is to be justified, then the proposed system must provide the clinician or patient with at least the same level of information as the original test format. The utility of reverse iontophoresis therefore relies, at least in part, on the ability to use the reading obtained at the skin surface as an indicator of the concentration of the analyte of interest in the blood. This is a key challenge, and many view it as the Achilles heel of the technology. It is therefore worthy of discussion and we will examine some of the technical challenges that have hampered efforts to establish robust correlations between blood and skin levels of an analyte.

5.2.2 Lag

A significant criticism of transdermal technologies that rely on sampling interstitial fluid, such as reverse iontophoresis, is that there is a lag time in detection of the molecule at the skin interface (Kulcu et al., 2003). It is known that blood glucose changes can occur rapidly in the blood (Pickup & Williams, 1997). A lag time of around 20 minutes was reported for the GlucoWatch (Tamada et al., 1995) although other studies suggest that shorter lag times of around 5 min may be possible (Kurnik et al., 1998). So it is not yet clear that lag time is an insurmountable problem for reverse iontophoresis approaches. It is also worth noting, that the relative importance of lag time can be viewed as being dependent on the molecule of interest. Given that attention has largely focused on glucose measurement thus far, it is perhaps not surprising that this problem has received considerable attention. However, there are other applications where the impact of lag time would present a much less significant problem. When one considers therapeutic drug monitoring for instance, a reverse iontophoresis patch may be applied to the skin for several hours before a measurement is made to estimate the final concentration of the drug within the blood (Leboulanger et al., 2004). Similarly, it is of little apparent clinical benefit to measure disease marker molecules continuously, or over an extended duration. Rather, the purpose of such detection would be to provide a snapshot to inform diagnosis, enabling treatment or prevention measures to be initiated. It is therefore clear that one must consider the molecule, and the intended use of the information, since both will impact the extent to which existing reverse iontohporesis technologies can usefully be applied. The point has already been made earlier in this chapter, but this reinforces the value of clinician input at the very earliest stages of device development.

5.2.3 Gel properties

Up until this point, our discussion on lag has focused on what is happening within the different compartments of the body, notably the relationship between blood and interstitial fluid analyte concentrations. The following discussion now considers what happens within the gel that collects the molecule at the skin surface. There are several challenges associated with this aspect of the technology. The first relates to irritation and this has been covered in previously in the text. The second relates to the diffusion profile within the gel environment and ultimately the systems sensitivity. The diffusion characteristics of small molecules within solutions and gels are relatively well described in the literature (Wesselingh, 1993; Westrin et al., 1994). However, the impact of molecular diffusion within the gels used in reverse iontophoresis has so far been examined in only a limited number of studies (Künzelmann & Böttcher, 1997; Kurnik et al., 1998).

Let us first consider what happens within existing reverse iontophoresis gels. The molecule of interest is extracted across the skin and collects in a gel reservoir. At some point following application of the current, the molecule will have reached a level that is detectable using an embedded sensor. The first point to make is that this introduces a lag time, meaning that the sensor response will be delayed. Figure 6 illustrates this concept in practice for a hydroxypropylmethylcellulose gel reservoir of approximately 5mm depth, with an embedded glucose biosensor at the bottom of the gel reservoir which we developed for testing gel behaviour (McColl, 2001). The time between addition of glucose to the gel surface and the first sensor response can be as much as one hour (Fig 6(b)). The use of a reduced gel concentration, with a consequent increase in the diffusion coefficient (from 2.44 x 10^{-11} to 6.87 x 10^{-11} m^2 / s), reduces this lag time to around 30 minutes (Fig6 (a)).

The time required for accurate detection will be related to gel volume, diffusion coefficient, molecule size and mobility, and gel thickness. Since the properties of the parameter of interest are necessarily fixed, modification of the gel properties is the main option for improving detection performance. We have shown in Figure 6 that diffusion time can be reduced by selecting a gel with a high diffusion coefficient. In addition, reducing gel volume and thickness will also reduce lag time. Indeed, lag times of 5-10 minutes were reported in an experimental study, which examined glucose diffusion in the type of thin gel layers (127μm) used in the Glucowatch (Kurnik et al., 1998). Future designs are likely to make use of gel printing technology which will enable the manufacture of very thin gel layers to reduce measurement lag time. This will also lead to enhanced sensitivity by reducing the dilution of the molecule in the gel reservoir. Taken together with the developments in enhanced skin permeation methods described earlier, advances in this area may help pave the way for near zero current, diffusion dominated transdermal extraction systems.

A second important element of diffusion in transdermal systems is the diffusion profile of the analyte to the sensor. It is important to work on the sensor design to enhance diffusion sensor profiles at the sensor interface and to calibrate the sensor carefully in situ. The gel improvements described above may be sufficient for the continuous detection of molecules where the concentration is relatively unchanging over short time periods (hours). As an example, it can be envisaged that for a molecule of relatively constant concentration, such as sodium, measurement within the gel could take place after a specified time, t, and the blood concentration inferred by a relatively simple algorithm based on an initial calibration. However, for molecules such as glucose, there is high variability in the blood levels of the molecule which can change rapidly over a period of minutes (Pickup and Williams, 1997). Since the diffusion profile of the molecule through the gel is essentially uncontrolled in

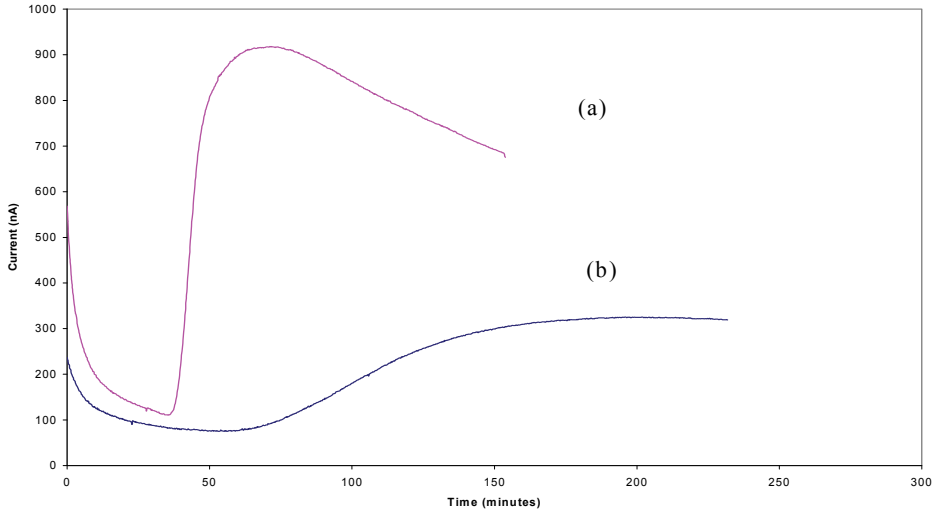

Fig. 6. Anodic current recorded from 2 individual electrodes in 2% HPMC gel (a) and 4% HPMC gel (b). At time zero, glucose was added to one end of the gel slab. The profile indicates the glucose dependent amperometric response observed at a sensor positioned at the opposite end of the gel slab.

existing systems, this means that continuous measurement and responses to rapid reductions/increases are difficult to measure. It is in this context that more sophisticated gel extraction systems are called for in the future.

5.2.4 Calibration

Whatever the parameter to be measured, it is clear that what is measured at the skin surface must provide an indication of the blood level of the molecule. Most reverse iontophoresis-based detection systems developed to date have relied on calibration of the device with the use of a finger stick blood sample. In recent years, research effort has been dedicated to the use of what is collectively known as an 'internal standard'. The basic requirement for an internal standard is that it must be small enough to be extracted using reverse iontophoresis, and that its concentration within blood should be relatively unchanging, and independent of the molecule of interest. The internal standard was first proposed in 1993 (Numajiri et al., 1993). Since then, there have been several alternative molecules proposed (Leboulanger et al., 2004; Sieg et al., 2004a; Sieg et al., 2003; Sieg et al., 2004b). Of these, the most widely studied to date has been sodium. Sodium is a small, and highly mobile, cation that is present in blood at a concentration of around 133mM. It has been examined as an internal standard for glucose measurement calibration in a previous *in vitro* study (Sieg et al., 2003). Using excised porcine ear skin, it was shown that the ratio of sodium to glucose fluxes was correlated to the concentration of glucose within the test chamber, indicating the potential utility of sodium to act as an internal standard for sample free glucose calibration. However, in the subsequent follow up study in a selected set of human volunteers (n=12) it was found that the promising correlations observed *in vitro* were not replicated *in vivo*, with the authors concluding that, "sodium, as the major charge carrier across the skin is not very sensitive to relatively subtle differences in skin

charge. As such it is a less than ideal internal standard for glucose monitoring."(Sieg et al., 2004a). In the same study, it was reported that potassium flux varied among individuals and within the same experiment although no data were provided. The reasons for the apparent failure of sodium as an internal standard remain to be elucidated, and we will return to this later in this chapter.

5.3 Reverse Iontophoresis – future prospects

In the above discussion, we have outlined limitations around comfort, irritation, sensitivity, and calibration with reverse iontophoresis systems developed to date. We will now go on to describe some of the most recent technical solutions that are being developed in response to these limitations.

There are several possible approaches whereby the current level used in reverse iontophoresis may be reduced. One potential method of achieving this is through the use of permeability enhancers. If the permeability of the skin is increased then a greater flux of the analyte can move across the skin for detection. In the case of reverse iontophoresis, this provides the opportunity for a reduction in the amount of current required for analyte extraction. There are many methods that can be used to achieve this, including chemical, mechanical, and electrical permeation enhancement methods. There are many different chemical enhancers used, with varying mechanisms of action. It is beyond the scope of the present discussion to go into each method in detail, and the reader is referred to a review of the area by Thong et al., 2007, which outlines the range of chemicals commonly used, and provides a list of FDA approved skin patches utilizing this approach for transdermal drug delivery (Thong et al., 2007). Mechanical permeation enhancement has been described previously in the text and includes: ultrasound; radiofrequency ablation; and epidermal tape stripping (Lademann & Hadzija, 2009; Ruddy et al., 1995). Iontophoresis and Electroporation lie within the realm of electrical permeation methods and have been also been described elsewhere. The synergistic use of a variety of the above enhancement methods has been well documented in the literature (Mitragotri, 2000).

In identifying further opportunities for improvements to transdermal technologies, and minimally invasive sensing more generally, it is instructive to revisit the concept of the internal standard and to consider the reasons why no candidate has yet proven successful in a commercial device. We have previously described the *in vivo* study by Sieg et al., 2004a, which demonstrated that sodium could not reliably be used as an internal standard for glucose measurement by reverse iontophoresis. Despite sodium flux being constant across all subjects, the glucose flux was an order of magnitude lower in 4 out of the 12 subjects studied. In addition, the constant sodium flux observed in the same subject over the course of a year did not reflect the high variation in glucose flux observed, over the same period in the same subject. Specifically, large decreases in electroosmosis were observed in the winter months. One potential explanation for the discrepancy between glucose and sodium fluxes is that the barrier properties of the skin are not constant between subjects and can indeed be variable from day to day within the same person. The question is therefore, how can such variations in skin permeability to different molecules be controlled for?

5.3.1 Skin permeability

Skin is a highly complex barrier, and it is well known that human skin permeability is highly variable (Cevc & Vierl, 2010; Cornwell & Barry, 1995). Large differences in

permeability can be observed between different body sites on an individual. In addition to this intra-individual variability there also exists an additional large inter-individual variability. For example, significant differences exist between individuals of different race, age, gender etc. Differences in skin permeability can be at least partially explained by structural factors such as stratum corneum thickness, intercellular lipid composition and the density of skin appendages. *In vivo*, biological factors such as skin metabolism and skin surface temperature may also have an impact. Finally, as well as naturally existing skin differences, individuals treat their skin with a variety of soaps moisturisers and other cosmetics. Given that skin permeability is crucial for reverse iontophoresic transport, and that this parameter is highly variable, then it is highly likely that accurate calibration will only be achieved by controlling for this variable.

There are a variety of non- or minimally-invasive methods that are available to characterise variations in skin properties. These have been the subject of review elsewhere, and have been summarized in this current chapter. A detailed description of the routes of in-vivo molecular transport across human skin, with a focus on the influence of iontophoresis was provided by Riveiere & Heit, 1997. The following discussion will consider the utility of impedance measurements, and will be focused within the context of calibrating transdermal extraction processes. The discussion will then be broadened out to the use of impedance in other minimally invasive monitoring and diagnostic applications, including hydration monitoring, and cancerous tissue detection, before concluding with a brief exploration of other similar technologies for measuring tissue properties minimally invasively which are useful in diagnostics and patient monitoring.

The human body is made up of trillions of cells containing, and surrounded by, electrolyte solutions of multiple cations and anions (sodium and chloride are the most abundant). The lipid membranes of these cells together with the proteins and fats of the body form a complex electrical domain worthy of study and characterization in the quest to understand person to person tissue variability.

5.3.2 Skin impedance calibration

The electrical impedance of the skin is dominated by two components, resistance and capacitance. Skin impedance is represented mathematically as a phasor quantity, or as two components represented by real and imaginary numbers. In its simplest form we can think of the real term as accounting for resistive elements in the skin, and the imaginary term as largely representing capacitative features of the tissue. It is a field of study in its own right and the reader is referred to two review articles, which serve as a useful introduction to the technique and how it can be applied in medicine (Rigaud et al., 1996; Valentinuzzi, 1996). For the purposes of the current chapter, it is sufficient to recognize that the values of the real and imaginary components are dependent on the properties and structures of the underlying biological tissue. When this concept is applied to skin, we see that different elements in the skin give rise to different components of the overall impedance signal. For example, the sweat glands and hair follicles are predominantly resistive in nature, whilst the lipid laden regions of the dermis are dominantly capacitive in nature. The skin can therefore be modeled as a series of resistors and capacitors (Figure 7). Applying this model to skin, it is easy to see how the skin impedance is dependent on a whole host of anatomical and physiological variables within the skin structure.

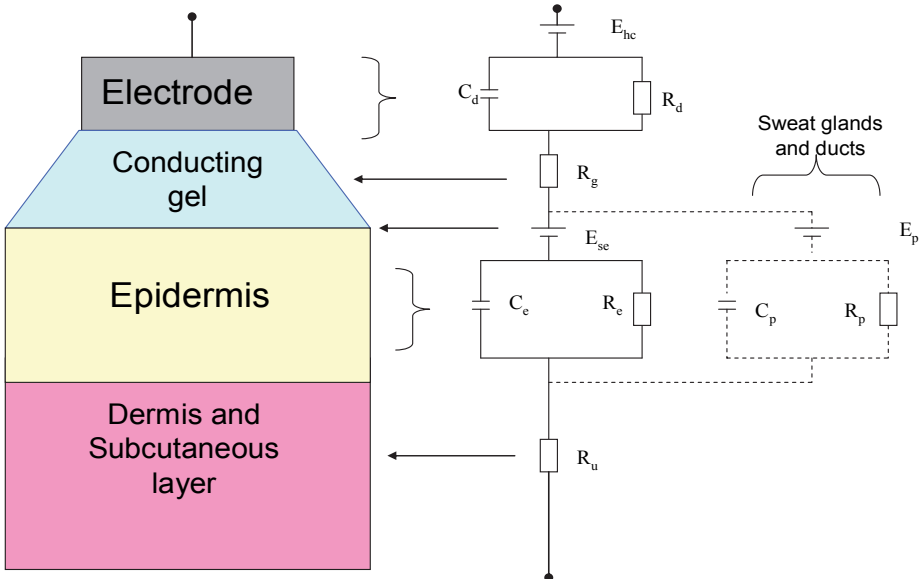

Ehc – electrode half cell potential, Cd and Rd – electrode double layer capacitance and resistance, Rg - gel resistance, Ese – potential due to ionic differences between gel and stratum corneum (SC), Ep - potential developed due to skin pores (release of ions in sweat), Ce and Re – capacitance and resistance of SC, Cp and Re – capacitance and resistance of skin pores, Rg – dermis and subcutaneous resistance.

Fig. 7. One representation of how skin can be modeled electrically.

Our specific interest has been in examining how skin impedance might be usefully deployed in the calibration of minimally invasive transdermal sensing applications. Briefly, we consider that the flux, F, of any given molecule across the skin will be a function of skin permeability, P, such that,

$$F = C \times P + k$$

Where C is the molecule concentration in blood/interstitial fluid, and k is a constant to be determined.

Given the impracticality of measuring P in people, we have been investigating if various impedance derived parameters (Z values), taken from measurements of human skin *in vivo* can be used to provide an indication of the variation in P from person to person and day to day. Our results indicate that this approach may be able to provide individual permeability values that are parameter and person specific, thus removing the requirement for the time consuming and often invasive calibration methods which are limitations of all existing transdermal monitoring devices. In one recent study in diabetic patients completed in 2009, we have shown that the rate of transdermal potassium flux collected in the gel of iontophoresis electrodes placed on the skin of a diabetic patient can be directly related to a normalized impedance parameter, measured through the same

electrodes. Figure 8 shows that the normalized impedance on patient skin can be correlated with transdermal flux. This opens the debate again on the possible uses of electrolytes as internal standards that can be used to calibrate iontophoresis systems for skin permeability and transdermal extractions.

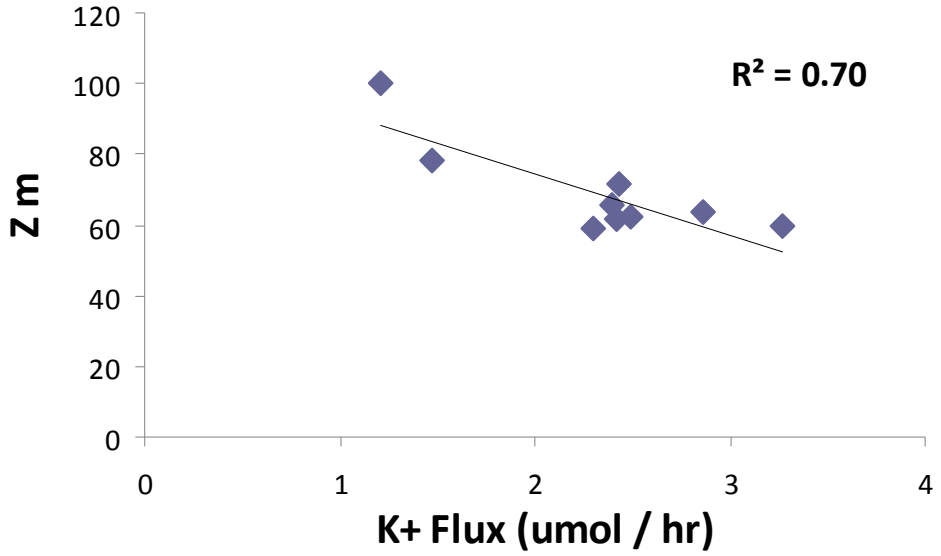

Fig. 8. Normalised impedance parameter, Zm, versus transdermal potassium ion flux in a Type II Diabetes patient group (n = 9).

6. Conclusion

Demand for clinical diagnostics in the home and community will grow as disease states develop in an increasingly aged world population. As yet biosensors have not overcome the challenges that host responses to implantation generate for sensor systems and therefore long term implantation of sensors for diagnostic monitoring is not a reality. Minimally invasive monitoring via the transdermal route is open to further development for wearable or point of care systems and combining know how from drug delivery research and miniaturised sensors opens new possibilities in device design for clinical monitoring. A key aspect of successful deployment of devices in this field will be the creation of multidisciplinary working groups that cross the clinical interface and the resolution of issues around calibration of devices.

7. References

Acierno, MJ, Johnson, ME, Eddleman, LA, Mitchell, MA (2008) Measuring statistical agreement between four point of care (POC) lactate meters and a laboratory blood analyzer in cats. *Journal of Feline Medicine & Surgery* 10 (2): 110-114

Arora, A, Prausnitz, MR, Mitragotri, S (2008) Micro-scale devices for transdermal drug delivery. *Int J Pharm* 364(2): 227-236.

Badugu, R, Lakowicz, JR, Geddes, CD (2005) Fluorescence sensors for monosaccharides based on the 6-methylquinolinium nucleus and boronic acid moiety: potential application to ophthalmic diagnostics. *Talanta* 65(3): 762-768.

Badugu R, Lakowicz JR, and Geddes CD (2003) A Glucose Sensing Contact Lens: A Non-Invasive Technique for Continuous Physiological Glucose Monitoring. *Journal of Fluorescence* 13 (5)

Cancel, LM, Tarbell, JM, Ben-Jebria, A (2004) Fluorescein permeability and electrical resistance of human skin during low frequency ultrasound application. *Journal of pharmacy and pharmacology* 56: 1109–1118

Cevc, G, Vierl, U (2010) Nanotechnology and the transdermal route: A state of the art review and critical appraisal. *Journal of Controlled Release* 141(3): 277-299.

Ching, CTS, Buisson, Y, Connolly, P (2008a) The effect of pulsed bipolar dc on the simultaneous extraction of glucose and lactate by reverse iontophoresis. *Sensors and Actuators B: Chemical* 129(2): 504-509.

Ching, TS, Connolly, P (2008b) Simultaneous transdermal extraction of glucose and lactate from human subjects by reverse iontophoresis. *Int J Nanomedicine* 3(2): 211-223.

Chizmadzhev, YA, Indenbom, AV, Kuzmin, PI, Galichenko, SV, Weaver, JC, Potts, RO (1998) Electrical properties of skin at moderate voltages: contribution of appendageal macropores. *Biophys J* 74(2 Pt 1): 843-856.

Cornwell, PA, Barry, BW (1995) Effects of penetration enhancer treatment on the statistical distribution of human skin permeabilities. *International Journal of Pharmaceutics* 117(1): 101-112.

Cox, M (2009) An Overview of Continuous Glucose Monitoring Systems. *Journal of Pediatric Health Care* 23 (5): 344-347

Curdy, C, Kalia, YN, Guy, RH (2001) Non-invasive assessment of the effects of iontophoresis on human skin in-vivo. *J Pharm Pharmacol* 53(6): 769-777.

Curdy, C, Kalia, YN, Guy, RH (2002) Post-iontophoresis recovery of human skin impedance *in vivo*. *European Journal of Pharmaceutics and Biopharmaceutics* 53(1): 15-21.

Daniel, KD, Kim, GY, Vassiliou, CC, Galindo, M, Guimaraes, AR, Weissleder, R, Charest, A, Langer, R, Cima, MJ (2009) Implantable diagnostic device for cancer monitoring. *Biosens Bioelectron* 24(11): 3252-3257.

Delgado-Charro, MB, Guy, RH (1994) Characterization of convective solvent flow during iontophoresis. *Pharm Res* 11(7): 929-935.

Delgado-Charro, B, Rodriguez-Bayn AM, Richard H. Guy (2005) Iontophoresis of nafarelin: effects of current density and concentration on electrotransport *in vitro*. *Journal of Controlled Release* 35: 35—40

Escobar-Chavez, JJ, Bonilla-Martinez, D, Villegas-Gonzalez, MA, Rodriguez-Cruz, IM, Dominguez-Delgado, CL (2009) The use of sonophoresis in the administration of drugs throughout the skin. *J Pharm Pharm Sci* 12(1): 88-115.

Ferrante do Amaral, CE, Wolf, B (2008) Current development in non-invasive glucose monitoring. *Medical Engineering & Physics* 30(5): 541-549.

Gifford, R, Kehoe, JJ, Barnes, SL, Kornilayev, BA, Alterman, MA, Wilson, GS (2006) Protein interactions with subcutaneously implanted biosensors. *Biomaterials* 27(12): 2587-2598.

Girardin, CM, Huot, C, Gonthier, M, Delvin, E (2009) Continuous glucose monitoring: a review of biochemical perspectives and clinical use in type 1 diabetes. *Clin Biochem* 42(3): 136-142.

Howard, JP, Drake, TR, Kellogg, DL, Jr. (1995) Effects of alternating current iontophoresis on drug delivery. *Arch Phys Med Rehabil* 76(5): 463-466.

HSBC Global Research (2006) Medtronic, Diabetes: sizing the market for real time continuous glucose monitors. HSBC Research, 22 June 2006 http://www.research.hsbc.com/midas/Res/RDV?p=pdf&key=ate2b8rygn&name=127057.PDF

Kissinger, PT (2005) Biosensors-a perspective. *Biosens Bioelectron* 20(12): 2512-2516.

Künzelmann, U, Böttcher, H (1997) Biosensor properties of glucose oxidase immobilized within SiO2 gels. *Sensors and Actuators B: Chemical* 39(1-3): 222-228.

Kost J, Mitragotri S, Gabbay RA, Pishko M, Langer R. Transdermal monitoring of glucose and other analytes using ultrasound. *Nat Med* 2000; 6: 347–350.

Kulcu, E, Tamada, JA, Reach, G, Potts, RO, Lesho, MJ (2003) Physiological differences between interstitial glucose and blood glucose measured in human subjects. *Diabetes Care* 26(8): 2405-2409.

Kurnik, RT, Berner, B, Tamada, J, Potts, RO (1998) Design and Simulation of a Reverse Iontophoretic Glucose Monitoring Device. *Journal of The Electrochemical Society* 145(12): 4119-4125.

Lademann, J, Jacobi, U, Surber, C, Weigmann, HJ, Fluhr, JW (2009) The tape stripping procedure--evaluation of some critical parameters. *Eur J Pharm Biopharm* 72(2): 317-323.

Leboulanger, B, Guy, RH, Delgado-Charro, MB (2004) Non-invasive monitoring of phenytoin by reverse iontophoresis. *Eur J Pharm Sci* 22(5): 427-433.

Ledger, PW Skin biological issues in electrically enhanced transdermal delivery. *Advanced Drug Delivery Reviews* 9(2-3): 289-307.

Liberty, HJ, Johnson, BD, Fortner, N, Randolph, D (2003) Detecting crack and other cocaine use with fastpatches. *Addict Biol* 8(2): 191-200.

Liu, H, Li, H, Ying, T, Sun, K, Qin, Y, Qi, D (1998) Amperometric biosensor sensitive to glucose and lactose based on co-immobilization of ferrocene, glucose oxidase, [beta]-galactosidase and mutarotase in [beta]-cyclodextrin polymer. *Analytica Chimica Acta* 358(2): 137-144.

Manabe, E, Numajiri, S, Sugibayashi, K, Morimoto, Y (2000) Analysis of skin permeation-enhancing mechanism of iontophoresis using hydrodynamic pore theory. *Journal of Controlled Release* 66 (2-3): 149-158

Marbach, R, Koschinsky, Th, Gries, FA, Heise, HM (1993) Noninvasive Blood Glucose Assay by Near-Infrared Diffuse Reflectance Spectroscopy of the Human Inner Lip. *Applied Spectroscopy* 47 (7): 875-881

McColl, D (2001) A glucose biosensor for a hydrogel environment. University of Strathclyde, MSc Thesis

Meurin, Ph, Tabet, JY, Monchi, M, Weber, H, Fabre, C, Gibier, B, Renaud, N Ben Driss, A (2009) Accuracy of a portable international normalized ratio monitor for patients receiving a low molecular weight heparin as a bridge pending full oral anticoagulant efficacy. *Thrombosis Research* 125 (2): 192-195

Mitragotri, S, Coleman, M, Kost, J, Langer, R (2000) Transdermal extraction of analytes using low-frequency ultrasound. *Pharm Res* 17(4): 466-470

Mitragotri, S (2000) Synergistic effect of enhancers for transdermal drug delivery. *Pharm Res* 17(11): 1354-1359.

Moschou, EA, Sharma, BV, Deo, SK, Daunert, S (2004) Fluorescence Glucose Detection: Advances Toward the Ideal *In vivo* Biosensor. *Journal of Fluorescence* 14 (5): 535-47

Mukerjee, EV, Collins, SD, Isseroff, RR, Smith, RL (2004) Microneedle array for transdermal biological fluid extraction and in situ analysis. *Sensors and Actuators A: Physical* 114(2-3): 267-275.

Newman, JD, Turner, AP (2005) Home blood glucose biosensors: a commercial perspective. *Biosens Bioelectron* 20(12): 2435-2453.

Numajiri, S, Sugibayashi, K, Morimoto, Y (1993) Non-invasive sampling of lactic acid ions by iontophoresis using chloride ion in the body as an internal standard. *J Pharm Biomed Anal* 11(10): 903-909.

N. S. Oliver, C. Toumazou, A. E. G. Cass and D. G. Johnston (2009) Glucose sensors: a review of current and emerging Technology, Diabetic Medicine, 26(3): 197-210

Pantelopoulos, A, Bourbakis, NG (2010) A Survey on Wearable Sensor-Based Systems for Health Monitoring and Prognosis. *Systems, Man, and Cybernetics, Part C: Applications and Reviews, IEEE Transactions on* 40(1): 1-12.

Pellett, MA, Hadgraft, J, Roberts, MS (1999) The back diffusion of glucose across human skin *in vitro*. *International Journal of Pharmaceutics* 193(1): 27-35.

Pickup, JC, Williams, G (1997) Textbook of Diabetes 2nd Edition. Blackwell Science Ltd, Oxford

Pickup, JC, Hussain, F, Evans, ND, Rolinski, OJ, Birch, DJ (2005) Fluorescence-based glucose sensors. *Biosens Bioelectron* 20(12): 2555-2565.

Posnett, J, Franks, PJ (2008) The burden of chronic wounds in the UK. *Nurs Times* 104(3): 44-45.

Rigaud, B, Morucci, JP, Chauveau, N (1996) Bioelectrical impedance techniques in medicine. Part I: Bioimpedance measurement. Second section: impedance spectrometry. *Crit Rev Biomed Eng* 24(4-6): 257-351.

Riviere, JE, Heit, MC (1997) Electrically-assisted transdermal drug delivery. *Pharm Res* 14(6): 687-697.

Ruddy, SB, Hadzija, BW (1995) The role of stratum corneum in electrically facilitated transdermal drug delivery. I. Influence of hydration, tape-stripping and

delipidization on the DC electrical properties of skin. *Journal of Controlled Release* 37(3): 225-238.

Saby, C, Mizutani, F, Yabuki, S (1995) Glucose sensor based on carbon paste electrode incorporating poly(ethylene glycol) -modified glucose oxidase and various mediators. *Analytica Chimica Acta* 304(1): 33-39.

Santi, P, Guy, RH (1996a) Reverse iontophoresis -- parameters determining electro-osmotic flow. II. Electrode chamber formulation. *Journal of Controlled Release* 42(1): 29-36.

Santi, P, Guy, RH (1996b) Reverse iontophoresis -- Parameters determining electroosmotic flow: I. pH and ionic strength. *Journal of Controlled Release* 38(2-3): 159-165.

Sato, N, Okuma, H (2006) Amperometric simultaneous sensing system for d-glucose and l-lactate based on enzyme-modified bilayer electrodes. *Analytica Chimica Acta* 565(2): 250-254.

Schrader, W, Meuerb, P, Popp, J, Kiefer, W, Menzebach, JU, Schrader, B (2005) Non-invasive glucose determination in the human eye. Journal of Molecular Structure 735–736: 299–306

Sieg, A, Guy, RH, Delgado-Charro, MB (2004a) Noninvasive glucose monitoring by reverse iontophoresis *in vivo*: application of the internal standard concept. *Clin Chem* 50(8): 1383-1390.

Sieg, A, Guy, RH, Delgado-Charro, MB (2003) Reverse iontophoresis for noninvasive glucose monitoring: the internal standard concept. *J Pharm Sci* 92(11): 2295-2302.

Sieg, A, Guy, RH, Delgado-Charro, MB (2004b) Simultaneous extraction of urea and glucose by reverse iontophoresis *in vivo*. *Pharm Res* 21(10): 1805-1810.

Sieg, A, Jeanneret, F, Fathi, M, Hochstrasser, D, Rudaz, S, Veuthey, JL, Guy, RH, Delgado-Charro, MB (2009) Extraction of amino acids by reverse iontophoresis *in vivo*. *Eur J Pharm Biopharm* 72(1): 226-231.

Sintov, AC, Krymberk, I, Daniel, D, Hannan, T, Sohn, Ze, Levin, G (2003) Radiofrequency-driven skin microchanneling as a new way for electrically assisted transdermal delivery of hydrophilic drugs. *Journal of Controlled Release* 89(2): 311-320.

Tamada, JA, Bohannon, NJ, Potts, RO (1995) Measurement of glucose in diabetic subjects using noninvasive transdermal extraction. *Nat Med* 1(11): 1198-1201.

Tezel A, Sens A, Tuchscherer J, Mitragotri S (2001) Frequency Dependence of Sonophoresis. *Pharmaceutical Research* (18) 12: 1694-1700

Thong, HY, Zhai, H, Maibach, HI (2007) Percutaneous penetration enhancers: an overview. *Skin Pharmacol Physiol* 20(6): 272-282.

Tierney, MJ, Tamada, JA, Potts, RO, Jovanovic, L, Garg, S (2001) Clinical evaluation of the GlucoWatch biographer: a continual, non-invasive glucose monitor for patients with diabetes. *Biosens Bioelectron* 16(9-12): 621-629.

Tura, A, Maran, A, Pacini, G (2007) Non-invasive glucose monitoring: assessment of technologies and devices according to quantitative criteria. *Diabetes Res Clin Pract* 77(1): 16-40.

Turner, APF, Karube, I, Wilson, GS, Worsfold, PJ (1987) Biosensors: fundamentals and applications : OUP, Oxford, 1987 (ISBN 0-19-854724-2). xvi+770 pp. Price £60.00. *Analytica Chimica Acta* 201: 363-364.

Ueda, H, Sugibayashi, K, Morimoto, Y (1995) Skin penetration-enhancing effect of drugs by phonophoresis. *Journal of Controlled Release* 37(3): 291-297.

Uemura, N, Harkey, MR, Nath, RP, Henderson, GL, Mendelson, JE, Jones, RT (2004) Delayed disposition of cocaine in sweat patches and in skin blister: cocaine may migrate from plasma to sweat patches via interstitial fluid. *Clin Pharmacol Ther* 75(2): P44-P44.

UK Prospective Diabetes Study Group (1998a) Effect of intensive blood-glucose control with metformin on complications in overweight patients with type 2 diabetes (UKPDS 34). *The Lancet* 352(9131): 854-865.

UK Prospective Diabetes Study Group (1998b) Efficacy of atenolol and captopril in reducing risk of macrovascular and microvascular complications in type 2 diabetes: UKPDS 39. *BMJ* 317(7160): 713-720.

UK Prospective Diabetes Study Group (1998c) Intensive blood-glucose control with sulphonylureas or insulin compared with conventional treatment and risk of complications in patients with type 2 diabetes (UKPDS 33). *The Lancet* 352(9131): 837-853.

UK Prospective Diabetes Study Group (1998d) Tight blood pressure control and risk of macrovascular and microvascular complications in type 2 diabetes: UKPDS 38. *BMJ* 317(7160): 703-713.

U.S. Food and Drugs Adminstration, Summary of safety and effectiveness, in Pre Market Approval, P990026, 01 April 2011, http://www.accessdata.fda.gov/cdrh_docs/pdf/P990026b.pdf

U.S. Food and Drugs Adminstration, Summary of safety and effectiveness, in Pre Market Approval, P990026S008b, 01 April 2011, http://www.accessdata.fda.gov/cdrh_docs/pdf/P990026S008b.pdf

Vaddiraju, S, Tomazos, I, Burgess, DJ, Jain, FC, Papadimitrakopoulos, F (2010) Emerging synergy between nanotechnology and implantable biosensors: a review. *Biosens Bioelectron* 25(7): 1553-1565.

Valentinuzzi, ME (1996) Bioelectrical impedance techniques in medicine. Part I: Bioimpedance measurement. First section: general concepts. *Crit Rev Biomed Eng* 24(4-6): 223-255.

Vanbever, R, Preat, VV (1999) *In vivo* efficacy and safety of skin electroporation. *Adv Drug Deliv Rev* 35(1): 77-88.

Walsh, JM, Terdiman, JP (2003) Colorectal cancer screening: scientific review. *JAMA* 289(10): 1288-1296.

Watt, BE, Proudfoot, AT, Vale, JA (2004) Hydrogen peroxide poisoning. *Toxicol Rev* 23(1): 51-57.

Wesselingh, JA (1993) Controlling diffusion. *Journal of Controlled Release* 24(1-3): 47-60.

Westrin, BA, Axelsson, A, Zacchi, G (1994) Diffusion measurement in gels. *Journal of Controlled Release* 30(3): 189-199.

Wickramasinghe, Y, Yang, Y, Spencer, SA (2004) Current problems and potential techniques in *in vivo* glucose monitoring. *J Fluoresc* 14(5): 513-520.

WHO, 2004. Diabetes Action Now: an Initiative of the World Health Organisation and the International Diabetes Federation. WHO, Geneva, Switzerland.

WHO, 2006. The Global Burden of Disease 2004-Update. WHO, Geneva, Switzerland.Lima.

WHO, 2008, The World Health Report 2008 - primary Health Care (Now More Than Ever). WHO, Geneva, Switzerland.

19

Biosensors for Monitoring Autophagy

Dalibor Mijaljica, Carlos J Rosado, Rodney J Devenish and Mark Prescott
Monash University, Department of Biochemistry and Molecular Biology
Victoria
Australia

1. Introduction

1.1 Prologue

Autophagy ("self-eating") is a highly conserved intracellular degradation process. Recently, an astonishing number of connections to human physiology and disease for autophagy have been made. Thus, autophagy plays a critical role during development and differentiation, in cancer, neurodegeneration, combating viral and microbial infections, and has been linked to life span extension and ageing. For these reasons, the ability to follow autophagy in living mammalian cells is of particular interest, both in terms of developing better understanding at a mechanistic level and in terms of possible future clinical applications.

In this chapter our intention is not to summarise the available autophagy assays, but to highlight the application of biosensors used to monitor autophagic processes in live cells. Firstly, we briefly outline current knowledge about the molecular mechanism and function of autophagy (Section 1.2). Then, we outline how autophagy can be measured in live cells in a non-invasive manner and indicate some of the advantages and disadvantages of the biosensor-based assays of autophagy currently in use (Section 2). In particular we focus here on the design and use of Rosella - a dual wavelength emission biosensor based on a fusion of fluorescent proteins whose use exploits alterations in pH during autophagy. The advantages of this approach will be highlighted (Section 2.3) and illustrated by applications to follow autophagy both in yeast, an important eukaryotic model organism (Section 2.3.1) and mammalian cells (Section 2.3.2). Finally, we address the future prospects for application of alternative approaches (Section 3) to the measurement of autophagy based on the use of novel probes.

1.2 Autophagy - different pathways, mechanism and selectivity

The biological importance of autophagy is such that the molecular mechanism is the focus of intense research efforts (reviewed in Yang & Klionsky, 2010). Three distinct autophagic pathways have been shown to operate in eukaryotic cells namely, macroautophagy, microautophagy and chaperone-mediated autophagy-CMA (Orenstein & Cuervo, 2010). In order to understand the rationale of biosensor design and function it is necessary to have a basic understanding of the particular process to be monitored. The key aspects of each of the three different forms of autophagy are shown in **Fig. 1**.

The morphological hallmark of macroautophagy (hereafter referred as autophagy) is the formation of a double-membrane structure called an autophagosome, encapsulating the

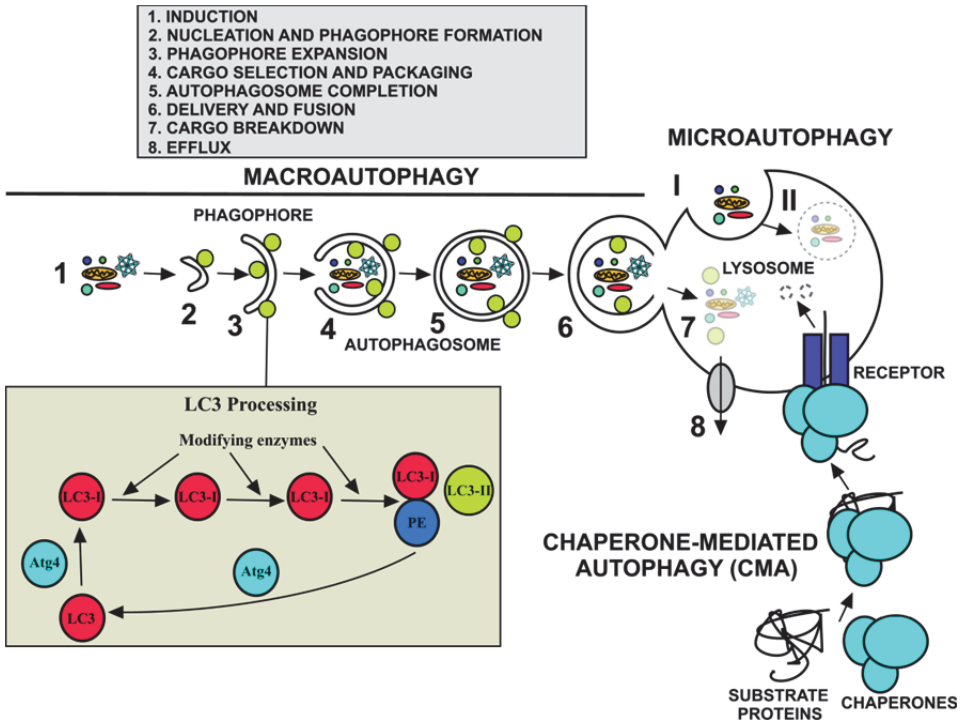

Fig. 1. Three main types of autophagy.
Three morphologically and mechanistically distinct types of autophagy have been described in cells: macroautophagy, microautophagy and chaperone-mediated autophagy (CMA). Microautophagy is best described in yeast cells and CMA is restricted to mammalian cells. The degradative vacuole in yeast cells is large, whereas the lysosomes are much smaller and far more numerous. In this diagram the lysosome is not drawn to scale in order to illustrate the three processes that deliver material to it. Microautophagy can be considered a two-step process: lysosomal membrane invagination (I) followed by cargo breakdown (II). The individual steps of macroautophagy are numbered (see shaded box for key). Inset (LC3 processing) summarises the steps leading to the recruitment of LC3-II (green spheres) to the forming autophagosome. Completed autophagosomes fuse with lysosomes, after which LC3-II on the cytoplasmic face of autolysosomes is delipidated through the activity of Atg4 and recycled. LC3-II located on the internal surface of autophagosomes is degraded in the autolysosomes. The association of LC3-II with autophagosomes has been widely exploited as a marker for autophagy. LC3, microtubule-associated protein 1 light chain 3; PE, phosphatidylethanolamine.

material for degradation (reviewed in Xie & Klionsky, 2007). The pathway consists of a number of distinct steps and includes: (1) induction, (2) nucleation and phagophore formation, (3) phagophore expansion, (4) cargo selection and packaging, (5) autophagosome completion, (6) cargo delivery and fusion of the autophagosome with the lysosome/vacuole, (7) breakdown of the sequestered cargo and (8) efflux (reviewed in Lagakis & Klionsky, 2006) **(Fig. 1)**. Upon autophagy induction, that is tightly regulated by Tor (target of

rapamycin kinase), a double membrane structure termed the phagophore is initiated and expands to engulf the cargo. The sequential expansion of the phagophore allows the cell to adjust the size of the autophagosome to sequester cellular components over a wide size range and can include organelles such as a mitochondrion (reviewed in He & Klionsky 2009; Kanki & Klionsky, 2010). The ends of the phagophore membrane fuse to form the autophagosome, thereby, sequestering the cargo from the rest of the cell. The outer-membrane of the autophagosome then fuses with the membrane of the lysosome (mammalian cells) or the vacuole (yeast cells) to deliver the cargo into to the acidic lumen (~pH 4.5-6). Cargo is degraded through the action of resident hydrolases to basic polymer building blocks (e.g., nucleotides, amino acids, sugars) which are exported to the cytosol for recycling by the cell (reviewed in Yorimitsu & Klionsky, 2005).

Autophagy is regulated by the autophagy-related genes (*ATG*) together with some other particular gene products required for selective sequestration and degradation of specific cargos (see below). Among the 35 *ATG* genes identified through pioneering studies in yeast, 15 are required for core autophagy functions, while others play particular roles in one or more types of autophagy (reviewed in Kanki & Klionsky, 2010). Homologues for many of these genes (~15) have been identified in mammals (Tanida, 2010; Tanida, 2011). Although the order of action and interactions between *ATG* gene products have been determined (reviewed in Legakis & Klionsky, 2006; Chen and Klionsky, 2011) few of the proteins encoded by the *ATGs* have motifs that provide insights into their function, and the precise mechanism of action of many remains unknown.

Nevertheless, details of how a number of individual gene products function in the process is emerging. Some of the gene products act sequentially in two ubiquitin-like conjugation systems (Atg8 and Atg12) that are involved in vesicle expansion and completion (Chen & Klionsky, 2011). *ATG8* and *ATG4* are of particular significance as their gene products have been exploited in a number of assays for autophagy (Section 2.2). In mammals the equivalent genes (of which there are several) encode LC3 (microtubule-associated protein 1 light chain 3) and autophagins (e.g., Atg4b), respectively (Tanida, 2010). LC3 in mammalian cells is immediately modified post-translation by the cysteine protease activity of an autophagin to form LC3-I, a soluble protein found throughout the cytosol. When autophagy is induced LC3-I is lipidated by the addition of PE (phosphatidylethanolamine) to form LC3-II and associates with the phagophore membrane. After completion of the autophagosome and during fusion with the vacuolar/lysosomal membrane, LC3-II is recycled from the outer-membrane by the action of an autophagin. Since LC3-II remains on the inner autophagosome membrane, when fused to GFP it can be used to track fusion of autophagosomes with the lysosomes, if the latter are appropriately labelled **(Fig. 1; Inset)** (reviewed in Mizushima et al., 2010).

Autophagy plays a role in the degradation of a wide range of cellular components, including long-lived proteins, protein complexes and aggregates, macromolecules (ribosomes, lipids), organelles (the endoplasmic reticulum, peroxisomes, the nucleus and mitochondria) and even intracellular pathogens (bacteria and viruses) (reviewed in Klionsky et al., 2007a). Although starvation-induced autophagy is thought to act non-selectively in the degradation of bulk cytoplasm, it can be highly selective in cargo selection. Protein aggregates (Rubinsztein, 2006), nuclear components (Krick et al., 2008; Roberts et al., 2003) or superfluous, damaged/stressed or nutritionally-challenged organelles, such as mitochondria (Kanki et al., 2011; Youle & Narendra, 2011) may be targeted. Selective autophagy is best characterised in yeast (reviewed in Farré et al., 2009; van der Vaart et al.,

2008) and includes other modes not described in mammalian cells such as the cytoplasm to vacuole targeting (Cvt) pathway (reviewed in Lynch-Day & Klionsky, 2010) and the vacuolar import and degradation (vid) pathway (Brown et al., 2010).
Cargo sequestration can take place through microautophagy, but the limiting/sequestering membrane in this case is the vacuolar/lysosomal membrane itself, which invaginates to form tubules or vesicles that pinch off into the lysosomal lumen **(Fig. 1)**. Our current understanding of microautophagy mechanism and regulation is largely based on studies in yeast. Microautophagy remains poorly understood in mammals (Mijaljica et al., 2011; Shpilka & Elazar, 2011).
Delivery of cargo via CMA does not require formation of intermediate vesicle compartments or membrane fusion. Instead, the substrates, soluble proteins, are translocated from the cytosol into the lysosomal lumen directly across the membrane in a process mediated by a translocation protein complex that requires activity of chaperones, substrate unfolding and the presence of receptors on the lysosomal membrane **(Fig. 1)**. CMA occurs only in mammalian cells (reviewed in Orenstein & Cuervo, 2010).

2. Approaches for monitoring autophagy

"Static measurements" of a particular biological process can be limiting in terms of the insights they provide. Autophagy is a complex, highly regulated and dynamic process involving membrane rearrangement events including formation of the autophagosome and fusion of intracellular membranes. Monitoring such dynamic events represents a challenge and biosensors specific for many of the selective forms of autophagy in particular are yet to be developed. The lack of suitable biosensors likely underlies many of the misconceptions in our understanding of the function of autophagy, mammalian autophagy in particular.
Nevertheless, new techniques have been developed both to monitor autophagy as a dynamic process and to modulate autophagy to facilitate probing its function in a given cellular process (reviewed in Klionsky et al., 2008; Mizushima, 2004; Mizushima et al., 2010; Mizushima & Yoshimori, 2007; Rubinsztein et al., 2009). Key components of the molecular mechanism have been identified, many of which have the potential to be exploited as useful reporters **(Fig. 1)**.
As interest in selective modes of autophagy gains momentum, it is increasingly important to have access to probes able to follow events in a selective manner. Since it is likely that some cellular targets are present in only small quantities, biosensors that allow monitoring of autophagy at low levels are required. Such a biosensor is also likely to facilitate the detection of autophagy at early stages after induction. It is often important to follow biological processes in living cells, tissues or organisms requiring the application of non-invasive techniques. Such applications are based commonly on the use of light-based probes that rely on the chemical production of light, or are based on fluorescence emission. Autophagy is a temporally and spatially dynamic process; therefore, it is desirable that biosensor outputs do not persist or accumulate in a way that would prevent successive cycles of activity to be detected. A single ideal biosensor fulfilling each of these requirements has yet to be developed.
Biosensor-based approaches for monitoring autophagy can be considered to fall into either of two major categories **(Fig. 2)**, examples of which have been reported in the literature (reviewed in Klionsky et al., 2007b; Klionsky et al., 2008; Mizushima et al., 2010). In the first category, autophagic activity can be assessed by monitoring the behaviour, modification or activity of key molecules involved in the molecular mechanism of autophagy (Section 2.2).

Alternatively, the fate of the target material itself can be followed either by monitoring delivery to the lysosome/vacuole, or its degradation (Section 2.3). In order to follow the fate of the target material itself, it is crucial to be able to identify or selectively label the target. This can be achieved to a limited extent by visualising characteristic staining patterns of particular targets such as mitochondria or intracellular pathogens using electron microscopy (Klionsky et al., 2007b; Klionsky et al., 2008; Mizushima et al., 2010), or by labelling with dyes suitable for detection by fluorescence microscopy. The scope for labelling autophagic targets is greatly expanded if genetically encoded probes such as fluorescent proteins (FPs) are considered. Genetic fusions of target proteins with FPs can be readily expressed in cells allowing the delivery of targets to the lysosome or vacuole to be tracked using fluorescence microscopy in individual cells. FPs are remarkably stable molecules and persist as

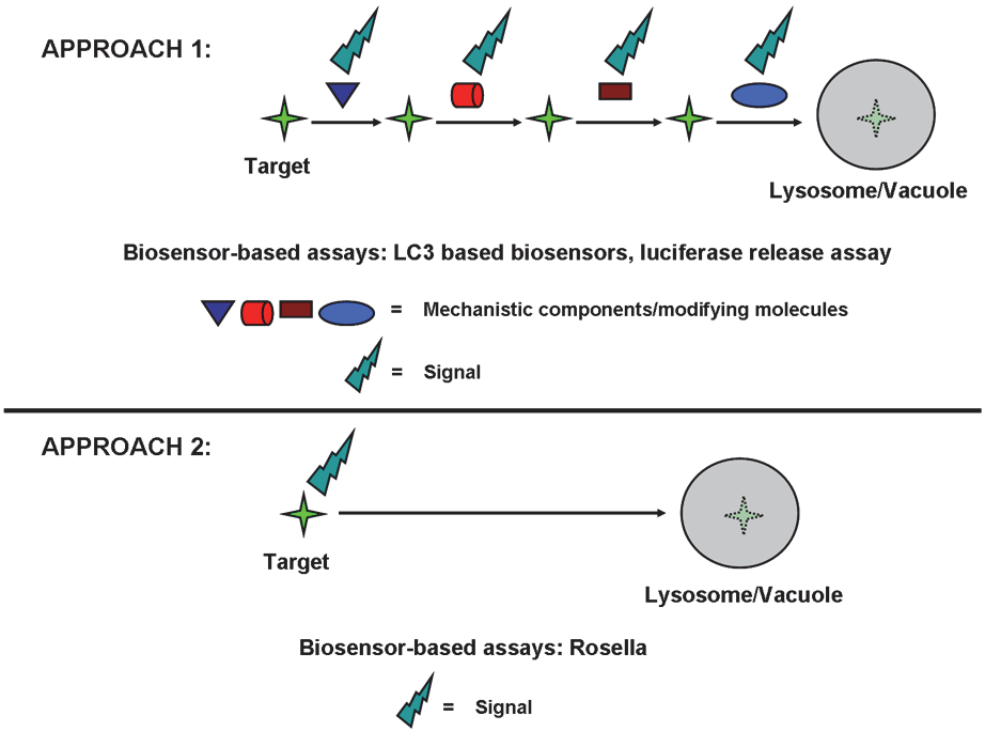

Fig. 2. Approaches for monitoring autophagy.
The molecular mechanism of autophagy may be exploited to monitor the process by tracking the modification or activity of key molecules in the pathway (Approach 1). For example, post-translational modification of LC3 or its recruitment to the autophagosome is commonly used. This approach does not provide information on the identity of the cargo, which must also be labelled if selective forms of autophagy are to be tracked. Alternatively, (Approach 2) labelling the target with a biosensor (e.g., Rosella) that continually senses and reports on the environment of the target material allows for monitoring of selective autophagy. However, this approach does not provide information on the mechanistic aspects of the particular process involved.

fluorescent forms in the degradative organelle long enough to detect their presence (Katayama et al., 2008). Furthermore, the fate of such genetic fusions can be followed in populations of cells using western blots to follow changes in sizes of the fusion produced by proteolytic degradation within the degradative organelle (Mizushima et al., 2010; Klionsky et al., 2008). In specific cases, enzymatic activities can also be used to follow delivery to the lysosome/vacuole (Ketteler et al., 2008; Ketteler & Seed, 2008; Kimura et al., 2007; Klionsky et al., 2007b; Klionsky et al., 2008; Mizushima et al., 2010). As new forms of selective autophagy are reported in the literature approaches that label and follow the target material for autophagy are becoming the focus of attention.

2.1 Fluorescence-based biosensors for monitoring autophagy in live cells

Monitoring autophagic activity or flux in cells, tissues or organs is of considerable interest to many researchers, and is a technology undergoing continual development. In recent years, methods for detection of autophagy suitable for *in vivo* applications have been developed (Ketteler & Seed, 2008; Mizushima et al., 2010). Nevertheless, ideal methods for any one particular application may not yet exist (Klionsky et al., 2008).

In the following section, we describe some of the available biosensors suitable for analysis of autophagy/autophagy-related pathways *in vivo*. These biosensors exploit fluorescent proteins or luciferase as reporters to generate a readily detectable light signal. The first category (as discussed above) exploits Atg8/LC3 and autophagin Atg4b (Section 2.2), key proteins in the molecular mechanism, whilst the second relies on direct labelling of the autophagic cargo (e.g., mitochondria, the nucleus) using the Rosella biosensor (Section 2.3).

2.2 LC3

LC3 (or Atg8 in yeast), fused at its N-terminus to one of a number of different colour FPs including GFP, CFP (Ravikumar et al., 2010) or mCherry (Axe et al., 2008; Klionsky et al., 2008; Mizushima et al., 2010), has been used with great success to monitor autophagy in a number of different model organisms including *Saccharomyces cerevisiae* (Klionsky et al., 2008; Xie et al., 2008), *Caenorhabditis elegans* (Klionsky et al., 2008; Meléndez et al., 2003), *Dictyostelium discoideum* (Klionsky et al., 2008; Otto et al., 2003), *Drosophila melanogaster* (Klionsky et al., 2008; Rusten et al., 2004; Scott et al., 2004), *Arabidopsis thaliana* (Klionsky et al., 2008; Yoshimoto et al., 2004), zebrafish (He et al., 2009) and mice (Mizushima et al., 2004; Mizushima et al., 2010). Transgenic mice expressing GFP-LC3 and mCherry-LC3 in a systemic or tissue-specific manner have been used to show alterations in autophagic activity under disease and stress conditions (Iwai-Kanai et al., 2008; Mizushima et al., 2010). LC3-based approaches underpin assays in current use to measure autophagic flux (Mizushima et al., 2010).

When viewed using fluorescence microscopy, the diffuse cytosolic GFP-LC3-I is converted to GFP-LC3-II upon induction of autophagy, which subsequently associates with the phagophore membrane and appears as bright fluorescent puncta in the cytoplasm. The number of puncta in a cell has been used as a measure of autophagic activity (Kabeya et al., 2000; Klionsky et al., 2008; Mizushima et al., 2010). GFP-LC3 on the outer surface of the completed autophagosome is removed by action of an autophagin just prior to its fusion with the degradative organelle. Fluorescence due to GFP-LC3 residing on the internal membrane of the autophagosome can persist in the autolysosome until degraded, dependent on the identity of the FP and pKa of its chromophore (Section 2.3).

Image based assays can be time consuming, labour-intensive and require experience for accurate interpretation. Fluorescence activated cell sorting (FACS) allows the rapid acquisition of large datasets and has been used to monitor autophagy by following the time–dependent decrease in the cellular GFP-LC3 signal as it is consumed during autophagy in live cells (Shvets et al., 2008).

Fusing LC3 to a red fluorescent protein (mRFP) and a GFP (EGFP) in tandem to form tfLC3, represents an approach that allows the environment of the probe to be monitored (Kimura et al., 2007; Klionsky et al., 2008). The fluorescence emissions of these two FPs differ in their response to pH such that mRFP remains highly fluorescent in the acidic lumen of the lysosome, whereas EGFP emission is essentially quenched. tfLC3 enables simultaneous estimation of both the induction of autophagy and flux through autophagic compartments without the need to use inhibitors and inducers of autophagy or any other drug treatment (Kimura et al., 2007).

An approach has been developed that monitors the enzymatic activity of Atg4b using LC3 fused to luciferase as a substrate (Ketteler et al., 2008; Ketteler & Seed, 2008). The luciferase is expressed fused at its C-terminus to LC3 and in turn to β-actin. Anchored to actin, the modified *Gaussia* luciferase cannot exit the cell into the growth medium unless it is first released by the action of Atg4b on the LC3 moiety, the preferred substrate (Ketteler et al., 2008). The growth medium is assayed for the presence of luciferase activity. In the future, transgenic mice expressing the luciferase release reporter system may provide convenient, tractably quantitative, mouse models of autophagy (Ketteler & Seed, 2008).

2.3 Rosella: a biosensor for selective autophagy

The growing interest in understanding the regulation and mechanism of selective forms of autophagy (reviewed in Farré et al., 2009; van der Vaart et al., 2008) demands the use of approaches that provide information on specific or individual cargos. However, each of the forgoing assays (Section 2.2) report on the activity of a component of the autophagic pathway, and require the use of additional probes in combination if individual autophagic cargo is to be followed. We have established an alternative approach that senses and reports delivery of the target material to the lysosome or vacuole **(Fig.2)**. The assay is based upon a genetically encoded dual colour-emission biosensor, Rosella, the fusion of a relatively pH-stable fast-maturing variant of the red fluorescent protein, DsRed.T3 with a pH-sensitive variant of green fluorescent protein, pHluorin **(Fig. 3A)** (Devenish et al., 2008; Rosado et al., 2008). By virtue of it being targeted to specific cellular compartments or fused to an individual protein, the biosensor provides information about the identity of the cellular component being delivered to the lysosome or vacuole for degradation. Importantly, the pH-sensitive dual colour fluorescence emission provides information about the environment of the biosensor **(Fig. 3B)** (Devenish et al., 2008; Rosado et al., 2008).

We have already shown that the Rosella biosensor can be used to follow autophagic degradation of specific cargo (cytosol, mitochondria and the nucleus) in yeast cells (Devenish et al., 2008; Mijaljica et al., 2010; Nowikovsky et al., 2007; Rosado et al., 2008) by fluorescence microscopy and FACS analysis (Devenish et al., 2008; Mijaljica et al., 2010; Rosado et al., 2008). Here, we extend those findings and demonstrate the use of Rosella to study reorganisation of the nuclear membrane in mutant yeast strains. We also show that Rosella can be used for monitoring both non-selective autophagy (cytosol) and selective autophagy (mitochondria) in mammalian cells highlighting the benefits of use of this biosensor.

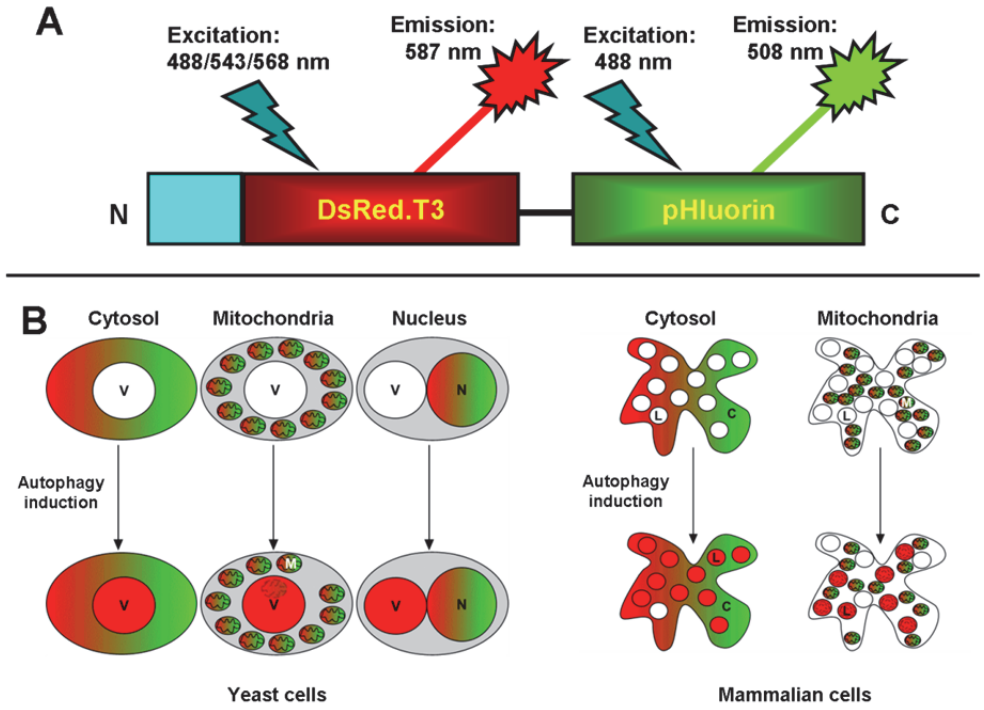

Fig. 3. Rosella can be used to monitor autophagy of different cellular compartments in yeast and mammalian cells.
(A) A schematic of Rosella. The components of Rosella are as follows: targeting sequence for subcellular localisation (cyan box) or other protein to which it is fused; red fluorescent protein (DsRed.T3); polypeptide linker (black bar) and a pH-sensitive GFP variant (pHluorin). A targeting sequence is not required for cytosolic Rosella. The wavelength of lasers suitable for excitation of each component fluorescent protein is indicated. The λ_{max}^{em} (maximum emission wavelength) of each FP is indicated.
(B) Appropriately targeted Rosella can be used to monitor delivery of cytosol, mitochondria or nucleus to the vacuole of yeast cells or cytosol and mitochondria to the lysosome of mammalian cells. When autophagy is induced, increased amounts of Rosella which fluoresces both red and green outside of the acidic vacuole or lysosome (indicated by red and green colour) accumulate in these compartments (indicated by red colour), whereby the green fluorescence emission is quenched. C, cytosol; L, lysosome; M, mitochondria; N, nucleus; V, vacuole.

2.3.1 Monitoring nucleophagy in yeast cells using Rosella

Nucleophagy in the yeast *S. cerevisiae* can occur by a microautophagic process based on the morphological distinction that the cargo destined for degradation within a nuclear bleb is directly engulfed and sequestered into an invagination of the vacuolar membrane rather than being packaged into autophagosome-like vesicles. This process has been referred to as micronucleophagy and piecemeal microautophagy of the nucleus (PMN). Upon nutrient

deprivation of cells (e.g., nitrogen starvation) PMN is initiated at nuclear-vacuolar (NV) junctions and promoted by the interaction of specific membrane-bound proteins (Krick et al., 2008; Kvam & Goldfarb, 2007; Roberts et al., 2003). PMN takes place through a series of morphologically distinct steps. First, an NV junction forms at which the nuclear envelope, coincident with an invagination of the vacuolar membrane bulges into the vacuolar lumen. Later, a fission event releases into the vacuolar lumen a nuclear-derived vesicle (PMN vesicle) filled with nuclear material enclosed by both nuclear membranes. Eventually, the PMN vesicle is degraded by resident vacuolar hydrolases (Krick et al., 2008; Kvam & Goldfarb, 2007; Roberts et al., 2003).

n-Rosella is a variant of Rosella targeted to the nucleus. Under growing conditions, wildtype yeast cells expressing n-Rosella exhibit fluorescent labelling of the entire nuclear lumen (nucleoplasm), which appears as a single red and green body **(Fig. 4)** (Devenish et al., 2008; Mijaljica et al., 2007; Mijaljica et al. 2010; Rosado et al., 2008). When incubated in nitrogen starvation medium for 24 h, cells show red and green fluorescence of the nucleus as well as markedly visible accumulation of red fluorescence in the vacuole indicative of autophagy (nucleophagy) **(Fig. 4A)**.

n-Rosella labelling allows both the morphology of the nucleus to be readily visualized and its own accumulation inside the vacuole. The biosensor can also be used to monitor intermediate steps in the process, using yeast cells lacking expression of particular *ATG* genes (**Fig 4B**). In this example blebbing of the nucleus into the vacuole can be seen. Since the bleb remains both red and green fluorescent, we can conclude that the bleb has a relatively high pH, and the membrane structures required to isolate the vesicle within the acidic vacuolar compartment have not yet been completed. This observation highlights that the pH sensing capabilities of Rosella can be used to monitor membrane continuity or integrity, although we do not have the optical resolution in these experiments to observe the ultrastructural organisation of the membranes themselves.

Mutant yeast cells lacking specific vacuolar enzyme activities required for efficient disassembly of membranes delivered by autophagy (e.g., *atg15Δ*) when starved of nitrogen accumulate a large number of Rosella labelled vesicles **(Fig. 4C)**. Some of these vesicles are both red and green indicating high pH whilst others appear only red indicating that they have a low pH-internal environment typical of the vacuole lumen. These results indicate that autophagic vesicles delivered into the lumen can retain their membrane integrity within the milieu of the resident hydrolases in the absence of the *ATG15* gene product, a putative lipase (Epple et al., 2001).

2.3.2 Monitoring autophagy in mammalian cells using Rosella.

The yeast vacuole is a relatively large and readily recognisable organelle, often accounting for much of the cell volume **(Fig. 4)**. Monitoring delivery of fluorescent cargo to the vacuole therefore is relatively simple. In contrast, the internal membrane structure of the mammalian cell is considerably more intricate and constitutes a profusion of vesicular compartments of various sizes. The mammalian lysosome is a much smaller organelle compared to the vacuole, usually present in large numbers that are distributed throughout the cytosol. The task of visualising delivery of cellular material to the lysosome is accordingly more complex and often requires specific labelling of the acidic organelle with proprietary dyes such as Lysotracker or Lysosensor (Klionsky et al., 2007b). The pH–sensing capability of Rosella allows the delivery of labelled material to be followed without the use

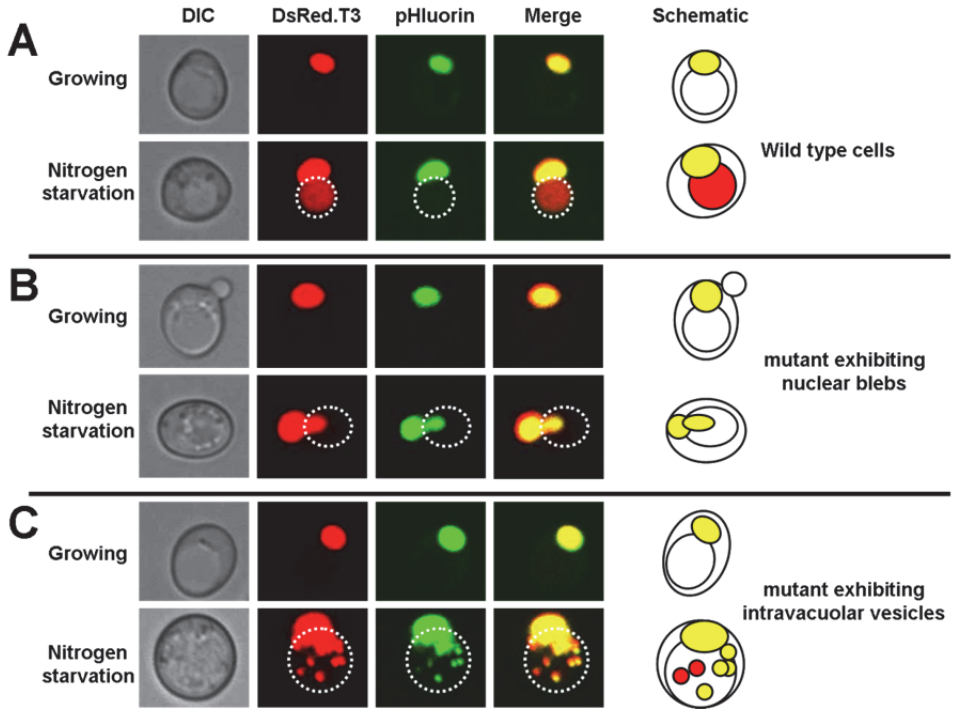

Fig. 4. n-Rosella in yeast: (A) Wild type cells expressing n-Rosella were imaged using fluorescence microscopy under growing and nitrogen starvation conditions. Accumulation of diffused red fluorescence in the vacuole after 24 h of commencement of nitrogen starvation indicates nucleophagy. (B) The absence of expression a particular gene product essential for nucleophagy influences nuclear morphology and abrogates correct delivery of n-Rosella to the vacuole. Nuclear blebs remain red and green indicating high pH environment. (C) The absence of the *ATG15* gene abolishes degradation of n-Rosella derived vesicles in the vacuole. Some intravacuolar vesicles are both red and green (indicating high pH environment) whereas others are only red (indicating low pH environment). The schematic (right) represents an interpretation of the image data. White dashed circles highlight the limits of the vacuole.

of additional probes to highlight the location of the lysosome. We next demonstrate in mammalian cells that Rosella can be used to monitor delivery of the cytosol or mitochondrion to the lysosome.

HeLa cells maintained in a replete growth medium and transfected with an expression vector encoding c-Rosella (Rosella without any additional targeting sequence) **(Fig. 3B)** when imaged using fluorescence microscopy showed both strong red and green fluorescence distributed throughout the cytosol. Rosella appears to have restricted access to the nuclear compartment (less intense staining) and is completely excluded from other compartments **(Fig. 5)**. Importantly, only 1-2 red and weakly green puncta/cell were observed **(Fig. 5A,** white arrows) suggesting that Rosella has accumulated in a relatively acidic compartment such as a lysosome. These puncta correspond to autophagolysosomes,

and represent fusion of an autophagosome carrying the Rosella cargo and a lysosome. Low numbers of puncta observed under growth conditions are consistent with basal autophagic activity and the homeostatic role of autophagy under these conditions.

Rapamaycin, an inhibitor of mTor (mammalian Tor), has been used in numerous studies to induce autophagy in HeLa cells (Ravikumar, et al., 2006). Following 4 h incubation in the presence of rapamycin (0.2µg/ml) a ~10-fold increase in the number of strongly red fluorescent puncta that were only weakly green fluorescent and corresponding to autophagolysosomes was observed **(Fig. 5A**, white arrows**)**.

The lysosome can be independently labelled using acidotropic dyes that accumulate in the lumen of the organelle (Klionsky et al., 2007b). The blue fluorescence emission of LysoTrackerBlue-White (LTBW) in the lysosome can be imaged together with the red and green emission of Rosella. In a separate experiment, prior to treatment with rapamycin to induce autophagy, lysosomes in Rosella-transfected HeLa cells were labelled with LTBW

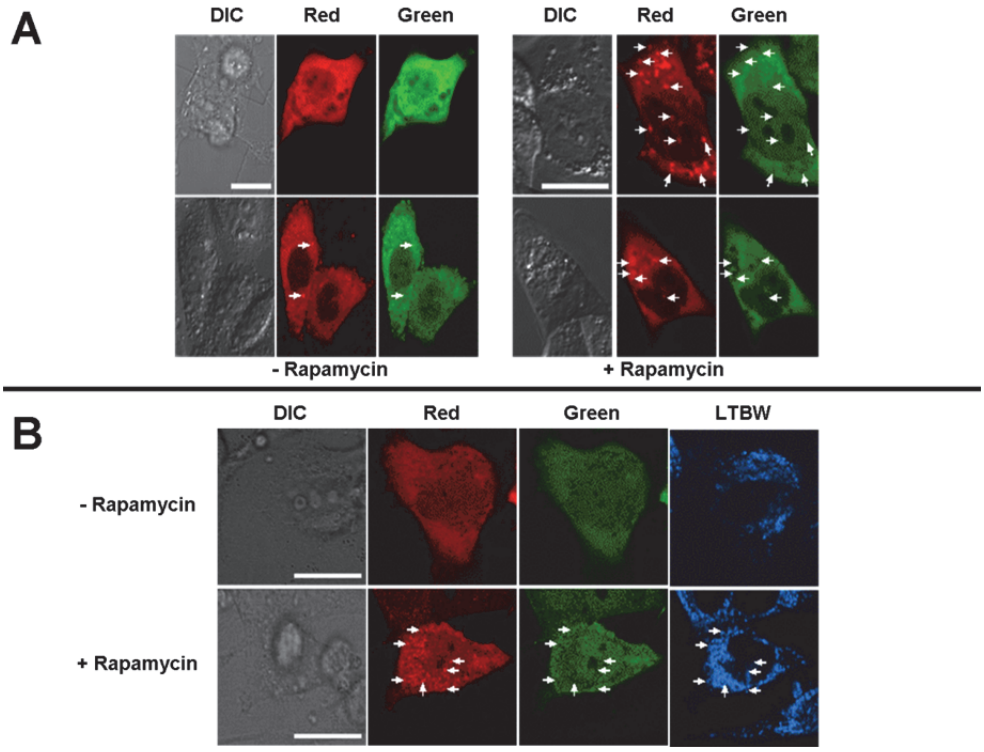

Fig. 5. Rosella can monitor autophagy in HeLa cells.

(A) HeLa cells expressing c-Rosella were imaged 24 h post-transfection for red and green fluorescence (left panel). 1-2 red puncta (white arrows) lacking green fluorescence and corresponding to uptake of cytosolic Rosella are visible in each cell. The number of red puncta lacking green fluorescence increased after incubation in the presence of rapamycin (0.2µg/ml) for 4 h (right panel). (B) In a separate experiment cells were incubated with LysoTrackerBlue-White (LTBW) to label lysosomal compartments. The scale bar is 20 µm.

(Fig. 5B). The puncta were both red and blue fluorescent, but not green fluorescent suggesting that these vesicles represent lysosomal derived compartments.
We next investigated whether Rosella was suitable for monitoring mitophagy in HeLa cells. For these experiments mt-Rosella (a variant of Rosella fused at its N-terminus to the mitochondrial targeting sequence of subunit VIII of cytochrome *c* oxidase; **Fig. 3B)** was expressed in HeLa cells grown in replete growth medium and visualised by fluorescence microscopy. Images of individual live cells show both bright red and green fluorescence restricted to a filamentous network distributed throughout the cell, consistent with a mitochondrial location **(Figs. 6A & 6B)**.

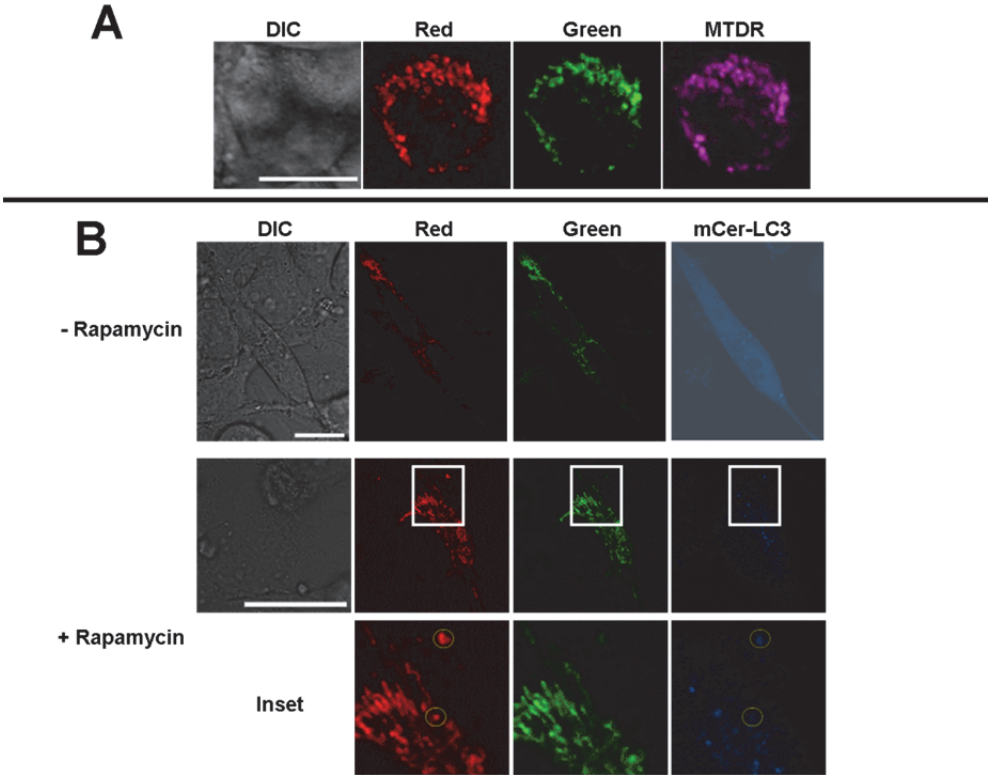

Fig. 6. Rosella can be used to monitor mitophagy in mammalian cells.
(A) DIC and fluorescence images are shown for HeLa cells transfected with an expression vector encoding m-Rosella. Cells were labelled after transfection with a far-red fluorescent mitochondrial probe, MitoTracker Deep Red (MTDR), whose emission is distinct from those of Rosella. (B) HeLa cells were co-transfected with expression vectors encoding m-Rosella and mCer-LC3, and subsequently incubated for 12 h in growth medium containing 0.2µg/ml rapamycin (+ Rapamycin) to induce autophagy. Control cells were not treated with the inducer (-Rapamycin). The white outlined inset region is shown enlarged. Yellow circles highlight red vesicles that co-localise with mCer-LC3, but contain little or no green fluorescence emission. The scale bar is 20 µm.

To confirm efficient targeting of mt-Rosella to the mitochondrion, transfected cells were incubated with the far-red fluorescent mitochondrial probe MitoTracker Deep Red (MTDR) **(Fig. 6A)** (Hallap et al., 2005). The far-red fluorescence emission of MTDR was observed to co-localise with the red and green fluorescence of mt-Rosella. Collectively, these results show that Rosella is efficiently imported into mitochondria, and subsequently becomes both red and green fluorescent.

Next, HeLa cells were co-transfected with expression vectors encoding mt-Rosella or a cyan FP (mCer) fused to the N-terminus of LC3. mCer-LC3 labels the autophagosome for reasons indicated in Figure 1. Transfected cells were cultured for 12 h without (control) or with the addition of rapamycin (0.2μg/ml) and imaged by fluorescence microscopy **(Fig. 6B)**. In control cells not stimulated with rapamycin, the presence of 1-2 cyan puncta per cell indicates autophagy occurring at a low homeostatic level. Since LC3-II will label autophagosomes resulting from both non-selective and selective autophagy, both of which will be induced by rapamycin, it is not expected that the puncta would exhibit the red fluorescence of mt-Rosella. Images of cells stimulated with rapamycin showed the presence of numerous cyan puncta indicating the recruitment of the LC3-II to the autophagosome **(Fig. 6B)**. Selected regions of the image (inset) are enlarged to highlight several autophagosomes that co-localise with bright red fluorescence, and therefore contain mitochondrial material labelled with Rosella. Green fluorescence emission is very weak or non-existent indicating that the pH inside the vesicles is relatively low and suggests that these autophagosomes have fused with lysosomes to form autophagolysosomes. Collectively, these data indicate that mt-Rosella can be used to monitor the delivery of mitochondrial contents to the lysosome.

3. Conclusions and alternative approaches

A better understanding of the molecular mechanism of autophagy in living cells and tissues is essential for the development of new therapeutic strategies to treat disease (Fleming et al., 2011). Accordingly, there is a need for the validation of reliable, meaningful and quantitative assays to monitor autophagy in live cells (Klionsky et al., 2007b; Klionsky et al., 2008; Mizushima et al., 2010).

Increased interest in selective forms of autophagy highlights the need to develop biosensors suitable for monitoring autophagy of specific targets. Exploiting components of the molecular mechanism such as LC3 to follow autophagy have proven to be particularly useful strategy, and LC3 tagged with a fluorescent protein remains the most commonly used marker of the autophagosome. However, such approaches involve additional labelling to identify target material. Labelling the target with Rosella allows delivery of the material to the acidic vacuole/lysosome to be followed by exploiting the unique pH-sensitive dual emission properties. Nevertheless, scope remains to improve development of new selective probes.

Biosensors suitable for high throughput, high content applications such as large scale drug or genetic screens are required. Although in some experimental regimes (e.g., yeast nucleophagy) the dual emission output Rosella can be analysed using conventional FACS analysis, sensitivity is somewhat reduced as the spatial information is lost and the assay relies on integrating the total red and green fluorescence emission from each cell (Rosado et al., 2008). New instrument technology such as imaging flow cytometry, an example of which is manufactured by the Amnis Corporation (https://www.amnis.com/autophagy.html),

would provide access to both spatial and colour information in cell populations (Lee et al., 2007). Our preliminary experiments in yeast cells suggest that this approach has potential but requires further validation and improvements under both physiological and autophagy-induced conditions (Rosado et al., 2008).

The development of biosensors with considerably improved signal-to-noise ratio may be possible using alternative probe technologies based on fragment complementation. Fragment complementation for a variety of different fluorescent proteins is now available (Kerpolla, 2006). The technology might be implemented to measure autophagy in one of several ways. For example, yeast cells in which one FP fragment is targeted to the mitochondrion and the complementing fragment targeted to the vacuole might be expected to have strongly fluorescent vacuoles *only* when mitophagy has occurred. Delivery of mitochondrial material including the FP fragment to the vacuole would allow re-constitution of a functional FP by fragment complementation. Cells would be otherwise non-fluorescent providing for a high signal-to-noise ratio. A similar and considerably more sensitive biosensor might be developed along similar lines if the FP is substituted for a member of the light-emitting luciferase family (Villalobos et al., 2010). Finally, it may be possible for an inactive pro-enzyme such as acid protease to be used to label targets. The enzyme would be proteolytically activated in the acidic lumen of the vacuole which would then be detected by incubation of cells with a cell permeant quenched fluorescent peptide substrate.

Given the interest in autophagy, it is likely in the near future that some of these ideas will result in the development of new sensitive and selective probes for this process.

4. Acknowledgment

This work was supported in-part by Australian Research Council Grant (DP0986937) awarded to R. J. Devenish.

5. References

Axe, E.L., Walker, S.A., Manifava, M., Chandra, P., Roderick, H.L., Habermann, A., Griffiths, G. & Ktistakis, N.T. (2008). Autophagosome formation from membrane compartments enriched in phosphatidylinositol 3-phosphate and dynamically connected to the endoplasmic reticulum. *J Cell Biol*, Vol. 182, No. 4, (August 2008), pp. 685-701, PMID: 18725538.

Brown, C.R., Dunton, D. & Chiang, H.L. (2010). The vacuole import and degradation pathway utilizes early steps of endocytosis and actin polymerization to deliver cargo proteins to the vacuole for degradation. *J Biol Chem*, Vol. 285, No. 2, (January 2010), pp. 1516-1528, PMID: 19892709.

Chen, Y. & Klionsky, D.J. (2011). The regulation of autophagy-unanswered questions. *J Cell Sci*, Vol. 124, No. Part 2, (January 2011), pp. 161-170, PMID: 21187343.

Devenish, R.J., Prescott, M., Turcic, K. & Mijaljica, D. (2008). Monitoring organelle turnover in yeast using fluorescent protein tags. *Methods Enzymol*, Vol. 451, pp. 109-131, PMID: 19185717.

Epple, U.D., Suriapranata, I., Eskelinen, E.L. & Thumm, M. (2001). Aut5/Cvt17p, a putative lipase essential for disintegration of autophagic bodies inside the vacuole. *J Bacteriol*, Vol. 183, No. 20, (October 2001), pp. 5942-5955, PMID: 11566994.

Farré, J.C., Krick, R., Subramani, S. & Thumm, M. (2009). Turnover of organelles by autophagy in yeast. *Curr Opin Cell Biol*, Vol. 21, No. 4, (August 2009), pp. 522-530, PMID: 19515549.

Fleming, A., Noda, T., Yoshimori, T. & Rubinsztein, D.C. (2011). Chemical modulators of autophagy as biological probes and potential therapeutics. *Nat Chem Biol*, Vol. 7, No. 1, (January 2011), pp. 9-17, PMID: 21164513.

Hallap, T., Nagy, S., Jaakma, U., Johannisson, A. & Rodriguez-Martinez, H. (2005). Mitochondrial activity of frozen-thawed spermatozoa assessed by MitoTracker Deep Red 633. *Theriogenology*, Vol. 63, No. 8, (May 2005), pp.2311-2322, PMID: 15826692.

He, C. & Klionsky, D.J. (2009). Regulation mechanisms and signaling pathways of autophagy. *Annu Rev Genet*, Vol. 43, (2009), pp. 67-93, PMID: 19653858.

He, C., Bartholomew, C.R., Zhou, W. & Klionsky, D.J. (2009). Assaying autophagic activity in transgenic GFP-Lc3 and GFP-Gabarap zebrafish embryos. *Autophagy*, Vol. 5, No. 4, (May 2009), pp.520-526, PMID: 19221467.

https://www.amnis.com/autophagy.html, Amnis®.

Iwai-Kanai, E., Yuan, H., Huang, C., Sayen, M.R., Perry-Garza, C.N., Kim, L. & Gottlieb, R.A. (2008). A method to measure cardiac autophagic flux in vivo. *Autophagy*, Vol. 4, No. 3, (April 2008), pp. 322-329, PMID: 18216495.

Kabeya, Y., Mizushima, N., Ueno, T., Yamamoto, A., Kirisako, T., Noda, T., Kominami, E., Ohsumi, Y. & Yoshimori, T. (2000). LC3, a mammalian homologue of yeast Apg8p, is localized in autophagosome membranes after processing. *EMBO J*, Vol. 19, No. 21, (November 2000), pp. 5720-5728, PMID: 11060023.

Kanki, T. & Klionsky, D.J. (2010). The molecular mechanism of mitochondria autophagy in yeast. *Mol Microbiol*, Vol. 75, No. 4. (February 2010), pp. 795-800, PMID: 20487284.

Kanki, T., Klionsky, D.J. & Okamoto, K. (2011). Mitochondria autophagy in yeast. *Antioxid Redox Signal*, (March 2011), Epub ahead of print, PMID: 21194379.

Katayama, H., Yamamoto, A., Mizushima, N., Yoshimori, T. & Miyawaki, A. (2008). GFP-like proteins stably accumulate in lysosomes. *Cell Struct Funct*, Vol. 33, No. 1, (February 2008), pp. 1-12, PMID: 18256512.

Kerpolla, T.K. (2006). Design and implementation of bimolecular fluorescence complementation (BiFC) assays for the visualization of protein interactions in living cells. *Nat Protoc*, Vol. 1, No. 3, pp1278-1286, PMID: 17406412.

Ketteler, R. & Seed, B. (2008). Quantification of autophagy by luciferase release assay. *Autophagy*, Vol. 4, No. 6, (August 2008), pp. 801-806, PMID: 18641457.

Kettele, R., Sun, Z., Kovacs, K.F., He, W.W. & Seed, B. (2008). A pathway sensor for genome-wide screens of intracellular proteolytic cleavage. *Genome Biol*, Vol. 9, No. 4, (April 2008), pp. R64, PMID: 18387192.

Kimura, S., Noda, T. & Yoshimori, S. (2007). Dissection of the autophagosome maturation process by a novel reporter protein, tandem fluorescent-tagged LC3. *Autophagy*, Vol. 3, No. 5, (September-October 2007), pp. 452-460, PMID: 17534139.

Klionsky, D.J., Cuervo, A.M., Dunn, W.A. Jr., Levine, B., van der Klei, I. & Seglen PO. (2007a). How shall I eat thee? *Autophagy*, Vol. 3, No. 5, (September-October 2007), pp. 413-416, PMID: 17568180.

Klionsky, D.J., Cuervo, A.M. & Seglen, P.O. (2007b). Methods for monitoring autophagy from yeast to human. *Autophagy*, Vol. 3, No. 3, (May-June 2007), pp. 181-206, PMID: 17224625.

Klionsky, D.J., Abeliovich, H., Agostinis, P., Agrawal, D.K., Aliev, G., Askew, D.S., et al. (2008). Guidelines for the use and interpretation of assays for monitoring autophagy in higher eukaryotes. *Autophagy*, Vol. 4, No. 2, (February 2008), pp. 151-175, PMID: 18188003.

Krick, R., Muehe, Y., Prick, T., Bremer, S., Schlotterhose, P., Eskelinen, E.L., Millen, J., Goldfarb, D.S. & Thumm. M. (2008). Piecemeal microautophagy of the nucleus requires the core macroautophagy genes. *Mol Biol Cell*, Vol. 19, No. 10, (October 2008), pp. 4492-4505, PMID: 18701704.

Kvam, E. & Goldfarb, D.S. (2007). Nucleus-vacuole junctions and piecemeal microautophagy of the nucleus in *S. cerevisiae*. *Autophagy*, Vol. 3, No. 2, (March-April 2007), pp. 85-92, PMID: 17204844.

Lee, H.K., Lund, J.M., Ramanathan, B., Mizushima, N. & Iwasaki, A. (2007). Autophagy-dependent viral recognition by plasmacytoid dendritic cells. *Science*, Vol. 315, No. 5817, (March 2007), pp. 1398-1401, PMID: 17272685.

Legakis, J.E. & Klionsky, D.J. (2006). Overview of autophagy. In: *Autophagy in Immunity and Infection. A Novel Immune Effector*, V. Deretic, (Ed.), pp. 3-17. Wiley-VCH, ISBN: 978-3-527-31450-8 Weinheim.

Lerena, M.C., Vázquez, C.L. & Colombo, M.I. (2010). Bacterial pathogens and the autophagic response. *Cell Microbiol*, Vol. 12, No. 1, (January 2010), pp. 10-18, PMID: 19888990.

Lynch-Day, M.A. & Klionsky, D.J. (2010). The Cvt pathway as a model for selective autophagy. *FEBS Lett*, Vol. 584, No. 7, (April 2010), pp. 1359-1366, PMID: 20146925.

Meléndez, A., Tallóczy, Z., Seaman, M., Eskelinen, E.L., Hall, D.H. & Levine, B. (2003). Autophagy genes are essential for dauer development and life-span extension in *C. elegans*. *Science*, Vol. 301, No. 5638, (September 2003), pp. 1387-1391, PMID: 12958363.

Mijaljica, D., Prescott, M. & Devenish, R.J. (2007) Nibbling within the nucleus: turnover of nuclear contents. Cell Mol Life Sci, Vol. 46, No. 5 (March 2007), pp. 581-588. PMID: 17256087.

Mijaljica, D., Prescott, M. & Devenish, R.J. (2010). The intricacy of nuclear membrane dynamics during autophagy. *Nucleus*, Vol. 1, No. 3, (May 2010), pp. 213-223, PMID: 21327066.

Mijaljica, D., Prescott, M. & Devenish, R.J. (2011). Microautophagy in mammalian cells: revisiting a forty year old conundrum. *Autophagy*, Vol. 7, No. 7, (January 2011), Epub ahead of print.

Mizushima, N. (2004). Methods for monitoring autophagy. *Int J Biochem Cell Biol*, Vol. 36, No. 12, (December 2004), pp. 2491-2502, PMID: 15325587.

Mizushima, N. & Yoshimori, T. (2007). How to interpret LC3 immunoblotting. *Autophagy*, Vol. 3, No. 6, (November-December 2007), pp. 542-545, PMID: 17611390.

Mizushima, N., Yoshimori, T. & Levine, B. (2010). Methods in mammalian autophagy research. *Cell*, Vol. 140, No. 3, (February 2010), pp. 313-326, PMID: 20144757.

Nowikovsky, K., Reipert, S., Devenish, R.J. & Schweyen, R.J. (2007). Mdm38 protein depletion causes loss of mitochondrial K+/H+ exchange activity, osmotic swelling

and mitophagy. *Cell Death Differ*, Vol. 14, No. 9, (September 2007), pp. 1647-1656, PMID: 17541427.

Orenstein, S.J. & Cuervo, A.M. (2010). Chaperone-mediated autophagy: molecular mechanisms and physiological relevance. *Semin Dev Cell Biol*, Vol. 21, No. 7, (September 2010), pp. 719-726, PMID: 20176123.

Otto, G.P., Wu, M.Y., Kazgan, N., Anderson, O.R. & Kessin, R.H. (2003). Macroautophagy is required for multicellular development of the social amoeba *Dictyostelium discoideum*. *J Biol Chem*, Vol. 278, No. 20, (May 2003), pp. 17636-17645, PMID: 12626495.

Ravikumar, B., Berger, Z., Vacher, C., O'Kane, C.J. & Rubinsztein, D.C. (2006). Rapamycin pre-treatment protects against apoptosis. *Hum Mol Genet*, Vol. 15, No. 7, (April 2006), pp. 1209-1216, PMID: 16497721.

Ravikumar, B., Moreau, K., Jahreiss, L., Puri, C. & Rubinsztein, D.C. (2010). Plasma membrane contributes to the formation of pre-autophagosomal structures. *Nat Cell Biol*, Vol. 12, No. 8, (August 2010), pp. 747-757, PMID: 20639872.

Roberts, P., Moshitch-Moshkovitz, S., Kvam, E., O'Toole, E., Winey, M. & Goldfarb, D.S. (2003). Piecemeal microautophagy of the nucleus in *Saccharomyces cerevisiae*, *Mol Biol Cell*, Vol. 14, No. 1, (January 2003), pp. 129-141, PMID: 12529432.

Rosado, C.J., Mijaljica, D., Hatzinisiriou, I., Prescott, M. & Devenish, R.J. (2008). Rosella: a fluorescent pH-biosensor for reporting vacuolar turnover of cytosol and organelles in yeast. *Autophagy*, Vol. 4, No. 2, (February 2008), pp. 205-213, PMID: 18094608.

Rubinsztein, D.C. (2006). The roles of intracellular protein-degradation pathways in neurodegeneration. *Nature*, Vol. 443, No. 7113, (October 2006), pp. 780-786, PMID: 17051204.

Rubinsztein, D.C., Cuervo, A.M., Ravikumar, B., Sarkar, S., Korolchuk, V., Kaushik, S. & Klionsky, D.J. (2009). In search of an "autophagomometer". *Autophagy*, Vol. 5, No. 5, (July 2009), pp. 585-589, PMID: 19411822.

Rusten, T.E., Lindmo, K., Juhász, G., Sass, M., Seglen, P.O., Brech, A. & Stenmark, H. (2004). Programmed autophagy in the Drosophila fat body is induced by ecdysone through regulation of the PI3K pathway. *Dev Cell*, Vol. 7, No. 2, (August 2004), pp. 179-192, PMID: 15296715.

Scott, R.C., Schuldiner, O. & Neufeld, T.P. (2004). Role and regulation of starvation-induced autophagy in the Drosophila fat body. *Dev Cell*, Vol. 7, No. 2, (August 2004), pp.167-178, PMID: 15296714.

Shpilka, T. & Elazar, Z. (2011). Shedding light on mammalian microautophagy. *Dev Cell*, Vol. 20, No. 1, (January 2011), pp. 1-2, PMID: 21238917.

Shvets, E., Fass, E. & Elazar, Z. (2008). Utilizing flow cytometry to monitor autophagy in living mammalian cells. *Autophagy*, Vol. 4, No. 5, (July 2008), pp. 621-628, PMID: 18376137.

Tanida, I. (2010). Autophagosome formation and molecular mechanism of autophagy. *Antioxid Redox Signal*, (December 2010), Epub ahead of print, PMID: 20712405.

Tanida, I. (2011). Autophagy basics. *Microbiol Immunol*, Vol. 55, No. 1, (January 2011), pp. 1-11, PMID: 21175768.

van der Vaart, A., Mari, M. & Reggiori, F. (2008). A picky eater: exploring the mechanisms of selective autophagy in human pathologies. *Traffic*, Vol. 9, No. 3, (March 2008), pp. 281-289, PMID: 17988219.

Villalobos, V., Naik, S., Bruinsma, M., Dothager, R.S., Pan, M.H., Samrakandi. M., Moss, B., Elhammali, A. & Piwnica-Worms, D. (2010). Dual-color click beetle luciferase heteroprotein fragment complementation assays. *Chem Biol*, Vol. 17, No. 9, (September 2010), pp. 1018-1029, PMID: 20851351.

Xie, Z. & Klionsky, D.J. (2007). Autophagosome formation: core machinery and adaptations. *Nat Cell Biol*, Vol. 9, No. 10, (October 2007), pp. 1102-1109, PMID: 17909521.

Xie, Z., Nair, U. & Klionsky, D.J. (2008). Atg8 controls phagophore expansion during autophagosome formation. *Mol Biol Cell*, Vol. 19, No. 8, (August 2008), pp. 3290-3298, PMID: 18508918.

Yang, Z. & Klionsky, D.J. (2010). Eaten alive: a history of macroautophagy. *Nat Cell Biol*, Vol. 12, No. 9, (September 2010), pp. 814-822, PMID: 20811353.

Yorimitsu, T. & Klionsky, D.J. (2005). Autophagy: molecular machinery for self-eating. *Cell Death Differ*, Vol. 12, No. Suppl 2, (November 2005), pp. 1542-1552, PMID: 16247502.

Yoshimoto, K., Hanaoka, H., Sato, S., Kato, T., Tabata, S., Noda, T. & Ohsumi, Y. (2004). Processing of ATG8s, ubiquitin-like proteins, and their deconjugation by ATG4s are essential for plant autophagy. *Plant Cell*, Vol. 16, No. 11, (November 2004), pp. 2967-2983, PMID: 15494556.

Youle, R.J. & Narendra, D.P. (2011) Mechanisms of mitophagy. *Nat Rev Mol Cell Biol*, Vol. 12, No. 1, (January 2011), pp. 9-14, PMID: 21179058.

20

Amperometric Biosensors for Lactate, Alcohols and Glycerol Assays in Clinical Diagnostics

Oleh Smutok[1] et al.[*]
[1]*Institute of Cell Biology, NAS of Ukraine, Lviv, Ukraine*

1. Introduction

Biosensors are bioanalytical devices which transform a biorecognition response into a measurable physical signal. Although biosensors are a novel achievement of bioanalytical chemistry, they are not only a subject of intensive research, but also a real commercial product (Kissinger, 2005). The estimated world analytical market is about $20 billion per year of which 30 % is in the healthcare field. The biosensors market is expected to grow from $6.72 billion in 2009 to $14.42 billion in 2016 (http://www.marketresearch.com, Analytical Review of World Biosensors Market).

Although up to now IUPAC has not accepted an official definition of the term biosensor, its electrochemical representative is defined as "a self-contained integrated device, which is capable of providing specifc quantitative or semi-quantitative analytical information using a biological recognition element (biochemical receptor) which is retained in direct spatial contact with an electrochemical transduction element'' (Thevenot et al., 2001). Generally, the biosensor is a hybrid device containing two functional parts: a bioelement (an immobilized biologically active material) and a physical transducer. As bioelements pieces of tissue, microbial cells, organelles, natural biomembranes or liposomes, receptors, enzymes, antibodies and antigens, abzymes, nucleic acids and other biomolecules and even biomimetics which imitate structural and functional features of the natural analogue can be used. The bioelement is a recognition unit providing selective binding or biochemical/metabolic conversion of the analyte that result in changes in physical or physico-chemical characteristics of the transducer (Scheller et al., 1991; Schmidt & Karube, 1998; Gonchar et al., 2002; Nakamura & Karube, 2003; Sharma et al., 2003; Investigations on Sensor Systems and Technologies, 2006). The bioelement in such constructions is usually prepared in immobilized form and often covered with an outer membrane (or placed between two membranes in a sandwich manner), which either prevents the penetration of

[*]Galina Gayda[1], Kostyantyn Dmytruk[1], Halyna Klepach[1], Marina Nisnevitch[3], Andriy Sibirny[1,2], Czesław Puchalski[2], Daniel Broda[2], Wolfgang Schuhmann[4], Mykhailo Gonchar[1,2] and Vladimir Sibirny[2]
2 University of Rzeszow, Rzeszow-Kolbuszowa, Poland
3 Ariel University Center of Samaria, Ariel, Israel
4 Ruhr-Universität Bochum, Bochum, Germany

interfering substances into a sensitive bioselective layer and the transducer surface, or creates a diffusion barrier for the analyte. Such membrane structures increase the stability of the biorecognition element, enhance its selectivity and provide the diffusion limitations for biochemical reactions. Electrochemical, optical, piezoelectric, thermoelectric, transistor, acoustic and other elements are used as transducers in biosensor systems. Electrochemical (amperometric, potentiometric, conductometric) and optical (surface plasmon resonance) devices are the most exploited transducers in commercially available biosensors (Commercial Biosensors, 1998).

Basically, biosensors can be regarded as information transducers in which the energy of biospecific interactions is transformed into information about the nature and concentration of an analyte in the sample. The most essential advantages of biosensors are excellent chemical selectivity and high sensitivity, possibility of miniaturization and compatibility with computers. Their drawbacks are limited stability and a rather complicated procedure for preparation of the biologically active material.

Enzyme biosensors are the most widespread devices (Zhao & Jiang, 2010); many of them are produced commercially. Enzyme biosensors are characterized by their high selectivity. They also provide fast output due to high activity and high local enzyme concentration in a sensitive layer. The drawbacks of enzyme biosensors are insufficient stability and the high price of purified enzymes. Cell sensors, especially microbial ones, have been actively developed only in recent years (Shimomura-Shimizu & Karube, 2010a, 2010b; Su et al., 2011). Cell biosensors have a range of considerable advantages when compared to their enzyme analogues: availability of cells, low price and simple procedure of cell isolation, possibility to use long metabolic chains, avoiding purification of enzymes and coenzymes, advanced opportunity for metabolic engineering, integrity of the cell response (important in assaying total toxicity and mutagenic action of environmental pollutants), possibility to retain viability of sensoring cells and even to provide their propagation, and, in some cases, higher stability of cell elements compared to enzyme ones. The main drawbacks of microbial biosensors are a rather low signal rate due to a lower concentration of enzymes involved in cellular response, as well as low selectivity of cell output (e.g. in the case of microbial O_2 electrode sensors due to a broad substrate specificity of cellular respiration).

These drawbacks are not absolute, taking into account recent progress in genetic engineering and the possibility to over-express the key analytical enzyme in the cell (Gonchar et al., 2002).

Most biosensors have been created for clinical diagnostics (D'Orazio, 2003; Song et al., 2006; Belluzo et al., 2008). They exploit enzymes as biocatalytic recognition elements and immunoreagents and DNA fragments as affinity tools for biorecognition of the target analytes (metabolites, antigens, antibodies, nucleic acids) coupled to electrochemical and optical modes of transduction. For simultaneous detection of multiple analytes, microarray techniques are developed for automated clinical diagnostics (Seidel & Niessner, 2008). For continuous monitoring of living processes, reagentless implantable biosensors have been developed (Wilson & Ammam, 2007).

Biosensors are regarded as very promising tools for clinical cancer testing (Rasooly & Jacobson, 2006; Wang, 2006). New genomic and proteomic approaches are being used for revealing cancer biomarkers related with genetic features, changes in gene expression, protein profiles and post-translational modifications of proteins.

Recent progress in nanobiotechnology allows using nanomolecular approaches for clinical diagnostic procedures (Salata, 2004; Jain, 2007). The most important applications are

foreseen in the areas of biomarker monitoring, cancer diagnosis, and detection of infectious microorganisms. Analytical nanobiotechnology uses different nanoscaled materials (gold and magnetic nanoparticles, nanoprobes, quantum dots as labels, DNA nanotags) for molecular detection (Baptista et al., 2008; Medintz et al., 2008; Sekhon & Kamboj, 2010). The use of nanomaterials in biosensors has allowed the introduction of many new signal transduction technologies into biosensorics and the improvement of bioanalytical parameters of the nanosensors - selectivity, response time, miniaturization of the biorecognition unit (Jianrong et al., 2004; Murphy, 2006).

2. Development of L-lactate-selective biosensors based on L-lactate-selective enzymes

Lactate, a key metabolite of the anaerobic glycolytic pathway, plays an important role in medicine, in the nutritional sector, as well as in food quality control. Amperometric biosensors offer a sensitive and selective means to monitor organic analytes like lactate. Here, different aspects of amperometric lactate biosensor construction are described: electrode materials, biorecognition elements, immobilization methods, mediators and cofactors as well as fields of application.

Biosensors for the detection of L-lactate are often based on either NAD^+-dependent lactate dehydrogenase (LDH) from mammalian muscles or heart (EC 1.1.1.27) (Arvinte et al., 2006; Hong et al., 2002), bacterial lactate oxidase (LOX) (EC 1.13.12.4) (Hirano et al., 2002; Iwuoha et al., 1999) or bi-enzyme systems combining peroxidase (HRP) and LOX (Herrero et al., 2004; Zaydan et al., 2004; Serra et al., 1999). Some approaches let to commercially available L-lactate sensors (Luong et al., 1997; http://www.johnmorris.com.au/html/Ysi/ysi1500.htm; http://www.fitnessmonitors.com/ecstore/cat111.htm). However, due to the non-advantageous equilibrium constant of the LDH-catalysed reaction and the need to add free diffusing NAD^+ as well as problems arising from the generally high working potentials of LOX-based amperometric biosensors, there is still a need to develop alternative sensor concepts for the determination of L-lactate. To decrease the impact of interfering compounds, related sensor's electrodes were, for example, covered with an additional permselective membrane (Madaras et al., 1996). Despite the more complex sensor preparation, this pathway is unsuitable for the development of L-lactate sensors due to the fact that negatively-charged L-lactate is simultaneously prevented from reaching the electrode surface through negatively charged membranes.

Besides LDH and LOX, another enzyme is known for participating in the lactic acid metabolism in yeasts, namely L-lactate-cytochrome *c* oxidoreductase (EC 1.1.2.3; flavocytochrome b_2, FC b_2) (Brooks, 2002), which catalyses the electron transfer from L-lactate to cytochrome *c* in yeast mitochondria. The protein can be isolated from *Saccharomyces cerevisiae* and *Hansenula anomala* (Labeyrie et al., 1978; Haumont et al., 1987; Silvestrini et al., 1993) as a tetramer with four identical subunits, each consisting of FMN- and heme-binding domains. FC b_2 has absolute specificity for L-lactate, moreover, it functions *in vitro* without regard to the nature of electron acceptors which makes this enzyme very promising for analytical biotechnology. However, until now application of FC b_2 from baker's yeast in bioanalytical devices was hampered by its instability and difficulties in purification of the enzyme (Labeyrie et al., 1978). Here, we describe the use of a purified FC b_2, isolated from the wild-type and recombinant thermotolerant *Hansenula polymorpha* yeast cells that overproduce this enzyme as a biological recognition element in amperometric biosensors.

2.1 Construction of biosensors using purified FC b_2 from the wild type *Hansenula polymorpha* 356

Prior to the electrochemical investigations, we have performed considerable microbiological, biochemical and analytical investigations. We have screened 16 yeast species as possible sources of the stable form of FC b_2. The thermostability test was performed at different temperatures and time periods. The study of enzyme activity by two procedures, including our own method for FC b_2 activity visualization in PAA-gels (Gaida et al., 2003), has shown that only FC b_2 from *H. polymorpha* 356 remained as a native tetramer during a 10 min-incubation of cell-free extract at 60˚C or 3 min at 70˚C (Smutok et al., 2006a). For preparative purification of FC b_2 from the cells of *H. polymorpha* 356, we modified a scheme that was developed for this enzyme from the yeast *H. anomala* (Labeyrie et al., 1978). The scheme of purification includes lysis of the cell's pellet by *n*-butanol followed by extraction of cell's debris with 1% Triton X-100; ion-exchange chromatography on DEAE–Toyopearl 650M (TSK-GEL, Japan). The enzyme yield after chromatographic purification was near 80 % (Smutok et al., 2006c). The highest specific FC b_2 activity in some fractions was 20 μmol·min^{-1}·mg^{-1} protein (U·mg^{-1}). After ammonium sulfate was added up to 70% saturation, the specific activity was increased to 30 U·mg^{-1}. FC b_2 preparations have been used to develop L-lactate-sensitive biosensors (Smutok et al., 2006a).

Amperometric FC b_2-based biosensors were evaluated using constant-potential amperometry in a three-electrode configuration with a Ag/AgCl/KCl (3 M) reference electrode and a Pt-wire counter electrode. Amperometric measurements were carried out with a bipotentiostat (EP 30, Biometra, Göttingen, Germany) or a potentiostat PGSTAT302 (Autolab, Netherlands). As working electrodes, graphite rods (type RW001, 3.05 mm diameter, Ringsdorff Werke, Bonn, Germany) were applied, which were sealed in a glass tube using epoxy, thus forming disk electrodes. Before sensor preparation, the graphite electrodes were polished on emery paper and on a polishing cloth using decreasing sizes of alumina paste (Leco, Germany). The polished electrodes were rinsed with water in an ultrasonic bath.

Although FC b_2 provides very specific electron transfer from L-lactate to cytochrome *c* in the respiratory chain of native yeast cells, theoretically, it could be supposed *in vitro* a direct electrochemical communication between the reduced heme-binding domain and the electrode surface. This hypothesis has been approved by using cyclic voltammetry (Fig. 1).

The obtained cyclic voltammogram (Fig. 1A) shows a small peak at a potential of +250 mV versus Ag/AgCl in the presence of L-lactate which can be attributed to the accessibility of the heme site of the enzyme for direct electron exchange reactions with the electrode surface. Obviously, the first monolayer of the enzyme is able to directly exchange electrons with the electrode surface, providing a favorable orientation with the accessible heme site towards the electrode.

The related hydrodynamic voltammograms at increasing L-lactate concentrations (0.5, 1 and 4 mM) are shown in Fig. 1B. The peak current is highest at a potential of about +300 mV versus Ag/AgCl; hence, all the experiments concerning direct electron transfer were performed at this working potential.

In yeast cells, mitochondrial FC b_2 catalyses the dehydrogenation of L-lactate to pyruvate, transferring the electrons from L-lactate *via* FMN as the primary electron acceptor, to the heme site of the enzyme and finally to cytochrome *c* as the terminal electron sink. No detectable direct electron transfer is possible from the reduced $FMNH_2$ inside the intact enzyme to cytochrome *c*, avoiding the intermediate storage of the electrons in the heme site (Ogura & Nakamura, 1966). However, it is known that a number of free-diffusing redox

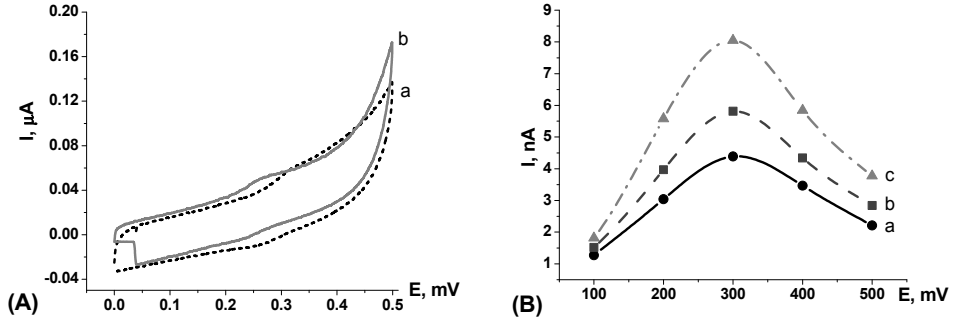

Fig. 1. (A) Cyclic voltammogram at a graphite electrode modified with adsorbed FC b_2 (a) in the absence and (b) in the presence of 20 mM L-lactate (0 to +500 mV at a scan rate of 5 mV/s in 20 mM phosphate buffer, pH 7.2). (B) Hydrodynamic voltammograms obtained from a graphite electrode modified with adsorbed FC b_2 in the presence of (a) 0.5 mM; (b) 1 mM; (c) 4 mM L-lactate in the absence of any electron-transfer mediator.

mediators can be used to transfer electrons from FC b_2 to electrodes, while direct electron transfer was not yet approved experimentally. Hence, we investigated the L-lactate-dependent current response of FC b_2-modified electrodes in the absence and presence of various electron-transfer mediators (Figs. 2 and 3).

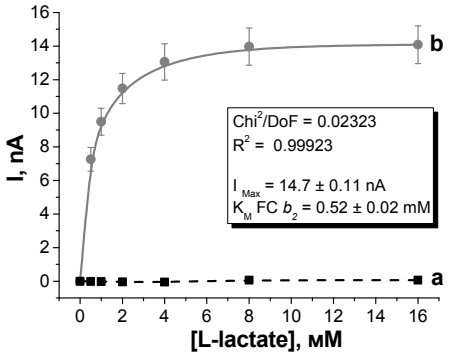

Fig. 2. Lactate calibration curve of a graphite electrode modified with adsorbed FC b_2 at a potential of +300 mV and pH 7.2 in the absence of any redox mediator (b). Control experiment with a bare graphite electrode (a).

In the absence of any free-diffusing redox mediator, direct electron transfer is only possible from those enzyme molecules which are located in a monolayer in direct contact with the electrode surface, while being orientated to allow the heme site to be situated at a productive electron-transfer distance. Although the efficiency of the direct electron transfer reaction is comparatively low, the response clearly exceeds the noise signal of the control electrode without immobilized enzyme (Fig. 2). These limitations lead to a maximum current of 14 nA at L-lactate saturation. In contrast, in the presence of the most effective free-diffusing redox mediator (phenazine ethosulfate) the response is enhanced 28 times, reaching a maximum value of 390 nA at substrate saturation.

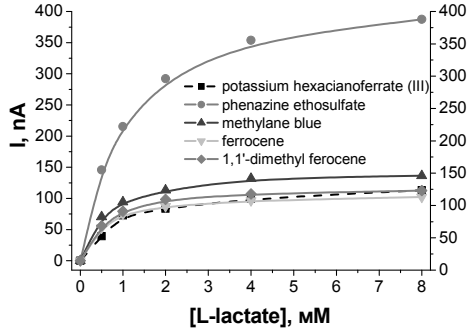

Fig. 3. Lactate calibration curves obtained with a graphite electrode modified with adsorbed FC b_2 in the presence of different free-diffusing electron-transfer mediators (+ 300 mV, pH 7.2).

As demonstrated in Fig. 3, all free-diffusing and adsorbed redox mediators used in the study accelerated the investigated oxidation of L-lactate catalyzed in the FC b_2 reaction. Phenazine ethosulfate exceeds the efficiency of the other mediators by up to 2.7–3.6 times. Hence, phenazine ethosulfate was used for all further experiments as a free-diffusing redox mediator. A variety of different immobilization techniques were applied for the preparation of the enzyme electrodes, with the aim to achieve optimal stability, the highest possible sensitivity and selectivity, and a low detection limit. FC b_2 was immobilized on graphite surfaces using some different strategies: physical adsorption; electrodeposition by anodic paint *Resydrol AY*; entrapment in a polymer layer of a precipitated cathodic paint *GY 83-0270 00054*; cross-linking by glutardialdehyde vapour (Smutok et al., 2005); electrodeposition by osmium-modified anodic paint (*AP-Os*); entrapment in a layer of cathodic paint (*CP-Os*) (Fig. 4).

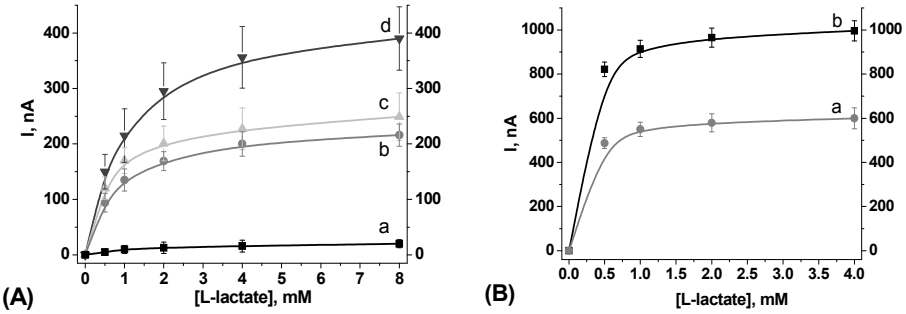

Fig. 4. (A) Lactate calibration curves obtained with graphite electrodes modified with FC b_2 using different enzyme immobilization methods in the presence of 1 mM phenazine ethosulfate as free-diffusing electron-transfer mediator (+300 mV, pH 7.6). (a) Entrapment in the anodic electrodeposition paint "Resydrol AY"; (b) entrapment in the cathodic electrodeposition paint "GY 83-0270 00054"; (c) cross-linking of the adsorbed enzyme in glutardialdehyde vapour; (d) physical adsorption. (B) electrodeposition of FC b_2 with an osmium-modified anodic paint (*AP-Os-FC* b_2) (a); entrapment of FC b_2 in a layer of a cathodic paint (*CP-Os-FC* b_2) (b).

All obtained biosensors were investigated concerning their substrate-dependent current response. As shown in Fig. 4A, the maximal responses of the different enzyme electrodes were 439 ± 3.2, 263 ± 3.1, and 237 ± 1.1 nA for physical adsorption, glutardialdehyde immobilization and cathodic paint precipitation, respectively. In the case of the anodic paint *Resydrol AY* the maximal current value was much lower (20 nA). The use of the electrodeposited osmium-complex modified anodic paint performed two functions: electron transfer and film immobilization. Therefore, this variant of enzyme immobilization looks most promising, especially since its signal value was 600 nA (Fig. 4B). However, we have shown that the activity of FC b_2 strongly depends on the process of electro-deposition in the presence of anodic paint. High voltage impulses of electrodeposition (+2200 mV) resulted in the inactivation of FC b_2, probably due to the very fast generation of protons and a decrease of pH values (Fig. 5A).

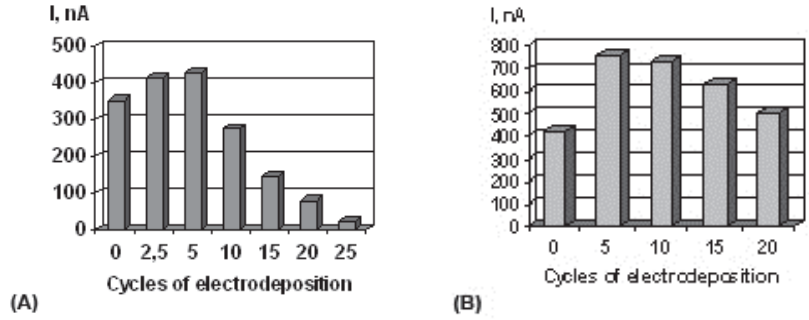

Fig. 5. (A) Dependence of sensor's output on cycles of anodic (A) and cathodic (B) schemes of electrodeposition of FC b_2 (+ 300 mV, pH 7.2 in the presence of 1 mM phenazine ethosulfate).

On the other hand, FC b_2 should have been more resistant at higher pH values according to its enzymological properties in solution (Smutok et al., 2006a). Therefore, in subsequent experiments, a cathodic paint was used as a matrix for the entrapment of FC b_2. No remarkable negative influence on the FC b_2 activity was observed at potentiostatic pulses to potentials as low as –1200 mV. Hence, this potential was used for the cathodic paint precipitation (Fig. 5B).

The sensor with *CP-Os-FC* b_2 architecture gave the highest output; 1000 nA (Fig. 4B). Therefore, in the subsequent experiments this structure was used in conjunction with free-diffusing mediators, to cross-link immobilized FC b_2 by glutaraldehyde vapour. In the case of covalently-bound mediator, the electroinduced immobilization by *CP-Os-FC* b_2 technique has been selected as the best.

Bioanalytical characteristics of the developed *FC* b_2-based biosensor in conjunction with free-diffusing mediators have been investigated. The calculated value for the apparent Michaelis-Menten constant K_M^{app} as derived from the calibration graphs in the presence of 1 mM phenazine ethosulfate for FC b_2 was about 1.0±0.02 mM. The response time was rather fast: 50 % of the signal value is achieved after 3 sec and 90 % after 6 sec (Fig. 6A).

The level of selectivity was estimated in relative units (%), as a ratio to the value of L-lactate response. No interference by L-malate, pyruvate, L,D-isocitrate or acetate on FC b_2-modified

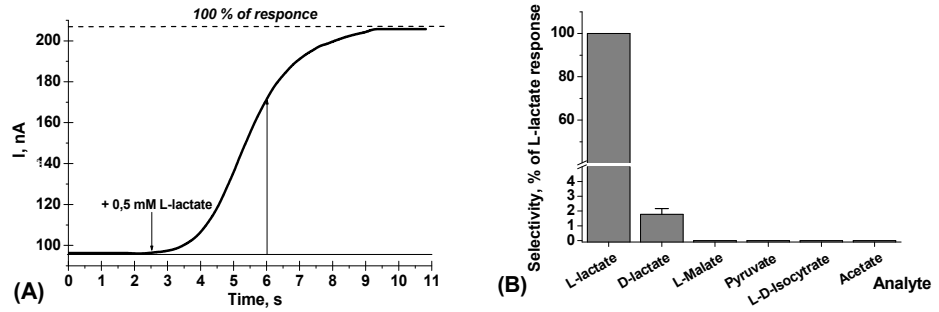

Fig. 6. (A) Development of the sensor's response with time upon addition of 5 mM L-lactate (potential +300 mV vs Ag/AgCl/3M KCl) in phosphate buffer, pH 7.2 in the presence of 1 mM phenazine ethosulfate (a). (B) Selectivity of FC b_2-modified electrodes (response to 4 mM analyte).

electrodes was observed, but the sensor did show a low signal to D-Lactate (1.8 ± 0.3 %). This fact can be explained by the incomplete purity of the FC b_2 sample, and its possible contamination with D-lactate cytochrome *c*-oxidoreductase. In spite of this fact, the developed sensor was highly selective to L-lactate (Fig. 6B).

The temperature and pH-dependence of the obtained biosensors were evaluated and the optimal temperature of 35-38 ^{0}C at the optimal pH-value of 7.5-7.8 was derived (Fig. 7). These values are governed by the properties of the enzyme itself and are not significantly altered by the used immobilization procedure.

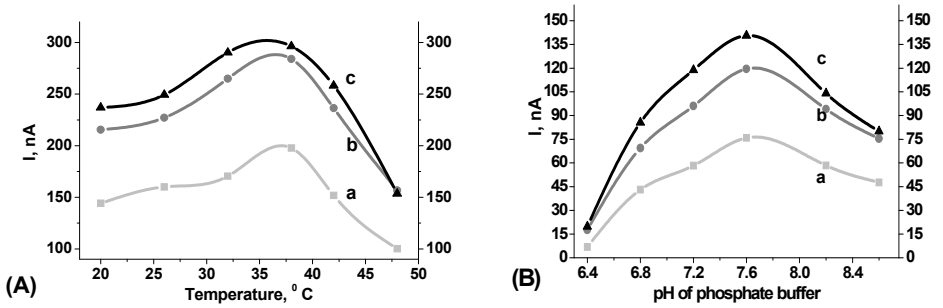

Fig. 7. Temperature- (A) and pH-dependence (B) of the biosensor's response to L-lactate: 0.5 mM (a); 2 mM (b) and 8 mM (c). Experimental conditions: +300 mV vs Ag/AgCl/3 M KCl, pH 7.6, 1 mM phenazine ethosulfate.

Simultaneous with the investigation of the sensor architecture comprising free-diffusing mediators, the main characteristics of the sensor formed by electrodeposition paint were determined. The maximal detected signal values were 1100 nA for the sensor architecture *CP-Os-FC* b_2 and 650 nA for *AP59-Os-FC* b_2-modified electrodes (Fig. 8).

The apparent Michaelis-Menten constants (K_M^{app}) for L-lactate calculated from the calibration curves were 0.141±0.001 mM and 0.135±0.003 mM, respectively. The sensor response time, selectivity, optimal temperature and pH values were the same as for the biosensor based on free-diffusing redox mediators.

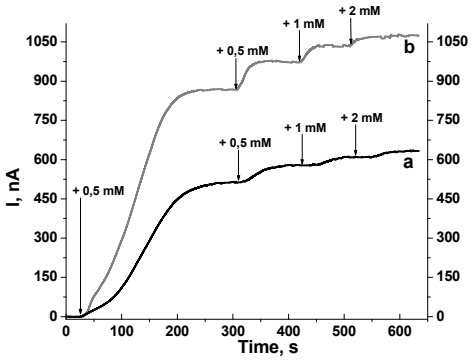

Fig. 8. Chronamperometric current response upon subsequent additions of L-lactate aliquots for sensors with FC b_2 entrapped in a layer of osmium-complex modified anodic paint (*AP-Os-FC* b_2) (a) and an osmium-complex containing cathodic paint (*CP-Os-FC* b_2) (b).

The operation and storage stabilities of the developed sensors have been evaluated. The electrodes prepared at optimal conditions were tested at 24 ^{0}C with respect to their stability. Solutions of 1 mM L-lactate (for experiments of operational stability) and 4 mM L-lactate (for the storage stability) were used in these experiments. The operational stability of the obtained microbial sensors was evaluated using a previously described automatic sequential-injection analyzer (*"OLGA"*) system (Schuhmann et al., 1995) and 15 measurements per hour were done (Fig. 9A).

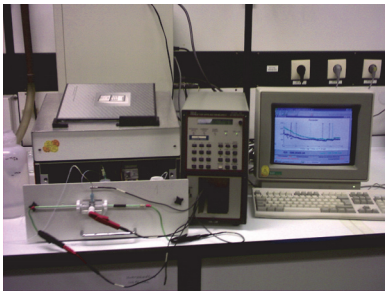

(**A**)

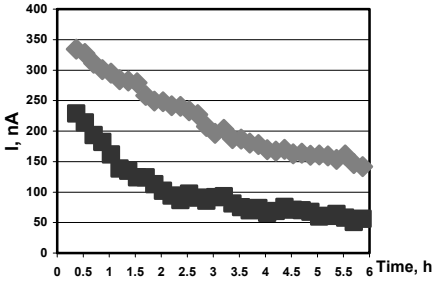

(**B**)

Fig. 9. Flow injection "OLGA" analyzer system with integrated bioelectrodes (A) and operation stability of the sensor obtained by "OLGA" (1 mM L-Lactate, flow-rate 5 ml min^{-1} , 24 ^{o}C and detection of results every 4 min) (B).

Two variants of the working electrodes showed some differences in the initial response values to L-lactate. There were also some differences in the kinetics of sensor inactivation. The initial sensor output for the *CP-Os-FC* b_2 variant of the working electrode was near 350 nA and decreased after 5.5 hours (82 measurements) to 175 nA (half-life). The *AP-Os-FC* b_2 variant of the sensor showed a lower initial output (250 nA) and after 5.5 hours of work revealed a lower signal (75 nA) as compared to the first sensor.

The storage stability of the constructed *CP-Os-FC* b_2 biosensor was found to be satisfactory over more than 7 days and a half-life activity of the sensor was observed at the 5th day of storage (Fig. 10).

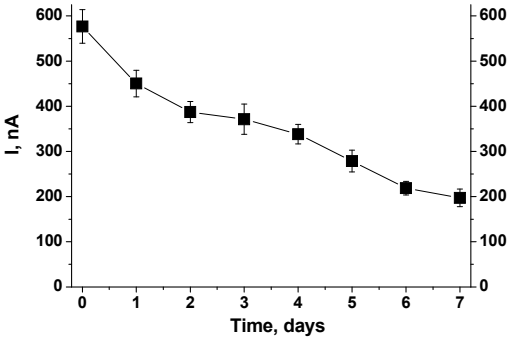

Fig. 10. Storage stability of the *CP-Os-FC* b_2 sensor architecture (4 mM L-Lactate, 24 ^{0}C).

2.2 Development of microbial amperometric biosensors based on the cells of flavocytochrome b_2 over-producing recombinant yeast *H. polymorpha*

Currently, four different enzymes are known as biological recognition element for L-lactate detection: lactate oxidase (LOD) (Karube et al., 1980), lactate monooxygenase (LMO) (Mascini et al., 1984), lactate dehydrogenase (LDH) (Wang & Chen, 1994) and flavocytochrome b_2 (Staskeviciene et al., 1991). However, microorganisms provide an ideal alternative to enzymes, providing certain advantages in comparison with enzyme-based biosensors: for example, avoiding isolation and purification steps for enzyme preparation; prolonged shelf-life of the sensor due to improved stability of the biorecognition element in the intact biological environment. Previous bacterial biosensors for L-lactate were successfully constructed using the whole cells of *Paracoccus denitrificans* (Kalab & Skladal, 1994), *Acetobacter pasteurianus* (Luong et al., 1989), *Alcaligenes eutrophus* (Plegge et al., 2000) and *Escherichia coli* (Adamowicz & Burstein, 1987). Physical robustness of yeasts in comparison to bacteria and superior tolerances to pH, temperature and osmolarity/ionic strength make them the preferred microorganisms, with the potential to be used as biological recognition elements for cell-based biosensors (Baronian, 2004). The application of the yeast *H. anomala* to oxidise L-lactate was investigated earlier by Racek et al. using a platinum electrode, polarised to the potential of +350 mV vs. Ag/AgCl using potassium ferricyanide as a soluble mediator (Racek & Musil, 1987a, 1987b), and later by Kulys et al. using carbon paste electrodes and different mediators (potassium ferricyanide, phenazine methosulfate, organic salt of TMPD/TCNQ, methylene green, Mendola's blue) at potentials of +50-300 mV vs. SCE (Kulys et al., 1992). Garjonyte implemented *S. cerevisiae* yeast cells for the construction of the biosensor for L-lactate using carbon paste electrodes and potassium ferricyanide, phenozine methosulfate, 2,6-dichlorophenolindophenol sodium salt hydrate, 1,2-naphthoquinone-4-sulfonic acid salt or *p*-benzoquinone as free-diffusing mediators at potentials of 0-+300 mV vs. Ag/AgCl (Garjonyte et al., 2006; Garjonyte et al., 2008).

In the meantime, the genomes of some yeast species (*S. cerevisiae*, *H. polymorpha*) were completely sequenced and gene engineering methods allowed for the tailoring of these microorganisms to enhance the activity of specific enzymes (Walmsley & Keenan, 2000). Genetically modified yeast cells of *S. cerevisiae* were successfully used for the construction of genotoxicity biosensors (Walmsley et al., 1997; Billinton et al., 1998), or biosensors for estrogen (Tucker & Fields, 2001), dibenzo-*p*-dioxins (Sakaki et al., 2002) and copper (Lehmann et al., 2000) detection. *H. polymorpha* mutants were implemented for the

development of biosensors for formaldehyde (Korpan et al., 1993) and ethanol/methanol (Gonchar et al., 1998).

Alteration of the target enzymatic pathway may cause other additional metabolic changes in the cell metabolism. Thus, cells have the ability to adjust their metabolism in order to adapt to changing conditions and to survive the imposed stress. A good example of yeast cells exhibiting such adaptation behavior was observed in genetically modified yeast cells of *H. polymorpha*, used for the detection of ethanol/methanol (Gonchar et al., 1998). A defect in the gene responsible for catalase synthesis, forced the cells to develop the mechanism of hydrogen peroxide depletion through its extrusion from the cell. Thus, the excreted hydrogen peroxide, which is a product of catalytic oxidation of alcohol in the yeast cell, was used as an analytical signal for methanol detection.

In the present study, genetically-modified yeast cells of *H. polymorpha*, over-expressing the enzyme L-lactate:cytochrome *c*-oxidoreductase (FC b_2) were used for the construction of a mediator-free biosensor for L-lactate. The recombinant cells were previously used for the construction of amperometric biosensor with improved sensitivity to L-lactate. The developed biosensor was using permeabilised cells, and the free-diffusing mediator phenazine methosulfate was used for the electrical communication between FC b_2 and the electrode surface (Smutok et al., 2007). Simultaneously we report the detection of L-lactate based on the monitoring of L-lactate-dependent respiration of intact genetically-modified cells of *H. polymorpha* with an increased content of FC b_2 within the cells of the recombinant strain (Shkil et. al., 2009).

2.2.1 Construction of free-diffusing microbial amperometric sensor using permeabilized cells of flavocytochrome b_2 over-producing recombinant yeast *H. polymorpha*

Construction of the recombinant *H. polymorpha* strain over-producing FC b_2 included several stages. The recombinant plasmid pGLG61_CYB2, which is based on the plasmid pGLG61 for multicopy integration (Fig. 11A, *b*), was transformed to the recipient strain *H. polymorpha* C-105 (*gcr1 catX*) avoiding glucose repression and catalase activity. The transformants were grown on YPD medium in the presence of increasing concentrations of geneticin G418. The highest concentration of G418 which allows the transformants to grow was 1 mg ml^{-1}. The transformants were stabilized by cultivation in non-selective media for ten to twelve generations with further shifting to the selective media with G418. The presence of the expression cassette in the stable transformants was examined by PCR using corresponding primers and genomic DNA of stable transformants as a template. Fragments of predictable size (~ 3.3 kb) were obtained (data not shown).

The level of FC b_2 activity in cell-free extracts of the recombinant strain "tr1" was compared with the recipient strain *H. polymorpha* C-105. As shown in Fig. 11B, the FC b_2 activity in the cell-free extracts of the transformed strain "tr1" was about 3.2 U mg^{-1} protein, while the recipient strain *H. polymorpha* C-105 under the same growth conditions had a much lower enzyme activity of only 0.6 U mg^{-1} protein. The transformant showed 5.2 fold higher FC b_2 activity as compared to the recipient strain. After permeabilization the cells of this FC b_2-over-producing strain were used as biorecognition element for the construction of a microbial L-lactate-selective amperometric biosensor.

In order to evaluate the developed L-lactate biosensor based on permeabilized cells, phenazine methosulphate (PMS) was used as a free-diffusing redox mediator for establishing the electron transfer between FC b_2 located at the mitochondria membrane and

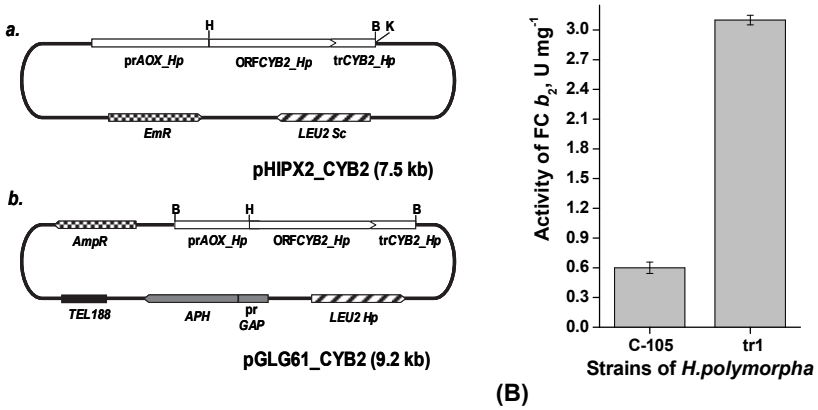

Fig. 11. (A) Circular schemes of the plasmids (*a*) pHIPX2_CYB2 (7.5 kb) and (*b*) pGLG61_CYB2 (9.2 kb). The *HpAOX* promoter and *CYB2* ORF with the terminator region are shown as open boxes. The *LEU2* genes of *S. cerevisiae* or *H. polymorpha* are shown as hatched boxes. Genes *EmR* and *AmpR* conferring resistance to erythromycin and ampicillin are shown as chequered boxes. The *H. polymorpha* truncated glyceraldehyde-3-phosphate dehydrogenase *(GAP)* promoter and the geneticin resistance gene (*APH*) are shown as grey boxes, the tellomeric region (*TEL188*) as black box. Restriction sites: H - *Hind*III; B - *Bam*HI; K - *Kpn*I. (B) Comparison of FC b_2 activity in cell-free extracts of *H. polymorpha* C-105 (recipient strain) and of the recombinant strain "tr1".

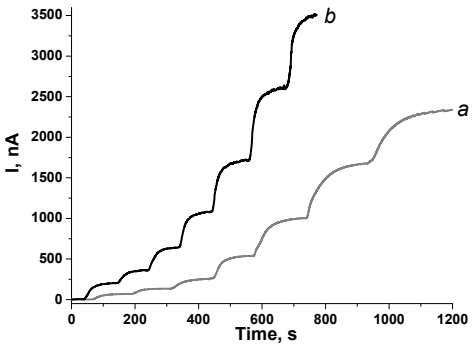

Fig. 12. Chronamperometric current response upon subsequent additions of L-lactate aliquots obtained with microbial sensors based on permeabilized cells of the recombinant strain of *H. polymorpha* ("tr1"). (a) Immobilization of cells by means of physical entrapment behind a dialysis membrane. (b) Entrapment of cells within a layer of a cathodic electrodeposition polymer CP9. (3.05 mm diameter graphite disk electrode; 0 mV *vs.* Ag/AgCl).

the electrode surface. It was supposed that PMS can easily diffuse into the permeabilized cell and back to the electrode. 3.05 mm graphite rod electrodes at a potential of 0.0 mV were chosen for PMS oxidation (Garjonyte et al., 2006). Since it has been shown previously that isolated FC b_2 exhibits only a limited stability (Smutok et al., 2005), it was suggested that the application of intact cells with the inherent ability to keep the enzyme protected in a membrane-bound state would significantly improve the properties of the sensors.

Two different immobilisation methods were evaluated, namely, the physical fixation of permeabilized cells behind a dialysis membrane and the entrapment of the cells within an electrodeposition paint layer which is formed in the presence of the cells. A typical sensor response for both sensor architectures is shown in Fig. 12. The output of the sensor prepared by electrochemically induced precipitation of the cathodic electrodeposition polymer *CP9* under simultaneous entrapment of the permeabilized cells within the hydrogel layer exhibits a higher current response upon addition of L-lactate. In addition, due to the favourable diffusion of the substrate and the mediator to the polymer entrapped cells these sensors showed a faster response time. The rate of the sensors' response to 0.1 mM L-lactate is about 190 nA·min^{-1} for the polymer entrapment system and 60 nA·min^{-1} for the system with a dialysis membrane, respectively.

To evaluate the impact of the genetic modifications performed on the bioanalytical characteristics of the cells, L-lactate sensors based on either permeabilized cells of the recombinant strain "tr1" or cells of the recipient strain "C-105" entrapped within the cathodic electrodeposition paint were compared. Since the difference between both strains is determined mainly by the FC b_2 content, it was expected that the current response of the sensor based on the genetically engineered cells was significantly enhanced.

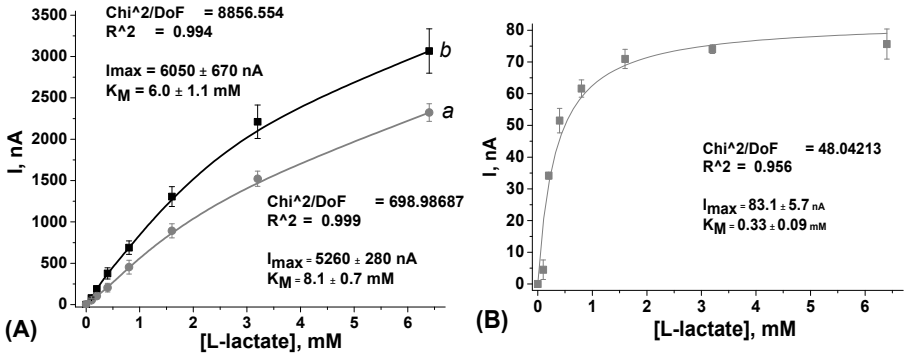

Fig. 13. (A) L-lactate calibration graphs for two types of sensors modified by genetically engineered *H. polymorpha* "tr1" cells (*a* - physical entrapment behind a dialysis membrane; *b* - electrochemically induced entrapment within a cathodic electrodeposition polymer *CP9*); (B) L-lactate calibration graph for sensor modified by *H. polymorpha* "C-105" cells by physical entrapment behind a dialysis membrane.

As clearly shown in Figure 13, a significantly increased current response is observed upon L-lactate addition for the sensors based on the genetically engineered cells "tr1" as compared with the wild-type strain "C-105". The maximal current I_{max} at substrate saturation for the "C-105" cells-based sensor was 83.1 ± 5.7 nA, while the "tr1" cell-based electrode showed an I_{max} of 5260 ± 280 nA under the same conditions. These results indicate that the maximum contribution of other L-lactate oxidizing enzymes within the cells, which should be similarly present in both the "tr1" and "C105" cells, does not exceed 80 nA at substrate saturation. This value represents only about 1.5 % of the maximum sensor output of 5260 nA. It could be hence concluded that most of the contribution to the sensor current originates from the added FC b_2 activity of the recombinant strain.

In addition, sensors based on genetically engineered "tr1" cells exhibit a 20 to 25 times higher K_M value irrespective of the immobilization method. The calculated values for K_M^{app} derived from the calibration plots are 0.33±0.09 mM for sensors based on "C-105" cells and 8.0±0.66 mM for "tr1"cells. To investigate whether the K_M values of the cell-based sensors depend on the differences in properties of FC b_2 itself or are dominated by the significantly higher enzyme loading in the case of the "tr1" cells, a L-lactate sensor based on FC b_2 isolated from "tr1" cells was prepared using physical entrapment of the enzyme behind a dialysis membrane for enzyme immobilization (Fig. 14).

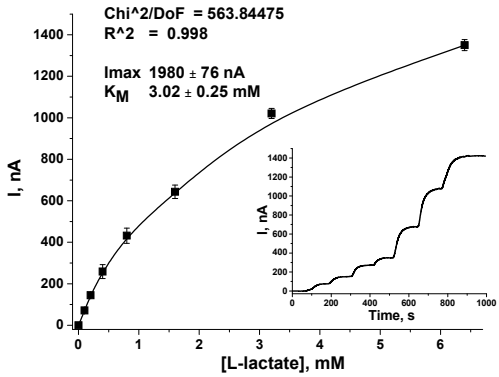

Fig. 14. L-lactate calibration curve and chronoamperogram (insert) of a biosensor based on isolated FC b_2 isolated from recombinant "tr1"cells.

The K_M^{app} of FC b_2 purified from recombinant "tr1" cells was determined from the calibration graph as 3.02 ± 0.25 mM (toward L-lactate) which is about 10 times higher than the K_M^{app} value of the sensor using permeabilized "C-105" cells. Obviously, restriction of the diffusion mass transfer through the permeabilized cells cannot be the reason for the observed increase in the K_M^{app} value. Hence, the structure of FC b_2 produced by the recombinant cells must be modulated, leading to a significantly decreased affinity of the active site of the enzyme for complementary binding of L-lactate. This may be due to errors caused by the *Taq* DNA-polymerase *in vitro*, which may lead to minor changes in the primary structure of the PCR product and consequently may result in amino acid substitutions in the FC b_2 molecule. The observed increased K_M^{app} value for recombinant cells and the enzyme isolated from these cells had a positive impact on the biosensor properties due to the increase of the linear range for L-lactate determination, up to 1.6 mM. The increased linear detection range is better adapted to the typical concentration range of L-lactate in real samples, thus avoiding dilution steps. The detection limit of the sensor is low (about 6 µM L-lactate). The optimal pH-value for the developed L-lactate biosensor based on the recombinant cells is in the range of 7.5 to 8.2, with an optimal temperature between 36 and 42 ^{0}C.

For the application of the L-lactate biosensor in real samples, the selectivity with respect to potential substrates/interferents such as D-lactate, pyruvate, succinate, L-malate, citrate, α-ketoglutarate, urate, D-glucose and ethanol is of great importance. Hence, the amperometric current response of the cell-based L-lactate sensor was evaluated with respect to the above mentioned compounds (Fig. 15).

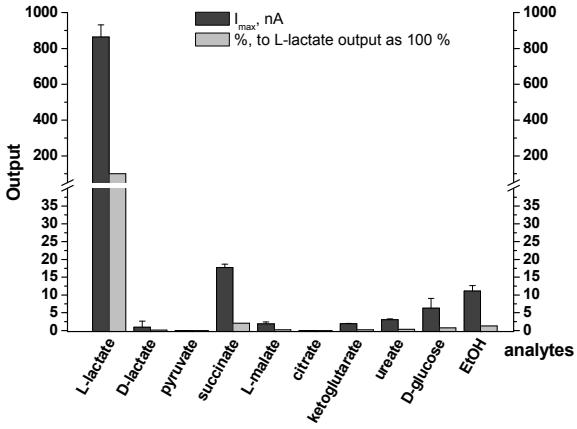

Fig. 15. Selectivity of the L-lactate biosensor (863 nA; 100 %) based on electrochemically immobilized *H. polymorpha* "tr1" cells. The current and the relative response of 1 mM solutions of D-lactate (0.92 nA; 0.1 %), pyruvate (0.0 nA; 0 %), succinate (17.7 nA; 2 %), L-malate (1.88 nA; 0.22 %), citrate (0.0 nA; 0 %), α-ketoglutarate (1.9 nA; 0.22 %), urate (3.07 nA; 0.36 %), D-glucose (6.29 nA; 0.73 %), and ethanol (11.1 nA; 1.29 %) are displayed.

The cell-based biosensor exhibits minor cross-sensitivity to most of the tested compounds. With the exception of succinate, D-glucose and ethanol the relative cross-sensitivity is below 1 %. Thus, the impact of these compounds will be insignificant for the determination of L-lactate in the real samples where the above mentioned components may be present.

The operational and storage stabilities of the L-lactate sensor were investigated. Biosensors were prepared following the optimal preparation protocol for both immobilization techniques of the permeabilized "tr1" cells. The stability tests were performed at a constant temperature of 24 ^{0}C using 1 mM solutions of L-lactate in 50 mM phosphate buffer, pH 7.8, for the investigation of the operational stability, and a 3 mM L-lactate solution - for the evaluation of the storage stability. The operational stability was evaluated using an automatic sequential injection analyzer (W. Schuhmann et al., 1995). The sensors were integrated into a flow-through electrochemical cell, and 15 injections of 500 µl of a 1 mM L-lactate standard solution per hour were performed automatically. Fig. 16 shows the peak currents of the different L-lactate sensors upon sample injection over a period of about 24 hours (approximately 360 individual measurements).

Both types of cell-based sensors demonstrated a linear decay of the current response during continuous operation over 24 hours (360 injections of 1 mM L-lactate solutions). In another experiment the peak currents decayed to 50 % of the initial sensor output after about 26-30 hours of continuous operation. Despite the continuous decrease of the sensor output the developed biosensors exhibited satisfactory operational stability for L-lactate determination in model samples, especially when integrated in the sequential injection analyser that allows for a repetitive recalibration.

Next, the storage stability of the different sensor configurations was tested. For this, the sensors were stored between amperometric L-lactate determinations at + 4°C (Table 1). The measurements were performed at room temperature in 50 mM phosphate buffer, pH 7.8,

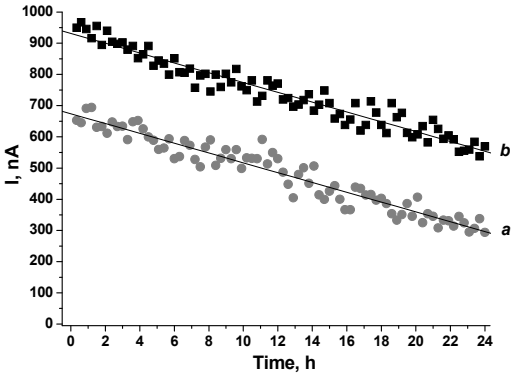

Fig. 16. Operational stability of the *H. polymorpha* "tr1" cells based L-lactate biosensors tested in an automatic sequential injection analyser (flow-rate 5 ml min^{-1}; sample injection every 4 min). (*a*) permeabilized cells physically entrapped behind a dialysis membrane; (*b*) permeabilized cells entrapped within a cathodic electrodeposited polymer.

Remaining response, % from the initial output	Time of storage, days									
	0	2	4	6	8	10	12	14	24	40
Physical entrapment behind a dialysis membrane	100	109	103	98.6	93.8	90.7	86.2	83	76.8	----
Entrapment within a cathodic electrodeposition polymer	100	99.8	98.3	98.8	97	94.4	90.5	89.3	80.1	67.2

Table 1. Storage stability of the recombinant cells-based biosensors

containing 0.2 mM PMS and 3 mM L-lactate. Both types of sensors proved to be stable for more than 24 days under storage conditions. After one day of storage in buffer solution, the detected signal of dialysis membrane-based sensor was increased by about 10 % over the initial response. This effect is often observed for amperometric biosensors and can be explained by the equilibration of sensor architecture and, especially, by a final swelling of the dialysis membrane facilitating diffusional access of the substrate to the immobilized cells. After about 24 days of storage, sensors of this type failed due to damage of the dialysis membrane. The sensors based on entrapment of the permeabilized cells within a cathodic electrodeposition polymer could be used for more than 40 days, with intermittent storage in buffer in the refrigerator.

The significantly improved stability of the developed L-lactate sensors as compared with similar sensors using the isolated enzyme (Smutok et al., 2005) may be accounted for by the use of the thermotolerant yeast *H. polymorpha* for the genetic modification and overexpression of FC b_2. Moreover, during cell permeabilization and the following washing steps, low molecular weight proteinases may be at least partly removed from the cells, thus

preserving FC b_2 activity. In addition, the overexpressed holoenzyme FC b_2 may be stabilized in its native environment in the mitochondria membrane.

2.2.2 Mediator-less L-lactate-selective microbial sensor based on modified *H. polymorpha* yeast cells overexpressing flavocytochrome b_2

A typical approach to target redox enzymes of bacterial or yeast cells involves the addition of a shuttle molecule, called a mediator that is recycled between the electrode and the target enzyme inside the cells. However this method requires the permeabilization of the cell membrane to facilitate the diffusion process. The usage of such soluble mediators restricts the practical application of the biosensor.

Another way to monitor the cells metabolism and specific internal processes is based on examining cell respiration, performed using an oxygen electrode, typically a Pt electrode (polarized at -600 mV vs. Ag/AgCl), a technique known to be used in first-generation biosensors. However, this method has serious drawbacks, mainly, the limited availability of soluble oxygen and an inverse relationship between the concentration of the analyte and the sensor response. Moreover, the involvement of the oxygen consumption processes within the cells (mainly through the respiratory chain) limits the selectivity of the method in detecting the analyte of interest, since there are multiple pathways that might be used to pump electrons through Complex IV, the site where the oxygen reduction process takes place. In the present study, some of the above mentioned drawbacks are overcome by specific approaches: i) using a potential of -300 mV; ii) over-expression of FC b_2 for increasing the selectivity; iii) using yeast cells instead of bacterial cells as done previously (Kalab & Skladal, 1994; Luong et al., 1989; Plegge et al., 2000; Adamowicz & Burstein, 1987) for the construction of biosensors for L-lactate detection which improves the tolerance to external conditions.

Since the method of L-lactate detection presented herein is based on the competition for oxygen consumption between a polarized electrode and the respiration process in yeast cells, the reaction at the electrode equally influences the sensor performance. Therefore, an evaluation of the oxygen reduction reaction using various types of electrode materials, such as gold, platinum and graphite was considered. Additionally, the biocompatibility of yeast cells with a specific electrode material has to be taken into consideration in order to provide good stability and reproducibility of the sensor.

The sensor's response in dependence from the applied electrode potential was evaluated in the presence and absence of L-lactate, as shown in Fig. 17.

The three different electrode materials show specific particularities in terms of on-set potential and reaction rate for oxygen reduction, as well as the sensitivity of L-lactate detection. The platinum electrode exhibits a high on-set potential for oxygen reduction, -200 mV, which is seen as a drawback due to the generation of high background noise. On the other hand, both graphite and gold electrodes exhibit on-set potentials of -100 mV, thus limiting the contribution of possible interferences to the overall reduction current. Despite this decrease in background current, the gold electrode, upon addition of L-lactate, leads to a minimum variation of the sensor response, meaning it rates poorly for sensitivity. The graphite electrode, in addition to its high sensitivity to variation in oxygen concentration, represented in Fig. 17 by the differences between opened and filled symbols (see corresponding arrows), is additionally preferred over other electrodes due to its unspecific reduction of oxygen, whereas the gold electrode is known to reduce oxygen mainly to H_2O_2,

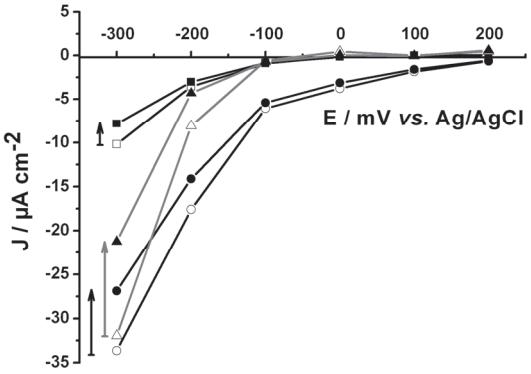

Fig. 17. Hydrodynamic voltammograms presenting the dependence of the sensor response for different electrode materials (gold - square, platinum - circles and graphite - triangles) modified with *H. polymorpha* "tr1" cells, recorded in the presence (filled symbols) and in the absence (opened-symbols) of L-lactate.

and Pt efficiently reduces oxygen to H_2O, however at the expense of a much lower reduction potential, usually at around -600 mV. Tuning the competition between electrode and yeast cells by varying the applied potential leads finally to improved selectivity and sensitivity, with an emphasis on the decrease of signal interference. Thus, as a compromise between background noise, sensor sensitivity and biocompatibility of yeast cells to the electrode material and their tolerance to exposure to products of oxygen reduction, a graphite electrode at an applied potential of -300 mV was selected for further study.

To demonstrate the novelty of the present biosensor for L-lactate, two sensors were built, one based on the wild-type strain 356, and the other based on the recombinant strain "tr1". The resulting biosensor performances are compared and presented in Fig. 18.

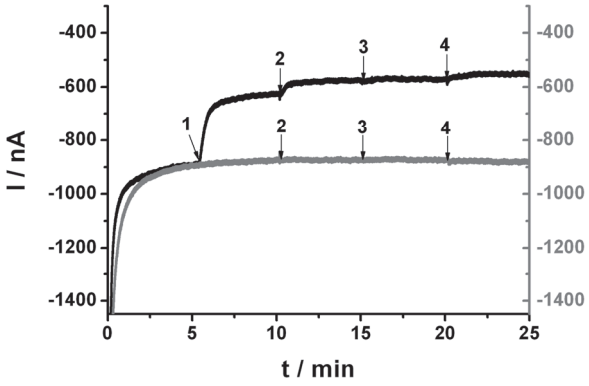

Fig. 18. Chronoamperometric response (in current density values) upon consecutive additions of L-lactate for two biosensors based on wild type (black line) and recombinant (grey line) *H. polymorpha* cells. Working electrode (graphite) polarized at -300 mV *vs.* Ag/AgCl 3M KCl. Additions 1-4, respectively: 1; 2.5; 5; 10 mM L-lactate.

As can be seen, the addition of L-lactate to the sensor based on the wild-type cells does not induce any effect on the level of oxygen concentration. Only the genetically modified yeast cells, overexpressing the FC b_2, produce a drastic change in the cell respiratory process, and thus L-lactate respiration contributes significantly to the depletion of oxygen at the electrode surface, seen here as a drop of the oxygen reduction current, proportional to the concentration of L-lactate (Fig. 18). The overexpression of FC b_2 *does* not only result in a tremendous increase in sensitivity to L-lactate (250 nA·mM^{-1} L-lactate), but also in the modulation of the selectivity of the sensor due to the specificity of oxygen consumption of the cell almost exclusively *via* L-lactate respiration. The addition of any other cell nutrients (*e.g.* glucose, etc.) does not have any effect on the background current.
Thus, by performing genetic modification, it is possible not only to inducing the synthesis of a higher amount (five times higher) of the target enzyme FC b_2, but also to influencing the metabolic pathways, in which this enzyme is involved. That makes the application of genetically modified yeast cells advantageous for L-lactate detection over wild-type cells.

3. Development of a reagentless bienzyme amperometric biosensor based on alcohol oxidase/peroxidase and Os-complex modified electrodeposition paints

Determination of ethanol is important in food technology, fermentation and wine industries, as well as in clinical chemistry (Alexander et al., 1998; Esti et al., 2003; Watson et al., 1998). Classical methods such as refractometry (Pen'kovskii et al., 2004) or densitometry (Bavcar & Kosmerl, 2003) of the distilled samples, as well as gas chromatography (Schmitt & Aderjan, 2004) which are routinely used in in clinics and industry are time- and labour-consuming procedures. In order to replace these methods, a variety of enzymatic and biosensor approaches were developed based on alcohol-specific enzymes isolated from different microbial species: NAD^+-dependent alcohol dehydrogenase (Ivanova et al., 2003; Gautier et al., 1990), quinohemoprotein alcohol dehydrogenase (Niculescu et al., 2002), or alcohol oxidase (Gibson et al., 1992; Gonchar et al., 2001, 2002; Patel et al., 2001) were proposed and applied for the determination of ethanol in complex samples. Alcohol biosensors based on NAD^+-dependent alcohol dehydrogenase (ADH) usually exhibit high selectivity, however, due to the need to add the coenzyme NAD^+ to the sample, ethanol determination is quite expensive using these types of biosensors. Even more important, ADH-based sensors showed limited operational stability (Rebelo et al., 1994).
Alternatively, alcohol oxidase (AOX), a flavoprotein, was used for the construction of alcohol biosensors. AOX exhibits an inherent non-selectivity since other primary alcohols as well as hydrated formaldehyde are enzymatically converted by this enzyme. For some real samples, this property is not crucial, because of the high abundance of a single analyte, e.g. ethanol in wine (Esti et al., 2003; Niculescu et al., 2002; Hasunuma et al., 2004). However, AOX based sensors suffer also from a limited stability and from the rather high working potential (+600 mV vs Ag/AgCl) which has to be applied for the oxidation of enzymatically-generated H_2O_2. In order to overcome these limitations, bi-enzyme sensors coupling a H_2O_2 generating oxidase reaction with the peroxidase-catalyzed H_2O_2 reduction were proposed (Castillo et al., 2003; de Prada et al., 2003). The low working potential (-50 mV vs Ag/AgCl) and the possibility to wire the peroxidase via suitable redox polymers to the electrode surface in order to provoke fast electron transfer make bi-enzyme sensor architectures a target of research (Castillo et al., 2003; de Prada et al., 2003; Vijayakumar et al., 1996). However, the main problem remains the inherent instability of AOX which often leads to a dramatic

decrease of activity during the immobilization process. Although the presence of stabilizers was shown to partially overcome this problem (Esti et al., 2003), there is still a need for the development of improved alcohol sensors with significantly increased operational stability.

3.1 Development of a reagentless bienzyme amperometric biosensor based on alcohol oxidase/peroxidase and Os-complex modified electrodeposition paints

The development of an alcohol bi-enzyme biosensor is reported which is based on AOX isolated from a genetically constructed mutant strain *Hansenula polymorpha* C-105 (Smutok et al., 2006b) or mutated AOX with decreased affinity toward substrates (Dmytruk et. al., 2007) coupled with commercial peroxidase (HRP). For immobilization of the enzymes, a non-manual electrochemically-induced precipitation procedure was applied using a new type of Os-complex modified electrodeposition paints (EDP) for the immobilization of horseradish peroxidase in a first layer and a cathodic EDP for the immobilization and stabilization of AOX in a second layer. The used redox EDP assures fast electron transfer between the integrated peroxidase and the electrode surface at a low working potential.

The electrochemical communication between immobilized enzymes and redox polymers was analyzed before sensor construction. There is no evidence that artificial electron acceptors other than O_2 are able to re-oxidize the reduced form of AOX in solution (Geissler et al., 1986), and hence AOX activity is strongly dependent on the availability of dissolved molecular oxygen. Nevertheless, possibilities for direct electron transfer between adsorbed AOX and the electrode surface as well as wiring of the enzyme by means of the Os-complex EDP were investigated. Formation of reduced AOX was induced by ethanol addition under strictly anaerobic conditions (after saturation of the system by argon for at least 1 hour). However, in accordance with previous results, neither direct electron transfer nor an Os-complex mediated wiring of the enzyme was observed for reduced AOX. Most probably, due to the complicated octameric structure of the enzyme, the polymer-bound Os-complexes were not able to approach the enzyme-integrated $FADH_2$ moiety to allow for fast electron transfer kinetics.

The integration of AOX into films of EDP was evaluated with respect to possible inactivation of the enzyme. Anodic deposition paints (*AP*) are precipitated on the electrode surface by applying potential pulses of up to +2200 mV (vs. Ag/AgCl), leading to the generation of protons in the diffusion zone in front of the electrode. After electrochemical-induced precipitation of the redox polymer *AP-Os* (anodic paint covalently linked with osmium-complexes) in the presence of AOX at such high potentials, no residual immobilized enzyme activity could be observed. Apparently, since AOX is unstable at pH-values below 6.5, the enzyme was denatured due to local proton generation. On the other hand, as suggested by the properties of AOX in solution (Woodward, 1990; Patel et al., 2001), AOX should be resistant to alkaline pH-values. Thus, integration of AOX into a cathodic EDP (*CP*) was performed using potential pulses to -1200 mV (vs. Ag/AgCl), leading to the generation of OH^--ions close to the electrode surface. No detectable deterioration of AOX activity was observed using this immobilization procedure.

In addition, due to the fact that high H_2O_2 concentrations limit AOX stability, it is essential that enzymatically generated H_2O_2 is removed as fast as possible. Thus, we have designed a bi-enzyme sensor architecture using a first layer containing horseradish peroxidase (HRP) integrated within an Os-complex modified EDP film (*AP-Os*) enabling fast electron transfer between the oxidized active site of HRP and the electrode surface, concomitantly decreasing AOX inactivation by high local H_2O_2 concentrations. On top of this layer, a second layer was

precipitated, consisting of AOX integrated within an electrochemically precipitated *CP9* layer. Alternatively, a mixture of HRP and AOX was integrated within the second layer. Thus, ethanol oxidation by means of AOX in the outer layer is coupled with the peroxidative oxidation of Os-complexes bound to the backbone of an anodic paint, followed by the final reduction of the mediator at the working electrode surface. The sensor architecture and the anticipated electron-transfer pathway are shown in Fig.19.

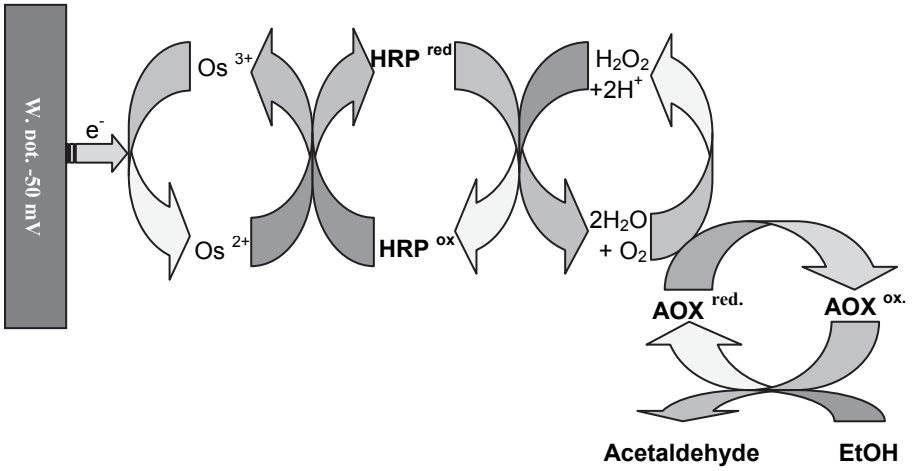

Fig. 19. Reaction scheme and electron-transfer pathway from ethanol *via* AOX, enzymatically generated H_2O_2, HRP, and polymer-bound Os-relays to the electrode.

The possibility of HRP to productively accept electrons from the Os-complexes coordinatively attached to the backbone of the anodic paint (*AP-Os*) was evaluated by means of cyclic voltammetry (Fig. 20).

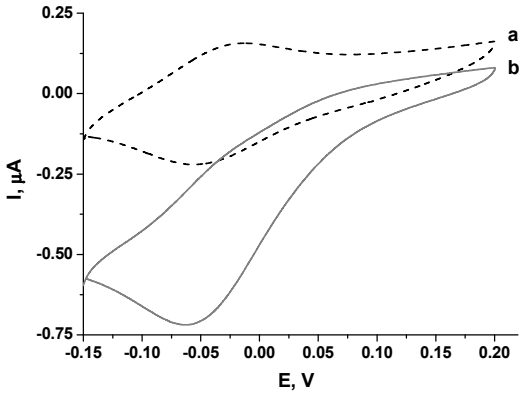

Fig. 20. Cyclic voltammogram at a graphite electrode modified with a layer containing HRP-*AP-Os* in the absence (a) and in the presence (b) of 1 mM H_2O_2. Potentials *vs.* SCE: -150 mV to –200 mV; scan rate 7 mV/s in 100 mM phosphate buffer, pH 7.6.

In the presence of H_2O_2, the reduction peak at a potential of about -50 mV *vs* SCE clearly reveals the accessibility of the heme site within HRP by the polymer-bound redox relays and the electron exchange with *AP-Os*.
Different electrode materials were investigated in combination with the optimal bi-enzyme sensor architecture (Fig. 21).

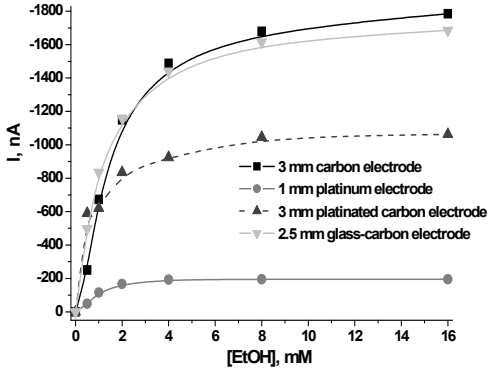

Fig. 21. Ethanol calibration graphs at *HRP-AP-Os//AOX-CP9* bi-enzyme sensors on different electrode materials.

The current densities calculated by dividing the maximal current at substrate saturation by the geometric electrode area were 244.5 nA mm^{-2} for graphite electrodes, 248.6 nA mm^{-2} for Pt electrodes; 145.5 nA mm^{-2} for electrochemically platinized graphite electrodes, and 343.6 nA mm^{-2} for glassy carbon electrodes (Fig. 21). Most probably, the platinization prevents good contact between the redox EDP or the HRP with the electrode surface, thus leading to a somewhat decreased current density. Since the current density at the Pt surface is similar to the one at the graphite surface, it can be assumed that the majority of electron transfer occurs *via* the polymer-bound Os centers, with only minor contributions by direct electron transfer from the surface adsorbed HRP.

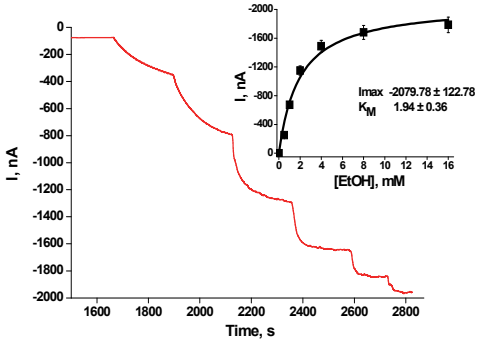

Fig. 22. Chronamperometric determination of ethanol using a *HRP-Ap-Os//AOX-CP* bi-enzyme sensors and the derived calibration graph (graphite electrode; -50 mV *vs* Ag/AgCl).

The apparent Michaelis-Menten constant K_M^{app} derived from the calibration curve shown in Fig. 22 is 1.94±0.37 mM for EtOH, a value which is in good agreement with the value of 2.7 mM for AOX in solution (Woodward et al., 1990). The typical signal rise time (95 % of the steady state value at an ethanol concentration of 4 mM) was determined to be 45 s. The optimal working pH value in phosphate buffer was determined to be 7.6.
The selectivity of the *HRP-Ap-Os//AOX-CP* bi-enzyme sensor was evaluated by determination of the concentration-dependent current response curves for different analytes, which are structurally similar to ethanol. The related calibration graphs for primary alcohols as well as formaldehyde are shown in Fig. 23.

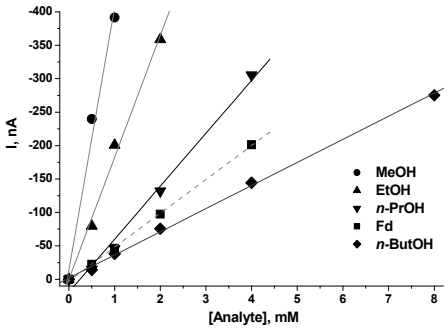

Fig. 23. Linear dynamic range of the response of *HRP-Ap-Os//AOX-CP* bi-enzyme sensors to primary alcohols and formaldehyde (graphite electrode; -50 mV vs Ag/AgCl).

The sensitivity of the sensor to the different analytes represents the affinity of AOX in solution, with the highest sensitivity for methanol (0.48 $\mu A \cdot mM^{-1}$) and ethanol (0.2 $\mu A \cdot mM^{-1}$). This sensitivity is significantly higher than that reported earlier for other AOX-based amperometric sensors, which were in the range from 0.006 to 0.03 $\mu A\ mM^{-1}$ (Patel et al., 2001). The linear dynamic range was found to be about 1 mM for methanol, 2 mM for ethanol, 4 mM for *n*-propanol and formaldehyde, and 8 mM for *n*-butanol.
As pointed out above, the main challenge in the development of alcohol biosensors is the limited operational and storage stability of the previously reported sensors. A significant improvement in the stability of the newly constructed alcohol sensor was expected due to the use of AOX from a genetically constructed mutant strain of the thermotolerant yeast *H. polymorpha* and the fast removal of enzymatically produced H_2O_2. The operational and storage stability of the *HRP-Ap-Os//AOX-CP* bi-enzyme sensor prepared under optimal conditions was tested at 24 ^{0}C. The operational stability was evaluated using a previously described automatic sequential injection analyzer (Schuhmann et al., 1995) repetitively injecting a 2 mM ethanol solution. More than 1000 injections were performed, and the obtained current peak heights were plotted against the analysis time (Fig. 24).
For the *HRP-AP-Os//AOX-CP9* bi-enzyme sensor, the current decreased from an initial peak height of 900 nA to 540 nA after 51 h. The inactivation constant of the sensor was 6.1×10^{-4} $\mu A \cdot min^{-1}$.
The storage stability of the constructed biosensor was detected by repeated sensor tests with the sensor being stored in buffer solution at 4 ^{0}C. The biosensor was stable for more than 16 days, however after about 14 days of storage there was a 50 % drop in current output. The

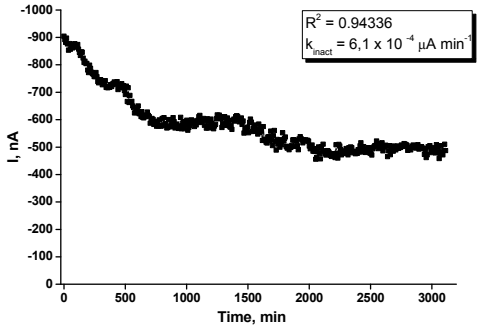

Fig. 24. Operation stability of alcohol bi-enzyme sensors evaluated by means of an automatic sequential injection analysis system.

significantly improved stability of the developed bi-enzyme sensor can be explained by their generic "sandwich" architecture using anodic and cathodic EDPs incorporating different enzymes according to their specific properties, namely, pH stability under electroprecipitation conditions.

3.2 Development an amperometric biosensor based on mutated alcohol oxidases from the yeast *H. polymorpha* with decreased affinity toward substrates

Yeast alcohol oxidase (AOX; alcohol:O_2 oxidoreductase, EC 1.1.3.13) has been extensively used for the determination of lower primary alcohols and formaldehyde (Alpeeva et al., 2005; Shkotova et. al., 2006). Significant progress in the selection of optimal transducers, and the immobilization and stabilization of the enzyme has been achieved. However, the affinity of AOX to ethanol is rather high, and direct AOX-based measurements of a target analyte, *e.g.* ethanol in real samples of wines, beers or fermentation cultures, is complicated and economically disadvantageous due to the necessity of diluting the samples. This is especially important in automatic electrochemical devises such as biosensors, since the additional step of sample dilution significantly increases the cost of analysis. In order to overcome this inconvenience, obtaining modified forms of AOX with a decreased affinity towards substrates and a wide range of linear responses is highly desirable.

Here, we describe the selection of methylotrophic yeast *H. polymorpha* mutants which produce a modified AOX with decreased affinity towards substrates, and the construction of an amperometric biosensor with a broadened linear range towards primary alcohols and aldehydes.

To isolate the mutant forms of AOX (mAOX) having decreased affinity to substrates, a positive selection procedure was developed. Allyl alcohol was used as the selective agent in the medium, with methanol as the sole carbon and energy source. The rationale for the selection scheme was as follows: since the oxidation of allyl alcohol by AOX is accompanied by the formation of the highly toxic molecule acrolein, in medium of methanol (0.5 %) and allyl alcohol (minimal inhibitory concentration was found to be 0.3 mM), mutants lacking AOX could not survive. Only mutants producing lower amounts of acrolein and enough formaldehyde for growth will survive and could be selected. One of the reasons for such an event would be the decreased affinity of AOX toward substrates while retaining a high enough reaction rate. This selection scheme would produce few or no mutants with a decreased rate of AOX reaction, as they would not grow efficiently due to the negligible

amount of formaldehyde produced. Altogether, 125 mutants of the *H. polymorpha* strain DL-1-356 that were able to grow in allyl alcohol containing medium were chosen for further selection. Mutants with decreased enzyme affinity towards ethanol were screened by a plate colony assay for AOX activity. Finally, two positive colonies (strains CA2 and CA4) which stained in the presence of 15 mM ethanol, but not 5 mM or 10 mM ethanol, were selected.
The kinetic parameters of AOX from the selected mutant strains were evaluated. K_M values for methanol from the parental strain and the CA2 and CA4 mutants were calculated as 0.62, 2.48, and 1.10 мМ, respectively (Table 2). At the same time, the values of V_{max} (recalculated per mg of protein) for AOX from the aforementioned strains were 27.4, 66.7 and 31.3 μmol of atomic O $\cdot min^{-1} \cdot mg^{-1}$ at 20 ^{0}C, respectively (Table 2). Thus, allyl alcohol/methanol-based selection is suitable for obtaining *H. polymorpha* mutants with decreased AOX affinity toward the substrate and without decreased maximal rate of the specific enzyme reaction.

H. polymorpha strain	K_M, мМ	V_{max}, μmol of atomic O $\cdot min^{-1} \cdot mg^{-1}$ of protein at 20^{o}C	Sigma factor, σ	Linear regression coefficient R for reciprocal plot
DL-1-356	0.62	27.4	0.084	0.992
CA2	2.48	66.7	0.040	0.958
CA4	1.10	31.3	0.130	0.990

Table 2. K_M and V_{max} values of AOX towards methanol for natural and mutant *H. polymorpha* strains

The construction of a bioselective layer of the sensor was performed according to the techniques described above. The structure of the bi-enzyme electrode was configured as *HRP-AP-Os//AOX(CA2)-CP* and included two layers: the inner, with horseradish peroxidase (*HRP*) electrochemically precipitated in the presence of a carboxylate-containing polymer modified with an osmium complex (*AP-Os*), and the outer, with mutated mAOX(CA2), immobilized *via* cathodic precipitation in the presence of an amino-containing polymer (*CP*). Platinized graphite rods were used as working electrodes. The characterisation of the enzymatic

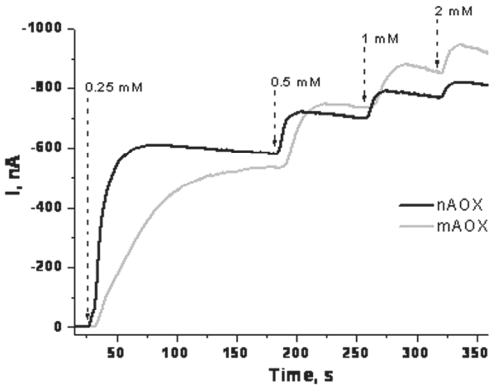

Fig. 25. Chronoamperometric assay of ethanol by *HRP/Os-Ap59//AOX/CP9* biosensors based on the natural (nAOX) and mutated (mAOX) forms of alcohol oxidase. Arrows indicate step-wise addition of ethanol in different concentrations.

properties of mAOX was performed using natural (wild type) nAOX as a reference. The typical dynamic ranges for AOX-modified sensors to ethanol are presented in Fig. 25.
In addition to alcohols (*e.g.*, ethanol or methanol), formaldehyde is also a substrate for AOX (Verduyn et al., 1984). The calibration curves of the biosensors response to ethanol and formaldehyde clearly show the lower affinities toward both substrates of mAOX compared to wild-type enzyme (Fig. 26A).

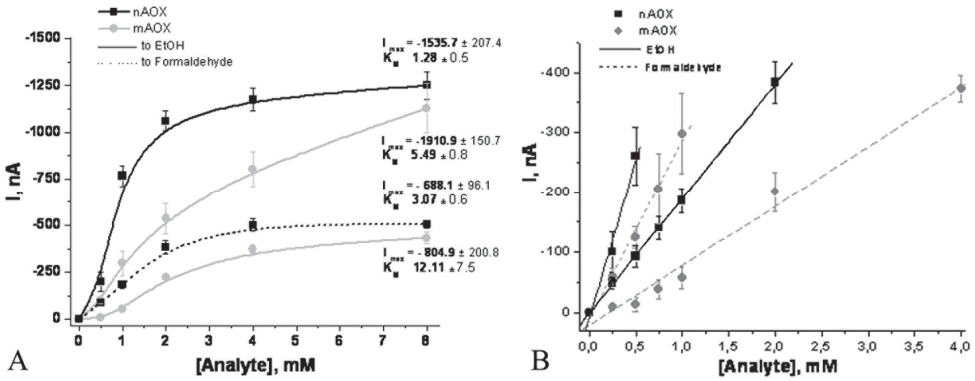

Fig. 26. Calibration curves and calculated K_M values of sensors based on the different forms of AOX toward ethanol (EtOH) and formaldehyde (A) and dynamic linear ranges of the corresponding sensors towards both analytes (B).

As previously mentioned, the natural and mutant forms of AOX differ in K_M value towards methanol in solution: the mutant enzyme possesses a 4-fold increased K_M value and thus, decreased substrate affinity (Table 2). The results obtained using amperometric sensors with immobilized AOXs show a good agreement with those obtained with AOXs in solution. The K_M values of a nAOX-baesd sensor were 1.28 mM for ethanol and 3.07 mM for formaldehyde, whereas these values for the mAOX-based electrode were increased to 5.40 mM for ethanol and 12.1 mM for formaldehyde. These results also show that mutant AOXs have a decreased affinity not only to the physiological substrate methanol, but also to other substrates, such as ethanol and formaldehyde. It is interesting to note that the I_{max} values for ethanol and formaldehyde of nAOX and mAOX-based electrodes were 1536/1911 nA and 688/805 nA, respectively. The I_{max} values of the sensors did not differ significantly (Fig. 26A). In addition, the linear dynamic range of the mAOX-based electrode for ethanol was 4 mM as compared to 0.5 mM for the nAOX-based electrodes (Fig. 26B).
The study of operational stability and inactivation kinetics of the constructed biosensors revealed that the sensors based on either mutant or natural (wild type) enzymes are very similar (Fig. 27).
Both sensors retained 50 % of their activity after 5 h of continuous operation in a sequential-inhection analyzer. The biosensors were stable for more than 16 days, however, after 14 days of storage there was a 50 % drop in current output (data not shown). In conclusion, the constructed amperometric biosensor based on mAOX(CA2) was characterised by a decreased affinity towards the analyzed substrates without altered operational stability of the sensor.

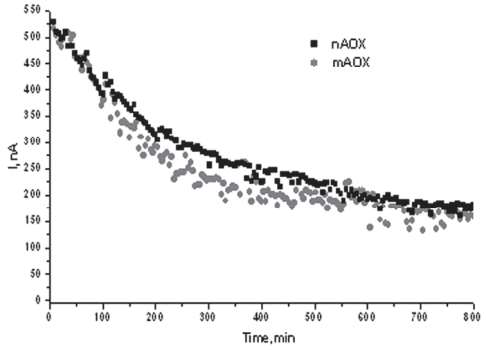

Fig. 27. Comparison of an operational stability of nAOX and mAOX-modified electrodes.

4. Amperometric biosensors for glycerol determination

Glycerol determination is important in clinical diagnostics for control of the triacylglycerides (TG) level in blood. The monitoring of these components has a prognostic value to drop the risks of diseases of the cardiovascular system. An elevated TG level in blood is a strong risk factor for arteriosclerosis. At high level of TG some malignancies, namely, coronary insufficiency and infarction occur more frequently. So, the development of a quick and reliably method for TG/glycerol determination is very important.

The known and used methods for TG determination are based on the enzymatic hydrolyses of TG by means of lipases/esterases and determination of the released glycerol.

The main principles for amperometric detection of glycerol are based on the detection of the formed NADH or mediators, on the use of oxygen or hydrogen peroxide electrodes, conductive organic salts and wiring of enzymes to electrodes (Fig. 28).

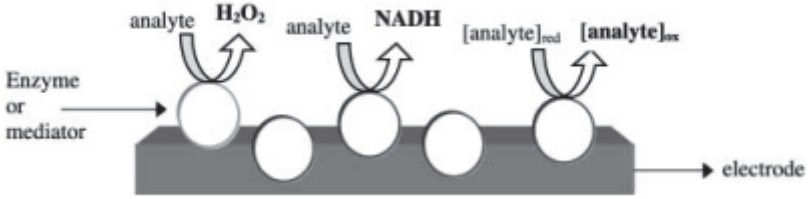

Fig. 28. Schematic representation of various types of amperometric biosensors (Prodromidis et al., 2002)

Many materials, namely, platinum (Goriushkina et al., 2010), gold (Gamella et al., 2008), glassy carbon (Guo et al., 2010), different types of graphite (Haghighi et al., 2010; Pournaghi-Azar et al., 2010), screen-printed electrodes (Ben Rejeb et al., 2007; Radoi et al., 2007; Ricci et al., 2007; Gurban et al., 2008), rigid carbon-polymer biocomposites (Alvarez-González et.al., 2000; Liao et al., 2008), zeolites, clays, and polymeric membranes (Katrlik et al., 2006; Rozlosnik et al., 2009) were previously used for the construction of glycerol-selective electrodes. Various strategies of enzyme immobilization (Prodromidis et al., 2002), including physical or covalent binding, gel entrapment, electropolymerization, sol-gel techniques

(Gurban et al., 2008; Haghighi et al., 2010; Guo et al., 2010; Pournaghi-Azar et al., 2010; Liao et al., 2008) and self-assembled architectures (Gamella et al., 2008) were employed for biosensors construction.

4.1 Glycerol-selective enzymes

Different methods, such as liquid chromatography and spectrophotometric approach based on chemical and enzymatic reactions (West, 1998; Wu et al., 2005; Hinsch et al., 1980; Minakshi et al., 2008), in particular, oxidase-peroxidase method (Gonchar & Sybirny, 1991; Gonchar, 1998) have been proposed for glycerol determination.

The test-kits for enzymatic analysis of glycerol produced by Boehringer Mannheim and Sigma are rather expensive, because they require several enzymes and coenzymes or co-substrates. For example, the multienzymatic system (West S.I.,1998) involves three enzymes: glycerol kinase (GK), pyruvate kinase (PK) and lactate dehydrogenase (LDH), and requires the presence of the coenzyme NADH and two co-substrates, namely, ATP and phosphoenolpyruvate:

$$\text{glycerol + ATP} \xrightarrow{GK} \text{glycerol-3-phosphate + ADP} \tag{1}$$

$$\text{phosphoenol pyruvate} + \text{ADP} \underset{\longleftarrow}{\overset{PK}{\longrightarrow}} \text{pyruvate} + \text{ATP} \tag{2}$$

$$\text{pyruvate} + \text{NAD}H\left(H^+\right) \underset{\longleftarrow}{\overset{LDH}{\longrightarrow}} \text{lactate + NAD}^+ \tag{3}$$

In this method, the glycerol concentration is determined by a decrease in the consumed NADH registered photometrically at 340 nm.

In the two-enzyme variant, GK (see eq. 1) and glycerol-3-phosphate dehydrogenase (GPD) are used. The reaction is also monitored photometrically by recording the generation of NADH(H^+) at 340 nm:

$$\text{glycerol-3-phosphate + NAD}^+ \xrightarrow{GPD} \text{NADH}\left(H^+\right) \text{ + dihydroxyacetone phosphate (DHAP)} \tag{4}$$

In another variant of the two-enzyme method, glycerol-3-phosphate-oxidase (GPOx) and peroxidase (HRP) are used instead of GPD. This variant was applied as a basis of diagnostic kit for glycerol determination.

$$\text{glycerol-3-phosphate} + O_2 \xrightarrow{GPOx} \text{DHAP} + H_2O_2 \tag{5}$$

$$H_2O_2 + \text{chromogen}\ (-2H) \xrightarrow{\text{HRP}} \text{dye} + 2H_2O \tag{6}$$

The third, dehydrogenase method, is based on the determination of NADH(H^+) generated in the enzymatic reaction catalyzed by glycerol dehydrogenase (GDH):

$$\text{glycerol} + \text{NAD}^+ \underset{\longleftarrow}{\overset{GDH}{\longrightarrow}} \text{DHA + NAD}H\left(H^+\right) \tag{7}$$

The application of this method in analytical practice is problematic since the glycerol oxidation by GDH is a reversible reaction, and the selectivity of the enzyme is insufficient.

The enzyme glycerol oxidase (GO) oxidizes glycerol in the presence of oxygen under formation of hydrogen peroxide and glyceraldehyde:

$$\text{glycerol} + O_2 \xrightarrow{GO} \text{glyceraldehyde} + H_2O_2 \quad (8)$$

GO is produced by cultivation of fungi: *Aspergillus*, *Penicillium* (Uwajima et al., 1979), *Neurospora* (Hill & Martin, 1975), *Botrytis* (Kupletskaya, 1996) and actinomycetes. GO is revealed in numerous mycelia fungi, but a highly purified enzyme preparation was isolated only from *Aspergillus japonicus* (Uwajima, 1984; Patent US US*4409328*(A), 1983), *Penicillium sp.* (Lin et al., 1996) and *Botrytis allii* (Patent 2117702C1, 1998; Pavlishko et al., 2004; Gayda et al., 2006).

Traditional enzymatic approaches for glycerol determination are disadvantageous due to either unsatisfactory selectivity, like in case of dehydrogenase reactions, or high cost of their everyday laboratory application. Therefore, the development of valid, selective, quick and cheap methods for glycerol analysis in clinical diagnostics is important.

4.2 Amperometric biosensors for glycerol determination

A number of biosensors for glycerol determination have been designed and investigated. They are based on the use of GDH (Kiba et al., 1996; Laurinavicius et al., 1996) and GK co-immobilized with GPOx (Compagnone et al., 1998). The latter sensor showed insufficient stability: after three days of storage in a working buffer only 10 % of the enzymes remained active. The key disadvantage of the use of GDH in amperometric biosensors is the necessity to add NAD^+ to the system which raises the price of the analysis substantially. Besides, NAD^+ can easily diffuse out of the enzyme membrane, causing a remarkable drop in biosensor sensitivity (Laurinavicius et al., 1996).

Lipase activity against TG has been measured using an amperometric GDH/NADH-based biosensor. A Prussian blue (PB) modified screen-printed electrode (SPE) was selected as a carrier for the two enzyme system. The obtained glycerol biosensor was investigated in a lipase activity assay in real samples and for detection of fatty acids. It demonstrated a good agreement with reference methods (Ben Rejeb et al., 2007).

Biosensors for NADH determination has been assembled using stable NADH oxidase (NAox) from *T. thermophilus* covalently immobilized on electrodes (Radoi et al., 2007; Serban & Murr , 2005). The NAox uses O_2 as its natural electron acceptor and produces H_2O_2 in a two-electron process. The possibility to measure glycerol with NAox-Prussian Blue bulk-modified screen-printed electrodes was investigated (Radoi et al., 2007). Various parameters: pH dependence (range of stability – pH 3.0–10.5, optimal - pH 5.0), response time (12 s) and operational stability (120 injections) were evaluated and optimised. The detection and quantification limits were 1.1×10^{-7} and 3.6×10^{-7} M, respectively, and the linear working range was comprised between 1 and 400 μM. The proposed biosensor was stable for 2 months (preserved in 50 mM phosphate buffer, pH 6.8, at 4 °C). Another high sensitive NADH amperometric biosensor based on co-immobilized NAox in combination with a redox mediator (hydroxymethyl ferrocene) and HRP was proposed (Serban & Murr , 2005) with a linear range from 5×10^{-6} M in reduction until 2×10^{3} M in oxidation.

For estimation of the glycerol content in complex biological fluids two enzyme biosensor systems, based on GDH/DP and GK/GPOx/HRP, immobilized on interchangeable membranes by a prepolymer technique, were developed. A flow-injection assay of the glycerol content was performed in the presence of ferricyanide/NAD^+ or ferrocyanide/ATP. The

biosensors were characterized by a linear range of 0.01–1 or 0.01–1.5 mM glycerol, and a sensitivity of 6.02 or 1.42 $mA \cdot M^{-1} \cdot cm^{-2}$ and with a signal loss of 40 % after 90 h or 30 % after 16 h during continuous operation at a sample throughput of 10 injections/h for GDH/DP or GK/GPOx/HRP-containing membranes, respectively. The operational stability of the described biosensor systems was sufficient for monitoring and control of fermentation processes for up to 24 h, with several months of storage stability (Katrlik et al., 2006).

Modified SPE for amperometric detection of H_2O_2 and NADH at low applied potential were obtained by modifying the working electrode surface with Prussian Blue (PB-SPE). The coupling of this sensor with phenazine methosulfate (PMS) in the working solution gives the possibility of measuring both NAD(P)H and H_2O_2. PMS reacts with NADH producing PMSH, which in the presence of oxygen, gives an equimolar amount of H_2O_2. This allows the measurement of both analytes with similar sensitivity (357 $mA \cdot M^{-1} \cdot cm^{-2}$ for H_2O_2 and 336 $mA \cdot M^{-1} \cdot cm^{-2}$ for NADH) and similar limit of detection (5×10^{-7} M for H_2O_2 and NADH). Results obtained with a variety of dehydrogenases (alcohol, malic, lactate, glucose, glycerol and glutamate dehydrogenase) for the detection of their substrates or the enzymatic activity were performed demonstrating the sutability of the proposed method for future biosensor applications (Ricci et al., 2007).

To improve the NADH detection biosensors based on NAox/FMN and Prussian blue (PB) modified SPE have been developed. The catalytic effect, the sensitivity and the stability of PB-SPEs were studied at different pH values and different potentials ranges in cyclic voltammetry and amperometric measurements. NAox and FMN were immobilised on the PB-SPEs by entrapment in a sol–gel, PVA-AWP polymer matrices or using glutaraldehyde. The amperometric detection of NADH was performed at +250 mV *versus* Ag/AgCl, and co-enzyme was entrapped with NAox in the biocatalytic layer using sol–gel matrix. The sensitivity was 4.57 $mA \cdot M^{-1} \cdot cm^{-2}$ (R.S.D. = 9.2 %, n = 4), the linear range up to 1.61 mM and the detection limits about 1.17 μM. These biosensors revealed a good long term and operational stability, the response decreased from 3.4 % after 2 days, to 50 % of the analytical signal after 6 months (Gurban et al., 2008).

GDH and NAD^+ were co-immobilized in a carbon paste electrode using an electropolymerized layer of non-conducting poly(*o*-phenylenediamine) (PPD). After partial oxidation of the immobilized NAD^+, the modified electrode allows the amperometric detection of the enzymatically generated NADH at an applied potential above 0 V (Ag/AgCl). The resulting biosensor shows a fast and linear response to glycerol within the concentration range of 1.0×10^{-6}-1.0×10^{-4} M with a detection limit of 4.3×10^{-7} M. The amperometric response remains stable for at least 3 days. The biosensor was applied to the determination of glycerol in a plant-extract syrup, with results in good agreement with those for the standard spectrophotometric method (Alvarez-González et. al., 2000).

For glycerol determination two different biosensor configurations have been evaluated: one based on the GDH/DP bienzyme system, and another using GK/GPOx/HRP. Both enzyme systems were immobilized together with the mediator tetrathiafulvalene (TTF) on a 3-mercaptopropionic acid (MPA) self-assembled monolayer (SAM)-modified gold electrode by using a dialysis membrane. After 51 days of use, the GDH/DP biosensor still exhibited 87 % of the original sensitivity, while the GK/GPOx/HRP biosensor yielded a 46 % of the original response after 8 days. Linear ranges of $1.0 \cdot 10^{-6}$ to $2.0 \cdot 10^{-5}$ or $1.0 \cdot 10^{-6}$ to $1.0 \cdot 10^{-5}$ M glycerol and sensitivities of 1214±21 or 1460±34 $\mu A \cdot M^{-1}$ were obtained with GDH/DP and GK/GPOx/HRP-based biosensors, respectively. The calculated detection limits were $4.0 \cdot 10^{-7}$ and $3.1 \cdot 10^{-7}$ M, respectively (Gamella et al., 2008).

The development of nanoscience and nanotechnology has inspired scientists to continuously explore new electrode materials for constructing an enhanced electrochemical platform for sensing. A Pt nanoparticle (NP) ensemble-on-graphene hybrid nanosheet (PNEGHNs) was proposed as new electrode material. The advantages of PNEGHNs modified glassy carbon electrode (GCE) (PNEGHNs/GCE) are illustrated from comparison with the graphenes (GNs) modified GCE for electrocatalytic and sensing applications. The electrocatalytic activities toward several organic and inorganic electroactive compounds at the PNEGHNs/GCE were investigated, all of which show a remarkable increase in electrochemical performance relative to GNs/GCE. Hydrogen peroxide and trinitrotoluene (TNT) were used as two representative analytes to demonstrate the sensing performance of PNEGHNs. It is found that PNEGHNs modified GCE shows a wide linear range and low detection limit for H_2O_2 and TNT detection (Guo et al., 2010).

An iridium nanoparticle modified carbon bioelectrode for the detection and quantification of TG was successfully carried out. TG was hydrolyzed by lipase and the produced glycerol was catalytically oxidized by GDH producing NADH in a solution containing NAD^+. Glyceryl tributyrate, a short chain TG, was chosen as the substrate for the evaluation of this TG biosensor in bovine serum and human serum. A linear response to glyceryl tributyrate in the concentration range of 0 to 10 mM and a sensitivity of 7.5 $nA \cdot mM^{-1}$ and 7.0 $nA \cdot mM^{-1}$ in bovine and human serum, respectively, were observed. The conditions for the determination of TG levels in bovine serum using this biosensor were optimized, with sunflower seed oil being used as an analyte to simulate the detection of TG in blood. The experimental results demonstrated that this iridium nano-particle modified working electrode based biosensor provided a relatively simple means for the accurate determination of TG in serum (Liao et al., 2008).

Prussian blue nanoparticles (PBNPs) immobilized on the surface of a graphite electrode was covered with a layer of Nafion. The sensor showed a good electrocatalytic activity toward H_2O_2 reduction, and it was successfully used for the amperometric detection of H_2O_2. The calibration curve for H_2O_2 determination was linear from 2.1×10^{-6} to 1.4×10^{-4} M with a detection limit (S/N = 3) of 1.0×10^{-6} M (Haghighi et al., 2010). Further modification of the proposed sensor with different enzymes, namely, GO, was discussed as a perspective for the fabrication of a glycerol biosensor.

For hydrodynamic amperometry of H_2O_2 at μM concentration level, an aluminum electrode plated by a thin layer of metallic palladium and modified with Prussian blue (PB/Pd–Al) was developed. It was found that the calibration graph is linear with the H_2O_2 concentration in the range from 5×10^{-6} to 34×10^{-6} M with a correlation coefficient of 0.999. The detection limit of the method was about 4×10^{-6} M. The method was successfully used for the monitoring of H_2O_2 in saliva and environmental samples (Pournaghi-Azar et al., 2010).

New natural materials, such as egg shells, were proposed as enzymes carrier in bioselective membranes for triglyceride (TG)-selective amperometric biosensors. A mixture of commercial lipase, GK and GPOx was co-immobilized at an egg shell membrane through covalent coupling. Maximum current was obtained at a working potential of +400 mV. The biosensor showed optimum response within 10 sec at pH 7.0 and 35 °C. The linear range was from 0.56 to 2.25 mM TG and the detection limit was 0.28 mM. A good correlation (r=0.985) was obtained between the TG level determined by the standard enzyme-based colorimetric test and the proposed sensors. Serum compounds (urea, uric acid, glucose, cholesterol, ascorbic acid and pyruvic acid) did not interfere with the sensor response. The stability of enzyme electrode was determined to be 200 measurements over a period of 70

days without any considerable loss of activity, when stored at 4°C between the measurements (Narang et al., 2010).
Conducting polymer-based electrochemical sensors have shown numerous advantages in a number of areas related to human health, such as the diagnosis of infectious diseases, genetic mutations, drug discovery, forensics and food technology, due to their simplicity and high sensitivity. One of the most promising group of conductive polymers is poly(3,4-ethylenedioxythiophene); PEDOT or PEDT) and its derivatives due to their attractive properties: high stability, high conductivity (up to 400-600 S/cm) and high transparency (Rozlosnik et al., 2009; Nikolou et al., 2008). Organic transistors based on PEDT doped with poly(styrene sulfonic acid) (PEDT:PSS) offer enormous potential for facile processing of small, portable, and inexpensive sensors ideally suited for point-of-care analysis. They can be used to detect a wide range of analytes for a variety of possible applications in fields such as health care (medical diagnostics), environmental monitoring (airborne chemicals, water contamination, etc.), and food industry (smart packaging). These transistors are considered to be excellent candidates for transducers for biosensors because they have the ability to translate chemical and biological signals into electronic signals with high sensitivity. Furthermore, fuctionalization of PEDT:PSS films with a chemical or biological receptors can lead to high specificity (Nikolou et al., 2008).

4.3 Bioanalytical application of Glycerol oxidase (GO) as bioselective element of amperometric biosensors

The enzymatic glycerol transformation using oxidases results in generating of electrochemically active hydrogen peroxide. An amperometric GO-based biosensor is considered to be an attractive alternative over other biosensors. To construct glycerol selective biosensors, a GO preparation with a specific activity of 5.7 $\mu mole \cdot min^{-1} \cdot mg^{-1}$ of protein were used for immobilization on electrodes. The enzyme was purified from a cell-free extract of the fungus *B. allii* by anion-exchange chromatography and stabilized with 5-10 mM Mn^{2+}, 1 mM EDTA and 0.05 % polyethylene imine (Gayda et al., 2006).

4.3.1 Immobilization of GO on platinum printed electrode (Goriushkina et al., 2010)

Different methods of GO immobilization on the surface of printed platinum electrodes (SensLab, Leipzig, Germany) were compared: electrochemical polymerization in polymer PEDT, electrochemical deposition in Resydrol and immobilization using glutaraldehyde vapors.
The monomer 3,4-ethylenedioxythiophene (EDT) and poly(ethylene glycol) (MM = 1450) were used for the electrochemical polymerization. A mixture consisting of 10^{-2} M EDT, 10^{-3} M polyethylene glycol, and GO solution was prepared in 20 mM phosphate buffer, pH 6.2. EDT was polymerized by application of a potential from +200 to +1500 mV at a rate of 0.1 V/s during 15 cycles. Homogenous PEDT films were obtained on the surface of the working electrode. Film formation is enhanced in aqueous and possibly hydrophilic polymers such as polyvinyl pyrrolidone (PVP) or polyethylene glycol (PEG), which are dissolved in the electropolymerization solution. The entrapment of PVP or PEG results in an increased hydrophilicity of the deposited polymer film.
The commercial resin Resydrol (Resydrol AY 498 w/35WA) and glutaraldehyde were also used as a polymer matrix for the enzyme immobilization.
GO-based biosensors with the enzyme immobilized within a Resydrol layer or using glutaraldehyde vapor, are characterized by a narrow dynamic range and a lower response

in comparison with the biosensor based on GO immobilized in PEDT. The limit of detection for glycerol for all these biosensors is about the same (Table 3). The developed GO-PEDT-based biosensor is characterized by a linear response on the glycerol concentration in the range from 0.05 to 25.6 mM with a detection limit of 0.05 mM glycerol (Fig. 29). The stability of the GO-PEDT-based biosensor was evaluated and showed a decrease in its response value by about 2.5 % daily with almost no response after 50 days of storage. The pH optimum of the GO-PEDT-based biosensor was determined to be 7.2.
An analysis of the impact of buffer capacity and concentration of the base electrolyte showed feeble influence of their change on the response value (Fig. 30) which is typical for enzyme amperometric biosensors.

Immobilization method	Detection limit for glycerol, mM	Linear range, mM	Maximum response, nA	Storage stability
Entrapment of GO in poly(3,4-ethylenedioxythiophene) (PEDT) by electrochemical polymerization	0.05	0.05 to 25.6	1405	75% activity after 15 days, 14% after 40 days
Entrapment in Resydrol by means of electrochemically induced polymer precipitation	0.05	0.05 to 0.4	400	38% activity after 2 weeks, 13% after 40 days
Glutaraldehyde vapour	0.05	0.05 to 0.2	130	10% after 1 day

Table 3. Comparative analysis of laboratory prototypes of amperometric biosensors based on different methods of glycerol oxidase immobilization

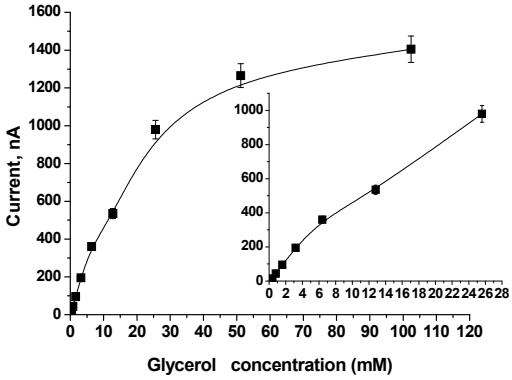

Fig. 29. The calibration curve of the GO-PEDT-based amperometric biosensor. Measuring conditions: 100 mM phosphate buffer, pH 7.2, potential of +300 mV versus the intrinsic reference electrode.

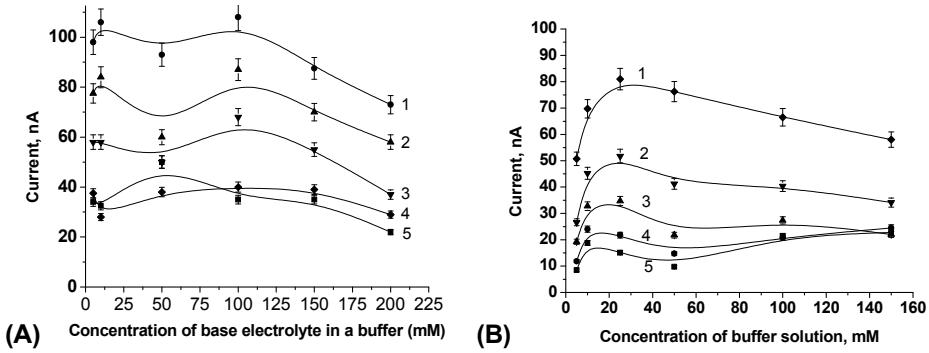

Fig. 30. Response of GO-PEDT-based amperometric biosensor on concentrations of the base electrolyte in buffer (A) and on the concentration of the buffer solution (B). Measuring conditions: 100 mM phosphate buffer, pH 7.2, potential of +300 mV *versus* the intrinsic reference electrode. Glycerol concentrations in a measuring cell: A - 6.4 mM (1); 3.2 mM (2); 1.6 mM (3); 0.8 mM (4); 0.4 mM (5); B - 1.6 mM (1); 0.8 mM (2); 0.4 mM (3); 0.2 mM (4); 0.1 mM (5).

4.3.2 Co-immobilization of glycerol oxidase and peroxidase on carbon electrode

Immobilization of glycerol oxidase (GO) in combination with horseradish peroxidase (HRP) was conducted on platinised carbon electrodes by electrodeposition in a mixture of the osmium-complex containing cathodic paint (*CP-Os*) according to the scheme which was developed by us for the immobilization of yeast alcohol oxidase (Smutok et al., 2006). Electrodeposition of the enzymes at the working electrode surface was performed in an electrochemical microcell using controlled potential pulses to -1200 mV for 0.2 sec with an interval of 5 sec for 10 cycles. The electrode was washed with 50 mM borate buffer, pH 9.0, before measurements.

Measurements were performed at room temperature in a glass cell with the volume of 50 ml, filled with 25 ml of buffer at intense stirring. After the bachground current was attained, glycerol was stepwise added to the measuring cell in increasing concentrations, and the amperometric signal was recorded. Fig. 31 shows current response of the bi-enzyme sensor *HRP-GO-CP-Os* upon stepwise addition of glycerol. The linear concentration range for the developed sensor was up to 5 mM of the analyte.

5. Conclusion

In this review, the development of enzyme- and cell-based amperometric biosensors is described aiming on monitoring of L-lactate, alcohols, and glycerol using genetically constructed over-producers of enzymes as well as wild type microorganisms. Novel, recombinant or mutated enzymes (L-lactate:cytochrome *c* oxidoreductase, alcohol oxidase, glycerol oxidase) were used as bioselective elements for the above mentioned biosensors. Most genetic manipulations have been done using the thermotolerant yeast *Hansenula polymorpha*. Enzymes isolated from this source demonstrated improved stability when

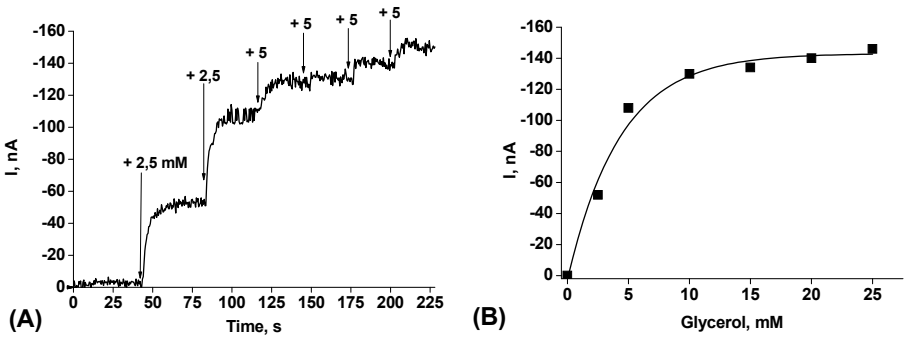

Fig. 31. Amperometric response (A) and calibration graph (B) obtained with a bi-enzyme sensor upon stepwise addition of glycerol at increasing concentrations. Experimental conditions: working potential –50 mV, 10 cycles of electrodeposition, 50 mM borate buffer, pH 9.0.

compared to non-thermotolerant yeasts. On the other hand, directed protein modification allowed increasing K_M values of the enzymes (flavocytochrome b_2 and alcohol oxidase) resulting in a wider linear range of the related biosensors. Recombinant yeast cells overproducing the target enzyme were used as the sources of the corresponding enzymes, as well as directly as microbial biorecognition elements in the sensors. For the different bioselective components (enzymes, cells or cell debris) different immobilization procedures were developed and optimized: physical adsorption, fixation behind a dialysis membrane, entrapment in a polymer layer of an anodic or cathodic electrodeposition paints, cross-linking with glutardialdehyde vapour *etc*. The developed biosensors are characterized by an in general high sensitivity, sufficient or improved selectivity, as well as improved long term operational and storage stability.

6. Acknowledgement

This work was partially supported by CRDF, project # UKB2-9044-LV-10 and in part by the Samaria and Jordan Rift Valley Regional R&D Center (Israel) and by the Research Authority of the Ariel University Center of Samaria (Israel), by NAS of Ukraine in the field of complex scientific-technical Program "*Sensor systems for medical-ecological and industrial-technological needs*". Some experiments were performed by the use of equipment granted by the project ''Centre of Applied Biotechnology and Basic Sciences'' supported by the Operational Program ''Development of Eastern Poland 2007-2013'', No. POPW.01.03.00-18-018/09.

7. References

Adamowicz, E. & Burstein, C. (1987). L-lactate enzyme electrode obtained with immobilized respiratory chain from Escherichia coli and oxygen probe for specific determination of L-lactate in yogurt, wine and blood. *Biosensors*, Vol.3, pp. 27–43, ISBN 978-953-7619-99-2

Alexander, P.W.; Di Benedetto, L.T. & Hibbert, D.B. (1998). A field-portable gas analyzer with an array of six semiconductor sensors. Part 1: quantitative determination of ethanol. *Field Analytical Chemistry and Technology*, Vol.2, No.3, pp. 135-143, ISSN 1520-6521

Alpeeva, I.S.; Vilkanauskyte, A.; Ngounou, B.; Csöregi, E.; Sakharov, I.Y.; Gonchar, M. & Schuhmann, W. (2005). Bi-enzyme alcohol biosensors based on genetically engineered alcohol oxidase and different peroxidases. *Microchimica Acta*, Vol.152, pp. 21-27, ISSN 1436-5073

Alvarez-González, M.I.; Saidman, S.B. & Lobo-Castañón, M.J. (2000). Electrocatalytic detection of NADH and glycerol by NAD(+)-modified carbon electrodes. *Anal. Chem.,* Vol. 72, No 3, pp. 520-527, ISSN: 0003-2700

Arvinte, A.; Gurban, A.; Rotariu, L.; Noguer, T. & Bala, C. (2006). Dehydrogenases-based biosensors used in wine monitoring. *Revista de Chimie*, Vol. 57, pp. 919-922, ISSN 0034-7752

Baptista, P.; Pereira, E.; Eaton, P.; Doria, G.; Miranda, A.; Gomes, I.; Quaresma, P. & Franco R. (2008). Gold nanoparticles for the development of clinical diagnosis methods. *Analytical & Bioanalytical Chemistry*, Vol.391, pp. 943-950, ISSN 1618-2650

Baronian, K.H.R. (2004). The use of yeast and moulds as sensing elements in biosensors. *Biosensors and Bioelectronics*, Vol.19, pp. 953–962, ISSN 0956-5663

Bavcar, D. & Kosmerl, T. (2003). Determination of alcohol content, volatile substances and higher alcohols of spirit beverages. *Slovenski Kemijski Dnevi*, Maribor, Slovenia, pp. 291-297 ISBN 86-435-0565-X

Belluzo, M.S.; Ribone; M.E. & Lagier, C.M. (2008). Assembling amperometric biosensors for clinical diagnostics. *Sensors*, Vol.8, pp. 1366-1399, ISSN 1424-8220

Ben Rejeb, I.; Arduini, F. & Amine, A. (2007). Amperometric biosensor based on Prussian Blue-modified screen-printed electrode for lipase activity and triacylglycerol determination. *Analytica Chimica Acta,* Vol. 594, Is. 1, pp. 1-8, ISSN: 0003-2670

Billinton, N.; Barker, M.G.; Michel, C.E.; Knight, A.W.; Heyer, W.D.; Goddard, N.J.; Fielden, P.R. & Walmsley, R.M. (1998). Development of a green fluorescent protein reporter for a yeast genotoxicity biosensor. *Biosensors and Bioelectronics*, Vol.13, pp. 831–838, ISSN 0956-5663

Brooks, G.A. (2002). Lactate shuttles in nature. *Biochemical Society Transactions*, Vol.30, No.2, pp. 258–264, ISSN 1470-8752

Carralero, S.V.; Luz, M.M. & Gonzélez-Cortès A. (2005). Development of a tyrosinase biosensor based on gold nanoparticles-modified glassy carbon electrodes. Application to the measurement of a bioelectrochemical polyphenols index in wines, *Analytica Chimica Acta,* Vol. 528, pp. 1–8, ISSN: 0003-2670

Castillo, J.; Gaspar, S.; Sakharov, I. & Csoregi, E. (2003). Bienzyme biosensors for glucose, ethanol and putrescine built on oxidase and sweet potato peroxidase. *Biosensors and Bioelectronics*, Vol.18, No.5-6, pp. 705-714, ISSN 0956-5663

Commercial Biosensors: Applications to Clinical, Bioprocess, and Environmental Samples. (1998) (Ed. Graham Ramsay), *Wiley-Interscience*, 304 p, ISBN-10: 047158505X

Compagnone, D.; Esti, M. & Messia, M.C. (1998). Development of a biosensor for monitoring of glycerol during alcoholic fermentation, *Biosensors Bioelectron*., Vol .13, pp. 875-880, ISSN: 0956-5663

Creanga C. & Murr N. E. (2011). Development of new disposable NADH biosensors based on NADH oxidase. *J. Electroanal. Chem.* In Press, Corrected Proof, Available online 1 December 2010, doi:10.1016/j.jelechem.2010.11.030, ISSN 0022-0728

de Prada, A.G.; Pena, N.; Mena, M.L.; Reviejo, A.J. & Pingarron, J.M. (2003). Graphite-Teflon composite bienzyme amperometric biosensors for monitoring of alcohols. *Biosensors and Bioelectronics*, Vol.18, No.10, pp. 1279-1288, ISSN 0956-5663

Dmitruk, K.V.; Smutok, O.V.; Gonchar, M.V. & Sibirnyĭ, A.A. (2008). Construction of flavocytochrome b2-overproducing strains of the thermotolerant methylotrophic yeast Hansenula polymorpha (Pichia angusta). *Microbiology* (Moscow), Vol.77, No.2, pp. 213-218, ISSN 1608-3237

Dmytruk, K.V.; Smutok, O.V.; Ryabova, O.B.; Gayda, G.Z.; Sibirny, V.A.; Schuhmann, W.; Gonchar, M.V. & Sibirny, A.A. (2007). Isolation and characterization of mutated alcohol oxidases from the yeast Hansenula polymorpha with decreased affinity toward substrates and their use as selective elements of an amperometric biosensor. *BMC Biotechnol*ogy, Vol.7, No.1, pp. 33, ISSN 1472-6750

D'Orazio, P. (2003) Biosensors in clinical chemistry. *Clinica Chimica Acta*, Vol.334, pp. 41-69, ISSN 0009-8981

Dzyadevych, S.V., Arkhypova, V.N.; Soldatkin, A.P.; El'skaya, A.V.; Martelet, C. & Jaffrezic-Renault, N. (2008). Amperometric enzyme biosensors: Past, present and future. *IRBM*, Vol.29, pp. 171-180, ISSN 1959-0318

Esti, M.; Volpe, G.; Compagnone, D.; Mariotti, G. & Moscone, D.P.G. (2003). Monitoring alcoholic fermentation of red wine by electrochemical biosensors. *American Journal of Enology and Viticulture*, Vol.54, No.1, pp. 39-45, ISSN 0002-9254

Gayda, G.Z.; Pavlishko, H.M. & Smutok, O.V. (2006). Glycerol oxidase from the fungus *Botrytis allii*: purification, characterization and bioanalytical application. *Investigations in the field of sensor systems and technologies* (ed. A. El'skaya, V. Pokhodenko. - Kyiv: Academperiodyka, pp. 126 -133, ISBN: 966-02-4155-0

Gaida, G.Z.; Stel'mashchuk, S.Ya.; Smutok, O.V. & Gonchar, M.V. (2003). A new method of visualization of the enzymatic activity of flavocytochrome b_2 in electrophoretograms. *Applied Biochemistry and Microbiology*, V.39, No.2, pp. 221-223, ISSN 1608-3024

Gamella, M.; Campuzano, S.; Reviejo, A.J. & Pingarrón, J.M. (2008). Integrated multienzyme electrochemical biosensors for the determination of glycerol in wines. *Analytica Chimica Acta,* Vol. 609, Is. 2, pp. 201-209, ISSN: 0003-2670

Garjonyte, R.; Melvydas, V. & Malinauskas, A. (2006). Mediated amperometric biosensors for lactic acid based on carbon paste electrodes modified with baker's yeast Saccharomyces cerevisiae. *Bioelectrochemistry*, Vol.68, pp. 191–196, ISSN 1567-5394

Garjonyte, R.; Melvydas, V. & Malinauskas, A. (2008). Effect of yeast pretreatment on the characteristics of yeast-modified electrodes as mediated amperometric biosensors for lactic acid. *Bioelectrochemistry*, Vol.74, pp. 188–194, ISSN 1567-5394

Gautier, S.M.; Blum, L.J. & Coulet, P.R. (1990). Fibre-optic biosensor based on luminescence and immobilized enzymes: microdetermination of sorbitol, ethanol and oxaloacetate. *Journal of bioluminescence and chemiluminescence*, Vol.5, No.1, pp. 57-63, ISSN 1099-1271

Geissler, J.; Ghisla, S. & Kroneck, P. (1986). Flavin-dependent alcohol oxidase from yeast. Studies on the catalytic mechanism and inactivation during turnover. *The Journal of Biochemistry*, Vol.160, pp. 93-100, ISSN 1756-2651

Ghosh, S.; Rasmusson, J. & Inganas, O. (1998). Supramolecular self-assembly for enhanced conductivity in conjugated polymer blends: ionic crosslinking in blends of Poly (3,4-ethylenedioxythiophene)-Poly (styrenesulfonate) and Poly (vinylpyrrolidone). *Adv. Mater*., Vol .10, No 14, pp. 1097-1099, ISBN: 0935-9648

Gibson, T.D.; Higgins, I.J. & Woodward, J.R. (1992). Stabilization of analytical enzymes using a novel polymer-carbohydrate system and the production of a stabilized, single reagent for alcohol analysis. *Analyst*., Vol. 117, pp. 1293-1297. ISSN 0003-2654

Gonchar, M.V. (1998). Sensitive method of quantitative determination of hydrogen peroxide and oxidase substrates in biological objects. *Ukr. Biochem. J.*, V.70, № 5, pp. 157-163 (Ukrainian)

Gonchar, M.V.; Maidan, M.M.; Moroz, O.M.; Woodward, J.R. & Sibirny, A.A. (1998). Microbial O2- and H2O2-electrode sensors for alcohol assays based on the use of permeabilized mutant yeast cells as the sensitive bioelements. *Biosensors and Bioelectronics*, Vol.13, pp. 945–952, ISSN 0956-5663

Gonchar, M.; Maidan, M.; Korpan, Y.; Sibirny, V.; Kotylak, Z. & Sibirny A. (2002). Metabolically engineered methylotrophic yeast cells and enzymes as sensor biorecognition elements. *FEMS Yeast Research*., Vol.2, pp. 307-314, ISSN 1567-1364

Gonchar, M.V.; Maidan, M.M.; Pavlishko, H.M.; Sibirny A.A. (2001). A new oxidase-peroxidase kit for ethanol assays in alcoholic beverages". *Food Technol. Biotechnol*., Vol. 39, No 1, pp. 37-42. ISSN 1330-9862

Gonchar, M.; Maidan, M.; Pavlishko, H.; Sibirny, A. (2002). Assay of ethanol in human serum and blood by the use of a new oxidase-peroxidase-based kit. *Visnyk of L'viv Univ*., *Biology Series*., Is. 31, pp. 22-27

Gonchar M.V.; Sybirny A.A. Method of determination of peroxydase activity of biological objects // Patent № 1636773 USSR, МКИ[5] G 01 N 33/52. / (USSR); № 4363857/14; Appl. 13.01.88; Publ. 23.03.91; № 11. – 6 p. (in Russian)

Goriushkina, T.B.; Shkotova, L.V. & Gayda G.Z. (2010). Amperometric biosensor based on glycerol oxidase for glycerol determination. *Sens. Actuat. B: Chem.,* Vol. 144, Is. 2, pp. 361-367, ISSN: 0925-4005

Guo, S.; Wen, D. & Zhai, Y. (2010). Platinum nanoparticle ensemble-on-graphene hybrid nanosheet: one-pot, rapid synthesis, and used as new electrode material for electrochemical sensing. *ACS Nano,* Vol. 4, No 7, pp. 3959-3968, ISSN: 1936-0851

Gurban, A.-M.; Noguer, T.; Bala C. & Rotariu L. (2008). Improvement of NADH detection using Prussian blue modified screen-printed electrodes and different strategies of immobilisation. *Sensors and Actuators B: Chemical*, Vol. 128, Is. 2, pp. 536-544, ISSN: 0925-4005

Haghighi, B.; Hamidi, H. & Gorton, L. (2010). Electrochemical behavior and application of Prussian blue nanoparticle modified graphite electrode. *Sensors and Actuators B: Chemical*, Vol. 147, Is. 1, pp. 270-276, ISSN: 0925-4005

Hasunuma, T.; Kuwabata, S.; Fukusaki, E. & Kobayashi, A. (2004). Real-time quantification of methanol in plants using a hybrid alcohol oxidase-peroxidase biosensor. *Analytical Chemistry*, Vol.76, No.5, pp. 1500-1506, ISSN 1520-6882

Haumont, P.Y.; Thomas, M.A.; Labeyrie, F. & Lederer, F. (1987). Amino-acid sequence of the cytochrome-b5-like heme-binding domain from Hansenula anomala flavocytochrome b_2. *European Journal of Biochemistry*, Vol.169, No.3, pp. 539–546, ISSN 1432-1033

Harwood, G. W. J. & Pouton, C. W. (1996). Amperometric enzyme biosensors for the analysis of drugs and metabolites. *Advanced Drug Delivery Reviews,* Vol. 18, Is. 2, pp. 163-191, ISSN: 0169-409X

Herrero, A.M.; Requena, T.; Reviejo, A.J. & Pingarron, J.M. (2004). Determination of l-lactic acid in yoghurt by a bienzyme amperometric graphite–Teflon composite biosensor. *European Food Research and Technology*, Vol.219, pp. 557-560, ISSN 1438-2385

Hill, P. & Martin, S.M. (1975). Cellular proteolytic enzymes of *Neurospora crassa*. Purification and some properties of five intracellular proteinases, *Eur. J. Biochem.,* Vol. 56, No 1, pp. 271-281, ISSN 0014-2956

Hinsch, W.; Ebersbach, W. -D. & Sundaram, P. V. (1980). Fully enzymic method of plasma triglyceride determination using an immobilized glycerol dehydrogenase nylon-tube reactor. *Clinica Chimica Acta,* Vol. 104, Is. 1, pp. 95-100, ISSN: 0009-8981

Hirano, K.; Yamato, H.; Kunimoto, K. & Ohwa, M. (2002). Novel electron transfer mediators, indoaniline derivatives for amperometric lactate sensor. *Sensors and Actuators B: Chemical*, Vol.86, pp. 88-93, ISSN 0925-4005

Hong, M.; Chang, J.; Yoon, H. & Kim, H. (2002). Development of a screen-printed amperometric biosensor for the determination of l-lactate dehydrogenase level. *Biosensors and Bioelectronics*, Vol.17, pp. 13-18, ISSN 0956-5663

http://www.marketresearch.com/product/display.asp?productid=2700316. Analytical Review of World Biosensors Market

http://www.johnmorris.com.au/html/Ysi/ysi1500.htm

http://www.fitnessmonitors.com/ecstore/cat111.htm

Investigations on Sensor Systems and Technologies / Edited by Anna V. El'skaya, Vitaliy D. Pokhodenko, Kyiv: Institute of Molecular Biology and Genetics of NAS of Ukraine, 2006, 373 pp., ISBN 966-02-4155-0

Isobe K. (1995). Oxidation of ethylene glycol and glycolic acid by glycerol oxidase. *Biosci. Biotechnol. Biochem.,* Vol. 59, No 4, pp. 576-581, ONLINE, ISSN: 1347-6947. PRINT, ISSN: 0916-8451

Ivanova, E.V.; Sergeeva, V.S.; Oni, J.; Kurzawa, Ch.; Ryabov, A.D. & Schuhmann, W. (2003). Evaluation of redox mediators for amperometric biosensors: Ru-complex modified carbon-paste/enzyme electrodes. *Bioelectrochemistry*, Vol.60, No.1-2, pp. 65-71, ISSN 1567-5394

Iwuoha, E.I.; Rock, A. & Smyth, M.R. (1999). Amperometric L-Lactate Biosensors: 1. Lactic Acid Sensing Electrode Containing Lactate Oxidase in a Composite Poly-L-lysine Matrix. *Electroanalysis*, Vol.11, pp. 367-373, ISSN 1040-0397

Jain, K.K. (2007). Application of nanobiotechnology in clinical diagnostics. *Clinical Chemistry*, Vol.53, pp. 2002-2009, ISSN 1530-8561

Jianrong, C.; Yuqing, M.; Nongyue, H.; Xiaohua, W. & Sijiao L. (2004). Nanotechnology and biosensors. *Biotechnology Advances*, Vol.22., pp. 505-518, ISSN 0734-9750

Kalab, T. & Skladal, P. (1994). Evaluation of mediators for development of amperometric microbial bioelectrodes. *Electroanalysis*, Vol.6, pp. 1004–1008, ISSN 1040-0397

Karube, I.; Matsunga, T.; Teraoka, N. & Suzuki, S. (1980). Microbioassay of phenzlalanine in blood sera with a lactate electrode. *Analytica Chimica Acta*, Vol.119, pp. 271–276, ISSN 0003-2670

Katrlík, J.; Mastihuba V. & Voštiar I. (2006). Amperometric biosensors based on two different enzyme systems and their use for glycerol determination in samples from biotechnological fermentation process. *Analytica Chimica Acta,* Vol. 566, Is. 1, pp. 11-18, ISSN: 0003-2670

Kiba, N.; Azuma, N. & Furusawa, M. (1996). Chemiluminometric method for the determination of glycerol in wine by flow-injection analysis with co-immobilized glycerol dehydrogenase/NADH oxidase. *Talanta*, Vol. 43, pp. 1761-1766, ISSN: 0039-9140

Kissinger, P.T. (2005). Biosensors – a perspective. *Biosensors and Bioelectronics*, Vol.20, pp. 2512-2516, ISSN 0956-5663

Korpan, Y.I.; Gonchar, M.V.; Starodub, N.F.; Shul'ga, A.A.; Sibirny, A.A. & El'skaya, A.V. (1993). A cell biosensor specific for formaldehyde based on pH-sensitive transistors coupled to methylotrophic yeast cells with genetically adjusted metabolism. *Analytical Biochemistry*, Vol.215, pp. 216–222, ISSN 1096-0309

Kulys, J.; Wang, L. Z. & Razumas, V. (1992) Sensitive yeast bioelectrode to L-lactate. *Electroanalysis*, Vol.4, pp. 527–532, ISSN 1040-0397

Kupletskaya, M. B. & Likhachev, A. N. (1996). Glyceroloxidase activity of fungi of *Botrytis* micheli species. *Mikologiya and phitopatologiya* (*Mycology and plant pathology*)., Vol. 30, No 5-6, pp. 55–58, ISSN*:* 00263648

Kurzawa, C.; Hengstenberg, A. & Schuhmann, W. (2002). Immobilization method for the preparation of biosensors based on pH shift-induced deposition of biomolecule-containing polymer films, *Anal Chem.*, Vol. 74, No 2, pp. 355 – 361, ISSN*:* 0003-2700

Labeyrie, F.; Baudras, A. & Lederer, F. (1978). Flavocytochrome b_2 or L-lactate cytochrome c reductase from yeast. *Methods in Enzymology*. Vol.53, pp. 238–256 ISSN: 0076-6879

Laurinavicius, V.; Kurtinaitiene, B. & Gureiviciene, V. (1996). Amperometric glyceride biosensor, *Anal. Chim. Acta,* Vol .330, pp. 159-166, ISSN*:* 0003-2670

Lehmann, M.; Riedel, K.; Adler, K. & Kunze, G. (2000). Amperometric measurement of copper ions with a deputy substrate using a novel Saccharomyces cerevisiae sensor. *Biosensors and Bioelectronics*, Vol.15, pp. 211–219, ISSN 0956-5663

Liao, W.Y. ; Liu, C.C. & Chou, T.C. (2008). Detection of triglyceride using an iridium nano-particle catalyst based amperometric biosensor. *Analyst.* Vol. 133, No 12, pp. 1757-1763, ISSN: 0003-2654

Lin, S.F.; Chiou, C.M. & Tsai, Y.C. (1996). Purification and characterization of a glycerol oxidase from Penicillum sp. TS–622., *J. Enzyme Microb. Technol*., Vol. 18, pp. 383-387, ISSN: 0141-0229

Luong, J.H.; Mulchandani, A. & Groom, C.A. (1989). The development of an amperometric microbial biosensor using Acetobacter pasteurianus for lactic acid. *Journal of Biotechnology*, Vol.10, pp. 241–252, ISSN 0168-1656

Luong, J.H.T.; Bouvrette, P. & Male, K.B. (1997). Developments and applications of biosensors in food analysis. *Tibtech*, Vol.15, pp. 369–377, ISSN 0167-7799

Madaras, M.B. & Buck, R.P. (1996). Miniaturized biosensors employing electropolymerized permselective films and their use for creatine assays in human serum. *Analytical Chemistry*, Vol.68, pp. 3832-3839, ISSN 1520-6882

Mascini, M.; Moscone, D. & Palleschi, G. (1984). A lactate electrode with lactate oxidase immobilized on nylon net for blood-serum samples in flow systems. *Analytica Chimica Acta*, Vol.157, pp. 45–51, ISSN 0003-2670

Medintz, I.; Mattoussi, H. & Clapp, A.R. (2008). Potential clinical application of quantum dots. *International Journal of Nanomedicine*, Vol.3, pp. 151-167, ISSN 1178-2013

Minakshi, Pundir, C.S. (2008) Co-immobilization of lipase, glycerol kinase, glycerol-3-phosphate oxidase and peroxidase on to aryl amine glass beads affixed on plastic strip for determination of triglycerides in serum. *Indian J. Biochem. Biophys.,* Vol. 45, No 2, pp. 111-115, ISSN: 0301-1208

Mizutani, F.; Yabuki, S. & Katsura T. (1993). Amperometric enzyme electrode with the use of dehydrogenase and NAD(P)H oxidase. *Sensors and Actuators B: Chem.* Vol. 14, Is. 1-3, pp. 574-575, ISSN 0925-4005

Murphy, L. (2006). Biosensors and bioelectrochemistry. *Current Opinion in Chemical Biology*, Vol.10, pp. 177-184, ISSN 1367-5931

Nakamura, H. & Karube I. (2003). Current research activity in biosensors. *Analytical & Bioanalytical Chemistry,* Vol.377, pp. 446-468, ISSN 1618-2642

Narang, J.; Minakshi, Bhambi, M. & Pundir, C.S. (2010). Determination of serum triglyceride by enzyme electrode using covalently immobilized enzyme on egg shell membrane. *Int. J. Biol. Macromol.,* Vol. 47, No 5, pp. 691-695, ISSN: 0141-8130

Niculescu, M.; Erichsen, T.; Sukharev, V.; Kerenyi, Z.; Csoregi, E. & Schuhmann, W. (2002). Quinohemoprotein alcohol dehydrogenase-based reagentless amperometric biosensor for ethanol monitoring during wine fermentation. *Analytica Chimica Acta*, Vol.463, No.1, pp. 39-51, ISSN 0003-2670

Nikolou, M. & Malliaras, G.G. (2008). Applications of poly(3,4-ethylenedioxythiophene) doped with poly(styrene sulfonic acid) transistors in chemical and biological sensors. *Chem Rec*., Vol. 8, No 1, pp. 13-22, ISSN (printed): 1527-8999. ISSN (electronic): 1528-0691

Ogura, Y. & Nakamura, T. (1966). Kinetic studies on the oxidation and reduction of the protoheme moiety of yeast L(+)-lactate dehydrogenases. *The Journal of Biochemistry*, Vol.60, No.1, pp. 77–86, ISSN 1756-2651

Patel, N.G.; Meier, S.; Cammann, K. & Chemnitius, G.C. (2001). Screen-printed biosensors using different alcohol oxidases. *Sensors and Actuators B: Chemical*, Vol.75, No.1-2, pp. 101-110, ISSN 0925-4005

Pat. US4409328 (A) Method and reagent for the determination of glycerol. Ziegenhorn J.; Bartl, K. & Roeder, A. Publ.983-10-11. C12N9/04; C12Q1/26; C12Q1/44

Pat. US 4399218 (A) Method and reagent for the determination of glycerin Gauhl, H.; Seidel, H. & Lang, G. Publ. 1983-8-16

Patent 2117702C1, Russia, МПК⁶ C12N 9/04//(C12N9/04, C12R1:645). Method of production of glycerol oxidase /ООО «Impact» (Russia); № 95115005/13; Appl. 22.08.95; Publ. 20.08.98 (Russian)

Pavlishko, H.M.; Gayda, G.Z. & Gonchar, M.V. (2004). Screening producer strains, purification and primary characterization of glycerol oxidase from mould fungi, *Visnyk of L'viv Univ.* (In Ukrainian), Biology Series, Is. 38, pp. 67-73

Pen'kovskii, A.I.; Gusikhin, A.V.; Fedorov, E.I.; Volkov, R.I.; Filatov, M.I.; Safina, R.A.; Nikolaeva, L.A.; Khamelin, D.D. & Vereshchagin, V.I. (2004). Refractometer and refractometric analysis of vodka. CODEN: RUXXE7 RU 2241220 C2 20041127 Patent written in Russian. Application: RU 2001-134083 20011213. CAN 141:410165

Piro, B.; Pham, M-C. & Ledoan, T. (1999). Electrochemical method for entrapment of oligonucleotides in polymer-coated electrodes, *J. Biom. Mat. Res.,* Vol. 46, No 4, pp. 566-572, ISSN: 0884-2914

Plegge, V., Slama, M.; Süselbeck, B.; Wienke, D.; Spener, F.; Knoll, M. & Zaborosch, C. (2000). Analysis of ternary mixtures with a single dynamic microbial sensor and chemometrics using a nonlinear multivariate calibration. *Analytical Chemistry*, Vol.72, pp. 2937–2942, ISSN 1520-6882

Pournaghi-Azar, M.H.; Ahour, F. & Pournaghi-Azar F. (2010). Simple and rapid amperometric monitoring of hydrogen peroxide in salivary samples of dentistry patients exploiting its electro-reduction on the modified/palladized aluminum electrode as an improved electrocatalyst. *Sensors and Actuators B: Chemical*, Vol. 145, Is. 1, pp. 334-339, ISSN: 0925-4005

Prodromidis, M., I. & Karayannis M.I. (2002). Enzyme based amperometric biosensors for food analysis. *Electroanalysis,* Vol. 14, N. 4, pp.241-260, ISSN: 1521-4109

Racek, J. & Musil, J. (1987, A). Biosensor for lactate determination in biological fluids. I. Construction and properties of the biosensor. *Clinica Chimica Acta*, Vol.162, pp.129–139, ISSN 0009-8981

Racek, J. & Musil, J. (1987, B). Biosensor for lactate determination in biological fluids. 2. Interference studies. *Clinica Chimica Acta*, Vol.167, pp. 59–65, ISSN 0009-8981

Radoi, A.; Compagnone, D.; Devic, E. & Palleschi, G. (2007). Low potential detection of NADH with Prussian Blue bulk modified screen-printed electrodes and recombinant NADH oxidase from *Thermus thermophilus*. *Sensors and Actuators B: Chemical*, Vol. 121, Is. 2, pp. 501-506, ISSN: 0925-4005

Radoi, A. & Compagnone, D. (2009). Recent advances in NADH electrochemical sensing design. *Bioelectrochemistry.* Vol. 76, No 1-2, pp. 126-134, ISSN: 1567-5394

Ramsay, G. (1998) *Commercial Biosensors: Applications to Clinical, Bioprocess, and Environmental Samples*, John Wiley & Sons, Inc., ISBN: 0-471-58505-X, New York

Rasooly, A. & Jacobson, J. (2006). Development of biosensors for cancer clinical testing. *Biosensors and Bioelectronics*, Vol.21, pp. 1851-1858, ISSN 0956-5663

Rebelo, J.F.; Compaguone, D. & Guilbault, G.G. (1994). Alcohol electrodes in beverage measurements. *Analytical Letters*, Vol.27, pp. 3027-3037, ISSN 1532-236X

Ricci, F.; Amine, A.; Moscone, D. & Palleschi, G. (2007). A probe for NADH and H_2O_2 amperometric detection at low applied potential for oxidase and dehydrogenase based biosensor applications. *Biosensors and Bioelectronics.,* Vol. 22, Is. 6, pp. 854-862, ISSN: 0956-5663

Rozlosnik, N. (2009). New directions in medical biosensors employing poly(3,4-ethylenedioxy thiophene) derivative-based electrodes. *Anal Bioanal Chem.,* Vol. 395, No 3, pp. 637-645, ISSN: 1618-2642

Sakaki, T.; Shinkyo, R.; Takita, T.; Ohta, M. & Inouye, K. (2002). Biodegradation of polychlorinated dibenzo-p-dioxins by recombinant yeast expressing rat CYP1A subfamily. *Archives Biochemistry and Biophysics*, Vol.401, pp. 91–98, ISSN 0003-9861

Salata, O.V. (2004). Applications of nanoparticles in biology and medicine. *Journal of Nanobiotechnology*, Vol.2, pp. 1-6, ISSN 1477-3155

Scheller, F.W.; Hintsche, R.; Pfeiļer, D.; Schubert, F.; Riedel, K. & Kindervater, R. (1991). Biosensors: fundamentals, applications and trends. *Sensors and Actuators B: Chemical*, Vol.4, pp. 197-206, ISSN 0925-4005

Schmidt, R.D. & Karube, I. (1998). Biosensors and 'Bioelectronics'. In: *Biotechnology*, VCH Verlagsgesellschaft, Weinheim, Vol. 6b, pp. 317-365, ISBN: 3527278664

Schmitt, G. & Aderjan, R. (2004). Blood alcohol analysis - validation and determination of the measurement inaccuracy according to international standards. *Blutalkohol*, Vol.41, No.4, pp. 299-318, ISSN 0006-5250

Schuhmann, W.; Wohlschläger, H.; Huber, J.; Schmidt, H.L. & Stadler, H. (1995). Development of an extremely flexible automatic analyzer with integrated biosensors for on-line control of fermentation processes. *Analytica Chimica Acta*, Vol.315, pp. 113-122, ISSN 0003-2670

Seidel, M. & Niessner, R. (2008). Automated analytical microarrays: a critical review. *Analytical & Bioanalytical Chemistry*, Vol.391, pp. 1521-1544, ISSN 1618-2642

Sekhon, B.S. & Kamboj, S.R. (2010). Inorganic nanomedicine – Part 1. *Nanomedicine: Nanotechnology, Biology and Medicine*, Vol.6, No.4, pp. 516-522, ISSN 1549-9634

Serban, S. & Murr, N. E. (2006). Redox-flexible NADH oxidase biosensor: A platform for various dehydrogenase bioassays and biosensors. *Electrochimica Acta,* Vol. 51, Is. 24, pp. 5143-5149, ISSN: 0013-4686

Serra, B.; Reviejo, A.J.; Parrado, C. & Pingarron, J.M. (1999). Graphite-Teflon composite bienzyme electrodes for the determination of L-lactate: application to food samples. *Biosensors and Bioelectronics*, Vol.14, pp. 505-513, ISSN 0956-5663

Sharma, S.; Sehgal, N. & Kumar, A. (2003). Biomolecules for development of biosensors and their applications. *Current Applied Physics*, Vol.3, pp. 307-316, ISSN 1567-1739

Shimomura-Shimizu, M. & Karube, I. (2010, A). Yeast based sensors. *Advances in Biochemical Engineering/Biotechnology*, Vol.117, pp. 1–19, ISSN 0724-6145

Shimomura-Shimizu, M. & Karube, I. (2010, B). Applications of microbial cell sensors. *Advances in Biochemical Engineering/Biotechnology*, Vol.118, pp. 1–30, ISSN: 0724-6145

Shkil H.; Stoica L.; Dmytruk K.; Smutok O.; Gonchar M.; Sibirny A.; Schuhmann W. (2009). Bioelectrochemical detection of L-lactate respiration using genetically modified Hansenula polymorpha yeast cells overexpressing flavocytochrome b_2. *Bioelectrochemistry*, Vol. 76, No 1-2, pp. 175-179, ISSN: 1567-5394

Silvestrini, M.C.; Teogoni, M. & Celerier, J. (1993). Expression in Escherichia coli of the flavin and the haem domains of Hansenula anomala flavocytochrome b_2 (flavodehydrogenase and b_2 core) and characterization of recombinant proteins. *Biochemical Journal,* Vol.295, No.2, pp. 501–508, ISSN 1470-8728

Shkotova, L.V.; Soldatkin, A.P.; Gonchar, M.V.; Schuhmann, W. & Dzyadevych, S.V. (2006) Amperometric biosensor for ethanol detection based on alcohol oxidase immobilised within electrochemically deposited Resydrol film. *Materials Science and Engineering: C*, Vol.26, pp. 411-414, ISSN 0928-4931

Smutok, O.; Gayda, G.; Gonchar, M. & Schuhmann W. (2005). A novel L-lactate-selective biosensor based on the use of flavocytochrome b_2 from methylotrophic yeast Hansenula polymorpha. *Biosensors and Bioelectronics*, Vol.20, pp. 1285-1290, ISSN 0956-5663

Smutok, O.V.; Osmak, H.S.; Gayda, G.Z. & Gonchar M.V. (2006a). Screening of yeasts producing stable L -lactate cytochrome c oxidoreductase and study of the regulation of enzyme synthesis. *Microbiology* (Moscow), Vol.75, No.1, pp. 20-24, ISSN 1608-3237

Smutok, O.; Ngounou, B.; Pavlishko, H., Gayda, G.; Gonchar, M. & Schuhmann, W. (2006b). A reagentless bienzyme amperometric biosensor based alcohol oxidase/peroxidase and an Os-complex modified electrodeposition paint. *Sensors and Actuators B: Chemical*, Vol.113, No.2, pp. 590-598, ISSN 0925-4005

Smutok, O., Gayda, G., Shuhmann W. & Gonchar, M. (2006c). Development of L-lactate-selective biosensors based on thermostable yeast L-lactate: cytochrome c-oxidoreductase. *Investigations on sensor systems and technologies* (ed. A. El'skaya, V. Pokhodenko. - Kyiv: Academperiodyka, pp. 39-45, ISBN: 966-02-4155-0

Smutok, O.; Dmytruk, K.; Gonchar, M.; Sibirny, A. & Schuhmann, W. (2007). Permeabilized cells of flavocytochrome b_2 over-producing recombinant yeast Hansenula polymorpha as biological recognition element in amperometric lactate biosensors. *Biosensors and Bioelectronics*, Vol.23, pp. 599–605, ISSN 0956-5663

Song, S. ; Xu, H. & Fan, C. (2006). Potential diagnostic application of biosensors: current and future directions. *International Journal of Nanomedicine*, Vol.1, pp. 433-440, ISSN 1178-2013

Staskeviciene, S.L.; Cenas, N.K. & Kulys, J.J. (1991). Reagentless lactate electrodes based on electrocatalytic oxidation of flavocytochrome b2. *Analytica Chimica Acta*, Vol.243, pp. 167–171, ISSN 0003-2670

Su, L.; Jia, W.; Hou, C. & Lei, Y. (2011). Microbial biosensors: a review. *Biosensors and Bioelectronics*, Vol.26, pp. 1788-1799, ISSN 0956-5663

Thevenot, D.R.; Toth, K.; Durst, R.A. & Wilson, G.S. (2001). Electrochemical biosensors: recommended definitions and classification. *Biosensors and Bioelectronics*, Vol.16, pp. 121-131, ISSN 0956-5663

Tkác, J.; Navrátil, M.; Sturdík, E. & Gemeiner, P. (2001). Monitoring of dihydroxyacetone production during oxidation of glycerol by immobilized Gluconobacter oxydans cells with an enzyme biosensor. *Enzyme Microb Technol.*, Vol. 28, No 4-5, pp. 383-388, ISSN: 0141-0229

Tucker, C. L. & Fields, S. (2001). A yeast sensor of ligand binding. *Nature Biotechnology*, Vol.19, pp. 1042–1046, ISSN 1546-1696

Uwajima T.; Akita H., & Ito, K. (1979). Some characteristics of new enzyme "Glycerol Oxidase", *Agric. Biol. Chem.*, Vol. 43, pp. 2633-2634, ISSN: 0002-1369

Uwajima, T.; Shimizu, Y.; Terada, O. (1984). Glycerol oxidase, a novel copper hemoprotein from *Aspergillus japonicus*. Molecular and catalytic properties of the enzyme and its application to the analysis of serum triglycerides. *J. Biol. Chem*. Vol .259, pp. 2748-2753, ISSN: 0021-9258

Verduyn, C.; Dijken, J.P. & Scheffers, W.A. (1984). Colorimetric alcohol assays with alcohol oxidase. *Journal of Microbiological Methods*, Vol.2, pp. 15-25, ISSN 0167-7012

Vijayakumar, A.R.; Csoeregi, E.; Heller, A. & Gorton, L. (1996). Alcohol biosensors based on coupled oxidase-peroxidase systems. *Analytica Chimica Acta*, Vol.327, No.3, pp. 223-234, ISSN 0003-2670

Walmsley, R.M.; Billinton, N. & Heyer, W.D. (1997). Green fluorescent protein as a reporter for the DNA damage-induced gene RAD54 in Saccharomyces cerevisiae. *Yeast*, Vol.13, pp. 1535–1545, ISSN 1097-0061

Walmsley, R.M. & Keenan, P. (2000). The eukaryote alternative: advantages of using yeasts in place of bacteria in microbial biosensor development. *Biotechnology and Bioprocess Engineering*, Vol.5, pp. 387–394, ISSN 1976-3816

Wang, J. & Chen, Q. (1994). Lactate biosensor based on a lactate dehydrogenase/nicotinamide adenine dinucleotide biocomposite. *Electroanalysis*, Vol.6, pp. 850–854, ISSN 1040-0397

Wang, J. (2006). Electrochemical biosensors: towards point-of-care cancer diagnostics. *Biosensors and Bioelectronics*, Vol.21, pp. 1887-1892, ISSN 0956-5663

Watson, R.R.; Solkoff, D.; Wang, J.Y. & Seeto, K. (1998). Detection of ethanol consumption by ELISA assay measurement of acetaldehyde adducts in murine hair. *Alcohol*, Vol.16, No.4, pp. 279-284, ISSN 0741-8329

West, S.I. (1998). Analitical enzymes: diagnostics. (1996). London: Macmillan Press Ltd., pp. 63-68

Wilson, G.S. & Gifford, R. (2005). Biosensors for real-time in vivo measurements. *Biosensors and Bioelectronics*, Vol.20, pp. 2388-2403, ISSN 0956-5663

Wilson, G.S. & Ammam, M. (2007). In vivo biosensors. *FEBS Journal*, Vol.274, pp. 5452-5461, ISSN 1742-4658

Woodward, J. (1990). Biochemistry and applications of alcohol oxidase from methylotrophic yeasts, In: *Autotrophic microbiology and one-carbon metabolism*. Codd, G.A., Dijkhuizen, L. & Tabita, F.R., pp. 193-225, Springer, ISBN 0-7923-0656-2

Zaydan, R.; Dion, M. & Boujtita, M. (2004). Development of a new method, based on a bioreactor coupled with an L-lactate biosensor, toward the determination of a nonspecific inhibition of L-lactic acid production during milk fermentation. *Journal of Agricultural and Food Chemistry*, Vol.52, pp. 8-14, ISSN 1520-5118

Zhao, Z. & Jiang, H. (2010). Enzyme-based electrochemical biosensors. In: *Biosensors*, (Ed.), Serra, P.A., pp. 1-21, *InTech*, ISBN 978-953-7619-99-2

21

P450-Based Nano-Bio-Sensors for Personalized Medicine

Camilla Baj-Rossi, Giovanni De Micheli and Sandro Carrara
EPFL - École Polytechnique Fédérale de Lausanne
Switzerland

1. Introduction

Cytochromes P450 (P450s or CYPs) belong to a multigene family of more than 3,000 heme proteins which catalyse the NADPH-dependent monooxygenation and other about 60 distinct classes of biotransformation reactions. Cytochromes P450 are known to be involved in the metabolism of over 1,000,000 different xenobiotic and endobiotic lipophilic substrates (Shumyantseva, Bulko, Archakov, 2005). Cytochrome P450s carry out a wide array of metabolic activities that are essential to homeostasis, apart from their roles in steroid biosynthesis and biotransformation and drug or toxin clereance. In figure 1, the tridimensional structure of cytochrome P450 3A4 is reported.

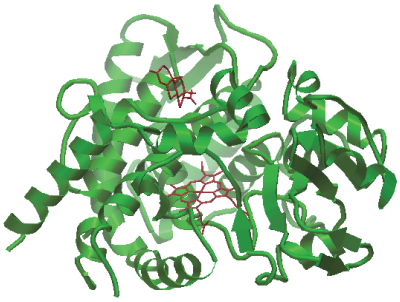

Fig. 1. Structure of cytochrome P450 3A4 (obtained by PDBe Protein Databank Europe http://www.ebi.ac.uk/pdbe/).

The liver is the main organ responsible for the biotransformation of drugs and chemicals, even if the gut metabolizes many drugs, and the CYPs and other metabolizing enzymes reside in the hepatocytes (Fig. 2). Basically, the primary function of CYPs and other biotransforming enzymes is to make very oil-soluble molecules highly water-soluble, so that they can be easily cleared by the kidneys into urine and they will be finally eliminated. When the drugs or toxins reach the hepatocytes in the liver, they basically flow inside the walls of the tubular structure of the smooth endoplasmic reticulum (SER), entering into the path of the CYP monooxygenase system. This is a highly liphophilic environment that keeps the liphophilic molecules away from the aqueous areas of the cell and allows the CYPs to metabolize them into more water-soluble agents (Coleman, 2010).

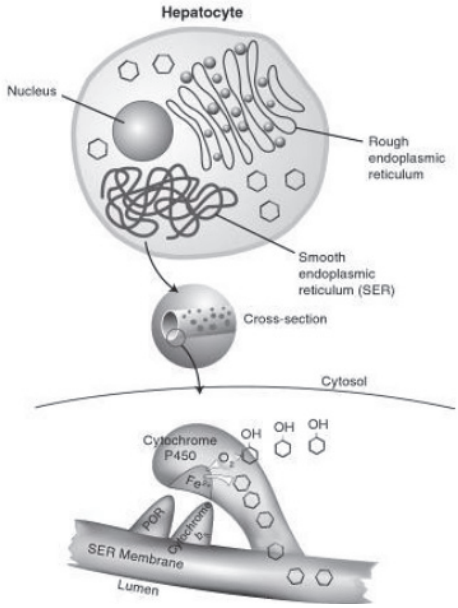

Fig. 2. Location in the hepatocyte of CYP enzymes and their redox partners, cytochrome b_5 and P450 oxidoreductase (POR), (Coleman, 2010). Reprinted with permission from Coleman, 2010. Copyright 2010 Wiley-Blackwell (John Wiley & Sons, Ltd).

Cytochromes P450 are enzymes involved in the metabolism of ~75% of all drugs (Figure 3A). Of the 57 human P450s, five are involved in ~95% of biotransformation reactions (Figure 3B), and each one is specific for a certain fraction of reactions which involved different substrates (Guengerich, 2008). In all living things, over 7,700 individual CYPs have been described and identified, although only 57 have been identified in human hepatocytes; of these, only 15 metabolize drugs and other chemicals.

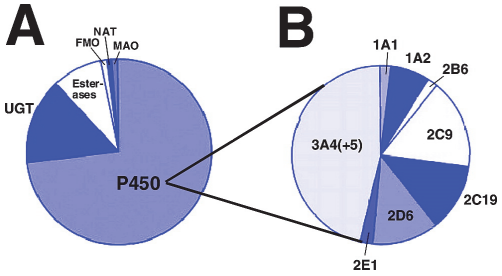

Fig. 3. Contributions of enzymes to the metabolism of marketed drugs. (A) Fraction of reactions on drugs catalyzed by various human enzymes. FMO, flavin-containing monoxygenase; NAT, Nacetyltransferase; and MAO, monoamine oxidase. (B) Fractions of P450 oxidations on drugs catalyzed by individual P450 enzymes (Guengerich, 2008). Reprinted with permission from Guengerich, 2008. Copyright 2008 American Chemical Society.

2. Cytochrome P450: classification and polymorphism

Cytochromes P450 are classified according to their amino acid sequence homology, that is, if two CYPs have 40 per cent of the full length of their amino acid structure in common they are thought to belong to the same 'family'. More than 780 CYP families have been found in nature in total, but only 18 have been identified in humans. Subfamilies are identified as having 55 per cent sequence homology and there are often several subfamilies in each family (Coleman, 2010). The nomenclature for P450s is based on naming cytochromes P450 with CYP followed by a number indicating the gene family (such as CYP1, CYP2, CYP3, etc.), a letter indicating the subfamily (i.e. CYP1A, CYP2A, CYP2B, CYP2C, etc.) and a number for the gene that identify the so named 'isoform'. In order to have the same gene number the genes must have the same function and exhibit high conservation (Ingelman-Sundberg, 2004). That is, two isoforms (e.g. CYP1A1 and CYP1A2) have 97 per cent of their general sequence in common. The completion of the sequence of the human genome revealed the presence of about 107 human P450 genes: 59 active and about 48 pseudogenes (Ingelman-Sundberg, 2004). The majority of genes exhibit a certain polymorphism (which is generally defined as 1% frequency of an allelic variant in a population) which leads to classify the CYPs even according to these allelic differences. A polymorphic form of a CYP is usually written with a * and a number for each allelic variant, or translated version of the gene. Regarding the polymorphic forms, they might contain one or more single nucleotide polymorphism (SNP, i.e. a change in one nucleotide of the genetic code) in the same allele (Coleman, 2010). For example, CYP2B6 has eight other significant allelic variants besides its major form, and among this variants, CYP2B6*4 has just one SNP, whilst CYP2B6*6 possesses two SNPs. The clinically most important polymorphism is seen with CYP2C9, CYP2C19 and CYP2D6. The functional importance of the polymorphisms of the xenobiotics metabolizing CYPs is summarized in Table 1.

The mutations in the CYP genes can cause the enzyme activity to be abolished, reduced, altered or increased, with substantial consequences in drug metabolism (Ingelman-Sundberg, 2004). Based on the composition of the alleles, the affected individuals might be divided into four major phenotypes: poor metabolizers (PMs), having two nonfunctional genes, intermediate metabolizers (IMs) being deficient on one allele, extensive metabolizers (EMs) having two copies of normal genes and ultrarapid metabolizers (UMs) having three or more functional active gene copies (Ingelman-Sundberg, 2004; Rodriguez-Antona, 2006). Phenotyping usually involves administering a single probe drug for a particular enzyme and measuring clearance and comparing it with data from other patients. The clinical influence of differences in CYP activity can be schematized as reported in figure 4. In this model example, only EMs and PMs are reported as the general population of interest. Referring to the EMs metabolizers (upper panel in figure 4), it is visible that after drug administration the plasma concentration rises to a peak ($C_{p,max}$) following the first dose and then decrease to a lower level prior to the next dose. With subsequent doses, the plasma concentration remains within this region and yields the desired pharmacological effect. Without prior knowledge about a problem with this drug, the PM (lower panel of Figure 4) and EM would be administrated the same dose. For PMs, a limited metabolism would occur between doses, and the plasma concentration of the drug will rise to an unexpectedly high level. The simplest effect would be an exaggerated and undesirable pharmacological response (Ortiz de Montellano, 2005).

CYP enzyme	Substrates	Polymorfism		
		Frequency	Functional effects	Most important polymorphic variants
CYP1A1	Carcinogens	Relatively high	-	-
CYP1A2	Drugs, carcinogens	High	Some	CYP1A2*1F, CYP1A2*1K
CYP2A6	Nicotine, drugs, carcinogens	High in orientals, less frequent in Caucasians	Important for nicotine metabolism	CYP2A6*1B, CYP2A6*4, CYP2A6*9, CYP2A6*12
CYP2B6	Drugs	High	Reduced drug metabolism	CYP2B6*5, CYP2B6*6, CYP2B6*16
CYP2C8	Some drugs	High	Reduced drug metabolism	CYP2C8*3
CYP2C9	Drugs	Relatively low	Very significant	CYP2C9*2, CYP2C9*3
CYP2C19	Drugs	High	Very significant	CYP2C19*2, CYP2C19*3, CYP2C19*17
CYP2D6	Drugs	High	Very significant	CYP2D6*2, CYP2D6*4, CYP2D6*5, CYP2D6*10, CYP2D6*17
CYP2E1	Carcinogens, solvents, few drugs	Low	No	-
CYP3A4	Drugs, carcinogens	Low	No or small	CYP3A4*1B

Table 1. Polymorphic cytochromes P450 of importance for drugs and carcinogens metabolism (Guengerich, 2001; Ortiz de Montellano, 2005).

At present state-of-the-art the only available monitoring system for personalized therapy is a check of the genetic predisposition of patients. In order to know which patient is at risk of having sub-therapeutic or toxic drug concentrations, a genetic test is done on alleles, which correspond to patient genetic predisposition for expressing the CYP proteins (Kirchheiner & Seeringer, 2007). A genetic test based on microarray has been introduced into the market by Roche: the Amplichip CYP450 (Amplichip, Figure 5).
It is the first FDA-cleared test for analysis of CYP2D6 and CYP2C19, two genes in the cytochrome P450 system that can greatly influence drugs metabolism. This test identifies the patient's genotype group and predicts his phenotype in order to classify patients as an either poor, intermediate, extensive, or ultra-rapid metabolizer. It was proven that this classification affects the actual amount of mean plasma concentration after a single drug dose (Lin, 2007).
However, the Amplichip can only "predict" the patient's phenotype and can only allow the adjustment of drug dose according to patient's genotype (as schematized in Figure 6). In Fig. 6, the theoretical dosages for different genotypes including ultrarapid, extensive, intermediate or slow metabolic activity are reported. They have been calculated from the differences in pharmacokinetic parameters and are depicted as schematic genotype-specific dosages, in order to have the same plasma-concentration course for all genetic group (Kirchheiner & Seeringer, 2007). Thus, in order to individually optimize an ongoing drug therapy, it is required to know how the patient metabolize drugs at the moment of the pharmacological cure, i.e. it is necessary to measure the plasma concentrations of drugs or their metabolites after the administration. This is a strong need since still most effective drug therapies for major diseases provide benefit only to a fraction of patients, typically in the 20 to 50% range (Lazarou et al., 1998).

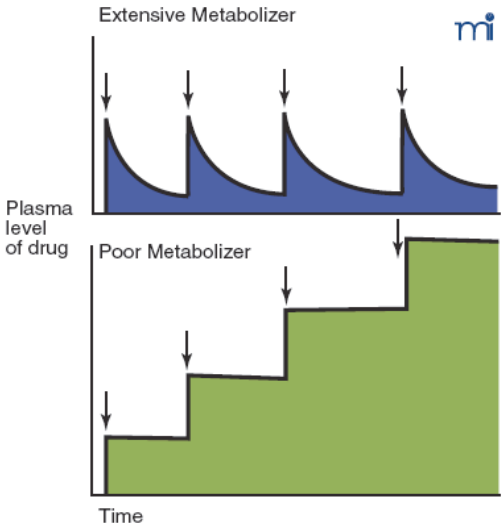

Fig. 4. Examples of unexpectedly low metabolism of a drug by P450s. The typical pattern seen with the majority of the population (extensive metabolizers) is shown in the upper panel, where the plasma level of the drug is maintained in a certain range after the administration of several consecutive doses (arrows indicate multiple doses). Unusually slow metabolism (lower panel) occurs when a poor metabolizer receives the same dose, resulting in unexpectedly high plasma level of the drug (Guengerich, 2003). Reprinted with permission from Guengerich, 2003. Copyright 2003 Molecular Interventions Online by the American Society for Pharmacology and Experimental Therapeutics.

Fig. 5. Amplichip CYP450 (Roche). ROCHE and AMPLICHIP are trademarks of Roche. AFFYMETRIX and POWERED BY AFFYMETRIX are trademarks of Affymetrix, Inc.

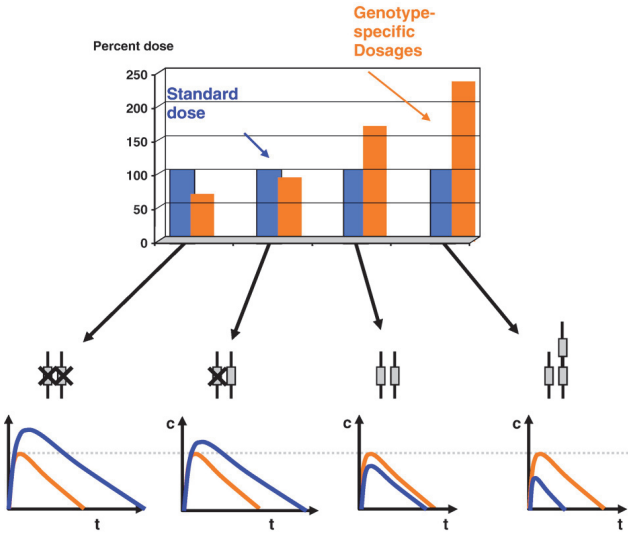

Fig. 6. Principle of calculation of genotype based dose adjustments based upon differences in pharmacokinetic parameters such as clearance and AUC. (Kirchheiner & Seeringer, 2007). Reprinted from Biochimica et Biophysica Acta, Vol. 1770, Julia Kirchheiner, Angela Seeringer , "Clinical implications of pharmacogenetics of cytochrome P450 drug metabolizing enzymes", Pages No. 489–494, Copyright (2007), with permission from Elsevier.

In general, there are only three CYP families which are mainly involved in drug and toxin biotransformation for humans, including:

- *CYP1 family (CYP1A1, CYP1A2 and CYP1B1);*
- *CYP2 family (CYP2A6, CYP2A13, CYP2B6, CYP2C8, CYP2C9, CYP218, CYP219, CYP2D6, CYP2E1);*
- *CYP3 family (CYP3A4, CYP3A5, CYP3A7).*

It is known that the 90% of marketed drugs are metabolized by only five of these isoforms (CYP1A2, CYP2C9, CYP2C19, CYP2D6, CYP3A4/5), (Ingelman-Sundberg, 2004).

3. Active-site structure of P450 enzymes

Although CYPs in general are capable of metabolizing almost any chemical structure and catalyse around 60 different classes of biotransforming reactions, they have a number of features in common, including (Coleman, 2010):

a. Most mammalian CYPs exist in the lipid smooth endoplasmic reticulum (SER) microenvironment, being partially embedded in the liphophilic membrane of the SER and their access channels are actually positioned inside the membrane ready to receive substrates, which are normally liphophilic (see Figure 2).
b. CYPs possess in their inner structure a heme group in their active site containing iron, which is a highly conserved part of their structures, and it is crucial for their catalytic activity. This active-site area is quite rigid, but it is surrounded by much more flexible complex binding areas, which can be regulated with different conformational changes in order to allow the entrance of different-size molecules.

c. CYPs have one or more binding area inside their active site, which determine for most part their variations and their ability to metabolize specific groups of chemicals.
d. Thanks to the heme group, CYPs exploit the ability of a metal to gain or lose electrons, thus catalyzing substrate oxidations and reductions, according to the NADPH-monooxygenation pathway.
e. All CYPs have closely associated redox partners, the cytochrome b_5 and P450 oxidoreductase (POR), able to supply them with electrons for their catalytic activities (Figure 2).
f. All CYPs bind and activate oxygen in their catalytic cycle as part of the metabolism process, but they are also able to carry out reduction reactions that do not require the presence of oxygen.

CYP enzymes share a common overall fold and topology (Figure 7) despite the differences in the genetic sequences and the genetic polymorphism. The conserved CYP structural core is formed by a four-α helix bundle composed of three parallel helices labelled D, L, and I and one antiparallel helix E (Denisov et al., 2005). The whole enzyme structure is usually anchored in the membrane of the smooth endoplasmic reticulum by an N-terminal α helix. The α helices hold in place the active site of the enzyme, the heme-iron group. In most CYPs the heme group is a relative rigid part of the protein's structure. The heme moiety (Figure 8), also known as ferriprotoporphyrin-9, has a highly specialized lattice structure that supports a iron molecule, which is the core of the enzyme and is the responsible of the substrate oxidation (Coleman, 2010).

Fig. 7. Ribbon representation (distal face) of cytochrome P450s fold. Substrate recognition sites (SRS) are shown in black and labelled. α-Helixes are labelled with capital letters (Denisov et al., 2005). Reprinted with permission from Denisov et al., 2005. Copyright 2005 American Chemical Society.

The iron atom is normally bound to five other molecules which keep it secured; four of them are pyrrole nitrogens and hold it in the horizontal plane while the fifth group, a sulphur atom from a cysteine amino acid residue links the iron in a vertical plane. This structure, known as the pentacoordinate state, represent the resting state, whilst the hexacoordinate state occurs when the iron binds another ligand. In this latter configuration, the iron atom appears to move 'upwards' and draws level with the nitrogens to bind a water molecule which is hydrogen bonded to an amino acid residue and is involved in the movement of protons during the catalytic activity. The ferriprotoporphyrin-9 is held in place by hydrogen bonding and a number of amino acid residues. The iron is crucial to the catalytic function of CYP enzymes.

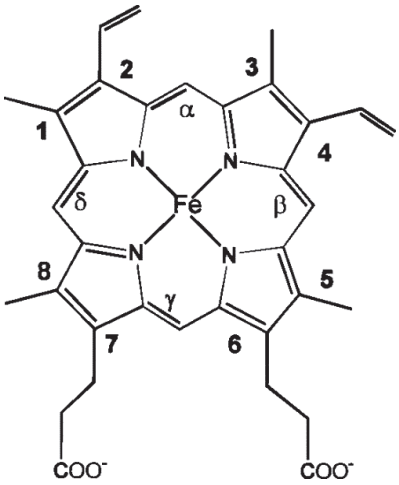

Fig. 8. Heme group chemical structure (Sono et al., 1996). Reprinted with permission from Sono et al., 1996. Copyright 1996 American Chemical Society.

The other helices that cover the active site are the flexible regions of the structure. They are normally partially clenched, but can open out to accommodate large substrates. The liphophilic substrate molecules diffuse through the membrane and enter the isoform through a sort of access path, which is defined as the widest, shortest and usually the most liphophilic pathway to reach the heme iron active site. The active site is supplied with electrons by the dual redox partners, the cytochrome b_5 and P450 oxidoreductase (POR), trough another access channel from the other side of the CYP (see Figure 9). These redox partners are also embedded in the smooth endoplasmic reticulum membrane right next to the CYP (see Figure 2). After the catalytic reaction, the transformed products naturally exit the isoform trough another channel (Coleman, 2010). Figure 9 shows the structure of cytochrome P450 14α-sterol demethylases (CYP51) with the open substrate access channel between the β-sheet and helical domains (channel 2) oriented approximately 90° relative to CYP51 channel 1. Those channels, delimited by the F, G, and H helices and loops in between, are known to undergo synchronized motions in CYPs when substrate binds. This synchronization allows the channel 1 to open, whereas channel 2 remains closed, thus providing a means for substrate to enter one channel and product to depart from the other (Podust et al., 2001).

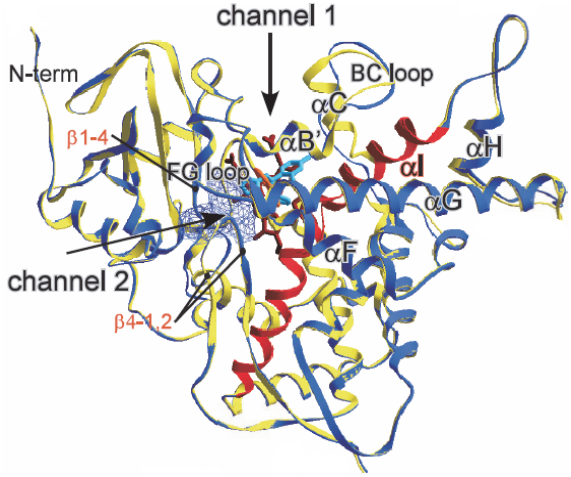

Fig. 9. Ribbon representation of the CYP51 structures with the azole inhibitors bound (Podust et al., 2001), which shows the two access channels (channel 1 and 2). Reprinted with permission from Podust et al., 2001. Copyright (2001) National Academy of Sciences, U.S.A.

3.1 Substrate binding in CYPs

The active site of an enzyme usually refers to a binding area which holds the substrate in a proper orientation capable to present the molecule to the structure of the enzyme that catalyze the reactions. In many enzymes, the dimensions and properties of the active and binding sites are quite well defined and mapped in detail, but crystallographic studies (Coleman, 2010), have shown that in the case of CYPs is difficult to define what constitutes the active binding site and to correctly identify their structure. As an example, it is known that CYP3A4, CYP2C8 and CYPC29 have very large active sites, whilst that of CYP2A6 is quite small. Cytochrome P450 undergo big changes in movement and binding area to accommodate substrates of differing sizes, thanks to the small-intermediate hydrophobic pockets placed into the CYP active site, with the capability as the α-helices to extend its area to bind larger substrates. The hydrophobic pocket (Figure 10) includes many amino acid residues that can bind a molecule with hydrogen bonding, weak van der Waals forces, or other interactions between electron orbitals of phenyl groups, such as π-π bond stacking. It is known that the isoform CYP3A4 can increase its active site area by 80 per cent to accommodate erythromycin (Coleman, 2010).

The presence of several amino acid residues allows the active site to provide a grip on the substrate in a number of places in the molecule preventing excessive movements while, when not binding substrates, CYP active site area is full of water molecules displaced upon the binding site. Moreover the substrate binding may occur in the interior and exterior structure of the isoform, and also the binding may involve internal rearrangement of the isoform or involve simultaneous binding of other substrates. At the simplest structural level it is possible to identify six different active sites or "substrate recognition sites" (SRS, see Figure 7), which predetermine CYP substrate specificity (Denisov et al., 2005). It has been reported that several CYP isoforms, including 3A4, 1A2, 2E1, 2D6, and 2C9, exhibit allotropic kinetics in vitro (Atkins, 2005). This atypical kinetic behaviour is typical of the enzymes that shows multiple substrate recognition sites in their active site, as CYPs, and is basically due to the conformational or chemical changes that occur in the active site of the enzyme after binding a first substrate (the effector). These changes in the conformation of

enzyme tertiary and quaternary structure result in the enzyme catalytic activity alteration which can affect the metabolism of a second substrate (Houston & Galetin, 2005).

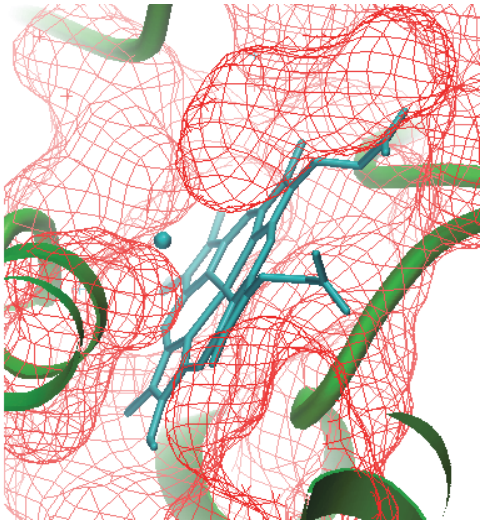

Fig. 10. The substrate binding cavity (meshed surface) of human cytochrome P450 3A4 (obtained by PDBe Protein Databank Europe, http://www.ebi.ac.uk/pdbe/). Molecular oxygen is reduced by the heme prosthetic group (the cyan stick figure) to form a reactive intermediate that oxygenates the substrate.

3.2 Redox partners and electron transport system

In catalyzing monooxygenation reactions of a substrate RH, CYP is able to utilize either NADH or NADPH (nicotinamide adenine dinucleotide and nicotinamide adenine dinucleotide phosphate respectively) as the electron donor (equation 1).

$$RH + O_2 + NAD(P)H + H^+ \rightarrow ROH + H_2O + NAD(P)^+ \quad (1)$$

However, the two electrons derived from NAD(P)H must be transferred to CYP via electron transport proteins called redox partners. The main CYP redox partners are the P450 oxidoreductase and the cytochrome b_5 (Sevrioukova et al., 1999):

a. *P450 oxidoreductase (POR*) is a flavoprotein complex, that consists of a large butterfly-shaped protein which locates and binds two flavins that work as electron carriers, FAD (flavin adenine dinucleotide) and FMN (flavin mononucleotide) in two separate lobes of the P450 oxidoreductase structure. The oxidative system, which consumes the glucose in the liver by the pentose phosphate pathway, produces NADPH to power all reductive reactions related to CYPs, and other reactions. P450 oxidoreductase complex operates as follows (Figure 11): electrons from reduced *NADPH (*released as NADP+*)*, are taken up by the FAD moiety, which is reduced to $FADH_2$. Then $FADH_2$ reduces FMN to $FMNH_2$, which in turn passes its two electrons to the CYP heme group, which is associated with the P450 oxidoreductase by electrostatic interactions (Huang et al., 2008). This electron transfer becomes a current of electron that P450 oxidoreductase must supply in the presence of high substrate concentrations.

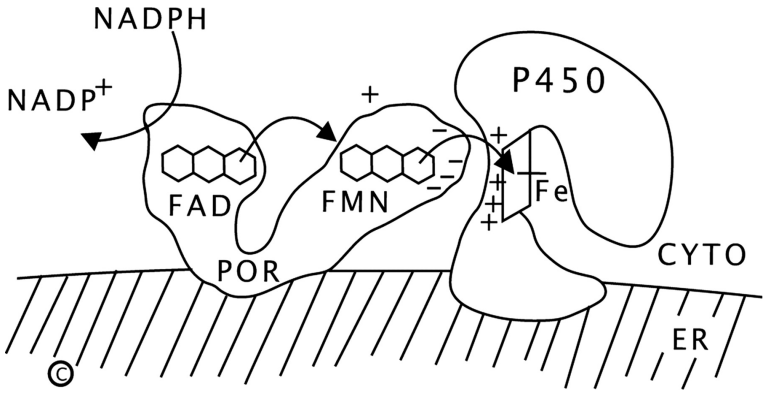

Fig. 11. Relationship of P450 oxidoreductase to a microsomal cytochrome P450 enzyme (Huang et al., 2008). ER is the endoplasmic reticulum and CYTO is the cytoplasm. Adapted from (Miller, W.L., 2005). Reprinted with permission from Huang et al., 2008. Copyright (2008) National Academy of Sciences, U.S.A.

b. *Cytochromes b_5 (Figure 12)* are electron transport hemeproteins which, similarly to cytochrome P450, are built around a central heme group. In nature these proteins convert in the cells NADH to NAD^+, building up proton gradients which stimulate the flow of electrons. There are numerous forms and structures of cytochrome b_5, but the microsomal cytochrome b_5 is of greatest interest in drug metabolism. Microsomal cytochrome b_5 is anchored by a helix into the smooth endoplasmic reticulum membrane (see Figure 2), but its heme structure, which is not-covalently linked with its CYP isoform, is closely associated with P450 oxidoreductase. Cytochrome b_5 has a complex but also essential role in CYP function. The standard CYP catalytic cycle (see paragraph 4) requires two electrons to reach a complete turn. The second electron is the rate limiting step in the enzymatic catalytic activity, and the cytochrome b_5 can supply this electron with high speed, even quicker than the system composed by P450 oxidoreductase and NADPH (Coleman, 2010).

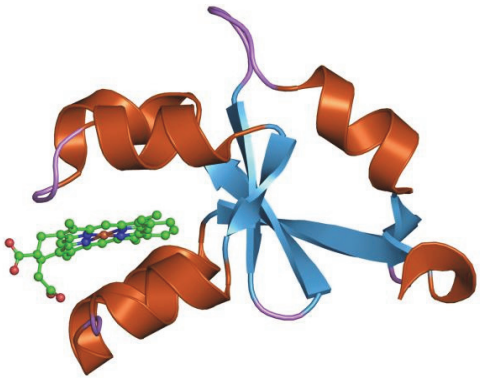

Fig. 12. Cytochrome b_5 structure (obtained by PDBe Protein Data Bank Europe, http://www.ebi.ac.uk/pdbe/).

4. Cytochrome P450 catalytic cycle

After having understand the complex structure of these enzymes, it is necessary to know that all of them essentially function in the same way, despite the genetic differences. CYPs can carry out substrate (RH) reductions through a catalytic cycle after substrate and oxygen binding. However, their main function is to insert an oxygen molecule into a usually stable and hydrophobic compound, and the global reaction can be schematized with the following equation (Coleman, 2010):

$$\text{Hydrocarbon (-RH)} + O_2 + 2 \text{ electrons} + 2H^+ \rightarrow \text{alcohol (-ROH)} + H_2O \quad (2)$$

The CYP reduction activity is carried out through the so-called catalytic cycle (figure 13), which will be briefly reported in a simple way, considering the many details involved in this complex process (Sligar, 1976).

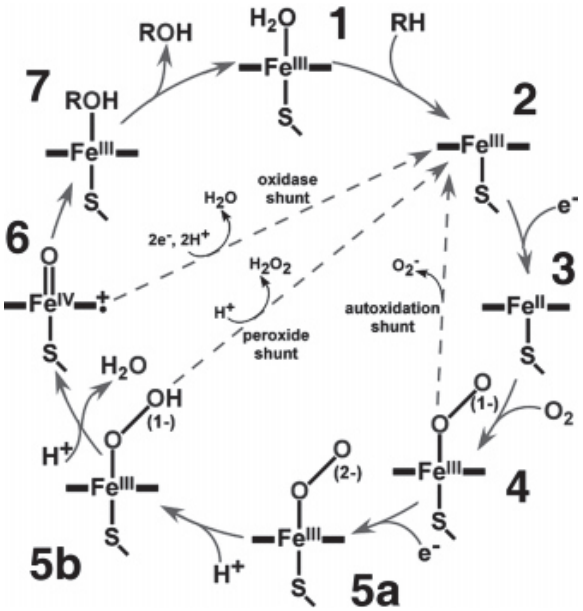

Fig. 13. CYP catalytic cycle (Denisov et al., 2005). Reprinted with permission from Denisov et al., 2005. Copyright 2005 American Chemical Society.

a. Substrate binding (1-3). The first step is the binding and orientation of the substrate molecules. The iron is usually in the ferric form when the substrate is bond*:*

$$Fe^{3+} - RH$$

The substrate binds to the active site of the enzyme, in close proximity to the heme group. The bound substrate induces a change in the conformation of the active site, displacing a water molecule from the distal axial coordination position of the heme iron, and changing the state of the heme iron from a low-spin (LS) to an high-spin (HS) substrate-bound complex (2). The HS ferric enzyme (Fe^{3+}) has a more positive reduction potential and thus in CYP is much easier reduced. Once the substrate has been bound,

the next stage is to receive the first of two electrons from the redox partners, so reducing the iron to its ferrous state Fe^{2+} (3):

$$Fe^{2+} - RH$$

b. *Oxygen binding (3-4).* The next stage involves the binding between ferrous substrate-bound complex and molecular oxygen. This process is usually faster than the previous one, since in the cell there is much more oxygen than substrate*:*

$$O_2 - Fe^{2+} - RH$$

Oxygen binding leads to a slow rearrangement of the $Fe^{2+}O_2$ complex to form an oxy-P450 complex (4), which is the last relatively stable intermediate in this cycle:

$$O^- - O - Fe^{3+} - RH$$

However, this sometimes allows the bond to dissociate, trough the so-called "autoxidation shunt", releasing a reactive superoxide radical, with the return of the enzyme to its resting state, thus interrupting the catalytic cycle (Denisov et al., 2005).

c. *Oxygen scission (splitting), (4-5$_a$).* This is the crucial stage that decides if the substrate will be oxidized or not and it is the rate-limiting step of the cycle. A second electron supplied by the redox partners feeds into the complex and forms *a peroxo-ferric intermediate (5$_a$):*

$$O^{2-} - O - Fe^{3+} - RH$$

As explained earlier, cytochrome b_5 may supply this second electron faster than NADPH reductase.

d. *Protonation of peroxo-ferric intermediate (5$_a$-6).* The peroxo group formed in the previous step is rapidly protonated by surrounding amino-acid side chains forming an hydroperoxo-ferric intermediate (5_b) and then is secondly protonated at the distal oxygen atom. Then, a subsequent heterolysis of O-O bond occurs with the release of a mole of water and the formation of a highly reactive iron (IV)-oxo species (6).

e. *Insertion of the oxygen into substrate (6-7).* Depending on the substrate and enzyme involved, P450 enzymes can catalyse a wide variety of reactions (a complete list is reported in Figure 14). A hypothetical hydroxylation is shown in the illustration (Sono et al., 1996). The substrate can be activated by either removing hydrogen (hydrogen abstraction) or an electron (e.g. from nitrogen atoms), from the substrate molecule. The hydrogen abstraction leaves the carbon with a spare electron making it a reactive radical (6) and then much more likely to react with the hydroxyl group. The final stage is the reaction between the newly created hydroxyl group and the carbon radical, leading the alcohol formation (7).

f. *Release of product (7-new cycle).* Now the substrate, converted to a metabolite, has changed both structurally and chemically and cannot be longer bound to the active site of the CYP. The product is thus released and the CYP isoform returns to its original resting state (1), with a water molecule returning to occupy the distal coordination position of the iron nucleus, now ready for binding another substrate molecule.

In addition the P450 reaction cycle contains at least three branch points, where multiple side reactions are possible and often occur under physiological conditions. The three major abortive reactions are *(i) autoxidation (autoxidation shunt)* of the oxy-ferrous enzyme (4) with

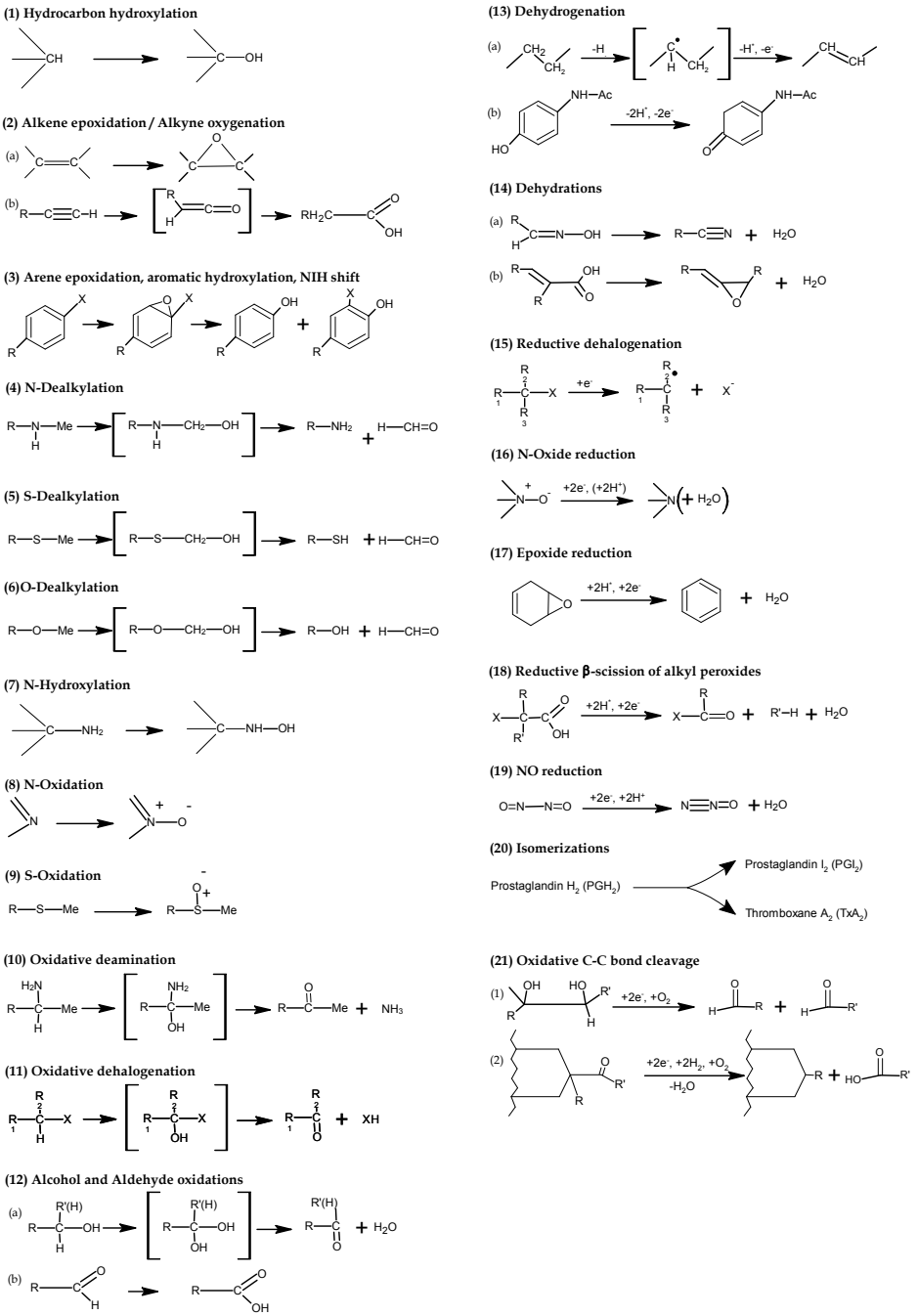

Fig. 14. Schematic summary of the diverse P450-catalyzed reactions (Sono et al., 1996).

the production of a superoxide anion and return of the enzyme to its resting state (2), *(ii) a peroxide shunt*, where the hydroperoxide anion (5_b) dissociates from the iron forming hydrogen peroxide, thus completing the unproductive reduction of oxygen, without substrate turnover, and *(iii) an oxidase uncoupling* wherein the ferryl-oxo intermediate (6) is oxidized to water, which results effectively in the reduction of dioxygen molecule with the formation of two molecules of water. These processes are often categorized together and referred to as uncoupling reactions (Denisov et al., 2005). Cytochrome P450 catalyzes different types of reactions, illustrated in the Figure 14, which are all based on the same catalytic cycle.

5. Cytochrome P450 for drug-biosensor

Electrochemical investigations are usually performed on enzymes to determine fundamental parameters, such as the redox potential, and the electron transfer between the enzymes and the electrodes (Armstrong & Wilson, 2000). Electrochemical studies of cytochromes P450 are of great interest due to the possibility of developing applications such as biosensors for analyte detection and electrochemical catalysis for product synthesis (Honeychurch, 2006). CYPs ability to metabolize a broad spectrum of endogenous substances, e.g., fatty acids, steroid hormones, prostaglandins and foreign compounds (e.g. drugs and environmental toxins), has made this enzyme family interesting as recognition element for biosensing (Bistolas et al., 2005). At the present state-of-the-art, methods such as gas chromatography-mass spectrometry and high-performance liquid chromatography are used for in vitro quantifying the levels of drugs and their metabolites in blood and plasma. These commercially-available methods are time-consuming and expensive. Although with these methods is possible to obtain rapid quantitative in vitro diagnosis with high accuracy, they require time-consuming sample preparation. Thus, these techniques are not so widely spread for practical industrial and medical applications (Iwuoha et al., 2007; Shumyantseva et al., 2004). A cytochrome P450 biosensor may be a promising alternative that would provide quick measurements for drugs and metabolites with a cheap, simple to use, rapid and in some instances disposable equipment, which also supply good selectivity, accuracy and sensitivity.

After the first studies in the 1970s (Bistolas et al., 2005), when CYPs contained in intact hepatocytes and microsomes were used in extracorporal detoxification reactions, choosing as target a wide range of substrates which are subjected to hydroxylation by CYPs, many attempts were carried out in order to built up a CYP-based biosensor for the detections of molecules of interest and drugs. In order to provide stability to the enzyme-system and in order to avoid the need of the regeneration of cofactor NADH and NADPH, which naturally provide electrons to the cytochrome active site, amperometric biosensors of second and third generations (Figure 15) were thought to be the most suitable for such applications and were designed. Some attempts have been recently made to improve the electron transfer between the CYP-enzymes and the electrodes, through the employment of en electrochemically active mediator and using cathodic current for the substrate reduction, thus obtaining highly efficient electrochemical second-generation biosensor (Shumyantseva et al., 2000). As found in literature, cobalt(III) sepulchrate trichloride was used as mediator for the electrocatalytical reduction of proteins containing different cytochrome P450s and NADPH-P450 reductase for catalyze the hydroxylation of steroids and the N-demethylation of drugs (Estabrook et al., 1996). Otherwise mediators such as FMN, FAD or riblofavins

(Shumyantseva et al., 2000, 2001) were covalently bound to cytochrome P450 2B4 and 1A2 cross-linked onto a screen-printed rhodium graphite electrode for direct amperometric measurement of cholesterol or aminopyrine. Unfortunately, this kind of redox mediators used in conjunction with redox enzymes facilitates not only the electron transfer between electrode and enzyme but also other various interfering reactions, resulting in a low-specificity detection.

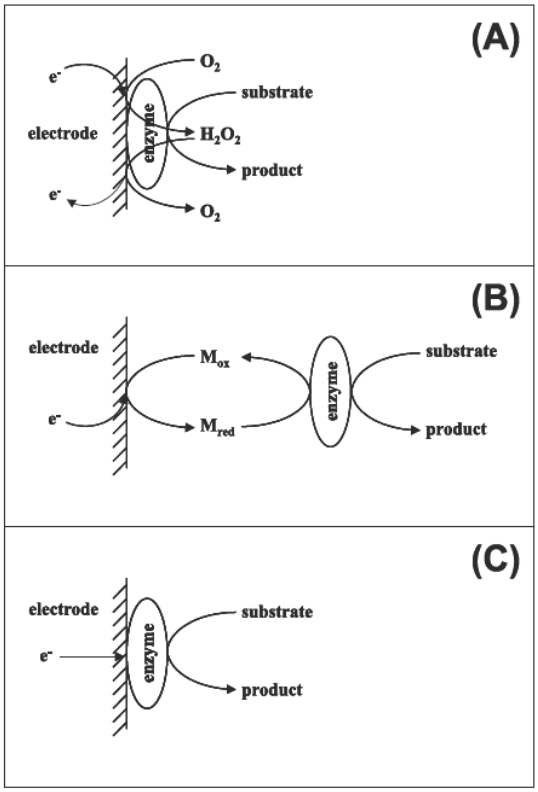

Fig. 15. Representation of three different amperometric biosensors generations (Freire et al., 2003). The first-generation biosensors (Fig. 15 A) are based on direct electrochemical detection of substrate or product of the enzyme reaction, while in the second and third-generation biosensor the detection is based on the quantification of the electron transfer. In the second-generation biosensors (Fig. 15 B), molecular oxygen is replaced with other reversible oxidizing agents, called mediators M_{ox}, which, are small redox active molecules (e.g., ferrocene derivates, ferricyanide, conducting organic salts and quinones) that could react both with the active site of the enzyme and with the electrode surface, realizing the electron transfer between the enzyme and the electrode. In the third generation-biosensors (Fig. 15 C) a direct electron transfer occurs, without using any kind of mediators. In third generation-biosensors several enzymes able to catalyse direct (mediatorless) electron transfer are used. Reprinted with permission from Freire et al., 2003. Copyright 2003 Sociedade Brasileira de Química.

The most suitable approach for the design of a CYP-based biosensor is the direct mediatorless electron supply from an electrode to the redox active group of the CYP, thus leading a direct flow of electrons between the enzyme and the electrode. This kind of biosensor (third-generation biosensors) usually offers better selectivity, because they are able to operate in a potential range closer to the redox potential of the enzyme itself, becoming less exposed to reactions with interferents. The electrode is used as electron source for the CYP cathodic reduction which is coupled with the substrate transformation. The generation and the measurement of a catalytic current is the direct indicator of CYP-dependent electrocatalysis. In the figure 16 is reported a scheme for the electrocatalytic oxygenation reaction of a substrate (RH) bound to CYP immobilized onto the electrode surface. In this scheme is possible to observe the active role of electrode as electron source in the P450 catalytic cycle.

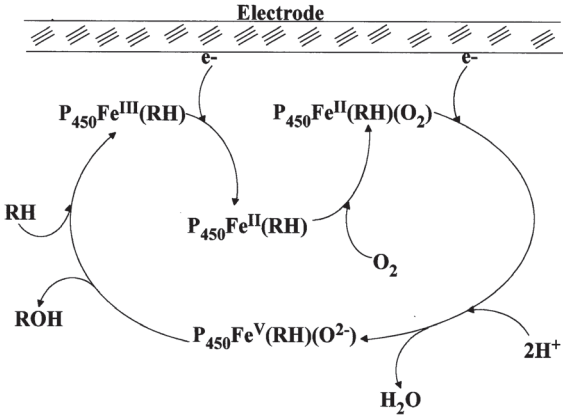

Fig. 16. Suggested scheme for the electrocatalytic oxygenation reaction of substrate-bound cytochrome P450 (Iwuoha et al., 1998). Reprinted from Journal of Pharmaceutical and Biomedical Analysis, Vol. 17, Emmanuel I. Iwuoha, Shiba Joseph, Z. Zhang, Malcolm R. Smyth, Uwe Fuhr, Paul R. Ortiz de Montellano, "Drug metabolism biosensors: electrochemical reactivities of cytochrome P450cam immobilised in synthetic vesicular systems", Pages No. 1101–1110, Copyright (1998), with permission from Elsevier.

In the development of this mediator-less approach, the immobilization of CYP onto the electrode surface has to be deeply controlled in order to obtain a high probability for the protein to be attached to the electrode in a proper orientation that could optimize the electron transfer to the heme group since it is deeply immerged in the cytochrome structure. In addition, the immobilization techniques of CYPs onto the electrode should avoid the formation of an insulating protein layer which prevents electron transfer, due to the adsorptive denaturation of proteins onto metal electrodes (Eggins, 2003).

5.1 CYPs immobilization techniques

The electron transfer between the enzyme and the electrode depends mostly on the technique used for the protein immobilization, on the electrode material or on the method used for modify the electrode surface, because all these factors change the orientation and the distance of the protein from the electrode. A variety of metal electrodes such as Au, Pt,

Tin oxide, oxide electrodes (such as In_2O_3), as well as non-metal electrodes such as glassy carbon, graphite (pyrolytic graphite and edge-plane graphite), and carbon cloth has been used for the fabrication of CYP-based amperometric biosensors (Bistolas et al., 2005; Eggins, 2003). Electrodes fabricated by screen-printed technology have been widely used for the design of amperometric-enzyme biosensors, thanks to their high selectivity and sensitivity, low cost, portable field–based size and their great versatility in the wide range of ways in which the electrodes can be modified (Renedo et al., 2007). Enzymes tend to denature and to passivate the electrode on not-modified metal electrodes, forming an insulating protein layer which prevents electron transfer. Electrochemical measurements has been carried out with CYPs immobilized onto bare electrode (Bistolas et al., 2005), showing that CYPs were absorbed onto the electrode surfaces but the electron transfer estimated with these systems was low and poorly efficient (Fantuzzi et al., 2004). It is necessary to keep under control both the concentration at the electrode surface and the orientation of the enzyme, in order to improve the sensor sensitivity. The inclusion of CYPs in an appropriate medium like a conductive polymer or the non-specific absorption of CYPs onto metal electrode modified with nanomaterials, can lead to the formation of a non-controllable and randomly orientated layer of enzymes. On the other hand, an orientated packed enzyme-monolayer covalently bonded to the electrode surface could be realized through the specific functionalization of both the CYPs ends and the metal surface. More in general, there are different techniques for the CYPs immobilization and the electrode surface modification which depend on the applications, but all of them avoid protein denaturation and preserve an appropriate orientation thus increasing electron transfer. Here, the main techniques used for modify the electrode surfaces are reported:

a. *Clay nanoparticles-modified electrodes.* Clay minerals are usually ion-exchangeable aluminosilicates, very widespread in geologic deposits. The mineral group of clays includes sodium montmorillonite, smectite, laponite, kaolinite, talc, goethite and orche. Clay particles are very small and their size is comparable with protein sizes so that they are really effective for mediate the electron transfer between electrode and biocomponent. In aqueous solutions clay produces colloid solutions with 1-100 nm size. Thus, clay materials can form films by dropping, casting and drying of a colloidal clay suspension, while with ionic surfactants they can generate biomembrane-like structures (Eggins, 2003; Shumyantseva et al., 2004) or can create protein-films by layer-by-layer technique. For instance, direct electrochemistry of cytochrome P450 at layer-by-layer clay modified carbon electrode was achieved (Lei et al., 2000). Sodium montmorillonite, kaolinite, talc, goethite and orche have been used to modify electrodes and investigate the electrochemistry of heme proteins (Bistolas et al., 2005).
b. *Phospholipid and vesicle-systems modified electrodes.* In order to mimic the physiological environment of CYP enzymes, i.e. the hydrophobic environment in the endoplasmic reticulum of cell, synthetic phospholipids has been used for the construction of biosensors. These films which mimic the cellular membrane structure are surfactant or bilayer lipid films made by didodecyldimethylammonium bromide (DDAB), dimeristoyl-l-phosphatidylcholine (DMPC), dilauroylphosphatidylethanolamine (DLPE) and distearoyl-phosphatidyl-ethanolamine (DSPE). The phospholipid layer-structure may facilitates electron transfer between the enzymes redox centre and the electrode. Stable films can be cast onto surfaces from solution of surfactants in

organic solvents or from aqueous vesicle dispersion, since the surfactants are insoluble in water. Then evaporation of solvent leads the surfactant to auto-assembly into phospholipid biomembrane-like films (Wu & Hu, 2007). In some studies (Iwuoha et al., 1998), CYPs were incorporated in vesicle dispersion of the synthetic material DDAB and then immobilized by cross-link onto glassy carbon electrode. Other applications involving CYPs for biosensor production used glutaraldehyde and synthetic phospholipids for the immobilization of semisynthetic flavocytochromes based on CYP2B4, CYP1A2 and mitochondrial P450scc onto rhodium-graphite electrodes (Shumyantseva et al., 2001), or films of surfactants with CYP176A (Aguey-Zinsou et al., 2003).

c. *Electrodes modified with multilayer films.* In order to improve the direct electron transfer between electrodes and heme proteins like CYP, multilayer-deposition techniques, such as layer-by-layer (LBL) polyionic films of CYPs, have been studied (Bistolas et al., 2005). The repetition of cycles of enzyme and polyion adsorption alternately with intermediate washing provides multilayer stable films with reproducible amounts of enzyme in each layer and namometer-scale control of thickness. More than 20 enzymes and proteins have been incorporated into films by this electrostatic layer-by-layer self-assembly technique. Synthetic polyions, metal oxide nanoparticles, and biological polyions such as DNA have been used to alternate with the enzyme layers. Some examples are (i) Au and pyrolytic graphite electrodes modified by LBL film of poly-(styrenesulfonate) (PSS) and/or branched poly(ethyleneimine) (PEI) and CYP101 thus creating CYP101-multilayer films (Munge et al., 2003), (ii) PSS-CYP1A2 multilayers grown on carbon cloth electrodes (Estavillo et al., 2003), (iii) LBL enzyme films on Au electrodes by alternate adsorption of a layer of CYP3A4 on top of a layer of PDDA (poly(dimethyl diallyl) ammonium chloride), (Joseph et al., 2003), and (iv) Polyaniline (Pan)-doped glassy carbon electrode (GCE) and CYP2D6 (Iwuoha, Wilson, Howel, Mathebe, Montane-Jaime, Narinesingh, Guiseppi-Elie, 2000).

d. *Nanomaterials.* Materials in the nanometric size regime display size-dependent optical, electronic, and chemical properties. Nanoparticles have several advantages, such as large surface area, high-powered catalysis, excellent affinity, and also their nanometric-size, since is comparable with protein size, influence the rate of electron transfer thus enhancing the electrochemical catalytic activity of enzymes. Several material nanoparticles have been used to immobilize proteins, including gold, colloidal gold (Wu & Hu, 2007), SiO_2 (He et al., 2004; Liu et al., 2004), MnO_2, ZrO_2 (Liu et al., 2008; Peng et al., 2008) and TiO_2 nanoparticles and carbon nanotubes (see paragraph 5.2.1). The immobilization of protein on gold nanoparticles can help the protein to keep a favoured orientation or to create conducting channels between the prosthetic groups and the electrode surface, thus reducing the effective electron transfer distance (Wu & Hu, 2007). It has been demonstrated (Shumyantseva, Carrara, Bavastrello, Riley, Bulko, Skryabin, Archakov, Nicolini, 2005) that gold nanoparticles improve the sensitivity of cholesterol biosensor with cytochrome P450scc. Other studies (Liu et al., 2008; Peng et al., 2008) showed the feasibility in enhance redox current of CYP2B6 to be incorporated into films made by zirconium dioxide nanoparticles and platinum components (Peng et al., 2008) and into a chitosan modified colloidal gold nanoparticles (Liu et al., 2008).

e. *Self-Assembled monolayers (Figure 17) and Langmuir-Blodgett protein films.* Redox proteins can be adsorbed via electrostatic interaction or covalently immobilized on Self-assembled monolayers (SAM), which can lead to a better-controlled electron transfer between the protein and the electrode (Yang et al., 2009). With SAMs is possible to regulate the distance between the heme group of CYP and the electrode surface, changing the chain length (the so called 'tail') of SAMs which allow the film to be tightly packed and oriented on the surface thanks to the weak interactions between the tails. Usually alkane-thiol or other thiol-terminated chains covalently bind the self-assembled molecule to the metal surface of the electrode. At the other end of the chains a group is able to specifically interact with a group on the protein surface, thus adding selectivity to the modified electrode for particular proteins. Figure 17 shows the model of CYP2C9 bonded to the Gold-SAM electrode surface. The Langmuir-Blodgett technique allows one to form highly ordered amphiphilic lipid monolayers at the air–water interface which can be used to study the interaction of proteins and phospholipids and to immobilize enzymes such as CYPs onto the electrode surface. LB monolayers offer high thermal stability thanks to the close packing of molecules and it has been demonstrated that its behaviour on electrodes is dependent on the number of monolayers (Nicolini et al., 2001). Recombinant and wild types of CYP11A1 (cytochrome P450scc) have been immobilized onto electrode surfaces with LB technique for cholesterol biosensing (Nicolini et al., 2001). Other cytochrome P450 isoforms were immobilized by the LB technique, and used as biological recognition element for biosensor fabrication. The substrates chosen for the detection utilized were clozapine for CYP1A2, styrene for CYP2B4, and cholesterol for CYP11A1 (Paternolli et al., 2004).

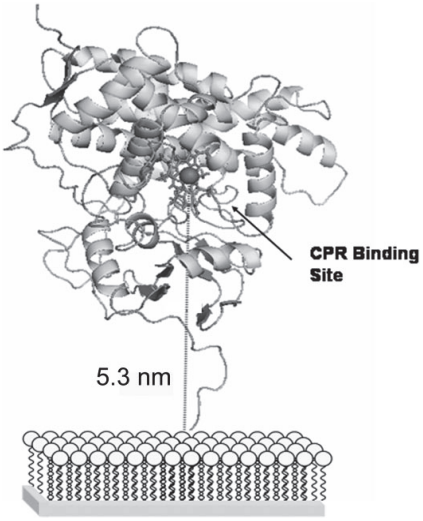

Fig. 17. Model of CYP2C9 bonded to the Gold-SAM electrode. The gold surface/SAM to iron atom separation is shown (Yang et al., 2009). Reprinted with permission from Yang et al., 2009. Copyright 2003 Drug Metabolism and Disposition by American Society for Pharmacology and Experimental Therapeutics.

f. *Sol-Gel matrix systems.* This kind of bioelectrode is suitable for applications in organic phases. In the sol–gel immobilization onto electrode, the silicate matrix is formed through the acid or base hydrolysis of an alkoxide precursor, such as tetramethyl orthosilicate (TMOS), or more in general of the silane monomer followed by condensation reaction, which generate a high-density silica gel. Therefore, if a protein is added after the partial hydrolysis of the TMOS precursor, a porous matrix is formed around the protein molecule, entrapping it in an aqueous microenvironment similar to that of an aqueous solution of protein (Eggins, 2003). The resulting sol-gel has been reported to be chemically, thermally and structurally stable, with a various pore-size structure which is large enough to allow substrate/product diffusion into and out of the sol-gel network but still being small enough to prevent leaching of the enzyme. In a study (Iwuoha, Kane, Ania, Smyth, Ortiz de Montellano, Fuhr, 2000), a composite amperometric biosensor has been prepared by encapsulating a cytochrome P450cam /didodecyl-dimethylammonium bromide (DDAB) liquid crystal system in a methyltriethoxysilane (MTEOS) sol-gel.

5.2 Electrochemical characterization of cytochrome P450 for drug sensing

Using an amperometric biosensor, it is possible to follow the catalytic cycle of CYP by the quantification of the electron transfer between the electrode and the enzyme. Thus it is possible to indirectly measure the concentration of the drug or metabolites present in the sample by measuring the current in the electrochemical cell. There are several electroanalytical techniques for the measure of substrate concentration, such as cyclic voltammetry, square wave voltammetry and amperometry (Thévenot et al., 2001). Cyclic voltammetry (CV) is one of the mostly considered technique in electrochemistry for biosensing applications. Compared to other electroanalytical techniques, CV is the most appropriate in the case of CYP, because of the uncertainty of CYP peaks potential and because with CV is possible to identify more substrate molecules at a time with the same biological recognition element (Eggins, 2003). The biosensing is carried out by the measurement of the current-peaks height found in the voltammograms resulting from the application of a potential scan, since the height of the peaks is proportional to the drug/metabolite concentration, while its position in potential gives information on the substrate chemistry. Several attempts to measure the presence of drugs in sample have been carried out with cytochrome P450-based biosensors (Bistolas et al., 2005). Table 2 reports peaks position of different CYPs obtained trough cyclic voltammetry. It is important to know that the redox potential mostly depends on the method used for the CYP immobilization onto the electrode surface.

Cyclic voltammograms registered with a CYP-based biosensor have different shape depending on some factors, such as the pH and the ionic strength of the buffer solution, the temperature, the immobilization technique and the scan rate, but mostly on the presence/absence of oxygen (O_2), and obviously of the substrate (Johnson et al., 2005).

In the absence of the CYP substrate, the mechanism of the reaction between the CYP immobilized onto electrode surface and O_2 is outlined as follows (Guengerich, 2001):

$$P - Fe^{III} + H^+ + e^- \rightleftarrows P - Fe^{II} \quad (3)$$

$$P - Fe^{II} + O_2 \rightleftarrows P - Fe^{II} - O_2 \quad (4)$$

$$P - Fe^{II} - O_2 + e^- + H^+ \rightleftarrows P - Fe^{III} + H_2O_2 \quad (5)$$

In the absence of oxygen in the buffer solution, one electron is first transferred from the electrode to the immobilized CYP (P is for the protein), leading to the reduction of the ferric heme iron (Fe^{III}) to the ferrous form (Fe^{II}), according to the equation (3). This is a reversible electrode reaction, where one proton and the iron heme ion participate in the electron transfer process (Liu et al., 2008). In the presence of dissolved oxygen, the shape of the cyclic voltammogram visibly changed with an increase of the reduction peak current and the decrease of the oxidation peak current (Fig. 18). The mechanism of the reaction between the CYP and O_2 is reported in the equations 4 and 5. Following CYP reduction, the ferrous heme iron of CYP (Fe^{II}) quickly binds to O_2 to form the ferrous–dioxygen complex (Fe^{II}-O_2, equation 4). This unstable highly-reactive ferrous–dioxygen complex can easily accept a second electron to be oxidized back to its ferric form, while the oxygen is catalytically reduced to H_2O_2 (Estavillo et al., 2003). The CYP ferric form could be reduced again, resulting in pronounced reduction currents observed that are typical for electrocatalytic oxygen reduction (Liu et al., 2008; Peng et al., 2008). In figure 18 a comparison between cyclic voltammograms obtained with argon-saturated buffer, air-saturated buffer and air-saturated buffer in presence of the CYP2B6 substrate, is reported (Shumyantseva et al., 2004).

CYP species	Electrode modification	E° potential	Reference
CYP1A2	Multilayer with PSS-Carbon cloth	-310mV(vs SCE)	(Estavillo et al., 2003)
	PEI(/PSS/CYP) multilayer on pyrolytic graphite	-330mV(vs Ag/AgCl)	(Krishnan et al., 2009)
CYP2B4	DDAB/Au/CYP	-323mV(vsAg/AgCl)	(Shumyantseva et al., 2009)
CYP2B6	ZrO_2/Pt/PLL-film	-449mV(vsAg/AgCl)	(Peng et al., 2008)
	CYP/Au-chitosan/GCE	-454mV(vsAg/AgCl)	(Liu et al., 2008)
CYP2C9	DDAB/CYP film on PGE electrode	-41mV(vs NHE)	(Johnson et al., 2005)
CYP2C18	DDAB/CYP film on EPG electrode	-70mV(vs NHE)	(Shukla et al., 2005)
CYP2C19	DDAB/CYP film on EPG electrode	-45mV(vs NHE)	(Shukla et al., 2005)
CYP2D6	Polyaniline doped GCE	-120mV(vs SCE)	(Bistolas et al., 2005)
CYP2E1	PEI(/PSS/CYP) multilayer on pyrolytic graphite	-347mV(vs Ag/AgCl)	(Krishnan et al., 2009)
CYP3A4	Au-MPS-PDDA multilayers	-470mV(vs Ag/AgCl)	(Joseph et al., 2003)
	Pt-CYP-DDAB-BSA-Glu multilayers	-689mV(vs Ag/AgCl)	(Ignaszak et al., 2009)
CYP11A1	Langmuir Blodgett films ITO glass plate	-295 to -318mV (vs Ag/AgCl)	(Bistolas et al., 2005)

Table 2. List of CYP used for biosensor and their electrochemical parameters obtained with cyclic voltammetry technique.

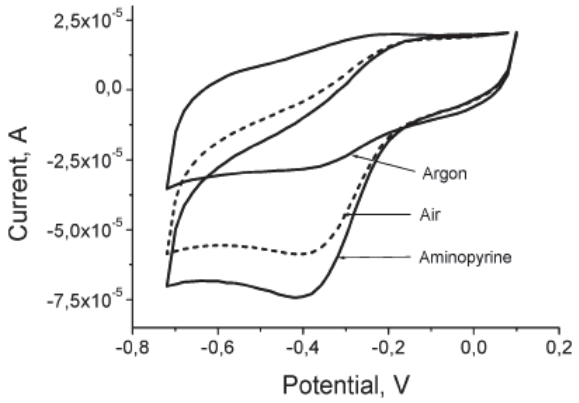

Fig. 18. Effect of oxygen and aminopyrine on the CYP2B4 electrode with mixed film of CYP2B4, Tween 80, and clay (Shumyantseva et al., 2004). Reprinted with permission from Shumyantseva et al., 2004. Copyright 2004 American Chemical Society.

When the drugs (substrates) are added to a buffer solution in presence of oxygen, a further increase of the CYP reduction current is observed (Fig. 18, spectrum of Aminopyrine), (Shumyantseva et al., 2004). It is known that the binding of substrates to the ferric CYP (Fe^{III}) induces a change in spin state, from low spin to high spin and this change in spin state makes the redox potential of the enzyme shift towards more positive values, thus thermodynamically facilitating the transfer of the fist electron from the electrode (Liu et al., 2008). So, the binding of the drug substrate to the enzyme promote the CYP reduction to its ferrous form, resulting in a faster oxygen binding and making more favorable the transfer of the second electron to the ferrous–dioxygen complex (Liu et al., 2008; Peng et al., 2008).
It is possible to conclude that the coupling of the bioelectrocatalytic oxygen reduction current and the bioelectrocatalytic substrate conversion occurs when the substrate is added to a buffer solution in presence of oxygen. Indeed, this phenomenon has been verified for a number of different P450 enzymes in solution, including CYP101, CYP102 and CYP11A1 (Johnson et al., 2005), and for a number of different CYPs immobilized onto electrodes, such as CYP2C9 (Johnson et al., 2005), CYP2B4 (Shumyantseva et al., 2004,2007), CYP3A4 (Joseph et al., 2003), CYP2B6 (Liu et al., 2008; Peng et al., 2008), CYP2D6 (Iwuoha et al., 2007), and CYP1A2 (Antonini et al., 2003; Estavillo et al., 2003). The simplified reaction scheme reported in figure 19, explains both the bioelectrocatalytic oxygen reduction current and the bioelectrocatalytic substrate conversion (Shumyantseva et al., 2004).
The first three reactions reported in Figure 19 are respectively the substrate binding (reaction 1), the first electron transfer (reaction 2) and the oxygen binding (reaction 3), with the formation of the dioxygen-ferrous complex. The latter accepts a second electron (reaction 4), leading to the formation of an highly reactive peroxy intermediate. The addition of protons H^+ to this intermediate results in the insertion of an oxygen atom into the substrate (ROH), which is then released and the CYP is restored to its starting ferric state (reaction 5). The uncoupling can occur on the level of the dioxygen (reaction 6) or peroxy complex (reaction 7). The catalytic oxygen reduction (with the peroxide formation), regenerates the ferric enzyme, which may again be reduced in a further reaction cycle (reaction 2), thus enhancing the electrochemical reduction (Estabrook et al., 1996).

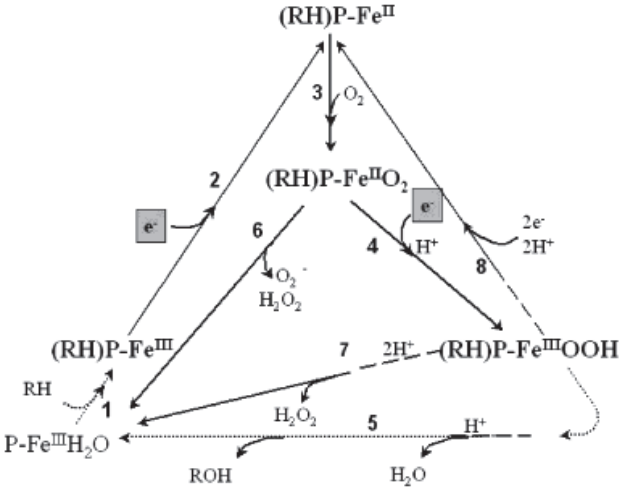

Fig. 19. General scheme of the electrocatalytic reaction of CYP in presence of oxygen and its substrate (RH), (Shumyantseva et al., 2004). Reprinted with permission from Shumyantseva et al., 2004. Copyright 2004 American Chemical Society.

Biosensors based on individual P450 proteins have already been proposed to develop novel tools for drug detection in human serum (Bistolas et al., 2005; Cavallini et al., 2010; Ghindilis, 2000). The biosensing is mainly based on the biochemical reaction schematized in figure 20 where a cytochrome P450 transform the redox form of a drug (the Cyclophosphamide in the example) in its oxidized form by using one oxygen molecules and two electrons.

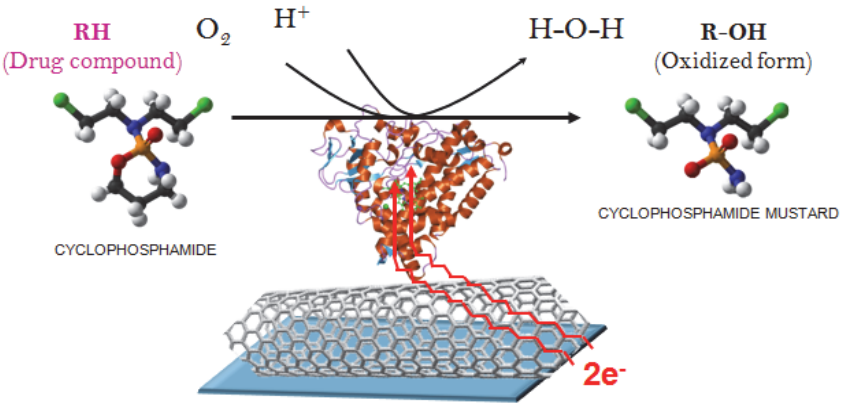

Fig. 20. The oxidation of a drug (Cyclophosphamide) catalyzed by the cytochrome P450.

The two electrons (which in nature are provided by the NADPH molecules) are supplied by the flowing current from the electrode. As explained previously, is possible to measure this catalytic current and, thus, to indirectly measure the drug concentration through the

CYP species	Drugs	Description	Reduction potential (vs Ag/AgCl)	Reference
CYP1A2	Clozapine	Antipsychotic for schizophrenia	-265mV	(Antonini et al., 2003)
	Ftorafur	Anticancer	-430mV	*
CYP2B4	Aminopyrine	Analgesic, anti-inflammatory and antipyretic	-400mV	(Shumyantseva et al., 2004)
	Benzphetamine	Anorectic	-250mV	(Shumyantseva et al., 2007)
CYP2B6	Bupropion	Antidepressant	-450mV	(Liu et al., 2008)
	Cyclophosphamide	Anticancer and immunosuppressive	-450mV	(Liu et al., 2008)
	Ifosfamide	Anticancer and immunosuppressive	-430mV	* (Peng et al., 2008)
	Lidocaine	Anesthetic and antiarrhythmic	-450mV	
CYP2C9	Diclofenac	Analgesic and anti-inflammatory	-41mV	(Johnson et al., 2005)
	S-Warfarin	Anticoagulant	-36mV	(Johnson et al., 2005)
	Sulfaphenazole	Antibacterial	-41mV	(Johnson et al., 2005)
	Tolbutamide	Stimulator for insulin secretion (treatment of type II diabetes)	-37mV	(Johnson et al., 2005)
	Torsemide	Diuretic	-19mV	
CYP2D6	Fluoxetine	Antidepressant	-327mV	(Iwuoha, Wilson, Howel, Mathebe, Montane-Jaime, Narinesingh, Guiseppi-Elie, 2000) (Iwuoha et al., 2007)
	Sertaline	Antidepressant	-275mV	
CYP2E1	P-Nitrophenol	Intermediate in the synthesis of paracetamol	-300mV	(Fantuzzi et al., 2004)
CYP3A4	Cyclophosphamide	Anticancer and immunosuppressive	-450mV	*
	Erythromycin	Antibiotic	-625mV	(Hendricks et al., 2009)

	Ifosfamide	Anticancer and immunosuppressive	-435mV	*
	Indinavir	Anti-HIV	-750mV	(Ignaszak et al., 2009)
	Midazolam	Anxiolytic, anaesthetic, sedative, anticonvulsant, and muscle relaxant	-	(Joseph et al., 2003)
	Quinidine	Beta blocker	-	(Joseph et al., 2003)
	Progesterone	Steroid hormone	-	(Joseph et al., 2003)
	Verapamil	For the treatment of hypertension, angina pectoris, cardiac arrhythmia	-100mV	

* Measurements obtained in studies performed by the authors, immobilizing CYPs isoforms onto carbon nanotubes.

Table 3. List of CYPs used for the detection of drugs for common diseases and their reduction potential obtained with cyclic voltammetry technique.

analysis of reduction peaks obtained in the cyclic-voltammograms. The electron transfer can be enhanced by electrodes nanostructuring, as using metallic or zirconium dioxide nanoparticles, carbon-nanotubes (Bistolas et al., 2005; Eggins, 2003), or other techniques for the enzyme immobilization onto the electrode surface, which have been already explained in the previous pharagraph. Different studies demonstrated that carbon-nanotubes (schematized in figure 20) promote the electron transfer between the CYP active site and the electrode and enhance biosensor sensitivity (Lyons & Keeley, 2008; Wang, 2005). In table 3 a list of a target drugs which have been detected with several CYP isoforms used as biological recognition element of biosensors is reported.
So, the cytochromes P450 may be used to detect drug compounds commonly used in medical treatments by using nanoparticles or carbon nanotubes for improving the device sensitivity to reach the therapeutic ranges found in the patients' serum. Since for the treatments some of the most common diseases, as in anti-cancer therapies, more than one drug are administrated contemporaneously, an array-based biosensor able to measure multiple-drug concentrations at the same time, by using different CYP isoforms, would be very useful and it would find several practical applications. The development of such as biosensor has to overcome several difficulties, first of all the fact that each cytochrome P450 isoform detects many drugs and that different isoforms can detect the same drug (Carrara et al., 2009).

5.2.1 Carbon Nanotube (CNTs)

CNTs can be described as sp^2 carbon atoms arranged in graphitic sheets wrapped into cylinders and can have lengths ranging from tens of nanometers to several microns (Lyons & Keeley, 2008). CNTs can display metallic, semiconducting and superconducting

electron transport, possess a hollow core suitable for storing guest molecules and have the largest elastic modulus of any known material. CNTs can be made by chemical vapour deposition, carbon arc methods, or laser evaporation (Wang, 2005) and can be divided into single-walled carbon-nanotubes and multi-walled carbon-nanotubes (see figure 21). Single-walled carbon nanotubes (SWCNTs) provide good chemical stability, mechanical strength and a range of electrical conductivity. They are around ten times stronger and six times lighter than steel and they can behave as metals, semiconductors or insulators depending on their chirality and diameter (Lyons & Keeley, 2008). The chirality of the SWNT is related to the angle at which the graphene sheets are rolled up (Gooding, 2005). It has been also demonstrated (Gooding, 2005) that the conductivity properties of SWNTs can depend by the presence of catalytic particles, deriving from the fabrication process, the presence of defects in their chemical structure, ion-doping and side-wall functionalizations.

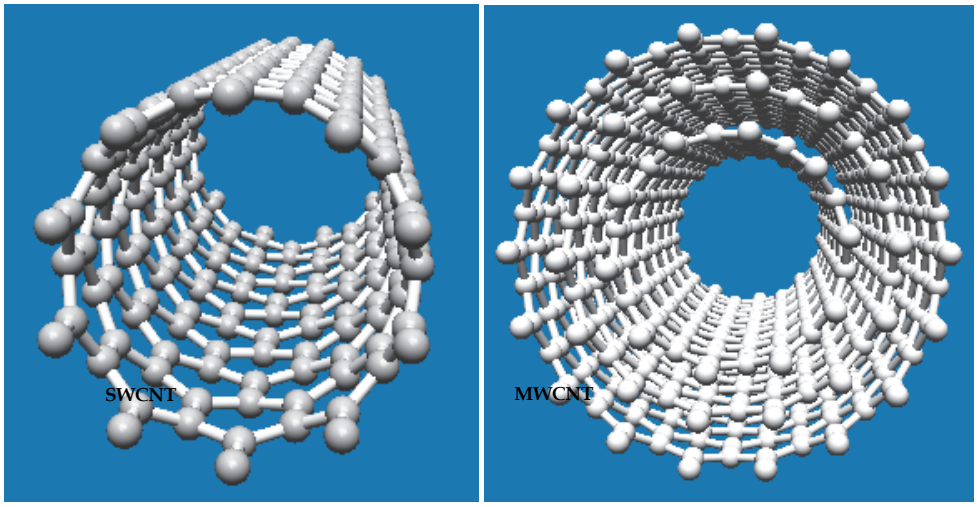

Fig. 21. MWCNT and SWCNT (obtained with Nanotube Modeler © JCrystalSoft, 2010).

Due to their high surface energies, SWCNTs are usually found in bundles or small aggregates composed of 10-100 tubes in parallel and in contact with each other. Multi-walled carbon nanotubes (MWCNTs) are composed of several layers of concentric graphitic cylinders. They are regarded entirely as metallic conductors, making them more suitable for electrochemical applications (Lyons & Keeley, 2008). Anyway, thanks to their electrochemical properties, both multi and single-walled carbon nanotubes could be excellent candidates for the nanostructuration of electrodes used in amperometric biosensor devices. Pre-treatments of CNTs before their deposition onto electrode surfaces, cause the formation of open-ended tubes with oxygenated functional groups, crucial for the electrochemical properties of CNTs. Because of the hydrophobicity due to the CNT walls, in aqueous solution or in polar solvents the tubes have a tendency to rapidly coagulate. Thus, dispersing tubes is usually performed in non-polar organic solvents such as in dimethylformamide (DMF) or chloroform, or with the aid of surfactants or polymers, such as Nafion. The difficulty in dispersing nanotubes in aqueous solution though has been used

as an advantage in preparing nanotube modified electrodes where nanotubes dispersed in an organic solvent are dropped onto an electrode surface and the solvent allowed evaporating. It has been demonstrated that this kind of CNT deposition allows the nanotubes to be strongly adsorbed onto the electrode surface (Gooding, 2005).

5.2.1.1 Electron transfer CNTs-protein

The best strategy for successful enzyme biosensor fabrication is to devise a configuration by which electrons can directly transfer between the redox center of the enzyme and the underlying electrode. This is achievable because the physical adsorption or covalent immobilization of enzymes onto the surface of immobilized carbon nanotubes allows a direct electrical communication between the electrode and the active site of redox-active enzymes. It has been reported (Wang, 2005) that a redox enzyme, such as the glucose oxidase or cytochrome P450, adsorbs preferentially to edge-plane sites on nanotubes. Such sites contain a significant amount of oxygenated functionalities such as hydroxyl groups or carboxylic moieties formed during the purification of CNT, which provide sites for covalent linking of CNT to biorecognition elements (or other materials) or for their integration onto polymer surface structures (Wang, 2005). Other oxygenated moieties, useful for the protein immobilization, can be also formed by the breaking of carbon-carbon bonds at the nanotube ends and at defect sites present on the side-walls. The nanotubes and enzyme molecules are of similar dimensions, which facilitate the adsorption of the enzyme without significant loss of its shape or catalytic function. It is thought that the nanotube directly reaches the prosthetic group such that the electron tunnelling distance is minimized. In this way, loss of biochemical activity and protein denaturation are prevented (Lyons & Keeley, 2008).

5.2.1.2 Nanostructuring electrode surfaces with carbon nanotubes

There have been a number of approaches to randomly distributing the CNTs on electrodes by dispersing the nanotubes with a binder such as dihexadecyl-hydrogen phosphate or Nafion, forming the nanotube equivalent of a carbon paste which can be screen printed, forming a nanotube-teflon composite, drop coating onto an electrode without any binders, preparing a nanotubes paper as the electrode and abrasion onto the basal planes of pyrolytic graphite. The resultant electrode has randomly distributed tubes with no control over the alignment of the nanotubes. To better control the alignment of nanotubes a more versatile approach to producing aligned carbon nanotube arrays is by self-assembly, by using self-assembled monolayers (after the functionalization of the carboxylic-ends of CNTs with carbodiimide groups and thiols), or by directly growing of aligned nanotubes onto the surface. To do this plasma enhanced chemical vapor deposition using a nickel catalyst on a chromium coated silicon wafer can be used (Gooding, 2005). Advantages in using this method are the robustness of these electrodes and also the control over the density of the CNT film by controlling the distribution of the catalyst on the surface (Salimi et al., 2005). Figure 22 reports a comparison between SEM images of MWCNTs (on the bottom) and MWCNTs covered by 1 layer of CYP3A4 (on the top). The CNTs has been deposited by drop casting technique onto the electrode surface (30μL of a solution 1mg/ml of MWCNTs in chloroform). In the figure is visible the increase of apparent CNTs diameter due to the presence of a layer of CYP3A4 (on the top), that has been deposited by drop casting onto the CNT-surface.

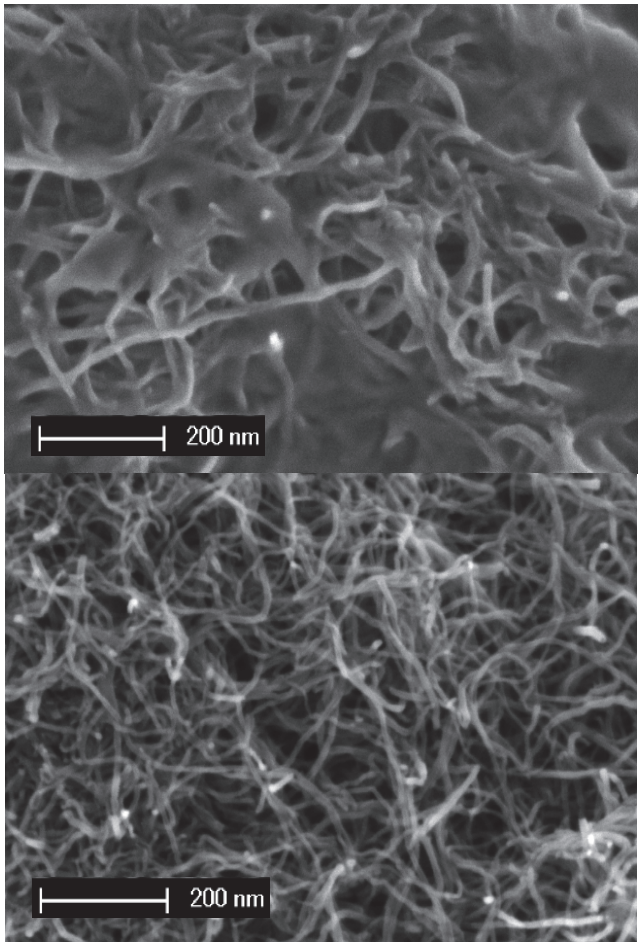

Fig. 22. Comparison between SEM images of MWCNTs (on the bottom) and MWCNTs covered by 1 layer of CYP3A4 (on the top), both at 80,000X of magnification.

5.2.1.3 Enhancement of catalytic current with CNTs

The chemical modification of electrode surfaces with carbon nanotubes has enhanced the activity of electrode surfaces with respect to the catalysis of biologically active species such as hydrogen peroxide, dopamine and NADH. Furthermore, multi-walled carbon nanotubes have exhibited good electronic communication with redox proteins where not only the redox center is close to the protein surface such as in Cytochrome c (Zhao et al., 2005) and horseradish peroxidase, but also when it is deeply embedded within the glycoprotein such as is found with glucose oxidase (Gooding, 2005). A recent study (Carrara et al., 2008) demonstrated the enhancement of the catalytic current in a P450-based enzyme sensor in the case of electrodes modified with MWCNT, with respect to the case of both the bare electrodes and the electrode modified with gold nanoparticles. In figure 23, a comparison between cyclic voltammograms of screen-printed bare electrode (1), electrode modified with

Au nanoparticles and CYP11A1 (2) and with MWCNTs and CYP11A1 (3) is reported. In these voltammograms, a huge increase of the current peak is observable in the case of the P450 working electrode modified with gold nanoparticles respect to the bare electrode, but a further enhancement of the peak current is clearly visible in the case of MWCNTs-modified electrode with P450 (Carrara et al., 2008).

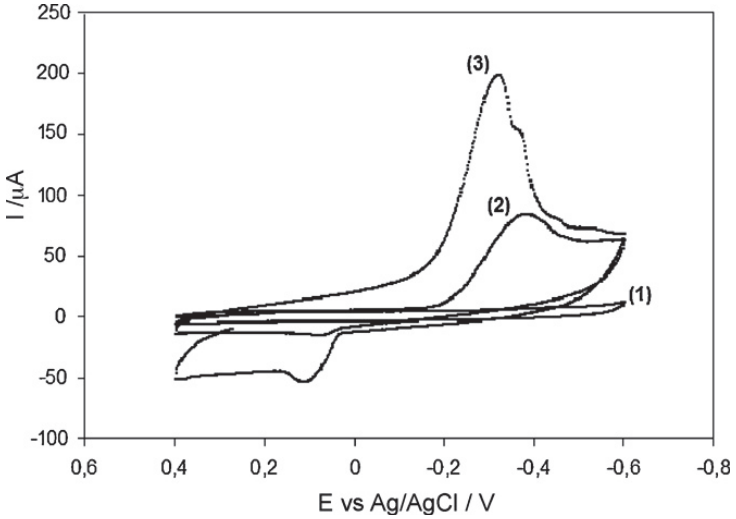

Fig. 23. Cyclic voltammograms of screen-printed bare electrode (1), electrode modified with Au nanoparticles and CYP11A1 (2) and with MWCNTs and CYP11A1 (3), (Carrara et al., 2008). Reprinted from Biosensors and Bioelectronics, Vol. 24, Sandro Carrara, Victoria V. Shumyantseva, Alexander I. Archakov, Bruno Samorì, "Screen-printed electrodes based on carbon nanotubes and cytochrome P450scc for highly sensitive cholesterol biosensors", Pages No. 148–150, Copyright (2008), with permission from Elsevier.

This is the direct proof that the CNT improve the electron transfer between the electrodes and the heme groups of the cytochromes. Moreover, in the presence of MWCNT, the peak is shifted in the positive direction of the voltage axis, because P450 is easier reduced in the presence of CNT, i.e. it is easier to reduce the heme iron incorporated in the protein core.

6. Conclusions

In this chapter the feasibility of cytochrome P450 as probe molecule for the design of an electrochemical biosensor for drug detection in biological fluids has been investigated. Cytochromes P450 have been chosen since they are known to be involved in the metabolism of over 1,000,000 different xenobiotic and endobiotic liphophilic substrates, in particular in the metabolism of ~75% of all drugs. The majority of cytochromes involved in drug metabolism exhibits a certain genetic polymorphism, i.e. mutations in the CYP genes that can cause the enzyme activity to be abolished, reduced, altered or increased, with substantial consequences in drug metabolism, such as an exaggerated and undesirable pharmacological response. In order to individually optimize an ongoing drug therapy, it is required to measure the plasma concentrations of drugs or their metabolites after the

administration. This is needed for really understand how the patient metabolize drugs at the moment of the pharmacological cure. It is a strong need since most effective drug therapies for major diseases still provide benefit only to a fraction of patients, typically in the 20 to 50% range. At the present state-of-the-art the technology allows only to check the genetic predisposition of patients to metabolize a certain drug, without taking into account the many factors that can influence drug metabolism, such as lifestyle, drug-drug interactions and cytochrome P450 daily variation of the polymorphism. Although CYPs are capable in general of catalyse around 60 different classes of reactions, they have a number of features in common, such as the overall fold structure, the presence in their active site of the heme group, that allow the electron transfer to catalyze substrate oxidations and reductions, and the typical catalytic cycle which requires oxygen and electrons as part of the process of metabolism.

CYPs ability to metabolize a broad spectrum of endogenous substances, e.g., fatty acids, steroid hormones, prostaglandins and in particular foreign compounds such as drugs, has made this enzyme family interesting as recognition element for biosensing. P450-based biosensors are of great interest due to the possibility of developing applications such as the detection of analytes and drugs, since the currently-available methods used for in vitro quantifying the levels of drugs in biological fluids are time-consuming and expensive. A cytochrome P450 biosensor may be a promising alternative that would provide quick measurements for drugs and metabolites with a cheap, simple to use, rapid and, in some instances, disposable equipment, which also supplies good selectivity, accuracy and sensitivity. The most suitable approach for the design of a CYP-based biosensor is the direct mediatorless electron supply from an electrode to the redox active group of the CYP, thus leading a direct flow of electrons to the enzyme. In the development of this mediator-less approach, the immobilization of CYP onto the electrode surface has to be deeply controlled in order to obtain a high probability for the protein to be attached to the electrode in a proper orientation that could optimize the electron transfer to the heme group. In this chapter different techniques for the immobilization of CYPs onto the electrode surface have been described as reported in literature, focusing the attention also on the use of nanostructures (e.g. carbon nanotubes), to improve the biosensor sensitivity.

Finally, a list of drugs which have been detected with several CYP isoforms has been reported with data found in literature as well as data obtained by the authors. It is possible to conclude that cytochromes P450 may be used to detect drug compounds also reaching the therapeutic ranges found in the patients' blood, thanks to improved performances due to nanostructured-electrodes. Since for the treatments of some of the most common diseases (e.g. in anti-cancer therapies), more than one drug are administrated contemporaneously, an array-based biosensor able to measure multiple-drug concentrations at the same time, by using different CYP isoforms, would find several practical applications and it could be a first step toward the development of a real chip for personalized-medicine. Electrode miniaturization is the next mandatory step in order to test the real feasibility of this cytochrome-based biosensor as a fully-implantable device for the detection of drugs and metabolites, as much as the evaluation of the biocompatibility of all chip's components, with particular regard to nanostructures and cytochrome citotoxicity. Finally, kinetics studies of drugs should be carried out in order to better understand drug-drug interaction phenomena and the reactions between drugs and cytochrome P450, with regard to enzyme heterotropic kinetics and its effects on drug metabolism.

A cytochrome P450-based biochip for drug detection should be a very powerful platform for personalization of drug therapy thanks to the key role of P450. However, as it has been shown in this chapter, different P450 isoforms may have the same drug compound as substrate and different drugs may be substrates of the same P450 protein. Proper strategies to develop the multiplexing P450-based biosensor arrays must be studied, considering problems due to multiple enzyme-substrate interactions and in the meanwhile maintaining high reliability and low cost of experimentation.

7. Acknowledgments

The SNF Sinergia Project, code CRSII2_127547/1 and title "Innovative Enabling Micro-Nano-Bio-technologies for Implantable systems in molecular medicine and personalized therapy" financially supported this research.

8. References

Aguey-Zinsou K.F; Bernhardt,P.V.; De Voss, J.J. & Slessor, K.E. Electrochemistry of P450cin: new insights into P450 electron transfer. *Chem. Commun*. Vol.(2003), pp.418-419

Antonini, M.; Ghisellini, P.; Pastorino, L.; Paternolli, C. & Nicolini, C. (2003). Preliminary electrochemical characterisation of cytochrome P4501A2-clozapine interaction. *IEE ProC.-Nanobiotechnol*. Vol.150, (June 2003), No.1

Armstrong, F.A. & Wilson, G.S. (2000). Recent developments in faradaic bioelectrochemistry. *Electrochimica Acta.* Vol.45, (2000), pp. 2623–2645

Atkins, W. (2005). Non Michaelis Menten Kinetics in Cytochrome P450-Catalized Reactions. *Ann Rev Pharmacol Toxicol*. Vol.45, (2005), pp 291-310

Bistolas, N.; Wollenberger, U.; Jung, C. & Scheller, F.W. (2005). Cytochrome P450 biosensors—a review. *Biosensors and Bioelectronics.* Vol.20, (2005), pp. 2408–2423

Carrara, S.; Cavallini, A.; Garg, A. & De Micheli, G. (2009). Dynamical Spot Queries to Improve Specificity in P450s based Multi-Drugs Monitoring. *Conference Proceedings of IEEE CME2009*, Tempe (US), 9-11, April, 200

Carrara, S.; Shumyantseva, V.V.; Archakov, A.I. & Samorì, B. (2008). Screen-printed electrodes based on carbon nanotubes and cytochrome P450scc for highly sensitive cholesterol biosensors. *Biosensors and Bioelectronics*. Vol.24, (2008), pp. 148–150

Cavallini, A.; Carrara, S.; De Micheli, G. & Erokhin, V. (2010). P450-mediated electrochemical sensing of drugs in human plasma for personalized therapy. *Ph.D. Research in Microelectronics and Electronics (PRIME), 2010 Conference on* , pp.1-4, ISBN 978-1-4244-7905-4, Berlin, Germany, July, 18-21, 2010

Coleman, M.D. (2010). *Human drug metabolism – An Introduction* (ed.2). Wiley-Blackwell.

Denisov, I.G.; Makris, T.M.; Sligar, S.G. & Schlichting, I. (2005). Structure and Chemistry of Cytochrome P450. *Chem. Rev*.,Vol.105, (2005), pp. 2253-2277

Eggins, B.R. (2003). *Chemical Sensors and Biosensors*. Wiley

Estabrook, R.W.; Faulker, K.M.; Shet, M.S. & Fisher, C.W. (1996). Application of electrochemistry for P450-catalyzed reactions. *Methods Enzymol.* Vol.272, (1996), pp.44–51

Estavillo, C.; Lu, Z.; Jansson, I.; Schenkman, J.B. & Rusling, J.F. (2003). Epoxidation of styrene by human cyt P450 1A2 by thin film electrolysis and peroxide activation compared to solution reactions. *Biophysical Chemistry*. Vol.104, (2003), pp. 291–296

Fantuzzi, A.; Fairhead, M. & Gilardi, G. (2004). Direct Electrochemistry of Immobilized Human Cytochrome P450 2E1. *Journal of the American Chemical Society*. Vol.126, (2004), No.16, pp. 5040-5041

Freire, R.S.; Pessoa, C.A.; Mello, L.D. & Kubota, L.T. (2003). Direct Electron Transfer: An Approach for Electrochemical Biosensors with Higher Selectivity and Sensitivity. *J. Braz. Chem. Soc*. Vol.14, (2003), No.2, pp. 230-243

Ghindilis, A. (2000). Direct electron transfer catalysed by enzymes: application for biosensor development. *Biochemical Society Transactions*. Vol.28, (2000), pp.84–89

Gooding, J.J. (2005). Nanostructuring electrodes with carbon nanotubes: A review on electrochemistry and applications for sensing. *Electrochimica Acta*. Vol.50, (2005), pp.3049–3060

Guengerich, F.P. (2001). Common and Uncommon Cytochrome P450 Reactions Related to Metabolism and Chemical Toxicity. *Chem. Res. Toxicol*., Vol.14, (2001), No. 6, pp. 611-650

Guengerich, F.P. (2003). Cytochromes P450, drugs, and diseases. *Molecular interventions*, Vol.3, No.3, (2003), pp. 194-204

Guengerich, F.P. (2008). Cytochrome P450 and Chemical Toxicology. *Chem. Res. Toxicol*., Vol.21, (2008), pp. 70–83

He, P.; Hu, N. & Rusling, J.F. (2004). Driving Forces for Layer-by-Layer Self-Assembly of Films of SiO_2 Nanoparticles and Heme Proteins. *Langmuir*. Vol.20, (2004), pp.722-729

Hendricks, N.; Waryo, T.T.; Arotiba, O.; Jahed, N.; Baker, P.G.L. & Iwuoha, E.I. (2009). Microsomal cytochrome P450-3A4 (CYP3A4) nanobiosensor for the determination of 2,4-dichlorophenol—An endocrine disruptor compound. Electrochimica Acta. Vol.54, (2009), No.7, pp. 1925-1931

Honeychurch, M. (2006). The direct electrochemistry of cytochrome P450. What are we actually measuring?. m.honeychurch@uq.edu.au, (2006)

Houston, B. & Galetin, A. (2005). Modelling atypical CYP3A4 kinetics: principles and pragmatism. *Archives of Biochemistry and Biophysics*, Vol.433, (2005), pp 351-360

Huang, N.; Agrawal, V.; Giacomini, K.M. & Miller, W.L. (2008). Genetics of P450 oxidoreductase: Sequence variation in 842 individuals of four ethnicities and activities of 15 missense mutations. *PNAS*. Vol.105, (2008), No.5, pp. 1733-1738

Ignaszak, A.; Hendricks, N.; Waryo, T.; Songa, E.; Jahed, N.; Ngece, R.; Al-Ahmed, A.; Kgarebe, B.; Baker, P. & Iwuoha, E.I. (2009). Novel therapeutic biosensor for indinavir—A protease inhibitor antiretroviral Drug. *Journal of Pharmaceutical and Biomedical Analysis*. Vol.49, (2009), pp.498–501

Ingelman-Sundberg, M. (2004). Human drug metabolising cytochrome P450 enzymes: properties and polymorphisms. *Naunyn-Schmiedeberg's Arch Pharmacol*.,Vol.369, (2004), pp. 89–104

Iwuoha, E.I.; Joseph, S.; Zhang, Z.; Smyth, M.R.; Fuhr, U. & Ortiz de Montellano, P.R. (1998). Drug metabolism biosensors: electrochemical reactivities of cytochrome P450cam immobilised in synthetic vesicular systems. *Journal of Pharmaceutical and Biomedical Analysis*. Vol.17, (1998), pp. 1101–1110

Iwuoha, E.I.; Kane, S.; Ania, C.O.; Smyth, M.R.; Ortiz de Montellano, P.R & Fuhr, U. (2000). Reactivities of Organic Phase Biosensors 3: Electrochemical Study of

Cytochrome P450cam Immobilized in a Methyltriethoxysilane Sol-Gel. *Electroanalysis*. Vol.12, (2000), No.12, pp.980-98

Iwuoha, E.I.; Ngece, R.; Klink, M. & Baker, P. (2007). Amperometric responses of CYP2D6 drug metabolism nanobiosensor for sertraline: a selective serotonin reuptake inhibitor. *IET Nanobiotechnology*. Vol.1, (2007), No.4, pp. 62-67

Iwuoha, E.I.; Wilson, A.; Howel, M.; Mathebe, N.G.R.; Montane-Jaime, K.; Narinesingh, D. & Guiseppi-Elie, A. (2000). Cytochrome P4502D6 (CYP2D6) Bioelectrode for Fluoxetine. Analytical Letters. Vol.37, (2000), No.5, pp. 929–941

Johnson, D.L.; Lewis, B.C.; Elliot, D.J.; Miners, J.O. & Martin, L.L. (2005). Electrochemical characterisation of the human cytochrome P450 CYP2C9. Biochemical Pharmacology. Vol.69, (2005), pp. 1533–1541

Joseph, S.; Rusling, J.F.; Lvov, Y.M.; Friedberg, T. & Fuhr, U. (2003). An amperometric biosensor with human CYP3A4 as a novel drug screening tool. *Biochemical Pharmacology*. Vol.65, (2003), pp.1817–1826

Kirchheiner, J. & Seeringer, A. (2007). Clinical implications of pharmacogenetics of cytochrome P450 drug metabolizing enzymes. *Biochimica et Biophysica Acta.* Vol.1770, (2007), pp.489–494

Krishnan, S.; Abeykoon, A.; Schenkman, J.B. & Rusling, J.F. (2009). Control of Electrochemical and Ferryloxy Formation Kinetics of Cyt P450s in Polyion Films by Heme Iron Spin State and Secondary Structure. *J. Am. Chem. Soc*. Vol.131, (2009), pp.16215–16224

Lazarou, J.; Pomeranz, B.H. & Corey, P.N. (1998). Incidence of Adverse Drug Reactions in Hospitalized Patients. *JAMA*. Vol. 279, (1998); No.15, pp 1200-1205

Lei, C.; Wollenberger, U.; Jung, C. & Scheller,F.W. (2000). Clay-Bridged Electron Transfer between Cytochrome P450cam and Electrode. Biochemical and Biophysical Research Communications. Vol.268, (2000), pp. 740–744

Lin, J.H. (2007). Pharmacokinetic and Pharmacodynamic Variability: A Daunting Challenge in Drug Therapy. *Current Drug Metabolism*. Vol.8, (2007), pp. 109-136

Liu, S.; Peng, L.; Yang, X.; Wu, Y. & He, L. (2008). Electrochemistry of cytochrome P450 enzyme on nanoparticle-containing membrane-coated electrode and its applications for drug sensing. *Analytical Biochemistry*. Vol.375, (2008), pp. 209–216

Liu, H.; Rusling, J.F. & Hu, N. (2004). Electroactive Core-Shell Nanocluster Films of Heme Proteins, Polyelectrolytes, and Silica Nanoparticles. *Langmuir.* Vol.20, (2004), pp.10700-10705

Lyons, M.E.G. & Keeley, G.P. (2008). Carbon Nanotube Based Modified Electrode Biosensors. Part 1.Electrochemical Studies of the Flavin Group Redox Kinetics at SWCNT/Glucose Oxidase Composite Modified Electrodes. *Int. J. Electrochem. Sci*. Vol.3, (2008), pp.819–853

Miller, W.L. (2005). Minireview: Regulation of Steroidogenesis by Electron Transfer. *Endocrinology*. Vol. 146, (2005), pp.2544-2550

Munge, B.; Estavillo, C.; Schenkman, J.B. & Rusling, J.F. (2003). Optimization of Electrochemical and Peroxide-Driven Oxidation of Styrene with Ultrathin Polyion Films Containing Cytochrome P450cam and Myoglobin. *ChemBioChem*, Vol.4, (2003), pp. 82-89

Nicolini, C.; Erokhin, V.; Ghisellini, P.; Paternolli, C.; Ram, M.K. & Sivozhelezov, V. (2001). P450scc Engineering and Nanostructuring for Cholesterol Sensing. *Langmuir*. Vol.17, (2001), pp.3719-3726

Ortiz de Montellano, P.R. (2005). *Cytochrome P450*, Kluwer Academic/Plenum Publishers, New York.

Paternolli, C.; Antonini, M.; Ghisellini, P. & Nicolini, C. (2004). Recombinant Cytochrome P450 Immobilization for Biosensor Applications. *Langmuir*. Vol.20, (2004), pp.11706-11712

Peng, L.; Yang, X.; Zhang, Q. & Liu, S. (2008). Electrochemistry of Cytochrome P450 2B6 on Electrodes Modified with Zirconium Dioxide Nanoparticles and Platin Components. *Electroanalysis*. Vol.20, (2008), No.7, pp.803–807

Podust, L.M.; Poulos, T.L. & Waterman, M.R. (2001).Crystal structure of cytochrome P450 14α-sterol demethylase (CYP51) from *Mycobacterium tuberculosis* in complex with azole inhibitors. Vol.98, (2001), No.6, pp. 3068-3073

Renedo, O.D.; Alonso-Lomillo, M.A. & Arcos Martinez, M.J. (2007). Recent developments in the field of screen-printed electrodes and their related applications. Vol.73, (2007), No.2, pp. 202-219

Rodriguez-Antona, C. & Ingelman-Sundberg, M. (2006). Cytochrome P450 pharmacogenetics and cancer. *Oncogene*. Vol.25, (2006), pp. 1679–1691

Salimi, A.; Noorbakhsh, A. & Ghadermarz, M. (2005). Direct electrochemistry and electrocatalytic activity of catalase incorporated onto multiwall carbon nanotubes-modified glassy carbon electrode. *Analytical* Biochemistry. Vol.344, (2005), pp.16–24

Sevrioukova, I.F.; Li, H.; Zhang, H.; Peterson, J.A. & Poulos, T.L. (1999). Structure of a cytochrome P450–redox partner electron-transfer complex. *PNAS*. Vol.96, (1999), No.5, pp.1863-1868

Shukla, A.; Gillam, E.M.; Mitchell, D.J. & Bernhardt, P.V. (2005). Direct electrochemistry of enzymes from the cytochrome P450 2C family. *Electrochemistry Communications*. Vol.7, (2005), pp.437–442

Shumyantseva, V.V.; Bulko, T.V. & Archakov, A.I. (2005). Electrochemical reduction of cytochrome P450 as an approach to the construction of biosensors and bioreactors. *Journal of Inorganic Biochemistry,* Vol.99, (2005), pp. 1051–1063

Shumyantseva, V.V.; Bulko, T.V.; Bachmann, T.T.; Bilitewski, U.; Schmid, R.D. & Archakov, A.I. (2000). Electrochemical Reduction of Flavocytochromes 2B4 and 1A2 and Their Catalytic Activity. *Archives of Biochemistry and Biophysics*. Vol.377, (2000), pp.43–48

Shumyantseva, V.V.; Bulko, T.V.; Kuznetsova, G.P.; Samenkova, N.F. & Archakov, A.I. (2009). Electrochemistry of Cytochromes P450: Analysis of Current–Voltage Characteristics of Electrodes with Immobilized Cytochromes P450 for the Screening of Substrates and Inhibitors. *Biochemistry*. Vol.74, (2009), No.4, pp. 438-444.

Shumyantseva, V.V.; Bulko, T.V.; Usanov, S.A.; Schmid, R.D.; Nicolini, C. & Archakov, A.I. (2001). Construction and characterization of bioelectrocatalytic sensors based on cytochromes P450. *Journal of Inorganic Biochemistry*. Vol.87, (2001), pp.185–190

Shumyantseva, V.V.; Bulko, T.V.; Yu.O.; Rudakov, G.P.; Kuznetsova, N.F.; Samenkova, A.V.; Lisitsa, I.I.; Karuzina, & Archakov, A.I. (2007). Electrochemical properties of cytochroms P450 using nanostructured electrodes: Direct electron transfer and electro catalysis. *Journal of Inorganic Biochemistry*. Vol.101, (2007), pp.859–865

Shumyantseva, V.V.; Carrara, S.; Bavastrello, V.; Riley, D.J.; Bulko, T.V.; Skryabin, K.G.; Archakov, A.I. & Nicolini, C. (2005). Direct electron transfer between cytochrome P450scc and gold nanoparticles on screen-printed rhodium–graphite electrodes. *Biosensors and Bioelectronics*. Vol.21, (2005), pp.217–22

Shumyantseva, V.V.; Ivanov, Y.D.; Bistolas, N.; Scheller, F.W.; Archakov, A.I. & Wollenberger, U. (2004). Direct Electron Transfer of Cytochrome P450 2B4 at Electrodes Modified with Nonionic Detergent and Colloidal Clay Nanoparticles. *Analytical Chemistry*. Vol.76, (2004), No.20, pp. 6046–6052

Sligar, S.G. (1976). Coupling of spin, substrate, and redox equilibriums in cytochrome P450. *Biochemistry*. Vol.15, (1976), No.24, pp. 5399–5406

Sono, M.; Roach, M. P.; Coulter, E.D. & Dawson, J.H. (1996). Heme-Containing Oxygenases. *Chem. Rev*.,Vol.96, (1996), pp. 2841-2887

Thévenot, D.R.; Toth, K.; Durst, R.A. & Wilson, G.S. (2001). Electrochemical Biosensors: recommended definitions and classification. *Analytical Letters*. Vol.34, (2001), No.5, pp. 635-659

Wang, J. (2005). Carbon-Nanotube Based Electrochemical Biosensors: A Review. *Electroanalysis*. Vol.17, (2005), No.1, pp. 7-14

Wu, Y. & Hu, S. (2007). Biosensors based on direct electron transfer in redox proteins, *Microchim Acta*. Vol.159, (2007), pp. 1–17

Yang, M.; Kabulski, J.L.; Wollenberg, L.; Chen, X.; Subramanian, M.; Tracy, T.S.; Lederman, D.; Gannett, P.M. & Wu, N. (2009). Electrocatalytic Drug Metabolism by CYP2C9 Bonded to A Self-Assembled Monolayer-Modified Electrode. *Drug Metabolism and Disposition*. Vol.37, (2009), No.4, pp. 892–899

Zhao, G.C.; Yin, Z.Z.; Zhang, L. & Wei, X.W. (2005). Direct electrochemistry of cytochrome c on a multi-walled carbon nanotubes modified electrode and its electrocatalytic activity for the reduction of H_2O_2. *Electrochemistry Communications*. Vol.7, (2005), pp.256–260

PDBe Protein Data Bank Europe, Available from http://www.ebi.ac.uk/pdbe/

Roche Molecular Diagnostic, Available from http://molecular.roche.com/diagnostics/genomics_oncology/ampliChip_CYP450.html

22

Development of Potentiometric Urea Biosensor Based on *Canavalia ensiformis* Urease

Lívia Maria da Costa Silva[1], Ana Claudia Sant'Ana Pinto[1], Andrea Medeiros Salgado[1] and Maria Alice Zarur Coelho[2]
[1]*Laboratory of Biological Sensors/EQ/UFRJ*
[2]*BIOSE/EQ/UFRJ*
Biochemical Engineering Department, Chemistry School, Technology Center, Federal University of Rio de Janeiro
Brazil

1. Introduction

The increasing number of potentially harmful pollutants in the environment calls for fast and cost-effective analytical techniques to be used in extensive monitoring programs. Additionally, over the last few years, a growing number of initiatives and legislative actions for environmental pollution control have been adopted in parallel with increasing scientific and social concern in this area (Rogers & Gerlach, 1996; Rodriguez-Mozaz et al., 2004; Rodriguez-Mozaz et al., 2005; Rogers, 2006). Nitrogen compounds are pollutant found in several industrial effluents, being its determination of extreme environmental importance.
Several methods are used to urea determination, including spectrophotometry, fluorimetry, potentiometry and amperometry. But some of these require a pretreatment or are unsuitable for monitoring in situ. For this reason there has been growing interest in the development of biosensors for these determinations.
The requirements for application of most traditional analytical methods to environmental pollutants analysis, often constitute an important impediment for their application on a regular basis. The need for disposable systems or tools for environmental applications, in particular for environmental monitoring, has encouraged the development of new technologies and more suitable methodologies. In this context, biosensors appear as a suitable alternative or as a complementary analytical tool. Biosensors can be considered as a subgroup of chemical sensors in which a biological mechanism is used for analyte detection (Rogers & Gerlach, 1996; Rodriguez-Mozaz et al., 2005; Rogers, 2006).
A biosensor (Figure 1) is defined by the International Union of Pure and Applied Chemistry (IUPAC) as a self-contained integrated device that is capable of providing specific quantitative or semi-quantitative analytical information using a biological recognition element (biochemical receptor), which is retained in contact direct spatial with a transduction element (Thévenot et al., 1999). Biosensing systems and methods are being developed as suitable tools for different applications, including bioprocess control, food quality control, agriculture, environment, military and in particular, for medical applications. The main classes of bioreceptor elements that are applied in environmental

analysis are whole cells of microorganisms, enzymes, antibodies and DNA. Additionally, in the most of the biosensors described in the literature for environmental applications electrochemical transducers are used (Thévenot et al., 1999).

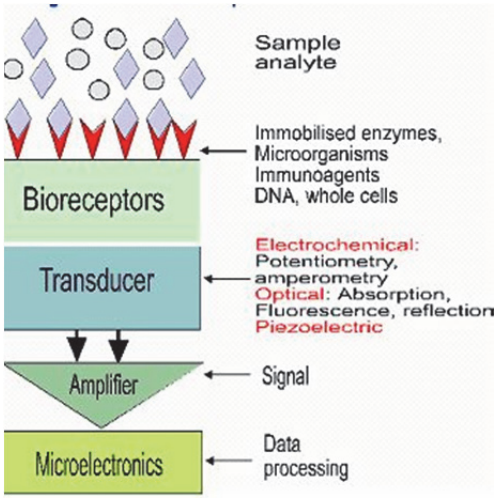

Fig. 1. Biosensor scheme.

For environmental applications, the main advantages offered by biosensors over conventional analytical techniques are the possibility of portability, miniaturization, work on-site, and the ability to measure pollutants in complex matrices with minimal sample preparation. Although many of the developed systems cannot compete yet with conventional analytical methods in terms of accuracy and reproducibility, they can be used by regulatory authorities and by industry to provide enough information for routine testing and screening of samples (Rogers & Gerlach, 1996; Rogers, 2006; Sharpe, 2003). Biosensors can be used as environmental quality monitoring tools in the assessment of biological/ecological quality or for the chemical monitoring of both inorganic and organic priority pollutants.

Due to great variety of vegetal tissues Brazil constitutes an inexhaustible enzyme source, which can be used in the most diverse areas of the knowledge, amongst them in the development of the biosensors. James B. Sumner (Sumner, 1926) crystallized the enzyme urease from jack bean, *Canavalia ensiformis* (Fabaceae), a bushy annual tropical american legume grown mainly for forage, in 1926, to show the first time ever that enzymes can be crystallized. Urease is abundant enzyme in plants and, moreover, it can be found at numerous of eukaryotic microorganisms and bacteria. The bacterial and plant ureases have high sequence similarity, suggesting that they have similar three-dimensional structures and a conserved catalytic mechanism.

Ureases (urea amidohydrolase, EC3.5.1.5) catalyzes the hydrolysis of urea to yield ammonia (NH_3) and carbamat, the latter compound decomposes spontausly to generate a second molecule of ammonia and carbon dioxide (CO_2) (Takishima et al., 1988) (Figure 2).

So, the main objective of this study was to optimize the operating conditions to obtain the final configuration of the urease biosensor for environmental application.

$$H_2N - CO - NH_2 + H_2O \xrightarrow{urease} NH_3 + H_2N - CO - OH$$
$$H_2N - CO - OH + H_2O \rightarrow NH_3 + H_2CO_3$$
$$H_2CO_3 \leftrightarrow H^+ + HCO_3^-$$
$$2NH_3 + 2H_2O \leftrightarrow 2NH_4^+ + 2OH^-$$

Fig. 2. Urea hydrolysis catalyzed by urease.

2. Material and methods

2.1 Biocomponent: jack beans (*Canavalia ensiformis*)

The biocomponent, jack beans, Canavalia ensiformis, as show in Figure 3, was donated by Seeds & Associate Producers on Earth by Brazilian Agricultural Research Company (EMBRAPA). It is a vegetal plant tissue rich in the urease (Luca & Reis, 2001). The jack beans were being used as a powder, with a particle size less than or 3mm, in free form or immobilized. When the powder was not in use, it was stored in refrigerators, till further use.

Fig. 3. Jack beans.

2.2 Ammonium ion-selective electrode calibration

For biosensor system development, an ammonium ion-selective electrode (*Orion Ammonia Electrode* 95-12 Thermo) was used as transducer. A calibration curve of the electrode potential (mV) vs. urea concentration (ppm) is constructed, using ammonium chloride solution (NH_4Cl) (1000 ppm) as stock solution. The standard solutions were prepared from the stock solution in range of 5 to 1000 ppm.

2.4 Best conditions of the fresh jack bean urease

The tests for optimization the enzymatic reaction conditions of fresh urease of jack beans monitored the urea hydrolysis to ammonia by ion-selective electrode response under different conditions. The conditions tested were: the jack bean amount (0.1, 0.2, 0.3, 0.4 and 0.5 g); the pH of sample standard solution (6.0, 7.0 and 8.0) and reaction temperature (20, 25, 30 and 40°C).

The assay consisted in adding the desired amount of powder in 5.0 mL of the standard solutions (several urea concentrations prepared from stock solution in potassium phosphate buffer with desired pH) and 100 µL of ISA (ionic strength adjustor buffer solution). Then the ammonium ion-selective electrode was immersed in the solution, monitoring the enzymatic reaction by the potential difference (mV) caused by urea hydrolysis.

2.5 Urease immobilization

The enzyme (powdered jack bean) immobilization using glutaraldehyde was performed according Junior (1995). **The final configuration of procedure, i**n brief, urease was covalently immobilized on nylon screen according to the following procedure: 0.2 g of powdered beans was placed under a nylon screen and 200 mL of glutaraldehyde solution (12.5%) were added. Then, another nylon screen was placed on top (Figure 4). After 20 minutes, the set was immersed in distilled water for 20 minutes and then in potassium phosphate buffer pH 7.0 at the same time. The immobilized biocomponent was used after storage for 24 hours in the refrigerator, at 4°C.

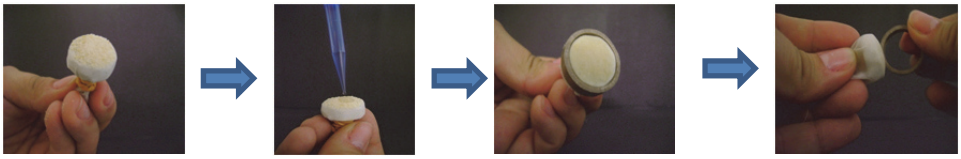

Fig. 4. Procedure step sequence of powdered jack bean immobilization.

2.6 Urease activity assay

Alkalimetric method is based on the observation made by Kistiakowsky & Shaw (1953, as cited in Comerlato, 1995) which the initial pH neutral of unbuffered solution of urea-urease rapidly increases to pH 9.0, and then remains approximately constant. The reaction products in this pH are usually ammonium carbamate, ammonium carbonate and bicarbonate as shown in the following Figure 5:

$$H_2NCONH_2 + 2H_2O \rightarrow (NH_4)^+ + (NH_2CO_2)^- + H_2O$$
$$\rightarrow 2(NH_4)^+ + (CO_3)^-$$
$$\rightarrow (NH_4)^+ + NH_3 + (HCO_3)^-$$

Fig. 5. Urea hydrolysis by urease.

In this method, the urease activity was assayed by adding 1mL of urea solution, immobilized urease and 10mL of deionised water. Incubation was carried out at 25°C (room temperature) and low agitation for a constant interval. Withdrew an aliquot (2 mL) of mixture solution and terminated with hydrochloric acid solution. Then, the reaction mixture was back-titrated with sodium hydroxide solution, methylorange being used as an indicator. The blank test was assayed under the same conditions above, using 1mL of urea solution and 11 mL of deionised water.

These end products of the reaction are a buffer system that maintains the pH constant as the reaction proceeds. So using the substrate initially buffered at pH 9.0, avoids the subsequent change in pH. The addition of excess hydrochloric acid in the final time disrupts the reaction and converts the carbamate and ammonia to ammonium ions. Therefore, back-titration with sodium hydroxide measures the acid did not react (Comerlato, 1995).

To calculate the enzyme activity, first is necessary to calculate the volume of sodium hydroxide (vol. NaOH) wich is given by: *vol. NaOH = vol. NaOH blank – vol. NaOH test*. So the urease activity calculated using the equation below:

$$\frac{(NaOH\ molarity)x(vol.NaOH)x(1000)x(df)}{time\ reaction\ (minutes)x\ amount\ of\ jack\ beans\ (g)} = {Units}/{amount\ of\ jack\ beans\ (g)}$$

where:

$$vol.NaOH = Volume\ (in\ milliliters)of\ sodium\ hydroxide\ solution\ used\ in\ the\ back\ titration$$

$$1000 = Conversion\ factor\ from\ millimoles\ to\ micromoles$$

$$df = Dilution\ factor$$

2.7 Kinetics parameters of urease

The kinetic parameters (K_m and V_{max}) for free and immobilized urease were determined by using Lineweaver–Burk plot. The substrate was urea, and its concentrations were 0.05 to 10.00% (w/v). The reaction rates were determined according to the method mentioned above in Section 2.4, with the established best reaction conditions. Based on Lineweaver–Burk plot Michaelis constant and maximal rate were calculated.

2.8 Instrumentation: biosensor system

The schematic set-up for biosensor system for urea analysis is presented as Figure 6. The set up consists of a peristaltic pump (2), reaction chamber (3) made from PVC pipe with biocomponent (immobilized urease) (4), transducer (ion-selective electrode) (5), potentiostat and data recorder (6). Standard sample and discard sample are numbered in Figure 5 as 1 and 7, respectively. Silicone tubing was used for connections.

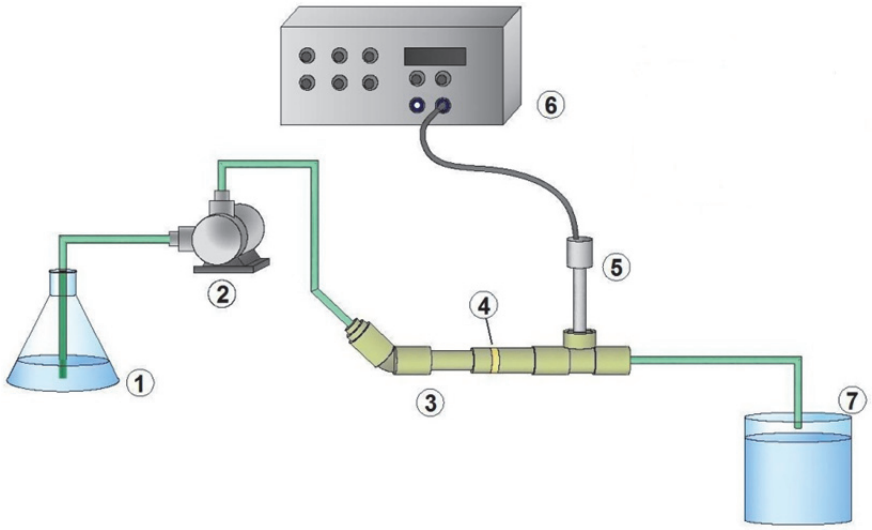

Fig. 6. Schematic set-up for biosensor system for urea analysis.

2.8.1 Procedure

For urea analysis, calibration standards were prepared by dilution of urea stock solution in potassium phosphate buffer, pH 6.0. All measurements were carried out by injection of 25.00 mL standard sample (0.50 a 50.00 ppm) at a flow rate of 40.00 $mL.min^{-1}$. After the sample has completed the reaction chamber, the pump was turned off and 200 mL of ISA was added and electrode was immersed. Then, data were collected throughout the reaction time, in order to analyze the response time of instrument. After each sample analysis, the system was thoroughly rinsed with distilled water for 2 minutes. The potentiometric measurements were made at room temperature (25°C).

A corresponding change of potential against the urea concentration could be observed. Different urea concentrations would cause different potential changes, due to ammonia generation. The values (mV) found with the transducer were converted into ammonia concentration through the equation of calibration curve of ammonium ion-selective electrode (Section 2.2). Thereby, the calibration curve of urea concentration versus ammonium generated was obtained.

2.9 Stability studies

2.9.1 Reusability

The immobilized urease was tested for its reusability by checking the biosensor response using assay as described in Section 2.8.1 at time intervals (days). After every use, biocomponent was washed properly with distilled water and stored in potassium phosphate buffer, pH 7.0 at 4ºC, till further use.

2.9.2 Storage stability

The immobilized urease was stored in potassium phosphate buffer, pH 7.0 at 4ºC. The activity was determined and recorded at regular intervals for stored urease using assay procedures described in Section 2.6. The values of activity were plotted against the number of days.

2.10 Protein assay

The amount of protein in the wash solutions after urease immobilization and biosensor system procedure were determined as described by Bradford (1976) with bovine serum albumin (BSA) as a standard.

2.11 Reproducibility

The reproducibility of ammonium ion-selective electrode response was checked by measuring this response when it was inserted into a 2% (w/v) urea solution with jack bean immobilized under over 2 minutes of enzymatic reaction. The assay was developed in potassium phosphate buffer, pH 6.0 at 25ºC.

3. Results

3.1 Best conditions of the jack bean urease (fresh and immobilized)

Table 1 shows the values of ammonia concentration (ppm) generated by urea hydrolysis in 2 minutes of enzymatic reaction in experiments with several fresh jack beans weight with urea solutions of 0.05% to 10.00% (w/v).

Ammonia concentration (ppm)					
Urea concentration % (w/v)	**Jack beans weight (g)**				
	0.1	0.2	0.3	0.4	0.5
0.05	33.02	38.69	22.40	5.57	11.67
0.10	3.73	60.97	37.73	52.24	42.25
0.50	21.97	96.29	77.79	77.23	120.85
1.00	67.44	107.99	161.70	161.48	201.22
2.00	76.16	119.96	141.96	170.66	167.56
4.00	100.88	183.08	204.64	313.02	265.61
6.00	90.11	134.24	218.96	218.86	234.95
8.00	77.73	120.84	214.76	1690.26	157.23
10.00	48.09	104.86	130.99	157.26	195.89

Table 1. Results of experiments to choose the best jack beans amount analyzing the ammonia generation according Secion 2.4.

The table data are shown in the graph below (Figure 7). The curves of Figure 7 show that after the urea concentration of 4% (w/v) regardless of the jack beans amount was a saturation of the enzymatic reaction.

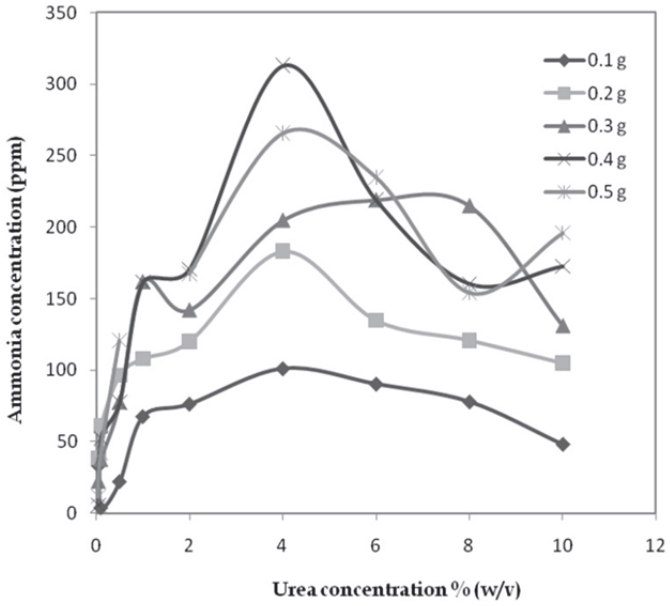

Fig. 7. Influence of jack beans amount on enzymatic reaction monitored (ammonia generation) by ammonium ion-selective electrode according Secion 2.4.

Figure 8 shows the pH dependence of buffer solutions on the potentiometric response of the transducer of fabricated urea biosensor. In the present work, the best response could be observed at pH 6.0 which was subsequently utilized in further experimental investigations.

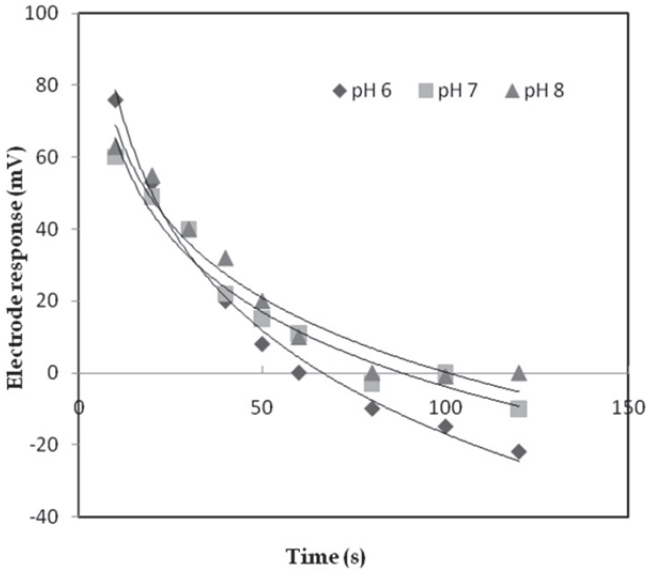

Fig. 8. Influence of buffer solution pH on the urea hydrolysis. Variation along the time of the ammonium ion-selective electrode (mV) response to a 2% (w/v) urea solution.

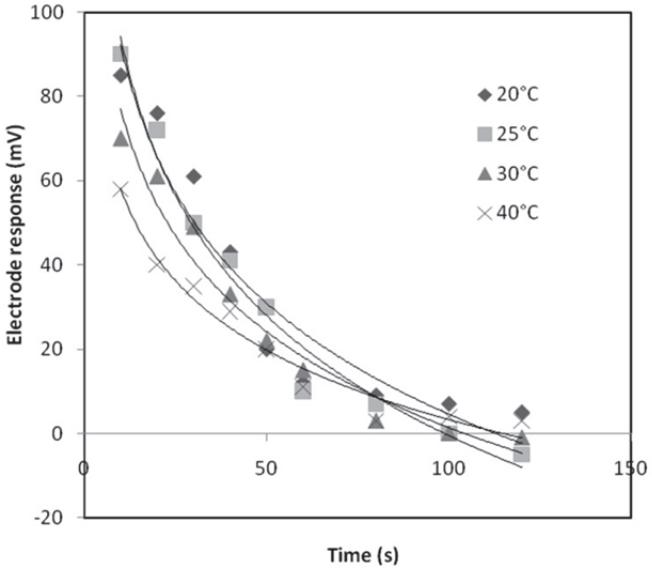

Fig. 9. Effect of temperature on the urea hydrolysis. Variation along the time of the ammonium ion-selective electrode (mV) response to a 2% (w/v) urea solution.

Furthermore, the effect of temperature of the buffer solution on the response of urea biosensor was studied in the range of 20–40°C. Figure 9 shows the ammonium ion-selective electrode against the buffer solution temperature. The 25°C was chosen the best temperature and utilized in further experimental investigations.

Through the tests using the fresh biocomponent, the best pH solution and test temperature were chosen. Furthermore, two jack beans amount (0.2 and 0.3 g) were chosen to be immobilized as Section 2.5 and used in the further tests. Although the 0.3 g jack bean weight has presented a better result as show in Figure 7, it was noted that 0.3 g did not have to be immobilized satisfactory results, and then the 0.2 g jack bean mass was also tested.

The powder of jack beans (urease source) was immobilized in different matrices (different screen materials), but the best results of mass retention were achieved with the screen nlyon (80% mass retention) (data not shown). So, this material was chosen to be used in the immobilization method in this work. Table 2 shows the values of ammonia concentration (ppm) generated by hydrolysis urea in 2 minutes of enzymatic reaction in experiments with 0.2 and 0.3 g of immobilized jack beans with urea solutions of 0.05% to 10.00% (w/v).

Ammoia concentration (ppm)		
Urea concentration % (w/v)	**Jack beans weight (g)**	
	0.2	**0.3**
0.05	62.13	42.29
0.10	258.61	205.31
0.50	30.24	243.77
1.00	525.73	271.94
2.00	675.31	371.47
4.00	981.44	533.27
6.00	1136.77	537.30
8.00	1200.35	583.23
10.00	1192.95	582.47

Table 2. Results of experiments to choose the best immobilized jack beans amount (0.2 or 0.3 g) analyzing the ammonia generation according Secion 2.4.

The table data are shown in the graph below (Figure 10). Figure 10 shows that the mass of 0.2 g had a higher urea hydrolysis into ammonia, whereas the immobilization of 0.3 g of jack bean on the nylon screen formed a thick film, hindering the mass transfer phenomena. So 0.2 g of jack bean was chosen as amount to be immobilized and utilized in further experimental investigations.

After the optimal pH of buffer solution, reaction temperature and immobilized amount of jack beans were chosen, the reproducibility of the ion-selective electrode response when inserted into 2% (w/v) urea solution was investigated under Section 2.11. Figure 11 shows a response variation, an average, of 11% over the eight times.

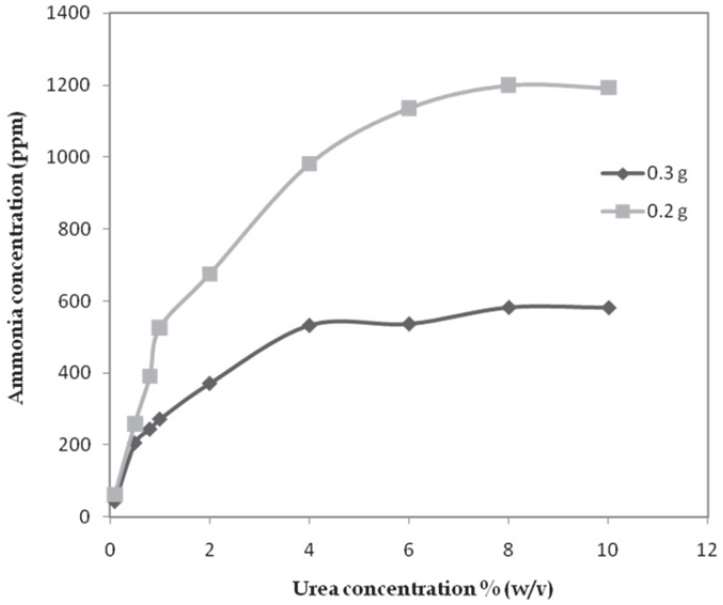

Fig. 10. Enzymatic reaction tests by jack bean immobilized mass variation (0.2 and 0.3 g), along the substrate (urea) concentration variation (0.05 to 10% (w/v)), pH 6.0, 25°C.

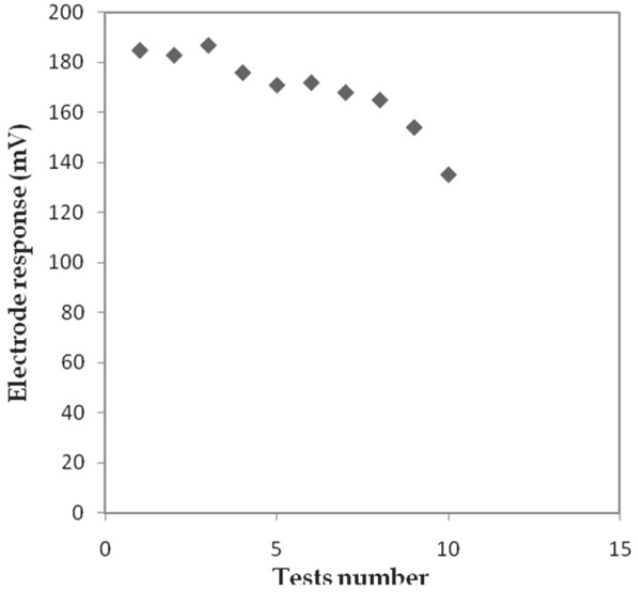

Fig. 11. Assay for reproducibility investigation according to Section 2.11.

3.2 Kinetic parameters determination

The kinetic parameters (K_m and V_{max}) were determined through the conventional Lineweaver–Burk plot, by varying the urea concentration between 0.05 to 10.00% (w/v) (Figure 12). The Km is an approximate measure of the affinity of the substrate for the enzyme. So the Km values for the free and immobilized ureases were also calculated. According to the results, the Km values were 19.10 mM and 411.39 mM for the free and immobilized urease, respectively.

This is a common result, because normally an increase of Km for an immobilized enzyme is expected. The difference of Km values suggests that substrate is easier to enter the active site of free urease because the enzyme immobilization may influence the diffusion of the substrate or product during reaction process. The K_m values found are within the range described in the literature (Verma & Singh, 2002) that lies between 2.08Mm for *Bacillus sp.* up to 100mM for *Bacillus pasteurii*. Therefore, it is noted that the study material (*Canavalia ensiformis* urease) has a good affinity with the substrate (urea) under the conditions tested.

Moreover, V_{max} values for the free and immobilized ureases were also calculated. According to the results, the V_{max} values were 3.76 mM/min and 31.26 mM for the free and immobilized urease, respectively. The value increase can be explained by enzymatic structure changes bye immobilization process that may have made the active sites more exposed to the substrate (urea).

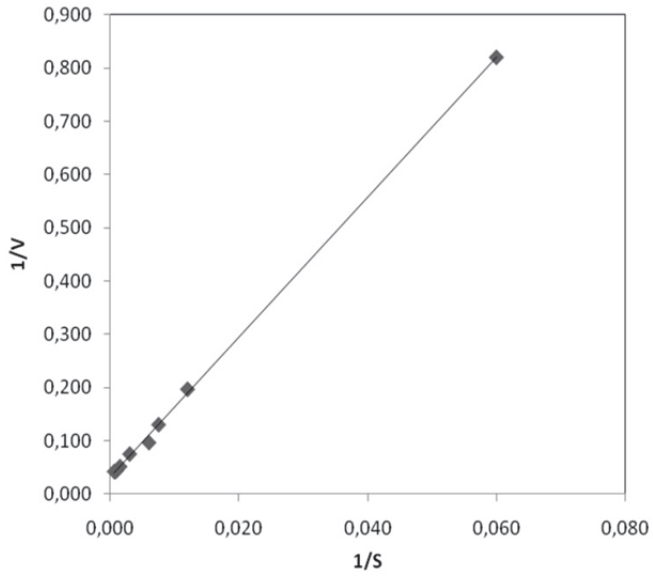

Fig. 12. Plot of 1/V against 1/[S] for immobilized urease (0.2 g of jack bean, pH 6.0, at 25°C).

3.3 Calibration curve of biosensor system and Reusability

The preliminary tests with the biosensor system were aimed in order to find the response time and linearity range of linearity of the instrument. For this, the range of 0.5 to 50.0 ppm of urea was chosen. Figure 13 shows that in all experiments, linearity range was observed in 1.0 to 20.0 ppm of the substrate. The best response time for the biosensor system was chosen 315 seconds. Moreover, water washing process between analysis samples did not cause

mass loss of immobilized biocomponent according to protein assay (Section 2.10). Calibration curve of protein assay is show in Figure 14.

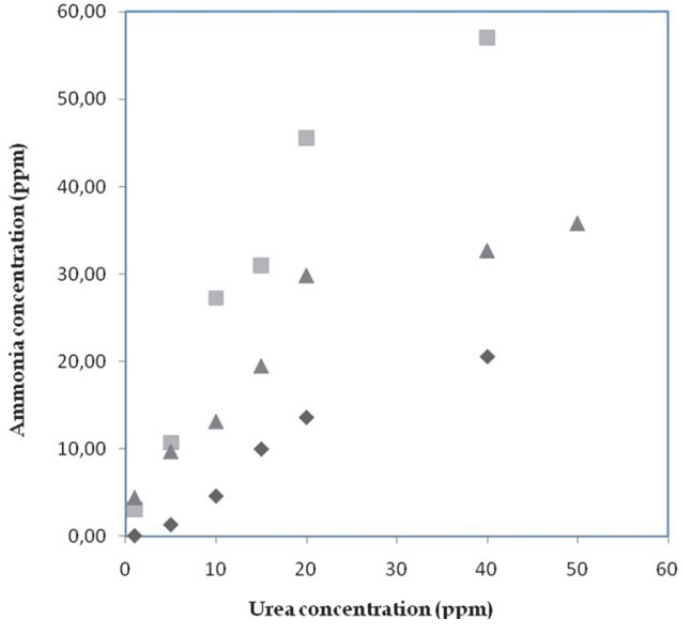

Fig. 13. Ammonia concentration variation over the urea range studied (0.5 to 50 ppm) using a biosensor system as a Section 2.8.1 for 317 seconds.

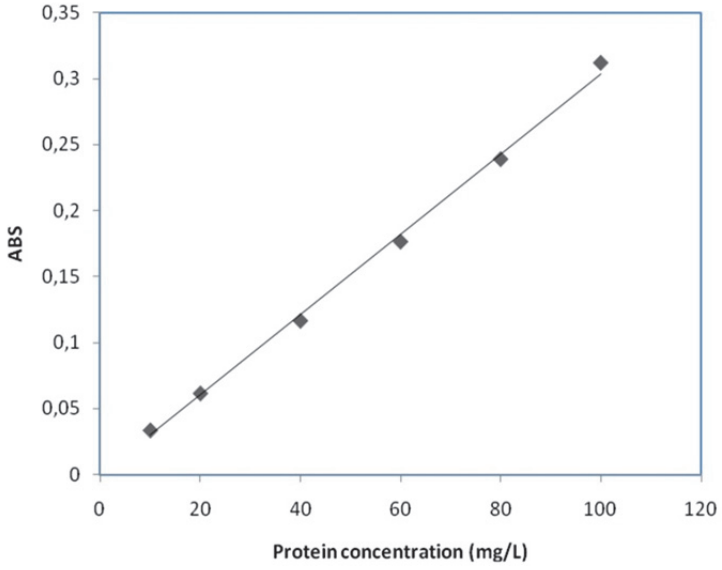

Fig. 14. Calibration curve of protein assay according Section 2.10.

Thereafter, to study the immobilized biocomponent reuse in biosensor system, assays were designed using the same immobilized urease along the days as Section 2.9.1. Figure 15 shows the results over 29 days using immobilized biocomponent in biosensor system. However, according to Table 3, it was found that up to 72 days of biocomponent use, the biosensor system has linearity range 1.0 to 20.0 ppm of urea, although the difference between the slopes of straight line, due to the urease activity of the immobilized jack bean powder.

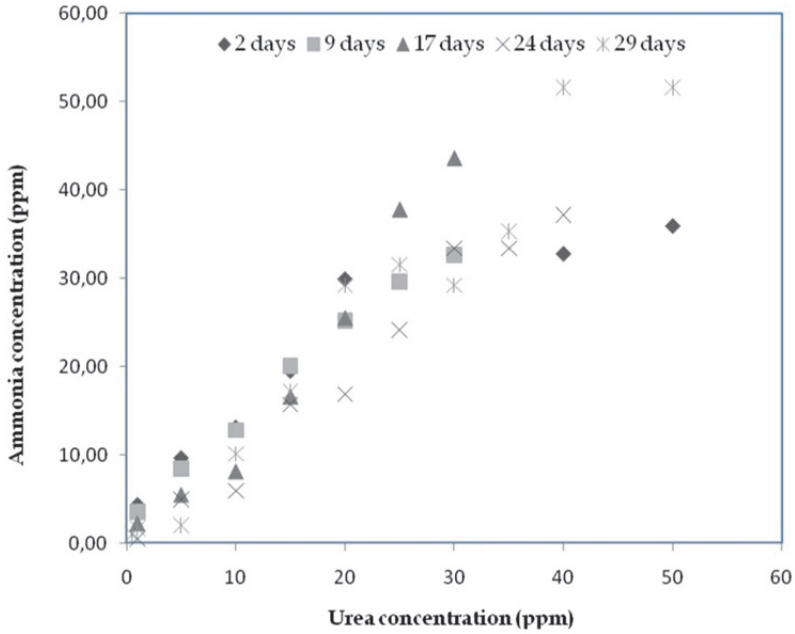

Fig. 15. Ammonia concentration variation over the urea range studied (0.5 to 50 ppm) using a biosensor system as a Section 2.8.1 for 29 days.

3.4 Storage stability

Figure 16 shows the storage stability of the three immobilized *Canavalia ensiformis* urease (as shown in Figure 4) stored at refrigerator (4°C) throughout the 1 month (30 days). The operational stability of a biosensor response may vary considerably depending upon the sensor geometry, method of preparation, biological recognition reactions etc. From Figure 16, it can be seen that the performance of the urea sensor stored under this conditions is not good. A pronounced decrease in the initial urease activity was observed over a nine days of stored.

4. Conclusion

In this study, for urease biosensor development, the urease was covalent immobilized on nylon screen by glutaraldehyde and the ammonia produced as a result of enzymatic reaction was monitored by potentiometry. The enzyme employed was from a rather non-

Storage time (days)	Linearity range of urea concentration (ppm)	Linear equation	R^2
02	1-20	y = 1.698x + 2.3518	0.9653
09		y = 1.1469x + 2.2988	0.9952
17		y = 1.2064x – 0,7344	0.9480
24		y = 0.9041x – 0,4318	0.9262
29		y = 1.4746 - 2,9956	0.9442
52		y = 2.0587x + 1,1672	0.9928
69		y = 0.963x - 2,2472	0.9699
72		y = 0.5912e0,13x	0.9908

Table 3. Characteristics of some calibration curves using system biosensor along the 72 days.

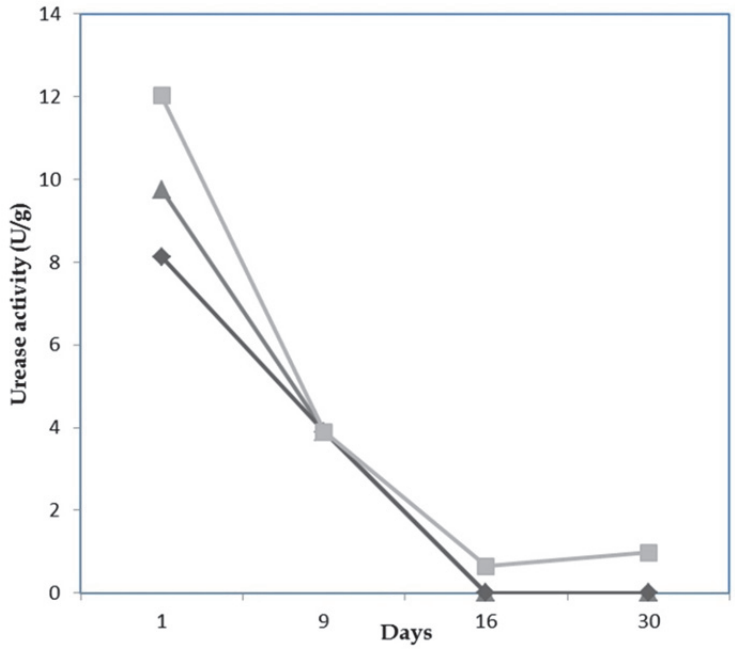

Fig. 16. Storage stability of the three immobilized *Canavalia ensiformis* urease stored at refrigerator (4°C) throughout the 1 month (30 days).

expensive and readily available source (jack beans). Some parameters had been analyzed aiming at to optimize the functioning of the biosensor. Through the results, in average, of storage the biological component activity declined more than 90% and the urea biosensor working range was 1-20ppm urea with a response time of 315s.

The developed instrument has become an inexpensive and practical tool for urea analysis in standard sample. Next step is biosensor application in environmental samples and industrial effluents, since it is necessary to monitor the nitrogen compounds concentration in waterbody to avoid problems such as eutrophication.

5. Acknowledgment

The authors thank the financial support of the National Council for Scientific and Technological Development (CNPq) and the Foundation for Research of the State of Rio de Janeiro (FAPERJ), the Brazilian Agricultural Research Company (EMBRAPA) for jack beans and the undergraduate students Juliana Christina C.V. Pereira and Rafaela Oliveira Flores for research assistance.

6. References

Bradford, M. (1976) A Rapid and Sensitive Method for the Quantitation of Microgram Quantities of Protein Utilizing the Principle of Protein-Dye Binding. *Anal. Biochem*., Vol.6, pp. 248-254.

Comerlato, M.H. (1995) Imobilização de enzimas no suporte crisotila. Tese de doutorado, Universidade Estadual de Campinas, São Paulo, Brasil.

Junior, L.R. (1995) Construção e Avaliação de Biossensor Potenciométrico para Determinação de Uréia, com eletrodo íon-seletivo a amônio, usando Canavalias Brasiliensis com fonte Enzimática. Dissetação de Mestrado, Universidade Estadual de Campinas, São Paulo, Brasil.

Luca, G.C. & Reis, B.F.(2001) Sistema em fluxo para determinação espectrofotométrica de uréia em plasma de sangue animal empregando leguminosas como fonte natural da enzima urease. *Química Nova*, Vol. 24, No. 2, pp. 191-194.

Rodriguez-Mozaz, S.; Marco, M-P.; Alda, M.J.L. & Barceló, D. (2004) Biosensors for environmental applications: future development trends. *Pure Appl. Chem*., Vol. 76, pp. 723-752.

Rodriguez-Mozaz, S.; Marco, M-P.; Alda, M.J.L. & Barceló, D. (2005) A global perspective: Biosensors for environmental monitoring. *Talanta*, Vol. 65, pp. 291-297.

Rogers, K.R. (2006) Recent advances in biosensor techniques for environmental monitoring. *Anal. Chim. Acta*., Vol. 568, pp. 222-231.

Rogers, K.R. & Gerlach, C.L. (1996) Environmental biosensors: A status report. *Environ. Sci. Technol*., Vol. 30, pp. 486-491.

Sharpe, M. (2003) It's a bug's life: Biosensors for environmental monitoring. *J. Environ. Monit*., Vol. 5, pp. 109-113.

Sumner, J.B. (1926) The isolation and crystallization of the enzyme urease. *J. Biol. Chem*., Vol. 69, pp. 435-441.

Takishima, K.; Suga, T. & Mamiya, G. (1988) The structure of jack bean urease. *European Journal of Biochemistry*, Vol. 175, pp. 151-165.

Thévenot, D.R.; Toth, K.; Durst, R.A. & Wilson, G.S. (1999) Electrochemical biosensors: Recommended definitions and classification. *Pure Appl. Chem*., Vol. 71, pp. 2333-2348.

Verma, N. & Singh, M. (2002) A disposable microbial based biosensor for quality control in milk. *Biosens. Bioelectron*, Vol. 18, pp.1219-1228.

23

Biosensors for Cancer Biomarkers

Zihni Onur Uygun[1] and Mustafa Kemal Sezgintürk[2]
[1]*Çanakkale Onsekiz Mart University*
[2]*Namık Kemal University,*
Turkey

1. Introduction

The cancer is experessed as a disorder of chaos which cause an impairment of biochemical pathways in living metabolisms. In particular, mulfunctioning of the controls of cells throught the human body is mostly observed breakdown in cancer. Actually, this is not single way to form cancer such that there are many chance to initiate cancer in the body. We know that most of our cells carry their own genetic materials which give them an opportunity to multiply once more. And this condition describes why the proliferation of uncontrolled cells in countless parts of the body is extremely important. In fact, a terrible cell turnover involving death and replacement of cell, consists everlastingly in many tissues in human body.The presantation, development, and outcome of the cancer are extremely different and complex from one patient to other. Moreover the cellular and molecular levels of the cancer show the similar heterogenity and uncertainty. During cancer process cells undergo serious metabolic changes which give rise to proliferate in an excessive and untimely way. Also these changes allow to cancer cells escape surveillance by immune system (Merlo et al., 2006). Mutations originate in the DNA sequences should initiate cancer (Herceg and Hainaut, 2007). A single base change results in a changing aminoacid to be integrated into a protein synthesized. This is enough to extremely change the three dimensional structure of that protein. Besides the activity of the protein will change dramatically. A large number of bases can be converted by other DNA differentiations. This will lead to synthesis of abnormal proteins. Significantly, these alterations can be monitored by sequencing the DNA of the cell and used to detect of cancer.

2. Cancer biomarkers

There is no standard definition for "biomarker" that is universally used. In 1999, the US National Institutes of Health/Food and Drug Administration Working Group drafted a definition of a biomarker as a characteristic that is objectively measured and evaluated as an indicator of normal biological processes, pathogenic processes or pharmacological response to a therapeutic intervention. Biomarkers could be found in body and they are quantifiable molecules such as proteins, metabolites, DNA, or RNA. The abnormal concentrations of such biomarkers are indicator for a pathological condition in body, such as cancer. A biomarker also could be a molecule occured as a specific response of the metabolism to the presence of cancer. Every type of cancer could be associated with gene modifications and alterations in protein function. These gene modifications and protein changes can be useful

indicators of any cancer types. Besides they could be used to idetify prognosis, progression and therapeutic response of the disease(Sriwastava, 2007). For development, evaluating, and validating biomarkers guding principles known as the five-phase approach has been established by the US National Cancer Institute's Early Detection Network (http://www.cancer.gov/edrn). The guidelines are very important for the usage of biomarkers in clinical applications. The five phases mentioned above ensure the principles and study design foundations for validating biomarkers for clinical use in early diagnosis of cancer. Phase 1 is the discovery pahse. Phase 2 is the validation phase in which the biomarkers are verified to determine their capacity for distinguishing between people with cancer and those without. In Phase 3, the capacity of a biomarker to detect preclinical disease is investigated. Phase 4 comprehends screening tests. And the last phase 5, focuses on the large-scale population experiments that appreciate the role of the biomarker for detection of cancer (Pepe et al., 2001).

3. Transducers used for detection of cancer biomarkers

Early diagnosis of cancer plays a major role for treatment(Yuan et al., 2001; Faraggi and Kramar, 2000; Zhang et al., 2007; Wu et al., 2007). The analytical techniques which are improved for detection of biomarkers are based on highly specific molecular recognition between antibody and antigen to form immunocomplex (Andrey et al..1998). In Addition these analytical methods are used for clinical researches(Itoh and Ichhara,2001; Trull 2001; Worwood, 2002) and biochemical analysis (Panteghini, 2000; Rossier et al., 2002; Sato et al., 2003). Because of highly specific molecular recognition characteristics of antigen and antibody, immunosensors are based on the interaction between antigen and antibody which are widely used for quantitative detection of biomarkers(Liu and Ju, 2005; Huang et al., 2010; Rusling et al., 2009; Tang et al., 2008a). Transducers are devices that are employed for preparation of immuosensors and transform the biomolecular recognition signals into electrical signals. Transducers can be divided into three main groups due to their sensing signal type; electrochemical, optic, and piezoelectric (Tothill, Turner, 2003). Choosing the exact transducer depends on a biomarker which is investigated and a signal which is occurred by biomarker reaction. It is very important to choose the correct transducer in routine utilization, for this reason the measurement principle of transducers are supposed to be proper for fabrication and commercial usage. Recently necessity of this kind of practical and economic devices by the public makes biosensors more important and attractive. Therefore the utilizing of biosensors for development of clinical researches and self-using by patients increase all over the world.

In this section; it is discussed that biosensor systems which are developed for the detection of biomarkers. The discussion will be focuses on the types of transducers used in the biosensor systems. First; brief information about cancer biomarkers which are diagnosed by the biosensor developed will be given, and after that the biosensor systems, that are developed for the detection any cancer marker, are discussed deeply.

3.1 Electrochemical transducers

Electrochemical biosensors are used in point-of-care devices since they were portable, simple, easy to use, cost effective and in most cases disposable. The electrochemical instruments used with the biosensors have been miniaturised to small pocket size devices which make them applicable for home use or the doctor's surgery (Tothill, 2009). As a result

of antigen antibody interaction forms electroanalytical signals. Immunosensors based on measurement of these signals are widely used for clinical applications(Liu et al., 2001; S´anchez and Garc´ıa, 1999; Dai et al., 2003; Andrey et al., 1998). Electrochemical transducers divided into four groups due to their sensing signal type; amperometric, potansiometric, conductometric and impedimetric.(Liu et al., 2001; Zhang et al., 2004; Hianik et al., 1999; Ruan et al., 2002). However sensing the signals, which are formed by bioaffinity interactions, is possible to detect in narrow electrochemical techniques. Below of this passage, electrochemical biosensors those are developed for cancer biomerkers as now, are discussed.

3.1.1 Electrochemical immunosensors developed for detection of Alfa-Fetoprotein

Alfa-fetoprotein(AFP) is a normal serum protein that is synthesized by liver, yolk sac and gastrointestinal tract. AFP, a glycoprotein, is about 70 kDa weight and AFP contains an asparagines coupling residue. This biomarker levels are about 3mg/mL when pregnancy occurs then decreases dramatically after birth and reaches 10ng/mL. When overexpression occurs by AFP synthesizing tissues that indicates liver cancer. In addition to this situation points out an evidence of the risk of gamet cell cancer %75-80 positively(Bisceglie et al., 2005; Yuen and Lai, 2005; Zinkin et al. 2008). Consequently the detection of AFP levels in lower levels is very important.

J.-H. Maeng et al. developed a novel microfluidic immunosensor system which measured AFP levels. In this system, a PDMS-glass microbiochip was used, this microbiochip can detect AFP antigen antibody interactions by using electrical signals. There were platinum electrodes to gain electrical signals, a microchannel and pillar-type microfilter to blockade sample flow. These microbeads, microfilters and immune-gold silver coated complexes(IGSS) were used to amplify the response signal(Baschong and Stierhof, 1998; Lackie, 1996; Weipoltshammer et al., 2000); thus more sensitive signals obtain. For the detection AFP levels; microbeads were conjugated with streptavidine, antibodies were conjugated with biotins. AFP was added on these conjugates and AuNPs were conjugated with these conjugates on microchannels. After these experiment steps, secondary antibody was added on these conjugates. Eventually a silver enchancer solution was flowed to the system to amplify electrical signal. A microfilter was deployed on this PDMS-glass hybrid immunoassay microchip adjacent to platinum electrode. Therefore; firstly streptavidin-biotin-AFP-Ab_2 conjugates injected into the PDMS-glass hybrid microchip, secondly this conjugate move to the filters, the filters hold the conjugate solution and a bulk of conjugates formed on the Platinum electrode. Consequently, not only grater mass of bulk obtains and amplify signal, but also silver enchancer coated more conjugates and increased the conductivity and sensitivity. In addition simple to modify, high reaction efficiency and both molecular and cellular level analysis potantials make this immunosensor individual AFP sensing system(Bienvenue et al., 2006; Choi et al., 2002; Lim and Zhang, 2007; Sato et al., 2002). A schematic representation of the biosensor is given in figure 1.

The effect of incubation time and flow rate of conjugate solution are effective parameters for working of this immunosensor. The important points; minimum incubation time and antigen binding time are individual parts of this system. Nanoparticles, which are used for coating, have a nucleation sites that catalyze silver ion reduction(Liang et al., 2004; Su et al., 2001; Xue et al., 2002), therefore this effect of reduction leads to elevated background signal which hides results and microbeads are coated silver enchancer to ignore self-nucleation. Because of using silver enchancer decreases the system's conductivity between 1-10 kΩ

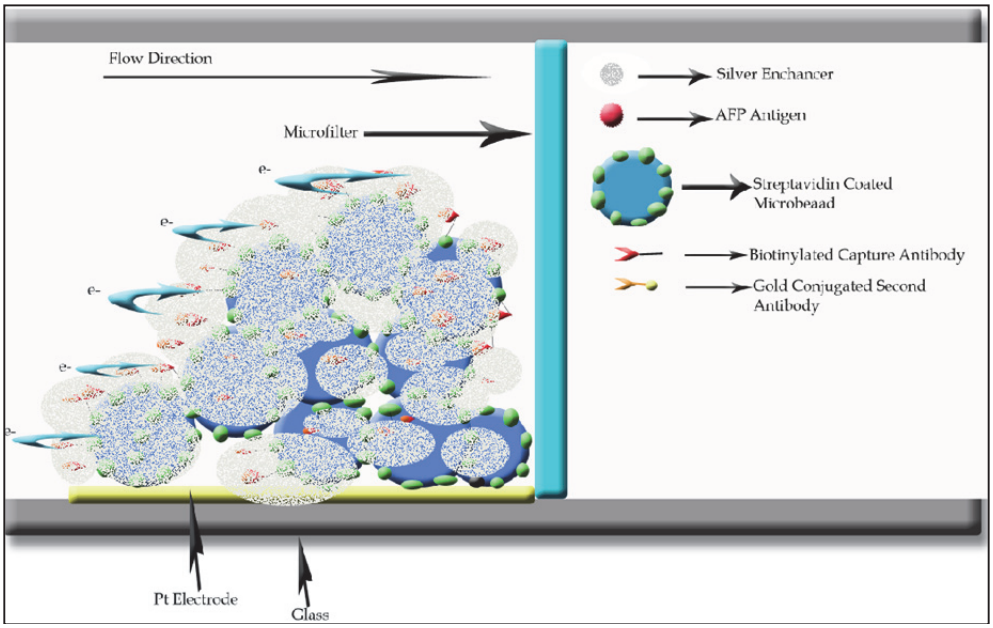

Fig. 1. A schematic representation of AFP sensing by a microfluidic immunosensor system

furthermore doesn't allow to form non-spesific binding, hence the system doesn't need any pretreatment for measurement. Preparation of the immunosensor, incubation time and measurement time totally took less than 1 hour. Minimum detection limit of AFP is 1-10^3 ng/mL and the correlation coefficient is 0.9746.

Wei et al. aimed to develop a label free detection of an immunsensor. Graphene and thionin nanocomposit film were employed on immunosensor. Recently graphene sheets that consist of single carbon atoms in hexagonal shape, are single layer phenomenon(Kauffmann, 2007). Graphene sheets show stability and resistant to higher electrical potentials, due to these properties they are in use for biosensor technologies(Wu et al.,2010; Lin et al., 2009; Liu et al. 2010; Shan et al. 2010; Wang et al. 2009; Babya et al. 2010). Because of nanomaterials's high surface/volume ratio, nanomaterials provide high molecular loading surface. Furthermore these properties amplify electroactivity of thionin. This composition which is located on biosensor increases sensitivity. Graphene sheets were prepared according to Hummer method(Liu et al. 2008) graphene oxide was reduced a method improved by Y. Wang et al. (Y. Wang et al. 2009). Antibodies were immobilized on graphene sheets by a cross-linker agent glutaraldehyde. For prevention of non-spesific boundings, BSA was used to block the reactive aldehyde groups. AFP linear detection limit was between 0.05 and 2 ng/mL. The low detection limit was obtained 5.77 pg/mL(S/N=3). According to Wei et al. there were two factor that provided very low detection limit, firstly; because of high surface area of graphene adsorbed high number of TH and increased antibody conjugation, secondly; conjugation of GS-TH thin film layer increased electroactivity for detection low concentration limits. Three electrode system was used for this experiment. This immunosensor more sensitive than other systems which are employed nanomaterials(Su, 2009 et al.; Sun et al., 2009; Wang, 2009). As it known that reproductivity is one of important

characteristics of an ideal biosensor. For the detection of 1ng/mL AFP, the relative standart deviation of measurements for five prepared electrode was 5.0% in which suggested precision and reproducibility of immunosensor was quite good. For the selectivity tests IgG, Vit. C, glucose and BSA were used and electrode respond was less than 5%, consequently selectivity of this biosensor was quite good. The stability test of this biosensor was stored 3 weeks and the RSD result was 4.9%. The advantageous of the biosensor were simple to prepare, label free and practical measurement system.

Tang et al. was developed another AFP detection immunosensor system which was based on conductometric and was employed carbon nanoparticles as label. The most important advantages of conductometric immunosensors are low prices, high sensitivity and low energy consumption in compliance with the micro system is perfect. Therefore; the novel biosensor designs often come from among the preferred methods(Hnaiein et al., 2008). Conductometric enzyme immunoassay principle of measurement systems, based on conductometric changing that results from a reaction occurs between two electrodes(Watson et al. 1987). According to the measurement system, most of antigen-antibody interactions are not able to occur any electrochemical signal. Thus the characteristics of electrochemical signaling enzymes (HRP, ALP, etc.) used for labeling the production of the signal obtaining to increase the low signal. In this manner; the technique could be used for development of many different measurement techniques. However some antibodies are limited to carry an enzyme. To solve this problem nanomaterials are combined with bioanalytical systems which decrease these limitations(Hiep et al,, 2010; MinhHiep et al.,2010; Yoo et al.,2010). Because of carbon nanoparticles used in this study (CNPS), the remarkable properties of amorphous sp^2-π electrons is quite noteworthy(Dumitrescu et al., 2009). In this study, CNP-HRP-anti-AFP, sandwiches were prepared on the basis of the method and conductometric determination of AFP was carried out as measurement system. Developed by the physical properties of nanoparticles used in this method can connect a maximum level of biomolecules with a created micro environment. Measurement of HRP to determine the concentration of iodine from the environment as a result of conversion is based on peroxide. According to electrochemical measurements carried out in a rapid increase in the reduction and oxidation current was observed that a sharp decline. According to Tang et al. the CNP-HRP-anti-AFP conductometric signal is higher than the building of the reasons for conjugation; CNPS high surface area / volume ratio due to the creation of further conjugation with HRP, HRP-anti-AFP according to this ratio is less than just a result of the addition of AFP (not clear what is required), as has been reported. This optimization stages of the conductometric response of the system was prepared by increasing the electrodeposition time decreased. Linear range of the method is 0.1 to 500 ng / mL, as determined and Immunosensors 50 pg / mL, has a lower limit of determination. A summarize for AFP detection is given in Table 1 below.

3.1.2 Electrochemical Immunosensors developed for detection of Annexin-II

Lung cancer is a disease which is one of the worst ended cancer types. The symptoms of lung cancer and CT X-ray scattering of the disease with only four of process can be observed. The first stage of biomarker identification for diagnosis of lung cancer in recent years, based on the methods researched and began to develop rapidly (Heighway et al., 2002, Hirsch et al., 2001 and Qiao et al., 1997; Singhalet al., 2005; Belinsky, 2004). Annexin II, also known as Annexin encoded by the gene ANXA2 used in the diagnosis of lung

Table Of Electrochemical Transducers For Detection of AFP				
Measurement Technique	Immobilization Technique	Low Detection Limit	Lineer Detection Limit	Reference
Conductometric	Microfluidic immunosensor system	1ng/mL	1 to 10^3 ng/mL	Maeng et al., 2008
Amperometric	Graphene and thionin nanocomposit film	5.77pg/mL	0.05 to 2 ng/mL	Wei et al., 2010
Conductometric	CNP-HRP-anti-AFP, sandwiches	50 pg / mL	0.1 to 500 ng/mL	Tang et al., 2011

Table 1. Electochemical Immunosensors for AFP detection

cancer(Takahashi et al., 1994). In terms of lung cancer, Annexin II what is a secreted protein, is not found in people with a solid, especially the stage of disease (Kim et al., 2007). In addition, the normal bronchial cells that secreted by intact lung bronchial epithelial cells can be used for the determination of the MUC5AC (Hovenverget al., 1996, Koo et al., 1999). Amperometric based electrochemical biosensors were developed for the early diagnosis of lung cancer biomarkers to determine the real-time mode (Wang et al., 1998; Darain et al., 2005; Shiddiky et al., 2007a, b). Biosensors allow to determine specific molecules. For this reason, recently nanomaterials such as CNTs QDS AuNPs can be used to improve the performance of biosensors. Nanomaterials, high surface area / volume ratio, high electrocatalytic activity and can easily be modified in a manner compatible with biomolecules are very useful in terms of their use in biosensor technology (Shiddiky et al., 2007a, b). Annexin II, as well as in electrochemical signal to give some of the biomarkers is not possible in theory, so biomarker is used for the determination of some special labeling.

D.-M, Kim et al. developed an immunosensor system for the analysis of MUC5A and AnnexinII for early diagnosis of lung cancer. This system is based on amperometric measurement using a label as a AnnexinII biomerker. The system consists of glucose oxidase as a label(Shankaran and Shim, 2002; Shiddiky et al., 2007b) have been appointed as amperometric. Glucose oxidase(Shankaran and Shim, 2002; Shiddiky et al., 2007b) was employed instead of the enzyme HRP to reduction of the glucose and was immobilized on surface the hydrazine was used to provide stabilization(Rahman et al., 2005). Immunosensor's measurement system is based on third-generation dendrimers immobilization with a covalent bond connection the foundation of hydrazine to polyclonal antibodies which are treated with AuNPs on the GCE (Rahman et al., 2005, Wang et al., 2007; Katz and Willner, 2004). The use of amine dendrimers increases the sensitivity of the system two or three times(Shiddiky et al., 2007b). First, gold nanoparticles were electrodepozited on the GCE, and then polymerized with TTCA by electropolymerization. Carboxyl groups on the poly-TTCA were activated with NHS and EDC(Shiddinky et al.) with amine groups on the poly-TTCA method of forming the amine groups are activated with glutaraldehyde for further bindings. After these ends are bond to the activated hydrazine sulfate. After measurement, the system is ready for the immobilization of anti-Annexin, Annexin II is required for the measurement of system pointing step of GOx, GOx solution of glutaraldehyde added to biomarker (Annexin II) activated on the connected

ends, after this steps the active sides to block the amino acids lysine (pH = 7 neutral) were used. The prepared immunosensor to verify the measurement controlled on biological fluids measurement should be made on the prepared normal bronchial cell cultures(Koo et al., 1999). Anti-Annexin II / Hyd / AuNP / Den / Polt-TTCA / AuNP-modified electrode in a solution of glucose measurement was carried out depending on the interaction of Annexin-GOx. The signal decreases the presence of free biomarker Annexin II, therefore, must be disposed of amperometric measurement of free as possible. This brought the measurement results have shown that 0.03 to 3 ng / mL Annexin II, the amount to be determined as linear. Dynamic range was measured in the 0.1 to 1 ng / mL. R.S.D. 2.2% (n = 5) and measuring the amount of the minimum 0.051 ng / ml, respectively. As we have seen extremely high sensitivity. Prepared bronchial cell cultures containing liquids examined of each species experiments of biomolecules to the response of immunosensor. Annexin II, a signal was not observed in normal cells, the addition of fluids with QCM measurements showed that the frequency change. The standard of the examination, with the added amount of Annexin II, 280 ± 8 pg / mL was measured. As a result, D.-M, Kim et al. have developed a measurement system was extremely sensitive for early diagnosis of lung cancer. Sensitive measurement techniques such as QCM and impedance method with proven accuracy.

3.1.3 Electrochemical immunosensors developed for the detection of CEA

Carcinoembriyonic Antigen (CEA) is a biomarker occurring in cases of colon cancer, pancreatic cancer, uterine cancer and stomach cancer(Benchimol et al., 1989; Oikawa et al., 1989, Goldenberg et al., 1976). CEA is an acidic glycoprotein is approximately 200 kDa molecular weight. Most of this glycoprotein synthesized during the formation of cancer(Benchimol et al., 1989; Schlageter et al., 1998). During the early diagnosis of cancer over-Express is vitally important. CEA is <2.5 ng / ml for a non-smoker man, while non-smokers <5ng/mL are around. In the presence of cancer is higher than 5 times this amount(Duffy, 2001).

W. Shi and Z. A reported a biosensor system based on electrostatic interaction for determination of CEA. The system shows good biocompatibility with immobilization materials have been chosen as, contains many amino group, a linear polysaccharide(Liu et al., 2010a, b) with negative charged groups on the chitosan(Liu et al., 2005) a good film layer observed due to form the nafion film. The main purpose of this system, a new membrane was prepared redox species is to adsorb on the film. Polietilendiamin were used to immobilization of antibody cross-linked on the electrode membrane and created with the electrolytic solution to facilitate the transfer of electrons between the AuNPs. Thus, antigen binding by blocking the electron transfer of redox-based measurement system's response was declined. (Liu and Gooding, 2009). AuNPs to be in 15 nm diameter(Yang et al. 2009) were prepared and were treated nafion to formed nafyon-AuNP complex. Ferrocene mixed with chitosan by sonication(Grabar et al. 1995). PEI treated with glutaraldehyde to modified electrode forming and the anti-CEA bound aldehyde ends. Nafyon-AuNP prevented leakage of ferrocene from system. With that of the secondary amine and negative charged Nafion and positively charged PEI to have facilitated the coexistence of two species via electrostatic interaction. A change in current density occurred after incubation with CEA. Stopping the transmission of electrical signals blocked electrostatic properties of electroactive layer of CEA. This was confirmed by a decrease in current. Prepared in conductivity compared to the control and AuNP-free sensor is determined to be less. In other words, the presence of AuNP increased the sensitivity of the system. Immunosensor

offers 0.01 to 150 ng / mL linear measurement. For the control of the prepared AuNP-free sensor showed a narrower range of measurement 0.03 to 100 ng / mL. RSD value of the sensor is 6%. Because of these properties prepared by different techniques, a measurement technique that has proved to be more effective than most Immunosensors (Wu et al., 2006, Pan and Yang, 2007; Mauritz and Moore, 2004; Limbut et al., 2006, Tan et al., 2006; Tang and Rhine, 2008, Tang et al., 2008, Zhang et al., 2008, He et al., 2008, Zhang et al., 2007, Liu et al., 2010a, b, ; Thomson et al., 1969, Yang et al., 2010, Lin et al., 2004).

X. Li et al. developed an immunosensor the poly-sulphanilic acid (PSAA) modified a glassy carbon electrode, due to the electrostatic interaction strategy. PSAA contains negative charge to interact the positively charged toluidine blue as a mediator and nano-Au as conductive agent facilitated binding of the anti-CEA in this system. HRP was used instead of BSA to prevent non-specific binding of the system. This is both non-specific bindings to blocked(Zhang et al., 2005; Zhuo et al., 2005, in press) and to use of TB as a mediator and H_2O_2 as a result of reduction feature makes the system more sensitive(Yang et al., 1998; Zhang et al., 2005). Radical cation method was used SAA to bond on GCE electrode(Cheng et al., 2001, Liu et al., 2000; Downard and Mohamed, 1999) to the PSAA / GCE modified electrode forming. Sulfonate groups of the modified electrode has been created with TB treatment. AuNP solution then immersed electrode to increase the surface area, this step was followed by immobilization with anti-CEA. Finally, the electrode immersed in HRP solution is ready for use as anti-CEA/HRP Immunosensors. All steps were followed by using the EIS. As is known, the electrode interface impedance spectroscopy is an effective method used in monitoring binding properties(Colvin et al., 1992, Gu et al., 2001). According to Fig 2 impedance spectroscopy a) bare GCE, b) the PSAA / GCE, c) the TB / PSAA / GCE, d) Au / TB / PSAA / GCE, and e) anti-CEA/Au/TB/PSAA/GCE modified electrode impedance shows the spectra. Electron transfer resistance showed a decrease, in the presence of Ferri/Ferro redox probe, TB and Au's.

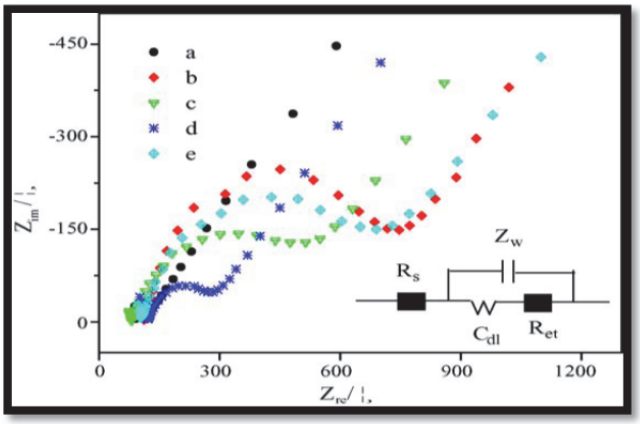

Fig. 2. Electrochemical impedance spectrums of glassy carbon electrode modified by poly-sulphanilic acid (Li et al., 2005)

It has been reported to the CV peaks increases in peroxide reduction when cyclic voltammetry studies of HRP in H_2O_2 solution. Incubation with CEA resulted in the reduction of CV peak current. The center of the electron transfer mediator in the formation

of Immunocomplex blocked impedance and CV studies has been proven again. In this system, the biosensor preparation strategy is based on electrostatic interactions, control of pH during preparation is considered to be very important. In addition, the pH of the enzyme can cause a change in the operation and characteristics of TB, the mediator. BSA and HRP As a blocking agent to prevent non-specific binding on prepared biosensors of two different proteins and their performances were compared. HRP was used the linear measurement range of the CEA were between 0.5 to 5ng/mL when BSA was used 0.8 to 5 ng / mL. Lower determination limit of 0.2 ng / ml. X. Li et al. developed instead of BSA as blocking agent, the use of HRP, the system has become more sensitive. CEA determination of H_2O_2 in the environment didn't show a differentiation of both blocking agent. Selectivity experiments in the studies with the AFP and hepatitis B, 2.38% and 3.24% RSD values, respectively. 20-day storage stability test of immunosensor, 20th day 97.5% initial activity remained at the end of the day persent.

Z. Liu et al. developed an immunosensor system was modified nano-Au/PTC-NH2/PB biocompatible composite film and CEA were determined by the composite film forming. High chemical stability of the system, a well-known redox characteristics of Prussian Blue was chosen because it is advantageous in terms of low price, and magnetic properties(Xian et al., 2007). Some of the disadvantages of immobilization on the surface of the PB electrode is noticeable. Among these various techniques, electrode surface immobilized PB(Zakharchuk et al., 1995; Mario et al., 2003; Lupu et al., 2002, Yu et al., 2007) depending on the electrode surface leakage to the solution(Haghigi et al., 2004, Yuan et al. 2007). In this study, a new organic compound was synthesized to create a semiconductor film. With ethylene diamine 3,4,9,10-perilentetracarboxylicanhydrite selective and sensitive to the formation of a layer of PTC-NH2 formed. Because of the well-known electronic properties of PTCDA (Gustafsson et al., 2006; Forrest, 1997) investigated the advantages of the production of a new substance derived in this matter. PTC-NH2 in the gaps on the creation of the PB film of organic-inorganic moved to create a component that has led to the surface because of the abundance of the amino ends of the leakage is prevented. Another advantage brought on the AuNPs, adsorbed by aminogroups, high specific surface area and lead to amplification of the response of the sensor by creating a structure that is biocompatible. Nano-Au / PTC-NH2/PB/GCE electrode of the recent anti-CEA-treated with BSA to prevent nonspecific binding. Impedance and CV datas were used to investigate for electrode interface. Modification of the electron transfer to the PB resistence reduced with the PTC-NH2 modification as a result of increased resistance. Modification with anti-CEA increased resistance so successfully. For electrochemical sensor prepared and covalent bond-free Immunosensors effecting parameter was pH. The temperature is also a defective factor that denatured biomolecules. Prepared immunosensor for CEA determination in linear range is between 0.05 to 2 ng / mL and the lower limit of determination is 0.018 ng/mL, $R^2 = 0.995$. Selectivity experiments carried out with the hepatitis B antigen, CEA, AFP, ascorbic acid, L-cysteine, L-lysine, L-glutamic acid and 1.4% BSA, CV experiments showed that this differentiation is also acceptable. 60-day storage stability of the prepared immunosensor observed and RSD value is 4.1%. Liu et al. developed by the PTC-NH2 compound produced in this system by increasing the stability of PB increased the accuracy of the method. Consequently lower limit of determination, and the fabrication steps produced quite simple.

Song et al. developed an immunosensors system for the determination of CEA to interface the gold nanoparticles and Prussian Blue with the nanoparticle/nanocomposite multi-layer structure. Advantage of this system nanomaterials and composite forms based on made of

chitosan and the immobilization of gold nanoparticles and multiwalled carbon nanotube (MWCNT) interface was used. MWCNTs are widely used in recent years because of high chemical stability, good electronic properties and mechanical stabilities(Wang and Musameh, 2003). MWCNTs can not show dissolution most of the features in environments containing water, to facilitate the dissolution of chitosan(CS) utilized in this study(Lu et al., 2005). In this way, the CS-MWCNT nanocomposite have shown very good agreement for potential applications(Liu et al., 2008, Spinks et al., 2006). In this way, the CS-MWCNT as a result of modification of amino groups on chitosan AuNP binding brought in a structure that allows for the convenience, the sensitivity of the system with a combination of both MWCNT and AuNPs were increased. Showing the redox activity of immune molecules are mostly used in the analysis of protein analysis, amperometric, redox activity of the PB in this study were chosen because of the well-known properties(Fiorito et al., 2005, Zhang et al., 2007). MWCNTs were activated by acid solution and then mixed in an ultrasonic bath CS and AuNPs after this stage of the nanocomposites structure formed. Liu et al. Synthesized PBNPs according to the method developed by(Liu et al., 2002). In this study, using the CS-MWCNTs-AuNPs-PBNPs as redox probe modified composite structure was immobilized on the AuNPs and nitrile groups by electrostatic interactions. CS-MWCNTs-AuNPs solution of suspension was spread on the GCE electrode after the modification of GCE-PBNPs was performed with the above principle. BSA used to block non-specific binding of anti-CEA solution was prepared by immersion and CV measurements confirmed that the immobilization of impedimetric as expected. Developed Immunosensors system of linear measurement range 0.3 to 120 ng / ml range, R2 = 0.9976, and the lower limit of determination 0.1 ng / mL. The best results are given for sensitivity, specificity and reproducibility. Song et al. were developed an anti-CEA/AuNPs/PBNPs/CS-MWCNTs-AuNPs/GCE modified electrode system in this study. By increasing the surface area of nanocomposite structure with PBNPs of the amount of the substance and the immobilization increased sensitivity and leakage could be prevented and thus can be used for clinical studies.

Y. Wang et al. Developed a Molecular imprinting-based potentiometric sensor system for the determination of cancer biomarker. Molecular imprinting process that artificial materials use of a very large area of the molecules determine to use(Pauling, 1940; Sellergren, 2001; Piletsky et al. 2001; Cram, 1988; Bartsch & Maeda, 1998; Mosbach, 1994; Sellergren & Shea, 1994; Haupt, 2003; Vlatakis meat al., 1993; Wulff, 1995). Used on a layer of polymer molecule imprinting method according to pattern creates a cavity, cavity's geometric pattern that is similar to the properties of the molecule carrying the groove to be connected. SAM is used as a surface molecular imprinting in this system. As the hydrophobic and hydrophilic groups of the SAM shown to interact with protein domains. Gold-coated silicon chip technique on a Au-S bond via alkenthiol molecules containing hydroxyl end is connected to water, this may very well organized in a single layer(Porter et al., 1987, Bain et al., 1989). If the target molecule to the surface during the binding of this molecule in the formation of monolayer taking place within the matrix of SAM forms imprinted. As a result of the removal of the mold layer also leaves behind a cavity. In terms of surface molecule template is compatible with the appropriate specificity by showing mold cavity is connected to the molecule performs and thus measured. The amount of potential to change the amount of binding molecule with the environment, as a result of decreasing the measured potentiometrically(Janata, 1975). Surface characterization studies performed by XPS and AFM. This study was carried out to determine CEA in colorectal cancer cell cultures. Linear determination is between 2.5 and 75ng/mL. Specificity studies of the electrode response

were observed in an experiment with bovine hemoglobin. While the normal human cell cultures in the system of measurement used in the CEA and CEA than the amount of excess. CEA concentration increase not only determines the speed, but also increases the potency increases differentiation. The sensor response time were obtained in 1 hour. If the protein is smaller than the thickness of the SAM molecule, the mold is only a small portion will be sufficient to interact(Porter et al., 1987, Boehm et al., 1996; Brayer et al., 1995). Both the hydrophobic and hydrophilic surface of CEA(Duffy, 2001;) and gold adsorption ability of proteins(Ostuni et al., 2001; Hook et al., 1998, Kaufman et al., 2007, Tang et al., 2004) with a molecular shot has to be strong.

Vismanathan et al. Developed a MWCNT and liposome technique for the determination of CEA was prepared by using ferrocene to screenprinted electrode system developed with the use of single-use electrochemical Immunosensors. Recently, on the screen printed electrode-based electrochemical immunosensors extremely useful, because of designed for single use and portable use(Valat et al., 2000, Wu et al., 2006, Gao et al., 2003). Nanomaterials, especially carbon nanotubes, have high strength, thermal and electrical properties because of the very useful, biosensor immobilization materials that increase the limits of sensitivity (Hansen et al., 2006, Pathak et al., 2001). Vismanathan et al. CEA levels in serum and saliva was arrested in his study polietilenimin Screen Printed MWCNT modified electrode and ferrocene carboxylic acid, encapsulated CEA were used in liposomes. Ferrocene labels used in preparation of liposomes were prepared by the method of reverse phase to blow (Ho and Hsu, 2003; Ho and Huang, 2005; Ho et al., 2007). Liposomes dipalmitoil phosphatidylcholine(DPPC) and phosphatidyl dipalmitoil glycerol (DPPG) have been prepared. Thiolat groups, where created on the liposomes, were incubated with CEA and unreacted thiol groups were blocked by the etilenmaleimid. Carboxylic acid, sulfuric acid and nitric acid oxidized MWCNT functionalize MWCNT was obtained(Tseng et al., 2007). PEI was modified with MWCNT suspension drops on the SPE. Modified electrode was immobilized covalently antibodies with glutaraldehyde. Non-specific binding ends of the unreacted aldehyde prevented by BSA. Liposomes were created to be characterized by determining the homogeneity of the lipid results were obtained from each liposome(eq 1). aL per lipid head group surface area, d is the hydrodynamic radius, t the thickness of the lipid bilayer (Singh et al., 1996).

$$N_{tot}=\frac{\pi}{aL}[d^2 + (d-2t)^2] \quad (1)$$

Thus, the number of CEA on the liposome can be calculated theoretically. From these data, the lipid molecule is connected to the CEA, 2 or 3. As a molecule of about 3900 that correspond to molar 0.023. One was entrapped in a liposome, the liposome containing ferrocene $1x10^{13}$ to 0.2 M was calculated for per milliliter. MWCNT on the negative ends of the positively charged PEI chains were interacted. Thus, measuring the limits of the modified electrode 5 pg / ml and 500 ng / ml, respectively. Reproducibility of immunosensor to submit actual samples for accurate determinations shows promise in clinical trials is available

Xiang et al. have developed a ultrasensitive CEA immunosensor stratified layer by layer to determine the multi-enzyme system. In this study with the creation of multi-enzyme layer on the SWCNT with an increase of the enzymatic reaction to enhance signal. LBL (layer-by-layer) will be marking technique, allows to the amounts enzyme catalytic activity to an increase in the signal(Munge et al., 2005, Wang et al., 2006, Zhao and Ju, 2006). On the other hand the connection of multi-layer enzyme dramatically increases the analytical

signal(Limoges et al., 2008; Limoges et al., 2006, Bauer et al., 1996; Schelde et al., 2001 and Mak et al., 2003, Kwon et al., 2008). Primarily on the preparation of SWCNT multienzyme LBL layer was prepared by modification of immunosensor(Munge et al., 2005, Zhou and Zhang, 2009). Alkaline phosphatase was immobilized on SWCNT has been modified with PDDA. SWCNT-(PDDA / ALP), conjugation was repeated several times, and thus the same system SWCNT-(PDDA / ALP)$_4$ bioconjugate the structure formed. This was adsorbed on PDDA conjugates negatively charged layer by repeating the same step again to add ALP binding immunosensors Ab_2 was formed. GCE electrode surface was modified with immobilization o-ABA solution was prepared containing H_2SO_4(Preechaworapuna et al., 2008). Reactive carboxylic Nb1 ends activated NHS, EDC after the modified electrode was treated to blocked by ethanolamine. After SWCNT-(PDDA-ALP)$_4$-PDDA-PSS-AB_2 bioconjugates was immobilized on electrode surface. ALP's isoelectric point is above this point will be charged pozitively easily adsorbed by PDDA. Enzyme layers by increasing the limit of determination decreased to very low values of the signal also increased the use of coenzyme is as follows: 0.1 to 1000 pg / mL defined as linear, the lower limit of determination in the FMA has dropped to 0.2. Specificity studies of myoglobin and lyzozme are not experienced a significant increase immunosensor responce these experiments also showed that high selectivity. Immunosensor's RSD value is 6.9% in the good results showed that the reproducibility and accuracy. As a result of prepared immunosensor for clinical trials because of it is quite susceptible to use the results. Table 2 summarizes the electrochemical immunosensors used for detection of CEA below.

Table Of Electrochemical Transducers For Detection Of CEA				
Measurement Technique	Immobilization Technique	Low Detection Limit	Lineer Detection Limit	Reference
Amperometric	anti-CEA/ PEI/Nafyon-AuNP/Fec/	0.01ng/mL	0.01 to 150 ng / mL	Shi and Ma, 2011
Voltammetric And Impedimetric	anti-CEA /Au / TB / PSAA / GCE	0.2 ng / mL	0.5 to 5ng/mL	Li et al., 2006
Voltammetric	Anti-CEA-BSA/Nano-Au / PTC-NH2/PB/GCE	0.018 ng/mL	0.05 to 2 ng / mL	Liu et al., 2008
Voltammetric	anti-CEA/AuNPs/PBNPs/CS-MWCNTs-AuNPs/GCE	0.1 ng / mL	0.3 to 120 ng/mL	Song et al., 2010
Potentiometric	SAM-CEA/Au Electrode Molecular Imprinting	2.5ng/mL	2.5 to 75ng/mL	Wang et al., 2010
Amperometric	MWCNT and ferrocene labeled liposome on SPE	5 pg/mL	5 pg/mL to 500ng/mL	Vismanathan et al., 2009
Amperometric	SWCNT-(PDDA / ALP)$_4$-Ab_2	0.1pg/mL	0.1 to 1000 pg /mL	Xiang et al.,

Table 2. Electrochemical Immunosensor for Detection of CEA

3.1.4 Electrochemical immunosensors developed for the detection of CRP And TNF

C-reactive protein is a biomarker that is118kDa and is circulating in the blood, the biomarker synthesized by interlokin6, in the liver (http://www.scrippslabs.com/datatables/proteinabsorbance.html, 2007; Weinhold and Rüther, 1997). Plasma levels are lower than normal human, 3µg/mL (Hu et al., 2006; Verma and Yeh, 2003). Used to determine levels of CRP as a prognostic indicator of gastric cancer.

M.-H. Lee et al. developed the source and drain electrodes placed on the surface potential measurement was carried out under a layer of semiconductor SiNW field-effect transistors in the system. Nanotechnology-based sensors through the mechanisms determining the limits and sensitivity have increased in recent years nested. Direct labeling of biomolecules and nano-structures provide an ultra-sensitive manner possible to determine. Foundations this type SiNW Fet transistor and connecting the surface of the positive or negative charge on the surface accumulation of a protein based on the principle of conductivity decrease or increase(Patolsky et al., 2006). This mechanism allows the realization of high sensitivity and real-time measurement. In this study, silicon nano-wires single-crystal substrates were prepared according to the method of thermal oxidation of p-type substrate, n type substrate and n-type substrate to face grain orientation(Lee et al., 2007). Gold colloids were prepared reduction of sodium citrate(Frens, 1973). Aldehyde-ended single-layer surface modification of SiNW surface is the principle of creation. In general, the use of oxygen plasma as a chemical reaction of the hydroxyl group is based on creating a glutaraldehyde solution(Patolsky et al., 2006). In this study, oxygen plasma cleaning to be surrounded by the surface amine performs a mapping of the surface silanol. Then aldehyde groups formed and paired with CRP bound to the antibody on the created surface. CRP and CRP antigen SiNW after reaction with gold nanoparticles formed to conjugate. This system is designed to work in a flow system, containing two PDMS micro-pump system, created a flow to input and output channels, microchannels 600 micrometers in length in the flow of the system by performing the analysis of the protein has led to measurement area. In this study, the actual serum samples from patients were used. Isoelectric point of CRP between 5 to 6, which is negatively charged in solution is neutral for this reason, flow to p-type SiNW Fet. Previous studies which Fet SiNW are used, to determine the lower limits of s have dropped to 1fmole. In addition, the observing effect of sodium chloride in the SiNW youth initiative. 13 CRP-positive patients, the diagnosis of gastric cancer biomarkers combined CEA and CA19-9 can be determined. Measurements of serum donors SiNW Fet between 3.2 to 10.4 micrograms/milliliter were measured. Despite the biomarkers measured in this system of measurements to be made so sensitive that low sensitivity of the system determines limitations. According to the results presented in this SiNW Fet signals proportional to the levels of CRP. Therefore, the diagnosis of gastric cancer, especially in the early stages, the determination provides a great asistance.

Qureshi et al. was developed Immunosensors system by using unlabeled array capacitors combined with gold for the determination of multiple biomarkers will be integrated biosensor systems have evolved to the surface of silicon oxide. Capacitive immunoassays are phenomenon immunochemical tests in recent years, the development and manufacture of hand-held devices used for personal use. Affinity-based capacitive sensors that can respond to even very low levels the opportunity to direct analyte measurement techniques. Changes in dielectric properties of the measurement basis on or load distribution depend on the conductivity change in the exchange of antigen-antibody interaction on the surface of the electrode. Recently, the label was developed the redox mediator used in capacitive

biosensors in this system(Carrara et al., 2009; de Vasconcelos et al., 2009; Saravan et al., 2008). In this study, the covalent bonding on an optimized GID is connected antibodies via epoxy-silanisation(Saravan et al. 2008), this method is less prone to sensitivity, the other less cheap silicon dioxide with a high-sensitive measurement applied to nanocrystalline diamonds(Quershi et al. , 2009). GID arrays of silicon oxide surface with a thick layer of tungsten, first a thin gold layer is coated in advance to allow for the creation of an easier way. According to this structure, the capacitor arrays includes 24 fingers GID(Quershi et al., 2010). First, arrays were treated with MPA to SAM created layer free carboxyl groups was activated by NHS / EDC and antibody is ready for immobilization. Phase of antibody immobilization was created in two formats: the first method, each GID capacitor with a pure antibody, while the second method, equal amounts of multiple antibodies (CRP, TNF and IL-6) was co-immobilized. Dielectric parameters of different antigens were treated arrays were prepared. BSA was used as a non-specific protein for a negative control. Limits for the determination of biomarkers measured in linear; 25pg/mL to 25ng/mL. The complex dielectric constant is a result of the change in dipole momenttes of biomolecules which differences amino acid sequence of elements that can bring about change in the dipole momentte(Antosiewicz, 1995). To the determination of several biomarkers of cancer as it is known to determine the accuracy of diagnosis of cancer is increasing. Most of the other proteins secreted as a result of the cancer biomarker can be found in a unified manner. Quareshi et al. developed for multiple analyses by allowing the disease to other single-analyte immunosensors advantageous and gives accurate results in this array technology. In addition, the silicon oxide background is fast, simple and sensitive measurements, allowing the hand-held personal devices allows the development of diagnostic devices. Table 3 summarizes the electrochemical biosensors for analysis of CRP and TNF.

Table Of Electrochemical Transducers For Detection Of CRP and TNF				
Measurement Technique	Immobilization Technique	Low Detection Limit	Lineer Detection Limit	Reference
Potentiometric	Anti-CRP/SiNW Fet	3.2µg/mL	3.2 to 10.4 µg/mL	Lee et al., 2010
Capacitance	Anti-CRP/MPA/Au Electrode	25pg/mL	25pg/mL to 25ng/mL	Qureshi et al., 2010

Table 3. Electochemical Immunosensor For Detection of CRP

3.1.5 Electrochemical immunosensors developed for detection of PSA

Prostate cancer is one of the most common cancers in men in most types of cancer among the three leading causes of death (Jemal et al., 2006). For this reason, the most important part of treatment of the disease is diagnosed early. Early detection of protein-based biomarkers for biosensor technology in the last few years as it is known to be very beneficial for the early diagnosis of determination. Prostate-specific antigen (PSA), to determine the most common tumor marker is used on prostate cancer(Benson et al., 1992, Bradford et al., 2006; Brawer, 1999, Stephan et al., 2006). PSA is a glycoprotein of 32-33 kDa single chain (Landis et al., 1999, Cesar et al., 2004;), a part of 93% sugar residue peptide also contains the rest of it is produced by the prostate tissues(Loeb and Cantolona, 2007).

Y.-Y. Lin et al. developed an immunochromatographic/electrochemical biosensor system which is nanoparticle-labeled for the determination of the PSA. This study obtains two steps; the first step rapid immunochromatographic assay with a combination of simple and sensitive immunoassay with a diagnosis after the device. As is well known a specific binding substance chromatography after moving from the principle of signal, depending on the diagnosis has been developed. Very fast measurement system offers the possibility of one or two minutes. In the first part of the design is based on the visual judgement, by using a dye or a gold nanoparticle provides a quick and qualitative determination (Jin et al., 2005; Nagatani et al., 2006, Zhang et al., 2006, Fernandez-Sanchez et al., 2005) . But not only is not sufficient for the qualitative determination of the correct results therefore reveal its high sensitivity due to the sensitivity of a combined electrochemical immunoassays permit designed to provide a more accurate result. Advantages brought by nanotechnology in recent years began to develop nanoparticle-based Immunosensors thus increase the signal trace of biomarkers to identify and obtain a more precise measurement is possible(Georganopoulou et al., 2005; Huhtinen et al., 2004; Jain, 2005, Liu et al., 2006, Liu and Lin, 2007, Liu et al., 2007, Nam et al., 2003, Wang et al., 2006). Y.-Y. Lin et al. developed to increase the signal in this system made of CdSe @ ZnS quantum dots (QDS) are used to mark the anti-PSA antibodies. Quantum dots can contain hundreds of very useful particles and biocompatible terms of marking, and signal enhancement. In order to take the measurement Y.-Y. Lin et al. anti-PSA-QD prepared (Wu et al., 2007; Wang et al., 2008). Then, immunochromatographic/electrochemical biosensor prepare, the system includes immunochromatographic strip and this strip is composed of three parts; sample loading area, the second part of the anti-PSA-QD loaded contact area, the third of the area consists of covalently bound anti-PSA to Screen Printed electrodes were placed under the test area. Modifications by using diaminothiofen to form the membrane with the space arms. Thus, the modified nitrocellulose membranes were later activated by glutaraldehyde, then incubated with the anti-PSA solution. Horizontal flow in the system, BSA and Tween blocking dried using a membrane with N_2 gas. Anti-PSA-QD conjugates were dried by applying the last part of the glass fiber. PSA application of this system was performed in various advantageous immunochromotographic primarily be facilitated removal of the extra buffer, other advantage, ten minutes of the measurement is performed. CdSe quantum dotls created the nucleus and shell contains ZnS. The sample is applied to the system as part of the walk by the PSA QD-labeled anti-PSA-QD complex consists of an complex. Membrane was adsorbed on the anti-PSA-QD bound to act on the membrane with anti-PSA to PSA, which itself depends on covalent, QD marked when the test section consists of a sandwich complex. Here, an appropriate reaction (1M HCl), QD complex is dissolved and the remaining free cadmium ions in the electrochemical measuring system to provide to be quantify. This system is ideally suited for making quantitative measurements and the signal gain is proportional to the amount of the PSA. PSA's linear measuring range between 0.05 to 4 ng / mL in this system and $R^2 = 0.995$ was determined. RSD value of reproducibility was 6.4% and the lower limit of determination of 0.02 ng / ml. This combined and developed system is cheap, fast and sensitive due to the use of devices developed for clinical applications, and paved the way for personal use.

J.F. Rusling et al. developed electrochemical sensor technology by other nanomaterials have been used. As is well known properties of carbon nanotubes are extremely useful materials that show metallic or semiconductivity (Munge et al., 2005). SWCNTs were used in the sensor at the two stages; electrode surface with higher conductivity and higher surface area

to provide more adhesion to the surface with analyte signals to be more sensitive and are used to mark the second part, by moving a larger amount of enzyme, and secondary antibodies amperometric signal is used as to increase(Mung et al., 2005). In this study, the surface of the carbon nanotube electrode has been modified by creating forest. SWCNT on the surface to be more intense forest electrode coated with a thin film layer nafyon. The second stage used for the oxidation of carbon nanotubes formed by acid carboxyl ends of the enzyme, peroxidase, and secondary antibody was immobilized. According to this approach, the CNT in each 100nm enzyme are 170 HRPs (Jensen et al., 2008). This also provides a determination of ultra-low levels of PSA (4 pg / ml) (Yu et al., 2006). Limitations of the generated results were extremely sensitive for nantube forests. The fact that nanotubes together with separation is difficult and increasing heterogeneity among the problems to be tackled. Depending on these results, Rusling et al. nanoparticles modified electrodes have deposited layer by layer(Lvov, 2001). First a polycationic molecule immobilized on ultrathin pyrolytic graphite electrode surface, after a negatively charged gold nanoparticles were immobilized. In the preparation of the negatively charged AuNPs modified with AuNPs glutatyondaki glutathione cysteine and glycine with glutamic acid at the carboxyl ends of the gold bond to make out the orientation created by the nucleus (Zheng and Huang, 2004). Carboxyl ends of the surfaces of nanoparticles created by HRP conjugate binding to form an amide bond with the HRP. This structure responds to a previous study, an electrochemical 0.28μA/μMlık 0.18μA/μM health changes in more than 40%. Detection limit of the results showed that more than 3 times. These two tests on samples of infected people in the experiments showed a good correlation with ELISA tests. This study showed that the province of AuNP with nanomaterials, especially with the system established SWCNT due to the sensitivity and accurate results have proven that they are suitable for clinical studies. The biggest problem with layers of polymer systems with non-specific binding problem should be in front of non-specific binding.

Wei et al. developed an immunosensor system by electrochemical measurement of the amount of PSA performed using Au-Fe3O4 nanoparticle labels. In this study, gold nanoparticles on a metal oxide support in support of holding a synergistic effect between metal and metal oxide showed higher catalytic activity(Valden et al., 1998, Wang et al., 2009, Zheng and Stucky, 2006; Comotti et al., 2006 ; Liu et al., 2006, Lee et al., 2010a). Similarly, Wang et al. their study of the structure of Pt-Fe3O4 showed higher catalytic activity than single PtNPs determined (Wang et al., 2009b). In this study, dumbbell-like Au-Fe_3O_4 was used to perform catalysis synergistic effect on H_2O_2. Created a dumbbell-like Au-Fe_3O_4 on the secondary antibody binding to PSA measurement was carried out. Immobilization on the surface of the electrode material used a graphene layer in this study. Carbon atoms of graphene layers tightly packed, flat two-dimensional honeycomb-like, with a high surface area nanomaterials(Geim and Novoselov, 2007, Ohta et al., 2006; Aleiner and Efetov, 2006). Because of these features of graphene layers increases the surface area of the installation of the primary antibodies, showing a good conductivity of H_2O_2 helps to determination(Du e al., 2010). Graphene layers of graphite oxide was prepared by the method of thermal exfolation(McAllister et al., 2007). Graphite oxide, graphene has been modified according to the method Hummer(Liu et al., 2008). Au-Fe_3O_4 dumbbell-like particles, Lee et al. prepared and developed method(Lee et al., 2010a) into the secondary antibody solution was added to conjugation. Graphene layers are created on the carboxyl groups with amide bonds linked with anti-PSA (primary antibody) was created with the GS-conjugate-anti-PSA, BSA was used to generated non-specific binding of conjugate to avoid dropping the surface of GCE.

On the modified electrode was incubated with PSA at the end on the previously prepared were incubated with the addition of Au-Fe_3O_4-AB_2. Peroxide electrode was prepared by adding the signal from the Au-Fe_3O_4 structure as a result of peroxide reduction by the amount of PSA was measured. The amount of PSA in the system increases, the increase in flow has occurred. Bi-linear system, the measurement of PSA concentration in the range 0.01 to 10 ng / mL, calculated as the lower limit of determination was found to be 5pg/mL. According to Wei et al. there are three factors to determine low amounts that are based on the large surface area of graphene layers has increased the installation of the primary antibody, Au-Fe_3O_4 dumbbell-like particles as a result of the high value of the catalytic reduction of peroxide increased the conductivity of the layers with the creation of very efficient in terms of lower limits were determined. 6.3% RSD value of the system is determined, the electrode stability is due to the long-term stability of the NPS Au-Fe_3O_4. The same procedures developed with the ELISA method is less than the deviations between the values was observed compared Immunosensors. As a result, the GS large surface area, high stability and catalytic activity of Au-Fe_3O_4 particles of the system has to be sensitive.

N. Triroj et al. developed miniaturized nanoelectode arrays with microfluidic biochemical analysis of the PSA sensor technology. As is well known properties of nano-sized materials due to different measurement systems are developed extremely sensitive, fast and easy. For instance, the interface in terms of molecular nano-electrodes are stable and electroactive molecules are easy to access the center for more sensitive measurements(Shi et al., 2007; Shi and Yeh, 2007; Kovochich et al., 2007, Yeh et al., 2007). This is small electrodes on the surface of the electrode double layer, increasing the loading materials and diffusion electrochemical reactions can be controlled more easily to make the execution. On the other hand, micro-electrode surface facilitates the mass transport(Norton et al., 1990). High mass transfer is important because in this way; biomolecules to the electrode surface of the catalytic reaction as a signal to come together and this association creates the first condition can not be controlled by diffusion(Armstrong, 2005). The electronic transmission of uniform nano-sized electrodes plays a role in increasing signal. Micro-electrode platform, the previous configurations(Triroj et al., 2006) unlike in this study as working electrode between the electrode arrangement of a micrometer pore is designed to be5x5 and 5nm. PSA determination for the design of microarrays as a sensor electrode surface is primarily the formation of the SAM procedure(Achim et al., 2009, Yeh et al., 2010a, b) which was carried out with mercaptopropionic acid. Free carboxyl ends of SAM layer activated by NHS / EDC, metallized peptide and nucleic acid-incubated with anti-PSA. PNA-ant-regulation of PSA(Achim et al., 2009, Yeh et al., 2010a, b) facilitated the immobilization of the electrode surface. After the surface of the microarray was incubated with PSA marked with GOx, this step was supported by CV datas. Because of the high surface area of microarray, the PSA levels in a sensitive way to be determined 4-10ng/mL. Such as the measurement of the enzyme suggests the preparation of the electrode marked with the signal extraction based on the conversion to glucose. Accordingly, the lower limit is determined as 10pg/mL.

Qu et al. developed immunosensor based on the marking technique with silica nanoparticles for determination of total PSA in human serum. Co-functionalized SiNPs-antibodies with alkaline phosphatase measurement principle of silver electrodeposition measure of the PSA. Silicon nanoparticles have been prepared by the method of emulsion, Triton X-100 and hydrophilic silica nanoparticles formed by the addition of hexanol in the cyclo hexane (Qu et al., 2008). Solved by adding an appropriate amount of the nanoparticles in APTES, glutaric anhydride into the solution containing nanoparticles formed by adding

functionalize silicon binding to ALP. Gold electrode was modified with cysteamine solution and the amino ends activated with glutaraldehyde that were incubated with the antibody, to prevent non-specific binding of aldehyde ends are blocked with BSA. The electrode made of silicon nanoparticles drops were modified for sandwich method. On this method, 0.76 ng / ml PSA concentrations were determined in lower determination. ALP of the ascorbic acid 2-phosphate conversion of electrons with the silver particles deposited on the surface of the stacked electrode and consequently the signal was measured. For increasing the catalytic activity of ALP as a result of the concentration increase has occurred in response to electrode. Excess amounts of ALP can help to prevent the sandwich method of attachment.

Li et al. developed to detection of cancer biomarkers by using nitrodopamin (NDA) with functionalized Fe_3O_4 particles to increase the signal of the electrochemical determination of electrochemical immunosensor. The NDA system with a strong anchor agent is a material that for immobilization of iron oxide formed by capturing nanoparticles(Young et al., 2009). The immobilization material is used to bind both the primary antibodies and secondary antibodies. Thionine complex with Fe_3O_4 and created HRP-AB_2 in the presence of peroxide is the mediator with Thionine reduce the signal. Fe_3O_4 nanoparticles synthesized according to the method developed by Xu et al.(Xu et al., 2009). NDA was prepared according to the study of Malisova et al.(Malisova et al., 2010). NDA-Fe_3O_4 with the primary antibody was immobilized on the modified GCE. This action on the NDA-Fe_3O_4 modified electrode was activated with glutaraldehyde and primary antibody binding blocked with BSA and the free ends of the steps to be included. After this containing the solution of PSA in different concentrations applied to the surface of the electrode and electrode was incubated for 1 h. Finally, the separately prepared solution of NDA-Fe_3O_4-TH-HRP-Ab_2 drops was measured. Because of HRP with a weak signal, Fe_3O_4 particles increased signal and shown better conductivity in this system. NDA can increase the loading of antibody and HRP has a positive effect on signal. NDA-Fe_3O_4 formation on the surface of the electrode, CV datas also shows that because of attachment the peak would give successfuly. Looking at the performance level of immunosensor, 4mM allows the determination of peroxide. This is accomplished to the use of TS as the mediator. NDA-Fe_3O_4 and Fe_3O_4 was prepared with the control experiment, two NDA conjugates shown better measurement limit than 5 times. This method is similar to the methods(Qu et al., 2008; Chikkaveeraiah et al., 2009, Yu et al., 2006, Liu et al., 2007) compared with measurements carried out have proven much more sensitive. The linear detection limit for PSA was in the range of 0,005 to 50 ng / ml. These values fall into the range where the normal human values(Lilja et al., 2008). Sensitivity determination of immunosensor; IgG, BSA, α-1-fetoprotein (AFP) and glucose 8% of the trials showed less interference. Repeatability and reproducibility studies showed for this immunosensor that acceptable.

Yang et al. developed ultrasensitive immunosensor which is modified with a layer of graphene. Graphene layers are 2-dimensional structures with high surface area material that provides excellent conductivity and stability is described in previous studies. Graphene layers for this study is to make the system more sensitive to both the primary antibody immobilization and secondary antibodies. Primary antibody immobilization of the 1-pyrenebutanoic acid adsorbed on graphene layers have been immobilized by using sucsinimidyl esters. π-π stacked with the primary antibody attached to the graphene layers on the suksinimidyl esters. In graphene layers of graphite oxide was prepared by the method of thermal extrafolation(McAllister et al., 2007). Secondary antibody binding stage on graphene layers are mixed with thionine by glutaraldeyde to built TH conjugates formed

with the active aldehyde residues, on top of them are bond HRP and anti-PSA via aldehyde. Primary antibodies were adsorbed on the graphene-1-pyrenebutanoic acid; esters sucsinimdyl graphene layers are created with non-specific binding of BSA. This structure is attached to the PSA is about to be immobilized on the GCE, and lastly a conjugate addition of secondary antibodies were measured by sandwich method. CV scans showed that the addition of thionine to facilitate the electron transfer effect. According to Yang et al. there are three reasons for this immunosensor for showing high sensitivity, this can be high because it is a large amount of surface area of graphene layers with the binding of HRP and TH increased signal, HRP showed high catalytic activity and electron transport in graphene layers used for the increasing effect of mediator between the TS of the peroxide with HRP. Catalytic reaction occurs, the current increases linearly. Linear measurement of PSA concentration in the range 0.002 to 10 ng / mL were determined, lower determination limit is 1 pg / ml, respectively. The obtained values showed a normal human and cancer patients fall into a range of standard values(Lilja et al., 2008). Depending on the sensitivity of the use of graphite oxide is used as the GS immunosensor 100 times faster than that observed. Children showed a narrower measure by graphite oxide is 0.2 to 2 ng / ml. TH provided the reasons for this stability in the long time molecule layer on the graphene π-π jam with increased stability of immunosensor, the secondary antibody and HRP on the GS in the covalent bonding increases stability. As a result, stability and conductivity of nanomaterials used in this study for the immobilization of molecules led to the introduction of ultra-sensitive immunosensors.

According to Yang et al. developed another quantum dot functionalized graphene layers as a label by the employed for electrochemical immunosensor systems. Graphene layers wide surface/volume ratio is preferred because of the reasons stated in previous studies(Liu et al., 2010, Wu et al., 2010). Graphene layer immobilization of the study, the primary antibodies and secondary antibodies, QD functionalized graphene sheets are used for labeling. Designed of immunosensor on graphene layers of graphite oxide were prepared by the method of thermal extrafolation(McAllister et al., 2007). GS-QD-AB_2 conjugates to be done; QD $CdCl_2$ solution preparation stage in the mixed acid solution mercaptoundecanoik acid and Cd^{2+} GS functionalized layer was created. Onto this conjugation Na_2S solution added when the CdS (QD) funtionalized GS consists of layers. Activated by NHS / EDC with secondary antibody that was prepared by adding layers of anti-PSA-QD conjugate to GS-formed. GS primary antibody reaction with the surface of the PBSE based amidation succinimidyl esters of secondary antibodies were carried out the immobilization via amine groups. BSA was used to block non-specific interactions. Secondary antibodies then bond to the PSA solution which was prepared after the electrode surface by applying the electrochemical measurement were ready. Having a large surface area of the GS with a lot of QD increased sensitivity. Electrochemical measurement principle depends on the determination of cadmium release from the system. PSA to be determined as a linear concentration range 0005 to 10 ng / ml, the lower limit of determination at 3 pg / ml. With low limits and Cd^{2+} ions to determine the QDS functionalized graphene layer is based on the determination by showing good conductivity. Graphene oxide layer was prepared with 50 times more sensitive than other immunosensor system. Repeatability of the electrode as the experiments was 7.9% RSD value. Selectivity studies, human IgG, BSA, lysozyme and glucose molecules are showing on the initiative of the experiments, the signal has changed by 7%. Additionally, the accuracy of this immunosensor showed that good correlation with ELISA tests. In table 4, a summary for biosensors developed for detection of PSA is given below.

Table Of Electrochemical Transducers For Detection Of PSA				
Measurement Technique	Immobilization Technique	Low Detection Limit	Lineer Detection Limit	Reference
Immunochromatographic and Electrochemical	anti-PSA-QD/nitrocellulose membranes	0.02 ng/mL	0.05 to 4 ng/mL	Lin et al., 2011
Amperometric	Au-Fe_3O_4-AB_2/PSA/GC	5pg/mL	0.01 to 10 ng / mL	Wei et al., 2010
Amperometric	anti-PSA/ PNA/GOx/MPA/MicroArray	10pg/mL	4 to 10ng/mL	Triroj et al., 2011
Amperometric	anti-PSA-ALP/Cys/AuElectrode	0.76 ng/mL	1 to 35 ng/mL	Qu et al., 2008
Amperometric	NDA-Fe_3O_4-TH-HRP-Ab_2	0,005ng/mL	0,005 to 50 ng/mL	Li et al., 2011
Amperometric	Anti-PSA/HRP-TH/PBA/GC	1 pg/mL	0.2 to 2 ng/mL	Yang et al., 2010
Conductance	GS-QD-anti-PSA	3 pg/ml	0005 to 10 ng/mL	Yang et al., 2010

Table 4. Electochemical Immunosensors developed for Detection of PSA

3.1.6 Electrochemical immunosensors developed for the determination of VEGF

Vascular endothelial growth factor has an important role in tumor growth and a biomarker metastas. Inordinate amount of time metastasis of VEGF that is structure containing five glycoprotein and synthesized large amounts(Augustin et al., 2009). Receptor binding as a result of this biomarker of endothelial cells in tissue secreted the excitation function with cascade mechanism(Kranz et al., 1999; Kurebayashi et al., 1999; Ruohola et al., 1999, Zhai et al., 1999). Rapid proliferation of tumor cells to increased amount of VEGF production. Lung, thyroid, breast, gastrointestinal system, kidney and bladder cancer was observed when production increases (Ferrara and Davis-Smyth, 1997).

Prabhulkar et al. developed an amperometric immunosensors system for the determination of VEGF. Unfortunately, most of the signal can not be given by non-electroactive biomarker, for this reason the use of a marker and a further reaction must be performed by measurement. Developed in the measurement of VEGF in this system with ferrocene monocarboxylic acid used for labeling, ferrocene monocarboxylic acid was measured by using its well known electrochemical properties(Zhang et al., 2008). Ferrocene monocarboxylic acid is not given intermediate product of a molecule that can be determined by creating fast voltammetric techniques which are very useful. In this study, the carbon fiber electrode with high sensitivity, high S / N ratio and increasing the mass transport is preferred due to the its good properties. In addition, this type of in-vivo measurements paves the way for the use of electrodes. Prepared carbon fiber electrode reported(Ates et al.,

2008). 4V immersed in the solution containing the carbon fiber electrode potential under alylphenol for isolation(Strein and Ewing, 1992). Fc-conjugates of anti-VEGF; first Fc dissolved in the buffer, after activated the NHS / EDC and treated anti-VEGF(Lim and Matsunaga, 2001). Carbon fiber electrode modification on the mapping carboxylic acid is a bifunctional linker was used(Jeffamine). The advantage of using immobilized antibodies bind to the effect of Jeffamine was more effective than other linkers(Cao et al., 2007). Immobilized antigen-antibody regulation also allows you to fine orientation. Thus, Fc-derived anti-VEGF was immobilized on the electrode surface. Surface characterization was confirmed by SEM scans. Immobilizations are determined by electrochemical CV data. Stabilization of covalently immobilized on the surface of the electrode increased. Incubation time and amount of anti-VEGF are two major factors in the study. Carbon fiber electrode surface, a maximum of 50 to 750 pg / ml antibody binds to the Fc-immobilized with anti-VEGF; this value rises to 800pg/mL. Lower limit of determination of VEGF 38 pg / ml, respectively. The maximum value of RSD 8.9%. Specificity studies of this immunosensor was carried out with IgG and did not give an important signal.

Kim et al. developed for the determination of VEGF in another study, indium tin oxide layer on the metal nanoparticles electrochemical measurement system. Recently metal nanoparticles on biosensor technology with immobilized electrodes are used widely. In this study, AuNPs / ITO electrode modified with the VEGF level was measured. AuNPs primarily prepared in accordance with the protocol developed by Kumar et al.(Kumar et al., 2008). Then attached to the surface of the electrode modified with AuNPs by APTES(Seiwert et al., 2008). ITO electrode modified with AuNPs of VEGF after treatment were immersed in a solution of BSA to prevent non-specific binding. VEGF gold nanoparticles were covalently modified with thiol groups to connect to the 2-MEA was obtained to be rendered. This is anchored on thiol groups of VEGF with sorrowful AuNPs VEGFantibodyfragment / AuNPs / APTES / ITO modified electrode formed. Fc-fragments of anti-VEGF prepared after modification is as follows: Fc condition with anti-VEGF conjugate formed through the activation of the anhydride(Kossek et al., 1996). This conjugate was prepared by applying the modified electrode surface was measured. One of the important points of the steps of immobilization induced by 2-MEA that is the process of purification of fragments. Electrochemical analysis of measurement systems used in the CV and DPV. Lower determination limit was determined as 100pg/mL. Table 5 shows voltammetric based immunosensors for PSA.

Table Of Electrochemical Transducers For Detection Of PSA				
Measurement Technique	Immobilization Technique	Low Detection Limit	Lineer Detection Limit	Reference
Voltammetric	Fc-derived-anti-VEGF /Jeffamine/CFE	38 pg/mL	50 to 750 pg/mL	Prabhulkar et al., 2009
Voltammetric	AuNPs/VEGFantibodyfragment/ AuNPs /APTES/ITO modified electrode	100 pg/mL	100 to 600 pg/mL	Kim et al., 2009

Table 5. Voltammetric Immunosensors For Detection of PSA

3.2 Optic transducers

Especially in the field of optical transducers; fluorescence, inferometry, optical wave spectroscopy, and surface plasmon rezonance used in sensor systems(Tothill, 2009). Usually the light emissions of fluorescence signal to realize biocomponents, QD etc. are used to create the signaling molecules. Especially in recent days at the molecular level without need to label the SPR technology allows the immunochemical analysis. Determination was carried out in very specific, allowing real-time analysis(Keusgen, 2002, Yang et al., 2005; Vaisocherova et al., 2007). Nanocrystals are used for labeling luminescent molecules for molecular and cellular imaging(Maxwell et al., 2002; Gerion et al., 2001; Gerion et al., 2002, Kim et al., 2004).

3.2.1 Development of the optical Immunosensors for the determination of AFP

Bi et al. developed for the determination of biomarker AFP multilayer enzyme-coated ultrasensitive chemiluminescent immunoassay system. In this system, the carbon nanaotubes are used for immobilization material. Besides the high stability and luminescence properties of the surface area of carbon nanotubes in the winning offers impressive features(Sumpter et al., 2008, Shen et al., 2004; Tasis et al., 2006). The study functionalize carbon nanotubes with carboxyl groups can be treated primarily by acid, and they were now ready for immobilization(Mung et al., 2005). On the carboxyl groups formed on the MWCNT then coated with PDDA. The positively charged PDDA was immobilized on the negatively charged HRP (HRP / PDDA) n / MWCNT multilayer structure of the enzyme were continued several times in this study by creating layered system formed. HRP immobilized on the PDDA-MWCNT after the negatively charged PSS adsrobe on this structure on the then secondary AFP antibodies were added and MWCNT-(PDDA / HRP)$_4$-PDDA/PSS-Ab$_2$ modification prepared. MBs with the primary antibody conjugated with the method have been developed by the Imato and colleagues (Zhang et al., 2007a, b). LBL films as a result of sandwich type immuno complex, depending on the enzyme activity by measuring the permeability values of the system. In this system, the amount of 1ng/mL was determined at the level of AFP. AFP linear measurement is between 0.02 to 2 ng / ml. A successful realization of the system as a result of the signal by increasing the light interaction with the CNT-LBL bio pointer by measuring the high sensitivity, good accuracy and operational stability as a result offers the possibility to analyze very large amounts.

3.2.2 Immunosensors based SPR for detection of CRP

CRP, a biomarker, is very well known. As mentioned in previous sections of early diagnosis is extremely important. Meyer et al. developed to allow different samples to be analyzed in combination with SPR sensor technology. SPR is an optical instrument and proteins, binding of antigen and antibodies used in monitoring processes. The biggest advantage of up to eight analyte by a measurement provides for a shorter time(Meyer et al., 2006). In this study, the biotin-coated gold electrodes used with a layer of APTES(Davidson et al., 2004; Phadtare et al, 2004; Yakovleva et al., 2003), thus creating an amino surface with biotin-NHS match ends formed. On this layer and biotinylated streptavidin antibody(Milka et al., 2000) on the application of CRP measurement was carried out by applying the secondary antibody. K_{dis}, antigen-antibody method, the values can be determined easily. For this purpose, Edwards and Leatherbarrow method(1997) was used. BSA is used to prevent non-specific binding of the system. Whether the application shows a significant increase in signal for 1µg/mL

example. In this case, the signal has been more than 4 times the noise and the lower limit of determination. Dynamic and linear measuring range 2 mg / ml to 5 mg / mL were determined. SPR sensor was developed in two different CRP antibody (C2 and C6) have the possibility of measurement separately. SPR sensor, two different epitope of these two biomolecule identification of features of the high specificity can be determined. Designed using the most important feature of the SPR biosensor is that has no limitations, such as ELISA, sample color, origin, or allow the possibility of measurement can yield without affecting the matrix.

3.2.3 SPR based biosensors developed for determination of CEA

Ladd et al. developed SPR-based measurement system for direct determination of CEA. As is known in real-time SPR, and do not need to label the quantitative determination of biomolecules is a measurement technique that allows each opportunity. Cancer diagnosis is very important in the early diagnosis offers the possibility to analyze. In this study the clone ovarian cancer in terms of levels of anti-CEA levels were used to determine by SPR sensor. In order to verify the measurement system, the data obtained from samples were confirmed by ELISA. The sensor is based on the measurement of total reflectance method(Boozer et al., 2004, Ladd et al., 2004). Polychromatic light source, optical prism reflecting light rays emitted from a thin metal layer after the reflected rays fall on the four independently collected by the spectrophotometer so that allows you to create 4 different measurement channels. In this study, 2nm thick Cr and 55nm thick gold electrode surface is covered electron beam evaporation. After cleaning the electrode surface with UV COOH-oligoetilenglikol: PGP solution is created with the SAM. Functionalized with COOH groups on the SAM layer, activated NHS / EDC and proteins were immobilized. After this process was the determination of CEA antibody in serum samples were applied to the electrode surface by the flow system. In the second sample solution containing the secondary antibodies anti-human IgG-HRP conjugate was applied. Compared with the ELISA method for direct analysis of the SPR signal of study of molecules has a higher response. ELISA and SPR studies that there are two different cases of non-specific binding Ladd et al. determinism which causes the application of surface chemistry and the sample. Surface modification and protein immobilization of the SPR and ELISA is shown by the many differences. SPR analysis of CEA as a result the basic purpose of this study consisted of developing immunosensor and ELISA tests for confirmation of the results of CEA was measured directly.

3.2.4 SPR based biosensors developed for determination of HER-2

Gohring et al. developed very different system for the determination of HER-2 for the diagnosis of breast cancer, opto-fluidic biosensor system using the ring resonator. As is known, the most common cancer among women is breast cancer, only 200,000 women in the USA affected by breast cancer(Cheng et al., 2009; Lippman, 2008; Jemal et al., 2006). The early diagnosis of cancer in recent years to study protein basis biomarkers the most widely used on the issue(Kearney and Murray, 2008; Gullick, 2001). Excessive secretion of growth factor receptor in human epidermis occurs during breast cancer. HER-2 levels in healthy people are between 2 to 15 ng/mL, sick people are between the 15 to 75ng/mL(Capobianco et al, 2008). For this reason, the quantitative detection of biomarkers need to be fast and responsive. Ring resonator was used for analysis in this study, thin high-Q ring resonator on

microfluidic system used to support the capillary walls. In this experiment by heating the desired radius under OFRRs silica glass door until it pulled carbon dioxide laser has been extended to increase the sensitivity of HF were treated with less than 3µm around to 5µm thickness were produced(White and Oveys, 2006, Zhu et al., 2008, White et al ., 2008). Interact with light in a fiber ring connecting the cable OFRR resonance, known as whispering gallery mode(WGM) creates. 1550nm laser diode used in this experiment can be adjusted in length (Fig. 3).

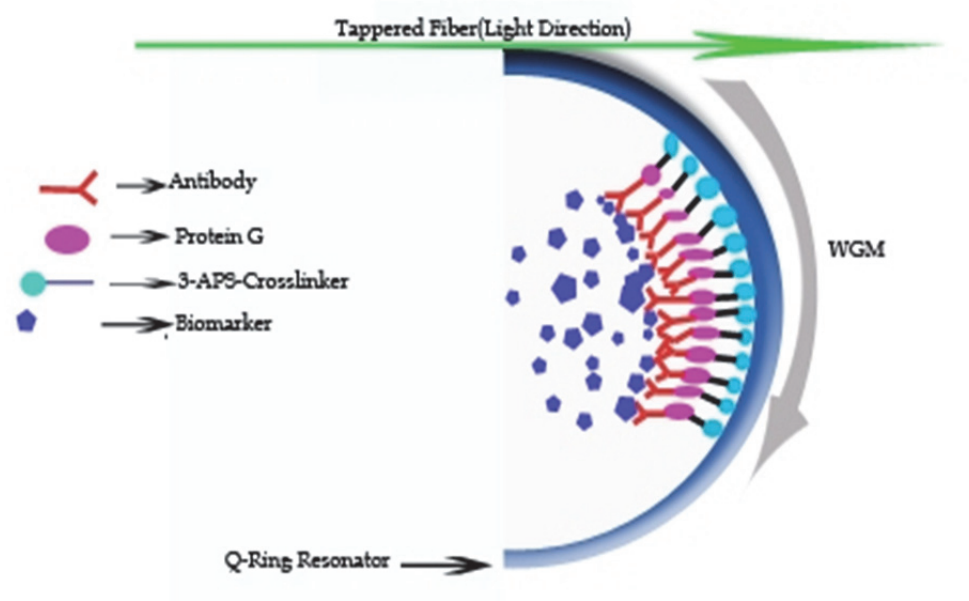

Fig. 3. A schematic representation of AFP sensing by a microfluidic immunosensor system

Nanometer size of measurement unit as a measure of sensitivity to OFRR each diffraction measurement of the index unit (RUI). OFRR inner surface (Fig. 3) the preparation should be modified to show the great sensitivity with small concentrations. First of all HF from the surface through the surface will be loaded. Then, the surface layer of 3-APS is obtained by passing an aminosilan. After passing through the DMP, then the creation of a layer of cross-linking of recombinant protein G immobilized on aminosilan surface, immobilization of this protein, the G antibodies provided orientation. In order to prevent non-specific binding, casein was used in blocking agent. HER2 biomarker 13, 16, 20, 25, 33, 50, 75, 100 and 250 ng / ml, all experiments were completed in 30 minutes, the ring was cleaned after each use with the HF. Casein-bound or loosely linked with HER2 after treatment with antibodies were to remove the casein solution from the system. This is a specially designed syringe pump is used for transactions. Lower determination of limit is 10ng/mL. 0.3pm is observed as a negative shift of the shift measurements, the sample is applied, showed that 4.5 pm shift. The only disadvantage of the system haven't been found better biomolecule to prevent non-specific binding of system. Conclusion Gohring et al. by responding to the rapid, sensitive and reproducible system was developed quickly.

3.3 Piezoelectric transducers

Hereinafter piezoelectric quartz crystals to provide mass to hear the transducers unlabeled measurements and the electrode on the surface of the gold-coated sensors are designed using the small mass changes depending on the measurement of change are based on the crystal resonance differences(Sullivan and Guilbault, 1999). Label was using a variety of recently developed systems for QCM immunosensors(Kurosawa et al., 2004, McBride and Cooper, 2008). QCM sensors, the biggest disadvantage of solution matrix applied to any kind of analyte.

3.3.1 QCM based biosensors developed for determination of CRP

Kim et al. QCM-based indirect competitive immunosensor systems developed for the determination of CRP. In this system, an indirect competitive QCM immunosensor system (IC) as the startup process as a monoclonal anti-CRP antibody was immobilized and was measured in serum biomarkers. Transducer in the system for measuring the surface has been prepared according to the method developed by Park and Kim (Park and Kim, 1998). QCM surface was treated separately, first sodym hydroxide and hydrochloric acid. The sensor surface is covered with sulfo-LC-SPDP is prepared for immobilization of antigen to be taken as a result of previous studies that suggested the best sensitivity (Park and Kim, 1998). Mixed with sulfo-LC-SPDP dithioeritrol CRA and CRP reacted with the latest sensor QCM gold electrode surface was prepared by treatment. High ionic strength was chosen to minimize the false positive signal and time of CRP measurement(Kim et al., 2004). In this study, a relatively high concentration of immobilized antigen-antibody binding and measurement is good. After that, the sensor response to an antigen-antibody interaction is between 0010 to 0.5 mg / mL antibody concentration was determined. Specificity studies with BSA bind to the surface of the sensor, almost no binding was observed with BSA. 0,130 to 25,016, depending on the time sensitivity of the sensor were examined ng / mL, in a linear range to be determined. IC, according to the response of the sensor decreases with increasing concentration of CRP (Hamalek et al., 2002; Adanyi et al., 2007). Prepared by the same enzyme system in the 0.3 ng / mL lower limit determined in this study, moreover, a close 87fM validation coefficient was calculated as 0.9893.

Kim et al. Immunosensors QCM gold nanoparticle-based systems have developed that increase the signal. In this study with the help of AuNPs the signal was amplified significantly. Streptavidin-coated gold nanoparticlws complexation of antigen antibody was measured by the IC assay format. Anti-CRP buffer by dissolving into the sulpho-NHS-LC-biotin was carried out by adding antibodies. QCM surface, hydro-chloric acid and sodium hydroxide in a separate location after being treated with sulpho-LC-SPDP to conjugate CEA was created by mixing the solution after the mixture was incubated with dithioeritrol tihol groups that hosts on the conjugated CRP, QCM was immobilized on the drops. Established a system of micro-flow system with the help of dispersing peristalsis sample pump is smart. At this point the resonance frequency was obtained from stationary phase. After a series of solution containing biotinylated that anti-CRP applied to 0.1pM between 0.53nM. According to the obtained resonance shift and bonded CRP measurement was carried out by the changes resulting from the resonance shift observed. In this study, performance of immunosensor is increased with the implementation of the nanomaterials. As for the sensitivity of the system on chip, 2 mg / mL antigen coated, biotinilated and competitive reaction between the free CRP, decreased concentration brings increased differentiation frequency (Halamek et al., 2002). Accordingly, the relative rate of antibody binding

decreases. These values indicate that antibodies bound on AuNPs attached with a mass deposition. According to the data being compared with the control value obtained by adding the shift 1pm shift control measurement of CRP is less than that observed. Based on this data to determine the lower limit is determined as 0.1pM. AuNPs on the surface have increased the sensitivity of the sensor. This method is more sensitive compared with other measurement methods based on related data have shown that (Meyer et al., 2002, Meyer et al., 2007; Vikholm-Lundin et al., 2006). 87fM be determined until this study, low-range signal. Verification of the system is determined as coefficient of 0.9796. Thus, the use of modified antibodies with increased sensitivity of the IC immunosensor QCM decreased to low levels of CRP measurement limits. Table 6 summarizes immunosensors based QCM for CRP detection.

Table Of QCM Transducers For Detection Of CRP				
Measurement Technique	Immobilization Technique	Low Detection Limit	Lineer Detection Limit	Reference
QCM	CRP/DTHE/sulfo-LC-SPDP/QCM	0.3 ng / mL (87fM)	0010 to 0.5 mg/mL	Kim et al., 2010
QCM	Anti-CRP/sulpho-NHS-LC-biotin/QCM	2 mg / mL (0.1pM)	0.1pM to 0.53nM	Kim et al., 2009

Table 6. QCM Immunosensor For Detection Limits Of CRP

3.3.2 QCM based biosensors developed for determination of PSA

Another study using the QCM Immunosensors Uludağ and Tothill developed an immunosensor based on the measurement of the amount of PSA using nanoparticles in human serum (75%). As is well known that is important early diagnosis of cancer which death rate among men with prostate cancer is known to be high, and confirmed by the WHO datas(Panini et al., 2008). In this study, a simple and rapid determination of the PSA is designed to carry out the QCM biosensor. As is well known among the QCM contains two electrode in a couple of thin layers of quartz (wafer). Mass loss or a mass connected to the surface by measuring the change in frequency allows the analysis. Although the analyte solution, the viscosity of the system are affected in the determination of the serum samples were carried out on the biomarker in this study. To minimize the matrix effect; the detergent, salt and other substances were used to measure the PSA and PSA-ACT complex. First, gold nanoparticles formed, were treated with anti-PSA conjugate. After the QCM gold disc for the purpose of the creation of a MUA SAM layer is covered with all night long. After NHS / EDC activation with anti-PSA and on the SAM-coated chip for controlling the flow rate used in the IgG molecule 80µl/min to be applied. Connecting to BSA and ethanolamine were used to block the non-active carboxyl groups. Frequency measurement was carried out in two minutes after the injection of proteins. PSA complex in serum is in conjunction with the ACT. This is a combination of two molecules by the presence of total PSA (tPSA) can be quantified. In this study, accurate measurement of this complex due to the mixing ratio of 1:1 was used PSA and PSA-ACT complex. After this process of IgG binding to the anti-PSA and then to 380 and 520 Hz frequency change of the order have

been observed. BSA surface with no frequency change is observed during the application of surface blocked were good in terms of measurement. PSA is given to the method of Sandwich, first applied to the surface of the electrode only sample of anti-PSA in 5Hz frequency change was recorded accordingly. Linear measurement range of the experiments with PSA 2.3 to 150 ng / mL was determined. With this method, sandwich method to determine, direct determination limit is more sensitive 4 times. As is well known for quartz disk viscosity is affected when applied to the buffer and serum samples showed different results. Sample is applied to determine the lower limit of 10% serum containing 10.2 ng / ml to 18.1 ng /ml. Non-specific binding of carboxymethyl dextran is used to prevent non-specific binding of the surface decreased by 88% (Choi et al., 2006, Yin et al., 2005). In this study, experiments in human serum with 75% diluation as a result of the realization of the measurement process as a linear 150ng/mL hesaplanmıı 100% to determine the serum ratio of 0:29 was determined as the 0.39ng/mL. In this study, the rate of change in the measurement of serum with additives will be examined and analyzed by 98% of non-specific binding of different additives were crossed in front.

4. Conclusion

It is vitally important to diagnose cancer early for treatment patients succesfully. Consequently there will always be a need to develop more sensitive, economical, and simple diagnostic biosensors because new cancer biomarkers are discovered continuously. Biosensors have the potentiality to diagnose cancer sensitively, simply, and economically. Unfortunatelly the biosensor based measurement systems need to be further developed to use these devices in analyzing of many cancer biomarkers simultaneously. Consequently, as a future prospestive, biosensor technology should gear to adapt these systems for multi target analysis by the help of microfluidics technologies. Beside using of the newly discovered nanomaterials in the development of biosensors can increase the sensitivity and selectivity of these devices.

5. References

Achim, C.; Shi, H.; Yeh, J.I. (2009) March 5. Biosensors and related methods. United States patent application US 2009/0061451.

Adányi, N.; Levkovets, I.A.; Rodriguez-Gil, S.; Ronald, A.; Váradi, M.; Szendro I. (2007) Development of immunosensor based on OWLS technique for determining Aflatoxin B1 and Ochratoxin A, Biosens. Bioelectron. 22, 797–802.

Aleiner, I.L.; Efetov, K.B.; (2006) Effect of Disorder on Transport in Graphene, Physical Review Letters 97:2323, 236801, American Physical Society, 12.

Andrey, L.G.; Plamen, A.; Michael, W.; Ebtisam, W.; (1998). Immunosensor: electrochemical sensing and other engineering approaches. Biosens. Bioelectron. 13, 113.

Antosiewicz, J. (1995). Computation of the dipole moments of proteins ,Biophysical Journal, 69, 4, 1344-1354

Armstrong, F.A.; (2005) Recent developments in dynamic electrochemical studies of adsorbed enzymes and their active sites, Current Opinion in Chemical Biology, 9, 2, 110-117

Ates, M.; Sarac, A.; Sezai; Wolfgang S.; (2008) Carbon fiber microelectrodes electrocoated with polycarbazole and poly(carbazole-co-p-tolylsulfonyl pyrrole) films for the detection of dopamine in presence of ascorbic acid, 160, 1-2, pp.247 251.

Augustin, H.G.; Koh, G.Y.; Thurston, G.; Alitalo. (2009) Control of vascular morphogenesis and homeostasis through the angiopoietin-Tie system. Nat Rev Mol Cell Biol 10:165-77. B. Haghighi, S. Varma, F.M.Alizadeh,Y. Yigzaw, L. Gorton, Prussian bluemodified glassy carbon electrodes—study on operational stability and its application as a sucrose biosensor, Talanta 64 pp. 3–12.

Babya, T.T.; Aravinda, S.S.J.; Arockiadossa, T.; Rakhia, R.B.; Ramaprabhu, S. (2010). Metal decorated graphene nanosheets as immobilization matrix for amperometric glucose biosensor, Sens. Actuators B: Chem. 145 71–77.

Bain, C.D.; Troughton, E.B.; Tao, Y.T.; Evall, J.; Whitesides, G.M.; Nuzzo, R.G.; (1989). Formation of monolayer films by the spontaneous assembly of organic thiols from solution onto gold, Journal of the American Chemical Society, 111,321–335.,

Barbora, M.; Samuele, T.; Marcus, T.; Karl, G.; Stefan, Z. (2010). "Poly(ethylene glycol) Adlayers Immobilized to Metal Oxide Substrates Through Catechol Derivatives: Influence of Assembly Conditions on Formation and Stability"., Langmuir, 26 (6), 4018–4026.

Bartsch, R.A.; Maeda, M. (1998) Molecular and Ionic Recognition with Imprinted Polymers, American Chemical Society, Washington, DC.

Baschong, W; Stierhof, Y.D. (1998) Preparation, use, and enlargement of ultrasmall gold particles in immunoelectron microscopy. Microsc Res Tech. 42:66-79.

Bauer, C.G.; Eremenko, A.V.; Ehrentreich-Forster, E.; Bier, F.F.; Makower, A.; Halsall, H.B.; Heineman, W.R.; Scheller, F.W. (1996). Zeptomole-detecting biosensor for alkaline phosphatase in an electrochemical immunoassay for 2,4- dichlorophenoxyacetic acid, Anal. Chem., 68, 2453–2458.

Belinsky, S.A. (2004) Gene-promoter hypermethylation as a biomarker in lung cancer. Cancer ;4,1-11

Benchimol, S.; Fuks, A.; Jothy, S.; Beauchemin, N.; Shirota, K.; Stanners, C.P. (1989). Carcinoembryonic antigen, a human tumor marker, functions as an intercellular adhesion molecule Cell, 57, 2, 327-334

Benson, M.C.; Whang, I.S.; Olsson, C.A.; Mcmahon, D.J.; Cooner, W.H. (1992). The use of PSA density to enhance the predictive value of intermediate levels of serum PSA. Journal Of Urology 147, 817–821.

Bi, S.; Zhou, H.; Zhang, S.S. (2009). Multilayers enzyme-coated carbon nanotubes as bio-label for ultrasensitive chemiluminescence immunoassay of cancer biomarker, Biosens. Bioelectron. 24, 2961–2966.

Bienvenue, J.M.; Duncalf, N.; Marchiarullo, D.; Ferrance, J.P.; Landers, J.P. (2006). Microchip-based cell lysis and DNA extraction from sperm cells for application to forensic analysis. J. Forensic Sci. 51, 266-273.

Boehm, M.K.; Mayans, M.O.; Thornton, J.D.; Begent, R.H.J.; Keep, P.A.; Perkins, S.J. (1996). Extended glycoprotein structure of the seven domains in human carcinoembryonic antigen by X-ray and neutron solution scattering and an automated curve fitting

procedure: implications for cellular adhesion, Journal of Molecular Biology. 259, 718–736.

Boozer, C.; Ladd, J.; Chen, S.F.; Yu, Q.; Homola, J.; Jiang, S.Y. (2004) DNA directed protein immobilization on mixed ssDNA/oligo(ethylene glycol) self-assembled monolayers for sensitive biosensors, Analytical Chemistry, 76, 6967–6972.

Bradford, T.J.; Tomlins, S.A.;Wang, X.J.(2006). Chinnaiyan, A.M., Molecular markers of prostate cancer. Urol. Oncol-Semin. Ori. Inves., 24, 538–551.

Brawer, M.K., (1999). Prostate-specific antigen: current status. CA Cancer J. Clin., 49, 264–281.

Brayer, G.D.; Luo, Y.G.; Withers, S.G. (1995). The structure of human pancreatic alphaamylase at 1.8 angstrom resolution and comparisons with related enzymes, Protein Science, 4, 1730–1742.

Capobianco, J.A.; Shih, W.Y.; Yuan, Q.; Adams, G.P.; Shih, W. (2008). Label-free, allelectrical, in situ human epidermal growth receptor 2 detection, Rev. Sci. Instrum., 79, 076101.

Carrara, S.; Bhalla, V.; Stagni, C.; Benini, L.; Ferretti, A.; Valle, F.; Gallotta, A.; Ricco, B.; Samori, B.; (2009). Sens. Actuator B: Chem., 136 (1), 163–172.

Celestino, P.; Grubelnik, A.; Tiefenauer, L. (2000). Ferrocene–avidin conjugates for bioelectrochemical applications., Biosensors & Bioelectronics, 15, 431–438

Cello, J.; Paul, A.V.; Wimmer, E. (2002) Chemical synthesis of poliovirus cDNA: generation of infectious virus in the absence of natural template, Science, 297, 1016–1018.

César Fernández-Sánchez, Ana M. Gallardo-Soto, Keith Rawson, Olle Nilsson and Calum J. McNeil. Quantitative impedimetric immunosensor for free and total prostate specific antigen based on a lateral flow assay format., Electrochemistry Communications, Volume 6, Issue 2, February 2004, Pages 138-143

Cheng, H. D.; Shan, J.; Ju, W.; Guo, Y.; Zhang, L. (2009) Automated breast cancer detection and classification using ultrasound images: a survey, Pattern Recogn., 43, 299–317.

Cheng, H.D.; Shan, J.; Ju, W.; Guo, Y.; Zhang, L. (2009) Automated breast cancer detection and classification using ultrasound images: a survey, Pattern Recogn., 43, 299–317.

Cheng, L.; Pacey, G.E.; Cox, J.A.; (2001). Carbon electrodes modified with ruthenium metallodendrimer multilayers for the mediated oxidation of methionine and insulin at physiological Ph. Anal. Chem., 73, 5607–5610.

Chikkaveeraiah, B.V.; Bhaskara, V.C.; Bhirde, A.; Malhotra, R.; Patel, V.; Gutkind, J.S.; Bhirde, A.; Malhotra, R.; Patel, V.; Gutkind, J.S. and Rusling, J.F. (2009) Single-wall carbon nanotube forest arrays for immunoelectrochemical measurement of four protein biomarkers for prostate cancer, Anal Chem, 81: 9129-9134.

Choi, J.W.; Kang, D.; Jang, Y.H.; Kim, H.H.; Min, J.; Oh, B.K. (2008) Ultra-sensitive surface plasmon resonance based immunosensor for prostate-specific antigen using gold nanoparticle–antibody complex., Colloids and Surfaces A: Physicochemical and Engineering Aspects, 313-314, 655-659.

Choi, J.W.; Kim, Y.K.; Kim, H.J.; Lee, W.; Seong, G.H. (2006) Lab on a Chip for monitoring the quality of raw milk, J. Microbiol. Biotechnol., 16, 1229–1235.

Choi, J.-W.; Oh, K.W.; Thomas, J. H.; Heineman, W. R.; Halsall, H. B.; Nevin, J. H.; Helmicki, Henderson H. T. and Ahn C. H., (2002) "An integrated microfluidic biochemical

detection system for protein analysis with magnetic bead-based sampling capabilities," Lab Chip, 2, 27–30, (5.821).

Corso, C.D.; Stubbs, D.D.; Lee, S.; Goggins, M.; Hruban, R.; Hunt, W.D. (2006) Real-time detection of mesothelin in pancreatic cancer cell line supernatant using an acoustic wave immunosensor Cancer Detection and Prevention, 30, 180–187.

Cram, D.J. (1988). The design of molecular hosts, guests, and their complexes (Nobel lecture), Angewandte Chemie-International Edition in English, 27, 1009–1020.

Dai, Z.; Yan, F.; Yu, H.; Hu, X.; Ju, H. (2004). Novel amperometric immunosensor for rapid separation-free immunoassay of carcinoembryonic antigen. Journal of Immunological Methods, 287, 1-2, 13-20.

Darain, F.; Park, D.-S.; Park, J.-S.; Chang, S.-C.; Shim, Y.-B. (2005).A separation-free amperometric immunosensor for vitellogenin based on screen-printed carbon arrays modified with a conductive polymer Biosens. Bioelectron, 20, 1780–1787

Davidsson, R.; Genin, F.; Bengtsson, M.; Laurell, T.; Emneus, J.; (2004). Microfluidic biosensing systems. Part I. Development and optimisation of enzymatic chemiluminescent micro-biosensors based on silicon microchips. Lab Chip 5, 481–487.

de Vasconcelos, E.A.; Peres, N.G.; Pereira, C.O.; da Silva, V.L.; da Silva, E.F. Jr.; Dutra, R.F. (2009) Potential of a simplified measurement scheme and device structure for a low cost label-free point-of-care capacitive biosensor. Biosens Bioelectron.,25, 4, 870-6

Downard, A.J.; Mohamed, A.B.; (1999). Suppression of protein adsorption at glassy carbon electrodes covalently modified with tetraethylene glycol diamine. Electroanalysis 11, 418– 423.

Du, D.; Zou, Z.X.; Shin, Y.S.; Wang, J.; Wu, H.; Engelhard, M.H.; Liu, J.; Aksay, I.A.; Lin, Y.H. (2010). "Sensitive Immunosensor for Cancer Biomarker Based on Dual Signal Amplification Strategy of Graphene Sheets and Multienzyme Functionalized Carbon Nanospheres," Anal. Chem. 82, 2989-2995

Duffy, M.J. (2001). Carcinoembryonic antigen as a marker for colorectal cancer: is it clinically useful, Clinical Chemistry 47, 624–630.

Dumitrescu, I.; Unwin, P.; MacPherson, J. (2009) Electrochemistry at carbon nanotubes: perspective and issues, Chem. Commun., 45, 6886–6901.

Edwards, P.R.; Leatherbarrow, R.J.; (1997). Determination of association rate constants by an optical biosensor using initial rate analysis. Anal. Biochem. 246, 1–6.

Ferrara, N.; Davis-Smyth, T. (1997).The biology of vascular endothelial growth factor. Endocr. Rev. 18, 4–25.

Fiorito, P.A.; Gonzales, V.R.; Ponzio, E.A.; Torresi, S.I.C.D. (2005). Synthesis, characterization and immobilization of Prussian blue nanoparticles. A potential tool for biosensing devices., Chem. Commun. 3, 366.

Forrest, S.R. (1997). Ultrathin organic films grown by organic molecular beam deposition and related techniques, Chem. Rev. 97,1793–1896.

Frens, G.; (1973) Controlled nucleation for the regulation of the particle size in monodisperse gold suspensions. Nat Phys Sci;241:20-2.

Gao, Q.; Ma, Y.; Cheng, Z.; Wang, W.; Yang, X. (2003). Flow injection electrochemical enzyme immunoassay based on the use of an immunoelectrode strip integrate immunosorbent layer and a screen-printed carbon electrode., Analytica Chimica Acta, 488, 1, 61-70.

Geim, A.K.; Novoselov, K.S. (2007) The rise of graphene . Nat. Mater. 6, 183–191.

Georganopoulou, D.G.; Chang, L.; Nam J.M.; Thaxton, C.S.; Mufson, E.J. (2005) Nanoparticle-based detection in cerebral spinal fluid of a soluble pathogenic biomarker for Alzheimer`s disease, Proc. Natl. Acad. Sci. USA 102,2273-2276.

Gohring, J.T.; Dale, P.S.; Fan, X (2010= Detection of HER2 breast cancer biomarker using the opto-fluidic ring resonator biosensor.,Sensors and Actuators B: Chemical, 146, 1, 226-230.

Goldenberg, D.M.; Sharkey, R.M.; Primus, F.J. (1976). Carcinoembryonic antigen in histopathology: immunoperoxidase staining of conventional tissue sections. J. Natl. Cancer Inst. 57, 11–22.

Grabar, K.C.; Freeman, R.G.; Hommer, M.B.; Natan, M.J. (1995). Preparation and Characterization of Au Colloid Monolayers,Analytical Chemistry , 67, 4, 735-43.

Gullick, W.J. (2001). Update on HER-2 as a target for cancer therapy: alternative strategies for targeting the epidermal growth factor system in cancer. Breast Cancer Res. 3, 390–394.

Gustafsson, J.B.; Moons, E.; Widstrand, S.M.; Johansson, L.S.O. (2006). Growth and characterization of thin PTCDA films on 3C-SiC(0 0 1)c(2×2), Surf. Sci., 600, 4758–4764.

Halámek, J.; Makower, A.; Skládal, P.; Scheller, F.W. (2002). Highly sensitive detection of cocaine using piezoelectric immunosensor, Biosens. Bioelectron., 17, 1045–1050.

Hansen, J. A.; Wang, J.; Kawde, A.-N.; Xiang, Y.; Gothelf, K. V.; Collins, G. (2006) Quantum-Dot/Aptamer-Based Ultrasensitive Multi-Analyte Electrochemical Biosensor. J. Am. Chem. Soc., 128, 2228-2229

Haupt,K. (2003), Imprinted polymers—tailor-made mimics of antibodies and receptors. Chemical Communications, 2, 171–178.

He, X.; Yuan, R.; Chai, Y.; Shi, Y. (2008). A sensitive amperometric immunosensor for carcinoembryonic antigen detection with porous nanogold film and nano-Au/chitosan composite as immobilization matrix. Journal of Biochemical and Biophysical Methods, 70, 6, 823-829.

Heighway, J.; Kmapp, T.; Boyce, L.; Brennand, S.; (2002). Field J.K., Betticher D.C., Ratschiller D., Gugger M., Donovan M., Lasek, A. and Rickert P. Expression profiling of primary non-small cell lung cancer for target identification Oncogene 21, 7749-7763.

Hiep, H.; Kerman, K.; Endo, T.; Saito, M.; Tamiya, E. (2010) Nanostructured biochip for label-free and real-time optical detection of polymerase chain reaction, Anal. Chim. Acta, 661,111–116.

Hiep, H.M.; Yashikawa, H.; Tamiya, E. (2010). Interference localized surface plasmon resonance nanosensor tailored for the detection of specific biomolecular interactions, Anal. Chem., 82, 1221–1227.

Hirsch, F. R.; Franklin, W. A.; Gazdar, A. F. and Bunn, P. A. Jr. (2001). Early detection of lung cancer: clinical perspectives of recent advances in biology and radiology. Clin Cancer Res,7: 5-22.

Hnaiein, M.; Hassen, W.; Abdelgani, A.; Fournier-Wirth, C.; Coste, J.; Bessueille, F.; Leonard, D.;Jaffrezic-Renault, N. (2008). A conductometric immunosensor based on functionalized magnetite nanoparticles for E. coli detection, Electrochem. Commun. 10, 1152–1154.

Hook, F.; Rodahl, M.; Kasemo, B.; Brzezinski, P. (1998). Structural changes in hemoglobin during adsorption to solid surfaces: effects of pH, ionic strength, and ligand binding, Proceedings of the National Academy of Sciences of the United States of America, 95, 12271–12276.

Hu, W.P.; Hsu, H.Y.; Chiou, A.; Tseng, K.Y.; Lin, H.Y.; Chang, G.L.; Chen, S.J. (2006). Immunodetection of pentamer and modified C-reactive protein using surface plasmon resonance biosensing. Biosens. Bioelectron. 21, 631–1637.

Huang, K.J.; Niu, D.J.; Xie, W.Z.; Wang, W. (2010). A disposable electrochemical immunosensor for carcinoembryonic antigen based on nano-Au/multi-walled carbon nanotubes–chitosans nanocomposite film modified glassy carbon electrode., Analytica Chimica Acta, 659, 1-2, 102-108.

Huhtinen, P.; Soukka, T.; Lövgren, T.; Härmä, H. (2004) Immunoassay of total prostate-specific antigen using europium(III) nanoparticle labels and streptavidin–biotin technology., Journal of Immunological Methods, 294, 1-2, 111-122.

Itoh, Y.; Ichihara, K.; (2001). Standardization of immunoassay for CRM-related proteins in Japan: from evaluating CRM 470 to setting reference intervals. Clin. Chem. Lab. Med. 39, 1154.

Jacobs, C.B.; Peairs, M.J.; Venton, B.V; (2010). Review: Carbon nanotube based electrochemical sensors for biomolecules. Analytica Chimica Acta, 662, 2, 105-127.

Jain, K.K. (2005) Nanotechnology in clinical laboratory diagnostics., Clinica Chimica Acta, 358, 1-2, 37-54.

Janata, J. (1975). Immunoelectrode, Journal of the American Chemical Society, 97,2914–2916.

Jemal, A.; Siegel, R.; Ward, E.; Murray, T.; Xu, J.; Smigal, C.; Thun, M.J.; (2006) Cancer Statistics, CA Cancer J. Clin. 56 (2006) pp. 106–130.

Jemal, R.; Siegel, E.; Ward, T.; Murray, J.; Xu, C.; Smigal, M.J.; Thun, (2006) Cancer Statistics 2006, CA Cancer J. Clin. 56, 106–130.

Jensen, G.C.; Yu, X.; Munge, B.; Bhirde, A.; Gong, J.D.; Kim, S.N.; Papadimitrakopoulos, F.; Rusling, J.F. (2008). Characterization of multienzyme-antibody–carbon nanotube bioconjugates for immunosensors, J. Nanosci. Nanotechnol., 8, 1–7.

Jin, Y.; Jang, J.W.; Han, C.H.; Lee, M.H.; (2005) Development of ELISA and immunochromatographic assay for the detection of gentamicin. J. Agric. Food Chem. 53, 7639–7643.

Katz, E.; Willner, I. (2004). Integrated nanoparticle-biomolecule hybrid systems: Synthesis, properties and applications., Angew. Chem. Int. Ed., 43, 6042-6108.

Kauffman, C.A.; Malani, A.N.; Easley, C.; Kirkpatrick, P. (2007). The rise of graphee, Nat. Mater., 6, 183–191.

Kaufman, E.D.; Belyea, J.; Johnson, M.C.; Nicholson, Z.M.; Ricks, J.L.; Shah, P.K.; Bayless, M.; Pettersson, T.; Feldoto, Z.; Blomberg, E.; Claesson, P.; Franzen, S. (2007). Probing protein adsorption onto mercaptoundecanoic acid stabilized gold nanoparticles and surfaces by quartz crystal microbalance and zeta-potential measurements, Langmuir, 23, 6053–6062.

Kearney, A.J.; Murray, M.; (2008). Breast cancer screening recommendations: is mammography the only answer? J. Midwife. Women Health 54 pp. 393–400.

Kim, D.M.; Noh, H.; Park, D.S.; Ryu, S.H.; Koo, J.S.; Shim, Y. (2009). Immunosensors for detection of Annexin II and MUC5AC for early diagnosis of lung cancer., Biosensors and Bioelectronics, 25, 2, 456-462

Kim, G.; Kim, K.; Oh, M.; Sung, Y.; (2010) Electrochemical detection of vascular endothelial growth factors (VEGFs) using VEGF antibody fragments modified Au NPs/ITO electrode . Biosensors and Bioelectronics, 25, 7, 1717-1722.

Kim, N.; Ji, G.E. (2006) Modulatory activity of Bifidobacterium sp. BGN4 cell fractions on immune cells, J. Microbiol. Biotechnol. 16, 584–589.

Kim, N.; Kim, D.K.; Cho, Y.J. (2009). Development of indirect-competitive quartz crystal microbalance immunosensor for C-reactive protein., Sensors and Actuators B: Chemical, 143, 1, 444-448.

Kim, N.; Kim, D.K.; Cho, Y.J. (2010) Gold nanoparticle-based signal augmentation of quartz crystal microbalance immunosensor measuring C-reactive protein., Current Applied Physics, 10, 4, 1227-1230.

Kim, N.; Park, I.S.; Kim, D.K. (2004). Characteristics of a label-free piezoelectric immunosensor detecting Pseudomonas aeruginosa, Sens. Actuators B: Chem. 100, 432–438.

Kim, N.; Park, I.S.; Kim, W.Y. (2007). Salmonella detection with a direct-binding optical grating coupler immunosensor, Sens. Actuators B: Chem. 121, 606–615.

Kim, P.Y.; Lee, B.Y.; Lee, J.; Hong, S.; Sim, S.J. (2009) Enhancement of sensitivity and specificity by surface modification of carbon nanotubes in diagnosis of prostate cancer based on carbon nanotube field effect transistors.,Biosensors and Bioelectronics, 24, 11, 3372-3378.

Kim, S.W.; Cheon, K.; Kim, C.H.; Yoon, J.H.; Hawke, D.H.; Kobayashi, R.; Prudkin, L.; Wistuba, I.I.; Lotan, R.; Hong, W.K.; Koo, J.S. (2007) Proteomics-based identification of proteins secreted in apical surface fluid of squamous metaplastic human tracheobronchial epithelial cells cultured by three-dimensional organotypic air-liquid interface method. Cancer Res. 67, 14, 6565-6573.

Koo, J.S.; Yoon, J.H.; Gray, T.; Norford, D.; Jetten, A.M.; Nettesheim, P.; (1999). Restoration of the mucous phenotype by retinoic acid in retinoid-deficient human bronchial cell cultures: changes in mucin gene expression., Am. J. Respir. Cell Mol. Biol. 20, 1, 43-52.

Koskinen, J.O.; Vaarno, J.; Meltola, N.J.; Soini, J.T.; Hänninen, P.E.; Luotola, J.; Waris, M.E.; Soini, A.E. (2004) Fluorescent nanoparticles as labels for immunometric assay of C-reactive protein using two-photon excitation assay technology, Anal. Biochem., 328, 210–218.

Kovochich, M.; Xia, T.; Xu, J.; Yeh, J.I.; Nel, A.E.; (2007). In: M. Weisner, (Ed.), Toxicological Impact of Materials. Principles and Methods for the assessment of nanomaterial toxicity. Journal of the American Chemical Society 62, 1940, 2643–2657.

Kranz, A.; Mattfeldt, T. and Waltenberger, J. (1999). "Molecular mediators of tumor angiogenesis: enhanced expression and activation of vascular endothelial growth factor receptor KDR in primary breast cancer." Int J Cancer 84, 293-8.

Kumar, S.; Aaron, J.; Sokolov, K.; (2008). Directional conjugation of antibodies to nanoparticles for synthesis of multiplexed optical contrast agents with both delivery and targeting moieties. Nat. Protoc. 3, 2, 314–320.

Kurebayashi, J.; Tang, C. K.; Otsuki, T.; Kurosumi, M., Yamamoto, S.; Tanaka, K.; Mochizuki, M.; Nakamura, H. and Sonoo, H. (1999). Isolation and characterisation of a new human breast cancer cell line, KPL-4, expressing the Erb B family receptors and interleukin-6. Br. J. Cancer, 79, 707–717.

Kurosawa, S.; Nakamura, M.; Park, J.W.; Aizawa, H.; Yamada, K.; Hirata, M. (2004). Evaluation of a high-affinity QCM immunosensor using antibody fragmentation and 2-methacryloyloxyethyl phosphorylcholine (MPC) polymer, Biosens. Bioelectron. 20, 1134–1139.

Kwon, S.J.; Yang, H.; Jo, K.; Kwak, J. (2008). An electrochemical immunosensor using p-aminophenol redox cycling by NADH on a self-assembled monolayer and ferrocene-modified Au electrodes, Analyst 133, 1599–1604.

Lackie, P.M. (1996) Immunogold silver staining for light microscopy. Histochem Cell Biol 106:9–17

Ladd, J.; Boozer, C.; Yu, Q.M.; Chen, S.F.; Homola, J.; Jiang, S. (2004) DNA-directed protein immobilization on mixed self-assembledmonolayers via a streptavidin bridge, Langmuir, 20, 8090–8095.

Ladd, J.; Lu, H.; Taylor, A.D.; Goodell, V.; Disis, M.L.; Jiang, S. (2009) Direct detection of carcinoembryonic antigen autoantibodies in clinical human serum samples using a surface plasmon resonance sensor., Colloids and Surfaces B: Biointerfaces, 70, 1, 1-6.

Landis, S.H.; Murray, T.; Bolden, S.; Wingo, P.A. (1999) Cancer statistics., CA Cancer J Clin. 49, 1,8-31, 1.

Lee, K.N.; Jung, S.W.; Shin, K.S., Kim, W.H.; Lee, M.H.; Seong, W.K. (2007) Fabrication of suspended silicon nanowire arrays. 4, 642-8.

Lee, M.H.; Lee, D.H.; Jung, S.W.; Lee, K.N.; Park, Y.S.; Seong, W.K. (2010) Measurements of serum C-reactive protein levels in patients with gastric cancer and quantification using silicon nanowire arrays., Nanomedicine: Nanotechnology, Biology and Medicine, 6, 1, 78-83.

Lee, Y.; Garcia, M.A.; Huls, N.A.F.; S, Sun. (2010). "Synthetic Tuning of Catalytic Properties of Au-Fe_3O_4 Nanoparticles". Angew. Chem. Int. Ed. 49, 1271.

Li, H.; Wei, Q.; Wang, G.; Yang, M.; Qu, F.; Qian, Z. (2011). Sensitive electrochemical immunosensor for cancer biomarker with signal enhancement based on nitrodopamine-functionalized iron oxide nanoparticles., Biosensors and Bioelectronics, 26, 6, 3044-3049.

Li, X.; Yuan, R.; Chai, Y.; Zhang, L.; Zhuo, Y.; Zhang, Y. (2006). Amperometric immunosensor based on toluidine blue/nano-Au through electrostatic interaction for determination of carcinoembryonic antigen. Journal of Biotechnology, 123, 3, 356-366.

Liang, R.Q.; Tan, C.Y.; Ruan, K.C. (2004). Colorimetric detection of protein microarrays based on nanogold probe coupled with silver enhancement., Journal of Immunological Methods, 285, 2, 157-163.

Liao, Y.; et al. (2010). Immunosensor based on Nf–Cys composite membrane Anal. Biochem. 402, 47–53.

Lilja, H.; Cronin, A.M.; Scardino, P.T.; Dahlin, A.; Bjartell, A.; Berglund, G.; Ulmert, D.; Vickers. A.J. (2008) A Single PSA Predicts Prostate Cancer Up To 30 Years Subsequently, Even In Men Below Age 40., The Journal of Urology, 179, 4, 206-207.

Lim, C.T.; Zhang, Y. (2007) Bead-based microfluidic immunoassays: The next generation.,Biosensors and Bioelectronics, 22, 7, pp. 1197-1204.

Lim, T.K .; Matsunaga T. (2001). Construction of electrochemical flow immunoassay system using capillary columns and ferrocene conjugated immunoglobulin G for detection of human chorionic gonadotrophin. Biosensors and Bioelectronics, 16, 9-12, 1063-1069.

Limoges, B.; Marchal, D.; Mavré, F.; Savéant, J.M. (2006). High amplification rates from the association of two enzymes confined within a nanometric layer immobilized on an electrode: modeling and illustrating example, J. Am. Chem. Soc. 128 pp.6014–6015.

Limoges, B.; Marchal, D.; Mavré, F.; Savéant, J.M. (2008). Theory and practice of enzyme bioaffinity electrodes. chemical, enzymatic, and electrochemical amplification of in situ product detection, J. Am. Chem. Soc. 130 pp.7276–7285.

Lin, W.J.; Liao, C.S.; Zhang,J.H.; Tsai, Y.C. (2009). Graphene modified basal and edge plane pyrolytic graphite electrodes for electrocatalytic oxidation of hydrogen peroxide and nicotinamide adenine dinucleotide. Electrochem. Commun. 11, 2153–2156.

Lin, Y.Y.; Wang, J.; Liu, G.; Wu, H.; Wai, C.M.; Lin, Y. (2008). A nanoparticle label/immunochromatographic electrochemical biosensor for rapid and sensitive detection of prostate-specific antigen. Biosensors and Bioelectronics, 23, 11, 1659-1665.

Lippman, M.E.; Harrison's Principles of Internal Medicine, 2008.

Liu, C.; Alwarappan, S. ; Chen, Z.F.; Kong, X.X.; Li, C.Z. (2010) Membraneless enzymatic biofuel cells based on graphene nanosheets, Biosens. Bioelectron., 25, 1829–1833.

Liu, G.; Gooding, J.J. (2009) Towards the fabrication of label-free amperometric immunosensors using SWNTs., Electrochemistry Communications, 11, 10, 1982-1985.

Liu, G.; Lin, Y. (2007). Nanomaterial labels in electrochemical immunosensors and immunoassays., Talanta, 74, 3, 308-317.

Liu, G.; Lin, Y.Y.; Wang, J.; Wu, H.; Wai, C.M. and Lin Y. (2007). "Disposable Electrochemical Immunosensor Diagnosis Device Based on Nanoparticle Probe and Immunochromatographic Strip." Analytical Chemistry 79, 20, 7644-7653.

Liu, J.; Cheng, L.; Liu, B.; Dong, S.J.; (2000). Covalent modification of a glassy carbon surface by 4-aminobenzoic acid and its application in fabrication of a polyoxometalates-consisting monolayer and multilayer films. Langmuir 16, 7471–7476.

Liu, K.G.; Yuan, R.; Chai, Y.Q.; Tang, D.P.; An, H.Z. Chiral resolution of phenylalanine by d-Phe imprinted membrane considering rejection property Bioprocess and Biosystems Engineering, 33, (1), 79-86.

Liu, K.P.; Zhang, J.J.; Yang, G.H.; Wang, C.M.; Zhu, J.J. (2010). Direct electrochemistry and electrocatalysis of hemoglobin based on poly(diallyldimethylammonium chloride) functionalized graphene sheets/room temperature ionic liquid composite film, Electrochem. Commun. 12, 402–405.

Liu, M.; Jia, C.; Jin, Q.; Lou, X.; Yao, S.; Xiang, J.; Zhao, J. (2010) Novel colorimetric enzyme immunoassay for the detection of carcinoembryonic antigen., Talanta, 81 , 4-5, 1625-1629.

Liu, S.; Zhang, X.; Wu, Y.; Tu, Y.; He, L. (2008). Prostate-specific antigen detection by using a reusable amperometric immunosensor based on reversible binding and leasing of HRP-anti-PSA from phenylboronic acid modified electrode., Clinica Chimica Acta, 395, 1-2 , 51-56.

Liu, S.Q.; Xu, J.J.; Chen, H.Y. (2002). Electrochemical behavior of nanosized Prussian blue self-assembled on Au electrode surface Electrochemistry Communications, 4, 5, 421-425.

Liu, Y.; Lei, J.; Ju, H. (2008). Amperometric sensor for hydrogen peroxide based on electric wire composed of horseradish peroxidase and toluidine blue-multiwalled carbon nanotubes nanocomposite. Talanta, 74, 4, 965-970.

Liu, Y.; Wang, M.; Zhao, F.; Xu, Z.; Dong, S. (2005). The direct electron transfer of glucose oxidase and glucose biosensor based on carbon nanotubes/chitosan matrix. Biosensors and Bioelectronics, 21, 6, 984-988.

Liu, Z.; Robinson, J.T.; Sun, X.; and Dai, H. (2008). PEGylated Nanographene Oxide for Delivery of Water-Insoluble Cancer Drugs. J. Am. Chem. Soc. 130, 10876–10877.

Liu, Z.; Yuan, R.; Chai, Y.; Zhuo, Y.; Hong, C.; Yang, X. (2008). Highly sensitive, reagentless amperometric immunosensor based on a novel redox-active organic–inorganic composite film. Sensors and Actuators B: Chemical, 134, 2, 625-631.

Lu, G.; Jiang, L.; Song, F.; Liu C. and Jiang, L. (2005) Determination of uric acid and norepinephrine by chitosan-multiwall carbon nanotube modified electrode, Electroanalysis 17, 901–905.

Lupu, S.; Mihailciuc, C.; Pigani, L.; Seeber, R.L.; Totir, N.; Zanardi, C. (2002). Electrochemical preparation and characterisation of bilayer films composed by Prussian Blue and conducting polymer, Electrochem. Commun. 4, 753–758.

Lvov, Y. (2001). Thin-film nanofabrication by alternate adsorption of polyions, nanoparticles, and proteins, in: R.W. Nalwa (Ed.), Handbook of Surfaces and Interfaces of Materials, 3, Academic Press, San Diego, 170-189.

Maeng, J.H.; Lee, B.C.; Ko, Y.J.; Cho, W.; Ahn, Y.; Cho, N.G.; Lee, S.H.; Hwang, S.Y. (2008). A novel microfluidic biosensor based on an electrical detection system for alpha-fetoprotein. 1319–1325 .

Mak, K.W.; Wollenberger, U.; Scheller, F.W.; Scheller; Renneberg; (2003). An amperometric bi-enzyme sensor for determination of formate using cofactor regeneration, Biosens. Bioelectron. 18, 1095–1100.

Mario, P.; Ali, T.; Wanqin, J.; Judit, S.; Bernd, T. (2003) Self-assembled films of prussian blue and analogues: optical and electrochemical properties and application as ion-sieving membranes, Chem. Mater. 15, 245–254.

Mauritz, K. A.; Moore, R. B. (2004) "State of understanding of Nafion." Chem. Rev., 104, 4535 4585.

McAllister, M. J.; Li, J. L.; Adamson, D. H.; Schniepp, H. C.; Abdala, A. A.; Liu, J.; Herrera-Alonso, M.; Milius, D. L.; CarO,R.; Prud'homme, R. K. (2007). Single Sheet Functionalized Graphene by Oxidation and Thermal Expansion of Graphite. Chem. Mater., 19, 4396–4404.

McBride, J.D.; Cooper, M.A. (2008). A high sensitivity assay for the inflammatory marker C-reactive protein employing acoustic biosensing, J. Nanobiotechnol., 6, 5.

Meyer, M.H.F.; Hartmann, M.; Krause, H.J.; Blankenstein, G.; Mueller-Chorus, B.; Oster, J.; Miethe, P.; Keusgen, M. (2007). CRP determination based on a novel magnetic biosensor, Biosens. Bioelectron. 22, 973–979.

Meyer, M.H.F.; Hartmann, M.; Keusgen, H.J. (2006)SPR-based immunosensor for the CRP detection—A new method to detect a well known protein., Biosensors and Bioelectronics, 21, 10, 1987-1990.

Meyer, M.H.F.; Hartmann, M.; Keusgen, M. (2006). SPR-based immunosensor for the CRP detection – A new method to detect a well known protein, Biosens. Bioelectron. 21, 1987–1990.

Milka, P.; Krest, I.; Keusgen, M.; (2000). Immobilization of alliinase on porous aluminium oxide. Biotechnol. Bioeng. 3, 344–348.

Mosbach,K. (1994). Molecular imprinting. Trends in Biochemical Sciences 19, 9–14.

Mukundan, H.; Kubicek, J.Z.; Holt, A.; Shively, J.E.; Martinez, J.S.; Grace, K.; Grace, W.K.; Swanson, B.I. (2009) Planar optical waveguide-based biosensor for the quantitative detection of tumor markers., Sensors and Actuators B: Chemical, 138, 2, 453-460

Munge, B.; Liu, G.; Collins, G.; Wang, J. (2005) Multiple enzyme layers on carbon nanotubes for electrochemical detection down to 80DNAcopies, Anal. Chem. 77 pp. 4662–4666.

Munge, B.; Liu, G.; Collins, G.; Wang, J. (2005). Multiple enzyme layers on carbon nanotubes for ultrasensitive electrochemical detection down to 80 DNA copies, Anal. Chem. 77 pp.4662–4666.

Nagatani, N.; Tanaka, R.; Yuhi, T.; Endo, T.; Kerman, K.; Takamura, Y.; Tamiya, E. (2006). Gold nanoparticle-based novel enhancement method for the development of highly sensitive immunochromatographic test strips., Science and Technology of Advanced Materials, 7, 3, 270-275.

Nam, J.M.; Thaxton, C.S.; Mirkin, C.A.; (2003) Nanoparticle-Based Bio–Bar Codes for the Ultrasensitive Detection of Proteins., Science 301, 1884.

Norton, J.D.; White, H.S.; Feldberg, S.W. (1990) Effect of the electrical double layer on voltammetry at microelectrodes., *J. Phys. Chem.*, 94 (17), 6772–6780.

O'Sullivan, C.K.; Guilbault, G.G. (1999) Commercial quartz crystalmicrobalances—theory and applications. Biosens Bioelectron. 14,663–70.

Ohta, T.; Bostwick, A.; Seyller, T.; Horn, K.; Rotenberg, E. (2006) Controlling the Electronic Structure of Bilayer Graphene. Science 313, 951–954.

Oikawa, S.; Inuzuka, C.; Kuroki, M.; Matsuoka, Y.; Kosaki, G.; Nakazato, H. (1989) Cell adhesion activity of non-specific cross-reacting antigen (NCA) and carcinoembryonic antigen (CEA) expressed on CHO cell surface: Homophilic and heterophilic adhesion., Biochemical and Biophysical Research Communications, 164, 1, 39-45.

Ostuni, E.; Chapman, R.G.; Holmlin, R.E.; Takayama, S.; Whitesides, G.M. (2001). A survey of structure–property relationships of surfaces that resist the adsorption of protein, Langmuir, 17, 5605–5620.

Panini, N.V.; Messina, G.A.; Salinas, E.; Fernández, H.; Raba, J. (2008). Integrated microfluidic systems with an immunosensor modified with carbon nanotubes for detection of prostate specific antigen (PSA) in human serum samples., Biosensors and Bioelectronics, 23, 7, 1145-1151.

Panteghini, M.; (2000). Present issues in the determination of troponins and other markers of cardiac damage. Clin. Biochem. 33, 161.

Park, I.-S.; Kim, N. (1998). Thiolated Salmonella antibody immobilization onto the gold surface of piezoelectric quartz crystal, Biosens. Bioelectron. 13, 1091–1097.

Park, I.-S.; Kim, N.; (2006) Development of a chemiluminescent immunosensor for chloramphenicol, Anal. Chim. Acta, 578, 19–24.

Pathak, S.; Choi, S.K.; Arnheim, N; Thompson, M.E. (2001) Hydroxylated quantum dots as luminescent probes for in situ hybridization. J. Am. Chem. Soc.123, 4103-4104.

Patolsky, F.; Zheng, G.; Hayden, O.; Lakadamyali, M.; Zhuang, X.; Lieber, C.M. (2004) Electrical detection of single viruses. Proc Natl Acad Sci U S A, 101, 14017-22.

Patolsky, F.; Zheng, G.; Lieber, C.M. (2006). Fabrication of silicon nanowire devices for ultrasensitive, label-free, real-time detection of biological and chemical species. Nat Protocol.,1, 1711-24.

Pauling, L. (2009). A theory of the structure and process of formation of antibodies, redox multi-wall carbon nanotube composite, Electrochim. Acta 54, 4149–4154.

Phadtare, S.; Vinod, V.P.; Mukhopadhyay, K.; Kumar, A.; Rao, M.; Chaudhari, R.V.; Sastry, M.; (2004). Immobilization and biocatalytic activity of fungal protease on gold nanoparticle–lodaed zeolite microspheres. Biotechnol. Bioeng. 6, 629–637.

Piletsky, S.A.; Alcock, S. Turner, A.P.F. (2001) Molecular imprinting: at the edge of the third millennium, Trends in Biotechnology 19, 9–12.

Porter, M.D.; Bright, T.B.; Allara, D.L.; Chidsey, C.E.D. (1987). Spontaneously organized molecular assemblies. 4. Structural characterization of normal-alkyl thiol monolayers on gold by optical ellipsometry, infrared-spectroscopy, and electrochemistry, Journal of the American Chemical Society 109, 3559–3568.

Prabhulkar, S.; Alwarappan, S.; Liu, G.; Li, C.Z. (2009). Amperometric micro-immunosensor for the detection of tumor biomarker., Biosensors and Bioelectronics, 24, 12, 3524-3530.

Preechaworapuna, Z.; Dai, Y.; Xiang, O.; Chailapakulb, J.; Wang, (2008). Investigation of the enzyme hydrolysis products of the substrates of alkaline phosphatase in electrochemical immunosensing, Talanta 76, 424–431.

Qian, J.; Zhou, Z.; Cao, X.; Liu. S. (2010) Electrochemiluminescence immunosensor for ultrasensitive detection of biomarker using $Ru(bpy)_3^{2+}$-encapsulated silica nanosphere labels., Analytica Chimica Acta, 665, 1, 32-38.

Qiao, Y.L.; Tockman, M.S.; Li, L.; Erozan, Y.S., Yao, S.X.; Barrett, M.J.; Zhou, W.H.; Giffen, C.A.; Luo, X.C.; Taylor, P.R. (1997). Risk factors and early detection of lung cancer in a cohort of Chinese tin miners. Cancer Epidemiol. Biomarkers Prev. 6, 893–900.

Qu, B.; Chu, X.; Shen, G.; Yu, R.; (2008). A novel electrochemical immunosensor based on colabeled silica nanoparticles for determination of total prostate specific antigen in human serum.,Talanta, 76, 4, pp. 785-790.

Qu, B.; Chu, X.; Shen, G.; Yu, R.; (2008). A novel electrochemical immunosensor based on colabeled silica nanoparticles for determination of total prostate specific antigen in human serum., Talanta, 76, 4, pp.785-790.

Quershi, A.; Gurbuz, Y., Kang, W.; Davidson J.L.; (2009) A novel interdigitated capacitor based biosensor for detection of cardiovascular risk marker., Biosensors and Bioelectronics, 25, 4, pp. 877-882.

Qureshi, A.; Niazi, J.; Kallempudi, S.; Gurbuz, Y.(2009). Label-free capacitive biosensor for sensitive detection of multiple biomarkers using gold interdigitated capacitor arrays. Biosensors and Bioelectronics, 25, 10, pp. 2318-2323.

Rahman, A.; Won, M.S.; Shim, Y.B. (2005). The potential use of hydrazine as an alternative to peroxidase in a biosensor: comparison between hydrazine and HRP-based glucose sensors., Biosensors and Bioelectronics, 21, 2, 257-265.

Rossier, J.; Reymond, F.; Michel, P.E.; (2002). Polymer microfluidic chips for electrochemical and biochemical analyses. Electrophoresis 23, 858.

Ruohola, J.K.; Valve, E.M.; Karkkainen, M.J.; Joukov, V.; Alitalo, K.; Härkönen, P.L. (1999). Vascular endothelial growth factors are differentially regulated by steroid hormones and antiestrogens in breast cancer cells., Molecular and Cellular Endocrinology, 149, 1-2, 29-40.

Rusling, J.F.; Sotzing, G.; Papadimitrakopoulosa, F. (2009). Designing nanomaterial-enhanced electrochemical immunosensors for cancer biomarker proteins., Bioelectrochemistry, 76, 1-2, 189-194

Sánchez, C.F.; Gallardo-Soto, A.M.; Rawson, K.; Nilsson, O.; McNeil, C.J. (2004). Quantitative impedimetric immunosensor for free and total prostate specific antigen based on a lateral flow assay format ., Electrochemistry Communications, 6, 2, 138-143

Sánchez, C.F.; Gallardo-Soto, A.M.; Rawson, K.; Nilsson, O.; McNeil, C.J.; Leung, H.Y.; Gnanapragasam, V. (2005) One-step immunostrip test for the simultaneous detection of free and total prostate specific antigen in serum., Journal of Immunological Methods, 307, 1-2, 1-12

Saravan, K.S.; Gul, O.; Basaga, H.; Sezerman, U.; Gurbuz, Y. (2008). C-reactive protein as a risk factor versus risk marker.,Sens. Lett. 6 (6), 873–877.

Sato, K.; Yamanaka, M.; Takahashi, H.; Tokeshi, M.; Kimura, H.; Kitamori, T.; (2002). Microchip-based immunoassay system with branching multichannels for simultaneous determination of interferon-γ. Electrophoresis 23, 734–739.

Scheller, F.W.; Bauer, C.G.; Makower, A.; Wollenberger, U.; Warsinke, A.; Bier, F.F. (2001) Coupling of immunoassays with enzymatic recycling electrodes, Anal. Lett., 34, 1233–1245.

Scripps Laboratories, http://www.scrippslabs.com/datatables/proteinabsorbance.html, 2007.

Seiwert, B.; Karst, U. (2008). Ferrocene-based derivatization in analytical chemistry. Anal. Bioanal. Chem. 390 (1), 181–200.

Sellergren, B. (2001) Molecularly Imprinted Polymers, Man-made Mimics of Antibodies and Their Application in Analytical Chemistry, Elsevier, New York,.

Sellergren, B.; Shea, K.J. (1994). Enantioselective ester hydrolysis catalyzed by imprinted polymers, Tetrahedron-Asymmetry 5 pp.1403–1406.

Shan, C.S.; Yang, H.F.; Song, J.F.; Han, D.X.; Ivaska, A.; Niu, L. (2009). Direct electrochemistry of glucose oxidase and biosensing for glucose based on grapheme, Anal. Chem., 81, 2378–2382.

Shankaran, D.R.; Shim, Y.-B. (2002). An amperometric sensor for hydrogen peroxide based on a (3-mercaptopropyl)trimethoxysilane self-assembled layer containing hydrazine. Electroanalysis 14, 704–707.

Shi, H.; Xia, T.; Nel, A.E.; Yeh, J.I.; (2007). Part II: coordinated biosensors--development of enhanced nanobiosensors for biological and medical applications. Nanomedicine 2 (5), 599–614.

Shi, W.; Ma, Z. (2011). A novel label-free amperometric immunosensor for carcinoembryonic antigen based on redox membrane. Biosensors and Bioelectronics, 26, 6 , 3068-3071.

Shiddiky, M.J.A.; Rahman, M.A.; Shim, Y.-B. (2007a). Trace Analysis of DNA: Preconcentration, Separation, and Electrochemical Detection in Microchip Electrophoresis Using Au Nanoparticles. Anal. Chem. 79, 3724–3733.

Shiddiky, M.J.A.; Rahman, M.A.; Shim, Y.B. (2007b) Hydrazine-Catalyzed Ultrasensitive Detection of DNA and Proteins. Anal. Chem. 79, 6886–6890.

Singh, A.K.; Kilpatrick, P.K.; Carbonell, R.G. (1996). Application of Antibody and Fluorophore-Derivatized Liposomes to Heterogeneous Immunoassays for D-dimer. Biotechnol. Prog. 12, 272–280.

Song, Z.; Yuan, R.; Chai, Y.; Yin, B.; Fu, P.; Wang, J. (2010). Multilayer structured amperometric immunosensor based on gold nanoparticles and Prussian blue nanoparticles/nanocomposite functionalized interface., Electrochimica Acta, 55, 5, 1778-1784.

Spinks, G.M.; Shin, S.R.; Wallace, G.G.; Whitten, P.G.; Kim, S.I.; Kim, S.J. (2006) Mechanical properties of chitosan/CNT microfibers obtained with improved dispersion., Sensors and Actuators B: Chemical, 115, 2, 678-684.

Stephan, C.; Klaas, M.; Muller, C.; Schnorr, D.; Loening, S.A.; Jung, K. (2006) Interchangeability of measurements of total and free prostate-specific antigen in serum with 5 frequently used assay combinations: an update. Clin. Chem., 52, 59 - 64

Strein, T.G.; and Ewing, A.G. (1992). "Characterization of submicron-sized carbon electrodes insulated with a phenol-allylphenol copolymer." Analytical Chemistry, 64, 1368-1373.

Su, H.L.; Yuan, R.; Chai, Y.Q.; Zhuo, Y.; Hong, C.L.; Liu, Z.Y.; Yang, X. (1995) Multilayer structured amperometric immunosensor built by self-assembly of a graphite electrodes with mechanically immobilized Prussian Blue, J. Electroanal. Chem., 398, 23–35

Su, X.D.; Li, S.F.Y.; and O'Shea, S.J. (2001). Gold nanoparticle and silver enhancement reaction amplified microgravimetric biosensor., Chemical Communications , 8, 755-756.

Sun, S.J.; Yao, Y.Z.; Wang, T.; Li, Y.C.; Ma, X.L.; Zhang, L.Y. (2009). Nanosilver, DNAfunctionalized immunosensing probes for electrochemical immunoassay of alpha-fetoprotein, Microchim. Acta 166, 83–88.

Takahashi, S.; Reddy, S.V.; Chirgwin, J.M.; Devlin, R.; Haipek,C.; Anderson, J.; Roodman, G.D. (1994). "Cloning and identification of annexin II as an autocrine/paracrine factor that increases osteoclast formation and bone resorption". J. Biol. Chem. 269 (46): 28696–701. PMID 7961821

Tan, F.; Yan, F.; Ju, H.X. (2006). A designer ormosil gel for preparation of sensitive immunosensor for carcinoembryonic antigen based on simple direct electron transfer. Electrochem Commun, 8:1835–9.

Tang, D.; Ren, J. (2008). In Situ Amplified Electrochemical Immunoassay for Carcinoembryonic Antigen Using Horseradish Peroxidase-Encapsulated Nanogold Hollow Microspheres as Labels. Anal. Chem. 80, 8064–8070.

Tang, D.;Yuan, R.; Chai, Y. (2008). Ultrasensitive Electrochemical Immunosensor for Clinical Immunoassay Using Thionine-Doped Magnetic Gold Nanospheres as Labels and Horseradish Peroxidase as Enhancer. Anal. Chem. 80, 1582–1588.

Tang, H.; Chen, J.; Nie, L.; Kuang, Y.; Yao, S. 2007) A label-free electrochemical immunoassay for carcinoembryonic antigen (CEA) based on gold nanoparticles (AuNPs) and nonconductive polymer film., Biosensors and Bioelectronics, 22, 6, 1061-1067.

Tang, J.; Huang, J.; Su, B.; Chen, H.; Tang, D.; (2011). Sandwich-type conductometric immunoassay of alpha-fetoprotein in human serum using carbon nanoparticles as labels., Biochemical Engineering Journal, 53, 2, 223-228.

Tang, Q.; Xu, C.H.; Shi, S.Q.; Zhou, L.M. (2004). Formation and characterization of proteinpatterns on the surfaces with different properties, Synthetic Metals 147, 247–252.

Thomson, D.M.P.; Krupey, J.; Freedman, S.O.; Gold, P. (1969). The carcinoembryonic antigen (CEA) radioimmunoassay. Proc. Natl. Acad. Sci. 64, 161–167.

Tiefenauer, L.X.; Kossek, S.; Padeste, C.; Thiébaud, P. (1997) Towards amperometric immunosensor devices., Biosensors and Bioelectronics, 12, 3, 213-223.

Tothill, I.E.; Turner, A.P.F. (2003). Biosensors. In: B Caballero, L Trugo , P Finglas, (Eds) Encyclopaedia of food sciences and nutrition. 2nd ed. Academic Press; ISBN: 0-12-227055-X.

Triroj, N.; Jaroenapibal, P.; Shi, H.; Yeh, J.I.; Beresford, R. (2011) Microfluidic chip-based nanoelectrode array as miniaturized biochemical sensing platform for prostate-specific antigen detection., Biosensors and Bioelectronics, 26, 6, 2927-2933.

Tseng, C.-H.; Wang, C.C.; Chen, C.-Y. (2007). Functionalizing Carbon Nanotubes by Plasma Modification for thenPreparation of Covalent-Integrated Epoxy Composites. Chem. Mater. 19, 308–315.

Uludağ, Y.; Tothill, I.E. (2010). Development of a sensitive detection method of cancer biomarkers in human serum (75%) using a quartz crystal microbalance sensor and nanoparticles amplification system. Talanta, 82, 1, 277-282.

Valat, C.; Limoges, B.; Huet, D.; Romette, J.L. (2000). Functionalizing Carbon Nanotubes by Plasma Modification for the Preparation of Covalent-Integrated Epoxy Composites. Anal. Chim. Acta 404, 187–194.

Valden, M.; Lai, X.; Goodman, D.W. (1998). Onset of Catalytic Activity of Gold Clusters on Titania with the Appearance of Nonmetallic Properties. Science 281, 1647–1649.

Verma, S.; Yeh, E.T. (2003). C-reactive protein and atherothrombosis-beyond a biomarker: an actual partaker of lesion formation, Am. J. Physiol. 285, R1253–R1256.

Vikholm-Lundin, I.; Albers, W.M. (2006) Site-directed immobilization of antibody fragments for detection of C-reactive protein, Biosens. Bioelectron. 21, 1141–1148.

Viswanathan, S.; Rani, C.; Anand, A.V.; Ho, J.A. (2009). Disposable electrochemical immunosensor for carcinoembryonic antigen using ferrocene liposomes and MWCNT screen-printed electrode., Biosensors and Bioelectronics, 24, 7, 1984-1989.

Vlatakis, G.; Andersson, L.I.; Muller, R.; Mosbach, K. (1993) Drug assay using antibody mimics made by molecular imprinting, Nature, 361, 645–647.

Wang, A.; Liang, X.; McAllister, J.P.2nd.; Li, J.; Brabant, K.; Black, C.; Finlayson, P.; Cao, T.; Tang, H.; Salley, S.O.; Auner, G.W.; Simon, Ng.K. (2007). Stability of and inflammatory response to silicon coated with a fluoroalkyl self-assembled monolayer in the central nervous system. J Biomed Mater Res A ,81(2):363-72.

Wang, C.; Daimon, H.; Sun, S.H. (2009). Dumbbell-like Pt−Fe_3O_4 Nanoparticles and Their Enhanced Catalysis for Oxygen Reduction Reaction. Nano Lett. 9, 1493–1496.

Wang, C.; Xu, C.J.; Zeng, H.; Sun, S.H. (2009). A General Approach to Noble Metal−Metal Oxide Dumbbell Nanoparticles and Their Catalytic Application for CO Oxidation. Adv. Mater. 21, 3045–3052.

Wang, H.L.; Li, W.; Jia, Q.X.; Akhadov, E. (2007). Tailoring Conducting Polymer Chemistry for the Chemical Deposition of Metal Particles and Clusters. Chem. Mater. 19, 520–525.

Wang, J.; Liu, G.; Jan, M.; (2004) Ultrasensitive electrical biosensing of proteins and DNA: carbon-nanotube derived amplification of the recognition and transduction events, J. Am. Chem. Soc.,126, 3010–3011.

Wang, J.; Pamidi, P.V.A.; Rogers, K.R. (1998). Sol–gel-derived thick-film amperomertic immunosensors. Anal. Chem. 70, 1171–1175.

Wang, J; Krause, R.; Block, K.; Musameh, M.; Mulchandani, A.; Schöning, M.J. (2003). Flow injection amperometric detection of OP nerve agents based on an organophosphorus–hydrolase biosensor detector Original Research Article Biosensors and Bioelectronics, 18, 2-3, 255-260

Wang, L.; Gan, X.X. (2009). Antibody-functionalized magnetic nanoparticles for electrochemical immunoassay of _-1-fetoprotein in human serum, Microchim. Acta 164, 231–237.

Wang, Y.; Lu, J.; Tang, L.H.; Chang, H.X.; Li, J.H. (2009). Graphene oxide amplified electrogenerated chemiluminescence of quantum dots and its selective sensing for glutathione from thiol-containing compounds. Anal. Chem. 81, 9710–9715.

Wang, Y.; Zhang, Z.; Jain, V.; Yi, J.; Mueller, S.; Sokolov, J.; Liu, Z.; Levon, K.; Rigas, B.; Rafailovich, M.H. (2010) Potentiometric sensors based on surface molecular imprinting: Detection of cancer biomarkers and viruses. Sensors and Actuators B: Chemical, 146, 1, 381-387.

Wang, Y.D.; Joshi, P.P.; Hobbs, K.L.; Johnson, M.B.; Schmidtke, D.W. (2006). Nanostructured biosensors built by layer-by-layer electrostatic assembly of enzyme-coated single-walled carbon nanotubes and redox polymers. Langmuir 22, 9776–9783.

Wang,J.; Liu, G.; Engelhard, M.H.; and Lin, Y. (2006). "Sensitive Immunoassay of a Biomarker Tumor Necrosis Factor-[alpha] Based on Poly(guanine)-Functionalized Silica Nanoparticle Label." Analytical Chemistry 78(19):6974-6979.

Watson, L.; Maynard, P.; Cullen, D.; Sethi, R.; Brettle, J.; Lowe, C. (1987). Microelectronic conductimetric biosensor, Biosensors. 3, 101–115.

Wei, Q.; Mao, K.; Wu, D.; Dai, Y.; Yang, J.;Du, B.; Yang, M.; Li, H. (2010) A novel label-free electrochemical immunosensor based on graphene and thionine nanocomposite., Sensors and Actuators B: Chemical, 149, 1, 314-318.

Wei, Q.; Xiang, Z.; He, J.; Wang, G.; Li, H.; Qian, Z.; Yang, M.; (2010). Dumbbell-like Au-Fe_3O_4 nanoparticles as label for the preparation of electrochemical immunosensors., Biosensors and Bioelectronics, 26, 2, 627-631.

Weinhold, U.R. (1997). Interleukin-6-dependent and -independent regulation of the human C-reactive protein gene. Biochem. J. 327, 425–429.

Weipoltshammer, K.; Schöfer,C.; Almeder,M.; and Wachtler,F. (2000). Signal enhancement at the electron microscopic level using Nanogold and gold-based autometallography. Histochem Cell Biol 114, 489-495.

White, I.M.; Gohring, J.; Fan, X. (2007). SERS-based detection in an optofluidic ring resonator platform, Opt. Express. 15, 17433–17442.

White, I.M.; Oveys, H.; Fan, X. (2006) Liquid-core optical ring-resonator sensors, Opt. Lett. 31, 1319–1321.

Wu, H.;Liu, G.;Wang, J.; Lin, Y. (2007). Quantum-dots based electrochemical immunoassay of interleukin-1α ., Electrochemistry Communications, 9,7, 1573-1577.

Wu, J.; Tang, J.; Dai, Z.;Yan, F.;Ju, H.; Murr, N.E. (200& A disposable electrochemical immunosensor for flow injection immunoassay of carcinoembryonic antigen., Biosensors and Bioelectronics, 22, 1, 102-108.

Wu, J.F.; Xu, M.Q.; Zhao, G.C. (2010) Graphene-based modified electrode for the direct electron transfer of cytochrome c and biosensing, Electrochem. Commun. 12 (2010) 175–177.

Wu, J.F.; Xu, M.Q.; Zhao, G.C. (2010) Graphene-based modified electrode for the direct electron transfer of cytochrome c and biosensing, Electrochem. Commun., 12, 175–177.

Wu, Y.; Liu, S.; He, L. (2010). Activators generated electron transfer for atom transfer radical polymerization for immunosensing. Biosensors and Bioelectronics, 26, 3, 970-975.

Wulff, G. (1995). Molecular imprinting in cross-linked materials with the aid of molecular templates—a way towards artificial antibodies, Angewandte Chemie-International Edition in English, 34,1812–1832.

Xian, Y.Z.; Hua, Y.; Liu, F.; Xian, Y.; Feng, L.J.; Jin, L.T. (2007). Template synthesis of highly ordered Prussian blue array and its application to the glucose biosensing. Biosens. Bioelectron. 22, 2827–2833.

Xu, Z.C.; Shen, C.M.; Hou, Y.L.; Gao, H.J.; Sun, S.H. (2009). Oleylamine as Both Reducing Agent and Stabilizer in a Facile Synthesis of Magnetite Nanoparticles. Chem. Mater. 21, 1778.

Xue, M. ; Li, J.; Lu, Z.; Ko, P. K. and Chan M. (2002) "Array-Based Electrical Detector of Integrated DNA Identification System for Genetic Chip Applications", Proceedings of the 32nd European Solid-State Device Research Conference (ESSDERC 2002), 483-486, Firenze, Italy

Yakovleva, J.; Davidsson, R.; Bengtsson, M.; Laurell, T.; Emneus, J. (2003). Microfluidic enzyme immunosensors with immobilised protein A and G using chemiluminescence detection. Biosens. Bioelectron. 19, 21–34.

Yang, F.; Ruan, C.M.; Xu, J.S.; Lei, C.H.; Deng, J.Q. (1998). Anamperometric biosensor using toluidine blue as an electron transfermediator intercalated in a-zirconium phosphate-modifiedhorseradish peroxidase immobilization matrix. Fresenius J. Anal.Chem. 361, 115–118.

Yang, L.; Ren, X.; Tang, F.; Zhang, L. (2009). A practical glucose biosensor based on Fe_3O_4 nanoparticles and chitosan/nafion composite film., Biosensors and Bioelectronics, 25, 4, 889-895.

Yang, M.; Javadi, A.; Li, H.; Gong, S. (2010). Sensitive electrochemical immunosensor for the detection of cancer biomarker using quantum dot functionalized graphene sheets as labels Sensors and Actuators B: Chemical,In Press, Corrected Proof, Available online 2 December 2010.

Yang, M.; Javadi, A.; Li, H.; Gong, S. (2010). Ultrasensitive immunosensor for the detection of cancer biomarker based on graphene sheet.,Biosensors and Bioelectronics, 26, 2, 560-565.

Yang, X.; Guo, Y.; Wang, A. (2010). Luminol/antibody labeled gold nanoparticles for chemiluminescence immunoassay of carcinoembryonic antigen., Analytica Chimica Acta, 666, 1-2, 91-96.

Yeh, J.I.; Du, S.; Xia, T.; Lazareck, A.; Kim, J-H.; Xu, J.; and Nel, A.E. (2007). Coordinated Nanobiosensors for Enhanced Detection: Integration of Three-Dimensional Structures to Toxicological Applications. ECS Transactions 3(29), 115-126.

Yeh, J.I.; Shivachev, B.; Rapireddy, S.; Gil, R.R.; Du, S.; Ly, D. (2010). Crystal Structure of Chiral γPNA with Complementary DNA Strand: Insights into the Stability and Specificity of Recognition and Conformational Preorganization. J. Am. Chem. Soc. 132 (31), 10717–10727.

Yin, X.B.; Qi, B.; Sun, X.; Yang, X.; Wang, E. (2005). 4-(Dimethylamino)butyric acid labeling for electrochemiluminescence detection of biological substances by increasing sensitivity with gold nanoparticle amplification. Anal. Chem. 77, 3525–3530.

Yin, Z.; Liu, Y.; Jiang, L.P.; Zhu, J.J. (2011). Electrochemical immunosensor of tumor necrosis factor α based on alkaline phosphatase functionalized nanospheres. Biosensors and Bioelectronics, 26, 5, 1890-1894.

Yoo, S.; Kim, D.; Park, T.; Kim, E.; Tamiya, E.; Lee, S. (2010). Detection of the most common corneal dystrophies caused by BIGH3 gene points mutations using multispot gold-capped nanoparticle array chip, Anal. Chem. 82, 1349–1357.

Young, K.L.; Xu, C.J.; Xie, J.; Sun, S.H. (2009). Conjugating Methotrexate to magnetite (Fe_3O_4) nanoparticles via trichloro-s-triazine. J. Mater. Chem. 19, 6400.

Yu, H.; Sheng, Q.L.; Li, L.; Zheng, J.B. (2007) Rapid electrochemical preparation of a compact and thick Prussian blue film on composite ceramic carbon electrode from single ferricyanide solution in the presence of HAuCl4, J. Electroanal. Chem., 606, 55–62.

Yu, X.; Kim, S.N.; Papadimitrakopoulos, F.; Rusling, J.F. (2005).Protein immunosensor using single-wall carbon nanotube forests with electrochemical detection of enzyme labels. Mol. Biosyst. 1, 70–75.

Yu, X.; Munge, B.; Patel, V.; Jensen, G.; Bhirde, A.; Gong, J.; Kim, S.; Gillespie, J.; Gutkind, S.; Papadimitrakopolous, F.; Rusling, J.F. (2006). Carbon nanotube amplification strategies for highly sensitive immunosensing of cancer biomarkers in serum and tissue. J. Am. Chem. Soc. 128, 11199–11205.

Yuan, Y.R.; Yuan, R.; Chai, Y.Q.; Zhuo, Y.; Shi, Y.T.; He, X.L.; Miao, X.M. (2007). A reagentless amperometric immunosensor for alpha-fetoprotein based on gold nanoparticles/TiO2 colloids/prussian blue modified platinum electrode. Electroanalysis 19, 1402–1410.

Zakharchuk, N.F.; Meyer, B.; Hennig, H.; Scholz, F.; Jaworski, A.; Stojek, Z. (1995). A comparative study with Prussian-Blue-modified graphite paste electrodes and solid graphite electrodes with mechanically immobilized Prussian Blue, J. Electroanal. Chem. 398, 23–35.

Zhai, Y.; Yu, J.; Iruela-Arispe, L.; Huang, W.Q.; Wang, Z.; Hayes, A.J.; Lu, J.; Jiang, G.; Rojas, L;, Lippman, M.E. (1999). Inhibition of angiogenesis and breast cancer xenograft tumor growth by vegi, a novel cytokine of the tnf superfamily. Int. J. Cancer 82, 131–136.

Zhang, G.P.; Wang, X.N.; Yang, J.F.; Yang, Y.Y.; Xing, G.X.; Li, Q.M.; Zhao, D.; Chai, S.J.; Guo., J.Q. (2006) Development of an immunochromatographic lateral flow test strip for detection of β-adrenergic agonist Clenbuterol residues., Journal of Immunological Methods, 312, 1-2, 27-33.

Zhang, L.Y.; Yuan, R.; Chai, Y.Q.; Li, X.L.; Zhong, X.; Zhu, Q. (2005). An amperometric immunosensor for rubella vaccine. Anal. Lett. 38, 1549–1558.

Zhang, N.; Wilkop, T.; Lee S. and Cheng, Q. (2007). Bi-functionalization of a patterned Prussian blue array for amperometric measurement of glucose via two integrated detection schemes, Analyst 132, 164–172.

Zhang, S.; Du P.; Li F. (2007). Detection of prostate specific antigen with 3,4-diaminobenzoic acid (DBA)–H_2O_2–HRP voltammetric enzyme-linked immunoassay system. Talanta, 72, 4, 1487-1493.

Zhang, S.; Zheng, F.; Wu, Z.; Shen, G.; Yu, R. (2008). Highly sensitive electrochemical detection of immunospecies based on combination of Fc label and PPD film/gold nanoparticle amplification., Biosensors and Bioelectronics, 24, 1, 129-135.

Zhang, X.; Wu, Y.; Tu, Y.; Liu, S. (2008). A reusable electrochemical immunosensor for carcinoembryonic antigen via molecular recognition of glycoprotein antibody by phenylboronic acid self-assembly layer on gold. Analyst 133, 485–492.

Zhao, H.T.; Ju, H.X. (2006) Multilayer membranes for glucose biosensing via layer- by-layer assembly of multiwall carbon nanotubes, Anal. Biochem., 350, 138–144.

Zheng, M.; Huang, X. (2004) Nanoparticles comprising a mixed monolayer for specific bindings with biomolecules, J. Am. Chem. Soc. 126, 12047–12054

Yin Z.; Liu, Y.; Jiang, L.P.; Zhu, J.J. (2011). Electrochemical immunosensor of tumor necrosis factor α based on alkaline phosphatase functionalized nanospheres., Biosensors and Bioelectronics, 26, 5, 1890-1894.

Song, Z.; Yuan, R.; Chai, Y.; Yin, B.; Fu, P.; Wang, J. (2010). Multilayer structured amperometric immunosensor based on gold nanoparticles and Prussian blue nanoparticles/nanocomposite functionalized interface., Electrochimica Acta, 55, 5, 1778-1784.

Liu, Z.; Yuan, R.; Chai, Y.; Zhuo, Y.; Hong, C.; Yang, X. (2008). Highly sensitive, reagentless amperometric immunosensor based on a novel redox-active organic–inorganic composite film., Sensors and Actuators B: Chemical, 134, 2, 625-631.

Zhu, H.; White, I.M.; Suter, J.D.; Zourob, M.; Fan, X. (2008). Opto-fluidic micro-ring resonator for sensitive label-free viral detection, Analyst, 133, 356–360.

Liu, Z.; Robinson, J.T.; Sun, X. and Dai, H. (2008). PEGylated Nanographene Oxide for Delivery of Water-Insoluble Cancer Drugs., J. Am. Chem. Soc. 130, 10876–10877.

Zhuo, Y., Yuan, R., Chai, Y.Q., Tang, D.P., Zhang, Y., Wang, N., Li, X.L., Zhu, Q., 2005. A reagentless amperometric immunosensor based on gold nanoparticles/thionine/Nafion-membranemodified gold electrode for determination of _-1-fetoprotein. Electrochem. Commun. 7, 355–360.

Zhuo, Y.; Yuan, R.; Chai, Y.Q.; Tang, D.P.; Zhang, Y.; Wang, N.; Li, X.L.; Zhu, Q. (2005). A reagentless amperometric immunosensor based on gold nanoparticles/thionine/Nafion-membranemodified gold electrode for determination of _-1-fetoprotein. Electrochem. Commun. 7, 355–360.

Zinkin, N.T.; Grall, F.; Bhaskar, K.; Otu, H.H.; Spentzos, D.; Kalmowitz, B.; Wells, M.; Guerrero, M.; Asara, J.M.; Libermann, T.A.; Afdhal, N.H. (2008) Serum proteomics and biomarkers in hepatocellular carcinoma and chronic liver disease, Clin. Cancer Res. 14, 470–477.

Zong Dai, Feng Yan, Hua Yu, Xiaoya Hu, Huangxian Ju., Novel amperometric immunosensor for rapid separation-free immunoassay of carcinoembryonic antigen., Journal of Immunological Methods, Volume 287, Issues 1-2, April 2004, Pages 13-20

Part 3

Biosensors for Environment and Biosecurity

24

A New Biosensor to Enumerate Bacteria in Planktonic and Biofilm Lifestyle

Maria De Giusti[2], Francesca Berlutti[1], Fabrizio Pantanella[1], Lucia Marinelli[2], Alessandra Frioni[1], Tiziana Natalizi[1], Daniela Tufi[2] and Piera Valenti[1]
Sapienza University of Rome, Faculty of Pharmacy and Medicine
Department of Public Health and Infectious Diseases
[1]Microbiology Unit,
[2]Hygiene Unit
Italy

1. Introduction

Remarkable interest for human health concerns the microbiological risk assessment due infections by bacteria possessing the ability to adhere to host cell or abiotic surfaces as well as to live in aggregated and biofilm lifestyle. Biofilm is multicellular bacterial community held together by a self-produced extracellular matrix in response to several factors. These factors may include recognition of specific or non-specific attachment sites on cell surfaces, electrostatic interactions on abiotic surfaces, nutritional cues, or in some cases, exposure to stress conditions in the environment as well as into the host.
Biofilm lifestyle is comparatively more common than the planktonic one and it has been shown that biofilm plays a crucial role in human health (Brady et al., 2008; Bryers, 2008). As matter of fact, the eradication of bacterial biofilm by administration of antibiotics often fails due to the high drug resistance of bacteria in this lifestyle. Since 2008, European Centre for Disease Prevention and Control reports epidemiological data on the increasing of antimicrobial resistance constituting an important concern in public health hazard.
For this reason, rapid assays to determine biofilm susceptibility to antibacterial drugs can significantly improve the outcome of infected patients by enabling a fast selection of efficient antibiotic treatments, thus decreasing the period and the related costs of hospitalization, as well as the incidence of morbidity and mortality (Gfeller et al., 2005).
Therefore, a fundamental prerequisite in studying, counteracting and eradicating biofilm is the possibility to quantify the actual number of bacteria involved. Bacterial counts have deep implications in microbiological diagnosis and therapeutic treatments (Bryers, 2008), in water and food quality analysis (Ramalho et al., 2001; Lee et al., 2007; Rueckert et al., 2005), in environmental applications and consumers' safety.
The standard method used to evaluate the number of bacteria, based on determination of Colony Forming Units (CFUs) (ISO method), can be considered fully appropriate only when bacteria are in planktonic lifestyle but it is unreliable to count bacteria in aggregated, adherent and biofilm lifestyle (Berlutti et al., 2003, Pantanella, 2008; Berlutti, 2008 a; Frioni,

2010). Even if different analytical strategies have been attempted to enumerate bacteria in biofilm, the detection of the actual number of bacteria in aggregated, adherent and biofilm lifestyle is still a great challenge for microbiologists.

The analytical assays alternative to CFU count have been classified in direct and indirect methods.

Direct methods including microscopic observation of bacteria adherent to surfaces through the use of optical, scanning electron, and transmission electron microscopes (Verheyen et al. 1993; John et al. 2001; Vacheethasanee et al. 2000) have been employed. Two main inadequacies characterize microscopic examinations: assessing cell viability and counting bacteria in aggregated or biofilm lifestyle. However, the detection of bacterial viability can be obtained by microscopic observation of the samples stained with specific fluorescent stain which allows highlighting viable bacteria (Boulos et al.1999; Hope et al. 2002). In particular, the LIVE/DEAD Viability Kit (Bac-Light) together with laser scanning confocal microscopy is able to reliably discriminate live from dead adherent bacteria (Gottenbos et al., 2002). On the contrary, the enumeration of adherent bacteria in aggregated and biofilm lifestyle through microscopic examinations is unreliable even when several microscopic fields are evaluated. As matter of fact, Atomic Force Microscopy has well shown biomaterial's imperfections which influence bacterial colonization and biofilm development different from microscopic field to field (Dorobantu, 2010).

Indirect methods suggest to detach bacteria in adherent and biofilm lifestyle by vortex or sonication and successively to count detached bacteria by CFU counts (Ceri et al., 1999; Sandoe et al., 2006). These procedures present disadvantages as they may not detach all bacteria or may alter bacterial viability leading to erroneous counts.

Other indirect methods count bacteria in biofilm through assays based on staining the firmly adherent cells (Christensen et al., 1985) or on spectrophotometrically measuring the dye eluted from stained bacteria (Merritt et al., 1998). These methods, too, are subject to uncertainties: the bacteria could be non homogeneously stained, or the dye also could be adsorbed and difficultly eluted from abiotic materials.

Indirect assays counting bacteria on the basis of their metabolism as the biologic reduction of the redox indicator 2,3,5 triphenyl tetrazolium chloride by metabolically active microorganisms or colorimetric detection of CO_2 produced by viable microorganisms (Bochner et al., 1977; Thorpe et al., 1990) are semi-quantitative methods.

If this were not enough, there is another pivotal problem for human health: the bacterial count and the antibiotic therapy against bacteria adherent in biofilm on the catheters or medical devices (Bestul and Vandenbussche, 2005; Falagas et al., 2007). Usually, the bacterial count is not executed and antibiotic treatment of catheter-related infections is based on antibiotic susceptibility test performed on planktonic counterpart detached from catheters or medical devices instead of on biofilm (Ceri et al., 1999; Sandoe et al., 2006). It is well known that microorganisms organized in biofilm exhibit higher levels of antibiotic resistance than in planktonic form, so that a great part of therapeutic regimens based on susceptibility of planktonic forms fails to eradicate biofilm infections (Carratalà, 2002; Pascual et al.,1993). Some laboratories employs the Calgary Biofilm Device, the most popular method (Ceri et al., 1999) which determines the minimal biofilm eradication concentration (MBEC) as the concentration of antibiotic killing 100% of bacteria in biofilm. Unfortunately, this method does not detect the actual number of bacteria in biofilm used as inoculum in MBEC tests. As inoculum size influences the results of susceptibility tests (Egervarn et al., 2007), MBEC values determined using the above mentioned methods, could be mistaken.

Taken together the data reported, it is imperative to setup a reliable method to detect the number of bacteria in biofilm.
Here, we describe a novel biosensor, named BioTimer Assay (BTA), which allows easily counting bacteria in adherent, aggregated and biofilm lifestyle without any manipulation of samples.

2. Biosensor - BioTimer Assay

BioTimer assay (BTA) is a new biosensor that allows counting bacteria both in planktonic, aggregated, adherent and biofilm lifestyle. BTA employs original reagents containing specific indicators able to switch as a consequence of bacterial metabolism.
As matter of fact, living bacteria release one or more metabolites that induce color switching of BTA indicators. Therefore, BTA can be classified as an indirect method counting bacteria independently on their lifestyle (i.e.: planktonic, aggregated, adherent and biofilm lifestyle) by detecting the time required for indicator switching induced by a metabolic product specific for each bacterial genus. The time for color switching of indicators is inversely related to the number of living bacteria present in the sample. Interestingly, BTA is a simple, easy to perform method to count bacteria without any manipulation of samples.
At now two main indicators have been selected and added to specific original reagents of BTA: phenol red specific to count fermenting bacteria and resazurin to count non-fermenting bacteria.
The reagent, named BioTimer Phenol Red (BT-PR), contains phenol red and it appears clear and red after sterilization, i.e. in the absence of living bacteria (Fig. 1, insert of Panel A) (Berlutti et al., 2003). In the presence of bacteria, BT-PR reagent switches red-to-yellow due to metabolism of fermenting bacteria. Optical absorbance of BT-PR in the absence or in the presence of bacteria is shown in Figure 1 (Panel A, continuous and dotted line, respectively).
The other BTA reagent, named BioTimer Resazurin (BT-RZ) contains resazurin and it appears clear and blue after sterilization i.e. in the absence of living bacteria (Fig. 1, insert of Panel B) (Frioni et al., 2010). In the presence of bacteria, BT-RZ switches blue-to-pink due metabolism of non-fermenting bacterial. Optical absorbance of BT-RZ in the absence or in the presence of bacteria is shown in Figure 1 (Panel B, continuous and dotted line, respectively).
As above mentioned, the time required for color switch of BT-PR and BT-RZ reagents is inversely related to initial bacterial concentration. Therefore, the time required for color switching (t*) determines the initial number of bacteria (N_0) present in a sample at time = 0 (t_0) through specific correlation lines. To draw the correlation lines, serial dilutions of both fermenting and non-fermenting planktonic bacteria are counted by CFUs and used to inoculate BT-PR and BT-RZ reagents, respectively. The inoculated reagents are incubated at proper temperature and the color of the reagents monitored.
The switching time (t*) needed for the color switching of BT-PR (red-to-yellow) and BT-RZ (blue-to-pink) reagents is recorded. The t* and the corresponding CFU counts are used to construct the correlation lines. All correlation lines are obtained by linear regression analysis, and linear correlation coefficients are calculated from the equation (1)

$$r = (n\sum xy - \sum x \sum y)/(sqrt((n\sum x^2 - (\sum x)^2)(n\sum y^2 - (\sum y)^2))). \quad (1)$$

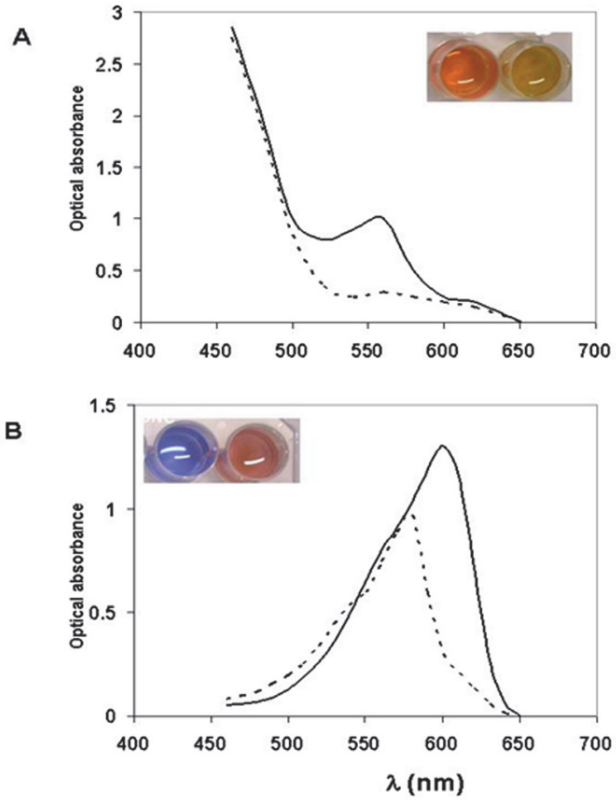

Fig. 1. Color switching of indicator specific for fermenting (A) and non-fermenting (B) bacteria contained in original reagents of BioTimer Assay (Frioni et al., 2010). Optical absorbance of BT-PR (Panel A) and BT-RZ (Panel B) indicators in the absence (solid line) or in the presence of bacteria (dotted line) at different λ as well as the color of BT-PR and BT-RZ reagents (insert of Panel A and Panel B, respectively) in the absence or in the presence of bacteria (left and right image of the inserts, respectively) are shown.

The switching time t* is inversely proportional to the logarithm of the initial value N_0, according to the following equation

$$t^* = -a \log N_0 + b \tag{2}$$

where a, b > 0 are correlation parameter depending on the environmental conditions and bacterial genus, respectively. In Figure 2, a typical correlation line is shown.
Several correlation lines have been drawn for different bacterial genera and species. In Table 1 the equations of correlation lines and the corresponding linear correlation coefficients to count fermenting and non-fermenting bacteria in several BTA applications are shown. The sensitivity of BTA theoretically corresponds to N_0 = 10−20 CFUs, even if the stochastic fluctuations for low values of N_0 will influence the standard deviation similarly to that observed using CFU method (Goel & Richter-Dyn, 1974).

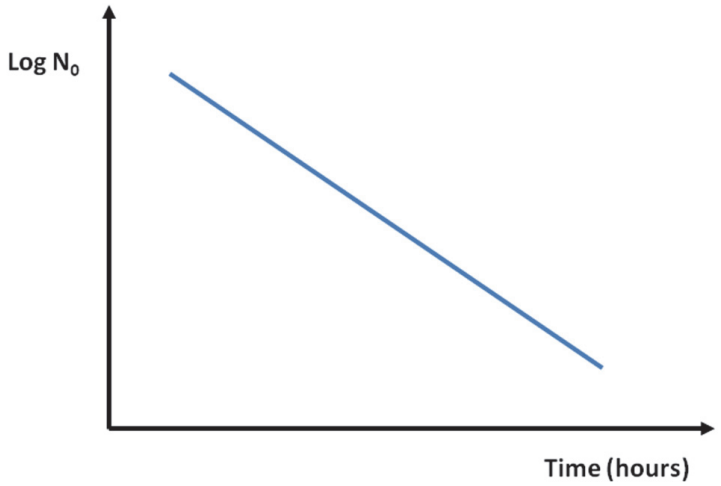

Fig. 2. BioTimer Assay correlation line. The typical BTA correlation line correlating the time (t*) for color switching of BTA indicator and the log of number of bacteria initially present in the samples (N_0) is described by the linear equation $t^* = -a \log N_0 + b$.

Moreover, the Eq (2) takes into account not only the t* of switching of different indicators, but also the composition of different reagents through "a" parameter. As shown in Figure 3 the correlation lines for *Lactobacillus rhamnosus* performed using BT-PR reagent containing glucose or lactose, as carbon source, differ only for "a" parameter involving the switching time (t*) for the same number of bacteria (N_0)..

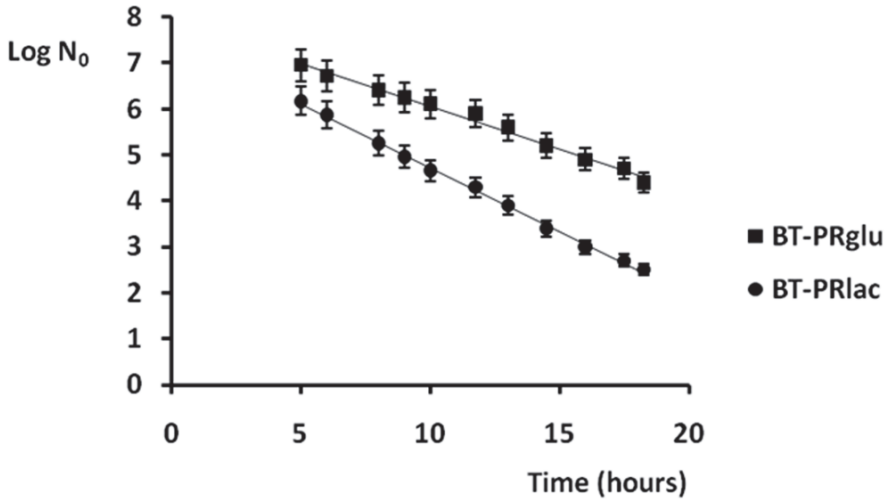

Fig. 3. Correlation lines of *Lactobacillus acidophilus* obtained using a BioTimer Assay Phenol Red (BT-PR) specific reagent with 1% glucose (BT-PRglu) or 1% lactose (BT-PRlac).

Bacterial species	BTA reagent	Equation of correlation line	*r*	Application	Reference
Streptococcus sobrinus	BT-RP	-0.3056x + 8.2608	0.9997	Adhesion to dental polymers	Berlutti et al., 2003
Streptococcus oralis	BT-RP	-0.301x + 9.0615	0.9999	Adhesion to dental polymers	Berlutti et al., 2003
Lactobacillus acidophilus	BT-RPglu	-0.1857x + 7.9174	0.9903	Control of lyophilized probiotic preparation	Valenti et al., personal data
	BT-RPlac	-0.2773x + 7.4984	0.998	Control of lyophilized probiotic preparation	Valenti et al., personal data
Staphylococcus aureus	BT-RP	-0.5903x + 8.7219	0.9973	Adhesion to dental polymers	Berlutti et al., 2003
	BT-RPMH	-0.597x + 10.28	0.9990	Antibiotic susceptibility of biofilm	Pantanella et al., 2008
Staphylococcus epidermidis	BT-RPMH	-0.633x + 9.267	0.9980	Antibiotic susceptibility of biofilm	Pantanella et al., 2008
Enterococcus faecalis	BT-RP	-0.4767x + 10.022	0.9975	Laser disinfection of dental root canals	Berlutti et al., personal data; Telesca, Master Thesis, 2010
Escherichia coli	BT-RP	-0.9678x + 10.347	0.9955	Adhesion to dental polymers	Berlutti et al., 2003
	FBTA	-0.8723+14.428	0.9970	Fecal contamination of food	Berlutti et al., 2008
Pseudomonas aeruginosa	BT-RZ	-0.4675x + 8.5841	0.9996	Adhesion to dental polymers; adhesion to SWCNT-structured surfaces	Berlutti et al., 2003; Frioni et al., 2010
Burkoldheria cenocepacia	BT-RZ	-0.415x + 9.018	0.9610	None	Berlutti et al., personal data

Table 1. Correlation lines.

Likely, Eq.(2) takes into account also bacterial genera/species through "b" parameter. As shown in Figure 4 the correlation lines for *Staphylococcus aureus* and *Streptococcus sobrinus or S. oralis* performed using the same BTA reagent differ only for "b" parameter involving the different metabolic activity specific for each bacterial genera/species.

Summarizing, in the BTA applications, the number of living planktonic bacteria in a sample is determined inoculating the specific BTA reagent. The color switching of BTA indicator is monitored and the time (t*) for color switching is recorded and used to determine the log N_0 through the specific correlation line.

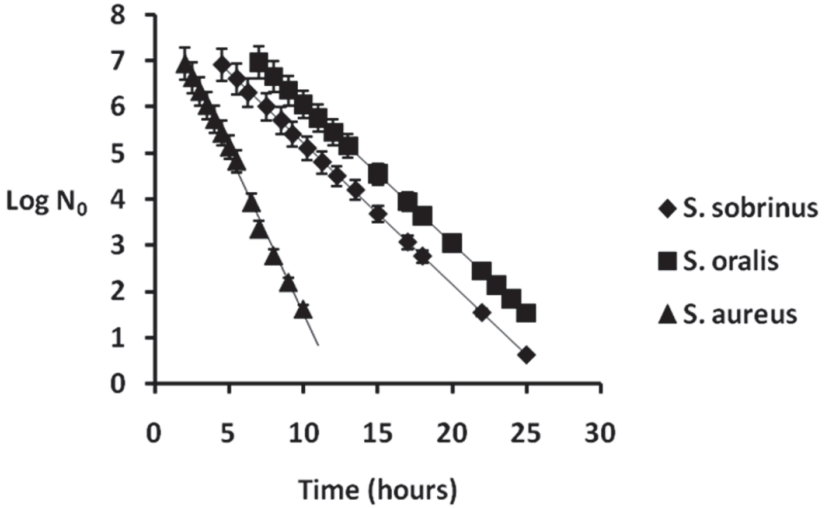

Fig. 4. Correlation lines of Streptococcus sobrinus, Streptococcus oralis and Staphylococcus aureus obtained using BT-PR reagent.

Similarly, it is possible to count bacteria in aggregated, adherent and biofilm lifestyle by inoculating BTA reagents with sample containing aggregated bacteria or solid supports/materials on which bacteria adhere or form biofilm (colonized material) without sample manipulation. As the Eq. 2 describes the correlation between the time for color switching of BTA indicators present in the original reagents and the CFUs (N_0) of planktonic bacteria, the number of bacteria in aggregated, adherent and biofilm lifestyle counted using BTA can be defined as planktonic-equivalent CFUs (PE-CFUs).

However, it is possible to object that the metabolic rate of the same bacterium in different lifestyle can be different and consequently the counts by BTA can be influenced by lifestyle. In order to answer to this objection, S. *sobrinus* has been chosen as bacterial model because it produces lactate as the principal end product of carbohydrate metabolism (Madigan, 2008; Burne, 1998), which is easily detectable by high performance liquid chromatography system (Berlutti, 2008; personal data). Planktonic and biofilm lifestyle *S. sobrinus* was cultured in complete medium for 24 h at 37°C, in the absence or in the presence of glass beads, respectively. *S. sobrinus*, indeed, colonizing the glass beads forms biofilm in 24 hours of incubation. Both planktonic bacteria and colonized glass beads were used to inoculate BT-PR reagents. The time for color switching of BT-PR reagents as well as the lactate concentrations (c_{lac}) at the moment of the color switching were recorded.

The values of lactate concentration c_{lac} at the moment of color switching of BT-PR reagents inoculated with different concentrations of planktonic N_0 were similar and corresponded to a mean value of 770±33 mg/l (Table 2).

The values of c_{lac} at the moment of color switching of BT-PR reagents inoculated with 1, 5, 10 colonized beads were similar and corresponded to a mean value of 760±45 mg/l (Table 2). Therefore, the concentration of lactate needed for inducing color switching of the indicator is independent from bacterial lifestyle. The sole difference observed among the samples was the time required for color switching, the parameter pivotal for bacterial counts by BTA (Berlutti et al., 2008 a; Valenti, personal data).

Lifestyle	Inoculum	c_{lac} (mg/l)	t* (hours)
Planktonic (log N_0) [a]	5	761±42	10.2
	6	773±42	7.5
	7	777±20	4.5
Biofilm (N_{GB})	1	805 ±48	4.5
	5	710±52	2.7
	10	740±45	1.5

Table 2. Lactate concentration (c_{lac}) and switching time (t*) of BT-PR reagents inoculated with *Streptococcus sobrinus* in planktonic and biofilm lifestyle. Legend: [a] planktonic inoculum is prepared from broth cultures; biofilm inoculum is obtained utilizing colonized glass beads (N_{GB}).

Similarly to that demonstrated in counting planktonic bacteria by BTA, the time required for BTA indicator switching is inversely related to the increasing of colonized glass bead (N_{GB}) number and consequently to the number of bacteria in biofilm (Table 2).
Therefore, the switching time t* is inversely proportional to the logarithm of the initial N_{GB}, according to the following equation

$$t^* = -a_{GB} \log N_{GB} + b_{GB} \quad (3)$$

which is equivalent to the Eq. (2) describing the correlation line for bacteria in planktonic lifestyle.

3. BioTimer Assay applications

It is important to again underline that the counts of bacteria in aggregated, adherent and biofilm lifestyle, through BTA, do not require any manipulation of the samples, and this characteristic represents an important advantage of BTA respect to other methods. However, in the absence of a validated reference method, the number of bacteria in aggregated, adherent and biofilm lifestyle carried out by BTA cannot be compared with those obtained by other methods of bacterial enumeration in biofilm. This lack is a disadvantage for all novel methods. Notwithstanding, BTA has been successfully applied to enumerate bacteria in biofilm adherent on abiotic materials, on different foods and recently, to detect the susceptibility of biofilm to antibiotics as well as the microbiological quality of nano-particles to be in vivo administered.

3.1 BioTimer Assay to enumerate bacteria in adherent and biofilm lifestyle on abiotic materials

The actual quantitative determination of bacteria in adherent and biofilm lifestyle on abiotic materials is a concern for microbiologists. BTA has been successfully employed to estimate bacterial population colonizing a variety of abiotic materials.
The first report concerned the evaluation of adhesion ability of different Gram-positive and Gram-negative species on different adhesive poly(HEMA)-based hydrogels to be utilized in dental restorative procedures (Berlutti et al., 2003). As matter of fact, the use of dental polymers is a standardized practice in dental restorative procedures. However, bacteria

potentially causing oral pathologies may colonize these polymers. It is therefore of great importance to evaluate both the susceptibility of the polymers to colonization by resident and transient bacterial genera, and the importance of chemical factors triggering bacterial adhesion. The study reported data of adhesion efficiency and biofilm formation of *S. sobrinus* and *Streptococcus oralis* representing bacterial resident species, and *Staphylococcus aureus, Escherichia coli,* and *Pseudomonas aeruginosa* considered transient bacteria in the oral cavity. The dental polymers were prepared with 2-hydroxyethyl methacrylate (HEMA) and different molar ratios of 2-acrylamido-2-methylpropane-sulfonic acid (AMPS) and/or 2-methacryloyloxyethyl-tri-methyl-ammonium chloride (METAC) co-monomers.
In conditions mimicking those present in the oral cavity, all tested bacteria showed similar adhesion percentages on the same dental polymer and different adhesion percentages on the different dental polymers (Fig. 5). As matter of fact, the physico-chemical characteristics of poly-HEMA based hydrogels are the major factors promoting bacterial adhesion. In particular, the adhesion efficiency increased with increasing water content in the swollen polymers and reached maximal values on cationic polymers. The highest adhesion efficiency was recorded for the polymer p(HEMAco-METAC) (10:1) that showed also the highest swelling ratio in double-distilled water.
BTA has been further employed in several microbiological studies in dentistry and, in particular, to demonstrate the antibacterial efficiency of laser treatment of experimental infections of dental root canals.

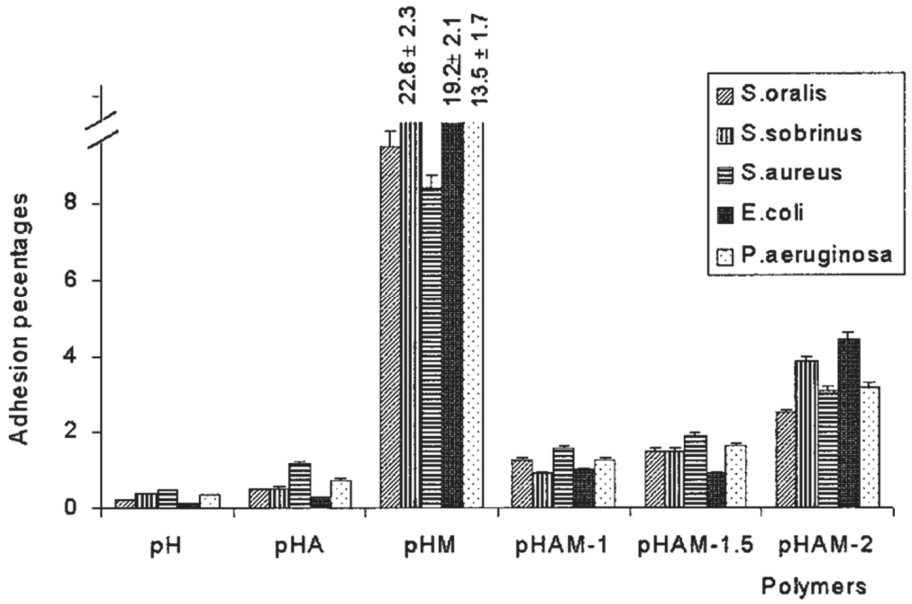

Fig. 5. Bacterial adhesion to different polymers. Adherent bacteria are expressed as percentages of the cells initially present in the saliva-polymer mixtures. The polymers used were: pH: p(HEMA); pHA:p(HEMA-co-AMPS) (10:1); pHM:p(HEMAco-METAC) (10:1); pHAM-1:p(HEMA-co-AMPS-co-METAC) (10:1:1); pHAM-1.5:p(HEMA-co-AMPS-co-METAC) (10:1:1.5); pHAM-2:p(HEMA-co-AMPS-co-METAC) (10:1:2). (Berlutti et al., 2003)

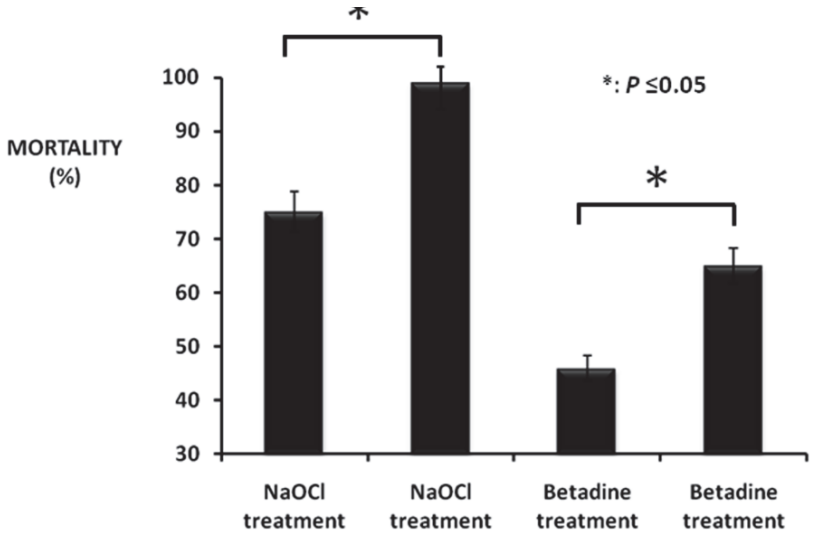

Fig. 6. Bactericidal activity of diode laser 808 nm treatment against *Enterococcus faecalis* CCM 2541 adherent on dental root canals. Dental roots were infected with *Enterococcus faecalis* CCM 2541(2.5 ± 0.7 x 10^6 CFUs). After 3 hours of incubation, dental root canals were treated with 808 diode alone or in combination with NaOCl or betadine.

It is well known that dental root canals may be infected with different bacteria causing endodontic as well as apical periodontitis and pulpitis. The treatment of canal and apical periodontal infections consists in eradicating microbes or in reducing the microbial load and preventing re-infection by orthograde root filling. The disinfectant treatment has a remarkably high degree of success even if it cannot be excluded some fail (Mohammadi &Abbott, 2009; Nair 2004). *Enterococcus faecalis* is associated with a significant number of refractory endodontic infections (Vidana et al., 2010; Ricucci & Siqueira, 2010). Recently, a different therapeutic approach for endodontic infections based on laser therapy has been exploited (Schwarz et al, 2009; Romeo et al., 2003). BTA has been applied, using a correlation line specific for *E. faecalis,* to evaluated the killing efficiency of the combined use of diode 808nm laser and betadine or NaOCl disinfectants against *E. faecalis* adherent on dental root canals after 3 hours of contact (Table 1) (Berlutti & Romeo, personal data). Results have showed that the both disinfectants did not kill all adherent bacteria while the combined use of disinfectants and diode 808nm laser significantly increased their antibacterial activity, even if at different extent (Fig. 6).
Further experiments were carried out to evaluate the efficiency of treatments carried out using diode 808nm and Er: YAG 2940nm laser against *E. faecalis* biofilm developed for 72 hours on dental root canals (Telesca V, European Master Degree On Oral Laser Applications Thesis). The results, obtained counting bacterial population in biofilm by BTA, showed that laser treatments significantly reduced bacterial number (Fig. 7).

3.2 BioTimer Assay to enumerate *Escherichia coli* in planktonic, adherent and biofilm lifestyle on different foods and surfaces: applications in HACCP

Food safety is a global health goal. U.S. Food and Drug Administration (FDA) has developed a comprehensive 'Food Protection Plan' in which food must be considered as a

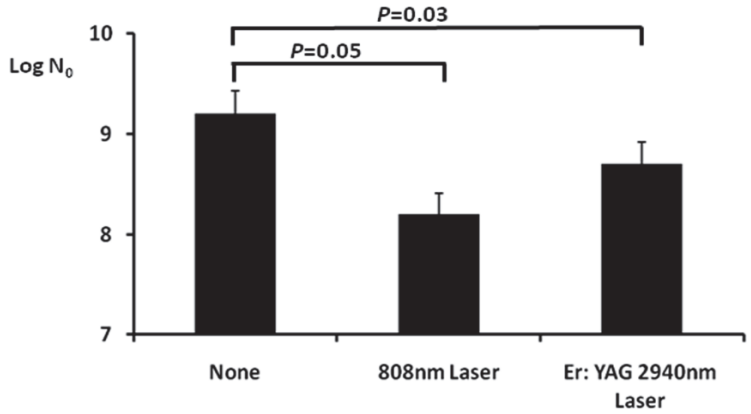

Fig. 7. Bactericidal activity of 808 diode and Er: YAG laser treatment on *Enterococcus faecalis* CCM 2541 biofilm developed on dental root canals. Dental roots were infected with *Enterococcus faecalis* CCM 2541 (2.5 ± 0.7 x 10^6 CFUs). After 72 hours of incubation, dental root canals were not treated (CTRL) or treated with 808 diode or Er: YAG laser. P values ≤0.05 were considered significant.

potential vehicle for intentional contamination (FDA, Food Protection Plan, 2007). Such intentional contamination of food could result in human or animal illnesses and deaths, as well as economic losses.

The European legislation through EC Regulation 852/2004 on the Hazard Analysis and Critical Control Point (HACCP) application in primary and secondary food productions indicates the systematic approach for food safety management. EC Regulation 2073/2005 followed by EC Regulation 1441/2007 identifies " microbiological criteria for food and foodstuffs" and indicated that "…foodstuffs should not contain microorganisms or their toxins or metabolites in quantities that present an unacceptable risk for human health".

In developed countries changes in the epidemiology of traditional infections have been observed: in USA in 2008 the incidence of *Salmonella* serotype *Typhimurium* is decreased, whereas the incidence of serotypes *Newport*, *Mississippi*, and J*aviana* is increased. In the same year in European Economic Area/European Free Trade Association countries, the two most common *Salmonella* serovars (*S. enteritidis* and *S. typhimurium)* representing 56 % and 22 %, respectively, were found. Moreover, the increasing of incidence of re-emerging and emerging pathogens like *Escherichia coli* O157, *Listeria monocytogenes, Campylobacter jejuni, Norovirus* and Hepatitis A virus, responsible for majority of food-borne outbreaks was observed (*De Giusti* et al., 2007; *Velusamy* et al. 2010; MMWR, 2008; ECDC. 2008).

Therefore, the food industry is strongly involved in real methods to detect the presence of pathogenic microorganisms, as failure or delay in detecting bacterial pathogens may lead to a dreadful effect.

Preparation and handling of safe food products requires the observance of hazard analysis and critical control point (HACCP) principles including : 1- to carry out the hazard analysis; 2- to determine the critical control points (CCPs); 3- to establish the critical limits; 4- to monitor the procedures; 5- to carry out the corrective actions; 6- to verify the procedures, and 7- to establish record-keeping and documentation procedures (EC Regulation 852/2004). In particular, this

Regulation reassesses the application of the HACCP procedure by extending it to the control of primary production and reinforces the role of Good Manufacturing Practice.
The Commission Regulation on the Microbiological Criteria for Foodstuffs (EC Regulation 1441/2007 amending EC Regulation 2073/2005) identifies *Escherichia coli* as indicator of good hygienical practice defining different limits of *E. coli* load in diverse foods and food handling procedures. Therefore, *E. coli* plays a pivotal role in performing corrective hygienic actions at CCPs to fit microbiological criteria of food safety as well as manufacturing, handling and distribution processes. The EC Regulation 1441/2007 indicates also the standard methods to count and identify *E. coli (*ISO 16649-2:2001). Conventional microbiological analyses (ISO methods) such as bacterial culture, colony forming unit (CFU) and other techniques as immunology-based and polymerase chain reaction-based methods have been used to evaluate food safety. However, all these techniques provide results after relatively long time spans (up to 72 hours) and many materials are needed. Moreover, ISO methods analyse a small amount of food samples (up to 0.1 g) that may not be representative of the actual bacterial contamination and they not guarantee reproducible and real results except for bacteria in planktonic lifestyle.
As matter of fact, many bacterial pathogens are able to grow, survive and persist in foods as well as to adhere both to catering surfaces and utensils also in biofilm lifestyle (Wilks et al., 2005, 2006). Biofilm in foods shows high resistance to disinfectants or biocides (Byun et al.,2007), thus causing food borne infections and diseases in humans (Gandhi, 2007; Oliver, 2005).
In foods, standardized enumeration of bacteria is based on CFUs count and on the most probable number (MPN) method (EC Regulations 2073/2005 and 1441/2007). Even if MPN could overcome the problem of counting bacteria in biofilm, it cannot be applied to count bacteria on surfaces and, moreover, it is manual labour and time consuming. Therefore, the development of microbiological methods allowing rapid and reliable detection of bacteria in biofilm for evaluating bacterial contamination of food and surfaces is highly desirable.
For this purpose, BTA has been specifically modified for the detection of *E. coli* as biological indicator of faecal contamination of food and surfaces. The modified BTA, named FoodBTA (FBTA), utilizes the phenol red indicator, a reagent specific for *E. coli*, and its corresponding correlation line (Table 1).
FBTA has been used for the evaluation of *E. coli* recovery in 122 food and surface samples. FBTA results compared with those of reference method (CFU/g or CFU/cm^2, respectively) showed high overall agreement percentage (97.54%) as identical results were obtained in 119 out 122 samples and discordant results concerned only three samples (1 food, 2 surfaces). Among the three discordant results, the food sample was positive using FBTA and negative using reference method. It should be underlined that FBTA allows analysing a 10-fold greater amount of food sample than reference method thus increasing the chance to detect *E. coli* contamination. Moreover, FBTA counts a greater *E. coli* number in 8 out 9 positive food samples than reference method. Concerning surface samples, the discrepancies could depend on fact that samples were collected in nearby surfaces that may be differently contaminated. The time required to achieve the results on *E. coli* contamination for all samples was 3-fold shorter using FBTA than reference method (Fig. 8, panel A). The trend of promptness in the results (Fig. 8, Panel B) clearly showed that FBTA may be considered very effective for HACCP application, as corrective actions at CCPs can be quickly taken (Berlutti et al., 2008b). Actually, using FBTA method, *E. coli* contamination can be detected in few hours and, in particular, the time will be shorter in the presence of higher than lower *E. coli* contamination.

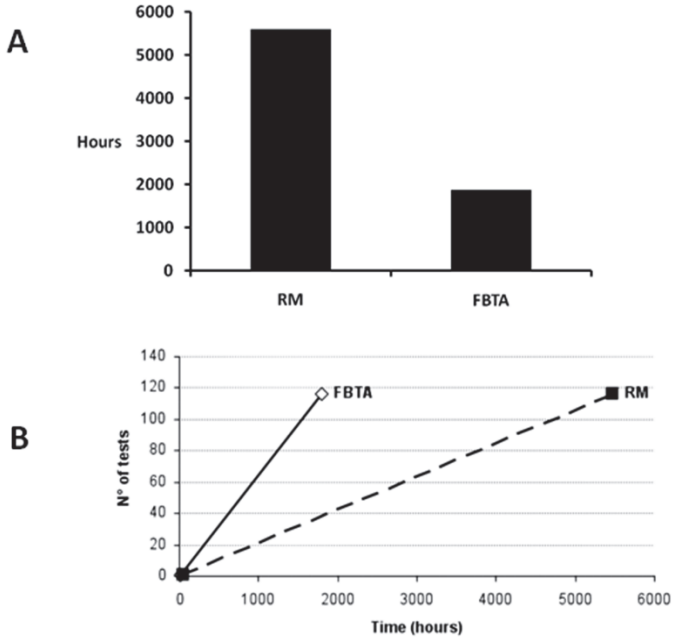

Fig. 8. Total time required to detect *Escherichia coli* contamination in all samples (Panel A) and trend of promptness of the analyses by FBTA and Reference Method (RM) (Panel B) (Berlutti et al., 2008b).

3.3 BioTimer Assay to detect the susceptibility of bacteria in planktonic and biofilm lifestyle to antibiotics

Staphylococcus aureus and *S. epidermidis* biofilm represent great challenge for medicine as they are involved in device- and specially catheter-related infections (Falagas et al., 2007). Usually, antibiotic treatment of catheter-related infections is based on antibiotic susceptibility tests performed on planktonic form of the clinical isolates instead on biofilm. It is well known that microorganisms organized in biofilm exhibit higher levels of antibiotic resistance than in planktonic form, so that a great part of therapeutic regimens based on susceptibility of planktonic forms fails to eradicate biofilm infections (Carratalà, 2002; Pascual et al., 1993). Therefore, it is imperative to set up a reliable method to detect antibiotic susceptibility of clinical isolated bacteria in biofilm, rather in planktonic lifestyle. At now, few methods are available to determine microbial antibiotic susceptibility of bacteria in biofilm. The Calgary Biofilm Device is the most popular method (Ceri et al., 1999), determining the minimal biofilm eradication concentration (MBEC) as the concentration of antibiotic required killing 100% of bacteria in biofilm. Unfortunately, none of these methods detects the actual number of bacteria in biofilm used as inoculum in MBEC tests. As inoculum size influences the results of susceptibility tests (Egervarn et al., 2007), MBEC values determined using the above mentioned methods, could be mistaken.

BTA has been applied to evaluate antibiotic susceptibility of *Staphylococcus* biofilm and for the contemporaneous enumeration of viable bacteria after exposure to sub-inhibitory doses

of antibiotics (Pantanella et al., 2008). For these experiments, BT-PR Muller Hinton (BT-PRMH) specific reagent has been set up to reliably determine antibiotic activity, and a specific correlation line has been determined (Table 1). Moreover, a work flow of BTA method to determine the minimal inhibitory concentration of a 24-hour-old *Staphylococcus* biofilm has been presented (Fig. 9).

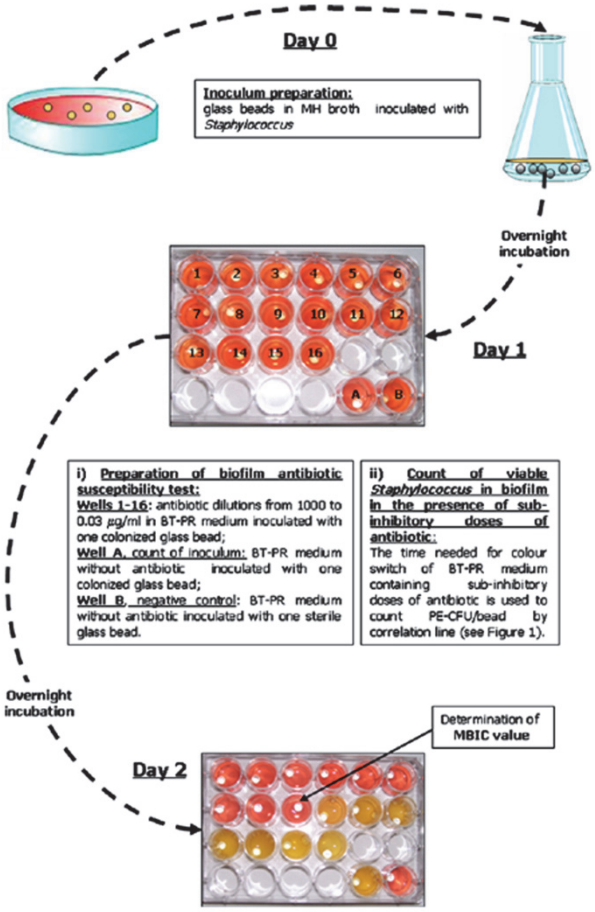

Fig. 9. Work flow of BioTimer Assay to determine the minimal inhibitory concentration of a 24-hour-old *Staphylococcus* biofilm (Pantanella et al., 2008).

Preliminary results obtained using BTA and reference antibiotic susceptibility test in evaluating MICs of planktonic *Staphylococcus* agree at 100% thus demonstrating the BTA reliability. Thereafter, BTA has been applied to study susceptibility of *Staphylococcus* biofilm to four antibiotics chosen as prototypes of different mechanisms of action. In this set of experiments, *Staphylococcus* biofilm has been developed on glass beads for 24, 48, and 72 hours. Colonized glass beads has been used as inoculum in antibiotic susceptibility assays in BT-RPMH specific reagent (Table 1).

Antibiotics susceptibilities determined by BTA confirmed a greater resistance of biofilm than of planktonic form according to the worldwide accepted literature (Lewis, 2001). Unlikely to all antibiotic susceptibility tests, BTA is the first method allowing to know the number of viable bacteria in the presence of sub-MBICs of antibiotics. This peculiar ability of BTA method may have a great importance for clinicians in evaluating also the putative therapeutic impact of sub-inhibitory doses of antibiotics against bacterial biofilm as they may favor biofilm development (Mirani & Jamil,, 2010)
Moreover, the possibility to count viable bacteria in biofilm could also be employed to study new anti-biofilm drugs. As matter of fact, the reported data show that antibiotics differently kill bacteria in biofilm and that the killing is dependent on biofilm age (Donlan & Costerton, 2002). Sub-MBICs of gentamicin and ampicillin, for example, reduce the number of viable *Staphylococcus* at higher extent in younger than older biofilm unlikely to sub-inhibitory doses of ofloxacin and azithromycin (Pantanella et al., 2008). Therefore BTA could be useful adopted in a wide range of microbiological laboratories to determine MBECs as well to evaluate the anti-biofilm activity of new antibacterial drugs.

3.4 BioTimer Assay to detect the microbiological quality of nano-particles to be in vivo administered

Infectious disease is one of the most important causes of mortality. Despite the great life expectancy related to advanced health care, the increasing numbers of complicating health-care infections remain a significant public health challenge. Biofilm lifestyle, more common than planktonic one, plays a crucial role in human health despite the therapeutic use of antibiotics (Brady et al., 2008; Bryers, 2008; Donlan & Costerton,, 2002). Moreover, biofilm-mediated infections are very difficult to treat when biofilm develops on medical devices and implanted biomaterials (Janatova,2000; Shunmugaperumal, 2010; Høiby et al., 2010). Therefore, the possibility to counteract bacterial colonization of medical device and biomaterial surfaces represents a crucial issue in human health. In the past few years nanotechnology has broken into Medicine as tsunami involving in researchers with different skills. Nano-structured materials have been recently proposed as pragmatic approach for the development of new biomaterials able to counteract bacterial colonization and biofilm development (Aslan et al., 2010). A fundamental prerequisite in studying bacterial adhesion and biofilm formation on abiotic surfaces is the quantitative evaluation of the actual bacterial number. The susceptibility of nano-structured medical devices and biomaterials to microbial colonization and biofilm formation has not been thoroughly considered as well as the sterility in process of manufacturing and storage of nano-structured medical devices. The underestimation of the potential risk of contamination by adherent bacteria and/or biofilm formation on nano-structured surfaces can lead to the unwanted onset of bacterial infections likely to what happened in the early biomaterial era.
The ability of *S. mutans* to adhere and form biofilm on glass beads coated with single wall carbon nano-tubes (SWCNTs-GBs) has been verified by atomic force microscopy (AFM) (Figure 10).
The number of *S. mutans* adherent on SWCNTs (3 hours of incubation) and the number of bacteria in biofilm (24 hours of incubation) has been detected by BTA. Results showed that BTA was reliable to evaluate the number of *S. mutans* in adherent and biofilm lifestyle to SWCNTs-GBs as well as to control the sterility of SWCNTs (Table 3).

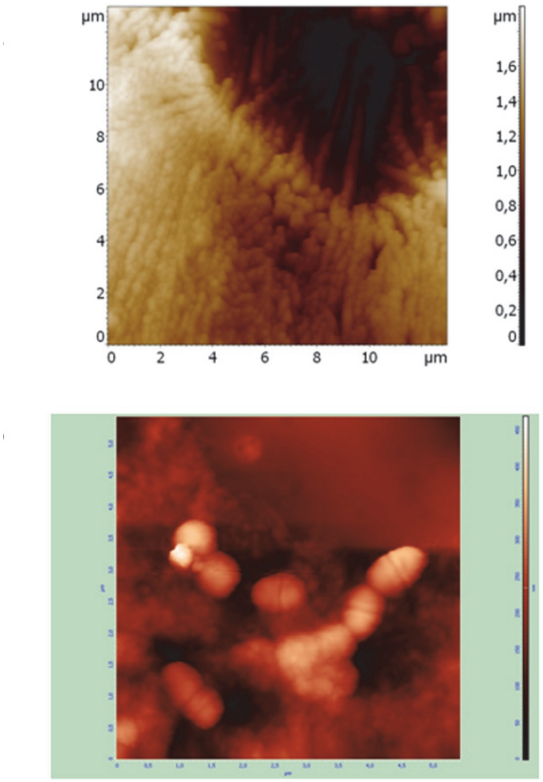

Fig. 10. Atomic force microscopy of sterile (A) and colonized (B) glass beads coated with single wall carbon nano-tubes.

Bacterial inoculum (N_0)	Number of bacteria adherent to SWCNTs (3 h of incubation)	Number of bacteria adherent in biofilm to SWCNTs (24 h of incubation)
0	0	0
$3.2*10^5$	$1.3±0.2*10^5$	$3.4±0.5*10^8$
$4*10^6$	$1.8±0.1*10^6$	$2.8±0.4*10^8$
$4.5*10^7$	$2.0±0.1*10^7$	$3.1±0.3*10^8$
$4.2*10^8$	$2.5±0.3*10^7$	$3.7±0.1*10^8$

Table 3. Enumeration of *Streptococcus mutans* in adherent and biofilm lifestyle on SWCNTs-GBs.

4. Conclusions and future perspectives

The quantitative microbiological risk assessment is an actual problem for analytical assays and public health as well as for drug therapy to eradicate biofilm related infections.

Despite the efforts to discover novel microbiological protocols involving multidisciplinary approaches, at now none validated method is available other than the CFU and MPN protocols that are unreliable to quantitative evaluate bacteria in adherent and biofilm lifestyle.

BTA utilizes original reagents specific for specific bacterial genera able to accelerate their metabolism. In fact, BTA exploits the synthesis of different metabolites produced by fermentative and non-fermentative bacteria evidenced by the switching of specific indicators. Moreover, this novel quantitative microbiological assay inversely correlates the time required for the switching of specific indicators with the number of bacteria present in the samples at time 0. For this reason, even if BTA is a very sample microbiological method, it requires a deep study to accurately define the composition of the reagents and the indicators specific for the bacterial genera to be counted. Importantly, BTA does not require any manipulation of the samples as well as it is not limited by the size and nature of the samples.

On the basis of above reported data, even if BTA is not validated method, it should be considered a useful tool in counting bacteria in planktonic, aggregated and biofilm lifestyle present in fluid phase or adherent to abiotic or cell surfaces.

Therefore, BTA being a versatile method has been utilized to detect bacterial load on a variety of samples.

In the study of the adhesion efficiency of bacteria to different biomaterials, BTA has been successfully applied thus allowing a real control on new biomaterials to be in vivo applied.

In the food industry FBTA has been usefully applied to enumerate bacterial indicators of good hygienically practice without any manipulation of samples. *E. coli* contamination has been detected by BTA in significant shorter time than the reference methods thus allowing to rapidly applying corrective majors at CCPs, to prevent food hazard and decrease economic loss. Moreover, FBTA method has been also employed for the screening of food samples at different steps of the food chain and for the determination of the safety of final food products according to the recent Microbiological criteria for foodstuffs and to track food products.

Concerning clinical application, the principal advantage of BTA is related to its employment in the evaluation of antibiotic susceptibility of bacteria in biofilm lifestyle. At now BTA is the first method that not only allows to determine the bactericidal concentrations of antibiotics against biofilm, but also to count the number of bacteria resistant to antibiotic treatments. This aspect of BTA performance could be helpful in order to evaluate the efficacy of antibiotic treatment in eradicating biofilm.

Recently, BTA has been found to be reliable in quantitative evaluation of bacteria adherent to nano-coated materials. This last BTA performance should be particularly relevant in the microbiological risk assessment related to the present and increasing future use of nano-materials to be in vivo applied.

Summarizing, BTA is an easy-to-perform and reliable biosensor which does not require a sophisticated apparatus as well as a complex experimental procedure after drawing correlation lines specific for each bacterial genus to be tested.

At now the main disadvantage of BTA is related to the lacking of a validated reference method, which limits the possibility to compare its reliability, efficiency, and sensitivity with reference methods, pivotal requisite for its validation and legal applications.

5. References

Aslan, S., Loebick, C.Z., Kang, S., Elimelech, M., Pfefferle, L.D., Van Tassel, P.R. (2010). Antimicrobial biomaterials based on carbon nanotubes dispersed in poly(lactic-co-glycolic acid). *Nanoscale*, Vol. 2, No. 9, pp. 1789–1794, ISSN 2040-3364, PMID 20680202

Berlutti, F., Pantanella, F., De Giusti, M., Tufi, D., Valenti, P., Boccia, A.(2008). FoodBioTimerAssay: a new microbiological biosensor for detection of *Escherichia coli* food contamination. *Italian Journal of Public Health*, Vol. 5, pp. 233-240, ISSN 1723-7815

Berlutti, F., Pantanella, F., Giona, M., Pagnanelli, F., Valenti, P. (2008) Indirect, easy-to-use and reliable method for counting bacteria in biofilm. Proceedings of Biofilms III: 3rd International Conference, p. 103, 6 - 8 October, Munich, Germany. Available from http://files.dropbox.com/u/107928/proceedings_biofilmsiii_final.pdf

Berlutti, F., Rosso F., Bosso P., Giansanti ,F., Ajello, M., De Rosa, A., Farina, E., Antonimi,G., Valenti, P. (2003). Quantitative evaluation of bacteria adherent to polyelectrolyte hema-based hydrogels. *Journal of Biomedical Materials Research.* Vol. 67 , No. 1, pp. 18-25, ISSN 0021-9304, PMID 14517857

Bestul, M.B., Vandenbussche, H.L. (2005). Antibiotic lock technique: review of the literature. *Pharmacotherapy*. Vol. 25, No 2, pp.211-27, ISSN 0277-0008, PMID 15767236

Bochner, B.R., Savageau, M.A. (1977). Generalized indicator plate for genetic, metabolic, and taxonomic studies with microorganisms. *Appl Environ Microbiol*., Vol. 33, No. 2, pp. 434-444, ISSN 0099-2240, PMID 322611

Boulos, L., Prevost, M., Barbeau, B., Coallier, J., Desjardins, R. (1999). LIVE/DEAD BacLight: Application of a new rapid staining method for direct enumeration of viable and total bacteria in drinking water. *J Microbiol Meth*., Vol. 37, No 1, pp. 77-86, ISSN 0167-7012, PMID 10395466

Brady, R.A., Leid J.G., Calhoun, J.H., Costerton, J.W., Shirtli, M. E. (2008). Osteomyelitis and the role of biofilms in chronic infection. *FEMS Immunol. Med. Microbiol*., Vol. 52, No. 1, pp. 13-22, ISSN 0928-8244, PMID 18081847

Bryers, J.D. (2008). Medical biofilms, *Biotechnol. Bioeng*., Vol. 100, No. 1, pp 1-18, ISSN 0006-3592, PMID 18366134

Burne, R. A. (1998). Oral streptococci: products of their environment. *J. Dent.Res.,* Vol. 77 No. 3, pp. 445–452, ISSN 0022-0345, PMID 9496917

Byun, M.W., Kim, J.H., Kim, D.H., Kim, H.J., Jo, C. (2007). Effects of irradiation and sodium hypochlorite on the micro-organisms attached to a commercial food container. *Food Microbiology*, Vol. 24, No. 5, pp. 544-548, ISSN 0740-0020, PMID 17367688

Carratalà, J. (2002). The antibiotic-lock technique for therapy of 'highly needed' infected catheters. *Clin Microbiol Infect*., Vol. 8, No. 5, pp. 282–9, ISSN 1723-7815, PMID 12047405

Ceri, H., Olson, M.E., Stremick, C., Morck, D.W., Read, R.R., Buret, A.G. (1999). The Calgary Biofilm Device: new technology for rapid determination of antibiotic susceptibilities of bacterial biofilms. *J Clin Microbiol*., Vol. 37, No. 6, pp. 1771–6, ISSN 0095-1137, PMID 10325322

Christensen, G.D., Simpson, W.A., Younger, J.J., Baddour, L.M., Barrett, F.F., Melton,bD.M., Beachey, E.H. (1985). Adherence of coagulasenegative staphylococci to plastic tissue culture plates: A quantitative model for the adherence of staphylococci to

medical devices. *J Clin Microbiol*., Vol. 22, No. 6, pp. 996-1006, ISSN 0095-1137, PMID 3905855

De Giusti, M. , De Medici, D., Tufi, D., Marzuillo, C., Boccia, A. (2007). Epidemiology of emerging foodborne pathogens. *Italian Journal of Public Health*, Vol 4, No 1, pp. 24-31, ISSN 1723-7815

Donlan, R.M., Costerton, J.W. (2002). Biofilms: survival mechanisms of clinically relevant microorganisms. *Clin. Microbiol. Rev.,* Vol. 15, pp. 167-193, ISSN 0893-8512, PMID 11932229

Dorobantu, L.S., Gray, M.R. (2010). Application of atomic force microscopy in bacterial research. *Scanning*, Vol 32, No 2, pp. 74-96. ISSN 0161-0457, PMID 20695026

Egervarn, M., Lindmark, H., Roos, S., Huys, G., Lindgren, S. (2007). Effects of inoculum size and incubation time on broth microdilution susceptibility testing of lactic acid bacteria. *Antimicrob Agents Chemother*., Vol 51, No. 1, pp. 394-6, ISSN 0066-4804, PMID 17060527

European Centre for Disease Prevention and Control (2010). ECDC, ISSN 1830-6160, Available from http://www.ecdc.eu.int/

Directive (EC) No. 7/2006 of the European Parliament and of the Council of 15 February 2006 concerning the management of bathing water quality and repealing Directive 76/160/EEC Official Journal of the European Union 4.3.2006 EN L 64/37

Falagas, M.E., Fragoulis, K., Bliziotis, I.A., Chatzinikolaou, I. (2007). Rifampicin-impregnated central venous catheters: a meta-analysis of randomized controlled trials. *J Antimicrob Chemother*., Vol 59 No. 3 pp. 359-369, ISSN 0305-7453, PMID 17255143

FDA, Food Protection Plan. Department of health and human services. Maryland: U.S. Food and Drug Administration; 2007. Available from www.fda.gov

Frioni ,A., Natalizi,T., Tendini, M., Fraveto, A., Pantanella, F., Berlutti, F., Pietropaoli, M., Passeri, D., Terranova, M. L., Rossi, M., Valenti, P. (2010). Biotimer Assay for counting bacterial biofilm. *Biophysics and Bioengineering Letters*, Vol. 3, No. 2, pp. 1-9, ISSN 2037-0199

Gandhi, M., Chikindas, M.L. (2007). Listeria: A foodborne pathogen that knows how to survive. *Int J Food Microbiol.,* Vol. 113, No. 1, pp.1-15, ISSN 0168-1605, PMID 17010463

Goel, A.S. and Richter-Dyn, N. (1974). Stochastic models in biology, *Academic Press* New York, 1974. ISBN 0124192505

Gottenbos, B., van der Mei, H.C., Klatter, F., Nieuwenhuis, P., Busscher, H.J. (2002). In vitro and in vivo antimicrobial activity of covalently coupled quaternary ammonium silane coatings on silicone rubber. *Biomaterials*, Vol. 23, No. 6, pp. 1417-1423, ISSN 0142-9612, PMID 11829437

Høiby, N., Bjarnsholt, T., Givskov, M., Molin, S., Ciofu, O. (2010). Antibiotic resistance of bacterial biofilms. *Int J Antimicrob Agents*., Vol.35, No. 4, pp. 322-32, ISSN 0924-8579, PMID 20149602

Hope, C.K., Clements, D., Wilson ,M. (2002). Determining the spatial distribution of viable and nonviable bacteria in hydrated microcosm dental plaque by viability profiling. *J Appl Microbiol*., Vol. 93, No. 3, pp. 448-455, ISSN 1364-5072, PMID 12174043

International Organization for Standardization (ISO). Microbiology of food and animal feeling stuffs. Horizontal method for the enumeration of β- glucuronidase-positive

Escherichia coli. Part.2: Colony-count technique at 44°C using 5-bromo-4-chloro-3-indolyl β –D-glucuronide. ISO 16649-2:2001

Janatova, J. (2000). Activation and control of complement, inflammation, and infection associated with the use of biomedical polymers. *ASAIO J.*, Vol. 46, No. 6, pp. 53-62, ISSN 1058-2916, PMID 11110295

John, T., Kopstein, A.B., John, O.C., Lai, C.I., Carey, R.B. (2001). In vitro adherence of Staphylococcus epidermidis to silicone punctual plugs and collagen implants. *J Cataract Refract Surg.*, Vol. 27, No. 8, pp. 1298-1302, ISSN 0886-3350, PMID 11524204

Gfeller, K.Y., Nugaeva, N., and Martin H. (2005). Rapid Biosensor for Detection of Antibiotic-Selective Growth of *Escherichia coli*. *Applied and Environmental Microbiology.*, Vol. 71, No. 5, pp. 2626–2631, ISSN 0099-2240, PMID 15870354

Lee, D.G., Park, S.J., Kim, S.J. (2007). Influence of pipe materials and VBNC cells on culturable bacteria in a chlorinated drinking water model system. *J Microbiol Biotechnol.*, Vol. 17, No. 9, pp. 1558–62, ISSN 1017-7825, PMID 18062238

Lewis, K. (2001). Riddle of biofilm resistance. *Antimicrob. Agents Chemother.,* Vol. 45, No. 4, pp. 999–1007, ISSN 0066-4804, PMID 11257008

Madigan, M,, Martinko, J., Dunlap, P., Clark, D. (2008). Brock biology of microorganisms. 12th *Pearson Ed*. Ltd. UK. ISBN-10 0321536150

Merritt K., Gaind A., Anderson J.M. (1998). Detection of bacterial adherence on biomedical polymers. *J Biomed Mater Res.*, Vol. 39, No. 3, pp. 415-422, ISSN 0021-9304, PMID 9468050

Mirani, Z.A., Jamil, N. (2010). Effect of sub-lethal doses of vancomycin and oxacillin on biofilm formation by vancomycin intermediate resistant Staphylococcus aureus. *J Basic Microbiol.*, Oct 21. [Epub ahead of print]) ISSN 0233-111X, PMID 20967790

Morbidity and Mortality Weekly Report. (June 2010). Summary of Notifiable Diseases — United States, 2008. Vol. 57, No. 54, Available from http://www.cdc.gov/mmwr/pdf/wk/mm5754.pdf

Mohammadi, Z., Abbott, P.V. (2009). Antimicrobial substantivity of root canal irrigants and medicaments: a review. *Aust Endod J.,* Vol. 35, No. 3, pp. 131-9, ISSN 1329-1947, PMID 19961451

Nair, P.N. (2004). Pathogenesis of apical periodontitis and the causes of endodontic failures. *Crit Rev Oral Biol Med,* Vol. 15, No. 6, pp. 348-81, ISSN 1329-1947, PMID 15574679

Oliver, S.P., Jayarao, B.M., Almeida, R.A (2005). Foodborne pathogens in milk and the dairy farm environment: food safety and public health implications. *Foodborne Pathog Dis*, Vol. 2, No. 2, pp. 115-29, ISSN 1535-3141, PMID 15992306

Pantanella, F., Valenti, P., Frioni, A., Natalizi, T., Coltella, L., Berlutti. F. (2008). BioTimer Assay, a new method for counting *Staphylococcus* spp. in biofilm without sample manipulation applied to evaluate antibiotic susceptibility of biofilm. Journal of Microbiological Methods. *J Microbiol Methods,* Vol. 75, No. 3, pp. 478-84, ISSN 0167-7012, PMID 18721833

Pascual, A, de Arellano, E.R., Martı´nez-Martı´nez L et al (1993). Effect of polyurethane catheters and bacterial biofilms on the in vitro activity of antimicrobial agents against *Staphylococcus epidermidis*. *J Hosp Infect*, Vol. 24, No. 3, pp. 211–18, ISSN 0195-6701, PMID 8104211

Ramalho, R., Cunha, J., Teixera, P., Gibbs, P.A. (2001). Improved methods for the enumeration of heterotrophic bacteria in bottled mineral waters. *J Microbiol Methods*, Vol. 44, No. 2, pp. 97–103, ISSN 0167-7012, PMID 11165338

Regulation (EC) No. 1441/2007 modified of EC Regulation No. 2073/2005 of the European Parliament and of the Council of 5 december 2007 on microbiological criteria of foodstaffs, Official Journal of the European Union 7.12.2007 L322/12.

Regulation (EC) No. 178/2002 of the European Parliament and of the Council of 28 January 2002 on laying down the general principles and requirements of food law, establishing the European Food Safety Authority and laying down procedures in matters of food safety. Official Journal of the European Union 1.02.2002 L31/1.

Regulation (EC) No. 2073/2005 of the European Parliament and of the Council of 15 november 2005 on microbiological criteria of foodstaffs, Official Journal of the European Union 22.12.2005 L338/1. Official Journal of the European Union 7.12.2007 L 322/12.

Regulation (EC) No. 852/2004 of the European Parliament and of the Council of 29 April 2004 on the hygiene of foodstuffs.Official Journal of the European Union 30.4.2004 L 139/1.

Ricucci, D., Siqueira, J.F. Jr (2010). Biofilms and apical periodontitis: study of prevalence and association with clinical and histopathologic findings. *J Endod,* Vol. 36, No. 8, pp. 1277-88, ISSN 0099-2399, PMID 20647081

Romeo, U., Palaia, G., Pacifici, L., Ripari, F., Gambarini, G., Moroni, C., Tarsitani, G., Petti,. S. (2003). Antimicrobial activity of Nd:YAG laser in endodontics. *J Dent Res* , Vol. 82 (Spec. Iss. B) 184, No 1378, ISSN 0022-0345

Rueckert, A., Ronimus, R.S., Morgan, H.W. (2005). Development of a rapid detection and enumeration method for thermophilic bacilli in milk powders. *J Microbiol Methods*, Vol. 60, No. 2, pp. 155–167, ISSN 0167-7012, PMID 15590090

Sandoe Jonathan, A. T., Wysome, J., Andrew, P., West, Heritage, J. and Wilcox, M. H.. (2006). Measurement of ampicillin, vancomycin, linezolid and gentamicin activity against enterococcal biofilms. *Journal of Antimicrobial Chemotherapy,* Vol. 57, No. 4, pp. 767–770, ISSN 0305-7453, PMID 16464896

Schwarz, F,, Aoki, A., Sculean, A., Becker, J. (2009). The impact of laser application on periodontal and peri-implant wound healing. *Periodontol 2000,* Vol. 51, pp. 79-108. ISSN 0906-6713, PMID 19878471

Shunmugaperumal, T. (2010). Microbial colonization of medical devices and novel preventive strategies. *Recent Pat Drug Deliv Formul,* Vol. 4, No. 2, pp. 153-73, ISSN 1872-2113, PMID 20236065

Telesca, V. (2010). Interaction of 810nm and 2940nm lasers with endodontic bacterial pathogens. Thesis in European Master Degree On Oral Laser Applications (EMDOLA), November 5, 2010, Tutors: Prof Umberto Romeo, Prof Francesca Berlutti, Dr Gaspare Palaia.

Thorpe, T.C., Wilson, M.L., Turner, J.E., Di Guiseppi, J.L.,Willert, M., Mirrett, S., Reller, L.B. (1990). BacT/Alert: An automated colorimetric microbial detection system. *J Clin Microbiol*, Vol. 28, No. 7, pp. 1608-1612, ISSN 0095-1137, PMID 2116451

Vacheethasanee, K., Marchant, R.E. (2000). Surfactant polymers designed to suppress bacteria (*Staphylococcus epidermidis*) adhesion on biomaterials. *J Biomed Mater Res*, Vol. 50, No. 3, pp. 302-312, ISSN 0021-9304, PMID 10737871

Velusamy, V., Arshak, K.., Korostynska, O., Oliwa, K.., Adley, C. (2010). An overview of foodborne pathogen detection: In the perspective of biosensors. *Biotechnology Advances*, Vol. 28, No. 2, pp. 232–254, ISSN 0734-9750, PMID 20006978

Vidana, R., Sullivan, A., Billström, H., Ahlquist M., Lund B. (2010). Enterococcus faecalis infection in root canals - host-derived or exogenous source? *Lett Appl Microbiol*, Vol. 52, No. 2, pp. 109-15, ISSN 0266-8254, PMID 21155997

Wilks, S.A., Michels, H., Keevil, C.W. (2006). Survival of *Listeria monocytogenes* Scott A on metal surfaces: implications for cross-contamination. *Int J Food Microbiol* , Vol. 111, No. 2, pp. 93-98, ISSN 0168-1605, PMID 16876278

Wilks, S.A., Michels, H., Keevil, C.W. (2005). The survival of *Escherichia coli* O157 on a range of metal surfaces. *Int J Food Microbiol*, Vol. 105, No. 3, pp. 445-454, ISSN 0168-1605, PMID 16253366

25

Indirect Amperometric Determination of Selected Heavy Metals Based on Horseradish Peroxidase Modified Electrodes

Philiswa N. Nomngongo[1], J. Catherine Ngila[1,2] and Titus A. M. Msagati[2]
[1]*School of Chemistry, University of KwaZulu Natal*
[2]*Department of Chemical Technology, University of Johannesburg*
South Africa

1. Introduction

Due to the high toxicity of heavy metals, it is crucial to detect ultra low levels of the metals, especially in drinking water. The common techniques include spectrometric techniques such as inductively coupled plasma- atomic emission spectroscopy, ICP-AES (Bettinelli et al. 2000; Rahmi et al. 2007; Tuzen et al. 2008) as well as anodic stripping voltammetry (Brainina et al. 2004). Even though ICP techniques have low detection limits (ranges from parts per billion, ppb to parts per trillion, ppt (Berezhetskyy et al. 2008), however, they are unsuitable for in-situ analysis, they are expensive, sophisticated and require skilled operators. For these reasons, the development of alternative techniques such as electrochemical biosensor techniques, offer alternative methods because they are sensitive, low cost and simple to operate (Wang et al. 2009b).

Recent developments have shown the use of electrochemical biosensors as indirect methods for detection of Cd^{2+}, Cu^{2+}, Cr^{3+}, Zn^{2+}, Ni^{2+} and Pb^{2+} using urease biosensor (Ilangovan et al. 2006; Tsai et al. 2003); Cd^{2+}, Co^{2+}, Zn^{2+}, Ni^{2+} and Pb^{2+} using alkaline phosphatase (Berezhetskyy et al. 2008); Cd^{2+}, Cu^{2+}, Zn^{2+} and Pb^{2+} by glucose oxidase (Ghica and Brett 2008); Hg^{2+} using glucose oxidase invertase and mutarose (Mohammadi et al. 2005); Cu^{2+}, Cd^{2+}, Mn^{2+} and Fe^{3+} using acetylcholinesterase (Stoytcheva 2002); and Cu^{2+}, Cd^{2+}, Zn^{2+} and Pb^{2+} by nitrate reductase (Wang et al. 2009b).

Horseradish peroxidase (HRP) biosensor has so far only been reported for detection of mercury (Han et al. 2001). This study sought to extend its application for detection of other metals such as lead, cadmium and copper. We have chosen cadmium due to its similarities with mercury with regards to toxicity as both metals, belong to the same group. In addition, we have also chosen copper and lead because of their common occurrence in environmental matrices (Pb from leaded petrol and Cu from wiring activities). Furthermore, copper is reported to show interaction with biological systems (Cecconi et al. 2002; Uriu-Adams and Keen 2005) and therefore interesting to see how it interacts with HRP enzyme.

The main aim of this present work is to investigate the inhibition of HRP enzyme by Cd, Pb and Cu, a phenomenon that can be employed for their indirect determination. Kinetic studies were done to determine the nature of enzyme inhibition (whether it is reversible or irreversible and if reversible whether it is competitive or noncompetitive). The apparent

Michealis-Menten constant (K_M^{app}) as well as maximum current (I_{max}) values in the absence and the presence of metal inhibitor were investigated. The developed biosensor was applied for determination of the Cd, Pb and Cu in tap water and landfill leachate sample.

2. Methodologies, results and discussion

2.1 Experimental reagents

All the chemicals used in this work were of analytical grade unless otherwise stated. Horseradish peroxidase (E.C. 1.11.1.7, 169 Units mg^{-1} powder, Sigma) aniline (99%), hydrochloric acid (37%), N,N-dimethylformamide (DMF), disodium hydrogen phosphate (dehydrated) and sodium dihydrogen phosphate (dehydrated) were all obtained from Sigma-Aldrich (South Africa). Cadmium and copper stock solutions (1000 ppm) were obtained from KIMIX Chemicals & Lab Supplies; and lead stock solution (1000 ppm) was obtained from Saarchem-Holpro Analytic (PTY) Ltd. Working solutions of hydrogen peroxide were prepared from 30% v/v stock solution obtained from Merck Chemical (PTY) Ltd.. Phosphate buffer (PBS, 0.1 M, pH 7.0) was used as a supporting electrolyte as per Songa et al. 2009.

3. Instrumentation

All electrochemical experiments were performed using BAS100W Electrochemical Analyzer (Bioanalytical Systems, West Lafayette, IN, USA). A 15 mL electrochemical cell consisting of Pt working electrode (A = 0.018 cm^2), Pt wire auxiliary electrode and Ag/AgCl (saturated 3 M NaCl) reference electrode. Supporting electrolyte solutions was degassed with argon gas before measurements performed at room temperature (20-25 °C). The PANI film was characterized using both Perkin Elmer Spectra 100 FT-IR Spectrometer (attenuated total reflectance, ATR) and UV-Vis Perkin Elmer Spectra spectrophotometer (PANI in DMF solution in quartz cuvette). UV photolysis of the leachate water sample was carried out by UV digester 705 equipped with a 500 W Hg lamp from Metrohm (Herisau, Switzerland). Inductively coupled plasma optical emission spectroscopy (ICP-OES) analysis of Cd, Cu, and Pb was performed using an Optima 5300 ICP-OES system (Perkin Elmer LLC, 761 Main Avenue, Norwalk, USA) equipped with AS 93plus autosampler.

4. Preparation of polyaniline (PANI) film modified electrode

Aniline was distilled before use. The platinum working electrode was first polished thoroughly with successive alumina slurries particle size of 1.0, 0.3 and 0.05 µm, and then rinsed with distilled water after each polishing step followed by 10 min sonication with ethanol and then water. The polyaniline (0.2 M aniline in 1.0 M HCl degassed in argon for 10 min) was electrochemically deposited on the platinum electrode (-200 mV to +1100 mV at 50 mVs^{-1} for 20 cycles). The PANI- modified electrode was rinsed with water before use. The modified electrode was used in subsequent biosensor fabrication.

5. Enzyme immobilization

The PANI film was reduced in PBS at a constant potential of –500 mV until the current signal reached a steady state value. This was followed by the oxidation at +0.65 V for 20 min

in the presence of HRP solution (50 µl of 2.0 mg ml^{-1} in 1.0 ml fresh PBS). During the oxidation process, the heme protein of HRP became electrostatically attached onto the PANI film (Songa et.al. 2009; Mathebe et al. 2004) .The biosensor was stored in PBS at 4 °C when not in use.

6. HRP Biosensor response to hydrogen peroxide

The response of the biosensor (Pt//PANI/HRP) to H_2O_2 was studied at pH 7.0 in PBS. Cyclic voltammetric (CV), differential pulse voltammetry (DPV) and amperometric responses of the biosensor were recorded by adding small aliquots of 0.01-0.05 M H_2O_2.

7. Determination of Cd^{2+}, Cu^{2+} and Pb^{2+} in model solutions

Amperometric measurements of HRP inhibition by cadmium, copper and lead were carried out in a cell containing 2.0 ml of 0.1 M PBS (pH 7.02) and constant concentration H_2O_2 (0.5 mM) with continuous stirring. The experiments were carried out at -0.20 V versus Ag/AgCl (3 M NaCl) and allowing the steady-state current to be attained. An appropriate volume (µl) of the inhibitor stock solution (10 ppm of each Cd^{2+}, Cu^{2+} and Pb^{2+}) was then added using a micropipette. After each experiment the enzyme electrode activity was regenerated by rinsing the electrode with distilled water.

8. Analysis of heavy metals in tap water and landfill leachate samples

Water samples were collected as follows: Tap water was collected from the Laboratory Tap at University of Western Cape, Bellville, Cape Town. Landfill leachate sample was collected from the Marrianhill landfill (Ethekwini municipal solid waste deposit). The leachate water sample was collected in polyethylene container and stored in the fridge at 4 °C.

Determination of heavy metals in tap water was achieved using standard addition method. The pH of the tap water samples was first adjusted from 8.90 to 7.04 before the analysis was carried out. The tap water sample (10 ml) was spiked with 0.1 ppm of each metal solution (Cd^{2+}, Cu^{2+} and Pb^{2+}) followed by amperometric analysis. For ICP-OES, the tap water sample was analysed without the addition of metal standards.

Leachate water sample is rich with organics; therefore prior electrochemical analysis, the organics were removed by passing the water sample through C-18 SPE column. The cartridges were first conditioned with 5 mL methanol followed by 5 mL water. The C-18 column retained the organics and the water sample containing inorganics was collected. The collected leachate water sample was spiked with 0.1 ppm of each metal solution (Cd^{2+}, Cu^{2+} and Pb^{2+}) followed by Pt/PANI/HRP biosensor analysis.

For ICP-OES analysis, the leachate samples were filtered with 0.45 µm pore size filter before they were subjected to UV digester. This procedure was done in order to destroy all dissolved organic matter in the landfill leachate sample. A UV digester 705 equipped with a 500 W Hg lamp from Metrohm was used. The quartz vessels were arranged concentrically around the Hg lamp with a distance of 2.5 cm. Ten mL of leachate samples were placed in quartz vessels and 100 µL H_2O_2 was added to each sample. The solution was irradiated with UV light for about 2 hour. The leachate water sample was then analyzed by ICP-OES.

9. Results and discussion

9.1 Electrosynthesis of PANI film

Multiscan voltammetry of Pt/PANI electrode was performed (result not shown). The redox peak currents increased with increasing scan rate while the peak potentials showed slight increase in positive potential. These observations shows that the polymer is electroactive and the peak currents are diffusion controlled (Mathebe et al. 2004). In order to calculate surface concentration of the PANI film, Γ^*_{PANI}, Brown-Anson equation (1) (Bard & Faulkner 2000) was used.

$$I_P = \frac{n^2 F^2 \Gamma^*_{PAN} A}{4RT} v \tag{1}$$

where n is the number of electrons (n = 2) transferred, F is the Faraday constant (96584 C mol^{-1}), Γ^*_{PANI} is the surface concentration of the PANI film (mol cm^{-2}), A is the surface area of the electrode (0.0177 cm^2), v is the scan rate (V s^{-1}), R is the gas constant (8.314 J $mol\ K^{-1}$), and T is the absolute temperature of the system (298 K). A graph of peak current versus scan rate was obtained and the slope of the curve was used to calculate the surface concentration of the PANI film. The surface concentration was found to be 7.8×10^{-7} mol cm^{-2}. The surface concentration obtained in our study was comparable to that reported by Mathebe et al. 2004 (1.85×10^{-7} mol cm^{-2}).

The Randles-Sevcik equation (2) was used to calculate the diffusion coefficient of the electrons within the polymer (Gau et al. 2005).

$$i_p = 2.69\times10^5 n^{3/2} A D_e^{1/2} C v^{1/2} \tag{2}$$

where i_p is the peak current (A), n is the number of electrons appearing in half-reaction for the redox couple, A is the area of the electrode (cm^2), D is the diffusion coefficient (cm^2/s), C is the concentration (mol/cm^3) and v is scan rate (V/s). Equation 2 was used to plot peak current versus the square root of the scan rate and the slope of the linear regression was used to estimate the diffusion coefficient of the electrons within the polymer (D_e) as $4.07\times10^{-8} cm^2\ s^{-1}$.

10. Spectroscopic characterization of polyaniline

The absorption spectrum of PANI (dissolved in DMF) shows two characteristic absorption peaks at 340 nm and 660 nm. The first absorption peak was assigned to π–π^* transition of the benzenoid rings and the second was attributed to the transition of benzenoid rings into quinoid rings (Laska & Widlarz 2005; Kan et al. 2006). The results (UV-Vis characterization of PANI) obtained in this study are in close agreement with the literature values (Laska &Widlarz 2005; Kan et al. 2006; Singh et al. 2008; Mazeikiene et al. 2007; Kang, Neoh & Tan 1998).

The FTIR absorption band at 3325 cm^{-1} was assigned to N-H stretching of the amine group of polyaniline (spectrum not shown). The peaks at 1596 and 1493 cm^{-1} which are characteristics of, polyaniline, were most likely due to the C=C stretching of quinoid and benzenoid groups, respectively (Lakshmi et al. 2009; Kim et al. 2001).

11. Cyclic Voltammetric (CV) and Differential Pulse Voltammetric (DPV) response of Pt/PANI/HRP biosensor to hydrogen peroxide

The electrochemical behaviour of Pt/PANI/HRP electrode in the absence and presence of H_2O_2 in PBS (0.1 M, pH 7.02) was studied using CV and DPV. Figure 1 shows CV (A) and DPV(B) of Pt/PANI/HRP electrode in different concentrations of H_2O_2 (0-6.9 mM) at scan rate of 10 mV s^{-1} and 20 mV s^{-1} for CV and DPV, respectively. The value used in this study for the optimum concentration of HRP was as per Ndangili et al. (2009) and Songa et al. (2009). The effect of pH on HRP electrode response was investigated by CV in the pH ranges from 5.5 to 8.5 in the presence of 1.0 mM H_2O_2. The HRP electrode response current achieved a maximum value at pH 7.0. Therefore, in order to obtain maximum sensitivity, 0.1 M PBS solution of pH 7.0 was used throughout this study.

As expected, in the absence of H_2O_2, no significant current was observed. However increasing the amount of H_2O_2 showed increased cathodic peak current intensity due to the reduction of H_2O_2. In order to confirm whether the change in current intensity observed was due to the enzymatic catalytic reduction of H_2O_2, control experiments in the absence of HRP were carried out. At both the bare electrode (Pt) and polymer modified surface (Pt//PANI) no H_2O_2 reduction current was observed at -200 mV. This is because, the reduction reaction of H_2O_2 at both electrodes in the absence of HRP, is very slow and usually occurs at higher potentials. The difference in the observations made for the control experiments (Pt and Pt/PANI) compared to that for Pt/PANI/HRP confirms that the increase in the cathodic current was due to the direct electron transfer between the HRP molecules and the electrode (Wang & Wang 2004). Moreover, PANI provides a suitable platform for the immobilization of HRP on the platinum electrode surface and it also mediates in electron transfer between HRP and the electrode (Gerard et al. 2002). Thus the reduction peak is an indication of the electrocatalytic activity of the enzyme on H_2O_2 (Sun et al. 2004).

Figure 2 shows the possible mechanism of electric transduction between the platinum electrode, PANI and HRP enzyme active site combined with electrocatalytic reduction process of H_2O_2 by HRP. It can be seen from figure 2 that H_2O_2 is reduced by HRP to form water and in turn HRP gets oxidized to form Compound I. The latter is converted to HRP through the formation of intermediate (Compound II) via a two-electron reduction step (Iwuoha et al. 1997). The reduction of Compound I is due to the direct electron transfer that takes place between the PANI modified electrode and the enzyme (Liu & Ju 2002).

The relatively low potential value for H_2O_2 reduction (-200 mV) in the presence of HRP, ensures minimal risk of interfering reactions of other electroactive species in solution as well as low background current and noise levels (Tong et al. 2007; Wang &Wang 2004).

12. Amperometric responses of Pt/PAN/HRP to H_2O_2

Amperometric responses of Pt/PANI/HRP biosensor were investigated by consecutively increasing the concentration of H_2O_2 at a working potential of -200 mV. Figure 3 presents a typical steady state current-time plots obtained with the fabricated biosensor upon successive additions of 10 µL of 0.001 M H_2O_2 into 2.0 mL PBS with the calibration plot as an inset. It was observed that, upon the addition of H_2O_2 into the PBS, the reduction current rises sharply to reach the steady state value. In addition, the biosensor attained 95% steady state current within 5 seconds after each addition of 10 µL 0.010 M H_2O_2. This observation

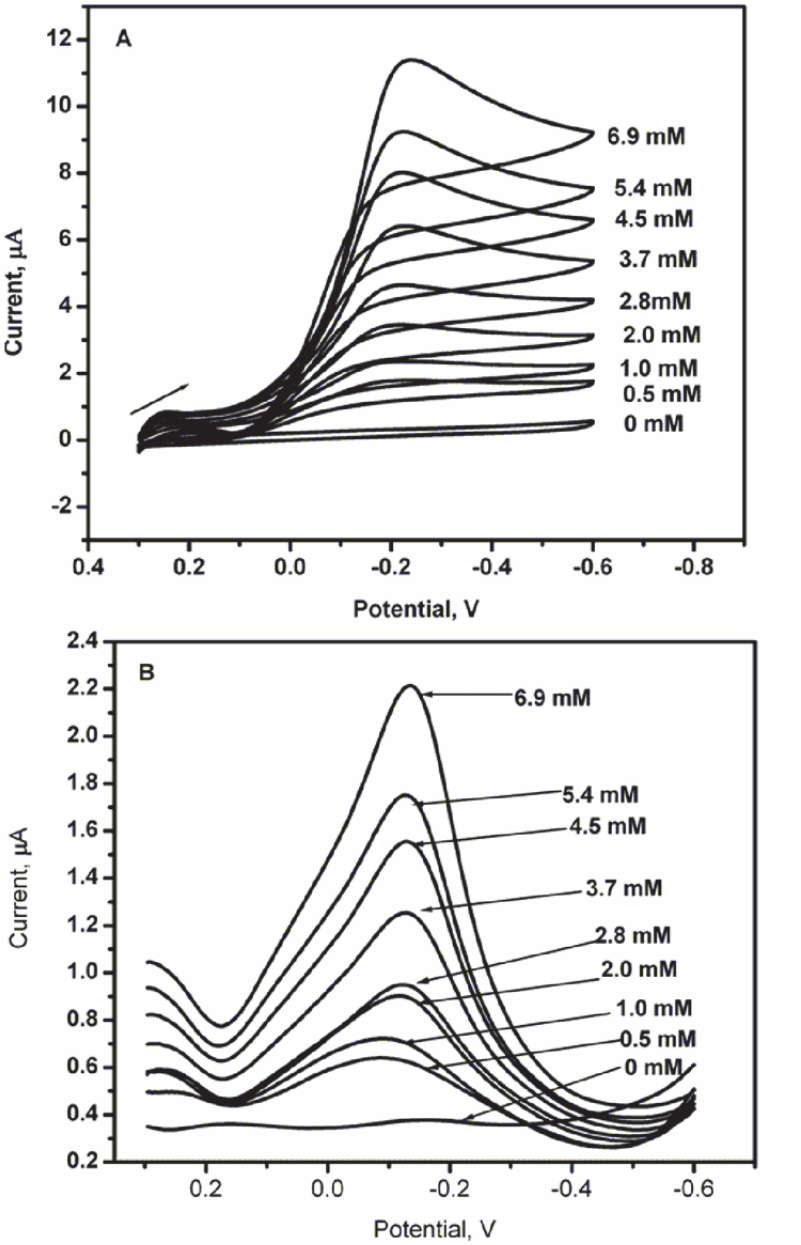

Fig. 1. Cyclic voltammograms and (B) Differential pulse voltammograms for the response of the biosensors (Pt/PANI/HRP) to different concentrations of H_2O_2 ranging from 0.5 to 6.9 mM made up in 0.1 M PBS (pH 7.02). CV experiments: scan rate, 10 mV/s; DPV experimental conditions were: scan rate 20 mV s^{-1} pulse width: 50 msec and pulse amplitude: 20 mV. Arrow (→) indicate direction of potential scan

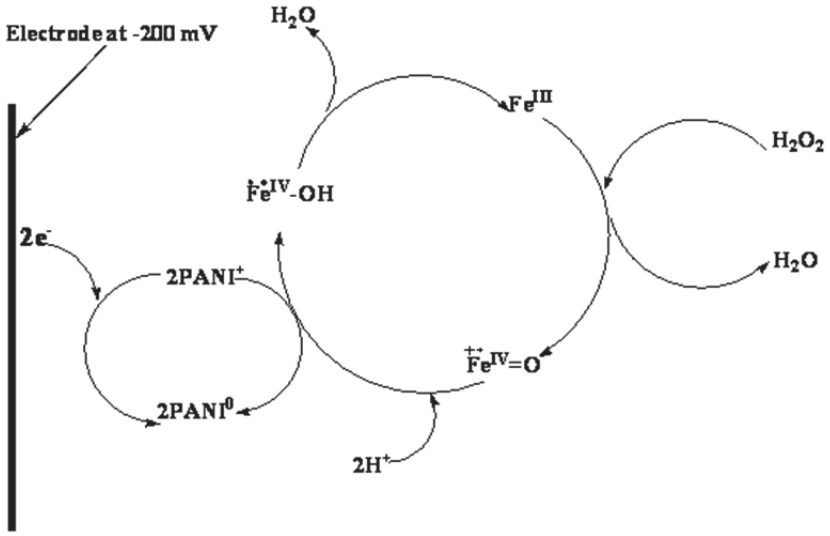

Fig. 2. Mechanism of electric transduction between the platinum electrode, PANI and HRP enzyme active site.

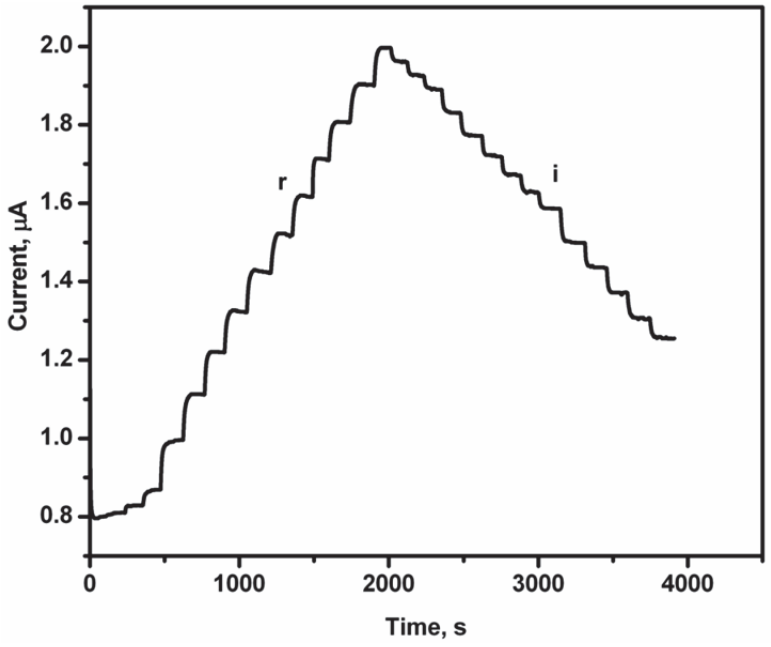

Fig. 3. Amperometric responses of Pt/PANI/HRP to successive additions of 10 μL 0.05 mM of hydrogen peroxide (inset shows the calibration curve). Potential: −0.2 V; supporting electrolyte: 0.1 M PBS (pH 7.02).

implied a fast response of the fabricated biosensor.The response currents at the biosensor were linear to H_2O_2 in the range from 0.05 to 3.17 mM with a correlation coefficient of 0.9991 (n = 18); sensitivity of 1.75 μA mM^{-1}; and a detection limit of 36.8 nM (0.0368 μM) (estimated at a signal-to-noise ratio of 3).

13. Kinetics of Pt/PANI/HRP electrode

A plot (not included) of the reciprocal of current versus the reciprocal of H_2O_2 concentration (Lineweaver–Burk plot) showed a linear relationship implying a kinetic behavior (Liu and Ju 2002; Wang, et al. 2009a). Using equation 3, Michaelis–Menten constant of the enzyme could be calculated as per previous studies (Liu, and Ju 2002; Mathebe, Morrin, and Iwuoha 2004):

$$\frac{1}{I} = \frac{1}{I_{\max}} + \left(\frac{K'_M}{I_{\max}[H_2O_2]} \right) \tag{3}$$

where I is the observed response current, $I_{\max}$ is the maximum steady state current that can be attained for the system (Pt//PAN/HRP biosensor), K_M^{app} is Michaelis–Menten constant and $[H_2O_2]$ is the concentration of H_2O_2 in the bulk solution. The *slope (*1.18 $\mu A^{-1}mM$*)* and the *y-intercept* (0.958 μA^{-1}) of the Lineweaver–Burk plot are equal to $I_{\max}$ and $\frac{K_M^{app}}{I_{\max}}$, respectively. The values of $I_{\max}$ and K_M^{app} were estimated as 1.04 μA and 1.23 mM, respectively. The K_M^{app} value obtained in our study was relatively better (lower) than previous studies (Wang et al. 2009a; Liu & Ju 2002; Ndangili et al. 2009. Since K_M^{app} is inversely proportional to the affinity of the enzyme for the substrate (Wang et al. 2009; Ansari et al. 2009), based on the value 1.23 mM it can be concluded that Pt/PANI/HRP electrode exhibited high affinity towards H_2O_2. The differences in the values obtained by different workers indicate that the affinity between H_2O_2 and HRP is plainly dependent on the immobilizing materials and procedure used (Wang et al. 2009).

14. Reproducibility, repeatability and stability of Pt/PAN/HRP biosensor

To evaluate the reproducibility of the HRP based biosensor, six biosensors were prepared under similar conditions separately. The amperometric responses of each biosensor to successive additions of H_2O_2 (0.05 to 0.30 mM) were recorded and gave a relative standard deviation (RSD) of 3.8% (n = 6). The precision (repeatability) of a selected biosensor was investigated by recording the response current using 0.05 mM H_2O_2 for replicate experiments (n = 10). The biosensor showed a high precision with a %RSD of 2.1%. The stability of the Pt/PANI/HRP electrode (stored in 0.1 M PBS at 4 °C in between measurements) was tested every two days by amperometric measurements in the presence of 0.05 mM H_2O_2. After two weeks, the biosensor retained > 95% of its initial response, indicating good stability. The latter implies that the HRP molecules were firmly immobilized in the PANI films which provided a biocompatible microenvironment.

15. Detection of heavy metals (Cd^{2+}, Cu^{2+} and Pb^{2+}) in model solutions

Heavy metals such as Cd^{2+}, Co^{2+}, Cu^{2+}, Fe^{3+}, Mn^{2+}, Ni^{2+} and Pb^{2+} as well as some organic and inorganic compounds such as sodium azide, cyanide, L–cystine, dichromate, ethylenethiourea, hydroxylamine, sulfide, vanadate, p–aminobenzoic acid are well-known inhibitors of horseradish peroxidase (Zollner 1993). Figure 4 (I) shows amperometric responses of Pt/PANI/HRP to successive additions of 0.05 mM H_2O_2 (denoted by r) followed by addition of Cd^{2+} (denoted by i). It can be observed that the current for the electrocatalytic reduction of H_2O_2 decreases upon the addition of Cd^{2+}. This observation clearly showed that the catalytic activity of HRP at Pt/PANI electrode is inhibited by Cd^{2+} by binding to the enzymes active sites. The inhibition of HRP activity was analyzed by monitoring the current decrease at -0.20 V using the following procedure: H_2O_2 was added to PBS (electrolyte solution) and the current response was recorded. After the stabilization of the steady-state current response, Cd^{2+} was added, leading to an immediate decrease in the biosensor response.

The other two heavy metal ions (Pb^{2+} and Cu^{2+}) showed the same behaviour. Calibration plots for the determination of the metals in the range 0.05 to 60.8 ppb were obtained. The linear ranges were established as 4.76-55.3 ppb for Cd^{2+} and Pb^{2+} while that for Cu^{2+} was 2.38-52.8 ppb. Limits of detection (LOD= $\frac{3\times SD}{m}$) and limits of quantification (LOQ= $\frac{10\times SD}{m}$)

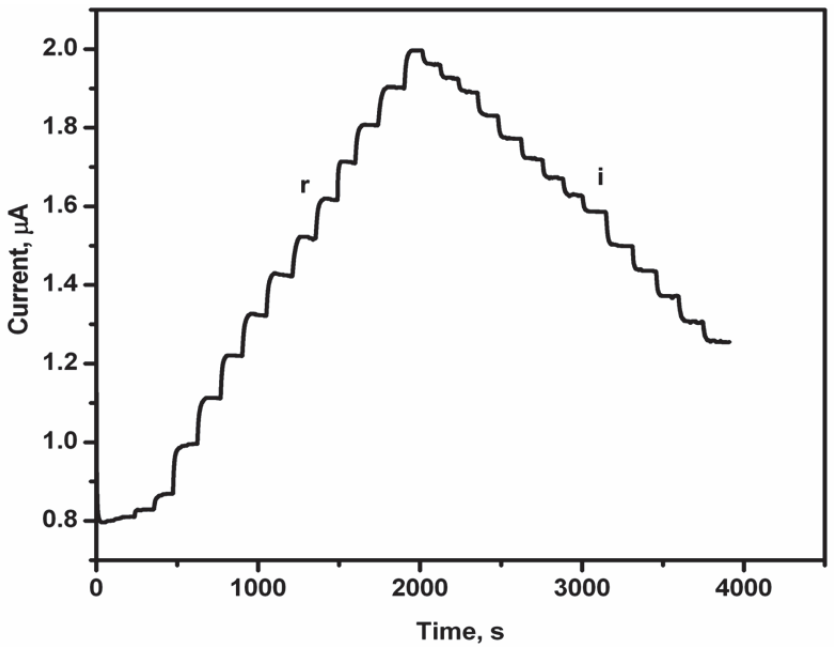

Fig. 4. Typical amperometric responses of Pt/PANI/HRP biosensor to successive additions of 0.05 mM hydrogen peroxide (r) and Cadmium (i). Applied potential: −0.20 V; supporting electrolyte: 0.1 M PBS (pH 7.02).

were calculated and their values are presented in Table 1. Where SD is standard deviation of the blank signal (n = 8) obtained in PBS (SD = 2.4×10^{-4} μA) and m is the slope of the calibration curve. The low LOD and LOQ values confirmed good sensitivity of the proposed biosensor method for the determination of heavy metals. Table 6 shows a summary of analytical response and linear regression characteristics of calibration curves for heavy metals. The inhibition of heavy metals to HRP enzyme is reversible, and the biosensor can be reused (beyond 10 runs) after rinsing with double distilled water.

Metal ion	Linear range/ppb	Slope/μAppb^{-1}	Correlation Coefficients (R^2)	LOD/ppb	LOQ/ppb
Cd^{2+}	4.76-55.3	7.945×10^{-3}	0.9985	0.091	0.30
Pb^{2+}	4.76-40.5	2.100×10^{-2}	0.9995	0.033	0.12
Cu^{2+}	2.38-52.8	7.230×10^{-3}	0.9990	0.10	0.33

Table 1. A summary of analytical characteristics and regression parameters for calibration curves for determination of heavy metals.

16. Inhibition studies

The values of the steady state current in the absence (I_0) and in the presence (I_i) of an inhibitor were determined from the recorded amperograms in Figure 4. The inhibition percentage ($I\%$) was calculated from the following expression (Nwosu et al. 1992):

$$I\% = \frac{I_0 - I_i}{I_0} \times 100\% \quad (4)$$

The $I\%$ values obtained were used to compare the inhibitory effects of the different metal ions on the activity of the immobilized HRP. Inhibition plots showing the effects of heavy metals on the activity of the immobilized HRP are presented in Figure 5. The order of inhibition was found to increase from Pb^{2+} (32.8 %), Cu^{2+} (43.4 %) to Cd^{2+} (51.1 %) in the presence of 0.95 mM H_2O_2. It should be noted that the higher the $I\%$ value the higher the degree of enzyme inhibition by the heavy metal.

There are two approaches that can be used for inhibition studies; incubation method and direct method (without incubation) and in this study the latter was employed. It was observed that when using the direct method, it is difficult to attain the concentration that causes 50% inhibition (IC_{50}) (Songa et al. 2009); this worked reasonably well for Cd^{2+} (51.1%) with the value for IC_{50} calculated as 3.13 ppm but was not successful for Pb^{2+} and Cu^{2+}. Therefore unlike Cd^{2+}, in order to attain the 50% inhibition (IC_{50} value) for Pb^{2+} and Cu^{2+}, either a higher concentration of the metal can be used or the incubation method can be employed.

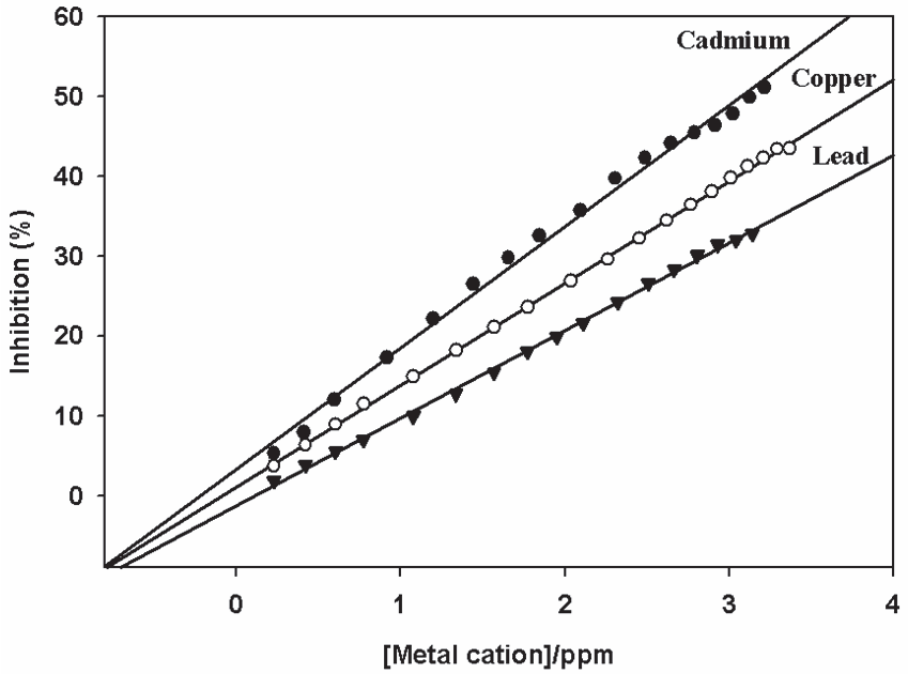

Fig. 5. Plots showing the Inhibition of Pt/PANI/HRP biosensor by heavy metals; Cd^{2+}, Cu^{2+} and Pb^{2+} .

After successfully obtaining the IC_{50} value for Cd^{2+} using direct approach, the results from the latter approach were used to investigate the inhibition kinetics and the type of inhibition (competitive or non-competitive).

17. Investigation of inhibition kinetics and mechanism

The amperometric response of the biosensor to various H_2O_2 concentrations (in 0.1 M PBS, pH 7.02) in the absence (0 ppm Cd^{2+}) and presence (3.13 ppm Cd^{2+}, IC_{50}) of an inhibitor was recorded at -200 mV (Figure 6A). The response of the biosensor to various H_2O_2 concentrations in the presence of an inhibitor was done as follows; HRP electrode was first incubated in PBS containing 3.13 ppm Cd^{2+} for 20 min followed by the successive addition of different concentrations of H_2O_2. A fast response of the biosensor to the additions of different concentrations of H_2O_2 was observed in the absence of Cd^{2+} whereas the presence of 3.13 ppm Cd^{2+} gave a slow response. Studies suggest that during incubation, Cd^{2+} slowly binds to the enzyme and leads to gradual conformational changes (Keyhani et al. 2003, **Tayefi-Nasrabadi et al. 2006**). Therefore, it can be suggested that the difference in background current could be due to the conformational changes of HRP. Figure 6B shows the Lineweaver–Burk plots for enzymatic reactions. The *slope* and the *y-intercept* values of the linear plots were used to calculate apparent Michealis-Menten constants K_M^{app} and maximum current (I_{max}) in the absence and the presence of Cd^{2+} (Table 2).

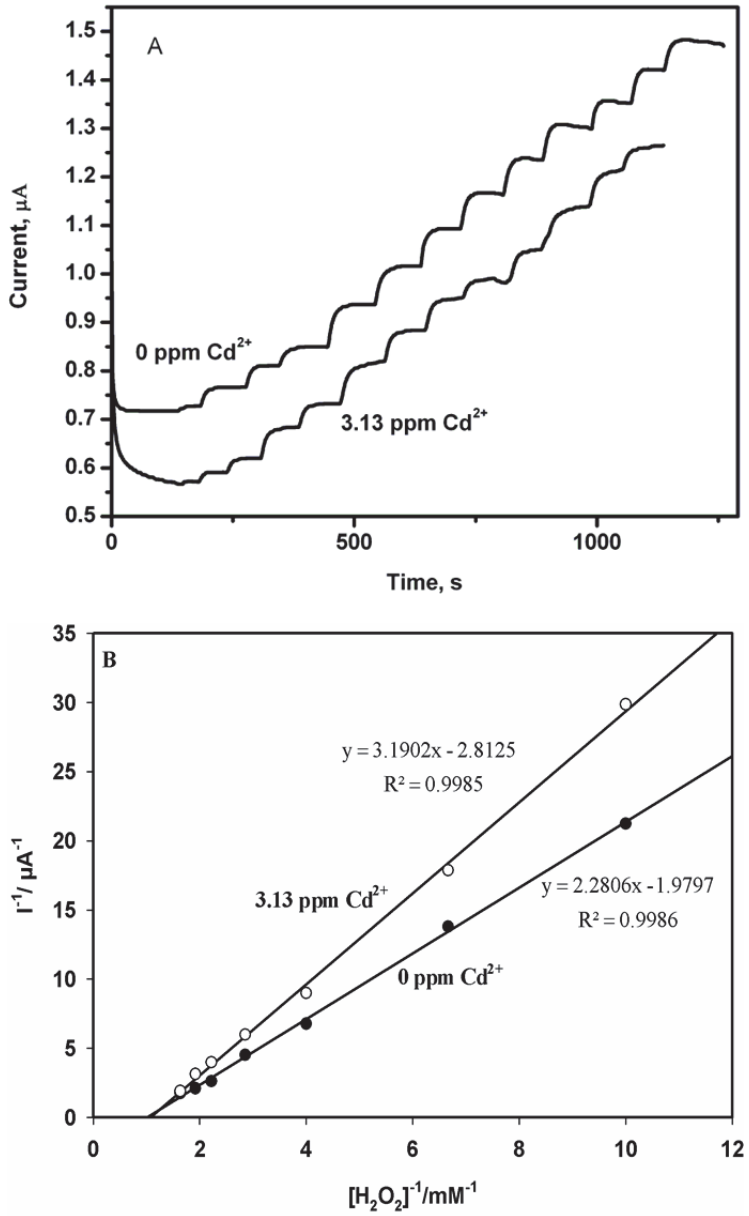

Fig. 6. (A) Pt/PANI/HRP biosensor response to successive additions of H_2O_2 in the absence and presence of heavy metals, at applied potential of -0.20 V. (B) Lineweaver- bulk plot for HRP response to H_2O_2 in the absence and presence of heavy metals.

Kinetic parameters	*0 ppm Cd^{2+}*	*3.125 ppm Cd^{2+}*
Slope μA^{-1}mM	2.28	3.19
y-intercept μA^{-1}	1.98	2.81
K_M^{app} /mM	1.16	1.13
I_{max} /μA	0.505	0.356

Table 2. Apparent Michealis-Menten constants (K_M^{app}) and I_{max} in the absence and the presence of Cd^{2+} (3.125 ppm).

The K_M^{app} values for Cd^{2+} in the absence (1.16 mM) and the presence (1.13 mM) of the inhibitor were not significantly different (based on statistical t-test, n =3, p = 0.05), whereas the I_{max} values decreased. The decrease in I_{max} indicates that the type of inhibition in this study is reversible and also non-competitive inhibition and the inhibition constant was found to be 27.8 μM (Amine et al. 2006; Stoytcheva 2002). Non-competitive inhibition occurs when the inhibitor binds to both the enzyme and enzyme-substrate complex. The possible mechanism of non-competitive inhibition can be seen in Scheme 1 (Amine et al. 2006); where E represents HRP enzyme, S represents H_2O_2, ES represents Compound I containing an oxyferryl centre with the iron in the ferryl state ($Fe^{IV}=O$), and a porphyrin π cation radical; EIS presents HRP-heavy metal-H_2O_2 complex; I represents heavy metal cation and P represents H_2O.

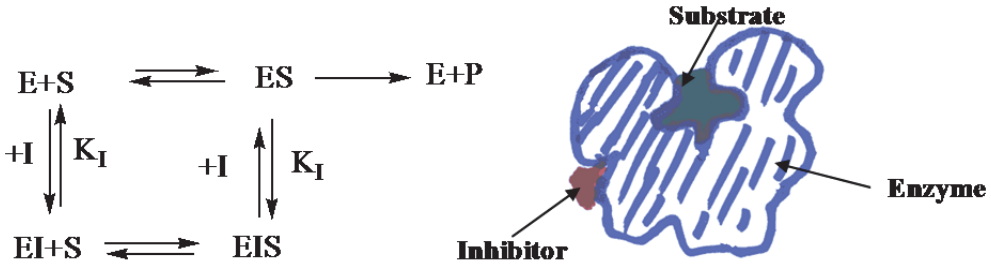

Scheme 1. Mechanisms for reversible non-competitive enzyme inhibition.

18. Selectivity of Pt/PAN/HRP biosensor

In order to show the selectivity of Pt/PANI/HRP biosensor, the response of possible interferences in tap water (drinking water) components on the determination of heavy metals were investigated. A range of cations were measured to examine if they interfered with the determination of heavy metal cations. The effect of possible interferences in drinking water such as Mg^{2+}, Zn^{2+}, Ca^{2+}, K^{+}, Fe^{3+} and Na^{+} was investigated by Pt/PANI/HRP biosensor under the same working conditions. Table 3 presents the possible interferences tested with the biosensor. It can be observed that most cations had minimal effect (<5%) on the determination of heavy metals apart from Fe^{3+} which also inhibit HRP activity. However, at the same concentration (1.0 ppm), the degree of inhibition by interferent is still less than that of the analyte cations

Interferent	Concentration (ppm) Added	%Inhibition
Fe^{3+}	1.0	7.46
Fe^{2+}	1.0	2.01
Zn^{2+}	1.0	1.86
Mg^{2+}	1.0	2.43
Na^{+}	1.0	2.58
K^{+}	1.0	2.06
Ca^{2+}	1.0	2.56

Table 3. Interference studies showing the effects of cations on the response of Cd^{2+}, Pb^{2+} and Cu^{2+}.

Apart from the degree of inhibition of the interfering species, the selectivity of the biosensor was also evaluated by two methods; mixed and separate solutions (Stefan et al. 2001; Macca & Wang 1995) with respect to Cd^{2+}, Cu^{2+} and Pb^{2+}. For the mixed solution method, the concentration of the interfering cation was 1.0 ppm and the concentration of the analyte was 0.5 ppm. In the case of separate solution method, the concentration of the analyte and that of interfering cation were equal (1.0 ppm). Amperometric selectivity coefficients and response ratio were calculated using equations (5) and (6) for mixed solutions and separate solutions (Macca & Wang 1995), respectively.

$$K_{i,j}^{amp} = \left(\frac{\Delta I_j}{\Delta I_t - \Delta I_j} \right) \times \frac{c_i}{c_j} \tag{5}$$

$$R_{i,j} = \frac{\Delta I_j}{\Delta I_i} \tag{6}$$

where ΔI_t, ΔI_j and ΔI_i are current values recorded for mixed solution, interfering cation and analyte of interest, respectively; c_j and c_i are concentrations of the interfering cation and

the analyte, respectively. The $K_{i,j}^{amp}$ and $R_{i,j}$ values in Table 4 suggest that Fe^{3+} is a strong interferent while the other cations species are relatively not interfering with the determination of cadmium, copper and lead. Therefore, the results suggest that Pt/PANI/HRP electrode can be used for the determination of cadmium, copper and lead in the presence of other cations except Fe^{3+}.

Table 4. Interference studies showing the effects of cations on the response of Cd^{2+}, Pb^{2+} and Cu^{2+} using mixed (amperometric selectivity coefficients, $K_{i,j}^{amp}$) and separate (response ratio, $R_{i,j}$) solution methods.

Interferent, j	Amperometric selectivity coefficient, $K_{i,j}^{amp}$			Response ratio, $R_{i,j}$		
	Cd	Cu	Pb	Cd	Cu	Pb
Fe^{3+}	0.80	1.33	2.28	0.56	0.74	0.89
Fe^{2+}	4.06×10^{-3}	4.72×10^{-3}	4.50×10^{-3}	1.10×10^{-2}	1.35×10^{-2}	1.61×10^{-2}
Zn^{2+}	5.69×10^{-3}	6.63×10^{-3}	6.31×10^{-3}	1.42×10^{-2}	1.42×10^{-2}	2.25×10^{-2}
Mg^{2+}	3.64×10^{-3}	4.23×10^{-3}	4.03×10^{-3}	9.12×10^{-3}	1.21×10^{-2}	1.24×10^{-2}
Na^{+}	3.64×10^{-3}	4.23×10^{-3}	4.03×10^{-3}	6.15×10^{-3}	1.12×10^{-2}	1.44×10^{-2}
K^{+}	4.15×10^{-3}	4.15×10^{-3}	3.95×10^{-3}	8.95×10^{-3}	1.19×10^{-2}	1.42×10^{-2}
Ca^{2+}	3.66×10^{-3}	3.66×10^{-3}	3.49×10^{-3}	7.90×10^{-3}	1.05×10^{-2}	1.25×10^{-2}

19. Application of Pt/PANI/HRP for analysis heavy metals in tap water and landfill leachate samples

The performance of the biosensor (Pt/PANI/HRP) was tested using both tap water and landfill leachate water samples. The latter were collected from Sensor Lab in the University of Western Cape (Cape Town, South Africa) and Marrianhill landfill in Durban (South Africa). The quantification of Cd^{2+}, Pb^{2+} and Cu^{2+} in water samples was achieved by employing the standard addition method. For tap water sample, the sample preparation was not required. This is because the possible interferences that are normally present drinking water samples did not have much effect on the catalytic activity of immobilized HRP. The procedure involved initially measuring the response of the biosensor after subsequent additions of 0.05 mM H_2O_2 followed by metal-spiked tap water (0.1 ppm metal ion solution), into the PBS solution containing H_2O_2 (0.5 mM). On addition of the water sample, current intensity was observed to decrease and the magnitude of the decrease was proportional to the amount of metal spiked. The decrease in the response current was most likely due to the inhibition of the enzyme by the metal ions. A possible dilution effect due to increased volume of added tap water was checked by setting a control experiment where deionized water was used instead of metal spiked tap water. The inhibition effect was not observed with the deionized water. In order to double-check the effect of metal inhibition, H_2O_2 was added into the mixture and resulted in an increase in current intensity. Similar

observations have been made by Han et al. (2001); Stoytcheva (2002) and Ghica & Brett (2008).

The concentrations of Cd^{2+}, Pb^{2+} and Cu^{2+} (0.4507 ppb Cd^{2+}, 0.2201 ppb Pb^{2+}, 41.77 ppb Cu^{2+}) in the tap water sample (analysed in triplicate for each metal) were calculated from the calibration curves and the results are presented in Table 5.

	Tap water sample		Landfill leachate water sample	
Cation	**Amperometric Biosensor**	**ICP-OES**	**Amperometric Biosensor**	**ICP-OES**
Cd^{2+}	0.46 ± 0.004	0.34 ± 0.05	ND	ND
Pb^{2+}	0.22 ± 0.0008	ND	ND	ND
Cu^{2+}	41.8 ± 0.07	41.5 ± 0.2	14.6 ± 0.09	14.0 ± 0.03

Concentrations were determined in ppb; ND: not detected, ± standard error ($SE_{\bar{x}} = \frac{s}{\sqrt{n}}$, where s is the sample standard deviation and n is the size of the sample).

Table 5. Comparison between the two analytical techniques: Amperometric biosensor and ICP-OES for determination of heavy metals in Tap water sample.

The values obtained were compared against the allowed MCLs by USEPA in drinking water. The MCLs are given as 5 ppb, 15 ppb and 1300 ppb for cadmium, lead and copper, respectively. The World Health Organization (WHO 2004) on the other hand has given the guideline values for cadmium, lead and copper in drinking water as 3.0 ppb, 10 ppb and 2000 ppb, respectively. It can be seen that the concentrations of Cd^{2+}, Pb^{2+} and Cu^{2+} obtained in this study are much lower than the USEPA and WHO guideline values, implying that the drinking water was not contaminated and therefore safe for human consumption.

In the case of landfill leachate water sample, sample preparation was performed. Solid phase extraction (amperometric biosensor) and UV digestion (ICP-OES) were used to minimize organic interferences. After removal of organics the same procedure that was applied for tap water sample was followed. Summary of the concentrations found by the fabricated biosensor are presented in Table 5.

Results of heavy metals obtained by amperometric biosensor and ICP-OES were compared statistically by Student t-test (two-tailed). At 95% confidence interval, the results by the two analytical techniques for the determination of Cu^{2+} were not significantly different ($p = 0.035 < 0.05$). However, the two methods differed significantly for the determination of cadmium, at 95% confidence interval ($P = 0.116 > 0.05$). The reason for this discrepancy could be the difference in limits of detection (LOD) capabilities by the two techniques. The detection limit for cadmium was 2.70 ppb with the ICP-OES and 0.091 ppb (91 ppt) with the biosensor. Thus the detection limit for Cd^{2+} obtained with the biosensor is lower by a magnitude of 30 to that by ICP-OES. It should be noted that the concentration of Cd^{2+} in the tap water sample was less than the LOD of ICP-OES (LOD = 2.70 ppb cited from ICP-OES operation manual). This explains the poor precision when the tap water sample was analyzed by ICP-OES in triplicate (3 repeated runs gave 0.41, 0.25 and 0.35 ppb). Lead on the other hand, was not

detected probably because its level was lower than 90 ppb (conc. of Pb^{2+} was 0.22 ppb by the biosensor). It can be concluded that the Pt/PANI/HRP biosensor technique is suitable for determination of ultra trace levels of heavy metals in drinking water.
The amount of copper in landfill leachate samples (Table 5) showed good correlation between the results obtained with the biosensor and the standard technique. Applying the Student t test, it was possible to verify that the averages obtained by the both methods are not significantly different at a confidence level of 95% ($P = 0.009 < 0.05$). With both methods, cadmium and lead were not detected.

20. Conclusions

An inhibition amperometric biosensor for the determination of selected heavy metals was fabricated on the base of the inhibition to horseradish peroxidase, which was immobilized on platinum-polyaniline electrode. Inhibition of HRP activity by heavy metals followed noncompetitive reversible mechanism. The HRP biosensor exhibited fast response, high sensitivity towards the determination of heavy metals (LOD of 0.091, 0.033 and 0.10 ppb for Cd^{2+}, Pb^{2+} and Cu^{2+}, respectively). The fabricated biosensor was applied for the determination of heavy metals in real samples (landfill leachate and tap water). The evaluation of the amperometric biosensor measurements against the standard technique (ICP-OES technique) verified the suitability of biosensor for rapid analysis of heavy metals. Moreover, the amperometric biosensor requires minimal sample preparation as compared to the tiresome sample pretreatment procedures required prior to metal determination by the conventional ICP-OES method.

21. Acknowledgement

The authors are grateful for NRF funding through grant-holder Dr Anna Soares. They also acknowledges the Sensor Lab at University of Western Cape where part of the work for this study was carried out as well as NRF sponsorships through grant-holder Prof E I Iwuoha

22. References

Amine, A., Mohammadi, H., Bourais I. & Palleschi G. (2006). Enzyme inhibition-based biosensors for food safety and environmental monitoring. *Biosensors and Bioelectronics* 21: 1405–1423.

Ansari, A. A., Solanki, P. R. & Malhotra, B. D. (2009). Hydrogen peroxide sensor based on horseradish peroxidase immobilized nanostructured cerium oxide film. *Journal of Biotechnology* 142: 179–184.

Baba, A., Tian, S., Stefani, F., Xia, C., Wang, Z., Advincula, R. C., Johannsmann, D. & Knoll, W. (2004). Electropolymerisation and doping/dedoping properties of polyaniline thin films as studied by electrochemical-surface plasmon spectroscopy and by the quartz crystal microbalance. *Journal of Electroanalycal Chemistry*. 562: 95–103.

Bard, A. J. & Faulkner, L. R. (2000). *Electrochemical Methods: Fundamentals and Applications*, 2nd ed., New York: J. Wiley and Sons.

Berezhetskyy, A. L., Sosovska, O. F., Durrieu, C., Chovelon, J-M., Dzyadevych, S. V. & Tran-Minh, C. (2008). Alkaline phosphotase conductometric biosensor for heavy metal ions determination. *ITBM-RBM* 29: 136-140.

Bettinelli, M., Beone, G. M. Spezia, S. & Baffi, C. (2000). Determination of heavy metals in soils and sediments by microwave-assisted digestion and inductively coupled plasma optical emission spectrometry analysis. *Analytica Chimica Acta* 424: 289–296.

Brainina, K. Z., Stozhko, N. Y., Belysheva, G. M., Nzhevatova, O. V., Kolyadina, L. I., Cremisini, C. & Galletti, M. (2004). Determination of heavy metals in wine by anodic stripping voltammetry with thick film modified electrode. *Analytica Chimica Acta* 514: 227-234

Cecconi, I., Scaloni, A., Rastelli, G., Moroni, M., Vilardo, P. G., Costantino, L., Cappiello, M., Garland, D., Carper, D. Petrash, J. M., Corso A. D. & Mura, U. (2002). Oxidative Modification of Aldose Reductase Induced by Copper Ion: Definition of the metal–protein interaction mechanism. *Journal of Biological Chemistry* 277: 42017-42027.

Gau, V., Ma, S-H., Wang, H., Tsukuda, J., Kible, J. & Haake, D. A. (2005). Electrochemical molecular analysis without nucleic acid amplification. *Methods* 37: 73–83.

Gerard, M., Chaubey, A. & Malhotra, B. D. (2002). Application of conducting polymers to biosensors: Review. *Biosensors and Bioelectronics* 17: 345-359.

Ghica, M. E. & Brett, C. M. A. (2008). Glucose oxidase inhibition in poly(neutral red) mediated enzyme biosensors for heavy metal determination. *Microchimica Acta* 163: 185-193.

Giardi, M. T., Koblızek, M. & Masojıdek, J. (2001). Photosystem II-based biosensors for the detection of pollutants. *Biosensors and Bioelectronics* 16: 1027–1033.

Han, S., Zhu, M., Yuan, Z. & Li, X. (2001). A methylene blue- mediated enzyme electrode for the determination of trace mercury (II), mercury (I), methylmercury, and mercury-glutathione complex. *Biosensors and Bioelectronics* 16: 9-16.

Ilangovan, R., Kranstanov, D. A., Zachariah, C. & Elizabeth, R. (2006). Enzyme based biosensor for heavy metals ions determination. *Biotechnology & Biotechnological Equipment* 184-189.

Kang, E. T., Neoh, K. G. & Tan, K. L. (1998). Polyaniline: A polymer with many interesting intrinsic redox states. *Progress in Polymer Science* 23: 211-324.

Kan, J., Zhou, S., Zhang, Y. & Patel, M. (2006.) Synthesis and characterization of polyaniline nanoparticles in the presence of magnetic field and samarium chloride. *European Polymer Journal* 42: 2004–2012.

Kenawy, I. M. M., Hafez, M. A. H., Akl, M. A. & Lashein, R. R. (2000). Determination by AAS of some trace heavy metal ions in some natural and biological samples after their preconcentration using newly chemically modified chloromethylated polystyrene-PAN ion exchanger. *Analytical Science* 16: 493-500.

Kim, B-J., S-G. Oh, M-G. Han & S-S. Im. (2001). Synthesis and characterization of polyaniline nanoparticles in SDS micellar solutions. *Synthetic Metals* 122: 297–304.

Lakshmi, G. B. V. S., Dhillon, A. Siddiqui, A. M., Zulfequar, M. & Avasthi, D. K. (2009). RF-plasma polymerization and characterization of polyaniline. *European Polymer Journal* 45: 2873–2877.

Lapkowski. M. (1990). Electrochemical synthesis of linear polyaniline in aqueous solutions *Synthetic Metals* 35 : 169-182.

Laska, J. & Widlarz, J. (2005). Spectroscopic and structural characterization of low molecular weight fractions of polyaniline. *Polymer* 46: 1485–1495.

Liu, S-Q. & Ju, H-X. (2002). Renewable reagentless hydrogen peroxide sensor based on direct electron transfer of horseradish peroxidase immobilized on colloidal gold-modified electrode. *Analytical Biochemistry* 307: 110–116.

Luo, X., Killard, A. J., Morrin, A. & M. R. Smyth. (2006). Enhancement of a conducting polymer-based biosensor using carbon nanotube-doped polyaniline. *Analytica Chimica Acta* 575: 39–44.

Malitesta, C. & Guascito, M. R. (2005). Heavy metal determination by biosensors based on immobilized by electropolymerisation. *Biosensors and Bioelectronics* 20: 1643-1647.

Martha, S. K., Hariprakash, B., Gaffoo, S. A., Trivedi, D. C. & A. K Shukla. (2006). A low-cost lead-acid battery with high specific-energy. *Journal Chemical Science* 118: 93–98.

Mathebe, N. G. R., Morrin A. & Iwuoha, E. I. (2004). Electrochemistry and scanning electron microscopy of polyaniline/peroxidase-based biosensor. *Talanta* 64: 115–120.

Mazeikiene, R.; Tomkute, V., Kuodis, Z., Niaura, G. and Malinauskas, A. (2007). Raman spectroelectrochemical study of polyaniline and sulfonated polyaniline of different pH. *Vibrational Spectroscopy* 44: 201-208.

Mohammadi, H., Amine, A., Cosnier S., & Mousty, C. (2005). Mercury-enzyme inhibition assays with an amperometric sucrose biosensor based on a trienzymatic –clay matrix. *Anal. Chim. Acta* 543: 143-149.

Mu, S., Chen, C. & Wang. J. (1997). The kinetic behaviour for the electrochemical polymerization of aniline in aqueous solution. *Synthetic Metals* 88: 249-254.

Ndangili, P. M., Waryo, T. T., Muchindu, M., Baker, P. G. L., Ngila, J. C. & Iwuoha, E. I. (2009). Ferrocenium hexafluorophosphate-induced nanofibrillarity of polyaniline–polyvinyl sulfonate electropolymer and application in an amperometric enzyme biosensor. *Electrochimica Acta* 55: 4267–4273.

Pournaghi-Azar, M. H. & Habibi, B. (2007). Electropolymerisation of aniline in acid media on the bare and chemically pre-treated aluminum electrodes: A comparative characterization of the polyaniline deposited electrodes. *Electrochim. Acta* 52: 4222–4230.

Prechthai, T., Parkpian, P. & Visvanathan C. (2008). Assessment of heavy metal contamination and its mobilization from municipal solid waste open dumping site. *Journal of Hazardous Material* 156: 86-94.

Rahmi, D., Zhu, Y., Fujimori E., Umemura, T. & Haraguchi H. (2007). Multielement determination of trace metals in seawater by ICP-MS with the aid of with aid of down-sized chelating resin packed microcolumn for preconcentration. *Talanta* 72: 600-606.

Ruzgas, T., Gorton, L., Emneus, J. & Marko-Varga G. (1995). Kinetic models of horseradish peroxidase action on a graphite electrode. *Journal of Electroanalytical. Chemistry*391: 41-49.

Seo, K-D., Lee, K-P, Gopalan, A. I., Chung, S. J., Lim, Y. T. & Choi S-H. (2007). Horseradish Peroxidase (HRP) Immobilized Poly(aniline-co-*m*-amino the electrocatalytic behaviour of the enzyme phenol) film electrodes–fabrication and evaluation as hydrogen peroxide sensor. *Sensors* 7: 719-729.

Singh, K., A. Ohlan, R. K. Kotnala, A. K. Bakhshi & Dhawan, S. K. (2008). Diectric and magnetic properties of conducting ferromagnetic composite of peolyaniline with γ-Fe_2O_3 nanoparticles. *Material Chemistry and Physics.* 112: 651-658.

Songa, E. A.; Arotiba, O. A., Owino, J. H. O., Jahed, N., Baker, P. G. L. & Iwuoha E. I. (2009). Electrochemical detection of glyphosate herbicide using horseradish peroxidase immobilized on sulfonated polymer matrix. *Bioelectrochemitry* 75: 117-123.

Stoytcheva, M., (2002). Electrochemical Evaluation of the Kinetic Parameters of a Heterogeneous Enzyme Reaction in Presence of Metal Ions. *Electroanalysis* 14: 923-927.

Sun, D., Cai, C., Li, X., Xing W. & Lu, T. (2004). Direct electrochemistry and bioelectrocatalysis of horseradish peroxidase immobilized on active carbon. *J. electroanalytical Chemistry* 566: 415-421.

Tayefi-Nasrabadi, H., Keyhani, E. & Keyhani J. (2006). Conformational changes and activity alterations induced by nickel ion in horseradish peroxidase. *Biochimie* 88: 1183–1197.

Tong, Z.; Yuan, R., Chai. Y., Chen, S., Xie, Y. (2007). Amperometric biosensor for hydrogen peroxide based on Hemoglobin/DNA/Poly-2,6-pyridinediamine modified gold electrode. *Thin Solid Films* 515: 8054–8058.

Tsai, H-C., Doong, R-A. Chiang, H. C. and Chen K. T. (2003). Sol-gel derived urease-based optical biosensor for rapid determination of heavy metals. *Analytica Chimica Acta* 481: 75-84.

Tuzen, M., Sayji, K. O. & Soylak, M. (2008). Solid phase extraction of heavy metal ions in environmental samples on multiwalled carbon nanotubes. *Journal of Hazardous Materials* 152: 632-639.

Uriu-Adams, J. Y. & Keen, C. L. (2005). Copper, oxidative stress, and human health. *Molecular Aspects of Medicine* 26: 268–298.

USEPA (1991), "USEPA Maximum contaminant level goals and national primary drinking water regulations for lead and copper; final rule", Federal Register, Vol. 56 110, 26460-9, 40 CFR Parts 141 and 142.

Wang, L. & Wang, E. 2004. Novel hydrogen peroxide sensor based on horseradish peroxidase immobilized on colloidal Au modified ITO electrode. *Electrochemical Communication* 6: 225–229.

Wang, P., Li, S. & Kan, J. (2009a). A hydrogen peroxide biosensor based on polyaniline/FTO. *Sensors and Actuators* B 137: 662–668.

Wang, X-J., Xia, S-Q., Zhao, J-F., Zhao, H-N. & Renault, N. J. (2009b). Inhibitive Determination of heavy metal ions by conductometric nitrate reductase biosensor. *Chemical Research in Chinese Universities* 25: 443-44.

World Health Organization (WHO) (2004), Guidelines for Drinking Water Quality, 3rd ed., Vol. 2, World Health Organization (WHO), Geneva.

Yin, H., Ai, S., Shi, W. & Zhu, L. (2009). A novel hydrogen peroxide biosensor based on horseradish peroxidase immobilized on gold nanoparticles–silk fibroin modified glassy carbon electrode and direct electrochemistry of horseradish peroxidase. *Sens. Actuators* B 137: 747–753.

Zhang, L. and Lian J. (2007). Electrochemical synthesis of copolymer of aniline and o-aminophenol and its use to the electrocatalytic oxidation of ascorbic acid. *J. Electroanalytical Chemitry* 611: 51–59.

26

Chemical Biosensors Based on Proteins Involved in Biomineralization Processes

Rayana R. Ruiz-Arellano[1], Hugo Javier Serrano-Posada[2], María Liliana Marín-García[3], Bernardo A. Frontana-Uribe[4,5] and Abel Moreno[1]
Universidad Nacional Autónoma de México
[1]Instituto de Química
[2]Instituto de Biotecnología
[3]FES-Cuautitlán
[4]Centro Conjunto de Investigación en Química Sustentable UAEM-UNAM
[5]Permanent position at the Instituto de Química-UNAM Circuito Exterior
Mexico

1. Introduction

Biomineralization processes are involved in bone and teeth formation, optical/acoustic/magnetic sensors (Mann, 2001), even as in pathological aspects like cardiovascular calcifications, renal or gallbladder stones and others (Narayana & Subramanian, 2010). A remarkable example is the formation of eggshell in avians. The eggshell is the only rigid part of an avian egg, made up of calcium carbonate and some biological macromolecules. The eggshell is a mineral structure with a highly specialized function (Lammie et al., 2005). The question about the role of individual matrix proteins in avian eggshell calcification is an important subject of investigation (Hincke et al., 1999). This is so because the role of individual matrix proteins in avian eggshell calcification is poorly understood, and has never been investigated as calcium or carbonate's biosensors have. Lakshminarayanan et al., (2005) have done a comparative study of the structure/function relationship of avian eggshell matrix ansocalcin and ovocleidin-17 (OC-17) proteins. These two proteins belong to the C-type lectin family, and share a high degree of similarity, though they interact differently with the growing calcium carbonate crystals, which suggest that their role in eggshell calcification is different as shown by Reyes-Grajeda et al., (2003).
Nowadays, an increasing number of studies in C-type lectin-like proteins contained in the avian eggshell matrix have been reported elsewhere (Drickamer, 1999) but they have not been considered as biological sensors for inorganic ions. In this way, Mann & Siedler have determined the amino acid sequence of OC-17, a major protein of the hen´s (*Gallus gallus*) eggshell (Mann & Siedler, 1999); later, struthiocalcin-1 and 2 (SCA-1 and SCA-2) present in ostrich (*Struthio camelus*) eggshell matrix (Mann & Siedler, 2004), and they have recently, elucidated the amino acid sequence of two proteins of emu (*Dromaius novaehollandiae*) dromaiocalcin-1 and 2 and two proteins in rhea (*Rhea americana*) rheacalcin-1 and 2 (Mann & Siedler, 2006). Mann suggested that the structure of the ostrich eggshell was very similar to that of avian eggshells; for example, ansocalcin had the same number of aminoacid

sequences. SCA-1 contained 132 amino acids, the mass determined by ESI mass spectrometry was 15,343.2 ± 4 Da, while SCA-2 contained 142 amino acids, the mass determined by electrospray ionization (ESI) mass spectrometry was 16,834.1 ± 2 Da (Mann & Siedler, 2004).

In this chapter, we report the purification and characterization of SCA-1 and 2, two proteins isolated from the intramineral part of the ostrich's eggshell, Ansocalcin (ANCA) found in goose eggshell matrix. In order to obtain a better insight about its solubility behavior at different temperatures in water, as well as in the presence of carbonate ions, Dynamic Light Scattering (DLS) experiments were carried out. The selectivity and chemical recognition of proteins present in the eggshell for carbonate ions (carbonate biosensors), was sorted out by means of electrochemical and dynamic light scattering methods. It was verified the influence of CO_3^{2-} concentration on the electrochemical and on the DLS responses using the intramineral proteins SCA-1, SCA-2, Ansocalcin (ANCA) and hen egg white Lysozyme (LYS), which is not intramineral and was used as protein control. The DLS experiments confirmed the protein-carbonate's interaction observed by means of electro-analytical methods.

2. Experimental

2.1 Protein purification

This was done following and modifying the procedure of Mann and Siedler (2004). The ostrich as well as goose's eggshells were treated with 5% (v/v) EDTA for one hour to facilitate the removal of the organic membranes. The calcified layer was then extracted with 10% acetic acid (20 ml/g of eggshell) at 4 ºC for 48 h stirring constantly. The solution was then filtered and concentrated using an ultra filtration cell (Amicon cellulose filter YM3) of 3KDa molecular weight cut. The concentrated solution was dialyzed against 5 x 10 vol. of 5% acetic acid. The dialyzed solution was saturated with ammonium sulfate in order to precipitate all proteins. After 24 h, the solution was centrifuged at 64,500g for 30 minutes. The supernatant was discarded and the pellet was resuspended and dialyzed against 5% (v/v) acetic acid in order to remove the ammonium sulfate. The resulting solution was filtered using PVDF filters (Millipore) of 0.45 µm. The resulting solution was injected into a Vydac C18 HPLC reverse phase column and eluted using a gradient of acetonitrile (100 %) with 0.1 % (v/v) TFA for 85 minutes at a rate flow of 1 mL min^{-1}. Along the purification step two proteins were observed, SCA-1 (Rt=58.765 min) at a higher concentration and SCA-2 (Rt=56.26 min) at a lower concentration as reported previously (Mann and Siedler, 1999). In the particular case of Ansocalcin, only one protein was obtained (Rt=58.0 min) using the same gradient as that reported for SCA-1 and SCA-2 adjusted to our experimental set up for chromatographic procedures. All proteins were purified in an Ultra Fast Liquid Chromatographer (UFLC, Shimadzu Model Prominence), and obtained in a high degree of purity as shown by the electrophoresis gel (Figure 1), highly pure Lysozyme (recrystallized six times) was purchased from Seikagaku Kogyo Co., Japan (Code 100940).

2.2 Dynamic light scattering

The analysis of the hydrodynamic radius and the degree of aggregation versus temperature were obtained from the Zeta Sizer software version 6.20 DTS (Nano) (Malvern, Ltd.). A Malvern Nano S apparatus with a NIBS laser technology was used. For these studies,

solutions of SCA-1, SCA-2, Ansocalcin, and Lysozyme (control) were prepared in distilled water. All these three intramineral proteins (SCA-1, SCA-2, ANCA) as well as Lysozyme were thermally analyzed in their aggregation behavior ranging from 5-30 ^{o}C in steps of 1^{o}C. For all proteins analyzed in dynamic light scattering the final concentration was 1.0 mg/mL.

2.3 Electrochemical investigations

The electro-analytical determinations of carbonate response for SCA-1 and SCA-2 were carried out by cyclic voltammetry (100 mVs^{-1}) in an AUTOLAB PGSTAT 30 potentiostat/galvanostat following the procedure published by Marín-García *et al*. (2008). For these experiments, all maximum currents for each addition of carbonate ions at different concentrations respect to a voltage of 1.3V vs SCE (Saturated Calomel Electrode) using the protein adsorbed carbon paste electrode, were divided by current of the pure carbon paste electrode to obtain a normalized curve I/I° vs carbonate concentration. This electrochemical procedure was suitable to detect the interaction between these proteins (10 µg included in the working electrode) and carbonate ions (ranging from 0 to 14 mM) for SCA-1 and SCA2. It is worth mentioning that in electrochemistry an inert electrolyte is always required for these types of experiments, so in all cases $LiClO_4$ 0.1 M was used as supporting electrolyte, and the electrochemical response (current) of the carbonate oxidation on the pure carbon paste electrode was used as the control experiment. The analyzed proteins did not show any electrochemical response in this medium. This electroanalytical methodology was not suitable to be applied to ANCA due to the limitation of amount of protein purified from the natural source, where the yield is very low compared to SCA-1 and SCA-2 from the ostrich eggshell.

3. Results and discussion

The purity of all the proteins used in this research were analyzed and characterized by means of biochemical methods as have been shown in the gel of electrophoresis (Figure 1). In order to verify the feasibility of constructing a carbonate's biosensor using these intramineral proteins contained in the avian eggshells, we based our electroanalytical analyses using the first prototype designed by Marín-García et al, (2008).

Nowadays, proteins play an important role in the development of novel electroanalytical devices because of their high selectivity for certain analytes. However, there is the possibility of using them for monitoring biomolecules during diagnostic tests in different clinical areas (Chien et al., 2009; Cosnier, 1999; Navratilova et al., 2006). Recently, the development of a protein biosensor used to detect a specific class of antibiotic or any other biological important species have been reported elsewhere (Amine & Palleschi, 2004; Li et al., 2006; Mechler et al., 2006). Most of the proteins, which have been used for these types of structural and biomedical research, need to be in a higher degree of purity.

In our experiments, for the electroanalytical results a clear final difference of the electrode response was observed after the protein adsorption on the surface of the electrode. An enhancement of the capacitive current and the change of the barrier potential were the most important features proving the presence of the protein. The stability of the adsorption was verified every 10 minutes using a cyclic voltammetry of the biosensor dipped into the electrolyte solution. The response of cyclic voltammetry for proteins SCA-1 and SCA-2 in period of one hour remained unchanged after protein-adsorption. Once the stability of the protein on the biosensor was checked, its electrochemical response towards the carbonate

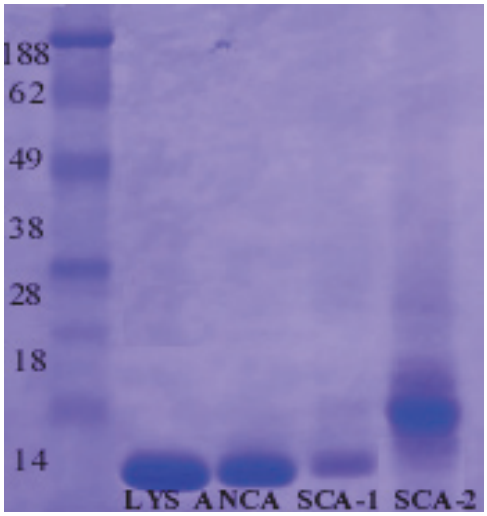

Fig. 1. SDS-PAGE electrophoresis gel for highly purified proteins used for this research: first lane corresponds to MW markers, the second to Lysozyme (lys), third to Ansocalcin (ANCA), the fourth and fifth for struthiocalcins 1 and 2 (SCA-1 and SCA-2) respectively.

ion was investigated. In Figure 2, the electrochemical response in terms of the normalized current measured at 1.3 V vs SCE (Saturated Calomel Electrode, anodic barrier) with respect to Na_2CO_3 concentration is shown. Due to the absence of an electrochemical peak to follow the electrochemical response, the current related to the anodic barrier, which corresponds to the oxidation of carbonate anions, was monitored. The protein SCA-1, for instance, showed a higher slope and a clear linear response (R^2=0.98) of the current when carbonate concentration in the solution was ranging from 10^{-3} to 10^{-2} M and a slope less remarkable for SCA-2. This range was selected to show the response of the biosensor with the isolated proteins from the eggshell, but it must be clarified that the biosensor could also give a good response at lower carbonate concentrations or higher sensibility.

The comparison of the slope values for these analyzed proteins demonstrated that the biosensor containing SCA-1 was 2.7 times more sensitive to carbonates, than the pure carbon paste electrode.

Although these experiments were highly sensitive for detecting protein-carbonate ions interactions, when applied to proteins SCA-1 and SCA-2, it was nevertheless a challenge to look for another methodology to detect these interactions (chemical recognition) using a simple experimental set up. By means of using photon correlation spectroscopy methods like dynamic light scattering (DLS) can be performed easily using higher amounts of carbonate ions ranging from 10mM to 100mM as those found in the intrauterine fluid in avian (Domínguez-Vera et al., 2000), and less amount of protein sample.

Many proteins aggregate to some extent when they are in pure water. At low ionic strength, the tendency to form aggregates is usually lower and became more soluble at certain pH values (salting-in effect). However, in a transparent solution, it is difficult either to evaluate the homogeneity or the inhomogeneity of the biological aggregates in solution. So, dynamic light scattering methods were used to characterize the homogeneity, the conformational stability, and thermal properties of these proteins. On the whole, the analyzed range of

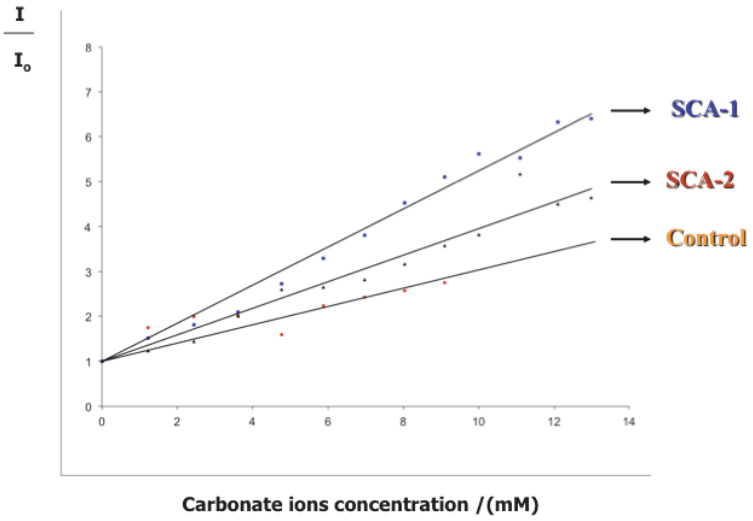

Fig. 2. Fig. 2. Plot of normalized (I/I_0) electrochemical response taken at 1.3V for all cyclic voltammograms versus concentration of carbonate ions using an electrode of carbon paste.

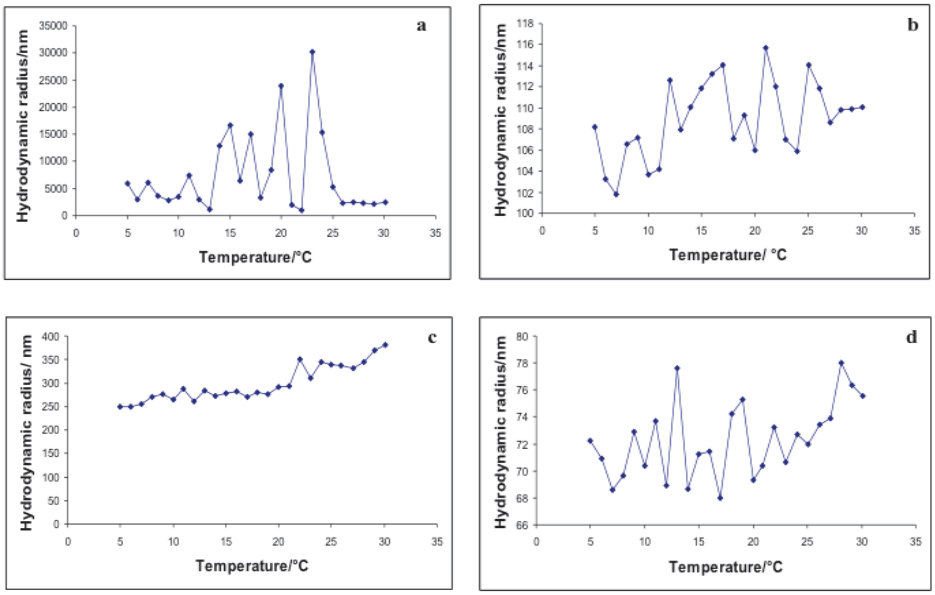

Fig. 3. Dynamic light scattering aggregation behavior for a) SCA-1, b) SCA-2, c) SCA-1 filtered, and d) SCA-2 filtered.

temperatures (5 to 30 ºC), dynamic light scattering experiments for SCA-1, SCA-2 showed a fully random aggregation behavior with huge aggregates (Figure 3a and 3b respectively). However, when filtering the protein solution a few small and slightly homogeneous aggregates were observed for SCA-1 in water as shown in Figure 3c (ranging from 250 to 350 nm in their hydrodynamic radii) when for SCA-2 these aggregates were small and inhomogeneous (Figure 3d).

On the other hand, when adding different concentrations of carbonate ions (10mM, 70mM and 100mM as shown in Figure 4 a-c respectively). This protein SCA-1 was stable showing a highly homogeneous particle size distribution (around 40 nm in hydrodynamic radius) when 70 mM sodium carbonate was added to the protein sample along the DLS analysis and thermal behavior (Figure 4 b). It is clearly observed that the particle size distribution is a function of carbonates concentration. The homogeneous hydrodynamic radius observed on these experiments could be explained in terms of a well-defined aggregation process that generates smallest species at 100mM and the biggest at 10mM. On the other hand, SCA-2 for instance, showed almost the same behavior (Figure 4 d-f) obtained for SCA-1, but at higher concentrations of sodium carbonate (ranging from 70 mM to 100mM) as shown in Figure 4 f. In this case the aggregate size distribution did not follow a clear tendency like in SCA-1 with the concentration, although the hydrodynamic radii were also function of carbonates concentration value, which demonstrates that the process to form them occurs but by different mechanism.

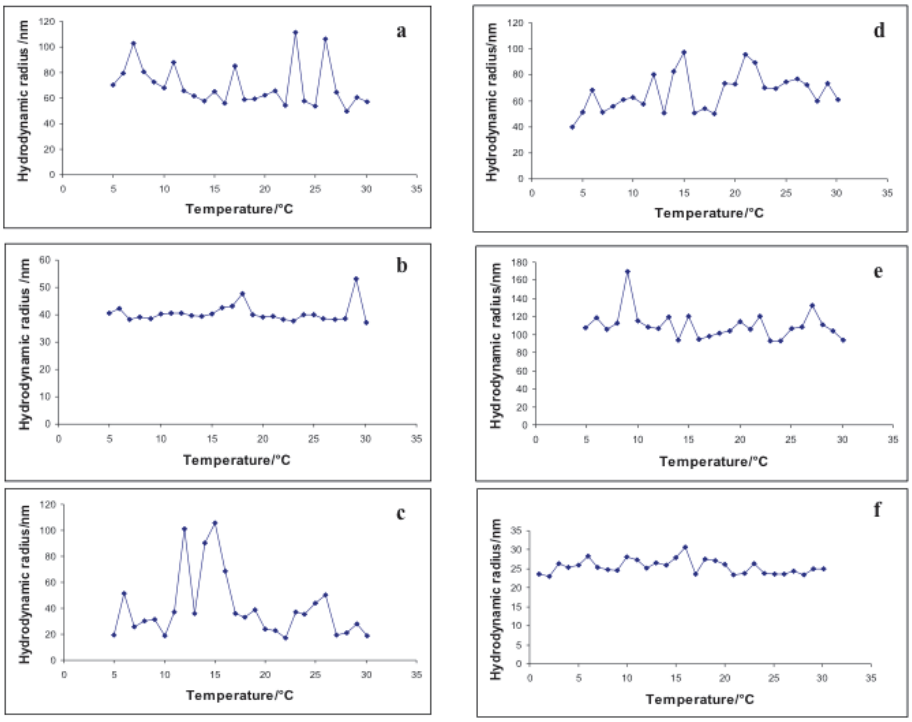

Fig. 4. Dynamic light scattering aggregation behavior for SCA-1 at a) 10mM, b) 70mM and c) 100mM sodium carbonate; the same for SCA-2 from d) 10mM, e) 70m, and f) 100mM.

In the particular case of Ansocalcin (Figure 5 a-d), this homogeneous size distribution behavior was obtained starting at 10ºC ranging from 10mM concentration of sodium carbonate as that obtained for SCA-1, from the filtered solution (Figure 5 a) to the addition of 10mM, 70mM, and 100mM sodium carbonate (Figure 5b, 5c, and 5d respectively). This protein did not show the aggregation trend observed for SCA-1 and SCA-2, which demonstrates that ANCA is less sensitive to the carbonate ions recognition. It is worth mentioning that goose eggshell contains only one intramineral protein (called ANCA). This result is particularly interesting in terms of the conformational stability, and chemical recognition function of these intramineral proteins as biological sensors for carbonate ions. While SCA-1 is very sensitive, ANCA is less sensitive in all range of specific concentrations of sodium carbonate (from 10mM to 70mM), and slightly more homogeneous at 70mM concentration, which is equivalent to those concentrations found in the intrauterine fluid in avian. The protein SCA-2 is sensitive at higher concentrations of carbonate ions (100 mM), which is probably less sensitive to carbonate ions interactions than SCA-1 (see Figure 4f). These dynamic light scattering experiments gave us a double check methodology to prove our electrochemical approach shown in Figure 2. However, the procedure via light scattering methods is less time-consuming, needs less amount of sample, and it is non-destructive for analyzing these protein-carbonate interactions.

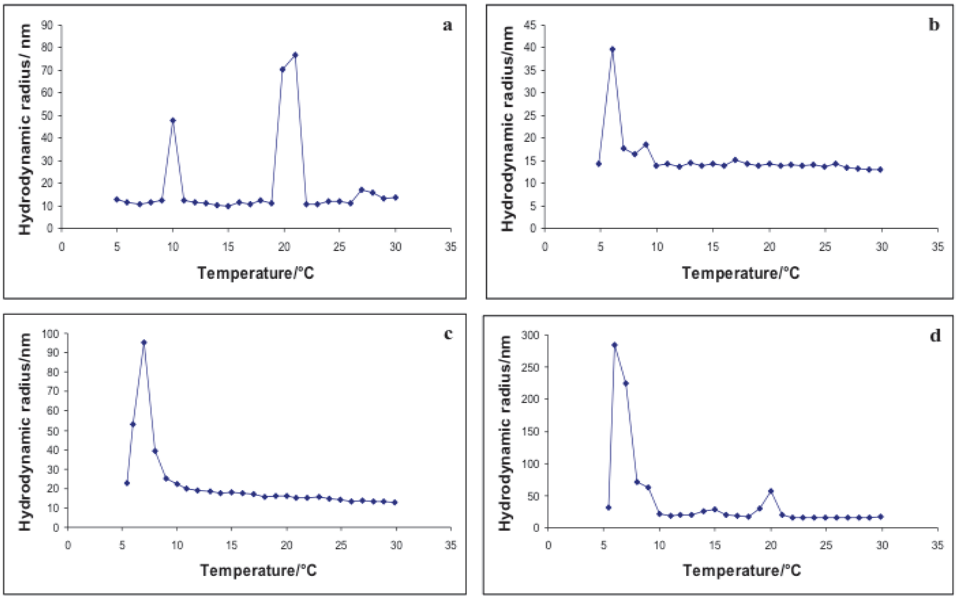

Fig. 5. Dynamic light scattering aggregation behavior for ANCA: a) filtered solution, b) in the presence of 10mM, c) 70mM, and d) 100mM of sodium carbonate respectively.

Based on the present results, it is also possible to propose that the mineralization of calcium carbonate (calcite) process that gives rise to avian eggshell formation is fostered by proteins like SCA-1 in ostrich or ANCA for goose eggshell (or from the biological point of view maybe controlled by some genes), which have an specific biological function during this process. These would give rise to crystalline arrays that favor the formation of highly

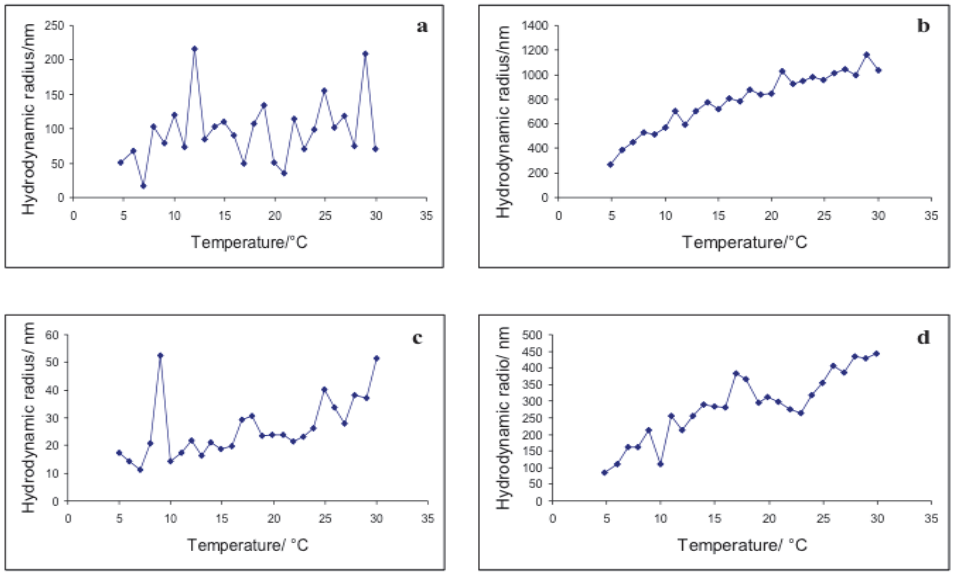

Fig. 6. Dynamic light scattering aggregation behavior for Lysozyme: a) filtered solution, b) in the presence of 10mM, c) 70mM, and d) 100mM of sodium carbonate respectively.

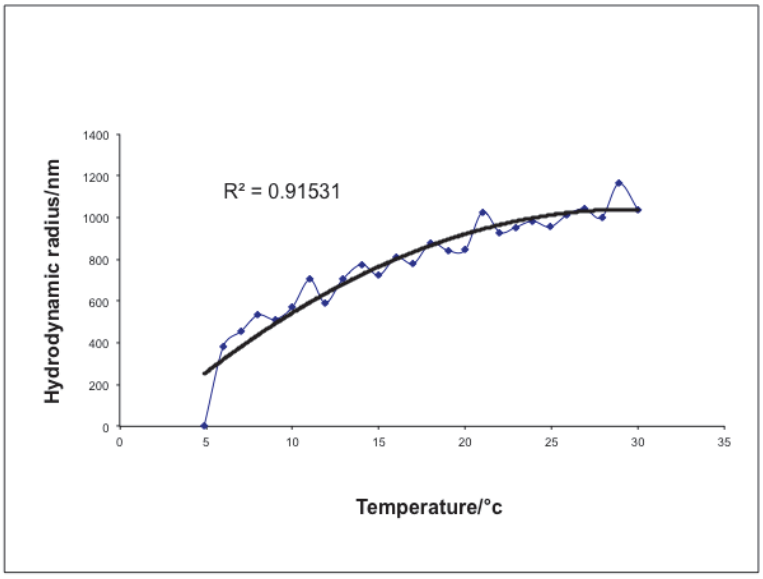

Fig. 7. Curve fitting of lysozyme aggregates growth for a cuadratic power of the hydrodynamic radius versus temperature. The fitting equation was $Y = -1.2945x^2 + 76.566x - 92.554$

selective polycrystalline aggregates, which have the specific features to develop the duties for which these rigid structures have being designed (Li & Stroff, 2007). Finally, hen egg white lysozyme, used as control, did not show a remarkable effect (Figure 6 a-d). This protein is not intramineral, nonetheless it could play an important role also in the calcification of eggshell as has been published recently (Wang et al., 2009). This can be assumed by looking at Figure 6b where 10 mM sodium carbonate was added and a trend was observed; the hydrodynamic radius varies from 200 to 1200 nm in the range of temperatures from 5 to 30°C compared to other values (Figure 6 c, d), where the random aggregates size distribution was ranging from 10 to 400 nm, when adding 70 mM and 100 mM sodium carbonate respectively. From the crystal growth point of view, this linear aggregation behavior for lysozyme is more related to the influence of the ionic strength to the growth of the nucleus of lysozyme than the carbonate ions recognition. The linear behavior of lysozyme aggregates (shown in Figure 6 b) was mathematically adjusted, and did show a quadratic growth fitting; when plotting a quadratic value or root square of the r_h (hydrodynamic radius) versus temperature (Figure 7).

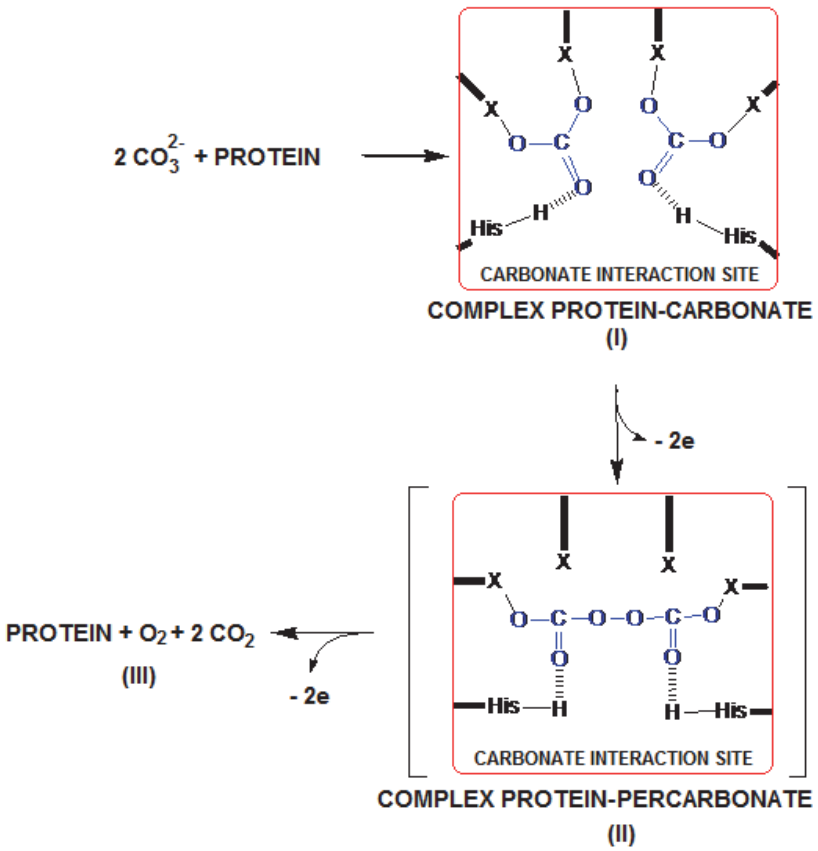

Scheme 1. Proposed carbonate oxidation process through an interaction protein-carbonate

The selectivity towards carbonate ion observed with these proteins in electrochemical and DLS experiments could be explained by an interaction mechanism where two carbonate anions are fixed into a protein cavity named carbonate interaction site (Scheme 1, step I). In the case of the electrochemical experiments, this mechanism facilitates the first oxidation process producing the percarbonate ion that remains fixed at this site (step II). It can suffer a second oxidation step yielding as final products oxygen and carbon dioxide molecules (step III). The current value is enhanced due to an enriched mass transfer during the oxidation process because both reactants are confined on the protein adsorbed on the electrode surface. Finally, based on Figures 3 to 5 those clearly show the solution of the dilemma about the selectivity of these proteins for carbonate ions. At least three of the intramineral proteins SCA-1, and SCA-2 (concentration dependent) as well as ANCA (less sensitive) interact directly with carbonate ions as proven by using electroanalytical methods (for SCA-1 and 2), and dynamic light scattering techniques for all of them. This fact opens the first possibility of explaining the mechanisms of calcite mineralization in the eggshell as well as the potential applications of SCA-1, SCA-2, and ANCA as plausible carbonate ions biosensors.

4. Conclusion

The idea of designing carbonate biosensors would be based on these types of experiments, which demonstrated interaction between SCA-1, SCA-2 and ANCA with carbonate anions. The electroanalytical characterization, and limits of the biosensor containing intramineral proteins could be estimated in this contribution combining both methods cyclic voltammetry, and photon correlation methods like dynamic light scattering.

5. Acknowledgment

The authors acknowledge financial support from the DGAPA-UNAM through projects No. IN201811 and IN212207-3. Rayana R. Ruiz Arellano acknowledges the scholarship for a PhD from C.L.A.F., and the Institute for Science and Technology of Mexico City (ICyTDF) and CONACYT (complementary scholarship as an assistant researcher for SNI 3). Finally, one of the authors (A.M.) acknowledges the partial support of CONACYT (Mexico) project No. 82888.

6. References

Amine, A., Palleschi, G. (2004) Phosphate, Nitrate, and Sulfate Biosensors. *Analytical. Letters* 37, pp. 1-19. ISSN 0003-2719.

Cosnier, S. (1999). Biomolecule immobilization on electrode surfaces by entrapment or attachment to electrochemically polymerization films. *Biosensors and Bioelectronics.* 14, pp. 443-456. ISSN 0956-5663.

Chien, Y.-C., Hincke, M.T., McKnee, M.D. (2009). Avian Eggshell Structure and Osteopontin. *Cells Tissues Organs*. 189 pp. 38-43. ISSN 1422-6405.

Dominguez-Vera, J. M., Gautron, J., Garcia-Ruiz, J. M., Nys, Y. (2000). The effect of avian uterine fluid on the growth behavior of calcite crystals. *Poultry Science* 79, pp. 901-907. ISSN 0032-5791.

Drickamer, K. (1999). C-type lectin-like domains. *Curr. Opin. Struct. Biol*. 9, pp. 585-590. ISSN 0959-440X.

Hincke, M.T., Gautron J., Tsang, Ch. P.W., McKnee, M.D., Nys, Y. (1999). Molecular Cloning and Ultrastructural Localization of the Core Protein of an Eggshell Matrix Proteoglycan, Ovocleidin-116, *Journal of Biological Chemistry* Vol. 274, pp 32915-32923. ISSN 0021-9258.

Lammie, D., Bain, M. M., Solomon S. E., Wess, T. J. (2005). The Physiology of Avian Eggshell, *Current Topics in Biotechnology*, Vol. 2, pp 65-74, ISSN 0972-821X. Lakshminarayanan, R., Joseph, J. S., Kini, R. M., and Valiyaveettil, S. (2005). Structure−Function Relationship of Avian Eggshell Matrix Proteins: A Comparative Study of Two Major Eggshell Matrix Proteins. Anocalcin and OC-17. *Biomacromolecules,* 6, pp. 741-751, ISSN 1525-7797

Li, H. & Estroff, L. A. (2007). Hydrogels Coupled with Self-Assembled Monolayers: An in Vitro Matrix To Study Calcite Biomineralization. *J. Am. Chem. Soc*. 129, pp. 5480-5483. ISSN 0002-7863.

Li, I. T., Pham, E., Truong, K. (2006). Protein biosensors based on the principle of fluorescence resonance energy transfer for monitoring cellular dynamics. *Biotechnoly Letters*. 28, pp. 1971-1982. ISSN 0141-5492.

Mann, K. & Siedler, F. (1999). The amino acid sequence of ovocleidin 17, a major protein of the avian eggshell calcified layer *Biochem. Mol. Biol. Int.* 47, pp. 997-1007. ISSN 1039-9712.

Mann, K. & Siedler, F. (2004). Ostrich (*Struthio camelus*) eggshell matrix contains two different C-type lectin-like proteins. Isolation, amino acid sequence, and posttranslational modifications. *Biochim. et Biophysics Acta*.1696, pp. 41-50. ISSN 09266585.

Mann, K. & Siedler, F. (2006). Amino acid sequences and phosphorylation sites of emu and rhea eggshell C-type lectin-like proteins. *Comparative Biochemistry and Physiology.* 143B, pp. 160-170. ISSN 1095-6433.

Mann, S. (2001). *Biomineralization. Principles and Concepts in Bioinorganic Materials Chemistry*, Oxford University Press, ISBN 0-19-850882-4, Oxford, UK.

Marín-García, L., Frontana-Uribe, B.A., Reyes-Grajeda, J.P., Stojanoff, V., Serrano-Posada, H.J., Moreno, A. (2008). Chemical recognition of carbonate anions by proteins involved in biomineralization processes and their influence on calcite crystal growth. *Crystal Growth and Design.* 8, pp. 1340-1345. ISSN 1528-7483.

Mechler, A., Nawaratna, G., Aguilar, M., Martin, L. L. (2006). A Study of Protein Electrochemistry on a Supported Membrane Electrode. *Int. J. of Peptide Research and Therapeutics* 12, No. 3 (2006) 217-224. ISSN 1573-3149.

Navratilova, I., Pancera, M., Wyatt, R. T., Myszka, D. G. (2006). A biosensor-based approach toward purification and crystallization of G protein-coupled receptors. *Analytical Biochemistry.* 353, pp. 278-283. ISSN 0003-2697.

Narayana K. & Subramanian N. (2010). Crystallization from Gels In: *Handbook of Crystal Growth*, Dhanaraj, G., Byrappa, K., Prasad, V., Dudley, M. (Ed), pp. 1607-1636 Springer-Verlag, ISBN 978-3-540-74182-4, Berlin, Germany.

Reyes-Grajeda, J. P., Moreno, A., Romero, A. (2004). Crystal Structure of Ovocleidin-17, a Major Protein of the Calcified *Gallus gallus* Eggshell. Implications in the calcite mineral growth pattern. *J. Biol. Chem*. 279, pp. 40876-40881. ISSN 0021-9258.

Wang, X., Sun, H., Xia, Y., Chen, C., Xu, H., Shan, H., Lu, J. R. (2009). Lysozyme mediated calcium carbonate mineralization. *Journal of Colloid and Interface Science* 332, pp. 96-103. ISSN 0021-9797.

27

Applicability of GFP Microbial Whole Cell Biosensors to Bioreactor Operations - Mathematical Modeling and Related Experimental Tools

Delvigne Frank[1], Brognaux Alison[1], Gorret Nathalie[2], Sørensen J. Søren[3], Crine Michel[4] and Thonart Philippe[1]
[1]*Université de Liège, Gembloux Agro-Bio Tech, Unité de Bio-industries/CWBI*
[2]*Université de Toulouse, INSA, INRA, UMR792*
Ingénierie des Systèmes Biologiques et Procédés
[3]*University of Copenhagen, Department of microbiology, Sølvgade 83H, 1307 Copenhagen*
[4]*Université de Liège, Chemical engineering laboratory*
[1,4]*Belgium*
[2]*France*
[3]*Denmark*

1. Introduction

Until now, whole cell microbial biosensors have been mainly used for the detection chemicals in different ecosystems (Sorensen, 2006). In this work, we propose to point out different features of microbial biosensors in the context of their applicability to monitor bioreactor operations. Indeed, large-scale bioreactors tend to be heterogeneous and it is now clear that these heterogeneities (e.g. in substrate, dissolved oxygen, pH, temperature,…) induce several kinds of physiological responses at the level of the exposed microbial cells, i.e., metabolic shift (Xu, 1999, Neubauer, 1995, Han L., 2002), mRNA synthesis (Schweder, 1999), stress protein synthesis (Schweder, 2004, Pioch, 2007), alteration of membrane integrity (Hewitt, 2000, Nebe-von-Caron G., 2000). In this context, the use of Green Fluorescent Protein (GFP) microbial whole cell biosensors is fully justified to their recognized advantages: characterization of the physico-chemical conditions at the micrometer scale when analyzed at the single cell level (Tecon, 2006, Southward, 2002), non invasive measurement and possibility to acquire online signal (Jones, 2004). Two main problems are encountered when extending the use of microbial biosensors for monitoring bioreactor efficiency, i.e. first the choice of an appropriate stress promoter for the detection of extracellular fluctuations and second the dynamics of the expression of the reporter system in front of the bioreactors hydrodynamics. This last issue is especially critical considering the particular dynamics of extracellular fluctuations encountered in the reacting volume depending on bioreactor mixing efficiency, circulation of microbial cells inside the broth and the dynamics of substrate consumption. Discussion will be supported by

mathematical simulations of the dynamics of GFP expression inside microbial biosensors and of the bioreactor hydrodynamics.

2. Basic microbial biosensor design and its application to bioreactor operations

2.1 Basic bioreactor design: the scaling-up problematic and the potential role of microbial biosensors

The main problem associated with bioprocesses scaling-up is the formation of concentration gradients inside large-scale bioreactors (Hewitt, 2007a, Lara, 2006, Enfors, 2001). These gradients induce various stresses at the level of microbial cells, such as glucose excess, glucose starvation, oxygen limitation, pH shock, leading to a deviation of the cells from the desired metabolism and in extreme case to a complete modification of the metabolism subsequent to a modification of the gene expression pattern. Studies have been mainly focused on glucose gradient appearing during fed-batch process, although other kinds of gradient have also been considered (Neubauer, 2010). The characterization of the exposure of microorganisms to gradients stress is not a trivial task, since several phenomena, including bioreactor mixing efficiency and microorganism's circulation, are involved (Fig. 1).

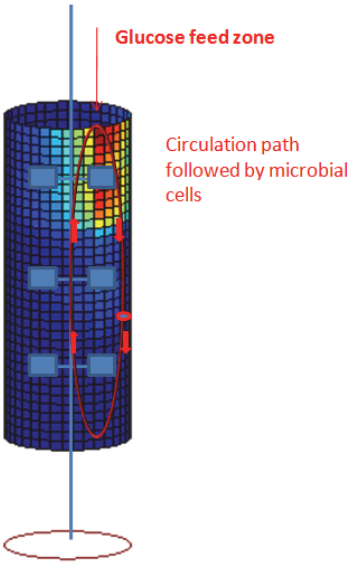

Fig. 1. Illustration of the exposure of microbial cells to glucose gradient concentration inside an industrial bioreactor operating in fed-batch mode. The color intensity is proportional to the glucose concentration and the figure shows that glucose accumulates at the level of the upper part of the bioreactor considering the lack at the level of the mixing efficiency of the system

Actually, because of the lack of appropriate sensors, bioprocess monitoring rely on indirect, global parameters, such as biomass evolution, substrate uptake profile, and these

parameters are not directly related to the cells physiological state (Deckwer, 2006, Pioch, 2007, Clementschitsch F., 2006). As reported in previous studies, stress genes can be used as marker in order to monitor the fitness of bacterial systems during industrial bioprocesses (Schweder, 2004). We propose thus to use several stress promoters linked with the GFP doing sequence and inserted in microbial cells in order to design some kind of "physiological tracer" for the determination of the biological impact of the mixing conditions met in heterogeneous bioreactors. These analyses will be performed by considering several *E. coli* strains carrying a Green Fluorescent Protein (GFP) reporter system. This kind of reporter system provides rapid detection of the promoter expression level (March, 2003), at a single cell level (by using flow cytometry) and by taking the population dynamics into account (Patkar, 2002). Indeed, previous studies have shown that microbial population can be very heterogeneous in a bioreactor, according to a particular cellular function (Hewitt, 2007b, Sundstrom, 2004, Roostalu, 2008). It is why a lare part of this work will be devoted to the demonstration of the usefulness of GFP reporter strains combined with a flow cytometry analytical tool in order to characterize the stress experienced by microorganisms in perturbed fed-batch bioreactors. As said before, this combination of biological and analytical techniques allows the observation of the consequences of stress at a single cell resolution among a microbial population. By comparison with inert tracer experiments used to characterize bioreactor hydrodynamics, the GFP reporter system takes into account the cell history, i.e. the displacement of the microbial particle along the concentration gradient. This reporter system is also linked with a direct physiological parameter, i.e. the protein synthesis related to an extracellular stimulus. It must be noted that, although protein synthesis is the final consequence of a physiological reaction (e.g., synthesis of a stress protein that redirect metabolic activity to better cope with stress conditions), the characteristic time constant associated with this biological reaction is rather high compared with circulation and mixing time inside bioreactors. The major challenge of this work is thus to demonstrate that useful information can be gained from the analysis of the GFP microbial biosensor dynamics after the response of the microbial population to various process-related perturbations.

2.2 Selection of an appropriate stress promoter

The critical step for an appropriate biosensor design, apart from the characteristics of the GFP itself, relies on the choice of a stress promoter. This is this part of the biosensor that will be sensitive to the extracellular conditions met by microbial cells inside bioreactors (Fig. 2).
According to their specificity, three classes of promoter can be considered in order to build the reporter system (Sorensen, 2006):

- Non-specific: the reporter gene coding for GFP is linked to a constitutive promoter. This kind of construction has been previously used to toxicants in various environments (Wiles, 2003, Bhattacharyy, 2005). Since the promoter is constitutively expressed, cells that are exposed to lethal dose of toxicants do not exhibit any fluorescence and can be easily distinguished from not exposed biosensors. Owing to their simplicity, non-specific reporters are the most widely used whole-cell biosensors.
- Semi-specific: the reporter gene is linked with a promoter responding to general conditions of stress. In this case, the biosensor is activated when cells are exposed to stressful conditions. Stress promoters can be selected on the basis of their belonging to well-known stress regulon, such as the heat shock or the general stress response regulons (e.g., *rpoS* regulon for several Gram negative bacteria, including *E. coli*).

- Specific: the biosensor specifically responds to the presence of a defined chemical. It implies the selection of a promoter that is tightly regulated by the presence of a specific chemical signal.

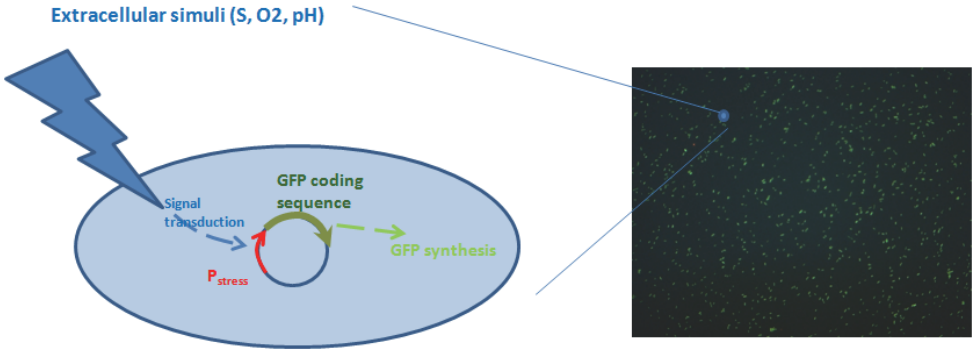

Fig. 2. Basic principle of GFP microbial biosensors. Photograph on the right shows the process of GFP synthesis inside *E. coli* biosensors

In bioreactor, the environment detected by the cells comprises multiple variables, such as substrate level, pH, dissolved oxygen and temperature. The use of specific biosensor is thus not adapted in bioreactor applications, although some studies involve the use of such system (e.g., the use of the *narZ* promoter coupled to the GFP coding sequence in order to detect local oxygen limitation in bioreactors (Garcia, 2009)). It must also point out that the reporter system governs the field of application of the considered microbial biosensor. Indeed, if GFP is used as signaling system, only aerobic processes can be investigated, considering that maturation of the GFP molecule requires an oxidation step promoted by the presence of oxygen in the medium (Tsien R.Y., 1998). In our case, we will select stress promoter responsive to carbon limitation. This stimulus is in fact mainly encountered in intensive fed-batch operation, one of the most used modes of operation at the industrial level considering its enhanced productivity. Then, in normal fed-batch mode it is expected that the microbial biosensor is fully activated and exhibit a given level of fluorescence according to the strength of the associated stress promoter, and when biosensor is exposed to deviation from the normal feeding profile, GFP level decreases. These considerations about the performances of fed-batch bioreactor will be explained more in details in section 4.

2.3 Dynamics of the microbial biosensor and method for GFP detection

When the appropriate stress promoter has been selected, the characteristic of the reporter molecule itself, i.e. GFP, must be kept into account. Indeed, GFP synthesis depends on a huge amount of factors, such as plasmid copy number (if the reporter system is carried by a plasmid), promoter strength, but also the rate of transcription and translation and the half-life of the GFP mRNA and proteins. One of the major drawbacks associated with the first version of GFP used as reporter system was its folding and maturation time of about 95 minutes (DeLisa, 1999), limiting the use of GFP to characterize the dynamics of microbial process in bioreactor. Until this, intensive researches have been provided in order to find out GFP variant of different colors (Shaner, 2005) and exhibiting significantly reduced

maturation time (Cormack, 2000). This has led to the GFPmut1, 2 and 3 variants with maturation of about 4 minutes. Another issue was the high stability of this variant. In fact, the stability of the gfpmut2 variant is so high that this protein exhibits half-life of more than 24 hours. In order to illustrate the previous statement, a model allowing the simulation of GFP synthesis has been set up. This model is partly inspired from (Thattai M., 2004) and take into account the essential step involved in GFP expression (Fig. 3).

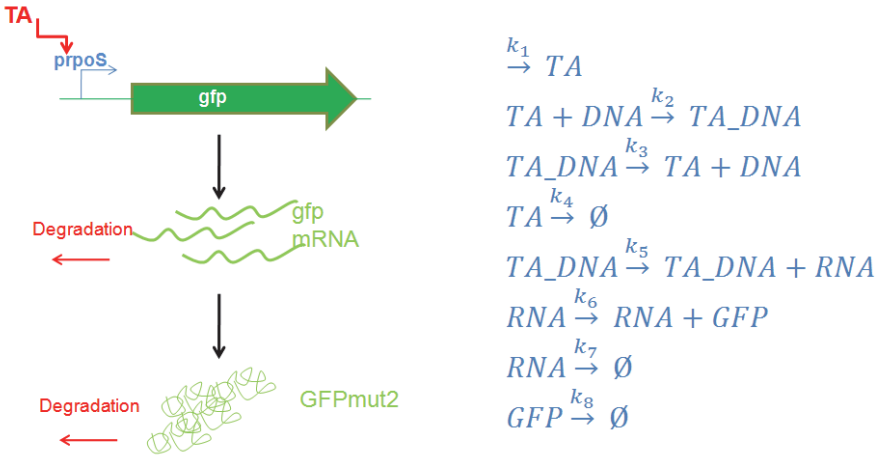

Fig. 3. Scheme showing the different steps involved for GFP synthesis and related chemical reactions with specific rates (from k1 to k8)

In our case, synthesis of transcription activator (TA) will depends on the exposure of microbial cells to heterogeneous conditions at the level of the bioreactor (Fig. 3). When TA is synthesized, it binds to the stress promoter (here, *rpoS* promoter has been chosen as an example) and the TA_DNA complex induces a cascade of reactions involving transcription of GFP-related mRNA and translation of this RNA to actively fluorescent GFP.
In this work, the gfpmut2 variant will be used (details about GFP biosensors will be given in section 3). The dynamics of our microbial biosensors will be experimentally characterized in section 4. The dynamics of this set of reactions can be mathematically modeled by 5 ordinary differential equations (ODEs) involving synthesis and degradation of the different chemicals involved (i.e. TA, TA_DNA, DNA, RNA and GFP):

$$\frac{dTA}{dt} = k_1 - k_2.TA.DNA - k_4.TA + k_3.TA_{DNA} \quad (1)$$

$$\frac{dTA\_DNA}{dt} = k_2.TA.DNA - k_5.TA\_DNA - k_3.TA\_DNA \quad (2)$$

$$\frac{dDNA}{dt} = k_3.TA\_DNA - k_2.TA.DNA \quad (3)$$

$$\frac{dRNA}{dt} = k_5.TA\_DNA - k_6.RNA - k_7.RNA \quad (4)$$

$$\frac{dGFP}{dt} = k_6.RNA - k_8.GFP \quad (5)$$

These equations can be used in order to predict the time required to reach a given GFP expression level after gene induction. Basically, GFP-related fluorescence can be monitored non-invasively and in a non-destructive way by a lot of equipments comprising excitation sources and appropriate photomultipliers (Randers-Eichhorn, 1997, Kostov, 2000). However, there are more and more GFP measurements carried out with flow cytometer (Patkar, 2002, Galbraith, 1999, Tracy, 2010, Diaz, 2010). This equipment allows the separation of cells prior to analysis, leading to single-cell measurements. The major reason for this increasing interest for flow cytometry relies on the fact that microbial cells are able to exhibit various phenotypes in a same culture broth. Many reasons have been identified to lead to this phenotypic heterogeneity, among which various intrinsic biological processes (cell cycle and division) and extrinsic physico-chemical conditions (impact of the environment on microbial cells) (Müller, 2010). In our case, the recognized stochasticity associated to gene expression (MacAdams H.H., 1997, Swain P.S., 2002) is of major importance since it affects directly GFP synthesis (Mettetal, 2006). To account for these random components, several stochastic models have been developed. Most of these modes are based on the Gillespie algorithm in order to include the stochasticity at the level of the biochemical reactions (Gillespie D.T., 2001). In order to demonstrate the potential impact of stochastic gene expression on GFP synthesis, equations (1) to (5) have been implemented at the level of the Gillespie algorithm. Simulation has been performed with the following parameters: k1 = 0.1 s^{-1}; k2 = 0.05 s^{-1} ; k3 = 0.045 s^{-1} ; k4 = 0.09 s^{-1} ; k5 = 0.1 s^{-1} ; k7=0.0058 s^{-1} ; k6=0.1155 s^{-1} ; k8=0.0002 s^{-1},and considers that the biosensor is activated after 1hour (Fig. 4). Simulated results show that GFP content at the single cell level can vary according to the random nature of the biochemical reactions (Fig. 3). This randomness has to be attributed to the extremely small reacting volume represented by the microbial envelope and the rather small amount of DNA and RNA molecules involved.

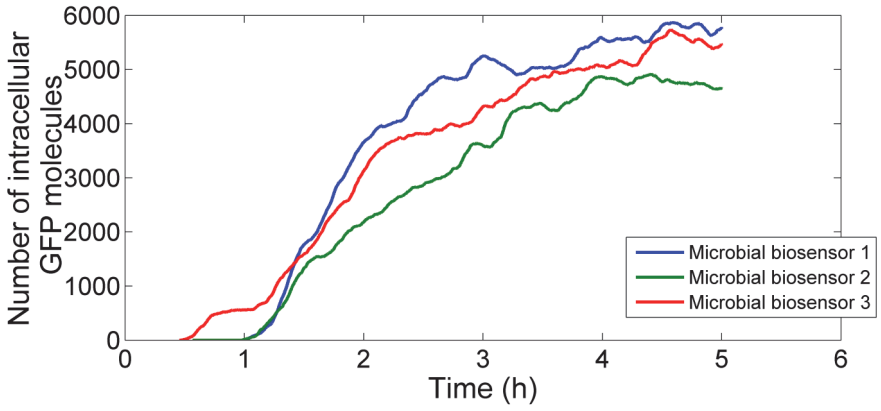

Fig. 4. Stochastic simulation of the GFP evolution at the single cell level according to the biochemical reaction scheme depicted at figure 3.

By repeating several time the simulation, it is possible to simulate the fate of GFP expression at the single cell level for a whole microbial population. By this way, phenotypic heterogeneity can be taken into account. Comparison with experimental results obtained by

flow cytometry is also possible by taking into account the background noise and the sensitivity of this equipment (Zhang, 2006) (Fig. 5).

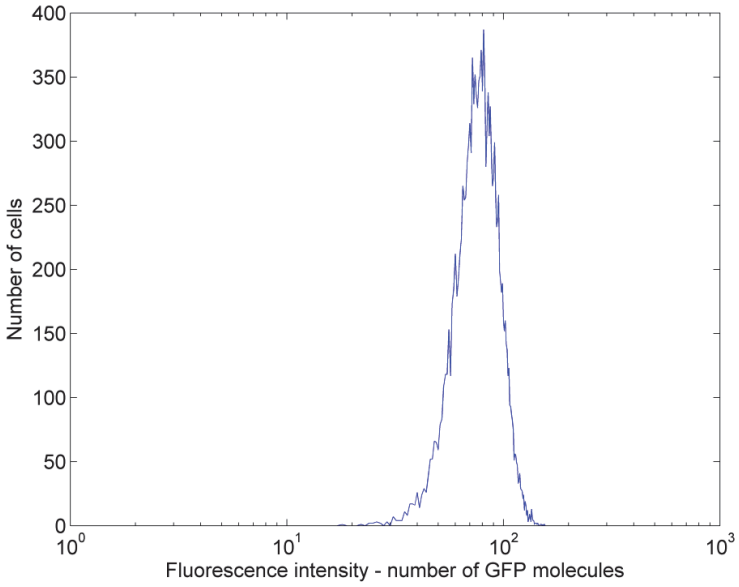

Fig. 5. Simulated histogram for the GFP content at the single cell level for a given time during bioreactor cultivation

The purpose of this work is to demonstrate the applicability for the use of microbial biosensor in a fluctuating reacting volume representative of that encountered in large-scale bioreactor. Single cell behavior will be investigated in order to highlight the impact of both intrinsic and extrinsic sources of noise at the level of GFP expression.

3. "Material and methods" items used in order to illustrate the principles covered in this chapter

The experimental results that will be used to illustrate this chapter come from an important set of experiments involving different *E. coli* GFP reporter strains coming from a public collection (Zaslaver, 2006). Two techniques have been used for GFP detection: a classical spectrofluorimeter and flow cytometry. Most of the experiments carried out in this work have been based on a fluorescence signal are measured by flow cytometry, considering the single cell capability of this techniques. This approach allows to interpret the data by considering the stochastic mechanisms (noise) inherent to GFP expression and to fluctuations met in heterogeneous environment (Müller, 2010, Patnaik, 2002, Patnaik P.R., 2006). Techniques are detailed in the following sections.

3.1 Strains and medium

E. coli K12 MG1655 bearing a pMS201 (4260 bp) plasmid with a stress promoter and a kanamycin resistance gene. The strains comes from a cloning vector library elaborated at the

Weizmann Institute of Science (Zaslaver, 2006). Three reporter strains have been selected from this library, according to the responsiveness of their promoter to carbon limitation, i.e. the general stress response promoter *rpoS*, the carbon starvation induced promoter *csiE* and the universal stress protein associated promoter *uspA*. A constitutive promoter *cyaA* has been used as a basis for comparison (Fig. 6). Microbial biosensors are maintained at -80°C in working seeds vials (2 mL) in solution with LB media and with 40% of glycerol. Precultures and cultures have been performed on a defined mineral salt medium containing (in g/L): K_2HPO_4 14.6, $NaH_2PO_4.2H_2O$ 3.6 ; Na_2SO_4 2 ; $(NH_4)_2SO_4$ 2.47, NH_4Cl 0.5, $(NH_4)_2$-H-citrate 1, glucose 5, thiamine 0.01, kanamycin 0.1. Thiamin and kanamycin are sterilized by filtration (0.2 µm). The medium is supplemented with 3mL/L of trace solution, 3mL/L of a $FeCl_3.6H_2O$ solution (16.7 g/L), 3mL/L of an EDTA solution (20.1 g/L) and 2mL/L of a $MgSO_4$ solution (120 g/L). The trace solution contains (in g/L): $CoCl_2.H_2O$ 0.74, $ZnSO_4.7H_2O$ 0.18, $MnSO_4.H_2O$ 0.1, $CuSO_4.5H_2O$, $CoSO_4.7H_2O$. Before each bioreactor cultivation experiment, a precultivation step is performed in 100 mL of the above mentioned medium in baffled shake flask at 37°C and under orbital shaking at 160 rounds per minute. Cell growth has been monitored by optical density (OD) at a wavelength of 600 nm. Cell dry weight has been determined on the basis of filtered samples (0.45 µm) dried during 24 hours at 105°C. Glucose concentration has been monitored by an electro-enzymatic system YSI.

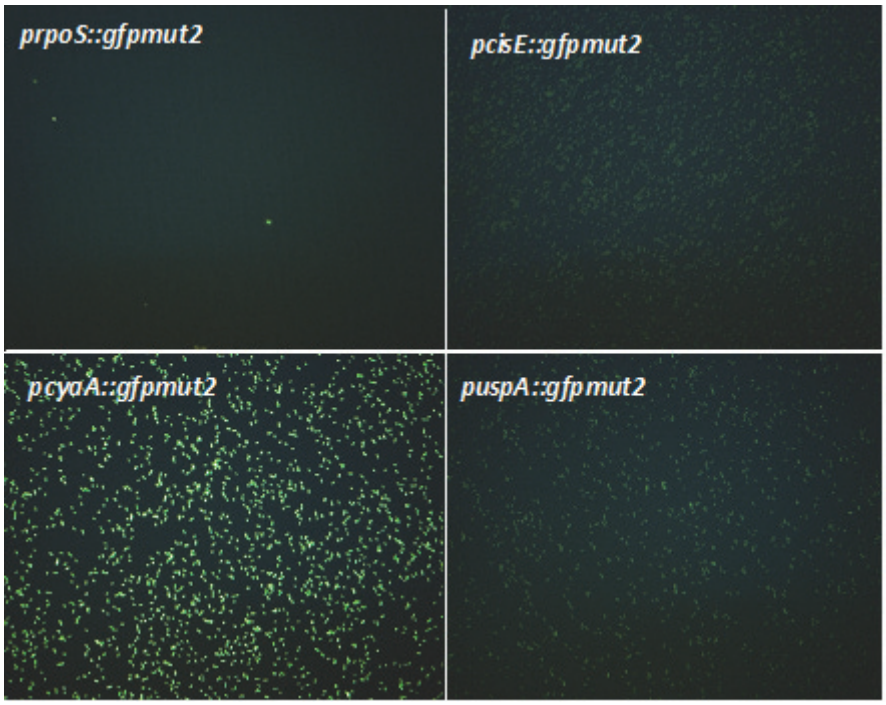

Fig. 6. Epifluorescence microscopy pictures showing the relative intensity of the basal level of GFP expression for the different microbial biosensors involved in this work

3.2 Bioreactor configurations

Microbial GFP biosensors have been cultivated in a lab-scale stirred bioreactors (Biostat B-Twin, Sartorius) operated in fed-batch mode (total volume: 3L; initial working volume: 1L; final working volume: 1.5L; mixing provided by a standard RTD6 rushton turbine). The bioreactor platform comprises 2 cultivation vessels in parallel monitored and controlled by the same control unit (remote control by the MFCS/win 3.0 software). For each reporter strains, experiments have been conducted in parallel by considering a culture performed in the classical stirred vessel and another one conducted with the stirred vessel connected to a recycle loop. This last apparatus correspond to a scale-down strategy allowing to reproduce heterogeneities expected in large-scale bioreactors (Hewitt, 2007a, Lara, 2006, Delvigne, 2006a). The scale-down reactor arrangement is based on the previously described stirred bioreactor connected to a recycle loop (silicon pipe; diameter 0.005m ; length 6m or 12m in order to modulate the residence time in the recycle loop). A continuous recirculation of the broth between the stirred reactor and the recycle loop is ensured by a peristaltic pump (Watson Marlow 323) with the glucose feed solution being added at the inlet of the recycle loop in order to generate a concentration gradient. Fed-batch is controlled on the basis of dissolved oxygen (setpoint : 30% above saturation). The dissolved oxygen in the recycle loop is monitored by a set of sterilizable optical probes (Flow-through cell, Presens). The sensor spot inserted in the flow-through cell contains a fluorogenic compound that is excited at a wavelength of 540 nm. The emission signal can then be recorded at 640 nm. The dissolved oxygen measurement is based on the properties that molecular oxygen is able to absorb a part of the emission energy. The relationship between dissolved oxygen and fluorescence intensity is nonlinear and can be expressed by the Stern-Volmer equation (John, 2003). The excitation and emission signals are generated / recorded at the level of a miniaturized set of excitation led and photomultiplier. The fluorescence signal coming from planar sensors is then processed and recorded at the level of an oxy-4 mini transmitter. During the experiments, pH was maintained at 6.9 (regulation by ammonia and phosphoric acid) and temperature at 37°C. Stirrer rate is maintained at 1000 rpm with a RDT6 impeller and air flow rate is set to 1 L/min at the beginning of the culture. When fed-batch is started agitation rate and air flow rate are progressively raised to 1300 rpm and 2 L/min respectively. Culture is fed with 500 mL of a solution containing 400 g/L of glucose diluted in mineral medium (see above for composition). Continuous cultures have also been performed on the basis of the same stirred bioreactor with the same settings. In this case, fresh culture medium is added continuously and spent medium is withdrawn in order to keep a constant volume. The fresh medium feed rate is modulated in order to reach dilution rate of 0.02 h^{-1} and 0.2 h^{-1}.

3.3 Flow cytometry

The analysis of the GFP expression level has been performed by Fluorescence Activated Cell Sorting (FACS) on a FACScan (Becton Dickinson) flow cytometer. Samples are taken directly from the reactor and are diluted in 900 µL of PBS and 100 µL of a chloramphenicol solution (50 µg/mL) in order to stop protein synthesis. For each measurement, 30,000 cells are analyzed. GFP is excited at 488 nm and emission signals are collected by using filters at 530 nm. The gfp-mut2 variant has been especially engineered to optimally match the excitation/emission range of the FACS instrument (Cormack, 1996). Considering that bacterial cells exhibit a high side scatter (SSC) signal(Galbraith, 1999), a threshold of 52 has been set up on the SSC channel in order to limit noise signal. The FSC, FL1, FL2 and FL3

channels are logarithmically amplified with the following settings: FSC E00, FL1 620, FL2 420, FL3 420. The results have been analyzed by the FlowJo version 7.6.1 software. Flow cytometry has also been used in order to determine the residence time distribution inside the recycle loop of the SDRs and the membrane permeability of the cells (see above).

3.4 Tracer test for the determination of the residence time distribution inside the recycle loop of the SDRs

Fluorescent microspheres (fluorosphere 1µm, molecular probes, invitrogen) have been used as representative tracer for the determination of the residence time distribution of the microbial cells inside the recycle loop of the SDRs. Indeed, tracer test involving particulate dye instead of soluble dye has been recently recognized as more relevant to describe the transport of microbial cells (Asraf-Snir, 2011). We have also use this method previously for the characterization of the transport of fluorescently labeled microbial cells in scale-down reactors (Delvigne, 2006b). Our methodology has been improved in the present work, mainly at the level of the method used to detect fluorescent particles. A tracer pulse of 1 mL containing 10^9 fluorescent beads has been injected at the inlet of the recycle loop. Samples of 3 mL are taken at different time intervals at the outlet of the recycle loop. Samples are analyzed by flow cytometry. Beads are easily detected according to their high green fluorescent level (FL1 detection). The analysis is performed for 30s and the number of events recorded during this period is used as a measure of the beads concentration. The number of events is gated on the basis of the FL1 parameter in order to make the distinction between fluorescent beads and background (software analysis performed on FlowJo 7.6.1.). The RTD curves are processed with MatLab to determine the following parameters:

$$t_R = \frac{\sum_i^{n-i} t_i.C_i.\Delta t_i}{\sum_i^{n-i} C_i.\Delta t_i} \quad (6)$$

$$\sigma^2 = \frac{\sum_i^{n-i} t_i^2.C_i.\Delta t_i}{\sum_i^{n-i} C_i.\Delta t_i} - t_R^2 \quad (7)$$

With t_R being the mean residence time of the RTD (s); C_i the number of beads detected during the time interval t_i and σ^2 the variance of the RTD (s^2).

The SDRs considered here comprise a well-mixed stirred bioreactor connected to a recycle loop. Glucose is injected at the inlet of the recycle loop in order to generate a concentration gradient. As stated in a previous work, the intensity of the concentration gradient, but also the frequency at which microbial cells are exposed to these gradients is important (Delvigne, 2006a). In order to assess the performances of the SDRs, the residence time distribution (RTD) of microbial cells has been determined by using an innovative tracer test. Mathematical treatment of the RTD curves led to the following results: in the case of the SDR with a recycle loop L = 6 m : mean residence time t_R = 38.2 s and variance σ^2 of 62.2 s^2 ; in the case of the SDR with a recycle loop L = 12 m : t_R = 79.8 s and σ^2 = 120.7 s^2.

3.5 Supernatant analysis: fluorescence, SDS-page and western blot

Samples coming from bioreactor are centrifugated at 12000 rpm for 3 minutes and filtered on 0.2 µm cellulose membrane in order to remove the cells. Fluorescence of the supernatant (samples of 200 µL on 96 wells black microtiter plate) is analysed by spectrofluorimetry (Victor³ V Wallac, Perkin Elmer). Proteins coming from the supernatant (7 µL) are separated

on 30% polyacrylamide gels (Biorad). Immunoblot is performed in order to detect the band corresponding to GFP (ECL plus detection system, Amersham).

3.6 Membrane permeability

Samples taken from bioreactor are diluted in PBS in order to reach an optical density of 4. Cells are stained by adding 10µL of propidium iodide solution (PI) for 15 minutes at 37°C. Samples are then analyzed by flow cytometry with the following settings : FSC E00, FL1 620, FL2 420, FL3 520.

3.7 Mathematical modeling

Mathematical modeling procedures allowing the simulation of the gradients experienced by microbial biosensors developed in this work will be explained directly in the text for the ease of understanding. All the codes are written in MatLab and are based on standard algorithm (notably the ode function has been used for the resolution of ODEs systems). Sample codes are provided in annex. Please refer to a reference book (e.g., (Finlayson, 2006)) for additional explanations about appropriate use of the .m codes.

4. Investigation of the dynamics of several GFP microbial biosensors responsive to substrate limitation

Two strategies, involving each a given bioreactor mode of operation, will be considered in order to assess the performance of selected microbial biosensors. The chemostat reactor allows to test the responsiveness of the microbial biosensor in fully stabilized conditions, whereas the scale-down reactor (SDR) allows to better reproduce the complex environmental perturbations encountered in industrial scale bioreactor operating in fed-batch mode.

4.1 Investigation in continuous bioreactors : chemostat mode

In order to assess the responsiveness of the microbial biosensor, a culture in chemostat mode has been performed by considering a sharp variation at the level of the dilution rate. Indeed, the *csiE* biosensor is supposed to be induced upon carbon limitation, a condition that can be easily implemented in a chemostat under controlled conditions (i.e., constant cell density and growth rate with constant environmental variables such as pH and dissolved oxygen). The culture is started by a batch phase and no evolution of the fluorescence is noticed during this phase according to the fact that microbial growth is not limited and substrate is in large excess. At the end of the batch phase, bioreactor is switched to continuous mode at a very low dilution rate of 0.02 h^{-1} (Fig. 7) At this stage, *csiE* promoter is activated and fluorescence level rises significantly and reach a constant value after 60 hours of culture (corresponding to the equilibrium time considered when using a D = 0.02 h^{-1}). When equilibrium is reached, dilution rate is rapidly switched to 0.2 h-1 leading to a shift of the environmental conditions to less limiting at the level of the carbon source. As expected, fluorescence level drops considering the decrease of the activation of the *csiE* promoter. However, fluorescence level does not go back to its initial basal level. As a last step of experiment, a glucose pulse of 5 g/L has been performed in order to relieve completely glucose limitation leading to the drop of fluorescence level to its initial state. This series of experiments validate the responsiveness of the *csiE* promoter to glucose limitation.

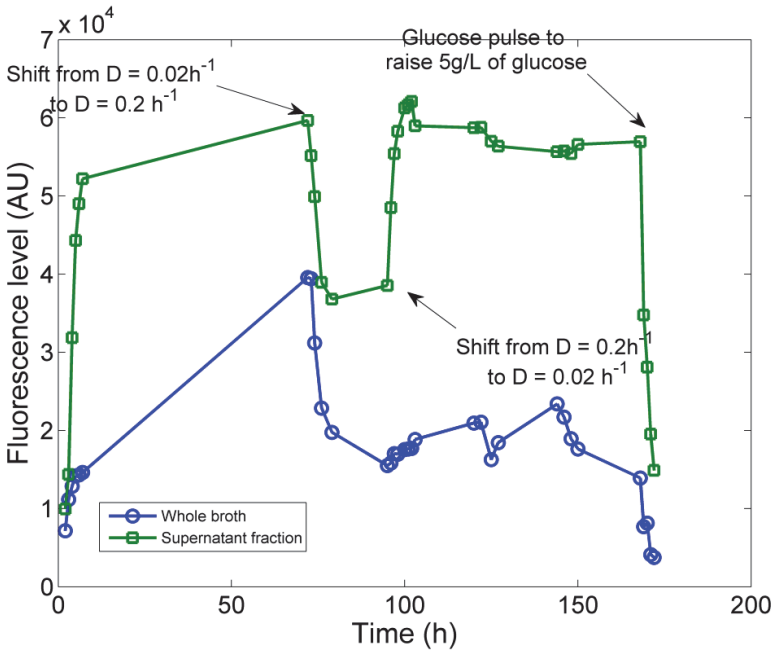

Fig. 7. Evolution of the global fluorescence for a culture carried out by using the *csiE* microbial biosensor in chemostat. Initial batch phase ends at 2 hours and is followed by a continuous mode of culture.

The GFP distribution among the microbial population has been determined by flow cytometry (Fig. 8). Results show that, even when all the microbial biosensors are cultivated under strictly constant environmental conditions, heterogeneity at the level expression is observed. This phenomenon has to be attributed to the stochastic mechanisms governing GFP expression (described as the intrinsic source of noise in section 2) and must be further taken into account to make the difference between intrinsic and extrinsic or environmental source of noise. The extrinsic source of noise will be experimentally generated at the level of a scale-down bioreactor.

4.2 Investigation in scale-down reactors (SDR)

In industrial bioreactor, the picture is by far more complex since extrinsic noise has to be added to the intrinsic one. Indeed, the drop of mixing efficiency induces the appearance of concentration gradient. In order to characterize the concentration fluctuations met by the microbial cells, the circulation process must be superimposed to the concentration gradient. However, it is well known that this circulation process is subject to stochasticity in large-scale bioreactor, and can be characterized by a circulation time distribution (Nienow A.W., 1998). This kind of stochastic process is at the basis of the extrinsic source of noise, i.e. the extracellular fluctuations experienced by the cells and potentially leading to a stress response (Müller, 2010). In order to take into account this extrinsic component, a two-compartment scale-down bioreactor experiment has been set up. In this kind of apparatus, the passage of the cells through the tubular section is an extrinsic stochastic phenomenon

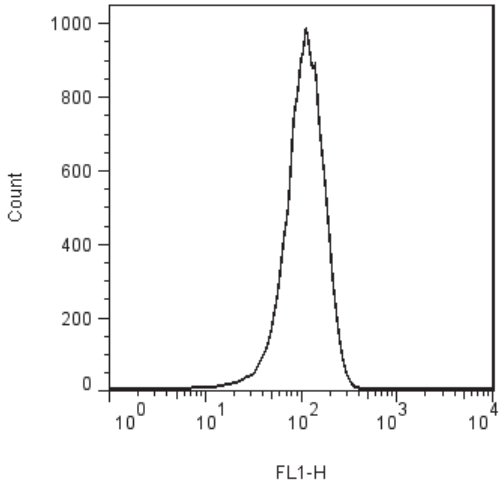

Fig. 8. Distribution of the GFP-related fluorescence determined by flow cytometry (green component of the fluorescence determined by the FL1 channel). Sample has been taken from a culture involving the csiE biosensor in a chemostat at D = 0.02 h^{-1}

that leads to the exposure to local glucose fluctuations. By this way, it is possible to expose the microbial cells belonging to the same population to extracellular fluctuations at different frequencies and intensities (Fig. 9).

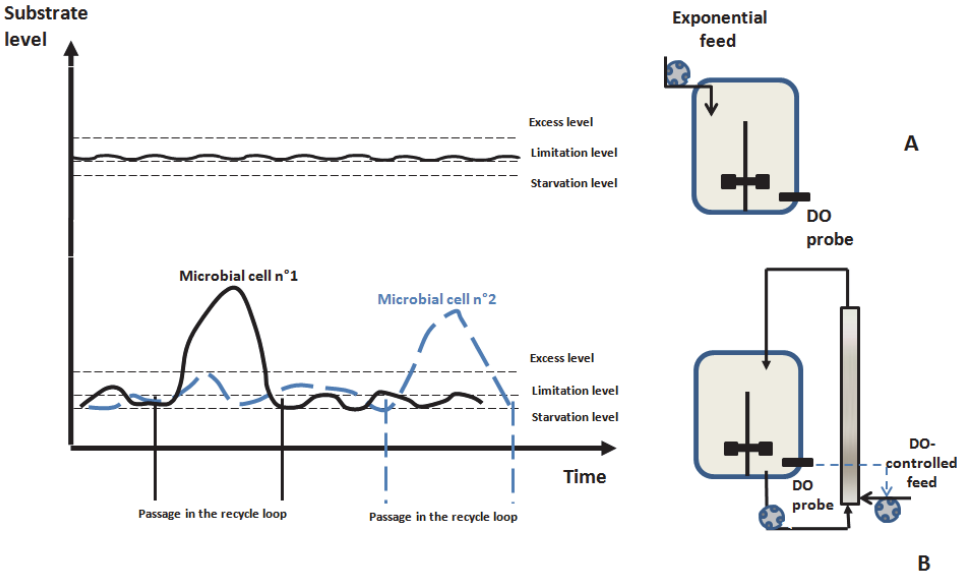

Fig. 9. Illustration of the scale-down reactor (B) principle and comparison with normal (A) mode of substrate addition during fed-batch

The dynamics of four GFP biosensors have been tested comparatively in a stirred bioreactor (considered as well-mixed) and a scale-down reactor with a recycle loop (Fig. 10).

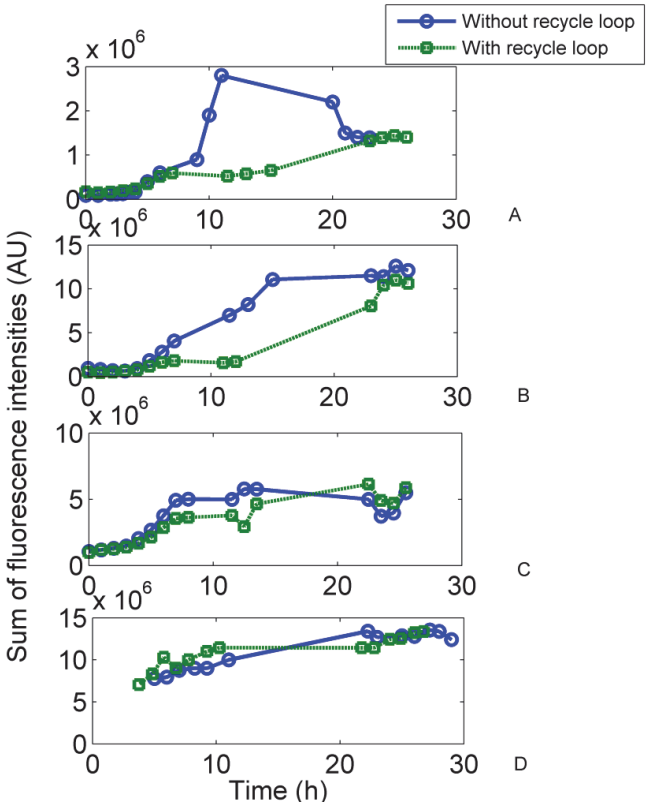

Fig. 10. Evolution of the GFP-related fluorescence for the *rpoS* (A), *csiE* (B), *uspA* (C) and *cyaA* (D) biosensor in lab-scale bioreactor and in SDR

The *cyaA* strain has been chosen as a reference and exhibits a strong constitutive GFP expression throughout the culture. In addition, GFP expression is not affected by the perturbations induced by the presence of the recycle loop in the case of the SDR experiment. For the three other reporter strains involving stress promoters, a significant induction is observed when the bioreactor is shift to the fed-batch mode after 4 hours of cultivation. The *rpoS* and *csiE* exhibits a very low basal level of GFP expression, whereas this basal level is high in the case of the *uspA* strain. This quite high basal level has been previously observed with an equivalent *lacZ* transcriptional reporter strain cultivated in fed-batch mode (Prytz, 2003). A significant difference has been noticed at the level of the induction profile between classical and scale-down bioreactor for the *rpoS* and *csiE* strains. This environmental condition seems to be met during the fed-batch culture when the carbon flow inside the bioreactor is limited in order to avoid dissolved oxygen limitation. In the case of the scale-down bioreactor experiments, glucose is injected at the level of the recycle loop and microbial cells are thus exposed to glucose fluctuations. In our case, these fluctuations tend

to slow down the induction dynamics of the promoters associated to the carbon starvation network. The *rpoS* promoter induces the expression of the sigma S factor, i.e. the master regulator of the general stress response when *E. coli* is carbon limited or starved (Storz, 2000). Interestingly, the *csiE* promoter is sigma S dependent (Marschall, 1995) and exhibits also a significant difference of level of induction when the corresponding reporter strain is cultivated in SDR. The *uspA* reporter strain shows no significant difference at the level of the GFP intensity when the culture is performed in classical bioreactor or in SDR. In all cases, the three stress promoters (the *cyaA* being considered as constitutive) show a significant increase in their level of induction when cultures are shifted to fed-batch mode. This observation can be attributed to the fact that the *rpoS*, *cisE* and *uspA* promoters are known to be induced in carbon limiting conditions which is the case in our fed-batch experiments. At this stage, it is important to relate biosensor response to environmental perturbations experienced in SDR. This point will be discussed in the next section.

5. Mathematical modelling of the local heterogeneities met by microbial cells in scale-down bioreactors

The characterization of the environmental fluctuations perceived by microbial biosensors is an essential step in order to understand the dynamics of GFP expression. However, the extracellular perturbations perceived at the single cell level involve several components including bioreactor hydrodynamics, but also the displacement of the microbial cells themselves along the gradient field. The purpose of the next two sections is to provide the reader with basic and advanced mathematical tools in order to simulate concentration fluctuations perceived at the single cell level in a SDR.

5.1 Simulation of the concentration gradient fields inside bioreactors

The appearance of concentration gradients (substrate, dissolved oxygen, pH,…) in large-scale bioreactors can have severe consequences at the level of the viability of the microorganisms and thus at the level of the bioprocesses performances. The characterization of these gradients in function of the bioreactor design modification and the up-scaling procedures is of particular importance and is generally achieved by the aim of structured hydrodynamic models that can be classified into three distinct classes with increasing level of complexity (Guillard F., 1999). The simplest structured hydrodynamic model is based on a rough compartimentalisation of the bioreactor in a few virtual fluid zones. This kind of model has been used with success to characterize axial concentration gradient in multi-impeller systems (Mayr B., 1993, Vrabel P., 2001, Machon V., 2000, Cui Y.Q., 1996, Vasconcelos J.M.T., 1995). The advantage of such model relies on its simple physical and mathematical representation, i.e. respectively mass balance and ordinary differential equations, for the expression of the time evolution of a given chemical species in each compartment, allowing to connect the hydrodynamic modeling procedure with complex microbial growth model (Vrabel P., 2001). However, the compartment model is limited by its poor spatial resolution. This problem has been overcome by the use of network-of-zones (NOZ) models. The NOZ model is based on the same physical and mathematical principles than for the compartment model, but in this case the number of virtual fluid zones has been significantly increased, allowing a higher spatial discretization of the bioreactor domain. NOZ models comprising up to 36,000 fluid zones have been used (Hristov H.V., 2004) and

have allowed to capture to some extent the complex liquid or gas-liquid flow patterns in stirred or pneumatically agitated bioreactors (Hristov H.V., 2004, Zahradnik J., 2001, Mann R., 1997). However, the elaboration of NOZ models is based on some prior knowledge, such as the streamlines pattern (Hristov H.V., 2004), which is difficult to obtain for complex turbulent flow. A second limitation is the hypothesis that all the circulation flows between the fluid zones have the same intensities, which can leads to the abstraction of local stagnant zones that can have a detrimental effect at the level of the bioprocess. The best representation of fluid flow phenomena is achieved by a more complex model based on the transport of momentum throughout the reactor called computational fluid dynamics (CFD). CFD is based on the Navier-Stokes equations and allows the determination of a large diversity of complex flow patterns, including the transition between flow regimes. However, the computational difficulties associated with the related partial-differential equations make it difficult to link with complex biological reaction. However, some significant results have been obtained by coupling CFD with biochemical reactions (Lapin A., 2006, Schmalzriedt S., 2003), but at a high computational cost. A new approach involves the integration of CFD data (mainly, the orientation of the flow vectors) to build the NOZ model (Bezzo, 2005). Such approach combines the power of CFD with the ease of use of the NOZ models. In this work, discussion will be focused on the application of NOZ based models.

The most critical parameter that has to be taken into account in order to simulate efficiently glucose gradients generated in the SDR is the pulse frequency of the feed pump. In general, different categories of behaviour can be depicted in function of the relative importance of the feed pump frequency and the mixing time of the SDR or the residence time inside the recycle loop:

- For a time interval between two pulses (T_{pulse}) smaller than the global mixing time of the system, the mean concentrations experienced by the microorganisms are very low. This is due to the fact that, between two pulses, the concentration gradient at the level of the mixed part of the SDR disappears.
- For T_{pulse} approximatively equal or superior to the mixing time of the scale-down reactor, concentration gradient is maintained. This concentration gradient persistence leads to the increase of the mean concentration experienced by the microorganisms, as well as an increase of the variance of the frequency distribution.

In our case, the glucose addition frequency is governed by a regulation loop involving the dissolved oxygen signal, i.e. when the DO signal raise above 30% from saturation, glucose is depleted and the feed pump is thus activated. On the opposite, when DO signal drops below 30% from saturation, glucose is accumulating in the broth and the oxygen transfer efficiency of the bioreactor is overwhelmed by the biological oxygen requirement, the feed pump is thus deactivated.

The SDR has been modelled following a defined scheme (Fig. 11). The stirred part is considered as a single perfectly mixed reactor, whereas the recycle loop exhibits a strong plug flow behaviour and must then be modelled as a series of perfectly mixed reactors. The hydrodynamics of the SDR has been experimentally determined (see section "material and methods") and the recycle loop (in the case of the SDR with a recycle loop of L = 12m) has been modelled as a series comprising n = 90 perfectly mixed reactor (backmixing flow rate has been taken into account).

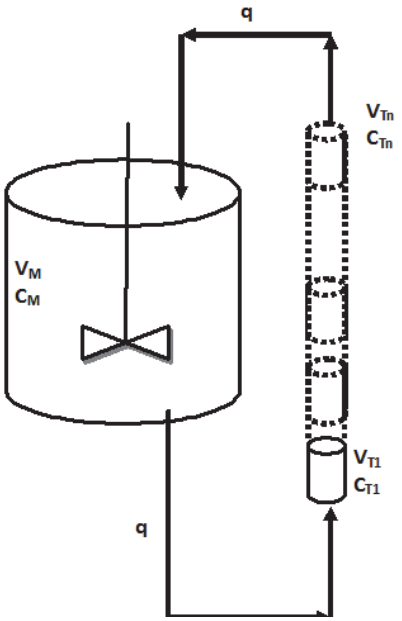

Fig. 11. Scheme of the hydrodynamic model showing the compartimentalization of the SDR into perfectly mixed fluid zones

In order to illustrate the principle of compartimentalization, the following equations can be considered. For the stirred part of the SDR, the evolution of concentration C (g/m^3) with time t (s) on the volume of the mixed part V_m (m^3) depends on the outlet and inlet flow rates q (m^3/s) :

$$V_M . \frac{dC_M}{dt} = q . C_{T6} - q . C_M \tag{8}$$

And for the recycle loop:

$$V_{T1} . \frac{dC_{T1}}{dt} = q . C_M - q . C_{T1} \tag{9}$$

$$V_{T2} . \frac{dC_{T2}}{dt} = q . C_{T1} - q . C_{T2} \tag{10}$$

$$V_{Tn} . \frac{dC_{Tn}}{dt} = q . C_{Tn-1} - q . C_{Tn} \tag{11}$$

Leading to in matrix form:

$$d\begin{bmatrix} C_M \\ C_{T1} \\ C_{T2} \\ \vdots \\ C_{Tn} \end{bmatrix} \Big/ dt = \begin{bmatrix} -q/V_m & 0 & 0 & 0 & 0 & 0 & q/V_m \\ q/V_{T1} & -q/V_{T1} & 0 & 0 & 0 & 0 & 0 \\ 0 & q/V_{T2} & -q/V_{T2} & 0 & 0 & 0 & 0 \\ 0 & 0 & \cdot & \cdot & 0 & 0 & 0 \\ 0 & 0 & 0 & \cdot & \cdot & 0 & 0 \\ 0 & 0 & 0 & 0 & : & \cdot & 0 \\ 0 & 0 & 0 & 0 & 0 & q/V_{Tn} & -q/V_{Tn} \end{bmatrix} . \begin{bmatrix} C_M \\ C_{T1} \\ C_{T2} \\ \vdots \\ C_{Tn} \end{bmatrix} \tag{12}$$

This system of equation (equ. 12) can be resolved numerically in order to simulate, for example, the dynamics of homogenization of a substance in the SDR. In our case, we will use the model is order to simulate the glucose concentration gradient experienced by microbial cells during a fed-batch reaction performed in the SDR. In order to simulate this process, additional equations, representing the glucose addition and consumption and biomass formation must be considered. Full sample codes written in MatLab are given in annex 1 and 2. Based on these equations, the dynamics of glucose inside the SDR can be simulated (Fig. 12).

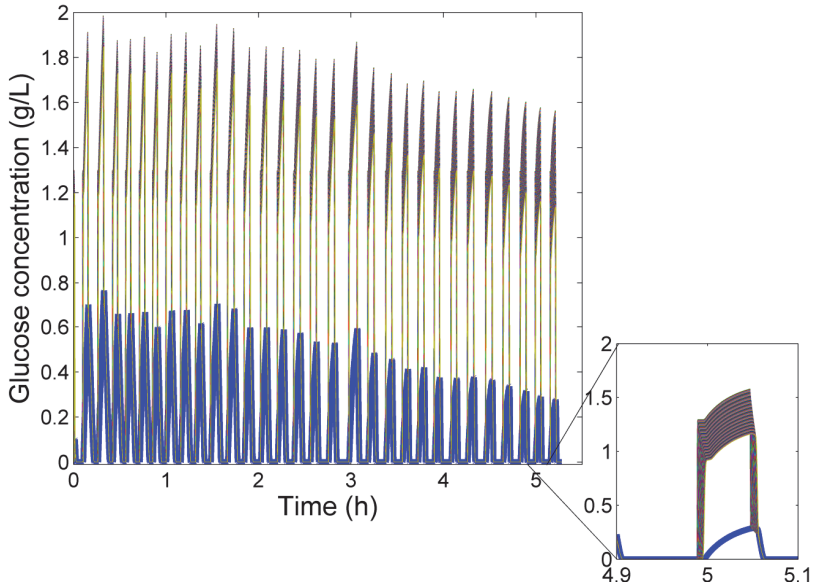

Fig. 12. Simulation of the dynamics of glucose gradient formation in SDR (in blue: glucose profile inside the stirred tank)

Compartimentalization of the SDR allows to take into account the formation of glucose concentration gradient. However, concentration perceived at the single cell cannot be simulated by this way. This issue will be resolved in the next section.

5.2 Stochastic simulation of the displacement of microbial cells along concentration field

The displacement of microbial cells in the environment and in engineered system such as a bioreactor can be represented roughly by convection and/or diffusion-based equations, according to the nature of the convoying medium. However, one of the biggest advantages of using whole cell biosensor is their ability to detect stress at the micrometer scale. If this kind of data as to be interpreted, the environmental fluctuations have to be described at the single cell level and the random component linked with the displacement of the cell has to be taken into account. In the case of bioreactor operations, such displacement can be described by a stochastic version of the hydrodynamic presented previously. Roughly, the same equations are kept but the algorithm used to perform the simulation is quite different

since the stochastic component of the process has to be added to the problem. The basic principle is to use the same model structure as used previously for the simulation of glucose gradient by integrating a random component. The matrix M containing the exchange flow rate (m^3/s) of the NOZ model will be assimilated as the generator matrix Q of the stochastic version of the model (Yin K.K., 2003):

$$M = Q = \begin{bmatrix} -q_{ii} & q_{ij} & 0 & 0 & 0 & 0 \\ q_{ij} & . & . & 0 & 0 & 0 \\ 0 & . & . & . & 0 & 0 \\ 0 & 0 & . & . & . & 0 \\ 0 & 0 & 0 & . & . & . \\ 0 & 0 & 0 & 0 & . & . \end{bmatrix} \quad (13)$$

Physically, Q contains the exchange rates (s^{-1}) between fluid zones. The main diagonal of Q contains the escape rate from the ith fluid zones and is described by the vector λ:

$$\lambda = \begin{bmatrix} q_{ii} \\ . \\ \vdots \\ . \end{bmatrix} \quad (14)$$

Considering mass balance:

$$q_{ii} = -\sum q_{ij} \quad (15)$$

This equation leads to the fact that the sum of each line of matrix Q (equ. 13) equal zero. This property can be used to verify mass balance of the system. Value of vector λ (equ. 14) can be used to compute the residence time distribution for a given fluid zone. This vector is then usually called sojourn time vector. For example, in the case of a fluid zone i :

$$P(x_i) = q_{ii} . e^{-q_{ii} . x_i} \quad (16)$$

The outlet flow rates λ_i will be used to define the occurrence of an event (i.e., in our case the displacement of a microbial biosensor from a fluid zone to another). The times at which events occur are determined from an exponential distribution:

$$T_i = -\frac{\ln(r)}{\lambda_i} \quad (17)$$

For which r is a random number determined from a uniform distribution on the interval [0 1]. When an event is determined, the displacement of the microbial biosensor, i.e. the coordinates of the incoming fluid zone, is determined from the generator matrix Q (equ. 13):

$$P = \frac{Q}{\lambda} + \begin{bmatrix} 1 & 0 & 0 & 0 & 0 & 0 \\ 0 & 1 & 0 & 0 & 0 & 0 \\ 0 & 0 & . & 0 & 0 & 0 \\ 0 & 0 & 0 & . & 0 & 0 \\ 0 & 0 & 0 & 0 & . & 0 \\ 0 & 0 & 0 & 0 & 0 & 1 \end{bmatrix} \quad (18)$$

In the algorithm, event is determined by generating a random number and by comparison with the probability value contained in the line of the P matrix (equ. 18) corresponding to the departure fluid zone.

A stochastic simulation for the displacement of micobial biosensor has been performed by using the SDR framework. Results of the stochastic simulation have been superimposed to the deterministic simulation of the glucose gradient field in the SDR (Fig. 12), leading to the glucose concentration profile experienced at the level of a single biosensor cell (Fig. 13).

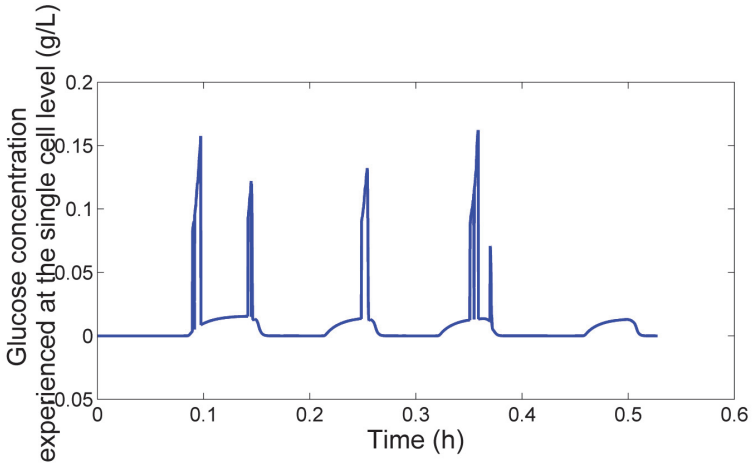

Fig. 13. Simulation of the glucose profile experienced by a microbial biosensor if the SDR

At this point, it is interesting to compare GFP synthesis simulation (Fig. 4) with the environmental fluctuations experienced by the biosensor in the SDR (Fig. 13).

6. Enhancing the usefulness the response of GFP microbial biosensor: measuring viability and protein leakage

6.1 Considering GFP biosensors as viability reporter

In another field of study, GFP biosensors have been used in order to assess microbial viability (Lehtinen, 2004). In their study, authors used unspecific whole cell microbial biosensors in which GFP is constitutively expressed. When cells are exposed to stressful conditions, intracellular GFP intensity is decreased following membrane damages and leakage to the extracellular medium. These findings suggest that GFP can be excreted to the extracellular medium following membrane permeation and/or cell lysis. Another study suggests that GFP can be excreted to the extracellular medium by mechanisms other than cell lysis. Indeed, *E. coli* export system can be involved in the GFP leakage (Fischer, 2008). The potential impact of GFP leakage will be investigated in the next section.

6.2 Protein leakage: what is the part of the secretome that has to be considered as indirect reporter of cell viability?

During cultivations, a significant release of GFP to the extracellular medium has been observed. It is known that about 30% of the proteome of Gram negative bacteria as extracellular protein, this fraction being described as the secretome (Song, 2009). The secretome fraction of *E. coli* comes from the leakage (and not from membrane lysis) of proteins generally found in the outer membrane compartment (Nandakumar, 2006). Protein

leakage can be attributed to the occurrence of stress and/or changes in growth conditions. There is indeed a strong correlation between growth rate, membrane stress and protein leakage (Shokri, 2002, Shokri, 2004, Ling H., 2003). More recently, a series of cultivation tests carried out in intensive fed-batch bioreactor validate the periplasmic origin of the secretome of *E. coli* and the fact that this secretome is modulated in function of cell density and growth phase (Xia, 2008). The purpose of this work is to determine if this release can be correlated to the extracellular fluctuations met in the scale-down bioreactors. At this level, relationship between GFP leakage and membrane permeability could also be a very interesting parameter to investigate, considering the fact that cell membrane integrity based assay is often used in order to assess microbial viability (Klotz, 2010). If the relationship with GFP leakage can be established, this information could be potentially used to expand to use GFP microbial biosensors for viability assessment. Although the proteome of *E. coli*, as well as its secretome fraction has been relatively well characterized in the literature (Han, 2006), only a few studies deal with the release of protein in process-related conditions. Only a single study involving the characterization of the *E. coli* secretome in high cell density culture with control of the main environmental variables (i.e. dissolved oxygen, glucose level, pH and temperature) has been performed so far (Xia, 2008). However, this study has been conducted in a lab-scale, well-mixed bioreactor. In industrial bioreactors, considering the drop at the level of the mixing efficiency, microbial cells are exposed to fluctuations at the level of the main environmental variables (Hewitt, 2007a, Enfors, 2001). It could be thus interesting to characterize the secretome fraction affected by these fluctuations since some studies suggest a strong modulation of the secretome in function of the environmental conditions (Pugsley, 1998).

In order to get a better insight at the level of the presence of extracellular GFP, as set of SDS-PAGE analysis followed by western blotting have been performed on supernatant coming from the different culture conditions (Fig. 14). Western blotting of the culture supernatant shows a band around 30 KDa in most of the cases. Generally this band appears more lately during the culture and is more pronounced in the case of the culture performed in classical bioreactor without recycle loop. This effect can be clearly observed in the case of the *csiE* strain cultivated in normal mode. In this case, a strong GFP band appears after 12 and 24 hours of culture. In the case of the cultures operated in SDRs, the GFP band is only recorded at the end of the process (24h) with a significantly lower intensity. The same relative observation can be made for the *rpoS* strain. For this strain, GFP band intensity is lower in all cases compared with the *csiE* strain, considering the level of expression previously observed. Although the protein secretion machinery is a well known component of the *E. coli* physiology (Pugsley, 1993), only a few studies are actually dealing with the secretion of GFP to the extracellular medium. GFP has been investigated as a secretory reporter in transgenic plant cells where this protein accounted for 30% of the total extracellular proteins (Liu, 2001). This observation highlights the transport potential of GFP to the extracellular medium. In microbial systems, GFP leakage has been considered as a marker for the detection of death cells (Lowder, 2000). According to the results obtained during these studies viable and viable but non culturable (VBNC) cells remained highly fluorescent, whereas death cells exhibited a highly reduced fluorescence level. The drop of fluorescence can be in this case attributed to the increase of the permeability of the compromised membrane of death cells. The release of protein has to be attributed in this case to the rupture of cell membrane under severe stress conditions (Klotz, 2010). If less severe stress conditions are considered, it has been shown that protein leakage is a phenomenon

correlated with nutrient level, growth rate and membrane structure (Liu, 1998, Shokri, 2002). Indeed, it has been observed that a model recombinant protein (β-lactamase (Shokri, 2002)) exhibited an optimal leakage at a dilution rate of 0.3 h^{-1} in chemostat. This observation has been correlated with a high membrane fluidity. This last observation makes the relation with studies involving the permeation of fluorescent product (including GFP) to assess microbial viability. At this point, it would be thus useful to determine if GFP is subjected to non specific leakage depending on the physiological state of the cell and more particularly on the state of the cellular membrane or if GFP is secreted to the extracellular medium by a specific pathway. The results obtained in this section tend to orientate our hypothesis towards a non specific leakage of GFP depending on the bioreactor operating mode. Indeed, there is no clear correlation indicating that GFP is secreted to the extracellular by a specific pathway allowing to keep a appropriate protein conformation (Fischer, 2008).This observation is supported by the fact that supernatant fluorescence levels are very low and not in accordance with the GFP concentrations recorded by western blotting.

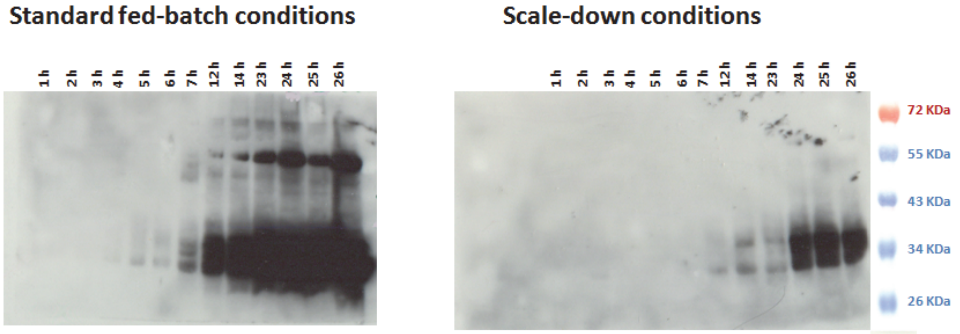

Fig. 14. SDS-PAGE, western blotting of the supernatant for the *csiE* biosensor cultivated in standard bioreactor and in SDR

Microbial cells cultivated in scale-down conditions tend to exhibit a lower PI permeability than those cultivated in normal mode. This result is in accordance with previous scale-down studies involving the determination of the *E. coli* viability by multi parameter flow cytometry (Hewitt, 2000, Hewitt, 2007a). In these works, a combination of PI and BOX staining it has shown a significant drop in cell viability for cultures conducted in lab-scale bioreactors, compared with those conducted in scale-down or industrial-scale bioreactors. It has been argued that this effect can be attributed to the stress associated with glucose limitation, since cultures performed in batch and continuous mode exhibited no significant drop in cell viability (Hewitt, 1999). Another mechanism could be also the adaptation of cells cultivated in SDRs to continuously changing environment and growing at a lower growth rate (Berney, 2006). Flow cytometry profiles (Fig. 15) have been divided into three distinct subpopulation : "PI - first stage" corresponding to microbial cells stained in exponential phase ; "PI - thermal stress" corresponding to cells exposed to 60°C for 30 minutes and between these two states an intermediate subpopulation depicted as "PI - second stage". It can be observed that the stressed fractions (PI-second stage and PI-thermal stress) decreased when cells are cultivated in SDRs instead of the normal mode and when residence time in the recycle loop of the SDR is increased. In general, it can be observed that

of GFP leakage (as shown by western blot analysis of the supernatant) is correlated with higher membrane permeability as shown by PI staining tests.

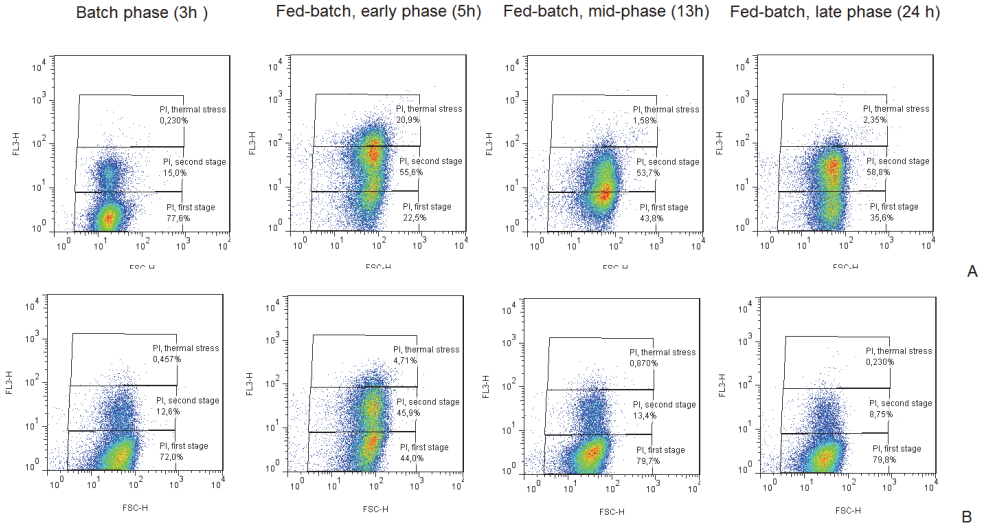

Fig. 15. Evolution of the PI-stained population inside A : standard fed-batch bioreactor B : SDR.

7. Conclusion and future outlook

Successful integration of microbial biosensors could be achieved by characterizing the physico-chemical fluctuations perceived at the single cell level. Modeling procedures described in this work allow the achievement this task, but some uncertainties remain at the level of the dynamics of the GFP biosensor itself. It has been shown that several side phenomena are interacting with the GFP synthesis, such as GFP leakage to the extracellular medium. Our mathematical analysis shows that there are several similarities between the biological and physical processes involved. One common feature is the stochastic mechanisms associated with biosensors circulation inside the bioreactor and GFP synthesis inside microbial biosensors. Both processes can be efficiently simulated by using the Gillespie algorithm leading to a homogeneous mathematical formulation including the biological and physical mechanisms. An important perspective of this work is the elaboration of such model and its validation by dedicated experimental techniques, such as flow cytometry.

8. Annex : MatLab .m files

Annex 1 : SDRdynamics.m file

```
function dydt = SDRdynamics(t,y)

%% Part1 : SDR hydrodynamics
```

```
% Part of the model representing the exchanges between
% n different fluid zones
% These exchanges are modelled in the matrix dF
n = 90; % number of fluide zones
V = 0.117/(n-1); % Volume of the fluid zones (recycle loop of the SDR)(in L)
q = 0.004;  % Estimated flow rate between zones (in L/s)
V2 = 1; %Volume of the stirred part of the SDR (in L)
dF1 = diag(ones(n,1)*(-q/V));
dF2 = diag(ones(n-1,1)*1*(q/V),-1);
dF3 = diag(ones(n-1,1)*0*(q/V),1);
dF = dF1+dF2+dF3;
dF(1,1) = -q/V2;
dF(1,n) = q/V2;
dF(1,2) = 0;

%% Part2 : microbial kinetics (fed-batch mode)

%Part of the model describing consumption and addition of substrate S
% and its conversion into biomass X following a Monod equation
X = y(1:n); % Biomass concentration (in g/L)
S = y(n+1:2*n); % Substrate concentration (in g/L)

Sa = 400; % Substrate concentration in the feed (in g/L)
Yxs = 0.46; % Substrate to biomass conversion yield
mumax = 0.6/3600;  % Maximum growth rate (in s-1)
Ks = 0.025; %Affinity constant for substrate S (in g/L)
Dmax = 0.000013; %Maximum feed flow rate (in L/s)

load oxybin3 %The vector oxybin contains a series of binary number (0 or 1)
             %corresponding to the activation of the feed pump during
             %a real fermentation run

rx = mumax*(S/(S+Ks))*X;
rs = rx./Yxs;
Qfeed = zeros(1,n);
Qfeed(2) = Dmax*Sa/V;
if oxybin3(round(t)+1)==0
  Qfeed(2) = 0;
end
dXdt = rx;
dSdt = ((dF*S)-rs+Qfeed');

dydt = [dXdt;dSdt];
```

Annex 2 : SDRdynamicsrun.m file

```
n = 90;
y0 = zeros(1,2*n);
y0(1:n)=10;

options = odeset('NonNegative',2:n);
[t y]=ode45('SDRdynamics',0:19000,y0,odeset);

figure(1)
plot(t/3600,y(:,n+1:2*n))
xlabel('Time (h)')
ylabel('Glucose concentration (g/L)')
```

9. References

ASRAF-SNIR, M., GITIS, V., 2011. Tracer studies involving fluorescent-dyed microorganisms - A new method for determination of residence time in chlorination reactors. *Chemical engineering journal,* 166**,** 579-585.

BERNEY, M., WEILENMANN, H.U., IHSSEN, J., BASSIN, C., EGLI, T., 2006. Specific growth rate determines the sensitivity of Escherichia coli to thermal, UV and solar disinfection. *Applied and environmental microbiology,* 72**,** 2586-2593.

BEZZO, F., MACCHIETTO, S., PANTELIDES, C.C., 2005. Computational issues in hybrid multizonal/computational fluid dynamics models. *AIChE journal,* 51**,** 1169-1177.

BHATTACHARYY, J., READ, D., AMOS, S., DOOLEY, S., KILLHAM, A., GRAEME, I. P., 2005. Biosensor-based diagnostics of contaminated groundwater: assessment and remediation strategy. *Environmental Pollution,* 134**,** 485-492.

CLEMENTSCHITSCH F., B. K. 2006. Improvement of bioprocess monitoring : development of novel concepts. *Microbial cell factories,* 5**,** 1-11.

CORMACK, B. P., VALDIVIA, R.H., FALKOW, R., 1996. FACS-optimized mutants of the green fluorescent protein (GFP). *Gene* 173**,** 33-38.

CORMACK, B. P., VALDIVIA, R.H., FALKOW, R., . 2000. *FACS optimized mutants of the green fluorescent protein (GFP)*.

CUI Y.Q., V. D. L. R. G. J. M., NOORMAN H.J., LUYBEN K.CH.A.M. 1996. Compartment mixing model for stirred reactors with multiple impellers. *Trans IChemE,* 74**,** 261-271.

DECKWER, W. D., JAHN, D., HEMPEL, D., ZENG, A.P., 2006. Systems biology approaches to bioprocess development. *Engineering in life sciences,* 6**,** 455-469.

DELISA, M. P., LI, J., RAO, G., WEIGAND, W.A., BENTLEY, W.E., 1999. Monitoring GFP operon fusion protein expression during high cell density cultivation of Escherichia coli using an on-line optical sensor *Biotechnology and bioengineering,* 65**,** 54-64.

DELVIGNE, F., DESTAIN, J., THONART, P., 2006a. A methodology for the design of scale-down bioreactors by the use of mixing and circulation stochastic models. *Biochemical engineering journal,* 28**,** 256-268.

DELVIGNE, F., LEJEUNE, A., DESTAIN, J., THONART, P., 2006b. Stochastic models to study the impact of mixing on a fed-batch culture of Saccharomyces cerevisiae. *Biotechnology progress,* 22**,** 259-269.

DIAZ, M., HERRERO, M., GARCIA, L.A., QUIROS, C., 2010. Application of flow cytometry to industrial microbial bioprocesses. *Biochemical engineering journal,* 48**,** 385-407.

ENFORS, S. O., JAHIC, M., ROZKOV, A., XU, B., HECKER, M., JÜRGEN, B., KRÜGER, E., SCHWEDER, T., HAMER, G., O'BEIRNE, D., NOISOMMIT-RIZZI, N., REUSS, M., BOONE, L., HEWITT ,C., MCFARLANE, C., NIENOW, A., KOVACS, T., TRÄGARDH, C., FUCHS, L., REVSTEDT, J., FRIBERG, P.C., HJERTAGER, B., BLOMSTEN, G., SKOGMAN, H., HJORT, S., HOEKS, F., LIN, H.Y., NEUBAUER, P., VAN DER LANS, R., LUYBEN, K., VRABEL, P., MANELIUS, A. 2001. Physiological responses to mixing in large scale bioreactors. *Journal of biotechnology,* 85**,** 175-185.

FINLAYSON, B. A. 2006. *Introduction to chemical engineering computing*, Wiley.

FISCHER, A. C., DELISA M.P., 2008. Laboratory evolution of fast-folding green fluorescent protein using secretory pathway quality control. *Plos One,* 3**,** e2351.

GALBRAITH, D. W., ANDERSON, M.T., HERZENBERG, L.A., 1999. Flow cytometry analysis and FACS sorting of cells based on GFP accumulation. *Methods in cell biology,* 58**,** 315-341.

GARCIA, J. R., CHA, H., J., RAO, G.G., MARTEN, M.R., BENTLEY, W.E., 2009. Microbial nar-GFP cell sensors reveal oxygen limitations in highly agitated and aerated laboratory-scale fermentors. *Microbial cell factories,* 8**,** 6.

GILLESPIE D.T. 2001. Approximate accelerated stochastic simulation of chemically reacting systems. *Journal of chemical physics,* 115**,** 1716-1733.

GUILLARD F., T. C. 1999. Modeling the performance of industrial bioreactors with a dynamic microenvironmental approach : a critical review. *Chemical engineering and technology,* 22**,** 187-195.

HAN L., E. S. O., HÄGGSTRÖM L. 2002. Changes in intracellular metabolite pools and acetate formation in Escherichia coli are associated with a cell density dependent metabolic switch. *Biotechnology letters,* 24**,** 483-488.

HAN, M. J., LEE, S.Y., 2006. The Escherichia coli proteome : past, present and future prospects. *Microbiology and molecular biology reviews,* 70**,** 362-439.

HEWITT, C. J., NEBE-VON CARON, G., AXELSSON, B., MC FARLANE, C.M., NIENOW, A.W., 2000. Studies related to the scale-up of high-cell-density E. coli fed-batch fermentations using multiparameter flow cytometry : effect of a changing microenvironment with respect to glucose and dissolved oxygen concentration. *Biotechnology and bioengineering,* 70**,** 381-390.

HEWITT, C. J., NEBE-VON CARON, G., NIENOW, A.W., MC FARLANE, C.M., 1999. The use of multi-parameter flow cytomerty to compare the physiological response of Escerichia coli W3110 to glucose limitation during batch, fed-batch and continuous culture cultivations. *Journal of biotechnology,* 75**,** 251-264.

HEWITT, C. J., NIENOW, A.W., 2007a. The scale-up of microbial batch and fed-batch fermentation processes. *Advances in applied microbiology.* Vol. 62.

HEWITT, C. J., ONYEAKA, H., LEWIS, G., TAYLOR, I.W., NIENOW, A.W., 2007b. A Comparison of High Cell Density Fed-Batch Fermentations Involving Both Induced and Non-Induced Recombinant Escherichia coli Under Well-Mixed Small-Scale and Simulated Poorly Mixed Large-Scale Conditions. *Biotechnology and bioengineering,* 96**,** 495-505.

HRISTOV H.V., M. R., LOSSEV V., VLAEV S.D. 2004. A simplified CFD for three-dimensional analysis of fluid mixing, mass transfer and bioreaction in a fermenter equipped with triple novel geometry impellers. *Trans IChemE,* 82**,** 21-34.

JOHN, G. T., KLIMANT, I., WITTMANN, C., HEINZLE, E., 2003. Integrated Optical Sensing of Dissolved Oxygen in Microtiter Plates: A Novel Tool for Microbial Cultivation. *Biotechnology and bioengineering,* 81**,** 830-836.

JONES, J. J., BRIDGES, A.M., FOSBERRY, A.P., GARDNER, S., LOWERS, R.R., NEWBY, R.R., JAMES, P.J., HALL, R.M., JENKINS, O., 2004. Potential of real-time measurement of GFP-fusion proteins. *Journal of biotechnology,* 109**,** 201-211.

KLOTZ, B., MANAS, P., MACKEY, B.M., 2010. The relationship between membrane damage, release of protein and loss of viability in Escherichia coli exposed to high hydrostatic pressure. *International journal of food microbiology,* 137**,** 214-220.

KOSTOV, Y., ALBANO, C.R., RAO, G., 2000. All solid-state GFP sensor. *Biotechnology and bioengineering,* 70**,** 473-477.

LAPIN A., S. J., REUSS M. 2006. Modeling the dynamics of E. coli populations in the three-dimensional turbulent field of a stirred bioreactor - A structured-segregated approach. *Chemical engineering science,* 61**,** 4783-4797.

LARA, A. R., GALINDO, E., RAMIREZ, O.T., PALOMARES, L.A., 2006. Living with heterogeneities in bioreactors - Understanding the effects of environmental gradients on cells. *Molecular biotechnology,* 34**,** 355-381.

LEHTINEN, J., NUUTILA, J., LILIUS E.M., 2004. Green fluorescent protein - propidium iodide (GFP-PI) based assay for flow cytometric measurement of bacterial viability *Cytometry Part A,* 60**,** 165-172.

LING H., E. S. O., HÄGGSTRÖM L. 2003. Escherichia coli high-cell-density culture: carbon mass balances and release of outer membrane components. *Bioprocess and biosystems engineering,* 25**,** 205-212.

LIU, S., BUGOS, R.C., DHARMASIRI, N., SU, W.W., 2001. Green fluorescent protein as a secretory reporter and a tool for process optimization in transgenic plant cell cultures. *Journal of biotechnology,* 87**,** 1-16.

LIU, X., FERENCI, T., 1998. Regulation of porin-mediated outer membrane permeability by nutrient limitation in Escherichia coli. *Journal of bacteriology,* 180**,** 3917-3922.

LOWDER, M., UNGE, A., MARAHA, N., JANSSON, J.K., SWIGGETT, J., OLIVER, J.D., 2000. Effect of starvation and the viable but nonculturable state on green fluorescent protein (GFP) fluorescence in GFP-tagged Pseudomonas fluorescens A506. *Applied and environmental microbiology,* 66**,** 3160-3165.

MACADAMS H.H., A. A. 1997. Stochastic mechanisms in gene expression. *Proc Natl. Acad. Sci.,* 94**,** 814-819.

MACHON V., J. M. 2000. Liquid homogenization in aerated multi-impeller stirred vessel. *Chem. eng. technol.,* 23**,** 869-876.

MANN R., V. D., LOSSEV V., VLAEV S.D., ZAHRADNIK J., SEICHTER P. 1997. A network-of-zones analysis of the fundamentals of gas-liquid mixing in an industrial stirred bioreactor. *Récents progrès en génie des procédés,* 11**,** 223-230.

MARCH, J. C., RAO, G., BENTLEY, W.E., 2003. Biotechnological applications of green fluorescent protein. *Applied microbiology and biotechnology,* 62**,** 303-315.

MARSCHALL, C., HENGGE-ARONIS, R., 1995. Regulatory characteristics and pormoter analysis of csiE, a stationary phase-inducible gene under the control of sigma S and the cAMP-CRP complex in Escherichia coli. *Molecular microbiology,* 18**,** 175-184.

MAYR B., N. E., HORVAT P., MOSER A. 1993. Modelling of mixing and simulation of its effect on glutamic acid fermentation. *Chem. Biochem. Eng. Q.,* 7**,** 31-42.

METTETAL, J. T., MUZZEY, D., PEDRAZA, J.M., OZBUDAK, E.M., VAN OUDENAARDEN, A., 2006. Predicting stochastic gene expression dynamics in single cells. *PNAS,* 103**,** 7304-7309.

MÜLLER, S., HARMS, H., BLEY, T., 2010. Origin and analysis of microbial population heterogeneity in bioprocesses. *Current opinion in biotechnology,* 21**,** 100-113.

NANDAKUMAR, M. P., CHEUNG, A., MARTEN, M.R., 2006. Proteomic analysis of extracellular proteins from Eschercihia coli W3110. *Journal of proteome research,* 5**,** 1155-1161.

NEBE-VON-CARON G., S. P. J., HEWITT C.J., POWELL J.R., BADLEY R.A. 2000. Analysis of bacterial function by multi-colour fluorescence flow cytometry and single cell sorting. *Journal of microbiological methods,* 42**,** 97-114.

NEUBAUER, P., AHMAN, M., TÖRNKVIST, M., LARSSON, G., ENFORS, S.O., 1995. Response of guanosine tetraphosphate to glucose fluctuations in fed-batch cultivations of Escherichia coli. *Journal of biotechnology,* 43**,** 195-204.

NEUBAUER, P., JUNNE, S., 2010. Scale-down simulators for metabolic analysis of large-scale bioprocesses. *Current opinion in biotechnology,* 21**,** 114-121.

NIENOW A.W. 1998. Hydrodynamics of stirred bioreactors. *Applied mechanics review,* 51**,** 3-32.

PATKAR, A., VIJAYASANKARAN, N., URRY, D.W., SRIENC, F., 2002. Flow cytometry as a useful tool for process development : rapid evaluation of expression systems. *Journal of biotechnology,* 93**,** 217-229.

PATNAIK P.R. 2006. External, extrinsic and intrinsic noise in cellular systems : analogies and implications for protein synthesis. *Biotechnology and molecular biology review,* 1**,** 121-127.

PATNAIK, P. R. 2002. Can imperfections help to improve bioreactor performance ? *Trends in biotechnology,* 20**,** 135-137.

PIOCH, D., JÜRGEN, B., EVERS, S., MAURER, K.H., HECKER, M., SCHWEDER, T., 2007. At-line monitoring of bioprocess-relevant marker genes. *Engineering in life sciences,* 7**,** 373-379.

PRYTZ, I., SANDEN, A.M., NYSTRÖM, T., FAREWELL, A.,WAHLSTRÖM, A., FÖRBERG, C., PRAGAI, Z., BARER, M., HARWOOD, C., LARSSON, G., 2003. Fed-batch production of recombinant beta-galactosidase using the universal stress promoters uspA and uspB in high cell density cultivations *Biotechnology and bioengineering,* 83**,** 595-603.

PUGSLEY, A. P. 1993. The complete general secretory pathway in Gram-negative bacteria. *Microbiological reviews,* 57**,** 50-108.

PUGSLEY, A. P., FRANCETIC, O., 1998. Protein secretion in Escherichia coli K-12: dead or alive? *Cell. Mol. Life Sci.,* 54**,** 347-352.

RANDERS-EICHHORN, L., ALBANO, C.R., SIPIOR, J., BENTLEY, W.E., RAO, G., 1997. On-line green fluorescence protein sensor with LED excitation. *Biotechnology and bioengineering,* 55**,** 921-926.

ROOSTALU, J., JOERS, A., LUIDALEPP, H., KALDALU, N., TENSON, T., 2008. Cell division in Escherichia coli cultures monitored at single cell resolution. *BMC microbiology,* 8**,** 68.

SCHMALZRIEDT S., J. M., MAUCH K., REUSS M. 2003. Integration of physiology and fluid dynamics. *Advances in biochemical engineering,* 80**,** 19-68.

SCHWEDER, T., HECKER, M., 2004. Monitoring of stress responses. *Advances in biochemical engineering/Biotechnology,* 89**,** 47-71.

SCHWEDER, T., KRÜGER, E., XU, B., JÜRGEN, B., BLOMSTEN, G., ENFORS, S.O., HECKER, M., 1999. Monitoring of genes that respond to process related stress in large-scale bioprocesses. *Biotechnology and bioengineering,* 65**,** 151-159.

SHANER, N. C., STEINBACH, P.A., TSIEN, R.Y., 2005. A guide to choosing fluorescent proteins. *Nature methods,* 2**,** 905-909.

SHOKRI, A., LARSSON, G., 2004. Characterisation of the Escherichia coli membrane structure and function during fedbatch cultivation. *Microbial cell factories,* 3**,** 9.

SHOKRI, A., SANDEN, A.M., LARSSON, G., 2002. Growth rate dependent changes in Escherichia coli membrane structure and protein leakage. *Applied microbiology and biotechnology,* 58**,** 386-392.

SONG, C., KUMAR, A., SALEH, M., 2009. Bioinformatic comparison of bacterial secretomes. *Genomics proteomics bioinformatics,* 7**,** 37-46.

SORENSEN, S. J., BURMOLLE, M., HANSEN, L.H., 2006. Making bio-sense of toxicity : new developments in whole-cell biosensors. *Current opinion in biotechnology,* 17**,** 11-16.

SOUTHWARD, C. M., SURETTE, M.G., 2002. The dynamic microbe: gree fluorescent protein brings bacteria to ligth. *Molecular microbiology,* 45**,** 1191-1196.

STORZ, G., HENGGE-ARONIS, E., 2000. *Bacterial stress response*, American Society for Microbiology.

SUNDSTROM, H., WALLBERG, F., LEDUNG, E., NORRMAN, B., HEWITT, C.J., ENFORS, S.O., 2004. Segregation to non-dividing cells in recombinant Escherichia coli fed-batch fermentation processes. *Biotechnology letters,* 26**,** 1533-1539.

SWAIN P.S., E. M. B., SIGGIA E.D. 2002. Intrinsic and extrinsic contributions to stochasticity in gene expression. *PNAS,* 99**,** 12795-12800.

TECON, R., VAN DER MEER, J.R., 2006. Information from single-cell bacterial biosensors: what is it good for? *Current opinion in biotechnology,* 17**,** 4-10.

THATTAI M., V. O. A. 2004. Stochastic gene expression in fluctuating environments. *Genetics,* 167**,** 523-530.

TRACY, B. P., GAIDA, S.M., PAPOUTSAKIS, E.T., 2010. Flow cytometry for bacteria : enabling metabolic engineering, synthetic biology and the elucidation of complex phenotypes. *Current opinion in biotechnology,* 21**,** 85-99.

TSIEN R.Y. 1998. The green fluorescent protein. *Annual review in biochemistry,* 67**,** 509-544.

VASCONCELOS J.M.T., A. S. S., BARATA J. M. 1995. Mixing in gas-liquid contactors agitated by multiple turbines. *Chemical engineering science,* 50**,** 2343-2354.

VRABEL P., V. D. L. R. G. J. M., VAN DER SCHOT F.N., LUYBEN K.CH.A.M., XU B., ENFORS S.O. 2001. CMA : integration of fluid dynamics and microbial kinetics in modelling of large-scale fermentations. *Chemical engineering journal,* 84**,** 463-474.

WILES, S., WHITELEY, A.S., PHILP, J.C., BAILEY, M.J. 2003. Development of bespoke bioluminescent reporters with the potential for in situ deployment within a phenolic-remediating wastewater treatment system. *Journal of microbiological methods,* 55**,** 667-677.

XIA, X. X., HAN, M.J., LEE S.Y., YOO, J.S., 2008. Comparison of the extracellular proteomes of Eschercihia coli B and K-12 strains during high cell density cultivation. *Proteomics,* 8**,** 2089-2103.

XU, B., JAHIC, M., BLOMSTEN, G., ENFORS, S.O., 1999. Glucose overflow metabolism and mixed-acid fermentation in aerobic large-scale fed-batch processes with Escherichia coli. *Applied microbiology and biotechnology,* 51**,** 564-571.

YIN K.K., Y. H., DAOUTIDIS P., YIN G.G. 2003. Simulation of population dynamics using continuous-time finite-state Markov chains. *Computer and chemical engineering,* 27**,** 235-249.

ZAHRADNIK J., M. R., FIALOVA M., VLAEV D., VLAEV S.D., LOSSEV V., SEICHTER P. 2001. A network-of-zones analysis of mixing and mass transfer in three industrial bioreactors. *Chemical engineering science,* 56**,** 485-492.

ZASLAVER, A., BREN, A., RONEN, M., ITZKOVITZ, S., KIKOIN, I., SHAVIT, S., LIEBERMEISTER, W., SURETTE, M.G., ALON, U., 2006. A comprehensive library of fluorescent transcriptional reporters for Escherichia coli. *Nature methods,* 3**,** 623-628.

ZHANG, Q., ANDERSEN, M.E., CONOLLY, R.B., 2006. Binary gene induction and protein expression in individual cells. *Theoretical biology and medical modelling,* 3**,** 18.